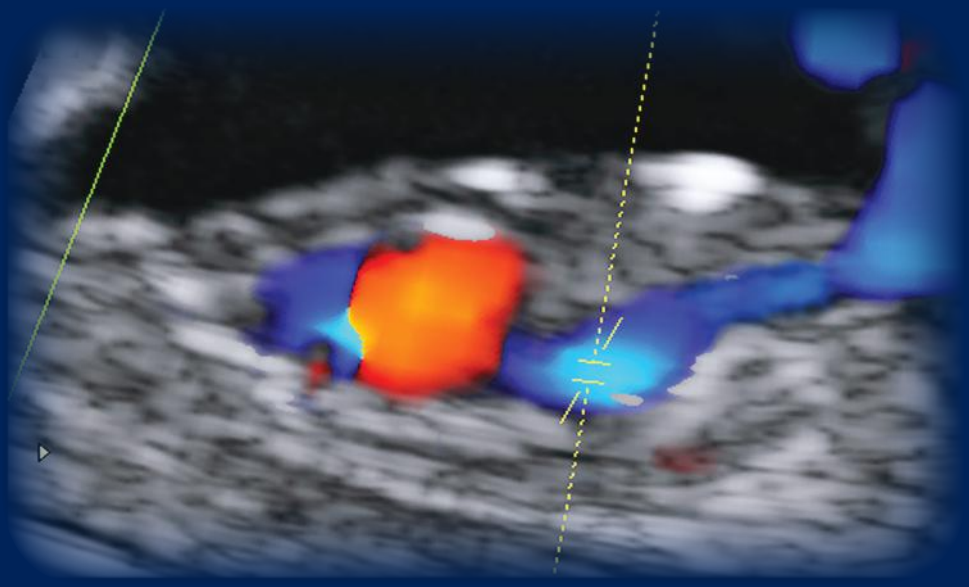
SECOND EDITION

ULTRASOUND OF CONGENITAL FETAL ANOMALIES

Differential Diagnosis and Prognostic Indicators



Dario Paladini • Paolo Volpe

CRC Press
Taylor & Francis Group

ULTRASOUND OF CONGENITAL FETAL ANOMALIES

SECOND EDITION

ULTRASOUND OF CONGENITAL FETAL ANOMALIES

Differential Diagnosis and Prognostic Indicators

Dario Paladini
Head, Fetal Medicine and Surgery Unit
Gaslini Childrens' Hospital, Genoa, Italy

Paolo Volpe
Head, Fetal Medicine Unit, Department of Obstetrics
and Gynecology, Hospitals Di Venere and Sarcone, Bari, Italy

Foreword by Yves Ville

CRC Press
Taylor & Francis Group
Boca Raton London New York

CRC Press is an imprint of the
Taylor & Francis Group, an **informa** business

CRC Press
Taylor & Francis Group
6000 Broken Sound Parkway NW, Suite 300
Boca Raton, FL 33487-2742

© 2014 by Taylor & Francis Group, LLC
CRC Press is an imprint of Taylor & Francis Group, an Informa business

No claim to original U.S. Government works
Version Date: 20140416

International Standard Book Number-13: 978-1-4665-9897-3 (eBook - PDF)

This book contains information obtained from authentic and highly regarded sources. While all reasonable efforts have been made to publish reliable data and information, neither the author[s] nor the publisher can accept any legal responsibility or liability for any errors or omissions that may be made. The publishers wish to make clear that any views or opinions expressed in this book by individual editors, authors or contributors are personal to them and do not necessarily reflect the views/opinions of the publishers. The information or guidance contained in this book is intended for use by medical, scientific or health-care professionals and is provided strictly as a supplement to the medical or other professional's own judgement, their knowledge of the patient's medical history, relevant manufacturer's instructions and the appropriate best practice guidelines. Because of the rapid advances in medical science, any information or advice on dosages, procedures or diagnoses should be independently verified. The reader is strongly urge to consult the relevant national drug formulary and the drug companies' printed instructions, and their websites, before administering any of the drugs recommended in this book. This book does not indicate whether a particular treatment is appropriate or suitable for a particular individual. Ultimately it is the sole responsibility of the medical professional to make his or her own professional judgements, so as to advise and treat patients appropriately. The authors and publishers have also attempted to trace the copyright holders of all material reproduced in this publication and apologize to copyright holders if permission to publish in this form has not been obtained. If any copyright material has not been acknowledged please write and let us know so we may rectify in any future reprint.

Except as permitted under U.S. Copyright Law, no part of this book may be reprinted, reproduced, transmitted, or utilized in any form by any electronic, mechanical, or other means, now known or hereafter invented, including photocopying, microfilming, and recording, or in any information storage or retrieval system, without written permission from the publishers.

For permission to photocopy or use material electronically from this work, please access www.copyright.com (http://www.copyright.com/) or contact the Copyright Clearance Center, Inc. (CCC), 222 Rosewood Drive, Danvers, MA 01923, 978-750-8400. CCC is a not-for-profit organization that provides licenses and registration for a variety of users. For organizations that have been granted a photocopy license by the CCC, a separate system of payment has been arranged.

Trademark Notice: Product or corporate names may be trademarks or registered trademarks, and are used only for identification and explanation without intent to infringe.

Visit the Taylor & Francis Web site at
http://www.taylorandfrancis.com

and the CRC Press Web site at
http://www.crcpress.com

To my boy, Alessandro, and Gloria

—DP

To my father

—PV

Contents

Foreword ix
Preface xiii
Acknowledgments xv

1. Anatomic survey of the fetus and early diagnosis of fetal anomalies 1
2. Central and peripheral nervous system anomalies 31
3. Craniofacial and neck anomalies 97
4. Cystic hygroma and nonimmune hydrops fetalis 137
5. Congenital heart disease 147
6. Thoracic anomalies 233
7. Anomalies of the gastrointestinal tract and of the abdominal wall 267
8. Anomalies of the urinary tract and of the external genitalia 307
9. Skeletal dysplasias and muscular anomalies: A diagnostic algorithm 347
10. Chromosomal and nonchromosomal syndromes 383
11. Ultrasound in fetal infection 437
12. Ultrasound in multiple pregnancy 453

Appendix 469

Foreword

FETAL IMAGING: Mor E ThAN MEETs ThE EyE

I have already had the honor and pleasure of praising the first edition of this book, and I am proud to introduce this new and augmented edition.

Ultrasound has come of age, and ultrasound in obstetrics has deeply changed the practice of clinical obstetrics and will hopefully do so even more in the next few years. However, this is not to say that one or more examinations during pregnancy will simply and directly influence perinatal outcome. Ultrasound is a powerful and very effective tool for fetal assessment, but its success or failure to deliver is intrinsically tied to sound indication and an appropriate management plan. Screening and diagnosis are the two main facets of fetal imaging. They differ mainly in their indications, the level of expertise they require, and, to a certain extent, the complexity of the technology supporting the imaging modality. These largely determine the availability of the investigation, its reproducibility, and accuracy. The number of examinations, and the gestational age at which these examinations are performed, are not only driven by technical and developmental factors but also by economic and social considerations, as well as legal aspects surrounding termination of pregnancy. As a result, screening has moved toward earlier gestations while diagnostic accuracy is increasing at later gestations, when termination of pregnancy (TOP) is either not an option or has stopped being relevant to the management of the pregnancy. Ultrasound screening in pregnancy can be seen as the offer to check the largest number of pregnancies, by the largest number of operators for simple and reproducible criteria in order to make important choices on the management of pregnancy and delivery. Most established screening programs claim figures of around 40%–70% sensitivity (for a 5% false-positive rate) for various conditions such as congenital heart defects and Down syndrome. However divergent their directions can be, both screening and diagnosis demand an ever-increasing knowledge of fetal development and mastering of the technology.

The impact of 3D ultrasound has gradually developed over and above that of a new look at already well-documented fetal structures. Outside a small group of pioneers, promotion of 3D technology has been perceived as an expensive and obsessive campaign to demonstrate that poor 2D images obtained with an inconveniently large transducer could be put together into a grumpy fetal face, to be presented as a breakthrough in fetal imaging. However, over the past five years, this ultrasound modality has overcome these technical, as much as cultural, challenges. Image quality has gained respect from the most demanding operators, and the commercial viability often has become diverse and competitive. At the same time, 3D-champions have moved away from baby-facing into virtual dissection of the relevant fetal anatomy. This approach is now continuously raising the level of diagnostic ultrasound expertise and perhaps more importantly, it is proving to be a remarkable incentive and tool for education. At the beginning of this century, a multiplanar approach of ultrasound was mostly considered eccentric or unnecessary, and rarely was this concept seen as either innovative or logical. In the past, registrars were often described as having either surgical or obstetric skills. However, many of us have noticed that we now also see ultrasound skills burgeoning in first-year trainees and a five-year follow-up often proves us right. It is not by chance that ultrasound has gradually moved away from being an exclusive and

select apprenticeship, to becoming a discipline that can be learned while providing the culture and the tools of quality assessment we have long been missing. The frontier between education and research is often subtle, especially owing to the critical importance of subjectivity and reproducibility, two extreme and antagonistic components of ultrasound examination. Education is, therefore, likely to remain the most significant individual contribution each one of us can make to the improvement of perinatal care. Screening and diagnosis address two different issues. However, there is a continuum between them, so much so that it is often difficult to draw a clear separation line. One aspect can benefit from the other when this continuum transforms into a progressive, pragmatic, and didactic approach of diagnosis. The diagnosis path is absent from most textbooks.

The essence of this book, "from the ultrasound sign to the diagnosis," clearly exposes these principles and makes this book an invaluable help in the ultrasound room, as well as an initial source for a thorough investigation of any particular anomaly or risk factor. The extensive use of illustrated flowcharts to highlight differential diagnoses, as well as identification of the abnormalities from specific ultrasound features, will become significant assets in prenatal diagnosis. Another strong point of this volume is the continuous effort to include 3D images for most diagnoses, especially those that are most likely to benefit from this development, including cranial sutures, skeleton, and fetal brain and heart.

In fact, what was long seen as alien with a most uncertain future within the 3D family has become the most spectacular and dynamic field of research and development. The fetal heart remains the greatest fantasy in the "brain" holding the transducer. Spatiotemporal image correlation (STIC) and all its by-products provide the best examples of both didactic and antiphobic tools that can help overcome the challenge fetal echocardiography throws at most sonologists and sonographers. The important distinctive feature of this book, in comparison with other textbooks presenting 3D ultrasound images, is that 3D ultrasound images are introduced only if they add value to the diagnosis or if relevant for multidisciplinary counseling purposes. Three-dimension-rendered images of craniofacial and brain anomalies, or cast-like reconstructions of cardiac defects, are shown only if they are useful and not just to demonstrate that 3D ultrasound can also be used for diagnosis. There is no reference to 3D if the diagnosis can be made confidently by 2D ultrasound. Whether 3D will facilitate important breakthroughs in ultrasound screening remains questionable. Fetal heart examination is likely to represent the most sensitive indicator of the effectiveness of screening policies. Although gestational age, which makes different countries very unequal, is a critical factor for performance, a technique that is both highly educational and accessible to telemedicine is more likely to succeed.

Finally, ultrasound–anatomical correlates presented side-by-side with 2D and/or 3D ultrasound images and relevant details of specimens from TOP from extensively documented cases are a great teaching tool. Rare chromosomal and nonchromosomal syndromes are also introduced and described using the same methodology, and thus are more likely to make an impact on the reader than the usual long and dry list of features usually encountered for these abnormalities.

The three main additions to this new edition deal with the first trimester, fetal infection, and multiple pregnancies. Ultrasound evaluation in the first trimester has achieved unprecedented results, thanks also to the introduction of intracranial translucency into clinical practice. Fetal infection is a topic that leads to the largest number of false ideas, and, unfortunately, ignorance causes the greatest prejudice against the fetus once the pregnant woman feels that the doctor is worried and uncertain, but largely unable to handle the situation through logical steps. Indeed imaging, and not only ultrasound, provides evidence to adequately manage these difficult situations only when good knowledge of virological parameters can refine its use.

Although multiple pregnancies account for around 2% of all births (but are rising), they account for 20% of all admissions to neonatal intensive care units and for over a third of the burden of prenatal diagnosis and fetal medicine. Becoming proficient with the specific aspects of multiple pregnancies is, therefore, critical to modern prenatal diagnosis, and ultrasound examination of these cases is at least twice as difficult as in singletons.

The only book worth displaying in our ultrasound rooms has long been *Smith's Recognizable Patterns of Human Malformation* by Kenneth Lyons Jones, chiefly for its ability to gather the critical number and description of the most common anomalies to be identified in utero. Let us be confident that this new edition of *Ultrasound of Congenital Fetal Anomalies*, already an exhaustive reference with a unique pedagogic format, will become an important landmark in the field and will smoothly reach classic status on the way to its third edition!

Yves Ville
Service of Obstetrics–Gynecology
Necker-Enfants-Malades Hospital, Paris, France

Preface

From ultrasound sign to final diagnosis is the mission of this book, for it is in this way the diagnostic process goes and not the other way round.

In this edition, we have followed the same philosophy that inspired us five years ago, which was mentioned in the preface to the first edition. In fact, the most frequently asked questions that confront the fetal medicine trainee/expert on a daily basis are "Is the finding real or merely an artifact?" and "Is the diagnosis correct?". However, to be able to find the description of an abnormal ultrasound finding in a textbook, one generally has to search by the definite diagnosis, which has not been done as yet! This uneasy feeling was the first factor that had pushed us to design the volume in its present format, that is, with an ample part dedicated to fetal anomalies "by scanning view." We have tried to describe, for all major ultrasound planes, what can be considered a normal view and what cannot; in other words, how each particular ultrasound view can differ from its normal appearance and what are the corresponding diagnoses. Truthfully, traveling the world and lecturing from China to the United States and back, passing through Italy and Europe, we have encountered colleagues in every country praising the usefulness of this layout, with several of them acknowledging the difficulties of our everyday routine as sonologists and experts in the ever-evolving field of fetal medicine. During the very same trips, we were reminded of the inevitable omissions, and this has been the cue for preparing this new edition, in which, thanks also to the support of the publisher, we were able to add three new chapters and significantly change images and drawings that may have been less explicative than we would have liked them to be. Brand new chapters of this new edition are dedicated to early detection of fetal anomalies (12–14 weeks), to ultrasound in fetal infections, and to ultrasound in twins. In Chapter 1 (early anomaly scan), in addition to the nuchal translucency issue, the newest intracranial translucency as well as the range of congenital anomalies detectable at this gestational age is dealt with extensively. The chapter on heart anomalies has been expanded (covering now also arrhythmias and early fetal echocardiography), and has become a "book within a book," being able now to compete with all fetal echocardiography manuals on the market. This is beneficial for readers, as they no longer need to purchase a separate text for fetal cardiology. Chapter 11 is dedicated to fetal infection. In this chapter, not only the sonographic signs of fetal infections but also detailed and concise information on the chances of infection according to the time of maternal seroconversion and on prenatal management are presented in a reader-friendly manner. Chapter 12 covers the issues of multiple pregnancy, with special focus on monochorionics and on their unique range of growth and vascular abnormalities. Finally, it also goes without saying that all chapters have been updated to include the more recent literature.

Acknowledgments

We thank the following colleagues for their invaluable help: Drs. Gianluca Campobasso, Valentina De Robertis, Brunella Muto, Georgios Rembouskos, Annalisa Tempesta, Beniamino Tormettino, and Nicola Volpe; Fetal Medicine Unit, Di Venere and Sarcone Hospitals, ASL Bari, Italy.

We also thank the following colleagues for providing us with the MRI scans contained in this book:

Professor Marco Salvatore and Dr. Mario Quarantelli
Biostructure and Bioimaging Institute
National Research Council
Naples, Italy

Chapter 1
Anatomic survey of the fetus and early diagnosis of fetal anomalies

The first chapter of this new edition is dedicated to first-trimester screening of aneuploidies and early detection of fetal anomalies. In addition, we have decided to underscore the evolving nature of some lesions, paying attention to the gestational age at which the different fetal abnormalities can be detected.

Ultrasound screening for congenital anomalies is carried out routinely, or only on demand, in the first or second trimester. However, in the vast majority of countries, the second-trimester (18–22 weeks) scan remains the standard of care for fetal anatomical evaluation in both low-risk and high-risk pregnancies. Thanks to high-quality equipment, specific settings for first-trimester evaluation of fetal anatomy, and even probe features, the most recent literature underlines the improvements made in the detection of fetal abnormalities as early as possible during pregnancy.

In keeping with the progress in the field of fetal imaging, in the last section of this chapter, we also have briefly illustrated the approach to 3D ultrasound, from the volume acquisition procedure to offline navigation and reconstruction.

FIrs T-Tr IMEsTEr U LTr Aso UNd

The main role of the first-trimester ultrasound examination was, initially, to confirm the diagnosis of pregnancy, to assess the implantation site, the number of embryos, their viability, and to date the pregnancy. In the early 1990s, the observation of a measurable fluid collection behind the fetal neck, named nuchal translucency (NT), and its correlation, when increased to aneuploidies and other fetal abnormalities, has changed the targets of the first-trimester scan [1,2].

Currently, the combination of different ultrasound markers for chromosomal abnormalities (NT, nasal bone calcification, fetal heart rate, tricuspid and ductus venosus [DV] blood flow) with maternal age, and both free β-human chorionic gonadotropin (free β-hCG) and pregnancy-associated plasma protein A (PAPP-A) levels in maternal blood, represents the screening test ("combined test") with the highest sensitivity for the detection of the most frequent fetal aneuploidies (up to 93%–95%), with a low false-positive rate (about 2%–3%) [1,3]. In comparison, older screening programs, based on either the biochemical markers in the second trimester, or the maternal age alone, show a considerably lower performance, due to lower sensitivity and higher false-positive rate [3,4]. Therefore, the national health systems of several countries have abandoned these low-performing screening methods, opting for the combined first-trimester screening, as more reliable and less harmful (lower collateral damage).

In fact, thanks to the increased knowledge on ultrasound and biochemical features of fetuses affected with Down syndrome and other aneuploidies (trisomies 13 and 18), it is now possible to calculate for each pregnancy a patient-specific risk of having a chromosomally abnormal baby [5–7].

A better performing screening allows for a more accurate selection of a high-risk population which should be offered an invasive test, with a lower rate of false-positive cases, which also means lower rate of invasive tests (and miscarriages) performed in normal pregnancies. In addition, an NT measurement above the 95th percentile, a tricuspid regurgitation (TR), and a reversed A-wave in the DV are actually considered to be an indication for a fetal cardiac sonographic evaluation, as it has been demonstrated that they are related as well to an increased risk for congenital heart defects (CHD) [8]. Furthermore, the maternal PAPP-A, assessed for the first-trimester

combined test, has been shown to be a useful marker not only for aneuploidies but also for predicting maternal preeclampsia (PE), pregnancy-induced hypertension (PIH), miscarriage/intrauterine demise, and fetal growth restriction [9–12]. For these reasons, the first-trimester examination has yielded the potential to predict not only for aneuploidies but also for several pregnancy complications, including miscarriage and intrauterine demise, preterm delivery, PE and PIH, fetal growth restriction, CHD, and severe structural abnormalities [6].

The screening for aneuploidies has become well-established and is performed all around the world at 11 to 13 weeks and 6 days. Early screening for PE, PIH, and growth restriction (impaired-placentation-related conditions) is easily integrated; the early evaluation of cardiac and other fetal abnormalities is one of the most interesting fields at the moment, showing increased performance during the past few years [13,14], as described in the dedicated section of this chapter.

scr EENING For A NEUpLo Id IEs

As described above, the combined screening has been initially based on a combination of maternal age, biochemical assessment (free β-hCG and PAPP-A), and NT measurement, with the detection of about 90% of trisomies 21, and about 5% of false-positives. This came about from the observation that the risk for Down syndrome increases proportionally with maternal age and NT thickness, and that Down's placentas produce higher amounts of free β-hCG and lower amounts of PAPP-A than normal [15]. In the past few years, aiming for even better accuracy, research has focused on additional ultrasound markers for Down syndrome, namely, nasal bone (NB), tricuspid valve, and DV. These markers have been found positive in a higher proportion of Down's fetuses than in the normal population. Similar to NT, the integration of these new markers permits a further calculation of risk based on their increased incidence in the affected population of fetuses compared with the population of normal ones. As is the case with NT, the assessment of all these additional ultrasound markers requires a specific technique and training [16]. Assessment of each of these ultrasound markers can be routinely integrated into the screening for aneuploidies, leading to a better performance of the screening itself, as previously described (detection of 93%–96% with a false-positive rate of 2%–3%).

The observation that fetuses with trisomy 13 and 18 are characterized during the first trimester by an increased NT, abnormally low levels of both free β-hCG and PAPP-A, and abnormal fetal heart rate (increased in the group of trisomy 13, slightly decreased for trisomy 18) [17] led to the extension of the screening for aneuploidies to these conditions as well. The performance of the screening for these two chromosomopathies reaches a detection of more than 95%, with a false-positive rate of 3%, using mainly the same markers already used for trisomy 21 [3].

NUch AL Tr ANsLUc ENcy

The association between nuchal edema and aneuploidies was described for the first time in 1987 by Benacerraf after having observed a thicker subcutaneous nuchal fold between 16 and 18 weeks of gestation, in fetuses referred for amniocentesis because of advanced maternal age [18]. The same data were described four years later by Nicolaides et al., who observed this earlier in pregnancy at 11 to 13 weeks and 6 days [19]. The observation of an NT behind the fetal neck, measurable at 11 to 13 weeks and 6 days, and the association between increased NT and chromosomal abnormalities (or other fetal conditions) represent the basis on which the first-trimester screening has been developed. The pathophysiology of the increased NT (Figure 1.1) is multifactorial. Possible causes are extracellular matrix anomalies, and cardiocirculatory and lymphatic abnormalities [15]. Some authors used to describe as "cystic hygroma" the cases of markedly increased NT, with septations within the translucency, and they used to consider this finding to be more severe than a simply increased NT, and different from it. Actually, these two pathologies have the same pathogenic mechanisms and similar pathologic correlations. The double nomenclature of the same pathology could cause misunderstandings, given that the two findings have the same management, and the seriousness of an increased NT simply depends upon how thicker than normal it is.



Figure 1.1 Increased nuchal translucency in a 12-week fetus.

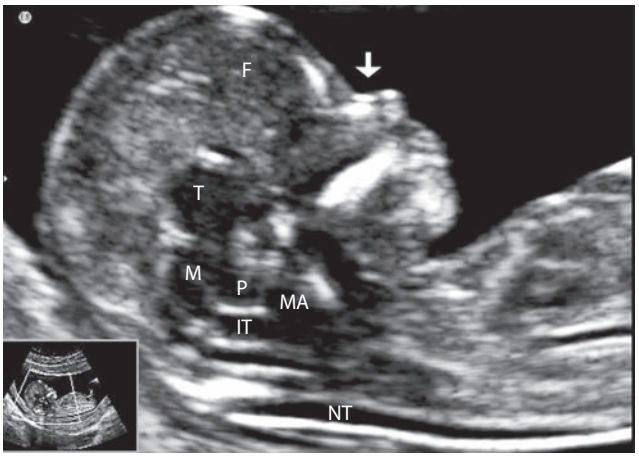


Figure 1.2 Midsagittal view of the fetal face (F) at 12 weeks: In this section, it is possible to visualize the nuchal translucency (NT) and the nasal bone (NB). There are three lines at the level of the fetal nose (arrow): two parallel lines ("equal sign") representing the NB (lower line, thicker and brighter) and the skin covering it (upper line), and a third distal line that represents the tip of the nose. It is possible to visualize also the intracranial translucency (IT), representing the IV ventricle; the thalamus (T), and the brain stem (midbrain [M], pons [P], medulla oblongata [MA]).

TEch NIqUE To MEASUr E ThE NT [16]

Section. Midsagittal; visualization of the fetal profile, NB, skin covering it and tip of the nose, diencephalon, NT, and exclusion of the frontal processes of the upper maxilla, also defined as "zygomatic bones" (Figure 1.2).

Magnification. Fetal head and upper thorax occupy the whole screen.

Fetal position. The fetus must be facing up, with the neck in a neutral position, neither hyperextended nor hyperflexed, to avoid a consequent overestimation or underestimation of the NT measurement, respectively.

Settings. Ultrasound and transducer settings should be optimized in order to clearly visualize the lines representing the borders of the nuchal space, with enough contrast to have no artifacts within the translucency.

Calipers positioning. "On to on"; the inner border of the horizontal crossbar of the calipers and the inner border of the two retronuchal lines should be perfectly superimposed; the horizontal crossbar should not be entirely embedded within the retronuchal white lines and, conversely, no part of it should be within the black NT space (Figure 1.3).

It is important, before measuring, to identify the amniotic membrane, in order to avoid erroneous measurements of the space between the skin and the amnion. In order to obtain a proper midsagittal view, it is necessary to search for the anatomic landmarks described above, visible only in this section. The exclusion of the cerebral lateral ventricles, and evidence of the structures of the posterior fossa (brain stem, fourth ventricle, and cisterna magna) could provide additional anatomic details to achieve a more accurate midsagittal section. The ultrasonic beam should be perpendicular to the lines of the NT, in order to have a clear image of the edges of these lines, and gain reduction could help to get rid of the fuzziness on the edges of these lines and the artifacts inside the translucency. The measurement has to be taken on the thickest

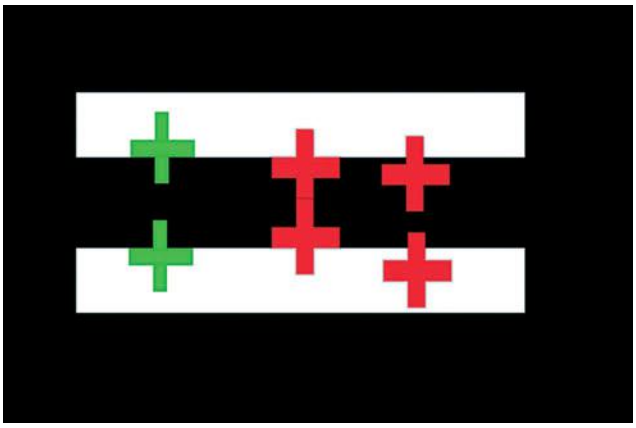


Figure 1.3 Position of the calipers for the measurement of the nuchal translucency (NT). The green calipers represent the correct position ("on to on"); the red ones are not correctly positioned.

part of the NT, carefully placing the calipers on the lines defining the NT rather than the amnion. We recommend, following the Fetal Medicine Foundation protocol, repeating the procedure to obtain more than one measurement, and then choosing the highest correct measurement. Sometimes, the umbilical cord is positioned around the fetal neck (nuchal cord), making the measurement technically difficult. The presence of a nuchal cord, usually, causes compression on the skin of the neck with subsequent redistribution of the nuchal fluid above (increased) and below (reduced) the compression site. In this case, we recommend measuring above and below the cord, and using the average of these two measurements to calculate the risk. This double measurement option in case of nuchal cord is also available in the FMF software.

NAsAL Bo NE

The NBs develop through an intramembranous ossification process and are usually not histologically demonstrable in fetuses with crown-rump length (CRL) less than 42 mm. The typical nasal hypoplasia is one of the features described by Langdon Down in 1866 in his manuscript "Observations on an ethnic classification of idiots." It is associated to a delayed ossification process that ultrasonographically corresponds to an absent NB at 11 to 13 weeks and 6 days and to an absent or hypoplastic NB in the second-trimester anomaly scan. An "absent nasal bone" is found in about 65% of Down's fetuses and 1%–3% of the normal fetuses during the first trimester [20].

TEch NIq UE To Ass Ess ThE NB [16,20]

Section. Midsagittal (Figure 1.2).

Magnification. Fetal head and upper thorax occupy the whole screen.

Fetal position. The fetus must be facing up, and the fetal nose must be perpendicular or slightly oblique to the ultrasound beam; if the insonation angle is greater than 45°, the NB is not clearly visible any longer. This is what happens when the neck of the fetus is hyperextended [21].

Settings. Same settings as used for the NT measurement.

Once the midsagittal plane has been obtained, it would be necessary to tilt gently the probe from one side to the other of the fetal face to ensure an adequate examination of the NB. The NB can be identified in a midsagittal or, when a gap between the NBs of 0.6 mm or more is present (9% of fetuses), in a slightly parasagittal plane [22]. It is possible to visualize three lines in particular: two proximal parallel lines, known as "equal sign," representing the NB (lower line) and the skin covering it (upper line), and a third distal line, representing the surface skin reaching the tip of the nose. In order to define this marker as "present," the NB must be brighter and thicker than the skin above it. It may be useful to note that the NB is visible on the scan, following the above-described technique, usually as a single line, even if the bones are actually two. The ultrasound signal of brightness due to the calcium present in the bones, simply overlaps, and therefore, the bones show up as a single bright line. As aforementioned, when the gap is greater than 0,6 mm, the NB may not be clearly visualized in a perfectly midsagittal view; in these circumstances, which account for 9% of the cases, the transducer should be carefully tilted to a parasagittal plane on either side of the midline to visualize the two NBs. The incidence of absent NB, as previously mentioned, is 1%–3% in normal fetuses, and it could depend on gestational age (more frequent around 11 weeks of gestation than later), ethnicity, and constitutional factors (Figure 1.4) [20].



Figure 1.4 Absent nasal bone at 12 weeks: absence of the "equal sign." Instead of two parallel lines it is possible to see only one line (the skin), the lower line (the bone) is not visible; the distal line represents the tip of the nose.

TRICUSPID VALVE

An association has been reported between fetal aneuploidies and abnormal tricuspid flow, i.e., tricuspid valve regurgitation (TR) [23]. The early examination of the fetal heart in high-risk patients led to the observation of a TR in about 55% of the Down's fetuses. If we consider that this finding is observed in just 1% of the normal fetuses, TR could be, therefore, used as an ultrasound marker for Down syndrome [24]. A correlation has also been found between TR and cardiac abnormalities even in chromosomally normal fetuses, which makes this finding a marker for congenital heart disease (CHD) as well [8,25].

TECHNIQUE TO ASSESS TR [16]

Section. Cardiac four chambers (Figure 1.5a).

Magnification. The fetal thorax occupies the whole screen.

Position of the heart. Apical; insonation angle less than 30°.

Settings. The pulsed Doppler sample must be 2–3 mm; Pulse Repetition Frequency (PRF) has to be set in order to visualize waves of up to 100 cm/s velocity; set sweep speed 2–3 cm/s in order to assess the wider waves better.

Position of the sample. The fetus should not be moving. The pulsed Doppler sample must be placed across the tricuspid valve, and the assessment has to be performed across three different parts of the valve (medial, central, and lateral) in order to interrogate the whole valve.

During the measurement, the Doppler trace could show not only the signal of the forward blood flow through the tricuspid valve but also the backward flow through the aortic/pulmonary valve, which could be erroneously interpreted as a regurgitation. This is a quite common confounding contamination that has a velocity generally less than 60 cm/s. Another common contamination is the small backward jet corresponding to the closure of the tricuspid valve, sometimes showing a velocity higher than 60 cm/s but usually lasting a very small part of the systole, never more than half of this period of the cardiac cycle. TR, on the other hand, is defined as a backward flow across the valve characterized by a velocity more than 60 cm/s and lasting more than half of the systole (Figure 1.5b). The careful assessment of these wave features is helpful in correctly differentiating a TR from a contamination.

DUCTUS VENOSUS

The DV represents an important shunt within the fetal circulation. The DV leads the oxygenated blood coming from the umbilical vein directly to the heart, bypassing the liver circulation. The blood flow is preferentially directed toward the interarterial septum, in order to reach the left atrium through the foramen ovale. The spectral Doppler waveform of the DV blood flow is characterized by a forward triphasic flow: the S, D, and A waves are representing respectively the systole, the early diastolic phase, and the atrial contraction (Figure 1.6a). A reversed A-wave in the DV (Figure 1.6b) has been shown to be associated with chromosomal abnormalities (about 65% of Down's fetuses) and cardiac malformations [8,25,26]. It is also possible to find a reversed DV in about 3% of euploid fetuses [26].

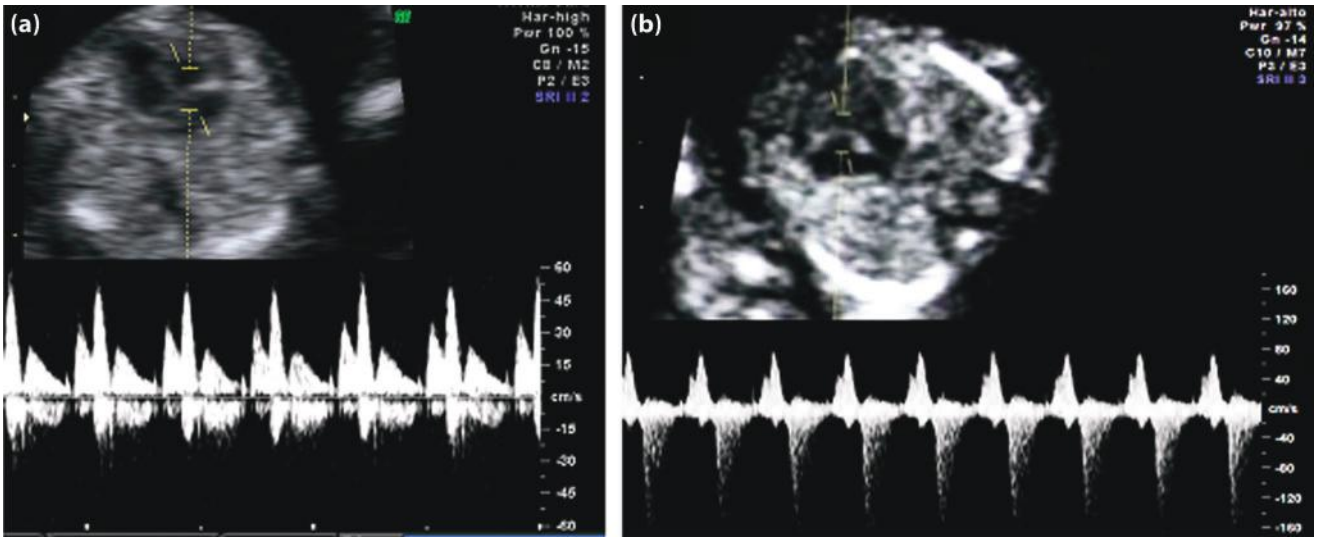


Figure 1.5 (a) Normal tricuspid flow. (b) Tricuspid regurgitation: the backward flow has a velocity higher than 60 cm/s and lasts more than half of the systole.

TEch NIq UE To Ass Ess ThE dV [16]

Section. Midsagittal (Figure 1.6).

Magnification. The fetal thorax and abdomen occupy the whole screen.

Position of the fetus. The fetus should be facing up and not moving.

Insonation angle. Less than 30° between the ultrasound beam and the blood flow direction in the DV.

Color Doppler. The umbilical vein, the ductus venosus, the descending aorta and the heart should be visualized with color Doppler. It is useful to use a PRF low enough to create aliasing only at the level of the ductus venosus. This facilitates identification of the vessel and following PWD sampling (see below).

Pulsed Doppler sample. Small sample (0.5–1 mm), filter set at a low frequency (50–70 Hz), and high sweep speed (2–3 cm/s). The sample has to be positioned on the aliasing representing the blood flow acceleration in the DV, between the umbilical vein and the inferior vena cava just below the right atrium.

The DV is a small vessel, and the signal coming from it easily overlaps with the ones coming from the nearby veins. The blood in the umbilical vein has a forward homogeneous and continuous flow that could overlap and cover the A-wave of the DV; the hepatic veins normally have a backward flow during the atrial contraction, which corresponds to a reversed A-wave, and the overlap with the DV A-wave could erroneously lead to the diagnosis of a reversed flow in the A-wave of the ductus. In order to avoid these contaminations as much as possible, we recommend reducing the sample size (usually to 0.5 mm).

The following two markers have been studied only very recently, and further research results are awaited in order to be used on a routine basis.

rIG hT sUBc LAVIAN Ar TEr y

The observation of an unusual pattern of the right subclavian artery (RSA) in Down syndrome fetuses has led to an increased interest in this vessel in the past few years. An aberrant right subclavian artery (ARSA) has been found in up to one-third fetuses, and is as well associated with the most common chromosomal

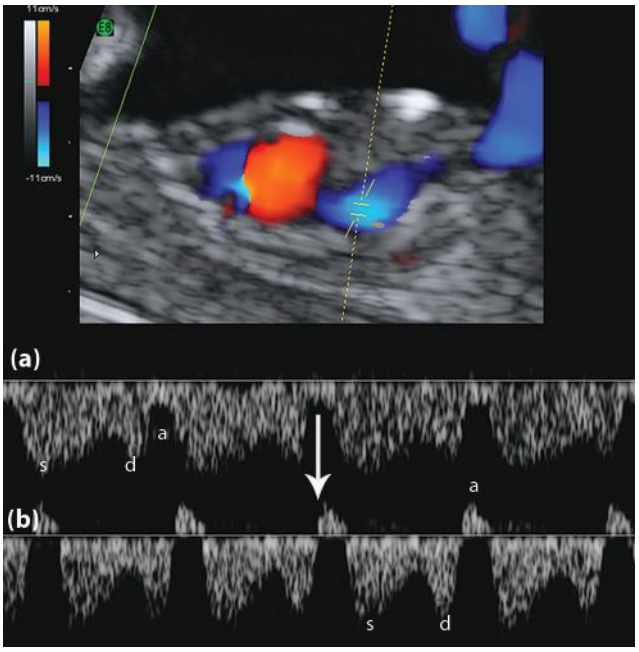


Figure 1.6 (a) Normal ductus venosus: systolic flow (s), protodiastolic flow (d) "a" wave positive. (b) Abnormal ductus venosus flow (the arrow indicates the reversed A-wave).

abnormalities [27–31]. An ARSA is found in about 1.5% of the normal euploid population, according to recent studies [27,31], and, therefore, when isolated would be correctly considered a normal variant. However, it has been reported that its presence could increase the risk for chromosomal abnormalities and CHD; for these reasons, it has been considered an ultrasound marker for chromosomal and cardiac abnormalities. This marker has been investigated not only in the routine second-trimester scan, but its assessment has been found feasible also in the first-trimester screening [28,31]; its association with genetic defects (i.e., 22q11.2 microdeletion) [31,32], and with anatomic anomalies (mainly cardiac abnormalities) [29,31], makes it very interesting and helpful in terms of pregnancy management.

TEch NIq UE To Ass Ess ThE rs A [31]

Section. Transverse view of the upper thorax, just above the "three vessels and trachea" view (Figure 1.7a).

Magnification. Fetal upper thorax occupies the whole screen.

Fetal position. The fetal clavicles should be pointing 6 o'clock and 12 o'clock; ideally, the right one should be pointing up. The fetal subclavian vessels should be, therefore, parallel to the ultrasound beam.

Settings. The color Doppler, and/or high sensitivity bidirectional power Doppler, should be used to visualize the RSA, by reducing the pulse repetition frequencies.

After the visualization of the "three vessels and trachea," the transducer should be moved slightly upward, to the level of the clavicles, to explore the vessels arising from the aortic arch, and rolled on the side, in order to have the clavicles pointing 12 o'clock and 6 o'clock, as described above. In this way, the blood flow in the subclavian arteries is parallel to the ultrasound beam, and it is possible to visualize their typical "S" shape. It is important to distinguish the RSA from the right subclavian vein (opposite blood direction). Then, it is necessary to focus on the color Doppler signal that shows the direction of the blood flow inside the subclavian vessels. The normal appearance of an RSA is an S-shaped vessel, with blood flow from the aortic arch toward the fetal shoulder, positioned in front of the trachea, rather than behind. In case of an ARSA, this vessel would be behind the trachea (Figure 1.7b), and the appearance would be quite different. It would be visible as a straight vessel, with flow toward the right shoulder, behind the trachea, arising from the aortic arch. In the same view, another straight vessel, in front of the trachea, with flow from the shoulder to the arch (the opposite direction than a normal RSA) can be seen, and it is the subclavian vein.

hEpATIc Ar TEr y

The blood supply to the fetal liver is provided mainly by the umbilical and portal vein (more than 90%) as well as by the hepatic artery (HA) [33]. The observation of an increased hepatic artery flow in fetuses with Down syndrome has been recently described [34,35]. In a recent study, in about 80% of fetuses with trisomy 21, the peak systolic velocity in the HA was found to be increased (above the 95th percentile),

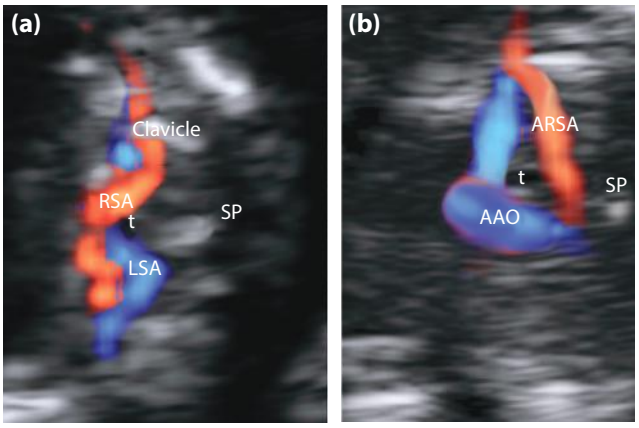


Figure 1.7 Comparison of color Doppler aspect of normal and aberrant right subclavian artery at the first trimester. (a) Both subclavian arteries (right: RSA; left: LSA) can be seen with a typical "S" shape. Arteries and veins are normally overlapping. (b) Aberrant right subclavian artery (ARSA) would be visible as a straight vessel, with flow toward the right shoulder, behind the trachea, arising from the aortic arch (AAO). t: trachea; SP: spine.

and the pulsatility index was found to be reduced [35]. A strong association with TR and reversed DV makes, potentially, the HA a marker more useful to characterize high or intermediate risk fetuses, rather than to be used as a single marker in a low-risk population.

TEch NIq UE To Ass Ess ThE hA

Section. Midsagittal (Figure 1.8a and b).

Magnification. The fetal thorax and abdomen occupy the whole screen.

Position of the fetus. The fetus should be facing up and not moving.

Insonation angle. Less than 30° between the ultrasound beam and the blood flow direction in the HA.

Pulsed Doppler sample. Sample of 1 mm, filter set at a high frequency (120 Hz) to avoid contaminations, high sweep speed (2–3 cm/s), pulsed wave PRF set low (2.2–3.3 Hz). The sample has to be positioned between the celiac trunk and the DV. The peak systolic velocity and pulsatility index ideally should be measured after three consecutive waves are obtained.

The section to assess the HA is the same as that used to assess the DV, but it is important to keep the insonation angle less than 30° (rolling the probe in order to have the fetal head at the same level or slightly higher than the bottom) and to set up the machine properly in order to optimize the visualization and the measurement accuracy. In the majority of euploid fetuses, the HA normally is difficult to visualize clearly by Doppler flow mapping. It becomes more visible when there is an abnormally increased flow, making the sampling easier. The HA is seen as the vessel coming in close contact with the DV and in continuity with the celiac artery, arising as the first anterior branch from the descending aorta [34]. One recommended option is to begin the measurement with a sample of 2 mm, including the signal from the DV, to make the sample positioning easier. The waves from the HA are visible on the same Doppler trace but in the opposite direction, underneath the waves coming from the DV, with a typical arterial pattern, and a partly absent diastolic wave. In any case, the measurement should be obtained with a sample of 1 mm, positioned just behind the DV, excluding the celiac trunk and the DV itself. This way, the Doppler trace shows just the waves coming from the HA. This can be obtained even when the color Doppler mapping does not show the precise position of the HA.

No NINVAs IVE pr ENATAL TEs TING

Next-generation DNA sequencing, analyzing cell-free DNA (cfDNA) in maternal blood, 5% of which is fetal/placental in origin, has recently shown highly accurate detection of common fetal autosomal trisomies [36–38]. It has been demonstrated that advanced technologies including

- DNA amplification, by polymerase chain reaction (PCR);
- Matrix-assisted laser desorption ionization time-of-flight mass spectrometry;
- Massive parallel shotgun sequencing;

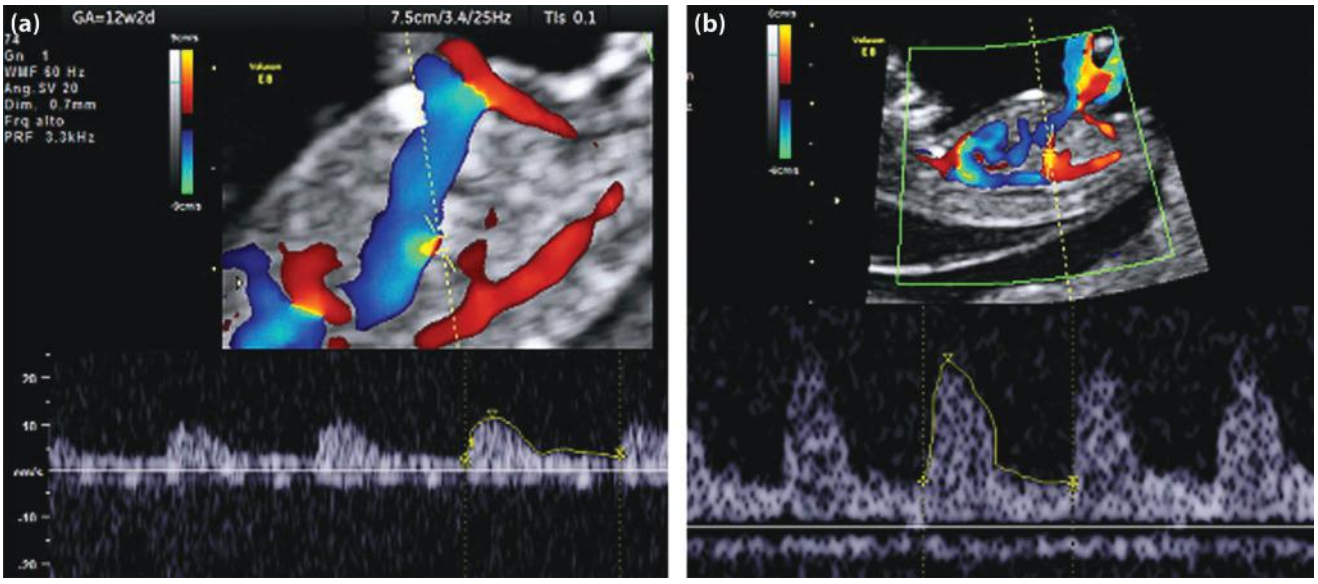


Figure 1.8 (a) Normal hepatic artery flow. (b) Abnormal hepatic artery flow in a fetus with trisomy 21: the peak systolic velocity is increased.

- Selective sequencing of loci from specific chromosomes under investigation

can potentially detect more than 99% of Down syndrome fetuses with a false-positive rate inferior to 1% [38]. These data still need to be validated prospectively in a large screening population. In any case, there is widespread agreement that NIPT should not replace the nuchal translucency scan, because aneuploidy screening represents only one of the scopes of this early ultrasound examination, which will remain as a complement to NIPT for those women who have opted for such aneuploidy screening method.

scr EENING For pr EEc LAMps IA

It has recently been shown that by combining maternal history (ethnicity, body mass index [BMI], parity, previous PE, etc.), mean maternal blood pressure, pulsatility index of the uterine arteries (Figure 1.9), and PAPP-A or PlGF concentration in maternal blood, it is possible, already in the first trimester, to select a group of pregnant women at high risk to develop PE [9,6].

These elements are easy to be included in the routine first-trimester screening for chromosomal abnormalities, as history taking and blood biochemical analysis for PAPP-A are already part of this examination; adding a few specific questions during history taking, as well as blood pressure measurement and uterine arteries assessment during the scan, it is possible to assess the patient-specific risk for PE within the same screening examination between 11 and 13 weeks and 6 days of gestation. The combination of the above-described clinical data is able to predict not only PE but also the other conditions related to an impaired placentation: PIH, fetal growth restriction, abortion, and intrauterine demise [9–12].

A combination of maternal characteristics, as well as biophysical and biochemical markers would lead to the early detection of more than 90% of the cases of early onset PE [9,12]. The most recent publications also focus on the role of Placental Growth Factor (PlGF) and show some improvement in the detection of PE [12].

Early detection of these conditions allows us to select a population of pregnant women suitable for prophylaxis at an earlier gestational age, in order to limit the pathologic mechanisms underlying the impaired placentation.

Several therapies (low-dose acetylsalicylic acid, calcium, and antioxidant vitamins) have been tested so far, during the second trimester, when these conditions already show symptoms, but without success. Recent studies show how an early treatment (starting before 16 weeks) based on low-dose acetylsalicylic acid could reduce the impact of placentation problems on pregnancy, improving the overall outcome and reducing the incidence of conditions such as PE by up to 50% [39].



Figure 1.9 Uterine artery Doppler at 12 weeks, normal waveform. In order to sample the uterine artery at 11–13^{+6}, it is necessary to obtain a sagittal section of the uterus, identify the cervical canal, gently tilt the transducer side-to-side, identify each uterine artery by color flow mapping, and sample them with the pulsed wave Doppler using a 2 mm gate.

Screening for PE is more effective at detecting early onset PE than late onset. In fact, the later the onset of PE during pregnancy, the more difficult it is to predict the condition using the above-mentioned markers for impaired placentation [9].

EVALUATIo N o F FETAL sTr Uc TUr AL ABNor MALITIEs

Fetal abnormalities are known to affect 3% to 5% of all pregnancies [40,41]. In the vast majority of countries, the second-trimester (18–22 weeks) scan remains the standard of care for fetal anatomical evaluation in both low-risk and high-risk pregnancies [42].

However, the most recent literature shows improvement in the detection of fetal abnormalities in the 1st trimester of pregnancy, thanks to high-quality equipment, specific settings for first-trimester evaluation of fetal anatomy, and even probe features [14,42]. Reported advantages include early detection and exclusion of many major anomalies, early reassurance to at-risk mothers, earlier genetic diagnosis, and easier pregnancy termination, if appropriate.

Recent publications suggest classifying fetal abnormalities into three groups according to the possibility of detection during the first-trimester examination: always detectable, potentially detectable, and undetectable abnormalities [14].

The "always detectable" abnormalities are those already present in the first trimester, and causing clearly visible alterations of the fetal structures even before 13 weeks and 6 days. The "undetectable abnormalities" usually are manifested only during the second or third trimester of pregnancy (Table 1.1) and, therefore, are not detectable at 11–13 weeks and 6 days. The "potentially detectable" malformations are usually those related to abnormalities of the fetal structure already present in the first trimester but not easily visualized. The detection of these abnormalities could depend on the expertise of the operator; the aims, indications, and standardization of the ultrasound examination; the time allocated for the scan; the equipment used; the presence of direct or indirect ultrasound markers of the malformation; and the evolution in the phenotypic expression of the abnormality with gestation [14]. We describe below which anatomic structures and fetal anomalies can be assessed during the first trimester.

Skull, Brain, and Spine

Ultrasound views. Transverse and midsagittal sections of the head and face; sagittal section of the spine.

Method. The examination should focus on the normal appearance of the skull (normal calcification and absence of distortions or disruptions); the absence of distortions or disruptions of the midline of the brain; the symmetry of the two halves of the brain, with choroid plexuses similar in size and appearance (butterfly sign) [43,44]. At 11 to 13 weeks and 6 days, the ultrasound aspect of the brain is characterized by the two prominent lateral ventricles that are filled with the choroid plexuses.

The two cerebral hemispheres are symmetrical in size divided by the falx, and the cortex is thin. Posterior fossa should be visualized in the axial and midsagittal view, with evaluation of the brain stem, fourth ventricle, and cisterna magna. In order to complete the examination of the central nervous system, it is necessary to use a sagittal section to check for distortions and disruptions of the spine and the skin covering it.

Always detectable abnormalities.

- **Acrania–exencephaly–anencephaly.** Already in the 1990s it was shown to be possible to detect up to 97% of cases of anencephaly during the second-trimester anomaly scan. The most recent publications show how it is possible to obtain such a detection rate already during the first-trimester scan [14,43].

Table 1.1 Average gestational age at diagnosis for most common anomalies

Congenital anomaly	<18 weeks	18–21 weeks	>28 weeks
Anencephaly	+++	–(+)	
Hydrocephaly	+	++	+++
Microcephaly	NP	+	+++
Holoprosencephaly	++	+++	
Agenesis of the corpus callosum	NP	+	+++
Dandy–Walker complex	+	+++	++
Spina bifida	+	+++	++
Congenital heart disease	+	+++	+++
Diaphragmatic hernia	+	++	++
CAML and sequestration	NP	+++	++
Esophageal atresia	NP	++	++
Duodenal atresia	NP	++	+++
Ileo-jejunal atresia	NP	+	+++
Omphalocele	+++	+++	++
Gastroschisis	+++	+++	++
Bilateral renal agenesis	+	+++	
ADPKD	–	++	++
Multicystic kidney	+	+++	++
Posterior urethral valves	+++	++	++
Limb reduction defects	+++	+++	
NIHF	++	+++	
Tumors (all sites)	NP	+	+++

ADPKD: autosomal dominant polycystic kidney disease; CAML: cystic adenomatoid malformation of the lung; NIHF: nonimmune hydrops fetalis; NP: assessment not possible; +++: more common; ++: average; +: less common; –: extremely rare.

Acrania–exencephaly–anencephaly (see Chapter 2) could be, therefore, considered as malformations always detectable in the first trimester, given that it is possible to find direct signs of these malformations in the above-described views. Most of the skull, and in particular parietal and occipital bones, are identifiable as echoic calcified structures from 11 completed weeks. Therefore, it is possible to assess quite clearly the skull shape and profile between 11 and 14 weeks. The observation of the absence of the ossified cranial vault (acrania), resulting in abnormal shape of the exposed brain (exencephaly) should lead to the early diagnosis of acrania–exencephaly (Figure 1.10).

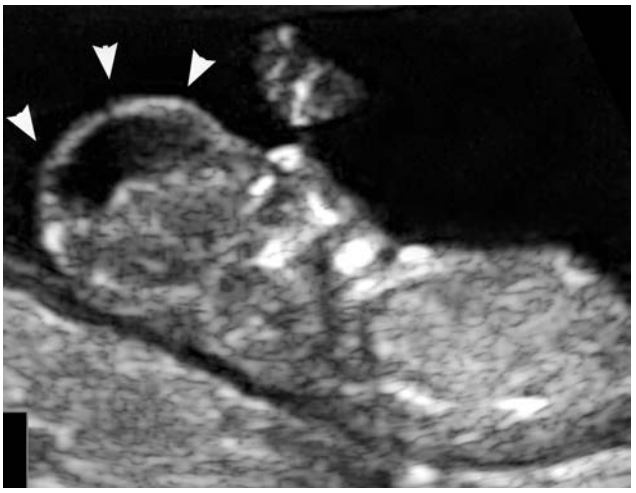


Figure 1.10 Acrania in a 12-week fetus. Cranial vault is absent and the brain is covered only by meninges (arrowheads).

The subsequent degeneration of the gray matter due to the exposure of the brain to the amniotic fluid leads to anencephaly with little or no brain remaining above the base of the skull.

- **Cephalocele.** This is characterized by protrusion of intracranial structures through a cranial bone defect. The herniated anatomic structures can consist of meninges only (meningocele) or meninges plus cerebral tissue (meningoencephalocele). Sonographic diagnosis is based on the recognition of a cystic (meningocele) (Figure 1.11) or complex (meningoencephalocele) formation of variable size protruding through a skull defect, often localized in the occipital region. This anomaly is usually revealed on axial views of the head. However, the *midsagittal view* of the fetal head, if obtainable with a posterior approach, may clearly demonstrate the relationship of the cephalocele with the remaining brain.
- **Holoprosencephaly.** Another malformation that confidently may be diagnosed in the first trimester is alobar/semilobar holoprosencephaly (see Chapter 2) [14,43]. It is caused by the impaired midline cleavage of the embryonic forebrain [43,45].

At 11 weeks, the falx is already present and evident on ultrasound, and, therefore, its complete or partial absence, which is one of the features typical of alobar and semilobar holoprosencephaly, can be reliably detected. The transverse view of the head will not show the typical butterfly sign (Figure 1.12a), but the fusion of the brain midline structures and of the cerebral lateral ventricles or its anterior part will be visible (Figure 1.12b). It is also important to take into account the strong correlation of this abnormality with trisomy 13 (about 66% of the cases diagnosed in the first trimester) [46].

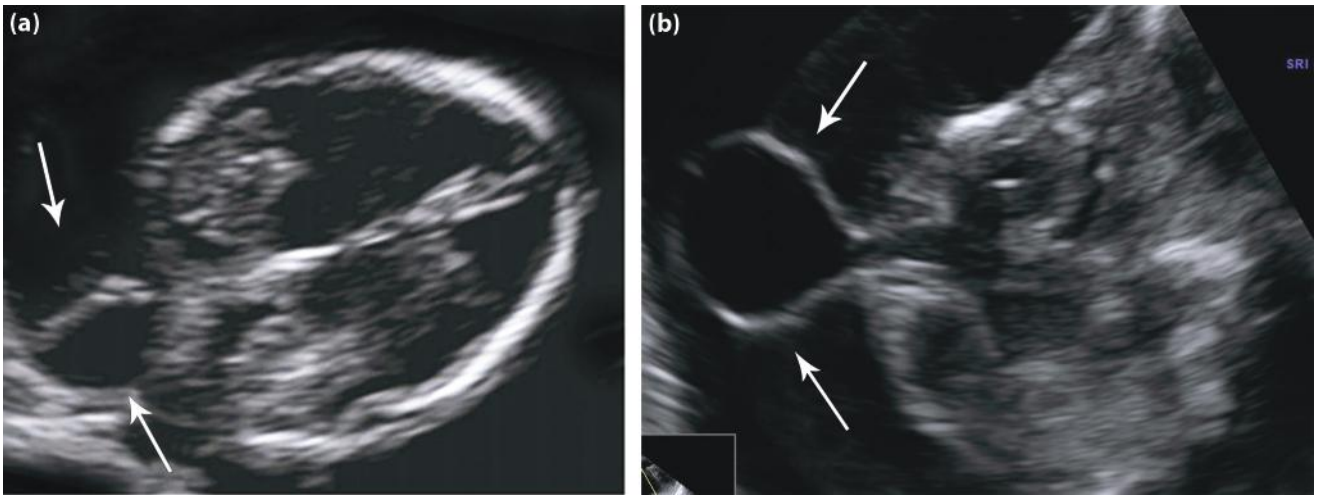


Figure 1.11 Meningocele in a 13-week fetus. (a) Axial and (b) midsagittal views of the fetal head showing a cystic formation (arrows) protruding through a skull defect, localized in the occipital region.

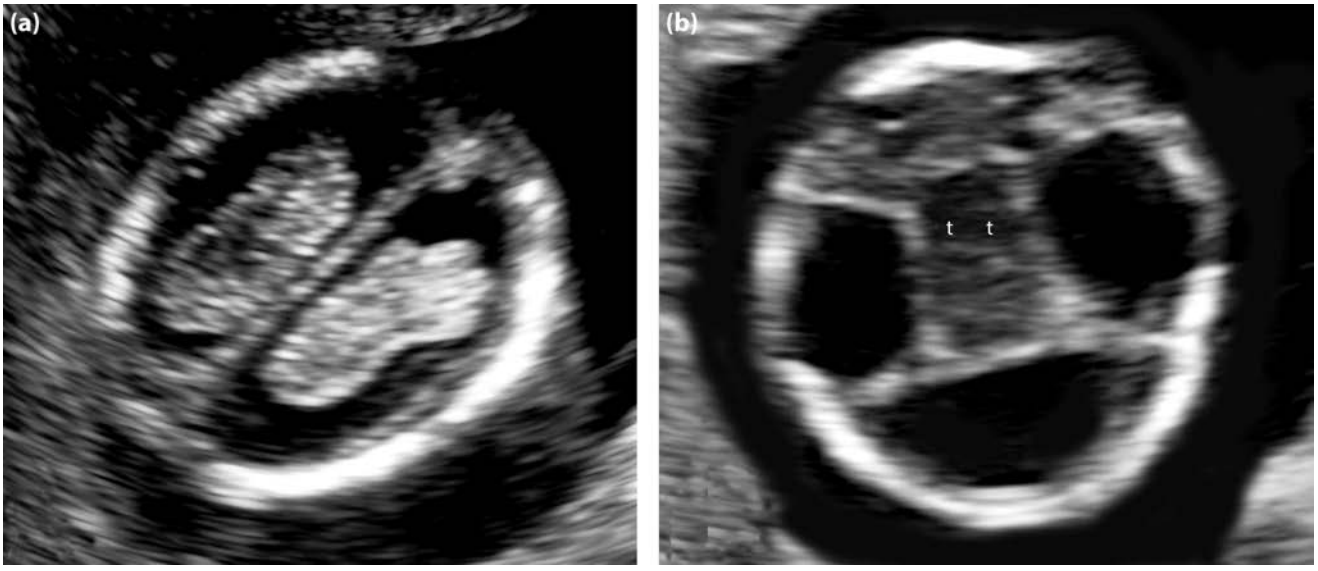


Figure 1.12 (a) Normal skull and brain at 13 weeks. Axial view of the head showing the normal calcification of the skull; the falx and the two choroid plexuses ("butterfly sign") are normal. (b) Alobar holoprosencephaly: transverse view of the head showing the fusion of the thalami and of the lateral ventricles.

Potentially detectable abnormalities.

- **Open spina bifida.** The evaluation of the spine, through the direct midsagittal visualization of the vertebral column and the skin covering it, allows the diagnosis of large myelomeningoceles, but a normal appearance during the first trimester cannot exclude open spina bifida, because the defect would not be sufficiently evident at this stage. The early detection of this defect could be improved by the recent description of a new ultrasound marker of open spina bifida (intracranial translucency) [47], detectable during the routine first-trimester scan: the midsagittal view of the fetal face and head allows, as already mentioned, the visualization of the main structures of the fetal posterior fossa, usually abnormal in the case of open spina bifida and almost always associated with Chiari II malformation. It is possible to visualize at 11 to 13 weeks and 6 days, three spaces within the posterior fossa, between the sphenoid and the occipital bones; these are the brain stem, the fourth ventricle (defined as the intracranial translucency), and the cisterna magna, in the same routine midsagittal view used to check the NT (Figure 1.2). Chiari II

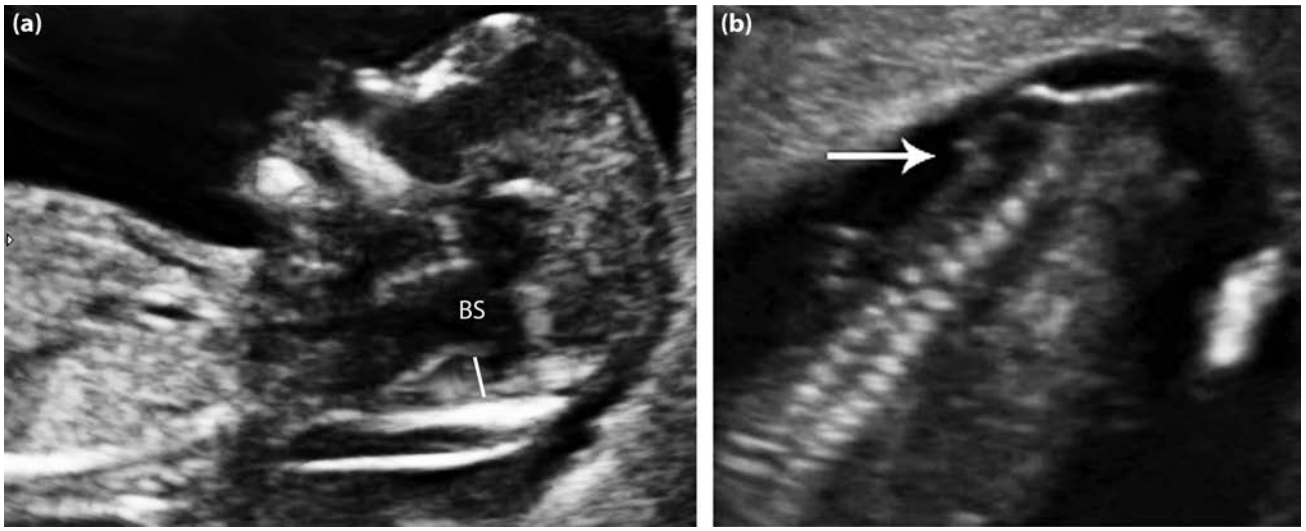


Figure 1.13 (a) Posterior fossa in a fetus with open spina bifida at 12^{+6} weeks: no typical intracranial translucency (IT) with clear borders is identifiable; the brain stem (BS) is thickened and the distance from the posterior border of the brain stem to the occipital bone (white line), is shorter than the brain stem diameter. (b) Midsagittal view of the spine showing a small lumbosacral myelomeningocele in the same fetus.

malformation is characterized by the caudal displacement of the brain stem and the compression of the fourth ventricle and cisterna magna, causing the obliteration and disappearance of the intracranial translucency/fourth ventricle, and the enlargement of the anechoic space representing the brain stem (Figure 1.13a) [47]. According to the most recent literature [48], it could be useful to measure the ratio between the brain stem and the fourth ventricle/cisterna magna complex in cases of suspected spina bifida (brain stem/brain stem-occipital bone diameters ratio is higher in fetuses with open spina bifida than in normal fetuses). In case of abnormal appearance or measurement of the structures of the posterior fossa, the operator could be alerted to accurately examine the anatomy of the spine, aiming for direct visualization of any spinal defects (Figure 1.13b), or evidence of normal appearance of the vertebral column and skin.

- **Posterior fossa major abnormalities.** Development of the posterior fossa structures is ongoing during the first trimester, and a proper assessment of the anatomy of these structures should be performed after 18–20 weeks. In particular, the cerebellar vermis is not completely formed in the first trimester, and a wide communication between the fourth ventricle and cisterna magna is normal at this stage. Therefore, a false-positive diagnosis of Dandy–Walker malformation (DWM) can be made if the normal development of the cerebellum is not taken into consideration. Even if the correct diagnosis of these abnormalities cannot be made this early, the evidence of a cystic posterior fossa (Figure 1.14a and b) [49] should raise suspicion of posterior fossa malformation in the first trimester. However, it should be kept in mind that, in this case, the diagnostic suspicion should be subsequently confirmed by a later scan, usually beyond 18 weeks of gestation.

  As mentioned above, in the case of spina bifida, the ratio between the brain stem and the fourth ventricle/cisterna magna complex is abnormal (brain stem/brain stem-occipital bone diameters ratio is higher in fetuses with open spina bifida than in normal fetuses).
- **Cerebral ventriculomegaly.** Ventriculomegaly may be secondary to brain destruction (congenital infection or a vascular mechanism); malformations; hydrocephalus; neoplasms; or a combination of two processes (i.e., hydrocephalus and malformation). The anatomy of the fetal brain is still developing at 14 weeks, and most of the aforementioned causes are usually related to a second or third-trimester ventriculomegaly, rather than a first-trimester one. However, significant dilation of the ventricular cavities (Figure 1.15a and b), due to hydrocephaly in the first trimester, has been reported [14,43,50]. Ventriculomegaly can be diagnosed relatively early if the choroid plexuses do not fill the ventricles.

Face

Ultrasound views. Midsagittal view of the face; transverse view at the level of the orbits and of the upper lip/hard palate; coronal view, to visualize the hard palate and retronasal triangle [51].

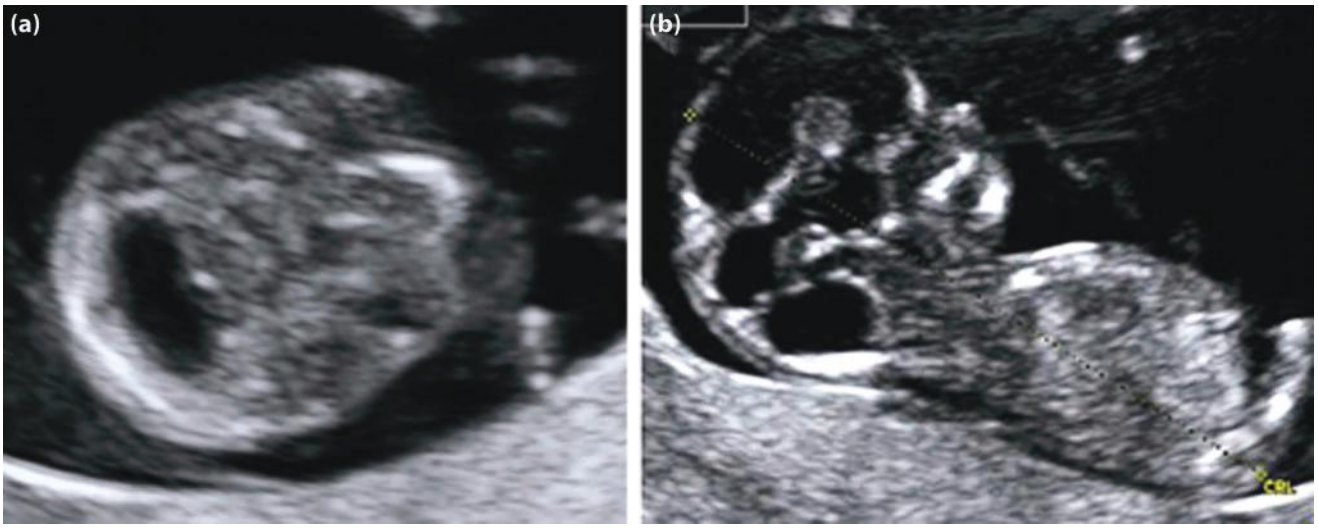


Figure 1.14 A cystic posterior fossa in a fetus at 12^{+6} weeks. The identification of a cystic posterior fossa in an axial scan (a) and sagittal scan (b) can raise the suspicion of Dandy–Walker malformation (DWM) or other cystic posterior fossa abnormalities. In this case, the suspicion of DWM was subsequently confirmed. Hydrocephaly was also present.

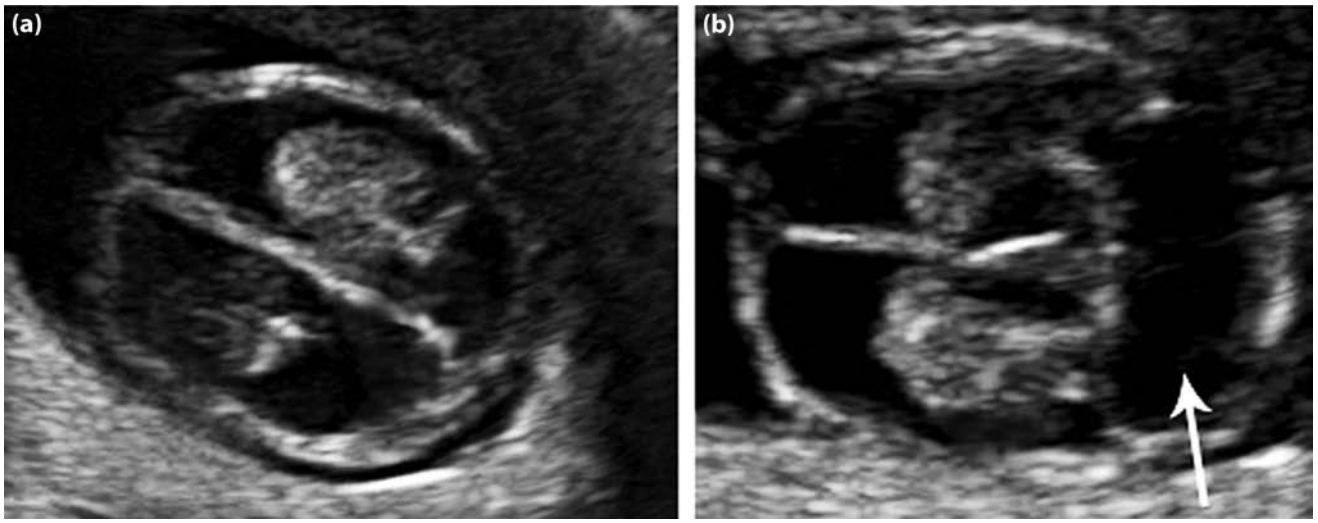


Figure 1.15 (a) Significant dilation of the ventricular cavities due to hydrocephaly in a 13-week fetus. (b) The arrow indicates the associated cystic posterior fossa.

Method. The examination of the face should be performed when the fetus is facing toward the probe. In the midsagittal view of the fetal face, it is necessary to focus on the normal appearance of the fetal profile (the calcification of the NB, the size of the chin, and the integrity of the upper lip). The transverse view of the orbits may show the two orbits, symmetric and normal in size/position. In the hard palate/upper lip view, the arch-shaped calcified palate and the upper lip above it should be visualized, without any evident disruption. A coronal view could be obtained aiming to assess the bony structures of the hard palate and the two frontal processes of the upper maxilla calcification nuclei, which form a bony retronasal triangle. The base of this triangle (hard palate) should be present and intact.

Potentially detectable abnormalities.

- **Micrognathia.** The examination of the fetal profile in the midsagittal view of the face may show a chin smaller than normal (Figure 1.16). This finding is usually not easily detected, because the size of the chin is generally not markedly smaller than normal at this stage; therefore, the micrognathia could remain undiagnosed, especially if isolated, during the examination. However, severe micrognathia, as seen

in primary mandibular dystostoses (see Chapter 3) may be detectable also at 12–13 gestational weeks (Figure 1.16). This finding should raise suspicions of chromosomal abnormalities (mainly trisomy 18) and genetic syndromes. When diagnosed, a detailed examination of the fetal anatomy should be encouraged.

- **Facial cleft.** The routine examination of the palate and lip could lead to an improved detection of facial cleftings. The usually difficult visualization of the lip and the small dimensions of these structures make the diagnosis possible only for the major defects (Figure 1.17). In selected cases, the transvaginal approach may contribute to improve the detection of these defects.

Thorax and Heart

The thorax, and several basic features of cardiac anatomy, can be evaluated during the first trimester. The chest normally contains lungs of homogeneous echogenicity on ultrasound, without evidence of cystic or solid masses.

It has been reported that an experienced sonographer can detect CHD with good accuracy at 11–14 weeks [13,52]. Routine examination of some ultrasound markers for chromosomal abnormalities has recently improved the early detection rates of fetal cardiac anomalies. This is first related to the association between increased NT and CHD even in euploid fetuses [14,52,53]. The same association is observed with the TR and reverse flow in the DV [25,26,31,54,55]. The need for further cardiac investigation in the presence of the aforementioned ultrasonographic markers (increased NT with normal karyotype, TR, and reversed DV A-wave) has led to the inclusion of these findings among the list of indications for fetal echocardiography at 18–22 weeks of gestation. Along these lines, an early echocardiography, within 16 gestational weeks, has been proposed in cases of NT measurements more than the 99th percentile (3.5 mm) or for the presence of two ultrasonographic markers simultaneously.

A screening strategy that includes routine first-trimester NT with tricuspid valve, DV, and direct fetal heart evaluation, and subsequent early and/or mid-trimester echocardiography in case of any abnormal finding, can increase significantly, together with the classic mid-trimester anomaly screening scan, our ability to detect CHD.

However, it should be kept in mind that a suspicious four-chamber view screening at 11–13 weeks and 6 days seems to be the single most sensitive and specific first-trimester marker of CHD. Combined with NT, TR, and examination, this finding can potentially lead to the early detection of about 70% of the major cardiac defects [13].

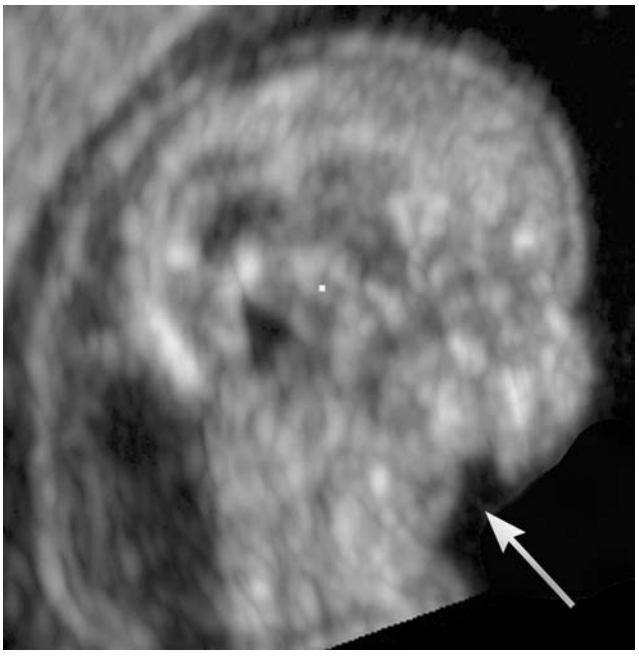


Figure 1.16 Micrognathia in a 12-week fetus. Three-dimensional Volume Contrast Imaging. Midsagittal view of the face showing very severe retromicrognathia (arrow).



Figure 1.17 Three-dimensional surface rendering of bilateral cleft lip and palate in a 13-week fetus.

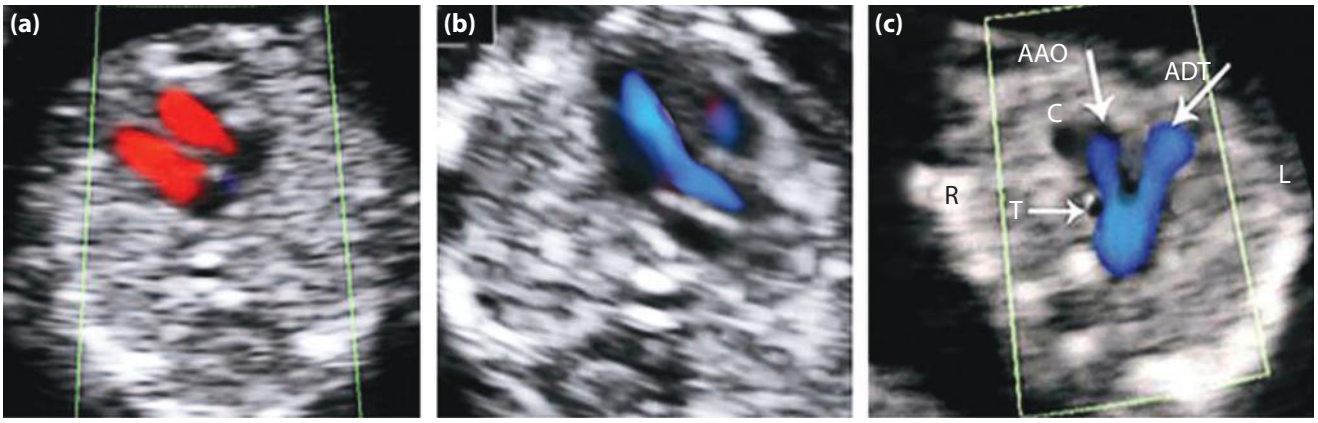


Figure 1.18 (a) Color Doppler of an apical four-chamber view at 12 weeks' gestation demonstrating diastolic flow from left and right atrium into left and right ventricle, respectively. The lumen of right and left ventricle separated by the interventricular septum can be clearly identified. (b) Color Doppler of a left outflow tract showing aortic blood flow in blue and the continuity of the medial wall of the aorta with ventricular septum. (c) Color Doppler of three-vessel and trachea view at 13 weeks' gestation. This transverse view provides important information on the direction of blood flow in the two arches and on the location and dimension of the aortic arch. (Modified from Volpe P et al. *Prenat Diagn* 2011; 31: 1054–61.)

Ultrasound views and method. The direct cardiac examination requires a rather different set of echocardiographic views from the second-trimester one. The principal first-trimester views should include:

- Four-chamber view (Figure 1.18a), preferably with the cardiac apex to the top of the screen. In this view, the assessment of the cardiac situs and its relation with the fetal stomach should be carried out. Also, an evaluation of the two atrioventricular connections by two-dimensional ultrasound and color flow mapping should be performed;
- Left outflow tract view (Figure 1.18b);
- Crossover view; this view is referred to in the first trimester as the "X-sign" [14] or "anterior V-sign" [13] on color flow mapping;
- Three vessels and trachea view; the ductal and aortic arches are depicted on color flow mapping as posterior "V-sign" (Figure 1.18c).

Always detectable abnormalities.

- **Situs abnormalities.** The transverse view of the chest, with the examination of the four-chamber view of the fetal heart, should always start with the assessment of the situs, by the definition of the fetal left side, and the evaluation of the position of the cardiac apex, pointing to the same side. In order to confirm the situs solitus, it is also important to check whether the fetal stomach is on left side of the fetus. Situs abnormalities could, therefore, already be detected in the first trimester, if we were to assess these structures and their position routinely.

Potentially detectable abnormalities.

- **Cardiac abnormalities.** Evaluation of the fetal heart allows us to detect, already in the first trimester, many major CHD (Figure 1.19a through c). Detection of these CHDs is still not easy, and in several cases, the defect might only be suspected in the first trimester and require further evaluation after a few weeks [13,56].
- **Diaphragmatic hernia.** The four-chamber view could reveal an abnormal position of the heart, due to compression by bowel loops or stomach or liver in case of congenital diaphragmatic hernia. Small defects of the diaphragm with small herniation of the abdominal structures are usually difficult to diagnose, and the association with other markers of chromosomal abnormalities (mainly trisomy 18) such as increased NT could improve the detection of this condition. However, an adequate evaluation of the heart position, and of the abdominal and thoracic organs position, may lead to the diagnosis of the majority of severe cases of diaphragmatic hernia, even if isolated. In a recent study, about half of the cases of diaphragmatic hernia had been diagnosed in the first trimester [14] (Figure 1.20).

Abdomen

Ultrasound views. Transverse and midsagittal views of the abdomen, including the visualization of the stomach, the outline of the abdominal wall, and cord insertion.

Method. The stomach must be shown in a transverse view, in order to assess the situs of this structure, as

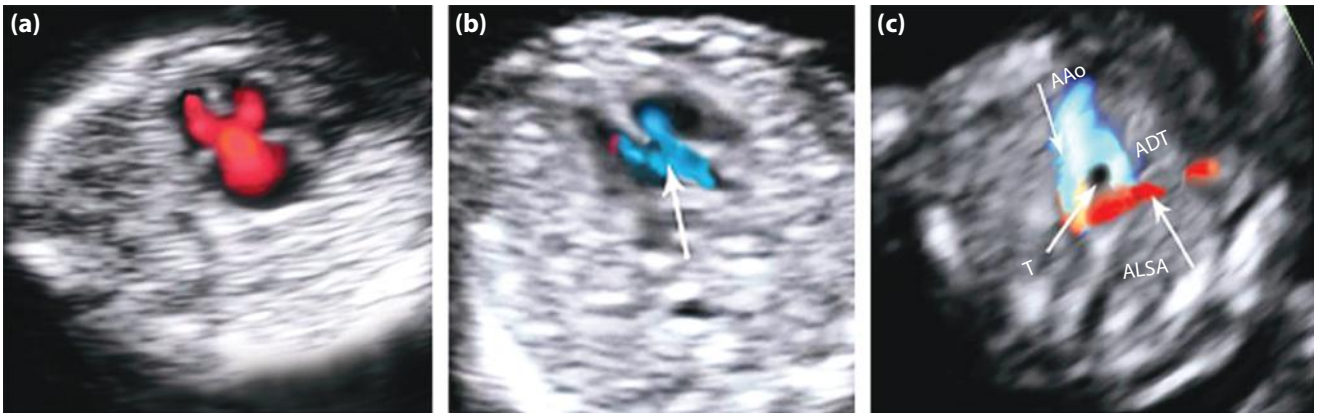


Figure 1.19 (a) Color Doppler image at 13 weeks demonstrating a complete atrioventricular septal defect. (b) Tetralogy of Fallot. Color Doppler image at 13 weeks demonstrating, in the five-chamber view, the ventricular septal defect with an overriding aorta (arrow). (c) Right aortic arch with an aberrant left subclavian artery and a left ductal arch (vascular ring). Color Doppler image at 12 weeks demonstrating the vascular ring. The trachea (T) is encircled by the right aortic arch (AAO), aberrant left subclavian artery (ALSA), and left ductal arch (ADT). (Modified from Volpe P et al. *Prenat Diagn* 2011; 31: 1054–61.)

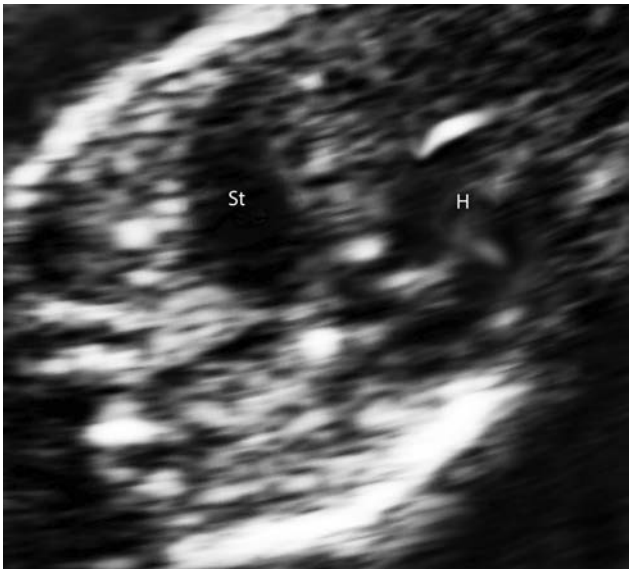


Figure 1.20 Left-sided congenital diaphragmatic hernia in a fetus at 12^{+3} weeks. The heart (H) is shifted to the right by intrathoracic viscera. The stomach (St) is herniated into the chest.

well as the normal size and position within the abdomen. The cord insertion can be visualized either in a transverse view or in a midsagittal one. In the latter view, the outline of the abdominal wall can be assessed to exclude any abdominal wall defects.

Always detectable abnormalities.

- **Exomphalos and gastroschisis.** Among abdominal wall malformations, both exomphalos (Figure 1.21a) and gastroschisis (Figure 1.21b), can be recognized early in gestation, because of the favorable fetal lie. In fact, before 14 weeks' gestation, the limbs are more frequently abducted, allowing a good view of the abdominal wall. However, care should be taken in diagnosing an exomphalos before 12 weeks, because the physiologic herniation of the bowel in the cord completely regresses only at the end of 11 weeks. Therefore, if an exomphalos containing only bowel loops is suspected at this gestational age, it is safer to wait 1 week in order to get a confirmation of the diagnosis. On the contrary, in case of liver herniation (Figure 1.21a), the diagnosis could be made already at 11 weeks. Sometimes, cord loops could give the impression of a bowel herniation and the color Doppler could be helpful in the differential diagnosis. It is important to differentiate between exomphalos and gastroschisis because of the strong association between exomphalos and chromosomal abnormalities, like trisomy 18 and 13 (about half of the cases) [46,57]. In case of exomphalos, the option of an invasive test could be consequently offered. In euploid fetuses, this condition could resolve spontaneously, if there is just herniation of the bowel [46,57] between 12 and 14 weeks. If herniation of the liver is already visible in the first trimester and the exomphalos does not resolve spontaneously, surgery is required after birth. Gastroschisis is not usually correlated with increased risk for chromosomal abnormalities, but this condition persists throughout the pregnancy, requiring postnatal treatment as well [58].
- **Pentalogy of Cantrell, limb–body wall complex, and ectopia cordis (Figure 1.22).** Pentalogy of Cantrell (PC) is a rare form of abdominal wall defect that consists of five associated anomalies including a midline anterior ventral wall defect, a diaphragmatic defect, a cleft distal sternum,

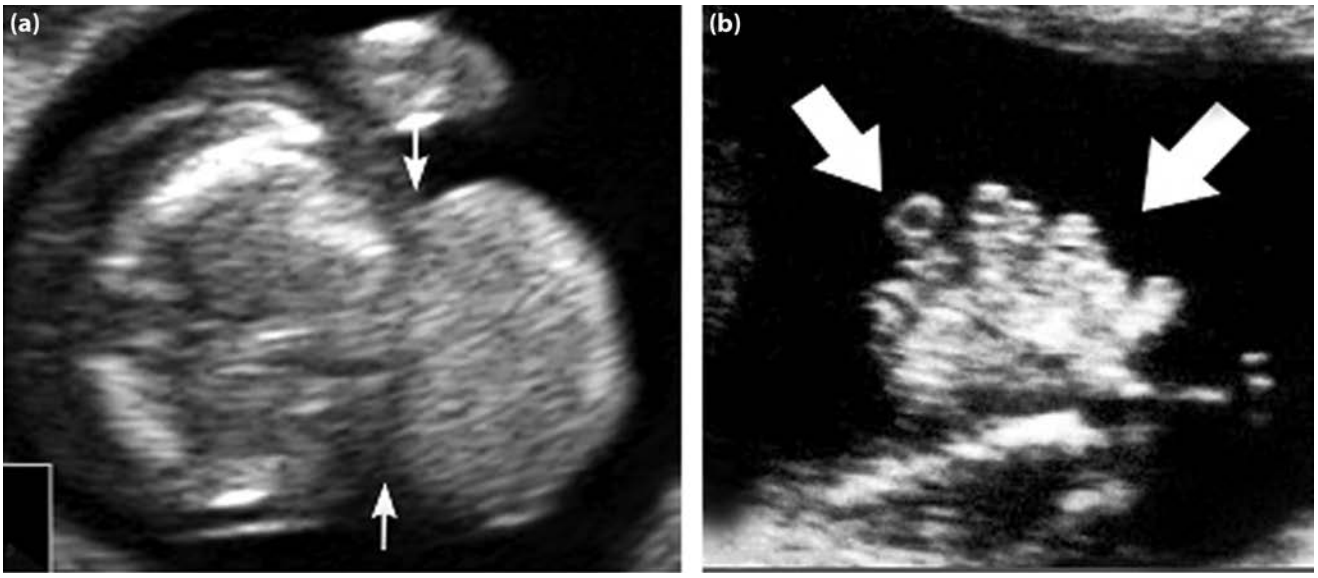


Figure 1.21 (a) Exomphalos at 11 weeks and 3 days. Transverse view of the fetal abdomen showing herniation of the liver in the sac (arrows). (b) Gastroschisis at 12 weeks. Typical appearance of bowel loops freely floating in the amniotic fluid (arrows).

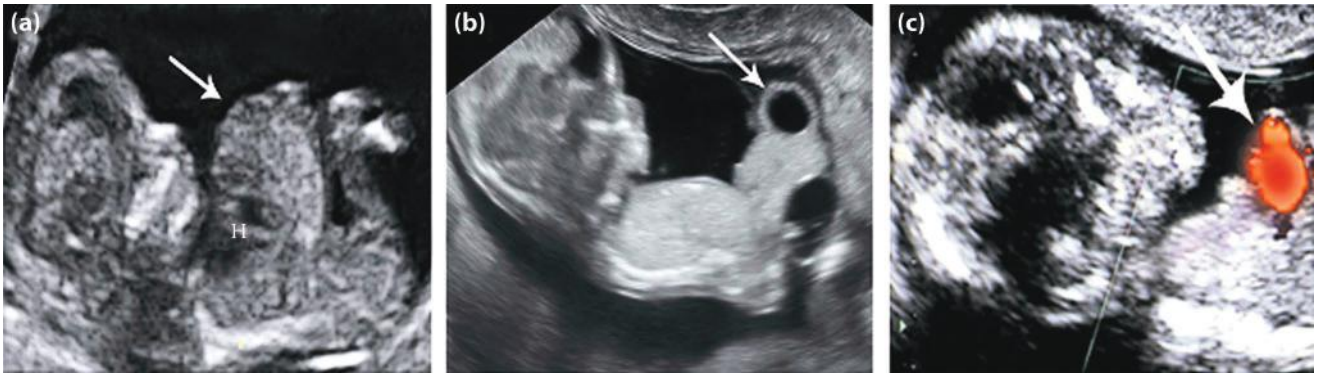


Figure 1.22 (a) Pentalogy of Cantrell: the typically supraumbilical omphalocele (arrow) and a slight displacement of the heart (H) at the base of the omphalocele can be clearly seen. (b) Limb-body wall complex: in a 13-week fetus, some of the eventrated organs and the umbilical cord are located in the extraembryonic coelomic cavity (arrow). (c) Ectopia cordis: a protrusion of the heart outside the chest can be clearly seen.

a defect of the apical pericardium with communication into the peritoneum, and an intracardiac defect. PC is also known as the "thoracoabdominal ectopia cordis," but this is in part a misnomer, given that the heart is always outside of the thorax in the latter case.

In limb–body wall complex (LBWC), a severely distorted fetus is adherent to placenta and no free-floating cord is present. Generally, the diagnosis is based on two of the three features below: exencephaly/cephalocele, abdominal wall defect/thoracoschisis, and limb defect.

In ectopia cordis, a term used interchangeably with PC, the heart protrudes through a cleft sternum, but no other defects usually are associated.

Urinary Tract

Ultrasound views. Transverse view of the pelvis, showing the fetal bladder between the umbilical arteries. Coronal view showing the kidneys.

Method. The bladder has to be clearly seen within the fetal pelvis, either in the midsagittal view or in a transverse view, which shows, as well, the umbilical arteries on its two sides. The kidneys are already visible in the first trimester, but they have similar echogenicity to the surrounding tissue; therefore, visualization is possible when good ultrasound equipment is available in favorable conditions (low maternal BMI, fetal position, etc). The visualization could be improved by transvaginal approach.

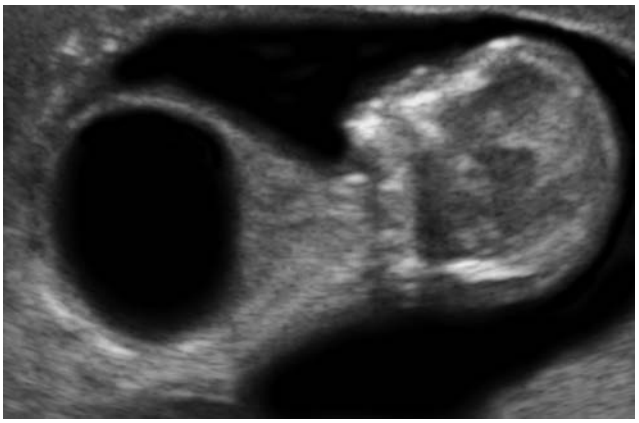


Figure 1.23 Megacystis. Midsagittal view of a fetus at 13 weeks showing massive dilatation of the bladder, occupying almost all the abdominal cavity.

Always detectable abnormalities.

- **Megacystis.** Megacystis is defined as a bladder measuring more than 7 mm. This finding is correlated with chromosomal abnormalities (mainly trisomy 13 and 18) in a significant number of cases [46,59,60]. We need to classify at least two different types of megacystis, both visible in the first trimester. A bladder diameter more than 15 mm is usually related to ureteral obstruction (complete urethral valves or urethral atresia) (Figure 1.23), and the outcome of these cases is usually poor [60]. This type of megacystis is strikingly evident at this stage, regardless of the rather normal amount of amniotic fluid, due to the severe enlargement of the bladder in the fetal abdomen, often occupying the whole abdomen of the fetus. When longitudinal diameter of the bladder is between 7 and 15 mm, it has been reported [60] that around 24% of fetuses have a chromosomal anomaly. However, if the karyotype is normal, spontaneous resolution of the megacystis occurs in about 90% of cases.

Potentially detectable abnormalities.

- **Bilateral renal agenesis.** It is difficult to diagnose this anomaly early in gestation. This difficulty arises because though the kidneys can be visualized, as previously mentioned, they cannot always be visualized as clearly as they ought to be. In addition, the important sign that always leads to this diagnosis in the second trimester, namely severe oligohydramnios, develops only after 16 weeks' gestation, because until that time the amniotic fluid is produced exclusively by ultrafiltration and the contribution of the fetal urine to its maintenance is marginal [61]. When the bladder is not visible during the routine first-trimester examination, even after waiting for enough time to allow the bladder to fill up, it is mandatory to clearly visualize the kidneys either transabdominally or, if necessary, transvaginally. If the kidneys are not visible, bilateral renal agenesis condition has to be suspected, and a further confirmation could be the impossibility to demonstrate the renal arteries by color or directional power Doppler with low PRF (Figure 1.24). In doubtful cases, it is advisable to wait until 16 completed weeks, when oligo-anhydramnios develops.

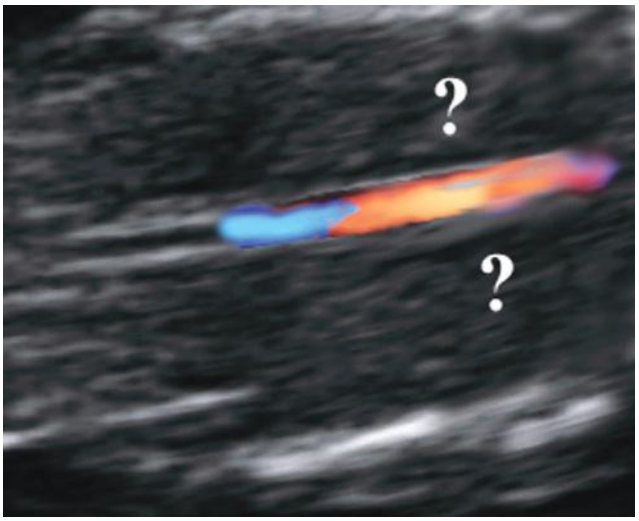


Figure 1.24 Bilateral renal agenesis in a fetus at 13 weeks. Both renal fossa are empty (?). The color Doppler can be helpful to confirm the absence of both renal arteries.

Extremities

Ultrasound views. Longitudinal view of the three segments of the four limbs. View of the hands and feet showing the fingers. Evidence of fetal movements.

Method. Basically, the examination of the limbs should aim to show the presence of all three segments of each limb: thigh, leg, and foot in both lower limbs; arm, forearm, and hand in both upper limbs. Also, within each segment, all bones should be checked for normal appearance and proportions. This check is obtained by longitudinal views of these segments. A closer examination, by dedicated views of the open hands and the foot soles, could show whether there are five fingers on each hand and five toes on each foot.

Potentially detectable abnormalities. Limb abnormalities such as transverse reduction defects and aplasia radii (Figure 1.25), as well as clubfoot and clenched hands, may be detected. The detailed examination of the hands and feet is not always feasible in the routine first-trimester scan, because these structures are small and difficult to see, especially in cases of unfavorable

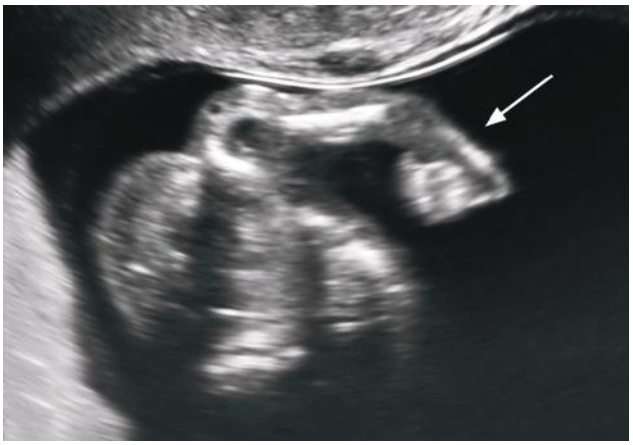


Figure 1.25 Radial aplasia. Ultrasound image showing a fetal arm with a normal humerus and a small forearm characterized by the presence of only one small bone (the ulna).



Figure 1.26 Three-dimensional surface rendering of a unilateral clubfoot (arrow) in a 13-week fetus.

fetal position. The diagnosis of limb abnormalities is easier when the condition is not isolated, such as in the case of clenched hands or clubfoot (Figure 1.26), which are often associated with chromosomal abnormalities usually showing other anomalies. The routine visualization of a midsagittal view of the leg, showing the normal relationship with the foot (the sole should be not visible in this view), could improve the detection of severe talipes, mainly when associated with chromosomal abnormalities (trisomy 18) or with early arthrogryposis [62]. The position of the foot in the earlier stages of embryologic development is actually intrarotated, making it difficult to differentiate pathological talipes from the positional one [62,63].

ThE MId-Tr IMEsTEr A No MALy sc AN

As already mentioned, in most countries, the screening for congenital anomalies is carried out in the second trimester, usually between 18 and 22 weeks of gestation. In this regard, the ideal time for the sonographic assessment of fetal anatomy should be at 24–26 weeks' gestation, to provide an optimal balance between the amount of amniotic fluid and the volume and developmental stage of the fetal organs.

If the timing of the anomaly scan differs, this is usually due to laws in countries where there is a legal time limit for termination of pregnancy; in these cases, upper time limit for the scan is usually set at 22–23 weeks' gestation, which represents the limit of fetal viability. Usually, the examination protocol includes:

- A biometric assessment usually consisting of biparietal diameter, head circumference, abdominal circumference, and femur length (Tables A.1 through A.8).
- Anatomic assessment that, depending on different national guidelines, consists of visualization of all or part of the following structures:
  - *Head*: skull, cerebral hemispheres, falx, cavum septi pellucidi, cerebellum and cisterna magna, lateral ventricles, orbits, lips, and facial profile;
  - *Thorax*: four-chamber view with outflows and lungs;
  - *Abdomen*: stomach, liver, bowel, kidneys and bladder, and abdominal wall;
  - *Limbs*: presence of the four limbs and of the extremities;
  - *Spine*.
- Evaluation of the fetal adnexa, placenta, and amniotic fluid.

Pretest information. Prior to the scan, the patient should be informed about the potential diagnostic accuracy of the examination, its screening nature, and the technical and practical limitations of the ultrasound examination. In addition, it is useful to inform the couple that the scan will not have a predefined duration, but rather will depend on several factors, including acoustic window limitations (e.g., maternal obesity) and fetal lie.

Acoustic window impairment. The diagnostic accuracy of mid-trimester screening for the detection of congenital anomalies will be illustrated below. Here, we wish to emphasize how important it is, for medicolegal reasons, to describe in the report and to express in the pre- and

posttest counseling the existence of any factor that may reduce the diagnostic accuracy of the ultrasound examination. These include maternal and fetal limitations.

Maternal causes of impaired acoustic window. The most important factor that may greatly reduce the diagnostic potential of a transabdominal ultrasound examination is the presence of *maternal obesity,* which, unfortunately, is becoming a real problem due to the increased prevalence of this condition in the populations of the developed countries [64]. The impairment of the acoustic window exhibits a positive linear correlation with the thickness of the abdominal subcutaneous adipose tissue. It is common experience, however, that in some cases resolution and penetration are also significantly reduced in the *absence of evident maternal overweight*, probably due to individual differences in subcutaneous adipose tissue, water, and fat content. Another factor that may limit the diagnostic accuracy of the mid-trimester scan is an *increased tone of the abdominal musculature*, usually due to maternal anxiety. The presence of *striae rubrae* from dysmetabolic conditions or of large *abdominal scars* or *burns* can also have a significant impact on the quality of the ultrasound examination. Finally, the most frustrating condition to be confronted with in the course of an ultrasound examination is, in our experience, a *previous abdominoplasty*. In this case, several concurrent factors contribute to the limitation of diagnostic accuracy: the extensive cleavage of the whole abdominal subcutaneous tissue from the underlying muscular fascia associated with a long cutaneous surgical wound scar; residual abdominal fat; and a dramatic increase in abdominal firmness. All represent a frustrating if not insurmountable problem.

Fetal causes of impaired acoustic window. The most common cause of (fortunately transient) impairment of the acoustic window is represented by an *unfavorable fetal lie*: an anterior spine, especially if associated with a transverse lie, often making assessment of the heart and the craniofacial area impossible. However, in these cases, it is often sufficient to rescan the woman after 20–60 min to allow the fetus to change its position and remove the cause of the acoustic window impairment.

Fetal crowding is also a potential cause of acoustic window impairment, with the degree of impairment increasing with the number of fetuses. Another factor that can significantly limit the diagnostic accuracy of the mid-trimester scan is an abnormal amount of amniotic fluid. In particular, *severe oligohydramnios*, from premature rupture of membranes or renal anomalies, and *severe polyhydramnios*, from fetal anomalies, twin-to-twin-transfusion syndrome, or idiopathic, can be responsible for an impairment of the acoustic window for different reasons. In oligohydramnios, the natural contrast agent represented by the amniotic fluid is absent and, in addition, the limbs are often adducted; these two factors usually limit assessment of the fetal limbs and heart. With severe polyhydramnios, the increased fetal movements and the significant increase in the distance between the transducer and the fetal body are the two main limitations.

The abdominal acoustic windows. It is useful to know that the normal anatomy of the human abdominal wall provides a few preferential "channels" to exploit in the case of an impaired acoustic window. These preferential points of access are characterized by a reduced amount of subcutaneous adipose tissue with a consequently reduced transducer–fetus median distance. Two of these anatomic regions are the *periumbilical area*, where there is virtually no adipose tissue and which may be exploited if no air is left between the transducer and the actual maternal umbilicus, and the *lateral regions of the abdomen* (i.e., iliac fossae), where the mean thickness of the abdominal adipose tissue is less than in the hypogastric area (between the symphysis and the umbilical area). To take advantage of this type of approach, the patient may be asked to roll onto one side (which one depends on the position of the fetus) in order to better expose the lateral abdominal area to the operator. Often, using this type of approach, the increased muscular resistance offered by some patients (see above) also tends to be reduced. A third preferential point of access is the *suprapubic area/fold*. In general, at 20–22 weeks with the fetus in the vertex position, the fetal head may be approached through the suprapubic area, while the craniofacial anatomy may be assessed through the periumbilical area. A useful hint may be to use the maternal bladder as a wedge: a full bladder will push the uterus (and the fetus) upward, toward the umbilical area; on the contrary, an empty bladder may allow the fetal head to descend into the pelvis, where it can be explored through the suprapubic window.

THE THIRD-TRIMESTER SCAN (TABLE 1.2)

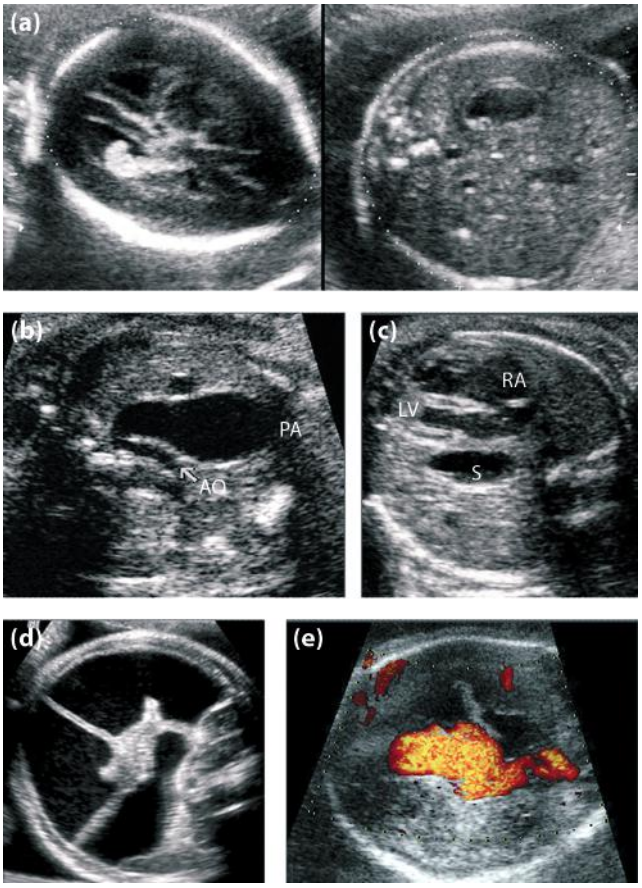
This ultrasound scan usually aims at the recognition of growth restriction. A second endpoint is the detection of late-onset congenital anomalies.

Evolving and late-onset malformations (**Figure 1.27 and Table 1.2**). The term "evolving" may indicate two conditions: (1) that a malformation may potentially

Table 1.2 The most common (but not all) late-onset (>24 weeks' gestation) malformations

Congenital anomaly	Always	In a significant number of cases	Also only after birth
Hydrocephalus		+	
Microcephaly		+	+
Agenesis of the corpus callosum		+	
Semilunar valve stenosis		+	+
Aortic coarctation		+	+
Cardiomyopathy	+		+
Premature closure of DA	+		
Patent DA	+		+
Diaphragmatic hernia		+	+
Esophageal atresia		+	+
Duodenal atresia		+	+
Ileo-jejunal atresia	+		
Meconium ileus		+	+
ARPKD		+	
ADPKD		+	+
Vesicoureteral reflux		+	+
Achondroplasia		+	
Arthrogryposis (FADS)		+	+
Vein of Galen aneurysm	+		
Tumors (all sites)	+		+

ADPKD: autosomal dominant polycystic kidney disease; ARPKD: autosomal recessive polycystic kidney disease; DA: ductus arteriosus.



arise late in gestation (late onset), due to an arrest in the development/growth of a given anatomic structure (e.g., microcephaly or semilunar valve stenosis); or (2) that it is already present at mid-trimester but has the potential to progress toward more severe stages in the third trimester (e.g., diaphragmatic hernia, semilunar valve stenoses, upper renal lesions, or gastrointestinal malformations). As a result, the mid-trimester anomaly can be unremarkable in all conditions covered by the former definition [65]. A partial list of the most common evolving lesions is given in Table 1.2.

Figure 1.27 Evolving (late-onset) malformations: A few examples of evolving lesions are shown. (a) Microcephaly: Compare the reduced head area (<3 standard deviations) with the normal abdominal area. (b) Aortic coarctation: The axial three-vessel view shows the severely hypoplastic aortic arch (tubular hypoplasia AO: aortic arch; PA: Ductal arch). (c) Left-sided congenital diaphragmatic hernia: The presence in the thorax of the stomach is evident LV: left ventricle; RA: right atrium; S: stomach). (d) Jejunal atresia: extremely severe dilatation of jejunal loops. (e) Aneurysm of the vein of Galen: On the transventricular view, the huge midline vascular lake, consistent with the diagnosis of aneurysm of the vein of Galen, is highlighted on power Doppler.

THREE-DIMENSIONAL ULTRASOUND

Three-dimensional (3D) ultrasound has become an integral part of the ultrasound assessment of a large number of fetal anomalies [66–70]. It represents for the new century what Doppler velocimetry represented for the 1980s and 1990s—an enormous contribution to the field of fetal medicine. Unfortunately, the clinical use of 3D ultrasound has been in part obstructed by its use (misuse?) to display portraits of the fetal face. The heavy marketing campaign launched some years ago by all producers of 3D ultrasound equipment has led to a misunderstanding in the population that because 3 is "better" than 2, then 3D ultrasound should *see more and better* than 2D ultrasound. Although this may be partly true in those cases in which a fetal malformation has been detected, though only for some organ systems, as explained in the various chapters, the use of 3D ultrasound in the screening setting so far has *not* been validated at all. In this section, we will illustrate briefly the approach to 3D ultrasound, from the volume acquisition procedure to offline navigation and reconstruction. Of all the currently available techniques and imaging modes, we will illustrate only those pertinent to the diagnosis of fetal malformations.

In addition, it should be pointed out that the names and the techniques used by the various manufacturers of 3D ultrasound systems differ. Because all 3D ultrasound images in this book have been obtained with General Electric–Kretz equipment, the terms and the procedures described here relate to the equipment and technologies developed by this manufacturer.

Volume acquisition procedure. The volume acquisition procedure is based on the particular technology of *volumetric transducers*. The acquisition of the volume is based on the movement of the array housed inside the transducer: when the procedure is activated, this array performs a slow single sweep, automatically recording one single 3D data set. This volume consists of a high number of 2D frames (or slices). Once the volume has been acquired, it can be processed directly on the ultrasound system or, more comfortably, offline on a PC, with the help of dedicated software.

Quality of the volume. The quality of the acquired volume depends first of all on all the usual limitations inherent to the physics of ultrasound (maternal obesity, fetal lie, etc.), which obviously apply to 3D ultrasound, too. In addition, the quality of the volume is conditioned by the presence/absence of fetal movements during the acquisition time: the more movements that occur, the less adequate is the acquired volume. Another important factor affecting the quality of the volume is involuntary movement of the hand holding the transducer during the acquisition. However, an easy and fast way to assess the quality of an acquired volume consists in assessing how many abnormal "waves" are present on the b window (the upper-right end-side one) on the multiplanar screen (Figure 1.28): the higher their number, the poorer is the volume quality.

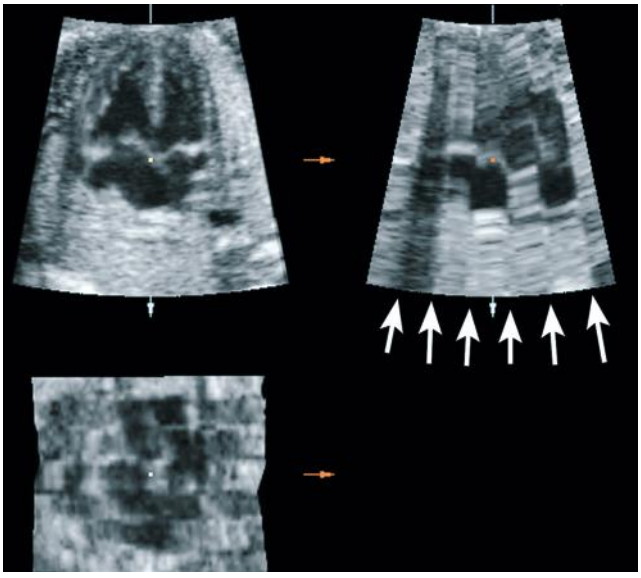


Figure 1.28 Overall quality of the volume. It is possible to assess the overall quality of the acquired volume by looking at the b window (top right). The number of vertical artifacts (arrows) corresponds to the number of gross fetal movements. In this case, from the regular rhythm of the artifacts it can be deduced that the STIC volume was acquired during a period of fetal breathing.

Multiplanar imaging. This image modality represents the key approach to the study of fetal anatomy in normal and abnormal conditions. In the three windows, the three orthogonal planes are displayed (Figure 1.29). Using the cursors, it is possible to navigate the volume, reproducing all possible views on the three planes; in addition, to better assess the relationships among different anatomic structures, it is possible to move the dedicated caliper on one plane and evaluate the corresponding changes on the other two planes.

Surface mode. From the acquired data set, it is possible to retrieve all the information needed to reconstruct the surface appearance of a given structure (*surface mode*). The combination of various filters and thresholds allows one to obtain the desired mixture of contrast, light, and transparency (Figure 1.30).

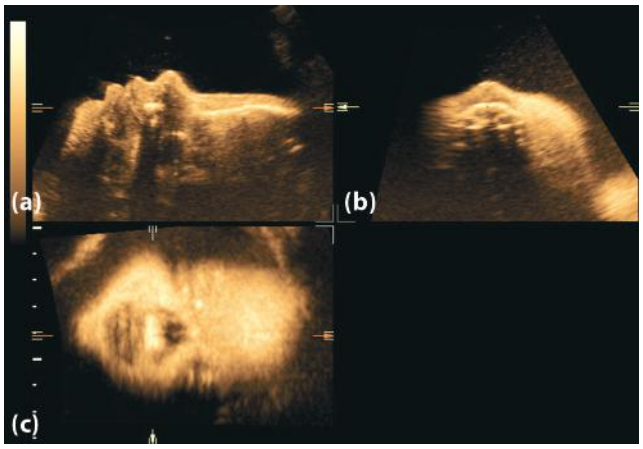


Figure 1.29 Three-dimensional ultrasound—multiplanar imaging. Once the 3D volume is opened, the three orthogonal planes are shown. By moving the small caliper, yellow in (a), red in (b), blue in (c), it is possible to assess in detail the anatomic structure of interest. This example illustrates the multiplanar rendering of a normal fetal face at 32 weeks of gestation.

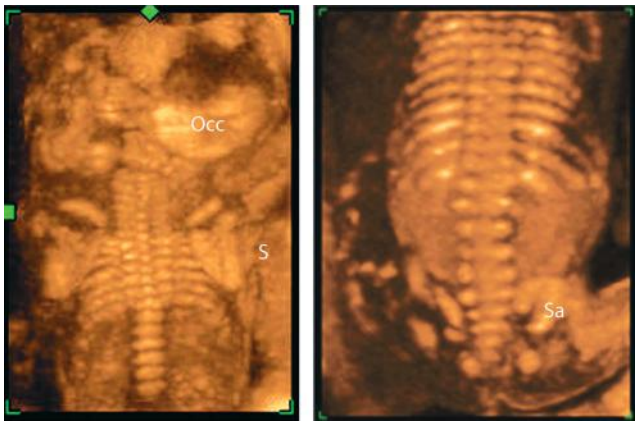


Figure 1.31 Three-dimensional ultrasound—maximum mode. This image modality allows one to "see through" the soft tissues, displaying the fetal bones. This example shows the upper spine with the occipital bone (Occ) and the scapulae (S) on the left and the lower spine with the iliac wings (Sa) on the right.

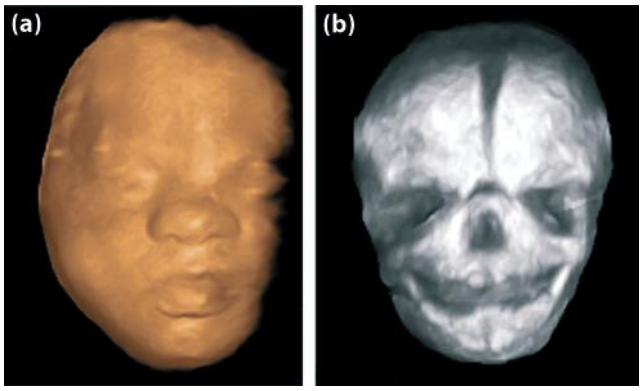


Figure 1.30 Three-dimensional ultrasound. (a) Surface mode. Using the surface mode, and adjusting threshold and filters, it is possible to display the surface of the fetal face. This example is the same as in Figure 1.28, a 32-week-old fetus. (b) Maximum mode of the same volume and with the same region of interest as (a). This example shows the skeleton of the face.

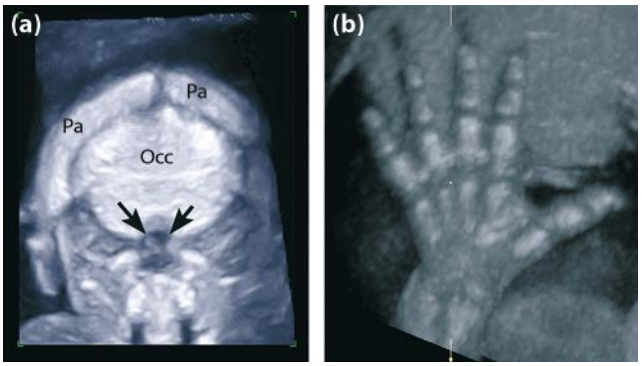


Figure 1.32 Volume contrast imaging C (VCI-C) (Coronal). (a) Occipital encephalocele at 19 weeks' gestation. The VCI-C shows the parieto-occipital sutures and the small cephalocele (arrows) (Occ: occipital bone; Pa: parietal bones) (b) detailed rendering of the bones and soft tissue of a fetal hand.

Maximum mode. If the degree of transparency is increased, and the maximum mode option is activated, the soft tissues become transparent and the fetal skeleton is displayed (Figure 1.31).

Volume contrast imaging C (coronal). This application allows quick display on screen. In gynecologic ultrasound, it is possible to provide impressive images of the normal and abnormal uterine cavity. In obstetrics, its use is of crucial importance for the assessment of cranial sutures (Chapter 3), thoracoabdominal topographic anatomy (Chapter 6), and of limb abnormalities (Figure 1.32).

Inversion mode. This is one of the latest developments. It can be used to assess sonolucent structures (vessels, cavities, etc.). In fact, its algorithm inverts the color code assigned to black and white pixels (voxels in 3D). The final output is a cast-like image of the studied structure; originally developed for the heart, it can also be applied to cystic structures (Figure 1.33).

B-flow rendering. B-flow imaging is a new technique that employs digitally encoded sonographic technology to provide direct visualization of blood flows in grayscale. It displays simultaneously both tissue morphology and blood flow using the same grayscale schemes. This leads to a higher frame rate and better spatial resolution in comparison with power and color Doppler.

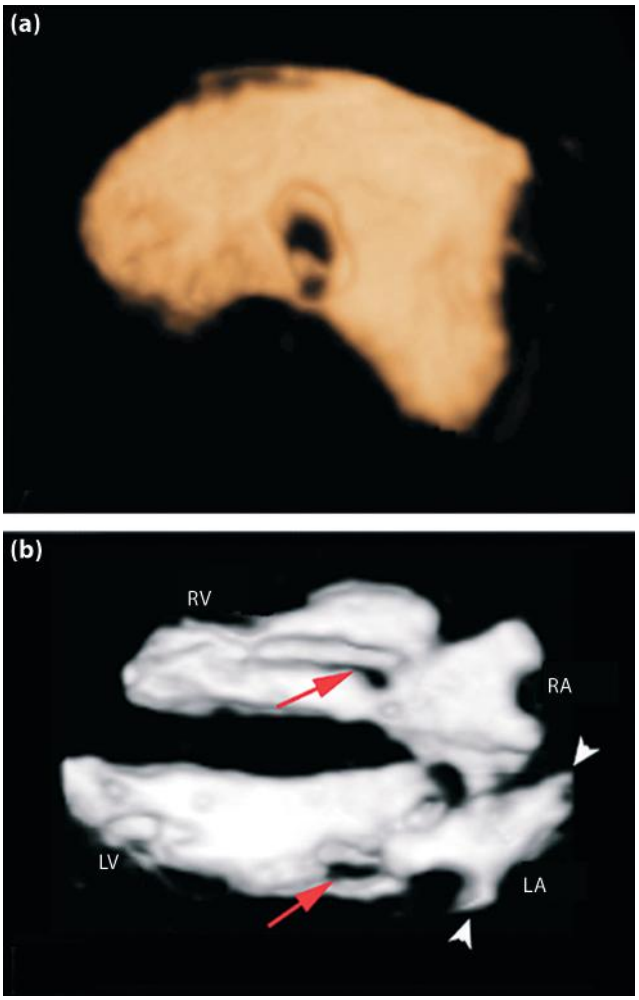


Figure 1.33 Three-dimensional ultrasound—inversion mode. This image modality allows one to create cast-like reconstructions of hollow anatomic structures. (a) Lateral cerebral ventricles in early onset severe hydrocephalus. Note the oval "defect" represented by the choroid plexus. (b) Four-chamber view of a normal heart. The arrows indicate the leaflets and the chordae tendineae of the atrioventricular valves. arrows: atrioventricualr valves; arrowheads: pulmonary veins; LA: left atrium; LV: left ventricle; RA: right atrium; RV: right ventricle

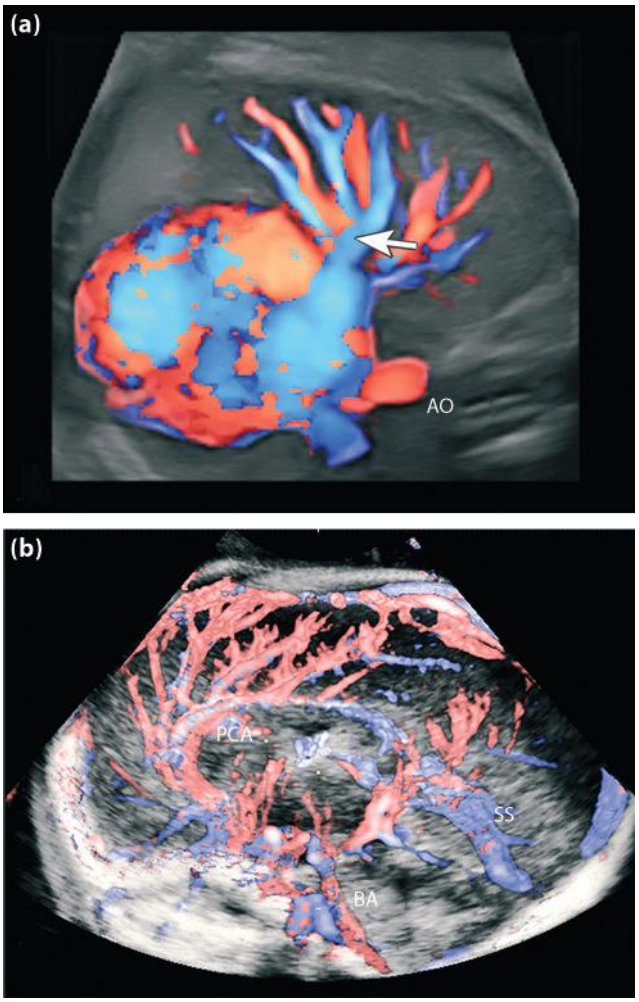


Figure 1.34 3D power Doppler. (a) Pulmonary intraparenchymal arterial and venous blood flow at 28 weeks' gestation (AO, descending aorta; arrow, intra-parenchymal pulmonary arteries and veins). (b) Transvaginal transfontanellar view of cerebral blood vessels at 24 weeks' gestation shows the anterior cerebral artery branching and giving rise to the pericallosal artery (PCA). Basilar trunk (BA), Sinus rectus (SS).

The rendering of B-flow facilitates obtaining of "digital casts" of the heart and vessels. This technique is briefly described in Chapter 5.

Glass-body rendering. This allows simultaneous viewing of the information from grayscale and color Doppler. This mode also is useful in the study of the cardiovascular system (Figure 1.34).

Sono-AVC. This technique, based on edge recognition, fills in hollow structures with color, creating casts of the structures. It has been used for three-dimensional follicular measurement in the IVF program. Now sono-automated volume count (AVC) shows application in fetal cardiology (Figure 1.35).

Tomographic ultrasound imaging. This image modality offers a new way of displaying diagnostic information contained in a static or dynamic 3D data set. In particular, it allows 2D slices to be displayed from any given volume, on any of the three orthogonal planes similar to CT or MR scans (Figure 1.36). This display mode can be advantageously used to demonstrate brain or cardiac fetal anomalies and to evaluate ovarian tumors or endometrial cavity abnormalities in gynecologic ultrasound.

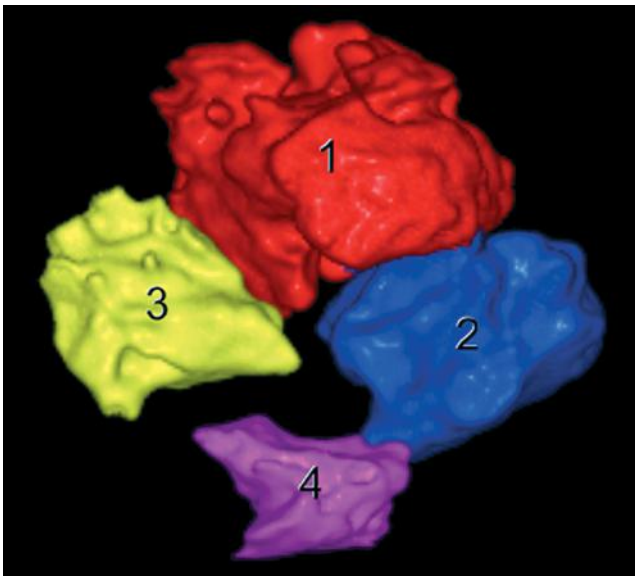


Figure 1.35 Sono-automated volume count (AVC). Images generated using spatiotemporal image correlation and sonography-based AVC, showing the four chambers in a fetus with coarctation of the aortic arch demonstrating ventricular disproportion (3: in yellow; 4: in purple; 1: in red; 2: in blue).

Other image modalities. Many possible combinations of rendering modes are available. The Cardio-spatiotemporal image correlation (STIC) technique developed for the study of the fetal heart is described in Chapter 5.

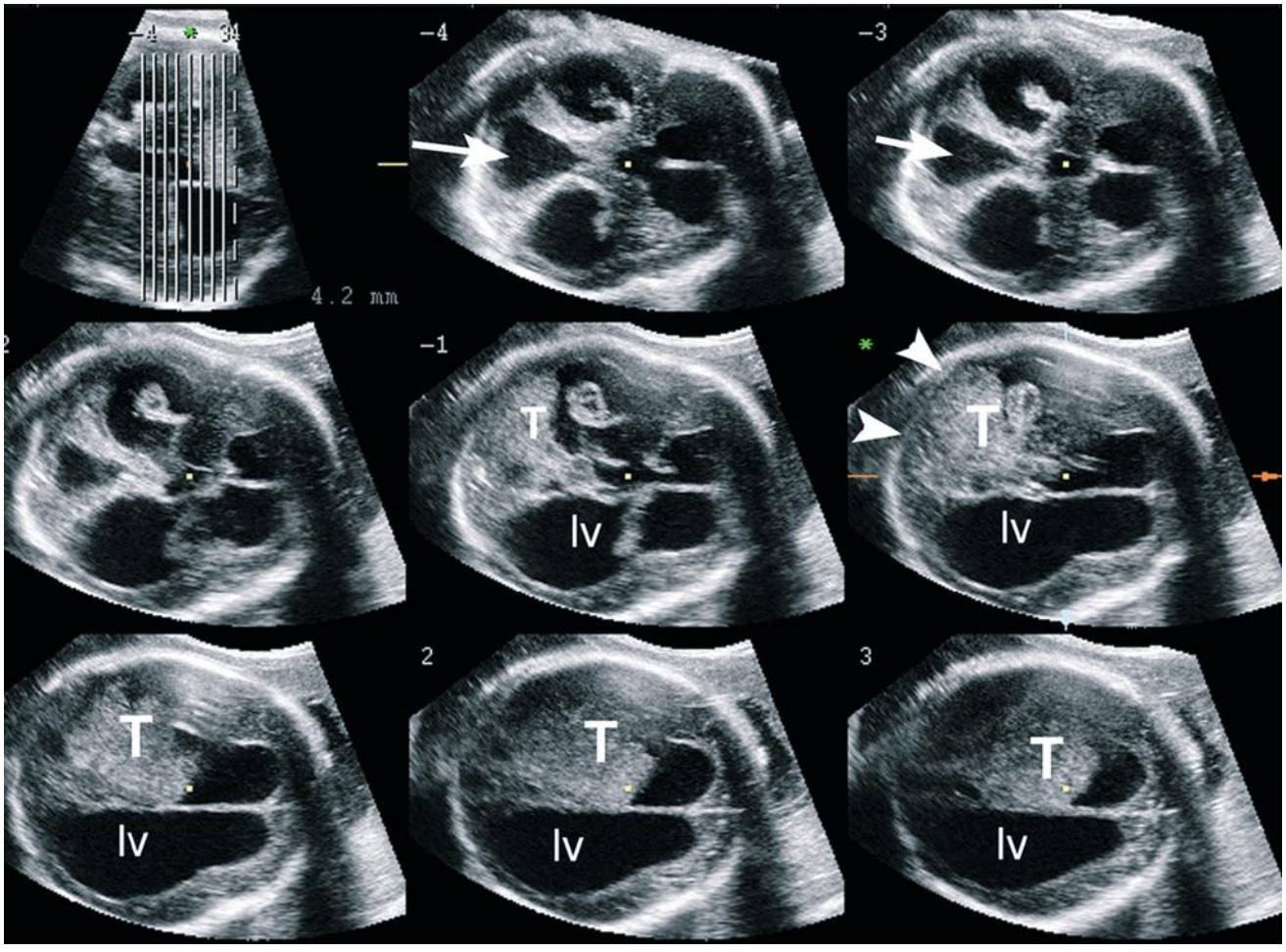


Figure 1.36 Tomographic ultrasound imaging. Carcinoma of the right choroid plexus at 35 weeks' gestation. The image shows the large malignant tumor (T) infiltrating the brain posteriorly (arrowheads) with secondary hydrocephalus (lv: lateral ventricles; arrow: fourth ventricle). The multi-slice, tomographic imaging allows assessment on the single panel of images, the extension of the tumor, and its relationship with the surrounding anatomic structures.

OUTLINE OF THIS BOOK

The rationale behind this book is the concept that, in everyday practice, what raises the suspicion of a fetal anomaly is an *abnormal view*—that is, the "non-normal" appearance of a conventional scanning view. This is why, in each chapter, the first part does not consist of the classic nosologic approach but rather of a section dedicated to the various ultrasound views necessary to assess each organ. Then, the abnormal aspect of each view is illustrated, and the anomalies possibly responsible for the abnormal aspect of the ultrasound view are illustrated. In several cases, the first part of the chapter is further enriched with diagnostic flowcharts that may help in the differential diagnosis by *sign*. For example, these flowcharts illustrate all anomalies to be ruled out in the case of *nonvisualization of the fetal stomach* (Figure 7.1) or *bladder* (Figure 8.1), or, in the case of *micromelia*, which additional signs should be sought to make a differential diagnosis among all skeletal dysplasias possibly associated with micromelia (Figure 9.1). The philosophy behind this approach—*from sign to diagnosis*—is maintained in all chapters. The second part of each chapter is dedicated to the illustration of the various abnormalities. Again, to maintain the practical approach, for each anomaly a summarizing box is given at the beginning, and the various headings then include *Definition; Etiology and pathogenesis; Ultrasound diagnosis; Risk of chromosomal anomalies; Risk of nonchromosomal syndromes; Obstetric management; Postnatal therapy;* and *Prognosis, survival, and quality of life*. Of particular interest, under the *Ultrasound diagnosis* heading, important subheadings give the differential diagnosis with anomalies featuring similar ultrasound signs and the ultrasound prognostic indicators.

In conclusion, we did not intend to write an extensive textbook on fetal anomalies—there are already excellent ones available—instead, our idea was to produce a versatile text that might be consulted in everyday practice and that might help in difficult situations.

REFERENCES

1. Nicolaides KH. Nuchal translucency and other first trimester sonographic markers of chromosomal abnormalities. *Am J Obstet Gynecol* 2004; 191: 45–67.
2. Souka AP, Von Kaisenberg CS, Hyett JA, Sonek JD, Nicolaides KH. Increased nuchal translucency with normal karyotype. *Am J Obstet Gynecol* 2005; 192: 1005–21.
3. Nicolaides KH. Screening for fetal aneuploidies at 11 to 13 weeks. *Prenat Diagn* 2011; 31: 5–7.
4. Cuckle H, Benn P, Wright D. Down syndrome screening in the first and/or second trimester: model predicted performance using meta-analysis parameters. *Semin Perinatol* 2005; 29: 252–7.
5. Kagan KO, Wright D, Valencia C, Mais N, Nicolaides KH. Screening for trisomies 21, 18 and 13 by maternal age, fetal nuchal translucency, fetal heart rate, free βhCG and pregnancy-associated plasma protein-A. *Hum Reprod* 2008; 23: 1968–75.
6. Nicolaides KH. Turning the pyramid of prenatal care. *Fetal Diagn Ther* 2011; 29: 183–96.
7. Tabor A, Alfirevic Z. Update on procedure-related risks for prenatal diagnosis techniques. *Fetal Diagn Ther* 2010; 27: 1–7.
8. Clur SA, Ottenkamp J, Bilardo CM. The nuchal translucency and the fetal heart: a literature review. *Prenatal Diagn* 2009; 29: 739–48.
9. Akolekar R, Syngelaki A, Sarquis R, Zvanca M, Nicolaides KH. Prediction of early, intermediate and late pre-eclampsia from maternal factors, biophysical and biochemical markers at 11–13 weeks. *Prenat Diagn* 2011; 31: 66–74.
10. Karagiannis G, Akolekar R, Sarquis R, Wright D, Nicolaides KH. Prediction of Small-for-Gestation Neonates from Biophysical and Biochemical Markers at 11–13 Weeks. *Fetal Diagn Ther* 2011; 29: 148–54.
11. Poon LCY, Akolekar R, Lachmann R, Beta J, Nicolaides KH. Hypertensive disorders in pregnancy: screening by biophysical and biochemical markers at 11–13 weeks. *Ultrasound Obstet Gynecol* 2010; 35: 662–70.
12. Poon LC, Syngelaki A, Akolekar R, Lai J, Nicolaides KH. Combined screening for preeclampsia and small for gestational age at 11–13 weeks. *Fetal Diagn Ther* 2013; 33:16–27.
13. Volpe P, Ubaldo P, Volpe N, et al. Fetal cardiac evaluation at 11–14 weeks by experienced obstetricians in a low-risk population. *Prenat Diagn* 2011; 31: 1054–61.
14. Syngelaki A, Chelemen T, Dagklis T, Allan L, Nicolaides KH. Challenges in the diagnosis of fetal non-chromosomal abnormalities at 11–13 weeks. *Prenat Diagn* 2011; 31: 90–102.
15. Nicolaides KH, Heath V, Cicero S. Increased fetal nuchal translucency at 11–14 weeks. *Prenat Diagn* 2002; 22: 308–15.
16. Internet course: *The 11–13 weeks scan*. Available from: www.fetalmedicine.com
17. Liao AW, Snijders R, Geerts L, Spencer K, Nicolaides KH. Fetal heart rate in chromosomally abnormal fetuses. *Ultrasound Obstet Gynecol* 2000; 16: 610–13.
18. Benacerraf BR, Gelman R, Frigoletto FD Jr. Sonographic identification of second-trimester fetuses with Down's syndrome. *N Engl J Med* 1987; 317: 1371–6.
19. Nicolaides KH, Azar G, Byrne D, Mansur C, Marks K. Fetal nuchal translucency: ultrasound screening for chromosomal defects in first trimester of pregnancy. *BMJ* 1992; 304(6831): 867–9.
20. Cicero S, Rembouskos G, Vandecruys H, Hogg M, Nicolaides KH. Likelihood ratio for trisomy 21 in fetuses with absent nasal bone at the 11–14-week scan. *Ultrasound Obstet Gynecol* 2004; 23: 218–23.
21. Rembouskos G, Cicero S, Longo D, Vandecruys H, Nicolaides KH. Assessment of the fetal nasal bone at 11–14 weeks of gestation by three-dimensional ultrasound. *Ultrasound Obstet Gynecol* 2004; 23(3): 232–6.

22. Peralta CF, Falcon O, Wegrzyn P, Faro C, Nicolaides KH. Assessment of the gap between the fetal nasal bones at 11 to 13 + 6 weeks of gestation by three-dimensional ultrasound. *Ultrasound Obstet Gynecol* 2005; 25(5): 464–7.
23. Faiola S, Tsoi E, Huggon IC, Allan LD, Nicolaides KH. Likelihood ratio for trisomy 21 in fetuses with tricuspid regurgitation at the 11 to 13 + 6-week scan. *Ultrasound Obstet Gynecol* 2005; 26: 22–7.
24. Kagan KO, Valencia C, Livanos P, Wright D, Nicolaides KH. Tricuspid regurgitation in screening for trisomies 21, 18 and 13 and Turner syndrome at 11+0 to 13+6 weeks of gestation. *Ultrasound Obstet Gynecol* 2009; 33(1): 18–22.
25. Pereira S, Ganapathy R, Syngelaki A, Maiz N, Nicolaides KH. Contribution of fetal tricuspid regurgitation in first-trime - ter screening for major cardiac defects. *Obstet Gynecol* 2011; 117(6): 1384–91.
26. Maiz N, Valencia C, Emmanuel EE, Staboulidou I, Nicolaides KH. Screening for adverse pregnancy outcome by ductus venosus Doppler at 11–13+6 weeks of gestation. *Obstet Gynecol* 2008; 112(3): 598–605.
27. Chaoui R, Thiel G, Heling KS. Prevalence of an aberrant right subclavian artery (ARSA) in normal fetuses: a new soft marker for trisomy 21 risk assessment. *Ultrasound Obstet Gynecol* 2005; 26: 356.
28. Borenstein M, Cavoretto P, Allan L, Huggon I, Nicolaides KH. Aberrant right subclavian artery at 11 + 0 to 13 + 6 weeks of gestation in chromosomally normal and abnormal fetuses. *Ultrasound Obstet Gynecol* 2008; 31: 20–4.
29. Borenstein M, Minekawa R, Zidere V, Nicolaides KH, Allan LD. Aberrant right subclavian artery at 16 to 23 + 6 weeks of gestation: a marker for chromosomal abnormality. *Ultrasound Obstet Gynecol* 2010; 36: 548–52.
30. Paladini D, Sglavo G, Pastore G, Masucci A, D'Armiento MR, Nappi C. Aberrant right subclavian artery: incidence and correlation with other markers of Down syndrome in second-trimester fetuses. *Ultrasound Obstet Gynecol* 2012; 39(2): 191–5.
31. Rembouskos G, Passamonti U, De Robertis V, et al. Aberrant right subclavian artery (ARSA) in unselected population at first and second trimester ultrasonography. *Prenat Diagn* 2012; 32(10): 968–75.
32. McElhinney DB, Clark BJ 3rd, Weinberg PM, et al. Association of chromosome 22q11 deletion with isolated anomalies of aortic arch laterality and branching. *J Am Coll Cardiol* 2001; 37: 2114–19.
33. Ebbing C, Rasmussen S, Godfrey KM, Hanson MA, Kiserud T. Hepatic artery hemodynamics suggest operation of a buffer response in the human fetus. *Reprod Sci* 2008; 15: 166–78.
34. Bilardo CM, Timmerman E, Robles de Medina PG, Clur SA. Low-resistance hepatic artery flow in first-trimester fetuses: an ominous sign. *Ultrasound Obstet Gynecol* 2011; 37(4): 438–43.
35. Zvanca M, Gielchinsky Y, Abdeljawad F, Bilardo CM, Nicolaides KH. Hepatic artery Doppler in trisomy 21 and euploid fetuses at 11–13 weeks. *Prenat Diagn* 2011; 31(1): 22–7.
36. Chiu RW, Akolekar R, Zheng YWL, et al. Non-invasive prenatal assessment of trisomy 21 by multiplexed maternal plasma DNA sequencing: large-scale validity study. *BMJ* 2011; 342: c7401.
37. Bianchi DW, Platt LK, Goldberg JD, Abuhamad AZ, Sehnert AJ, Rava RP. Genome-wide fetal aneuploidy detection by maternal plasma DNA sequencing. *Obstet Gynecol* 2012; 119: 1–12.
38. Nicolaides KH, Syngelaki A, Ashoor G, Birdir C, Touzet G. Noninvasive prenatal testing for fetal trisomies in a routinely screened first-trimester population. *Am J Obstet Gynecol* 2012; 207(5): 374.
39. Bujold E, Roberge S, Lacasse Y, et al. Prevention of preeclampsia and intrauterine growth restriction with aspirin started in early pregnancy. A meta-analysis. *Obstet Gynecol* 2010; 116: 402–14.
40. Bricker L, Garcia J, Henderson J, et al. Ultrasound screening in pregnancy: a systematic review of the clinical effectiveness, cost effectiveness and women's views. *Health Technol Assess* 2000; 4: 1–193.
41. Garne E, Dolk H, Loane M, Boyd PA. EUROCAT website data on prenatal detection rates of congenital anomalies. *J Med Screen* 2010; 17: 97–8.
42. Salomon LJ, Alfirevic Z, Bilardo CM, et al. ISUOG practice guidelines: performance of first-trimester fetal ultrasound scan. *Ultrasound Obstet Gynecol* 2013; 41: 102–13.
43. Grande M, Arigita M, Borobio V, Jimenez JM, Fernandez S, Borrell A. First-trimester detection of structural abnormalities and the role of aneuploidy markers. *Ultrasound Obstet Gynecol* 2012; 39(2): 157–63.
44. Sepulveda W, Dezerega V, Be C. First-trimester sonographic diagnosis of holoprosencephaly: value of the "butterfly sign. *J Ultrasound Med* 2004; 23: 761–5.
45. Volpe P, Campobasso G, De Robertis V, Rembouskos G. Disorders of prosencephalic development. *Prenat Diagn* 2009; 29(4): 340–54.
46. Kagan KO, Stamboulidou I, Syngelaki A, Cruz J, Nicolaides KH. The 11–13-week scan: diagnosis and outcome of holoprosencephaly, exomphalos and megacystis. *Ultrasound Obstet Gynecol* 2010; 36: 10–14.
47. Chaoui R, Benoit B, Mitkowska-Wozniak H, Heling KS, Nicolaides KH. Assessment of intracranial translucency (IT) in the detection of spina bifida at the 11–13-week scan. *Ultrasound Obstet Gynecol* 2009; 34(3): 249–52.
48. Lachmann R, Chaoui R, Moratalla J, Picciarelli G, Nicolaides KH. Posterior brain in fetuses with open spina bifida at 11–13 weeks. *Prenat Diagn* 2011; 31(1): 103–6.
49. Lachmann R, Sinkovskaya E, Abuhamad A. Posterior brain in fetuses with Dandy-Walker malformation with complete agenesis of the cerebellar vermis at 11–13 weeks: a pilot study. *Prenat Diagn* 2012; 32: 765–9.
50. Melchiorre K, Bhide A, Gika AD, Pilu G, Papageorghiou AT. Counseling in isolated mild fetal ventriculomegaly. *Ultrasound Obstet Gynecol* 2009; 34: 212–24.
51. Sepulveda W, Wong AE, Martinez-Ten P, Perez-Pedregosa J. Retronasal triangle: a sonographic landmark for the screening of cleft palate in the first trimester. *Ultrasound Obstet Gynecol* 2010; 35(1): 7–13.
52. Makrydimas G, Sotoriadis A, Huggon IC, et al. Nuchal translucency and fetal cardiac defects: a pooled analysis of major fetal echocardiography centers. *Am J Obstet Gynecol* 2005; 192: 89–95.
53. Hyett J, Perdu M, Sharland G, Snijders R, Nicolaides KH. Using fetal nuchal translucency to screen for major congenital cardiac defects at 10–14 weeks of gestation: population based cohort study. *BMJ* 1999; 318: 81–5.
54. Chelemen T, Syngelaki A, Maiz N, Allan L, Nicolaides KH. Contribution of ductus venosus Doppler in first-trimester screening for major cardiac defects. *Fetal Diagn Ther* 2011; 29 (2): 127–34.
55. Volpe P, Marasini M, Caruso G, et al. Prenatal diagnosis of ductus venosus agenesis and its association with cytogenetic/congenital anomalies. *Prenat Diagn* 2002; 22(11): 995–1000.
56. Volpe P, De Robertis V, Campobasso G, Tempesta A, Volpe G, Rembouskos G. Diagnosis of congenital heart disease by early and second-trimester fetal echocardiography. *J Ultrasound Med* 2012; 31(4): 563–8.

57. Khalil A, Arnaoutoglou C, Pacilli M, SzaboA, David AL, Pandya P. Outcome of fetal exomphalos diagnosed at 11–14 weeks of gestation. *Ultrasound Obstet Gynecol* 2012; 39: 401–6.
58. David AL, Tan A, Curry J. Gastroschisis: sonographic diagnosis, associations, management and outcome. *Prenat Diagn* 2008; 28(7): 633–44.
59. Sebire NJ, von Kaisenberg C, Rubio C, Snijders RJM, Nicolaides KH. Fetal megacystis at 10–14 weeks of gestation. *Ultrasound Obstet Gynecol* 1996; 8: 387–90.
60. Liao AW, Sebire NJ, Geerts L, Cicero S, Nicolaides KH. Megacystis at 10–14 weeks of gestation: chromosomal defects and outcome according to bladder length. *Ultrasound Obstet Gynecol* 2003; 21: 338–41.
61. Rabinowitz R, Peters MT, Vyas S, Campbell S, Nicolaides KH. Measurement of fetal urine production in normal pregnancy by real-time ultrasonography. *Am J Obstet Gynecol* 1989; 161: 1264–6.
62. Lauson S, Alvarez C, Patel MS, Langlois S. Outcome of prenatally diagnosed isolated clubfoot. *Ultrasound Obstet Gynecol* 2010; 35(6): 708–14.
63. Bar-Hava I, Bronshtein M, Orvieto R, Shalev Y, Stal S, Ben-Rafael Z. Caution: prenatal clubfoot can be both a transient and a late-onset phenomenon. *Prenat Diagn* 1997; 17(5): 457–60.
64. Paladini D. Sonography in obese and overweight pregnant women: clinical, medicolegal and technical issues. *Ultrasound Obstet Gynecol* 2009; 33: 720–9.
65. Malinger G, Lerman-Sagie T, Watemberg N, et al. A normal second-trimester ultrasound does not exclude intracranial structural pathology. *Ultrasound Obstet Gynecol* 2002; 2: 51–6.
66. Volpe P, Campobasso G, Stanziano A, et al. Novel application of 4D sonography with B-flow imaging and spatiotemporal image correlation (STIC) in the assessment of the anatomy of pulmonary arteries in fetuses with pulmonary atresia and ventricular septal defect. *Ultrasound Obstet Gynecol* 2006; 28: 40–6.
67. Chaoui R, Hoffman J, Heling KS. Three-dimensional (3D) and 4D color Doppler fetal echocardiography using spatio-temporal image correlation (STIC). *Ultrasound Obstet Gynecol* 2004; 23: 535–45.
68. Paladini D. Standardization of on-screen fetal heart orientation prior to storage of spatio-temporal-image correlation (STIC) volume data sets. *Ultrasound Obstet Gynecol* 2007; 29: 605–11.
69. Pilu G, Ghi T, Carletti A, et al. Three-dimensional ultrasound examination of the fetal central nervous system. *Ultrasound Obstet Gynecol* 2007; 30: 233–45.
70. Goncalves LF, Espinoza J, Lee W, et al. A new approach to fetal echocardiography: digital casts of the fetal cardiac chambers and great vessels for detection of congenital heart disease. *J Ultrasound Med* 2005; 24: 415–24.

Chapter 2
Central and peripheral nervous system anomalies

Normal anatomy of the brain: ultrasound approach, scanning planes, and diagnostic potential

Timing of examination. Although the most recent literature shows the improvements achieved in the detection of fetal abnormalities as early as possible during pregnancy (i.e., 12–14 weeks), ultrasound (US) screening for fetal brain malformations is commonly performed at 19–21 weeks' gestation. For the assessment of the fetal brain, the second-trimester anomaly scan includes the following axial planes: transthalamic, transventricular, and transcerebellar [1–3].

This has become the standard approach. However, some major developmental events occur in the second half of the gestational period, including neuronal proliferation, migration, and organization, and the same is true for acquired lesions, such as hemorrhage and tumors, which usually occur late in gestation. Therefore, although it is possible to detect most fetal brain anomalies in the second trimester, migration, proliferation, and organization [4,5] disorders, as well as acquired lesions can become apparent only in the third trimester.

Ultrasound approach and scanning planes. The screening or basic examination for anomalies of the central nervous system (CNS) is performed by transabdominal US. The examination should include evaluation of the fetal head and spine.

The fetal head is commonly evaluated using transverse scanning planes that are easily obtained. Coronal and sagittal views are more difficult to obtain; if the fetus is in the vertex position, a transvaginal scan may be required. Coronal and sagittal views may become necessary in a targeted examination, known as *fetal neurosonogram*, in patients with an increased risk of CNS anomalies [6–8].

Brain anomalies by scanning view. The axial scans used in the mid-trimester screening of brain malformations are as follows (Figure 2.1).

Axial transventricular view and related malformations. This is the most cephalad axial scan plane of the fetal head. It allows visualization of the sonolucent lateral ventricles with the echoic choroid plexuses, filling the ventricular bodies and atria (Figure 2.1a). They are separated medially by the cavum septi pellucidi (CSP). The CSP is a fluid-filled cavity between two thin membranes. In late gestation or the early neonatal period, these membranes usually fuse.

To exclude the presence of ventriculomegaly (VM), the width of the atria is measured at the level of the glomus. The measurement is made perpendicular to the ventricular axis by positioning the calipers on the inner sides of the echogenic ventricular walls (inner to inner borders) [8] (Figure 2.2) and should be less than 10 mm. The site for the measurement, at the level of the glomus, is chosen because, regardless of the etiology, dilatation of the lateral ventricle generally involves the caudal portion (atrium and posterior horn) first [2].

The 10 mm cutoff applies throughout gestation; any measurement of 10 mm or more indicates the presence of VM (Figures 2.3 and 2.4a). As mentioned above, the body of the choroid plexus typically occupies most of the ventricle; a separation of the choroid plexus from the medial ventricular wall by 3 mm or greater may represent another sign indicating the presence of VM.

Morphologic evaluation of the cerebral ventricles allows the sonologist to detect midline defects such as holoprosencephaly (single or partially separated ventricles) (Figures 2.3 and 2.4b) and to suspect agenesis of the corpus callosum (Figures 2.3 and 2.4c).

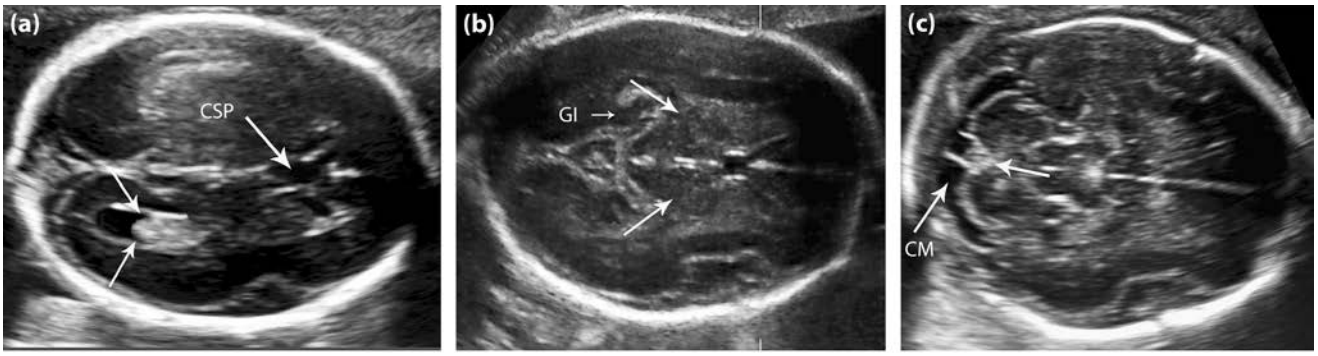


Figure 2.1 Axial views of the fetal head. (a) Transventricular plane, the arrows indicate the glomus of the choroid plexus; CSP: cavum septum pellucidi; (b) transthalamic plane, the arrows indicate the thalami; GI: hippocampal gyrus; (c) transcerebellar plane; CM: cisterna magna; the arrow indicates the vermis.

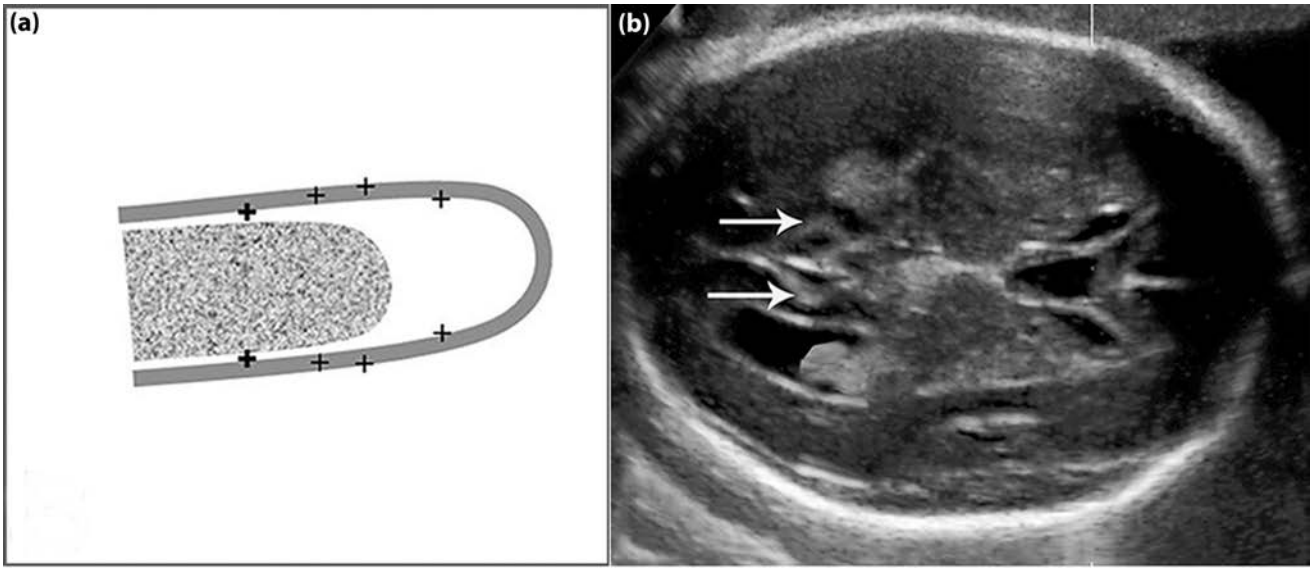


Figure 2.2 (a) Measurement of the atrium of the lateral ventricles. The calipers should be positioned at the level of the glomus of the choroid plexus, inside the echoes generated by the ventricular walls; the arrows indicate parieto-occipital fissures; (b) diagram to illustrate correct caliper placement for ventricular measurement. Calipers are correctly placed touching the inner edge of the ventricle wall at its widest part and aligned perpendicular to the long axis of the ventricle (in black). Incorrect placements include middle–middle, outer–outer, and placement that is too posterior in the narrower part of the ventricle or not perpendicular to the ventricle axis.

Alobar holoprosencephaly is, in fact, characterized by a single common ventricle, whereas in semilobar holoprosencephaly the ventricles are separated only posteriorly, where a rudimentary horn is present. The less frequent lobar variant is characterized by completely separated lateral ventricles except in the foremost portion, where there is fusion of the anterior horns. In corpus callosum agenesis, colpocephaly may be present; in addition, there is an increased distance between the "parallel" bodies of the lateral ventricle, and the third ventricle is enlarged and upwardly displaced in 50%–60% of cases. Some destructive brain lesions are detected on this axial scan, too: hydranencephaly, which is characterized by a large endocranial cyst, and porencephaly, which is characterized by a parenchymal cyst that commonly communicates with the ventricular system.

Brain anomalies characterized by the absence of the CSP are evident on transventricular and transthalamic views. Agenesis of CSP is a brain abnormality that can be isolated or be part of complex brain anomalies [9].

Axial transthalamic view and related malformations. The axial transthalamic view is the classic plane in which the biparietal diameter (BPD) and the fetal head circumference (HC) are measured. On this view, the CSP, the thalami, and the symmetry

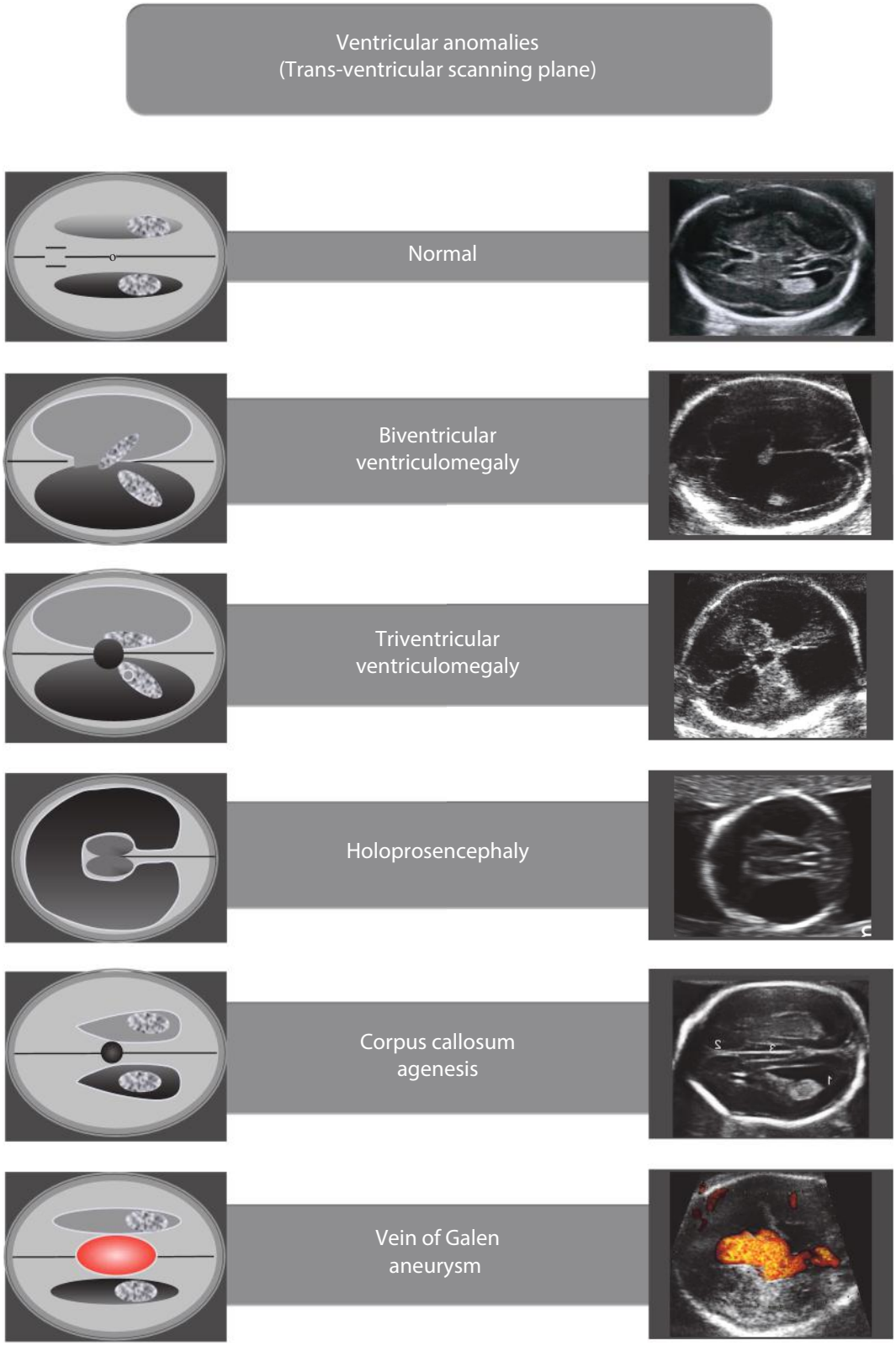


Figure 2.3 Ventricular anomalies evident on the axial transventricular scan.

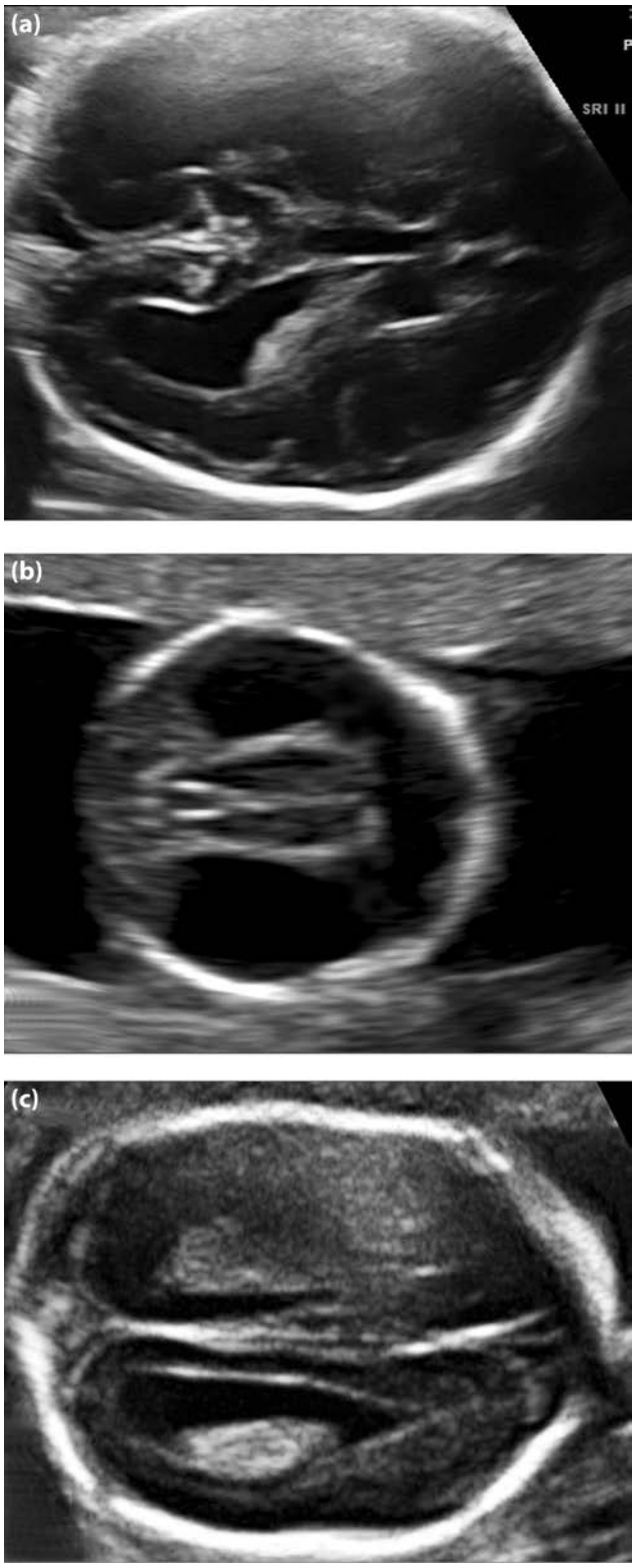


Figure 2.4 Transventricular scan of the fetal brain, showing: (a) mild dilatation of the distal lateral ventricle; (b) a single ventricular cavity; (c) mild dilatation of the posterior part of the lateral ventricle (colpocephaly) while the anterior part is normal.

of the cerebral hemispheres can also be assessed (Figure 2.1b). Hence, the various midline malformations associated with absence of the CSP can also be detected on this view. Although this plane does not add significant anatomic information to that obtained from the transventricular and transcerebellar planes, some neuronal proliferation and migration disorders can be more easily detected on the transthalamic view. These include microcephaly, which is characterized by a marked reduction of the fetal HC, and hemimegalencephaly (Figure 2.5), in which the two cerebral hemispheres are of different size, although a certain degree of asymmetry can also be present in some intracranial neoplasms. In the same plane, some skull deformities, due to craniosynostoses or to other anomalies of the CNS, can also be more easily recognized (Figures 2.5 and 2.6).

Axial transcerebellar view and related malformations (Figure 2.7). This plane is obtained at a slightly lower level than that of the transventricular plane and with a slight posterior tilting. This view is used to assess the posterior cranial fossa and the related structures, namely the cerebellum (including the vermis) and the cisterna magna (Figure 2.1c); with a slight caudal tilting, the fourth ventricle and the inferior vermis can be seen, too (Figure 2.8). The nomograms for the transverse cerebellar diameter are given in the Appendix Table A.10. As for the cisterna magna, the distance between the posterior margin of the cerebellar vermis and the internal occipital bone surface should be measured. The normal range is 3–10 mm. It should also be taken into consideration that in the early second trimester the cerebellar vermis has not covered the fourth ventricle; this may give the false impression of a defect of the vermis. In fact, a premature scan can mislead the sonologist and cause misinterpretation of a normal pattern: the still incomplete cerebellar vermis closure of the fourth ventricle can be misinterpreted as a vermian defect [10]. Therefore, the screening examination for the detection of posterior fossa abnormalities should not be performed before 19–21 weeks' gestation.

On the axial transcerebellar plane, the cisterna magna and the cerebellum (including the vermis) are displayed. It is, therefore, possible on this view to demonstrate the anomalies of these structures, such as abnormal width of the posterior cranial fossa (Chiari II malformation, Dandy–Walker malformation [DWM]) and/or the presence of a "cyst" in the posterior fossa (Figure 2.9). The study of the vermis should be performed with particular attention paid to its inferior portion: If the cerebellum is insonated with an excessive downward angle, the plane will cut through the

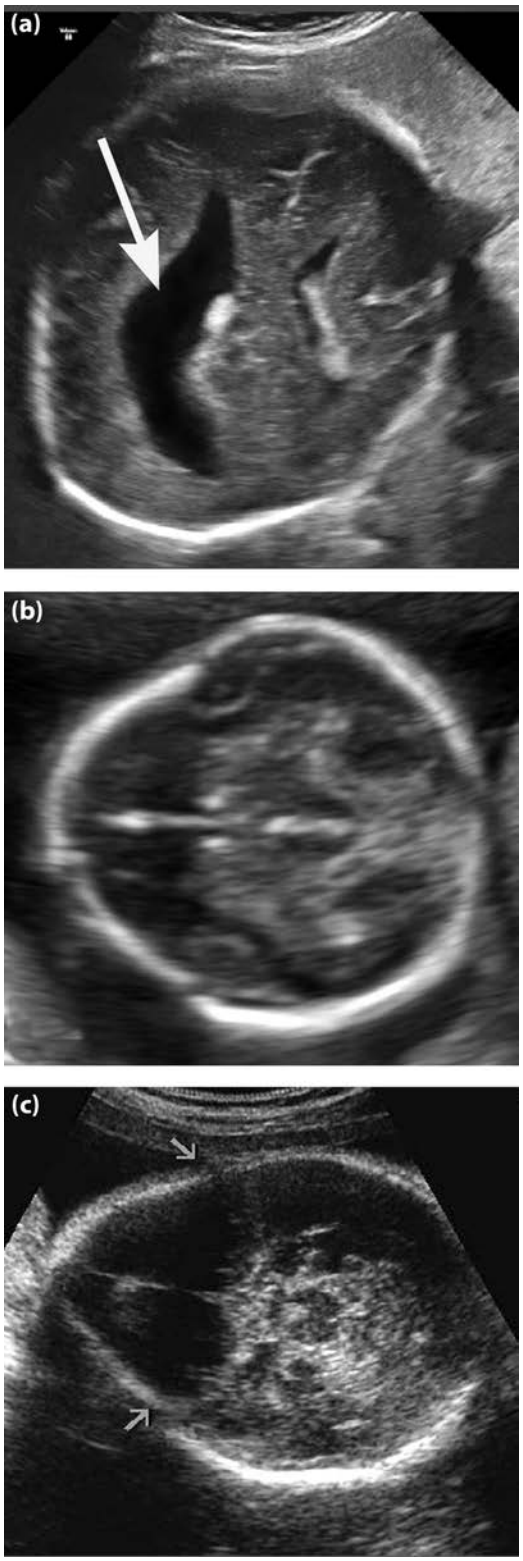


Figure 2.5 (a) Hemimegalencephaly. Axial scan of the fetal brain showing a shift in the midline echo, with overgrowth of one hemisphere and ipsilateral ventriculomegaly (arrow). (b) Strawberry-shaped cranium in a fetus with a trisomy 18. (c) Trigonocephaly, the arrows indicate the patent coronal sutures.

inferior part of the fourth ventricle rather than the vermis itself, erroneously suggesting an hypoplasia/partial agenesis of the cerebellar vermis (Figure 2.10). A likely explanation of this artifact may be the following: the fluid-filled vallecula cerebelli tends to expand slightly in the anterior aspect and has a very thin membranous roof that is impossible to visualize with the resolution currently available with US equipment. The juxtaposition of the vallecula with the adjacent cerebellar hemispheres creates the false impression of a continuum between the cisterna magna and the fourth ventricle, mimicking an hypoplasia/partial agenesis of the vermis.

In doubtful cases, and in those in which a posterior fossa cyst is detected, a midsagittal or median view will resolve the issue (see below) (Figure 2.11). The most important structure that needs to be carefully evaluated is the cerebellar vermis and its anatomy, because this is involved in a significant number of posterior fossa anomalies. Unfortunately, it is difficult to make a correct evaluation of vermian integrity when a cyst is present, particularly if its mass effect is significant.

Three-dimensional US navigation of the fetal brain. Axial views are extremely useful in the context of screening, but have significant diagnostic limitations. While examining the fetal brain, one of the most important views is the midsagittal or median plane: this view provides unique information on important midline intracranial structures such as the corpus callosum and the cerebellar vermis (Figure 2.11). Several authors have advocated the use of this scanning plane in the evaluation of fetal brain anatomy [6,7,11]. Unfortunately, scanning in this plane is difficult with two-dimensional US. Several approaches have been described, but they all require considerable manual skill, time, and, possibly, a transvaginal approach. Three-dimensional ultrasonography is now widely available, and one of its advantages is the possibility of obtaining a volume and "slicing" it along different directions from those used to acquire it. With this technique, obtaining midsagittal and other informative sagittal and coronal views has become much easier [11].

In fact, 3D US imaging allows visualization of a virtual midsagittal plane from a volume that has been acquired from an axial approach (Figure 2.12). It should be noted that the structures displayed best will be those perpendicular to the insonating beam when the volume is acquired. Finally, a new image modality allowing 2D slices to be displayed from any given volume similar to CT or magnetic resonance imaging (MRI) scans is represented by tomographic US imaging (TUI) (Figure 1.36).

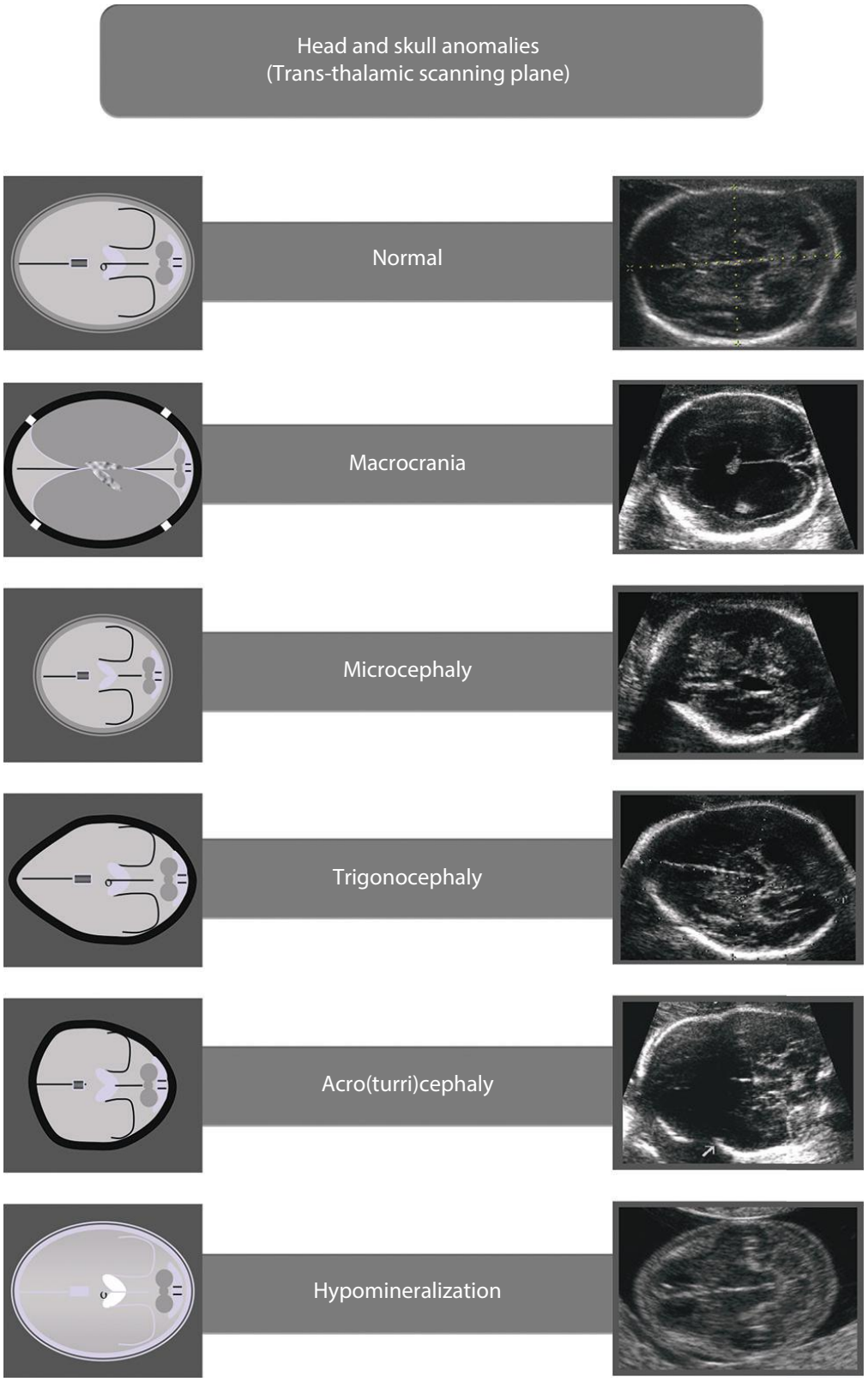


Figure 2.6 Cranial anomalies evident on the transthalamic view.

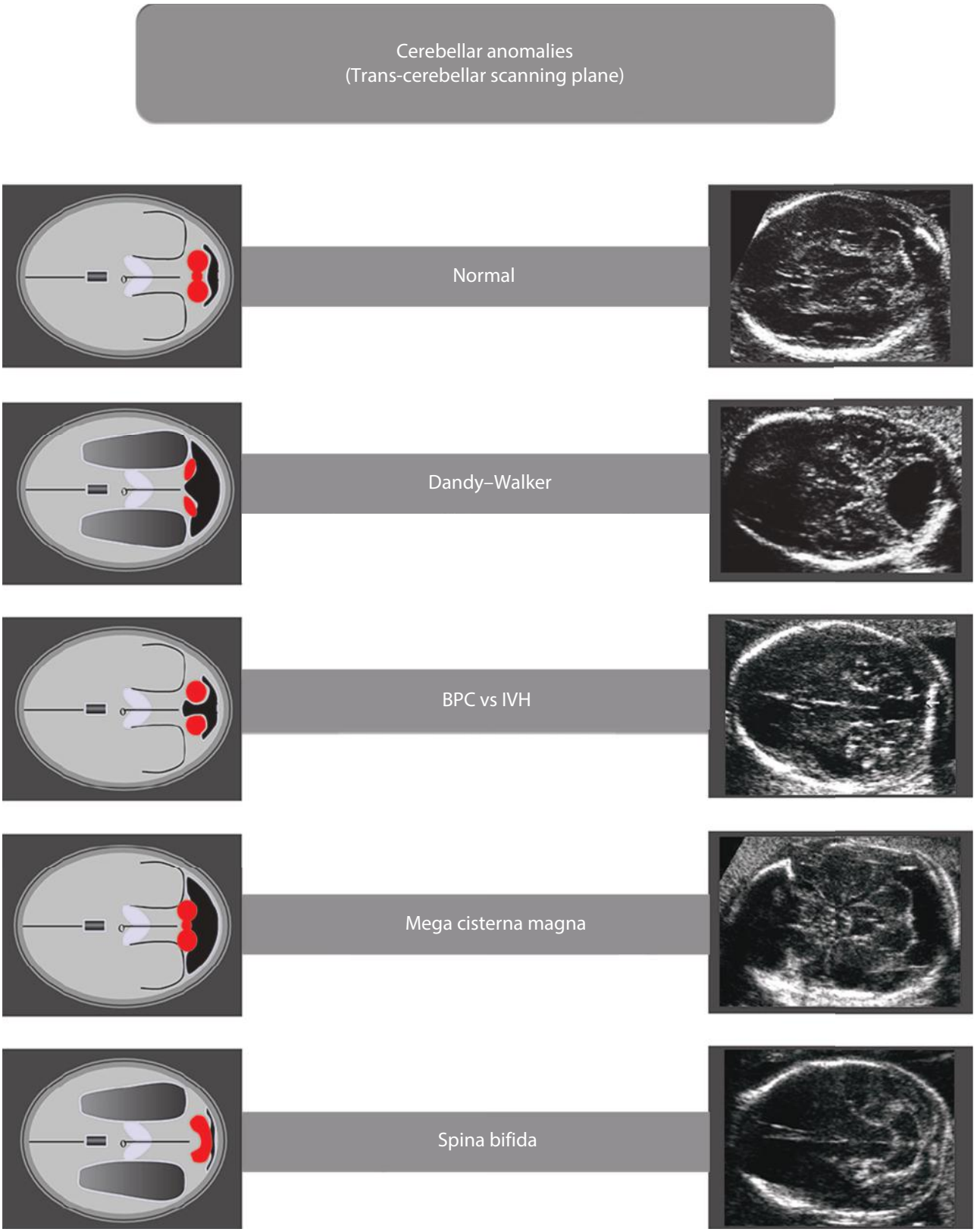


Figure 2.7 Posterior fossa anomalies evident on the axial transcerebellar view. BPC: Blake's pouch cyst; IVH: inferior vermian hypoplasia.

Fetal neurosonography. Fetal neurosonography is a diagnostic examination, requiring a grade of expertise, performed in patients with an increased risk of CNS anomalies, including cases in which the screening examination identifies suspicious findings. The basis of the neurosonographic examination of the fetal brain is the multiplanar approach including axial, coronal (Figure 2.13), and sagittal views (Figure 2.14) of the brain. Coronal and sagittal plane are more difficult to obtain and can require a transvaginal scan if the fetus is in cephalic presentation. However, it is advisable to employ the transvaginal approach whenever feasible, for it allows a greater definition of anatomical details of the fetal brain.

Evaluation of the spine is a part of the fetal neurosonography, too (see section "Neural Tube Defects").

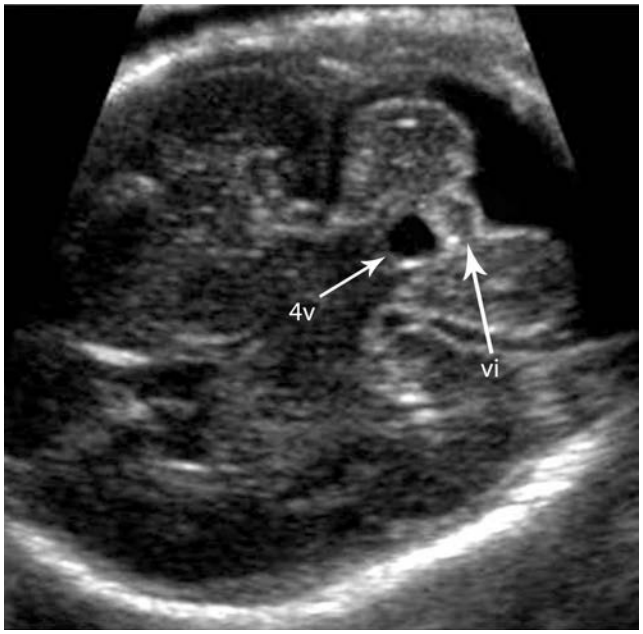


Figure 2.8 Posterior fossa: with a slightly steeper angulation of the scanning plane with regard to the standard transcerebellar plane, the fourth ventricle (4v) and inferior vermis(vi) can be clearly seen.

Midsagittal or median plane of the fetal head and related malformations. The midsagittal or median plane allows visualization of the corpus callosum with the CSP, the third ventricle, the tela choroidea, part of the mesencephalon, the cerebellar vermis, the fourth ventricle, and the cisterna magna (Figure 2.14). It, therefore, allows detection and characterization of agenesis of the corpus callosum, and vermian abnormalities.

Knowledge of vermian morphology is essential when assessing for vermian anomalies. At 21–22 weeks, primary fissure is present. The primary fissure delineates the anterior from posterior lobes of the vermis; the volume of the posterior lobe is greater than the volume of the anterior lobe (Figure 2.11b).

Right and left parasagittal views. Proximal parasagittal views allow study of the lateral ventricles with the choroid plexuses (Figure 2.14b). Outermost parasagittal views allow visualization of the insula and the parietal and temporal operculum.

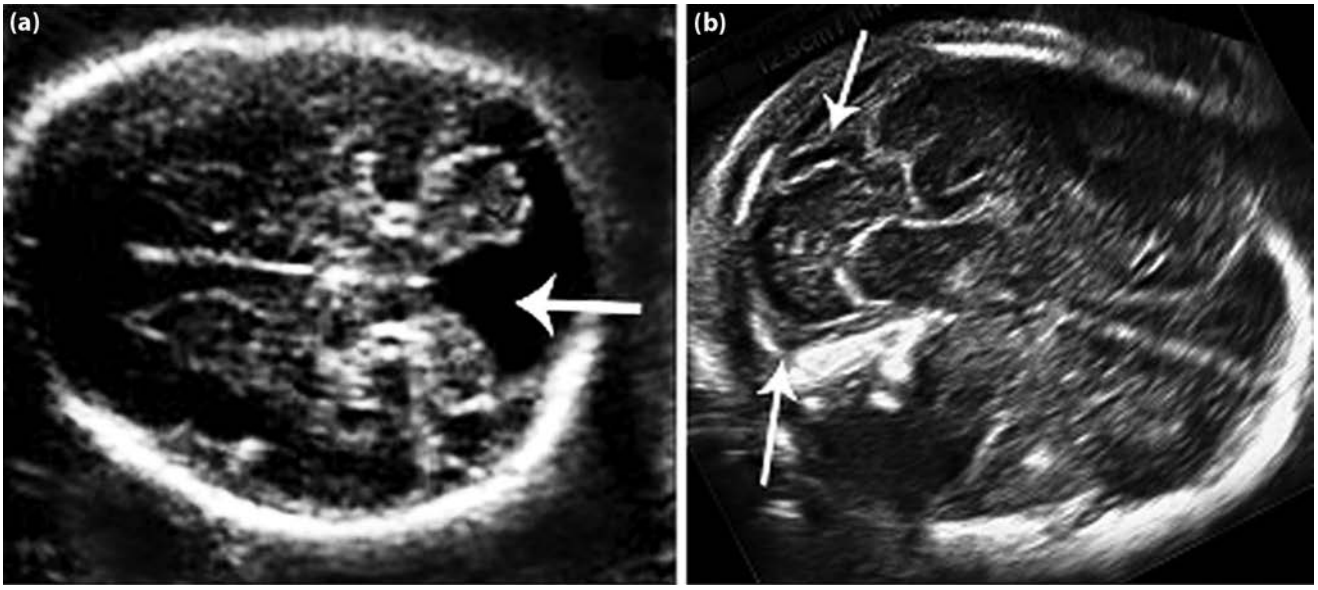


Figure 2.9 (a) DWM: the arrow indicates the cerebrospinal fluid collection in an enlarged posterior fossa; (b) Chiari II malformation; the arrows indicate the nulled posterior fossa.

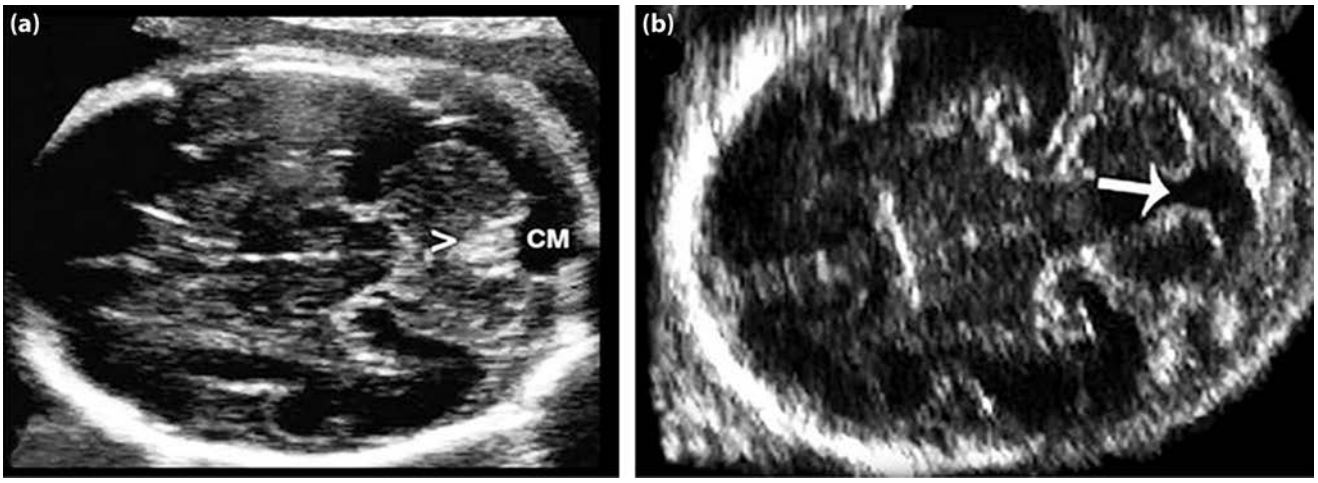


Figure 2.10 (a) The image shows a correct transcerebellar axial plane; the arrowhead indicates the cerebellar vermis. (b) The transcerebellar scan is too oblique downward. There seems to be a direct connection between the cisterna magna (CM) and the fourth ventricle (arrow), producing a false-positive image of partial absence of the cerebellar vermis.

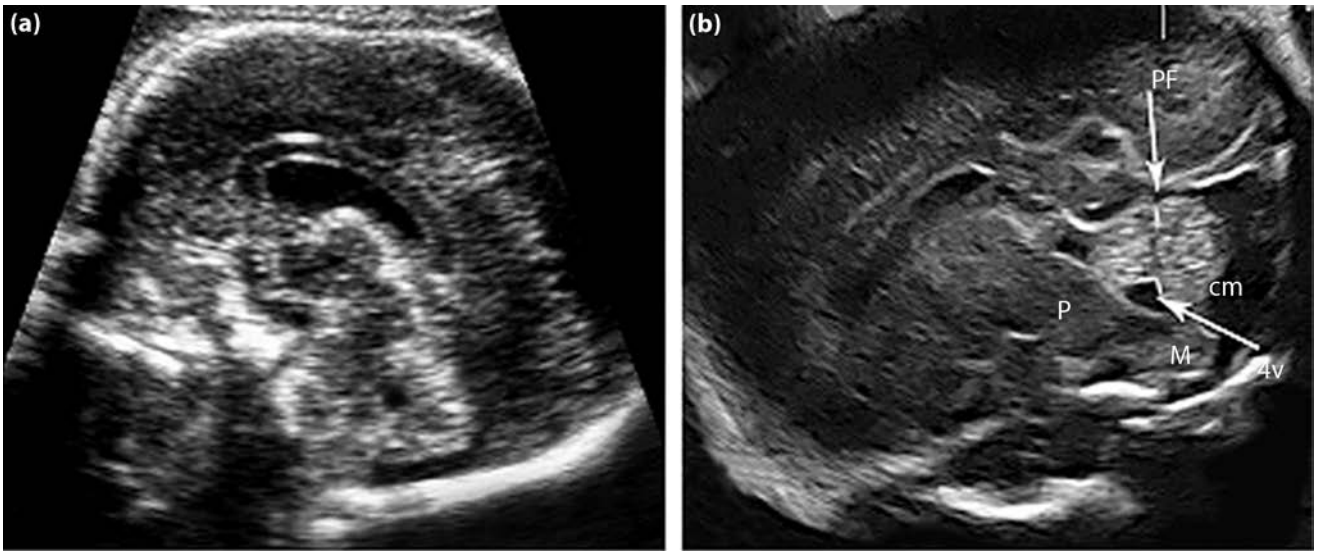


Figure 2.11 (a) Midsagittal view of the fetal brain obtained through the sagittal suture showing the corpus callosum and cerebellar vermis; (b) median view of the fetal brain obtained through the posterior fontanelle showing the fourth ventricle (inferior arrow), the fastigium, the primary fissure (PF) of the vermis (arrow), the cisterna magna (cm), the brainstem (including the pons, P, and the medulla, M). The PF, always visible at 21 weeks' gestation, delineates the posterior part of the vermis from the anterior part. The volume of the posterior vermis is greater than the volume of the anterior vermis.

Coronal views. The *transfrontal view* allows visualization of the interhemispheric fissur and the ocular orbits (Figure 2.13a). This view is rostral to the genu of the corpus callosum (CC).

The *midcoronal 1 or transcaudate view* allows visualization of the anterior horns, the genu of CC that interrupts the continuity of the interhemispheric fissure, the CSP, and the caudate nuclei (Figure 2.13c). On this view, the width of the corpus callosum can be measured (Table A.14).

In the *midcoronal 2 or transthalamic view*, both thalami are found in close apposition (Figure 2.13b). On the midsagittal view, the corpus callosum length (Table A.13) and the vermian height (Table A.11–12) can be measured.

The *transcerebellar* or posterior coronal view allows visualization of the occipital horns and the cerebellum, including the vermis, and the cistern magna (Figure 2.13d).

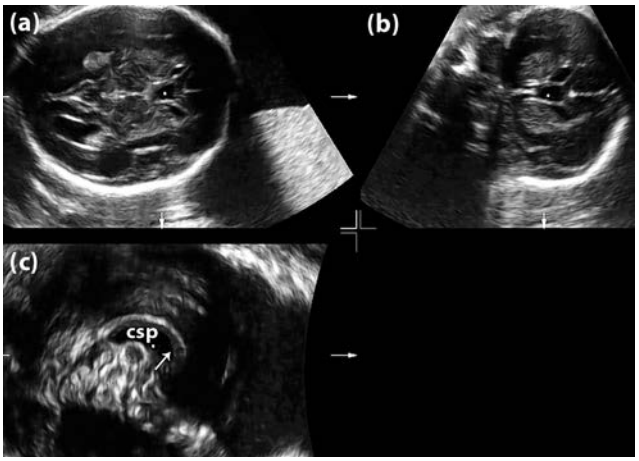


Figure 2.12 Multiplanar analysis of the ultrasound (US) volume obtained from an axial transventricular view of a 23-week fetal brain. The (a) plane corresponds to the axial plane, (b) to the coronal plane, and (c) to the sagittal plane. In (c), the reconstructed median plane allows recognition of the CC (arrow) as an hypoechoic stripe within a thin echogenic contour that separates it from the underlying cavum septi pellucidi (CSP). The position of the reference dot is within the CSP.

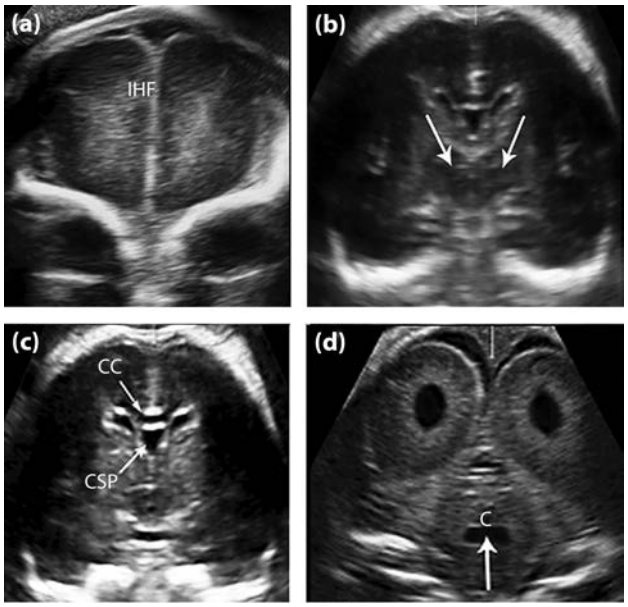


Figure 2.13 Coronal views of the fetal head showing: (a) transfrontal plane; (b) transthalamic plane; (c) transcaudate plane; (d) transcerebellar plane. CSP: cavum septi pellucidi; CC: corpus callosum; IHF: interhemispheric fissure; C: cerebellum.

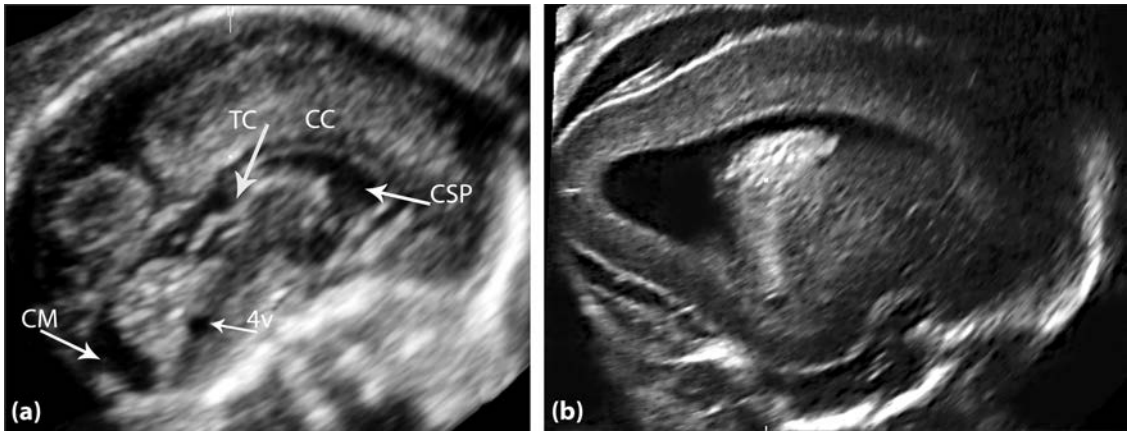


Figure 2.14 (a) Midsagittal view of the fetal head showing the corpus callosum (CC) with the cavum septi pellucidi (CSP), the third ventricle, the tela choroidea (TC), part of the mesencephalon, the cerebellar vermis, the fourth ventricle (4v) and the cisterna magna (CM). (b) Parasagittal view of the fetal head showing the lateral ventricle with choroid plexus.

cE r EBr AL VENTr Ic ULo MEGALy

Incidence. In the fetus, the incidence of mild ventriculomegaly (VM) is 1%. The incidence of severe VM is about 1:1000 newborns.

Ultrasound diagnosis. *Axial transventricular view.* Uni- or biventricular dilatation ≥ 10 mm. It can be isolated or associated with other congenital (DWM, CC agenesis) or acquired (hemorrhage, infections) CNS anomalies.

Risk of chromosomal anomalies. Moderate to high: 1.5%–12% for isolated VM; 9%–36% if VM is associated with other malformations; low if VM is associated with acquired lesions.

Risk of nonchromosomal syndromes. High.

Outcome. Variable, and depending on the etiology and associated lesions; poor, if associated with syndromes or other CNS anomalies.

Definition VM may be the consequence of a variety of conditions that can result in a dilatation of the cerebral ventricular system.

Fetal VM is the most common abnormal imaging finding leading to the diagnosis of cerebral malformations and is characterized by an atrial width of the lateral cerebral ventricles ≥ 10 mm. Mild ventriculomegaly is seen in 1% of fetuses. The incidence of severe VM is about 1:1000 newborns.

Etiology and pathogenesis. VM represents a common endpoint of various pathological processes with different prognoses. It may be secondary to brain destruction (congenital infection or a vascular mechanism), malformations, hydrocephalus, or a combination of two processes (i.e., hydrocephalus and malformation). It may also be related to a brain neoplasm or to a genetic abnormality not associated with a brain malformation. The well-known classic criteria for the diagnosis of hydrocephalus in the postnatal period cannot be completely extended to the fetus. Indeed, in utero, hydrocephalus may be present even with a normal HC, and the underlying cause of an altered flow of the cerebrospinal fluid (CSF) cannot be identified in all cases. However, progressive, severe fetal ventricular enlargement together with decreased or absent pericerebral space and parenchymal thinning can be presumed to be indicative of hydrocephalus. The mean ventricular size measurement is not reliable as a means of distinguishing between the different causes of VM. However, even if there is no statistically significant difference, the mean value is lower for fetuses with underlying genetic causes (excluding cerebral malformations) than for those in which hydrocephalus is due to destructive causes; indeed, a significant number of fetuses with mild VM have a chromosomal anomaly.

The presence of uni- or bilateral VM seems to be of some discriminatory value. VM tends to be unilateral in cases of destruction and bilateral in cases of malformation, and this difference is statistically significant [13].

In apparently isolated VM, we have to distinguish between mild and moderate-to-severe VM.

The term mild (or borderline) VM is commonly used to indicate cases characterized by an atrial width of 10–15 mm. Some authors have reported a different rate of abnormal neurologic outcome in fetuses with atria >12 mm compared with those with atria measuring 10–12 mm [14]. The higher incidence of this anomaly in male fetuses is related to the fact that their mean atrial size is slightly greater than that of females. Mild VM may resolve even before birth; however, in a significant number of cases, this finding can be the sign of brain lesion from heterogeneous causes, including primary cerebral maldevelopment (i.e., lissencephaly) or the earliest manifestation of a progressive, severe ventricular enlargement. Severe VM, especially if associated with decreased or absent pericerebral space and parenchymal thinning, is usually referred to as hydrocephalus and is defined on the basis of an atrial width of more than 15 mm. Aqueductal stenosis, regardless of its cause, severely hampers the progression of ventricular dilatation. Although it is generally a multifactorial disease, there can be an X-linked transmission characterized by mental retardation, spastic paraplegia, and adducted thumbs. Aqueductal stenosis can also be acquired, following intrauterine infection or intraventricular hemorrhage. Other causes of severe second-trimester VM revealing obstruction are related to pathologies of diencephalic, mesencephalic, and rhombencephalic differentiation.

Ultrasound diagnosis. We report the most common sonographic patterns of ventriculomegaly.

Ventriculomegaly associated with CNS malformations. As stated above, VM is associated with typical malformation patterns of the CNS. In the Chiari II malformation (Figure 2.15a), VM is associated with a small posterior fossa, a small dysmorphic cerebellum, an effaced cisterna magna, and a spinal defect with myelomeningocele; for a conclusive diagnosis, the latter defect must be detected. The association of VM with the presence of an enlarged posterior fossa, and complete or partial agenesis or hypoplasia of the cerebellar vermis is the typical sonographic sign of the DWM (Figure 2.15b). The "teardrop" appearance of the lateral ventricles (Figure 2.15c) with parallel bodies, which are shifted laterally, and upward displacement of the third ventricle suggest agenesis of the CC, the presence of which must be confirmed on coronal and sagittal views.

Ventriculomegaly associated with cerebral destruction. VM associated with destructive lesions can be unilateral or bilateral. The most common causes are hypoxia, infection, or vascular lesions. When VM is associated with hyperechogenic foci located in the brain and periventricular cysts, a fetal infection should be suspected. If multiple nodular subependymal calcifications, which sometimes group together to form periventricular hyperechogenic bands (Figure 2.16a), are present, cytomegalovirus (CMV) infection should be suspected. In addition, free-floating particles, consisting of exudate and shed ependymal cells, may be detected within the cerebral ventricles (Figure 2.16b), which are often dilated, because this particulate matter frequently obstructs ventricular foramina, leading to secondary

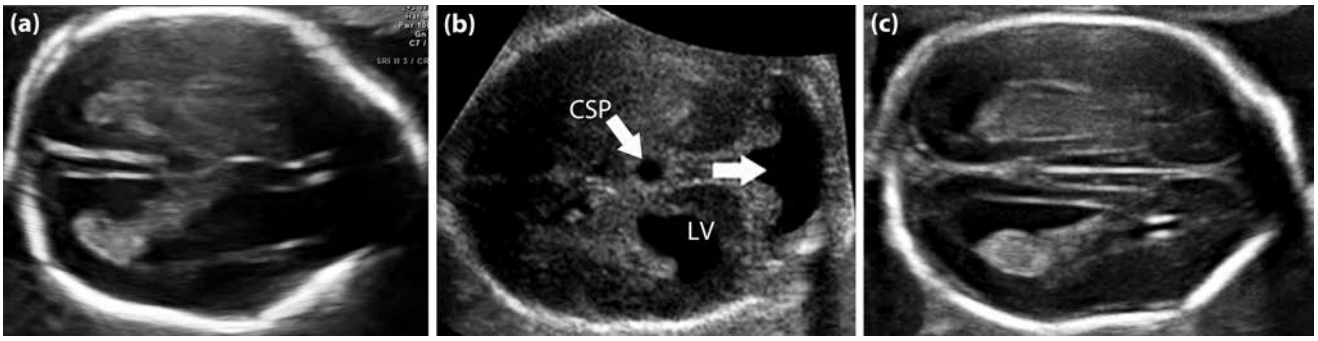


Figure 2.15 (a) Chiari II malformation: dilatation of the lateral cerebral ventricles and "lemon sign" are clearly seen. (b) Dandy–Walker malformation with ventriculomegaly: cystic dilatation of the fourth ventricle, cleft between the cerebellar hemispheres (arrow), and enlarged posterior fossa can be seen; cavum septi pellucidi (CSP) third ventricle (arrowhead); LV: lateral ventricle. (c) Agenesis of corpus callosum; axial transventricular scan showing the teardrop configuration of the lateral ventricle due to mild enlargement of its posterior part (colpocephaly). Note also the absence of the CSP.

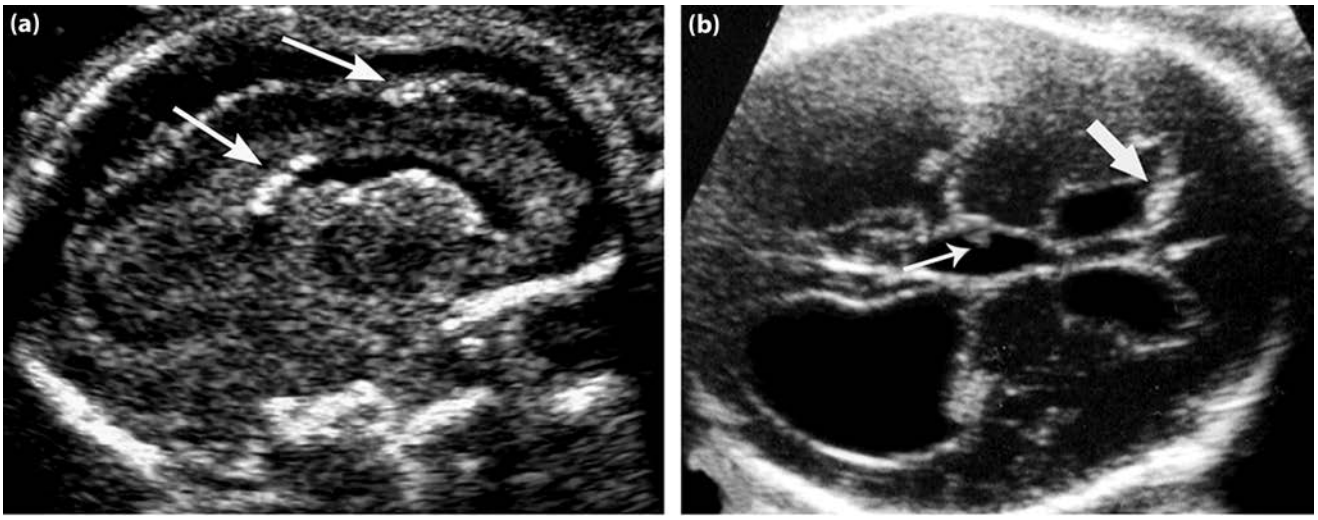


Figure 2.16 (a) Cytomegalovirus infection: a periventricular hyperechogenic band is clearly seen (arrow). (b) Axial scan of the fetal brain, showing hyperechoic clots within the frontal horn of the proximal lateral ventricle (arrow) and in the third ventricle (arrow).

obstructive hydrocephalus. In such cases, a differential diagnosis with intraventricular hemorrhage should be made: maternal serology for CMV and other infectious agents and the findings at earlier US examinations often resolve the differential diagnostic issue. In the case of hypoxia-induced hemorrhage, ventricular dilatation occurs in severe forms only, and is generally associated with intraventricular fibrin strands and/or blood clots (grade 3). If this is the case, then a hyperechoic hemorrhagic lesion (grade 4) is often found in the parenchyma; this will successively become hypoechoic, due to the liquefaction of the blood clot, and eventually disappears, leaving a poroencephalic cyst filled with CSF and in communication with the ventricular system.

Isolated ventriculomegaly. The diagnosis of isolated VM is made when there is no other associated sonographically detectable anomaly or markers of aneuploidy at the time of the initial presentation [12].

An atrial width of 10–15 mm is defined as *mild* ventriculomegaly [12] (Figure 2.4a). The terms "milder ventriculomegaly" and "moderate ventriculomegaly" have been used by some authors to indicate measurements of 10–12 mm and 13–15 mm, respectively [14].

Isolated mild VM may also be unilateral. It should be noted that ventricular asymmetry, defined as a difference in atrial size greater than 2 mm, without dilatation may be observed in normal fetuses.

Severe ventriculomegaly. Especially if associated with decreased or absence of pericerebral space and parenchymal thinning, severe VM is usually referred to as hydrocephalus, and is defined by an atrial width of more than 15 mm (Figure 2.17).

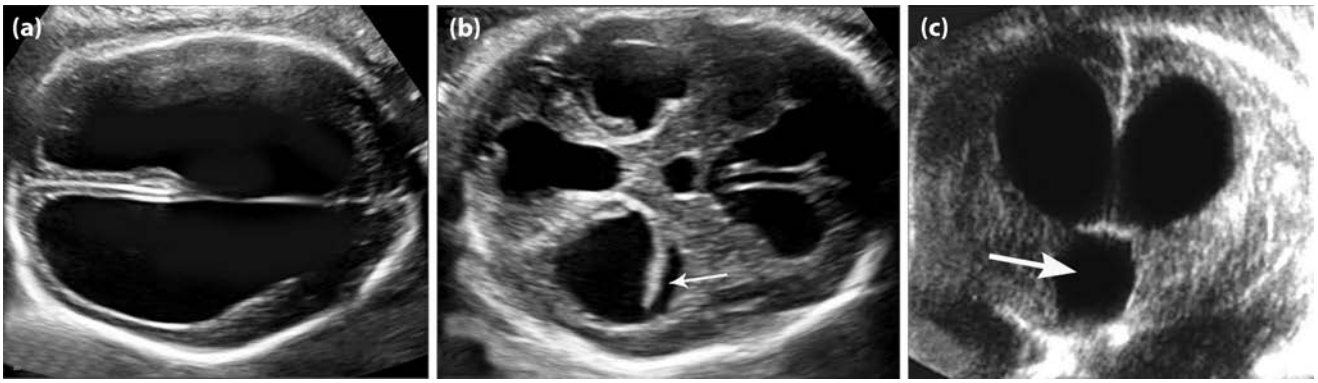


Figure 2.17 Severe ventriculomegaly. (a) Overall enlargement of both lateral ventricles. (b) Severe tetraventricular hydrocephaly with dangling choroid plexus (arrow). (c) Triventricular hydrocephalus: coronal scan of the fetal brain showing dilatation of the third ventricle (arrow) and lateral ventricles with a typical "Mickey Mouse" configuration.

Hydrocephalus may result either from overproduction of CSF or from obstruction to CSF flow or impaired resorption through the pacchionian granulations. Depending on whether CSF flow obstruction is intraventricular or extraventricular, obstructive hydrocephalus is categorized into noncommunicating and communicating. In the fetus, VM is more frequently the result of a noncommunicating hydrocephalus (as in aqueductal stenosis). The typical sonographic pattern of aqueductal stenosis is triventricular hydrocephalus with enlargement of the third and the lateral ventricles (Figure 2.17c). Hydrocephalus can also be related to abnormal differentiation of the diencephalon, mesencephalon, and rhombencephalon, which leads to obstruction of CSF flow. For these reasons, when facing severe isolated VM, whose sonographic features are suggestive of an obstructive mechanism, close examination of the third ventricle, thalami, sylvian aqueduct, and cerebellum may reveal pathological differentiation of the diencephalon, mesencephalon, or rhombencephalon, often in combination. Noncommunicating hydrocephalus also includes the bilateral and unilateral obstruction of foramina of Monro.

The term "communicating hydrocephalus" refers to failure of CSF absorption with dilatation of the ventricles. Obstruction to CSF flow is extraventricular, that is, within the subarachnoid space, either impeding the passage from around the cerebellum through the ambient cistern or at the arachnoid villi, impeding the resorption of CSF into the cerebral venous system at the superior sagittal sinus.

Hydrocephalus due to excessive production of CSF (i.e., in papilloma of the choroid plexus) is less frequent.

Differential diagnosis. Mild VM must be differentiated from colpocephaly, caused by agenesis of the CC. The sonographic findings useful for a correct differential diagnosis are described above.

Association with other malformations. The rate of association with other cerebral anomalies (holoprosencephaly, CC agenesis, and DWM) and extracerebral anomalies (myelomeningocele) ranges from 45% to 80%.

Risk of chromosomal anomalies. This is moderate to high. In particular, the rate of association with aneuploidy is 1.5%–12% in the case of isolated VM but is higher (9%–36%) if VM is associated with other malformations. Only in the case of VM associated with destructive lesions is the risk of associated chromosomal anomalies low.

Risk of nonchromosomal syndromes. This is high. The most common syndromes [16] are:

- *Miller–Dieker syndrome*: look for ► *ventriculomegaly* + lissencephaly + microcephaly + cardiac anomalies + facial anomalies + polydactyly;
- *Goldenhar syndrome*: look for ► *ventriculomegaly* + facial asymmetry + preauricular tag + vertebral anomalies + cleft lip and palate;
- *Meckel–Gruber syndrome*: look for ► *ventriculomegaly* + encephalocele + polydactyly + polycystic kidneys + other CNS anomalies;
- *Neu–Laxova syndrome*: look for ► *ventriculomegaly* + lymphedema of the limbs + lissencephaly + microcephaly + proptosis + intrauterine growth restriction + arthrogryposis + other CNS anomalies;
- *Walker–Warburg syndrome*: look for ► *ventriculomegaly* + eye anomalies (microphthalmia, cataract) + CNS anomalies (lissencephaly, midline anomalies + cerebellar anomalies + microcephaly + cephalocele);

- *Crouzon syndrome*: look for ► *ventriculomegaly* + craniofacial dysostosis + hypoplastic jaw bone;
- *Gorlin syndrome*: look for ► *ventriculomegaly* + facial anomalies, macrocephaly, and multiple neoplasms;
- *Kartagener syndrome*: look for ► *ventriculomegaly* + situs inversus.

Obstetric management. When ventricular dilatation is detected in utero, it is important to assess the cause and extent of VM (biventricular, triventricular, etc.), its degree (mild, moderate, or severe), and whether it is associated with any cerebral or/and extracerebral anomaly. Except for cases associated with acquired lesions (e.g., infections, tumors, hemorrhages) lesions, fetal karyotyping should be offered to the parents.

Fetal MRI has not been the subject of many studies, and it is difficult to establish its role on the basis of the small and heterogeneous series investigated. However, it seems to be helpful in detecting migrational abnormalities, parenchymal damage, infarctions, and hemorrhage eventually associated with VM [15]. Most of the above-mentioned anomalies are evolving, and the presence of late-onset lesions be recognized only from the late second trimester onward.

In the case of isolated mild fetal VM (atrial width measurement of 10–15 mm), the appropriate management remains controversial. However, this finding is frequently associated with CNS and extra-CNS anomalies, and so a careful evaluation of the fetal anatomy should be carried out using an expert US examination. Where available, fetal MRI is also indicated [12,15]. The likelihood ratio for trisomy 21 is about 9, and invasive testing for chromosomal analysis should be offered. Maternal serum CMV and *Toxoplasma* studies should be considered; measurement of anti-HPA antibodies may be justified if there is a suspicion of intracranial hemorrhage (ICH) [12].

Postnatal treatment. Aqueductal stenosis may be treated with a ventriculoperitoneal or ventriculoatrial shunt placed for decompression of hydrocephalus after delivery; unfortunately, shunt obstruction is common and a new operation may be needed. An endoscopic procedure (i.e., third ventricle cisternostomy) represents a valid alternative, which has yielded good results.

Prognosis, survival, and quality of life. It is difficult to establish a prognosis for VM because published studies have often been based on small case series and very heterogeneous patient cohorts. Despite these limitations, some prognostic factors can be outlined. The outcome of prenatally detected VM is worse than that of VM detected in the neonatal period [16]. There is a high rate of spontaneous abortion, in utero fetal demise, stillbirth, and neonatal death (up to 60%), especially if VM is associated with other brain anomalies. The mortality rate is much lower if the lesion is isolated, with a reported survival rate of about 80%, with 60% of these having normal neurologic development. Early detection and progressive increase of the VM are two factors indicating a less favorable prognosis [16]. An important factor influencing prognosis is the cause of the VM—for example, X-linked hydrocephalus is known to have an unfavorable prognosis. Considering apparently isolated only mild VM, the mortality and morbidity rates seem to be much lower [12].

In these cases, the strongest predictors of abnormal developmental outcome remain the cause of the VM, any unrecognized underlying defect, and the progression of the condition. Whether the atrial width is above or below 12 mm at presentation does play a role, but the risk attributable to this finding does not seem to be high [12]. The rate of neurodevelopmental delay in infants with a prenatal diagnosis of isolated mild VM is about 11%, and it is unclear whether this is increased over that in the general population. The most important prognostic factors in isolated mild VM are the association with other abnormalities undetected at the time of the first diagnosis (about 13% of cases) and progression of the ventricular dilatation (about 16% of cases) [12].

ho Lopros ENc Eph ALy

Incidence. One in 10.000–15.000 births have holoprosencephaly (HPE), but much higher in aborted fetuses (1 in 250).

Ultrasound diagnosis. Alobar and semilobar HPE: completely or partially fused thalami, single or partially fused ventricles, and absence of the CSP. Lobar HPE: fused frontal horns and absence of CSP.

Risk of chromosomal anomalies. High: An aneuploidy is associated in up to 47% of cases (especially trisomy 13).

Risk of nonchromosomal syndromes. Relatively high.

Outcome. Very poor in alobar and semilobar forms, better in lobar form.

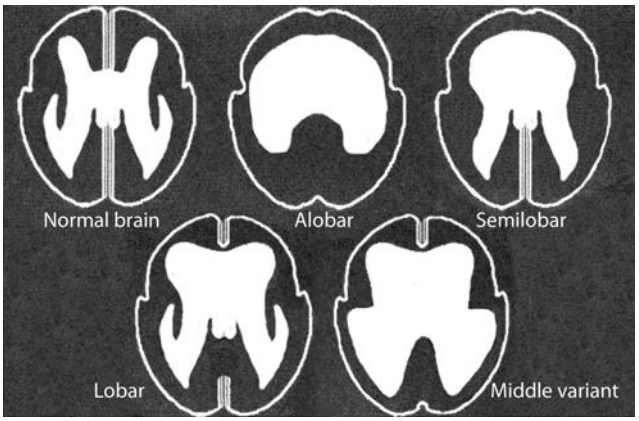


Figure 2.18 Graphical representation of the variants of holoprosencephaly, showing the different forms of the cerebral hemispheres with respect to the normal brain.

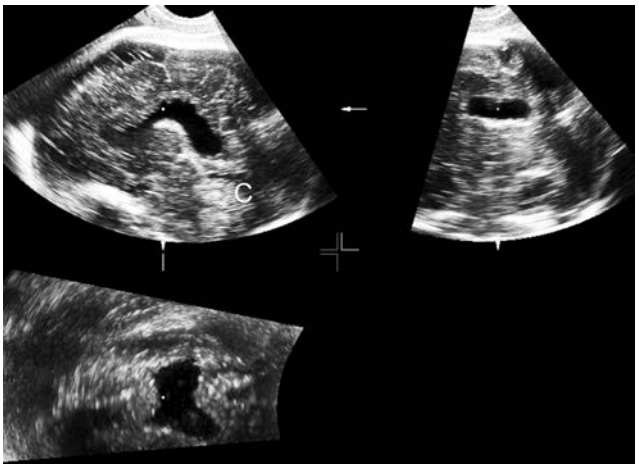


Figure 2.19 Middle interhemispheric variant of holoprosencephaly.

Definition The term "holoprosencephaly" refers to a group of complex abnormalities of the forebrain deriving from a failed cleavage of the prosencephalon that yields an incomplete division of the cerebral hemispheres and of the telencephalon from the diencephalon. The most widely accepted classification of holoprosencephaly recognizes three major varieties: the alobar, semilobar, and lobar types, according to the severity of the malformation [9] (Figure 2.18). However, there are no precise boundaries between the three variants, and intermediate cases may be identified Recently, another variant of HPE has been described: the middle interhemispheric variant (syntelencephaly), characterized by failure of cleavage of the posterior frontal and parietal regions of the brain. Whereas more anterior and occipital areas of the brain are fully cleaved, the interhemispheric fissure may be present both anteriorly and posteriorly [17] (Figure 2.19).

In alobar HPE, the prosencephalon fails to cleave sagittally into cerebral hemispheres, transversely into telencephalon and diencephalon, and horizontally into olfactory tracts and bulbs. It is characterized by a single primitive cerebral ventricle continuous with a large dorsal cyst. No midline structures, including the falx cerebri, the interhemispheric fissure, the SP (septum pellucidum), the CC and the third ventricle, are present and the thalami are fused on the midline.

The semilobar variety of HPE is characterized by the presence of rudimentary lateral ventricles with sketchy posterior horns, partial development of the interhemispheric fissure and of the falx cerebri, which are present only posteriorly. Partial fusion of the thalami and partial agenesis of the CC are present. SP is absent.

In the lobar variety, the hemispheres are almost completely divided. It is characterized by fusion of the frontal horns (particularly in their lower portion), which show ample communication with the third ventricle, partial agenesis of the CC and absence of the SP.

It has to be pointed out that HPE is the only brain malformation described in which the posterior CC forms in the absence of anterior callosal formation. Holoprosencephaly is usually associated with facial abnormalities [9,18,19].

The incidence of HPE is 1 in 10,000–15,000 births; it is higher in early termination of pregnancy [20] (1 in 250), indicating that most HPE fetuses are aborted.

Etiology and pathogenesis. HPE is the result of a ventral induction disorder, and is characterized by a defect in the development of the midline embryonic forebrain. The etiology of HPE is very heterogeneous (Table 2.1) [9]. Most cases are of unknown cause. The identified causes are chromosomal, monogenic, and teratogenic. Chromosomal abnormalities are present in 24% to 47% of all cases [9], most commonly trisomy 13. Monogenic inheritance of nonsyndromic HPE includes most commonly autosomal dominant transmission with variable expressivity and incomplete penetrance; autosomal recessive transmission and X-linked transmission have been also reported [18,19]. To date, 12 genes and their mutations are known to cause HPE in humans; however, the most common HPE-associated genes in which the HPE type (or lack thereof) is known are four: SHH, ZIC2, SIX3, TGIF [9].

Because various pathways are linked to the sonic hedgehog (SHH)-signaling network, most of the mutations are interrelated. SHH protein seems to be a developmental regulator of the ventral neural tube, important for its induction and differentiation [9,18,19]. During the past 20 years, it has become

Table 2.1 Causes and conditions associated with HPE

Cause/condition	Diagnostic aids
Chromosomal abnormalities	Fetal karyotyping
Trisomy 13	
Trisomy 18	
Triploidy	
Others:	
Duplications, Microdeletions	
Partial monosomy 14q	
Cryptic unbalanced aberrations	FISH, CGH array, parental karyotyping
Syndromic HPE	Associated US features—family history
Autosomal dominant	
Autosomal recessive	
X-linked	
Nonsyndromic HPE	Family history-examination of the parents to identify microforms of HPE and/or parental mutation analysis
Environmental factors	Prenatal history
Retinoic acid	
Ethyl alcohol	
Salicylates	
Estrogen/Progestin	
Anticonvulsants	
CMV	
Rubella	
Toxoplasma	
Metabolic disorders	Family history
Maternal diabetes	

Source: Modified from Volpe P et al., *Prenat Diagn* 29, 340–54, 2009.

clearer that a primary defect of induction and patterning of the rostral neural tube may be important and that the prechordal plate may play a major role in the genesis of HPE. Aberrancies in ventral midline SHH-expressing cells, or in the SHH pathway, both of which are critical to the normal development of the forebrain, appear to play a pivotal role in this disorder.

Some environmental and metabolic factors have also been implicated in HPE. In fact, diabetic embryopathy has been reported with HPE. Nevertheless, in about 60%–70% of cases, the molecular basis of the disease remains unknown, suggesting the existence of several other candidate genes and/or environmental factors [9,18].

Ultrasound diagnosis. Prenatal diagnosis of HPE by US has been reported and criteria for diagnosis are well established [9]. Early diagnosis of alobar HPE during the first trimester has also been reported based on the visualization of a single ventricle [21].

The visualization of cerebral ventricular abnormalities, on axial plane of the fetal brain, and of facial anomalies is usually the first step in the diagnostic process.

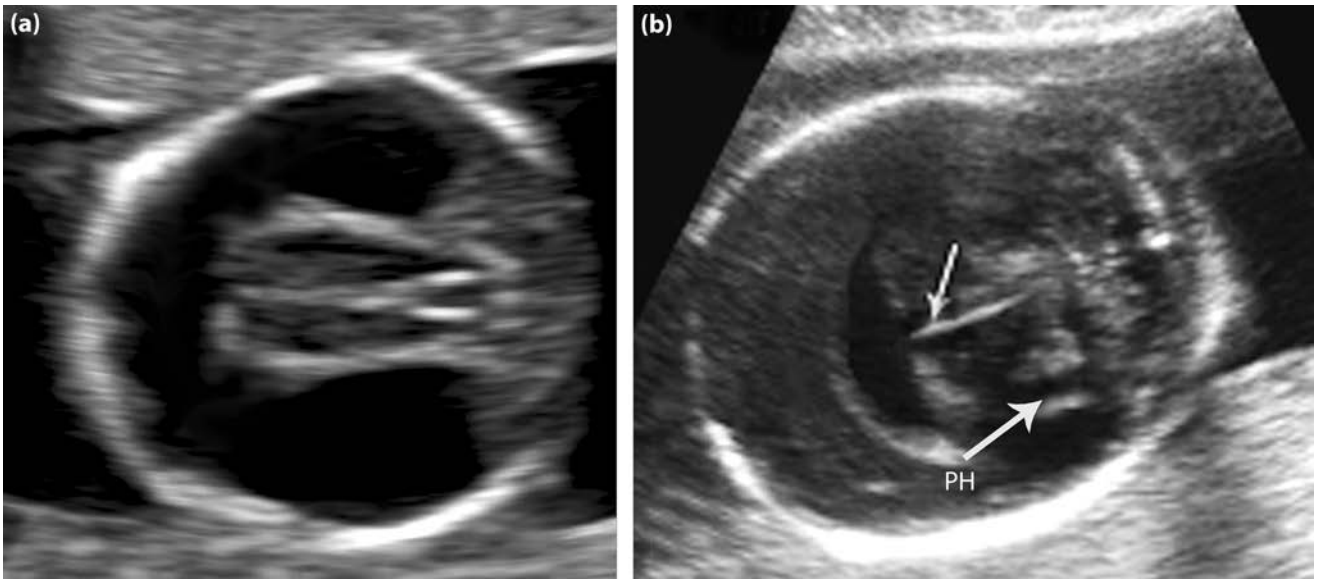


Figure 2.20 (a) Alobar holoprosencephaly: axial scan at the level of the thalamus showing the single ventricle, absence of midline structures, and fused thalamus; (b) Semilobar holoprosencephaly: ultrasound image showing the two cerebral hemispheres partially separated posteriorly; the rudimentary lateral ventricles with sketchy posterior horns (PH) and posterior falx cerebri can be seen.

In the alobar form of HPE, there are no midline structures of the brain. A single midline ventricle (Figure 2.20) (a crescent-shaped monoventricle), which often communicates with a dorsal cyst, can be clearly seen already in the first trimester. In the semilobar form, sketchy posterior horns and a hypoplastic third ventricle are usually present. Some portions of the posterior interhemispheric fissure, falx cerebri (Figure 2.20) and splenium of the corpus callosum can be identified. A dorsal cyst, less frequently than in alobar form, may be also present in the semilobar form.

In cases of lobar HPE, a definitive diagnosis is difficult. In fact, the diagnosis of the lobar form requires a midcoronal plane to demonstrate the absence of the CSP and the central fusion of the frontal horns (Figure 2.21) [9], which communicate with the third ventricle.

Differentiation between semilobar and the other two types of HPE can be sometimes prove difficult because no clear boundary exists between these forms. The differential diagnosis between semilobar and lobar types has been reported to be particularly difficult in some cases. However, if the third ventricle is completely formed and some frontal horn formation is present and the splenium and posterior part of the callosal body are completely formed, the HPE variant can be classified as lobar rather than semilobar.

In the case of HPE, sonographic assessment of the fetal face is mandatory. The spectrum of facial anomalies, caused by an abnormal development of the midline structures, ranges from cyclopia to mild dysmorphisms. The more severe the facial anomalies, the more pronounced the brain lesion [9,18,19] ("the face predicts the brain" approximately 80% of the time), but the reverse is not always true: About 15%–20% of alobar HPE cases are associated with only minor dysmorphisms.

The most frequent facial anomalies are usually classified into the following types: cyclopia, with a single midline orbit or absent eyes; arhinia, with or without a proboscis; ethmocephaly, with evident ocular hypotelorism and a proboscis located between the eyes; cebocephaly, with less pronounced ocular hypotelorism and a nose with a single nostril; (Figure 2.22) a median cleft lip and palate, with premaxillary agenesis; isolated premaxillary agenesis and slight anomalies that cannot be detected by US (e.g., a single central incisor).

Differential diagnosis. Alobar HPE should be distinguished from hydranencephaly: the presence of a dorsal sac, the fused thalami, and the evidence of a thin cerebral cortex and of facial anomalies may orient the diagnosis toward HPE.

It is also important to differentiate HPE from some forms of severe hydrocephalus in which an acquired communication between the lateral ventricles has occurred due to a disruption of the falx. The presence of the contralateral choroid plexus dangling across the ruptured falx, normally separated thalami, and the lack of midline facial anomalies are suggestive of hydrocephaly.

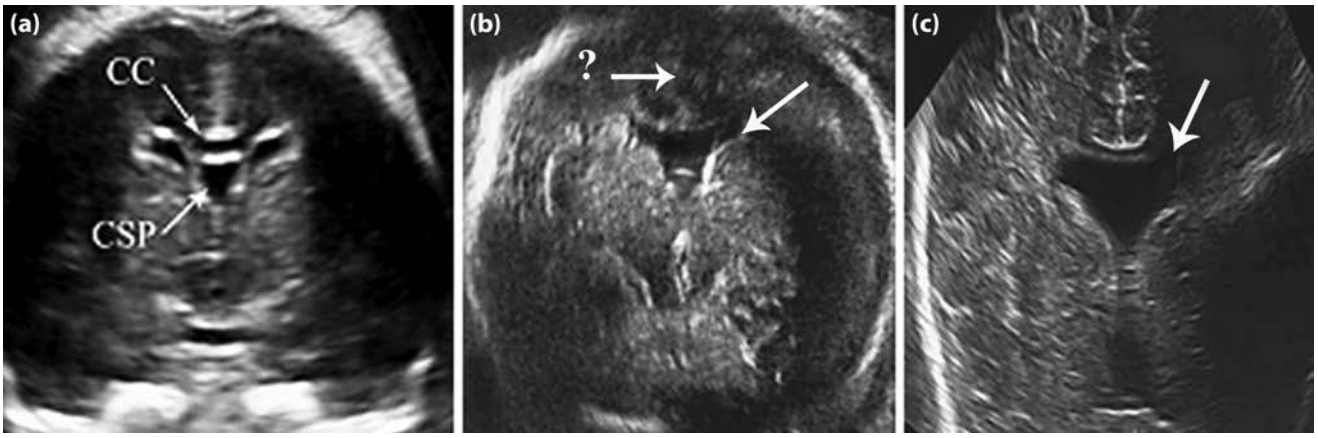


Figure 2.21 (a) Midcoronal view of the brain in a 23-week normal fetus showing the normally developed frontal horns, genu (CC), and cavum septi pellucidi (CSP). (b) Lobar holoprosencephaly. Midcoronal plane of a 30-week fetal brain showing absence of the CSP, the cingulate gyrus, and the anteriormost part of the interhemispheric fissure. The frontal horns are fused centrally (arrow) as are the fornices. (c) Agenesis of septum pellucidum. Midcoronal plane of a 34-week fetal brain shows the absence of the CSP with communicating frontal horns (arrow). The genu and cingulate gyrus are normally developed. (Modified from Volpe P et al., *Prenat Diagn* 29, 340–54, 2009.)

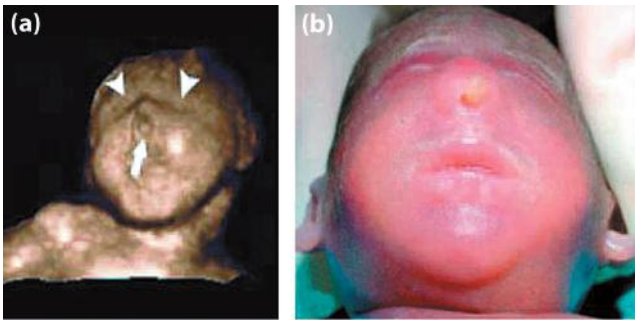


Figure 2.22 Cebocephaly. (a) Three-dimensional surface rendering of the fetal face showing marked hypotelorism (arrowheads) and a single-nostril nose (arrow). (b) Postmortem photograph confirming the marked hypotelorism and the single-nostril nose.

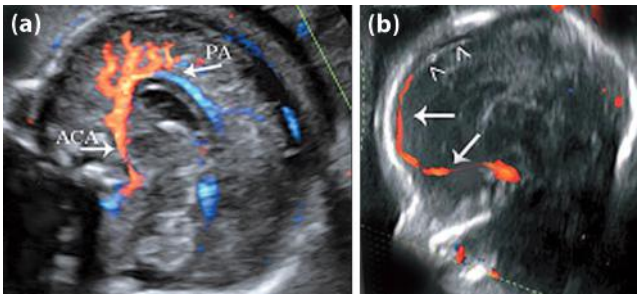


Figure 2.23 Sagittal scan of the fetal brain showing (a) the normal course of the anterior cerebral artery (ACA) and pericallosal artery (PA) and (b) the abnormal pathway of the anterior cerebral artery "crawling under the skull" (arrow). (Modified from Volpe P et al. *Diagn* 29, 340–54, 2009.)

In the case of lobar HPE, we have already reported the difficulty in differential diagnosis, between isolated agenesis of septum pellucidum (and septo-optic dysplasia [SOD]) and lobar holoprosencephaly. This differentiation is difficult because these malformations share the absence of the CSP and similar appearance of the frontal horns. The absence of a normally developed interhemispheric fissure between the anterior hemispheres helps to differentiate lobar HPE from isolated agenesis of SP (and SOD) (Figure 2.21). Recently, an additional sonographic sign has been used to differentiate between these anomalies: in lobar HPE, the anterior cerebral artery is often pushed anteriorly alongside the frontal bone by an abnormal bridge of cortical tissue between the two frontal gyri. This sign of a "snake under the skull" is clearly seen on the midsagittal view of the fetal brain (Figure 2.23).

Associated anomalies. The most frequently associated anomalies involve the CNS (microcephaly, macrocephaly, and DWM) the heart, the skeleton, and the gastrointestinal tract (omphalocele). When these associated anomalies are detected, the risk of chromosomal and genetic anomalies is very high.

Risk of chromosomal anomalies. This is high (especially trisomy 13): up to 47%.

Risk of nonchromosomal syndromes. This is relatively high. The most common syndromes are [16]:

- *Grote syndrome*: look for ► *holoprosencephaly* + ectrodactyly + absent tibiae + cardiac anomalies;
- *Steinfeld syndrome*: look for ► *holoprosencephaly* + median cleft lip + renal anomalies + short

forearms + absent thumbs + cardiac anomalies + absent gallbladder;
- *Holoprosencephaly-fetal akinesia syndrome*: look for ► *holoprosencephaly* + microcephaly + micrognathia + multiple contractures + talipes equinovarus;
- *Velocardiofacial syndrome*: look for ► *holoprosencephaly* + median cleft lip + cleft palate + cardiac defects;
- *Meckel–Gruber syndrome*: look for ► *holoprosencephaly* + encephalocele + polydactyly + polycystic kidneys + other CNS anomalies;
- *Pallister–Hall syndrome:* look for ► *holoprosencephaly* + polydactyly + imperforate anus.

Obstetric management. When an HPE is detected in a fetus, karyotyping should always be performed. In addition, the high risk of syndromic HPE strongly supports a careful search for additional structural anomalies.

If the fetal karyotype is normal, the parents should be referred for genetic counseling, including a detailed family history (with emphasis on pregnancy loss and neonatal deaths), clinical examination to identify microforms of HPE, and parental mutation analysis. In case of fetal abortion, a postmortem examination should also be performed. Genetic review is particularly important in women who have a euploid fetus with HPE to adequately counsel and estimate the risk of recurrence in a subsequent pregnancy, as well as initiating appropriate molecular studies. Identification of mutations responsible for HPE can confer significant recurrence risks, up to 20%, in a clinically normal family [9].

Postnatal therapy. No therapy is possible for neonates affected with the severest forms of HPE, considering the invariably poor prognosis.

Prognosis, survival, and quality of life. In the severest forms of HPE, the neurologic deficit is already evident in the neonatal period, in the form of generalized hypotonia, seizures, feeding problems, and mental retardation. Endocrine disorders, such as diabetes insipidus and growth hormone deficiency are commonly associated. Although many fetuses with HPE miscarry spontaneously, there is a common misconception that children with HPE do not survive beyond infancy. Although this is the case for the severest forms of HPE, a significant proportion of patients with milder forms of HPE will survive into childhood and beyond [22].

Life span is generally shorter if there are chromosomal abnormalities. Among affected patients with a normal karyotype, an inverse relationship exists between the severity of the facial phenotype and length of survival. A not insignificant number of patients with isolated milder form of HPE survive into the teenage years and are able to speak and function with mild cognitive impairment [22].

AGENESIS OF THE CORPUS CALLOSUM

Incidence. From 0.3%–0.7% in the general population to 2%–3% in the developmentally disabled population.

Ultrasound diagnosis. *Midsagittal view*: Complete or partial absence of the corpus callosum. *Axial views*: Colpocephaly, absence of the CSP (in complete agenesis). *Coronal views*: lateral convexity of and increased distance between the frontal horns.

Risk of chromosomal anomalies. High: 20%.

Risk of nonchromosomal syndromes. High.

Outcome. About 20%–30% rate of significant neurodevelopmental delay in isolated forms has been reported; in nonisolated form the prognosis is poor.

Definition Developmental abnormalities of the CC include hypoplasia, hyperplasia, agenesis, and dysgenesis. Agenesis of the corpus callosum (ACC) can be complete (CACC) or partial (PACC); the latter is also referred to as hypogenesis. The CC represents the major commissure between the two cerebral hemispheres; it extends from the frontal lobe anteriorly to above the collicular plate posteriorly. In the fetus, the leaves of the septum pellucidum enclose the space of the cavum of the septum pellucidum, which is located under the anterior portion of the CC. The other telencephalic commissures include the hippocampal commissure and the anterior commissure.

Etiology and pathogenesis. The prevalence of CC anomalies varies significantly in the different studies,

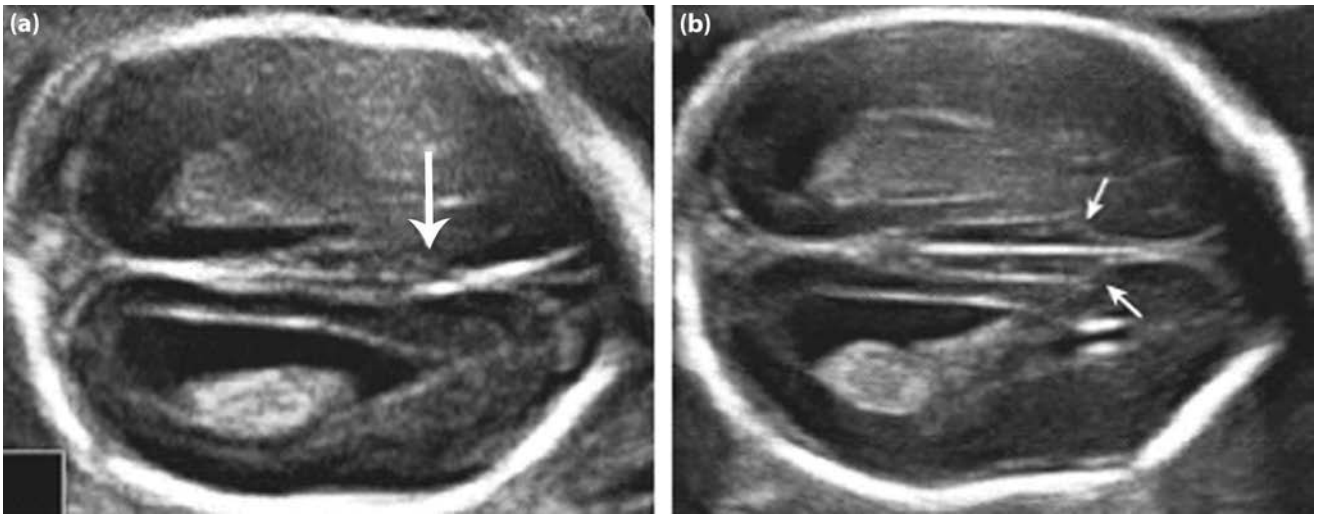


Figure 2.24 Agenesis of corpus callosum. Indirect signs: (a) axial scan of a 22-week fetal brain showing the absence of the CSP (arrow) and the teardrop shape of the lateral ventricle owing to dilatation of the atria and occipital horns (colpocephaly). (b) Arrows indicate increased separation of the hemispheres with the bodies of the lateral ventricles parallel to each other and shifted laterally. Colpocephaly is also present.

depending on the population and the diagnostic criteria. It ranges from 0.3% to 0.7% in the general population and from 2% to 3% in developmentally disabled individuals have been reported.

The formation of the CC starts with the development of the genu; the body and splenium develop at a later stage. If the normal developmental process is disturbed, the CC may be completely or partially absent (hypogenetic) [9,23]. Because the developmental process starts from the anterior part and progresses front to rear, when the CC is hypogenetic, usually the posterior portion is affected (the posterior body and the splenium).

There has been some debate about the timing of the development of the rostrum, the small frontal part of the CC. Although clinical observations seemed to agree that the rostrum should be the last portion to develop, more recent studies based on diffusion tensor MRI showed that the rostrum, the genu, and the anterior part of the body were already present at around 15 weeks' gestation [9]. The knowledge of the organogenetic process helps to differentiate a developmental injury (hypogenesis) from an acquired one (destruction). The latter mechanism usually occurs in association with hypoxic-ischemic injury and infectious causes.

The etiology of ACC is very heterogeneous. Identified causes are chromosomal, monogenic, and teratogenic. Chromosomal abnormalities are present in 20% of cases, especially trisomies 18 and 13. More than 100 syndromes involving ACC have been reported. Some environmental and metabolic factors also have been implicated in ACC, such as in utero cytomegalovirus and rubella infection and fetal alcohol exposure.

Ultrasound diagnosis. The CC can be visualized with US, but some degree of technical skill is required because it is not apparent using the standard axial planes, and additional coronal and particularly sagittal planes are required [6,7,24]. In fetuses in cephalic presentation, the transvaginal approach is preferred [6,7]; in fetuses in breech presentation, a transfundal approach is suggested. More recently, the use of three-dimensional multiplanar technique has also been proposed [11] because it offers a more accurate identification of the midsagittal plane, and navigation in the other two simultaneous orthogonal planes may permit a better evaluation of the midline prosencephalic structures (Figure 2.12). In axial planes, the diagnosis is based on the presence of some indirect signs. Because the CC shares a common anatomic and embryogenetic formation with the septum pellucidum, complete ACC is commonly associated with a hypoplastic or absent CSP (Figure 2.24).

Therefore, at the second-trimester anomaly scan, ACC may be suspected when the CSP is not visualized on the axial transventricular view (Figure 2.24). The suspicion of ACC is supported further by the recognition of other indirect signs, such as (1) colpocephaly (dilatation of the atria and occipital horns, "which is determined by the absence of the splenium and by a defect of the intrinsic association bundles of the occipital lobe) (Figure 2.24); and (2) increased separation of the hemispheres with the bodies of the lateral ventricles parallel to each other and shifted laterally (Figure 2.24).

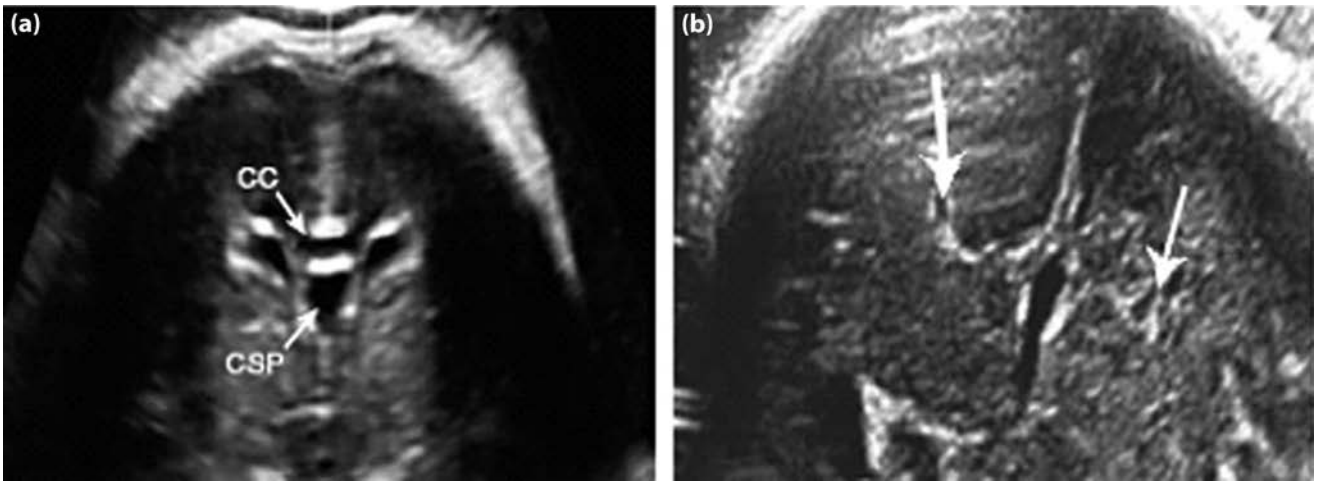


Figure 2.25 (a) Midcoronal view of the brain in a 23-week normal fetus shows the normally developed frontal horns, genu (CC), and cavum septi pellucidi (CSP). (b) Agenesis of the corpus callosum (ACC). Coronal scan of a 29-week fetal brain shows absence of the genu and increased distance between the frontal horns (arrows). The inner walls of the frontal horns are concave medially because of the medial compression exerted by the Probst bundles. Together with the lumen of the third ventricle, this makes up the typical appearance of a "bull's head."



Figure 2.26 (a) Median view of the fetal head in a 22-week fetus showing the entire corpus callosum. B: body; CSP: cavum septi pellucidi; G: genu; R: rostrum; S: splenium. (b) Midsagittal scan of the brain in a 22-week fetus with ACC showing the absence of the corpus callosum (?) and of the CSP. (c) ACC at 31 weeks' gestation. At this advanced gestational age, an atypical radiating appearance of the median sulci, which converge toward the third ventricle (3v), can also be seen.

Dorsal elevation of the third ventricle can be also present. On coronal sections of the fetal brain, the indirect signs are mainly characterized by the frontal horns, which are separated more than usual with inner walls that are concave medially (Figure 2.25). This appearance is due to the compression exerted by a conspicuously large longitudinal bundle of fibers that represent the callosal fibers, which fail to cross the hemispheres and instead are rerouted parasagittally, parallel to the midline. This abnormal bundle, called the *longitudinal bundle of Probst*, runs parallel to the medial walls of the lateral ventricles and invaginates their medial borders, especially at the level of the frontal horns. Each of these indirect signs can be present in isolation or become more apparent with advancing gestational age. This probably partly explains the frequent false-negative diagnosis of ACC (especially before 24 weeks).

A definitive diagnosis of ACC relies on recognition of direct signs [23–25], which consist of the demonstration of the absence of the CC on midsagittal and coronal views of the fetal brain. In particular, the midsagittal plane shows absence of the CC (Figure 2.26) and, in advanced gestation or postnatally, an atypical radiating appearance of the median sulci, which converge toward the third ventricle (Figure 2.26). In this view, usually no cingulate gyrus can be recognized, or it appears incomplete.

ACC may also be partial, resulting in more subtle US findings than those associated with the complete form. When the CC is incompletely formed, usually the posterior portion is affected (the posterior body and

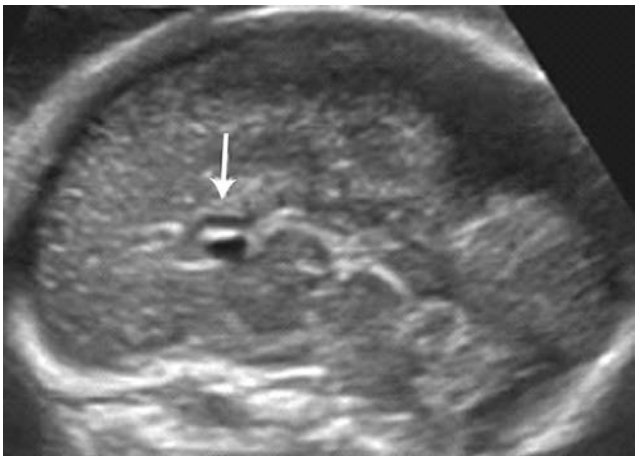


Figure 2.27 Partial agenesis of the corpus callosum (ACC). Midsagittal scan of the brain in a 24-week fetus. Genu and a small anterior part of the body are present (arrow), whereas the posterior part of the body and the splenium are absent.

the splenium); in this situation, the CSP can be present, and often the only indirect US sign is a mild colpocephaly. Sometimes the indirect signs of partial ACC may also be completely absent [23]. A sagittal view is the only way to make the diagnosis, visualizing a small CC that is lacking the posterior part (Figure 2.27) and only partially surrounds the third ventricle. Less frequently, the remaining structure is the genu; it can appear thin and barely discernible with gray-scale imaging and can be identified only when highlighted by the course of the pericallosal artery.

In cases of ACC, the use of color Doppler demonstrates that the semicircular loop, normally formed by the pericallosal artery along the superior surface of the CC, is lost (Figure 2.28). This sign may help to make the diagnosis of ACC. Its value is even greater in the case of partial ACC; in partial ACC, the pericallosal artery closely follows and depicts the small anterior part of the CC, often discernible with difficulty on gray-scale imaging [9,23]. Its course is then lost, being usually absent in the posterior part of the CC.

Interhemispheric cysts (Figure 2.29) associated with ACC are often considered as mere extensions of the ventricular system. These cysts have a variable appearance and can be divided into two main categories: one in which the cysts are herniations of the ventricular system, representing the dorsal expansion of the roof of the third ventricle, and the other in which they are clearly separated from the ventricles. Another median anomaly that may be associated with ACC is an intracranial lipoma, visible only in the third trimester as a hyperechogenic image under the inferior part of the interhemispheric scissure (Figure 2.29).

Differential diagnosis. ACC causes colpocephaly; this must be distinguished from other causes of mild VM. However, the presence of other indirect signs and the direct evidence of ACC on the midsagittal view of the fetal brain is diagnostic.

Association with other malformations. ACC is often associated with other cerebral and/or extracerebral malformations, including a number of syndromes and metabolic diseases. The risk of associated brain anomalies is extremely high (up to 80%) including Dandy–Walker complex, gyral anomalies, and neuronal heterotopia. The risk of associated extra-CNS abnormalities is high (up to 60%), including congenital heart disease and skeletal and genitourinary defects.

Risk of chromosomal anomalies. This is relatively high (20% of cases): trisomy 13 and 18, deletions [del(4)(p16), del(l6)(q23), del(X)(p22)], and duplications [dup(8)(p21–23), dup(11)(q23–qter)].

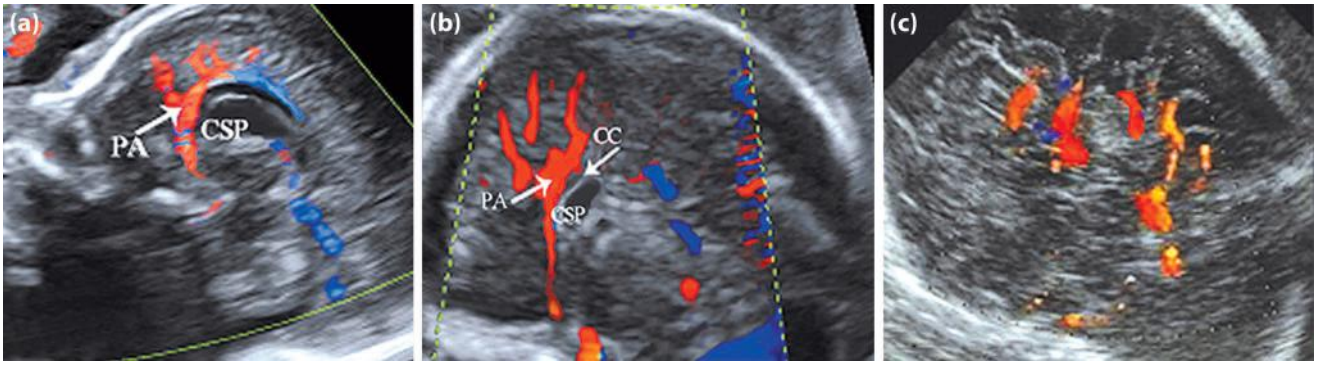


Figure 2.28 (a) Midsagittal view of a 22-week normal fetal brain. Color Doppler shows anterior cerebral artery branching giving rise to the pericallosal artery (PA). (b) Partially absent corpus callosum. Midsagittal view of a 22-week fetal brain. The small corpus callosum (CC) (arrow) is highlighted by the course of the PA. The PA closely follows the genu but loses its normal course where the CC disappears; it takes an upward posterior oblique direction. (c) Complete agenesis of the CC. Midsagittal view of a 30-week fetal brain shows the absence of the PA; its classic loop is not seen. CSP: cavum septi pellucidi.

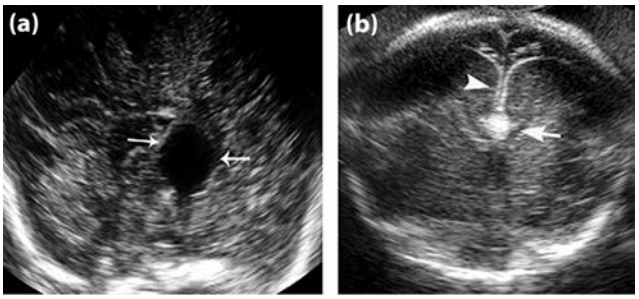


Figure 2.29 (a) Interhemispheric cyst (arrows) associated with agenesis of the corpus callosum (ACC). (b) Intracranial lipoma is visible as a hyperechogenic image (arrow) under the inferior part of the interhemispheric scissure (arrowhead).

Risk of nonchromosomal syndromes. This is high. The most common syndromes involving ACC are shown in Table 2.2.

Obstetric management. Should ACC be diagnosed in a fetus, karyotyping is mandatory, because of the high risk of chromosomal anomalies. In addition, the high rate of association with Mendelian-inherited syndromes dictates an accurate familial analysis and a careful search for additional structural anomalies (hematologic diseases, asplenia, anophthalmia, cleft lip/palate, albinism, bone lesions, congenital megacolon, and camptodactyly). A tissue sample should usually be preserved for a possible molecular diagnosis.

Fetal MRI (Figure 2.30) [23] is particularly useful in demonstrating possible additional cerebral anomalies, such as late sulcation, migration anomalies, and heterotopia [9,23]. However, in most cases, the presence of these anomalies can be recognized only from the late second trimester onward, with late development of the sulci and gyri.

Table 2.2 Syndromes associated with ACC

Syndrome	Transmission	Gene
Acrocallosal	AR	GLI 3
Aicardi	XLD	
Apert	AD	*FGFR2*
ATRX	XLR	*ATRX*
Basal cell nevus	AD	*PTCH2*
CRASH	XLR	*L1CAM*
Fukuyama	AR	*FCMD*
Kallmann	XLR/AD/AR	*KAL1*
Leopard	AD	*PTPN11*
Leprechaunism	AR	*INSR*
Neu-Laxova	AR	
Neurofibromatosi	AD	*NF1*
Rubinstein-Taybi	AD	*CREBBP*
Tuberous sclerosis	AD	*TSC1*, *TSC2*
Walker–Warburg	AR	Pomt/FKRP

AD: autosomal dominant; AR: autosomal recessive; XLR: X-linked recessive; XLD: X-linked dominant.

Prognosis, survival, and quality of life. It is not unusual for individuals with ACC to have no neurologic



Figure 2.30 (a) Magnetic resonance image (MRI). Sagittal view of the normal fetal brain (T2-weighted HASTE image). The corpus callosum is completely formed; it is evident as an intermediate signal due to the incomplete myelination. The black arrow indicates the cavum septi pellucidi (R: rostrum; G: genu; B: body; S: splenium). (b) Complete agenesis of the corpus callosum: MRI (sagittal view, T2-weighted HASTE image) of the fetal brain showing complete absence of the corpus callosum and the third ventricle communicating with the interhemispheric fissure. (c) Partial agenesis of the corpus callosum: MRI (sagittal view, T2-weighted HASTE image) of the fetal brain showing the presence of the genu and the anterior part of the body; the posterior part of the body and the splenium are absent and cisternal enlargement is evident. B: anterior part of the body; G: genu; ?, absence of the posterior part of the corpus callosum. (Modified from Volpe P et al., *Ultrasound Obstet Gynecol* 27, 509–16, 2006.)

problems, despite the absence of callosal fibers although a case series of children with postnatally diagnosed ACC reported that most of them suffered from developmental delay and often from seizures. However, in this study, there was a referral bias, since children without developmental anomalies were not studied. Several postnatal case series suggest a direct relationship between the occurrence of associated brain abnormalities and poor neurodevelopmental outcome. With isolated ACC, caution must be adopted when assessing the fetal/neonatal prognosis. In fact, considering the small number of fetal cases series reported in the literature, no general conclusions can be drawn, although some interesting points can be made. The first issue is that other CNS malformations (especially gyral anomalies, which are difficult if not impossible, to visualize on US) or extra-CNS malformations can be present even when ACC is apparently isolated on US /MRI, especially if the evaluation is carried out at 20–22 weeks [9,23].

The second point is that, regardless of the associated anomalies, significant neurodevelopmental delay develops in a consistent proportion of cases (20%–30%), even if ACC is confirmed postnatally to be isolated [3,23,24,26]. The same also applies to isolated partial ACC.

A final point that should be made is that even when the outcome is good, subtle neuropsychologic, perceptual, and motor defects can emerge later in life, because all individuals with CACC/PACC have some neuropsychological symptoms. Considering the presence of neurosensorial information transfer defects, no differences seem to exist between PACC and CACC in terms of the performance accuracy of the somatosensory functions.

However, the clinical relevance of such deficits should not be exaggerated, because the functions of the CC are not completely understood and it is difficult to assess correctly the neuropsychologic status of individuals with CACC/PACC and normal-range IQs, and the role of possible compensatory mechanisms. Nevertheless, a protracted follow-up (until around six years of age) is important to update the neurodevelopmental status of these patients, especially with regard to social interactions and school performance, in order to be able to provide better prognostic information to families.

The recurrence risk is 5% when syndromes are excluded.

ABsENT sEpTUM pELLUcIdUM ANd sEpTo-opTIc dysp LAsIA

Incidence. Unknown in the fetus.

Ultrasound diagnosis. The US findings are characterized by absent CSP with communicating frontal horns.

Risk of chromosomal anomalies. This is low.

Risk of nonchromosomal syndromes. This is low.

Outcome. Isolated absence of the septum pellucidum (ASP) is usually asymptomatic. The clinical presentation of SOD is variable. Visual disturbances may range from blindness to almost normal vision; hypothalamic-pituitary insufficiency, mainly characterized by growth deficit and diabetes insipidus, is seen in two-thirds of patients.

Definition The septum pellucidum is a single, vertically oriented structure, positioned between the medial border of the frontal horns and the bodies of the lateral ventricles. It is intimately related to the CC, which provides its rostral and superior boundaries. The body of the fornix forms its posterior-inferior part. The septum pellucidum does not contain organized gray matter and is not simply a membrane. It is made of two sheaths of white matter apposed to each other along the midline and has been shown to carry fibers In the fetus, a space is found between the pellucidal leaves, the well-known *cavum septi pellucidi*, with its occasional posterior recess between the splenium and hippocampal commissure, known as the *cavum vergae*.

Septal agenesis is a rare brain abnormality that can be isolated or be part of complex brain anomalies. Apparently isolated cases of ASP may be due to SOD or represent an isolated anomaly. SOD was first described by De Morsier [27] in an autopsy series of 36 patients; it is a highly heterogeneous condition that comprises a variable combination of optic nerve and pituitary gland hypoplasia, and absent septum pellucidum. It may be associated with cortical abnormalities (SOD-plus), especially bilateral schizencephaly and polymicrogyria.

Etiology and pathogenesis. Most cases of SOD are sporadic, and several etiologies have been suggested. However, numerous familial cases have been described, and the identification of mutations in key developmental genes, including *HESX1*, *SOX2*, and *SOX3*, in patients with SOD and associated phenotypes suggests

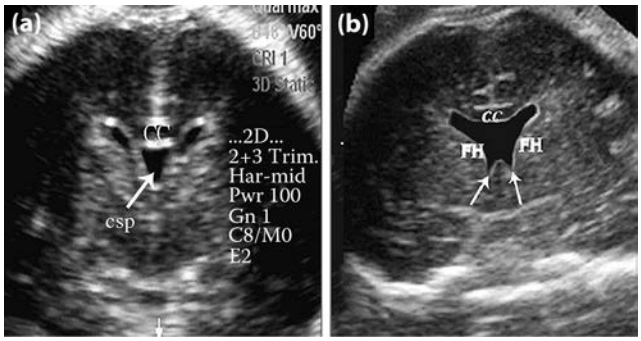


Figure 2.31 (a) Midcoronal view of the brain in a 23-week normal fetus shows the normally developed frontal horns, genu (CC), and cavum septi pellucidi (CSP). (b) Absent septum pellucidum. Midcoronal plane of a 29-week fetal brain shows the absence of the CSP with communicating frontal horns (FH). The typical aspect of the downward point of the frontal horns is clearly seen (arrows). The genu is normally developed (CC). (Modified from Volpe P et al. *Diagn* 29, 340–54, 2009.)

that a genetic causation is likely in the more common sporadic cases of the condition. The precise etiology of SOD is most likely multifactorial, involving contributions from environmental factors in addition to an important role for crucial developmental genes [9].

Ultrasound diagnosis. ASP can be diagnosed by US in the second trimester of pregnancy. The US findings are characterized by absent CSP with communicating frontal horns. On the coronal view, ASP results in a squared appearance of the frontal horns with inferior pointing (Figure 2.31). The CC usually is present, albeit it may be thinned. As reported above, an apparently isolated case of ASP may be due to SOD or may represent an isolated anomaly. In this case, the correct diagnosis is challenging. It may be attempted by evaluation of (1) maternal urine and serum estriol levels; (2) fetal blood assays for growth hormone, adrenocorticotropic hormone, and prolactin; and (3) optic nerves and chiasm size in the third trimester, as depicted by MRI and three-dimensional US.

Differential diagnosis. Isolated agenesis of SP and SOD should be differentiated from lobar holoprosencephaly. In fact, on US coronal view, the ASP results in a squared-off appearance of the frontal horns that resembles lobar holoprosencephaly. However, if the interhemispheric fissure is normally developed, and the CC and anterior cerebral arteries are normal in shape and position, this is suggestive of ASP without holoprosencephaly (Figure 2.21). In addition, MRI can be useful in clearly showing a ventral fusion of the frontal lobes in cases of lobar holoprosencephaly.

Associated anomalies. See Table 2.3.

Table 2.3 Fetal brain anomalies associated with absent septum pellucidum

Septo-optic dysplasia
Holoprosencephaly
Complete agenesis of corpus callosum
Bilateral polymicrogyria
Bilateral schizencephaly
Severe hydrocephaly

Risk of chromosomal anomalies. This is low.

Risk of nonchromosomal syndromes. This is relatively low.

Obstetric management. In the case of apparently isolated absence of CSP detected by US, MRI should be used to visualize the size of the optic nerves and chiasm (in late pregnancy) to exclude hypoplasia and to demonstrate possible associated cortical abnormalities (polymicrogyria and schizencephaly). Hypoplasia of the optic nerves or chiasm may be difficult to assess even with MRI and sometimes may develop only after birth. More recently, 3D US has been used to visualize the optic chiasm, but we reckon that making a diagnosis of absent/hypoplastic chiasm remains a rather challenging diagnosis, despite 3D US. In the presence of hypoplastic optic chiasm (and cortical abnormalities), the diagnosis of SOD has to be suspected and should be confirmed by the presence of maternal and fetal endocrinologic deficiencies. However, it must be kept in mind that the onset and extent of hormonal disorders in patients with SOD vary considerably. Endocrinologic deficiencies are found in 50% to 90% of cases during infancy [9]. For this reason, despite normal fetal pituitary function (and normal appearance of the optic tract on fetal MRI), SOD cannot be completely ruled out prenatally. However, the assessment of fetal pituitary function should be incorporated into the diagnostic work-up because pituitary dysfunction, when present, represents a typical sign of SOD.

Postnatal treatment. Postnatal treatment is symptomatic, and a multidisciplinary team with regular follow-up should manage patients with SOD. Hormone insufficiencies can be treated with hormone replacement therapy, but close monitoring is required as the hormone deficiencies evolve with age. Children may benefit from developmental programs for visually impaired individuals and from physical and occupational therapies.

Prognosis, survival, and quality of life. Isolated ASP is usually asymptomatic. However, prenatal detection of an isolated ASP does not preclude normal neurologic clinical status, owing to the possible presence of histopathologic brain anomalies not detectable by US and MRI.

The clinical presentation of SOD is variable. Visual disturbances may range from blindness to almost normal vision; hypothalamic-pituitary insufficiency, mainly characterized by growth deficit and diabetes insipidus, is seen in two-thirds of patients. Microphallus (in males) also can be present. In cases of SOD-plus, seizures or spastic motor deficit or both are also present. The prognosis of SOD is variable, depending on the severity of the disease.

pos TEr Ior c r ANIAL Foss A MALFor MATIo Ns

The classification of cerebellar malformations is controversial; no widely accepted agreement has been reached, despite many attempts by neuroradiologists, geneticists, and neuropathologists [28–31]. In particular, as far as the conditions associated with a defective vermis are concerned, there is no general consensus as to their categorization. In addition, cerebellar hemispheric and vermian malformations have been described but are poorly understood. Thus, the prognosis of patients with most cerebellar malformations is uncertain. Finally, it is often difficult to distinguish clearly, in an infant with signs and symptoms relating to the posterior fossa, between cerebellar or vermian atrophy, hypoplasia, or malformation. In the fetus, the situation is understandably even more confused, due to difficulties in the prenatal assessment of posterior fossa, both by US and by MRI. However, based on a morphologic US approach, it is at least possible to differentiate posterior fossa anomalies into two broad categories: (1) cystic malformations, characterized by the presence of an apparent CSF collection in the posterior fossa due to fourth ventricle/cisterna magna dilatation, or to true arachnoid loculations; and (2) noncystic malformations, in which there is no apparent CSF collection [31,32].

cys TIc pos TEr Ior Foss A

In this group we include the anomalies characterized, on the axial transcerebellar view, by the presence of an apparent CSF collection in the posterior fossa and/or by the fourth ventricle opening posteriorly and apparently communicating with the cisterna magna.

It must be kept in mind that the "closure" of the fourth ventricle, occurs at 18–20 weeks' gestation [33–35]. In fact, in the late first trimester, the fourth ventricle is large and a relatively small cerebellum is located on top of it. In the following weeks, the cerebellum grows to enfold the fourth ventricle completely. After 20 weeks, the vermis has normally "closed" the fourth ventricle and, therefore, the demonstration of an opening may be indicative of a posterior fossa anomaly [33–35]. However, a small fingerlike appendage of the fourth ventricle, the Blake's pouch (BP), is frequently seen protruding into the cisterna magna, caudal to the cerebellum [33–36]. Failed closure of the fourth ventricle seems to result from two potential processes: either arrest of vermian development so it does not cover the fourth ventricle at its inferior extent or failure of adequate fenestration of the fourth ventricular outflow foramina, leading to a secondary elevation of the vermis.

The failed closure of the fourth ventricle is characteristic of *Dandy–Walker malformation* (*DWM*), *Blake's pouch cyst (BPC),* and *vermian hypoplasia*.

An apparent CSF collection can also be due to *mega cisterna magna (MCM)* and a true arachnoid loculation (*arachnoid cyst*).

The *DWM* and related disorders—cerebellar/vermian hypoplasia, MCM, and BPCs—comprise a grouping of abnormalities of the cerebellum, its surrounding mesenchyme, and sometimes cerebral structures, a variable combination of features that has generated considerable confusion and controversy [28,37]. The mildest of these anomalies are the BPC and MCM. However, their differential diagnosis can be particularly difficult because recognizing the subtle anatomic features that differentiate them may be challenging. For accurate anatomic assessment of these malformations, a midsagittal plane of the fetal head is required. The mainstay of the diagnosis is represented by the assessment of a number of direct and indirect signs, including the following: the vermian biometry, position, and morphology, including the fastigial point and vermian fissures and the association with ventriculomegaly; the size of the posterior fossa; the position of the torcular/tentorium; and the morphology of the cyst and its relationship with the fourth ventricle and subarachnoid spaces. For these reasons, evaluation of the vermis—absent, hypoplastic, or intact—and of the fourth ventricle/cisterna magna (normal or enlarged) are important. The degree of upward vermian rotation is also relevant.

dANdy–W ALk Er M ALFor MATIo N

Incidence. Incidence of DWM is 1 in 25,000–30,000 live births.

Ultrasound diagnosis. It is characterized, on axial transcerebellar view, by an "open fourth ventricle" apparently communicating with the cisterna magna. An expansion of the posterior cranial fossa is also evident. On median view of the head, the vermis is small and upwardly rotated (usually more than 45°). An upward displacement of the tentorium/torcular is also evident.

Risk of chromosomal anomalies. High: up to 35% of cases.

Risk of nonchromosomal syndromes. This is high.

Outcome. Outcome is poor when associated with other malformations and syndromes; less severe if isolated.

Definition The term *Dandy–Walker malformation* was suggested to describe a malformation [38] consisting of a (1) complete or partial agenesis of the vermis; (2) cystic dilatation of the fourth ventricle that fills the posterior fossa and extends into the cisterna magna; (3) enlarged posterior fossa with upward displacement of the tentorium; and (4) upward rotation of the partial agenetic vermis.

On the basis of subsequent observations of DWM cases, it seems that the vermis in DWM was not necessarily incomplete, as reported in the pre-MRI era, but could be tiny and complete with a different prognosis. This relates to two different morphogenetic paths: hypoplasia vs. agenesia. VM develops in more than 50% of cases, especially in postnatal age.

Etiology and pathogenesis. It has been suggested that the DWM be considered in the group of mesenchymal-neuroepithelial signaling defects. In fact, several cerebellar growth factors are derived from the overlying leptomeninges [28,37]. Therefore, abnormalities of the cerebellar leptomeninges may result in abnormalities of the cerebellum itself, as well as abnormalities of the surrounding CSF spaces. This is the basis of development of the DWM: it requires abnormal development of the cerebellum itself and of the overlying leptomeninges.

Ultrasound diagnosis. On axial transcerebellar view, a triangular or square-shaped open fourth ventricle apparently communicating with cistern magna can be seen (Figure 2.32). An expansion of the posterior cranial fossa is also evident. To assess the presence, integrity, and position of the vermis and the position of the torcular/tentorium, a median view is required. On the median view, a small vermis (Figure 2.32b) with a normal or abnormal configuration (absence of fastigium and/or fissures) may be present. While an abnormal configuration usually indicates partial agenesis, a small vermis with a normal configuration indicates hypoplasia [34,35,39]. However, the distinction between these two entities is difficult The upward rotation of the small vermis usually exceeds 45° [35] (Figure 2.32) and

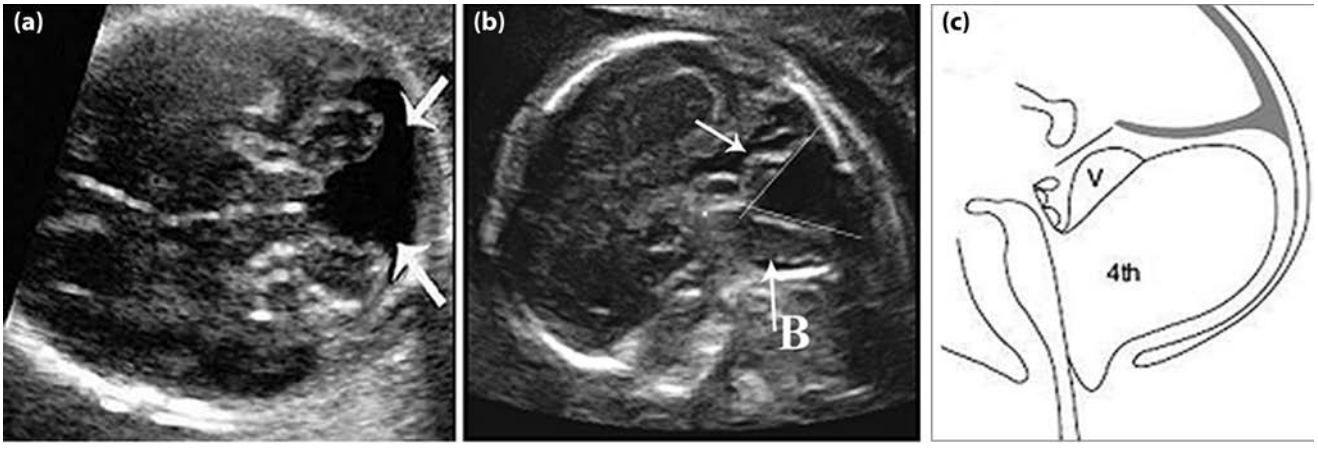


Figure 2.32 Dandy–Walker malformation. (a) Axial view of the posterior fossa showing a CSF collection (arrows) and a V-shaped cerebellum. (b) Midsagittal view of the posterior fossa showing an upward displacement of the small vermis (arrow) and an open fourth ventricle, communicating with the cisterna magna. The upward rotation of the small vermis exceeds 45°; B: brainstem. (c) Schematic diagram of the same finding.

a superior displacement of the torcular/tentorium is also present.

Differential diagnosis. The DWM should be differentiated from other cystic anomalies of the posterior fossa. As mentioned above, a median view of the fetal head is mandatory for an accurate assessment of the position and features of the vermis and of the characteristics of the CSF collection of the posterior fossa (fourth ventricle and cisterna magna). The presence of a apparent communication between the fourth ventricle and cisterna magna (open fourth ventricle) associated with a normal vermis is indicative of BPC. In this case, the rotation of the vermis is usually less pronounced.

The presence of a apparent communication between the fourth ventricle and cisterna magna (open fourth ventricle) associated with the hypoplastic vermis, normally inserted tentorium/torcular, and no expanded posterior fossa is indicative of vermian hypoplasia. In this case, the rotation of the vermis usually does not exceed 45° [35]. In case of mega cisterna magna, the cisterna magna is large but the cerebellum is intact and the fourth ventricle is closed.

Association with other malformations. Several malformations have been reported to be associated with DWM. The most commonly associated anomalies are other CNS anomalies (in 50%–60% of cases), including midline anomalies (ACC, holoprosencephaly, etc.). An association with facial clefts and other extra-CNS anomalies (especially congenital heart disease and urinary anomalies) has been described, often in the context of genetic syndromes.

Risk of chromosomal anomalies. This is high, with up to 35% of cases being associated with aneuploidy, mainly trisomies 18 and 13.

Risk of nonchromosomal syndromes. This is high. The most common syndromes that can be associated with DWM are:

- *Walker–Warburg syndrome*: look for ► *DWM* + eye anomalies + other CNS anomalies (lissencephaly, midline anomalies, microcephaly, and cephalocele);
- *Meckel–Gruber syndrome*: look for ► *DWM* + encephalocele + polydactyly + polycystic kidneys
- *Aicardi syndrome*: look for ► DWM + ACC + vertebral defects;
- *Neu–Laxova syndrome*: look for ► *DWM* + lissencephaly + microcephaly + proptosis + diffuse joint contractures + subcutaneous tissue edema + intrauterine growth retardation.

Obstetric management. Fetal karyotyping is mandatory, because of the high risk of chromosomal anomalies. In addition, a thorough anatomic scan should be performed by an expert because of the high risk of association with other CNS and extra-CNS malformations. Serial US monitoring is warranted to verify the possible onset of severe hydrocephalus. Delivery should take place in a tertiary referral center, for definitive diagnosis and adequate neonatal management.

Postnatal treatment. There is obviously no treatment for the primary vermian lesion. The virtually ubiquitous secondary obstructive hydrocephalus may be treated with a cystoperitoneal shunt.

Prognosis, survival, and quality of life. DWM is associated with late-onset hydrocephalus in more than 50% of cases. If hydrocephalus develops, whether in utero or in the neonatal period, there is an overall mortality rate of over 60%, with most survivors having a low IQ. When hydrocephaly is not associated, it has been suggested that the neurologic outcome is mainly related to the appearance of the cerebellar vermis. When the small vermis has a normal configuration a normal development has been reported in more than 50% of cases. Conversely, when the vermis is abnormally lobulated and/or there are associated cerebral anomalies, the prognosis is poor [34,39].

BLAkE's poUch cysT

Incidence. Unknown; it seems to be the most frequent fetal posterior fossa cystic anomaly.

Ultrasound diagnosis. On axial transcerebellar view it is characterized by an open fourth ventricle apparently communicating with the cisterna magna. On a median view of the fetal head, a normal but upwardly rotated cerebellar vermis is seen.

Risk of chromosomal anomalies. Relatively high, especially if associated with other anomalies.

Risk of nonchromosomal syndromes. If associated with other anomalies, it is relatively high.

Outcome. If isolated, it seems to be a normal variant. In less frequent cases associated with hydrocephaly, the prognosis depends on hydrocephaly.

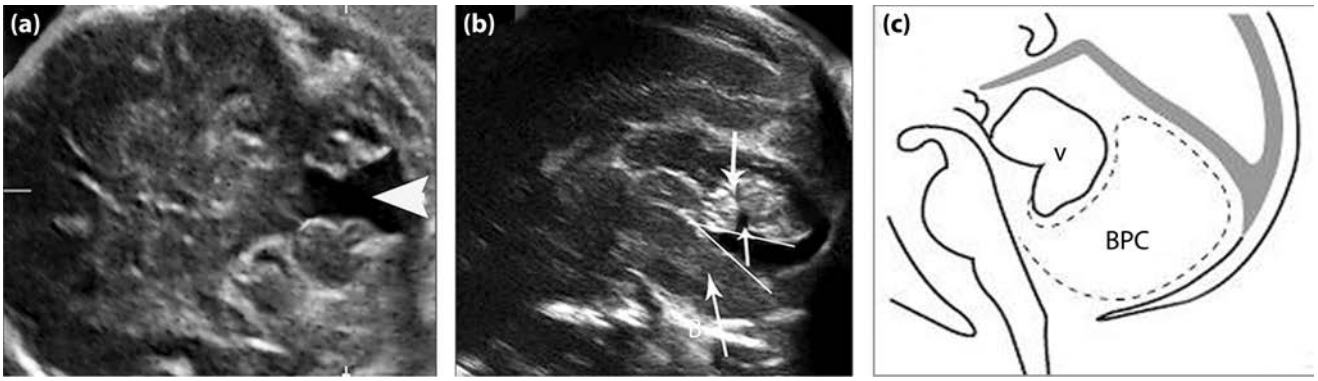


Figure 2.33 Blake's pouch cyst (BPC). (a) Axial scan of the posterior fossa showing an hourglass opening fourth ventricle (arrowhead). (b) Sagittal scan of the posterior fossa showing an upward displacement of a normal vermis (arrow) and an open fourth ventricle, communicating with the cisterna magna. The upward rotation of the vermis is mild; B: brainstem. (c) Schematic diagram of the same finding.

Definition and anatomy. BP is a normal, transient embryological structure, representing an evagination of the posterior membranous area (PMA), one of the two components of the rhombencephalic roof (the other being the anterior membranous area, AMA) [32,40] that initially does not communicate with the surrounding subarachnoid spaces. Subsequent spontaneous perforation of the pouch, by the 10th gestational week, forms the foramen of Magendie.

The term Blake's pouch cyst was originally introduced in infantile pediatric neuroradiology [41] to indicate a type of obstructive hydrocephalus secondary to failure of formation of the foramen of Magendie and Luschka, resulting in a compressive cyst of the posterior fossa displacing superiorly the cerebellar vermis. More recently, the term has been used in fetal imaging studies to indicate cases with a posterior fossa cyst displacing superiorly an intact cerebellar vermis, typically in association with a normal ventricular system and a normal size of the posterior fossa [30,34,35,42]. This finding has been interpreted as failed or delayed regression of the BP. The entity described in the original neonatal studies likely differs from the one later described in fetal studies, because the latter typically has a normal outcome and appears to be rarely associated with ventriculomegaly [34,35,42].

Ultrasound diagnosis. Sonographically, on the axial transcerebellar view, BPC is characterized by an hourglass opening (buttock sign) apparently communicating with the cisterna magna (Figure 2.33). On a median view of the fetal head, a normal but usually moderately upward-rotated vermis is evident [35] (Figure 2.33). The tentorium and torcular are in normal position. There may also be visualization of the BPC roof within the cisterna magna and a more translucent

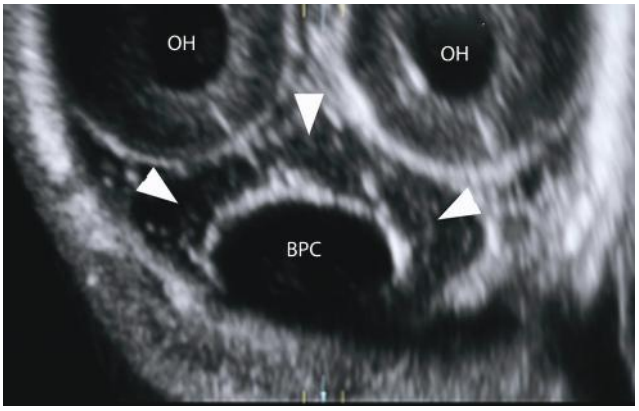


Figure 2.34 Blake's pouch cyst (BPC). A more translucent echogenicity of the cyst (BPC) content in comparison with the cisterna magna fluid can be clearly seen; OH: occipital horn.

echogenicity of the cyst content in comparison with the cisterna magna fluid (Figur 2.34).

Differential diagnosis. The BPC should be differentiated from other cystic anomalies of the posterior fossa. As mentioned above, in the case of apparent communication between the fourth ventricle and the cisterna magna (open fourth ventricle), on an axial transcerebellar view, such as in the case of BPC, a median plane of the fetal head is mandatory for an accurate assessment of the position and features of the vermis. The presence of a normal vermis rules out the possibility of a DWM and vermian hypoplasia. In addition, instead of DWM, in case of BPC the rotation of vermis is less pronounced. In case of mega cisterna magna, the cisterna magna is large but the fourth ventricle is closed.

Association with other malformations. About one-third of BPCs detected antenatally are associated with

other anomalies, including chromosomal aberrations (in most cases trisomy 21) [34,42].

Risk of chromosomal anomalies. It is significant especially when associated with other anomalies.

Risk of nonchromosomal syndromes. It is significant when associated with other anomalies.

Obstetric management. Fetal karyotyping is mandatory, especially in cases associated with other anomalies, because of the significant risk of chromosomal anomalies. In addition, a thorough anatomic scan should be performed by an expert because of the high risk of association with other CNS and extra-CNS malformations.

Postnatal treatment. In the rare cases associated with ventriculomegaly, the secondary obstructive hydrocephalus may be treated with a cystoperitoneal shunt.

Prognosis, survival, and quality of life. When the BPC is an isolated finding and the karyotype is normal, the outcome is usually good. Intrauterine remission occurs in a significant number of cases, and a normal developmental outcome is reported in nearly 100% of cases.

MEGA cISTEr NA MAGNA

Incidence. Unknown.

Ultrasound diagnosis. It is characterized by a CSF collection in the posterior fossa. The vermis is normal and the fourth ventricle is closed.

Risk of chromosomal anomalies. Relatively high, especially if associated with other anomalies.

Risk of nonchromosomal syndromes. Relatively high, if associated with other anomalies.

Outcome. If isolated, the prognosis is good. Fetuses with MCM associated with abnormal cerebral findings were found to have neurologic sequelae in about one-third of cases.

Definition and anatomy. MCM is defined as a cisterna magna larger than 10 mm. It is characterized by an intact vermis, an enlarged cisterna magna, and a normal-sized fourth ventricle. It has been suggested that the enlargement of the cisterna magna may be secondary to a distension of the BP, which, however, does not displace the cerebellar vermis superiorly [34,35].

Ultrasound diagnosis. On the axial transcerebellar view, a CSF collection is seen in the posterior fossa. The vermis is normal, and the fourth ventricle is closed (Figure 2.35) [35]. In most cases, the torcular and the tentorium are in normal position.

Differential diagnosis. The MCM should be differentiated from other cystic anomalies of the posterior fossa, especially AC. In fact, posterior fossa arachnoid cysts can mimic MCM but mass effect with asymmetric distortion of the cerebellum is usually associated. The presence of a normal vermis, such as in the case of MCM, rules out the possibility of a DWM and isolated vermian hypoplasia. The presence of a closed fourth ventricle and of a nonrotated vermis, such as in case of MCM, rules out the possibility of a BPC.

Association with other malformations. A significant number of associated anomalies have been reported. The most commonly associated anomalies are supratentorial anomalies (i.e., periventricular heterotopia).

Risk of chromosomal anomalies. When associated with other anomalies, it is significant

Risk of nonchromosomal syndromes. When associated with other anomalies, it is significant

Obstetric management. Fetal karyotyping is mandatory, especially in cases associated with other anomalies because of the risk of chromosomal anomalies. In addition, a thorough anatomic scan should be performed by an expert because of the high risk of association with other CNS and extra-CNS malformations.

Postnatal therapy. No treatment is required.

Prognosis, survival, and quality of life. In the absence of associated anomalies, the prognosis is good [34,35]. The vast majority of cases had normal development. However, these data may be biased by the limited follow-up. Fetuses with MCM associated with abnormal cerebral findings (i.e., periventricular heterotopias) were found to have neurologic sequelae, often mild, in about one-third of cases.

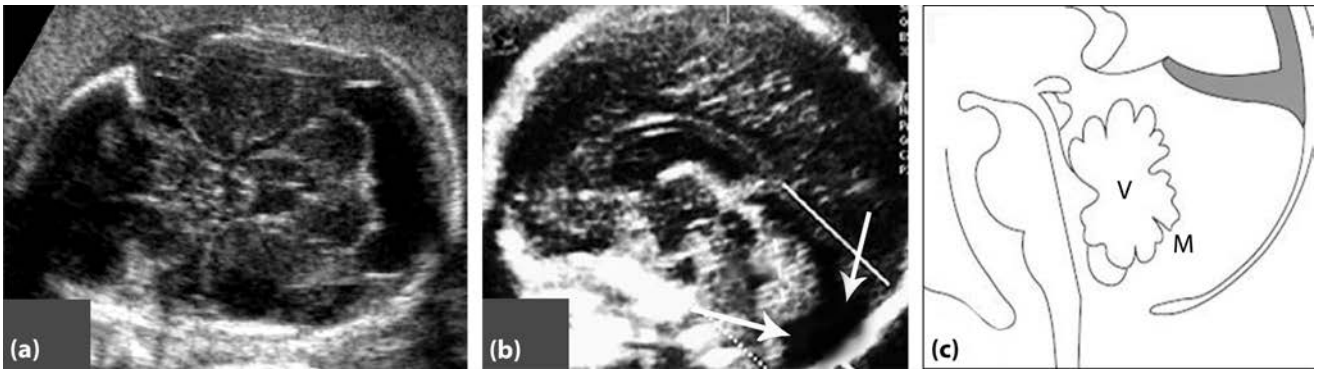


Figure 2.35 Mega cisterna magna. (a) Axial view of the posterior fossa showing enlargement of the cisterna magna; the cerebellar vermis appears intact. (b) Sagittal view of the posterior fossa demonstrating increased size of the cisterna magna (arrows), a closed fourth ventricle, and an intact vermis. (c) Schematic diagram of the same finding; V: cerebellar vermis; M: mega cisterna magna.

VErMIAN hypoplASIA

Incidence. Unknown.

Ultrasound diagnosis. It is characterized, on axial transcerebellar view, by an open fourth ventricle apparently communicating with the cisterna magna. Posterior cranial fossa is not expanded. On median view of the head, the vermis is small and upwardly rotated (usually less than 45°). Tentorium and torcular are positioned normally.

Risk of chromosomal anomalies. High, especially if associated with other anomalies.

Risk of nonchromosomal syndromes. High, especially if associated with other anomalies.

Outcome. Vermian hypoplasia is frequently a part of multiple anomalies and genetic syndromes. When isolated it may be asymptomatic, but precise risk figures are not available.

Definition and anatomy. Vermian hypoplasia, previously referred to as Dandy–Walker variant, is characterized by an isolated small vermis, usually upwardly rotated. It has been suggested that the term hypoplasia should be limited to cases in which the vermis is small but has a normal morphology (all the lobules are present); conversely, the term partial agenesis should be used in those cases in which a part, is absent [34,39]. However it can be difficult to differentiate, by ultrasound, between vermian agenesia and hypoplasia. In addition, hypoplasia or agenesia may affect any part of the vermis. The part of the vermis affected depends on the nature and timing of the insult.

Ultrasound diagnosis. On axial transcerebellar view, an open fourth ventricle apparently communicating with the cisterna magna is seen (Figure 2.36). Posterior cranial fossa is not expanded. On median view of the head, the small and upwardly rotated (usually not exceeding 45°) vermis can be seen [35]. Tentorium and torcular are positioned normally.

Differential diagnosis. The hypoplastic vermis should be differentiated from other posterior fossa anomalies characterized by an open fourth ventricle. The presence of a communication between the fourth ventricle (open fourth ventricle) and cisterna magna associated with a normal vermis is indicative of BPC (see Appendix Table A.11 and A.12). In this case, the rotation of the vermis is mild. The presence of a communication between the fourth ventricle (open fourth ventricle) and cisterna magna associated with a hypoplastic vermis, superiorly displaced tentorium/torcular, and expanded posterior fossa is indicative of DWM. In this case the rotation of the vermis usually exceeds 45° [35].

Association with other malformations. Numerous malformations have been reported to be associated with the vermian hypoplasia. The most commonly associated anomalies are other CNS anomalies including supratentorial anomalies.

Risk of chromosomal syndromes. This is high, especially if associated with other anomalies.

Risk of nonchromosomal syndromes. This is high, especially if associated with other anomalies.

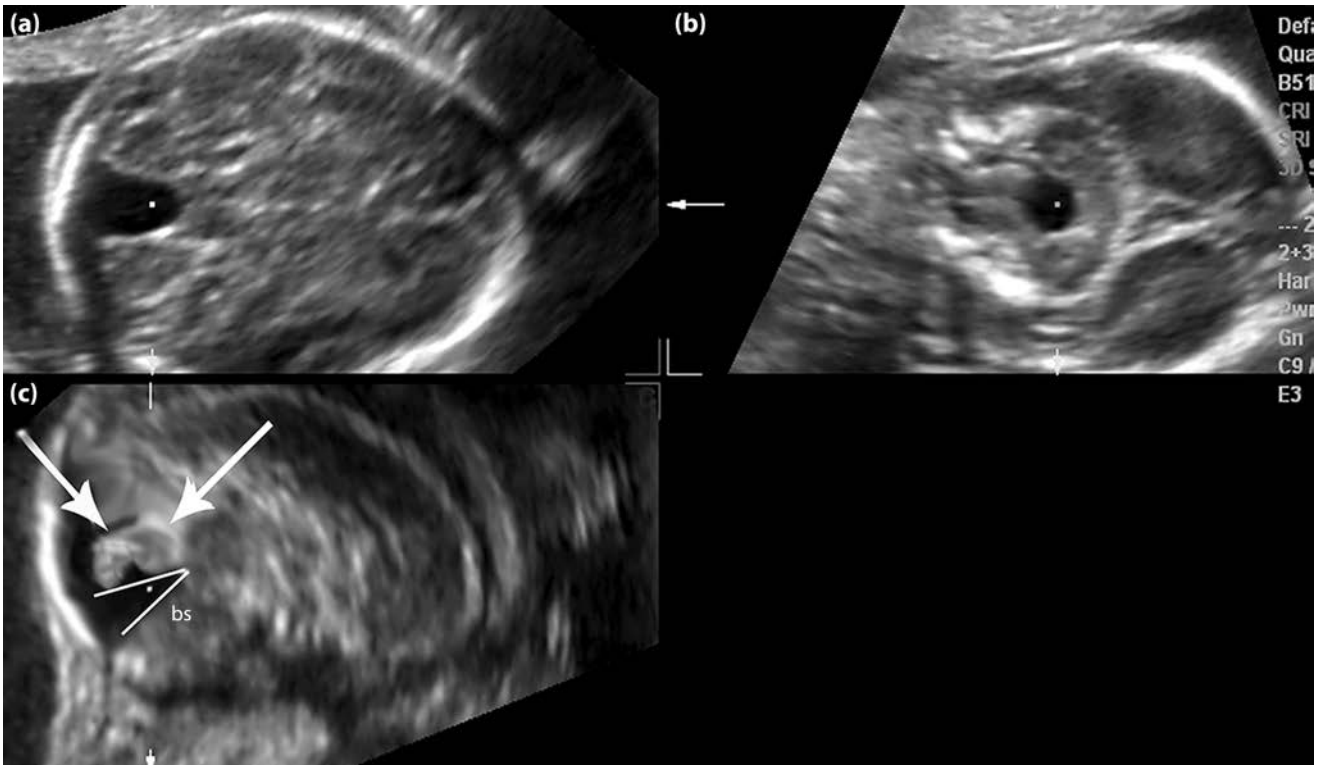


Figure 2.36 Vermian hypoplasia. On the axial transcerebellar view (a), an open fourth ventricle, communicating with the cisterna magna can be seen. (b) on the coronal view, the communication between the cisterna magna and the open 4th ventricle is shown. On the median view (c) of the head, the small and upwardly rotated (not exceeding 45°) vermis can be seen. (bs, brainstem); the arrows indicate the vermis.

In particular, Joubert syndrome is a very severe albeit rare condition featuring vermian hypoplasia in association with dysgenesis of the isthmic portion of the brainstem at the pontomesencefalic junction, a deep posterior interpeduncolar fossa with thick elongated superior cerebellar peduncles. The diagnosis can be made on MRI only, and the typical aspect of the abnormal superior cerebellar peduncles is referred to as "molar tooth sign", evident on axial MRI slices of the brain. Symptoms range from general hypotonia with a froglike posturing, hyperpnea/apnea, ataxia. Colobomas, nystagmus and strabismus are associated.

Obstetric management. Fetal karyotyping is mandatory, because of the high risk of genetic syndromes. In addition, a thorough anatomic scan should be performed by an expert because of the high risk of association with other CNS and extra-CNS malformations.

Postnatal therapy. There is obviously no treatment of the primary vermian lesion.

Prognosis, survival, and quality of life. Vermian hypoplasia is frequently a part of multiple anomalies and genetic syndromes [34,39]. When isolated, it may be asymptomatic but precise risk figures are not available [34,39]

Ar Ach No Id cys T

Incidence. Unknown.

Ultrasound diagnosis. Sonographically, a retrocerebellar arachnoid cyst appears as a sonolucent cystic mass. Compression on the cerebellum may be detected on the midsagittal view, in case of large cysts.

Risk of chromosomal anomalies. Low.

Risk of nonchromosomal syndromes. Low.

Outcome. The overall prognosis is good.

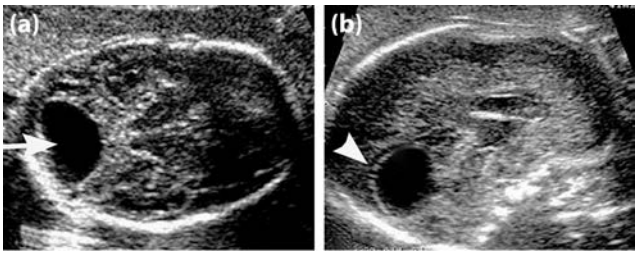


Figure 2.37 Retrocerebellar arachnoid cyst. (a) Axial view of the posterior fossa showing a sonolucent cystic mass. (b) Sagittal view of the posterior fossa showing a large arachnoid cyst.

Definition A retrocerebellar arachnoid cyst is a CSF collection that does not communicate with the surrounding subarachnoid spaces nor with the ventricular system and usually is not associated with brain malformations.

Ultrasound diagnosis. Sonographically, a retrocerebellar arachnoid cyst appears as a sonolucent cystic mass (Figure 2.37). Depending on its size, the cyst may compress and displace the cerebellum. In addition, large arachnoid cysts may obstruct the circulation of CSF, leading to secondary obstructive hydrocephalus.

Differential diagnosis. The AC should be differentiated from other cystic anomalies of the posterior fossa, especially MCM. In fact, posterior fossa AC can mimic MCM but mass effect with asymmetric distortion of the cerebellum is usually associated. In addition, instead of MCM, AC may cause hydrocephaly.

Association with other malformations. This is low.

Risk of chromosomal anomalies. This is low.

Risk of nonchromosomal anomalies. This is low.

Obstetric management. Management should be conservative with US monitoring. Standard obstetric care is advised, unless hydrocephalus/macrocrania occurs. In this case, a Cesarean section should be performed.

Postnatal therapy. Although controversy surrounds the treatment of AC, many Authors suggest using a cystoperitoneal shunt for decompression of symptomatic cysts [32].

Prognosis, survival, and quality of life. The overall prognosis is good, and the condition does not need treatment if compression on the cerebellum is absent or asymptomatic. In contrast, if the cyst is large and symptomatic, it may require surgery [32].

No Ncys TIc pos TEr Ior Foss A MALFor MATIo Ns

A large number of heterogeneous syndromes, some of which have a genetic background, fall into this category.

Pathologically, these conditions are mainly characterized by vermian dysgenesis (rhombencephalosynapsis, etc.) or by a small posterior cranial fossa (Arnold-Chiari malformation). Some, but not all, of the former conditions may be detected on US, while most of those in the second group are evident on the axial transcerebellar view, due to a very small posterior fossa, as in the Chiari II syndrome. However, it should be kept in mind that when global decreased cerebellar biometry is present, it requires that attention be focused on the brainstem anatomy in order to differentiate isolated cerebellar hypoplasia from pontocerebellar hypoplasia.

Cerebellar hypoplasia can be primitive or secondary to a chromosomal anomaly, infection, or a polymalformative syndrome.

r ho MBENc Eph ALosy NAps Is (r Es)

Incidence. Rare.

Ultrasound diagnosis. Hypoplastic cerebellar hemispheres fused on the midline.

Risk of chromosomal anomalies. Low.

Risk of nonchromosomal syndromes. Relatively high.

Outcome. Outcome is poor.

Definition and anatomy. This rare malformation is characterized by vermian agenesis associated with fusion of the cerebellar hemispheres, peduncles, and dentate nuclei. Kinking of the brainstem is often present [32].

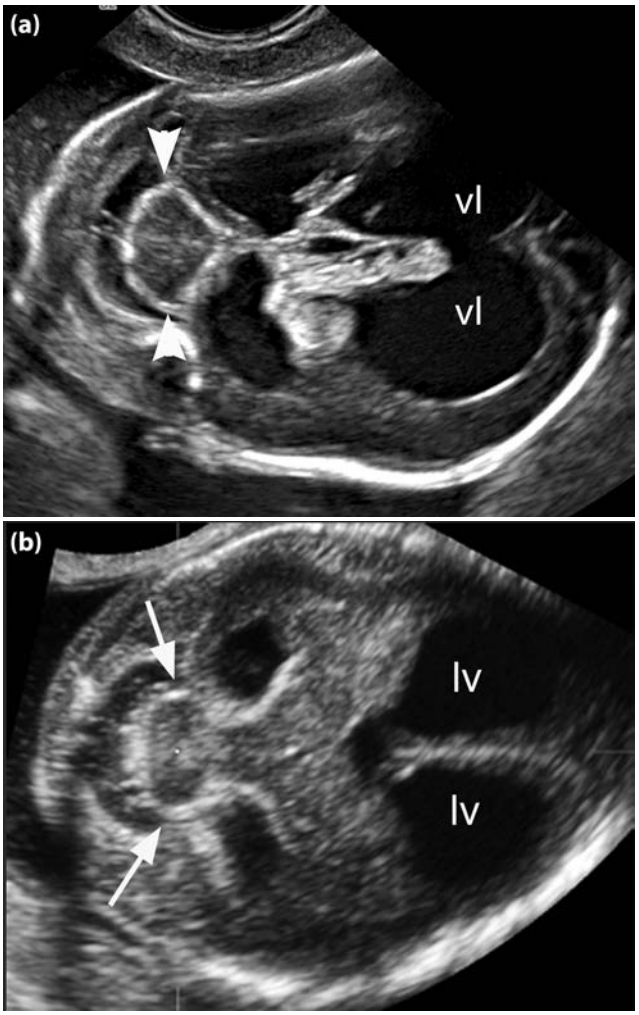


Figure 2.38 (a) Rhombencephalosynapsis. The vermis is absent and the hypoplastic cerebellar hemispheres are fused on the midline (arrowheads); the cerebellum has a rhomboid shape. Ventriculomegaly can be seen. vl: lateral ventricles. (b) Pontocerebellar hypoplasia. The cerebellum size is exceedingly small, but its shape is regular(arrows). lv: lateral ventricle.

Ultrasound diagnosis. On the axial transcerebellar view, the vermis is absent and the hypoplastic cerebellar hemispheres are fused on the midline. The posterior fossa is small (Figure 2.38), and associated supratentorial abnormalities—absent septum pellucidum, abnormal gyration, and hydrocephalus—may be present.

Differential diagnosis. Rhombencephalosynapsis should be differentiated from DWM. In DWM, a small upwardly rotated vermis is usually present and the brainstem is normal. Also, RES should be differentiated from ponto-cerebellar hypoplasia, because both entities can be associated with early onset severe obstructive hydrocephalus. However, in the former—on the axial view—the cerebellum has a rhomboid shape, due to the absence of the vermis; on the contrary, in pontocerebellar hypoplasia the shape of the cerebellum is regular, but the size is exceedingly small (Figure 2.38b)

Association with other malformations. Supratentorial anomalies including hydrocephaly are often present.

Risk of chromosomal anomalies. This is low.

Risk of nonchromosomal anomalies. This is relatively high.

- *Gomez–Lopez–Hernandez syndrome*: look for ► look for RES + turricephaly and facial anomalies.

Obstetric management. A thorough anatomic scan should be performed by an expert because of the high risk of association with other CNS anomalies.

Prognosis, survival, and quality of life. This is commonly poor, with most affected patients dying in childhood.

chIAr I II MALFor MATIo N

Incidence. 1 in 1000 live births.

Ultrasound diagnosis. Frontal scalloping, which is responsible for the "lemon sign" and obliteration of the cisterna magna, with abnormal curvature of the cerebellar hemispheres (the "banana sign"). Open spina bifida is invariably present.

Risk of chromosomal anomalies. Low.

Risk of nonchromosomal syndromes. Chiari II malformation represents per se a syndromic condition.

Outcome. See "Open spina bifida"

Definition and anatomy. This malformation is characterized by a small posterior fossa with downward displacement of the vermis, the brainstem, and the fourth ventricle into the foramen magnum or even into

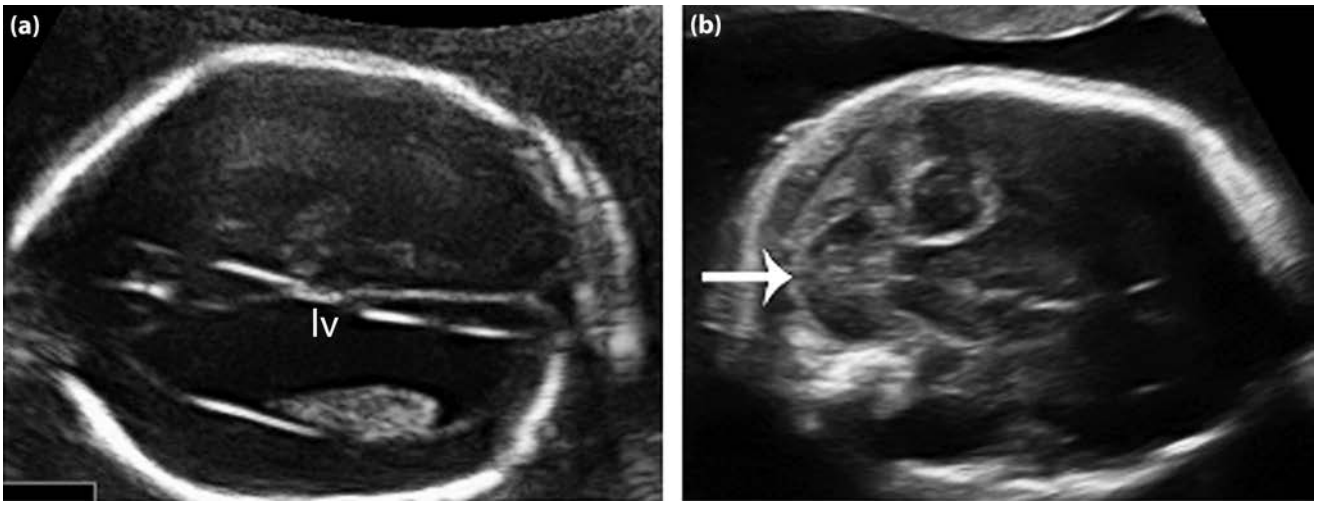


Figure 2.39 Chiari II malformation. (a) Axial view of the fetal head showing moderate ventriculomegaly (lv: lateral ventricle) and frontal scalloping (lemon sign). (b) The cerebellum is banana-shaped (arrow) as it wraps around the midbrain. The cisterna magna is obliterated.

the cervical spinal canal. An open spinal dysraphism is constantly associated [32].

Pathogenesis. Embryologically, during the fourth week, closure of the neural tube (day 25, posterior neuropore) results in an accumulation of ependymal fluid and dilatation of the three cerebral vesicles. If the closure of the neuropore fails (myelomeningocele), the physiologic dilatation of the rhombencephalic vesicle is impaired, and this, in turn, determines a small posterior fossa.

Eventually, the brainstem and the cerebellum, which have normal growth, are no longer contained in the small posterior fossa and herniate through the cervical canal behind the upper cervical cord; the cerebellum surrounds the brainstem and compresses the collicular plate.

Ultrasound diagnosis. In the second trimester, the US findings indicating the presence of the Chiari II malformation are frontal scalloping, which is responsible for the lemon sign (Figure 2.39), and obliteration of the cisterna magna, with abnormal curvature of the cerebellar hemispheres (the banana sign) (Figure 2.39b). In addition, moderate-to-severe ventriculomegaly develops in most cases (70%) during the second trimester, and worsens in the third trimester (Figure 2.39a). In the third trimester, US examination of the fetal posterior fossa is limited by increased calvarial mineralization; with this limitation, the cerebellum is often not visible, while the classic lemon sign is less reliable, being present only in up to 50% of cases.

Association with other malformations. See "Spina bifida"

Risk of chromosomal anomalies. This risk is relatively low.

Risk of nonchromosomal syndromes. Chiari II malformation represents per se a syndromic condition.

Obstetric management. See "Spina bifida"

Postnatal therapy. See "Spina bifida"

Prognosis, survival, and quality of life. See "Spina bifida"

ANo MALIEs o F NEUro NAL pro LIFEr ATIo N ANd M IGr ATIo N ANd o F c or TIc AL o r GANIz ATIo N

Any event that is able to alter neuronal proliferation, migration, or cortical organization can cause a cerebral cortex malformation. Neuroblast proliferation starts in the seventh week of gestation in the subependymal region around the walls of the lateral ventricle. This proliferation is particularly active between 13 and 26 weeks' gestation. After 26 weeks, the volume of the germinal zone rapidly decreases. Neuronal migration to the cerebral cortex starts around the eighth week and is completed by 20–24 weeks' gestation; glial cell migration continues until after birth. During this period, the neurons migrate from the germinal matrix

within the periventricular zone, on radial glial guides, toward the pial surface. Waves of migrating neuroblasts lead to the formation of a superficial cortical plate separated from the deep germinal layer by an intermediate zone containing concentric migrating cells. The migration waves form an "inside-out" six-layered cortex, in which the first wave of migrating neuroblasts forms the deepest cortical layer, while the later waves constitute the most superficial layer.

At the same time, the intermediate zone increases in width and forms the white matter. Recently, it has been shown that not all cerebral cortical neurons are generated in the germinal zones of the dorsal telencephalon and migrate radially to the developing cortex; in fact, a not insignificant number of cortical interneurons are generated in the lateral, medial, and caudal ganglionic eminences and migrate tangentially into the cerebral cortex. In addition, recent reports have made it clear that radial glia are much more active participants in cortical development. Indeed, radial glia are neuronal and glial precursors as well as guides and may, as well, have a role in orchestrating the entire migration process. Myelination, in contrast, starts only after birth. Gyration and sulcation occur during neuronal migration and continue until after birth. In this section, we describe the main *malformations of cortical development*. These are classified into three basic groups, based on the stage at which the developmental process is likely disturbed [43]. Group I (abnormal neuronal and glial proliferation/apoptosis) comprises microcephaly, megalencephaly, and cortical dysgenesis with abnormal cell proliferation. Group II (abnormal neuronal migration) includes various types of heterotopia and lissencephaly. Group III (abnormal postmigration development) includes polymicrogyria and schizencephaly, focal cortical dysplasia, and post migration microcephaly [43].

MIcroc Eph ALy

Incidence. 1 in 6250–8500 live births.

Ultrasound diagnosis. An HC below three standard deviations from the mean of the gestational age is considered a reliable indicator of microcephaly. A "slanting" forehead on the midsagittal profile view represents an additional sign.

Risk of chromosomal anomalies. Relatively high.

Risk of nonchromosomal syndromes. high.

Outcome. Outcome depends on etiology and association with other anomalies. In the isolated form, the severity of mental delay increases with the degree of impairment of HC.

Definition Microcephaly is defined as a small HC, that is more than three standard deviations below the mean for postnatal or gestational age. It is commonly characterized by a small size of the brain.

It can be divided into two major categories: primary (or genetic) and secondary (or nongenetic). Acquired microcephaly is presumed to result from brain injury, such as that associated with hypoxic-ischemic injury, intracranial infection, or metabolic disease; head size is initially normal but decreases as a result of brain injury. Primary microcephaly was originally described as a congenitally small but architecturally normal brain, with affected patients having nonprogressive mild mental retardation. As the interest in primary microcephaly and its genetic causes has grown, many such patients have been studied with MR imaging and have been found to have abnormalities of the cerebral cortex, characterized by a reduced number of gyri and shallow sulci [43,44]. This subgroup is referred to as having simplified gyral pattern microcephaly with simplified gyral pattern (MSG).

It must be kept in mind that the term "simplified gyral pattern," most often used to describe a reduced number of gyri and shallow sulci with a normal cortical thickness, can be confusing because other terms are sometimes used to describe malformations with too few gyri and too shallow sulci: lissencephaly, pachygyria, and microlissencephaly. However, these malformations result from different causes and developmental periods.

Although it is unclear whether primary microcephaly (with normal sulcation) and MSG are part of a phenotypic continuum, it is clear that microcephaly has heterogeneous clinical, radiologic, and genetic features.

Several reports have suggested that patients with MSG may have more severe mental retardation, neurodevelopmental delay, and associated CNS malformations than those with primary microcephaly.

The incidence of microcephaly varies between 1 in 6250 and 1 in 8500 births, and it increases during the first year of life.

Etiology and pathogenesis. Microcephaly is believed to result from decreased neuronal and glial proliferation/increased apoptosis [43]. A distinct group of microcephaly is characterized by patients born with normal to slightly small head size and developing severe microcephaly in the first one to two years after birth. They form a separate group designated postmigrational microcephaly [43]. Hence, the etiology of microcephaly is heterogeneous.

Primary microcephaly should be differentiated from microcephaly secondary to environmental insults. Primary microcephaly may be inherited with an autosomal recessive, or dominant or an X-linked pattern.

More than one hundred distinct familial syndromes characterized by microcephaly have been documented, with a significant number of these estimated to be genetic. Recent studies show that many of the proteins that are mutated in primary microcephalies localize to centrosomes for at least part of the cell cycle.

Ultrasound diagnosis. The main issue regarding the prenatal diagnosis of microcephaly is its difficult , due to the fact that microcephaly is of late onset in most cases, with the impairment in head growth becoming clearly evident in the third trimester or even only after birth. At present, the sonographic diagnosis is mainly based on biometric parameters. The most important diagnostic criterion is a HC below 3 standard deviations from the mean. Other biometric parameters, such as HC/abdominal circumference (HC/AC) ratio and HC/femur length (HC/FL) ratio, may be useful in doubtful cases (Figure 2.40, Appendix Table A.9). A nomogram of the normal dimensions of the frontal lobes has been proposed as a potential tool for the prenatal diagnosis of microcephaly, in view of the fact that the anterior lobes seem to be primarily involved in this malformation. Microcephaly also leads to a disproportion between the skull and the face, which is also due to the fact that the frontal lobes are severely hypoplastic; this causes a typical sloping forehead, which is present in most cases of this defect, especially from the late second trimester onward (Figure 2.41). Among the various signs described in some but not all cases of microcephaly are large subarachnoid spaces and an absent or reduced flow of the anterior cerebral arteries. As mentioned above, in a subgroup of fetuses affected by primary microcephalies, the gyral pattern is abnormal. However, the degrees of cerebral gyration and sulcation are difficult if not impossible to assess with prenatal US.

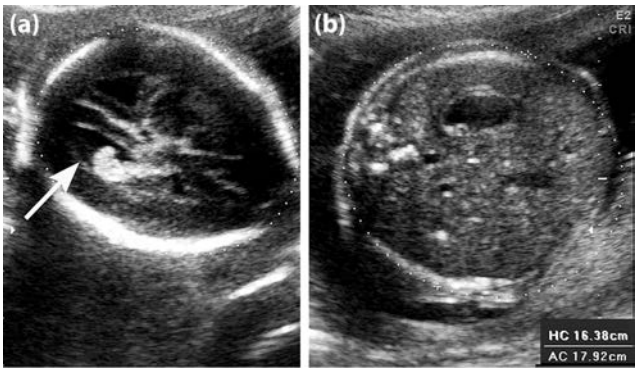


Figure 2.40 Microcephaly. (a, b) The sonographic diagnosis of microcephaly is based mainly on biometric parameters such as an HC/AC ratio below the first percentile. The arrow indicates the distal lateral ventricle

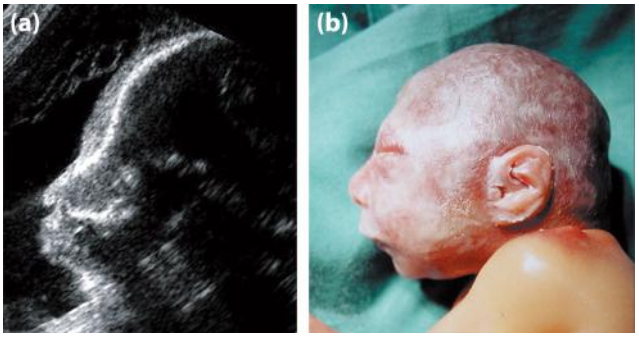


Figure 2.41 Microcephaly. (a) Side view of a 24-week fetus showing a typical sloping (or slanting) forehead. (b) Corresponding photograph after birth.

Differential diagnosis. This includes mainly the craniosynostoses, in which an indentation of the cranial outline is present.

Associated anomalies. Microcephaly is often associated with lissencephaly, ACC, and holoprosencephaly.

Risk of chromosomal anomalies. This risk is relatively high.

Risk of nonchromosomal syndromes. This risk is high. The syndromes most commonly associated with microcephaly are [16]:

- *Meckel–Gruber syndrome*: look for ► *microcephaly* + encephalocele + polydactyly + polycystic kidney + other CNS anomalies;
- *Walker–Warburg syndrome*: look for ► *microcephaly* + eye anomalies (microphthalmia and cataract) + CNS anomalies (lissencephaly, midline anomalies, and cephalocele);

- *Miller–Dieker syndrome*: look for ► *microcephaly* + lissencephaly + congenital heart disease + facial anomalies + polydactyly;
- *Smith–Lemli–Opitz syndrome*: look for ► *microcephaly* + genitourinary defects;
- *Seckel syndrome*: look for ► *microcephaly* + arachnoid cysts + intrauterine growth restriction + facial anomalies.

The empiric recurrence risk of microcephaly is 10%. In syndromic cases, the recurrence risk is that of the underlying syndrome.

Obstetric management. When microcephaly is suspected or diagnosed, it is necessary to assess brain structures carefully in order to rule out associated brain anomalies. In addition, a thorough anatomic scan should be performed by an expert, because of the association with extra-CNS anomalies. Karyotyping should also be performed, because of the relatively high risk of chromosomal anomalies. Finally, the high association rate with genetic forms supports the need for an accurate familial analysis.

Postnatal therapy. Treatment is only possible for microcephaly if it is due to craniosynostosis.

Prognosis, survival, and quality of life. The prognosis of microcephaly depends on the etiology, the associated anomalies, and the size of the head/brain. When microcephaly is isolated, the mental delay increases with the severity of the impairment of HC. However, clinically, microcephaly patients with MSG are more severely affected than those with normal gyral pattern. In addition, an association of the severity of microcephaly with the presence of a callosal anomaly has been reported. The most common signs are mental retardation, seizures, and developmental delay.

hEMIMEGALENc EphALy (hME)

Incidence. Very low.

Ultrasound diagnosis. It is based on asymmetry of the cerebral hemispheres with dilatation of the lateral ventricle on the affected side and a shift of the midline.

Risk of chromosomal anomalies. Low.

Risk of nonchromosomal syndromes. Relatively high.

Outcome. Very poor: severe mental retardation, seizures, and hemiplegia.

Definition HME is characterized by an overgrowth of one cerebral hemisphere, with gyral disorders and white matter gliosis. It can be isolated or associated with several neurocutaneous syndromes. The brainstem and cerebellum may also be affected.

Etiology and pathogenesis. HME is characterized by a primary disturbance in cellular lineage, differentiation, and proliferation, interacting with a disturbance in gene expression of body symmetry, with earlier onset than radial neuroblast migration.

Ultrasound diagnosis. The sonographic diagnosis is based on asymmetry of the cerebral hemispheres, with overgrowth of one cerebral hemisphere, dilatation of the ipsilateral ventricle, and a consequent shift of the midline (Figure 2.42). Gyral anomalies are commonly associated, but are difficult to identify on US. A detailed anatomic scan must be performed in order to detect associated corporeal hemihypertrophy and hamartomatous lesions, which may indicate the presence of an associated syndrome (see below).

Differential diagnosis. The hemisphere asymmetry can also be caused by a brain neoplasm and its mass effect. However, in this case, the tumor mass is easily detected on US.

Associated anomalies. Lissencephaly is frequently associated.

Risk of chromosomal anomalies. This risk is low.

Risk of nonchromosomal syndromes. This is relatively high. The syndromes most commonly associated with HME are [16]:

- *Klippel–Trenaunay–Weber syndrome*: look for ► *hemimegalencephaly* + hemangiomatosis of one or more limbs + soft tissue hypertrophy + cardiac anomalies + kidney agenesis + laryngeal atresia;

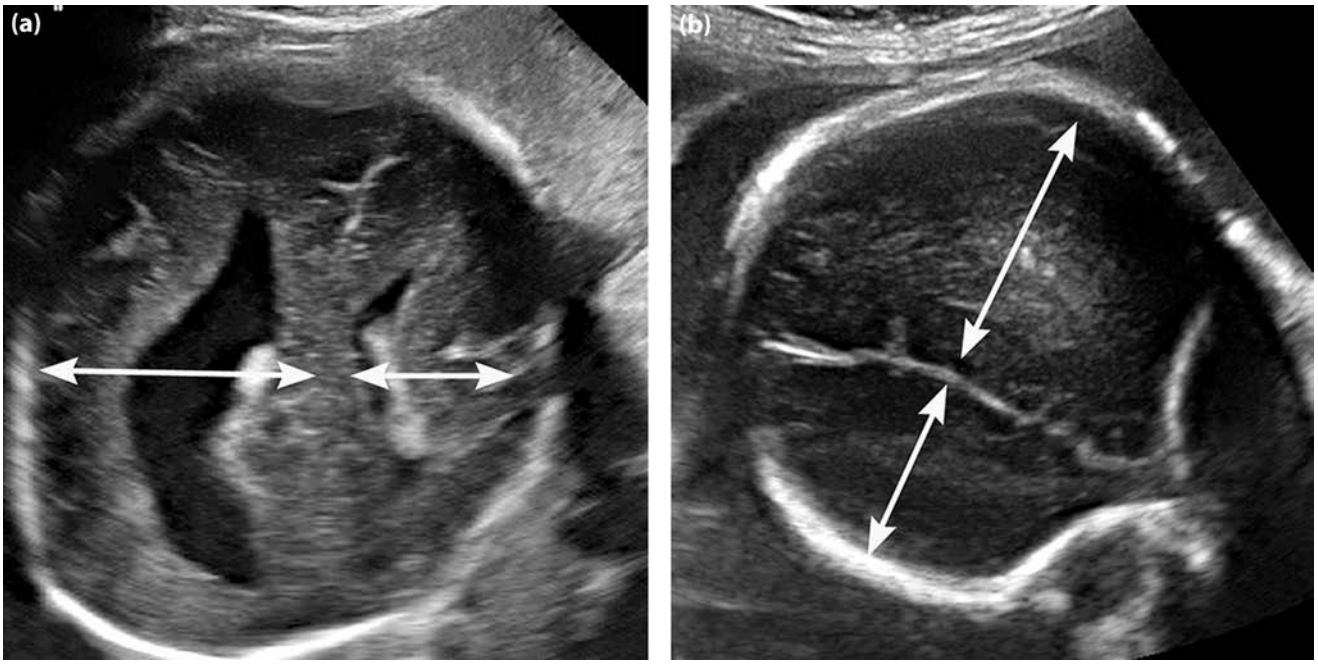


Figure 2.42 Hemimegalencephaly. (a) Coronal scan of the fetal brain showing an overgrowth of one hemisphere and ipsilateral ventriculomegaly. (b) Axial scan of the fetal brain showing a shift in the midline echo, with an overgrowth of one hemisphere arrows indicate hemisphere width.

- *Proteus syndrome*: look for ► *hemimegalencephaly* + partial gigantism of hands and feet + hemihypertrophy + subcutaneous hamartomatous tumors + macrocephaly.

Obstetric management. Considering the low risk and the very poor prognosis of HME itself, fetal karyotyping should be discussed with the parents. In the case of continuation of pregnancy, the perinatal management should also be discussed with the parents, for the same reasons.

Postnatal treatment. The only possible treatment consists of a hemispherectomy of the affected hemisphere. Often, this is the only way to control seizures.

Prognosis, survival, and quality of life. The prognosis is poor, with epilepsy unresponsive to treatment, severe mental retardation, and hemiplegia.

LIss ENc Eph ALy

Incidence. Unknown in the fetus.

Ultrasound diagnosis. In suspected cases, absence of normally present sulci, lack of opercularization of the sylvian fissure, or early abnormal sulcation can be seen. Mild VM is often present.

Risk of chromosomal anomalies. Relatively low.

Risk of nonchromosomal syndromes. Relatively high.

Outcome. Poor in most cases.

Definition The term "lissencephaly" refers to a smooth outer brain surface, characterized by a paucity of gyral and sulcal development. It encompasses a spectrum of gyral malformations ranging from complete agyria to regional pachygyria and includes subcortical band heterotopias [43,45]. Based on both brain imaging and pathology, lissencephaly has been traditionally classified into two distinct groups: classic (cLIS, formerly called lissencephaly type 1) and Cobblestone complex (CBSC, formerly called lissencephaly type 2).

The pattern of cortical brain involvement in cLIS typically is different from what is seen in "cobblestone

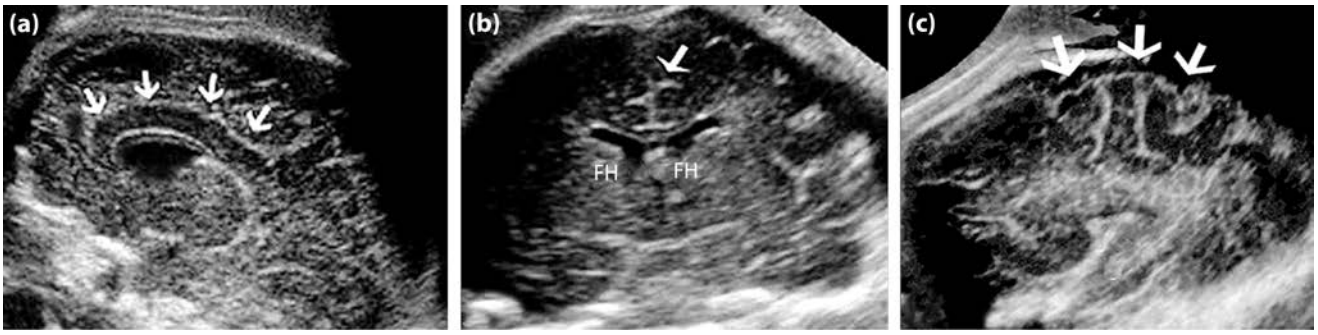


Figure 2.43 Fetal cerebral sulci and gyri. (a, b) Sagittal views of the fetal brain: images of a 30-week fetus showing ultrasound appearance of (a) cingulate sulcus (arrows), above the corpus callosum, (b) Coronal view of the fetal brain: image of a 30-week fetus showing the appearance of the cingulate sulcus (arrow) (FH: frontal horns), and (c) convex sulci (arrows).

malformations". The agyria/pachygyria complex seen in cLIS is mainly the result of incomplete migration of neurons, whereas CBSC is primarily a result of neuroglial overmigration into the arachnoid space. This results in the formation of an extracortical neuroglial layer responsible for the agyria and irregular "cobblestone" surface of the brain and, at the same time, of ventriculomegaly. The underlying mechanism is a disruption of the glia limitans, the outermost layer of the brain [43–45].

Heterotopia refers to arrested migration of normal neurons along the radial glial path between the ependyma of the lateral ventricle and the cortex. According to the location, it can be classified into subependymal, subcortical, and marginal glioneuronal heterotopia.

Etiology and pathogenesis. To date, several genes have been identified as causing or contributing to human cLIS, including LIS1, DCX, RELN, ARX, VLDLR, TUBAIA. The group caused by LIS1 gene mutations includes the Miller Dieker syndrome and shows a four-layered cortex (instead of the classic six-layered one) predominantly posterior with nodular heterotopia in the cerebellum, a normal three-layered cerebellar cortex, and normal to small pons.

Numerous genes have been identified in association with CBSC characterized by an irregularly bumpy and knobbed surface of the brain. Most affected patients have symptoms of congenital muscular dystrophies (CMDs), visual impairment, with CNS involvement. Among these disorders, three phenotypes are well-defined: Fukuyama congenital muscular dystrophy (FCMD), Walker–Warburg syndrome (WWS), and muscle–eye–brain disease (MEB). These phenotypes have been associated with mutations of multiple genes involved in *O*-glycosylation of α-dystroglycan, including *FCMD*, *FKRP*, *POMT1*, *POMT2*, *LARGE*, and *POMGNT1* [43,45].

Ultrasound diagnosis. Prenatal detection of lissencephaly remains a challenge even for the expert, and can be achieved only if the US examination is done from the late second trimester onward. In fact, due to the timing of normal neuronal development, lissencephaly cannot be reliably suspected before week 23–24 of gestation, when some normal gyri and sulci become well-defined

Familiarity with the normal US pattern of development of the fetal sulci (Figure 2.43), and especially of the parieto-occipital fissure and the sylvian fissure/insula (Figures 2.44 and 2.45), is of the utmost importance in allowing suspicion of lissencephaly as early as the late second trimester. In fact, the absence or abnormal appearance of a particular sulcus at the appropriate fetal age should raise suspicion about the possibility of abnormal or delayed cortical development [46]. A sulcus or fissure is first seen as a small dot on the surface of the brain; later, a V-shaped indentation forms and finally it deepens and is visible as an echogenic line that extends into the brain in a Y-shaped configuration. Since mild VM (Figure 2.46) can be the first sign of abnormal/delayed brain maturation, it has been suggested that a follow-up US examination be performed at 24–26 weeks for the assessment of cerebral sulci in fetuses with apparently "isolated" mild VM detected at the mid-trimester scan (19–21 weeks). However, currently, if no associated anomalies are present, the diagnosis is made prenatally in very few cases.

Moreover, although there have been recent reports describing sonographic criteria for the diagnosis of lissencephaly, it must be stressed that cerebral involvement may vary significantly in severity and extension in lissencephaly, and only the most severe forms can be suspected on US (Figure 2.46); milder degrees of cerebral involvement such as subcortical band heterotopia are very difficult, if not impossible, to diagnose. As reported by several authors, gyral anomalies and neuronal heterotopia are the anomalies most commonly missed on prenatal US due to technical limitations and/or to the fact that routine US is not usually performed late in gestation, when gyration and sulcation

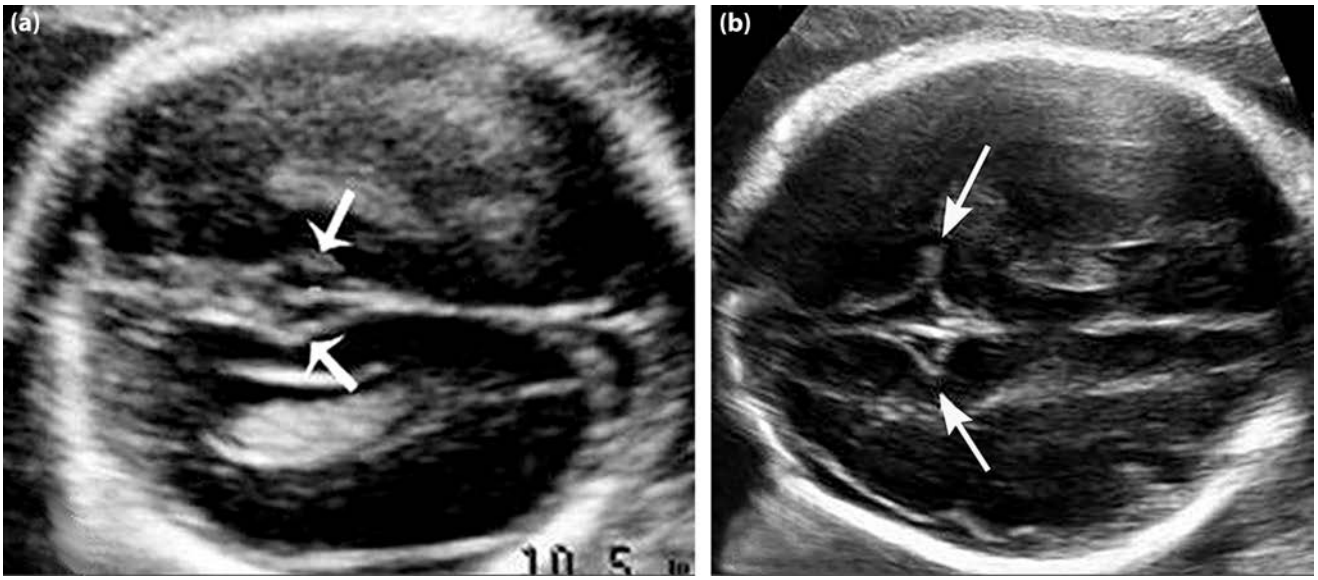


Figure 2.44 Axial views of the fetal brain: images showing ultrasound appearance of the parieto-occipital fissure (arrows) at (a) 20 weeks' and (b) 23 weeks' gestational age.

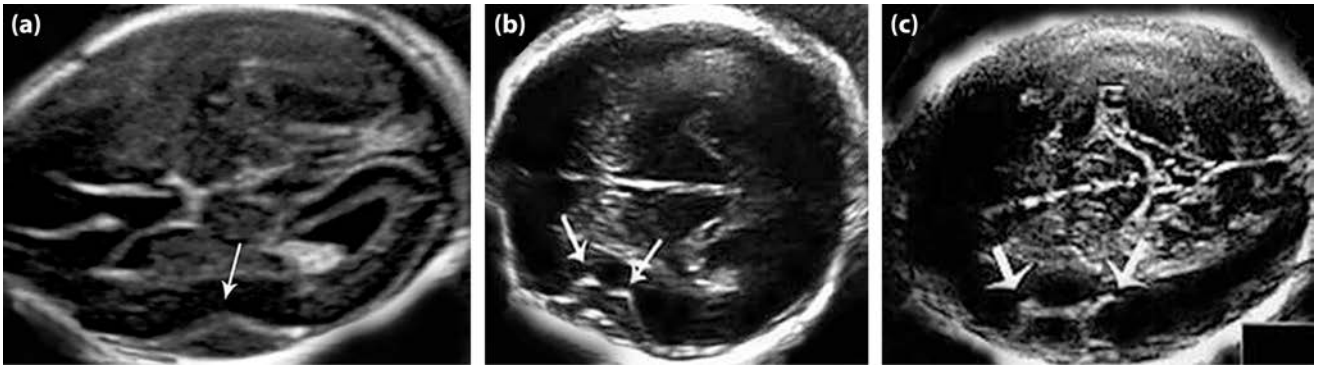


Figure 2.45 Axial views of the normal fetal brain. (a) Ultrasound appearance of a 19-week fetus showing a smooth sylvian fossa without any angularity (arrow). (b) Ultrasound image of a 23-week fetus showing a plateau-like sylvian fossa with obtuse posterior angulation (arrows) at the site of the developing circular sulcus. (c) Ultrasound image of a 26-week fetus showing further development of the sylvian fissure. The temporal operculum is overgrowing the insula and forms an acute angle posteriorly (arrows).

mainly occur. MRI represents a valuable diagnostic tool, being more accurate than US in the detection of gyral disorders. The optimal time for its use appears to be after 23–24 weeks' gestation.

Differential diagnosis. Care should be taken in diagnosing lissencephaly prior to 24 weeks gestation, because a smooth cerebral surface is a normal finding until 20–22 weeks.

Association with other malformations. Lissencephaly can be associated with ACC, DWM, micrognathia, omphalocele, polydactyly, coronary heart disease, urinary defects, and, frequently, polyhydramnios.

Risk of chromosomal anomalies. This is relatively low.

Risk of nonchromosomal syndromes. This is relatively high. The syndromes most commonly associated with lissencephaly are [16]:

- *Walker–Warburg syndrome*: look for ► *lissencephaly* + eye anomalies (microphthalmia, retinal dysplasia and cataract) + CNS anomalies (VM, midline anomalies, brain stem and cerebellar anomalies, and cephalocele);
- *Miller–Dieker syndrome*: look for ► *lissencephaly* + microcephaly + congenital heart disease + facial anomalies + polydactyly;

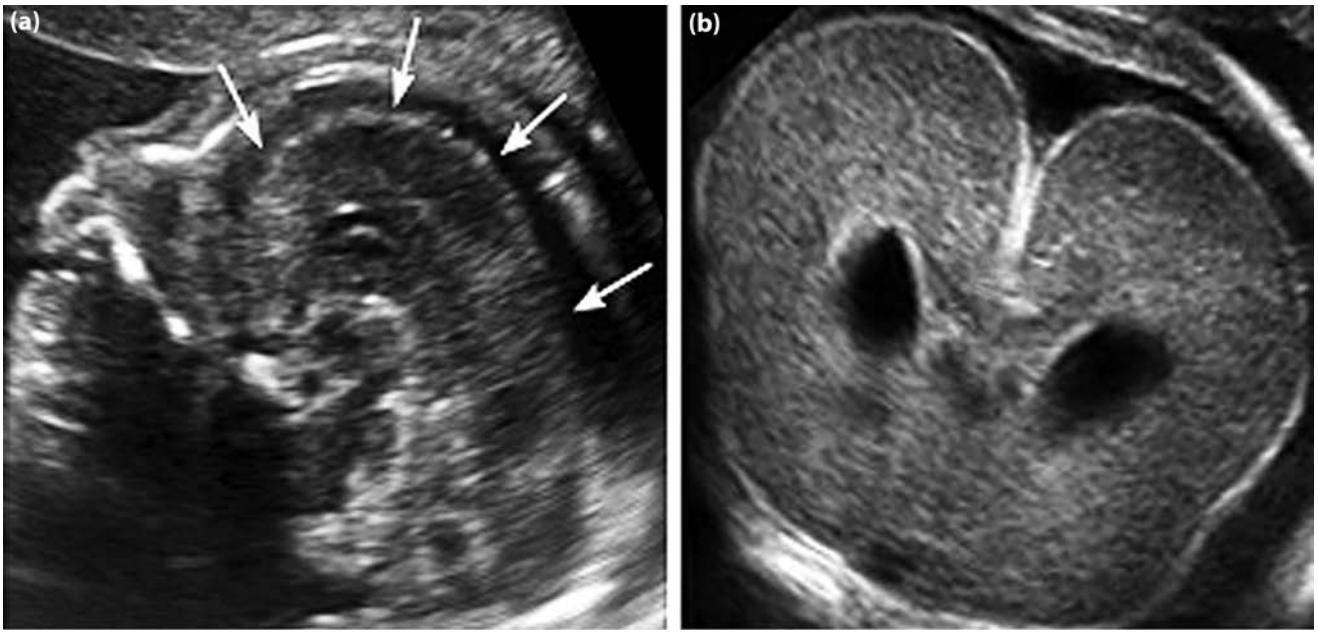


Figure 2.46 Lissencephaly type 1 at 26 weeks' gestation. (a, b) Agyric cortical surface (arrows) is evident. In (b) a mild ventriculomegaly and flattening of sylvian fissure can be seen.

- *Neu–Laxova syndrome*: look for ► *lissencephaly* + microcephaly + DWM + proptosis + diffuse joint contractures + subcutaneous tissue edema + intrauterine growth retardation.

Obstetric management. If abnormal sulcal development is suspected, further investigations should include MRI and genetic evaluation (fluorescence in situ hybridization (FISH) for 17p13.3 deletion (Miller–Dieker region).

Postnatal treatment. No treatment is available.

Prognosis, survival, and quality of life. The prognosis is usually poor, and is characterized by severe mental retardation, hypotonia, convulsions, and death during the first five years of lif The prognosis is less severe in the case of heterotopia. However, in these cases, postnatal outcome cannot be extrapolated from postnatal series, which usually include only symptomatic individuals who are referred to the specialist and ignore those patients who remain asymptomatic.

sch IzENc EphALy

Incidence. Unknown.

Ultrasound diagnosis. Characterized by the presence of CSF-filled clefts of cerebral hemispheres that extend from cortical surface to ventricle (pia mater to ependyma) lined by dysplastic gray matter.

Risk of chromosomal anomalies. Low.

Risk of nonchromosomal syndromes. Low.

Outcome. Outcome is variable in closed forms; poor in most cases of open schizencephaly.

Definition Schizencephaly is characterized by the presence of abnormal clefts in the part of the cerebral mantle that separates the lateral ventricles from the subarachnoid spaces. Clefts are lined by dysplastic gray matter, so that a loss of substance due to acquired causes, such as encephaloclastic porencephaly, can be ruled out. It can be uni- or bilateral, symmetric or asymmetric. Up to 50% of schizencephaly is bilateral; when bilateral, 60% are "open lipped" on both sides. Of the two types of schizencephaly, "closed lipped" schizencephaly shows very thin clefts (fused clefts), while open lipped schizencephaly has clefts filled with CSF and is often associated with VM.

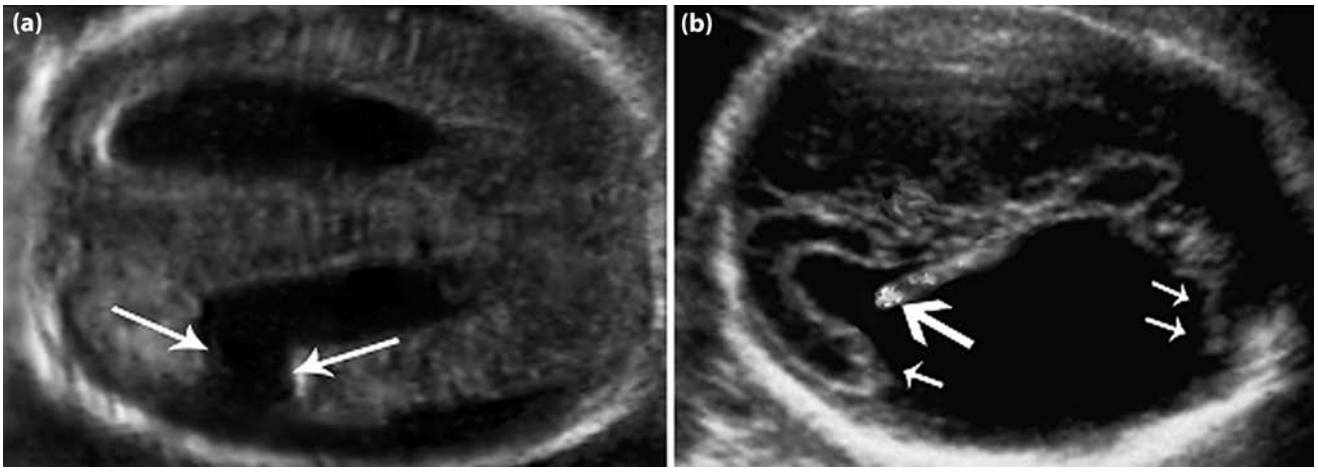


Figure 2.47 Open lips schizencephaly. (a, b) Axial scan of the fetal brain showing full-thickness clefts of the cortex (arrows), connecting the lateral ventricles with the subarachnoid space. In (b) the big arrow indicates the choroid plexus.

Etiology and pathogenesis. Schizencephaly is a malformation secondary to abnormal postmigrational development [43]. Although past work suggested that mutations of EMX2 are a common cause of schizencephaly, recent work has shown that EMX2 mutations are highly unlikely to be a cause of schizencephaly. Furthermore, a large population study found an association with young maternal age and with monozygotic twin pregnancies. In one-third of cases a non-CNS abnormality was present, over half of which could be classified as secondary to vascular disruption. For this reason, schizencephaly seems to be a disorder with heterogeneous causes, many of which are vascular disruptive in origin. It is unquestionably associated with polymicrogyria of disruptive etiology.

Ultrasound diagnosis. Only open lipped schizencephaly has been diagnosed in utero. It is characterized by the presence of a CSF-filled cleft of one or both cerebral hemispheres that extends from the subarachnoid spaces to the lateral ventricles (Figure 2.47). The lateral ventricles are often dilated and clearly visible on the transventricular view. The most common site of the cleft is the sylvian scissure, and it is often associated with septo-optic dysplasia.

Differential diagnosis. Differential diagnosis with a large sylvian porencephalic cyst is extremely difficult. However, type I porencephaly differs from schizencephaly not only in the smaller size of the lesion but also in both the unilaterality and the shape. In fact, schizencephaly is commonly wedge-shaped rather than round or irregular like the porencephalic cyst. Moreover, in schizencephaly, the cortical clefts are lined with gray matter. Due to the relatively frequent association with septo-optic dysplasia, a differential diagnosis with lobar holoprosencephaly and isolated septo-optic dysplasia should be made, since both share the fusion of the anterior horns and the absence of the CSP; the presence of the cleft is typical of schizencephaly.

Association with other malformations. Agenesis of the CC, septo-optic dysplassia, and ventriculomegaly are often associated. Non-CNS abnormalities, including bowel atresia and gastroschisis, have been reported in one-third of cases.

Risk of chromosomal anomalies. This is low.

Risk of nonchromosomal syndromes. This is low.

Obstetrical management. In cases of open bilateral schizencephaly, termination of pregnancy can be offered prior to viability, due to the extremely poor prognosis of schizencephaly.

Prognosis, survival, and quality of life. Unilateral closed schizencephaly is occasionally found incidentally in adults undergoing MRI for other reasons; in these cases, the affected individuals are asymptomatic or have minor symptoms. In contrast, open bilateral schizencephaly is generally associated with seizures and severe mental retardation. In fact, the presence of bilateral clefts and the association with other cerebral anomalies are poor prognostic indicators. The severity of the disease varies with the extension of the cortical lesion. Bilaterality of the anomaly is correlated with more serious psychomotor retardation. When it is associated with septo-optic dysplasia, blindness may also be present. Epilepsy is frequent.

dEsTrUcTIVE LEsIoNs

Independently of the cause, the outcome of a cerebral insult depends mainly on the age at which it occurs and on the severity of the insult itself. The main destructive anomalies are hydranencephaly, porencephaly, and multicystic encephalomalacia. To understand the meaning and the US pictures of these entities, it is necessary to consider that the reaction of the fetal brain to an insult changes according to the gestational age at which it occurs. Until the second trimester, the lesion is characterized by a scarce glial reaction; therefore, the necrotic tissue is completely reabsorbed and the final result is a smooth-walled cyst (porencephaly). In the third trimester, the glial reaction becomes more intense; consequently, the cyst will have irregular walls and small septa (multicystic encephalomalacia).

hydrANENcEphALy

Incidence. It occurs in 1–2.5 of 10,000 newborns.

Ultrasound diagnosis. A huge fluid collection fills the whole cranial cavity, with no recognizable cerebral cortex.

Risk of chromosomal anomalies. Low.

Risk of nonchromosomal syndromes. Low.

Outcome. Very poor.

Definition Hydranencephaly is characterized by a complete or almost complete absence of the cerebral cortex, with the normal brain tissue being replaced by a large fluid collection covered by leptomeninges and dura [32]. The presence of the falx and of the cranial nerves demonstrates that the hemispheres have developed but have subsequently been destroyed. The incidence at birth is 1–2.5 in 10,000.

Etiology and pathogenesis. The most accepted hypothesis to explain this particular lesion is interruption of the blood supply in early pregnancy. In fact, in animal models, this type of lesion can be induced by occluding the carotid arteries. Moreover, congenital infections such as toxoplasma and cytomegalovirus can have a similar effect by causing necrotizing vasculitis with consequent destruction of the cerebral tissue. It should be kept in mind that a number of situations can lead to an impairment of fetal brain perfusion. These include placental, maternal (hypoxia, abdominal trauma, etc.), and fetal (infection and coagulation factor deficits) causes. Finally, the twin–twin transfusion syndrome (TTTS), if severe, may also be responsible for hydranencephaly.

Ultrasound diagnosis. Hydranencephaly is characterized by a huge fluid collection filling the whole cranial cavity, with no recognizable cerebral cortex (Figure 2.48a).

The falx is usually present (Figure 2.48b); the meninges, thalami, basal ganglia, brainstem, and cerebellum may be normal.

Differential diagnosis. This includes alobar holoprosencephaly and severe hydrocephalus. In the former, the thalami are fused and residual cortex is visible.

In severe hydrocephalus, a layer of cortex can usually be seen and the falx is always present, even if it may have ruptured. Color Doppler can contribute to a correct diagnosis by showing absent flow in the anterior and middle cerebral artery in hydranencephaly.

Associated anomalies. In most cases, hydranencephaly is an isolated anomaly, although an association with renal dysplasia and cardiac defects has been reported.

Risk of chromosomal anomalies. This risk is low.

Risk of nonchromosomal syndromes. This is low. The most common syndrome possibly associated with hydranencephaly is:

- Fowler syndrome: look for ► *hydrocephalus/hydranencephaly* + arthrogryposis.

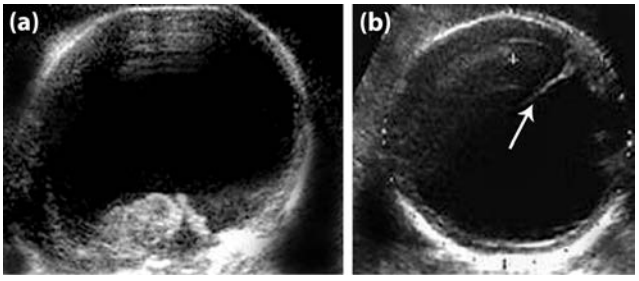


Figure 2.48 Hydranencephaly. (a) The image shows the typical features of hydranencephaly, with a large cystic mass filling the entire cranial cavity. (b) A midline falx is usually present, at least in part (arrow).

Obstetric management. Due to the poor prognosis, termination of pregnancy should be offered prior to viability.

Prognosis, survival, and quality of life. Prognosis is uniformly poor. Hydranencephaly is associated with severe psychomotor delay, nystagmus, optic atrophy, epilepsy, and hypothermia. Death usually occurs within the first two years of life.

por ENc Eph ALy

Incidence. Rare.

Ultrasound diagnosis. Cystic, usually unilateral, lesion communicating with the ipsilateral ventricle and/or the subarachnoid space.

Risk of chromosomal anomalies. Low.

Risk of nonchromosomal syndromes. Low.

Outcome. Outcome depends upon the extension of the lesion. However, in most cases outcome is poor. There can be psychomotor retardation, hemiparesis, and epilepsy.

Definition The term "porencephaly" includes every type of lesion with cavitary character, that is, a fluid-fille area within the brain that commonly communicates with the ventricles and, on very rare occasions, with subarachnoid spaces, or both [47,48]. It involves the destruction of previously developed brain tissue, with subsequent cavity formation. It may be isolated or associated with ventriculomegaly.

Etiology and pathogenesis. Some authors consider two types of porencephaly: type I is due to parenchymal damage followed by liquefaction/reabsorption (*encephaloclastic porencephaly*), resulting from an insult (ischemia, hemorrhage, etc.) during the late second trimester/third trimester. It is the more frequent type and the surface of the defect is often irregular and is not covered by a grey matter. When multiple cystic cavities are found within the brain, the term multicystic encephalomalacia is usually adopted. In this case, the injuries are late gestational or perinatal. Type II (*schizencephalic porencephaly*) is completely cystic with a smooth wall. It is the less frequent type.

Serious hemodynamic alterations can be responsible for the formation of porencephalic cysts, as in TTTS (usually in the recipient twin).

Ultrasound diagnosis. Porencephaly appears as a unilateral cystic lesion, usually communicating with the ipsilateral ventricle (Figure 2.49a) and/or the subarachnoid space. Due to destruction of brain tissue, it does not cause any mass effect. The cystic walls and the content of the cyst may vary according to the gestational age at which the insult occurs. If it is secondary to hemorrhage, it is possible to visualize a hyperechoic focus evolving into an anechoic CSF-filled cyst. When multiple cystic lesions are located in the cortex, the term multycystic encephalomalacia should be used.

Differential diagnosis. Type I porencephaly differs from schizencephaly not only in the smaller size of the lesion but also in its unilaterality and shape. In fact, schizencephaly is commonly wedge-shaped rather than round or irregular. Moreover, cortical clefts are lined with gray matter (detectable by MRI).

A single porencephaly cyst must also be differentiated from multicystic encephalomalacia, which results from a diffuse insult to the brain late in gestation, with a large portion of cortical tissue replaced by multiple and bilateral cystic lesions (Figure 2.49b). Unlike porencephaly, these cysts are separated by hyperechoic strands of glial tissue and may not communicate with the ventricles (Figure 2.49b).

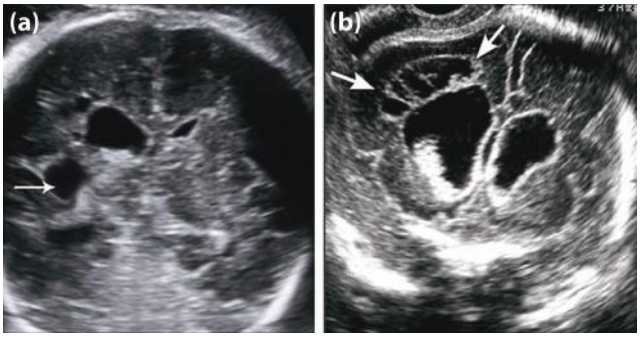


Figure 2.49 (a) Porencephaly. Midcoronal scan of the brain in a 28-week fetus showing a cystic cavity (arrow) in the brain that communicates with the ipsilateral ventricle. (b) Periventricular leukomalacia. Multiple cystic periventricular lesions (arrows) can be clearly seen.

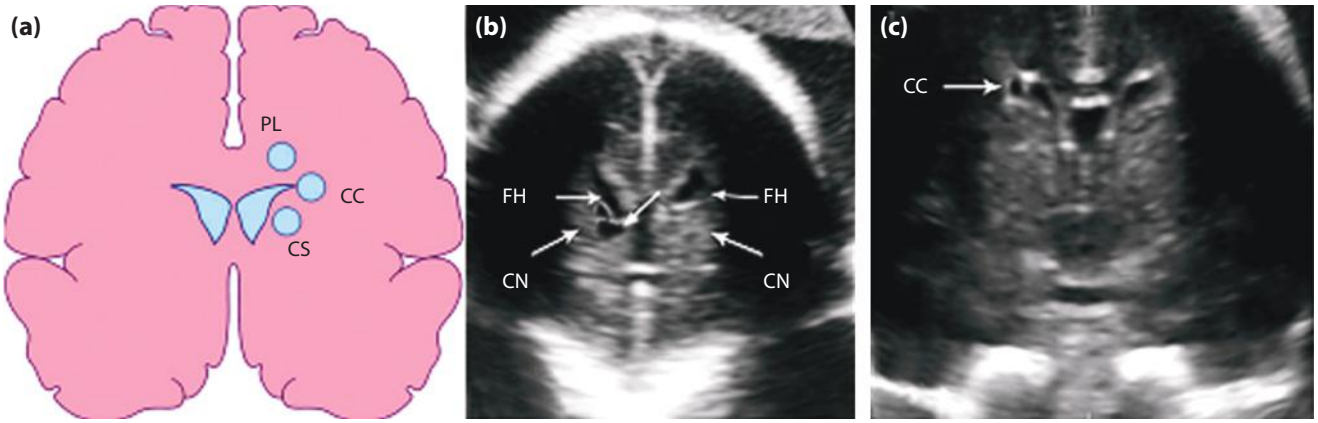


Figure 2.50 (a) Graphical representation of the differential diagnosis between the cystic lesions seen in connatal cyst (CC), subependymal cyst (SC), and periventricular leukomalacia (PL). (b) Subependymal cysts (arrow), located below the external angle and posterior to the foramen of Monro; CN: caudate nucleus; FH: frontal horn. (c) CC or frontal horn cyst, characterized by a cystic area (arrow) adjacent to the superolateral margin of the body and frontal horn of the lateral ventricle.

The difference with arachnoid cysts and tumors lies in the mass effect, which is present in both these entities and absent in porencephaly. *Arachnoid cysts* are usually smooth-walled, asymmetrical, do not communicate with the lateral ventricles, and as opposed to porencephaly, have a mass effect. *Cystic neoplasms* are rare. They usually have a mass effect with both solid and cystic components.

Other periventricular cysts. Depending on the exact location of some periventricular cysts, they may be classified as: (1) connatal cysts or frontal horn cysts: cystic areas adjacent to the superolateral margins of the body and frontal horns of the lateral ventricles (Figure 2.50c); in many cases they represent a normal variant due to approximation of the walls of the frontal horns of the lateral ventricles proximal to their external angles; (2) subependymal cysts: may be acquired, posthemorrhagic cysts or congenital cysts related to germinolysis, located below the external angle and posterior to the foramen of Monro (Figure 2.50b); (3) Periventricular leukomalacia (PVL) (Figure 2.49b) due to degeneration of white matter adjacent to the cerebral ventricles following cerebral hypoxia – ischemia should be considered when it is above the external angle.

Associated anomalies. The most frequently associated anomaly is VM.

Risk of chromosomal anomalies. This risk is low.

Risk of nonchromosomal syndromes. This risk is low. Type I porencephaly may be associated with:

- *Orofaciodigital syndrome [16]*: look for ► *type I porencephaly* + facial anomalies + tongue hamartoma + other CNS anomalies.

Obstetric management. In the less frequent bilateral form, it is necessary to look for other anomalies, whereas the unilateral form is usually isolated, having been due either to ischemia or to hemorrhage.

Prognosis, survival, and quality of life. These depend on the extent of the lesion. However, in most cases expectations are poor; there can be psychomotor retardation, hemiparesis, and epilepsy.

INTr Acr ANIAL hEMorrh AGE

Incidence. Rare; occurs in 1 in 10,000 pregnancies.

Ultrasound diagnosis. *Grade 1*: germinal matrix hemorrhage (usually undetectable prenatally). *Grades 2 and 3*: presence of hyperechoic clots, scattered in the ventricle(s) (grade 2) or filling them (grade 3). *Grade 4*: extension of the hemorrhage to the parenchyma as a hyperechoic area.

Risk of chromosomal anomalies. Low.

Risk of nonchromosomal syndromes. Low.

Outcome. Good for grades 1 and 2; relatively poor for grades 3 and 4 (neurologic sequelae can be present in >50% of cases).

Definition Based on the anatomic location, several types of hemorrhage can be distinguished: subdural, subarachnoid, intraparenchymal, subependymal, and intraventricular [49]. Although rare (1 in 10,000 pregnancies), the most frequent form in the fetus is the subependymal/intraventricular hemorrhage; it is also frequent in the premature neonate. In fact, in premature infants less than 32 weeks and below 1500 g weight, its incidence reaches 30%–40%.

Etiology and pathogenesis. The initial lesion is a bleeding episode in the germinative matrix, which has its maximal extension at about the 26th week, regressing thereafter. This is a highly vascularized region with thin-walled vessels, and because of this anatomic characteristic, very rarely can the hemorrhage be stopped or restrained. In a premature baby, with an immature autoregulatory system for vascular tone and consequently for cerebral blood flo , hypoxia and hypercapnia can cause an increase in blood flo , thereby distending the fragile vascular bed of the matrix. In the fetus, a number of conditions can lead to impairment of fetal brain perfusion. These can be of placental, maternal, or fetal origin. Among maternal causes, the following should be considered: history of recent abdominal trauma, anticoagulant therapy (e.g., warfarin), coagulation disorders, and hyperpyrexia (>38°C). Fetal predisposing conditions include congenital coagulation factor deficiency (mainly factors V and X), cerebral arteriovenous malformations, and severe TTTS. However, the most important determinant of fetal intracranial hemorrhage is represented by an autoimmune disease, namely, fetomaternal alloimmune thrombocytopenia (FMAIT). FMAIT is due to the maternal production of antibodies against paternal antigens present on fetal platelets that are not recognized by the maternal immune system. Maternal exposure to these antigens during pregnancy can lead to the production of various classes of immunoglobulins: the IgG antibodies are small enough to cross the placental barrier and enter the fetal circulation, causing severe thrombocytopenia. Unlike hemolytic disease of the newborn, FMAIT can also occur in the first pregnancy if there is parental incompatibility. Depending on the time of onset, the disease is referred to as FMAIT or NAITP (neonatal alloimmune thrombocytopenia). The former often leads to severe hemorrhage and even intrauterine death during the second or early third trimester, while the latter is the most common cause of severe thrombocytopenia in neonates. Among the various platelet antigens involved in FMAIT, immunization against human platelet antigen (HPA)-1a (P1A1) is by far the most common, accounting for 80%–85% of cases. The importance of recognizing this cause of fetal cerebral hemorrhage lies in the fact that it can be effectively treated, if disclosed prior to the hemorrhagic episode, with intravenous immunoglobulins and intrauterine transfusion of compatible platelets. In some cases, the cause of the hemorrhage remains unknown.

A simple classification divides intracranial hemorrhage into four grades based on severity [49]:

- *Grade 1*: the hemorrhage is limited to the germinative matrix;
- *Grade 2*: the hemorrhage diffuses from the matrix into the ventricle, which fills up with blood without distension;
- *Grade 3*: the hemorrhage distends the ventricles;
- *Grade 4*: there is extension of the hemorrhage to the parenchyma.

Ultrasound diagnosis. The US appearance varies with the size, location, and age of the hemorrhage. Grade 1 hemorrhage is rarely detectable; it can sometimes form a subependymal cyst, which represents an occasional finding Grade 2 and Grade 3 hemorrhage can be recognized by the presence of hyperechoic clots, which may fill the entire ventricle or be scattered within it (Figure 2.51a). It can be limited to one ventricle, but is often bilateral; the third ventricle may also be involved (Figure 2.51b). The ependymal walls appear hyperechoic and irregular due to chemical ventriculitis caused by the blood. The presence of VM can persist even after the disappearance of the clots due to obstruction of the ventricular outlets by the clot debris. Grade 4, which is the most severe form, is characterized by a clot in the parenchyma, which appears as a hyperechoic, usually oval area; this often evolves with time into a porencephalic cyst.

Differential diagnosis. The detection of clots inside the enlarged ventricles contributes to the identification of the hemorrhage as the cause of the VM. However, the most important condition that needs to be distinguished from hemorrhage is represented by cerebral lesions associated with infections—because, in some cases (e.g., cytomegalovirus), the infection itself may be responsible for intracranial hemorrhagic events. The differential diagnosis should rely on an accurate maternal obstetric history and on the results of blood tests, which will show recent seroconversion.

Obstetric management. The first concern is to determine the cause of the hemorrhage. It is, therefore, useful to obtain a careful clinical history to rule out recent trauma.

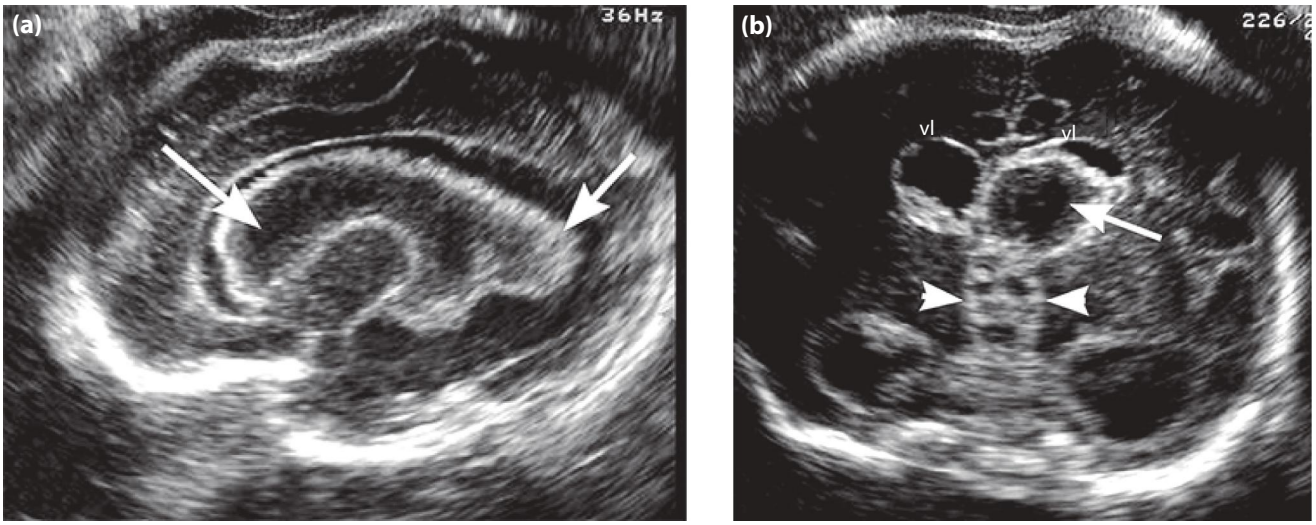


Figure 2.51 (a) Parasagittal view of fetal brain: hyperechoic clot fills the entire lateral ventricle (arrows). (b) Midcoronal view of the fetal brain showing hyperechoic clots (arrows) in both lateral ventricles (vl) and in the third ventricle (arrowheads).

Maternal testing for coagulation disorders/platelet antibodies has to be done in order to detect possible FMAIT or congenital coagulation disorders. In the case of FMAIT, fetal platelets or whole blood transfusion may be needed together with, in the former case, intravenous immunoglobulin (IVIG), with or without steroids. There has been much discussion regarding the best way to deliver a baby with an intracranial hemorrhage, because there are no clear data about the advantages of Cesarean section compared with vaginal delivery in fetuses with mild-to-moderate FMAIT.

Prognosis, survival, and quality of life. Survival is high and with a low percentage of neurologic sequelae for the first two degrees of hemorrhage, especially Grade 1 (there is a good outcome in 95%–100% of cases in Grade 1 and 65%–70% in Grade 2). In Grade 3, significant neurologic sequelae may be present in over 50% of cases, reaching 70%–90% in Grade 4. Grade 4 hemorrhage is also associated with a mortality rate between 30% and 70%. Posthemorrhagic hydrocephalus is a common complication of large hemorrhages. It should be emphasized that a couple having a firs child/fetus affected with FMAIT have a high risk (>80%) of a recurrence in the following pregnancy. To avoid recurrence, early monitoring and treatment with IVIG may succeed in reducing the severity of the recurrence.

spAc E-o cc Upy ING LEs lo Ns

The term "space-occupying lesion" refers to different kinds of disorders with a mass effect, compressing and/or altering normal intracranial anatomy. The best known entities are arachnoid cysts (CSF collections enclosed within layers of arachnoid), cerebral tumors (teratomas, neuroblastoma, craniopharyngioma, etc.), and vascular lesions (aneurysms of the vein of Galen).

Ultrasound diagnosis. The US aspect varies, depending on the type of lesion.

Arachnoid cysts. These are represented by extra-axial sonolucent cysts of variable dimensions, with regular walls, with or without septa (Figure 2.52), and which do not communicate with the ventricular

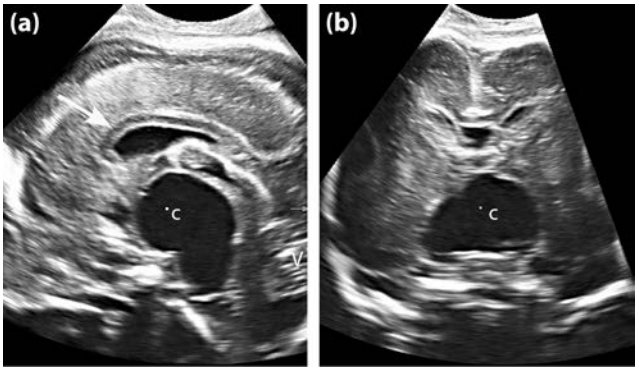


Figure 2.52 Arachnoid cyst: sagittal (a) and coronal (b) views of the fetal brain showing a large fluid prepontine cyst of the cisterna ambiens cyst; note the smooth contour of the cyst and its mass effect.

system [47,48]. The location may be supra- or, more rarely, subtentorial. Compression of the adjacent cerebral structures is evident in larger cysts. Secondary hydrocephalus develops when the foramen of Monro or the aqueduct is blocked by the cyst. Virtually all arachnoid cysts are identified in the third trimester.

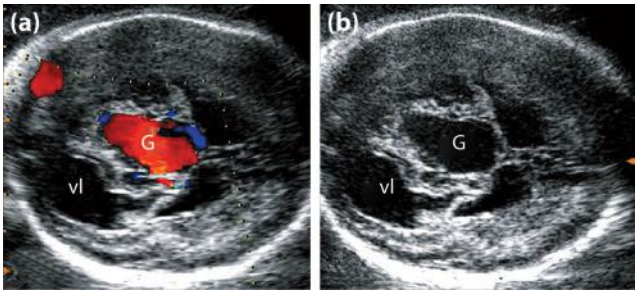


Figure 2.53 (a) Axial view of the fetal brain showing an apparent fluid interhemispheric cyst. (b) Color Doppler demonstrates the aneurysm of the vein of Galen G, aneurysm of the vein of Galen; vl: lateral ventricle.

Aneurysm of the vein of Galen. This consists of an enlarged midline vascular structure, extending from the quadrigeminal plate cistern posteriorly toward the occiput, showing typical turbulence on color Doppler (Figure 2.53). It may be associated with secondary hydrocephalus due to compression of the aqueduct and with high-output heart failure due to the arteriovenous fistula.

Cerebral tumors. The tumor has a predominantly solid or mixed echostructure, with irregular contours. The localization is more frequently supratentorial. Tumor growth is rapid, often leading to macrocrania, which may be associated with signs of disruption of the normal intracranial anatomy and possible secondary hydrocephalus (Figure 2.54). Polyhydramnios may

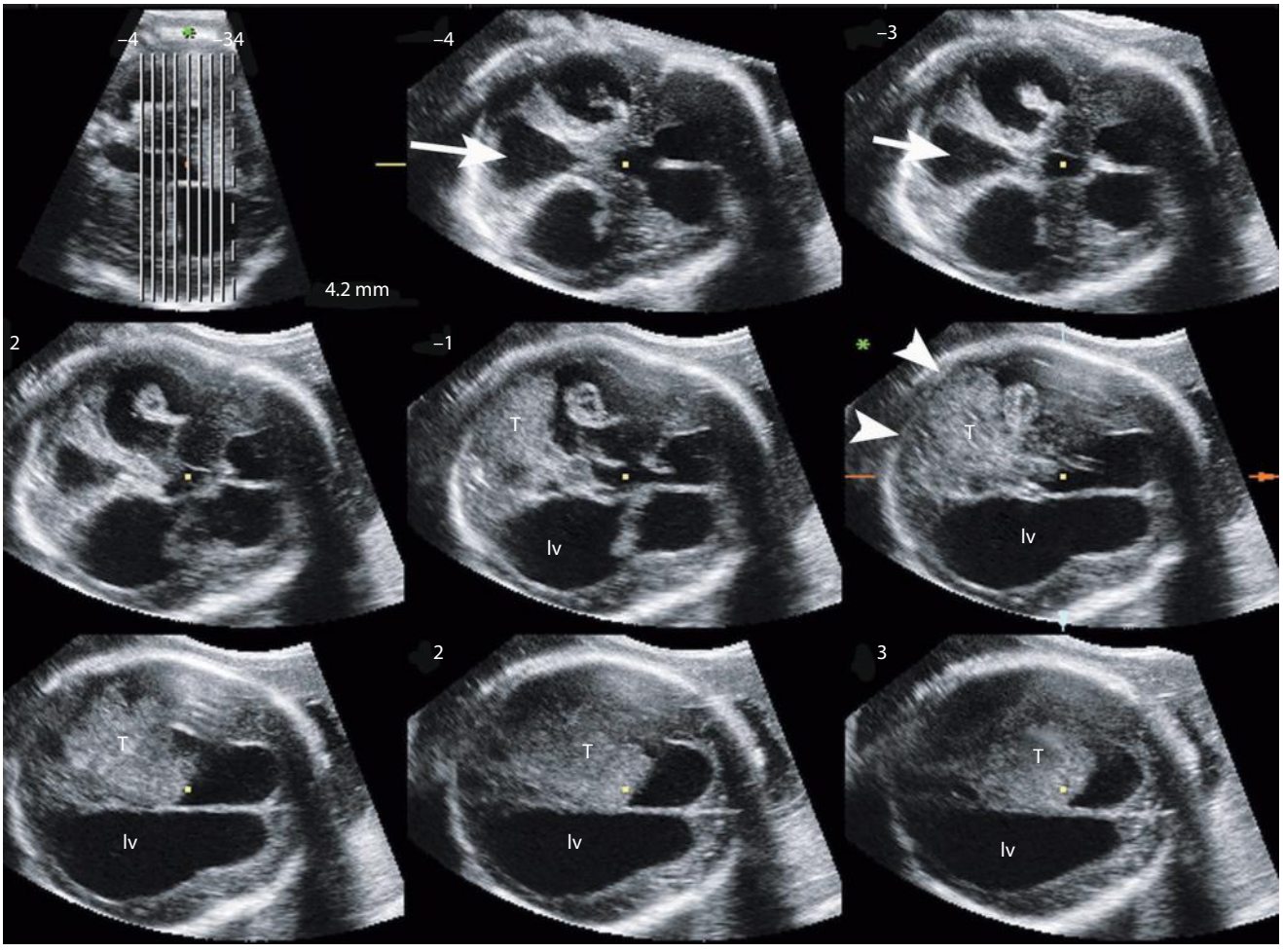


Figure 2.54 Tomographic ultrasound imaging (TUI). Carcinoma of the right choroid plexus at 35 weeks' gestation. The image shows the large malignant tumor (T) infiltrating the brain posteriorly (arrowheads) with secondary hydrocephalus; LV: lateral ventricles; arrow: fourth ventricle. The multi-slice, tomographic imaging allows the extension of the tumor and its relationship with the surrounding anatomic structures to be assessed on a single panel of images.

also be associated. According to the site of the tumor, a preliminary distinction between choroid plexus papilloma/papillocarcinoma (intraventricular), craniopharyngioma, and the other varieties (including teratoma, astrocytoma, and others) can be made. The most frequent brain tumor in utero is teratoma.

Prognosis, survival, and quality of life. These depend on the type of lesion. In particular, arachnoid cysts may be left in place, if asymptomatic, or be surgically removed or shunted if there are seizures or epilepsy or hydrocephalus. With regard to the relationship between location and prognosis, temporal cysts have the best prognosis, while subtentorial cysts in the posterior fossa are associated with the worst outcome. Aneurysms of the vein of Galen are associated with significant neonatal mortality, especially if cardiac failure is already evident in utero. An endovascular approach with embolizing agent and repeated procedures may provide a good outcome, especially if the anatomy of the lesion is favorable and if cardiac failure has not yet developed. The prognosis of cerebral tumors is generally poor, and depends on their histology and size.

NEUr AL TUBE dEFEcTs

The embryonic process that leads to the development of the neural tube—the precursor of the brain and spine—is called neurulation. The two phases of this process, primary and secondary neurulation, occur respectively during the weeks 3–4 and 5–6. In the first, the brain and the neural tube form from the cranial region to the upper sacral level, while in the second the distal sacral and coccygeal regions are formed. The failure of neurulation at any stage leads to the formation of a neural tube defect (NTD). In particular, approximately 18 days after conception, the neural plate forms a central (neural) groove and bilateral neural folds. From the cranial end of the neural tube the three components of the brain will form (forebrain, midbrain, and hindbrain); if the neural tube does not close at this level, anencephaly will occur. Along the same lines, the caudal end of the neural tube becomes the spinal cord, and a failure in the closure of the posterior neuropore results in spina bifi a.

The vertebral column forms around the cord from the sixth week proceeding with ossification during the following two weeks. Each vertebra presents three primary ossification centers, one at the level of the vertebral body and two in the neural arch, at the base of the transverse processes. The ossification process starts at the thoracolumbar junction and progresses cephalad and caudalad.

Ultrasound approach and scanning planes. Using two-dimensional US, the views of interest for screening and diagnosis of spina bifida and other NTDs include cranial and spinal planes.

Fetal Head. The planes of interest, as far as the recognition of NTD, have been described in the first section of this chapter.

Fetal Spine. The screening examination is carried out with two-dimensional US, whereas expert, targeted examination may benefit from the use of three-dimensional US. With the former, which represents the technique of choice, the spine and the single vertebrae can be studied in detail with sagittal, axial, and coronal views (Figure 2.55). If an abnormal intracranial anatomy, including banana sign and obliterated cisterna magna (indirect signs of open spina bifida) is present, a full detailed evaluation of the fetal spine, by axial, coronal, and sagittal views, is required. However, a full detailed evaluation of the fetal spine from every projection is not a part of the basic examination; in fact, with normal intracranial anatomy, only coronal and sagittal sections of the fetal spine are required. The axial plane (Figures 2.55 and 2.56) shows the three ossification centers of the vertebra. As for the sagittal views, it should be emphasized that, only the "midsagittal" view (Figure 2.56) of the spine allows a detailed assessment of the spinal cord and the cauda equina because in the mid-trimester fetus the spinous process of the vertebrae is unossified

In addition, it should be remembered that in the normal fetus, the conus medullaris reaches the sacrum at 18 weeks and lower lumbar vertebrae at 21–22 weeks. Conversely, the ossification process progresses caudalad, with a sacrum that still can be incompletely ossified up to 25 weeks' gestation.

Three-dimensional imaging is able to provide the sonologist with even more self-explanatory images of the fetal spine and rib cage. The main difference between two-dimensional US and three-dimensional US is that a volume data set of the whole spine is acquired with three-dimensional US. After acquisition, the sonologist can choose to navigate through this volume using multiplanar correlation imaging or by applying in postprocessing (using his/her laptop) a series of rendering modalities to highlight the skin contour or the bony skeleton.

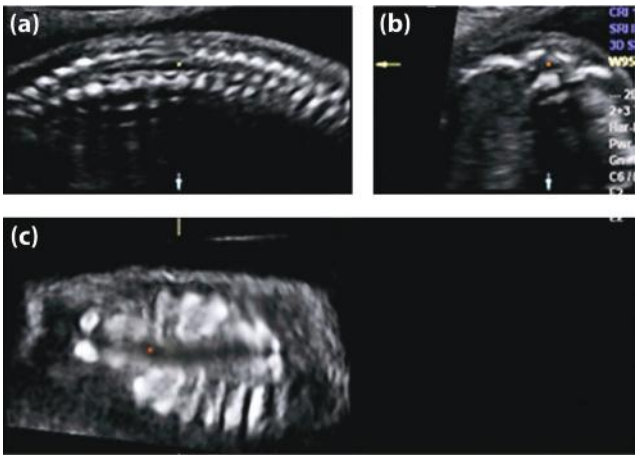


Figure 2.55 Three-dimensional multiplanar imaging of the fetal spine at 22 weeks of gestation. The (a) plane corresponds to the midsagittal plane, (b) to the axial plane, and (c) to the coronal plane. The position of the reference dot is within the neural canal.

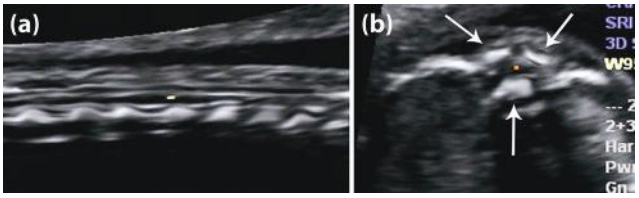


Figure 2.56 (a) Midsagittal and (b) axial view of the fetal spine at mid-gestation. Using the unossified spinous process of the vertebrae as an acoustic window, the contents of the neural canal are demonstrated. The arrows point to the three ossification centers of the vertebrae.

In most cases, a transabdominal approach suffices, but in obese women and in those in whom a breech fetal lie ensure a more direct approach to the spine, transvaginal scanning may provide dramatic images of spinal anatomy. It is important to emphasize that there is an increased risk of NTD in obese women; that this risk shows a positive linear correlation with increasing degrees of obesity [50]; and that the visualization of the fetal spine and cerebellum may be inadequate in these women [50]. This is why an higher level of attention should be provided while examining the fetal spine and posterior fossa in fetuses of obese women, despite the impaired acoustic window. However, it should be pointed out that, prior to the description of the cranial signs associated with open spina bifida—illustrated above—the detection rate of open spina bifida was very low, because it is extremely difficult and challenging to detect a spinal defect while directly assessing the spine. Only since the "lemon" and "banana" signs were described [51], has the detection rate of spina bifida progressively increased, to reach the current figure of about 90%, at least in developed countries. In fact, the above-mentioned signs are, in most instances, the first signs to orient the sonologist toward a more detailed assessment of the fetal spine in order to search for an open spina bifida that may have escaped recognition at first glance.

NTDs include anencephaly, encephalocele, and spinal dysraphisms. If the first two malformations represent clear-cut pathological entities, with little variation among cases, spinal dysraphisms include a wide spectrum of common (open spina bifida) and less common (closed spina bifida and notochord abnormalities), which have different functional prognoses and outcomes.

Acr ANIA – Ex ENc Eph ALy – ANENc Eph ALy

Ultrasound diagnosis. Absence of cranial vault with visible cerebral hemispheres (exencephaly) or complete absence of cerebral hemispheres (anencephaly).

Risk of chromosomal anomalies. Low (2%–11%).

Risk of nonchromosomal syndromes. Low.

Outcome. Uniformly fatal.

Definition. The term anencephaly generally refers to the final stage of a sequence of events due to a primary failure of cranial bones to develop (*acrania)*. In the early phase, usually visible at the end of the

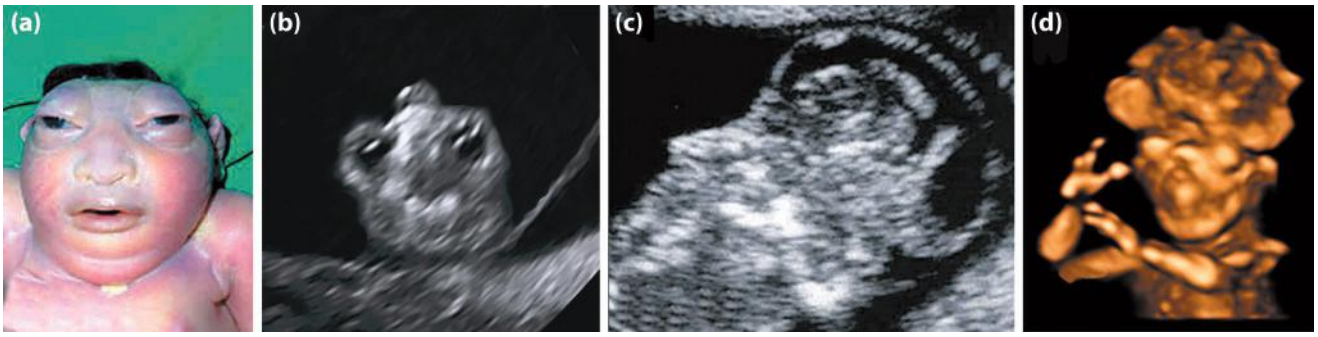


Figure 2.57 Anencephaly. (a) Pathologic finding of a term fetus with anencephaly. (b) The typical appearance is that of the so-called frog's face sign, because of the association of the absence of cerebral tissue and of cranial vault with concurrent macrophtalmos. (c) acrania–exencephaly at 13 weeks. The calvarium is absent, but the relatively intact brain is covered with pia mater. (d) Exencephaly: 3D rendering.

first trimester, the cerebral hemispheres have not yet been destroyed and are visible floating above the orbits in the amniotic fluid. This stage is called *exencephaly*. The full-blown anomaly—*anencephaly*—is characterized by the complete absence of the brain parenchyma, and is usually recognizable from the second trimester onward. The incidence of anencephaly was formerly reported as 1/1000 live births, but is dramatically decreasing due to an extremely high prenatal detection rate (at least in developed countries), which leads almost invariably to termination of pregnancy, in those countries in which this is allowed, and if the couple do not opt for continuing the pregnancy on religious or moral grounds.

Etiology and pathogenesis. The pathogenetic link with a folate deficiency status as well as with homocysteine metabolism errors has been fully uncovered during the past decades for all types of NTDs, and this has led to a significant reduction in the incidence of these defects following the worldwide strong recommendation for supplementation of folic acid in the periconceptional period. The sequence acrania–exencephaly–anencephaly is due to progressive destruction of the exposed fetal brain by chemical and traumatic insults in the amniotic fluid. The repeated trauma determined by active fetal movements leads to rapid destruction of the brain.

Ultrasound diagnosis. Currently, anencephaly is diagnosed at the time of the nuchal translucency scan (12–14 weeks) or even earlier [52] in the majority of cases (Figure 2.57). At this gestational age, the stage is that of exencephaly, with the cerebral hemispheres visible above the orbits, on a frontal or midsagittal view of the fetal head. Three-dimensional imaging is of limited value (Figure 2.57). A second-trimester diagnosis is becoming rarer and rarer. At 18–24 weeks, the diagnosis is straightforward, because when the sonologist tries to find the transthalamic plane to measure the biparietal diameter, he/she cannot find it and anencephaly is detected. On a frontal plane, the typical appearance is that of the so-called frog's face sign, because of the association of absent cerebral tissue and cranial vault with concurrent macrophtalmos and proptosis.

Differential diagnosis. Anencephaly is probably the easiest anomaly to detect and it cannot be confused with other abnormalities. On very rare occasions, in case of extensive cephaloceles, the abundant presence of brain outside the cranium may mimic exencephaly–anencephaly. However, in the former the cranial bones are present at least in part.

Associated abnormalities. These include spina bifida (27%) and iniencephaly. The association with cleft lip/palate, omphalocele, congenital heart disease, and/or limb anomalies constitutes the rare *thoracoabdominal syndrome*.

Risk of chromosomal anomalies. This risk is extremely low (2%–3%) if the lesion is isolated, but reaches 11% if associated with other malformations [16].

Risk of nonchromosomal syndromes. The single most important nonchromosomal condition not only associated with but often determining anencephaly is the amniotic band syndrome. In this condition, the presence of amniotic bands in the uterine cavity may be responsible for anencephaly, limb amputation, and huge abdominal wall defects (body wall complex).

The only real syndromic condition possibly associated with anencephaly is the:

- *Thoracoabdominal syndrome [16]*: look for ► *anencephaly* + cleft lip/palate + omphalocele + congenital heart disease, and/or limb anomalies.

Obstetric management. Termination of pregnancy can be considered as an option, considering that this anomaly is incompatible with life. In fact, only a few cases survive more than a week after birth.

Prognosis, survival, and quality of life. This anomaly is incompatible with life.

cEphALocELE

Incidence. 1 in 3500 to 1 in 5000 live births.

Ultrasound diagnosis. Cystic structure of variable dimensions protruding through a calvarial bone defect, most often in the occipital region, with (encephalomeningocele) or without (meningocele) brain tissue.

Risk of chromosomal anomalies. Relatively high, 14%–18%.

Risk of nonchromosomal syndromes. Relatively high.

Outcome. Postnatal mortality ranges from 30% to 50% for encephalocele and from 5% to 15% for meningocele.

Definition. Cephalocele is the protrusion of cerebral and/or meningeal structures through a cranial bone defect of variable size.

Etiology and pathogenesis. Cephalocele may result from failure in the fusion of the neural tube at specific closing sites or, according to other authors, it may be determined by abnormal mesenchymal induction in the postneurulation phase. Cephalocele may also be caused by amniotic bands, which secondarily disrupt normal brain development; in this case, the skull lesion is associated with other severe abnormalities, such as omphalocele and limb amputations. Cephaloceles are defined according to their anatomical location (frontal, parietal, occipital, frontoethmoidal, etc.); the occipital location is more common in Europe and the United States, whereas the frontal one is more frequent in Asia.

Ultrasound diagnosis. The cephalocele is characterized by a usually round cystic or partly solid mass seen protruding from the calvarial outline, most commonly at the level of the occipital region (Figures 2.58, 2.59). The size of the cephalocele may vary, and the small ones may also escape prenatal diagnosis, due to the fact that the extracranial component is extremely small. The diagnosis can be made as early as the 12th week of gestation. At diagnosis, the sonographic aspect of the herniated mass varies from completely anechoic to mixed echostructure, depending on whether only the meninges or also cerebral structures are involved. The herniation of the cerebellum through the skull defect is often referred to as *Chiari III malformation*. Occipital cephaloceles are usually revealed on a transthalamic view, but the midsagittal view of the fetal head, if obtainable with a posterior approach, or a coronal one, may clearly demonstrate both the bony defect and the myelomeningocele. Three-dimensional US has enhanced the prenatal characterization of these defects: multiplanar image correlation allows a detailed assessment of the skull defect, whereas surface and maximum-mode renderings can be used to further characterize the lesion (Figure 2.59). Frontoethmoidal cephaloceles are very rare, but they can be associated with frontonasal dysplasia. MRI is rarely needed prenatally to reach a final diagnosis of cephalocele; it may be used to assess its content and the overall development of the brain parenchyma and to rule out possibly associated neuronal migration and proliferation abnormalities.

Differential diagnosis. Cephalocele should be differentiated from cystic hygroma and hemangioma of the neck. The differential diagnosis is easily carried out considering that a cranial vault defect is absent in all but cephalocele, though a defect of the underlying bony plate has been found in a number of head hemangiomas in the fetus (Figure 2.60).

Associated anomalies. These are found in up to 80% of cases. They include mainly other CNS malformations, such as ACC, VM, holoprosencephaly, microcephaly, and spina bifida Extra-CNS anomalies reported in association with cephalocele include congenital heart disease and skeletal dysplasias. Of particular importance is the diagnosis of cephalocele

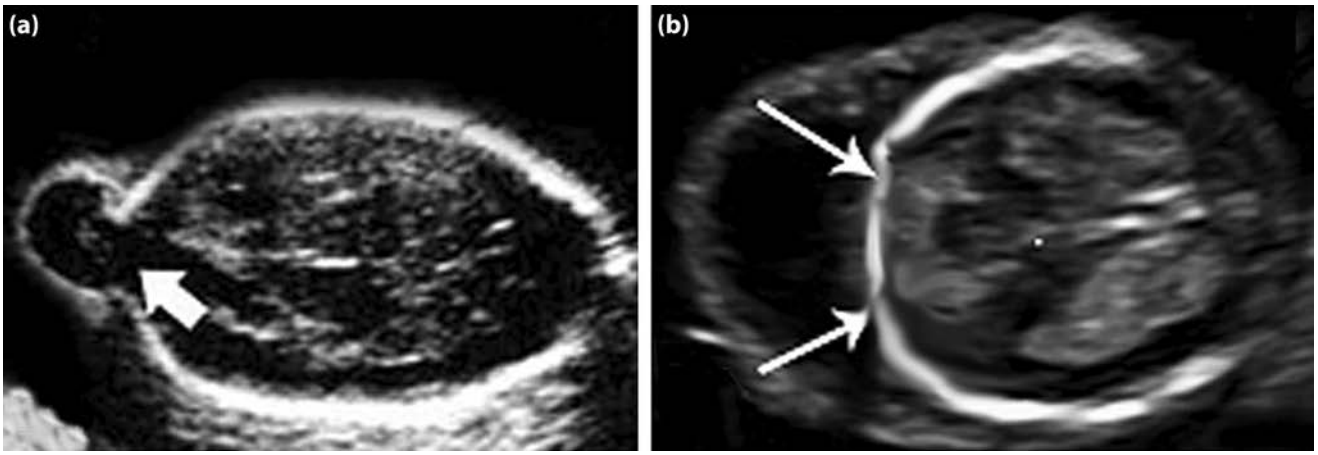


Figure 2.58 (a) Cephalocele. Cystic formation protruding through a skull defect (arrow), localized in the occipital region. (b) Small cystic hygroma; no calvarium defects are present (arrows).

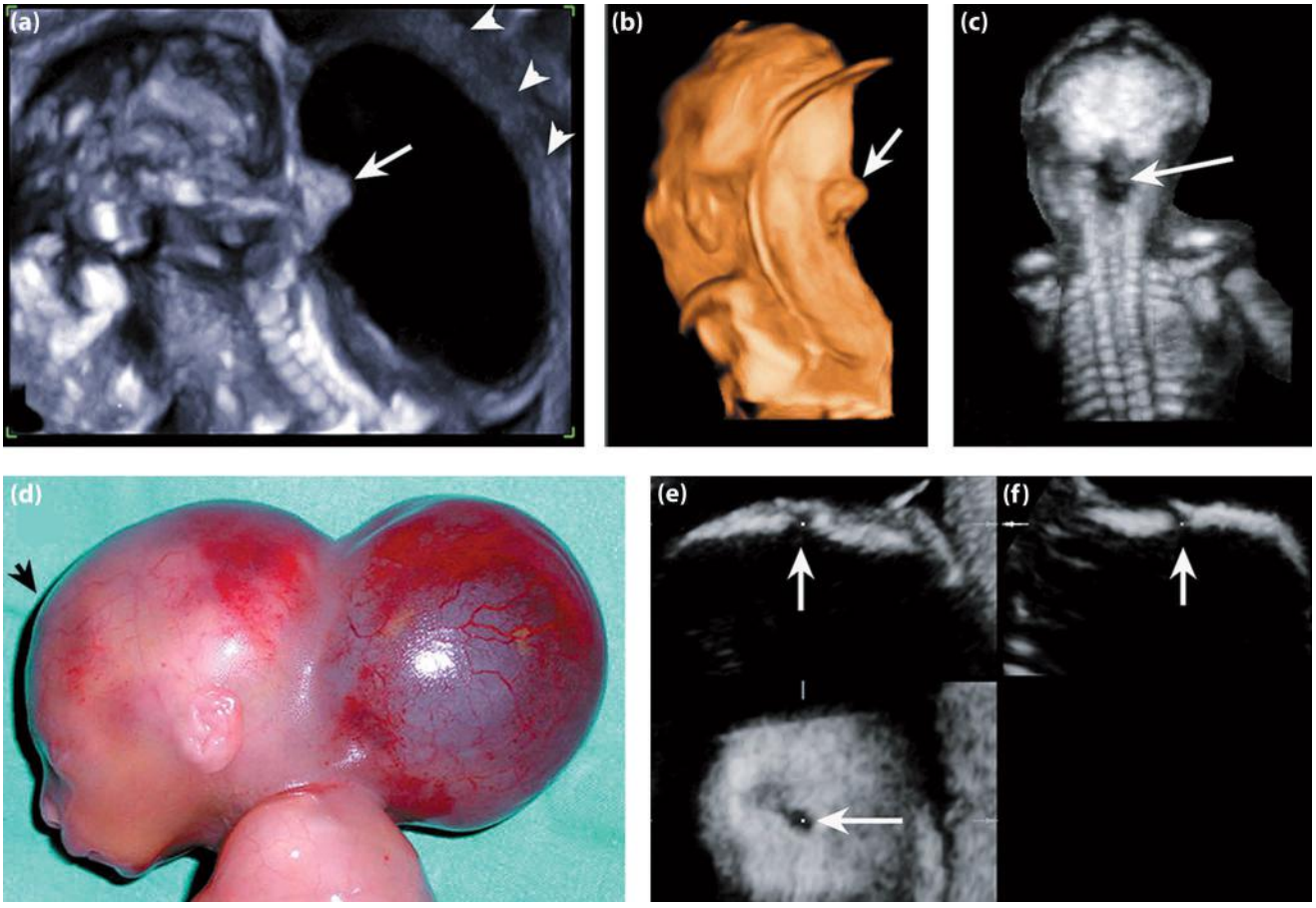


Figure 2.59 Meningoencephalocele. In this case (20 weeks' gestation), there is a huge meningocele with a very small occipital defect through which only the hypoplastic cerebellum has herniated. (a) Three-dimensional volume contrast imaging (VCI) rendering of the midsagittal view of the fetal head showing the meningocele (arrowheads) and the herniated hypoplastic cerebellum (arrow). (b) Three-dimensional surface rendering showing the herniated cerebellum (arrow). (c) Maximum-mode rendering showing the small occipital bony defect (arrow). (d) the fetus after termination of pregnancy: note the huge meningoencephalocele and the initial microcephaly with moderatly slanting forehead (arrow). (e)-(f) Multiplnar imaging, demonstrating the small bony defect (arrow) on the three orthogonal planes.

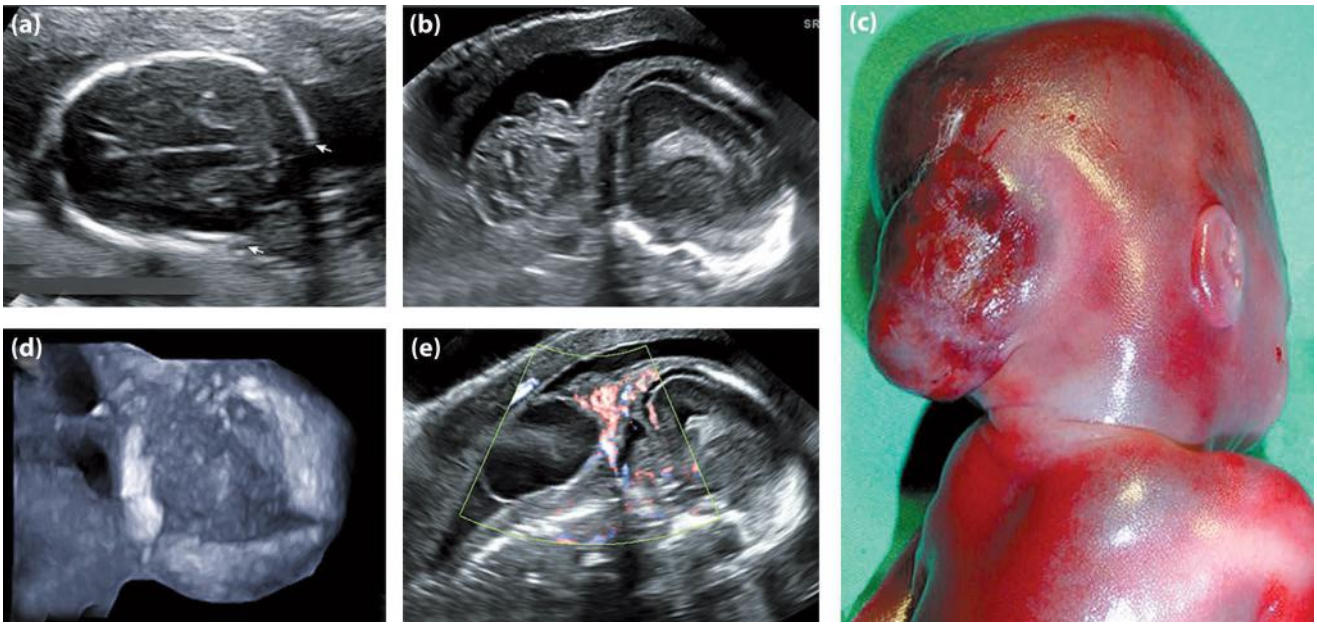


Figure 2.60 Occipital hemangioma may rarely mimic an occipital cephalocele, as in this case, in which a bony defect was associated with the hemangioma: both share a soft, possibly cystic, occipital mass. The only difference is that in hemangioma there is high vascularization of the mass, whereas in cephalocele the only vessels are found in the cerebral tissues. (a) on the axial, trans-thalamic view, the wide parieto-occipital bony defect is shown (arrows); (b) the occipital hemangioma, that may be mistaked for a cephalocele; (c) the specimen, after termination of pregnancy. Note the highly vascularized hemangioma of the occipital region. (d) the wide bony defect, as highlighted on three-dimensional maximum mode imaging; (e) power Doppler showing high vascularity of the lesion, orienting the diagnosis towards the hemangioma.

in the context of the Meckel–Gruber syndrome; this condition shows an autosomal recessive inheritance pattern and, therefore, subsequent pregnancies should be monitored as early as possible to rule out recurrence of the syndrome.

Risk of chromosomal anomalies. Risk is relatively high (7%–18%). Cephaloceles can be associated also with a significant number of nonchromosomal syndromic conditions [16], such as:

- *Amniotic band syndrome* ► *cephalocele* + amputation of digits or limbs + facial disruptions;
- *Frontonasal dysplasia* ► *cephalocele* + hypertelorism + anterior cranium bifidum occultum, widely set nostrils + median cleft lip/palate;
- *Meckel–Gruber syndrome* ► *cephalocele* + polydactyly + polycystic kidneys + other CNS anomalies.

Obstetric management. Obstetric management includes a thorough search for any associated structural anomalies, in order to rule out or confirm the presence of one of the syndromic conditions mentioned above. Karyotyping is recommended, especially if other anomalies are present. Neurosurgical consultation should be sought to give the parents a comprehensive idea of the defect and its possible outcome. In cases reaching term of gestation, delivery by Cesarean section is advisable to avoid trauma and infection (through the birth canal) of the exposed brain tissue.

Postnatal treatment. Very large lesions have an unfavorable prognosis—hence there is no benefit from treatment. Small cephaloceles can be corrected surgically.

Prognosis, survival, and quality of life. These depend on the dimensions and the location of the lesion, on the presence of cerebral tissue in the herniated sac, and on any association with hydrocephaly or microcephaly or other extracranial pathologies. The postnatal mortality rate varies from 30% to 50%, depending on the above-mentioned parameters. Meningocele and an anterior (frontal) location are associated with lower mortality rates (10%–25%).

opEN spINA BIFIdA

Incidence. 1 in 1000 at birth.

Ultrasound diagnosis. *Indirect cerebral signs:* Lemon sign (frontal bossing), banana sign (cerebellar dysmorphism), and effacement of the cisterna magna. *Direct signs*: "C" or "U" shape of the affected vertebra, which is due to absence of the dorsal arches; interruption of the cutaneous contour with/without a meningocele; splaying of the lateral processes.

Risk of chromosomal anomalies. Relatively high at 8%–16%.

Risk of nonchromosomal syndromes. Low.

Outcome. 14% to 20% of children with open spina bifida die within the 5 years of life due to shunt complications, in a significant number of cases. If brainstem disfunction related to Chiari II malformation is present the mortality rate rises to 35–40%. Motor disability depends on the level and complexity of the spinal defect.

Spinal dysraphisms. Spinal dysraphisms are divided into open spinal dysraphisms (OSDs), in which there is exposure of abnormal nervous tissues through a skin defect, and closed spinal dysraphisms (CSDs), in which there is complete skin coverage of the underlying malformation. OSDs basically include open spina bifida, with myelomeningocele, and other rare abnormalities such as myelocele and hemimyelo (meningo) cele. CSDs will be briefly described at the end of this chapter. The main difference between OSDs and CSDs is that in the former category there is a leakage of CSF within the amniotic cavity and the ensuing hypotension within the subarachnoid spaces triggers a cascade of events that eventually results in the Chiari II malformation [53]. In CSDs, there is no loss of CSF and, consequently, the cranial anatomy is unremarkable. Their prenatal diagnosis relies only on the direct recognition of the closed spinal defect.

Definitio . The term "spina bifida is still commonly used as a synonym for spinal dysraphism, although it properly refers to defective fusion of posterior spinal bony elements. The terms "spina bifida aperta" or "cystica" and "spina bifida occulta" are used to refer to OSD and CSD, respectively. Myelomeningoceles and myeloceles are characterized by exposure of the placode through a midline defect in the back. In myelomeningoceles, expansion of the underlying subarachnoid space results in elevation of the placode above the cutaneous surface (open spina bifida with dorsal cyst), whereas in myeloceles, the placode is flush with the cutaneous surface [53].

Etiology and pathogenesis. OSDs originate from defective closure of the primary neural tube, which leads to the persistence of a segment of nonneurulated placode. The overall majority of cases are located at the lumbosacral level, and the placode is terminal. Because neurulation does not occur, the cutaneous ectoderm does not detach from the neural ectoderm and remains in a lateral position. This results in a midline skin defect. Therefore, the external surface of the placode is directly visible upon inspection. In an antenatal series, 23% of the defects were sacral, 64% lumbosacral, 12% thoracolumbar, and only 1% cervical.

Ultrasound diagnosis. Until a few decades ago, the prenatal detection rate of spina bifida was relatively low, and was based mainly on serum screening in those countries, such as United States, where this mass screening program was available. The low detection rate for spina bifida on screening US was due to the fact that it is often difficult to obtain a diagnostic view of the fetal spine both in the longitudinal plane and in the axial one; in fact, the fetus often lies with its back along the uterine wall and this hampers the visualization of the fetal spine. Only after the recognition that *indirect cerebral signs* were present in the overwhelming majority of cases of open spina bifida did the detection rate of this severe anomaly increase sharply, to reach the current levels of nearly 90%. These *indirect signs* are related to the fact that in OSDs there is virtually always a Chiari II malformation. This malformation is characterized by a small posterior fossa associated with downward displacement of the dysmorphic vermis, the brainstem, and the fourth ventricle into the foramen magnum or even into the cervical spinal canal [53]. This cluster of events is triggered by the failed closure of the neuropore, which prevents the physiologic accumulation of fluid in the rhombencephalic vesicle responsible for its physiologic dilatation. As a result, the posterior fossa will be too small to accommodate the growing brainstem and cerebellum, and these will herniate through the cervical

canal behind the upper cervical cord. The US diagnosis of the Chiari II malformation is based upon the recognition of a series of signs including: 1) obliterarion of the cisterna magna; 2) dysmorphic and dysplastic cerebellum featuring an abnormal anterior curvature (banana sign); 3) frontal scalloping (lemon sign). The frontal scalloping (lemon sign) develops early, is inconstantly present (50% of the cases), and is lost in most cases by 24 weeks [51]. On the contrary, obliteration of the cisterna magna and the cerebellar banana sign are the most sensitive features, with the percentage of false positives being close to zero. These signs can be found from 16 weeks of gestation until term, though it should be considered that the US examination of the fetal posterior fossa is severely hampered in the third trimester by the increased calvarial mineralization.

VM is a relatively late-onset sign. In most cases (70%), it appears in the in the late second trimester (22–26 weeks.) and worsens thereafter (80%–90%). As mentioned, it is thanks to these *indirect cerebral signs* that the prenatal detection rate of open spina bifida in western countries has reached figures in the range of 68%–90%, with 68% of the diagnosis before 24 weeks of gestation. Once the suspicion of an OSD has been raised because of the recognition of indirect cerebral signs, then a direct approach to the spine is needed, to actually find the level and determine the extent of the spinal defect. It should be pointed out here that the sonographic assessment of the fetal spine is all but difficult even today, being strongly dependent upon the fetal lie. Direct sonographic recognition of the spinal defect requires systematic examination of each neural arch (Figure 2.61), from the cervical to the sacral ones. In particular, the *sagittal planes* can be used for an overall evaluation of the craniocaudal extension of the defect and to assess the dimensions of the myelomeningocele (Figure 2.61b). On *axial views*, it is possible to detect the interruption of the cutaneous contour at the level of the affected vertebrae, which will, therefore, show a "C" or "U" configuration, due to absence of the dorsal arches (Figure 2.61a). The *coronal planes* will demonstrate splaying of the lateral processes (Figure 2.61c). The three aspects just mentioned can be demonstrated advantageously on the same panel of images using the multiplanar display allowed by three-dimensional US. With this approach it is possible to recognize the level and the extent of the spinal defect very easily and at the same time very accurately. This information is of the utmost importance, because the level of the lesion correlates with the extent and the severity of motor and neurofunctional dysfunction. These findings can then be advantageously employed during the prenatal counseling session with the neurosurgeon. However, it should be

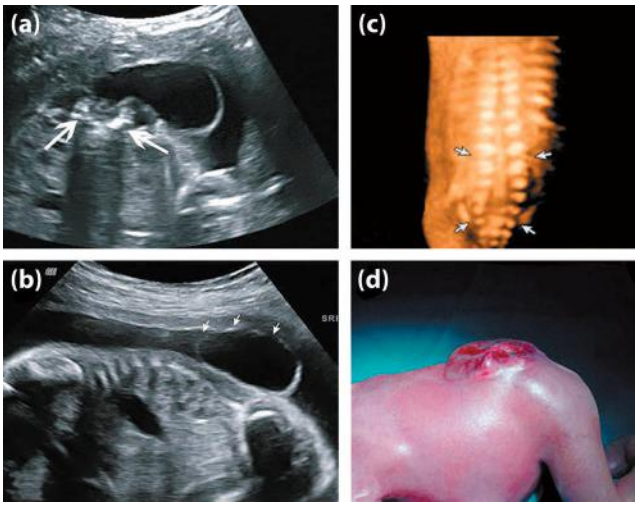


Figure 2.61 Spina bifida. (a) Axial scan of the lumbosacral spine demonstrating the open vertebra (arrows) and membranous coverage of the meningocele. (b) Sagittal view of the lumbar spine showing the bulging membranes of the myelomeningocele (arrows). (c) Maximum-mode rendering of the spine demonstrates lateral splaying of the lateral vertebral processes, with widening of the spinal canal (arrows). (d) Photograph of a fetus with spina bifida.

emphasized that the direct recognition of the defect is often challenging; in a significant number of cases the spinal lesion is missed on initial evaluation and is diagnosed only because the sonologist has detected the previously described *indirect signs* at the level of the fetal head. Conversely, CSDs are never associated with cranial signs and can only be recognized on direct inspection of the spine and only in some instances (see next heading) [53,54]. In some cases, the spina bifida is complicated by the presence of severe abnormalities of the affected segment; in particular, the lumbosacral tract of the spine may be severely distorted, showing acute posterior convexity.

The role of MRI in the prenatal assessment of open spina bifida is rather limited, especially because US is able to characterize open spinal defects accurately, as mentioned above and to diagnose the associated cerebral signs and their importance. On the contrary, it may be speculated that MRI might play a complementary role in the characterization of CSDs.

It is important to mention an important step forward toward an earlier diagnosis of OSD. Chaoui et al. [55] have described what they called the *Intracranial Translucency (IT)*. This evaluation is performed during the nuchal translucency scan (12–14 weeks) on the same median view of the fetal head on which the nuchal translucency is measured. In fetuses with OSDs, the IT cannot be recognized, and the distance between the thickened brainstem and the occipital bone is shorter

(see first chapter). Prospective trials have confirmed the clinical usefulness of this marker in the early detection of spina bifida.

Differential diagnosis. The only differential diagnosis of OSD is with sacrococcygeal teratoma. However, in the latter, both the indirect cerebral signs of OSD and the vertebral defects are absent.

Association with other malformations. Associated anomalies may be related to the spinal defect or be independent of it. The former category includes talipes (from contractures), bladder distension, and hydronephrosis (signs of neurofunctional damage). Extra-CNS anomalies often point to an underlying chromosomal aberration, which can be found in up to 16% of cases.

Risk of chromosomal anomalies. This risk is relatively high (8–16%).

Risk of nonchromosomal syndromes. This risk is relatively low.

Obstetric management. As far as obstetric management is concerned, the occurrence of associated anomalies should be excluded. Karyotyping is indicated, especially if the lesion is not isolated. Delivery by Cesarean section is considered recommendable by most, but not all, experts to avoid any trauma to, and possible infection of, the myelomeningocele during its transit through the birth canal.

Pre- and postnatal therapy. The need for ventriculoperitoneal shunting, the motor and functional sequelae, and the type and timing of surgery should be discussed with the neurosurgeon in the prenatal counseling session. In this regard, it should be pointed out that, after a series of frustrating experiences with intrauterine surgery, a randomized controlled trial has shown for the first time that open intrauterine surgery may reduce the need for ventriculoperitoneal shunting and improve motor outcome at 30 months [56]. However, this represents the first such study, though randomized, showing this improvement at the expense of serious maternal and fetal risks such as premature delivery, abruptio placentae, and chorioamnionitis. In addition, only 183 of the initial 1087 women undergoing preliminary screening eventually underwent randomization. Therefore, it is our belief that caution should be applied in interpreting the results of this nonetheless important study, and that we need these data to be supported by other series before accepting prenatal surgery of OSDs as a possibly better alternative to the conventional surgical approach after birth.

Prognosis, survival, and quality of life. Fourteen to Twenty percentage of children with open spina bifida die within the 5 years of life due to, in a certain number of cases, shunt complications. If brainstem disfunction related to Chiari II malformation is present the mortality rate rises to 35–40%. Early neonatal surgery is associated with the best survival rates, but cannot reduce or prevent disability. A long-term outcome study [57] of 117 liveborns with spina bifida carried out in the 1970s showed that by a mean age of 30 years, 51% had died. Of the survivors, 84% had a ventricular shunt, 70% had an IQ of 80 or more, 37% lived independently, 39% drove a car, 30% could walk more than 50 m, and 26% were employed. Normal intelligence was inversely related to presence of hydrocephalus and revision of the ventriculoperitoneal shunt. Infants who do not require ventricular shunting have a mean IQ of 104; if they require it and have no complications, mean IQ is 91; if the shunt needs to be revised, mean IQ is only 70. Hence, the presence of hydrocephalus represents a significantly negative prognostic factor; and it has been demonstrated that if fetuses with open spina bifida do not have a concurrent hydrocephalus at the time of diagnosis or before 26 weeks of gestation, which is indeed unlikely, there is only a 9% risk for them to develop it later.

c Los Ed sp INAL dysr Aph Is Ms (csd s)

CSDs are so named because the spinal defect is covered with skin, and are further categorized based on the association with spinal subcutaneous masses. CSDs with mass are represented by lipomyelocele, lipomyelomeningocele, meningocele, and myelocystocele. Closed CSDs without mass comprise simple dysraphic states and complex dysraphic states. The latter category further comprises defects of midline notochordal integration (basically represented by diastematomyelia) and defects of segmental notochordal formation (represented by caudal agenesis and spinal segmental dysgenesis) [53].

It should be emphasized that the prenatal detection rate of CSDs is decidedly lower in comparison with that of OSD, due to the absence in the former of the cranial indirect signs [54].

In the following headings, we will briefly review the prenatal diagnosis and outcome of some of the above-mentioned abnormalities. It should be emphasized here that MRI might play a significant complementary role in the characterization of these complex lesions: in fact, abnormal communications between the spinal canal and the enteric or urinary tract, which represent a key feature of complex CSDs such as split notochord syndrome, are difficult to detect with US and MRI may indeed contribute to a better characterization of these defects.

Closed spina bifida with subcutaneous mass: meningocele/lipoma.
Definitio . In this case, the cystic mass of the lower spine is skin-covered. This anomaly can be associated with a tethered cord or hydromyelia [53].

Ultrasound diagnosis. The diagnosis of a closed spina bifida is rather difficult given the absence of the cranial signs, and relies only on direct evidence of the lesion. This is why only some of the largest lesions are detected prenatally. They usually appear as a cystic backmass at the caudal end of the spine. With some attention, the continuity between the cystic mass and the spinal canal can also be seen. By definition the skin overlying the defect is intact (Figure 2.62). However, this sign can be difficult to demonstrate. On some occasions, a lipoma may be associated (lipomeningocele). However, in some cases the lipoma may escape prenatal recognition because its echogenicity is atypical. MRI is warranted in such cases to reach the final diagnosis and to ascertain, at the same time, the presence of a tethered cord, even though a lower than normal position of the *cauda equina* on a median US view of the fetal spine may suggest the presence of a tethered cord [54].

Outcome. The prognosis for closed spina bifida with meningocele/lipoma is better than that for OSP, although neurologic symptoms of variable entity are frequently present. In closed spina bifida there is usually much less involvement of the neural cord, and the Chiari II malformation does not develop. If the conus medullaris is in a normal position (around L2) and is not tethered, the outcome for infants with closed spina bifida seems to be good

Closed spina bifida without subcutaneous mass: Diastematomyelia.
Definitio . Diastematomyelia consists of complete or partial vertical clefting of the spinal cord into two symmetric or asymmetric hemicords, usually at the thoracolumbar level of the spine, with the cord that usually

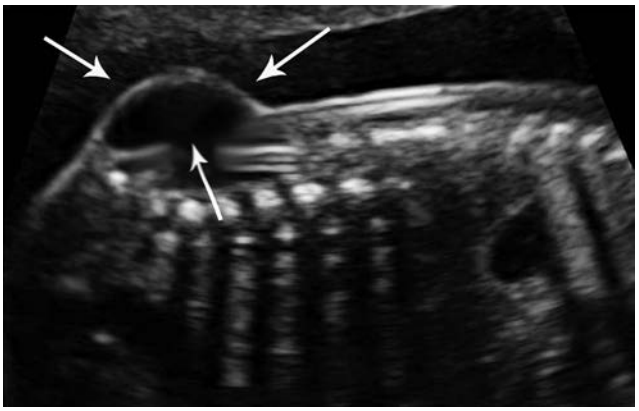


Figure 2.62 Closed spina bifida with lipoma, at 22 weeks' gestation. The cystic mass at the caudal end of the spine is clearly evident (arrows). The diagnosis of "closed" defect was made upon the absence of any associated cranial sign and the presence of continuity of fetal skin. Differential diagnosis with meningocele is extremely difficult. The lipoma is not usually clearly visible until the 3rd trimester.

reunites more distally [53]. Two subtypes of the lesions are recognized: in type A the two hemicords are contained within a single dural and arachnoid sheath without any fibrous or bony dividing spur, whereas in type B each hemicord has its own dural and arachnoid sac and there is a bony spur or a septum separating the two hemicords. Only the latter subtype can be recognized prenatally, and at that, only rarely. Cutaneous stigmata (hairy patch, capillary hemangioma, etc.) at the site of the anomaly are found after birth in roughly 30% of cases, but these are not detectable prenatally. Similarly, cord tethering and syringohydromyelia, that are also commonly associated, cannot be sonographically recognized in utero with certainty.

*Ultrasound diagnosis***.** Prenatal diagnosis of diastematomyelia has been reported in a limited number of cases and relies on the almost impossible demonstration of the separated cords in type A and on the more straightforward recognition of the bony spur in type B diastematomyelia. This type of diagnosis is made more confidentl with three-dimensional imaging (Figure 2.63). Since a tethered cord is associated in a significant percentage of cases, and its presence matters as to functional outcome, it would be of the utmost importance to detect this type of anomaly before birth. However, its presence can only be suspected at US if the cauda equina is located below L4-5 at 20–22 weeks of gestation. In this regard, MRI may be helpful. The importance of prenatal diagnosis is due to the fact that after birth the lesion can remain unrecognized if there are not cutaneous stigmata

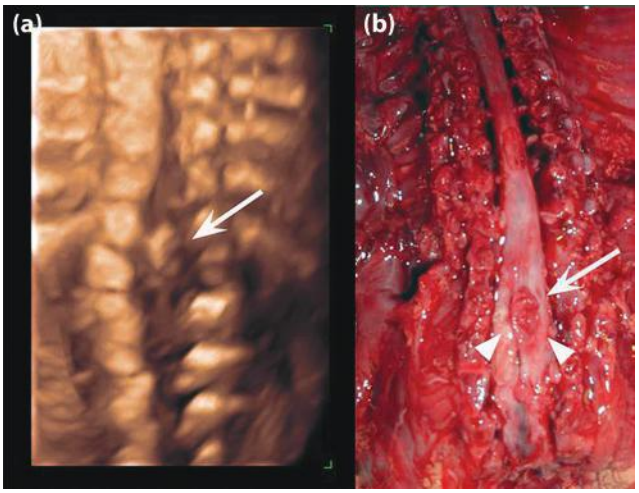


Figure 2.63 Diastematomyelia type B (30 weeks' gestation). (a) Magnified three-dimensional ultrasound. Coronal view showing the bony spur in the middle of the spinal canal (arrow). (b) Postmortem image. The posterior processes have been removed to show the cord. Note the bifurcation of the cord in the two hemicords at the level of the bony spur (arrow).

associated. And a delayed surgical relief of the tethered cord, with consequent damage of the cauda equina, has been shown to be the most important determinant of significant motor sequelae

Outcome. Diastematomyelia usually becomes symptomatic during childhood. The symptoms most frequently reported are sensorimotor deficits of the lower extremities, neurogenic claudication, sphincter dysfunction, and symptoms due to dysplastic development of the feet and legs in children, which are the result of the neurological deficit If diastematomyelia remains asymptomatic and undetected until adulthood, signs of the associated primary neuro-orthopedic (neurological deficit musculoskeletal deformities) or lumbar cutaneous malformation may be the only evidence to raise suspicion of a spinal anomaly.

Closed spina bifida without subcutaneous mass: Caudal regression sequence, sirenomelia.

Definitio . Caudal regression and sirenomelia share a significant number of anomalies, and probably the latter represents the extreme, full-blown form of the sequence. Caudal regression is characterized by partial or total agenesis of the sacrum (Figure 2.64) and, in some cases, of the lower lumbar part of the spine as well [53]. Genitourinary, gastrointestinal, and respiratory abnormalities may be associated, which points to the similarities with the VACTERL (Non-random association of Vertebral Ano-rectal, Cardiac, Tracheo-Esofageal, Renal, Limb anomalies) association (Figure 2.65). The exceedingly rare sirenomelia is the most severe form of caudal regression syndrome, in which the two legs are fused into a single abnormal limb (Figure 2.66). Both isolated sacral agenesis and the various stages of caudal regression are strongly associated with maternal diabetes. The Currarino syndrome is a form of caudal regression syndrome characterized by the classic triad of presacral mass, sacral bone defect, and anorectal malformation, which is inherited as an autosomal dominant tract, with mutation or deletion of the HLXB9 gene.

Ultrasound diagnosis. In caudal regression sequence, the backmass is usually large enough to be detected on screening US. Once referred, on targeted, expert US, it will be possible to recognize the complex spinal defect

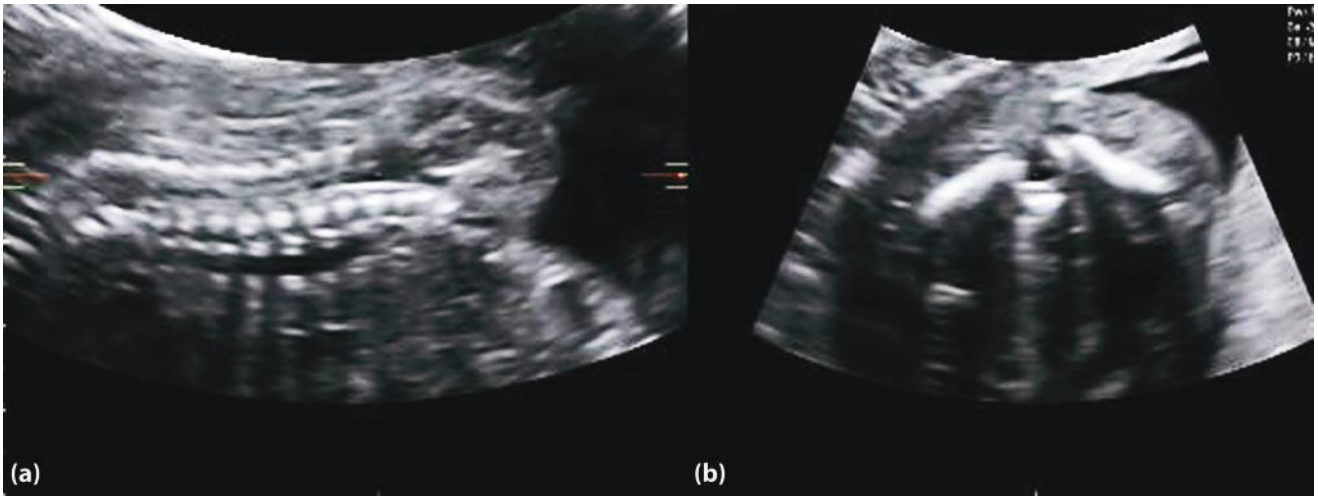


Figure 2.64 Caudal regression sequence at 21 weeks' gestation. Agenesis of the sacrum is seen on (a) sagittal and (b) axial views of the fetal spine.

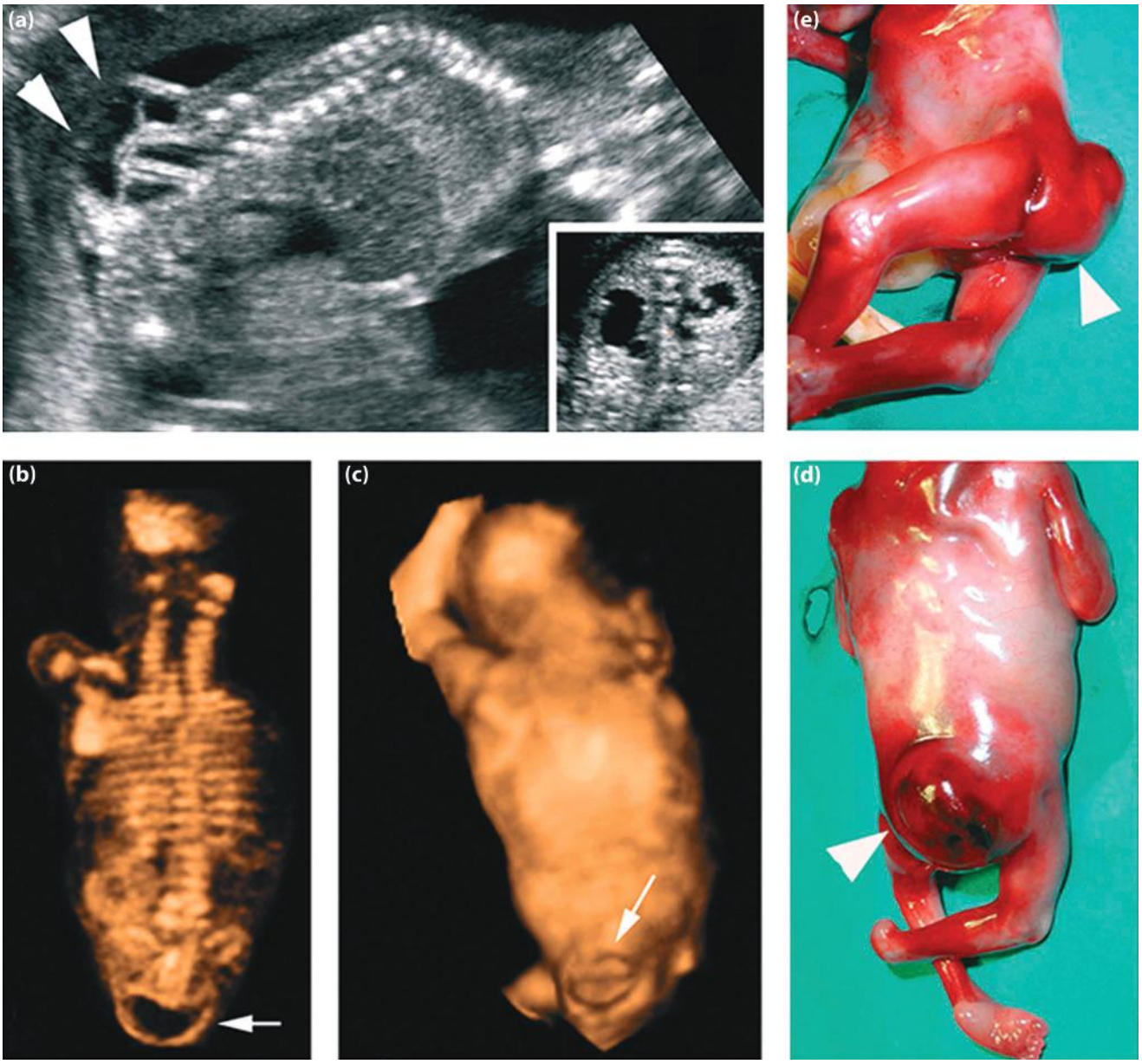


Figure 2.65 VA(C)TER(L) association. (a) Severe scoliosis due to a hemivertebra and a complex and large defect of the caudal part of the spine involving the lumbar and sacral tracts. The inset shows bilateral renal dysplasia. (b) 3D maximum-mode rendering demonstrating the vertebral anomalies and the wide sacral defect (arrow). (c) The same image, but with surface-mode rendering showing the cystic sacral lesion (arrow). (d, e) Confirmation at autopsy (compare with [b] and [c]).

and the concurrent renal abnormalities, if present. At the same time, significant abnormalities of the lower limbs will be detected. The recognition of the most severe form of the caudal regression syndrome, sirenomelia, should be straightforward, for in this case the two inferior limbs will be fused into a single one, even though the severe oligohydramnios due to the concurrent bilateral renal agenesis or maldevelopment may sometimes make the diagnosis of the gross limb anomaly challenging, if the sonologist does not think about it.

Outcome.

- *Caudal regression syndrome.* Both treatment and prognosis of this complex anomaly depend on the extent of the lesion. Morbidity is mainly related to genitourinary and neuromuscular complications, with management options centered around these two problems. In fact, usually extensive urologic and orthopaedic interventions are required. Longterm morbidity consists mostly of neurogenic bladder

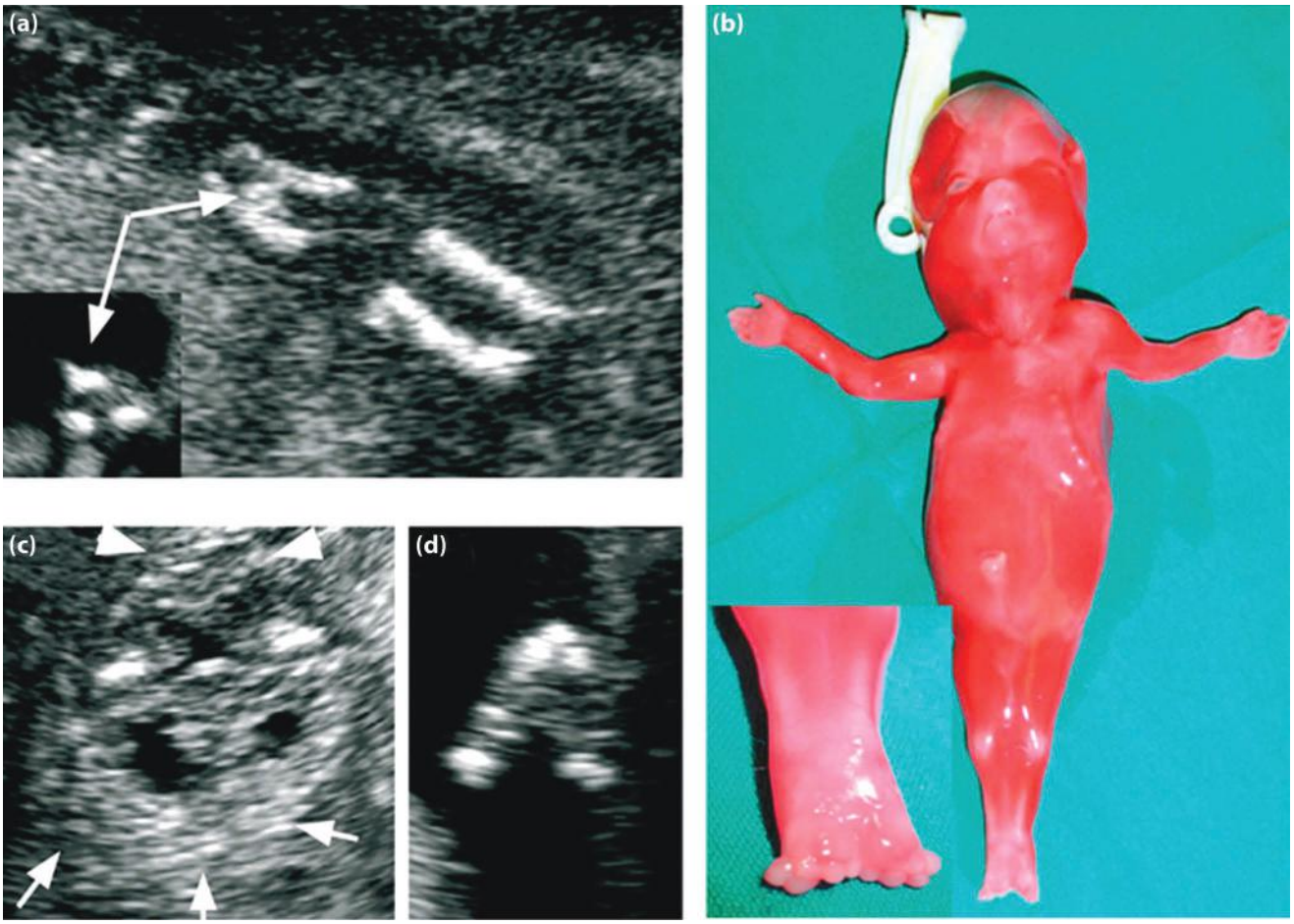


Figure 2.66 Sirenomelia. Ultrasound examination is difficult because of the constant severe oligohydramnios due to renal agenesis. In addition to this anomaly, the following malformations are found: (a) Fused lower limbs, with two sets of long bones but soft tissue fusion. In the inset, note the absence of the fibulas and the abnormal bone between the tibias (arrow). (b) Confirmation at autopsy: Note the single lower limb resulting from the fusion of the soft tissues of the two legs. The inset shows the fused feet (compare with [d] and [c]). On the axial view of the pelvis, it is possible to recognize a horseshoe kidney (arrows) and sacral agenesis (arrowheads): In fact, only the two iliac bones are visible above the kidney, with no sacral vertebrae appearing between them. (d) Axial view of the feet fused at the heels.

dysfunciton resulting in progressive renal damage and disabling deficits of the lower extremities.

- *Sirenomelia*. From the prognostic standpoint, the overwhelming majority of neonates with this complex anomaly die of renal insufficiency and/or lethal lung hypoplasia due to the prolonged absence of amniotic fluid. There are very few survivors; in them renal function was not completely absent and they underwent a complex surgical procedure to have the two legs separated.

sAcrococcy GEAL TEr ATo MA

Incidence. Extremely rare tumor.

Ultrasound diagnosis. Large mass arising from the sacrococcygeal area, with or without an intrapelvic component. It can be completely cystic, solid, or partly solid. High-output cardiac failure is frequently associated.

Risk of chromosomal anomalies. Low.

Risk of nonchromosomal syndromes. Low.

Outcome. The perinatal mortality rate is 30%–40%. Poorer prognosis is associated with solid, malignant, and large tumors.

Definition. Sacrococcygeal teratoma is a neoplasm arising probably from the pluripotent cells of Hensen's node, which is located anterior to the coccyx. Given that the cells of this node migrate into the embryo's tail during the first postconceptual week, this theory may explain why teratomas arise more frequently in the lower spinal area than in other parts of the body [16]. The most widely accepted classification recognizes the following four subtypes, according to the extension of the tumor: type 1 are predominantly external, with minimal presacral component; type 2 are predominantly external, with significant presacral component; type 3 are predominantly internal, with abdominal extension; and type 4 are entirely internal, with no external component. The first two subtypes account for more than 80% of cases [16].

Ultrasound diagnosis. Sacrococcygeal teratomas appear as large masses arising from the sacrococcygeal area. In general, the cases described in the fetus attain very large sizes and are mainly external (Figure 2.67). The echogenicity of the tumor may vary according to the component—from densely hyperechoic (Figure 2.67a) with sparse calcifications to completely cystic. Care should be taken in searching for an intrapelvic component, which may be difficult to identify due to bowel echogenicity. On color Doppler, high vascularization is usually detected in solid tumors. Signs of heart failure are frequently associated with solid and large tumors: hydrops, cardiomegaly, polyhydramnios, and subcutaneous edema. Hence, the poor prognostic indicators include a prevalently solid tumor, because of its strong association with high-output heart failure and hydrops (Figure 2.67b, d), and its higher malignant potential. Large size is another poor prognostic indicator, for the same reasons; as is a rapid growth rate, due to high mitotic index, which is a marker of likely malignant tumors. These will have a more abundant vascular supply than their benign counterparts, which leads to high-output cardiac failure in a significant proportion of cases, though this latter complication is not limited to malignant cases.

Differential diagnosis. The differential diagnosis should be made only for small and cystic tumors with other possible masses located in the sacral area, including lipomas and NTDs. In the latter, the spine is abnormal, whereas lipomas tend to be strictly associated with the lower spinal elements (not the coccyx).

Associated anomalies. Postnatal reports indicate a relatively high association rate (up to 25%) of sacrococcygeal teratomas with other malformations, without any particular organ system being preferentially involved.

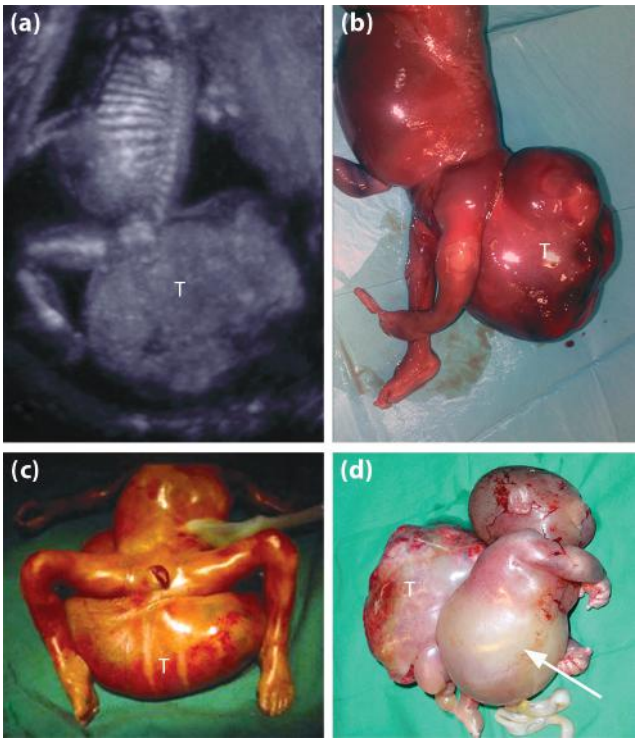


Figure 2.67 Sacrococcygeal teratoma (T). (a) large solid teratoma (28 weeks of gestation) causing high output cardiac failure responsible for fetal death; (b) confirmation after delivery of the stillborn; (c) a rare prevalently cystic sacrococcygeal teratoma: fetus after termination of pregnancy at 22 weeks' gestation; (d) another case of fetal death from severe hydrops in a 29 week old fetus affected with a large, solid, sacrococcygeal teratoma (T) (arrow: abdomen distended by ascites).

However, prenatally diagnosed cases do not appear to show the same relatively high risk of association, and the only frequent findings are cardiomegaly or hydrops from high-output cardiac failure.

Obstetric management. Would include a thorough search for other possibly associated malformations, as well as fetal echocardiography to assess the potential and stage of high-output cardiac failure, limited to solid tumors. Termination of pregnancy is an option, considering the poor prognosis of large and solid tumors and/or if cardiac failure (hydrops) is associated. Delivery should take place in a tertiary referral center in order to provide adequate neonatal management. A Cesarean section is always indicated in the case of solid and large tumors due to the high risk of soft tissue dystocia. A few attempts at reducing the vascular bed prenatally, with radiofrequency or laser coagulation, have been reported, but there was a high toll in terms of fetal deaths, and, therefore, this approach is currently not considered a valid therapeutic option.

Prognosis, survival, and quality of life. The overall prognosis of sacrococcygeal teratomas is guarded, with a 30%–40% neonatal mortality rate, which is mainly due to hydrops from cardiac failure. There is also a consistent intrauterine mortality, for the same reasons. The only indicators of good outcome are represented by small mainly cystic tumors, which are also predominantly benign.

rEFE r ENc Es

1. Filly RA, Cardoza JD, Goldstein RB, et al. Detection of fetal central nervous system anomalies: a practical level of effort for a routine sonogram. *Radiology* 1989; 172: 403–8.
2. Reece EA, Goldstein I. Three-level view of fetal brain imaging in the prenatal diagnosis of congenital anomalies. *J Matern Fet Med* 1999; 8: 249–52.
3. Nyberg DA. Reccomendations for obstetric sonography in the evaluation of the fetal cranium. *Radiology* 1989; 172: 309–11.
4. Toi A, Lister WS, Fong KW. How early are fetal cerebral sulci visible at prenatal ultrasound and what is the normal pattern of early fetal sulcal development? *Ultrasound Obstet Gynecol* 2004; 24: 706–15.
5. Malinger G, Lerman-Sagie T, Watemberg N, et al. A normal second trimester ultrasound does not exclude brain pathology. *Ultrasound Obstet Gynecol* 2002; 20: 51–6.
6. Timor-Tritsch IE, Monteagudo A. Transvaginal fetal neurosonography: standardization of the planes and sections by anatomic landmarks. *Ultrasound Obstet Gynecol* 1996; 8: 42–7.
7. D'Addario V, Pinto V, Di Cagno L, et al. The midsagittal view of the fetal brain: a useful landmark in recognizing the cause of fetal cerebral ventriculomegaly. *J Perinat Med* 2005; 33: 423–7.
8. ISUOG. Sonographic examination of the fetal central nervous system: guidelines for performing the 'basic examination' and the 'fetal neurosonogram'. *Ultrasound Obstet Gynecol* 2007; 29: 109–16.
9. Volpe P, Campobasso G, De Robertis V, et al. Disorders of prosencephalic development. *Prenat Diagn* 2009; 29: 340–54.
10. Babcook C, Chong B, Salamat M, et al. Sonographic anatomy of the developing cerebellum: normal embryology can resemble pathology. *AJR Am J Roentgenol* 1996; 166: 427–33.
11. Pilu G, Ghi T, Carletti A, et al. Three-dimensional ultrasound examination of the fetal central nervous system. *Ultrasound Obstet Gynecol* 2007; 30: 233–45.
12. Melchiorre K, Bhide A, Gika AD, et al. Counseling in isolated mild fetal ventriculomegaly. *Ultrasound Obstet Gynecol* 2009; 34: 212–24.
13. Girard N, Gire C, Mancini J, et al. Ventriculomegaly. *J Neuroradiol* 2002; 29: 1S8.
14. Signorelli M, Tiberti A, Valseriati D. Width of the fetal lateral ventricular atrium between 10 and 12 mm: a simple variation of the norm? *Ultrasound Obstet Gynecol* 2004; 23: 14–18.
15. Triulzi F, Manganaro L, Volpe P. Fetal magnetic resonance imaging: indications, study protocols and safety. *Pediatr Radiol* 2011; 116: 337–50.
16. Stevenson RE, Hall JG, Goodman RM. Brain. In: Stevenson RE, Hall JG, Goodman RM, eds. *Human Malformations and Related Anomalies*. Oxford: Oxford University Press; 1993, 2975–3012.
17. Lewis AJ, Simon EM, Barkovich AJ, et al. Middle interhemispheric variant of holoprosencephaly: a distinct cliniconeuroradiologic subtype. *Neurology* 2002; 59: 1860–5.
18. Gentile M, Volpe G, Volpe P. Genetics of brain malformations. *Ultrasound Rev Obstet Gynecol* 2003; 3: 97–103.
19. Dubourg C, Bendavid C, Pasquier L, et al. Holoprosencephaly. *Orphanet J Rare Dis* 2007; 2: 8.
20. Matsunaga E, Shiota K. Holoprosencephaly in human embryos: epidemiologic studies of 150 cases. *Teratology* 1977; 16: 261–72.
21. Blaas HG, Eriksson AG, Salvesen KA, et al. Brains and faces in holoprosencephaly: pre- and postnatal description of 30 cases. *Ultrasound Obstet Gynecol* 2002; 19: 24–38.
22. Plawner LL, Delgado MR, Miller VS, et al. Neuroanatomy of holoprosencephaly as predictor of function: beyond the face predicting the brain. *Neurology* 2002; 59: 1058–66.
23. Volpe P, Paladini D, Resta M, et al. Characteristics, associations and outcome of partial agenesis of the corpus callosum in the fetus. *Ultrasound Obstet Gynecol* 2006; 27: 509–16.
24. Pilu G, Sandri F, Perolo A, et al. Sonography of fetal agenesis of the corpus callosum: a survey of 35 cases. *Ultrasound Obstet Gynecol* 1993; 3: 318–29.
25. Malinger G, Zakut H. The corpus callosum: normal fetal development as shown by transvaginal sonography. *Am J Roentgenol* 1993; 161: 1041–3.
26. Moutard ML, Kieffer V, Feingold J, et al. Agenesis of corpus callosum: prenatal diagnosis and prognosis. *Childs Nerv Syst* 2003; 19: 471–6.
27. De Morsier G. Etudes sur les dystrophies cranio-encephaliques III. Agenesie du septum pellucidum avec malformation du tractus optique: la dysplasie septo-optique. *Schweiz Arch Neurol Neurochir Psychiatr* 1956; 77: 267–92.
28. Barkovich AJ, Millen KJ, Dobyns WB. A developmental and genetic classification for midbrain-hindbrain malformations. *Brain* 2009; 132: 3199–230.
29. Garel C, Fallet-Bianco C, Guibaud L. The fetal cerebellum: development and common malformations. *J Child Neurol* 2011; 26: 1483–92.
30. Guibaud L, des Portes V. Plea for an anatomical approach to abnormalities of the posterior fossa in prenatal diagnosis. *Ultrasound Obstet Gynecol* 2006; 27: 477–82.
31. Parisi MA. Clinical and molecular features of Joubert syndrome and related disorders. *Am J Med Genet C Semin Med Genet* 2009; 151C: 326–40.
32. Tortori-Donati P, Rossi A, Biancheri R. Brain malformations. In: Tortori-Donati, ed. *Pediatric Neuroradiology*. Berlin: Springer-Verlag; 2005, 121–98.
33. Robinson AJ, Goldstein R. The cisterna magna septa: vestigial remnants of Blake's pouch and a potential new marker for normal development of the rhombencephalon. *J Ultrasound Med* 2007; 26: 83–95.
34. Gandolfi Colleoni G, Contro E, Carletti A, et al. Prenatal diagnosis and outcome of fetal posterior fossa fluid collections. *Ultrasound Obstet Gynecol* 2012; 39: 625–31.
35. Volpe P, Contro E, De Musso F, et al. The brainstem-vermis and brainstem-tentorium angles allow accurate categorization of fetal upward rotation of the cerebellar vermis. *Ultrasound Obstet Gynecol* 2012; 39: 632–5.
36. Paladini D, Volpe P. Posterior fossa and vermian morphometry in the characterization of fetal cerebellar abnormalities: a prospective three-dimensional ultrasound study. *Ultrasound Obstet Gynecol* 2006; 27: 482–9.

37. Barkovich AJ. Developmental disorders of the midbrain and hindbrain. *Front Neuroanat* 2012; 6: 7.
38. Barkovich AJ, Kjos BO. Revised classification of posterior fossa cysts and cystlike malformations based on the results of multiplanar MR imaging. *AJR* 1989; 153: 1289–300.
39. Malinger G, Lev D, Lerman-Sagie T. The fetal cerebellum. Pitfalls in diagnosis and management. *Prenat Diagn* 2009; 29: 372–80.
40. Klein O, Pierre-Kahn A, Boddaert N, et al. Dandy-Walker malformation: prenatal diagnosis and prognosis. *Childs Nerv Syst* 2003; 19: 484–9.
41. Tortori-Donati P, Fondelli MP, Rossi A, et al. Cystic malformations of the posterior cranial fossa originating from a defect of the posterior membranous area. Megacisterna magna and persisting Blake's pouch: two separate entities. *Childs Nerv Syst* 1996; 12: 303–8.
42. Paladini D, Quarantelli M, Pastore G, et al. Abnormal or delayed development of the area membranacea posterior of the brain: the Blake's pouch cyst. Anatomy, ultrasound diagnosis, natural history and outcome in the fetus. *Ultrasound Obstet Gynecol*. 2012; 39: 279–87.
43. Barkovich AJ, Guerrini R, Kuzniecky RI, et al. A developmental and genetic classification for malformations of cortical development: update 2012. *Brain* 2012; 135: 1348–69.
44. Adachi Y, Poduri A, Kawaguch A, et al. Congenital microcephaly with a simplified gyral pattern: associated findings and their significance *AJNR* 2011; 32: 1123–9.
45. Jissendi-Tchofo P, Kara S, Barkovich AJ. Midbrain–hindbrain involvement in lissencephalies. *Neurology* 2009; 72: 410–18.
46. Fong KW, Ghai S, Toi A, et al. Prenatal ultrasound findings of lissencephaly associated with Miller-Dieker syndrome and comparison with pre- and postnatal magnetic resonance imaging. *Ultrasound Obstet Gynecol* 2004; 24: 716–23.
47. Pilu G, Falco P, Perolo A, et al. Differential diagnosis and outcome of fetal intracranial hypoechoic lesions: report of 21 cases. *Ultrasound Obstet Gynecol* 1997; 9: 229–36.
48. Epelman M, Daneman A, Blaser SI, et al. Differential diagnosis of intracranial cystic lesions at head US: correlation with CT and MR imaging. *Radiographics* 2006; 26: 173–96.
49. Garel C. Abnormalities of the Fetal Cerebral Parenchyma: Ischaemic and Haemorrhagic Lesions. In: Catherine Garel Ed. *MRI of the Fetal Brain*. 2004, Springer-Verlag, 247–62.
50. Paladini D. Sonography in obese and overweight pregnant women. *Ultrasound Obstet Gynecol* 200; 33: 720–9.
51. Nicolaides KH, Campbell S, Gabbe SG. Ultrasound screening for spina bifida: cranial and cerebellar signs. *Lancet* 1986; ii: 72–4.
52. Blautoris H-GK, Eik-Nes SH. Sonoembriology and early prenatal diagnosis of neural anomalies. *Prenat Diagn* 2009; 29: 312–25.
53. Rossi A, Biancheri R, Cama A, et al. Imaging in spine and spinal cord malformations. *Eur J Radiol* 2004; 50: 177–200.
54. Ghi T, Pilu GL, Falco P, et al. Prenatal diagnosis of open and closed spina bifida *Ultrasound Obstet Gynecol* 2006; 28: 899–903.
55. Chaoui R, Benoit B, Mitkowska-Wozniak H, et al. Assessment of intracranial translucency (IT) in the detection of spina bifida at the 11–13-week scan. *Ultrasound Obstet Gynecol* 2009; 34: 249–52.
56. Adzick NS, Thom EA, Spong CY. A randomized trial of prenatal versus postnatal repair of myelomeningocele. *N Engl J Med* 2011; 364: 993–1004.
57. Mapstone TB, Rekate HL, Nulsen FE, et al. Relationship of CSF shunting and IQ in children with myelomeningocele: a retrospective analysis. *Childs Brain* 1984; 11: 112–18.

Chapter 3
Craniofacial and neck anomalies

Normal Anatomy of the Face and Neck: Ultrasound Approach, Scanning Planes, and Diagnostic Potential

The fetal face represents one of the key anatomic regions from both a psychological and a clinical standpoint. Observing the fetal face on the screen of the scanner plays a central role in the development of maternal–fetal bonding, especially with recent developments in three-dimensional (3D) ultrasound (US). In addition, it has to be considered that a significant number of chromosomal and nonchromosomal syndromes are associated with major and/or minor anomalies of the face. Finally, the high social and cosmetic impact of isolated anomalies of the face, such as microphthalmia or micrognathia, is extremely important. All of these factors, together with the difficulties posed by US examination of an irregularly shaped anatomic region such as the fetal face, contribute to making the fetal face one of the most difficult and delicate areas to explore.

Timing of examination. The US appearance of the fetal face varies significantly throughout gestation, owing to the progressive accumulation of adipose tissue, especially at the level of the maxilla and the chin. This explains why the fetal face appears extremely thin and bony until 23–24 weeks; thereafter, the facial features will progressively smooth out to acquire individual features in the third trimester (30–32 gestational weeks) (Figures 3.1 and 3.2).

Ultrasound approach and scanning planes (views). As already mentioned, the fetal face represents an extremely irregular region to explore with US, when compared with regular geometric shapes such as the fetal cranium or limbs. This is why US examination of the fetal face has always posed significant problems in all attempts at a standardization of the US approach [1,2]. To overcome the above-mentioned significant limitations, it is necessary to have in mind an extremely detailed mental replica of the spatial position of the fetal face in relation to the limbs and the uterine cavity. With these significant limitations, we report below the reference scanning planes, classified as axial, coronal, sagittal, and oblique, and the anatomic structures assessable in each of these views. Furthermore, it has to be emphasized that the actual movements required of the hand holding the transducer to switch from one plane to the other are quite subtle and consist mainly of rotational and/or sweeping movements. With regard to the possible approaches, we should underscore the significant role played by US physics in obtaining a clear and artifact-free image: the better-displayed structures are those at 90° to the insonating beam. Thus, for example, if the orbits are displayed with a ventral approach, the lens and the orbicular muscles will be better imaged; on the contrary, with a lateral approach, the bony orbits, and their lateral and medial aspects, with the ethmoid between them, will be the structures displayed in the clearest fashion. Given that the fetal face consists of the anterior part of the head only, the feasible approaches are reduced to *lateral* and *ventral* (anterior). As already mentioned, the US planes usually employed in the assessment of the fetal face are the axial, coronal, sagittal, and oblique planes. The different views will be described separately afterward. Figure 3.3 summarizes the relevant axial planes.

Because the anomaly scan is carried out in most countries between 18 and 22 weeks' gestation [3], all US planes described and illustrated below refer to fetuses examined at that gestational age-range, unless otherwise specified.

1. **Axial views:** The following US planes are shown in Figure 3.3:
   A. Orbits—lateral approach (Figure 3.4);
   B. Orbits—ventral approach (Figure 3.5);
   C. Lower maxilla/upper alveolar ridge—ventral approach (Figure 3.6);
   D. Tongue/pharynx—ventral approach (Figure 3.7);

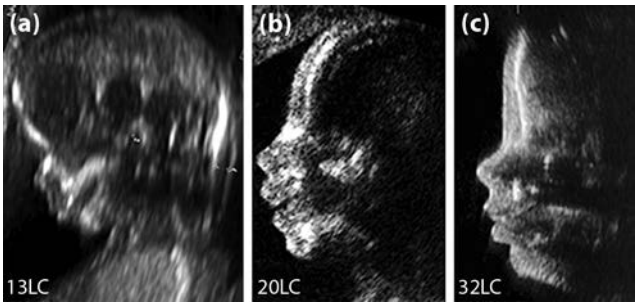


Figure 3.1 Fetal profile at different gestational ages on two-dimensional ultrasound. The progressive increase in subcutaneous fat is responsible for the significant changes in the sharpness of the facial features: (a) 13 gestational weeks; (b) 20 gestational weeks; and (c) 32 gestational weeks.

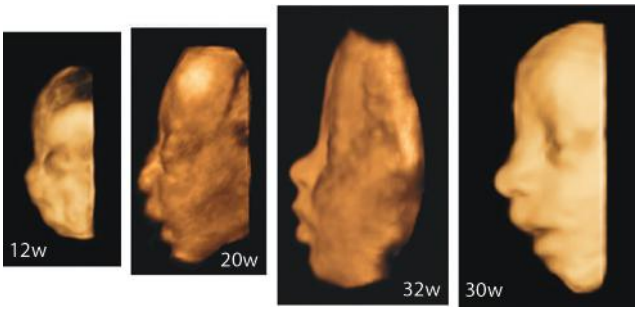


Figure 3.2 Fetal profile at different gestational ages on three-dimensional ultrasound. The progressive increase in subcutaneous fat is responsible for the significant changes in the sharpness of the facial features: (a) 12 gestational weeks; (b) 20 gestational weeks; (c) 32 gestational weeks. In the second part of gestation, three-dimensional ultrasound also allows the highlighting of some ethnic features: Compare the image of an Afro-Caribbean fetus at 32 weeks (c) with that of an eastern European one (d). This pronounced interethnic but also intra-ethnic variance in the phenotype should be considered while assessing the "normalcy" of a fetal profile.

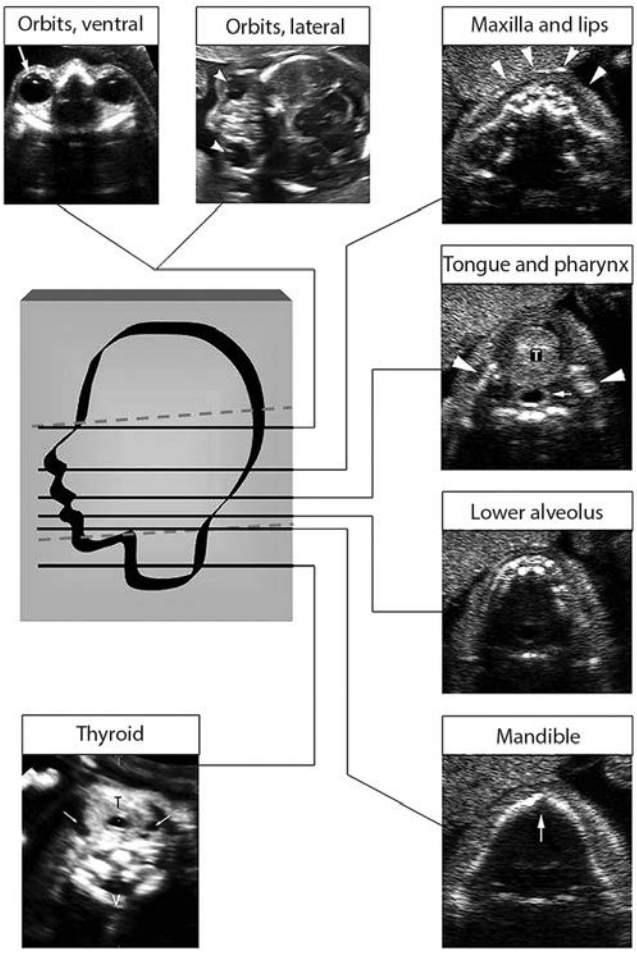


Figure 3.3 Axial ultrasound views for the assessment of the splanchnocranium. This figure illustrates the level of the scanning plane and the corresponding two-dimensional ultrasound image. All views are illustrated in detail in Figures 3.4 through 3.9.

E. Mandible/inferior alveolar ridge—ventral approach (Figure 3.8a);
F. Mandibular bone—ventral approach (Figure 3.8b);
G. Thyroid—ventral approach (Figure 3.9).

2. **Sagittal views:** The two reference planes are
   A. Facial profile—midline sagittal (Figures 3.10 and 3.11);
   B. Ear—parasagittal (lateral) (Figure 3.12).

The final scanning planes to complete the evaluation of the splanchnocranium are (Figure 3.13) as follows:

A. The coronal view of the face and palate (Figure 3.14);
B. The oblique view of the upper lip (Figure 3.15a);
C. The coronal/oblique view of the palate (Figure 3.15b).

FAc IAL ANo MALIEs By sc ANNING VIEW

Orbits (lateral approach) and related malformations (Figure 3.4). This represents the classic view for the assessment of the bony orbits and the measurement of the binocular and interocular diameters. The corresponding nomograms are given in the Appendix Table A.15 [4]. With reference to this view, and its



Figure 3.4 Axial view of the orbits—lateral approach. The lateral walls of the orbits and the midline structures (ethmoid) are clearly displayed. The lenses (arrowheads) are also visible in this case, though they are better displayed with a ventral approach (see Figure 3.5).

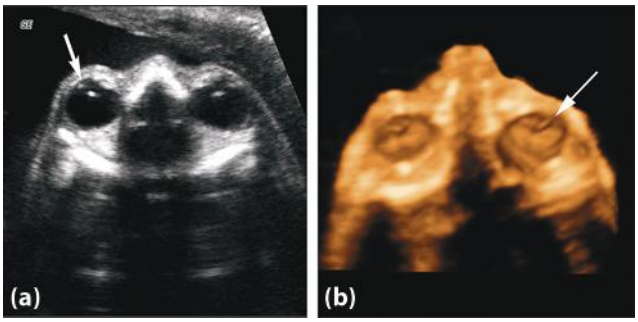


Figure 3.5 Axial view of the orbits—ventral approach. Both lenses and the whole of the eye bulb are clearly depicted (arrows). Posteriorly, the back of the bony orbit, which is accounted for by the sphenoid, can be seen (arrows). (a) Two-dimensional imaging. (b) Three-dimensional surface rendering.

corresponding drawing in Figure 3.3, it has to be underscored that, notwithstanding the fact that this view can also be achieved as a perfectly axial plane, it is common practice to obtain it with a minimal rotation of the transducer and that insonates the anterior aspect of the fetal head, starting from the axial transthalamic view. Hence, in practice, the view used for the assessment of the orbits with a lateral approach represents a slightly oblique view of the fetal head (Figure 3.3). As is evident from Figure 3.4, in this plane, the lateral and median aspects of the orbits are clearly visible, which allows correct measurement of binocular and interocular diameters. It should be emphasized that the above-mentioned measurement does not represent an integral part of the biometric assessment commonly carried out as part of the mid-trimester scan in all countries; in some, only the visualization of the orbits, but not their biometric assessment, is required. However, orbital biometry should be checked whenever there is a suspicion of orbital malformations such as hypertelorism, hypotelorism, or microphthalmia.

The orbital malformations that can be suspected and diagnosed on this view are as follows:

- *Microphthalmia/anophthalmia*: Complete absence or severe hypoplasia of one or both orbits
- *Hypertelorism/hypotelorism*: Increased/reduced interocular distance, with orbits of normal or abnormal dimensions
- *Macrophthalmia*: Increased orbital diameter, usually bilateral
- *Dacryocystocele*: Cystic enlargement of the lacrimal duct

On the basis of what has been said about US physics and insonation, it is useful to stress that the ocular bulbs, regardless of how normal or abnormal they may appear on this view, should be electively assessed on the ventral approach view (see below). On the contrary, the orbital anomalies reported above can also be detected on the ventral approach view. We have decided to describe the two views separately, in order to underscore the different accuracy with which the soft and hard tissues of the bony orbit and ocular bulb are displayed in each.

Orbits (ventral approach) and related malformations (Figure 3.5). As has been said, this view should be sought to assess the intraocular soft tissues, the lenses, and the posterior walls of the orbits, represented mainly by the anterior aspect of the sphenoidal wings. The lenses will appear as small echogenic circular structures within the eyes (Figure 3.5). Consequently, this represents the elective approach for the diagnosis of lens and ocular abnormalities; in addition, because the two nasal bones also are visible in cross-section, severe nasal anomalies also can be detected on this view.

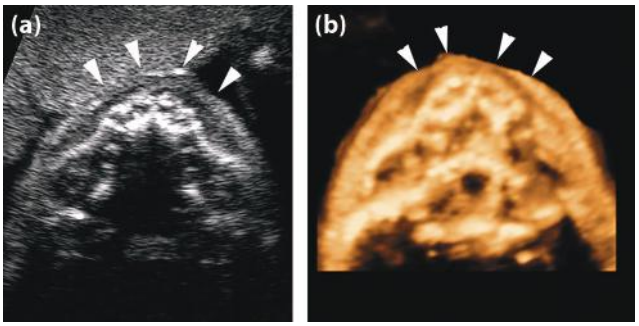


Figure 3.6 Lower maxilla/upper alveolar ridge—ventral approach. The alveoli of the upper teeth are positioned symmetrically in relation to the midline and the maxillary sinuses. In front of the upper alveolar ridge, the upper lip, displayed cross-sectionally, is visible (arrowheads). (a) Two-dimensional imaging. (b) Three-dimensional surface rendering.

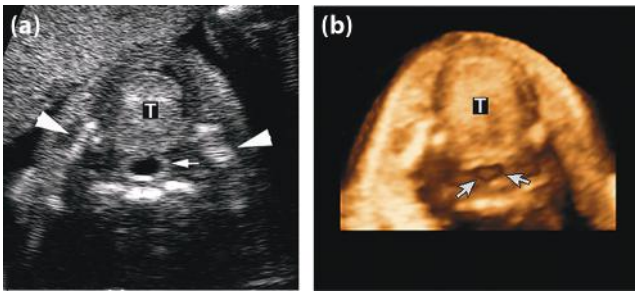


Figure 3.7 Tongue/pharynx—ventral approach. Just caudal to the upper alveolar ridge, the tongue (T) can be seen in the mouth. The oropharynx (arrows) is visualized posteriorly, in the prevertebral area. Lateral to the tongue, the two mandibular rami are seen in cross-section (arrowheads). Anteriorly, the upper lip is visible only if the plane is obtained with the mouth shut. (a) Two-dimensional imaging. (b) Three-dimensional surface rendering.

The malformations that can be anticipated and diagnosed on this view are as follows:

- *Cataract*: Partial/complete opacity of one or both lenses
- *Aphakia*: Congenital absence of the lens
- *Arhinia*: Absence of the nose (bones and soft tissues, nostrils included)
- *Microphthalmia/anophthalmia*: Complete absence or severe hypoplasia of one or both orbits
- *Hypertelorism/hypotelorism*: Increased/reduced interocular distance, with orbits of normal or abnormal dimensions
- *Macrophthalmia*: Increased orbital diameter, usually bilateral
- *Dacryocystocele*: Cystic enlargement of the lacrimal duct

Recently, some experts have reported on the possibility of using 3D US to perform a *virtual* eyeground. This approach has been employed to diagnose retinal coloboma in cases at risk (such as fetuses with suspected CHARGE association) [5].

Lower maxilla/upper alveolar ridge and related malformations (**Figure 3.6**). This plane cuts through the hard palate and the upper alveolar ridge, allowing the best possible view of the latter structure (Figure 3.6). Consequently, this view should be electively sought in order to assess the extent of the bony defect in cases of cleft lip/palate. It is important to note that isolated *cleft lip* (without associated cleft palate) can also be detected on this US plane, with the upper lip also evident on this view.

Tongue/pharynx and related malformations (**Figure 3.7**). If the transducer is moved caudally a few millimeters, the region of the mouth is displayed, with the tongue in the middle and the oropharynx posteriorly, in the prevertebral area (Figure 3.7). Therefore, in this view, the tongue diameters [6] can be measured in order to arrive at a diagnosis of *macro- or microglossia*.

Mandible/lower alveolar ridge/mandibular bone and related malformations (**Figure 3.8**). The axial view of the mandible allows, with minor angling movements of the transducer, display of the lower alveolar ridge (Figure 3.8a) and, below it, the bony mandible with the symphysis on the midline and the two mandibular branches laterally (Figure 3.8b). Therefore, this view allows confirmation of a suspicion of micrognathia, possibly raised while assessing the fetal facial profile In particular, it has been shown [7] that the two most reliable methods to detect also moderate micrognathia are the Jaw Index and the Inferior Facial Index. The former is given by the ratio of the anteroposterior mandibular diameter to the biparietal diameter: values less than 23 are indicative of micrognathia [8]. The Inferior Facial Angle (IFA) [9] is measured in a midsagittal view of the fetal profile at the crossing of two lines: one orthogonal to the vertical part of the forehead, drawn at the level of the synostosis of the nasal bones; and a second joining the tip of the mentum and the anterior border of the more protrusive lip. Its normal value is 65° (SD: 8°).

Thyroid and related malformations (**Figure 3.9**). This plane, which consists of an axial view of the fetal neck at the level of this gland, is relatively difficult to obtain, due to the fact that the operator has to wait for the fetus to extend the head slightly and to remain in that position to give a reliable display of the thyroid. In fact, with the fetal head in its most common position,

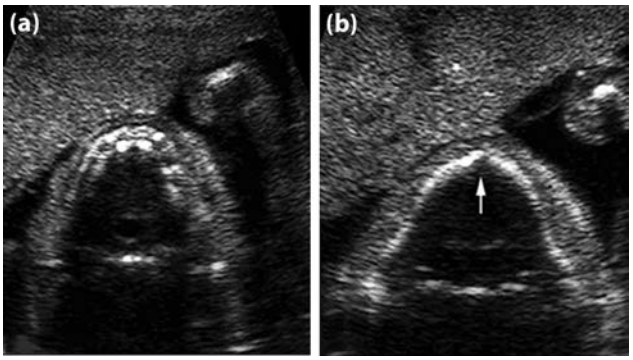


Figure 3.8 Mandible and inferior alveolar ridge—ventral approach. (a) In the plane just below the tongue, the lower horseshoe-shaped alveolar ridge can be seen. (b) Slightly caudalad, and by angling the transducer imperceptibly, the bony mandible comes into view, with its acute angle. The *symphysis mentis* can be seen on the midline (arrow).

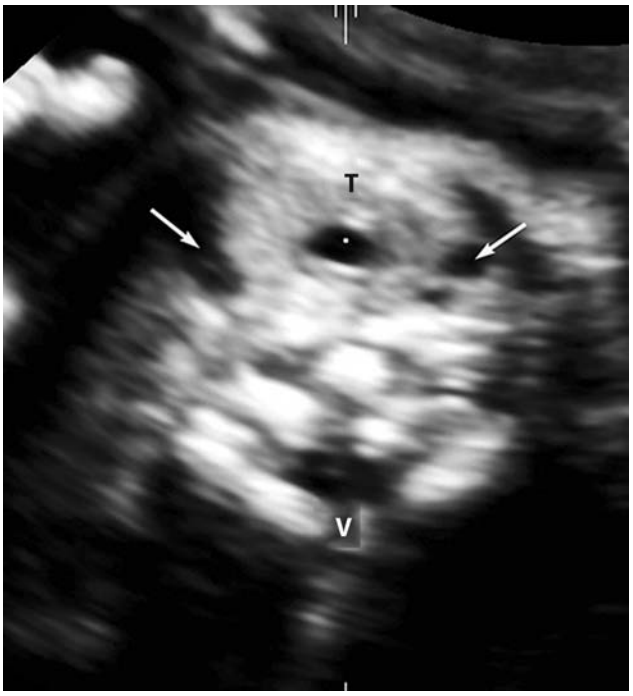


Figure 3.9 Thyroid—ventral approach. In this plane, the thyroid (T) appears as a weakly hyperechoic midline round structure surrounding the trachea (reference dot). This appears as a small round sonolucent area. The two jugular veins can be seen laterally, as small round sonolucent areas (arrows); posteriorly, the vertebral body (V) is visible.

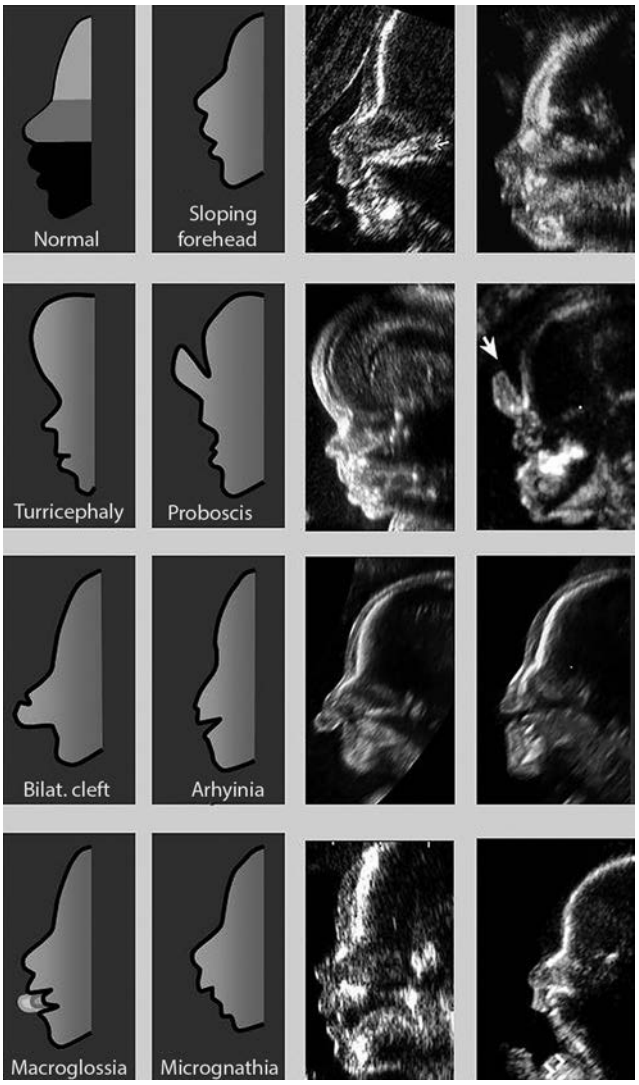


Figure 3.10 Summary of the most important anomalies of the fetal facial profile. A sloping forehead is typical of microcephaly. Proboscis and arhinia are associated with holoprosencephaly. Turricephaly, due to early closure of the coronal suture, is typical of Apert syndrome (acrocephalosyndactyly). In the case of a bilateral cleft lip/palate, there is commonly additional tissue on the philtrum, which becomes evident on the midsagittal view of the facial profile. Mild macroglossia can be found in trisomy 21 (Down syndrome), whereas severe macroglossia is typical of Beckwith–Wiedemann syndrome. Micrognathia is associated with trisomy 18 and with a considerable number of nonchromosomal syndromes (fetal akinesia deformation sequence [FADS], skeletal dysplasia, etc.).

acoustic shadowing of the mandible makes visualization of the thyroid impossible. With a compliant fetus, the thyroid, which surrounds the trachea, is seen in the center of the neck between the two jugular veins and carotid arteries, with the cervical vertebra posteriorly (Figure 3.9). This plane should be sought in order to diagnose the rare cases of fetal goiter or neck tumors.

Facial profile (midsagittal) and related malformations (Figures 3.10 and 3.11). This view, which is an extremely important one to obtain in order to get an overall idea of the anatomic proportions of the fetal face, represents a midsagittal plane, as already pointed out. Its importance is due to the fact that in this one plane, the three regions of the face (forehead,

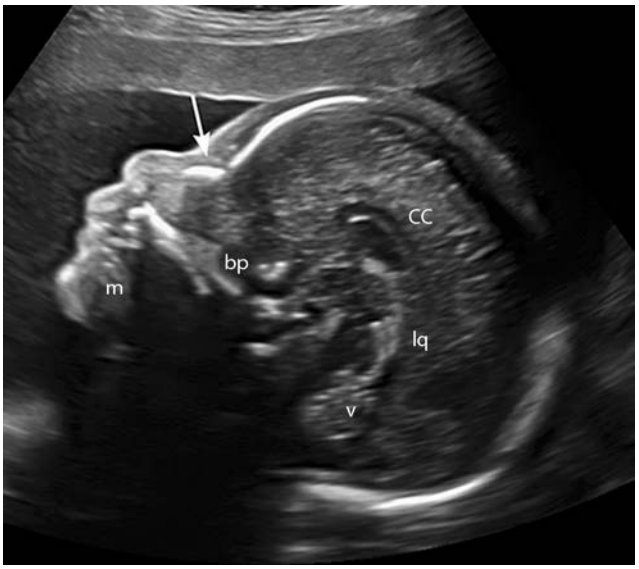


Figure 3.11 Midsagittal view of the fetal facial profile. In this view, the following structures can be recognized: the frontal area, the nasal root, the nose with the nasal bone (arrow), the lips with the bony palate (bp) in cross-section, and the chin, with the mandible (m) in cross-section. It should be noted that if the view is perfectly on the midline, as in this case, the orbits cannot be seen, this being a symmetric organ. In addition, due to the yet-unossified metopic suture, the ultrasound beam penetrates deep in the fetal head, allowing a good view of the corpus callosum (CC) with the cavum septi pellucidi beneath, the quadrigeminal plate, lamina quadrigemina (lq), and the cerebellar vermis (v).

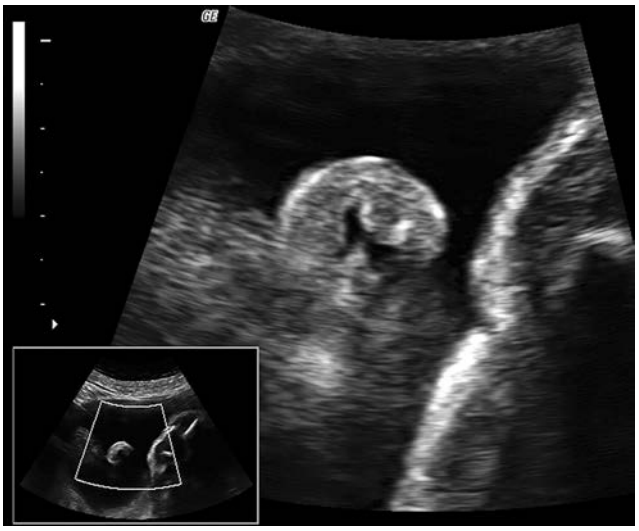


Figure 3.12 Parasagittal view at the level of the external ear. This view, which is often difficult to obtain with two-dimensional ultrasound, allows visualization of the external ear, which is abnormal or wrinkled in some syndromic conditions. The whole anatomy of the external ear is visible. This image was obtained in a 29-week-old fetus.

eyes and nose, and mouth and chin) are displayed together. The irregularity and the extreme phenotypic variability of the lines that make up the human face do not lend themselves easily to the creation of nomograms expressing the harmony and the correct mathematical or geometric relationships of the various elements composing the facial profile at least in the fetus [1]. Consequently, the diagnosis of generic profile abnormalities, such as a sloping forehead or a wide nasal root, is mainly based on a subjective assessment. In this US plane, the following aspects can be recognized (Figures 3.10 and 3.11): the echogenic curved shape of the frontal bone, with the overlying hypoechoic line represented by the soft tissues; the nasal area, with the nasal bone(s) in the upper part and the soft tissue of the tip of the nose; part of the hard palate; the lips, with the upper lip protruding slightly over the lower one; and the chin with the bony mandible. It is useful to note that, if the scanning view is perfectly on the midline, the insonating beam passes through the still open metopic suture, allowing a nice view of the brain, with the corpus callosum, the cavum septi pellucidi, the third ventricle, the quadrigeminal plate, and the cerebellar vermis (Figure 3.11; and see Chapter 2).

The major abnormalities detectable on this view are as follows (Figure 3.10):

- *Forehead, sloping forehead*: Due to the severe hypoplasia of the frontal lobes in microcephaly
- *Forehead, turricephaly*: Increased vertical diameter of the forehead, due to early closure of the sutures
- *Nose, arhinia*: Absence of the nose (bones and soft tissues, nostrils included); midline defect, associated with the holoprosencephaly sequence
- *Nose, proboscis*: Midline soft tissue appendix, protruding from the nasal root area; midline defect, associated with the holoprosencephaly sequence
- *Mouth, bilateral cleft*: Additional tissue on the philtrum, common in bilateral clefts
- *Mouth, macroglossia*: Increased volume of the tongue, usually protruding between the lips
- *Chin, micrognathia*: Hypoplasia of variable degree of the bony mandible, both in the anteroposterior diameter (retrognathia) and in the latero-lateral one

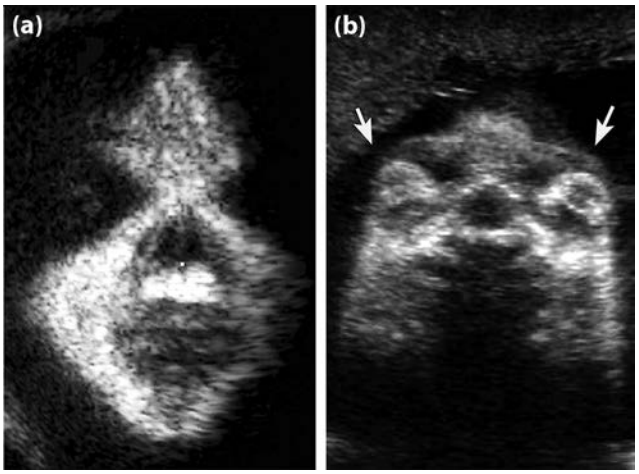


Figure 3.13 Coronal view of the face. (a) Normal fetus. (b) Syndromic fetus (22 weeks) with evident proptosis (arrows).

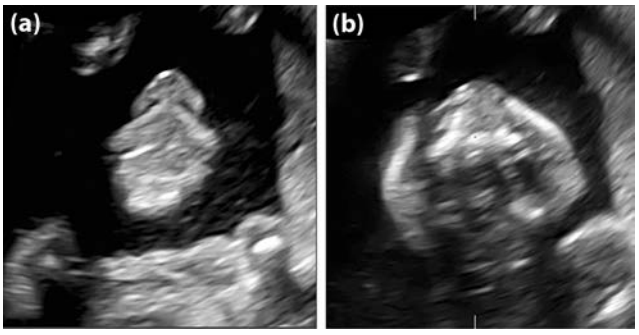


Figure 3.14 Oblique view of lips (a) and palate (b). (a) This represents the classic plane for assessment of the lips in normal and abnormal conditions: the lips, the nose with the nostrils, and the chin are displayed. (b) This plane is cut slightly deeper than the previous one; therefore, it allows recognition of the bony palate and its defects.

Ear (parasagittal) and related malformations. The most lateral sagittal plane of the fetal head is that passing for the external ear, which can be insonated with fine movements of the transducer (Figure 3.12). It is difficult to confirm a diagnosis of low-set ears, frequently associated with chromosomal abnormalities and nonchromosomal syndromes, but it is possible to confidently detect preauricular tags, which are also associated with rare syndromic conditions [10]. However, it should be emphasized that this parasagittal two-dimensional (2D) view has been replaced by the 3D surface-rendering image of the fetal face, which is much more readily obtained and, as far as ear abnormalities are concerned, also provides greater diagnostic accuracy (see Figure 3.29).

Face (coronal) and related malformations. In this coronal view, the fetal splanchnocranium is displayed *en face*, allowing an overall evaluation of the various anatomic structures (Figure 3.13). At the same time, this allows recognition of abnormally protruding anatomic structures, such as the eyes in the case of proptosis, bilateral cleft lip (additional tissue on the philtrum), or the tongue (macroglossia).

Lips (oblique) and related malformations. Oblique tangential views of the lips and palate are of fundamental importance for the detection of facial clefts and abnormalities of the nostrils associated with the holoprosencephaly sequence (arhinia or single nostril). An oblique view of the lips allows assessment of the philtrum in the middle of the upper lip, its relationship with the nostrils, the lower lip, and, inferiorly, the chin (Figure 3.14a). Therefore, this view allows diagnosis of single nostril, and median, unilateral, and bilateral clefts.

Palate (oblique) and related malformations. This view is parallel but deeper in comparison with the previous one (see Figure 3.15). It allows assessment of the upper alveolar ridge and, therefore, detection of defects of the hard palate and their relationships with the nasal cavity (Figure 3.14b).

The most significant malformations detectable on this view are as follows:

- *Single nostril*: Midline defect, associated with the holoprosencephaly sequence
- *Median cleft*: Midline defect, associated with the holoprosencephaly sequence
- *Unilateral cleft lip/palate*: Unilateral defect of the lip, alveolar ridge, and hard palate
- *Bilateral cleft lip/palate*: Bilateral defect of the lip, the alveolar ridge, and hard palate, commonly associated with additional tissue on the philtrum

Artifacts

Orbits. Because the orbits are symmetric organs, care should be taken to obtain a perfectly axial view. If this does not happen, a *false-positive diagnosis* of microphthalmia can be made (Figure 3.16a). In such a circumstance, it is necessary to reobtain the plane, making delicate sweeping and tilting movements, in order to achieve a correct symmetric positioning of the transducer to remove the artifact (Figure 3.16b).

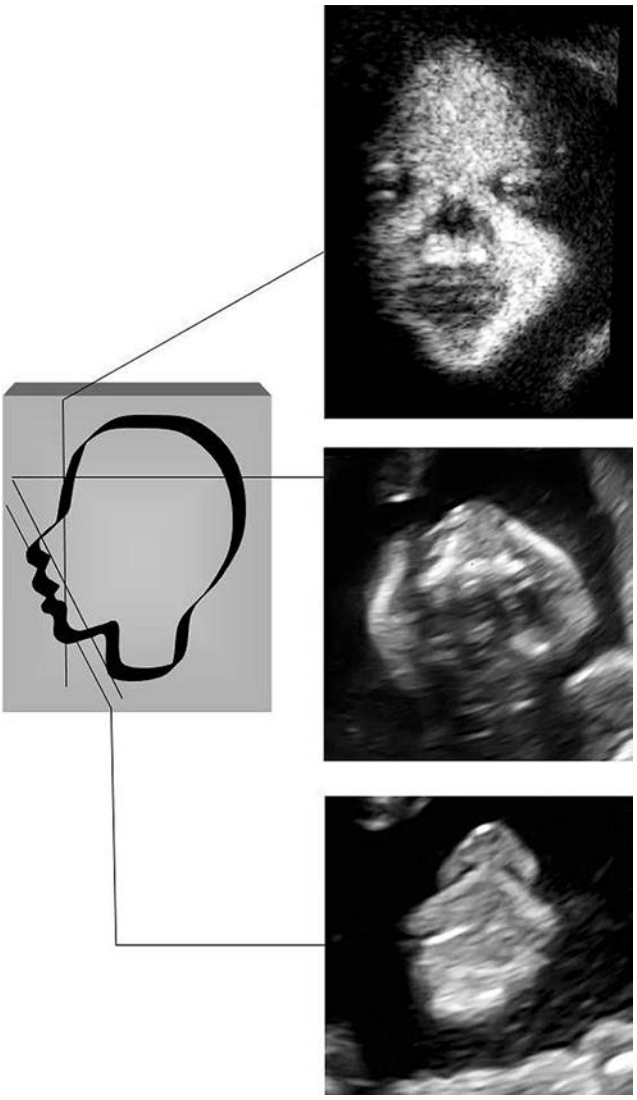


Figure 3.15 Coronal and oblique ultrasound views for the assessment of the splanchnocranium. This figure illustrates the level of the scanning plane and the corresponding two-dimensional ultrasound image. All views are illustrated in detail in Figures 3.13 and 3.14.

Lips. If the umbilical cord lies close to the upper lip, this can sometimes create the *false impression of a clefting* (Figure 3.17a). In this case, the lips should be checked again after a few minutes, to allow the fetus to move. Alternatively, power Doppler (or color Doppler with a relatively low pulse repetition frequency) may be used to discriminate between the cord lying on the lips and a real cleft lip/palate (Figure 3.17b).

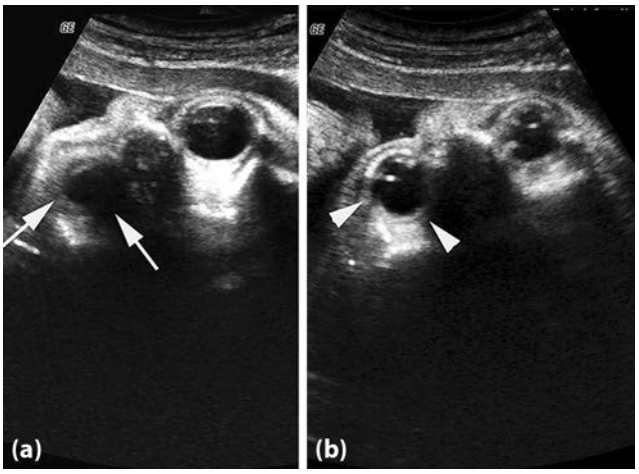


Figure 3.16 Artifact. A false-positive diagnosis of microphthalmia can be made if the plane for the visualization of the orbits is not perfectly axial. (a) One of the orbits (usually that distal to the transducer) appears smaller than the other (arrows). (b) It is sufficient to reobtain the axial plane with a correct angle to remove the artifact (arrowheads).

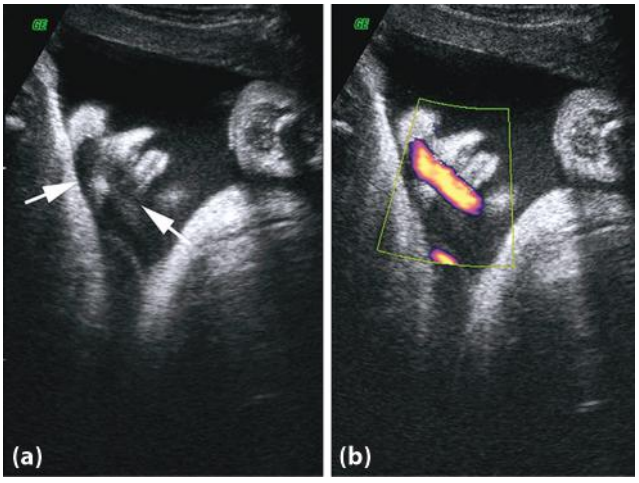


Figure 3.17 Artifact. A false-positive diagnosis of cleft lip/palate can be made if a cord loop is positioned in front of the lips. (a) The cord, lying vertically on the lips, can be mistaken for a cleft (arrows). (b) It is sufficient to wait for the fetus to move or, better, to switch on color/power Doppler to identify the umbilical blood flow and remove the artifact.

ThE r oLE oF 3d ULTr ASo UNd IN ThE Ass Ess MENT oF FAc IAL ABNor MALITIEs

Premises. The fetal face is one of the anatomic regions that benefits more from a 3D US approach, be this with multiplanar imaging or with surface rendering. In particular, the employment of 3D US represents the best

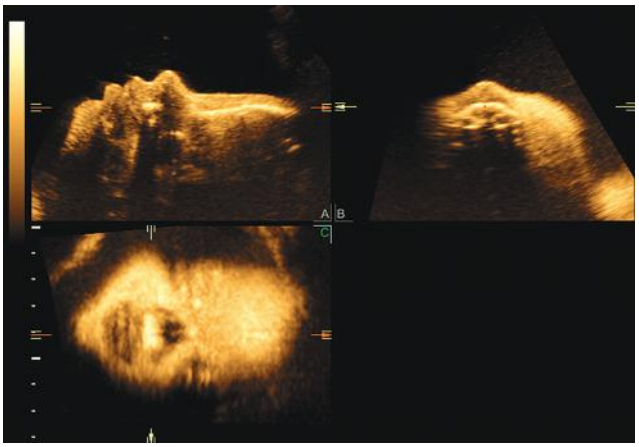


Figure 3.18 Multiplanar assessment of the face at 32 weeks' gestation. This image demonstrates the possibility of navigating the volume on the three orthogonal planes. Positioning the caliper at the level of the upper alveolus on the sagittal view, in window A, the axial view of the alveolar ridge will appear in window B, and the coronal view of the face in window C.

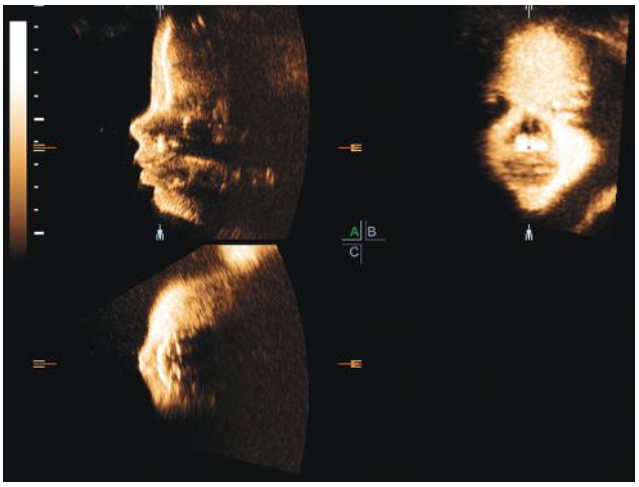


Figure 3.19 Multiplanar assessment of the face. This image shows the same volume as in Figure 3.18: on simply rotating the image in window A by 90°, the images in windows B and C change accordingly.

possible approach to the detailed characterization of craniofacial malformations, since this technique is able to effectively display anomalies of both the soft tissues and the bony structures. This is why we deem it is important to dedicate this part of the chapter to the description of the multiplanar and surface-rendering images of immediate clinical utility. It should be recalled here that a general introduction to the 3D technique is presented in Chapter 1, where the procedure of volume acquisition and rendering is explained—hereinafter, only the details regarding the use of 3D US for the assessment of craniofacial anomalies are described.

Lips and palate

Multiplanar imaging. The multiplanar mode represents the best approach for a detailed assessment of normal and abnormal facial anatomy. The volume acquisition is usually carried out having as a reference 2D plane the midsagittal view of the facial profile, described elsewhere in this chapter. However, if the region of interest is the oromandibular one, as in the case of facial clefting or micrognathia, the acquisition can also be advantageously made from an axial, ventral view of the face, at the level of the maxilla. Once the volume has been obtained, its study in multiplanar imaging allows a detailed evaluation of the bones and the soft tissues. For example, an acquisition obtained from the axial view at the level of the maxilla is shown in Figure 3.18. As is evident, the possibility to scroll the volume on one plane, checking how the views change on the other two planes, allows reliable identification of anatomic detail in normal and abnormal conditions. The utility of the multiplanar approach is demonstrated in Figure 3.19, obtained simply by rotating the image of "A" window of Figure 3.18, in order to display the facial profile in a vertical, more familiar position. In the case of complex cleftings, the use of multiplanar imaging allows a careful assessment of the extent and subtype of the defect, thanks to the correlation among the three orthogonal planes. The aspects in multiplanar imaging of a normal fetus, a fetus with unilateral cleft lip/palate, and a third with bilateral cleft lip/palate are shown in Figures 3.20 through 3.22: the features of the defects and their extent are evident.

Surface rendering. Having completed the anatomic assessment on multiplanar imaging, it is possible to switch to the surface-rendering mode, if the aim is the assessment of soft tissues (Figures 3.23 and 3.24a). If, however, the operator elects to study the bony structures, then the "maximum" mode should be employed: this filter adds transparency to the superficial, less echogenic tissues, letting the underlying bony skeleton show up (Figure 3.24b). Surface-rendering images of unilateral cleft lip/palate, bilateral cleft lip/palate, and isolated cleft lip are shown in Figures 3.25 through 3.27. In Figure 3.28, the maximum mode is used to demonstrate the bony cleft of the palate. Both rendering modes (surface and maximum) and multiplanar imaging can be advantageously employed during prenatal counseling sessions with the parents and for consultation with plastic surgeons.

Ear

Surface rendering. The external ear can, with some expertise, be imaged with 2D US, and there are reports in the literature of preauricular tags detected with this

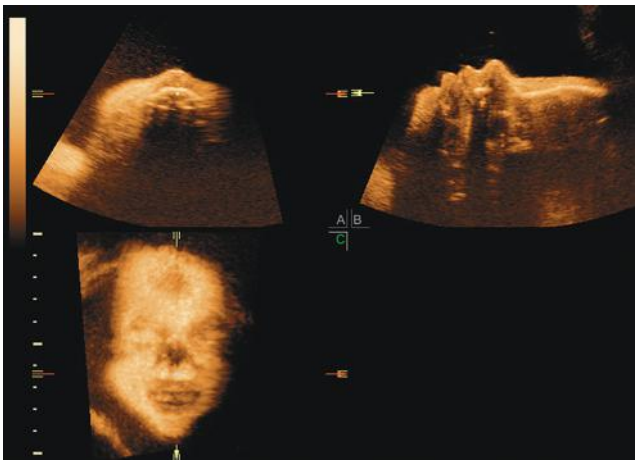


Figure 3.20 Multiplanar assessment of the face: normal fetus. To adequately study the lips and the whole area of the mouth, it is useful to display the axial plane in window A, so that the midsagittal profile view shows in B and the coronal view in C. Positioning the caliper at the level of the upper alveoli, the integrity of the hard palate can be assessed on the coronal plane (window C).



Figure 3.22 Multiplanar assessment of the face: bilateral cleft lip/palate (22 weeks' gestation). Also in this case, on positioning the caliper in the midline, behind the median remaining part of the alveolar ridge, on the axial view (top-left window), the additional tissue on the philtrum, characteristic of bilateral clefts, becomes visible in the sagittal plane (top-right window—arrow), while the bilateral ample palatal defect is visible in the coronal plane (lower-left window).



Figure 3.21 Multiplanar assessment of the face: unilateral cleft lip/palate (27 weeks' gestation). In this case, on positioning the caliper at the level of the bony defect (arrow) in the axial plane (top-left window), the abnormal communication between mouth and nose becomes visible in the coronal plane (lower-left window), with the caliper at the level of the palatal defect.

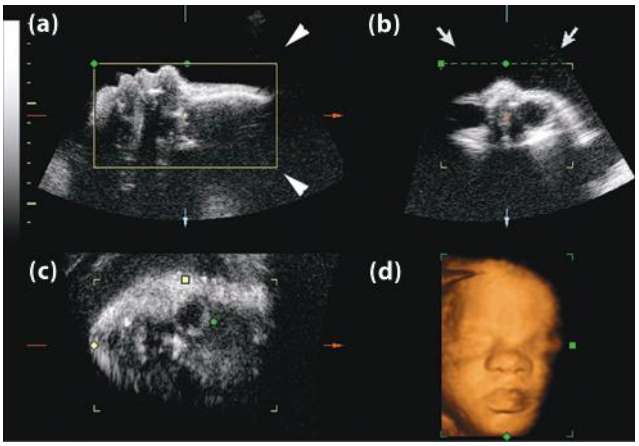


Figure 3.23 Surface rendering of the normal fetal face (same volume as in Figures 3.18 and 3.19, 32 weeks' gestation)—rendering mode for soft tissues (surface mode). The region of interest (ROI) box is positioned around the fetal face (window A, profile view) (arrowheads), with an adequate acoustic window, and on (b) the side of the green visualization bar is checked (arrows). In (d), the reconstructed three-dimensional image is displayed: this is a normal fetus of African American origin.

technique. However, we believe that 3D US and, above all, its surface-rendering mode, makes the assessment of the normal and abnormal external ear much easier and immediate [6]. In addition, this approach allows an opportunity to diagnose, with a good degree of accuracy, the occurrence of low-set ears, which represents a key feature in a significant number of chromosomal and nonchromosomal anomalies [10]. The 3D appearances of a normal ear and of various ear abnormalities are shown in Figure 3.29.

Cranial sutures and related abnormalities. The cranial sutures can be assessed only by 3D US, with the transparent maximum mode. The procedure and the appearance of normal and abnormal sutures is described at the end of this chapter.

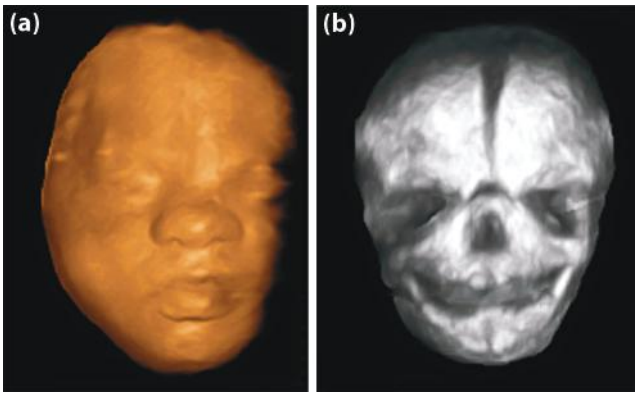


Figure 3.24 Renderings for soft tissues and bones. (a) Surface-mode rendering allows the display of the facial features (large nasal root, typical of the African American population). (b) Maximum-mode rendering is used to assess the bones: the metopic suture, between the frontal bones, the hard palate, and the mandible are all clearly displayed.

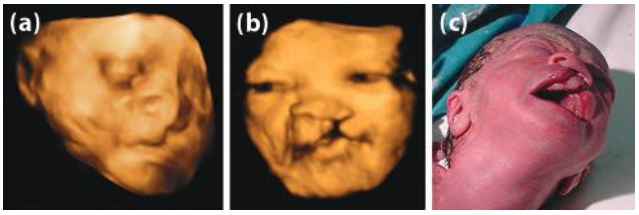


Figure 3.25 Surface-rendering reconstruction: unilateral cleft lip/palate. This is the same case as in Figure 3.21 (a) 27 weeks' gestation; (b) 35 weeks' gestation; (c) the appearance of the face, with the distortion of the alae nasi, is similar to the aspect at birth.



Figure 3.26 Surface-rendering reconstruction: bilateral cleft lip/palate. This is the same case as in Figure 3.22 (22 weeks' gestation). Also, in this case, the three-dimensional reconstruction of the bilateral cleft is similar to the autopsy finding.



Figure 3.27 Surface-rendering reconstruction: unilateral cleft lip. In this syndromic fetus (32 weeks), three-dimensional surface rendering allows demonstration of the small isolated cleft lip. The alveolar ridge was unaffected. On the right is the neonate at birth.

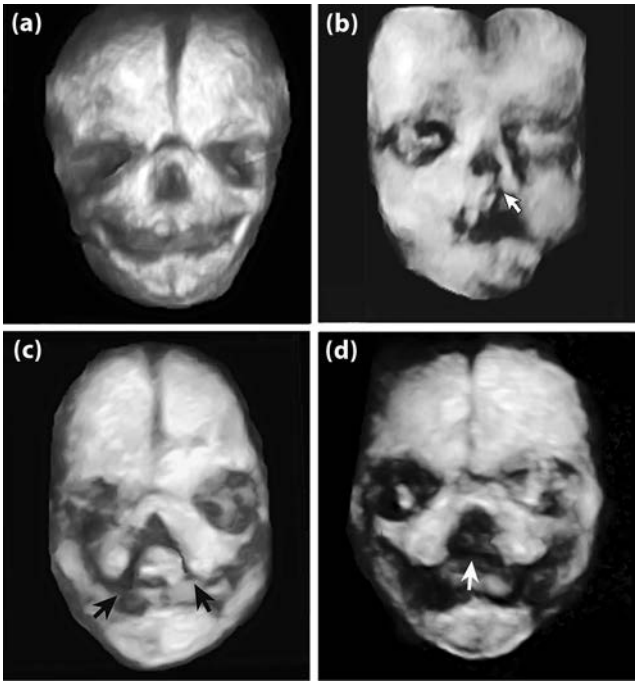


Figure 3.28 Maximum-mode rendering for the bones. The same volumes used for the images in Figures 3.20 through 3.22 are now processed with the maximum mode, in order to show the bony defects associated with cleft/palate (arrows): (a) normal palate; (b) unilateral cleft lip/palate; (c) bilateral cleft lip/palate; (d) large midline defect in a fetus with holoprosencephaly (21 weeks' gestation).

The fetal face

Surface rendering. Three-dimensional reconstruction of the fetal face has unfortunately represented for years the key marketing asset of 3D US both among professionals and in the media [11,12]. The number of articles appearing in women's magazines is almost comparable to the number of scientific publications in medical journals. The concept of fetomaternal bonding has been misused and abused in order to justify the wide use of 3D US. We have demonstrated above the clinical utility of such an approach in the characterization of fetal facial malformations, and we firmly believe that the clinical

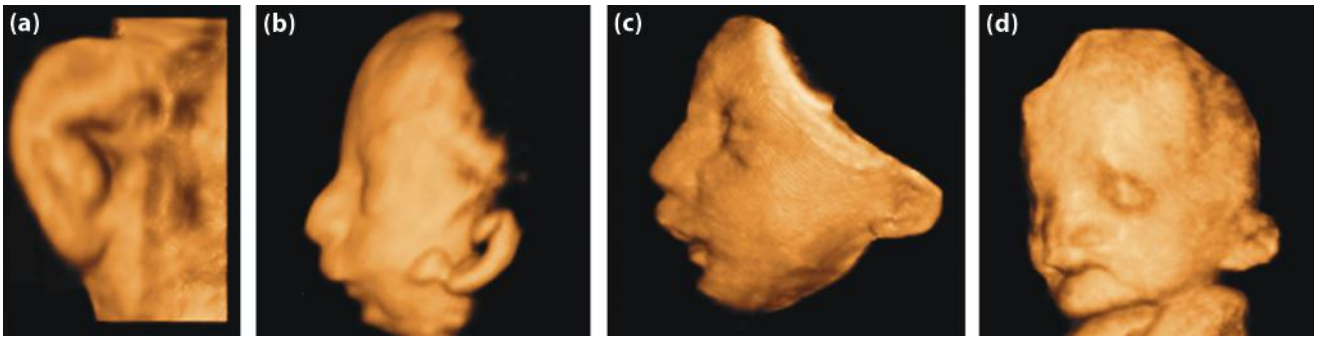


Figure 3.29 Surface-rendering reconstruction: external ear. (a) Magnification of a normal ear at 32 weeks' gestation; (b) syndromic fetus: low-set ears with preauricular tag; (c) syndromic fetus: low-set ears; (d) syndromic fetus: low-set ears and facial dysmorphism.

assessment of the abnormal fetus should be and should remain the key motivation for the use of 3D US.

"Scanning for pleasure," as Larry Platt [12] has said, or producing nice views of fetal facial expressions, should not be considered misuse—however, in our opinion, it should not be financially exploited without letting women know that fetal portraiture is not a medical procedure.

chArAcTErIzATIoN oF MAjor A NoMALIEs

ANoph ThALMIA/MIcroph ThALMIA

Incidence. Rare.

Ultrasound diagnosis. Reduced orbital diameter on the axial view of the orbits.

Risk of chromosomal anomalies. High.

Risk of nonchromosomal syndromes. Very high: Goldenhar, Cerebro-Oculo-Facio-Skeletal (COFS), Meckel–Gruber, Walker–Warburg.

Outcome. Depends on the general clinical context. Significant aesthetic impact also for isolated cases.

Definition Hypoplasia of variable degree of the bony orbit and the eye bulb.

Etiology and pathogenesis. Microphthalmia can be unilateral or bilateral. In both cases, it is often associated with severe chromosomal and nonchromosomal syndromes, the most common of which are described below.

Ultrasound diagnosis. This is made on the axial view of the orbits, regardless of the approach (lateral or ventral), as already described. The orbits appear small and hypoplastic—sometimes to such an extent that it is hard to identify them (Figures 3.30 through 3.32). In the case of moderate microphthalmia, the use of published nomograms [4] (see Appendix Table A.15) may be of help in establishing the diagnosis.

Note. In the case of misalignment of the US beam on the axial plane, a false-positive impression of microphthalmia can be created (see Figure 3.16).

Prognostic indicators. If the anomaly is bilateral, it is often syndromic and, as such, has a poorer prognosis. Isolated unilateral microphthalmia has a very high aesthetic impact and may or may not be associated with sight loss, according to the presence and functional status of the hypoplastic eye bulb. Aphakia (complete absence of the lens) may indicate complete absence of the eye bulb.

Association with other malformations. Microphthalmia is relatively often associated with cataract or lens opacity.

Risk of chromosomal anomalies. This is high. Microphthalmia is one of the most common features of trisomy 13 (in 50% of cases), especially if holoprosencephaly is also present.

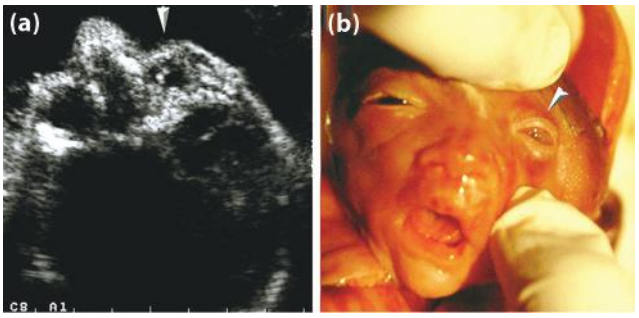


Figure 3.30 Unilateral microphthalmia with cataract. (a) The severe hypoplasia of the left orbit, which is associated with a corneal opacity (arrowhead), is evident. (b) The autopsy confirms both ultrasound findings, namely, unilateral microphthalmia and cataract.

Risk of nonchromosomal syndromes. This is high. The syndromes detectable in utero that can be associated with microphthalmia are as follows:

- *Goldenhar syndrome (oculo-auriculo-vertebral spectrum [OAVS]) [13,14]*: look for ► *microphthalmia* + unilateral cleft lip/palate + hemifacial microsomia (see Chapter 10);
- *Cerebro-oculo-facio-skeletal [COFS] syndrome [15]*: look for ► *microphthalmia, bilateral* + arthrogryposis + micrognathia (see Chapter 10);
- *Walker–Warburg syndrome [16]*: look for ► *microphthalmia, bilateral* + cataract + hydrocephaly + Dandy–Walker malformation;
- *Fraser syndrome [17]*: look for ► *microphthalmia, bilateral* + laryngeal atresia + cleft lip/palate + external ear anomalies + bilateral renal agenesis + congenital heart disease (see Chapter 10);
- *Meckel–Gruber syndrome [16]*: look for ► *microphthalmia, bilateral* + cephalocele + polycystic kidney + polydactyly (see Chapter 10).

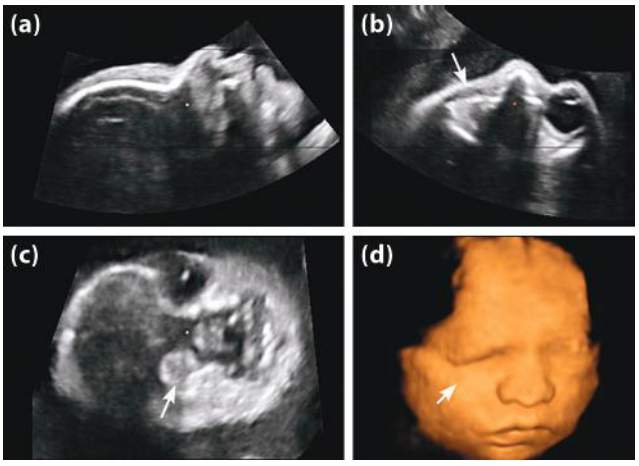


Figure 3.31 Unilateral anophthalmia. Multiplanar imaging (a–c). The reference dot is positioned on the midline, at the level of the orbits. There is no abnormality shown on the profile view (a). The axial (b) and coronal (c) views demonstrate the complete absence of the right orbit (arrow) and eye bulb. (d) On surface rendering, the defect is barely visible, with only mild enophthalmos and facial asymmetry evident.

Obstetric management. Should microphthalmia be detected in a fetus, fetal karyotyping is mandatory in order to exclude chromosome 13 anomalies (trisomy and long-arm deletion, del(13q)). In addition, a thorough anatomic scan should be performed by an expert, in order to detect major and/or minor signs possibly leading to the diagnosis of one of the above-mentioned syndromes. Obstetric care and mode and timing of delivery are unaffected.

Prognosis, survival, and quality of life. If the lesion is part of a syndrome, then overall survival is extremely poor, due to the severity of the above-mentioned syndromic conditions. On the other hand, in the case of

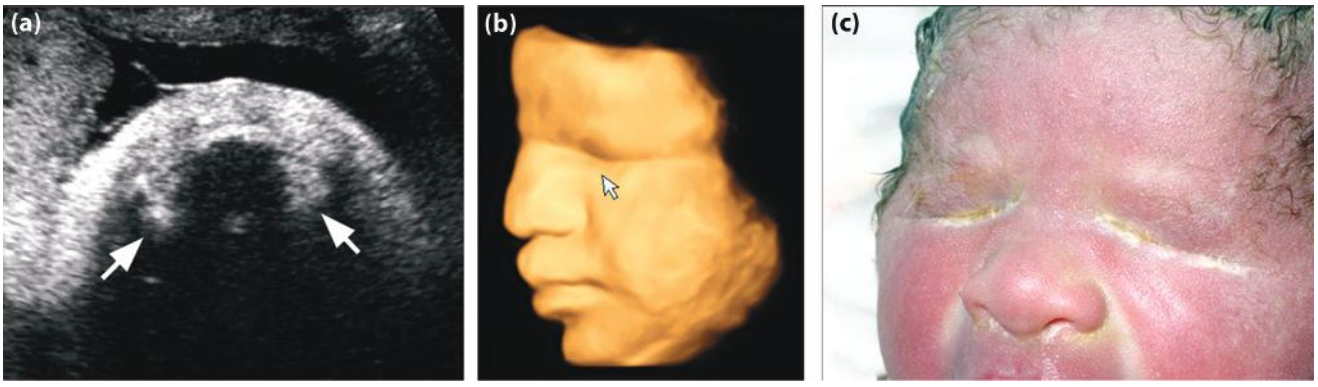


Figure 3.32 Bilateral microphthalmia (33 weeks' gestation). (a) Two-dimensional ultrasound: On this axial view of the orbits, the orbital cavities are replaced by whitish areas (arrows) and there is no sign of the eye bulbs. (b) Three-dimensional surface-rendering reconstruction of the fetal face showing the apparently sealed eyelid and the enophthalmos. (c) At birth: Both eyelids appear sealed and there is no sign of either orbits or eye bulbs.

isolated microphthalmia, the main problem, which may sometimes require cosmetic surgery only for psychologic reasons, is the significant aesthetic impact related to the facial dysmorphic features. The life span is unaltered, while the quality of life depends upon the degree of visual compromise of the affected eye.

cATAr Ac T

Incidence. Extremely rare.

Ultrasound diagnosis. Lens opacity, unilateral or bilateral, detected on the axial view of the orbits.

Risk of chromosomal anomalies. Low.

Risk of nonchromosomal syndromes. Extremely high: COFS, Walker–Warburg, Neu–Laxova, chondrodysplasia punctata.

Outcome. Depends on the general clinical context. Good outcome after surgery in nonsyndromic cases.

Definition Cataract denotes partial or total opacity of the eye lens. It can be unilateral or bilateral.

Etiology and pathogenesis. Cataract is an extremely rare lesion in the fetus. It can be the effect of first trimester maternal infections (rubella) or be due to the underlying presence of a syndrome. Isolated, unilateral, nonsyndromic cases have also been described. In this regard, a recent population case–control study [18] has found a positive correlation between maternal infl - enza/common cold/minor respiratory infections during early pregnancy and the occurrence of cataract in the fetus, but only if these minor illnesses were not treated with antifever drugs. These findings led the authors of the study to two conclusions: (1) congenital nonsyndromic cataract may be the result of transient maternal hyperthermia during organogenesis; (2) influenza vaccination and antifever therapy in common cold/minor respiratory infections in early pregnancy may reduce the incidence of congenital nonsyndromic cataract [18].

Ultrasound diagnosis. This is carried out on the axial view of the orbits, preferably with a ventral approach; at the level of one or both orbits, a hyperechoic, usually round, area is seen, as already described earlier in this chapter (Figures 3.30 and 3.33). Numerous authors have demonstrated that the recognition of a lens opacity is undeniably associated with cataract, while the reverse is not always true: the absence of any hyperechogenicity within the orbit in fetuses at risk of cataract does not allow one to exclude its presence.

Prognostic indicators. Bilateral cataracts are usually of syndromic origin, and, as such, have a poorer prognosis. Conversely, isolated, unilateral cases are more commonly due to intrauterine infections; in these cases, the final outcome depends on the spread and severity of the infection. If the cataract is associated with microphthalmia, this is more indicative of a syndrome. The isolated forms, which are not always detectable in utero because they are not constantly associated with lens hyperechogenicities, have a significantly better prognosis.

Association with other malformations. Microphthalmia is the most frequently associated anomaly.

Risk of chromosomal anomalies. This is low.

Risk of nonchromosomal syndromes. This is high, especially for bilateral forms. The in utero detectable syndromes that can be associated with cataract are as follows:

- *COFS syndrome [15]*: look for ► *cataract* + microphthalmia (bilateral) + arthrogryposis + micrognathia;
- *Walker–Warburg syndrome [16]*: look for ► *cataract* + microphthalmia + hydrocephaly + Dandy–Walker malformation;

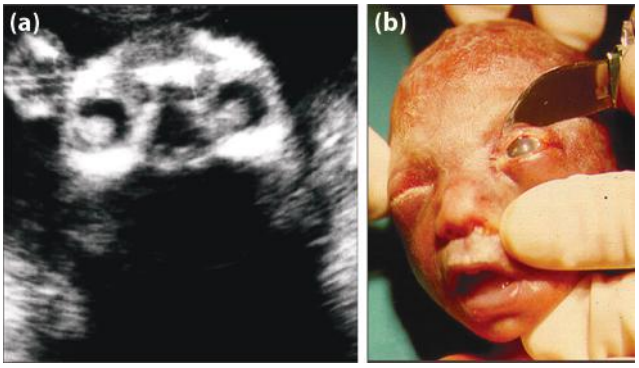


Figure 3.33 Bilateral cataract. In this case, bilateral cataract, detected at 20 weeks' gestation (a), was the only sonographically recognizable sign of a recurrent Walker–Warburg syndrome. (b) At autopsy, the occurrence of bilateral cataracts was confirmed. Note the opaque aspect of the lens.

- *Neu–Laxova syndrome [16]*: look for ► *cataract* + microcephaly + agenesis of the corpus callosum + severe cerebellar hypoplasia + hypertelorism + micrognathia + short limbs + syndactyly + joint contractures + early-onset fetal growth retardation + polyhydramnios (see Chapter 10);
- *Chondrodysplasia punctata [16]*: look for ► *cataract* + symmetric rhizomelic limb shortening + epiphyseal calcifications.

Obstetric management. Should cataracts be detected in a fetus, a thorough anatomic scan should be performed by an expert, in order to detect major and/or minor signs possibly leading to the diagnosis of one of the above-mentioned syndromes. Obstetric and delivery management should be changed accordingly.

Postnatal therapy. This entails lens aspiration and the use of contact lens, bifocal spectacles, and occlusion therapy (of the other eye, to stimulate the aphakic one), followed at a later stage by placement of a posterior chamber intraocular lens, with the latter procedure still being controversial [19,20].

Prognosis, survival, and quality of life. If additional anomalies and syndromes are absent, survival is unaffected and the quality of life unremarkable, although in selected cases visual axis reopacificatio can occur. In these cases, the intraocular lens should be replaced [19]. In syndromic cases, which are usually associated with microphthalmia, the perinatal mortality risk is extremely high, owing to the severe abnormalities that characterize the above-mentioned syndromes.

hyp Er TELor IsM

Incidence. Rare.

Ultrasound diagnosis. Increased (>95th percentile) interocular distance, often, but not always, associated with an increased binocular distance.

Risk of chromosomal anomalies. Low.

Risk of nonchromosomal syndromes. High: frontonasal dysplasia, Neu–Laxova, median facial cleft syndrome, Apert syndrome.

Outcome. Depends on the general clinical context.

Definition Increased (>95th percentile) interocular distance, often, but not always associated with an increased binocular distance.

Etiology and pathogenesis. Hypertelorism is rarely found in the fetus. Given that embryologically the ocular structures develop laterally and then start to migrate toward the midline to end up in their normal position, hypertelorism may be seen as a partial arrest in this migration process (as in the median facial cleft syndrome). Alternatively, it can be the result of an anterior cephalocele, which mechanically limits the migration process. Or it can be determined by anomalies in the development and growth of the cranial bones, as in Apert syndrome (see Chapter 10).

Ultrasound diagnosis. The diagnosis is made on the axial view of the orbits, with a lateral or ventral approach. In the rare cases of severe hypertelorism, the diagnosis is straightforward and does not need to be confirmed with the measurement of the binocular and interocular diameters (Figure 3.34). However, in most instances, the degree of hypertelorism is moderate or moderately severe. In these cases, the diagnosis of hypertelorism should always rely on the biometric assessment (binocular and interocular diameters >95th percentile see Appendix Table A.15).

Prognostic indicators. The recognition of a midline cystic structure, consistent with a diagnosis of an anterior cephalocele, represents a poor prognostic sign, because this anomaly is often associated with a bifid nose and median clefting (median facial cleft syndrome). The association with other abnormalities of the face and/or the central nervous system increases the syndromic risk exponentially.

Association with other malformations. There are no significant malformative clusters reported.

Risk of chromosomal anomalies. This is low. There have been a few cases of trisomy 13 and rare chromosomal arrangements.

Risk of nonchromosomal syndromes. This is high. The in utero detectable syndromes that can be associated with hypertelorism are as follows:

- *Neu–Laxova [16]*: look for ► *hypertelorism* + microcephaly + agenesis of the corpus callosum + severe cerebellar hypoplasia + cataract + micrognathia + short limbs + syndactyly + joint contractures + early-onset fetal growth retardation + polyhydramnios (see Chapter 10);

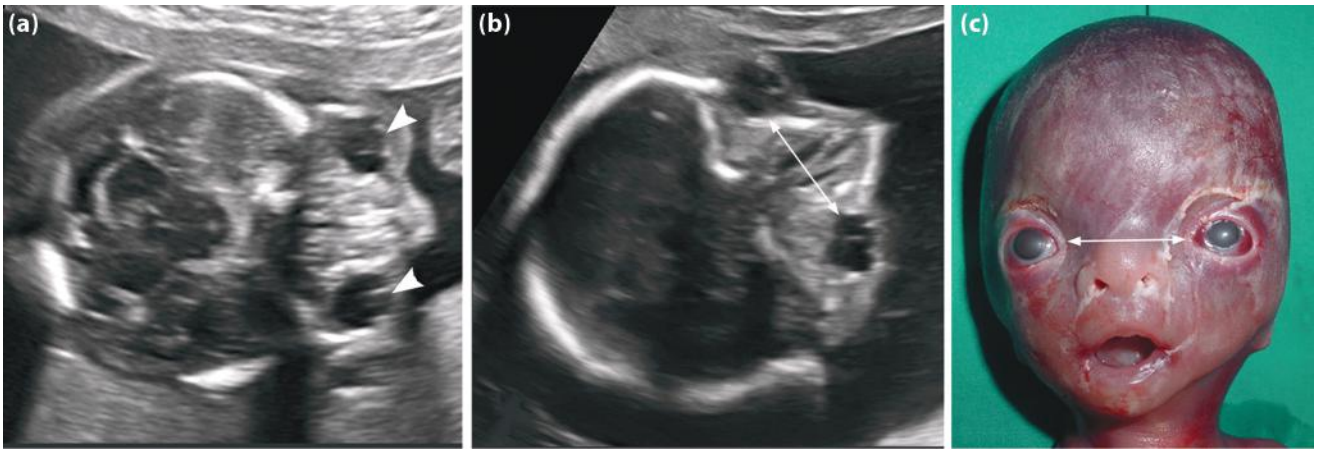


Figure 3.34 Hypertelorism. (a) Normal fetus at 22 weeks' gestation (arrowheads: lenses); (b) fetus with evident hypertelorism at 21 weeks' gestation. This fetus also had constantly open hands, leading to the final diagnosis of restrictive dermopathy. (c) The autoptic confirmation after termination of pregnancy. Note the fully opened eyelids, while at this gestational age these are always still sealed (arrows: increased interocular distance).

- *Median facial cleft syndrome [16]*: look for ► *hypertelorism* + midline facial clefting + anomalies of the nose;
- *Apert syndrome* (*acrocephalosyndactyly*) *[16]*: look for ► *hypertelorism* + turricephaly + macroglossia + syndactyly + fusion of cervical vertebrae + renal anomalies + congenital heart disease (see Chapter 10);
- *Frontonasal dysplasia [21]*: look for ► *hypertelorism* + anterior cephalocele + median cleft lip + bifi nose.

Obstetric management. Should hypertelorism be detected in a fetus, a thorough anatomic scan should be performed by an expert, in order to detect major and/or minor signs possibly leading to the diagnosis of one of the above-mentioned syndromes.

Prognosis, survival, and quality of life. The prognosis depends on the general clinical context, and on the nature of any underlying syndromic condition of which the hypertelorism is an expression.

hypo TELor IsM

Incidence. Rare.

Ultrasound diagnosis. Reduced (<5th percentile) interocular and binocular distances.

Risk of chromosomal anomalies. Extremely high and related to the almost constant association with holoprosencephaly.

Risk of nonchromosomal syndromes. Extremely high: trisomy 13.

Outcome. Extremely poor, if associated with holoprosencephaly.

Definition Hypotelorism refers to reduced interocular and binocular distances (<5th percentile).

Etiology and pathogenesis. The most common cause of hypotelorism is the migration defect underlying the frequently associated holoprosencephaly (see Chapter 2). The phenotypic expression of this midline migration defect ranges from severe hypotelorism to cyclopia.

Ultrasound diagnosis. This is carried out on the axial view of the orbits, with a ventral or lateral approach. It should be emphasized that the overwhelming majority of cases of hypotelorism detected in utero are associated with holoprosencephaly (Figure 3.35). As already pointed out for hypertelorism, the diagnosis is straightforward in the most severe cases, whereas in the less severe ones, measurement of the binocular and interocular diameters is of fundamental diagnostic importance (see Appendix Table A.15).

Prognostic indicators. The fact that holoprosencephaly is associated in 80% of the cases detected prenatally makes the association of this severe central nervous system developmental abnormality the key prognostic indicator.

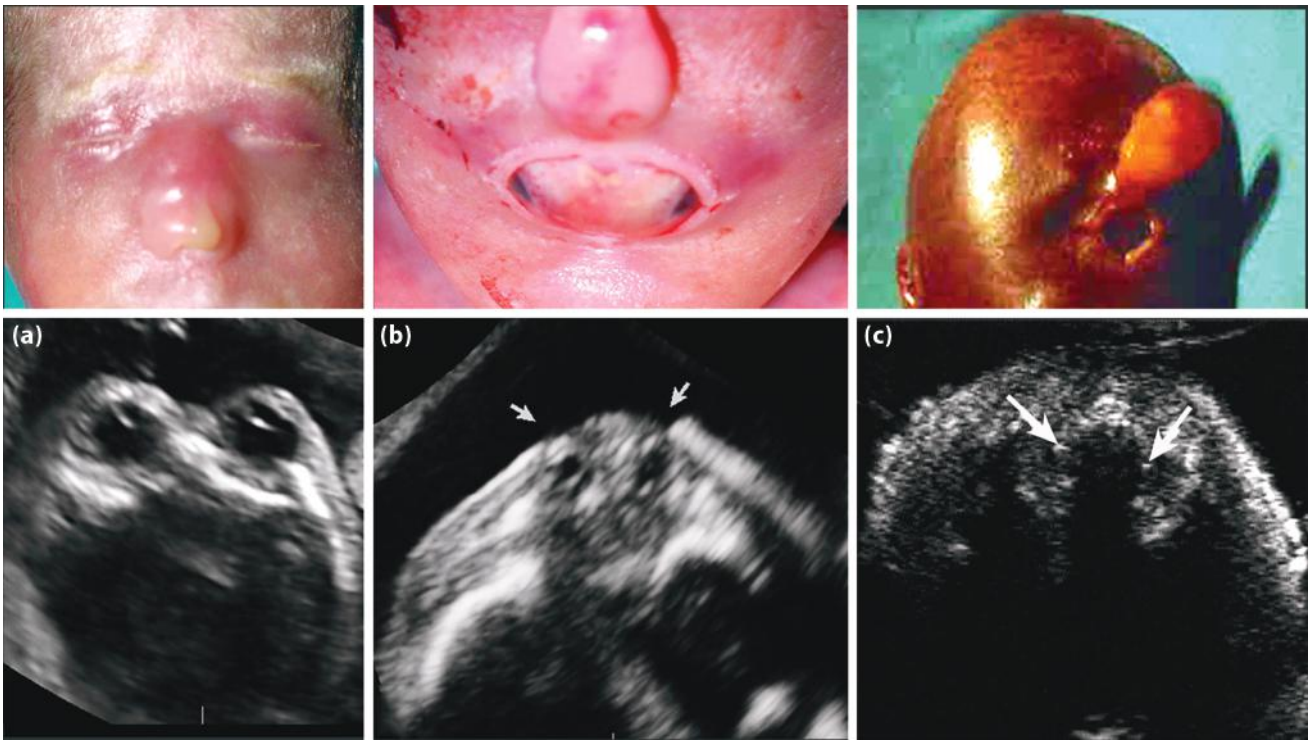


Figure 3.35 Hypotelorism. Three degrees of hypotelorism, which is in most instances associated with holoprosencephaly, are shown: (a) moderate hypotelorism associated with a single nostril (cebocephaly); (b) a single eye socket with two adjacent eye bulbs, associated with arhinia and proboscis; (c) cyclopia (single orbit and eye bulb), also associated with arhinia and proboscis.

Association with other malformations. The most frequent association is with holoprosencephaly.

Risk of chromosomal anomalies. This is high (about 40%). The most frequently associated chromosomal aberration is trisomy 13, given its high incidence in holoprosencephaly.

Risk of nonchromosomal syndromes. This is extremely high. In addition to the already mentioned holoprosencephaly, hypotelorism can also occur, less often, in Meckel–Gruber syndrome.

Obstetric management. Should hypotelorism be detected in a fetus, karyotyping is mandatory, because of the high risk of trisomy 13. In addition, a thorough anatomic scan should be performed by an expert, in order to detect the various defects characterizing the holoprosencephaly sequence.

Prognosis, survival, and quality of life. The prognosis is poor and the mortality rate high because of the high association with trisomy 13. In those cases in which the chromosomes are normal, the risk of severe mental retardation is strictly related to the subtype of holoprosencephaly (see Chapter 2).

ANo MALIEs o F ThE Nos E—1: pro Bosc Is, Arh INIA, sINGLE Nos Tr IL

Incidence. Extremely rare.

Ultrasound diagnosis. *Proboscis:* Fetal profile view: single midline mainly soft tissue formation departing from the nasal root area. *Arhinia:* Fetal profile view: complete absence of the nasal bones and soft tissues. *Single nostril*: oblique view of the lips: evidence of a single opening.

Risk of chromosomal anomalies. Extremely high and related to the constant association with holoprosencephaly (trisomy 13).

Risk of nonchromosomal syndromes. Extremely high and related to the constant association with holoprosencephaly.

Outcome. Extremely poor due to the constant association with holoprosencephaly.

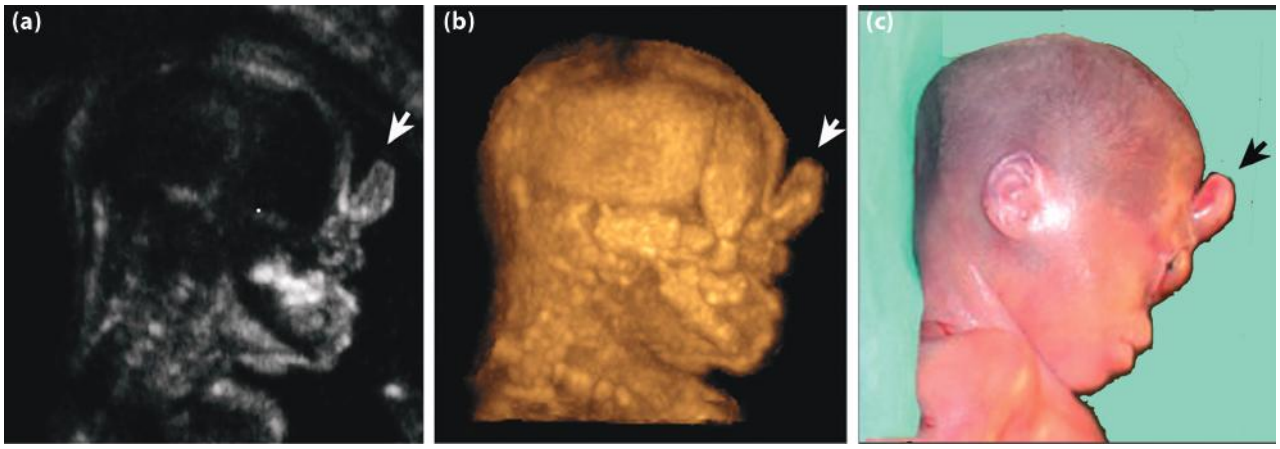


Figure 3.36 Proboscis in alobar holoprosencephaly. This midsagittal view of the facial profile shows the appendix (arrow) arising from the forehead: (a) two-dimensional ultrasound; (b) three-dimensional maximum-mode rendering; and (c) confirmation at autopsy.

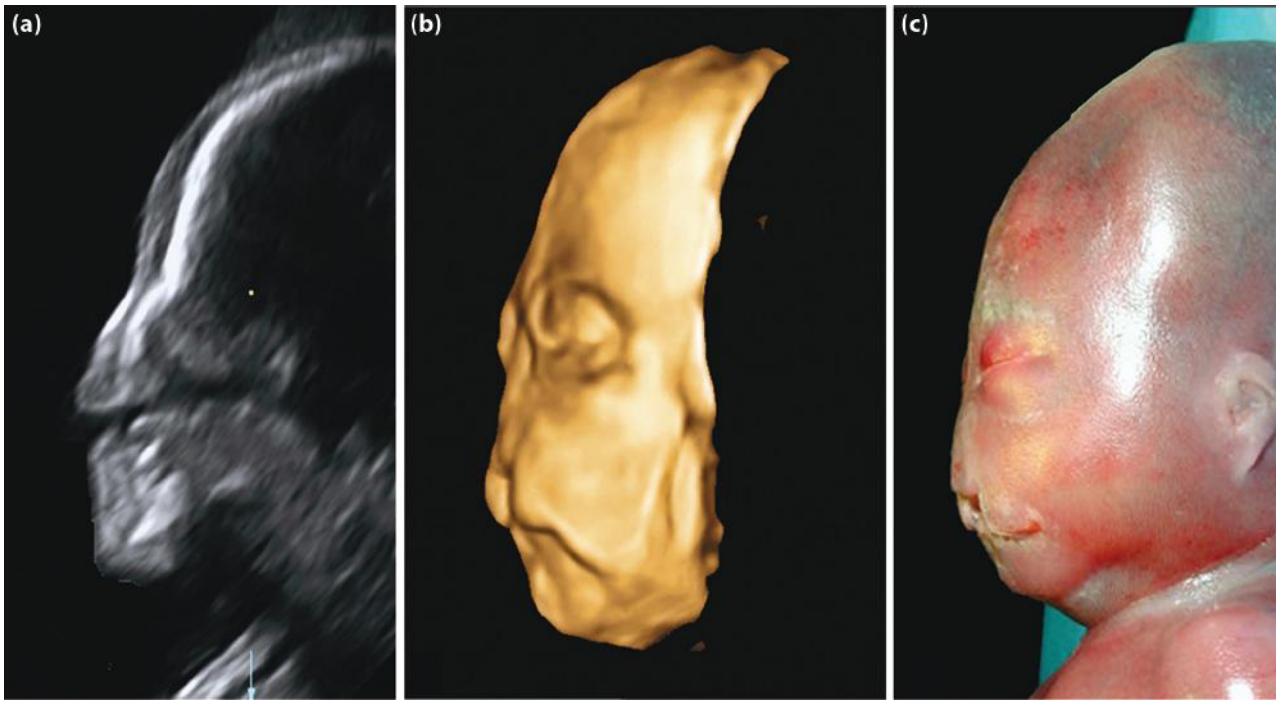


Figure 3.37 Arhinia in semilobar holoprosencephaly. On the midsagittal view, the absence of the nose with the completely flat profile is evident: (a) two-dimensional imaging; (b) three-dimensional surface-rendering imaging; (c) autoptic confirmation.

Definition Proboscis: single midline appendix of soft tissues (but can have a bony skeleton) departing from the nasal root area. Arhinia (ethmocephaly): complete absence of the nasal bones and of the nares. It can be associated or not with the proboscis. Single nostril (cebocephaly): evidence of a single nasal opening. It represents the less severe anomaly of the nasal area associated with holoprosencephaly.

Etiology and pathogenesis. As reported above, proboscis, arhinia, and single nostril are different expressions of the same midline developmental anomaly characteristic of holoprosencephaly; namely, a field developmental derangement of the prechordal mesoderm.

Ultrasound diagnosis. The diagnostic view is not the same for the various defects. The midsagittal plane of the fetal profile permits recognition of the proboscis and of the arhinia (Figures 3.10, 3.36, and 3.37). The axial view of the orbits (Figure 3.38) allows detection of arhinia only (the proboscis lies on another more cranial plane), while single nostril (cebocephaly),



Figure 3.38 Arhinia in semilobar holoprosencephaly (ethmocephaly). The absence of the nasal bones is also evident on this axial view of the orbits: Note the depressed area between the orbits (arrow).

which represents the less severe holoprosencephaly related developmental anomaly of the nasal placode, can only be recognized on the oblique view of the lips (Figure 3.39; see also Chapter 2). The diagnosis of all the aforementioned anomalies is straightforward and does not need any biometry.

Prognostic indicators. The fact that holoprosencephaly is constantly associated with these types of defects represents the most important negative prognostic factor.

Association with other malformations. There is a constant association with holoprosencephaly.

Risk of chromosomal anomalies. This is extremely high. It is obviously dependent on the constant association with holoprosencephaly and on the 40% chromosomal risk of this condition, mostly related to trisomy 13.

Risk of nonchromosomal syndromes. This is extremely high, because of the constant association with holoprosencephaly.

Obstetric management. Should these severe abnormalities of the nose be recognized on US, karyotyping is mandatory because of the high risk of trisomy 13. In addition, a thorough anatomic scan should be performed by an expert, in order to detect the various defects characterizing the holoprosencephaly sequence.

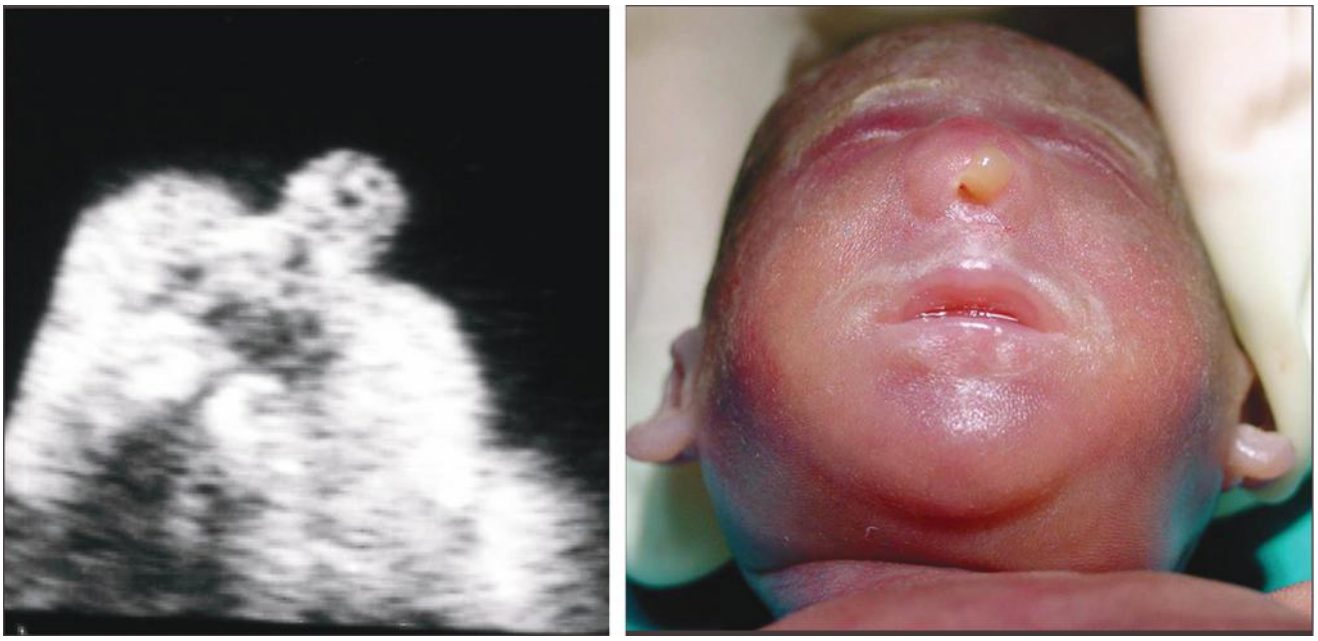


Figure 3.39 Single nostril in semilobar holoprosencephaly (cebocephaly). This oblique view of the lips allows demonstration of the single nostril. The confirmation at autopsy is shown on the right; also note the hypotelorism and microphthalmia.

Prognosis, survival, and quality of life. The prognosis is very poor and the survival minimal because of the association with holoprosencephaly and the 40% risk of a concomitant trisomy 13.

ANoMALIEs o F ThE Nos E—2: ThE "ABNor MAL" Nos E

Incidence. Very rare.

Ultrasound diagnosis. Fetal profile plane: minor abnormalities of the dimensions and the proportions of the nose; abnormal nasal root. Binder syndrome: small, vertical nose with midfacial hypoplasia.

Risk of chromosomal anomalies. High (absent nasal bone and flat profile in trisomy 21).

Risk of nonchromosomal syndromes. Variable. Binder syndrome + chondrodysplasia punctata.

Outcome. Depends on the overall clinical context.

Definition There is no generally accepted definitio of an "abnormal nose." This term has been created by the present authors. The aim of this small section is to draw the attention of the reader to the assessment of the overall aspect and harmony of the various components of the fetal profile and of the nose in particular.

In textbooks on human dysmorphology [16], as well as on the OMIM website (On-Line Mendelian Inheritance in Man: http://www.ncbi.nlm.nih.gov/entrez), the number of syndromes featuring minor abnormalities of the nose is enormous. Anomalies of the nose that can be detected in the neonate include a low or wide nasal bridge, a small nose with or without anteverted nares, hypoplasia of the alae nasi, midfacial hypoplasia, and choanal atresia. However, unfortunately (or luckily) virtually none of these minor anomalies of the nose can be diagnosed with certainty in the fetus. In addition, the extreme variability of the normal human phenotype has to be considered. It is of the utmost importance to explain this wide phenotypic variability to the parents of the possibly abnormal fetus. Nonetheless, we believe that, in an appropriate diagnostic framework, the careful evaluation of even minor or apparently insignificant anomalies of the fetal profile may help support, or rule out, a diagnostic hypothesis.

Etiology and pathogenesis. The minor developmental anomalies of the nose are determined by the underlying syndromic condition.

Ultrasound diagnosis. The key plane for the detection of minor anomalies of the nose is the midsagittal view of the fetal profile Once again, it must be emphasized that such a subjective approach to the assessment of the fetal nose appearance can be adopted only if a complex malformative cluster *has already been diagnosed* and there is a differential diagnostic doubt to be clarified In this context, such an approach, based on the descriptions of facial features reported in neonatal dysmorphology books, may help to resolve the issue. The same diagnostic process can also be applied a posteriori; in other words, when the recognition of a malformative cluster has already led to the identification of a likely diagnosis. In this circumstance, the confirmation that an anomaly of the nose described for that syndrome is indeed present in the index fetus further supports the diagnosis [22].

In case of Binder syndrome (also called maxillonasal dysplasia; see Chapter 10), there is significant hypoplasia of the maxilla and the nasal complex (midfacial hypoplasia), with a vertical short nose, flat nasal bridge, moderately hypoplastic maxilla, and prognathism [16,23] (Figure 3.40).

Prognostic indicators. The prognosis depends on the underlying syndromic condition, given that the anomalies of the nose described in this section are of no or mild clinical relevance.

Association with other malformations. As a general rule, syndromic conditions involving the face often present with anomalies of the lips and/or micrognathia; in case of Binder syndrome, chondrodysplasia punctata may be associated [23].

Risk of chromosomal anomalies. This is high, if we consider the strong risk of Down syndrome that carries the recognition of an absent or hypoplastic (<4.5 mm) nasal bone in the second trimester of pregnancy [24,25].

Risk of nonchromosomal syndromes. This is variable, depending on the clinical context. Midfacial hypoplasia characterizes Binder syndrome [16,23] that can be associated with chondrodysplasia punctata (see Chapter 10).

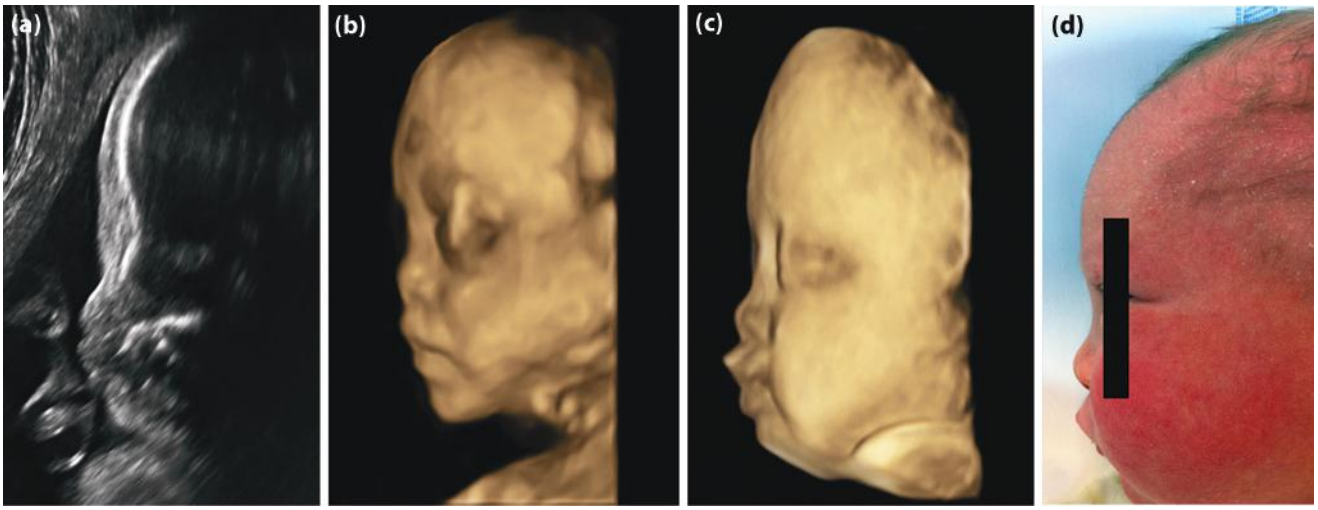


Figure 3.40 Binder syndrome. Midsagittal profile view. (a) Two-dimensional ultrasound, showing the flat profile and the small, vertical nose; (b) three-dimensional surface-rendering at 24 weeks; (c) three-dimensional surface-rendering at 34 weeks; and (d) the neonate at birth.

Obstetric management. Minor facial anomalies, such as an "abnormal" nose, are generally discovered after other significant malformations have already been diagnosed. If this occurs during the second trimester, and if, following the prenatal counseling session, the parents opt to continue the pregnancy, serial US examinations should be scheduled, as additional features may arise late in gestation.

If Binder syndrome has been diagnosed, sonographic follow-up is mandatory to discover possible signs of chondrodysplasia punctata, such as stippled epiphyses.

Prognosis, survival, and quality of life. The fina prognosis depends on the underlying syndromic condition. In general, syndromes associated with abnormal facial features relatively often carry a moderate-to-high risk of mental retardation. On the contrary, Binder syndrome, if isolated, may be compatible with a perfectly normal neurological outcome, but also with other underlying clinically important conditions [23].

cLEFT LIp/pALATE

Incidence. Relatively common.

Ultrasound diagnosis. Views able to display lips, upper alveolar ridge, and hard palate. On these views, the cleft appears as an interruption of the lip and/or the alveolar ridge/palate. It can be unilateral, bilateral, or median.

Risk of chromosomal anomalies. Extremely high, especially for the median (holoprosencephaly and trisomy 13) and the bilateral (trisomies 13 and 18) variants. Very low for the isolated unilateral cleft lip.

Risk of nonchromosomal syndromes. Very high: Goldenhar, Fraser, ectrodactyly–ectodermal dysplasia (EEC), Fryns, frontonasal dysplasia.

Outcome. Extremely unfavorable in syndromic cases. Good/extremely good for unilateral clefts. From acceptable to good for bilateral clefts.

Definition The defect may involve only the upper lip (cleft lip, CL), or extend to the alveolar ridge and, possibly, to the hard palate (cleft lip/palate, CLP). It can be unilateral, bilateral, or median. At birth, unilateral CL accounts for 29% of all clefts, unilateral CLP for 40%, bilateral CLP for 27%, and bilateral CL for the

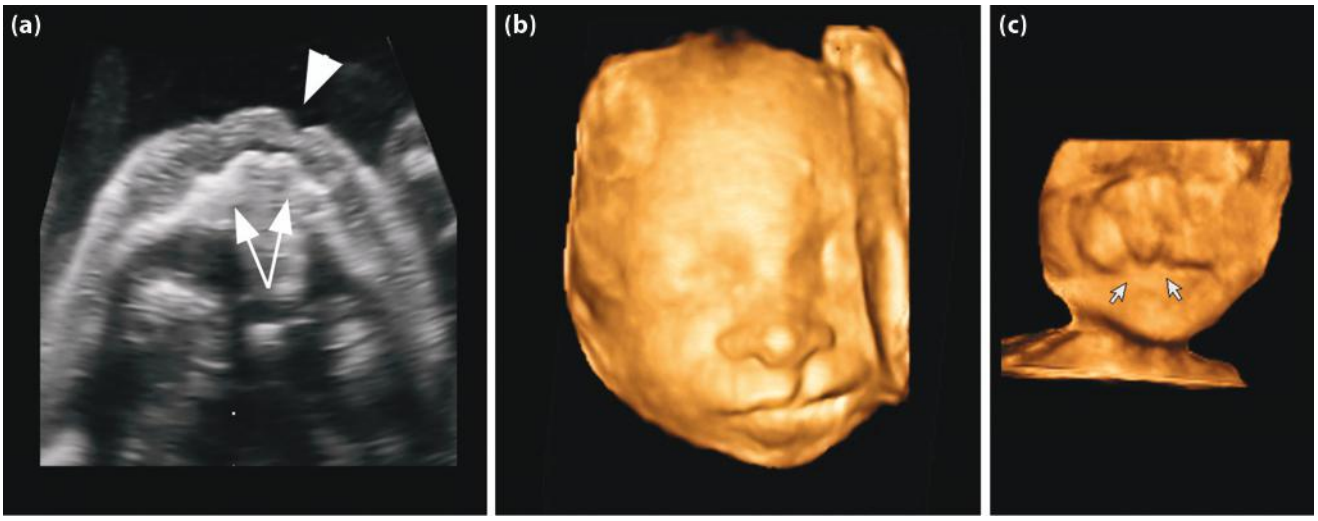


Figure 3.41 Isolated cleft lip. (a) On two-dimensional imaging, the axial view of the upper alveolar ridge shows an intact alveolus (arrows) and the small lateral cleft lip (arrowhead) in a 24-week-old fetus. (b) The corresponding three-dimensional surface-rendered image; (c) another case of bilateral isolated cleft lip (arrows) at 28 weeks' gestation.

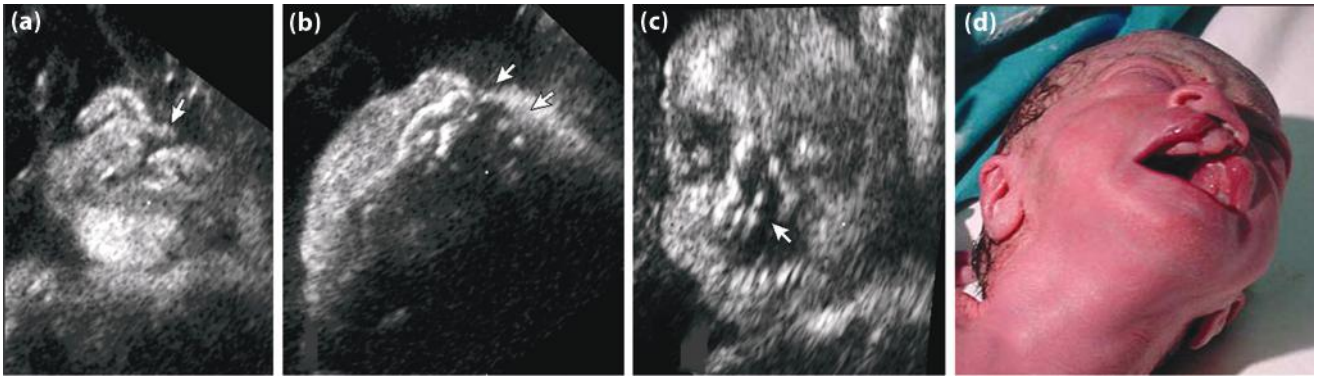


Figure 3.42 Unilateral cleft lip/palate. Unilateral cleft determining distortion of the alae nasi (27 weeks' gestation). (a) Oblique view, demonstrating the lip defect and the distortion of the alae nasi (arrow); (b) axial view, demonstrating the extent of the bony defect (arrows); (c) coronal view, demonstrating the abnormal communication between nose and mouth (arrow); (d) the appearance of the defect at birth.

remaining 5%. It should be noted that the more severe facial clefts classified according the Tessier scheme [26] are not considered in this section.

Etiology and pathogenesis. The lips and the palate originate from the first branchial arch between the 7th and the 12th week of gestation. In particular, the upper lip and the philtrum originate from the fusion of the medial nasal prominence with the lateral nasal prominences and the maxillary prominences. Similarly, the palate develops from the midline fusion of the secondary palatal shelves. If the lateral fusion process is blocked, then the lateral type of cleft lip/palate occurs; if, rather, it is the downward development of the medial nasal process that is arrested, this leads to the median type of cleft, which often extends laterally, since the absence of the median nasal process also prevents lateral fusion.

Ultrasound diagnosis. Even if the US diagnosis of CLP has been reported as early as the 12th week of gestation [27], the scant presence of facial soft tissues at this early stage of development poses significant limitations to diagnostic accuracy. The diagnosis of CLP is made using different views of the lower part of the face, as already mentioned. In particular, the cleft of the lip appears as a defect at the level of the upper lip (Figure 3.41). If this is not associated with hard palate defects, the alveolar ridge is intact and the maxilla unremarkable (Figure 3.41). If, on the contrary, the cleft involves the bony structures, an abnormal communication between the oral and nasal cavities is seen; in this latter instance, distortion of the alae nasi is common (Figure 3.42; see also Figures 3.21 and 3.25). In case of bilateral CLP, additional tissue at the level of the philtrum is commonly seen (Figure 3.43; see also

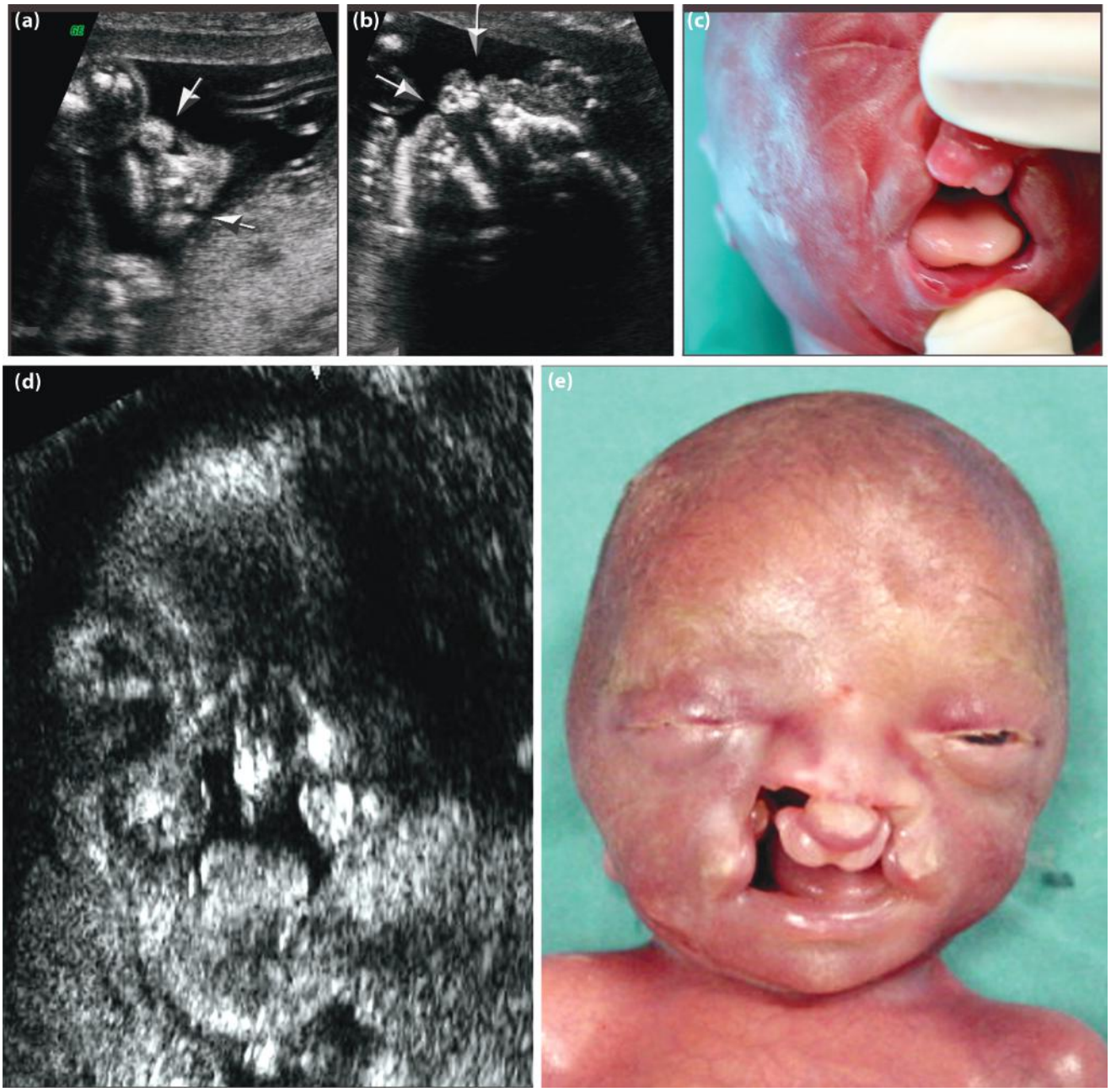


Figure 3.43 Bilateral cleft lip/palate. (a) Bilateral cleft lip/palate with additional tissue on the philtrum (22 weeks' gestation). Oblique view, demonstrating the double defect of the lip (arrows), and the additional tissue on the midline; (b) axial view of the same case, demonstrating the double bony defect (arrows); (c) the appearance of the defect after termination of pregnancy; (d) another case of syndromic bilateral cleft lip/palate. This coronal view demonstrates the double bony defect. (e) Confirmation at autopsy.

Figures 3.22 and 3.26). The diagnostic potential of the various US planes that can be employed for the assessment of the upper lip and palate is discussed below. The axial view of the maxilla allows direct recognition of the defect of the lip and the bony palate. If this view is obtained with a ventral (*anterior*) approach, the diagnostic accuracy is higher, because the US beam can penetrate through the defect up to the nasal cavity, and this gives a clearer idea of the width and the depth of the cleft (Figures 3.42 and 3.43). In comparison, the lateral approach allows detection of the defect of the upper alveolar ridge and of the palate, but does not usually allow assessment of the depth of the defect. In addition, in the case of bilateral CLP, the progressive absorption and refraction of US waves at the level of the defect closest to the transducer blurs

the visualization of the farther cleft. Oblique views of the lips and the palate can demonstrate the anomalies of the soft tissues and of the bony part, respectively. It should be emphasized that, in comparison with the axial views, the oblique views have the advantage of better displaying the spatial relationships between the lips and the nose, which can sometimes be distorted (Figures 3.42 and 3.43). Coronal views at the level of the face and the maxilla allow the best display of a median cleft, which is usually associated with holoprosencephaly (Figure 3.45). It should be noted that the midline sagittal view appears unremarkable in unilateral CLP, because the defect lies in another plane. Only in the case of bilateral CLP, does this view appear abnormal, due to the additional tissue present at the level of the philtrum (Figure 3.46). A summary of the US approach to the diagnosis of different types of CLP, listing the pros and cons of the various scanning views, is given in Table 3.1 [7].

Note. If the umbilical cord lies on the upper lip, this may raise the suspicion of a CLP: the vertical sonolucent area corresponding to the umbilical vein with its walls may sometimes lead to a false-positive diagnosis of CLP. It is sufficient to repeat the scan after a few minutes or to switch on the color/power Doppler to rule out a real defect (see Figure 3.17).

The Equals (=) sign. This sign refers to the appearance of the normal uvula on an axial view of the oropharynx (28). The fluid-solid-flui interfaces provide an enhancement of the echogenicity of the lateral edges of the uvula, which then resembles a "=" sign (Figure 3.44). In case of facial cleftings and in cases at risk of soft palate abnormalities, such view provides a relatively simple window on the normal appearance of the posterior palate. If the uvula is seen, then soft palate involvement in the clefting – as well as isolated cleft palate – may be excluded.

Prognostic indicators. The risk of chromosomal and nonchromosomal anomalies is higher for CLP than for CL, and higher for bilateral clefts than for unilateral ones. However, the worst prognosis is probably associated with the median cleft, because of its association with holoprosencephaly and/or other severe midline defects (frontonasal dysplasia). It also has to be considered that the cosmetic results depend upon the extent and the depth of the defect.

Association with other malformations. The single group of anomalies most frequently associated with CLP is represented by congenital heart disease.



Figure 3.44 The Equals sign. On an axial view of the oropharynx, obtained with a lateral approach, the uvula is displayed (arrow). The alternation of fluid-solid-fluid enhances the edges' echogenicity, creating the "Equals" (=) sign (ref.28) (arrowhead: upper lip; R: ramus of the mandible; T: tongue; V: cervical vertebral body.

The role of 3D ultrasound in the characterization of CLP. 3DUS has been extensively used over the past decades to characterize CLP. It has repeatedly shown that surface-rendering images facilitates the communication of the diagnosis to the parents, and this image modality together with transparent mode (in which the bony component is best appreciated) have allowed better prenatal consultation with the Plastic Surgeon. However, 3DUS shares with 2DUS the limitations regarding the assessment of the posterior, soft palate. This is due to the fact that, in most of the cases, the mandibule casts shadows right over the soft palate, making its evaluation challenging. Despite the several 3D approaches published in the Literature (Campbell S.: reversed face; Platt LD: flipped face; Pilu: oblique view), probably the simplest way to demonstrate integrity of the soft palate is by showing the uvula in the oropharynx, the Equal sign (fig.3.44) mentioned on page 109, which was described rather recently by Wilhem L et al.(28). See also the discussion earlier in this chapter on the role of 3D US and Figures 3.18 through 3.28.

Risk of chromosomal anomalies. This is very high for median clefts (holoprosencephaly) and for bilateral ones (15%–30%). It is moderately high for unilateral CLP (5%–15%), but minimal for isolated CL [29]. CLP can be associated with trisomies 13 and 18 and with other rarer chromosomal anomalies.

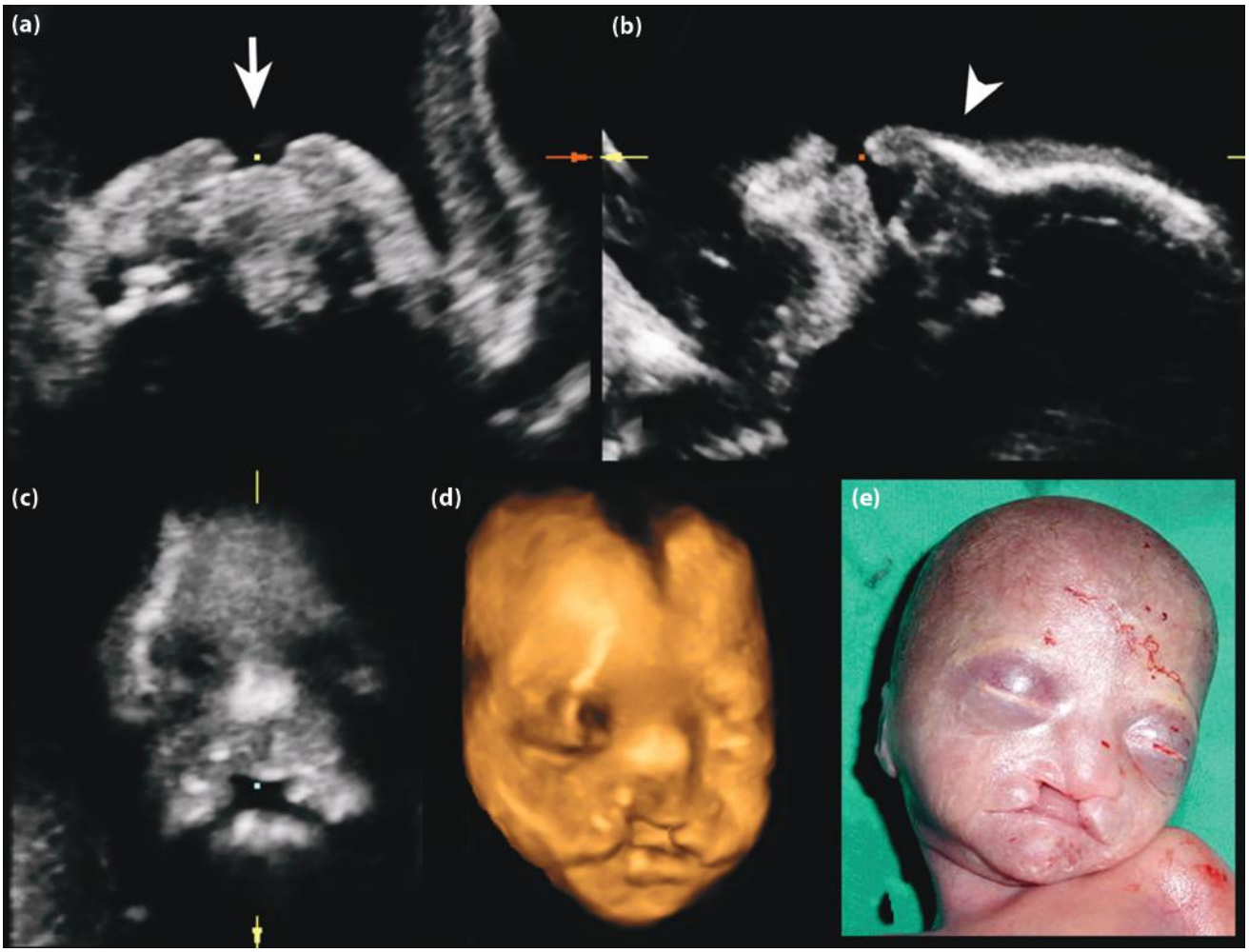


Figure 3.45 Median cleft lip/palate in lobar holoprosencephaly. (a) Axial view, demonstrating the midline defect of the lip and palate (arrow); (b) midsagittal view, demonstrating the arhinia and the absence of the upper alveolar ridge (arrowhead); (c) coronal view, demonstrating the abnormal communication between nose and mouth (caliper); (d) three-dimensional surface-rendering reconstruction demonstrating the midline defect; (e) the appearance of the defect at birth. Note also that such a severe midline defect of the face is rarely associated with lobar holoprosencephaly.

Risk of nonchromosomal syndromes. This is very high. The number of syndromes featuring CLP among the possible prenatally detectable signs is huge, and it would be of limited value to report all of them here. Before listing the syndromes with CLP most frequently detected in the fetus, it is important to emphasize that a CLP may sometimes represent the only prenatally detectable sign of various syndromes of clinical importance; we believe that this information should be given to the parents during the counseling session. The syndromes associated with CLP that are most frequently diagnosed in the fetus are as follows:

- *Goldenhar syndrome [13,14]*: look for ► *CLP, unilateral* + unilateral microphthalmia + hemifacial microsomia (see Chapter 10);
- *Fraser syndrome [17]*: look for ► *CLP, unilateral* + laryngeal atresia + congenital heart disease + microphthalmia + external ear anomalies + bilateral renal agenesis (see Chapter 10);
- *EEC (ectrodactyly–ectodermal dysplasia) syndrome [16]*: look for ► *CLP, unilateral* + ectrodactyly (lobster claw anomaly of hands and feet) + maxillary hypoplasia;
- *Frontonasal dysplasia [21]*: look for ► *CLP, median* + anterior cephalocele + hypertelorism;
- *Fryns syndrome [16]*: look for ► *CLP, unilateral* + diaphragmatic hernia + central nervous system anomalies.

Obstetric management. Should CLP be detected in a fetus, a thorough anatomic scan should be performed

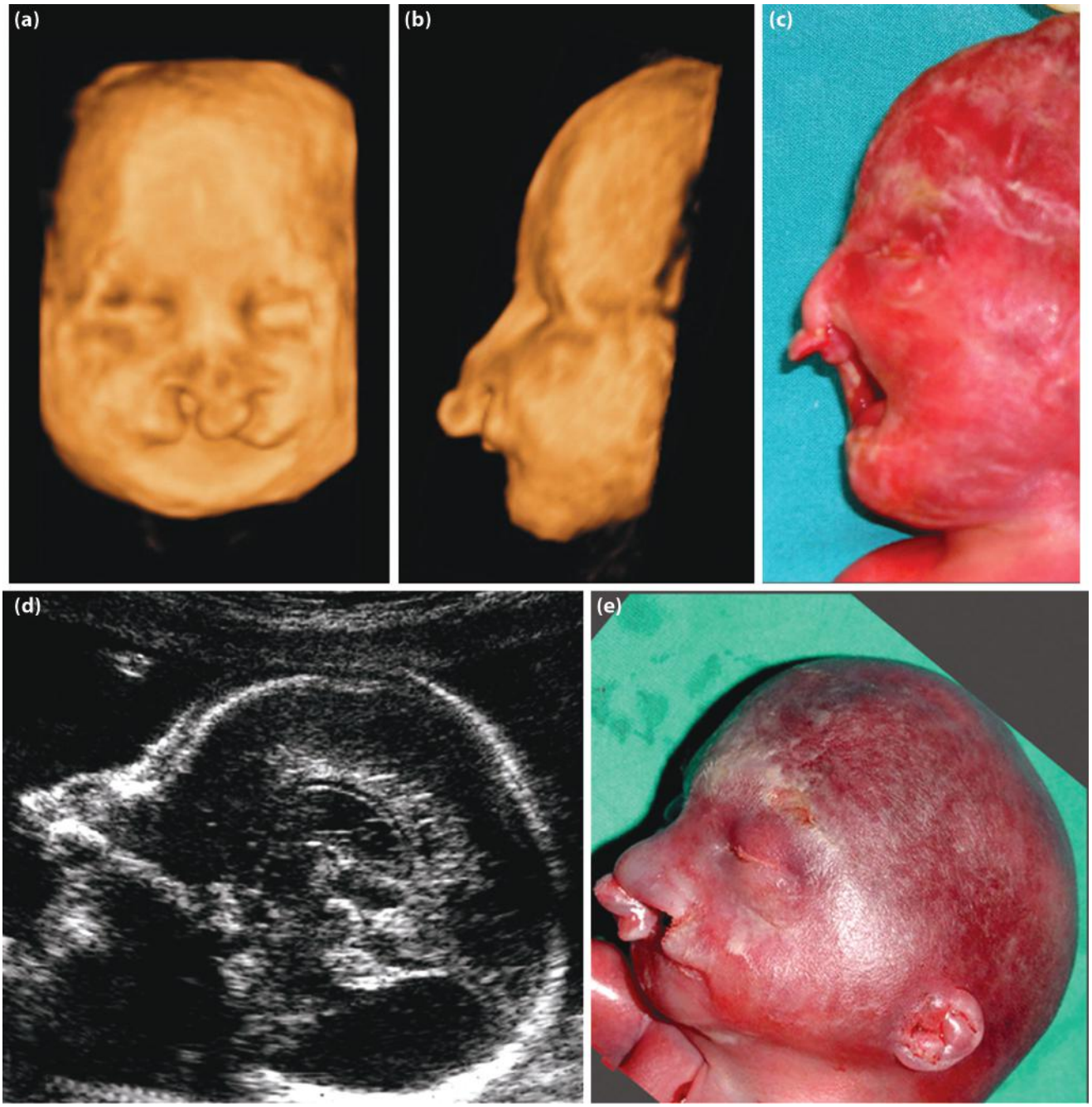
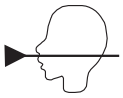


Figure 3.46 Bilateral cleft lip/palate. In these two cases, due to the presence of the additional tissue on the philtrum, the midsagittal view of the fetal facial profile is also abnormal, unlike in unilateral clefts, where it is unremarkable. (a–c) 21 weeks' fetus with trisomy 13: (a) the frontal approach shows bilateral microphthalmia and bilateral CLP; (b) on the profile view, the additional tissue on the philtrum is markedly evident; (c) autoptic confirmation after termination of pregnancy. (d–e): Another case of trisomy 13, showing similar features and Dandy–Walker malformation.

by an expert, in order to detect major and minor malformations possibly leading to the diagnosis of an underlying syndromic condition. Karyotyping is recommended, because of the relatively high risk of trisomy 13, especially in bilateral CLP. For isolated unilateral CLP and for CL, this option should be discussed with the parents. In the case of isolated CL/CLP, prenatal consultation with the reference surgeon, who may provide the parents with all necessary information regarding the timing and the

Table 3.1 Systematic approach to fetal face ultrasound. Pros and cons of the various scanning planes.

	Scanning plane	Pros	Cons
	Axial–ventral	Clear diagnosis of cleft extent and depth	Feasible only with the fetus in a favorable position
	Axial–lateral	Good assessment of the extent of the lip defect, less of the bony component	In bilateral clefts, inadequate definition of the defect located distal to the transducer
	Oblique lips	Excellent assessment of the lip defect and of possibly associated anomalies of the alae nasi	Feasible only with the fetus in a favorable position
	Oblique palate	Good assessment of the bony defect and of the relationships with the nasal cavity. It completes the previous view	Feasible only with the fetus in a favorable position. Does not give information on the lip component
	Coronal face	Good assessment of median nose and lip defects (holoprosencephaly)	Lateral defects do not show up on this view
	Midsagittal profil	Enables only detection of the additional tissue on the philtrum in bilateral clefts	No informations in unilateral clefts and in bilateral ones, except for the philtrum

results of the surgical procedure, is of the utmost importance.

Postnatal therapy. It is very important to explain to the parents that the surgical correction will not be carried out at birth. Only by fully understanding this piece of information will the parents be able to cope with the continuous confrontation with the defect at home. The use of presurgical plates and/or strapping is controversial. However, they may help feeding and, at the same time, contribute to narrowing the cleft, making surgery easier. If used, it is important that they be fitted soon after birth by an experienced orthodontist.

As far as the surgical approach is concerned, different protocols have been applied over the years in relation to the surgical technique and the timing of the surgical approach (also depending on the type of defect: unilateral versus bilateral, CL versus CLP, with or without distortion of the alae nasi). The classic "rule of 10" (10 months of age, 10 g/dL of hemoglobin, and 10 lb [about 4.5 kg] of weight) is not accepted by all surgeons. Currently, there is no uniform protocol for the surgical approach to CLP, but the repair of the various components (lip, soft palate, and hard palate) is carried out at different times and in various sequences: closure of the lip and hard palate, followed by closure of the soft palate; or closure of the lip and soft palate, followed by closure of the hard palate; or closure of the lip, soft palate, and hard palate together; or closure of the soft palate, followed by the hard palate, followed by lip reconstruction [30]. Any residual velopharyngeal dysfunction is managed with the help of speech therapists through speech and language therapy, possibly before school age. It is important to emphasize that different aspects are involved when assessing the surgical correction of facial cleftings: aesthetic, morphometric, functional (language, high airway, hearing, and jaw function), and psychological [31].

Prognosis, survival, and quality of life. The main prognostic determinant is the syndromic or isolated nature of the defect. In the latter instance, survival is unaffected, but the perceived quality of life is a function of the severity of the defect (bilateral vs. unilateral, CL vs. CLP) and of the consequent cosmetic and functional surgical outcome (speech, language, hearing, etc.) [31].

MIcro GNATh IA

Incidence. Common.

Ultrasound diagnosis. Fetal profile view: retrognathia/micrognathia; Inferior Facial Angle (IFA). Axial mandibular view: Jaw Index (see text).

Risk of chromosomal anomalies. Extremely high: trisomies 13 and 18.

Risk of nonchromosomal syndromes. Extremely high: FADS, multiple pterygium, Neu–Laxova, Nager, Treacher Collins, Pierre Robin, achondrogenesis, campomelic dysplasia, diastrophic dysplasia, femoral hypoplasia—unusual facies syndrome.

Outcome. Extremely unfavorable in the majority of syndromic cases. Variable in primary mandibular defects (Pierre Robin).

Definition Abnormal shape and arrested development of the mandible. The defect is defined as *retrognathia* if the most affected axis is the anteroposterior one; if the whole mandible is affected, then the defect is defined as *micrognathia*. In most cases, the two abnormalities are associated.

Etiology and pathogenesis. The mandible develops from the first branchial arch: the mandibular processes merge in the midline to form the mandible and, more superficiall , the lower lip. The normal development of the mandible can be blocked by genetic factors, as in chromosomal and nonchromosomal syndromes, or by environmental ones. The latter mechanism applies to the severe micrognathia characteristically present in neuromuscular conditions such as fetal akinesia deformation sequence (FADS) (see Chapter 10). In this case, it is the fixed contracture of the temporo-mandibular joint that prevents the opening of the mouth and consequently the normal development of the mandible. In severe cases, the same mechanism may also determine microstomia.

Ultrasound diagnosis. The US diagnosis of micrognathia is electively carried out on the sagittal view of the fetal profile In this plane, the absence of the last feature characterizing the fetal profile that is, the chin, is recognized. This finding is consistent with the diagnosis of micrognathia, which, in the most severe cases, can be associated with a retraction of the lower lip (Figure 3.47). The more severe cases of micrognathia are those related to primary mandibular dysostoses

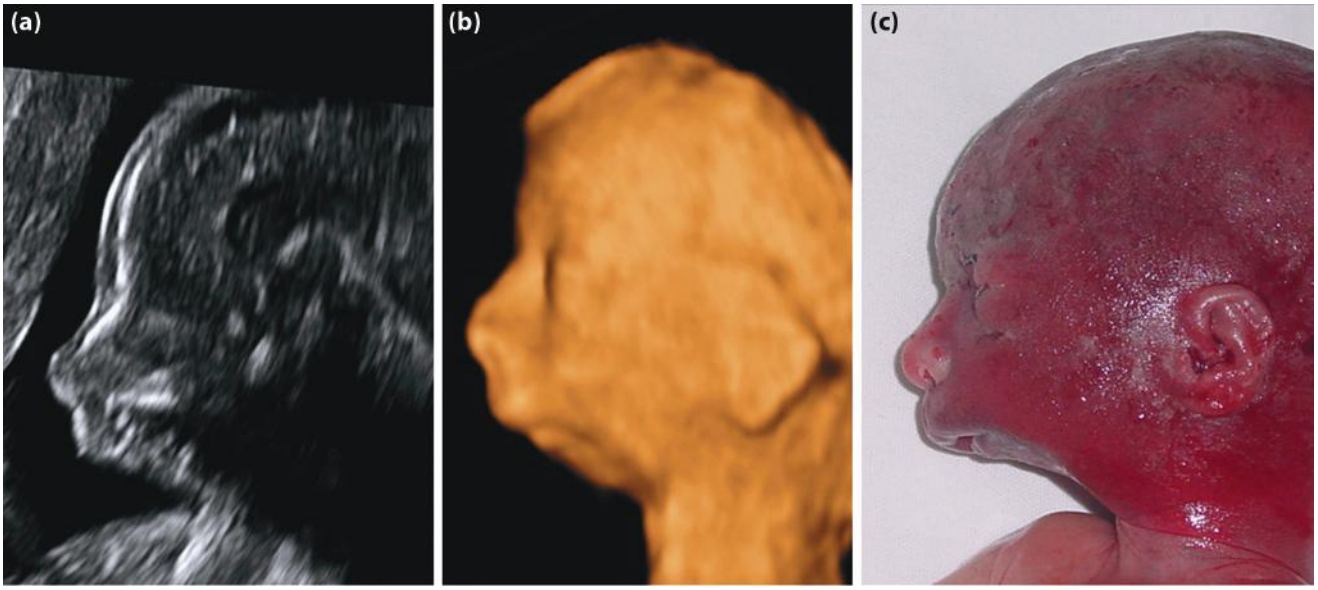


Figure 3.47 Severe micrognathia in oral-facial-digital syndrome, type II. Midsagittal profile view. The exceedingly severe degree of microretrognathia is evident, with the lower lip barely discernible. (a) Two-dimensional ultrasound; (b) three-dimensional surface-rendering; (c) autoptic confirmation.

Table 3.2 Syndromic conditions primarily involving the mandible

Syndromic condition	Other features potentially detectable in utero	Inheritance	Prenatal diagnosis reported
Acrofacial dysostosis			
Treacher Collins (Franceschetti) type	*Preaxial limb deficiencie* , CHD, CNS anomalies	AD	Yes
Rodriguez type	*Preaxial limb deficiencie* , CHD	AR	Yes
Nager type	Microcephaly, *preauricular tags*, CHD, *preaxial limb defects: radial aplasia, syndactyly, missing toes*	Sporadic	Yes
Miller (Genee–Wiedemann) type or POADS (postaxial)	Syndactyly, thumb hypoplasia, postaxial limb defects: absence of fifth digi	AR	—
Branchio-oculo-facial S.	Microcephaly, *ear anomalies*, hypertelorism, *microphthalmia*, renal anomalies, *polydactyly, vermian agenesis*	AD	Yes
Cerebro-costo-mandibular S.	*Microcephaly*, CHD, *small thorax, abnormal ribs*, renal ectopia, polyhydramnios	AD	Yes
Mandibuloacral dysplasia	Joint contractures, wide cranial sutures	AR	—
Orofaciodigital syndromes			
Type I	Facial asymmetry, bifid tongue polycystic kidney, *syndactyly, CNS anomalies*	X-linked dominant	Yes
Type II (Mohr)	Hypertelorism, polydactyly, porencephaly	AR	Yes
Oromandibular-limb hypogenesis spectrum	Acral hypoplasia, syndactyly	Sporadic	—
Otopalatodigital syndrome type II	Hypertelorism, omphalocele	X-linked dominant	—
Robin sequence	Glossoptosis, cleft palate		Yes

Source: Modified from Paladini , *Ultrasound Obstet Gynecol* 35, 377–84, 2010.
Most common signs in the fetus are in italics.
AD: autosomal dominant; AR: autosomal recessive; CHD: congenital heart defects; CNS: central nervous system; POADS: postaxial acrofacial dysostosis; S: syndrome.

(e.g., Pierre Robin anomaly or the various primary dysostoses; Table 3.2) [7], and in these cases, the anomaly is clearly detectable also at 12–13 weeks' gestation (Figure 3.48). In severe cases, this view alone is sufficien to subjectively diagnose micrognathia. However, less severe cases of micrognathia—such as those associated with chromosomal or neuromuscular syndromic conditions (Figures 3.49 and 3.50) [7]—can sometimes be reliably diagnosed only by applying biometric techniques. Nomograms of the various mandibular diameters have been published. Among these, the Jaw Index [8] and the IFA [9] show the best diagnostic accuracy [7]. The former is calculated as follows: Jaw Index = (anteroposterior mandibular diameter/BPD)/100. A value of 23 represents the 5th centile. Another advantage of the Jaw Index is that it is measured on the axial view of the mandible; therefore, it also allows detection of micrognathia if the facial profile view cannot be obtained because of an unfavorable position of the fetus. The IFA [9] is measured in a midsagittal view of the fetal profile at the crossing of two lines: one orthogonal to the vertical part of the forehead, drawn at the level of the synostosis

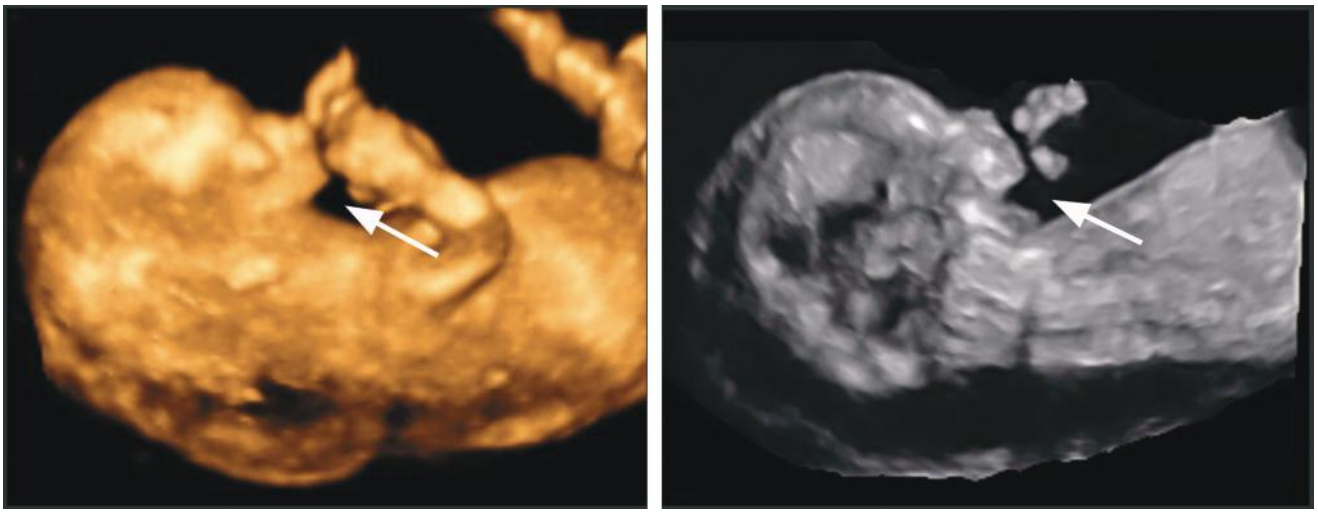


Figure 3.48 Severe micrognathia at 13 weeks. The sagittal view of the fetus clearly demonstrates the presence of severe micrognathia (arrow) as early as the 13th week of gestation. Also, note the conspicuously enlarged nuchal translucency. Karyotype was normal on Chorionic Villous Sampling (CVS).

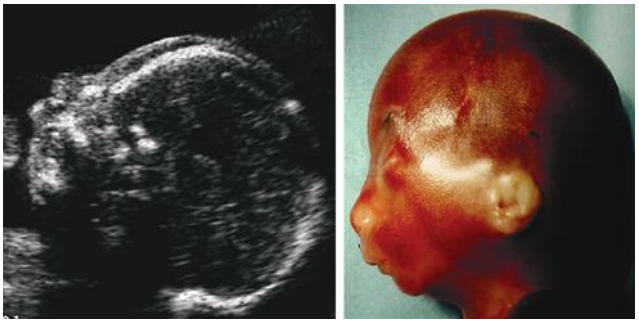


Figure 3.49 Moderate micrognathia in trisomy 18. On the midsagittal view of the fetal facial profile, the micrognathia is less evident than that in Figure 3.47. The confirmation at autopsy is shown on the right. Chromosomal and neuromuscular diseases feature less severe degrees of micrognathia than primary dysostoses (see also Table 3.2). (From Paladini D, *Ultrasound Obstet Gynecol* 35, 377–84, 2010.)

of the nasal bones; and a second, joining the tip of the mentum and the anterior border of the more protrusive lip. Its normal value is 65° (*SD*: 8°).

Note. As with the "abnormal nose" described earlier in this chapter, the variation of the normal human phenotype is also extreme in the shape, dimensions, and protrusion of the mandible. Again, it is safe practice to consider the phenotype of the parents in the scanning room prior to defining as certainly abnormal as the profile of the fetus that is under examination!

Prognostic indicators. The most severe forms of micrognathia are often syndromic. Also, if there is edema of the facial subcutaneous tissue, regardless of the degree of micrognathia, the risk of chromosomal and nonchromosomal syndromes is very high (Figure 3.50), and the prognosis consequently poorer.

Association with other malformations. Micrognathia is virtually never an isolated finding, being among the most common syndromic facial features. And in a significant number of those cases in which this apparently represents the only US abnormal finding, an underlying syndrome is often found after birth or at autopsy [16,32].

Risk of chromosomal anomalies. This is extremely high. Trisomies 18 and 13 are among the chromosomal aberrations most frequently associated with micrognathia. In particular, at autopsy, 70% of trisomy 18 cases show micrognathia of variable severity.

Risk of nonchromosomal syndromes. This is very high. A large number of nonchromosomal syndromes can be associated with micrognathia. We report in the following those most commonly encountered in the fetus, divided according to the pathogenetic mechanism.

The first group includes those characterized by a defect of neuromuscular transmission (arthrogryposes): the FADS, which also includes Pena–Shokeir syndrome [33], multiple pterygium syndrome, and Neu–Laxova syndrome. In this group, micrognathia is the consequence, as already mentioned, of masseter contracture, which blocks the temporomandibular joint. The second group includes primary defects of mandibular development, such as Pierre Robin anomaly (Table 3.2). Finally, there are the skeletal dysplasias, in which micrognathia represents the expression of a skeletal developmental derangement.

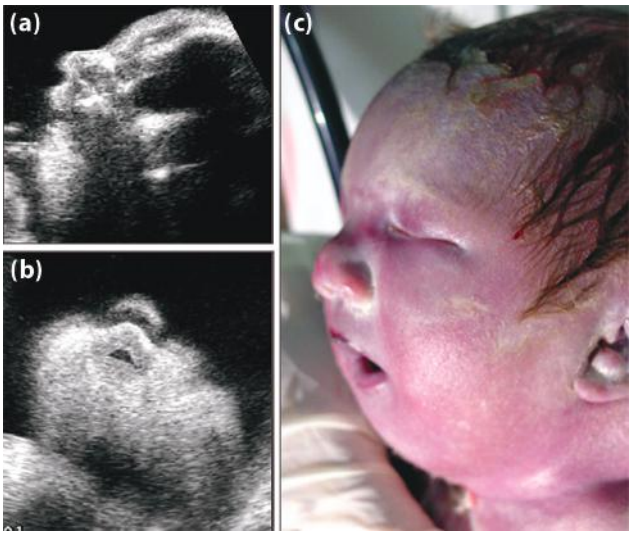


Figure 3.50 Micrognathia in FADS. (a) On the midsagittal view of the fetal facial profile, the severe micro/retrognathia is evident. (b) This oblique view of the lips demonstrates the associated microstomia, due to the block of the temporomandibular joint. (c) Confirmation of the diagnosis at birth (early neonatal death).

The most common skeletal dysplasias that feature, among other signs, micrognathia are campomelic dysplasia, the group of short-rib polydactyly syndromes, and thanatophoric dysplasia. It should be noted that all these syndromes are severe conditions with very high perinatal mortality rates, with the exception of the primary developmental defects of the mandible (Pierre Robin anomaly).

- *FADS, including Pena–Shokeir syndrome [33]*: look for ► *micrognathia* + diffuse joint contractures + thoracic hypoplasia + clubfeet + ulnar deviations of the hands + extremely reduced fetal movements (see Chapter 10);
- *Multiple pterygium syndrome [16]*: look for ► *micrognathia* + diffuse joint contractures + multiple pterygia at elbow and knee;
- *Neu–Laxova syndrome [16,34]*: look for ► *micrognathia* + microcephaly + agenesis of the corpus callosum + cerebellar hypoplasia (severe) + hypertelorism + short limbs + joint contractures + syndactyly + early-onset fetal growth retardation + polyhydramnios (see Chapter 10);
- *Nager syndrome [35]*: look for ► *micrognathia* + ectrodactyly + mesomelic hypoplasia + external ear anomalies;
- *Treacher Collins syndrome [16]*: look for ► *micrognathia* + external ear anomalies;
- *Pierre Robin anomaly [16]*: look for ► *micrognathia* + glossoptosis + cleft palate;
- *Achondrogenesis [16]*: look for ► *micrognathia* + micromelia + calvarial hypomineralization + hydrops (see Chapter 9);
- *Campomelic dysplasia [16]*: look for ► *micrognathia* + bowed and short femurs + tibiae (see Chapter 9);
- *Diastrophic dysplasia [16]*: look for ► *micrognathia* + micromelia + "hitchhiker" thumb + kyphoscoliosis (see Chapter 9);
- *Femoral hypoplasia/unusual facies syndrome [16,36]*: look for ► *micrognathia* + focal hypoplasia of one or both femurs + micrognathia + maternal insulin-dependent diabetes (see Chapter 10).

Obstetric management. When micrognathia is diagnosed in a fetus, a thorough anatomic scan should be performed by an expert, in order to detect major and minor anomalies, possibly leading to the disclosure of an underlying syndromic condition. Karyotyping is recommended, because of the relatively high risk of trisomies 13 and 18. Care should be taken in planning delivery in the case of primary mandibular defects, such as the Pierre Robin anomaly, in a tertiary referral center. In fact, life-threatening obstruction of the upper airways may occur at birth, and can lead to cerebral palsy from neonatal hypoxia if its occurrence is not predicted and adequately managed.

Prognosis, survival, and quality of life. Prognosis basically depends on the severity of the underlying syndrome. Survival is good only in the case of primary mandibular defects (e.g., Pierre Robin syndrome). Quality of life, which depends upon the success of reconstructive surgery, is fair in a significant percentage of cases

Ex TEr NAL EAr A No MALIEs

Incidence. Relatively common (but seldom detected).

Ultrasound diagnosis. *Parasagittal and axial views of the head*, at the level of the ears. Preauricular tags; abnormal auricles; crumpled ears.

Risk of chromosomal anomalies. Relatively high: autosomal trisomies.

Risk of nonchromosomal syndromes. Very high: Goldenhar, Fraser, Nager, Treacher Collins.

Outcome. Extremely unfavorable in syndromic cases.

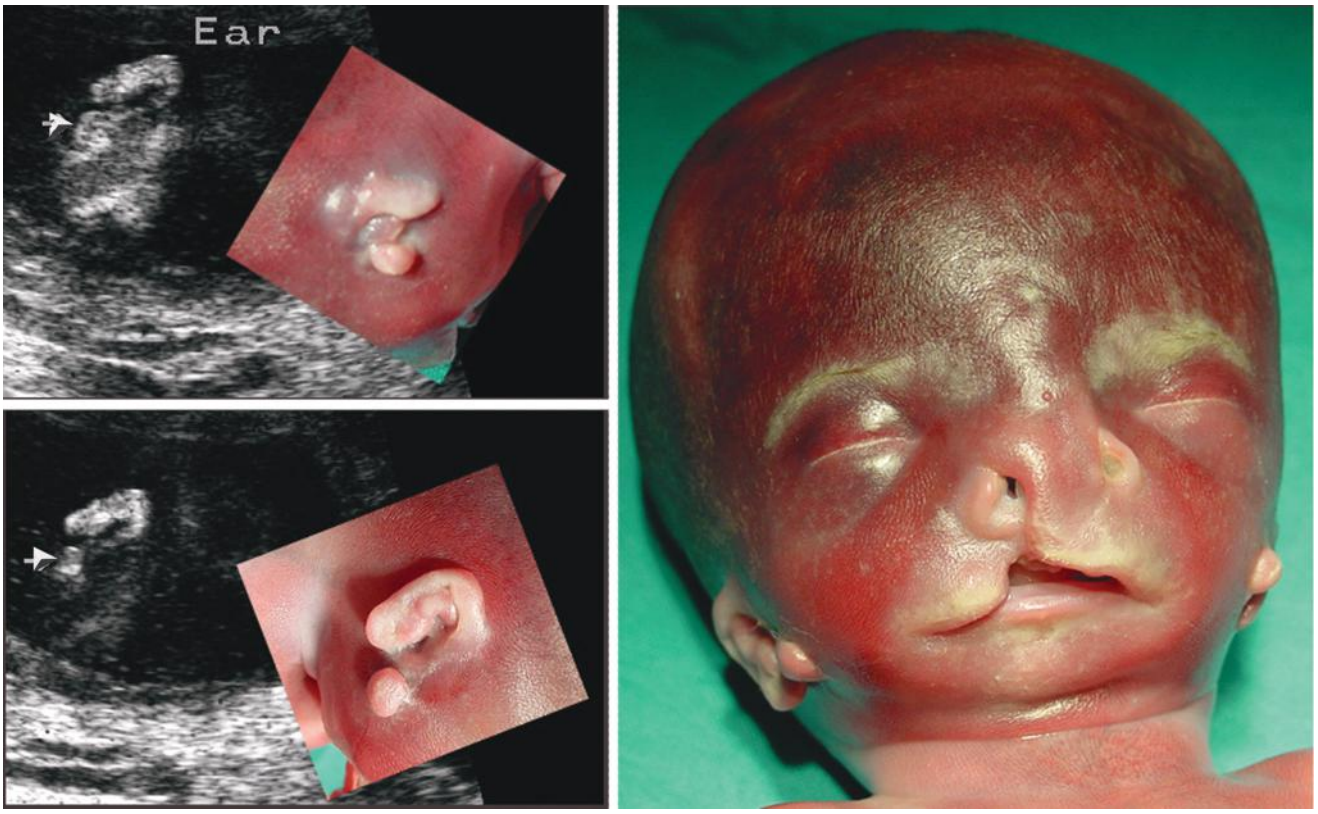


Figure 3.51 Preauricular tags, two-dimensional ultrasound. This parasagittal view at the level of the external ear demonstrates the abnormal preauricular appendices (arrows). The insets show the anatomic correlates. The dysmorphic features of the fetus after termination of pregnancy are shown on the right: Note also the cleft lip and the hypertelorism.

Definition The aim of this section is to draw the attention of the reader to the anomalies of the external ear. These anomalies can be detected by US, and this findin can be employed in the differential diagnosis of various syndromes. As a premise, it should be emphasized that the anomaly of the external ear most commonly associated with syndromic conditions, namely low-set ears, is not diagnosable with a good degree of certainty by 2D US. It has already been described how the use of 3D US has increased the diagnostic accuracy for this abnormal feature. Nomograms for the diameters of the external ear have been published (Appendix Table A.16) [37].

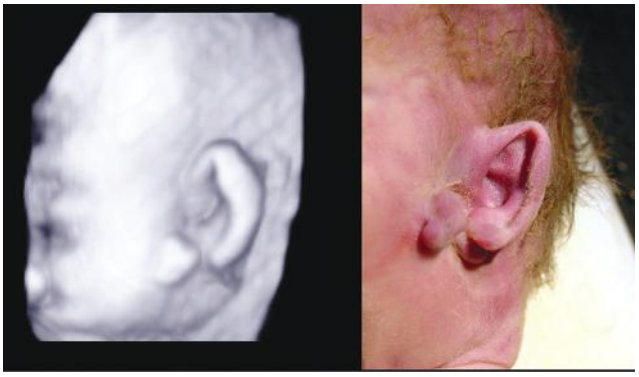


Figure 3.52 Preauricular tags, three-dimensional ultrasound. This surface-rendering reconstruction demonstrates the wrinkled ear and the preauricular tag in this 30-week-old fetus. The confirmation of the diagnosis at birth (40 weeks) is shown on the right.

Etiology and pathogenesis. The external ear originates from the first and second branchial arches. The preauricular tag represents an anomalous differentiation of these embryonic structures.

Ultrasound diagnosis. The diagnostic view is the most lateral anteroposterior view of the fetal head, which allows the whole external ear to be displayed (Figures 3.51 through 3.53; see also Figure 3.29). The occurrence of a preauricular tag can also be detected on the axial view of the orbits, because this plane displays the preauricular area where the tags would be, if present. Nomograms for the longitudinal ear diameter (Appendix Table A.16) [36] can be employed to confirm a diagnosis of microtia or, much more rarely, macrotia. The use of 3D US has also made this diagnosis much easier to achieve (Figures 3.29 and 3.51 through 3.53; see also Figure 10.12).

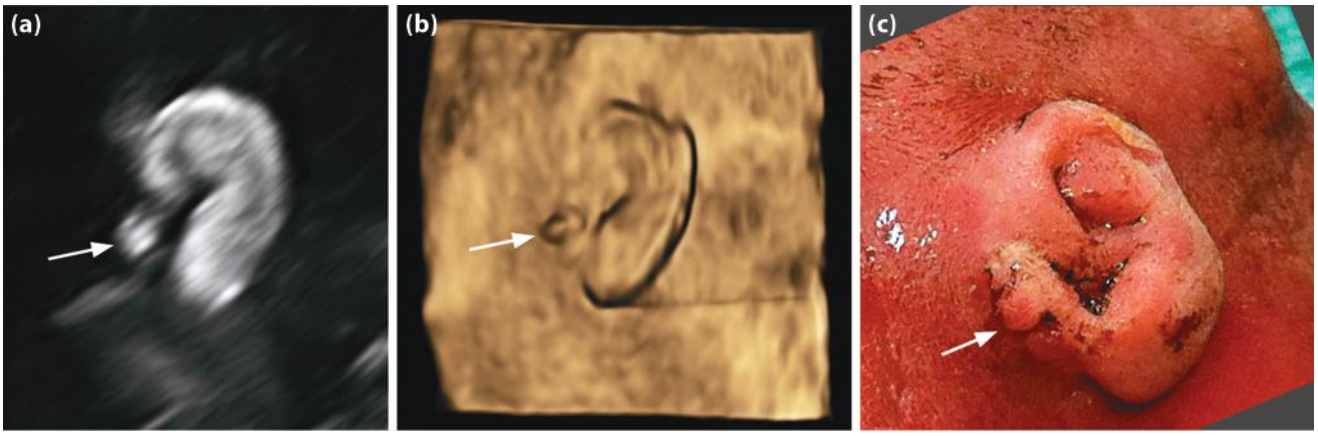


Figure 3.53 Preauricular tags in cat-eye syndrome (19 weeks). (a) Two-dimensional ultrasound; (b) three-dimensional surface-rendering ultrasound; and (c) autoptic confirmation (courtesy Dr Sansavini).

Prognostic indicators. Regardless of the shape of the external ear, it is the recognition of preauricular tags that represents the poorest prognostic sign, because of the high syndromic significance of this finding.

Association with other malformations. These include other developmental anomalies involving anatomic structures deriving from the first and second branchial arches, such as micrognathia and congenital heart disease.

Risk of chromosomal anomalies. This is relatively high. There is a close connection to the presence of trisomy 13 and, to a lesser extent, trisomy 18. Down syndrome fetuses tend to have small ears, but this does not represent a reliable marker for suspecting trisomy 21.

Risk of nonchromosomal syndromes. This is extremely high. Preauricular tags may be present in a significant number of syndromes. The syndromes associated with external ear anomalies that are most frequently diagnosed in the fetus are as follows:

- *Goldenhar syndrome [13,14,16]*: look for ► *external ear anomalies (or tags)* + hemifacial microsomia (unilateral) + microphthalmia + clefting (see Chapter 10);
- *Cat-eye syndrome (CES) [10,16]*: look for ► *preauricular tags (and/or wrinkled ears)* + heart defects, mainly abnormal pulmonary venous return (see Chapter 10);
- *Fraser syndrome [16,17]*: look for ► *external ear anomalies (or tags)* + laryngeal atresia + congenital heart disease + microphthalmia (unilateral) + facial clefting (see Chapter 10);
- *Nager syndrome [16,35]*: look for ► *external ear anomalies (or tags)* + ectrodactyly + micrognathia + mesomelic hypoplasia;
- *Treacher Collins syndrome [16]*: look for ► *external ear anomalies (or tags)* + micrognathia.

Obstetric management. The detection of severe external ear anomalies (tags, anotia, and small and wrinkled ears) usually follows the diagnosis of major fetal abnormalities. In the extremely rare cases in which the external ear anomaly represents the first abnormal finding on US, a detailed assessment of facial anatomy should be carried out, in order to disclose possible dysmorphisms. However, it should be kept in mind that moderate microtia/macrotia may represent a familial trait and, as such, may be devoid of any prognostic significance

Prognosis, survival, and quality of life. The prognosis depends upon the severity of the underlying syndrome. Survival and quality of life are normal in the case of familial macrotia or microtia.

CONGENITAL HIGH-AIRWAY OBSTRUCTION SYNDROME (CHAOS)

Incidence. Extremely rare.

Ultrasound diagnosis. *Facial profile view*: oropharyngeal and cervical masses obstructing the upper airways. *Axial view of the thorax:* Laryngeal/tracheal atresia.

Risk of chromosomal anomalies. Extremely low.

Risk of nonchromosomal syndromes. Extremely low, except for Pierre Robin syndrome (25%).

Outcome. Mainly unfavorable, unless the ex utero intrapartum treatment (EXIT) procedure is employed.

Definition Different types of congenital and acquired anomalies may cause the CHAOS sequence. These anomalies become a perinatal emergency when they completely block the high airway. In this case, survival can only be assured if the obstructing mass is removed or bypassed (tracheotomy). These anomalies include laryngeal atresia (see Chapter 6), tracheal atresia, obstructing laryngeal cysts, obstructing tumors of the oropharynx and the cervical region, large thoracic masses such as cystic adenomatoid malformations of the lung, and rare cases of diaphragmatic hernia.

Physiopathology. This group of anomalies is responsible for a partial or total obstruction of the upper airways at various levels. The obstruction can be located in the oropharynx (epignathus, lymphangiomas, etc.), or may involve more distal structures such as the larynx (laryngeal atresia) or the trachea (tracheal atresia and neck tumors). If these masses are very large, they can compromise swallowing of amniotic fluid relatively early in the course of the third trimester, causing severe polyhydramnios. At birth, the priority is to promptly re-establish the patency of the upper airways in order to ensure normal ventilation [38–40].

Ultrasound diagnosis. The most common anomalies possibly causing CHAOS are the following:

- *Epignathus*: This is a rare teratoma originating from the sphenoid bone or from the soft tissues of the oropharynx. It often achieves large dimensions, protruding from the mouth. It appears as an echogenic mass located in front of the mouth and nose of the fetus. The US diagnosis is straightforward and is made on the facial profile view. In the case of a dramatically fast-growing mass, the early compression can lead to developmental anomalies of the nose and the mouth (micrognathia and cleft palate).
- *Tumors of the tongue*: The tongue or, in general, the oral cavity, is an extremely rare location for a tumor. The mass will be prevalently cystic if of lymphangiomatous origin [41] or solid and hyperechoic in case of teratomas. If located in the oral cavity, the mass will grow within the mouth, eventually causing the lips to part (Figure 3.54). Only in the worst cases, such as in epignathus, will the mass continue its growth outside the fetal mouth. The US diagnosis is made on the midsagittal view of the fetal profile, for a general assessment; a detailed topographic study will then be carried out, employing axial views of the maxilla, the oral region, and the mandible, to assess possible involvement of the submandibular area and the anterior neck region.



Figure 3.54 Lymphangioma of the oropharynx. One of the anomalies potentially responsible for the CHAOS sequence. On the midsagittal view of the fetal face, the lips (LL) are pushed apart by the cystic intraoral mass (M) (F: forehead; N: nose). At birth, the lymphangioma (arrowheads) displaces the tongue.

- *Pierre Robin anomaly*: This condition has already been described among the primary developmental defects of the mandible. It is mentioned here because it can cause clinically significant obstruction of the upper airways if the degree of micrognathia and the concurrent glossoptosis are severe. The degree of micrognathia and glossoptosis are best evaluated on the midsagittal view of the fetal profile.

Risk of chromosomal anomalies. This is very low, because these lesions are primarily tumor masses.

Risk of nonchromosomal syndromes. This is low, except for the Pierre Robin anomaly, for which the association rate with syndromic conditions reaches 25% of cases. Of these, the syndromes potentially detectable in the fetus are diastrophic dysplasia (see Chapter 9), Beckwith–Wiedemann syndrome (see Chapter 10), and campomelic dysplasia (see Chapter 9).

Obstetric management and prognosis. The perinatal management of these conditions is complex and multidisciplinary. As already mentioned, upper-airway obstruction represents a neonatal emergency. There are two possible management options: (1) rapid delivery and immediate tracheotomy; and (2) the so-called EXIT (ex utero intrapartum treatment) procedure [38–40]. The latter is currently the most widely accepted option for CHAOS management and is described briefly here. Incision through the abdominal layers is carried out with the standard approach. After entering the abdominal cavity, intraoperative US is performed in order to locate the insertion site of the placenta, which has to be carefully avoided in the successive hysterotomy. The hysterotomy is generally carried out with staplers,

which ensure cutting and hemostasis of the myometrium at the same time. Amniorrhexis is then performed and the fetal head and neck are exposed. This is followed by intubation. Throughout this procedure, fetal well-being is monitored with oximetry and umbilical cord velocimetry. Once intubation has been completed, the umbilical cord is severed and the fetus delivered. If intubation fails, due to severe obstruction, then either a tracheotomy is performed or, according to the type of mass causing the obstruction, the tumor is removed surgically, if feasible. The outcome of the EXIT procedure depends mainly on the type of lesion causing the obstruction. It is very good for benign tumors of the neck (teratomas, etc.), but poor or very poor for extremely severe conditions such as laryngeal atresia or primary pulmonary hypoplasia [38–40].

oTherTUMors o F ThE NEck

Incidence. Extremely rare.

Ultrasound diagnosis. *Midsagittal view of the fetal profile; axial view of the thyroid region*: anterior neck masses (mesenchymal tumors, goiter).

Risk of chromosomal anomalies. Extremely low.

Risk of nonchromosomal syndromes. Extremely low.

Outcome. Variable, depending on the degree of upper-airway obstruction. Good for goiter (when due to maternal thyroid dysfunction).

Definition Although cystic hygromas account for most cervical masses in the fetus, there are other very rare entities that can originate at this level, such as anterior neck teratomas and goiter. Neck teratomas histologically show a prevalence of neuronal cells of ectodermal origin. Goiter consists of hypertrophic and hyperplastic thyroid follicles, and represents an expression of fetal hypothyroidism. The most common causes of fetal goiter are represented by maternal hyperthyroidism or, much more rarely, by maternal therapy with propylthiouracil.

Etiology and pathogenesis. As with most tumors, cervical teratomas are sporadic lesions.

Ultrasound diagnosis. The diagnosis is made on the midsagittal view of the profile but only when the head is extended, allowing the anterior neck region to be seen, and on the axial view of the thyroid, which allows direct assessment of the origin and the relationships of the mass with the other neck organs and vessels. Neck teratomas are usually solid and hyperechoic, or partly cystic, with possible calcified spots (Figure 3.55). Goiters appear as solid well-defined areas continuous with the thyroid gland, with which they share a weakly hyperechogenic appearance.

Prognostic indicators. The concurrent occurrence of evident polyhydramnios indicates the likely presence of esophageal compression. An abnormal and fixed hyperextension of the fetal head is a consequence of very large neck tumors.

Associations with other malformations. These are not known.

Risk of chromosomal anomalies. This is extremely low, as for all tumor masses. Goiters also do not show any additional risk of chromosomal anomalies.

Risk of nonchromosomal syndromes. This is extremely low, as for all tumor masses. Goiters also do not show any association with nonchromosomal syndromes.

Obstetric management. Should an anterior neck mass be diagnosed in a fetus, the occurrence of concurrent polyhydramnios should be evaluated. If present, this indicates the likely presence of esophageal compression and CHAOS. In these cases, an EXIT procedure (see above) should be considered [38–40]. If polyhydramnios is absent, operative delivery by Cesarean section is indicated due to the common occurrence of anomalous presentation and/or mechanical dystocia due to the neck hyperextension.

Postnatal treatment. The final treatment of neck tumors consists in their surgical removal. However, it should be noted that a significant percentage of mesenchymal tumors tend to regress after birth. Therefore, unless immediate surgery is indicated due to the malignant nature of the tumor, induced neck deformities (congenital wryneck, sternocleidomastoid muscle hypoplasia, etc.), or impairment of swallowing, then prolonged follow-up may be the approach of choice. More than one tumor has macroscopically disappeared or dramatically shrunken in a few months after birth, allowing

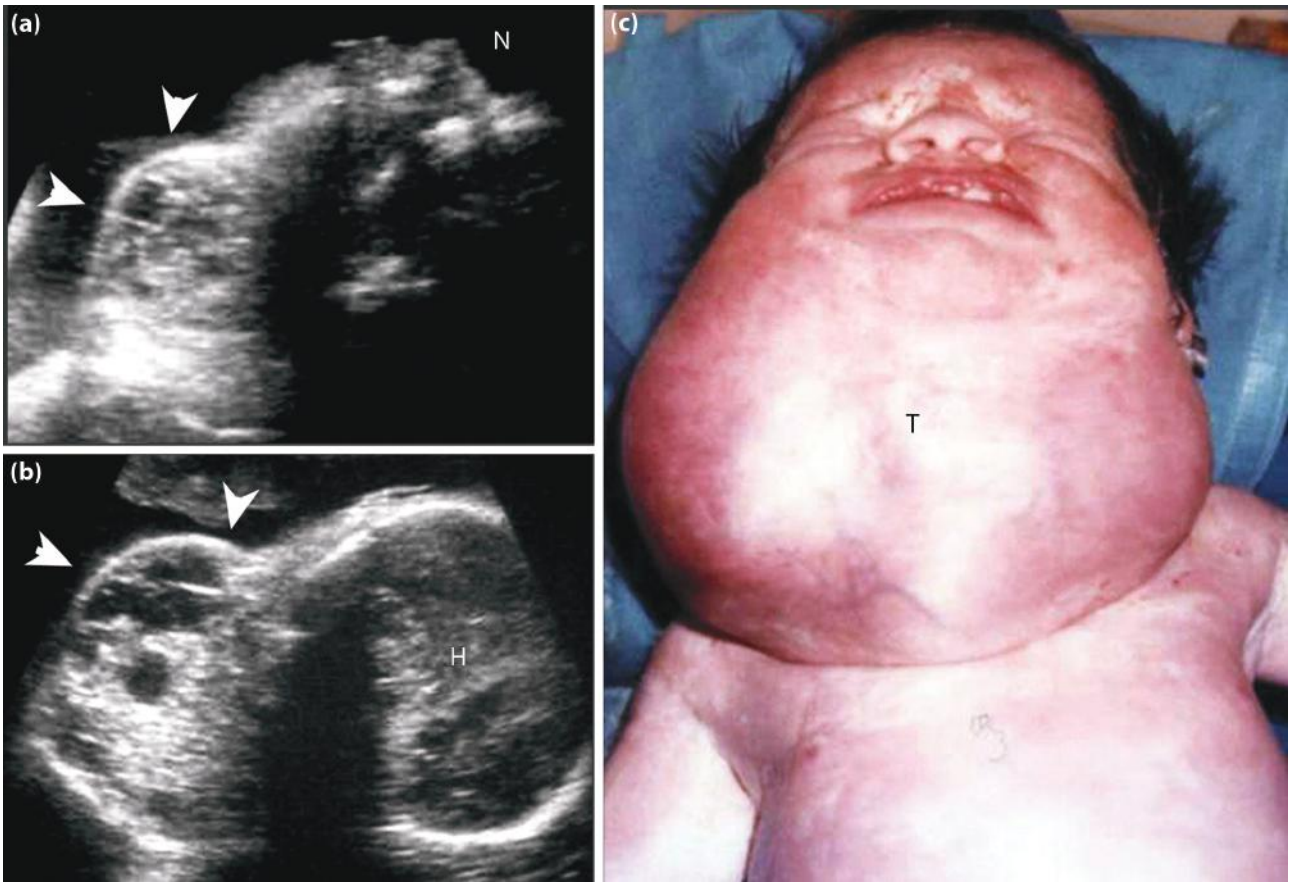


Figure 3.55 Neck teratoma. (a) On this midsagittal view of the fetal profile, the mass (arrowheads), located in the anterior neck region, appears to be causing severe hyperextension of the fetal head (N: nose); (b) An oblique view of the fetal neck demonstrating the mass (arrowheads) and the fetal head (H); and (c) the huge teratoma at birth.

easier and less invasive surgical removal. Some authors have claimed that the regression observed in the neonatal period for numerous mesenchymal benign tumors is due to the fact that their growth is sustained in utero by the maternal hormonal (estrogenic) milieu, which is claimed to represent a hyperplastic stimulus. As soon as this hormonal storm ceases, with delivery, the growth of the tumor is no longer stimulated and the mass shrinks significantl . Goiters can also undergo the same dramatic changes (partial or complete regression) once thyroid hormone receptors are no longer downregulated by maternal hyperthyroidism. Surgery is indicated in the rare cases in which significant esophageal compression occurs.

Prognosis, survival, and quality of life. Prognosis is usually good for both conditions, and quality of life is not affected in the absence of mechanical sequelae due to these masses. Congenital muscular torticollis (wryneck), temporomandibular joint anomalies, dental malocclusion, etc. may require orthopedic surgery, orthodontic procedures, and physiotherapy.

oTocEphALy

Incidence. Extremely rare.

Ultrasound diagnosis. *Midsagittal view of the fetal profile; ALL facial views are abnormal.* The mandible is not identifiable.

Risk of chromosomal anomalies. Extremely low.

Risk of nonchromosomal syndromes. Extremely low.

Outcome. Always lethal.

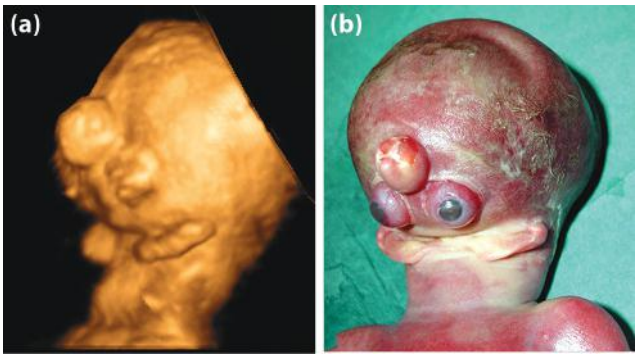


Figure 3.56 Otocephaly at 22 weeks' gestation. (a) The severe distortion of the facial anomaly is visible: The ears are horizontally placed below the eyes, and are partially fused; there is neither mouth nor mandible (agnathia). A midline proboscis replaces the nose; (b) autoptic confirmation.

Definition Otocephaly is characterized by agenesis or severe hypogenesis of the mandible (agnathia). The temporal bones are juxtaposed and the external ears are horizontally placed and/or fused.

Etiology and pathogenesis. The etiology is unknown. It can be associated with other midline defects, such as holoprosencephaly. The pathogenetic mechanism seems to be related to a complete failure of the mandibular development, possibly associated with inhibited or arrested migration of neural crest cells. Different degrees of severity have been described (synotia, agnathia, etc.).

Ultrasound diagnosis. The diagnosis is made on the midsagittal view of the profile but virtually all views of the fetal face are abnormal, due to the complete distortion of the facial anatomy. Three-dimensional US is often the only way to obtain an overall idea of the anomaly (Figure 3.56) [42].

Prognostic indicators. Otocephaly is always lethal.

Associations with other malformations. Holoprosencephaly, anencephaly, congenital heart disease, tracheoesophageal fistula.

Risk of chromosomal anomalies. This is not known, due to the extreme rarity of the anomaly. However, no association is reported.

Risk of nonchromosomal syndromes. Risk is not known, but presumably extremely low, or absent.

Obstetric management. Should such a rare anomaly be detected, termination of pregnancy should be offered, given that the anomaly is always lethal.

Postnatal treatment. This is not possible.

Prognosis, survival, and quality of life. Otocephaly is always lethal.

ABNor MALITIEs o F c r ANIAL sUTU r Es

Assessment of cranial sutures can only be performed using 3D US. All sutures and fontanelles can be displayed applying transparent maximum-mode rendering to previously acquired volumes of the fetal head. However, care should be taken in selecting an adequate approach for the study of each suture: due to the physics of US, only structures at an angle >45° (90° would be the optimum) with the insonating beam will be clearly displayed. Hence, the structure of interest should always be in front of the insonating beam. Volumes of the fetal face cannot be used to display the anterior fontanelle and, vice versa, volumes acquired with the objective to study the anterior fontanelle cannot be used to assess the metopic suture in detail. Normal images of the metopic, coronal, sagittal, and parieto-occipital sutures and of the anterior and posterior fontanelles are shown in Figure 3.57. The reliable assessment of sutures and fontanelles by 3D US has led to the recognition of their abnormalities. These include delayed fusion/ossification, premature fusion (synostoses), and presence of additional bones (Figure 3.58).

Recently, attention has focused on the aspect of the metopic suture, both for its intrinsic value and probably because it is easily studied retrospectively in stored volumes of fetal faces. Study of the metopic suture has demonstrated that ossification of the frontal bones starts at 9 weeks at the level of the supraorbital ridges, spreading them medially and laterally. At 12 weeks, the frontal bones are described as thick eyebrows. At 13 weeks, the frontal bones meet in the midline at the level of the nasal root, and the ossification then progresses upward. The gap between the two frontal bones starts to close at around 16 weeks in the supranasal region, and this fusion progresses with advancing gestation, so that at 32 weeks there is apparent closure of the metopic suture, starting from the glabella and then moving toward the anterior fontanelle [43]. It has recently been demonstrated that this process is delayed or altered in a number of pathologic conditions, ranging from central nervous system malformations (Dandy–Walker malformation), agenesis of the corpus callosum, and holoprosencephaly to Down syndrome and skeletal dysplasias [44–46]. In particular, recognized abnormal

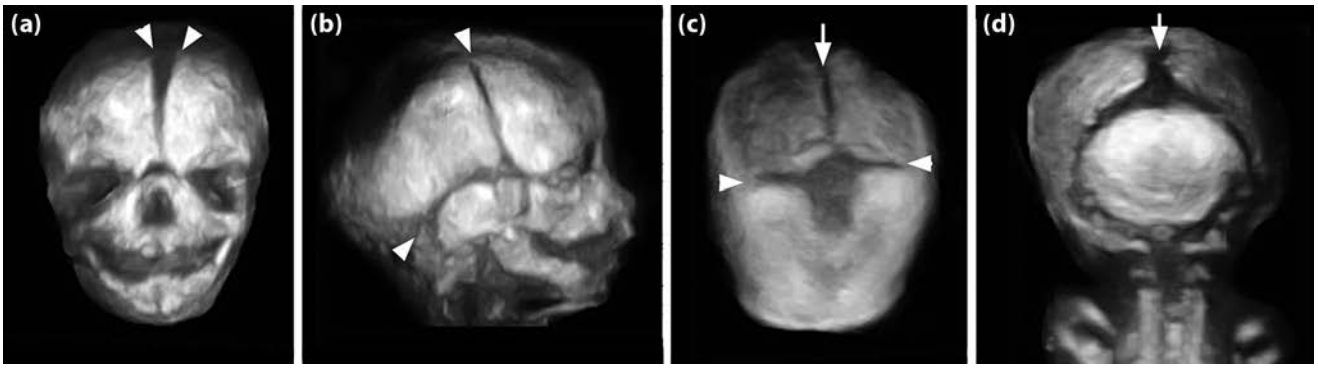


Figure 3.57 Normal cranial sutures and fontanelles. Three-dimensional maximum-mode rendering allows clear visualization of all cranial sutures and fontanelles. However, in order to obtain adequate images, care should be taken to maintain a perpendicular insonation angle with the suture of interest. These images are of a fetus at 22 weeks' gestation: (a) metopic suture (arrowheads); (b) coronal and temporoparietal sutures (arrowheads); (c) anterior fontanelle (arrowheads) and sagittal suture (arrow); (d) posterior fontanelle (arrow) and parieto-occipital suture.

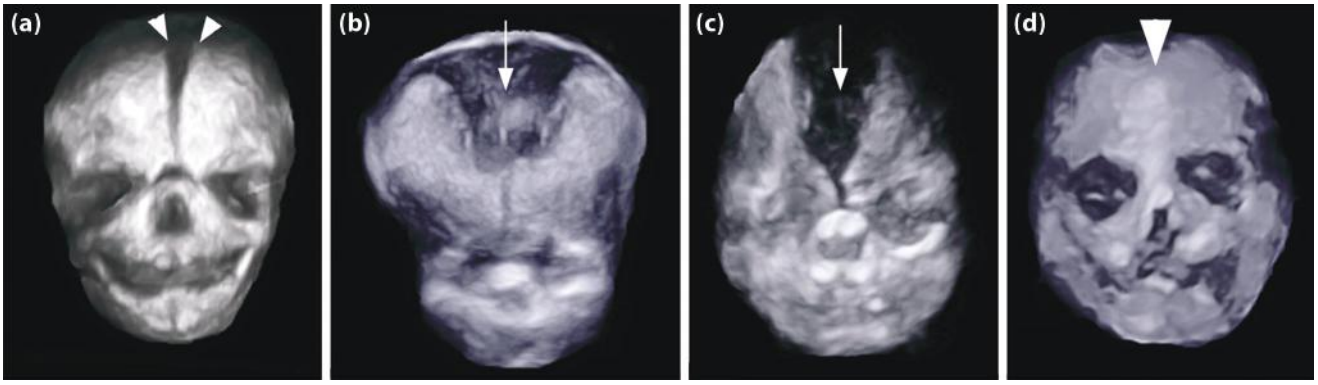


Figure 3.58 Abnormal cranial sutures. (a) Normal metopic suture at 22 weeks' gestation; (b) U-shaped metopic suture and severely unossified anterior fontanelle in severe hydrocephalus (22 weeks' gestation; note also incipient macrocrania); (c) U-shaped metopic suture in a fetus affected with Apert syndrome (23 weeks' gestation); (d) completely sealed metopic suture in a fetus affected with semilobar holoprosencephaly (20 weeks' gestation) (arrows and arrowheads indicate metopic suture and anterior fontanelle)

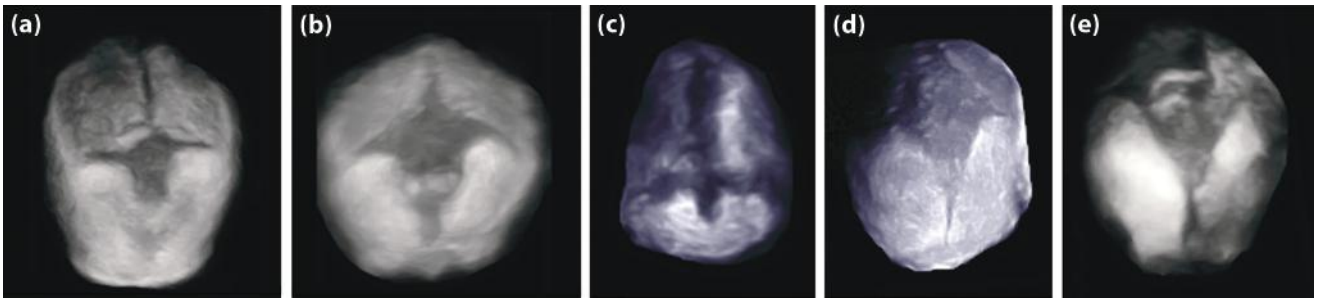


Figure 3.59 Abnormal fontanelles. (a) Normal anterior fontanelle at 22 weeks' gestation; (b) wide anterior fontanelle in severe hydrocephalus (22 weeks' gestation); (c) wide anterior fontanelle and underossified sagittal suture in another case of early hydrocephalus (19 weeks' gestation); (d,e) two cases of achondroplasia at 26 and 29 weeks' gestation respectively, showing extremely wide anterior fontanelles.

appearances of the metopic suture are a V- or Y-shaped suture, a U-shaped suture, premature closure, and additional bone. These aspects are shown in Figure 3.58. In addition to these findings, 3D US also allows the detection of synostoses, which are typical of some disorders associated with abnormal skull shape, such as Apert syndrome [47] and thanatophoric dysplasia. Abnormal development of the fontanelles can also be demonstrated with this technique: In our experience, ossification of the fontanelles is delayed in the case

of hydrocephalus and achondroplasia (Figure 3.59). In summary, a new diagnostic horizon has been opened by 3D US—namely, abnormalities of the cranial sutures. This diagnostic field has so far been only sampled, and the preliminary results are those reported here. However, this represents one of the most promising areas for investment in future research, considering that a significant number of syndromic conditions have among their typical signs a delayed ossification of the sutures, and of the metopic suture in particular. It is likely that other new interesting anomalies of the suture ossification process will soon be found.

rEFE r ENc Es

1. Jeanty P, Romero R, Staudach A, et al. Facial anatomy of the fetus. *J Ultrasound Med* 1986; 5: 607–16.
2. Rotten M, Levaillant JM. Two and three-dimensional sonographic assessment of the fetal face. 1. A systematic analysis of the normal face. *Ultrasound Obstet Gynecol* 2004; 23: 224–31.
3. Salomon LJ, Alfirevic Z, Berghella V, et al. Practice guidelines for performance of the routine mid-trimester fetal ultrasound scan. *Ultrasound Obstet Gynecol* 2011; 37: 116–26.
4. Jeanty P, Dramaix-Wilmet M, Van Gansbeke D, et al. Fetal ocular biometry by ultrasound. *Radiology* 1982; 143: 513–16.
5. Bault JP, Quarello E. Retinal coloboma: prenatal diagnosis using a new technique, the 'virtual fetal eyeground'. *Ultrasound Obstet Gynecol* 2009; 33: 495–6.
6. Kimes KR, Mooney MP, Siegel MI, et al. Size and growth rate of the tongue in normal and cleft lip and palate human fetal specimens. *Cleft Palate Craniofac J* 1991; 28: 212–16.
7. Paladini D. Fetal micrognathia: almost always an ominous fin - ing. *Ultrasound Obstet Gynecol* 2010; 35: 377–84.
8. Paladini D, Morra T, Teodoro A, et al. Prenatal diagnosis of micrognathia in the fetus. The jaw index. *Obstet Gynecol* 1999; 93: 382–6.
9. Rotten D, Levaillant JM, Martinez H, et al. The fetal mandible: a 2D and 3D sonographic approach to the diagnosis of retrognathia and micrognathia. *Ultrasound Obstet Gynecol* 2002; 19: 122–30.
10. Volpe P, Buonadonna AL, Campobasso G, et al. Cat-eye syndrome in a fetus with increased nuchal translucency: three-dimensional ultrasound and echocardiographic evaluation of the fetal phenotype. *Ultrasound Obstet Gynecol* 2004; 24: 485–7.
11. Chervenak FA, McCullough LB. An ethical critique of boutique fetal imaging: a case for the medicalization of fetal imaging. *Am J Obstet Gynecol* 2005; 192: 31–3.
12. Platt LD. Three-dimensional ultrasound, 2000. *Ultrasound Obstet Gynecol* 2000; 16: 295–8.
13. Martinelli P, Maruotti GM, Agangi A, et al. Prenatal diagnosis of hemifacial microsomia and ipsilateral cerebellar hypoplasia in a fetus with oculoauricolovertebral spectrum. *Ultrasound Obstet Gynecol* 2004; 24: 199–201.
14. Volpe P, Gentile M. Three-dimensional diagnosis of Goldenhar syndrome. *Ultrasound Obstet Gynecol* 2004; 24: 798–800.
15. Paladini D, D'Armiento MR, Ardovino I, et al. Prenatal diagnosis of the cerebro-oculo-facio-skeletal (COFS) syndrome. *Ultrasound Obstet Gynecol* 2000; 16: 91–3.
16. Lyon Jones K. *Smith's Recognizable Patterns of Human Malformation*. 6th ed. Philadelphia, PA: WB Saunders; 2006.
17. Maruotti GM, Paladini D, Agangi A, et al. Prospective prenatal diagnosis of Fraser syndrome variant in a family with negative history. *Prenat Diagn* 2004; 24: 69–70.
18. Vogt G, Puho E, Czeizel AE. Population-based case–control study of isolated congenital cataract. *Birth Defects Res Part A* 2005; 73: 997–1005.
19. Jeffrey BG, Birch EE, Stager DR Jr, et al. Early binocular visual experience may improve binocular sensory outcomes in children after surgery for congenital unilateral cataract. *J AAPOS* 2001; 5: 209–16.
20. O'Keefe M, Fenton S, Lanigan B. Visual outcomes and complications of posterior chamber intraocular lens implantation in the first year of life. *J Cataract Refract Surg* 2001; 27: 2006–11.
21. Martinelli P, Russo R, Agangi A, et al. Prenatal ultrasound diagnosis of frontonasal dysplasia. *Prenat Diagn* 2002; 22: 375–9.
22. Paladini D, Borghese AM, Arienzo M, et al. Prospective ultrasound diagnosis of Pallister–Killian syndrome in the 2nd trimester of pregnancy: the importance of the fetal facial profile *Prenat Diagn* 2000; 20: 996–8.
23. Levaillant JM, Moeglin D, Zouiten K, et al. Binder phenotype: clinical and etiological heterogeneity of the so-called Binder maxillonasal dysplasia in prenatally diagnosed cases, and review of the literature. *Prenat Diagn* 2009; 29: 140–50.
24. Vintzileos AM, Walters C, Yeo L. Absent nasal bone: a specific marker for second-trimester fetuses with Down syndrome. *Ultrasound Med Biol* 2003; 29: 5S.
25. Benoit B, Chaoui R. Three-dimensional ultrasound with maximal mode rendering: a novel technique for the diagnosis of bilateral or unilateral absence or hypoplasia of nasal bones in 2nd trimester screening for down syndrome. *Ultrasound Obstet Gynecol* 2005; 25: 19–24.
26. Tessier P. Anatomical classification facial, cranio-facial and latero-facial clefts. *J Maxillofac Surg* 1976; 4: 69–92.
27. Bronshtein M, Blumenfeld I, Kohn J, et al. Detection of cleft lip by early second trimester transvaginal sonography. *Obstet Gynecol* 1994; 84: 73–5.
28. Wilhelm L, Borgers H. The 'equals sign': a novel marker in the diagnosis of fetal isolated cleft palate. *Ultrasound Obstet Gynecol*. 2010 Oct; 36(4): 439–44
29. Nyberg DA, Sickler GK, Hegge FN, et al. Fetal cleft lip with and without cleft palate: US classification and outcome. *Radiology* 1995; 195: 677–80.
30. Sommerlad BC. The management of cleft lip and palate. *Curr Pediatr* 2002; 12: 43–50.
31. Timmons MJ, Wyatt RA, Murphy T. Speech after repair of isolated cleft palate and cleft lip and palate. *Br J Plastic Surg* 2001; 54: 377–84.
32. Vettraino IM, Wesley L, Bronsteen R, et al. Clinical outcome of fetuses with sonographic diagnosis of isolated micrognathia. *Am J Obstet Gynecol* 2003; 102: 801–5.
33. Paladini D, Tartaglione A, Agangi A, et al. Pena–Shokeir phenotype in three consecutive pregnancies. *Ultrasound Obstet Gynecol* 2001; 17: 163–5.
34. Manning MA, Cunniff CM, Colby CE, et al. Neu–Laxova syndrome: detailed prenatal diagnostic and post-mortem fin - ings and literature review. *Am J Med Genet A* 2004; 125: 240–9.
35. Paladini D, Tartaglione A, Lamberti A, et al. Prenatal ultrasound diagnosis of Nager syndrome. *Ultrasound Obstet Gynecol* 2003; 21: 195–7.

36. Paladini D, Maruotti GM, Sglavo G, et al. Diagnosis of femoral hypoplasia–unusual facies syndrome in the fetus. *Ultrasound Obstet Gynecol* 2007; 30: 354–8.
37. Chitkara U, Lee L, EI-Sayed YV, et al. Ultrasonographic ear length measurement in normal second – and third trimester fetuses. *Am J Obstet Gynecol* 2000; 183: 230–4.
38. Lim FY, Crombleholme TM, Hedrick HL, et al. Congenital high airway obstruction syndrome: natural history and management. *J Pediatr Surg* 2003; 38: 940–5.
39. Bouchard S, Johnson MP, Flake AW, et al. The EXIT procedure: experience and outcome in 31 cases. *J Pediatr Surg* 2002; 37: 418–26.
40. Hirose S, Harrison MR. The ex utero intrapartum treatment (EXIT) procedure. *Semin Neonatol* 2003; 8: 207–14.
41. Paladini D, Morra T, Guida F, et al. Prenatal diagnosis and perinatal management of a lingual lymphangioma. *Ultrasound Obstet Gynecol* 1998; 11: 141–3.
42. Chaoui R, Heling K, Thiel G, et al. Agnathia-otocephaly with holoprosencephaly on prenatal three-dimensional ultrasound. *Ultrasound Obstet Gynecol* 2011; 37: 745–8.
43. Faro C, Benoit B, Wegrzyn P, et al. Three-dimensional sonographic description of the fetal frontal bones and metopic suture. *Ultrasound Obstet Gynecol* 2005; 26: 618–21.
44. Chaoui R, Levaillant M, Benoit B, et al. Three-dimensional sonographic description of abnormal metopic suture in second and third-trimester fetuses. *Ultrasound Obstet Gynecol* 2005; 26: 761–4.
45. Paladini D. Vassallo M, Sglavo G, et al. Normal and abnormal development of the fetal anterior fontanelle: a three-dimensional ultrasound study. *Ultrasound Obstet Gynecol* 2008; 32: 755–61.
46. Paladini D, Sglavo G, Penner I, et al. Fetuses with Down syndrome have an enlarged anterior fontanelle in the second trimester of pregnancy. *Ultrasound Obstet Gynecol* 2007; 30: 824–9.
47. Faro C, Chaoui R, Wegrzyng P, et al. Metopic suture in foetuses with Apert syndrome at 22–27 weeks of gestation. *Ultrasound Obstet Gynecol* 2006; 27: 28–33.

Chapter 4
Cystic hygroma and nonimmune hydrops fetalis

cys TIc hy Gro MA (ch)

Incidence. Incidence of cystic hygroma (CH) is high (1/285 in first trimester).

Ultrasound diagnosis. It is usually characterized by bilateral cystic structures of the posterior neck separated by the nuchal ligament.

Risk of chromosomal anomalies. High (35%–50%): Turner syndrome; trisomies 21, 18, and 13; other rare chromosomal rearrangements.

Risk of nonchromosomal syndromes. High.

Outcome. Outcome is poor in most cases, especially for the high frequency of associated anomalies. Only 10% of cases survive without major morbidity.

Definition CH is defined as a congenital lymphatic abnormality, characterized by distended fluid-fille spaces, commonly affecting the fetal neck. It is classically defined as septated CH, in case of presence of septa within it.

Etiology and pathogenesis. CH etiology is not perfectly known, but it is thought to arise from impaired drainage of the jugular lymphatic sacs (JLS) or from altered lymphangiogenesis [1]. The JLS are the first part of the lymphatic system to develop: at the fifth week, the internal jugular veins give rise to lymphatic buds, which fuse and form the JLS. The peripheral lymphatic system is formed by sprouting from these sacs. The JLS in human fetuses normally reorganize into lymphatic nodes after ten weeks of gestation. The formation of the lymphatic system is completed by ingrowth of the thoracic duct into the left lymphatic sac, which thereby connects several lymphatic vessels. After reorganization of the JLS into lymphatic nodes, the connection of the thoracic duct to the internal jugular vein is the main site at which drainage of lymphatic fluid takes place. Any anomaly during the development of this lymphatic drainage system may cause enlargement of the JLS, resulting in CH [2].

Ultrasound diagnosis. CH typically develops late in the first trimester and is, therefore, usually diagnosed between 12 and 14 weeks. It is characterized by the presence of bilateral fluid-fille cavities in the fetal neck, considered as cystic dilatations of the JLS. An axial view of the fetal neck is required in order to make the diagnosis (Figures 4.1 and 4.2) [3]. There is an ongoing debate regarding the differentiation between increased nuchal translucency (NT) and CH in the first trimester of pregnancy. For this purpose, several authors have recently advocated the use of the axial plane of the fetal neck at the base of the skull to differentiate between the two conditions [3,4]. On this view, the presence of subcutaneous edema of the neck or diffuse thickening, with fine septations, should not be diagnosed as CH, but represents the anatomic spectrum of NT; on the contrary, the recognition of bilateral cystic JLS is typical of CH. However, in agreement with other authors (2), we consider CH and increased NT to be a single entity in the first trimester (Figure 4.3). It should be pointed out that the risk for chromosomal abnormalities and adverse outcome is related to the thickness of the retronuchal fluid rather than to its appearance and classification [5–6]. When detected in the first trimester, CH can evolve into different pictures: It can progress toward

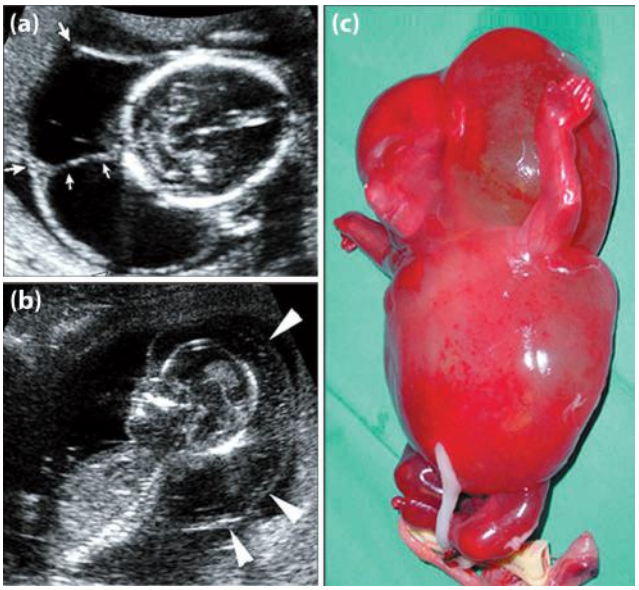


Figure 4.1 Cystic hygroma at 16 weeks' gestation—Turner syndrome. (a) On the axial view, the possible presence of septa (arrows) is evaluated. (b) On the midsagittal view, the extent of the retronuchal hygroma is assessed (arrowheads). (c) Confirmation at autopsy. In this case, significant subcutaneous edema was also present.

generalized hydrops, resolve completely, or persist in part as nuchal edema, irrespective of the fetal karyotype. The resolution of the hygroma has been related to an early partial and transient lymphatic obstruction or to a delay in jugular lymphatic connections that results in temporary lymphatic obstruction, which resolves with time. Lesions that persist into the second trimester are usually characterized by giant cysts that completely fill the amniotic cavity. Often, with increasing lymphedema of the upper trunk, neck, and base of the skull, fluid-fille regions with septa are found inside the skin. Eventually, the progression of the lymphedema leads to effusions in the body cavities.

Differential diagnosis. The main differential diagnosis of CH includes occipital meningocele (MC), cervical teratoma (see Chapter 3), increased nuchal fold, and cervical lymphangioma (see Chapter 3). In MC, a calvarial bone defect is present. In cervical teratoma, a solid mass is present (teratomas frequently arise in the anterior neck region). The increased nuchal fold is not a proper cystic lesion: it might represent an evolution of a previous CH, but should not be primarily regarded as CH. Figures 4.4 and 4.5 show the sonographic appearance of several conditions that should be differentiated from CH.

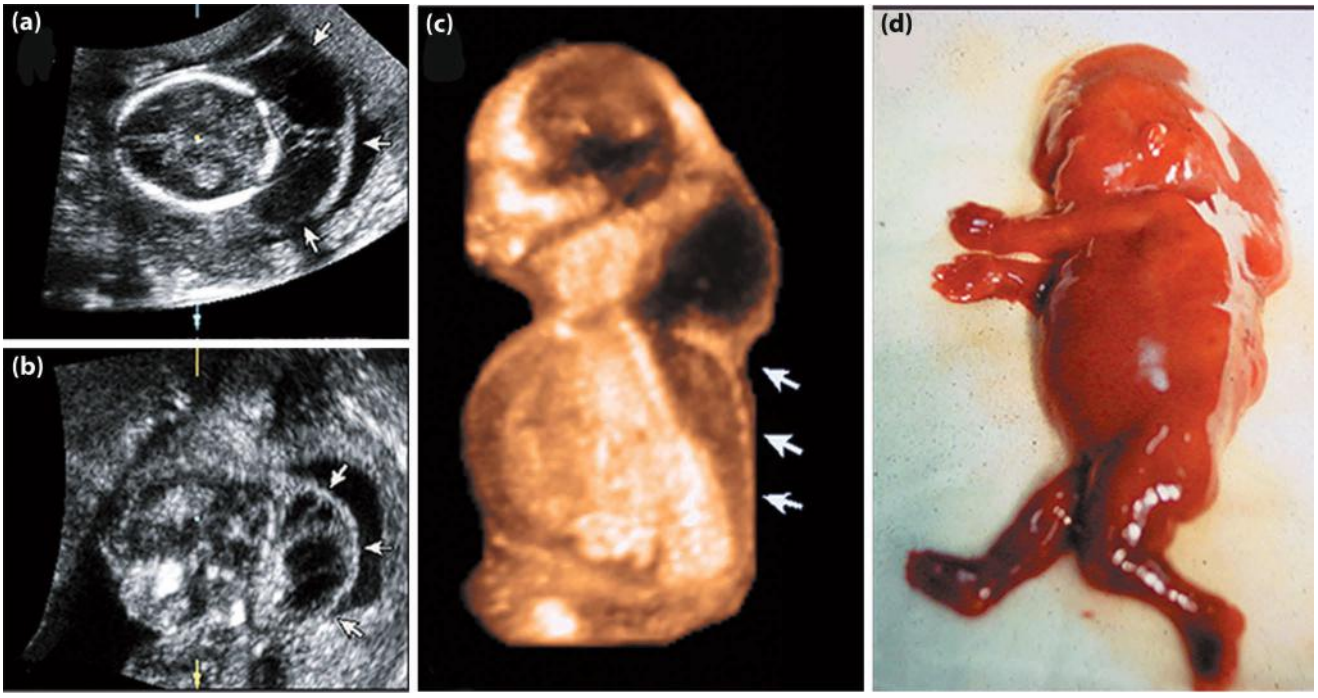


Figure 4.2 Cystic hygroma at 13 weeks' gestation. The multiplanar approach allows visualization of the severe septated hygroma (arrows) on the axial view (a) and midsagittal view (b); (c) three-dimensional surface rendering, demonstrating the thoracic extension of the lymphangiectasia (arrows); (d) confirmation at autopsy.

Prognostic indicators. Several studies have analyzed the prognostic significance of classifying hygromas into septate and nonseptate forms. Although some studies have suggested that the presence of septations predicts an increased likelihood of aneuploidy and poor fetal outcome [7], this concept has not been confirmed by other authors [8], who have noted that all the increased NTs have septations (when properly examined in terms of ultrasound planes and machine settings), and the risk of chromosomal abnormalities depends on the thickness rather than on other characteristics of the NT.

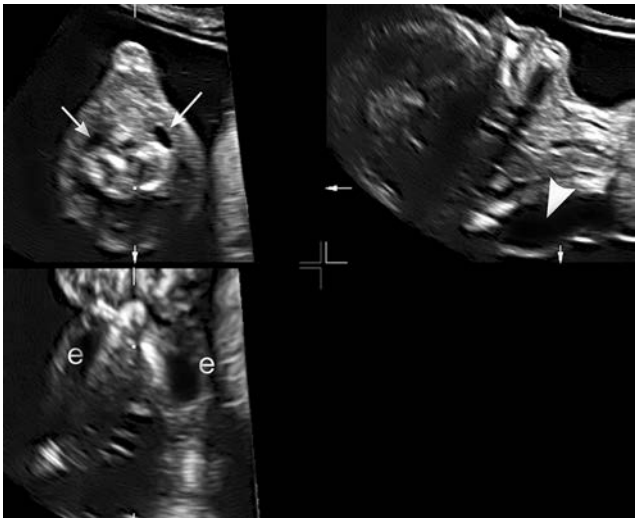


Figure 4.3 Multiplanar imaging of a fetus with increased nuchal translucency (NT) and enlarged jugular lymphatic sacs. The axial image (top left panel) shows mildly dilated jugular lymphatics (arrows). The midsagittal view (top right panel) shows enlarged NT (arrowhead). Enlarged jugular limphatic sacs are clearly seen on the lower left panel (e).

Association with other malformations. CH is associated with other malformations in up to 60% of cases, including cardiac defects, skeletal dysplasias, diaphragmatic hernia, and central nervous system (CNS) anomalies.

Risk of chromosomal anomalies. This risk is high. About 35%–50% cases of CH have an abnormal karyotype. In the second trimester, the most common chromosomal anomaly associated with a large CH, often with typical septations, is Turner syndrome. In the first trimester, there is the same proportion of trisomies 21 and 18 and Turner syndrome [4].

Risk of nonchromosomal syndromes. This risk is high. The most common syndromes associated with CH are as follows:

- *Noonan syndrome [9]*: look for ► *CH* + congenital heart disease (pulmonary stenosis and cardiomyopathy) + facial anomalies + fetal growth retardation (FGR);

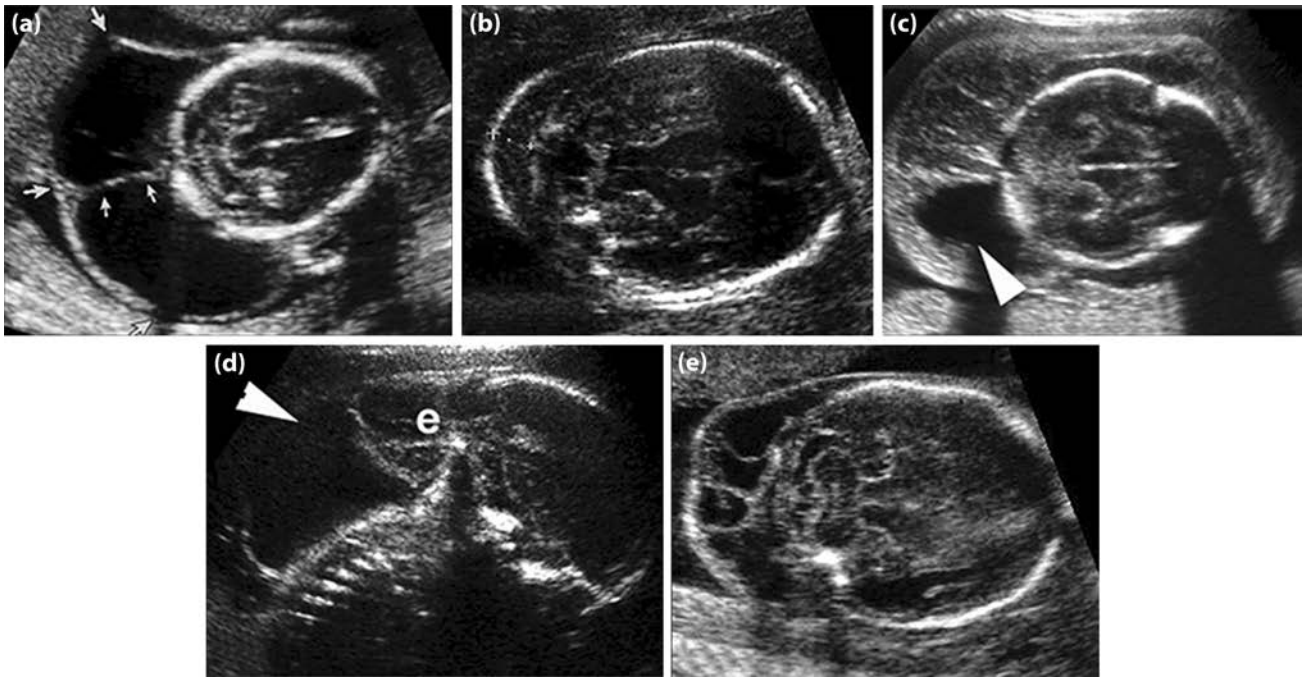


Figure 4.4 Differential diagnosis of retronuchal anomalies. (a) Septate cystic hygroma at 16 weeks' gestation. (b) Nuchal fold in trisomy 21 at 20 weeks' gestation. (c) Severe hydrops with subcutaneous edema and lymphangiectasia (arrowheads) at 19 weeks' gestation. (d) Occipital meningoencephalocele, with a large meningeal sac (arrowheads; e: herniated brain) at 21 weeks' gestation. (e) Retronuchal edema with lymphangiectasia in FADS (fetal akinesia deformation sequence) at 20 weeks' gestation.

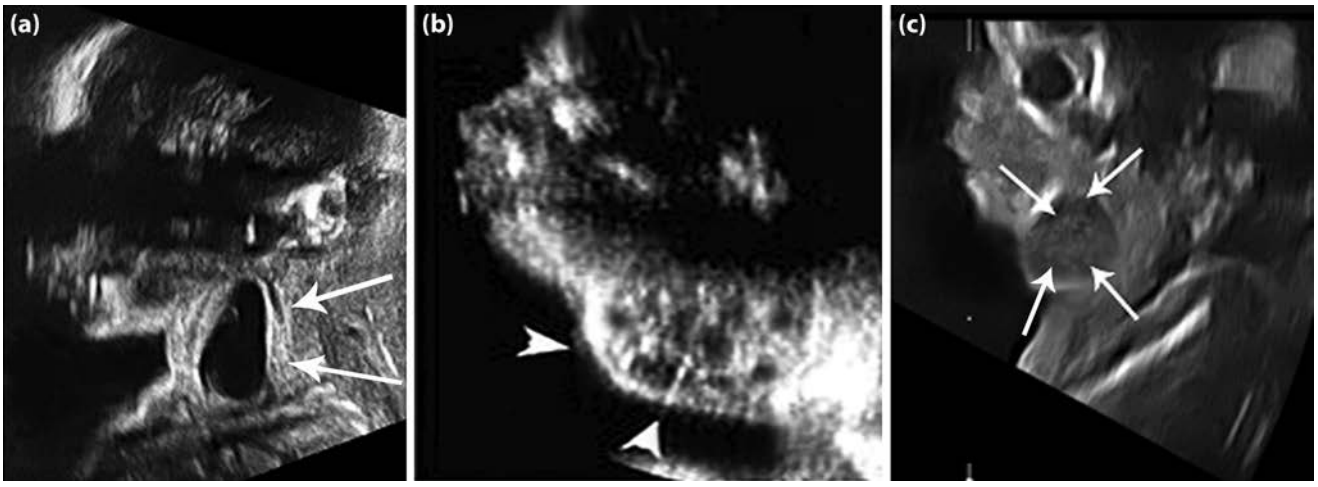


Figure 4.5 Differential diagnosis with other neck anomalies: (a) Neck limphangioma (arrows) is usually unilateral cystic tumor, often with intrathoracic extension; (b) neck teratoma is located anteriorly (and not posteriorly and/or laterally as in case of CH) and it is usually large and mixed -solid mass (arrowheads); (c) goiter is a homogeneous, echogenic mass (arrows) in the anterior part of the fetal neck.

- *Multiple-pterygium syndrome [9]*: look for ► *CH* + micrognathia + camptodactyly + arthrogryposis + pterygia at knees and elbows + FGR (See also Chapter 10);
- *Fryns syndrome [9]*: look for ► *CH* + diaphragmatic hernia + microphthalmia + CNS anomalies + distal limb anomalies;
- *Neu–Laxova syndrome [9]*: look for ► *CH* + CNS anomalies + microcephaly + arthrogryposis + micrognathia + edema in extremities + FGR (See also Chapter 10).

Obstetric management. The presence of CH is a strong indication for karyotyping, because of the high risk of aneuploidy. The sonographic detection of CH should prompt a detailed examination of fetal anatomy in order to detect associated anomalies and signs of hydrops. In particular, it is important to exclude skeletal anomalies, due to the frequent association with fetal akinesia deformation sequence (FADS), in view of its high recurrence risk. The disease course of a fetus with a CH detected in the first trimester may be unpredictable; in fact, there is no reliable method to predict which hygromas will regress and which will progress to frank nonimmune hydrops fetalis (NIHF). Also, if the karyotype is normal and no associated anomalies are found, the parents should still be counseled about the uncertain prognosis. If the pregnancy is continued, the fetus should be followed closely with detailed serial ultrasound. Large CH in fetuses reaching term of gestation can complicate obstetric and perinatal management. Infants with large prenatally detected hygromas may require delivery by Cesarean section. There are reports of successful vaginal delivery after intrauterine cyst decompression.

Postnatal therapy. At present, complete excision remains the treatment of choice for CH. It can be a difficult procedure due to the infiltrative nature of CH. However, before attempting excision of a CH, the extent of the lesion and its relationship to surrounding structures must be clearly defined by magnetic resonance imaging. Postoperative complications, including recurrence, wound seromas, infection, and nerve damage, occur in more than 30% of cases.

Prognosis, survival, and quality of life. Only 10% of fetuses with CH survive without major morbidity. In fact, CH is often associated with chromosomal anomalies, hydrops, and fetal death. Many fetuses with CH seen during the first trimester die spontaneously before 20 weeks' gestation. An even poorer prognosis is expected if CH is associated with other anomalies, including chromosomal aberrations [1,4]. CH is also a marker of numerous genetic syndromes with normal karyotype, and the poor survival rate in this condition is mainly due to its association with hydrops. In cases of CH with normal karyotype and no associated malformations, the parents should still be counseled about the prognosis. If an isolated CH not associated with chromosomal anomalies or any malformations has resolved, it is likely that the infant will be normal; however, resolution of the hygroma per se does not imply a good prognosis, because resolution has been documented in fetuses with genetic anomalies not detectable prenatally by ultrasound.

Nonimmune hydrops Fetalis

Incidence. It is a common anomaly with an incidence of 1 in 3000, but with a high intrauterine death rate.

Ultrasound diagnosis. Fluid collection in serosal cavities (ascites, hydrothorax, pericardial effusion); subcutaneous edema, prevalently of head and thorax, but sometimes also of limbs; polyhydramnios.

Risk of chromosomal anomalies. Risk is high: monosomy X, autosomal trisomies 21, 18, 13.

Risk of nonchromosomal syndromes. Risk is extremely high, and includes skeletal dysplasias, storage diseases, and infections.

Outcome. Outcome is extremely unfavorable, except for cases associated with potentially treatable causes, such as anemia from parvovirus B19 infection and supraventricular paroxystic tachycardia.

Definition Fetal hydrops represents an aspecific condition characterized by an increase of total body water content. In such a condition, the excess fluid collects by ultrafiltration in body cavities (pleural, pericardial, and peritoneal effusions) and/or in the subcutaneous tissue. Placental edema and polyhydramnios are frequently associated (30%–70%). Fetal hydrops is divided into two etiologic groups: *immune fetal hydrops* and *nonimmune hydrops fetalis*; the former is due to maternal Rhesus immunization, while the latter has a wide spectrum of possible causes. Immune hydrops was decidedly more frequent until prophylaxis against Rhesus immunization was implemented worldwide. Currently, very few cases of fetal hydrops are due to Rhesus immunization. In this chapter, only NIHF will be illustrated. By definition the term NIHF refers to fluid collections in at least two body cavities or involving just one body cavity plus diffuse subcutaneous edema.

Etiology and pathogenesis. The etiology of NIHF includes a huge number of different causes. Cardiac causes are those most frequently responsible for NIHF, accounting for 20%–40% of cases, whereas no cause (idiopathic hydrops)—or at least no sonographically recognizable cause—is found in 30%–50% of cases. A partial list of the numerous conditions associated with NIHF is given in Table 4.1. The etiology of NIHF comprises primarily four types of pathogenetically different causes:

1. *Cardiac failure and related conditions*. Cardiac failure can be due to a *low output* or to a *high output*. The former is caused by primary cardiac conditions, including functional and structural defects. Among the **functional causes**, severe bradyarrhythmias (complete heart block) and severe tachyarrhythmias (supraventricular parossistic tachycardia and atrial flutter) result in *low cardiac output* due to the extreme bradycardia and the impaired diastolic filling associated with increased preload, respectively. With regard to the **structural causes** (congenital heart disease), it should be noted that the presence of the *two shunts* represented by a patent ductus arteriosus and a patent foramen ovale reduces the hemodynamic impact of isolated obstructive lesions (tricuspid atresia or hypoplastic left heart) and septal lesions (atrioventricular or ventricular septal defects). In contrast, cardiac failure often develops in the case of severe volume overload due to severe valvular insufficiency (severe Ebstein's anomaly, critical aortic stenosis with mitral insufficiency, pulmonary atresia with intact ventricular septum, and tricuspid insufficiency). The basic cause of cardiac failure in these cases is the pump deficit. The same mechanism leads to cardiac failure and NIHF in the case of cardiomyopathies associated with severe impairment of the systolic function. Rare extracardiac conditions causing cardiac failure include large thoracic, cardiac, or pericardiac tumors/masses that could compress the vena cava and reduce the venous return to the heart. Among extracardiac conditions possibly responsible for *high output* heart failure and NIHF, it should be noted that the most common are those featuring *arteriovenous fistulas*. These include placental chorioangioma, sacrococcygeal teratoma, aneurysm of the vein of Galen, twin-to-twin transfusion syndrome (TTTS) (recipient twin). These conditions have in common an increased blood volume (e.g., perfusion of the tumor mass) that cannot be managed by the immature fetal heart, with consequent cardiac failure.
2. *Chromosomal anomalies*. The chromosomal anomaly most frequently associated with CH and NIHF is monosomy X (Turner syndrome). In this case hydrops is due to the commonly associated lymphatic dysplasia. Trisomy 21, and a significant number of other autosomal trisomies (13 and 18), can also be associated with early NIHF. Finally, it

Table 4.1 Cause of nonimmune hydrops in the fetus (NIHF) by anatomic region

Cause by region	Frequency of hydrops
Brain	
Cerebral hemorrhage	Low
Aneurysm of the vein of Galen	High
Cerebral tumors	Low
Heart	
CHD featuring valve insufficiency	Relatively high
CHD featuring impaired cardiac function (cardiomyopathies, myocarditis, tachyarrhythmias, CHB)	Relatively high
Cardiac tumors	Low
Thorax (heart excluded)	
Cystic adenomatoid malformation of the lung (CAML)	Low
Pulmonary sequestration	Moderate
Laryngeal atresia	High
Mediastinal tumors (teratomas, mainly)	Relatively high
Abdomen—gastrointestinal tract	
Diaphragmatic hernia	Low
Meconium peritonitis	Moderate
Hepatitis	High
Hepatic fibrosis	Moderate
Abdomen—genitourinary system	
Urethral obstruction	Moderate
Autosomal recessive polycystic kidney disease	Low
Renal vein thrombosis	High
Ovarian cyst torsion	Low
Tumors and conditions featuring high output cardiac failure	
Mediastinal teratoma	Relatively high
Neuroblastoma	Moderate
Hepatoblastoma	Moderate
Nephroblastoma	Moderate
Sacrococcygeal teratoma	High
Galen vein aneurysm	High
Placental chorioangioma	High
Twin-to-twin transfusion syndrome	High
Agenesis of the ductus venosus (with extrahepatic connection)	High
Hematologic/vascular causes of fetal anemia	
Cerebral, subdural hemorrhage	Low
Umbilical, renal, vena caval thrombosis	High
Autoimmune thrombocytopenia	Moderate
Alfa thalassemia	High

should be noted that Down syndrome might also be associated with late onset moderate hydrops, often involving pleural effusion and ascites, or subcutaneous edema. In these cases, the cause is thought to be local lymphatic obstruction.

3. *Skeletal dysplasias and syndromes*. The skeletal dysplasias most commonly associated with NIHF are the achondrogenesis, the hypophosphatasia, and the group of short-rib polydactyly syndromes. The type and number of nonchromosomal syndromes possibly associated with NIHF is enormous. It is useful to remember here the neuroarthrogryposes (FADS, Neu–Laxova syndrome, and multiple-pterygium syndrome), Fraser syndrome, oral-facial-digital syndrome, Beckwith–Wiedemann syndrome, and various storage diseases (mucopolysaccharidoses and mucolipidoses). Among the isolated conditions, very rarely, cystic adenomatoid malformation of the lung and pulmonary sequestration (see Chapter 6) can lead to hydrops due to vena caval compression. In contrast, laryngeal atresia is almost invariably associated with hydrops (see Chapter 10).
4. *Infections*. NIHF is a nonspecific sign of various infections vertically transmitted from mother to fetus, including both viral and nonviral infections. In the case of viral infections, the development of NIHF is probably due to different and synchronous mechanisms: inflammation, myocarditis with pump deficit, hemolytic anemia and/or hepatitis, and hepatitis-induced hypoproteinemia. The viruses most frequently associated with fetal hydrops are: parvovirus B19, coxsackievirus, herpes virus (varicella), cytomegalovirus (CMV), adenovirus, and influenza virus type B. Among the nonviral infections, the most common are syphilis, listeriosis, and toxoplasmosis.

   The final result of the various conditions mentioned above is a breakdown of equilibrium between intracapillary and extracapillary pressures, with consequent fluid ultrafiltration in the interstitial space.

Ultrasound diagnosis. NIHF can develop at any time during pregnancy, depending on its cause. If associated with syndromes and/or chromosomal aberrations it is usually of early onset, being apparent in the first trimester. If this is the case, it is often associated with CH and diffuse subcutaneous edema of the head and body, also known as "space suit." If NIHF is due to maternal infections or cardiac failure, its onset can also occur in the late second or third trimester. The fluid collections—in the abdomen, pleura, or pericardium—appear as sonolucent areas with different shapes characteristic of the different locations. Subcutaneous edema appears as a moderately echoic thickening of the soft tissue of the fetal face, trunk, and sometimes limbs. The diagnostic views depend on the site of the fluid collection. In the most severe cases, the *midsagittal view of the fetus*, at low magnificatio (Figure 4.6), can provide an overall idea of the regions involved, because it is possible to display simultaneously ascites, hydrothorax, pericardial effusion, and subcutaneous edema. The same plane also allows detection of the frequently associated CH. In moderate or initial hydrops, the fluid collection may be limited to one or two sites, and, therefore, its diagnosis needs dedicated planes. *Axial views of the head, neck, and thorax* may allow assessment of the extent and severity of the effusions (hydrothorax, pericardial effusion) and the subcutaneous edema (Figure 4.7). With regard to the ascites, it should be noted that, initially, the fluid collects in the pelvis only and, therefore, it should be sought in this region and not at the level of the liver. The axial view of the fetal abdomen at the level of the stomach and liver could be, therefore, not enough to detect initial ascites. In these cases, it is necessary to obtain a lower axial view at the level of the pelvis, or a longitudinal view in order to show both abdomen and pelvis.

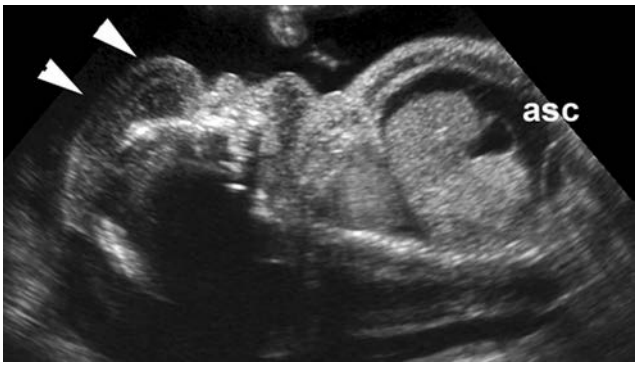


Figure 4.6 Nonimmune hydrops fetalis (NIHF). A midsagittal view of the fetal body at low magnification can provide an overall idea of the distribution and severity of hydrops. In this case, an extremely severe edema of the fetal head (arrowheads), ascites (asc), and polyhydramnios can be seen.

Differential diagnosis. NIHF should be differentiated from isolated effusions, which may have a completely different underlying cause (e.g., pericardial effusion in the case of congenital heart diseases).

Prognostic indicators. NIHF is per se a condition with poor prognosis. A positive prognostic indicator is recognition of a potentially treatable cause of the hydrops,

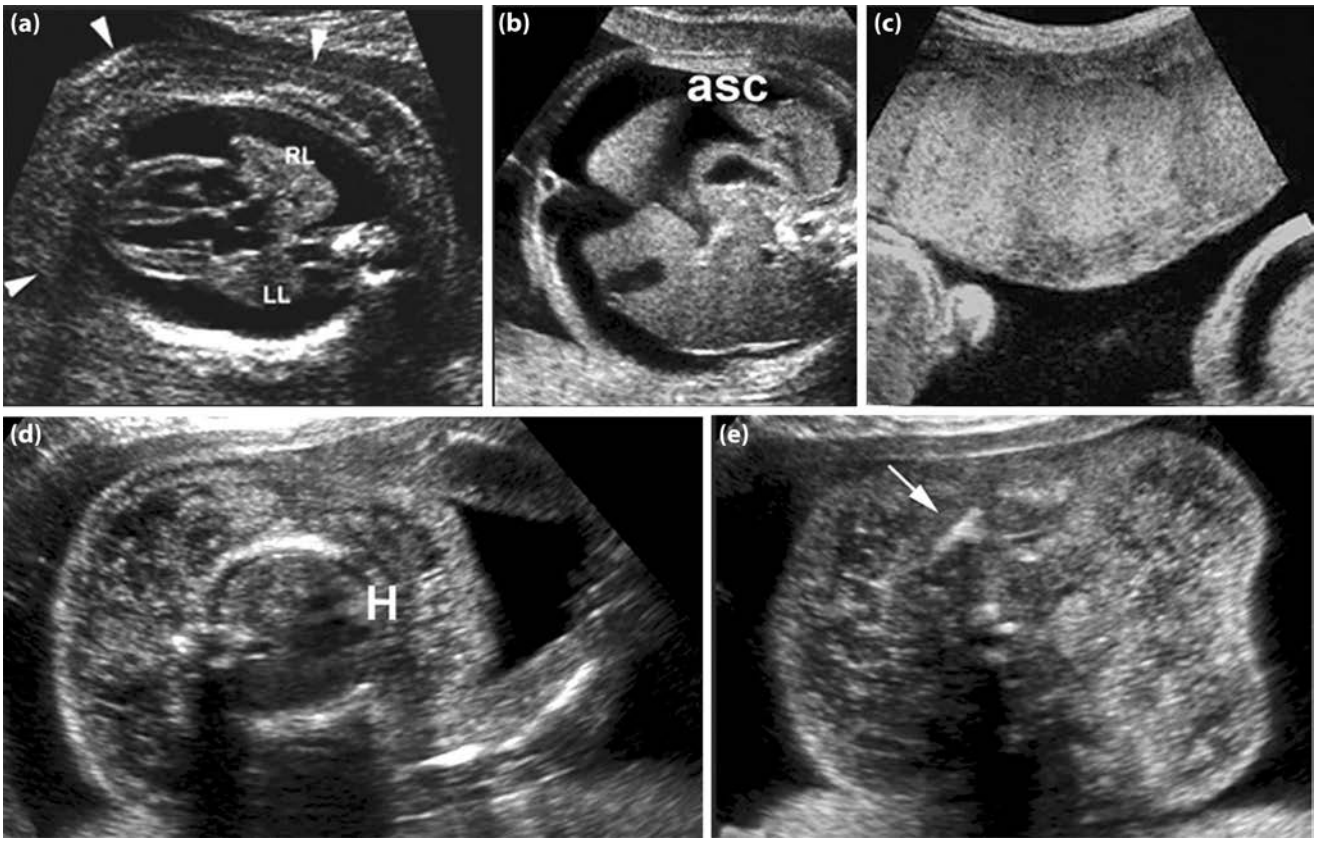


Figure 4.7 Nonimmune hydrops fetalis (NIHF). After the midsagittal view has provided an overall idea of the hydrops distribution, axial views may be used to assess in detail the various anatomic regions: (a) hydrothorax and subcutaneous edema (arrowheads) (LL: left lung; RL: right lung); (b) ascites (asc); (c) placental thickening and polyhydramnios in twin-to-twin transfusion syndrome (TTTS); (d) diffuse severe subcutaneous edema of the fetal trunk (H: heart); (e) diffuse severe subcutaneous edema of the cervical region, without hygroma (the arrow indicates the scapula).

such as parossistic tachycardia (usually responsive to antiarrhythmic drugs), or a parvovirus B19 infection (managed with intrauterine blood transfusion on the basis of measurements of the middle cerebral artery systolic peak velocity [8]).

Association with other malformations. See Etiology and pathogenesis.

Risk of chromosomal anomalies. This risk is high, especially for early onset NIHF (20%). The chromosomal anomalies most frequently associated with NIHF are Turner syndrome, autosomal trisomies (13, 18, and 21), and rarer aberrations, including partial deletions and unbalanced translocations.

Risk of nonchromosomal syndromes. This risk is extremely high (see Etiology and pathogenesis). It is not useful to list here the huge number of syndromes possibly associated with NIHF.

Obstetric management. Because few causes of NIHF can benefit from intrauterine treatment, a detailed assessment of all the possible causes previously listed should be performed; this entails a thorough anatomic scan and fetal echocardiography to confirm or rule out the most frequent determinant of NIHF, namely cardiac defects. Karyotyping is also mandatory, due to the high risk of aneuploidy. Maternal serological assessment should be carried out as well, in order to detect possible recent seroconversion for CMV, parvovirus B19, coxsackievirus, *Toxoplasma gondii*, and so on. It is necessary, as mentioned, to perform a careful examination of the fetal anatomy, in order to detect any structural or functional abnormality that could cause the hydrops, such as ductus venosus agenesis (with extrahepatic connection). In this case, the associated cardiac failure is due to severe volume overload or to high output [10].

Intrauterine therapy. The forms of NIHF potentially reversible following intrauterine treatment are only

those due to (1) tachyarrhythmias (supraventricular parossistic tachycardia and atrial flutter); and (2) parvovirus B19 infection with ascertained fetal anemia. In the former, transplacental or (in unresponsive cases) direct intraumbilical therapy with antiarrhythmic drugs can restore a sinus rhythm, with consequent clearance of the hydrops. In the case of severe fetal anemia, detected by Doppler velocimetry of the middle cerebral artery [11,12], due to parvovirus B19, intrauterine blood transfusions may help the fetus in the acute phase of the infection, with good neonatal outcome.

Prognosis, survival, and quality of life. The prognosis of NIHF is extremely poor. The intrauterine mortality rate is very high, and only the few treatable cases in which the aforementioned causes have been recognized can expect a better outcome.

References

1. Chevernak FA, Isaacson G, Blakemore KJ, et al. Fetal cystic hygroma. Cause and natural history. *N Engl J Med* 1983; 309: 822–5.
2. Bekker MN, Haak MC, Rekoert-Hollander M, et al. Increased nuchal translucency and distended jugular lymphatic sacs on first trimester ultrasound. *Ultrasound Obstet Gynecol* 2005; 25: 239–45.
3. Ville Y. Nuchal translucency in the first trimester of pregnancy: ten years on and still a pain in the neck? *Ultrasound Obstet Gynecol* 2001; 18: 5–8.
4. Kharrat R, Yamamoto M, Roume J, et al. Karyotype and outcome of fetuses diagnosed with cystic hygroma in the first trimester in relation to nuchal translucency thickness. *Prenat Diagn* 2006; 26: 369–72.
5. Snijders RJM, Noble P, Sebire N, et al. UK multicentre project on assessment of risk of trisomy 21 by maternal age and fetal nuchal translucency thickness at 10–14 weeks of gestation: Fetal Medicine Foundation First Trimester Screening Group. *Lancet* 1998; 351: 343–6.
6. Kagan KO, Avgidou K, Molina FS, et al. Relation between increased fetal nuchal translucency thickness and chromosomal defects. *Obstet Gynecol* 2006; 107: 6–10.
7. Bronshtein M, Bar-Hava I, Blumenfeld I, et al. The difference between septated and non-septated nuchal cystic hygroma in the early second trimester. *Obstet Gynecol* 1993; 81: 683–7.
8. Molina FS, Avgidou K, Kagan KO, et al. Cystic hygromas, nuchal edema, and nuchal translucency at 11–14 weeks of gestation. *Obstet Gynecol* 2006; 107 (3): 678–83.
9. Stevenson RE, Hall JC, Goodman RM, eds. *Human Malformations and Related Anomalies*. Oxford: Oxford University Press, 1993.
10. Volpe P, Marasini M, Caruso G, et al. Prenatal diagnosis of ductus venosus agenesis and its association with cytogenetic/congenital anomalies. *Prenat Diagn* 2002; 22 (11): 995–1000.
11. Hernandez-Andrade E, Scheier M, Dezerega V, et al. Fetal middle cerebral artery peak systolic velocity in the investigation of non-immune hydrops. *Ultrasound Obstet Gynecol* 2004; 23: 442–5.
12. Mari G, Adrignolo A, Abuhamad AZ, et al. Diagnosis of fetal anemia with Doppler ultrasound in the pregnancy complicated by maternal blood group immunization. *Ultrasound Obstet Gynecol* 1995; 5: 400–5.

Chapter 5
Congenital heart disease

Sequential anatomy and functional assessment of the heart: ultrasound approach, scanning planes, and diagnostic potential

The spectrum of congenital heart disease (CHD) that can be encountered in the fetus is wide, with a significant number of very complex defects. The description of these defects can benefit from a sequential segmental analysis, which consists of a step-by-step procedure that defines the central cardiovascular connections, beginning from the venous pole to the arterial one. Only in this way is it possible to understand and effectively describe the anatomy of complex fetal CHD. To perform a sequential segmental analysis of the fetal heart, the first step is the description of the visceroatrial situs. Then, the atrioventricular and ventriculoarterial connections are defined and described.

Situs. As a premise, it should be considered that, of all the anomalies occurring in the case of left or right isomerism (*situs ambiguous*), only those involving the venae cavae and, to a lesser extent, the pulmonary veins can be recognized in the fetus. Abnormalities in the spatial relationships between the bronchi and the pulmonary arteries and the number of pulmonary lobes cannot be detected in utero. With these limitations in mind, the *visceroatrial situs* can be described as follows [1,2].

Situs solitus. The liver and inferior vena cava are in the right hemiabdomen, and the spleen, stomach, and descending aorta are in the left. There is a trilobed lung with three bronchi on the right, and a bilobed lung with two bronchi on the left. The morphologic right atrium is on the right, and the morphologic left atrium on the left.

Situs inversus. This is a mirror image of situs solitus, and it is not usually associated with CHD, although there are some CHDs that can occur together with situs inversus.

Right atrial isomerism (asplenic syndrome). In this case, all left-sided structures are absent. The liver is centrally positioned due to the asplenia; the inferior vena cava and the aorta are usually close to one another and positioned on the same side of the spine. The lungs are both trilobed with three bronchi. Also, the atrial appendages are both morphologically right. Right atrial isomerism is frequently associated with complex CHD.

Left atrial isomerism (polysplenic syndrome). The liver is also centrally positioned in this case, but it is surrounded by several small splenic islets (polysplenia). The inferior vena cava is interrupted, and the systemic return is represented by an azygos continuation, adjacent to the descending aorta, which drains into the superior vena cava. Both lungs are bilobed with two bronchi. The atrial appendages are morphologically left. Major CHDs are associated in more than 50% of cases.

Atrioventricular connections

Atrioventricular concordance. This is the normal situation in which, with two atria and two ventricles, the right atrium connects to the morphologically right ventricle and the left atrium to the morphologically left ventricle. This relationship can occur within a situs solitus or inversus.

Atrioventricular discordance. In this abnormal situation, with two atria and two ventricles, the right atrium connects to the morphologically left ventricle and the left atrium connects to the morphologically right ventricle.

Double atrioventricular inlet. In this case, there are two atria connecting to the same ventricle. The second ventricular chamber is generally hypoplastic and sometimes connected to the dominant chamber through a ventricular septal defect (VSD). In this situation, the morphology

of the dominant ventricle should be assigned, whether of left ventricular, right ventricular, or (rarely) indeterminate morphology.

Single atrioventricular inlet. In this case, there is only one atrium, which connects to the dominant ventricle, while the second atrium connects only to the other atrium via the foramen ovale. The second atrioventricular connection is absent, due to atresia or imperforation of the ipsilateral atrioventricular valve. Also in this case, the second chamber is hypoplastic and may or may not communicate with the dominant ventricle. It should also be determined if the single ventricle is on the right, due to mitral atresia, or on the left, due to tricuspid atresia.

Atrioventricular valves. Once the type of atrioventricular connection has been determined, it is necessary to describe the possible anomalies of the atrioventricular valves: each valve can be imperforate, be atretic, be fused with the other (a *common atrioventricular valve*, as in the atrioventricular septal defect [AVSD]), or override a VSD.

Ventriculoarterial connections

Ventriculoarterial concordance. In this situation, with two ventricles and two great arteries, each artery is connected to its morphologically correct counterpart: the pulmonary artery arises from the morphologically right ventricle, and the aorta emerges from the morphologically left ventricle. These definitions of the ventriculoarterial junction apply regardless of the situs and the atrioventricular connection.

Ventriculoarterial discordance. In this situation, the pulmonary artery is connected to the morphologically left ventricle, and the aorta to the morphologically right ventricle.

Double outlet. In this case, more than 50% of each vessel is in connection with the same ventricle. It should then be determined if the double outlet occurs from a morphologically right (most common), morphologically left, or indeterminate ventricle.

Single outlet. In this case, there is only one arterial trunk connecting to the ventricles. This may occur due to pulmonary atresia, aortic atresia, or common arterial trunk (CAT).

In all cases, the ventricle(s) to which the single patent arterial vessel is connected should be defined.

Ventriculoarterial valves. In this case, the anomaly of the valve should be defined: atretic, imperforate, dysplastic, or overriding a VSD.

Additional anomalies. Any defects of the heart that have not been described in the sequential analysis can then be reported. These may include positional anomalies of the heart: levocardia, mesocardia, dextrocardia, or defects of the single segments (interatrial or interventricular defects, aortic coarctation, etc.).

TIMING o F ExAMINATIo N, ULTr Aso UNd Appro Ach, ANd sc ANNING pLANEs

Timing of examination. Assessment of the central cardiovascular connections is electively performed from 18 weeks of gestation onward [3]. However, major CHD can also be detected earlier (at 12–14 weeks) in high-risk cases.

Ultrasound approach and scanning planes (views). Complete assessment of fetal cardiac anatomy requires different views that are necessary to evaluate the central connections, from the veno-atrial junction to the ventriculoarterial one, and the ductal and aortic arches. Only by obtaining these views it is possible to confirm a normal sequential anatomy. The totality of these views constitutes fetal echocardiography, which also comprises a functional evaluation of the heart by color Doppler and, if necessary, pulsed-wave Doppler (PWD). However, in the midtrimester anomaly scan, only a partial assessment of the heart is generally required; this includes the four-chamber view and the outflow tract views [3]. In some countries, the three-vessel view also is part of the cardiac screening procedure. Since both the anomaly scan and fetal echocardiography are generally carried out in the second trimester, most of the sonographic images reported in this chapter have been taken at 19–22 weeks of gestation unless stated otherwise. The views can be summarized as follows:

- Axial views:
  - Four-chamber view (Figures 5.1 through 5.7)
  - Three-vessel view (Figures 5.8 through 5.11)
- Oblique views:
  - Long axis of the left ventricle (Figures 5.10 through 5.16)
  - Long axis of the right ventricle (Figures 5.12, 5.14 and 5.18)
  - Short axis of the right ventricle (Figures 5.17 and 5.18)
- Sagittal views:
  - Cavo-atrial junction (Figure 5.19)
  - Aortic arch (Figure 5.20)

c hd By sc ANNING pLANE

Fo Ur- c h AMBEr V IEW ANd rELA TEd M ALFor MATIo Ns

Atrial defects. Single atrium; atrial enlargement from severe atrioventricular insufficiency; type II atrial septal defects (ASD) (only the larger ones); congenital mega-atrium.

Septal defects. VSD; complete or partial AVSD.

Single atrioventricular inlet. Tricuspid atresia; mitral atresia; hypoplastic left heart syndrome (HLHS); single-inlet single ventricle; hypoplastic right heart.

Double atrioventricular inlet. Double-inlet single ventricle.

Ventricular disproportion. Aortic coarctation and interruption type A, prevalently; mitral stenosis; critical aortic stenosis; pulmonary atresia with intact ventricular septum (PAIVS) or critical stenosis.

Impaired contractility, unilateral. Critical aortic stenosis; PAIVS or critical stenosis.

Impaired contractility, bilateral. Cardiomyopathies.

Myocardial hypertrophy, bilateral. Cardiomyopathies.

This represents the key plane for the ultrasound (US) diagnosis of CHD: all anomalies of the atria, the atrioventricular valves, the septa (interatrial and interventricular—with the significant exception of the outlet and malalignment VSDs), and the ventricles are recognized in this view. At the same time, it allows a suspicion to be obtained of a significant number of the severe malformations affecting the ventriculoarterial junction.

Normal four-chamber view. This represents an axial view of the fetal thorax. It is defined as an *apical four-chamber view* (Figure 5.1a) if the cardiac apex is directed toward the transducer and the interventricular septum is aligned with the insonating beam, and as a *transverse four-chamber view* (Figure 5.1b) if the interventricular septum is at a 90° angle with the insonating beam. For a correct assessment of the four-chamber view, both approaches should be sought. In fact, due to the physics of US, only the anatomic structures at right angles (or at an acute angle) to the insonating beam will be correctly displayed on the screen. As a result, the atrioventricular plane and the posterior atrial walls are better assessed on the apical four-chamber view, whereas the septa, the myocardial walls, and the chordae tendinae are better displayed on the transverse four-chamber view. Assignment of the cardiac chambers is made following an anteroposterior axis connecting the spine posteriorly with the sternum anteriorly: in front of the spine is the descending thoracic aorta, and the cardiac chamber adjacent to the aorta is the left atrium, while the chamber located just below the sternum is the right ventricle. The remaining two chambers (the right atrium and left ventricle) are consequently assigned. A reliable marker that enables one to check the axiality of the four-chamber view is given by the ribs: in the fetus, these are horizontal, and therefore, if the four-chamber view is correctly aligned, one complete rib on each side of the thorax will appear. On the other hand, in case of ill alignment, several rib segments will be displayed on the screen. The following is a checklist of the anatomic structures to assess on the four-chamber view (Figure 5.2): (1) two-thirds of the heart in the left hemithorax; (2) the cardiac apex pointing to the left of the midline (levocardia) with a 45° (±20°) cardiac axis (this is calculated by tracing a line along the interventricular septum and measuring the angle between this line and the midsagittal line; it is traced between the sternum and the spine); (3) at least two of the four pulmonary veins draining into the left atrium; (4) two atria of similar size; (5) the flap of the foramen ovale opening into the left atrium; (6) two separate atrioventricular valves, with offset appearance (the septal leaflet of the tricuspid valve inserts just below the septal leaflet of the mitral valve) and regular excursion; (7) two ventricles of roughly similar size, with the right one slightly wider and rounder than the left, due to the presence of the moderator band in its apical part (the left ventricle forms the cardiac apex); (8) free right and left myocardial walls of similar thickness and with regular contractility; and (9) an intact interventricular septum. With regard to sonographic assessment of the interventricular septum, it should be noted that an artifact can occur if this structure is assessed on the apical four-chamber view: absorption of the US waves by the whole length of the septum creates a "dropout" artifact just below the atrioventricular plane, and this may be

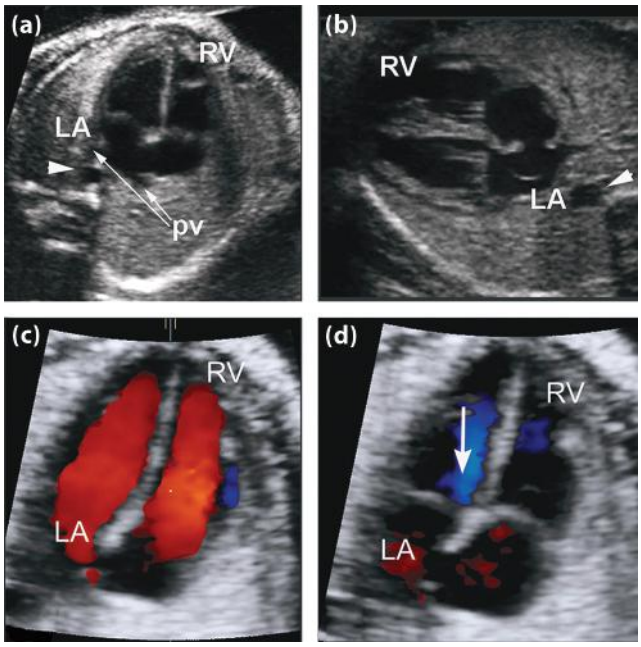


Figure 5.1 A four-chamber view. (a, b) Grayscale imaging; and (c, d) color Doppler imaging. (a) Apical four-chamber view. The atrioventricular plane and the drainage of two pulmonary veins are best imaged on this view. (b) Transverse four-chamber view. With the lateral approach, the best-insonated structures are the myocardial free walls, the interventricular septum, the interatrial septum with the foramen ovale flap, the chordae tendinae, and the papillary muscles of the atrioventricular valves. On this view, the diameters of the cardiac chambers and of the atrioventricular annuli can be measured, if necessary. For the assignment of the cardiac chambers, see this chapter's text. (c) During diastole, two blood columns with laminar blood flow are seen entering the two ventricles separately; and (d) during systole, the absence of atrioventricular valves' regurgitation and the acceleration of blood below the aortic outflow tract (arrow) can be seen. LA: left atrium; pv: pulmonary veins; RV: right ventricle; arrowhead: thoracic descending aorta.

mistaken for an inlet VSD. This is why the interventricular septum should be electively assessed on the transverse four-chamber view—at least for the part that is indeed visible on this plane. In fact, the interventricular septum wedges toward the aortic root, at the center of the heart, and this subaortic tract of the septum cannot be visualized on the four-chamber view, since it lies in another plane. To assess the subaortic tract of the septum, the long axis of the left ventricle should be visualized (as discussed in this chapter). Major anomalies recognizable on the four-chamber view are listed in Figure 5.3.

Atrial anomalies. A *common atrium* is associated in most instances with a complete AVSD (Figure 5.4a): there is generally no evidence of an interatrial septum (some remnants can sometimes be seen). In the case of type II ASD (of which only the largest can be suspected at US), there is a wide foramen ovale flap that float freely between the two atria, and often the septum primum is not identifiable as such, but the flap departs from the atrioventricular plane (Figure 5.4b). If a common atrium is suspected, the first step is to double-check the scanning view: if the plane is slightly posteriorized, the normal coronary sinus can be mistaken for an ostium primum ASD. The correct four-chamber view is just cranial to the view in which the coronary sinus is visible. If the impression of a common atrium persists, then the atrioventricular plane should be assessed, as an AVSD is the anomaly most commonly associated with a single atrium. If *atrial enlargement* is detected, this is almost always due to an insufficiency of the correspondent atrioventricular valve. It should be underlined that this finding of an increased atrial volume is much more commonly seen on the right side than on the left: the former finding can be associated with Ebstein's anomaly (Figure 5.4c) and with tricuspid dysplasia, which in turn is often associated with pulmonary atresia and critical stenosis. On the contrary, left atrial enlargement is due to mitral insufficienc , which is almost always associated with critical aortic stenosis. The final anomaly that can be detected while assessing the atria is the absence of the *septum primum*, usually in the context of a partial AVSD (Figure 5.4d).

Septal anomalies. A VSD can be recognized on the four-chamber view only if it involves the inlet perimembranous area or the muscular part of the septum (Figure 5.5a and b). The defects involving the outlet, subaortic portion can be detected only on the long axis of the left ventricle. A *muscular VSD* appears as an interruption of the septal continuity of variable dimensions, preferably shown on a transverse four-chamber view, because of the physics of US mentioned in the "Normal Four-Chamber View" section. An inlet *VSD*, on the contrary, is best appreciated on an apical four-chamber view, as a small absence of echoes just below the atrioventricular plane (Figure 5.5b). This type of defect is significantly associated with trisomy 21. An AVSD is defined as *complete* if there is only one atrioventricular valve deriving from the fusion of the two orifices (Figure 5.5c). The partial variant of AVSD is rarely diagnosed in the fetus, and it is characterized by a defect of the septum primum associated with loss of the normal offset appearance of the atrioventricular plane (Figure 5.4d).

Single atrioventricular inlet. A single inlet can be due to atresia and imperforation of the mitral or the tricuspid valve. The former is usually seen in the context of a HLHS (Figure 5.6a) (the isolated form of mitral

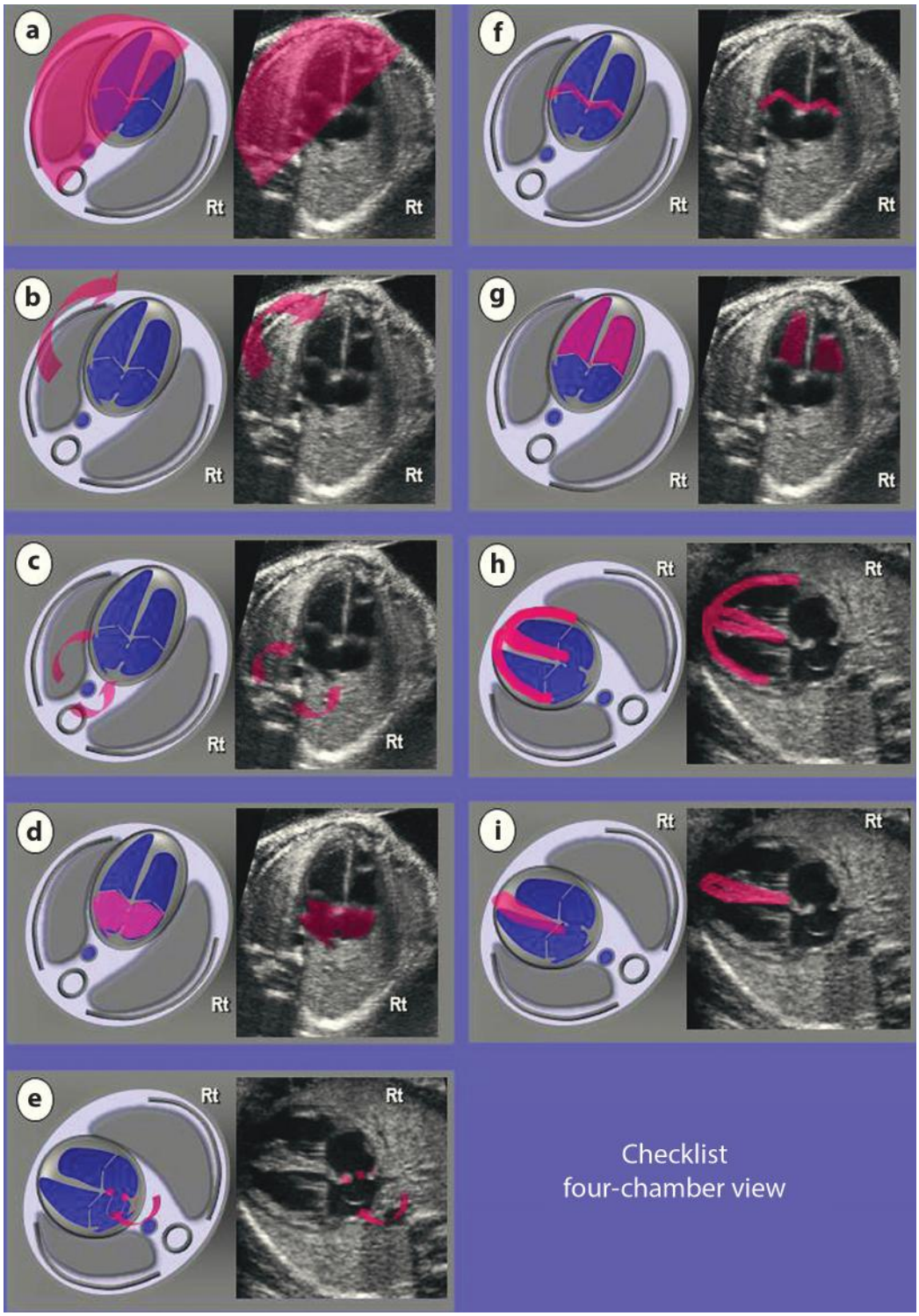


Figure 5.2 Checklist of the four-chamber view. (a) Two-thirds of the heart in left hemithorax. (b) Apex on the left, with 45° ± 20° cardiac axis (levocardia). (c) At least two pulmonary veins draining in the left atrium. (d) Two atria of similar size. (e) Foramen ovale flap opening into the left atrium, with evidence of the septum primum. (f) Presence of the crux of the heart, with offset aspect of the two atrioventricular valves, which show normal systo-diastolic excursion. (g) Two ventricles of similar diameter, with mild prevalence of the right one, which also shows a rounder appearance because of the presence of the moderator band. The left ventricle forms the cardiac apex. (h) Equal thickness of the free ventricular walls, with normal contractility. (i) Intact interventricular septum. In addition, the rhythm should be checked.

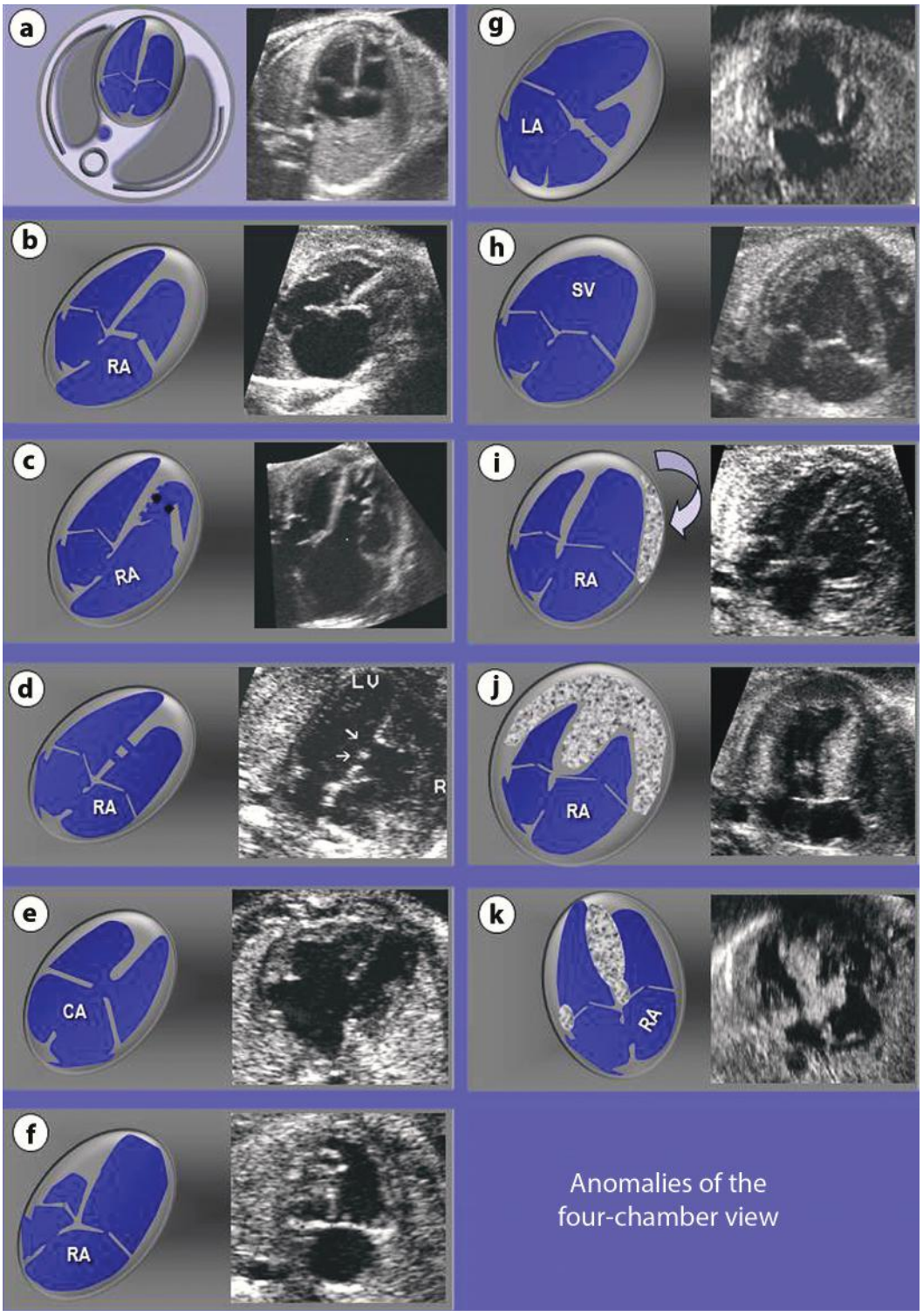


Figure 5.3 Anomalies recognizable on the four-chamber view. (a) Normal heart. (b) Right atriomegaly from tricuspid dysplasia and insufficiency. (c) Ebstein's anomaly, with apical displacement of the insertion of the tricuspid valve. (d) Ventricular septal defect. (e) Atrioventricular septal defect (with common atrioventricular valve). (f) Left ventricular hypoplasia and mitral atresia (hypoplastic left heart syndrome). (g) Right ventricular hypoplasia (plus ventricular septal defect) due to tricuspid atresia. (h) Double-inlet single ventricle. (i) Ventricular disproportion and moderate prevalence of the right ventricle (an indirect sign of aortic coarctation). (j) Biventricular hypertrophy (cardiomyopathy). (k) Tumors (rhabdomyomatosis). RA: right atrium; CA: common atrium; LA: left atrium; SV: single ventricle.

atresia is extremely rare). On the contrary, in the case of *tricuspid atresia* (Figure 5.6b), the ventricle is hypoplastic but the outflow (pulmonary artery) can be normal. However, if both the tricuspid and pulmonary valves are atretic, then the right ventricle is virtual and the defect, which is called *hypoplastic right heart*, is the mirror image of the HLHS. The final possibility is the *single-inlet single ventricle* (Figure 5.6c), a very rare anomaly in which a single atrium connects to a single dominant ventricle via a single patent atrioventricular valve.

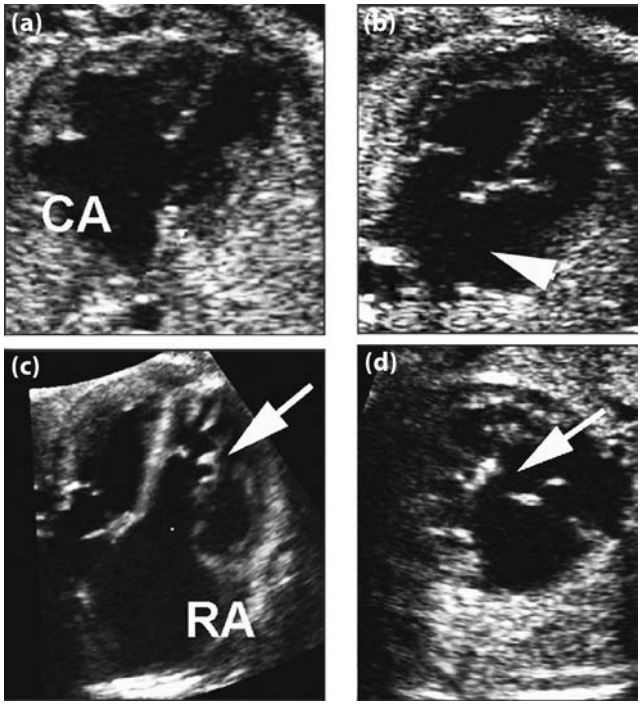


Figure 5.4 Atrial anomalies: four-chamber view. (a) Common atrium (CA) in complete atrioventricular septal defect. (b) Wide foramen ovale (arrowhead) in ASD type II (ostium secundum). (c) Severe right atriomegaly due to tricuspid insufficiency in Ebstein's anomaly. The arrow indicates the severe displacement of the septal and posterior tricuspid leaflets. RA: right atrium. (d) Absence of the septum primum (arrow), in partial atrioventricular septal defect.

Double-inlet single ventricle. In this rare anomaly (Figure 5.7a), there are two normal atria that connect to the same ventricle via two separate atrioventricular valves.

Ventricular disproportion. If the right ventricle is larger than the left ventricle, and the mitral annulus is significantly smaller than the tricuspid annulus, the defect can be a rare *mitral stenosis* (Figure 5.7b), which can be associated with aortic stenosis and coarctation in the Shone complex. However, the defect most commonly associated with ventricular disproportion (in which the right ventricle is larger than the left) is aortic coarctation (Figure 5.7c). Finally, it should be pointed out that the same appearance, with a right ventricle larger than the left, can also represent a transient benign finding that will regress spontaneously after birth.

Impaired contractility, unilateral. If unilateral, impaired contractility cannot be due to a primary myocardial disorder, but is the consequence of an increase in interventricular pressure and/or volume; if right-sided it is usually due to *pulmonary atresia* or *critical stenosis*; and if it is the left ventricular myocardial wall that is affected, then *critical aortic stenosis* is likely to be the underlying cause.

Impaired contractility, bilateral. If the whole myocardium is affected, then a primary disorder of cardiomyocytes (cardiomyopathy or myocarditis) is

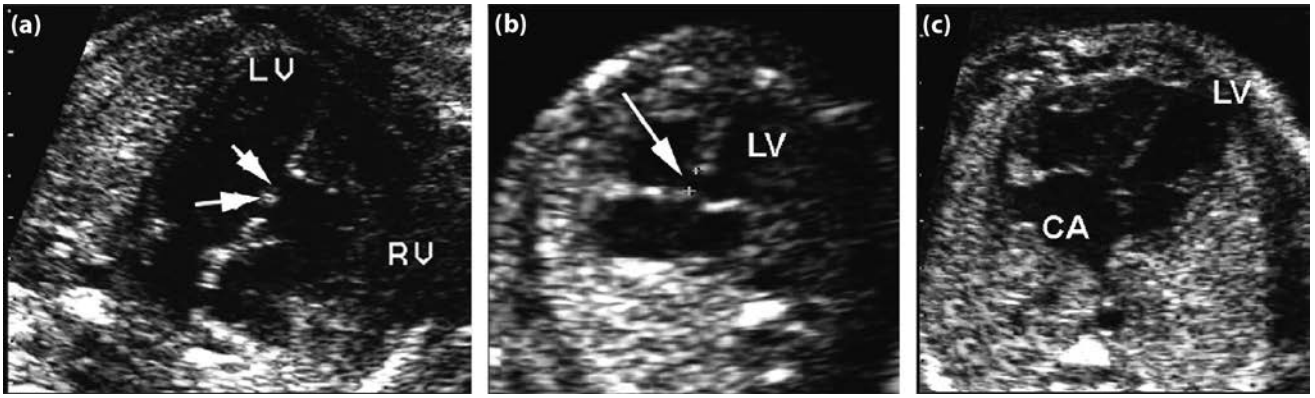


Figure 5.5 Septal defects: four-chamber view. (a) Double muscular ventricular septal defects (arrows). (b) Ventricular septal defect, inlet type (arrow). (c) Complete atrioventricular septal defect, with common atrioventricular valve and common atrium (CA). LV: left ventricle; RV: right ventricle.

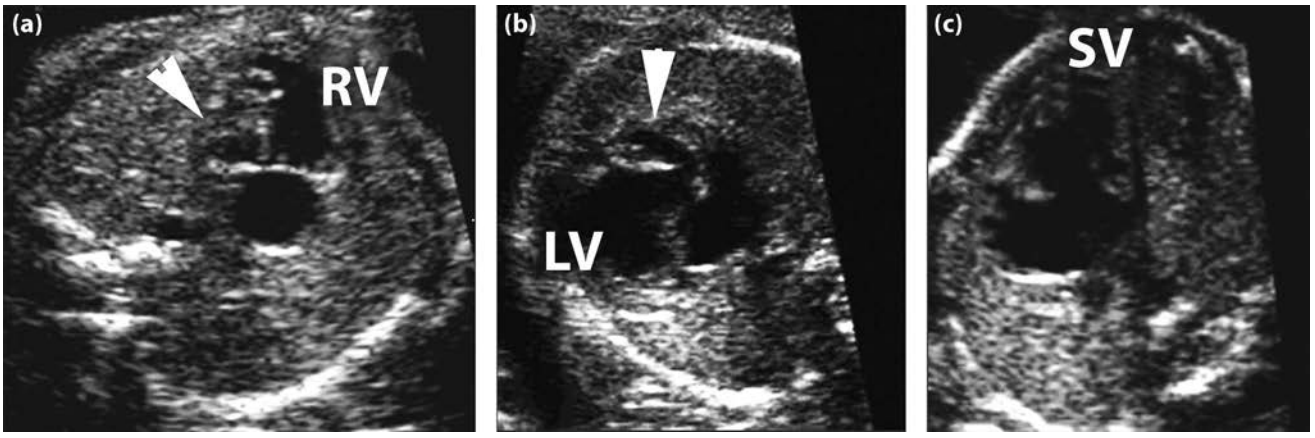


Figure 5.6 Single ventricular inlet: four-chamber view (a) Hypoplastic left heart: the mitral valve is atretic, and the left ventricle is extremely hypoplastic (arrowhead). (b) Tricuspid atresia: the tricuspid valve is atretic, and the right ventricle is hypoplastic (arrowhead). A small inlet ventricular septal defect connects the rudimentary right chamber with the left ventricle. (c) Single-inlet single ventricle: there is a single wide atrium connected through a single atrioventricular valve to a single ventricular chamber. LV: left ventricle; RV: right ventricle; SV: single ventricle.

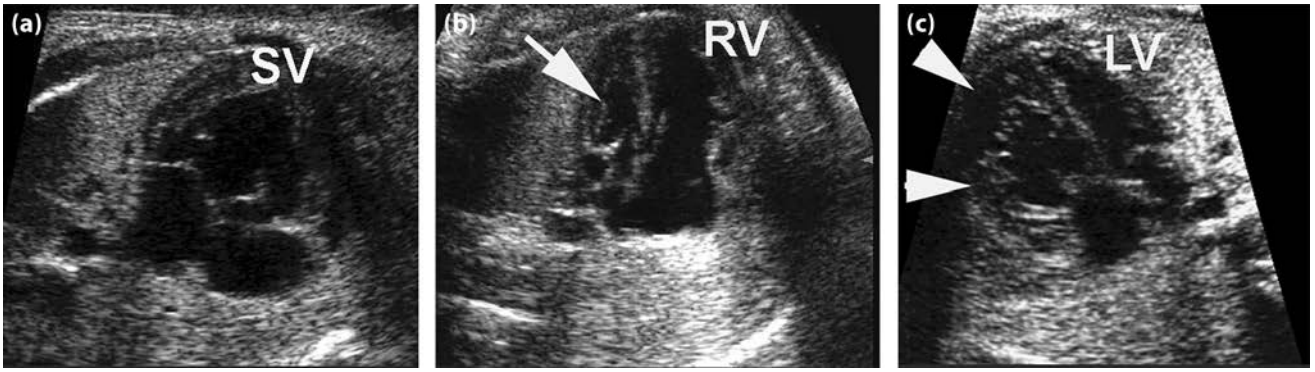


Figure 5.7 Ventricular anomalies: four-chamber view. (a) Double-inlet single ventricle: two atria connect with the same ventricle through two separate atrioventricular valves. (b) Moderate left ventricular hypoplasia (arrow) due to mitral stenosis (the annulus is reduced in size in comparison with the tricuspid one). Note also the moderately dilated coronary sinus, due to a concurrent persistence of the left superior vena cava draining into the coronary sinus (arrowhead). (c) Ventricular disproportion due to prevalence of the right chambers. This can be an indirect sign of aortic coarctation (arrowheads). LV: left ventricle; RV: right ventricle; SV: single ventricle.

likely to be present. In these cases, the myocardial walls are often thickened, the ejection fraction is reduced, and atrioventricular valvular regurgitation is often associated. In the case of myocarditis, the heart is usually dilated, the walls are less hypertrophied, and there should be serological evidence of maternal infection.

Myocardial hypertrophy, bilateral. This is usually due to primary or secondary *cardiomyopathy*.

Thr EE-VEss EL VIEW, Thr EE-VEss EL ANd Tr Ach EA VIEW, ANd r ELATEd MALFor MATIo Ns

Anomalies of the cavo-atrial junction. Persistence of the left superior vena cava; agenesis of the right superior vena cava.

Aortic and aortic arch anomalies. Aortic atresia; aortic coarctation; aortic arch interruption; right aortic arch (RAA); double aortic arch.

Pulmonary artery anomalies. Pulmonary atresia.

Thymus anomalies. Aplasia; hypoplasia.

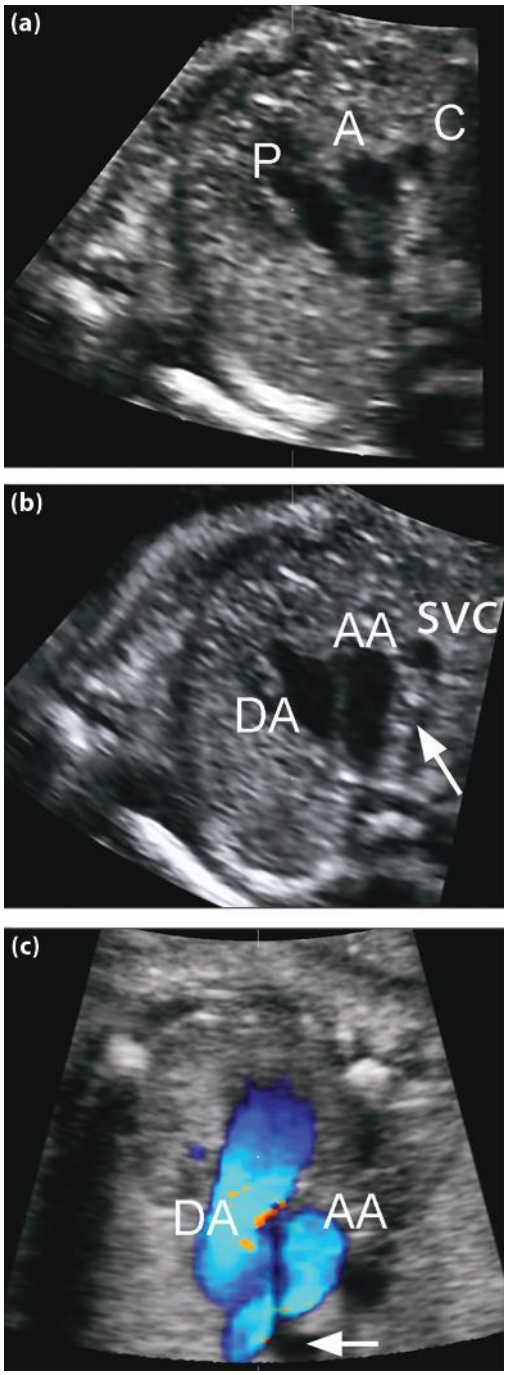


Figure 5.8 Three-vessel views. (a) Three-vessel view. This is obtained just cranial to the right outflow tract view: the pulmonary artery (P), the ascending aorta (A), and the superior vena cava (C) are seen in cross-section, between the thymus anteriorly and the spine and descending aorta posteriorly. (b) Slightly cephalad is the three-vessel and trachea view. On this plane, the ductal and aortic arches are visible, forming a "V" shape that is open anteriorly. The arches are both coursing to the left of the trachea (arrow). SVC: superior vena cava. (c) On color Doppler, the "V" shape is further highlighted and confirms that both the ductal arch (DA) and the aortic one (AA) are coursing to the left of the trachea.

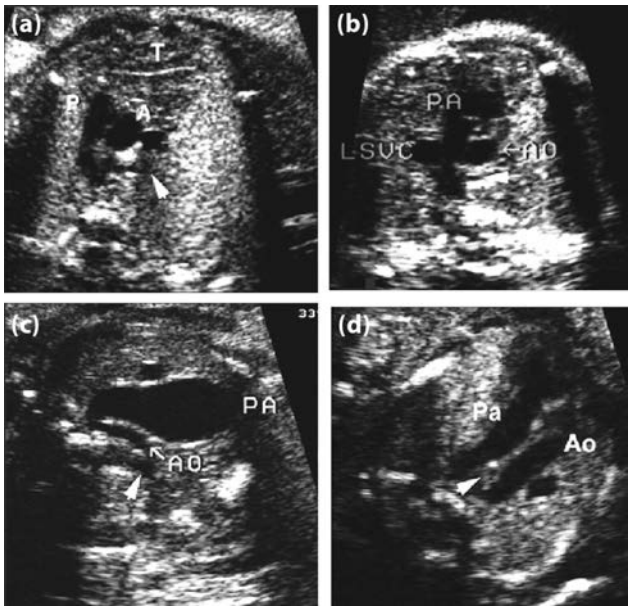


Figure 5.9 Anomalies of the three-vessel view. In all images, the arrowhead indicates the position of the trachea. (a) In the normal fetus, the thymus (T) is located in front of the three vessels, with the pulmonary artery (P) on the left, the aorta (A) in the middle, and the superior vena cava (SVC) on the right. (b) In the case of persistence of the left superior vena cava (LSVC), this vessel is found to the left of the pulmonary artery. In the case shown here, the concurrent agenesis of the right SVC led to the significant dilation of the former vessel. (c) In the case of severe aortic coarctation, the aorta, in the middle, appears extremely reduced in size in comparison with the adjacent ductal arch. Note the persistent left superior vena cava to the left of the ductal arch. (d) In the case of right aortic arch, which can be associated with the 22q11 microdeletion, the trachea is located between the ductal arch (on the left) and the aortic arch (on the right). AO: aortic arch; PA: ductal arch.

These represent two axial views of the upper mediastinum, which are obtained by sweeping the transducer from the plane of the four-chamber view cephalad. Following the two outflow tract views, first comes the three-vessel view, and just after that the three-vessel and trachea view (Figure 5.8). On these views, the presence and the relative size of the pulmonary artery, the ascending aorta, and the superior vena cava should be assessed in order to detect aortic coarctation (Figures 5.9c and 5.10c). In addition, these views are important because they allow one to detect aortic arch branching abnormalities. Also, it is important to underline that the abnormalities of the ventriculoarterial connections, such as transposition of the great arteries, cannot be directly diagnosed on the three-vessel view, as this plane is higher than the ventriculoarterial connection; however, in heart defects characterized by an absent crossover of the great arteries, often a single arterial vessel (and not two) is seen on this view (Figure 5.10a).

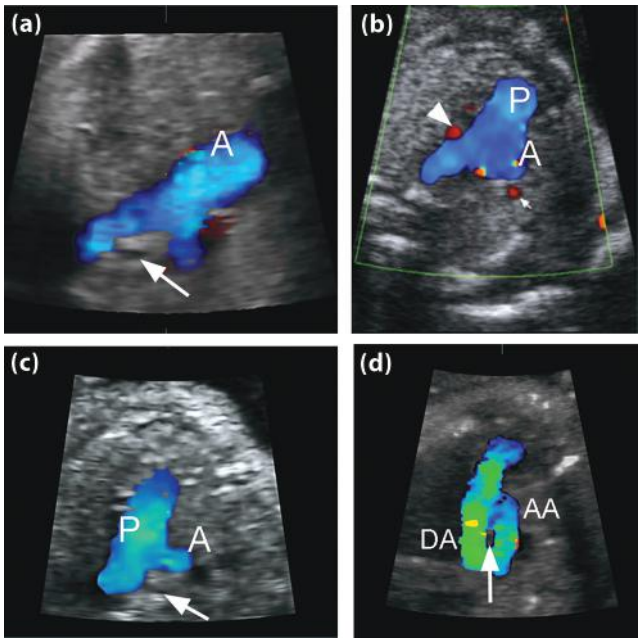


Figure 5.10 Anomalies of the three-vessel view. (a) In transposition of the great arteries, and in most CHDs characterized by an absent crossover of the great vessels, only one artery is visible on the three-vessel view. (b) In cases of persistent left superior vena cava, this vessel is seen to the left of the pulmonary trunk (arrowhead). However, care should be taken to reduce the PRF to have the color Doppler signal showing in the vessel, due to the low venous velocity. (c) In aortic coarctation, the size of the aortic arch is much smaller than that of the ductal arch. (d) In the right aortic arch, the trachea is trapped between the left-sided ductal arch and the right-sided aortic arch. A: aortic arch; arrow: trachea; DA: ductal arch; P: pulmonary artery.

Normal three-vessel and three-vessel trachea views (Figure 5.8a). As mentioned in this chapter, this is an axial view of the upper mediastinum; in particular, the three vessels are (from right to left) the superior vena cava, the aorta, and the pulmonary artery (Figure 5.8a). If the transducer is slightly tilted, the junction of the ductus arteriosus with the isthmic tract of the aortic arch becomes visible (Figure 5.8b and c). The thymus is also visible just behind the sternum, whereas the two arches are in the prevertebral area, on the left of the trachea (Figure 5.8c). As a result, the abnormalities of the great vessels, the aortic arch, and the thymus (aplasia and hypoplasia, typical of the 22q11 microdeletion) can be recognized on this view.

Anomalies of the cavo-atrial junction (Figures 5.9b and 5.10b). *Persistence of the left superior vena cava* may or may not be associated with agenesis of the right superior vena cava. If both vessels are present at the same time, then a fourth small vessel can be seen on the left of the pulmonary artery (Figures 5.9c and 5.10b); if the right superior vena cava is absent, then the left superior vena cava will be larger, as it will be the only venous return for the cerebral circulation; at the same time, the rightmost vessel (right superior vena cava) will be absent (Figure 5.9b).

Aortic arch anomalies (Figures 5.9c,d and 5.10c,d). In *coarctation of the aorta* (Figure 5.9c and 5.10c), the vessel in the middle, corresponding to the aorta, will be severely or moderately hypoplastic, according to the degree of coarctation. The differential diagnosis with *interruption*

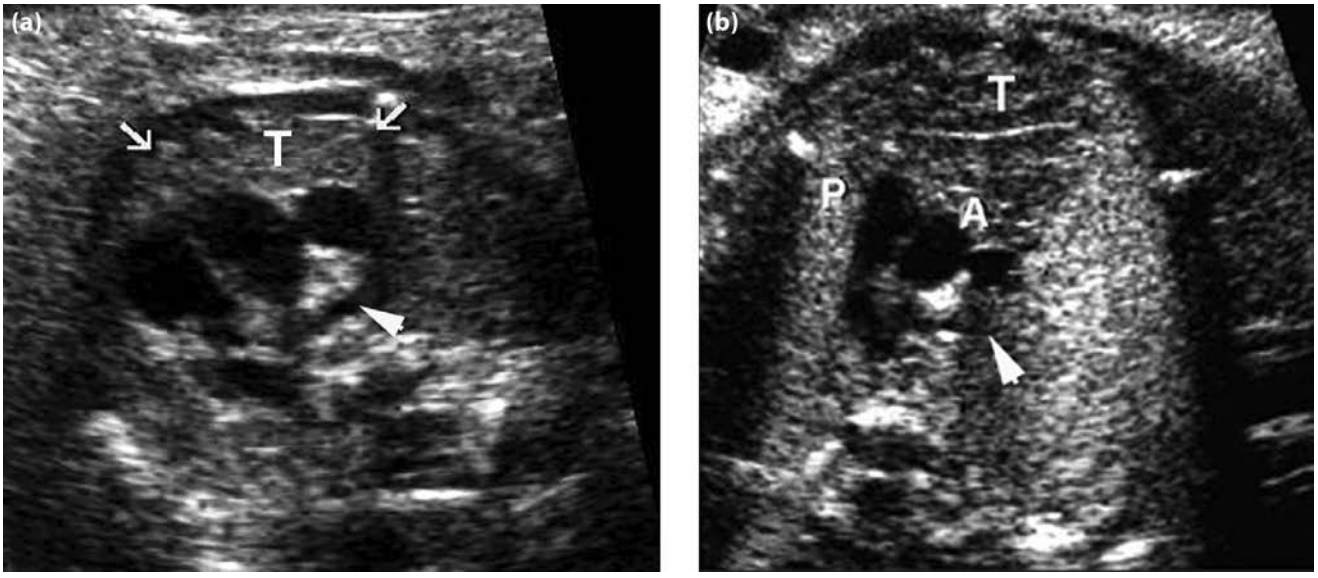


Figure 5.11 Anomalies of the three-vessel view. (a) Thymus hypoplasia, in a fetus at 34 weeks of gestation with tetralogy of Fallot and the 22q11 microdeletion. (b) Normal thymus at 33 weeks of gestation. Note the different dimensions. A: aortic arch; P: pulmonary artery; T: thymus.

of the aortic arch (IAA) can be made only if the three-vessel and trachea view (with the confluence of the two arches) is obtained. If the aortic arch is interrupted, the course of the ascending aorta is more vertical and the confluence of the ductal and the aortic arches cannot be demonstrated. In the case of a RAA, this will be on the right of the trachea, and the trachea will be between the pulmonary and aortic arches (Figures 5.9d and 5.10d).

Pulmonary artery anomalies. In *pulmonary atresia*, the leftmost vessel, corresponding to the pulmonary artery, shows a reduction in size.

Thymus anomalies (Figure 5.11). In the case of thymus aplasia, the three vessels are located just behind the sternum, and the thymus cannot be visualized.

Lo NG Ax Is o F Th E LEFT VENTr Ic LE ANd rELA TEd M ALFor MATIo Ns

Septal anomalies. Outlet VSD; *malalignment* VSD.

Anomalies of the aorta. Critical aortic stenosis; aortic atresia; CAT.

Absent crossover anomalies. Transposition of the great arteries; double-outlet right ventricle (DORV).

This is the second most important view after the four-chamber view.

Long axis of the left ventricle, normal (Figure 5.12a and c). According to various guidelines and fetal echocardiography manuals, this view can be obtained in two ways, the so-called *sweep* and *rotational* techniques [3]. According to the former technique, the transducer is swept slightly from the four-chamber view to insonate the very initial tract of the ascending aorta. In the past, this view was referred to as the "five-chamber view," the fifth chamber being the aortic root in the middle of the image. The second technique—*rotational*—is the one we recommend to use in any case and to get more acquainted with. The reason why we believe this technique is better than the other is because it aligns the transducer with the direction of the ascending aorta, allowing most of this vessel to be visible on the screen. This view is obtained by rotating the transducer slightly toward the right fetal shoulder, in order to visualize the ascending aorta: this vessel arises from the left ventricle and points toward the right shoulder prior to curving into the aortic arch (Figure 5.12a and c).

Checklist. This includes the following: (1) the presence of a vessel that connects with the morphologically left ventricle positioned on the left and that can be defined as the aorta (branching at a wide angle far from the semilunar valve); (2) septoaortic continuity; (3) the presence of a semilunar valve showing normal systo-diastolic excursion (the leaflets disappear completely during systole, being flattened on the aortic walls); (4) the presence of crossover: the direction of the aorta is at roughly 70° to the direction of the pulmonary trunk displayed on the long axis of the right

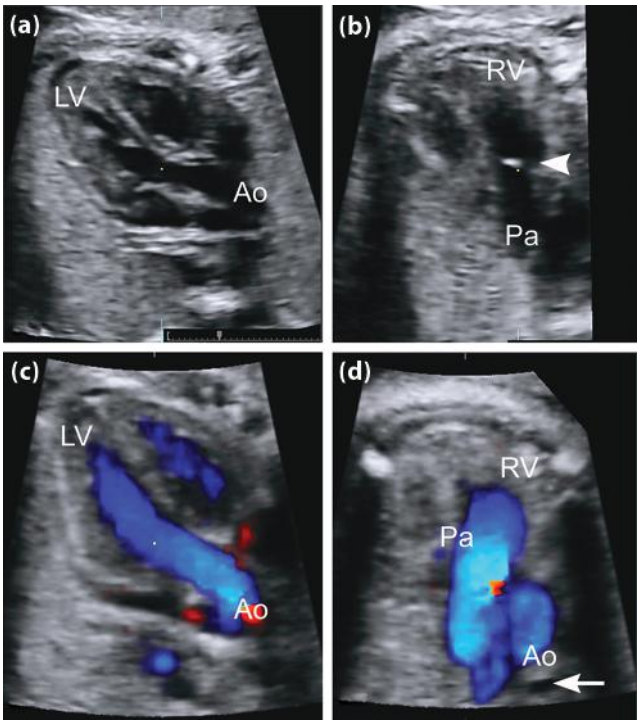


Figure 5.12 Left and right normal outflows. (a) Long axis of the left ventricle (rotational technique)—systole: the aorta emerges from the left ventricle, the mitral valve is closed, while the aortic semilunar valve is not visible since the cusps are flattened along the aortic walls. (b) Long axis of the right ventricle—diastole: the infundibular portion of the right ventricle is visible (RV), connected with the main pulmonary artery (Pa) through a (closed) semilunar valve (arrowhead). (c) Long axis of the left ventricle (rotational technique)—systole: the smoothly laminar blood flow from the left ventricle to the ascending aorta is seen. (d) Long axis of the right ventricle—systole: the smoothly laminar blood flow from the infundibular portion of the RV to the main pulmonary trunk (Pa) and the ductus arteriosus is visible. As is evident, this view is almost at the level of the three-vessel view (see Figure 5.8).

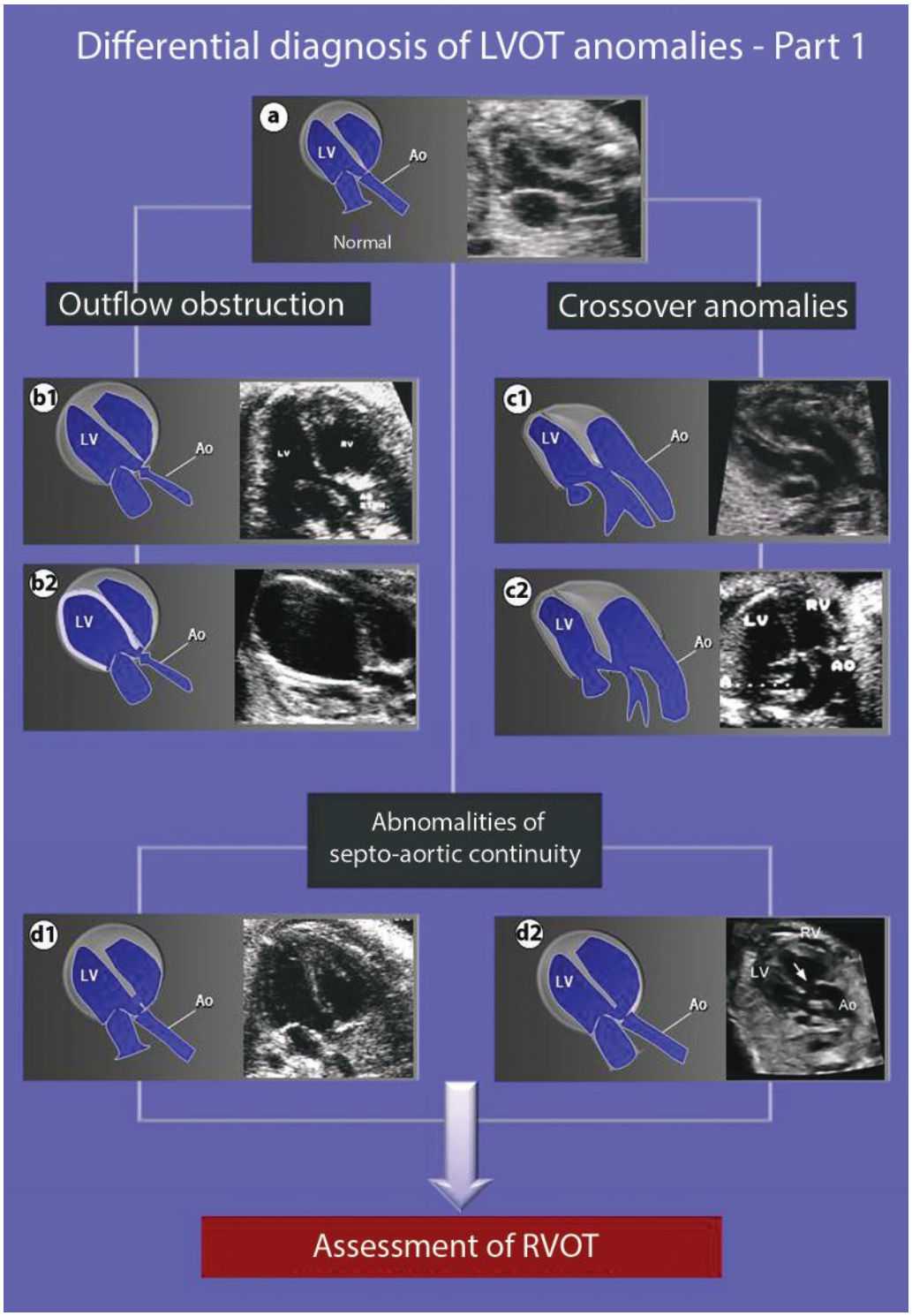


Figure 5.13 Diagnostic algorithm for the differential diagnosis of CHD detectable on the left outflow tract view. (a) Normal. (b) Anomalies of outflow: critical aortic stenosis, (b1) without gross anomalies of the left ventricle or (b2) with severe endocardial fibroelastosis. (c) Anomalies (lack) of crossover: (c1) transposition of the great arteries, if each vessel is connected with the contralateral ventricle (left ventricle-pulmonary artery and right ventricle -aorta; (c2) double-outlet right ventricle, if both great vessels are connected with the right (anterior) ventricle. (d) Anomalies of septoaortic continuity: (d1) simple outlet ventricular septal defect (VSD) if the septum is normally aligned with the anterior aortic wall; and (d2) malalignment VSD, if the infundibular septum is anteriorly displaced and the aorta overrides the defect. In this case, to reach the final diagnosis it is necessary to assess the right outflow (see Figure 5.14). Ao: aorta; LV: left ventricle; RV: right ventricle.

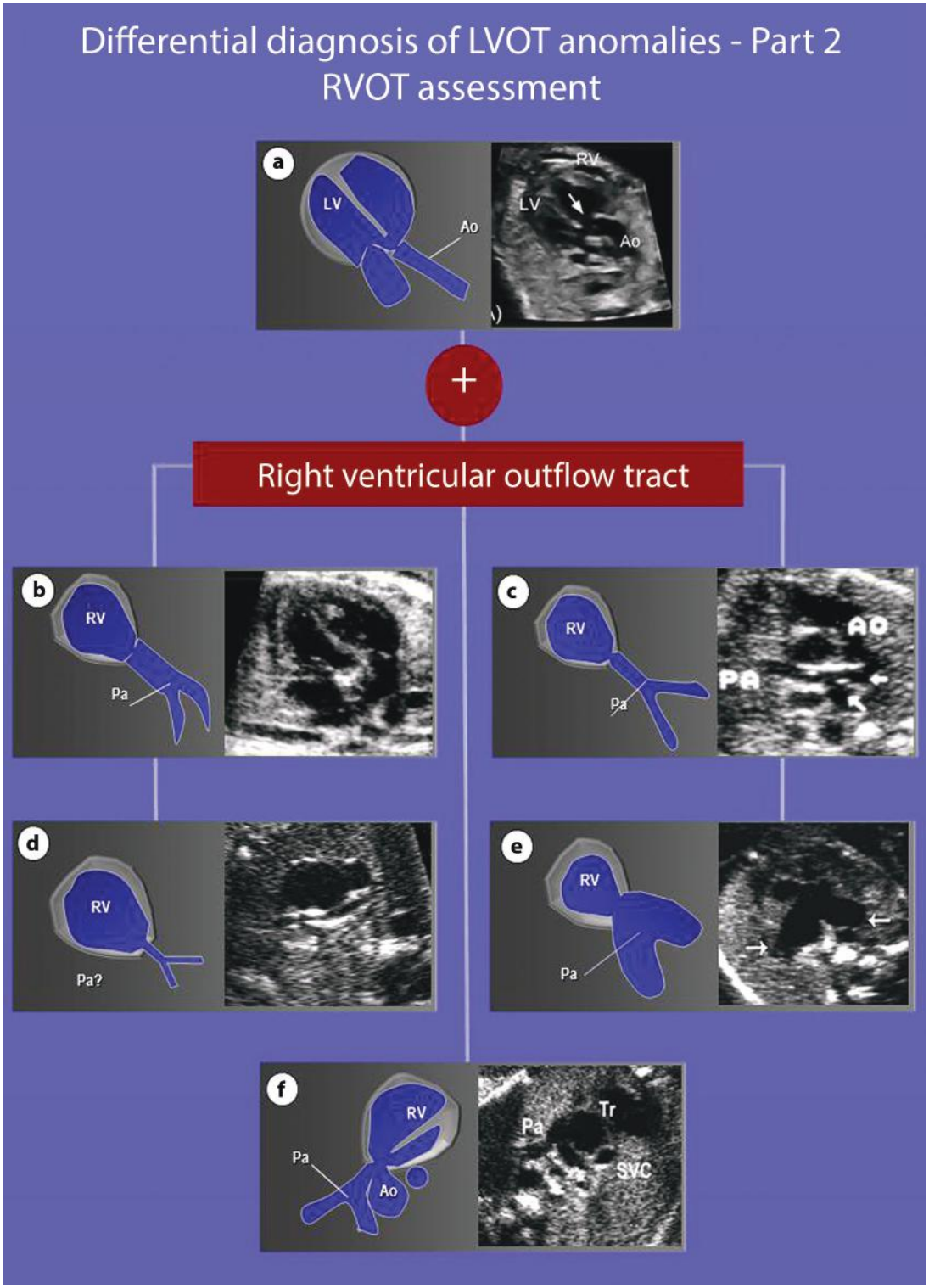


Figure 5.14 Diagnostic algorithm for the differential diagnosis of CHD featuring a malalignment ventricular septal defect (VSD), detected on the left outflow tract view (a) (see also Figure 5.13). (b) If the right outflow is normal, the diagnosis remains malalignment VSD. (c) If the right outflow is reduced in size, the diagnosis is classic tetralogy of Fallot. (d) If the right outflow is absent (atretic), the diagnosis is pulmonary atresia plus VSD. (e) If the pulmonary trunk and branches are severely dilated, the diagnosis is tetralogy of Fallot with a functionally absent pulmonary valve. (f) Finally, if the pulmonary artery does not arise from the right ventricle but rather from the aorta, the diagnosis is common arterial trunk. Ao: aorta; LV: left ventricle; RV: right ventricle; Pa: pulmonary artery; SVC: superior vena cava; Tr: common arterial trunk.

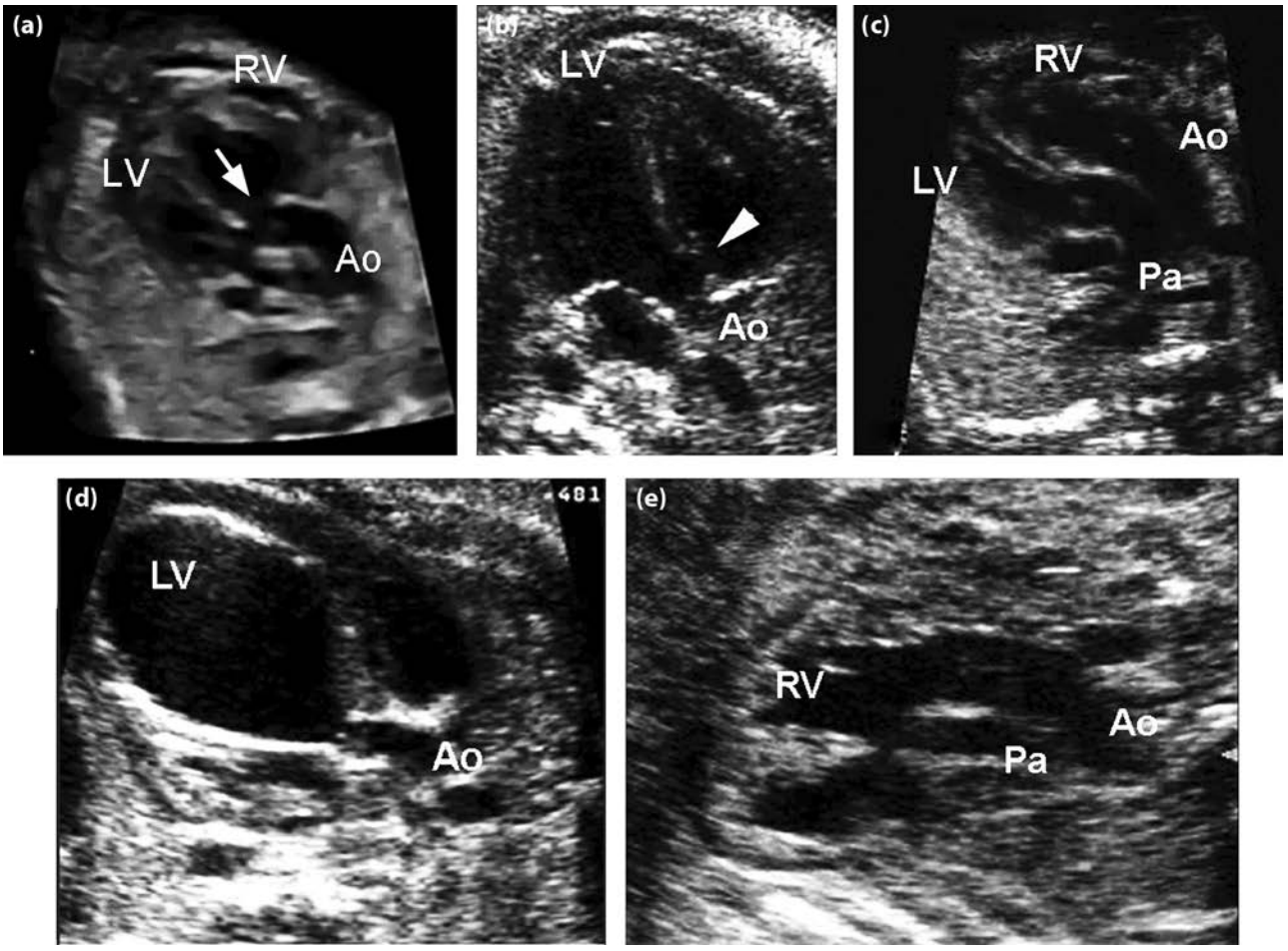


Figure 5.15 Left outflow tract anomalies. (a) Malalignment ventricular septal defect (VSD): the aorta overrides a wide septal defect (arrow). (b) Outlet VSD, consisting of a simple defect of the outflow perimembranous part of the septum. Note the normal alignment of the interventricular septum with the anterior aortic wall (arrowhead). (c) Transposition of the great arteries: two parallel vessels are seen arising, each from one ventricle. (d) Critical aortic stenosis: endocardial fibroelastosis and a hypoplastic aortic annulus are visible. (e) Double-outlet right ventricle: two vessels, both arising from the right (anterior) ventricle, are visible. In this condition, the pulmonary outflow is often stenotic, as in this case. Ao: aorta; LV: left ventricle; Pa: pulmonary artery; RV: right ventricle.

ventricle; and (5) the size of the vessel is similar to that of (here, slightly smaller than) the other vessel visualized on the long axis of the right ventricle. A diagnostic algorithm is shown in Figures 5.13 and 5.14. Abnormalities detectable on the left outflow tract view are shown in Figures 5.15 and 5.16.

Septal anomalies (Figures 5.15a,b). In a *malalignment* VSD, the infundibular septum is anteriorly displaced, and this leads to the aortic *overriding*. This feature is shared by most conotruncal anomalies, and, if detected, should prompt a thorough assessment of the right outflow for the differential diagnosis (Figures 5.13 and 5.14). On the contrary, in the case of a simple outlet VSD, there is only a discontinuity of the septum, but this is normally aligned with the anterior aortic wall.

Crossover anomalies (Figures 5.15c,e and 5.16c,d). If two parallel vessels are displayed on the long axis of the left ventricle, then an anomaly of crossover is present. In this case, if each vessel arises from one ventricle, then the diagnosis will be *transposition of the great arteries* (Figures 5.15c and 5.16c); if, on the contrary, both vessels are connected to the same ventricle, which is almost always the right one, then a DORV is diagnosed (Figure 5.15e). A *double-outlet left ventricle* is an extremely rare condition.

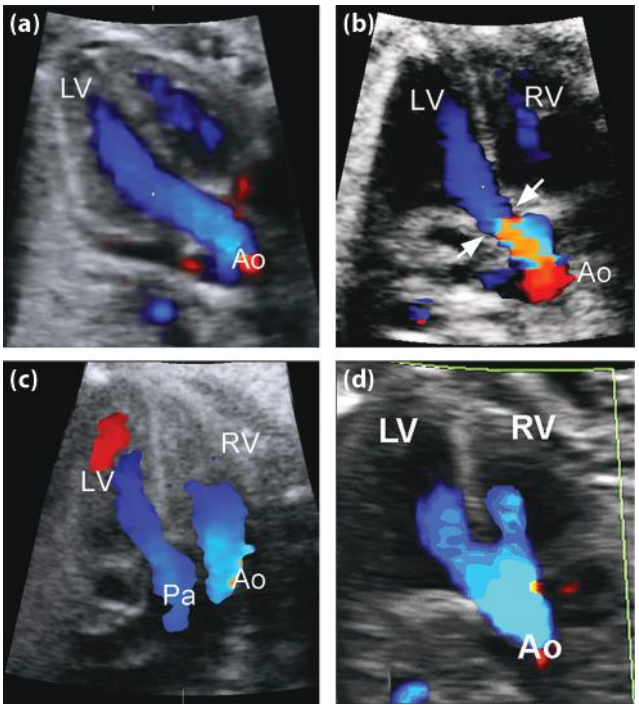


Figure 5.16 Left outflow tract anomalies. (a) Normal outflow, with a single connection between the left ventricle and the aorta, with normal septoaortic continuity and laminar blood flow. (b) Semilunar valve stenosis (moderate); note the sudden acceleration of blood at the annular level (arrows), with color showing turbulent flow, mosaic pattern, and aliasing. (c) Absence of crossover (transposition of the great arteries); note the two parallel arteries, typical of absent crossover. (d) Abnormal septoaortic continuity (malaligment ventricular septal defect); note the overriding of the aorta, which drains blood from both ventricles. Ao: ascending aorta; LV: left ventricle; Pa: main pulmonary artery; RV: right ventricle.

Anomalies of the aorta (Figures 5.15d and 5.16b). In most cases of *critical aortic stenosis*, the four-chamber view is significantly abnormal, and this leads to the diagnosis. On the long axis of the left ventricle, the aortic annulus is hypoplastic, and the dysplastic thickened valve remains in the lumen of the vessel throughout the cardiac cycle. The ascending aorta can be enlarged or hypoplastic. On the other hand, if the stenosis is moderate or moderately severe, the four-chamber view may be virtually normal. In this case, the anomaly is detected on the left outflow tract view, where the thickened semilunar valve is seen and the stenosis diagnosed on color Doppler (Figure 5.16b). In the case of a *CAT*, the main pulmonary artery or the two branches arise directly from the aortic vessel, which is overriding a malalignment VSD (Figure 5.14f). The truncal valve, which derives from the abnormal fusion of the two semilunar valves, is often dysplastic and insufficient

Lo NG ANd shor T Ax Es o F Th E rIG hT VENTr Ic LE ANd rELA TEd M ALFor MATIo Ns

Pulmonary trunk anomalies. Pulmonary atresia and stenosis; absent pulmonary valve syndrome (APVS).

Two different views may be used to assess the right outflow tract: the short and long axes of the right ventricle. The former is ideally more complete, since all connections of the right heart are displayed; however, it should be noted that this plane is easily achieved only if the fetus is lying with a posterior spine. On the contrary, the long axis, which depicts just the infundibular tract and the main pulmonary artery with the semilunar valve, can be obtained with virtually all fetal positions.

Long axis of the right ventricle, normal (Figure 5.12b and d). This view is obtained from the long axis of the left ventricle, by curving the transducer toward the fetal head.

Checklist. This includes the following: (1) the presence of a vessel that connects to the morphologically right ventricle positioned on the right and that can be defined as the pulmonary artery (acute-angle bifurcation); (2) the presence of a semilunar valve showing normal systo-diastolic excursion (the leaflets disappear completely during systole, flattening on the pulmonary artery walls); (3) the presence of crossover: the direction of the pulmonary artery is roughly 70° to the direction of the aorta displayed on the adjacent long axis of the left ventricle; and (4) the size of the vessel is similar to that of (here, slightly larger than) the aorta visualized on the long axis of the left ventricle.

Short axis of the right ventricle, normal (Figure 5.17). To obtain this view, from the four-chamber view, the transducer should perform a rotation mirroring that needed for the long axis of the left ventricle (i.e., toward the left fetal shoulder).

Checklist (same as for the long axis of the right ventricle). This includes the following: (1) the presence of a vessel that connects to the morphologically right

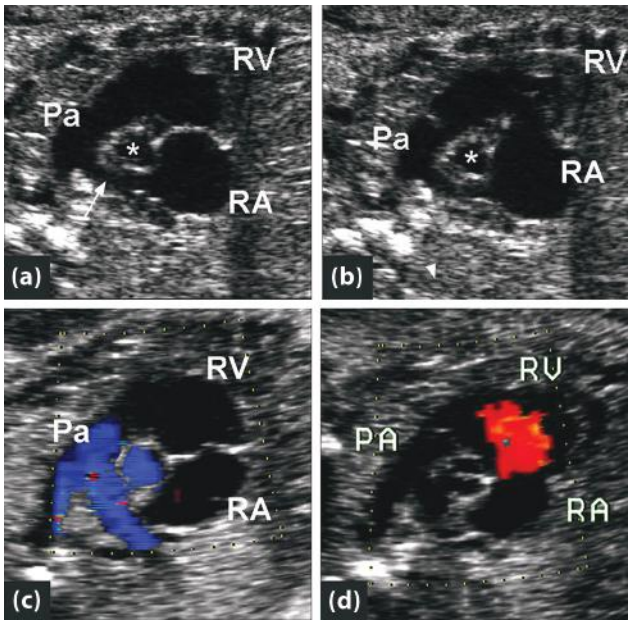


Figure 5.17 Short axis of the right ventricle, normal. (a) During systole, the tricuspid valve is closed, and the pulmonary valve open. The aorta is seen in cross-section at the center of the image (asterisk). The right branch of the pulmonary trunk is also visible (arrow). (b) During diastole, the tricuspid valve opens, while the semilunar valve (arrowhead) closes. (c) At color Doppler, during systole, laminar blood flow shows visible movement from the right ventricle into the main pulmonary artery (in blue). No regurgitation is visible at the level of the closed tricuspid valve in normal conditions. (d) During diastole, laminar blood flow enters the ventricle from the right atrium (in red), and no regurgitation should be visible across the closed semilunar valve. Pa: main pulmonary artery; RA: right atrium; RV: right ventricle.

ventricle positioned on the right and that can be defined as the pulmonary artery (acute-angle bifurcation); (2) the presence of a semilunar valve showing normal systo-diastolic excursion (the leaflets disappear completely during systole, flattening on the pulmonary artery walls); (3) the presence of crossover: the direction of the pulmonary artery is at roughly 70° to the direction of the aorta, which in this case is visible in the middle of the image, in cross section; and (4) the size of the vessel is similar to that of (here, slightly larger than) the aorta.

Pulmonary trunk anomalies. In the case of moderate *pulmonary stenosis* (Figure 5.18a), the semilunar valve is dysplastic and thickened, with incomplete opening during systole. Poststenotic ectasia of the pulmonary artery can be associated. On the contrary, in the case of *pulmonary atresia* (Figure 5.18b), the pulmonary trunk and the branches are often hypoplastic, although the vessel can appear to be of normal size if a formerly stenotic valve has become atretic only late in gestation, as may sometimes happen. In the case of *pulmonary atresia with VSD* (PAVSD), the main pulmonary artery may also be absent, with the two branches departing directly from the ductus arteriosus. Finally, in the case of *APVS with or without tetralogy of Fallot* (TOF) (Figure 5.18c), the pulmonary trunk and branches are severely dilated due to the conspicuous steno-insufficiency of the functionally absent pulmonary valve.

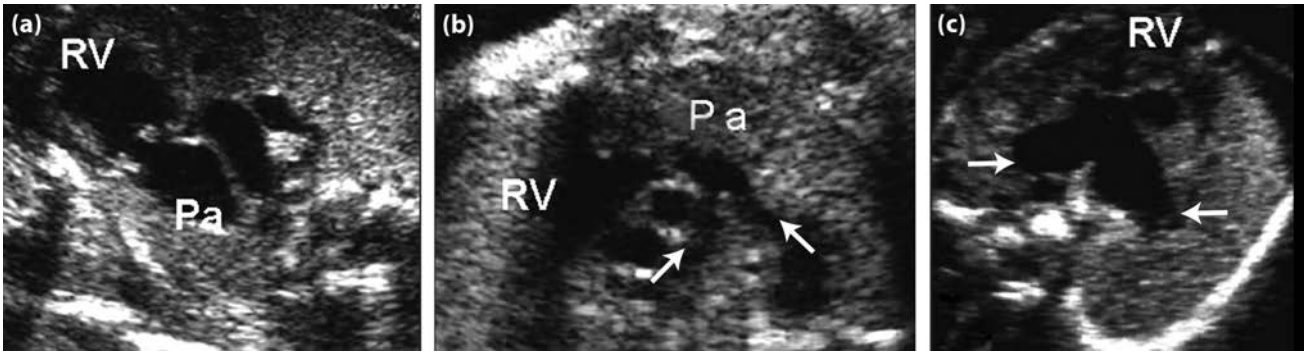


Figure 5.18 Right outflow tract anomalies. (a) Moderate pulmonary stenosis: note the thickened pulmonary valve cusps and the poststenotic ectasia. (b) Pulmonary atresia with intact ventricular septum: the pulmonary trunk and branches (arrows) are significantly hypoplastic, due to the valve atresia. Note also the thickened pulmonary valve. (c) Tetralogy of Fallot with absent pulmonary valve: the image shows severe dilation of the pulmonary trunk and branches, consequent to the severe insufficiency caused by the functional absence of the rudimentary pulmonary valve. RV: right ventricle.

CAVO-ATRIAL JUNCTION AND RELATED MALFORMATIONS

This is a longitudinal view of the fetal thorax, displaying the systemic venous returns. Therefore, the only anomaly that may be detected on this view is the rare absence of the inferior vena cava, replaced by an azygos continuation, which is typically associated with left atrial isomerism.

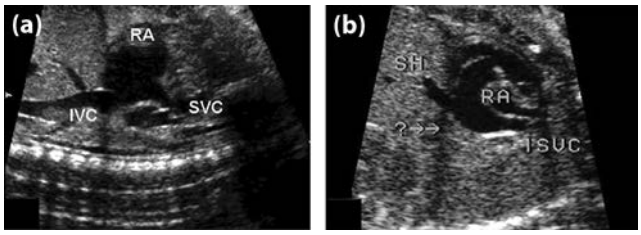


Figure 5.19 Cavo-atrial junction. (a) Situs solitus: normal venous return, with drainage of the superior and inferior venae cavae into the right atrium. (b) Situs ambiguous (left isomerism): the inferior vena cava (?) is absent and one suprahepatic vein (SH) drains directly into the right atrium. The systemic return is abnormal and consists of an azygos continuation (not visible in this image) draining into the superior vena cava and a persistent left superior vena cava (lSVC). IVC: inferior vena cava; RA: right atrium; SVC: superior vena cava.



Figure 5.20 Longitudinal view of the aortic arch (left: gray-scale; right: color Doppler). This view, obtained with a ventral approach, demonstrates the ascending aorta, the aortic arch with the neck vessels (arrowheads and numbers), and the descending aorta. The three neck vessels are the (1) innominate artery, (2) left carotid artery, and (3) left subclavian artery. IVC: inferior vena cava.

Cavo-atrial junction, normal (Figure 5.19a). In this longitudinal view of the fetal thorax, both venae cavae are seen entering the right atrium (*seagull wings view*).

Checklist. This includes (1) the presence of both venae cavae entering the right atrium; and (2) both venae cavae should have the same size.

Absence of the inferior vena cava (Figure 5.19b). In left atrial isomerism, the systemic return is abnormal: the inferior vena cava is absent, the suprahepatic veins drain directly into the right atrium, and there is an azygos continuation draining into the superior vena cava.

Lo NGITUd INAL VIEW o F Th E Aor TIc Arch

On this view, the whole course of the aortic arch, from the left ventricle to the abdominal aorta, is displayed. The neck vessels are also visible in most instances (Figure 5.20). In the case of transposition of the great arteries, the course of the aortic arch is wider than normal, due to the more anterior position of the ascending aorta, which arises from the substernal right ventricle. The two aspects of the normal arch and the transposed arch have been said to resemble an umbrella handle and a hockey stick, respectively.

Thr EE-dIMEN sIo NAL (3d) ANd Fo Ur- dIMEN sIo NAL (4d) F ETAL Echoc Ard Io Gr Aphy : cA rd Io- s TIc

Premise. 4D echocardiography—via spatiotemporal image correlation (STIC) or live with matrix arrays—is now used routinely in most fetal cardiology units, because it has been shown to contribute significantly to improving the characterization of a number of forms of CHD. The perception of the experts is that use of this technology adds clinically relevant data in 10%–15% of all cases seen at a referral unit. In addition, storage of 4D volume datasets contributes significantly to improving the quality of the teaching material.

Background and technique. In the fetus, the main factor limiting the 3D assessment of a dynamic organ such as the heart is absence of a *triggering source*, which in the adult allows coupling of the different frames acquired during the cardiac cycle. This problem has been overcome with the STIC protocol. In this technique, the array inside the transducer housing performs a single slow sweep, recording a single 3D dataset. This volume consists of a high number of two-dimensional (2D) frames. STIC derives the heart rate from the periodicity of the movements of the cardiac structures, and eventually a single *virtual* cardiac cycle, each frame of which is the result of the overlay of many acquired frames, is reconstructed. As a result, this technique cannot be used in case of fetal arrhythmias (transient or persistent), since the abnormal fetal heart rate would compromise the adequacy of the acquired volume. Once acquired, the volume is opened and can be used offline for multiplanar navigation and/or 4D image renderings using the various modes already described in other sections of this chapter.

Acquisition. The volume to acquire should include the whole thorax, from the subdiaphragmatic venous returns to the upper mediastinum (three-vessel view). With such a volume, all echocardiographic planes may be obtained

offline with the multiplanar mode. The best approach to acquire an adequate volume is to start the acquisition procedure while displaying an apical four-chamber view.

Modes of analysis. There are different rendering modes that may enhance the characterization of cardiac anatomy in normal and abnormal conditions.

Multiplanar mode. This represents the basic mode for exploration and navigation of the volume. The fetal heart can be thoroughly assessed, and all echocardiographic planes needed in fetal echocardiography can be achieved offline (Figure 5.21). It has to be underlined that the facility with which a beginner as well as an experienced operator can navigate the volume of the heart and great vessels contributes significantly to a better understanding of the three-dimensionality of the central cardiovascular structures [4,5].

Glassbody mode. The possibility of coupling a transparent mode for the grayscale image with a surface mode for the color Doppler signal allows a display on the same image of the diastolic filling of the ventricles and the systolic ejection of blood through the great vessels, giving a striking 3D cast of the crossover (Figure 5.22). This approach also contributes to the understanding of the relatively complex anatomy of the outflow tracts [5].

Surface mode. This mode is used to display, with different threshold and postprocessing filters, the anatomic structures of the four chambers and, less often,

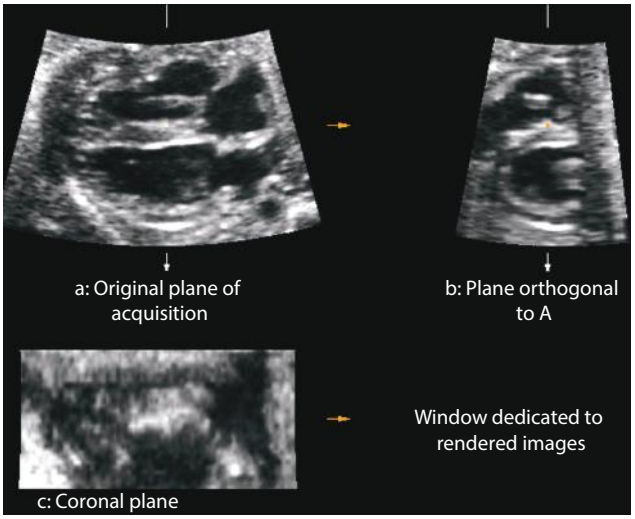


Figure 5.21 Cardio-STIC: grayscale multiplanar imaging. This image modality allows simultaneous visualization of the cardiac anatomic structures on the three orthogonal planes. By positioning the caliper on the structure of interest, it is possible to assess its characteristics on the three planes. The image is in motion and consists of a reconstructed virtual cardiac cycle played in a cineloop sequence.

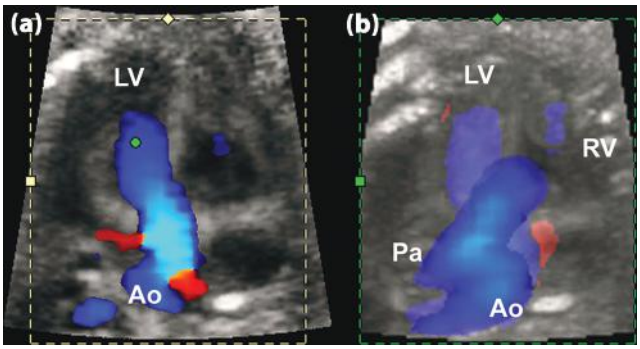


Figure 5.22 Cardio-STIC: color Doppler. Glassbody rendering with transparent maximum mode. This image modality allows a display of the 3D color Doppler, thanks to the transparency of the grayscale image. As a result, with appropriate adjustments of settings, it is possible to actually visualize the crossover of the great vessels. (a) Conventional color Doppler image of the left outflow: to check the crossover, in 2D imaging, it is necessary to image both the left and right outflows. (b) With the glassbody mode, the crossover is recognizable on a single image. Ao: ascending aorta; LV: left ventricle; Pa: pulmonary artery; RV: right ventricle.

of the outflows (Figure 5.23). In particular, this mode allows planes to be visualized that cannot be obtained with 2D US, such as the coronal view of the atrioventricular valves or the *en-face* view of the interventricular septum (Figure 5.23).

Tomographic ultrasound imaging. This image modality allows one to display on a single panel a variable number of reconstructed 2D sections, as in a computed tomographic or magnetic resonance imaging (MRI) scan. In particular, it displays parallel slices that are orthogonal to the plane of acquisition [6]. Therefore, if the acquisition is performed orthogonally to the fetal body (e.g., starting from the apical or transverse four-chamber view), and if the volume is sufficiently large, all consecutive slices from the transverse abdominal to the high mediastinum with the ductal and aortic arches will be displayed simultaneously and automatically (Figure 5.24).

B-flow. Finally, the B-flow mode is able to display casts of cardiovascular structures, starting from grayscale image, without the need for Doppler. This modality is very helpful in characterizing complex CHD (Figure 5.25) [7].

Diagnostic role of 4D echocardiography. The possible applications of 4D echocardiography are enormous. Its potential role in fetal cardiology teaching and training is huge: the possibility to display *live* and in three dimensions the four chambers and the outflows in normal and abnormal conditions significantly enhances the understanding of complex concepts such as impaired

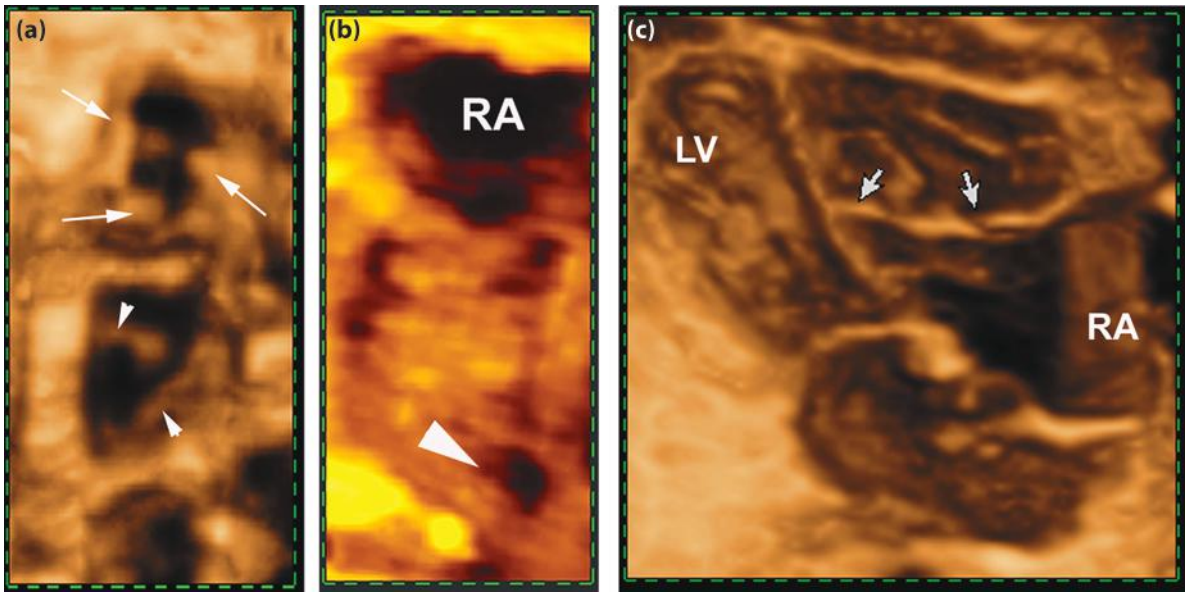


Figure 5.23 Cardio-STIC: surface rendering. (a) Coronal view of the atrioventricular valves. The three leaflets of the tricuspid valve (arrows) and the two leaflets of the mitral valve (arrowheads) are clearly visible with this technique. (b) *En-face* view of the interventricular septum, showing a small muscular septal defect (arrowhead) of the cardiac apex. (c) Ebstein's anomaly. The use of the surface mode allows one to visualize in detail the abnormal tricuspid valve, the dysplastic leaflets of which are plastered down along the interventricular septum (arrows). Note also the clear depiction of the foramen ovale and the abnormal chordae tendinae of the tricuspid valve (above the arrows, within the ventricular cavity). LV: left ventricle; RA: right atrium.

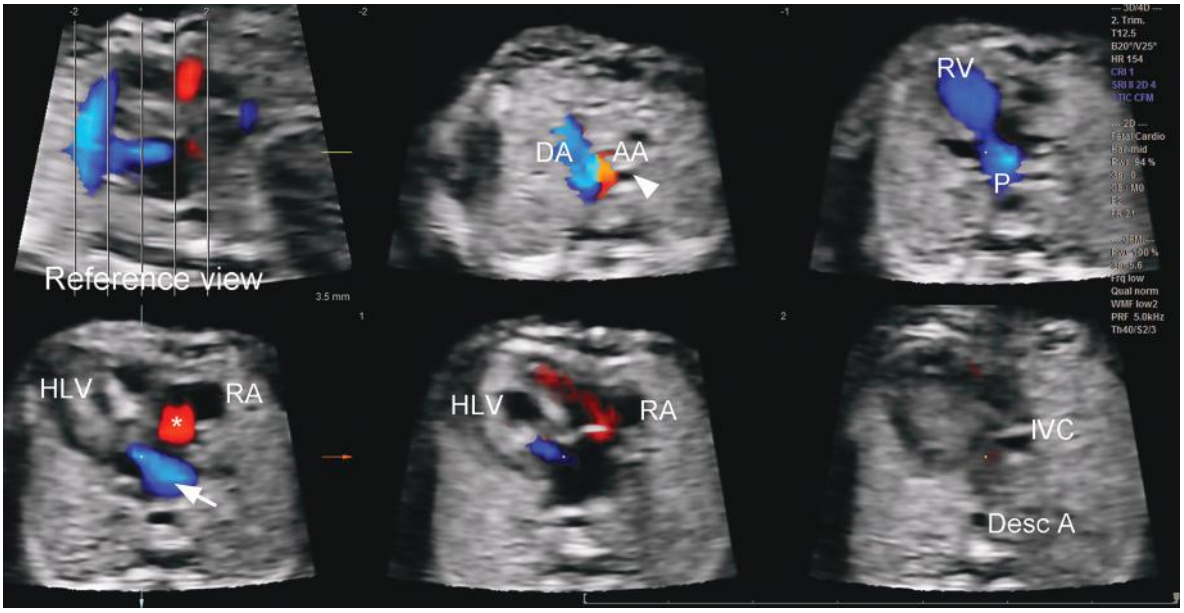


Figure 5.24 Cardio-STIC: tomographic ultrasound imaging (TUI). This image modality allows one to display on a single panel a variable number of parallel reconstructed 2D sections that are orthogonal to the plane of acquisition. Therefore, if the acquisition is performed orthogonal to the fetal body, and if the volume is sufficiently large, all consecutive slices from the transverse abdominal to the high mediastinum with the ductal and aortic arches will be displayed automatically. A case of hypoplastic left heart (21 gestational weeks) is shown. The sequential anatomy can be assessed, from the abdominal situs (lower row, right window) up to the aortic arch (upper row, central window). The following findings are shown: reverse flow across a severely hypoplastic aortic arch (central, top row); normal right ventriculoarterial connection (right, top row); mitral regurgitation (arrow) and reversed shunt (asterisk) across the foramen ovale (left, bottom row); and endocardial fibroelastosis, hypoplastic left ventricle, and bulging of foramen ovale flap into the right atrium (central, bottom row). Arrowhead: trachea; AA: aortic arch, hypoplastic; DA: ductal arch; Desc A: descending aorta; HLV: hypoplastic left ventricle; IVC: inferior vena cava: P: pulmonary trunk; RA: right atrium; RV: right ventricle.

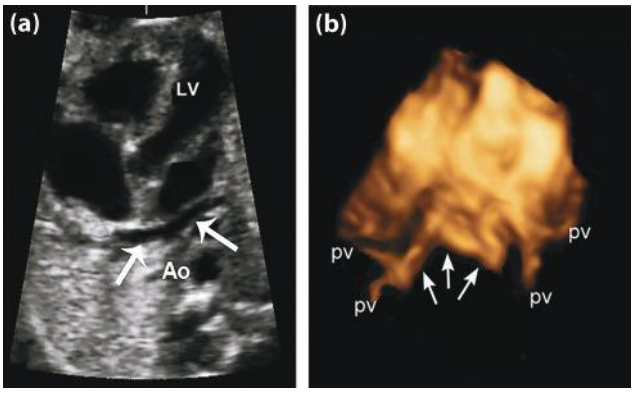


Figure 5.25 Cardio-STIC. B-flow imaging demonstrating a case of total abnormal pulmonary venous return (a): greyscale; (b): B-flow imaging. The rendered image (b) shows the four pulmonary veins (pv) draining into a collecting vein (arrows) that courses behind the left atrium without entering it. (Modified from Volpe P et al., *Ultrasound Obstet Gynecol* 2007; 30: 830–7).

contractility and pump failure. In this way, also, the learning curve for fetal echocardiography will dramatically improve. The use of cardio-STIC may also be beneficial if applied in the screening setting: the possibility to acquire a volume of the outflows rapidly while displaying a simple four-chamber view enables the operator to navigate it offline and extract the outflow tract views. In a diagnostic setting, the possibility of investigating cardiac defects using planes not obtainable by conventional 2D US, such as the coronal view of the atrioventricular valves, significantly increases the confidence with which some difficult diagnoses can be reached. In addition, the possibility of exploiting the potential of the various rendering modes in order to assess and display abnormal and hypoplastic vessels is likely to improve the characterization of rare anomalies. Finally, 4D echocardiography can be used advantageously also for peer review and second opinions, and the expert has the possibility to redo the fetal echocardiographic examination by navigating the volume.

When is it useful to use Cardio-STIC? We feel that it may represent a good rule, if there is such a possibility, to acquire at least one grayscale and one color Doppler volume of the fetal heart in each patient. This can then be used as archived material only or may become useful in case of medicolegal litigation or consultation. With regard to abnormal cases, in the following sections on CHD, 4D images will be illustrated and discussed whenever they may significantly improve diagnostic and/or prognostic accuracy.

chArAcTErIzATIoN oF MAjor chd

ANoMALoUs pULMoNAry VENoUs coNNEcTIoN

Incidence. 2% of CHD.

Ultrasound diagnosis. In the *apical four-chamber view*, the drainage of the pulmonary veins into the left atrium is not visualized. Often, a venous chamber or a venous collector is seen behind the left atrium.

Risk of chromosomal anomalies. Low.

Risk of nonchromosomal syndromes. High, if cardiosplenic syndromes are included.

Outcome. The prognosis depends on the association with other CHD, on the presence of obstructions, and on how early the postnatal diagnosis is made. If isolated and diagnosed early, mortality varies from 1% to 10%.

Definition The essential feature of the pulmonary veins when abnormally connected is that they drain into a site other than the morphological left atrium. Total anomalous pulmonary venous connection (TAPVC) accounts for approximately 2% of CHD in postnatal life. TAPVC is characterized by the anomalous drainage of all four pulmonary veins, whereas partial anomalous pulmonary venous connection (PAPVC) is characterized by the anomalous drainage of one, two, or three of the pulmonary veins.

A particular form of PAPVC is represented by *scimitar syndrome*. In this case, the venous drainage from the lower right lung is conveyed to the inferior vena cava (or the vena porta) by a vertical vein. Hypoplasias of various degrees of the right lung and the right pulmonary artery are associated.

Anatomy. Among the various classifications proposed, that by Darling et al. [8] is the most frequently used. In reference to the drainage anomaly, this classification distinguishes four types of TAPVC:

- *Type 1*: supracardiac (50% of cases). The four pulmonary veins drain into a venous collector located

behind the left atrium. This collector is traditionally termed the *confluence*. From this horizontal collector, a vertical vein runs up to reach the innominate vein; this then terminates in the right superior vena cava. At times, the vertical vein may be obstructed due to extrinsic compression by the bronchus and the ipsilateral pulmonary artery; these obstructions are rarely severe in the perinatal period.

- *Type 2*: cardiac (25% of cases). The pulmonary veins drain through the coronary sinus or, more rarely, directly into the right atrium. Usually, there is no obstruction.
- *Type 3*: infracardiac or infradiaphragmatic (20% of cases). The confluence of the pulmonary veins enters a descending vertical vein that passes into the abdomen through the esophageal orifice of the diaphragm. It then usually drains into the portal vein or, more rarely, into the ductus venosus or the inferior vena cava. When the infracardiac connection is to the portal venous system, the abnormal venous return is almost always obstructed.
- *Type 4*: mixed (5% of cases). The pulmonary veins drain separately to different anomalous sites.

Ultrasound diagnosis. Anomalous connection of the pulmonary veins is notoriously misdiagnosed prenatally, especially when isolated. In the few cases described prenatally, TAPVC is often associated with other cardiac anomalies in the context of *heterotaxy syndromes*. The diagnosis is suspected on the *four-chamber view*. Indirect signs of TAPVC are (1) moderate ventricular disproportion (Figures 5.25 and 5.26a), with the right sections larger than the left ones; and (2) a pulmonary artery significantly larger than the ascending aorta. The fetal echocardiographic clues to the diagnosis of TAPVC include failure to demonstrate a direct pulmonary venous connection to the left atrium, the detection of a venous confluence chamber behind the left atrium (Figure 5.26b), and the visualization of an ascending or descending vertical vein [9]. In cases of PAVPC, the visualization of at least one direct pulmonary venous connection to the left atrium (Figure 5.27a) makes the suspicion of this anomaly even harder to raise [10,11]. Color Doppler (with low-pulse repetition frequency (PRF) to detect the extremely low-velocity pulmonary venous flow) may be used to confirm the vascular nature of the sonolucent area behind the left atrium (differentiating it from the esophagus; Figure 5.26b). Spectral Doppler assessment can then be used to detect the typical pulmonary velocity waveform. Four-dimensional echocardiography can be advantageously used to locate normal and abnormal pulmonary venous returns [7] (Figure 5.27c).

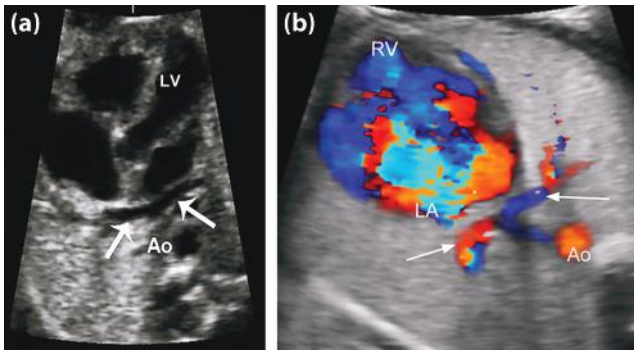


Figure 5.26 Total anomalous pulmonary venous connection. (a) The four-chamber view shows ventricular disproportion, with the right sections larger than the left ones. A venous collector (arrows) is seen passing behind the left atrium without entering it. (b) On color Doppler with very low PRF and high priority over grayscale, the pulmonary veins (arrows) are seen meeting behind the left atrium without entering it. Note also that the distance between the descending aorta and the atrial wall is increased: this has been described as an additional sign to suspect total abnormal pulmonary venous return. Ao: descending aorta; LA: left atrium; LV: left ventricle; RV: right ventricle, right atrium.

Scimitar syndrome represents a rare and particular form of partial abnormal pulmonary venous return. In this complex anomaly, the right lung is moderately or severely hypoplastic, and the venous drainage of the lower right lung lobe (or of two or even all three lobes) is abnormally connected to the systemic circulation at the level of the inferior vena cava or vena porta. The vertical vein draining into the systemic subdiaphragmatic venous system resembles a "scimitar" on MRI angio slides; from this aspect comes the name of this rare condition. On US, the initial abnormality to pick up on the four-chamber view is the mesocardia, due to the displacement of the heart toward the right, which is related to the relative hypoplasia of the right lung (Figure 5.27a). Then, on color Doppler with a low PRF (or bidirectional power Doppler), the absence of the connection between the inferior right pulmonary vein and the left atrium is detected (? on Figure 5.27a). The diagnosis is then finalized by getting the longitudinal view of the right lung and the inferior vena cava and looking for the abnormal venous connection with color Doppler (Figure 5.27b): an abnormal venous vessel is seen descending from the right lung to drain into the inferior vena cava (as in Figure 5.27b and c) or the vena porta. Four-dimensional US with B-flow may enhance the diagnosis by clearly showing the scimitar sign (Figure 5.27c).

Differential diagnosis. This should take into account other causes of atrioventricular disproportion, such as aortic coarctation (discussed further in this chapter).

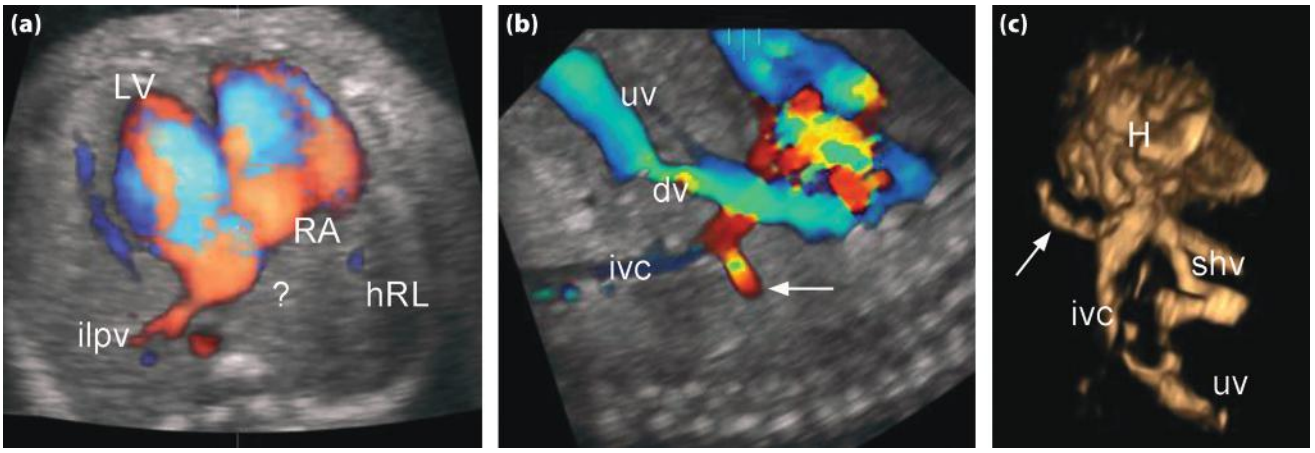


Figure 5.27 Scimitar syndrome (partial anomalous pulmonary venous return) at 21 gestational weeks. (a) The bidirectional power Doppler image of the four-chamber view demonstrates (1) mesocardia, due to moderate hypoplasia of the right lung (hRL); and (2) absence of the inferior right pulmonary vein (?) that is not seen entering the posterior wall of the left atrium as it should. (b) A longitudinal view of the inferior vena cava (ivc) showing the lower right pulmonary vein (arrow) entering the inferior vena cava. (c) B-flow reconstruction showing the "scimitar," represented by the abnormal pulmonary venous connection (arrow) to the inferior vena cava. The cava with the abnormal vessel and the suprahepatic veins on the other side represent the scimitar. dv: ductus venosus; hRL: hypoplastic right lung; ilpv: inferior left pulmonary vein; LV: left ventricle; RA: right atrium; shv: suprahepatic veins; uv: umbilical vein.

The recognition of at least one pulmonary vein entering the left atrium would rule out TAPVC; on the contrary, the detection of a venous chamber with typical pulmonary venous velocity waveform at Doppler assessment confirms the presence of TAPVC.

Prognostic indicators. The presence of an obstructive abnormal pulmonary venous return represents an unfavorable prognostic indicator because it is one of the few real neonatal emergencies due to a congenital cardiac defect. Also, the association with heterotaxy syndromes represents a poor prognostic sign.

Association with other malformations. TAPVC is often associated with complex cardiac anomalies, often in the context of heterotaxy syndromes.

Risk of chromosomal anomalies. This is low.

Risk of nonchromosomal syndromes. This is high if cardiosplenic syndromes are included; otherwise, it is low. TAPVC can be associated with rare syndromic conditions, such as cat-eye syndrome [10].

Obstetric management. In the few cases in which TAPVC is diagnosed prenatally, this should prompt in utero transfer to a tertiary referral center where cardiac surgery can be performed, because in the case of severe obstruction, it may be necessary to intervene in the first few hours of life

Postnatal therapy. Nonobstructed TAPVCs are usually asymptomatic at birth; nevertheless, they must be operated upon during the first two months of life in order to reduce operative risks to a minimum. As mentioned in this section, obstructed TAPVCs represent one of the few real emergencies in pediatric cardiac surgery. In fact, while nearly all the other critical heart defects can be pharmacologically (with prostaglandins, diuretics, etc.) or mechanically (via controlled mechanical ventilation) managed for 24–72 hours, immediate surgery represents the only option for severely obstructed TAPVCs. The neonate with TAPVC will show a combination of cyanosis, dyspnea, heart failure, anuresis, and acidosis. The operation consists of reconnecting the confluence of the pulmonary veins with the left atrium, and it is generally done via median sternotomy with hypothermy and circulatory arrest.

In cases of *scimitar syndrome*, early intervention is usually needed only in cases of obstruction of the infradiaphragmatic abnormal venous collector.

Prognosis, survival, and quality of life. In utero, TAPVCs have no hemodynamic consequences unless associated with complex heart defects (e.g., heterotaxy syndromes). After birth, the prognosis depends on the association with the above-mentioned heart anomalies, on the presence of obstruction, and on how early the postnatal diagnosis is made. In isolated TAPVC, regardless of the anatomic type, if the patient comes to surgery early and in good clinical condition, mortality and morbidity rates are not high (1%–10%) and long-term life expectancy is good. On the contrary, when the diagnosis and consequently surgery are delayed, the surgical mortality is high, similar to that characterizing heterotaxy syndromes.

ATr IAL sEpTAL dEFEc T: Typ E II

Incidence. Exceptionally detected in utero.

Ultrasound diagnosis. Ostium secundum: wide foramen ovale; intact septum primum.

Risk of chromosomal anomalies. Not assessable, due to the extremely low detection rate in the fetus. Relatively high in postnatal life (5%–15%).

Risk of nonchromosomal syndromes: Relatively high. 25%–30%. Holt–Oram.

Outcome. Very good.

Definition The normal development of the interatrial septum is complex and occurs in different stages, being completed only after birth with the closure of the foramen ovale. If the closure of the fossa ovalis is not complete, a type II ASD occurs. It should be noted that only a very limited number of ASDs can be suspected in utero, due to the normal patency of the foramen ovale in the fetus. In addition, we are aware of no reports describing the prenatal diagnosis of sinus venosus ASDs. Therefore, with the exception of the few reported diagnoses of ostium primum ASD (partial AVSD), the only type of ASD that can be (rarely) suspected in utero is that involving the septum secundum. It should also be underlined that it is not possible at all to discriminate in utero between this type of defect and the simple patent foramen ovale, which will close in most instances after a few months of life. Finally, it should be pointed out that a normal appearance of the interatrial septum does not rule out the possibility of an ASD.

Anatomy. According to the site of the defect, the ASD is classified as follows

- *ASD type II (ostium secundum)*: wide defect of the fossa ovalis, due to incomplete closure of the foramen ovale;
- *ASD, sinus venosus*: the defect extends toward the orifice of the superior or inferior vena cava;
- *ASD, coronary sinus*: the defect extends toward the coronary sinus, and is often associated with anomalies of the coronary sinus itself;
- *Septum primum defect*: partial AVSD —see the section on AVSD in this chapter.

Ultrasound diagnosis. Bearing in mind what has been underscored in this chapter, this section will consider the *suspicion* rather than the diagnosis of type II ASD. In our experience, there are two different aspects of the interatrial septum that may be associated with this type of ASD, on the *four-chamber view*: (1) an extremely wide foramen ovale: more than 7–8 mm in its maximum opening (Figure 5.28); and (2) nonvisualization of the flap "hinges," with a flap that starts bulging at its connection with the atrioventricular plane rather than at the upper edge of the septum primum, and up to its farther insertion at the level of the posterior atrial wall (Figure 5.28a). Functional assessment with color Doppler (with a low PRF for low-velocity venous flows) allows recognition of the wide interatrial shunt, sometimes with bidirectional flow (Figures 5.28c and 5.29).

Artifacts. If the presence of a type II ASD is suspected, the first step is always to double-check the scanning view: in fact, if the plane is slightly posteriorized, the normal coronary sinus can be mistaken for an ostium primum ASD. The correct four-chamber view is just cranial to the view in which the coronary sinus is visible, since this structure is positioned on the inferior surface of the heart, in the atrioventricular groove. This artifact is even more pronounced in the case of persistence of the left superior vena cava; in fact, this vessel usually drains into the coronary sinus, which dilates significantly to accomodate the increased venous flow coming from the cerebral area through the left superior vena cava (Figure 5.30a). A hint suggesting that the scanning view is not correct is the absence of the foramen ovale flap: if the transducer is moved a few millimeters toward the fetal head, the correct plane, with the interatrial septum *and* the foramen ovale flap comes into view (Figure 5.30b).

Differential diagnosis. This should include a partial AVSD (Figure 5.4d), which is characterized by a *septum primum defect*, located in the lower part of the interatrial septum, just above the atrioventricular plane; and the dilated coronary sinus typical of a persistent left superior vena cava (as discussed in this chapter).

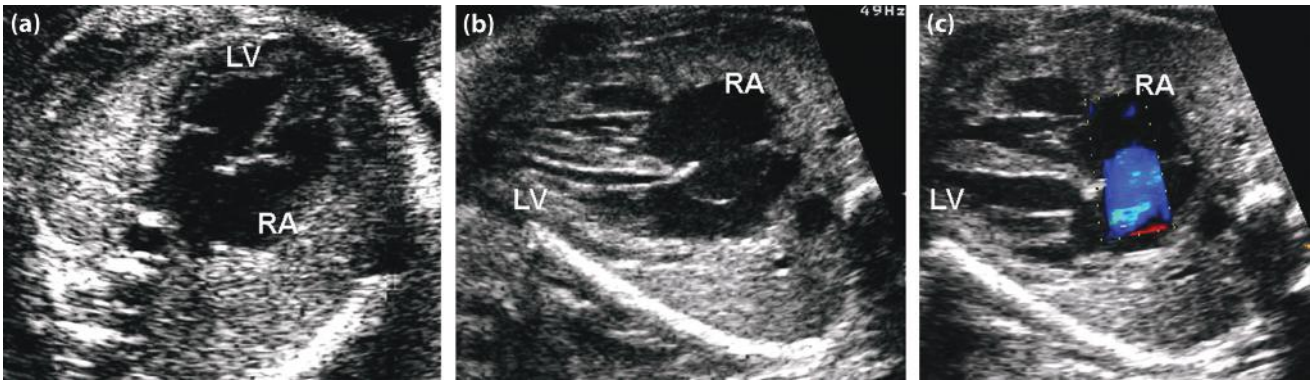


Figure 5.28 Atrial septal defect: two cases of ASD confirmed at birth. (a) On the apical four-chamber view, an extremely wide (8 mm) foramen ovale can be seen. (b) Also in this case, on the transverse four-chamber view, the large size of the foramen ovale is evident; the flap is seen in the left atrium. (c) Same case as in (b): color Doppler demonstrates the extent of the shunt. LV: left ventricle; RA: right atrium.

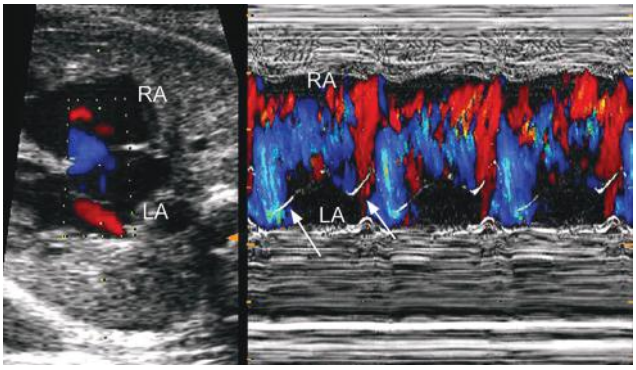


Figure 5.29 Atrial septal defect: this is the same case as in Figure 5.27 (b,c). The combined use of M-mode and color Doppler, positioning the cursor across the foramen ovale, allows demonstration of the bidirectional flow, with a significant left-to-right component (in red), which is normally absent. Arrow: foramen ovale flap; LA: left atrium; RA: right atrium.

Risk of chromosomal anomalies. This is relatively high in postnatal life (5%–15%, mainly trisomy 21). It is not assessable in the fetus due to the extremely low detection rate.

Risk of nonchromosomal syndromes. This is low but not absent in postnatal life. ASD can be associated with the following conditions [12]:

- *Holt–Oram syndrome (OMIM 142900):* look for ► *ASD* + syndactyly + positive family history;
- *Chondroectodermal dysplasia*: look for ► *ASD (or VSD/AVSD)* + thoracic hypoplasia + postaxial polydactyly (mainly, hands) + acromesomelia;
- *Alagille syndrome (OMIM 118450):* look for ► *ASD* + vertebral anomalies (hemivertebrae) + short ulnae;

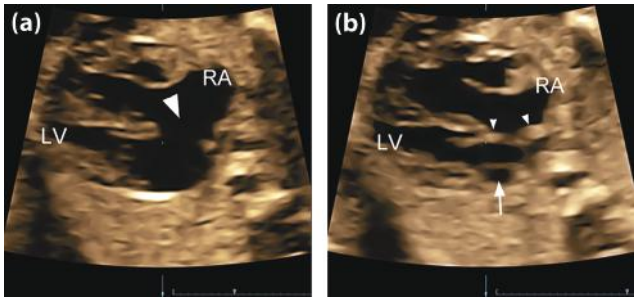


Figure 5.30 Artifact: false-positive atrial septal defect. In cases of a persistent left superior vena cava draining into the coronary sinus, the latter dilates significantly to accomodate the increased blood flow. As a result, it displaces the atria with the interatrial septum cranially, the coronary sinus being located in the atrioventricular groove. (a) On ultrasound, this condition can be mistaken for a large interatrial defect (?) and not (arrowhead), but what appears at the four-chamber view level is the dilated coronary sinus, and not the actual interatrial septum, which is displaced cranially. (b) If care is taken to obtain a more appropriate four-chamber view (just cranial to that shown in [a]), the artifact is removed, the normal interatrial septum is seen (arrowheads), and the dilated coronary sinus (arrow) becomes visible as a round sonolucent area on the lateral wall of the left atrium, just above the mitral valve.

- *Noonan syndrome (OMIM 163950):* look for ► *ASD* + (short stature + typical facies + pterygia).

Obstetric management. Should an ASD be suspected prenatally, a thorough search for possibly associated cardiac and extracardiac anomalies has to be carried out. If the suspected ASD is isolated, it should be underlined once more to the parents that a definite diagnosis will be made only after birth and that there is a consistent possibility that the presence of the defect will not be confirmed The obstetric management of the delivery is unchanged and the delivery can safely occur in a local

hospital, because there is no risk of neonatal emergencies. Echocardiography should be performed during the first week of life to assess the situation and, if necessary, schedule a follow-up scan (patent foramen ovale).

Postnatal therapy. A significant percentage of foramen ovale patencies will close during the first year of life. In those cases for which an interventional procedure is deemed necessary, closure using interventional catheterization has become the treatment of choice. Alternatively, surgical placement of a pericardial patch across the defect can be carried out. The procedure-related risks are extremely low.

Prognosis, survival, and quality of life. If the ASD is isolated, as in most instances, survival and quality of life are unaffected, regardless of the need for an interventional procedure. Only in the unlikely case in which an ASD is detected late, when it has already caused irreversible pulmonary hypertension, does the life expectancy decrease and there may be severe complications adversely affecting survival and quality of life.

VENTr Ic ULAr sEpTAL dEFE c T

Incidence. Very high. In postnatal life, VSDs account for 30% of all CHD. In utero, VSDs account for only 10% of detected CHD.

Ultrasound diagnosis. *Four-chamber view* and *left outflow view*: defect of the interventricular septum. It can involve the perimembranous (inlet or outlet) or the muscular part of the septum.

Risk of chromosomal anomalies. High (in utero). Extremely low after birth.

Risk of nonchromosomal syndromes. High (in utero).

Outcome. Very good, if the defect is isolated. Poor if associated with syndromes or other malformative clusters.

Definition VSDs represent one of the most important sources of false-negative diagnoses in utero. This accounts for the striking difference in the prevalence of this defect if fetal and neonatal series are compared: VSDs account for 30%–35% of all CHD detected after birth [13] but only for 10% of cases in fetal series [14,15]. In addition, in the fetus, VSDs are very often associated with chromosomal anomalies and/or syndromic conditions [16] whereas in the neonate, most VSDs are isolated and bear a relatively low risk of chromosomal anomalies. This consistent discrepancy is due to a selection bias: since the occurrence of a VSD does not conspicuously alter the four-chamber view, which represents the basic screening view for CHD in utero, isolated VSDs tend to be overlooked. On the contrary, if another extracardiac anomaly has already been recognized, it is likely that this will lead the operator to have a higher degree of suspicion, the four-chamber view will be more carefully evaluated or fetal echocardiography will be performed, and small VSDs may also be detected. The pathogenetic mechanism responsible for the VSD is a delay in the septal closure process: this is demonstrated by the fact that a high number of VSDs close during the first year of life or, also, in utero [16,17].

Anatomy. VSDs can be located anywhere in the interventricular septum; they can be single or multiple, and they range in size from 2 mm to several millimeters. VSDs are subdivided into *perimembranous* (of the inlet and outlet portions) and *muscular* types. Muscular VSDs can involve the inlet, trabecular, or outlet portions. Another, rarer type of VSD is the so-called doubly committed VSD, in which the roof of the defect, located in the infundibular portion, is represented by the fibrous annuli of the aortic and pulmonary valves. Finally, another type of VSD has a completely different origin and hemodynamics—the *malalignment* VSD. This type of defect will be described in the "Malalignment VSD" section, but it belongs to the conotruncal anomalies.

Ultrasound diagnosis. The diagnostic view depends on the site of the VSD: if this involves the inlet portion of the muscular-perimembranous component, it will be diagnosed on the *four-chamber view* (Figure 5.31); if the defect is located in the outlet portion, it will be evident on the *left outflow tract view* only (Figure 5.32a). Sonographically, the VSD appears as an interruption of the septum. Since the anatomic structures are better appreciated if they are at a 90° angle to the insonating beam, the best view to display the defect is a *transverse four-chamber view*. It should be underlined that a small muscular defect, especially if located at the apex, may not show up on grayscale US, and will become visible only when color Doppler is superimposed

(Figure 5.31b). As mentioned in this chapter, outlet VSDs (as well as malalignment VSDs) can be recognized on the left outflow tract view only (Figure 5.32), since the subaortic part of the septum is outside the plane of the four-chamber view. Care should be taken in assessing the alignment between the remaining part of the septum, caudal to the defect, and the anterior aortic wall: if the septum is correctly aligned with the anterior wall of the aorta, then the defect will be defined as a simple perimembranous outlet defect (Figure 5.32a); if, on the contrary, the infundibular septum is anteriorly displaced and the aorta overrides the septum, then the defect will be defined as a malalignment VSD (Figure 5.32b). On color Doppler, bidirectional flow across the VSD is found (Figure 5.31), unless another CHD that raises the pressure on one side of the heart is present at the same time (pulmonary atresia, aortic coarctation, etc.). PWD is not useful.

Four-dimensional echocardiography may be used to demonstrate the VSD on the *en-face* view of the interventricular septum, which is easily obtained through multiplanar imaging, whereas it is extremely difficult to display with 2D US [18,19]. On this view, the presence of a VSD can be reliably confirmed and its area easily measured (Figure 5.33).

Artifacts. An artifact can occur if the interventricular septum is assessed on the apical four-chamber view: the absorption of the US waves by the whole length of the septum creates a "dropout" artifact just below the atrioventricular plane, and this may be mistaken for an inlet VSD. This is why the interventricular septum should be electively assessed on the transverse four-chamber view—at least for the part that is indeed visible on this plane (Figure 5.34a). Should this doubt arise, it is sufficient to change the approach from ventral to lateral in order to remove the artifact. There are two other artifacts that can occur while displaying the left outflow tract. The first is a *pseudo-malalignment VSD*, which can be created if the left outflow is approached too laterally (Figure 5.34b). The second is a *false outlet VSD*, which is due to the shadow of the aortic annulus and/or to the origin of one of the coronary arteries: the doubt is solved when the level of the apparent defect is considered, as it is at the level or above the semilunar valve (Figure 5.34c). If the doubt persists, it is sufficient to approach the left outflow more laterally (from a transverse four-chamber view): in this way, the septum and the anterior aortic wall are insonated perpendicularly, and this removes all shadows and consequently the artifact.

Differential diagnosis. The first thing to rule out is a false VSD, as mentioned here. The only other type of CHD that can, to a certain extent, enter in the differential diagnosis is the AVSD, especially in its partial form (see Figure 5.4d): during systole, with the atrioventricular valve(s) closed, both a complete and (more so) a partial AVSD may be mistaken at first sight for a VSD. It is sufficient to reassess the heart during the next diastole to detect the wide atrioventricular communication in the complete form and to recognize the septum primum defect (which is obviously absent in the case of a simple VSD) in the partial atrioventricular canal. In addition, the normal offset appearance of the atrioventricular plane is lost in both variants of AVSD.

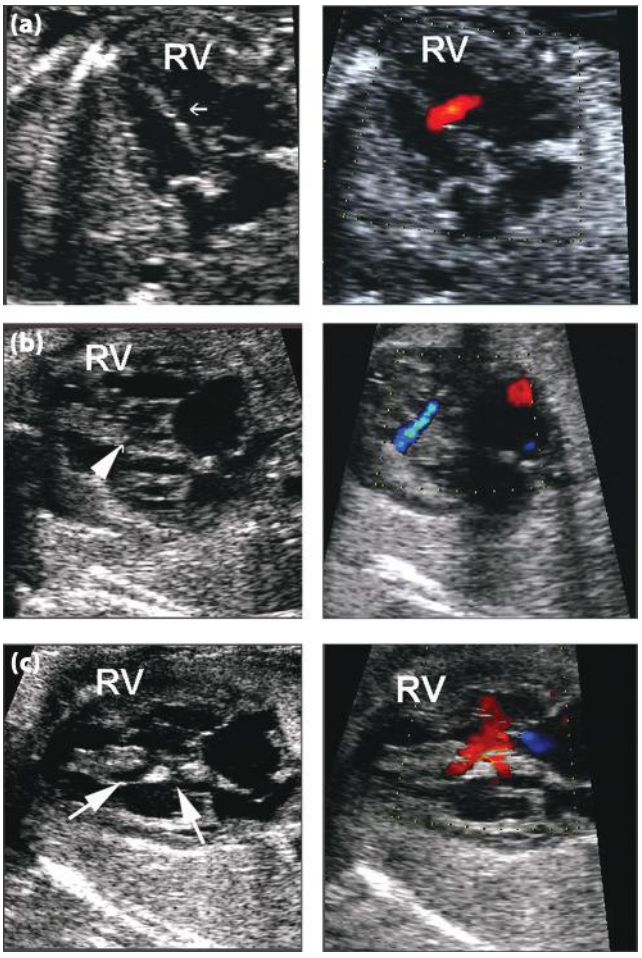


Figure 5.31 Ventricular septal defect (VSD). VSDs detectable on the four-chamber view include inlet and muscular defects. (a) Small muscular VSDs of the middle part of the septum, evident on both greyscale imaging and color Doppler (27 weeks of gestation). (b) Another small muscular VSD of the middle part of the septum, which is not clearly evident on greyscale ultrasound (left), but is demonstrated on color Doppler (31 weeks of gestation). (c) Double VSDs of the middle part of the septum, confirmed on color Doppler (right) (27 weeks of gestation). RV: right ventricle.

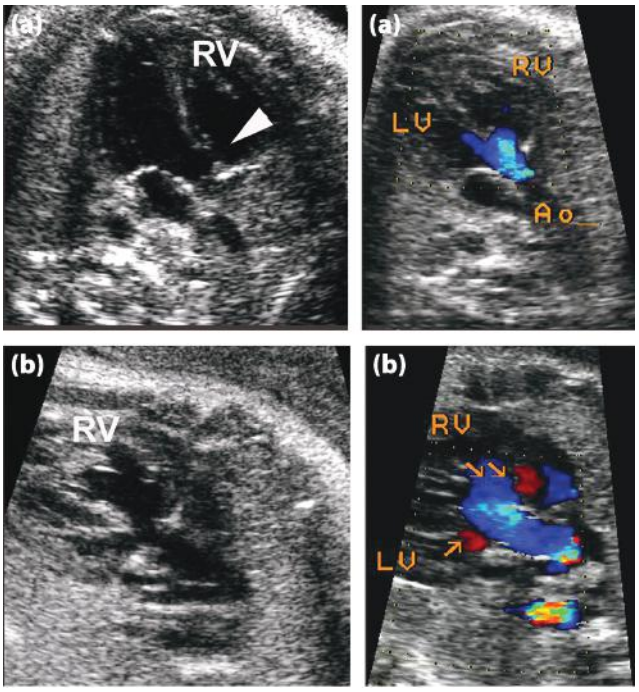


Figure 5.32 Ventricular septal defect (VSD). VSDs not detectable on the four-chamber view but only on the left outflow tract view which include (a) outlet subaortic perimembranous VSD (color Doppler demonstration on the right, 31 weeks of gestation); and (b) malalignment VSD, with the ascending aorta overriding the VSD (color Doppler demonstration on the right, 27 weeks of gestation). Ao: aorta; LV: left ventricle; RV: right ventricle.

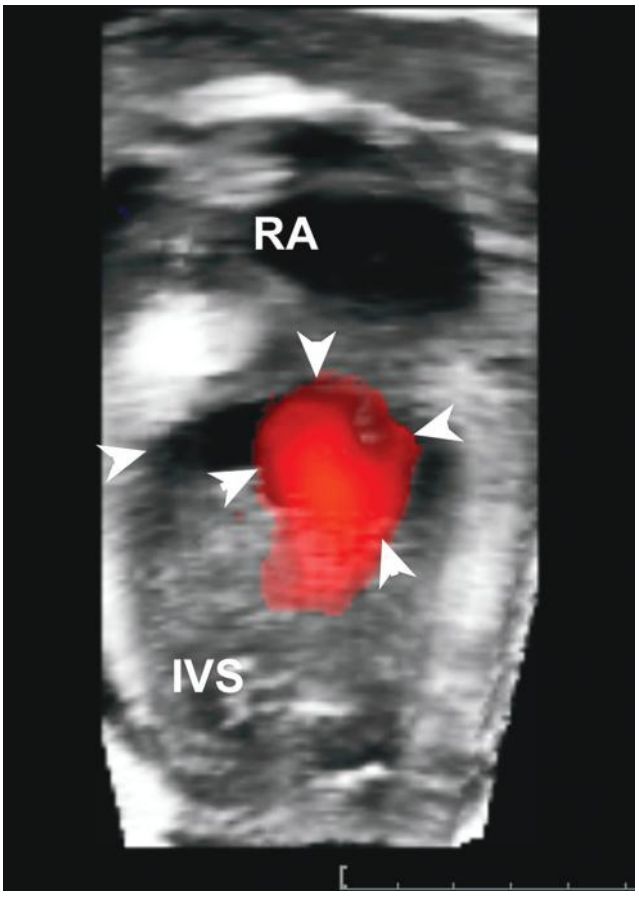


Figure 5.33 Ventricular septal defect (three-dimensional glass-body mode). With adequate adjustments of the settings, it is possible to actually visualize *en face* the interventricular septum and, in this case, the large defect (arrowheads) highlighted by the contrast offered by the color Doppler signal. IVS: interventricular septum; RA: right atrium.

Prognostic indicators. A distinction should be made between the *cardiac prognosis* and the *overall prognosis*. If isolated, a VSD has a very good prognosis; relatively negative prognostic signs include a large size (indicating that spontaneous closure is unlikely), a location adjacent to the conduction system (there is a risk of a surgical lesion with consequent need for a pacemaker), and the occurrence of malalignment (in which case it is no longer a simple VSD but also, from a hemodynamic point of view, a conotruncal anomaly). With regard to *overall prognosis*, the main prognostic indicator in the fetus is the site of the defect: in utero, inlet VSDs are associated with Down syndrome in up to 50% of cases, while malalignment VSDs are frequently associated with trisomies 18 and 13 [16]. In contrast, outlet VSDs are associated with a normal karyotype in most cases and are more likely to close spontaneously in utero, similarly to muscular VSDs [16].

Association with other malformations. No preferential association with any given type of extracardiac anomaly has been reported.

Natural history. The VSD is one of the few lesions that may disappear, by spontaneous closure, during prenatal life. This event usually occurs to the small perimembranous defects of the inlet and outlet areas and to the muscular ones [16,17]. Hence, it is possible that a VSD detected at 20 weeks of gestation will disappear by a follow-up scan during the third trimester. However, it should be considered that if a previously recognized VSD is no longer visible, it might actually have closed or it may also never have been there and may have represented a false-positive diagnosis at the previous scan.

Risk of chromosomal anomalies. This is high. Most common autosomal trisomies can be associated with VSDs: trisomies 21 (inlet) and 18 and 13 (malalignment). The interventricular septum also is often involved in cases of rare chromosomal arrangements or

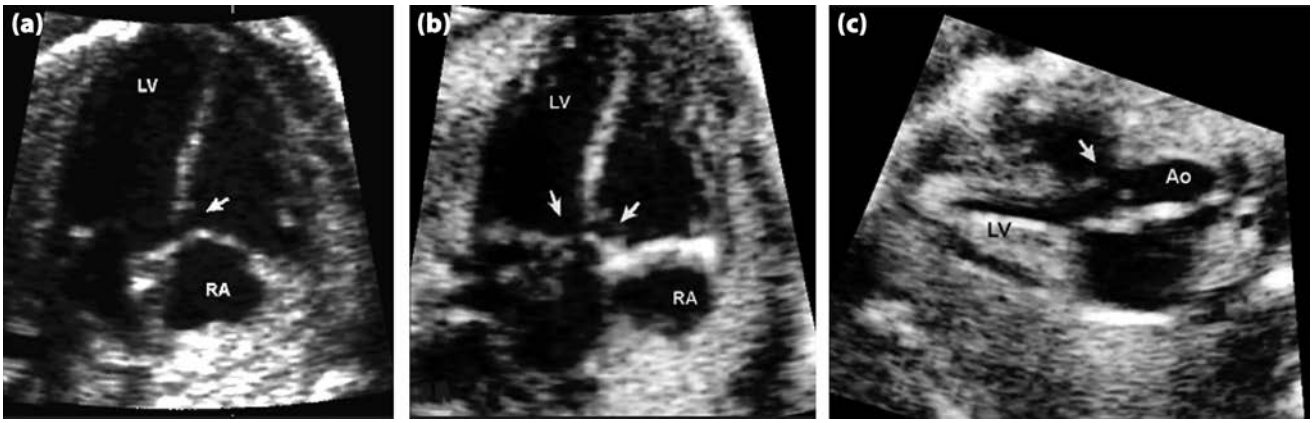


Figure 5.34 Artifact: false-positive VSD. (a) On the apical four-chamber view, the progressive ultrasound dropout across the interventricular septum creates a false appearance of an inlet VSD (arrow); it is sufficient to change the insonation approach and obtain a transverse four-chamber view to remove the artifact. (b) False appearance of malalignment VSD (below the closed aortic valve: arrows), due to a wrong insonation approach. In this case, it is sufficient to reobtain the left outflow tract with an adequate approach to remove the artifact. (c) False appearance of outlet VSD, due to ultrasound dropout caused by shadowing from the aortic valve annulus and/or by coronary arteries visualization: however, in this case, the false VSD is located at the level of or above the valve, which denotes the artifactual origin of the finding.

unbalanced translocations. In different fetal series, the risk of chromosomal anomalies for VSDs ranges from 20% to 40% [14–17].

Risk of nonchromosomal syndromes. This is extremely high. The number of syndromic conditions that feature a VSD among the typical signs is huge. There is no single syndrome that is exclusively associated with a VSD. On the contrary, it should be underlined that the interventricular septum is among the preferred targets for many genetic and chromosomal conditions.

Obstetric management. Should a VSD be detected in a fetus, a careful assessment of the cardiac and extracardiac anatomy should be carried out by an expert. Recommendation of fetal karyotyping is controversial: most perinatologists are in favor, while pediatric cardiologists are against it. Probably the best approach is to raise the issue discreetly during the initial counseling session and then act according to the wishes of the parents. The diagnosis of an isolated VSD does not alter the obstetric management, nor does it represent an indication for Cesarean section. The patient can deliver in the local hospital, since a VSD does not represent a neonatal emergency. The neonate should then be referred to a pediatric cardiology or cardiac surgery unit for management and follow-up.

Postnatal therapy. The timing of and the need for treatment depend basically on the size of the defect and on the consequent extent of the interventricular shunt. In most cases, the shunt is not severe enough to warrant operative closure during the first months of life. The natural history of VSDs has demonstrated that 40%–60% undergo spontaneous closure by 12 months of life [20]. However, if a VSD does not close spontaneously and the shunt is significant this causes an irreversible overload of the pulmonary circulation (Eisenmenger complex). To avoid this dangerous complication, surgical correction should be performed in those cases at risk. The most widely accepted approach to the closure of a VSD is based on the site and size of the defect: large defects (lesion diameter ≥ aortic diameter, right ventricular–left ventricular [RV/LV] pressure > 0.7) should be closed at three to six months of life. The closure procedure will be surgical for perimembranous, inlet, and infundibular subaortic defects. Defects of the muscular component and of the trabecular septum can be closed by interventional catheterization. In intermediate-size VSDs (lesion diameter < aortic diameter, RV/LV pressure < 0.5, pulmonary overload with QP/QS ≥ 2/1), the closure (surgical or with a device) should be done within the third year of life. Small VSDs (RV/LV pressure < 0.3, moderate pulmonary overload with QP/QS < 1.5) can be left alone or closed with a device. Finally, multiple VSDs can be closed after six months of life, if the shunt is not severe [21].

Prognosis, survival, and quality of life. In postnatal series, the prognosis for isolated VSDs is extremely favorable, with a high rate of spontaneous closure (up to 90% of cases, if the smallest muscular defects are included) and normal life expectancy both for untreated nonrestrictive VSDs and for large ones, if operated. In contrast, prenatal series show lower

survival rates, as is often the case when comparing prenatal and postnatal data for CHD: the intrauterine mortality rate can reach 11% and the neonatal mortality rate 31%, with a five-year survival rate of 40% [14–17]. It is clear that these data are affected by the selection bias mentioned under "Definition in this section, which leads to preferential recognition of VSDs associated with major extracardiac malformations. If all cases associated with chromosomal anomalies and nonchromosomal syndromes are excluded, the survival rate and quality of life are the same as those reported in postnatal cohorts.

Malalign Ment VSD

Incidence. Relatively high.

Ultrasound diagnosis. *Long axis of the left ventricle*: defect of the subaortic component of the septum, with anterior displacement of the infundibular septum and consequent aortic overriding.

Risk of chromosomal anomalies. Extremely high (50%).

Risk of nonchromosomal syndromes. Extremely high.

Outcome. Good if isolated, unfavorable if associated with syndromic and chromosomal disorders.

Definition Malalignment VSD is characterized by a malalignment between the infundibular septum, anteriorly displaced in relation to the underlying trabecular component, and the ascending aorta, with this vessel overriding the defect. Embryologically and anatomically speaking, malaligment VSDs do not belong to the septal defect group but rather to the conotruncal defect one. However, we have decided to illustrate this defect here because it may erroneously be placed in the former group by the less experienced reader.

Anatomy. In most cases, the malalignment VSD is a component of a conotruncal anomaly, such as TOF, a CAT, or the like (Figures 5.13 and 5.14). These CHDs are described in this chapter. Here, only isolated malalignment VSD will be described.

Ultrasound diagnosis. Malalignment VSD is detectable only on the long-axis view of the left ventricle, as mentioned in this section. The four-chamber view is unremarkable, unless other anomalies of the atrioventricular junction are associated. The defect appears as an interruption of the subaortic component of the interventricular septum, with the residual part of the septum pointing to the middle of the aorta (Figure 5.32b) rather than to the anterior aortic wall, as in simple outlet VSD (Figure 5.32a). The aorta will consequently override the defect. On color Doppler, the classic "Y" shape is detected, with the two arms of the "Y" corresponding to ejection of blood from both ventricles into the ascending aorta (Figure 5.32b). PWD is not useful.

Artifacts. As mentioned in this chapter, an artifact can occur when displaying the left outflow tract, that is, a *pseudomalalignment VSD*, which can be created if the left outflow is approached too laterally (Figure 5.34b). It is sufficient to change the sonographic approach, adopting a perpendicular insonation of the four-chamber and left outflow tract views to remove all artifacts

Differential diagnosis. The first issue is to distinguish malalignment VSD from simple outlet VSD: this is done by verifying the presence or absence of the normal alignment between the residual part of the interventricular septum and the anterior aortic wall (Figure 5.32a and b). Second, the possibility of an artifact should be ruled out. Finally, the most important issue is to exclude the presence of more complex conotruncal anomalies and confirm that the malalignment VSD is isolated (Figures 5.13 and 5.14).

Prognostic indicators. The main prognostic indicator is the presence or absence of associated chromosomal or nonchromosomal syndromes. If these are present, then the prognosis is unfavorable.

Association with other malformations. This occurs only in the context of chromosomal anomalies or syndromic conditions.

Risk of chromosomal anomalies. This is very high (50%), with trisomies 18 and 13 and some rare chromosomal arrangements. In a minority of cases, a malalignment VSD can also be associated with the 22q11 microdeletion.

Risk of nonchromosomal syndromes. This is extremely high. A large number of syndromic disorders may be associated with a malalignment VSD. In fact, the conotruncal area is often involved in the case of genetic or chromosomal conditions.

Obstetric management. Should a malalignment VSD be detected in a fetus, the first issue is to exclude the defect as being a component of a more complex conotruncal anomaly. In addition, due to the high risk of chromosomal anomalies and syndromic conditions, both karyotyping and a thorough anatomy scan should be performed. With regard to the karyotyping, if there are other anomalies suggesting the possible presence of the 22q11 microdeletion, such as thymus aplasia, then a fluorescence in situ hybridization (FISH) analysis of the DiGeorge critical region (DGCR) is warranted, in addition to classical G-banding. As with most CHDs, the presence of a malalignment VSD does not change the mode or timing of delivery. The lesion is not ductus dependent, but the left-to-right shunt can be significant and therefore the neonate should be transferred in the early neonatal period to a pediatric cardiology unit.

Postnatal therapy. A malalignment VSD, due to its architecture, cannot close spontaneously. Besides, the shunt is significant and this generally leads to the need for surgical closure by three to six months of age.

Prognosis, survival, and quality of life. If the defect is isolated, the prognosis is good, with optimal survival rates and normal quality of life. If chromosomal anomalies or syndromes are associated, the prognosis is very poor.

ATrIoVENTrICULAr sEPTAL dEFECT

Incidence. Very high.

Ultrasound diagnosis. *Four-chamber view*: Complete AVSD: common atrium; single atrioventricular valve; wide ventricular defect. Partial AVSD: ostium primum ASD; two separate atrioventricular valves with loss of offset appearance on the atrioventricular plane.

Risk of chromosomal anomalies. Extremely high (70%) for complete AVSD; about 30% for partial AVSD.

Risk of nonchromosomal syndromes. High.

Outcome. Cardiac outcome is good in isolated forms and in Down syndrome. It is much poorer in forms associated with cardiosplenic syndromes.

Definition AVSD is also called *atrioventricular canal defect* or *endocardial cushion defect*; the last term underlines the embryologic origin of the defect, which derives from an abnormal fusion of the endocardial cushions at an embryonic age of 34–36 days. The blood enters the ventricles through the common atrioventricular valve and then divides over the residual interventricular septum.

Anatomy. An AVSD consists of concurrent anomalies of the atrial septum, the atrioventricular plane, and the interventricular septum. The *complete form* is characterized by a common atrium; a single atrioventricular valve (usually with five leaflets) deriving from a lack of separation of the two atrioventricular annuli; and a wide defect of the interventricular septum. As a result, the central crux of the heart is lacking. Usually the two ventricles are of normal size, in which case the lesion is defined as *balanced AVSD*. If, on the contrary, one of the two ventricles is hypoplastic, the AVSD is defined as *unbalanced*. *Incomplete* or *partial AVSD* is characterized by an ostium primum ASD, two separate atrioventricular valves (with a cleft of the mitral valve, which is undetectable in the fetus), and, occasionally, a small VSD (*intermediate variant*). AVSD, especially if unbalanced, can be associated with cardiosplenic syndromes. If this is the case, then other cardiac anomalies, such as a DORV, complete heart block, or pulmonary atresia, may be associated. The association of AVSD with TOF is typical of Down syndrome. In a minority of cases, aortic coarctation can also be associated.

Ultrasound diagnosis. The US diagnosis is made on the *four-chamber view*.

Complete AVSD (Figure 5.35). There is a common atrium, due to the absence of the interatrial septum (scant remnants can be seen in some cases), and a common atrioventricular valve, deriving from the fusion of the two orifices. As a consequence, the normal offset aspect of the atrioventricular plane is lost, and this structure appears as a bar "doming" toward the ventricles during the systole. A defect of the interventricular

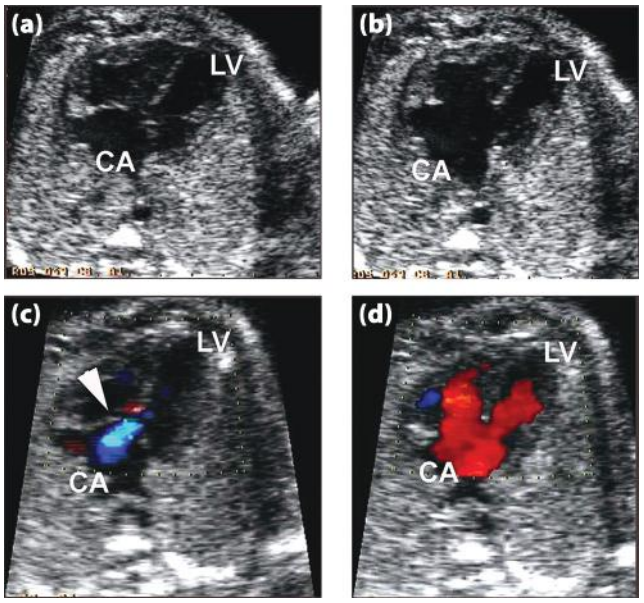


Figure 5.35 Atrioventricular septal defect (AVSD) complete, balanced (22 weeks of gestation). This is characterized by a common atrium, a single atrioventricular valve, and a "high" VSD of variable size. (a,b) On 2D ultrasound, during systole (a), the single atrioventricular plane, the loss of the normal offset appearance of the atrioventricular valves, and the interventricular and interatrial septal defects are seen. During diastole (b), the loss of the crux of the heart is seen. (c,d) On color Doppler, during systole (c), the insufficiency of the common atrioventricular valve can be seen, when present (arrowhead); and during diastole, (d), the classic Y-shaped sign of the ventricular inflow is shown. CA: common atrium; LV: left ventricle.

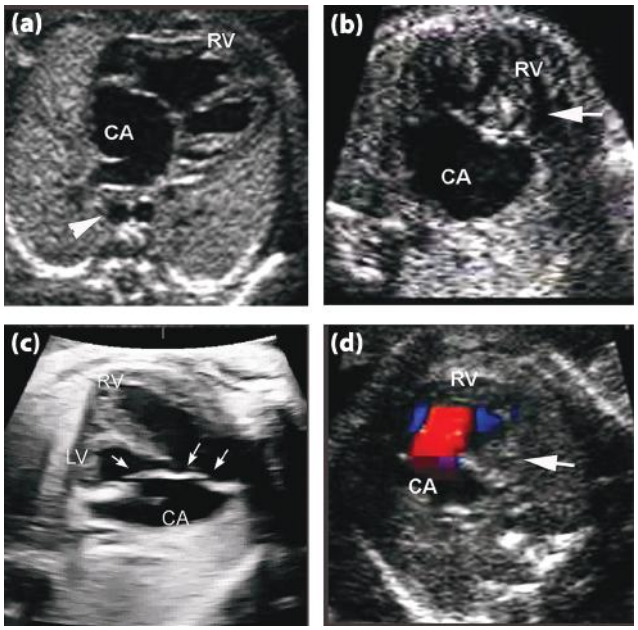


Figure 5.36 Atrioventricular septal defect (AVSD) complete, unbalanced in atrial isomerism (21–22 weeks of gestation). (a) Moderate ventricular disproportion (right ventricle larger than left). However, the azygos continuation (arrowhead) adjacent to the descending thoracic aorta should arouse suspicion of a situs abnormality. (b) Unbalanced AVSD, with severe hypoplasia of the right ventricle (arrow). (c) Unbalanced AVSD, with severe hypoplasia of the left ventricle (arrow). (d) In the same case as in (c), color Doppler demonstrates overriding of the atrioventricular valve and obstruction of the left part of the valve, responsible for the hypoplasia. CA: common atrium; RV: right ventricle.

septum is always associated. The two ventricles can be of normal size, or one of the two can be severely hypoplastic, especially in the case of cardiosplenic syndromes (Figure 5.36). The ventriculoarterial connections should be checked to rule out concurrent anomalies at this level, such as TOF and a DORV. Color Doppler assessment reveals, in a complete, balanced AVSD, the common atrioventricular diastolic filling, with a Y-shaped color Doppler image (Figure 5.35d). Insufficiency of the common atrioventricular valve should also be assessed (Figure 5.35c). In the case of unbalanced complete AVSD, color Doppler may help to define the degree of ventricular hypoplasia or, in the case of severely hypoplastic chambers, the absence of diastolic filling (Figure 5.36d). PWD may be used to quantify common valve regurgitation, if present. Four-dimensional echocardiography may be used to assess the anatomy of the atrioventricular common valve, although it plays a secondary role in this case.

Partial AVSD (Figure 5.37). This defect is rather subtle to pick up. The key features that lead to diagnosis are (1) loss of the classic *offset* appearance of the atrioventricular valves, which are not fused, as in the complete AVSD (Figure 5.37a and d); and (2) defect of the septum, above the atrioventricular plane (Figure 5.37c, e, and f). The former is visible on an apical four-chamber view, while the latter defect is better recognized on a *transverse four-chamber view.* Color Doppler with low PRF (and low priority of color signal on grayscale) or power Doppler may facilitate the recognition of the septum primum defect (Figure 5.37c and f).

Differential diagnosis. The differentiation from a simple inlet VSD is simple, as in the latter the atrial septum is normal and the offset aspect of the atrioventricular plane is unremarkable. With unbalanced AVSD, differentiation from a hypoplastic left heart or tricuspid atresia (according to the side of the hypoplastic ventricle) can be difficult (Figure 5.36c and d). Assessment of the atrioventricular plane, with recognition of the common valve and the presence in HLHS of an atretic threadlike aorta, may help to resolve any doubt. Partial AVSD is difficul to diagnose due to the fact that its sonographic appearance is strikingly similar to that of a normal heart.

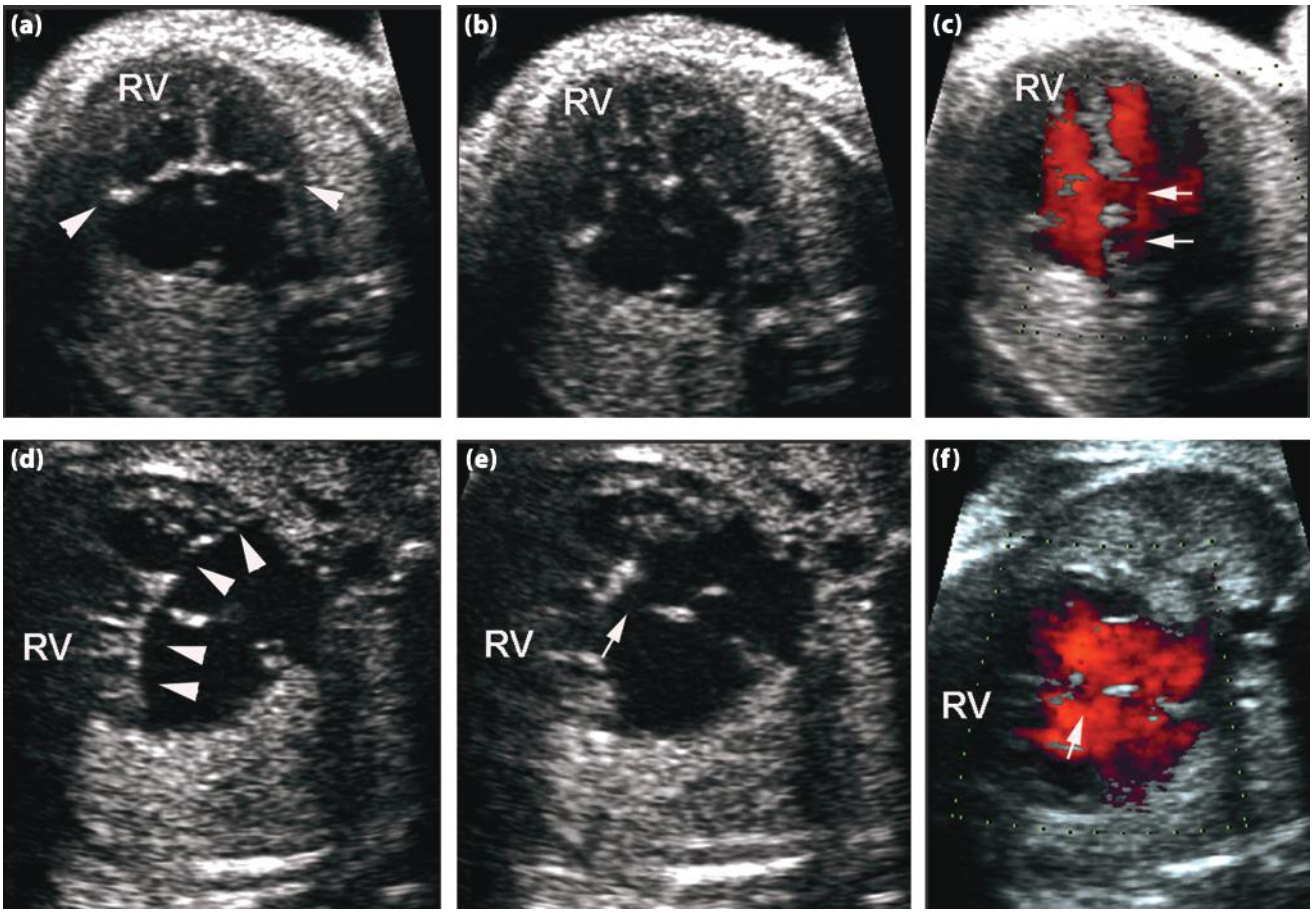


Figure 5.37 Atrioventricular septal defect (AVSD) partial (29 weeks of gestation). This is characterized by an atrial septal defect (ASD) of the ostium primum type (absence of the septum primum) with two atrioventricular valves, which do not show the normal offset aspect. (a,b) On 2D ultrasound, during systole (a), on the apical four-chamber view, the lack of the normal offset aspect is seen (arrowheads). In diastole (b), two separate atrioventricular valves are demonstrated. (c) Color Doppler helps to confirm the presence of the septum primum defect and, when present, of the VSD (arrows). (d) In systole, but on the transverse four-chamber view, the loss of the offset appearance of the atrioventricular valves is confirmed (arrowheads). (e) In diastole, the ostium primum defect is shown, just above the atrioventricular plane (arrow). (f) Color Doppler demonstrates flow across the ostium primum defect (arrow), across the normal foramen ovale (to the right of the ostium primum), and across the small VSD (to the left of the ostium primum). RV: right ventricle.

Prognostic indicators. The main poor prognostic indicator is the association with other CHD (especially cardiosplenic syndromes); significant regurgitation of the common atrioventricular valve can also represent a relatively bad prognostic indicator. If the AVSD is part of a complex syndrome, then the overall prognosis will be that of the underlying condition.

Association with other malformations. The association with cardiosplenic syndromes is consistent, ranging from 25% to 50% in most prenatal series [14,15,22–24].

Risk of chromosomal anomalies. This is very high (40%–70%). Complete balanced AVSD is the single anomaly most commonly associated with Down syndrome in the fetus [14,15,22,23]. Much more rarely, AVSD can also be associated with other autosomal trisomies (trisomies 13 and 18). On the contrary, if the AVSD is in the context of a cardiosplenic syndrome, the risk of a chromosomal anomaly is virtually absent, since this complex type of CHD seems to *protect* from such anomalies.

Risk of nonchromosomal syndromes. This is high. In addition to cardiosplenic syndromes, AVSD can be associated with other syndromic conditions and skeletal dysplasias [12]:

- *Chondroectodermal dysplasia*: look for ► *AVSD (or ASD)* + thoracic hypoplasia + postaxial polydactyly (hands) + acromesomelia;

- *Short rib–polydactyly*: look for ► *AVSD (inconstantly associated)* + micromelia + thoracic hypoplasia + postaxial polydactyly.

Obstetric management. If a balanced complete AVSD is detected in a fetus, and other cardiac defects are excluded (isomerism, DORV, etc.), karyotyping is mandatory because of the extremely high risk of Down syndrome, which in the fetus is 50%–70%. On the contrary, if the AVSD is a component of a cardiosplenic syndrome, karyotyping may be avoided. With regard to partial AVSD, the only published data we are aware of indicate a risk of association with Down syndrome of 13% and an overall risk of aneuploidy of 30% [25]. Obstetric management is not altered by detection of an AVSD: the lesion does not represent a neonatal emergency if other cardiac defects are not associated. There is no need for in utero transport to a referral center. After birth, the neonate should be referred to a pediatric cardiology unit, which will take care of the subsequent management and follow-up. However, if AVSD is associated with cardiosplenic syndromes and/or other CHD, the delivery should be arranged in a tertiary referral center to allow adequate perinatal management.

Postnatal therapy. Partial AVSD is generally asymptomatic, being basically an ASD. Only in a few cases is the cleft of the mitral valve (which is a component of the defect) so severe as to warrant treatment in the early neonatal period, especially if the left ventricle is hypoplastic: these are the worst cases, which need an early surgical approach. In complete balanced AVSD, radical surgery is generally performed between three and six months of life: the surgical procedures include closure of the VSD and ASD with a patch and reconstruction of the two atrioventricular valves. The approach to unbalanced AVSD is much more difficult—it is a surgical procedure similar to that needed in the case of a univentricular heart, especially if the dominant chamber is the right one: in this case, a Norwood three-stage procedure is needed (see the "Hypoplastic Left Heart Syndrome" section).

Prognosis, survival, and quality of life. The life expectancy of neonates with a partial AVSD is good, with a normal quality of life. The only cases with a significantly worse prognosis are those associated with a hypoplastic left ventricle and severe insufficiency of the abnormal mitral valve, which need early surgery. With respect to classic balanced complete AVSD, if surgical correction is performed when indicated (i.e., at three to six months of life), the operative mortality rate is less than 5%, with a similarly low incidence of complications (<5%) and an 89% intervention-free survival rate at 20 years. The association with Down syndrome does not alter life expectancy, and, conversely, the occurrence of an AVSD in individuals with Down syndrome does not seem to have any bad effect on prognosis, either. On the contrary, unbalanced AVSD has a very poor prognosis, with a high infant mortality rate, especially in the context of cardiosplenic syndromes [21,24].

Tr Ic Usp Id dysp LAs IA

Incidence. 1% of all CHD.

Ultrasound diagnosis. *Four-chamber view*: The tricuspid valve appears thickened and hyperechoic; the leaflets show limited systo-diastolic excursion. Color Doppler demonstrates the degree of valvular insufficiency.

Risk of chromosomal anomalies. Low.

Risk of nonchromosomal syndromes. Low.

Outcome. If the lesion is isolated and of moderate severity, survival is very good. If there is associated pulmonary atresia, the prognosis depends on the features of this anomaly.

Definition There is a wide range of heterogeneous lesions that can be defined as tricuspid dysplasia. In the most severe cases, the leaflets are severely dysplastic, the chordae tendinae are hypoplastic, and consequently the degree of insufficiency will be high. At the other end of the spectrum, there are benign cases showing only mild thickening and limited malfunction. The latter cases are compatible with a virtually normal life.

Anatomy. The mild forms may show only small nodular thickenings at the level of the free margins of the leaflets; in severely abnormal valves, the leaflet can be highly distorted, with anomalous insertion of the chordae

tendinae on the ventricular walls. Tricuspid dysplasia rarely occurs as an isolated lesion: it is often associated with Ebstein's anomaly and/or PAIVS.

Ultrasound diagnosis. On the *apical four-chamber view*, the leaflets of the tricuspid valve appear thickened and hyperechoic (Figure 5.38a) and show reduced systo-diastolic excursion with incomplete closure during systole. Color Doppler can be used to document the insufficiency of the dysplastic valve (Figure 5.38b): if the insufficiency is severe, the regurgitant high-velocity jet reaches the roof of the atrium and causes an inversion of the velocity waveform at the level of the ductus venosus. If tricuspid dysplasia is detected, it is of the utmost importance to assess the right pulmonary outflo , because pulmonary atresia is often associated. Spectral Doppler can be used to quantify the regurgitation. In the case of severe tricuspid insufficienc , cardiomegaly due to conspicuous right atrial enlargement and possibly signs of frank cardiac failure (e.g., pericardial effusion or hydrops) can be associated. It is important to note that the assessment of this type of lesion may benefit from 4D echocardiography: this technique allows a better appreciation of the anatomy and functional deficit of the dysplastic valve. In fact, 3D surface reconstruction allows visualization of the abnormal valve in planes that cannot be obtained with conventional 2D imaging (Figure 5.39).

Differential diagnosis. It is sometimes very difficult to differentiate some mild forms of tricuspid dysplasia from Ebstein's anomaly, but it should be noted that the outcome of the two lesions is similarly favorable. On the contrary, it is extremely important in the third trimester to differentiate moderate tricuspid dysplasia from premature constriction or closure of the ductus arteriosus: in both, the right ventricle and atrium can be dilated, but in the latter, the tricuspid valve is anatomically normal (the regurgitation is due to the high intraventricular pressure). Any doubt is solved when the three-vessel view is assessed with color and spectral Doppler: in the case of premature constriction of the ductus arteriosus, there is a high velocity across a small ductus and the velocity waveform is characterized by an extremely high peak velocity and a pulsatility index (PI) < 1.3, with high flow also during diastole [26]

Prognostic indicators. Poor prognostic signs are the presence of heart failure (hydrops, ascites, pericardial and pleural effusions, and polyhydramnios), tachyarrhythmia, massive right atrial enlargement from severe tricuspid insufficienc , and an absence of forward flow across the pulmonary valve (functional pulmonary atresia). However, these signs are usually present only

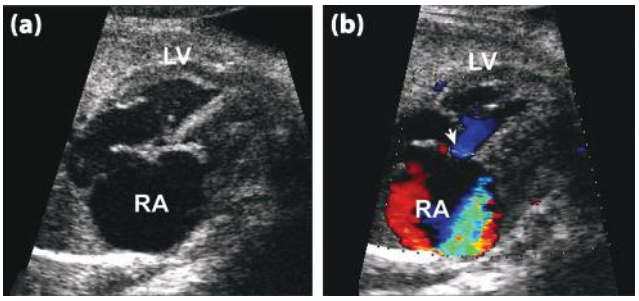


Figure 5.38 Tricuspid dysplasia (33 weeks of gestation). (a) A four-chamber view demonstrating right atrial enlargement due to the severe dysplasia of the tricuspid valve (thickened and hyperechoic leaflets). (b) Color Doppler demonstrates the severe systolic regurgitation: the high-velocity jet reaches the posterior atrial wall and curves along the atrial wall toward the foramen ovale. The arrow indicates the left outflow tract. LV: left ventricle; RA: right atrium.

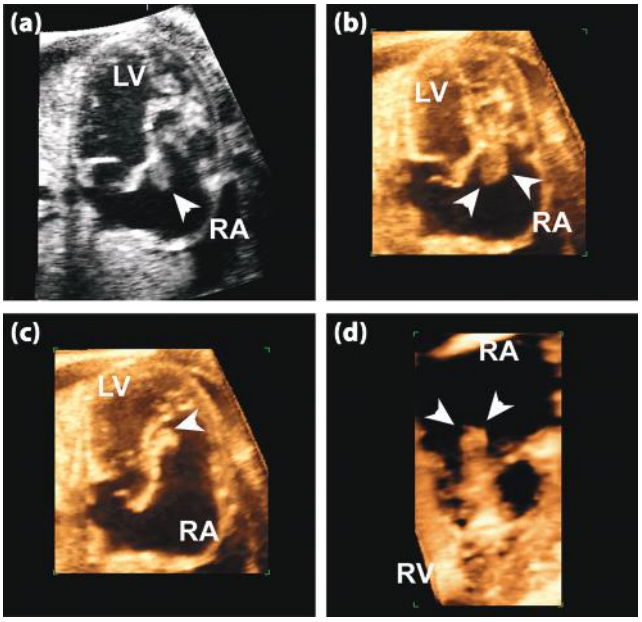


Figure 5.39 Tricuspid dysplasia with additional tissue on the valve, associated with pulmonary atresia with intact ventricular septum (33 weeks of gestation). 3D rendering enhances the visualization of dysplasia of the valve, the chordae tendinae, and the papillary muscles. (a) 2D imaging, showing the thickened and hyperechoic tricuspid valve, with additional tissue on the leaflet (arrows), which determines severe insufficiency and atriomegaly. (b) 3D surface rendering demonstrating the free movement of the additional tissue toward the atrium following the high-pressure regurgitant jet across the incompletely closed valve (arrow). (c) During diastole, the additional tissue is pushed within the right ventricle. (d) Positioning the region of interest within the right ventricle, it is possible to display the severe dyplasia, which involves the leaflets, the chordae tendinae, and the papillary muscles. The additional tissue is shown by the small arrows. LV: left ventricle; RA: right atrium; RV: right ventricle.

if the resulting dysplasia is associated with pulmonary atresia and critical stenosis. It should also be noted that, due to the physiopathology of the fetal heart, the tricuspid valve is also the first site to be involved in the case of cardiac overload from possible noncardiac causes of high-output cardiac failure, such as twin-to-twin transfusion syndrome or sacrococcygeal teratoma. Therefore, the presence of such conditions can be considered a very poor prognostic sign. Finally, it should be noted that trivial tricuspid regurgitation, usually not associated with an underlying valve dysplasia, has recently been included among the *soft markers* of Down syndrome in both the first and second trimesters [27]

Obstetric management. In the rare cases of severe tricuspid dysplasia with conspicuous insufficiency and heart failure, the perinatal mortality rate is very high: survival depends on delivery in a tertiary referral center, allowing prompt transfer of the neonate to a pediatric cardiac surgery unit and/or neonatal intensive care unit. For less severe cases, if the degree of regurgitation is deemed severe enough to cause cyanosis at birth, delivery should take place in a tertiary referral center with an intensive care unit. If tricuspid regurgitation is trivial, there is no need for in utero transport, and the neonate can be assessed echocardiographically and clinically after a few days of life.

Postnatal therapy. In the mild variant of tricuspid dysplasia, the simple switch from the fetal to the neonatal circulation, with consequent reduction of pressure levels in the right heart, leads to a dramatic improvement in the clinical situation, resulting in an immediate increase in oxygen saturation. On the contrary, the perinatal mortality rate is very high for the most severe cases, especially if heart failure is already present. However, isolated tricuspid dysplasia is rarely so severe as to cause heart failure.

Prognosis, survival, and quality of life. In mild to moderate cases, life expectancy and quality of life are virtually normal. The rare forms of severe tricuspid dysplasia causing heart failure are responsible for a high rate of perinatal death.

EBsTEIN's ANoMALy

Incidence. 1% of all CHD.

Ultrasound diagnosis. On the *apical four-chamber view*, the tricuspid valve is severely abnormal: the leaflets are thickened and hyperechoic, and the septal and posterior leaflets are plastered down into the right ventricular wall. Color Doppler investigation demonstrates the constant insufficiency of the valve. The frequently associated pulmonary atresia can be detected on the *right-outflow views*.

Risk of chromosomal anomalies. Low: 3%–5%.

Risk of nonchromosomal syndromes. Low.

Outcome. The prognosis is poor for most of the cases detected in utero. Mild Ebstein's anomaly is rarely detected before birth.

Definition Ebstein's anomaly is characterized by a malformative complex of the tricuspid valve. The valve is downwardly displaced into the right ventricle. As a consequence, a variable part of the right ventricle is atrialized.

Anatomy. The septal and posterior leaflets of the tricuspid valve do not insert at the annular level as usual, but remain adherent to the ventricular walls. These leaflets appear plastered down into the right ventricular wall, while the anterior leaflet which has a normal insertion at the level of the annulus, is redundant (spinnaker-like) and shows multiple attachments on the walls of the right ventricle, limiting its excursion. The valve is always severely dysplastic. As a result, in Ebstein's anomaly, the valve can be both stenotic and severely insufficient

Ultrasound diagnosis. In the most severe cases, on the transverse or *apical four-chamber view*, the first findin is conspicuous cardiomegaly, mainly due to right atrial enlargement (Figure 5.40a). The septal and posterior leaflets of the dysplastic tricuspid valve appear to be inserted lower than the atrioventricular plane (Figure 5.40a). The mean distance between the mitral and tricuspid attachments of the leaflet on the septum is ≥ 8 mm, but it can be lower in mild cases of Ebstein's anomaly. The tricuspid leaflets appear thickened and show reduced systo-diastolic excursion. The right ventricle can be hypoplastic or dilated if the valve is severely insufficient

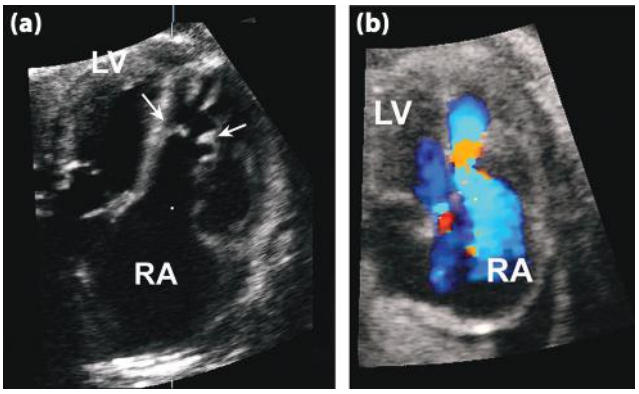


Figure 5.40 Ebstein's anomaly (35 weeks of gestation). (a) Image showing the significant displacement of the tricuspid annulus within the right ventricle, with the dysplastic posterior and septal leaflets adhering to the interventricular septum (arrows). The consequent severe insufficiency is responsible for the huge cardiomegaly. (b) Color Doppler demonstrating the severe tricuspid insufficiency, with aliasing and turbulence at the level of the downwardly displaced valve (orange area).

Color Doppler assessment allows quantification of the severity of the regurgitation (Figure 5.40b). Finally, the concurrent presence of pulmonary atresia should be confirmed or excluded by checking the right outflow tract. Four-dimensional echocardiography allows detailed characterization of the abnormalities of the tricuspid valve (see the "Pulmonary Atresia with Intact Ventricular Septum" section and Figure 5.23c).

Differential diagnosis. It is sometimes difficult to differentiate isolated tricuspid dysplasia from mild cases of Ebstein's anomaly, although there is little difference in terms of prognosis (what matters is the degree of insufficiency) What is important to differentiate from Ebstein's anomaly is premature closure of the ductus arteriosus: both share severe tricuspid insufficienc , but in premature closure, the tricuspid is normal and there is high-velocity turbulent flow across the ductus arteriosus, which is absent in Ebstein's anomaly. It is also important to differentiate the isolated form of Ebstein's anomaly from the tricuspid dyplasia and insufficiency that are frequently seen in PAIVS.

Prognostic indicators. Poor sonographic prognostic indicators are the presence of heart failure, with fetal hydrops; massive cardiomegaly due to severe right atrial enlargement; an enlarged right ventricle with thin and acontractile walls; and an absence of forward flow in the pulmonary artery, indicative of functional and/or anatomic atresia.

Association with other malformations. Ebstein's anomaly is usually sporadic and not associated with other major anomalies. As far as the heart is concerned, ASD and PAIVS are the defects most commonly associated.

Risk of chromosomal anomalies. This is relatively low (3%–5%).

Risk of nonchromosomal syndromes. This is low.

Obstetric management. Fetal karyotyping should be discussed with the parents, as the incidence of chromosomal anomalies is low. The mother should be referred to a tertiary center for delivery: the possibility of respiratory distress and/or of pump failure in severe cases may require resuscitation and active cardiovascular management.

Postnatal therapy. In severe cases, the neonate shows heart failure, cardiomegaly, and cyanosis. In favorable cases, with the fall in pulmonary resistance that occurs after a few days of life, the tricuspid regurgitation decreases significantly and the oxygen saturation improves. These cases usually remain asymptomatic for years, and surgical correction (tricuspid valvuloplasty with right ventricular folding and closure of the ASD) can be delayed for several years. The short- and long-term results of this elective surgery are good, with an early mortality rate of lesser than 5% and a 20-year survival rate of greater than 90%, with a reintervention rate of 5%. However, most of the cases detected in the fetus have a different course: they need intensive respiratory assistance, and nitric oxide and prostaglandin E1 infusion to decrease pulmonary resistance and prevent closure of the ductus arteriosus. If pulmonary atresia is associated, it may be necessary to proceed to radiofrequency or surgical opening of the pulmonary valve and to a systemic-to-pulmonary shunt (a modified Blalock–Taussig shunt) to maintain adequate pulmonary blood flo .

Prognosis, survival, and quality of life. Defining the outcome of Ebstein's anomaly is difficult bearing in mind that there are cases who die in utero and cases who live an almost normal life. As mentioned in this section, most of the cases detected in utero are at the worse end of the spectrum, often showing severe cardiomegaly and heart failure. This is due to the fact that only those cases in which the four-chamber view is severely abnormal are recognized in utero. In fetal series, the overall intrauterine mortality rate is as high as 40%; 20%–30% die in the neonatal period, and the remaining 30% survive more than one month. Neonates with Ebstein's anomaly requiring intensive care have a 50% mortality rate, but if they survive more than one month, then the life expectancy increases.

Tr Ic Usp Id ATr Es IA

Incidence Low. 0.7% in the fetus, roughly 2% in the neonate.

Ultrasound diagnosis. On the *four-chamber view*: the right atrioventricular valve is atretic, the right ventricle is hypoplastic, and a VSD is constantly associated. The *outflow tract views* should be sought to exclude ventriculoarterial discordance, which can be associated in 30% of cases.

Risk of chromosomal anomalies. Low. 2%.

Risk of nonchromosomal syndromes. Extremely low.

Outcome. Good. In cases without ventriculoarterial discordance, survival rates reach 65%–70% at 15 years. Life expectancy decreases in cases of ventriculoarterial discordance and/or if other malformations are associated.

Definition In tricuspid atresia, the right atrioventricular connection is absent due to complete atresia or imperforation of the tricuspid valve.

Anatomy. Tricuspid atresia is characterized by absence of the right atrioventricular connection. The valve can be completely atretic, with the connection being replaced by a fibrous bar or, rarely, can be imperforate. The small rudimentary right ventricle is displaced anterosuperiorly and fills through a constantly associated inlet VSD. The ventriculoarterial junction can be concordant or, less often, discordant. In rare instances, a double outlet from the left or the hypoplastic right ventricle can be associated. A type II (ostium secundum) ASD is often associated.

Ultrasound diagnosis. The diagnosis is made on the *four-chamber view*: there is a dominant left ventricle, a rudimentary right ventricular chamber, and a small VSD allowing filling of the right ventricle (Figure 5.41a). The tricuspid valve is absent and replaced by hyperechoic fibrous tissue. Color Doppler can be used to confirm the absence of right atrioventricular filling to demonstrate flow across the VSD, and to assess the ventriculoarterial connection (Figure 5.41b). Four-dimensional echocardiography may help in assessing the ventriculoarterial connection.

Differential diagnosis. The diagnosis of tricuspid atresia is relatively simple. However, care should be taken to identify the side of the hypoplastic chamber so as not to mistake a tricuspid atresia for a hypoplastic left heart (see the "Hypoplastic Left Heart Syndrome" section) or vice versa, given the completely different prognoses of the two lesions! Another rare anomaly to be differentiated from tricuspid atresia is an unbalanced complete AVSD with a dominant left ventricle: in this case, recognition of the common atrioventricular valve and the frequent association of cardiosplenic syndrome may orientate the diagnosis toward unbalanced AVSD.

Prognostic indicators. The association of ventriculoarterial discordance and/or of a double-outlet connection represents one of the most important poor prognostic factors. A restrictive VSD is also a relatively poor prognostic factor, possibly indicating the need for early surgery.

Association with other malformations. Except for the already-mentioned cardiac anomalies, there is no particular association with extracardiac malformations. Fetal growth retardation (FGR) is frequently observed in tricuspid atresia.

Risk of chromosomal anomalies. This is low (2%).

Risk of nonchromosomal syndromes. This is extremely low.

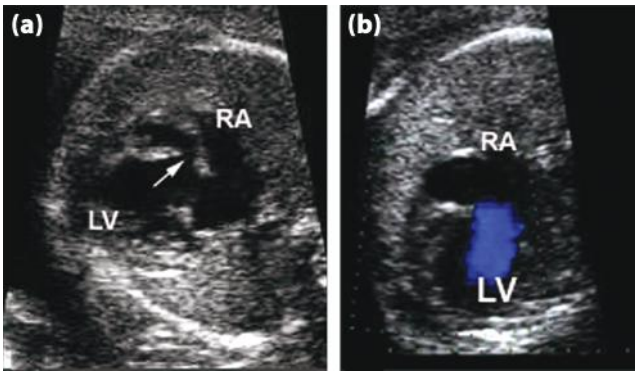


Figure 5.41 Tricuspid atresia (22 weeks of gestation). (a) On the four-chamber view, the atresia of the right atrioventricular valve, the hypoplastic right ventricle, and the small inlet VSD (arrow) are evident; note also the ASD (ostium secundum), which is frequently associated with tricuspid atresia. (b) On color Doppler, the absence of the right inflow is confirmed. LV: left ventricle; RA: right atrium.

Obstetric management. Fetal karyotyping should be discussed with the parents, as the incidence of chromosomal anomalies is low. Fetal growth should be monitored, given the relatively high incidence of FGR. It is advisable for delivery to occur in a tertiary referral center, although in most cases the VSD provides a wide enough shunt so that the lesion is not ductus dependent. However, in the few cases in which the VSD is restrictive, the lesion becomes ductus dependent and should be managed accordingly. In addition, the frequent association of impaired prenatal growth should further support the need for in utero transport to a tertiary referral center.

Postnatal therapy. Surgical corrective procedures aim at bypassing the hypoplastic right ventricle, creating a connection between the right atrium and the pulmonary trunk. The *Fontan operation* consists of a cavopulmonary shunt. This is obtained with the following steps:

- The pulmonary trunk is disconnected from its valve, and the two orifices are closed;
- The superior vena cava is cut prior to its entrance in the right atrium;
- The distal stump is then sutured to the upper wall of the right pulmonary artery, while the proximal stump is sutured to the inferior wall of the same artery;
- An ASD is created, and a synthetic Gore-Tex or Dacron conduct is placed in the right atrium to connect the inferior vena cava to the superior vena cava so that the whole of the systemic return is directed into the pulmonary artery;
- Alternatively, the pulmonary trunk can be connected directly to the roof of the right atrium.

In general, the Fontan operation is performed at 18–30 months of life; it cannot be done earlier due to the relatively high pulmonary pressures occurring in the neonate. As a result, if the neonate is severely hypoxic, or in case of contraindications to the Fontan operation (e.g., small pulmonary branches), the only chances of survival are related to a palliative systemic-to-pulmonary shunt, such as the *Glenn operation* (anastomosis between the superior vena cava and the right pulmonary artery).

Prognosis, survival, and quality of life. According to a number of authors, if candidates for the Fontan procedure are selected carefully, the three-year survival rate is 80%, with most patients in New York Heart Association (NYHA) class I/II. The best results, in terms of survival and cardiac function, are obtained if surgery is performed at four–seven years of age; survival decreases significantly if the correction is carried out later than seven years of age. According to other series, with long-term follow-up, the survival curve also continues to decrease several years after the correction, with survival rates of 70%, 65%, and 50% at 5, 10, and 15 years, respectively. This steady loss of patients is due to progressive deterioration of ventricular function. This makes the Fontan operation a good palliative procedure, but not a corrective operation. The operative mortality rates for palliative aortopulmonary shunting procedures are low, averaging 5%. If a successful Fontan operation cannot be performed, long-term survival is nonetheless reasonably good, with survival rates of 85% and 50% at 10 and 20 years, respectively.

pULMoNAry sTENosIs

Incidence. Very low in the fetus; up to 9% of all CHD in the neonate.

Ultrasound diagnosis. On the *right outflow tract views*, the pulmonary valve appears thickened and hyperechoic, with reduced systo-diastolic excursion. Poststenotic ectasia of the pulmonary trunk and moderate late-onset right ventricular hypertrophy can be present. On *color Doppler*, there is high-velocity turbulent flow across the pulmonary valve.

Risk of chromosomal anomalies. Extremely low.

Risk of nonchromosomal syndromes. Moderate.

Outcome. Favorable. In syndromic cases (Noonan), the overall prognosis depends on the underlying condition.

Definition Pulmonary stenosis is a narrowing of the pulmonary outflow due to a dysplastic semilunar valve. The critical form of pulmonary stenosis will not be described here but in the next section, together with PAIVS.

Anatomy. Pulmonary stenosis is usually due to partial fusion of the pulmonary valve cusps, which causes incomplete opening and a doming appearance of the semilunar valve during systole. Less frequently, the stenosis can be due to dysplasia and nodularity of

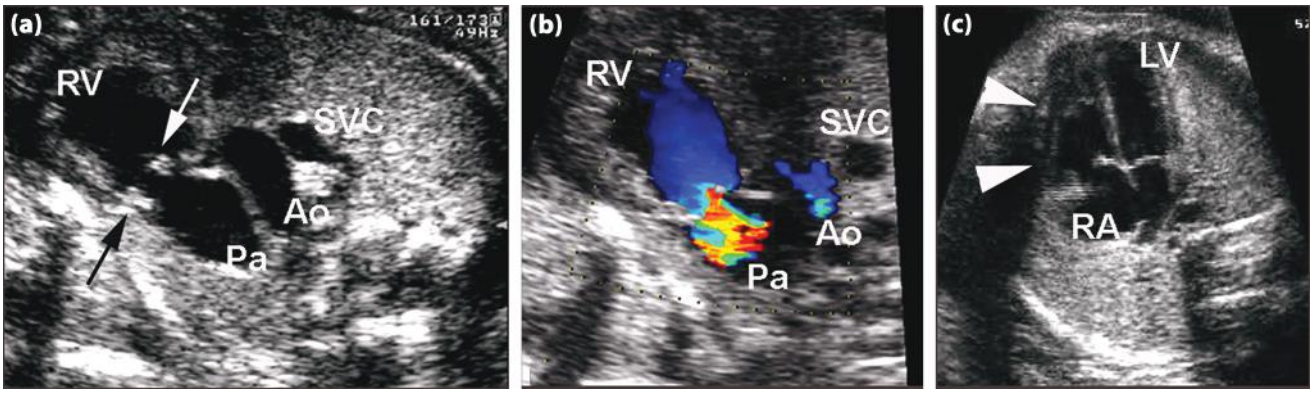


Figure 5.42 Moderate pulmonary stenosis (31 weeks of gestation). (a) 2D imaging demonstrates a dysplastic (hyperechoic and thickened) pulmonary valve (arrows), which does not open completely during systole. Note the slight poststenotic ectasia of the pulmonary trunk. (b) On color Doppler, the blood flow changes from laminar to turbulent, with aliasing and increased velocity when it passes through the stenotic valve. (c) Only in rare cases, and late in gestation, does moderate pulmonary stenosis cause hypertrophy of the free myocardial wall of the right ventricle (arrowheads)—evident on the four-chamber view. Ao: ascending aorta; LV: left ventricle; RV: right ventricle; SVC: superior vena cava; Pa: pulmonary artery.

cusps that are not fused. The degree of obstruction is variable and usually progressive. This tendency to worsen with time is present both in prenatal and in postnatal life [15,28], and also explains why pulmonary stenosis is frequently overlooked in utero. The right ventricle is usually unremarkable until late in gestation, when it may develop moderate myocardial hypertrophy. However, the classic tripartite aspect of the right ventricle is not lost (inlet, trabecular part, and outlet).

Ultrasound diagnosis. This is made on the *right outflow views* (long and short axis of the right ventricle): the pulmonary valve is thickened, hyperechoic, and hypomobile (Figure 5.42a). The valvular cusps remain visible in the lumen of the vessel throughout the cardiac cycle, while the normal valve disappears during systole as the cusps flatten along the arterial walls. Poststenotic ectasia of the pulmonary trunk is often associated (Figure 5.42a and b). On the *four-chamber view*, moderate late-onset right myocardial wall thickening and hypertrophy may be seen in a few cases of moderately severe stenosis; however, the ejection function is almost never depressed (Figure 5.42c). Color Doppler investigation of the right outflow tract demonstrates high-velocity flow across the pulmonary valve, with a color signal that shows laminar flow up to the annular level and turbulent flow with a mosaic pattern from the annulus onward (Figure 5.42b). In some cases, the dysplasia of the valve can also cause regurgitation, which is never severe. Spectral Doppler sampling allows quantification of the transvalvular gradient: mild to moderate stenoses are characterized by peak velocities of 1.5–2 m/s, whereas moderately severe stenoses show peak velocities of 3–3.5 m/s. Four-dimensional echocardiography may be used to study the abnormal pulmonary valve.

Differential diagnosis. This is virtually absent. If the valvular anomaly is overlooked, the right ventricular hypertrophy may be mistaken for an indirect sign of aortic coarctation (as discussed in this chapter).

Prognostic indicators. A doming, almost fixed valve recognized in the second trimester is likely to seal and become atretic later in gestation. A concurrent moderate nuchal thickening or simple hygroma is one of the fetal findings together with pulmonary stenosis, more commonly associated with Noonan syndrome.

Natural history. As already pointed out, pulmonary stenosis may actually appear only in the third trimester or worsen signficantly after 28–30 weeks of gestation, sometimes evolving into pulmonary atresia [15,28].

Risk of chromosomal anomalies. This is extremely low. Occasionally, pulmonary stenosis may be associated with Down syndrome.

Risk of nonchromosomal syndromes. This is moderate. The only risk is Noonan syndrome, which is not prospectively diagnosable in utero. Furthermore, when pulmonary stenosis occurs in the context of Noonan syndrome, it is usually of late onset.

Obstetric management. Should pulmonary stenosis be detected in a fetus, the need for karyotyping is questionable and should be discussed with the parents.

Obstetric and labor management are not changed and delivery can occur in a local hospital, unless the stenosis has evolved into pulmonary atresia at the last prepartum follow-up scan. After birth, the neonate should be referred to a pediatric cardiology unit for confirmation of the diagnosis and follow-up.

Postnatal therapy. Individuals with mild forms of pulmonary stenosis may remain asymptomatic and show no need for surgery. In those patients in which the stenosis worsens with time and for whom an intervention is deemed necessary, the procedure of choice is balloon valvuloplasty by interventional catheterization, which achieves good results in most cases. If the valve is difficult to dilate, surgical valvulotomy should be performed.

Prognosis, survival, and quality of life. The prognosis is extremely good, with normal life expectancy and quality of life in most cases.

PULMONARY ATRESIA WITH INTACT VENTRICULAR SEPTUM

Incidence. Relatively low: 1%–5% of all CHD.

Ultrasound diagnosis. On the *right outflow tract views*, the pulmonary valve is absent and imperforate, and the pulmonary trunk and branches may be moderately small or severely hypoplastic. On the *four-chamber view*, the right ventricle is hypoplastic if the tricuspid valve is atretic, and dilated if the tricuspid valve is insufficient.

Risk of chromosomal syndromes. Extremely low.

Risk of nonchromosomal syndromes. Extremely low.

Outcome. Moderate to good, despite the fact that surgery is only palliative in most cases.

Definition PAIVS is characterized by an absent right ventriculoarterial connection, often associated with concurrent significant anomalies of the tricuspid valve and the right ventricle.

Anatomy. In PAIVS, the whole right heart is abnormal, with a wide range of lesions. The primary lesion is atresia of the pulmonary valve: this can be completely absent or can be the consequence of a critical pulmonary stenosis in which the semilunar valve cusps have fused. In the former instance, the pulmonary trunk and branches will be severely hypoplastic, even threadlike; if the atresia is the final stage of a former critical stenosis, the pulmonary vessels can be moderately small or normal in size. In most cases of PAIVS, the tricuspid valve is atretic or severely dysplastic, with the type of abnormality determining the appearance of the right ventricle. If the tricuspid valve is atretic, the whole complex becomes a hypoplastic right heart syndrome (tricuspid and pulmonary atresia, and hypoplastic right ventricle), which is the mirror image of HLHS. On the contrary, if the tricuspid valve is dysplastic and severely insufficient as in most cases, the right ventricle will be severely dilated. It should be underlined that in about one-third of cases of PAIVS, fistulas connecting the right ventricular chamber with coronary circulation are found: these are indeed sinusoids, the difference being that the fistulas are acquired lesions, whereas the sinusoids are remnants of the embryonic circulation. When multiple, these sinusoids may cause severe coronary artery stenosis, and this in turn may be responsible for a dependency of the coronary circulation on the right ventricle, which represents a poor prognostic indicator (see "Postnatal Therapy" in this section).

Ultrasound diagnosis. The US diagnosis of PAIVS is not suspected on the views of the outflow tracts but on the *four-chamber view*, as for the left heart counterpart, represented by critical aortic stenosis (see critical aortic stenosis, later in this chapter). In fact, severe anomalies of the tricuspid valve and the right ventricle are associated in virtually all cases of PAIVS. Once the suspicion has been raised, direct evidence of pulmonary atresia is then sought on the *right outflow tract views*, where the absence or imperforation of the pulmonary valve together with the reduced size of the pulmonary trunk and branches are detected. The abnormalities found on the *four-chamber view* depend on the anatomy of the tricuspid valve (Figure 5.43): if the tricuspid valve is dysplastic, then severe right atrial enlargement and right ventricular dilation are usually present, due to the conspicuous insufficiency of the atrioventricular valve (Figure 5.43a). If, in contrast, it is atretic, the right ventricle will be extremely hypoplastic, with the whole cluster of right heart anomalies featuring the hypoplastic right heart syndrome (Figure 5.43c). On rarer occasions, the tricuspid valve may be only moderately involved, and in these cases the four-chamber view is not grossly abnormal (Figure 5.43b). Finally, in

some cases, pulmonary atresia may be associated with Ebstein's anomaly (Figure 5.43d).

Direct evidence of the primary lesion—namely, the atresia of the pulmonary valve—is then recognized and confirmed with color Doppler on *right outflow tract views* or on the *three-vessel and trachea view*: as mentioned here, if the valve is absent, the pulmonary trunk and branches will be barely visible (Figure 5.44a); if the atresia is the final stage of a critical stenosis, then the pulmonary vessels will be only moderately reduced in size or normal, while the valve will appear sealed and doming toward the pulmonary valve without opening (Figure 5.44b). On the *four-chamber view*, color Doppler is used to assess the degree of tricuspid valve regurgitation and to detect possible coronary sinusoids, if present (Figure 5.45). Spectral Doppler can be used to quantify the regurgitation of the tricuspid valve. Four-dimensional echocardiography allows characterization of the tricuspid valvular abnormalities (Figure 5.43d).

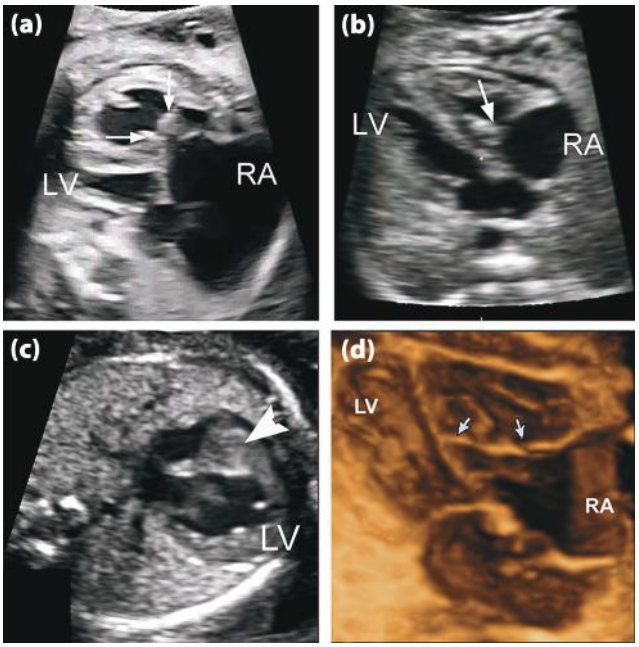


Figure 5.43 Pulmonary atresia with intact ventricular septum. The diagnosis is suspected on the four-chamber view, where the aspect of the right ventricle depends on the functional status of the tricuspid valve. (a) If the tricuspid valve is dysplastic (arrows) and severely insufficient, the right ventricle and atrium are usually extremely dilated (30 weeks of gestation). Note the thickened tricuspid leaflets (arrows) not coapting completely during systole. (b) If the tricuspid valve is only moderately dysplastic, the four-chamber view is not profoundly abnormal: only a moderate thickening of the tricuspid valve (arrow) associated with moderate right atriomegaly can be picked up by an expert eye; (c) if the tricuspid valve is atretic, then the ventricle is hypoplastic (arrowheads) and the whole malformative complex mirrors the hypoplastic left heart syndrome (tricuspid atresia, hypoplastic right ventricle, and pulmonary atresia—hypoplastic right heart; 21 weeks of gestation); and (d) if the tricuspid valve has an abnormal septal attachment (arrow), then there is an associated Ebstein's anomaly (24 weeks of gestation). LV: left ventricle; RA: right atrium.

Differential diagnosis. The main entity to be differentiated from PAIVS is PAVSD, which represents a completely different defect, both embryologically and hemodynamically. However, this task is easily carried out by displaying the interventricular septum on the *left outflow view*: if the septum is intact, the diagnosis will be PAIVS, whereas if there is a malalignment VSD with aortic overriding, then the diagnosis will be PAVSD (as discussed in this chapter). In the case of Ebstein's anomaly with severe tricuspid regurgitation and right atrial enlargement, it is sometimes hard to determine whether the pulmonary valve is patent and the forward flow is reduced due to the concurrent tricuspid insufficienc , which represents a low-pressure outlet for the blood in the right ventricle, or whether the pulmonary valve is indeed atretic. Careful evaluation of the pulmonary outflow with low-PRF color Doppler may help resolve the doubt.

Prognostic indicators. Poor prognostic indicators have been identified for PAIVS. First, it has been demonstrated that PAIVS has a worse prognosis if the right ventricle is dilated, whereas survival is higher if the ventricle is either moderately diminutive or hypoplastic [28]. Another poor prognostic factor is the presence of coronary sinusoids, because these may indicate the presence of a right ventricle–dependent coronary circulation. Finally, the Z-score of the tricuspid valve seems to be a very sensitive parameter in identifying the cases with a poorer prognosis. In particular, it has been shown that the Z-score of the tricuspid valve is highly indicative of the final anatomy of PAIVS (Table 5.1) [29]: a Z-score > –3 identifies all cases amenable after birth to biventricular repair and without a right ventricular–dependent coronary circulation; conversely, a Z-score ≤ –3 identifies 12/13 (92%) of cases undergoing univentricular repair but is not as predictive of a right ventricular–dependent coronary circulation.

Risk of chromosomal anomalies. This is extremely low.

Risk of nonchromosomal anomalies. This is extremely low.

Obstetric management. Should PAIVS be detected in a fetus, karyotyping should be discussed with the parents, due to the low risk of aneuploidy. The mother should be referred to a tertiary center for delivery, due

Table 5.1 Biventricular versus single-ventricle outcome and RVDCC versus non-RVDCC in midgestation by TV Z-score group

TV Z-score	Biventricular repair	Single ventricle	*P*	RVDCC	Non-RVDCC	*P*
≤ –3 (13 cases)	1	12	.001	8	5	.036
> –3 (5 cases)	5	0		0	5	

Source: Modified from Salvin JW et al., *Pediatrics* 118, e415–20.

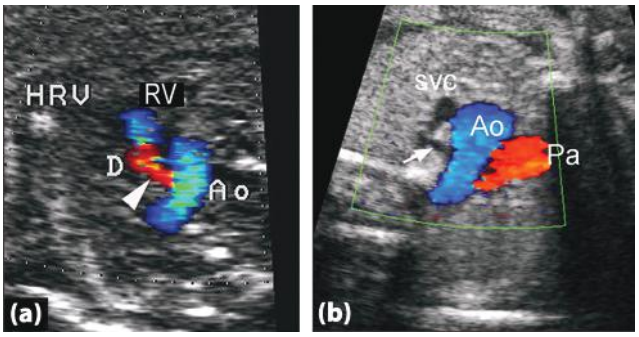


Figure 5.44 Pulmonary atresia with intact ventricular septum. The diagnosis, suspected on the four-chamber view (Figure 5.43), is confirmed on the three-vessel and trachea view. (a) Color Doppler demonstrates the severe hypoplasia of the pulmonary trunk, filling retrogradely from the ductus arteriosus (DA; arrowhead). (b) If the atresia of the pulmonary valve is a late evolutionary event of a former moderate stenosis, then the size of the pulmonary artery is not affected, and the atresia is demonstrated by reverse flow across a normally sized pulmonary artery (28 weeks of gestation). Ao: aorta; arrow: trachea; D: ductus arteriosus; HRV: hypoplastic right ventricle; PA: pulmonary artery; RV: right ventricle; svc: superior vena cava.

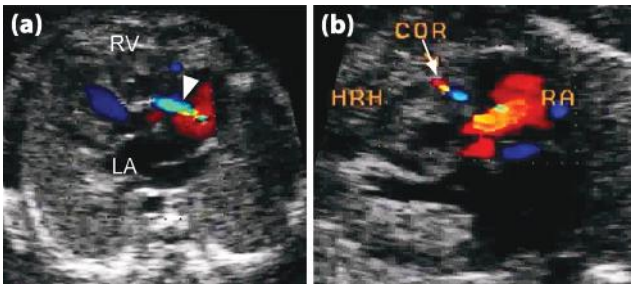


Figure 5.45 Pulmonary atresia with intact ventricular septum: coronary fistula. (a) The entity of the tricuspid regurgitation (arrowhead) is too small for the degree of tricuspid dysplasia; (b) in these cases, a coronary fistula (arrowhead) may be the preferential outlet from the right ventricle (arrow). This represents a poor prognostic sign, because it identifies a right ventricular–dependent coronary circulation (see this chapter's text). COR and arrow: coronary artery; LA: left atrium; HRH: ypoplastic right ventricle; RV: right ventricle.

to the ductus dependence of the pulmonary circulation. In fact, prostaglandin E1 (PGE1) infusion in the early neonatal period is mandatory to prevent closure of the ductus arteriosus until surgery is scheduled.

Postnatal therapy. The best approach to the neonate with PAIVS is still controversial, although most authors agree that, to attempt to rescue the right ventricle, prompt reopening of the right outflow is considered the top priority. This task can be carried out with a surgical valvulotomy, often associated with aortopulmonary shunting. This allows later reassessment of the functional recovery of the right ventricle, which is the key parameter to consider for the selection of the most appropriate surgical procedure. If the right ventricle is indeed functioning, then a biventricular repair can be perfomed (closure of the ASD and of the aortopulmonary shunt, associated with removal of the residual infundibular obstruction, if needed). Alternatively, if doubts about the right ventricular function are still present, a one-and-a-half ventricular repair can be selected (the same procedures as those discussed here, together with a cavopulmonary anastomosis). If the right ventricle remains hypoplastic or acontractile, then a univentricular Fontan-like repair is chosen. This multistep approach yields an early mortality rate of 15%–35% and a late mortality rate of 20%, with a 30% rate of biventricular repair, a 60% rate of one-and-a-half ventricular repair, and a 10% rate of univentricular repair. In recent years, perforation of the pulmonary valve with radiofrequency or laser via interventional catheterization, followed by balloon dilation, has become the procedure of choice. In this protocol, if after two–three weeks of PGE1 infusion the right ventricle does not regain its contractility and, despite a successful decompression, is unable to provide at least a 75% oxygen saturation at rest, an aortopulmonary shunt is additionally performed. This type of approach using interventional catheterization seems to yield better results than those obtained with the multistep protocol mentioned here: the early mortality rate is 0%–20%, and the rate of biventricular repair reaches 75%. However, if the hypoplasia of the right ventricle is severe (presence of the inlet part only—unipartite ventricle) or, in the case of right ventricle–dependent coronary circulation, the opening of the pulmonary valve is impossible or contraindicated, this would often lead to severe left ventricular ischemia. Both circumstances require a

Rashkind septostomy and an aortopulmonary shunt to warrant adequate pulmonary blood flo . Later, these patients may require a Fontan operation or, as a last resort, cardiac transplantation.

Prognosis, survival, and quality of life. PAIVS can cause intrauterine demise, if the degree of tricuspid insufficiency is severe and heart failure ensues relatively early in gestation. These cases show a 40% intrauterine mortality rate, with an additional early neonatal mortality rate of 35%–45%. On the contrary, if the tricuspid valve is atretic or only moderately dysplastic, the disease is well tolerated in utero and cardiac decompensation is rare. In fetal series, PAIVS is associated with an intrauterine mortality rate of 10% (excluding cases undergoing termination of pregnancy) and a survival rate beyond the first month of life of 63% [30]. Postnatal prognosis depends, as pointed out under "Prognostic Indicators" in this section, on the following:

- *The size of the right ventricle and the anatomy of the tricuspid valve*: In the case of moderate ventricular hypoplasia (tripartite right ventricle), the mortality rate is less than 5%, the life expectancy is almost normal, and additional surgical procedures are rarely necessary. In the case of severe ventricular hypoplasia, the mortality rate ranges from 15% to 35%, and both the life expectancy and the quality of life depend on the need for additional surgery.
- *The presence of severe coronary stenoses and/or of a right ventricle–dependent coronary circulation.*

These poor prognostic features are often found in cases with extremely hypoplastic right ventricles, in which the mortality rate can exceed 70%.

hypop LAsTIc L EFT hEAr T syNdro ME

Incidence. HLHS occurs in approximately 1 in 10,000 live births.

Ultrasound diagnosis. On the *four-chamber view*: complete absence of the left ventricle (mitral and aortic atresia) or a small globular left ventricle with endocardial fibroelastosis (aortic atresia and a hyposplastic but patent mitral valve). Retrograde flow in the aortic arch and ascending aorta is present on color Doppler.

Risk of chromosomal anomalies. High (up to 15%) in the fetus; 3%–4% in postnatal life.

Risk of nonchromosomal syndromes. Low.

Outcome. Poor, with high postnatal mortality and morbidity.

Definition HLHS includes a spectrum of heterogeneous conditions characterized by severe hypoplasia of the left ventricle and left ventricular outflow tract

Anatomy. There are two classic forms of HLHS: the first is characterized by mitral and aortic atresia, and the second by aortic atresia and a hypoplastic but patent mitral valve [31]. In the former type, there is no communication between the left atrium and the left ventricle due to mitral atresia or imperforation. As a result, the left ventricle is a virtual cavity, often recognizable only from the outside of the heart on the basis of the course of the anterior and posterior coronary branches (autopsy). In the other form of HLHS, the mitral valve is hypoplastic but patent; in this case, the left ventricle is hypoplastic but has a lumen that can be easily recognized. It should be stressed that other cardiac anomalies, characterized by severe hypoplasia of left cardiac sections, that are unable to support systemic circulation [32] are included under the term "HLHS." These are represented by some forms of critical aortic stenosis, by the Shone complex (which is characterized by anomalies of the mitral valve, coarctation of the aorta, and subaortic stenosis), and by unbalanced AVSD with marked right ventricular dominance. Aortic coarctation is associated in 70% of cases of HLHS.

Ultrasound diagnosis. On the *four-chamber view*, either a small globular ventricle with endocardial fibroelast - sis (Figure 5.46a) or a slitlike ventricle (mitral and aortic atresia; Figure 5.46b and c) is detected on the left side of the heart. By definition the hypoplastic left ventricle *never* reaches the apex of the heart (Figure 5.46). The mitral valve is atretic or with a hypoplastic annulus. On the *long-axis view of the left ventricle*, it is possible to observe with difficulty a threadlike ascending aorta and the extremely hypoplastic annulus of the aortic valve. On the *four-chamber view*, color Doppler confirm the absence of filling of the left ventricle (Figure 5.46c) and demonstrates reverse (left-to-right) flow across the foramen ovale and mitral regurgitation in those cases characterized by a patent and dysplastic mitral valve.

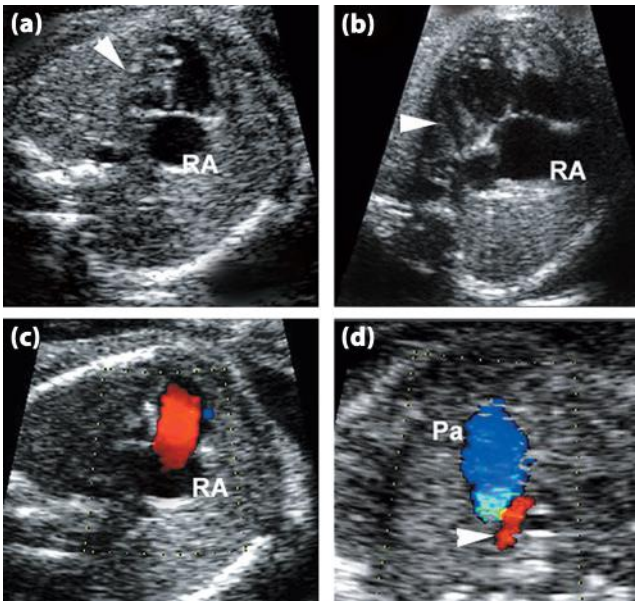


Figure 5.46 Hypoplastic left heart syndrome. (a) At 22 weeks of gestation, on the four-chamber view, the severe hypoplasia of the left ventricle, transformed into a virtual cavity due to the mitral atresia (arrowhead), is evident. (b) At 32 weeks of gestation, there is severe hypoplasia of the left ventricle, which is slitlike (arrowhead). (c) In the same case as in (a), color Doppler demonstrates the mitral atresia (absence of left ventricular filling). (d) On the three-vessel view, the reverse flow across the hypoplastic aortic arch (in red, arrowhead) (associated tubular hypoplasia) confirms the aortic atresia.

On the *three-vessel view*, color Doppler demonstrates the retrograde flow in the hypoplastic aortic arch (Figure 5.46d). Finally, it should be underlined that, due to the severity of the anomalies, HLHS is among the CHDs that may also be diagnosed at 12–16 weeks. Spectral Doppler may be used to support a diagnosis of restrictive foramen ovale by showing an abnormal pulmonary venous blood flow pattern, with a negative A wave. 4D echocardiography does not play a significan diagnostic role in this type of CHD.

Differential diagnosis. The differential diagnosis between critical aortic stenosis, severe coarctation, and HLHS may be difficult at times. Failure to demonstrate forward blood flow across the mitral or aortic valve favors the diagnosis of HLHS.

Prognostic indicators. The cases in which the size of the ascending aorta is more than 2 mm at birth can be selected for Norwood correction. However, most of the cases detected in utero do not belong to this group, having a severely hypoplastic threadlike ascending aorta. Furthermore, even though most fetuses with HLHS have a widely patent interatrial communication, in approximately 10%–20% of cases, there is an intact or highly restrictive foramen ovale. Prenatal echocardiographic diagnosis of atrial septal restriction is associated with a poor prognosis in the fetus. An abnormal pattern of pulmonary venous flow (namely, a decrease in the ratio of forward-to-reverse flow in the pulmonary veins) has been described as a marker of elevation in left atrial pressure [33].

Natural history. HLHS can occur as such from the beginning or can be the final evolved stage of critical aortic stenosis and, rarely, of aortic coarctation. In addition, there are anecdotal cases reported by centers of proven experience where a diagnosis of a normal heart at echocardiography performed at 20 weeks was followed by the recognition of HLHS in the third trimester.

Association with other malformations. Cardiac anomalies (dextrocardia and tricuspid dysplasia) and extracardiac anomalies (vertebral, urinary, and gastrointestinal anomalies) are associated in 15%–20% of cases.

Risk of chromosomal anomalies. This is relatively high (up to 15%) in the fetus, but it is lower in postnatal life (3%–4%). The most frequent chromosomal anomaly is monosomy X (45X), followed by trisomies 18 and 21.

Risk of nonchromosomal syndromes. This is low.

Obstetric management. Should HLHS be detected in the fetus, karyotyping is mandatory because of the high risk of aneuploidy. In the case of continuation of pregnancy, delivery should be planned in a tertiary referral center, as the systemic circulation is ductus dependent due to the aortic atresia.

Postnatal therapy. HLHS represents a neonatal emergency and therefore should be managed by infusion of prostaglandin E1 to keep the ductus patent until surgery. Severe atrial restriction remains almost uniformly lethal in the neonatal period; there have been reports of success with early balloon septostomy, atrial stent placement, or surgical septectomy in stabilizing the neonate with atrial septal restriction prior to surgery [34].

Surgical solutions to HLHS are neonatal heart transplantation or a series of palliative operations aiming in the beginning at reconstructing the systemic ventricular outflow using the only residual ventricular pump, represented by the right ventricle. However, as underlined here, a high proportion of fetal cases are excluded from any type of surgery because of the extreme degree of aortic hypoplasia. The three-stage Norwood palliation converts the cardiac system into a univentricular heart with

the systemic circulation supported by the reconstructed right ventricle, the Fontan circulation. The Norwood procedure is performed in three stages. **Stage I**, which is carried out soon after birth, consists of a complex prosthetic reconstruction of the entire ascending aorta, the arch, and the aortic isthmus, obtained by connecting the trunk of the pulmonary artery with the neo-aorta (after separation of the bifurcation of the pulmonary branches) and creating a pulmonary systemic shunt. **Stage II** is done at three–six months of age and consists of a direct terminolateral anastomosis between the superior vena cava and the right pulmonary artery: bidirectional cavopulmonary anastomosis. In **Stage III**, the two circulations are completely separated, directing the blood coming from the inferior vena cava toward the pulmonary arteries, usually through an extracardiac duct (total cavopulmonary).

Prognosis, survival, and quality of life. Despite the recent brilliant achievements of pediatric cardiosurgery, HLHS continues to be the congenital cardiac defect with the highest mortality. In the neonatal series, mortality rates between HLHS Stage I and Stage II surgery are significant and range from 5% to 10%, while surgical outcomes after Stages II and III are quite good, with close to 99% survival. Survival for the fetus diagnosed with HLHS is quite variable around the world, with recent reports describing continued poor outcome, with an overall survival rate below 40% [35]. The discrepancy between these data is justified by the fact that the neonatal series include a selected population of *ideal* candidates for the Norwood procedure, and not all neonates born with HLHS. In fact, a significant proportion of neonates with HLHS die before reaching a cardiology unit, and this presurgical mortality is often not accounted for in the surgical series. In addition, differences in patient selection may also influence survival statistics. A number of categorical risk factors are associated with poor prognosis in the fetus: the presence of any extracardiac, anatomic, genetic, or chromosomal anomalies; prematurity; and fetal echocardiographic identification of additional cardiac findings such as an intact or highly restrictive atrial septum. In a recent series of 240 fetuses, with a prenatal diagnosis of HLHS, overall survival was 65%–79% in the low-risk group versus 37% in the high-risk group. Increased early mortality in the high-risk group appears to occur in two phases: first there is a high rate of unexpected death, either intrauterine fetal demise or postnatal death prior to surgical intervention; second, survival of the Norwood surgery itself is much worse in the high-risk group [34].

Aor TIc sTENos Is

Incidence. About 3% of CHD.

Ultrasound diagnosis. On the *long-axis view of the left ventricle*, the aortic valvular cusps appear thickened and hypomobile; occasionally, a hypoplastic annulus and/or poststenotic dilation is present. On the *4-chamber view*, dilated hypocontractile left ventricle with endocardial hyperechoic lining consistent with fibroelastosis.

Risk of chromosomal anomalies. Low in the valvular form.

Risk of nonchromosomal syndromes. Low in the valvular form.

Outcome. Unfavorable in the critical forms already evident in the second trimester.

Definition Obstructions to left ventricular outflow can be classified on the basis of the site of the obstruction into valvular, subvalvular, and supravalvular stenosis. The single variant that is consistently detected in the fetus is the valvular one; in this case, the valvular ring is often of normal size, and the stenosis is the result of the valvular dysplasia.

Anatomy. In *valvular stenosis*, the anatomy of the valve may be completely distorted, with dysplastic cusps of mucoid appearance, or mostly preserved, with distinct valvular cusps that are fused along the commissures. The valve may have three cusps, be bicuspid, or, exceptionally, be mono- or quadricuspid. When associated with other anomalies of the left heart, the annulus is frequently hypoplastic. The spectrum of aortic stenosis varies from an isolated mild lesion to a severe lesion, critical aortic stenosis, which may lead to a HLHS [36,37].

Ultrasound diagnosis. The US picture of aortic valvular stenosis depends on the severity of the obstruction. On the *four-chamber view*, in moderate to severe aortic stenosis, the left ventricle appears globose and

hypertrophic, with a good systolic function. In critical aortic stenosis, the picture depends on the function of the mitral valve: if the mitral valve is damaged, either concurrently or secondary to the aortic valve lesion, then severe atrioventricular insufficiency is present, and this leads to severe left atrial enlargement (Figure 5.47a); if, on the contrary, the mitral valve is hypoplastic, then the valve is almost closed and only a reduced regurgitation is present (Figure 5.47b). The left ventricle is usually globose and dilated, and its contractility is severely impaired. In these cases, the ventricular endocardium and, to a lesser extent, the papillary muscles of the mitral valve are brightly hyperechoic because of secondary ischemia-induced fibroelastosis (Figure 5.47c). On the *long-axis view* of the left ventricle, the aortic valvular cusps appear thickened and almost immobile (Figure 5.47d). Occasionally, a poststenotic ectasia of the ascending aorta is seen, although, in the most severe forms, this vessel is frequently hypoplastic. In *critical aortic stenosis*, color Doppler can be used to assess mitral regurgitation (Figure 5.47b) and to reveal inversion of the interatrial shunt on the *four-chamber view*. It also allows demonstration of retrograde flow in the aortic arch on the *three-vessel view*. In *moderate to severe aortic stenosis*, color Doppler demonstrates, on the *long-axis view* of the left ventricle, the turbulent flo across the stenotic aortic valve. Spectral Doppler may be used to quantify the pressure gradient in moderate to severe aortic stenosis. Four-dimensional echocardiography may be used to demonstrate the impaired contractility and the severe dilation of the left ventricle in the most severe cases.

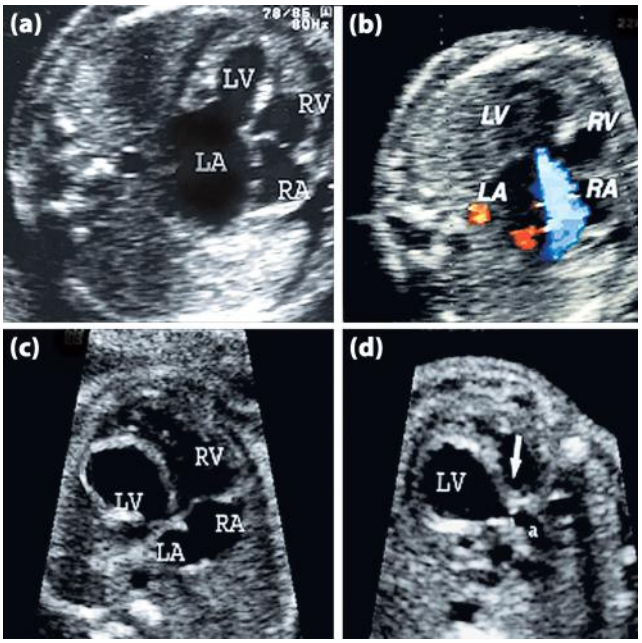


Figure 5.47 Critical aortic stenosis. Four-chamber view. (a) Variant associated with severe mitral dysplasia and insufficiency: the mitral valve apparatus is abnormal and hyperechoic, and the insufficiency determines the atriomegaly. (b) Color Doppler demonstrates the insufficiency of the mitral valve. (c) Variant associated with severe mitral stenosis: the extremely high intraventricular pressure, due to simultaneous obstruction of the mitral and aortic valves, leads to endocardial fibroelastosis (hyperechoic rim of the left ventricle) and dilation of the ventricle. (d) Direct evidence of severe annular stenosis is obtained from the left outflow view, which shows a moderately hypoplastic ascending aorta (a) and severe narrowing of the annulus (arrow). LA: left atrium; LV: left ventricle; RA: right atrium; RV: right ventricle.

Differential diagnosis. Isolated mitral dysplasia is extremely rare. Mitral regurgitation might suggest the presence of cardiomyopathy, but in this case the cardiac anatomy is unremarkable. Critical aortic stenosis and some forms of HLHS constitute a continuum, and thus a HLHS should be considered in the differential diagnosis. In HLHS, instead of critical aortic stenosis, the left ventricle never reaches the apex of the heart.

Prognostic indicators. Poor prognostic signs are the presence of endocardial fibroelastosis and an association with other anomalies of the left heart (Shone complex). In addition, progression of aortic stenosis to HLHS from the first to the second trimester [38] and from the second to the third trimester [39] has been reported. Abnormal features associated with progression to HLHS include (1) retrograde flow in the transverse aortic arch, (2) severe LV dysfunction, (3) monophasic and short mitral valve inflo , and (4) left-to-right flow across the foramen ovale [40].

Association with other malformations. In about 30%–40% of cases, aortic valvular stenosis is associated with mitral anomalies, subvalvular aortic stenosis, and aortic coarctation. Association with extracardiac anomalies is exceedingly rare.

Natural history. Aortic stenosis tends to progress during fetal life: the degree of obstruction can worsen, or it can evolve into a hypoplastic left heart [36,38,39]. US and Doppler findings heralding progression to HLHS are those listed elsewhere in this section [40].

Risk of chromosomal anomalies. This is low in the valvular form.

Risk of nonchromosomal syndromes. This is low in the valvular form.

Obstetric management. The evolving nature of critical aortic stenosis should be considered during prenatal counseling, especially with regard to the possibility of achieving a biventricular repair. In critical aortic stenosis, karyotyping is not mandatory and should be discussed with the parents. In the case of continuation of pregnancy, delivery should be planned in a tertiary referral center, in order to ensure adequate neonatal management. In fact, critical aortic stenosis is often ductus dependent.

Postnatal treatment. After birth, the key point, after removal of the valvular obstruction, is to evaluate whether or not the left ventricle will be able to maintain the systemic circulation. In fact, the surgical approach and the ultimate prognosis will depend on this parameter.

Prognosis, survival, and quality of life. In aortic stenosis, the prognosis depends on the severity and the gestational age at which the diagnosis is made. In fact, analysis of major prenatal case series reveals a truly ill-fated prognosis for cases of critical aortic stenosis recognized in the second trimester, with a significant risk of fetal death and low survival beyond the neonatal period [36,37]. After birth, the prognosis depends on the capability of the left ventricle to support the systemic circulation after removal of the obstruction of the left outflo . In the more favorable forms, the midterm mortality rate is as low as 10%. The marked difference in terms of mortality and morbidity among prenatal and postnatal cases is related to the greater severity of the lesions disclosed during the second trimester of pregnancy.

Recently, the option of in utero aortic valvuloplasty has been proposed to avoid progression of the midgestation fetal aortic stenosis into HLHS [39,40]. The goal of in utero valvuloplasty for aortic stenosis with evolving HLHS is to alter left heart physiology and growth to allow postnatal survival with a healthy biventricular circulation. In recently published experience, over 30% of patients who underwent technically successful aortic valvuloplasty for this indication had a biventricular circulation from birth, and another 8% were converted to a biventricular circulation after initial univentricular palliation [40]. However, fetal aortic valvuloplasty carries a significant risk of fetal demise. Furthermore, it has been shown that selection of possible candidates to prenatal treatment is very important: fetuses undergoing in utero aortic valvuloplasty with an unfavorable multivariable threshold score at the time of intervention are very unlikely to achieve a biventricular circulation postnatally [40].

c o Arc TATIo N o F ThE Aor TA

Incidence. About 4%–5% of CHD.

Ultrasound diagnosis. *Indirect signs*: significant prevalence of right cardiac sections over left ones and a prevalence of the pulmonary artery with respect to the ascending aorta. *Direct signs*: reduced size of the transverse aortic arch in comparison with the ductal arch.

Risk of chromosomal anomalies. Extremely high: 29%.

Risk of nonchromosomal syndromes. Relatively low.

Outcome. Good in isolated cases, especially if the transverse part of the arch is not involved.

Definition Coarctation of the aorta refers to an area of narrowing of the thoracic aorta in the region of insertion of the arterial duct, most commonly between the left subclavian artery and the ductus arteriosus (isthmus). Commonly, coarctation of the aorta encompasses a spectrum of lesions, ranging from segmental narrowing to severe tubular hypoplasia of the whole transverse arch. In particular, tubular hypoplasia refers to a uniform narrowing of the transverse arch, whereas segmental coarctation is usually determined by a localized shelf-like lesion, often with a degree of proximal tapering of the aortic arch toward the lesion; the two lesions are often associated [41].

Anatomy. From the anatomic standpoint, discrete coarctation is characterized by a posterior eccentric fold (posterior shelf) inside the isthmus, opposite to the orifice of the arterial duct. When this closes at birth or soon afterward, it causes further narrowing of the aortic lumen. In 30%–40% of cases, coarctation is

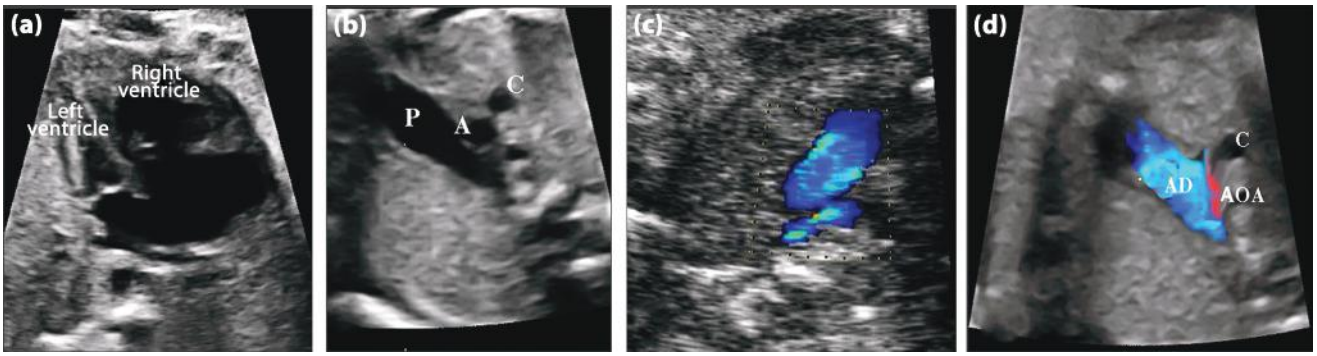


Figure 5.48 Coarctation of the aorta. (a) On the four-chamber view, the ventricular disproportion, which is an indirect sign of coarctation, is evident (the right ventricle is larger than the left). (b) The three-vessel view demonstrates the severe narrowing of the aorta (A), between the pulmonary artery (P) and the superior vena cava (C). (c) In this case, the coarctation was severe: the extreme discrepancy between the size of the ductal arch (DA) and that of the hypoplastic transverse part of the arch (AO) is evident. (d) In this case of critical coarctation (tubular hypoplasia), on color Doppler, a complete inversion of the flow in the distal part of a hypoplastic aortic arch (AOA) can be seen. AD: ductal arch.

an isolated heart defect (above all in infant and child forms), but in the remaining 60%–70% of cases, which account for the great majority of symptomatic patients in the first month of life, other cardiac anomalies (VSD, aortic and mitral valve anomalies, transposition of the great arteries, and DORV) are associated.

Ultrasound diagnosis. Even with good visualization of the fetal aortic arch, prenatal diagnosis of discrete coarctation is very difficult if not impossible. However, when associated with tubular hypoplasia of the entire arch, the US diagnosis is less difficult and can be reasonably made during the prenatal period. Sonographic findings possibly suggesting the presence of coarctation include direct and indirect signs, the latter being burdened with a significant percentage of false positives.

Indirect signs include a significant prevalence of the right cardiac sections over the left ones on the *four-chamber view* (Figure 5.48a) and of the pulmonary artery over the ascending aorta on the *outflow views* and on the *three-vessel view* (Figure 5.48b). *Direct signs* of coarctation, when possible, can be gathered by assessing the *three-vessel and trachea view*: on this plane, the ductal arch appears significantly larger than the aortic arch (Figure 5.48c). The transverse part of the aortic arch is severely reduced in size, especially if tubular hypoplasia of the whole arch is present (Figure 5.48c). On color Doppler, a complete or partial inversion of the flow in the distal part of the arch and/or in the ascending aorta (Figure 5.48d) and a left-to-right interatrial shunt can be seen. However, it should be recalled here that prenatal diagnosis of coarctation of the aorta remains challenging [14,15,40], with a high rate of false-positive and false-negative diagnoses. Spectral Doppler is of little use in coarctation but it may be employed to detect abnormal flow at the isthmus level. Four-dimensional echocardiography may be used to assess the discrepancy in the size of the aortic and ductal arches (Figure 5.49).

Artifacts. Particular attention should be paid when evaluating the aortic arch on longitudinal views in order to not mistake, in the case of severe coarctation, the prevalent and dilated ductal arch for a normal aortic arch. This is why the three-vessel and trachea view is currently the preferred option for the comparative assessment of the ductal and aortic arches.

Differential diagnosis. The marked prevalence of the right heart sections over the left on the *four-chamber view*, present in the critical form of coarctation, should be differentiated from HLHS and from TAPVC (see the Anomalous Pulmanary venous connection, page 156–158). However, the former is characterized by a sealed or atretic mitral valve, which is mainly normal in coarctation. In addition, color Doppler confirms normal left ventricular filling in diastole and thus differentiates aortic coarctation from HLHS. As far as TAPVC is concerned, the recognition of a single pulmonary vein entering the left atrium on color Doppler rules out this diagnosis. On the *aortic arch views* (transverse and longitudinal), coarctation should be differentiated from IAA: in the latter case, a malalignment VSD is almost always associated.

Prognostic indicators. Unfavorable prognostic indicators include the presence of other anomalies of the left

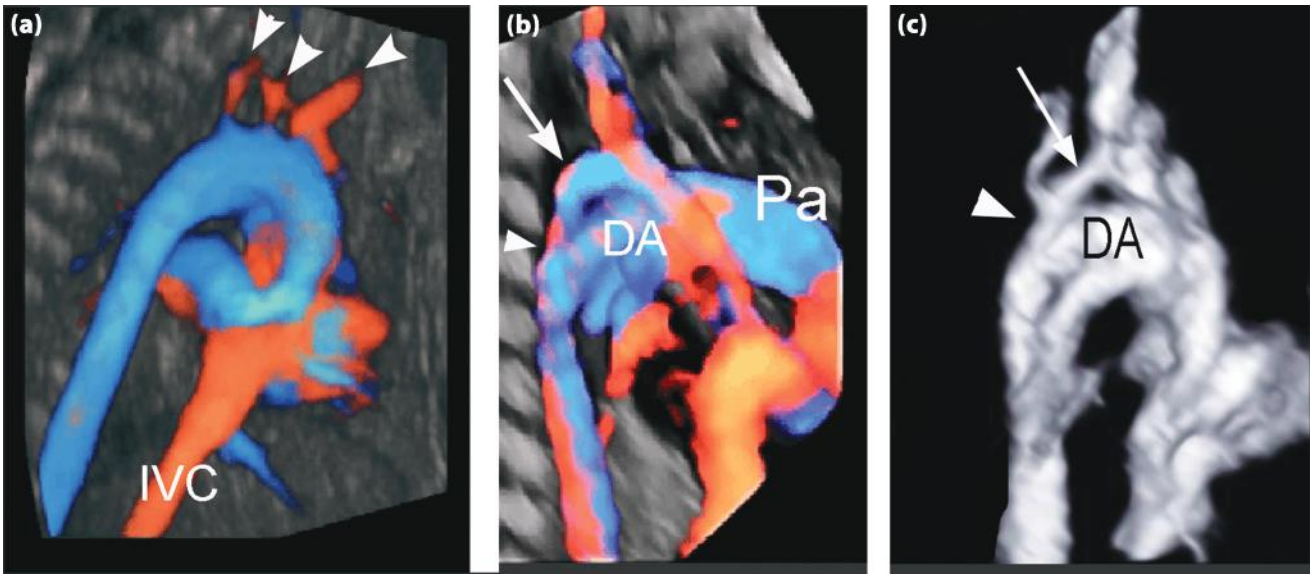


Figure 5.49 Coarctation of the aorta. Four-dimensional echocardiography (STIC) contributes to the characterization of aortic coarctation. Volumes should be acquired with a longitudinal ventral approach for adequate imaging. (a) Normal fetus at 22 weeks of gestation. Glassbody rendering shows the normal size of the aortic arch and the three neck vessels (arrowheads). The isthmic tract shows no indentation or reduction in caliber. (b) In a fetus with aortic coarctation (26 weeks of gestation), the same view demonstrates the tapered, hypoplastic aortic arch (arrow) and the much greater size of the ductal arch. The arrowhead indicates the shelf. (c) In another case of severe aortic coarctation, B-flow demonstrates (even more clearly than with glassbody) both the tapering (arrow) and the shelf (arrowhead), which represent classic findings in severe aortic coarctation. DA: ductal arch; IVC: inferior vena cava; Pa: pulmonary artery.

heart as well as association with extracardiac anomalies and low birth weight [43].

Associations with other malformations. Coarctation is often associated with other malformations of the left heart and with VSD [14,15,41–43]. In the presence of mitral valve anomalies and subaortic stenosis, it can be part of Shone syndrome. The presence of a persistent left superior vena cava has also been associated with coarctation of the aorta. Extracardiac malformations are frequently associated with coarctation (25%–30% of cases): these include urinary, gastrointestinal, central nervous system, and facial anomalies.

Risk of chromosomal anomalies. This is high, reaching 29% [42,43]—mainly monosomy X, but also trisomies 21 and 18 and 22q11 microdeletion.

Risk of nonchromosomal syndromes. This is relatively low.

Obstetric management. A detailed anatomic scan should be performed by an expert to exclude the presence of extracardiac anomalies. Karyotyping is indicated because of the high risk of chromosomal disorders. If there is a suspicion of any anomaly of the aortic arch, delivery should be planned in a tertiary referral center, in order to allow early transfer of the newborn to the pediatric cardiology unit for fina diagnosis and correct neonatal management; in fact, critical coarctation of the aorta is a ductus-dependent defect.

Postnatal treatment. The surgical techniques commonly used are resection of the coarcted tract with termino-terminal and terminolateral anastomoses, a subclavian flap and widened aortoplasty. Long-term follow-up studies (>five years) have reported a 20% recoarctation rate.

Prognosis, survival, and quality of life. The overall prognosis depends on the severity of the lesion, on the presence of associated cardiac and extracardiac lesions that can significantly influence operative mortality and the life expectancy, and on correct perinatal management. The overall mortality rate is less than 5% for isolated coarctation. In symptomatic neonatal cases with associated cardiac lesions, the mortality rate is about 20%, ranging from 2% in cases associated with VSD to 40% in cases associated with complex cardiac anomalies or when the preoperative clinical condition is poor.

INTErr UpTIoN o F ThE Aor TIc Arch

Incidence. About 1% of CHD.

Ultrasound diagnosis. *Indirect signs*: discrepancy in ventricular and great artery size is present in IAA type A and C (prevalence of the right ventricle over the left and of the pulmonary artery over the ascending aorta), whereas in type B, only a discrepancy in great vessel size is observed (prevalence of pulmonary artery over the ascending aorta). *Direct sign*: visualization of lack of continuity of the aortic arch on upper mediastinal views.

Risk of chromosomal anomalies. High (22q11 microdeletion).

Risk of nonchromosomal syndromes. Low.

Outcome. Preoperative death occurs in 5% of cases, and the survival rate at four years after repair is 63%.

Definition IAA is a rare, severe form of CHD characterized by complete anatomic discontinuity between two adjacent segments of the aortic arch.

Anatomy. IAA can be subdivided into three groups according to the site of interruption:

- *Type A*: the interruption is distal to the left subclavian artery;
- *Type B*: the interruption is between the left common carotid and left subclavian arteries;
- *Type C*: the interruption is between the innominate artery and the left common carotid artery.

Ultrasound diagnosis. Prenatal diagnosis of IAA and its subtypes depends on the observation of some reliable anatomic indicators that point to the correct differential diagnosis [44,45]. Since a significant number of cases of IAA type A and C have a left-right ventricular discrepancy, which is easily visualized on the *four-chamber view*, this sign should be considered as a hint to check the great vessels. In fact, angling toward the outflow tracts to image the great vessels reveals a significant discrepancy in the size of the great arteries and, in most cases, a VSD. In particular, the ascending aorta is significantly smaller than the main pulmonary artery. It should be noted that if the VSD is large and malaligned, as in IAA type B, only a significant discrepancy in great vessel size is observed. As for coarctation of the aortic arch, care must be taken on the longitudinal view not to mistake the prevalent ductal arch for a normal aortic arch. Again, the three-vessel and trachea view is the reference plane for detecting aortic arch anomalies. With regard to US differentiation of the various subtypes, type B can be difficult to distinguish from type A. In type B, the ascending aorta has a straighter course to the innominate and left carotid arteries, the typical "V" shape (Figure 5.50) [45], whereas in type A, there is a slight curvature after the origin of the innominate artery (Figure 5.51) [42] related to the persistence of the aortic arch segment between the origin of the left carotid and subclavian arteries [45]. A conal malalignment VSD with a leftward and posterior displacement of the conal septum is typically found in most cases of IAA, especially type B. In addition, as reported here, discrepancy in ventricular and great artery size is usually present in the setting of IAA type A and C, whereas in type B only a discrepancy in great vessel size is observed. The use of color Doppler may facilitate assessment of the continuity (or absence there of) of the ascending aorta with the descending part; it also facilitates assessment of the course of the ascending aorta and neck vessels. Spectral Doppler is of limited use, while 4D echocardiography has been demonstrated to facilitate the assessment of aortic arch anomalies, especially with B-flow [45]

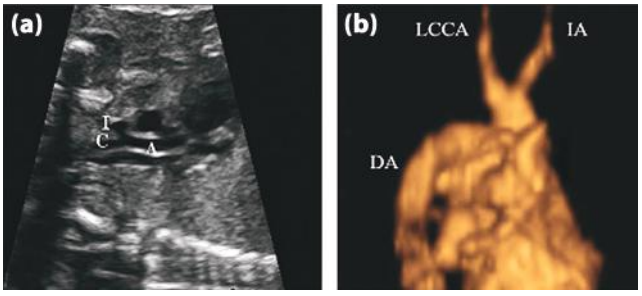


Figure 5.50 Interruped aortic arch (IAA), type B in a 21-week fetus. (a) Two-dimensional (2D) echocardiography showing how the ascending aorta (A) fails to curve, but courses straight, to divide into the innominate artery (I) and the left common carotid artery (C). (b) STIC-derived B-flow imaging shows the typical "V"-shaped configuration of the interrupted arch, due to the straight course of the ascending aorta bifurcating into the innominate artery (IA) and the left common carotid artery (LCCA). DA: descending aorta. (Modified from Volpe P et al., *Ultrasound Obstet Gynecol* 35, 302–9, 2010.)

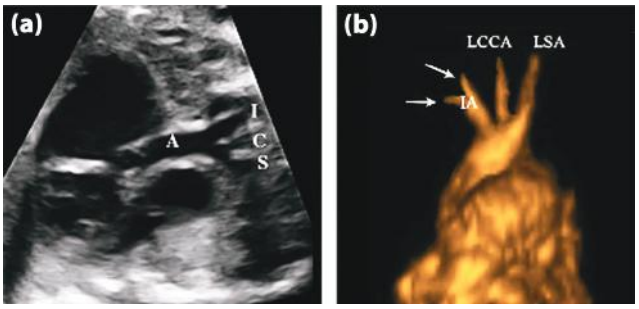


Figure 5.51 Interrupted aortic arch (IAA), type A, in a 24-week fetus. (a) Two-dimensional echocardiography showing slight curvature of the ascending aorta (A) after the origin of the innominate artery (I), related to the persistence of the aortic arch segment between the origin of the left carotid (C) and subclavian (S) arteries. (b) B-flow and spatiotemporal image correlation clearly showing a typical "W"-shaped configuration due to the aspect of the innominate artery (IA), the left common carotid artery (LCCA), and the left subclavian artery (LSA). The arrows indicate the right common carotid artery and the right subclavian artery. (Modified from Volpe P et al., *Ultrasound Obstet Gynecol* 35, 302–9, 2010.)

Differential diagnosis. It is possible to distinguish between IAA and coarctation of the aorta on US. In IAA, the ascending aorta runs with a straight course to its branches, unlike coarctation, where the aortic curvature is present, or even accentuated, and there is continuity with the descending aorta in any event.

Association with other malformations. VSD is almost always present. A right aortic arch (RAA) and anomalies of the left ventricular outflow are frequently associated in type B. Association with extracardiac anomalies (central nervous system, urinary, gastrointestinal, and facial) is more frequent in type B.

Risk of chromosomal anomalies. Type B IAA is associated with microdeletion 22q11 in about 50% of the cases, both prenatally and postnatally [44,46,47]. In fact, type B is usually syndromic, being the most common cardiac defect occurring in DiGeorge syndrome, a developmental disease characterized by thymic and parathyroid gland hypoplasia and aplasia associated with conotruncal malformations and due to the 22q11 microdeletion (see Chapter 10). The other subtypes of IAA are rarely associated with chromosomal anomalies.

Risk of nonchromosomal syndromes. This is low.

Obstetric management. Should IAA be detected in a fetus, a thorough anatomic scan should be carried out by an expert to detect possible additional anomalies, such as thymus hypoplasia, which increase the risk of 22q11 microdeletion even more [48,49]. Fetal karyotyping with FISH analysis for the 22q11 microdeletion is indicated in type B IAA. Timing and mode of delivery are unchanged, but the delivery should be planned in a tertiary referral center in order to reach a definite diagnosis and to adequately manage the situation in the neonatal period.

Postnatal treatment. The surgical management of IAA is controversial. Primary anastomosis and patch aortoplasties combined with end-to-end anastomosis have significant complications, including recurrence and aneurysm formation. Pulmonary autograft patch aortoplasty together with end-to-side anastomosis comprise an alternative approach to surgical management and do not require cardiopulmonary bypass. In a large case series [41], preoperative death occurred in 5% of cases, and the survival rate at four years after repair was 63%.

Prognosis, survival, and quality of life. Risk factors for postinterventional death are low birth weight and major associated cardiac anomalies. The discrepancies among the clinical features and, above all, the remarkable difference with regard to association with the 22q11 microdeletion suggest that type A and type B IAA could be two separate pathogenetic entities, with the latter type carrying a poorer prognosis.

Aor TIc Arch A No MALIEs (r IGh T Aor TIc Arch, d o UBLE Aor TIc Arch, ANd VAsc ULAr rING)

Incidence. Rare.

Ultrasound diagnosis. On the *three-vessel and trachea view*: *right aortic arch*: aortic arch on the right of the trachea; *double aortic arch*: "N" shape with bifurcation of the aortic arch in front of the trachea; *vascular ring*: abnormal retrotracheal vessel.

Risk of chromosomal anomalies. Relatively high for the right aortic arch with aberrant subclavian artery and for the double aortic arch (22q11 microdeletion).

Risk of nonchromosomal syndromes. Relatively low.

Outcome. Excellent in the case of isolated anomalies; if associated with major CHDs, final outcome will depend on the severity of these.

Definition Aortic arch anomalies comprise a variety of congenital abnormalities of the position, branching pattern, or both of the aortic arch. They result from aberrant development of one or more components of the embryonic pharyngeal arch system. These anomalies can be divided into those that cause a vascular ring around the trachea and esophagus, usually determining compression of both structures, and those that do not.

Anatomy. The left or right position of the aortic arch is defined in relation to the mainstem bronchus, which is crossed by the descending thoracic aorta, and does not refer to the side of the midline on which the aorta descends. In the left aortic arch, the descending thoracic aorta crosses over the left mainstem bronchus and descends left to the midline along the spine. Three vessels arise from the aortic arch: first the innominate artery branching into the right carotid and right subclavian arteries; second, the left carotid artery; and, third, the left subclavian artery. Usually, the first aortic arch vessel gives rise to the carotid artery, which is opposite to the side of the aortic arch (i.e., the right carotid artery in the left aortic arch and the left carotid artery in the right aortic arch (RAA)). The ductus arteriosus joints the aorta distal to the origin of the left subclavian artery. Normally, the ductus arteriosus can left-sided, bilateral, or right-sided. A RAA occurs in about 1 in 1000 of the general population.

The most common types of RAA *branching* are as follows:

- Mirror-image branching (left innominate artery, right carotid artery, and right subclavian artery);
- Retroesophageal left (aberrant) subclavian artery with a normal caliber;
- Retroesophageal diverticulum of Kommerell.

In the first case (mirror branching), the RAA is associated with major CHD (especially TOF) nearly 90% of the time. Usually, in this case the ductus arteriosus courses to the right of the trachea, and, therefore, there is no vascular ring. In fact, the presence or absence of a *vascular ring* in the setting of a RAA depends on the branching of the brachiocephalic vessels and the location of the ductus arteriosus: if these are located on the left of the trachea, this will create the retrotracheal sling; and, vice versa, if the ductus arteriosus courses to the right of the trachea, together with the right-sided aortic arch, then there is no vascular ring.

In the other two cases (i.e., with a retroesophageal left [aberrant] subclavian artery with or without a retroesophageal diverticulum of Kommerell), the RAA is associated with a left-sided ductus arteriosus. In this condition, the trachea is positioned between the transverse aortic arch and the ductus arteriosus, which represent the vascular ring (or retrotracheal sling). Commonly, this condition is associated with an aberrant course of the left subclavian artery, commonly from a retroesophageal diverticulum situated at the junction of the ductus arteriosus with the descending aorta, called a Kommerel diverticulum. This branching pattern is not usually associated with a major cardiac malformation. The tighter vascular ring is represented by the *double aortic arch*. In this case, both right and left aortic arches are present: the ascending aorta splits into two limbs, which encircle the trachea and esophagus to join at the level of the descending aorta. As to the size of the two aortic arches, the most common arrangement is with hypoplasia of the left arch, but cases with hypoplasia of the right arch or normal size of both have also been described. This anomaly is commonly associated with a patent ductus arteriosus.

Ultrasound diagnosis. As described here, the aortic arch can be examinated on the *three-vessel and trachea view* (Figure 5.52) [50]. A RAA is diagnosed when the transverse aortic arch is located to the right of the trachea on this axial view of the mediastinum. If the ductus arteriosus is left-sided, the RAA and the left ductal arch form a U-shaped configuration with the trachea located between them (Figures 5.9d, 5.10d, and 5.52b) [47–49]. In addition, any branch coursing behind the trachea (e.g., a right aberrant subclavian artery) should be considered as an abnormal aberrant branch (Figure 5.52d). Color Doppler is extremely useful to trace the course of the abnormal vessels in the upper mediastinum (Figure 5.52). Spectral Doppler may be used to differentiate the innominate vein from arterial vessels (e.g., aberrant subclavian arteries) [50] (see also Chapter 1). Four-dimensional echocardiography permits an easier diagnosis of all aortic arch anomalies. B-flow and, to a lesser extent, inversion mode are the renderings of choice.

Association with other malformations. RAA with mirror-image branching is often associated with other complex cardiac anomalies (TOF and CATs). VSD is the cardiac anomaly most commonly associated with a vascular ring.

Risk of chromosomal anomalies. This is relatively high. Vascular ring and isolated RAA can be associated with the 22q11 microdeletion [50].

Risk of nonchromosomal syndromes. This is low in cases of vascular ring.

Obstetric management. For isolated RAA, the option of fetal karyotyping with a FISH analysis for the 22q11 microdeletion should be discussed with the patient.

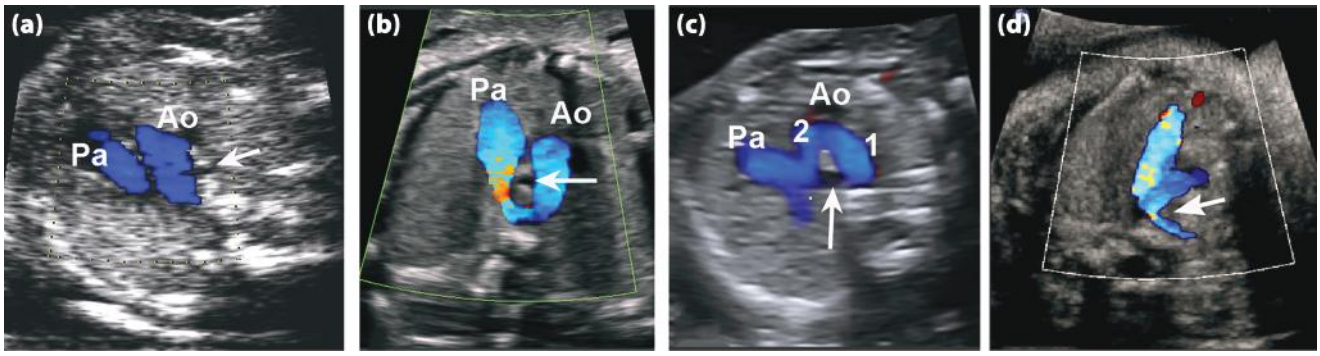


Figure 5.52 Aortic arch anomalies: three-vessel and trachea view. (a) In the normal spatial relationships, the trachea (arrow) is located on the right of the aortic arch. (b) In a right aortic arch, the trachea (arrow) is located between the aortic and ductal arches. Sometimes, as in this case, a retrotracheal vessel (sling) can be identified. (c) In a double aortic arch, the arches feature an upside-down "N," with the oblique bar of the "N" (2; 1 represents the first arch) representing the second arch. The trachea (arrow) in this case is located between the two aortic arches, although several spatial arrangements are possible. (d) In some cases, the aortic arch is normally positioned on the left of the trachea (arrow), but the neck vessels can have an abnormal origin and course. In this case, there was an aberrant retrotracheal right subclavian artery (arrowhead). See this chapter's text for details. Ao: aortic arch; Pa: pulmonary artery and ductus arteriosus.

Prognosis, survival, and quality of life. Vascular rings encircle the trachea and the esophagus, which can determine symptomatic compression of both structures, especially in cases of double aortic arch. Compression of the trachea causes upper airway obstruction that impairs inspiratory and, to a lesser degree, expiratory airflo . The extent of respiratory impairment depends upon the severity of compression, which can vary considerably. In addition to the airway symptoms, patients may experience swallowing problems related to the esophageal compression. The prognosis of patients with vascular rings depends on several factors, including the severity of tracheal and esophageal compression and the association with other cardiac and extracardiac anomalies.

TETr ALo Gy o F FALLo T

Incidence. Accounts for about 7%–9% of CHD in infants.

Ultrasound diagnosis. On the *long axis of the left ventricle*: an anterior malalignment VSD with overriding aorta. Sweeping further cephalad from this view, a small pulmonary artery should be detected.

Risk of chromosomal anomalies. High: 20%.

Risk of nonchromosomal syndromes. Relatively high.

Outcome. Good or extremely good in isolated cases. Poor if chromosomal and/or extracardiac anomalies are associated or in the case of unfavorable cardiac anatomy.

Definition TOF is a cardiac malformation characterized by the following:

- Subaortic VSD caused by malalignment between the infundibular and the trabecular septum;
- An aorta overriding the VSD;
- Obstruction of varying severity of the right outflow tract;
- Consequent hypertrophy of the right ventricle (after birth).

Its incidence reaches 9%–11% after birth, but due to the prevalence of complex cardiac anomalies, its incidence in utero is reduced to about 3%.

Anatomy. The extent of the anatomic obstruction to the right outflow tract is determined by the degree of deviation of the infundibular septum, the hypertrophy of the septum and anterior wall of the right ventricle, and the association of pulmonary valvular stenosis. In the fetus, because of the frequent absence of pulmonary stenosis

and the presence of physiologic shunts, the tetralogy often becomes a *di-* or *trilogy*, with the right ventricular hypertrophy being absent and the pulmonary stenosis present only in the more important cases and/or developing late in gestation. Although the TOF spectrum comprises numerous variants and subtypes, TOF with an absent pulmonary valve, which is characterized by severe dilation of the pulmonary trunk and branches due to severe stenosis and the insufficiency of the functionally absent pulmonary valve, certainly represents a well-known entity with an unfavorable prognosis, which needs to be addressed separately (see section "Absent Pulmonary Valve Syndrome").

Ultrasound diagnosis. As for most conotruncal anomalies, the *four-chamber view* is unremarkable, unless anomalies of the atrioventricular plane are associated. Only in TOF with absent pulmonary valve can the four-chamber view be abnormal due to the presence of cardiomegaly [51]. Classic TOF is diagnosed on the *long-axis views*. On the *long axis of the left ventricle*, a malalignment VSD with an overriding aorta can be seen (Figure 5.53a). Sweeping further cephalad from this view, on the *right outflow tract view*, the smaller pulmonary artery can be detected (Figure 5.53b). The pulmonary artery may have a diameter within the normal range, but the aorta–pulmonary artery diameter ratio will be abnormal. As mentioned here, the hypertrophy of the right ventricle is absent, whereas the infundibular stenosis is not a constant finding in the second trimester. Color Doppler can be used to demonstrate flow through the VSD toward the aorta (Figures 5.16d and 5.53c) from both left and right ventricles and flo through the smaller pulmonary outflow tract and arterial duct. In utero, it is unusual to detect pronounced acceleration of blood across the right outflow tract, even in the presence of an obvious reduction of the vessel size, due to the presence of the usually large shunt represented by the malalignment VSD. Moreover, stenosis is frequently absent at the time of diagnosis in the second trimester, but it becomes evident later on in gestation; in a few cases, a narrow pulmonary outflow may progress to atresia [52]. This is why serial US monitoring is important in order to demonstrate antegrade flow through the pulmonary artery late in gestation to exclude the potential need for prostaglandin therapy after birth. Spectral Doppler is of limited value, as is 4D echocardiography, even though there is recent evidence that a high peak systolic velocity of the pulmonary trunk may predict the need for early intervention [53]. The latter may be of help if anomalies of the aortic arch are associated.

Differential diagnosis. As already mentioned, in utero TOF cannot be differentiated from an isolated malalignment VSD if evident pulmonary stenosis is absent. Therefore, in the absence of pulmonary outflow obstruction, it is always necessary to consider the possible evolution from malalignment VSD in TOF. Another important concept is that the degree of aortic overriding is variable and cannot be fully appreciated in utero. Therefore, when the aorta emerges about 50% from the right ventricle, differentiation of TOF from a Fallot-like DORV can be difficult the two being distinguished only by the degree of aortic overriding. With regard to the differential diagnosis with other conotruncal anomalies, it should be considered that CAT and pulmonary atreria with VSD (PAVSD) share with TOF the presence of a malalignment VSD. Hence, if aortic overriding is found, the right outflow tract should be evaluated: if a small pulmonary artery is connected to the right ventricle, the diagnosis is TOF; if this is atretic, it is PAVSD; and if the pulmonary artery originates from the single emerging vessel, it is CAT (Figure 5.14).

Prognostic indicators. Unfavorable prognostic elements are the presence of extracardiac anomalies (including chromosomal anomalies), severe pulmonary artery stenosis, and the absent pulmonary valve variant (discussed in the "Absent Pulmonary Valve Syndrome" section). Recently, it has been demonstrated that a pulmonary valve peak systolic velocity > 87.5 cm/s at 19–22 weeks of gestation is highly indicative of the need for early intervention (sensitivity 100%, specificity 96%) [53]

Association with other malformations. Association with extracardiac anomalies is frequent, in particular gastrointestinal and thoracic ones (esophageal and duodenal atresia, and diaphragmatic hernia), even independently of chromosomal anomalies.

Risk of chromosomal anomalies. This is high (up to 20% in fetal case series), with equal distribution between trisomies 21 and 18 [14,15,54]. The association with microdeletion 22q11 is less frequent, unless a RAA is present. In the latter case, as well as in the variants with absence or atresia of the pulmonary valve, the association is very high (25%–35%) [51].

Risk of nonchromosomal syndromes. This is relatively high, even though there is not a preferential association with a single syndromic condition or a range of them.

Obstetric management. Should TOF be detected in a fetus, a detailed fetal anatomic scan should be performed by an expert to exclude the presence of extracardiac anomalies, bearing in mind the relatively high association rate. Fetal karyotyping, including FISH analysis for the 22q11 microdeletion, is indicated, especially if additional anomalies of the aortic arch are

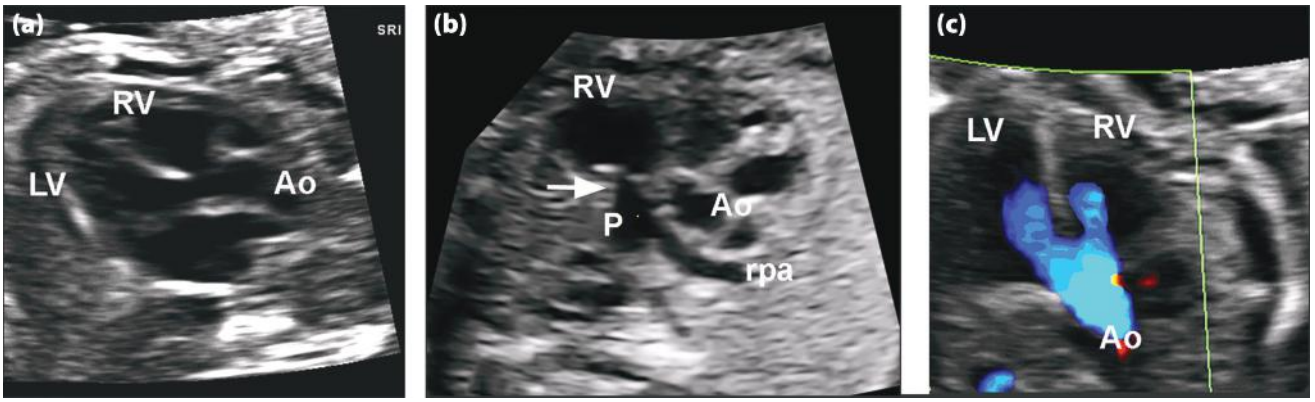


Figure 5.53 Tetralogy of Fallot (TOF): the typical signs of TOF are shown. (a) The left outflow tract view shows a malalignment VSD with an overriding aorta. (b) The right outflow tract view shows the narrowing of the pulmonary trunk, consistent with an infundibular stenosis (arrow). (c) On the left outflow tract, color Doppler demonstrates the overriding aorta draining from both ventricles. Ao: aorta; LV: left ventricle; P: pulmonary artery; rpa: right pulmonary artery; RV: right ventricle.

associated. Although the shunt is significant in classic TOF, it is better to plan the delivery in tertiary referral centers in order to warrant optimal multidisciplinary management of possible associated malformations. In addition, if the pulmonary outflow is significantly obstructed, a need for early shunting may arise.

Postnatal treatment. The treatment of this defect is surgical in all cases. However, the type of approach will depend on different anatomic features that may be ascertained only after birth. These include the degree of pulmonary trunk and branch stenosis, the presence of multiple VSDs, and the presence of coronary anomalies. All of these features have an impact on the type of treatment. In most cases, definitive surgical correction will be performed at three–six months of age, depending on the orientation of the reference cardiosurgical center, with a surgical mortality rate of less than 2.5%. The surgical approach includes removal of the outflow obstruction (infundibulectomy), together with closure of the VSD with a patch and, if necessary, pulmonary valvulotomy. However, if pulmonary outflow obstruction is significant, an early intervention is needed in order to ensure an adequate blood flow to the lungs and, consequently, an acceptable oxygen saturation. This is obtained with a palliative aortopulmonary shunting procedure, the modified Blalock–Taussig operation. This consists of the interposition of a Gore-Tex conduct between the left subclavian artery and the left pulmonary artery.

Prognosis, treatment, and quality of life. The overall prognosis will depend on several factors, including karyotype, associated extracardiac malformations, and cardiac anatomy. This last factor is extremely important as no two cases of TOF are identical, as Lev and Eckner [55] pointed out over 40 years ago. Prenatal counseling should therefore take into consideration all of these aspects in addition to the well-established fact that the pulmonary outflow obstruction may evolve during pregnancy [52]. With regard to survival, case series of patients with isolated TOF report long-term survival rates as high as 80%–90%. The variant with an absent pulmonary valve has significantly lower survival rates and will be discussed in the "Absent Pulmonary Valve Syndrome" section. In conclusion, if no unfavorable prognostic factors are found in utero and, above all, after birth, TOF is an easily correctable heart defect with excellent survival and good quality of life.

ABsENT pULMo NAr y VALVE syNdro ME

Incidence. It accounts for about 6%–9% of TOF cases, and less than 1% of CHD in fetuses.

Ultrasound diagnosis. On the *long axis of the left ventricle*: an anterior malalignment VSD with overriding aorta. On the *right outflow views*, very large pulmonary trunk and branches, sometimes seen also on the four-chamber view, due to severe dilation. Pulmonary valve functionally absent.

Risk of chromosomal anomalies. High (25%). Mainly but not only microdeletion 22q 11.

Risk of nonchromosomal syndromes. Low.

Outcome. Poor, if chromosomal and/or extracardiac anomalies are associated and for the risk of life-threatening tracheomalacia. Discrete or good in the other cases.

Definition APVS is a rare cardiac abnormality characterized by the existence of a dysplastic or rudimentary pulmonary valve, associated in most instances with severe dilation of the pulmonary trunk and branches due to the concurrent occurrence of valve stenosis and regurgitation. In most cases, this condition is associated with TOF and absence of the arterial duct, although cases with a patent ductus arteriosus and/or occurring as an isolated anomaly also have been reported in the fetus [51,56].

Anatomy. Two variants of APVS have been recognized in the fetus: the more frequent is characterized by an absent pulmonary valve with a severely dilated pulmonary trunk and branches associated with a malalignment VSD, overriding aorta (TOF), and ductal agenesis; the rarer variant is defined by the presence of an intact ventricular septum and a lower degree of pulmonary artery dilation, and it is associated in most instances with a patent ductus arteriosus. In this case, severe right ventricular hypertrophy is associated.

Ultrasound diagnosis. Unlike most conotruncal malformations, APVS can be suspected on the *four-chamber view*: evident cardiomegaly and an abnormal cardiac axis are the two key features; on some occasions, the pulmonary trunk may be so dilated that it also becomes visible on this view (Figure 5.54a). On the *left outflow view*, a malalignment VSD with an overriding aorta can be seen with difficult , due to the severe dilation of the pulmonary outflow tract; in fact, sweeping further cephalad from this view, severe dilation of the pulmonary trunk and branches appears (Figure 5.54b): the US aspect is so typical that, after being seen once, it will never be forgotten! Color Doppler allows detection of the severe stenosis and insufficiency of the functionally absent pulmonary valve (Figure 5.54c and d). Spectral Doppler can be used to quantify the steno-insufficiency of the rudimentary pulmonary valve. Four-dimensional echocardiography effectively demonstrates the degree of pulmonary artery dilation and can also be used to characterize the severely dysplastic pulmonary valve. The differential diagnosis is nonexistent, due to the very typical US aspect of APVS.

Very rare is the variant without TOF, in which the ductus arteriosus is present and the right ventricle is severely dilated with significant myocardial hypertrophy, due to the high intraventricular pressure (Figure 5.55).

Association with other malformations. The association with extracardiac (central nervous system and gastrointestinal) malformations is frequent—often in the context of a chromosomal aberration.

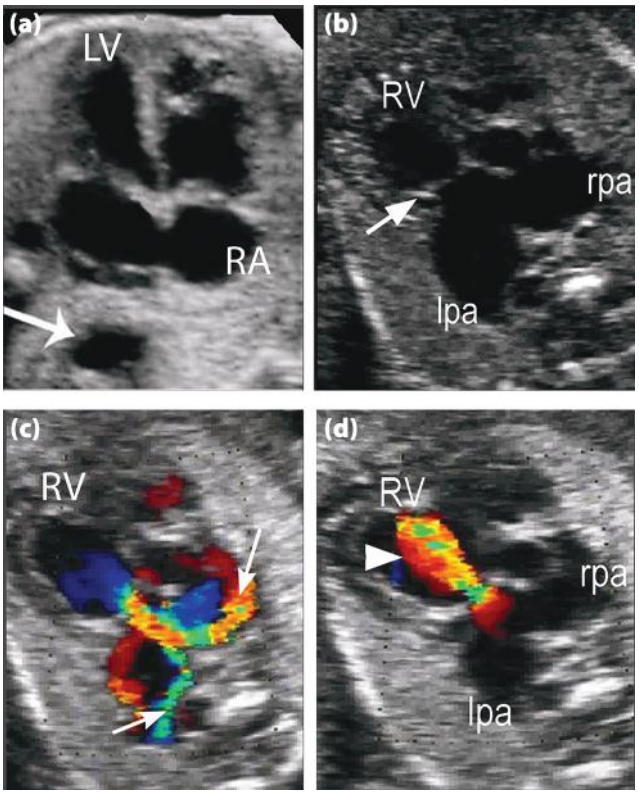


Figure 5.54 Absent pulmonary valve syndrome (APVS) with tetralogy of Fallot at 25 weeks of gestation. (a) On the four-chamber view, moderate cardiomegaly and increased cardiac axis are seen. Note also that part of the pulmonary trunk (arrow) is visible on this view, due to its severe dilation. (b) On the right outflow tract view, severe dilation of the main pulmonary trunk and the branches is visible. The fibrous pulmonary valve (arrowhead) persists in the lumen also during systole. (c) On color Doppler, during systole, the high-velocity and turbulent blood flow is seen entering the main pulmonary trunk and recircling along the walls of the pulmonary branches (arrows); and (d) during diastole, severe pulmonary insufficiency is detected (arrowhead). This is responsible for the volume overload leading to both cardiomegaly and dilation of the pulmonary arteries. lpa: left pulmonary artery; LV: left ventricle; RA: right atrium; rpa: right pulmonary artery; RV: right ventricle.

Risk of chromosomal anomalies. This is extremely high for APVS–TOF. There is a 20%–25% association rate with the 22q11 microdeletion; other severe aneuploidies may also be associated (trisomy 13 and triploidy) [51,56]. On the contrary, the variant with an intact ventricular septum is rarely associated with aneuploidies.

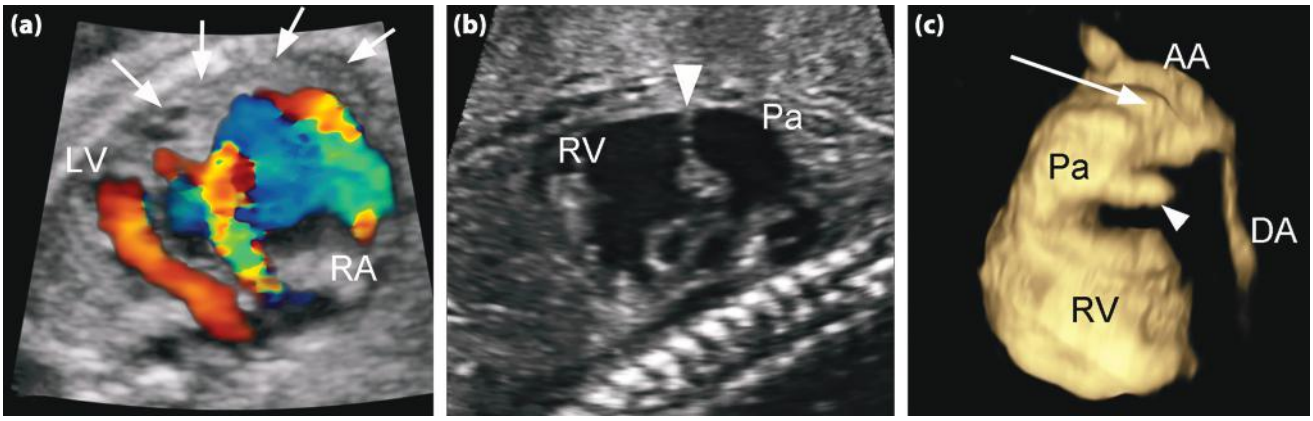


Figure 5.55 Absent pulmonary valve syndrome (APVS) at 23 weeks of gestation. On very rare occasions, APVS can occur as an isolated anomaly (not associated with tetralogy of Fallot). In this case, the ductus arteriosus is present (it is absent if APVS is associated with tetralogy of Fallot), and the right ventricle is severely hypertrophic due to the high pressure. (a) On the four-chamber view, color Doppler demonstrates the severe dilation and hypertrophy (arrows) of the right ventricle with high-velocity turbulent blood flow. Cardiomegaly (due to the volume overload) and an increased cardiac axis are also present. (b) The right outflow tract view demonstrates the severely dilated pulmonary trunk and the thickened valve (arrowhead) persisting in the lumen of the vessel also during systole. (c) Three-dimensional B-flow surface rendering demonstrating the severe dilation of the right ventricle and the pulmonary artery, with the presence of the ductus arteriosus (arrow) inserting onto the isthmic portion of the aortic arch. AA: aortic arch; DA: descending aorta; LV: left ventricle; Pa: main pulmonary artery; RA: right atrium; RV: right ventricle.

Risk of nonchromosomal syndromes. This is relatively low.

Obstetric management. Fetal karyotyping, including FISH analysis for the 22q11 microdeletion, is warranted in all cases of APVS–TOF. In this variant, a thorough search for associated extracardiac anomalies should also be carried out by an expert. Serial US monitoring should be provided in order to detect the possible prenatal onset of heart failure, which is due to the severe pulmonary insufficienc . The delivery should take place in a tertiary referral center in order to ensure adequate neonatal management, which may require resuscitation and, in some cases, tracheotomy.

Prognosis, treatment, and quality of life. The outcome of the cases detected prenatally is poor due to the severity of the defect and the frequent association with genetic and extracardiac anomalies. The overall prognosis is guarded, regardless of the surgical correction of the defect, due to the common occurrence of bronchomalacia. This life-threatening lesion is virtually ubiquitous if severe cardiomegaly and marked branch pulmonary dilation are present.

d o UBLE-oUTLET rIG h T VENTr Ic LE

Incidence. 3%–6% of CHD in the fetus; 2% in postnatal life.

Ultrasound diagnosis. Double ventriculoarterial connection from the right ventricle. VSD constantly associated. Variable spatial relationships of the great vessels. Pulmonary atresia, cardiosplenic syndromes and other major cardiac defects commonly associated.

Risk of chromosomal anomalies. Very high: 12%–45%.

Risk of nonchromosomal syndromes. Low.

Outcome. Extremely variable, depending on the cardiac anatomy and associated cardiac and extracardiac lesions.

Definition DORV encloses a spectrum of lesions characterized by a double ventriculoarterial connection originating from the right ventricle, a VSD, and a variable spatial relationship of the great arteries.

Anatomy. DORV is not a single defect but, rather, includes a wide range of lesions that may have completely different hemodynamic characteristics. The basic feature of DORV is the fact that both great vessels arise for more than 50% from the same ventricle. The spatial relationship of the two arteries is variable: they can show a normal relationship, with the aorta posterior and the pulmonary artery anterior and to the left, or they can be malposed, with the aorta arising behind the sternum and the pulmonary trunk posterior and above the VSD. The position and the commitment of the VSD are similarly variable: the defect can be subpulmonary, subaortic, doubly committed, or far from the two outlets for the interposition of the muscular septum (noncommitted). In addition, the pulmonary outflow or (much less frequently) the aortic outflow may be obstructed, due to pulmonary stenosis or atresia or due to aortic coarctation. The result of this significant anatomic variability is that DORV comprises cases that are hemodynamically similar to TOF and cases that share several features with transposition of the great arteries. The most frequent variants, in decreasing order of frequency, are the *Fallot type* (subaortic VSD, great vessels in normal spatial relationship, and pulmonary artery obstruction), the *Taussig–Bing type* (subpulmonary VSD and malposed great arteries), and the *type with subaortic VSD but without pulmonary stenosis*. In a significant number of cases, other major cardiac defects are associated: ventricular hypoplasia (almost always due to straddling and overriding of one of the two atrioventricular valves), aortic coarctation, AVSD, and cardiosplenic syndromes.

Ultrasound diagnosis. It should be noted that, as for all conotruncal anomalies, the *four-chamber view* is unremarkable. However, since DORV is one of the major CHDs more often associated with heterotaxy, it often can be found in association with a single ventricle or an AVSD. DORV is recognized on the *outflow tract views*: the crossover is lacking, and the great vessels have a parallel course and arise from the anterior ventricle (Figure 5.56). As already mentioned, the spatial relationship of the two vessels should be evaluated, as these may be in normal relationship or malposed (Figure 5.56a and b). The assignment of the great vessels is based on the following features:

- The pulmonary artery has an acute-angle bifurcation not far from the semilunar valve;

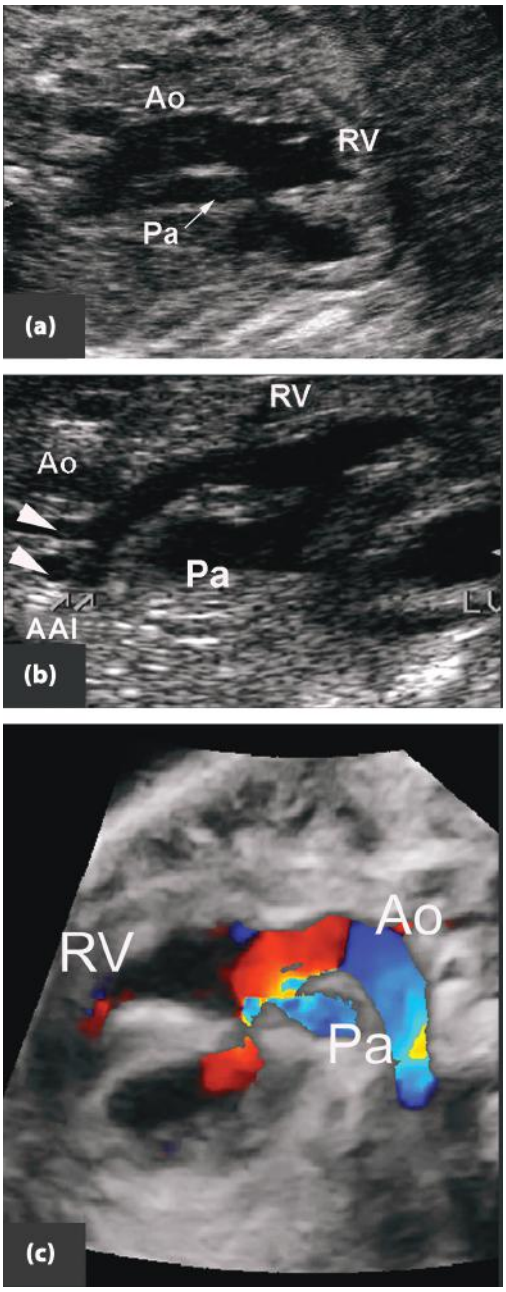


Figure 5.56 Double-outlet right ventricle (DORV). This comprises a spectrum of anomalies of the great vessels, which may have different sizes due to left or right outflow obstruction, in different spatial relationships (see text of this chapter). (a) DORV with an anterior malposed aorta and a posterior moderately stenotic pulmonary artery (arrow); this is one of the most common arrangements seen in the fetus. (b) DORV with an anterior malposed aorta, which is also reduced in size due to a concurrent interruption of the aortic arch; note the straighter course of the aorta and the "V" shape of the first neck vessels (arrowheads). (c) Color Doppler can be used to confirm the connection of the great vessels with the anterior ventricle, if there is any remaining doubt regarding the differential diagnosis with transposition of the great arteries. AAI: aortic arch interruption; Ao: ascending aorta; Pa: main pulmonary artery; RV: right ventricle.

- The aorta is characterized by the first neck vessel branching off at almost 90° at a certain distance from the semilunar valve (Figure 5.56b). Note that if one of the vessels is hypoplastic, it may be difficult to identify it.

Color Doppler may contribute to ascertaining the spatial relationship of the great vessels (Figure 5.56c) and the site of the VSD. However, it should be underlined that in the case of moderate pulmonary outflow tract obstruction, no transvalvular acceleration is seen on color Doppler. The diagnosis of outflow obstruction in DORV is based on comparison of the vessel size (Figure 5.56a and b) rather than on increased transvalvular velocity. The definition of the spatial relationship of the great vessels is of the utmost importance, since it identifies the type of surgical approach required, and this in turn affects the prognosis (discussed further in this section). Also, DORV may change through the course of pregnancy: in the third trimester, the degree of pulmonary outflow obstruction can worsen significantly, and, at the same time, ventricular hypoplasia can develop, especially if the atrioventricular valves show straddling or overriding. Spectral Doppler has a limited diagnostic role. Four-dimensional echocardiography may be used to confirm the absence of crossover and to ascertain possible associated anomalies of the aortic arch.

Differential diagnosis. The most difficult issue is the differentiation from the other conotruncal anomalies: in some cases, the distinction between DORV and TOF or a transposition of the great arteries may be challenging. However, it should be pointed out that the surgical approach and prognosis are similar for the DORV variants and the conotruncal lesions with similar hemodynamics. The differences lie in the rate of associated chromosomal and extracardiac anomalies.

Prognostic indicators. As for all CHD, the main negative prognostic determinant is the association with extracardiac or chromosomal anomalies. Second, if DORV is part of a cardiosplenic syndrome, the prognosis is significantly poorer than if it occurs in situs solitus. Finally, in cases of isolated DORV in situs solitus, at least four other anatomic features seem to represent negative prognostic indicators. In fact, in a recent study [57], abnormal relationship of the great arteries, subpulmonary VSD, unobstructed pulmonary blood flow at birth, and aortic coarctation were all associated with suboptimal postsurgical outcomes (OR 2.9, 6.0, 2.8, and 9.0, respectively).

Association with other malformations. There is a high risk of association with extracardiac (mainly gastrointestinal and central nervous system) anomalies, regardless of the association with chromosomal aberrations.

Risk of chromosomal anomalies. This is very high. The rate is 12%–45%, with a prevalence of trisomies 18 and 13 and, to a lesser extent, the 22q11 microdeletion and trisomy 21 [14,15,57].

Risk of nonchromosomal syndromes. This is low.

Obstetric management. Karyotyping is mandatory because of the high risk of chromosomal anomalies; a FISH for the DGCR is advisable, although not mandatory. In addition, a thorough search for associated cardiac and extracardiac anomalies should be performed. The changing nature of DORV during the course of pregnancy should be addressed in the prenatal counseling session. The delivery should be organized in a tertiary referral center, so that the neonate can be transferred to a pediatric cardiology unit for confirmation of the diagnosis and adequate management.

Postnatal therapy. The cardiologic management depends on the type of DORV: if the VSD is subaortic and there is no outflow obstruction, the lesion is not ductus -dependent; on the contrary, if aortic coarctation or pulmonary atresia is associated, DORV becomes a neonatal emergency. In the former case, the neonate will become symptomatic when the pulmonary resistances decrease. Early correction (closure of the VSD with a patch) avoids the need for pulmonary banding, which is done only if the neonate fails to thrive or develops unresponsive cardiac failure. In DORV with subaortic VSD and pulmonary outflow obstruction, the management is similar to that of TOF (as discussed in this chapter). In DORV with a subpulmonary VSD, the arterial switch operation or the REV (*Réparation à l'Etage Ventriculaire*) procedure is performed. In DORV with subpulmonary VSD and pulmonary outflow obstruction, most surgeons currently adopt the REV procedure modified by Rastelli

Prognosis, survival, and quality of life. The overall survival of DORV detected prenatally is 46%–50% (if terminations of pregnancy are excluded), due to the strong association with aneuploidy and extracardiac anomalies. If postnatal series are considered, the overall surgical mortality rate for biventricular repair is as low as 13%, while the ten-year survival rate is about 86%. The mortality is much higher if other major cardiac lesions are associated, which is not infrequent.

c o MMo N Ar TEr IAL Tr UNk

Incidence. Accounts for about 1% of CHD in utero and at birth.

Ultrasound diagnosis. On *the long axis of the left ventricle*: a malalignment VSD with overriding aorta and a dysplastic truncal valve can be seen; the pulmonary arteries are visualized—sometimes with difficulty—arising from the main trunk.

Risk of chromosomal syndromes. High: 15%–28%. Trisomes 13 and 18 and microdeletion 22q11.

Risk of nonchromosomal syndromes. Relatively high.

Outcome. Prognosis depends on the association with extracardiac anomalies and on unfavorable cardiac anatomy, if present.

Definition CAT is characterized by a single great artery arising from the base of the heart, which supplies the systemic, coronary, and pulmonary blood flo , and by a VSD.

Anatomy. CAT results from a septation failure during development of the ventricular outlets and the proximal arterial segment of the heart tube. According to the Collett and Edwards classification [58], CAT can be divided into different anatomical subtypes with respect to the origin of the pulmonary arteries:

- *Type I*: the main pulmonary trunk arises from the truncal artery just distal to the truncal valve;
- *Types II* and *III*: the pulmonary trunk is absent, and the two pulmonary branches arise from the posterior aspect of the truncus but close to each other (type II) or originating at different distance from the truncal valve (type III).

The former type IV of the original classification now corresponds to pulmonary atresia with ventricular septal defect (PAVSD—see the "Pulmonary Atresia with Ventricular Septal Defect" section). CAT accounts for 1% of cardiac lesions detected in fetal life. The frequency is similar to that reported in infancy, even though the type of lesion is not easily detected if obstetric US screening is limited to the four-chamber view, because in most cases only a moderate increase of the cardiac axis can be seen on this view. The intrauterine incidence of this type of CHD is probably higher than in postnatal life, but there is an increased rate of natural fetal wastage.

Ultrasound diagnosis. In CAT, the *four-chamber view* is usually normal; only a moderate increase of the cardiac axis can be seen on some occasions on this view. The constant malalignment VSD is best displayed on the *long-axis view of the left ventricle* (Figure 5.57). Although the truncal valve is commonly connected to both ventricles, it may sometimes straddle one ventricle preferentially, especially if there is dominance of one ventricle (Figure 5.57) [59]. Visualization of the pulmonary arteries is essential to distinguish CAT from PAVSD and to identify the CAT subtype. In fact, when the pulmonary arteries are visualized arising from the main trunk, the diagnosis of CAT is straightforward (Figure 5.57a). In the case of PAVSD, the hypoplastic pulmonary arteries are supplied by the ductus arteriosus and/or by the major aortopulmonary collateral arteries (MAPCAs). As noted here, in type I CAT, the main pulmonary trunk arises from the posterolateral aspect of the common trunk and bifurcates into two pulmonary arteries (Figure 5.57a). In types II and III, the pulmonary arteries arise separately. The truncal valve is often dysplastic, and it may be regurgitant or stenotic (Figure 5.57b and c). Color Doppler may be used to evaluate the steno-insufficiency of the truncal valve (Figure 5.57b and c) and to trace the course and connection of the pulmonary trunk and arteries. Spectral Doppler may help to quantify the degree of truncal valve stenosis and insufficienc . The use of 4D echocardiography has proved significantly helpful in the identification of the small pulmonary branches in types II and III CAT (Figure 5.58) and in the characterization of the pulmonary trunk anatomy in PAVSD.

Differential diagnosis. Differentiation of CAT from PAVSD is often difficult In fact, this differential diagnosis represents the most challenging task to be faced when diagnosing CAT in the fetus: types II and III CAT and PAVSD share reduced dimensions of the pulmonary branches and the prevalence of the aortic vessel. When doubts arise, the following anatomic details should be sought to make the final diagnosis: the aortic and truncal valve, the atretic pulmonary valve, and the direction of flow within the arterial duct. The semilunar valve is always dysplastic (from two to five cusps) and typically stenotic and/or insufficient in CAT (Figure 5.57b and c), whereas it is frequently unremarkable or only

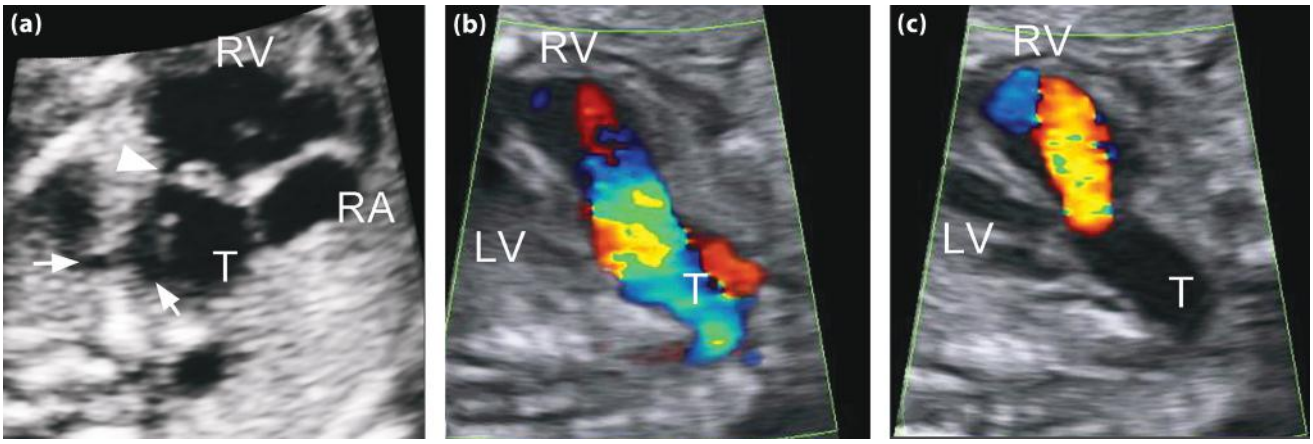


Figure 5.57 Common arterial trunk (CAT), type I, 23 weeks of gestation. (a) The main pulmonary artery with the two hypoplastic branches (arrowheads) is seen branching off the truncus (T) just above the truncal valve (arrowhead). (b) On the left ouflow tract view, color Doppler demonstrates (during systole) moderate stenosis of the truncal valve (aliasing and turbulence), due to a highly dysplastic truncal valve. Straddling of the truncus toward the right ventricle is also visible. (c) During diastole, massive insufficiency of the dysplastic truncal valve is visible. Note how the truncus is prevalently connected to the right ventricle due to the straddling. LV: left ventricle; RV: right ventricle; T: arterial trunk.

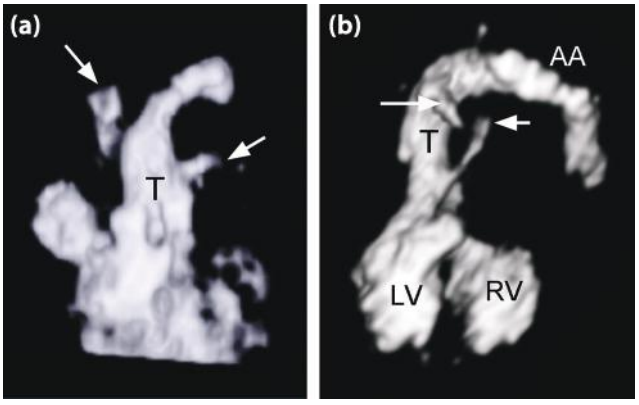


Figure 5.58 Common arterial trunk (CAT), type II versus III. Three-dimensional B-flow imaging is of help in the differential diagnosis of truncal type. (a) In type II, the two pulmonary branches arise directly and separately from the truncus, without a main pulmonary artery, at the same distance from the truncal valve; and (b) in type III, in this image with a posterior approach, the two pulmonary branches depart at different distances from the truncal valve. The overriding position of the truncus is also evident. AA: aortic arch; LV: left ventricle; RV: right ventricle; T: truncus arteriosus.

mildly abnormal in PAVSD. The atretic pulmonary valve is difficult to detect in PAVSD, but if it is demonstrated (in those infrequent cases in which the pulmonary trunk is not extremely hypoplastic), then CAT can be excluded. Finally, accurate color Doppler mapping of the great vessels may help one to detect reversed flow in the arterial duct and main pulmonary artery as well as aortopulmonary collaterals in PAVSD, or the branching point of the pulmonary arteries in the truncal vessel in types II and III CAT [59].

Association with other malformations. When CAT is diagnosed in a fetus, care should be taken to identify possible additional heart and great vessel anomalies, which occur in 20%–30% of cases. Associated cardiac defects include absence of ductus arteriosus (50% of cases), IAA, RAA, and atrioventricular valve atresia [59].

Risk of chromosomal anomalies. This is high. There is a high rate of association with the 22q11 microdeletion (20%–30% of cases) and, to a lesser extent, with trisomies 18 and 13 [59].

Risk of nonchromosomal syndromes. This is relatively high.

Obstetric management. A detailed fetal anatomic scan should be performed by an expert to exclude the presence of extracardiac and cardiac anomalies. Fetal karyotyping is warranted because of the high risk of chromosomal anomalies, and it should include FISH analysis for the 22q11 microdeletion. Delivery should take place in a tertiary referral center to ensure confirmation of the diagnosis and adequate neonatal management. In fact, in CAT there may be significant reduction of the pulmonary blood flow due to stenosis of the pulmonary branches, or aortic arch anomalies [e.g., interrupted aortic arch (IAA)] may lead to early surgical correction, which is otherwise scheduled after one–two months of life.

Postnatal therapy. Surgical repair should be done in the first two–three months of life. Operative repair consists of detachment of the pulmonary arteries from

the truncus and attachment to the right ventricle with a conduit, closure of the VSD, and repair of the truncal valve, if necessary. In recent series, the overall operative mortality rate is as low as 5%, if no severe truncal valve abnormalities are present. The association of IAA may lead to a need for earlier surgical correction.

Prognosis, survival, and quality of life. Prognosis depends on the presence of extracardiac and chromosomal anomalies and of unfavorable cardiac anatomy (e.g., severe truncal valve regurgitation, IAA, and straddling with ventricular hypoplasia).

PULMONARY ATRESIA WITH VENTRICULAR SEPTAL DEFECT

Incidence. PAVSD accounts for about 1% of CHD in the fetus.

Ultrasound diagnosis. On the *long axis of the left ventricle*, a malalignment VSD with overriding aorta can be seen. Sweeping further cephalad from this view, an atretic pulmonary artery can be detected with difficulty.

Risk of chromosomal anomalies. High: 13%–20%.

Risk of nonchromosomal syndromes. Relatively low.

Outcome. Prognosis is favorable in isolated PAVSD, if confluent pulmonary branches supplied by the ductus arteriosus are present.

Definition PAVSD is characterized by absence of the right ventriculoarterial connection. The pulmonary trunk is usually severely abnormal and can be completely absent in some cases, with the pulmonary branches dependent on the arterial duct or MAPCAs.

Anatomy. PAVSD can be considered an extreme form of TOF; it comprises a heterogeneous group of lesions sharing absence of the right ventriculoarterial connection. There is a malalignment VSD with an overriding aorta, while the right ventricular outflow tract is, in most cases, similar to that of TOF, with the muscular outlet septum being anteriorly displaced. In most cases, the muscular outlet septum fuses directly with the parietal musculature of the right ventricle, obliterating the ventriculopulmonary junction. The anatomy of the hypoplastic pulmonary vessels is variable. In the most frequent arrangement, the right and left pulmonary arteries may be confluent (communicating with each other) and supplied by the ductus arteriosus (with or without a threadlike main pulmonary artery). Alternatively, the central pulmonary arteries may be confluent and coexist with MAPCAs. The third pattern of arterial supply is complete absence of the central pulmonary arteries, the lungs being directly supplied by multiple MAPCAs [60].

Ultrasound diagnosis. The *four-chamber view* is usually normal; in some cases, minor leftward rotation of the cardiac axis and/or cardiomegaly can be appreciated (Figure 5.59a) [7]. The malalignment VSD is best visualized on the *long-axis view* of the left ventricle (Figure 5.59b). When the right and left pulmonary arteries are present, they are commonly smaller than normal and confluent with the characterstic appearance of a "flying seagull" (Figure 5.59c), and their size is usually dependent on the source of arterial supply [7,60]. The pulmonary vascular bed may be supplied with blood flow from a ductus arteriosus, from MAPCAs (Figure 5.59d), or from a combination of both. Color Doppler contributes to demonstrating the overriding of the aorta, and it demonstrates the retrograde blood flow across the ductus arteriosus, confirming the ductus dependence of the pulmonary circulation. The use of color Doppler is also important to demonstrate the presence of MAPCAs branching off the descending thoracic aorta, although B-flow imaging seems superior in this regard [7]. Spectral Doppler has a limited diagnostic role to play in PAVSD. Four-dimensional echocardiography has recently been demonstrated to be very helpful in the definition of the vascularization pattern of the pulmonary arteries [7]. In particular, the use of B-flow imaging can demonstrate the confluent pulmonary arteries and the MAPCAs better than 2D US (Figure 5.59d).

Differential diagnosis. Differentiation of PAVSD from CAT can be very difficult Types II and III CAT and PAVSD share the reduced dimensions of the pulmonary branches and the prevalence of the aortic vessel. When doubts arise, the following anatomic details should be sought to make the final diagnosis: the aortic and truncal valve, the atretic pulmonary valve, and the direction of flow within the arterial duct. The semilunar valve

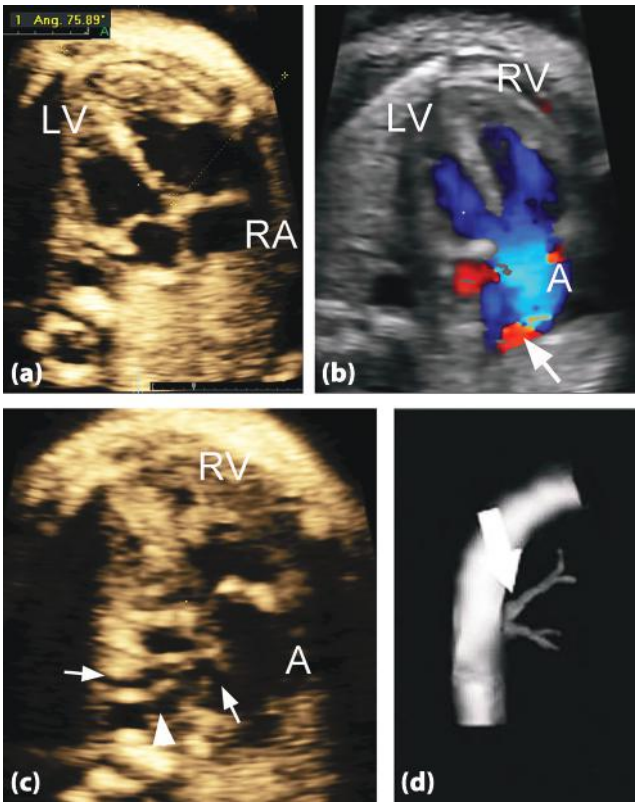


Figure 5.59 Pulmonary atresia with ventricular septal defect (PAVSD). (a) The four-chamber view shows only an increase in cardiac axis (75°; normal values 45° ± 20°), but the anatomy is unremarkable. (b) On the left outflow tract view, color Doppler shows the malalignment VSD with the overriding aorta. The red color at the arch level (arrow) indicates the reversed blood flow across the ductus arteriosus, due to the concurrent atresia of the pulmonary valve. (c) The right outflow is severely hypoplastic. In this case, the two pulmonary branches (arrows) are confluent and fill from the ductus arteriosus (arrowhead), while the main pulmonary trunk is absent. (d) With B-flow rendering, two MAPCAs (arrow) departing directly from the anterior wall of the descending aorta are clearly visible. A: ascending aorta LV: left ventricle; RA: right atrium; RV: right ventricle. (Modified from Volpe P et al., *Ultrasound Obstet Gynecol* 28, 40–46, 2006.)

is always dysplastic (from two to five cusps) and typically stenotic and/or insufficient in CAT, whereas it is frequently unremarkable or only mildly abnormal in PAVSD. The atretic pulmonary valve is difficult to detect in PAVSD, but if demonstrated (in those infrequent cases in which the pulmonary trunk is not extremely hypoplastic), CAT can be excluded. Finally, accurate color Doppler mapping of the great vessels may help to detect reversed flow in the arterial duct and main pulmonary artery as well as aortopulmonary collaterals in PAVSD, or the branching point of the pulmonary arteries in the truncal vessel in types II and III CAT [52].

Association with other malformations. Associated cardiac defects include absence of the ductus arteriosus (in about half of the cases), IAA, and right-sided aortic arch. Extracardiac malformations can also be associated, including central nervous system and gastrointestinal anomalies.

Risk of chromosomal anomalies. PAVSD is frequently associated with 22q11 microdeletion (20% of cases [7]). Association with trisomies 13 and 18 has also been reported.

Risk of nonchromosomal syndromes. This is relatively low.

Obstetric management. A detailed fetal anatomic scan should be performed by an expert to exclude the presence of extracardiac anomalies. Fetal karyotyping, including FISH analysis for the 22q11 microdeletion, is indicated. Delivery should take place in a tertiary referral center to allow proper neonatal management.

Postnatal therapy. The ultimate goal of surgical therapy is to construct completely separated, in series, pulmonary and systemic circulations [60]. This may be achieved as a single or staged procedure, depending on the complexity of the central pulmonary arteries and pulmonary blood supply, as well as institutional preference. The reported surgical mortality rate has been relatively low and good functional results have been achieved, especially when left and right pulmonary arteries are confluent and are supplied by the ductus arterious, but data obtained from pediatric series are likely to differ from fetal series, as usual, and therefore these results cannot be simply extended to the prenatally recognized cases.

Prognosis, survival, and quality of life. Along with the presence of extracardiac and genetic anomalies, the prognosis of PAVSD is greatly influenced by the anatomy of the pulmonary arteries and by the sources of the pulmonary blood supply, appreciation of which helps to provide fully informative prenatal counseling. Isolated PAVSD presents a difficult management plan, since variations in blood supply to the pulmonary arterial tree may be complex and create significant variations in the development of the pulmonary arteries. The presence of central pulmonary arteries of appropriate size and the relationship of the two branches are of surgical relevance. The central pulmonary arteries are considered "confluent when they maintain free communication with each other. The most favorable arrangement, from a surgical point of view, is that in which the two pulmonary branches are confluent and are supplied by

the arterial duct. On the contrary, a complete absence of the central pulmonary arteries, with the lungs being directly supplied by multiple MAPCAs, represents the worst scenario, being associated with a significantly poorer prognosis; also, it is the most difficult to treat postnatally.

coMpLETE TrANspos ITIoN oF ThE Gr EAT Ar TEr IEs

Incidence. Relatively frequent, accounting for 2%–5% of CHD in the fetus and the neonate.

Ultrasound diagnosis. Ventriculoarterial discordance, with the right ventricle connected to the aorta and the left connected to the pulmonary artery. VSDs, pulmonary stenosis, and arch abnormalities may be associated.

Risk of chromosomal anomalies. Virtually absent.

Risk of nonchromosomal syndromes. Virtually absent.

Outcome. Extremely good in classic forms; good in the case of less favorable cardiac anatomy.

Definition Complete transposition of the great arteries (TGA) is defined by the presence of a discordant ventriculoarterial connection, with the pulmonary artery arising posteriorly from the left ventricle and the aorta connected anteriorly to the right ventricle.

Anatomy. The basic anomaly is the ventriculoarterial discordance. TGA can be isolated (simple TGA) or can be associated with VSDs, pulmonary outflow obstruction, or aortic arch anomalies (coarctation or interruption). Much more rarely, atrioventricular valve abnormalities, including straddling and overriding, may be present. In two-thirds of the cases, significant anomalies of the coronary pattern, which are not diagnosable in utero, are associated.

Ultrasound diagnosis. The *four-chamber view* is unremarkable, as for all conotruncal anomalies, unless major anomalies of the atrioventricular junction are associated. The diagnosis is made on the *outflow tract views*: there is no crossover, and the two arteries follow a parallel course. The aorta arises from the anterior right ventricle, whereas the pulmonary artery is connected posteriorly with the left ventricle (Figure 5.60a and b). If present, the VSD can also be displayed on the *left outflow tract view*. The sizes of the vessels should be compared in order to detect possible obstructions, which consist mainly of valvular anomalies for the pulmonary artery and arch coarctation and interruption for the aorta. On *longitudinal views*, the aortic arch has a wider angle of curvature because of the anteriorized connection of the ascending aorta (a "hockey stick" aspect, in comparison with the "umbrella handle" aspect of the normal arch). Finally, particular attention should be paid, in the case of TGA with an intact ventricular septum, to signs indicative of a restrictive foramen ovale (bulging or thickening; Figure 5.60c) [61]. Color Doppler may help in the characterization of the ventriculoarterial connection (Figure 5.60b), in the recognition of small VSDs, and in the detection of pulmonary and aortic outflow obstruction. Spectral Doppler may be used to quantify the transvalvular gradient. Four-dimensional echocardiography can effectively demonstrate the absence of crossover and the parallel course of the great vessels. However, the most interesting use of 4D echocardiography (STIC) is when it is employed to reconstruct the coronal plane of the four cardiac valves in order to demonstrate the spatial relationships of TGA (Figure 5.61) [62]. In fact, this assessment is impossible or rather difficult with 2D echocardiography. The advantage of knowing the spatial orientation of the great arteries is due to the fact that an anomalous origin or course of the coronary arteries is strictly dependent on the former and coronary arteries abnormalities represent a poor prognostic indicator [62,63].

Differential diagnosis. This includes all CHDs sharing an absent crossover, namely, corrected TGA (cTGA: see the "Corrected Transposition of the Great Arteries" section) and DORV. cTGA can be differentiated from TGA, thanks to the atrioventricular discordance (which is absent in TGA) which can be detected on the four-chamber view. As far as the differentiation from DORV is concerned, doubts may arise when distinguishing TGA-like DORV, but in this case the outcome of the lesion is the same as for classic TGA. The differentiation from the other forms of DORV is based on the recognition, on 2D US, color Doppler, or 4D echocardiography, of the different connection of the two vessels in DORV (Figures 5.56 and 5.60).

Prognostic indicators. The occurrence of significant right outflow obstruction is a relatively poor prognostic indicator, being a contraindication to the classic arterial

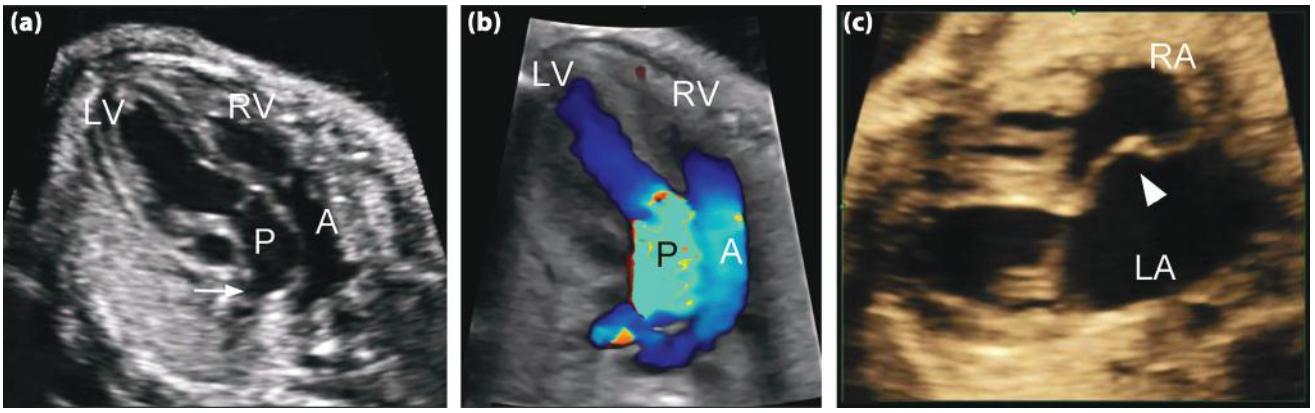


Figure 5.60 Transposition of the great arteries (TGA), 27 weeks of gestation. (a) On the left outflow tract view, the ventriculoarterial discordance and the absence of crossover (two parallel vessels) are demonstrated, with the pulmonary artery arising from the left ventricle and the anterior aorta arising from the right ventricle. (b) Color Doppler helps in defining the ventriculoarterial connection and the parallel course of the vessels. (c) In the case of TGA with an intact ventricular septum, a restrictive foramen ovale (arrowhead) indicates the need for immediate postpartum Rashkind atrioseptostomy (see this chapter's text).

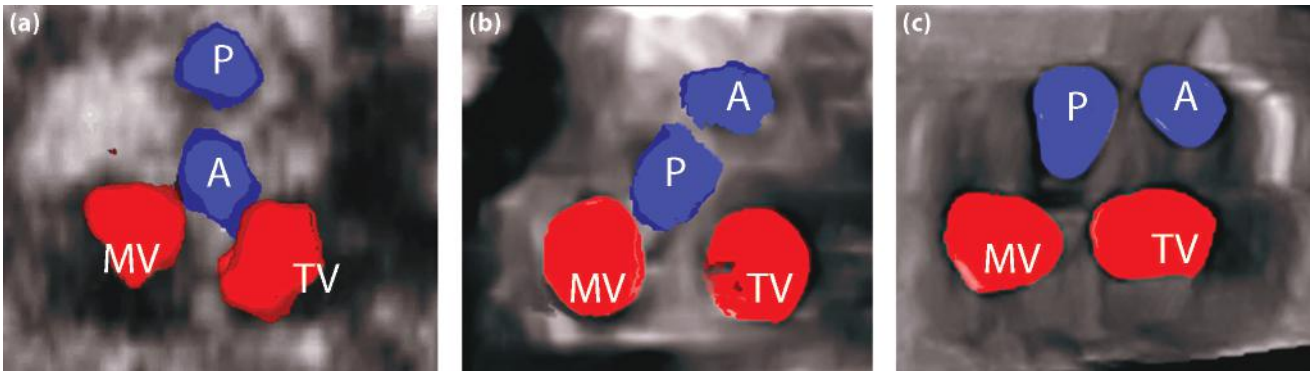


Figure 5.61 Transposition of the great arteries (TGA). Four-dimensional echocardiography (STIC) allows reconstruction of the coronal plane of the four cardiac valves. On this view, with color Doppler it is possible to identify the spatial relationships of the vessels in TGA (see this chapter's text). (a) In the normal heart, the aorta is wedged in between the two atrioventricular valves; (b) in TGA, the most common arrangement of the vessels is with the aorta anterior and to the right of the pulmonary artery; and (c) on rarer occasions, the vessels may arise "side by side," as demonstrated in this image. A: ascending aorta; MV: mitral valve; P: main pulmonary artery; TV: tricuspid valve.

switch operation. Also, an abnormality in the origin and/or pattern of the coronary circulation represents a complication that has been shown to have a negative impact on survival. As mentioned in this section, the incidence of coronary arteries' abnormalities depends strictly on the spatial arrangement of the great vessels, which can be studied with STIC echocardiography [62]. An important feature to diagnose in utero during the last weeks of pregnancy is the presence of a restrictive foramen ovale (Figure 5.60c). Its recognition before birth is of crucial importance for proper early neonatal management. In fact, in cases of restrictive foramen ovale, the Rashkind atrioseptostomy, a life saving procedure that is performed after birth in all cases of TGA with an intact ventricular septum, should be carried out as early as 15–30 minutes after birth, to avoid acute decompensation and immediate death of the neonate (see the "Obstetric Management" subsection) [61].

Association with other malformations. None is known.

Risk of chromosomal anomalies. Like cTGA and cardiosplenic syndromes, TGA seems to *protect* from aneuploidy.

Risk of nonchromosomal syndromes. This is extremely low.

Obstetric management. Karyotyping is not necessary, as the risk of chromosomal anomalies is very low. Similarly, the risk of associated extracardiac anomalies is trivial. Care should be take in differentiating TGA from cTGA,

considering the significantly different management of the two lesions. Serial follow-up scans are warranted, especially in the case of TGA with intact ventricular septum, in order to recognize a restrictive foramen ovale (if present). This diagnosis should prompt immediate transfer of the neonate to the interventional catheterization room in order to perform a life saving Rashkind atrioseptostomy. According to some authors, the delivery of a fetus diagnosed with TGA and a restrictive foramen ovale should be organized with a cardiac hemodynamist in the delivery room because of the high risk of immediate neonatal decompensation [61,64]. In cases of TGA with a VSD or nonrestrictive foramen ovale, the neonate may be transferred to the pediatric cardiology unit in the first hours of life in order to ensure assessment of oxygen saturation and proper planning of the Rashkind atrioseptostomy.

Postnatal therapy. In the case of TGA with an intact ventricular septum, the Rashkind procedure is always necessary to provide adequate oxygenation and proper planning of corrective surgery. Prostaglandin E1 infusion is always necessary to avoid closure of the arterial duct and increase oxygen saturation. The option of choice for surgical correction of TGA is the arterial switch operation, which consists of the following: (1) transection of the aorta and pulmonary artery from the ventricular outflows above the semilunar valves; (2) excision of the coronary arteries from the aortic root, with a cuff of aortic wall; (3) connection of the ascending aorta to the pulmonary root and of the coronary arteries to the repositioned aorta; (4) closure using a patch of the parietal defects of the aortic root from which the coronary arteries had been detached; and (5) connection of the pulmonary artery to the aortic root, with the interposition of a synthetic conduit if necessary. The arterial switch operation is performed during the first days of life in the case of TGA with intact ventricular septum, and in the first weeks in the case of TGA with a VSD. In particular cases only, the palliative atrial switch (the Senning or Mustard procedure) operation is performed, usually at three–six months of life. This type of surgery aims at redirecting the pulmonary venous blood flo toward the right ventricle, which becomes the systemic one, and, vice versa, diverting the caval blood flo toward the left ventricle. In cases of TGA with DIV plus severe pulmonary stenosis, an aortopulmonary shunt is performed. If the pulmonary outflow obstruction is moderately severe, the final intervention (*Réparation à l'Etage Ventriculaire*, or REV) will be performed at about 12 months of life. This surgical procedure consists of the following steps: resection of the infundibular septum, creation of a tunnel connecting the left ventricle with the aorta, and direct anastomosis of the right ventricle and the pulmonary artery. Alternatively, the Rastelli procedure consists of connection of the right ventricle with the pulmonary artery through a prosthetic conduit, widening of the VSD, and interposition of a patch connecting the aorta with the left ventricle. As for all procedures in which prosthetic conduits are used, patients will need one or more replacements of the conduit during their lives.

Prognosis, survival, and quality of life. TGA represents a keystone in the validation of prenatal screening of CHD, as it represents the ideal model of CHD to be screened: it has a high early neonatal mortality risk, which disappears if early neonatal management is properly planned; and, once corrected, this CHD has a greater than 90% long-term survival rate in good functional conditions. Bonnet et al. [61] have demonstrated that prenatal diagnosis does indeed make a difference, being responsible for a 13% reduction in surgical mortality in comparison with cases detected postnatally. Once corrected, patients with TGA experience a 15-year survival rate of 86%. In comparison, patients undergoing palliative surgical procedures (Mustard or Senning) have a 15-year survival rate of 80%, with an increased risk of major postoperative complications and sequelae (rhythm abnormalities, right ventricular dysfunction, and sudden death).

c orr Ec TEd Tr ANspos ITIo N o F TGA

Incidence. Very low: <1% of CHD.

Ultrasound diagnosis. On the *four-chamber view*: double atrioventricular and ventriculoarterial discordance. Frequent association with other CHDs, including VSD, Ebstein anomaly, outflow obstruction, and ventricular hypoplasia.

Risk of chromosomal anomalies. Virtually absent.

Risk of nonchromosomal anomalies. Virtually absent.

Outcome. Good short-term outcome. Poor in the long term because of the development of unresponsive heart failure.

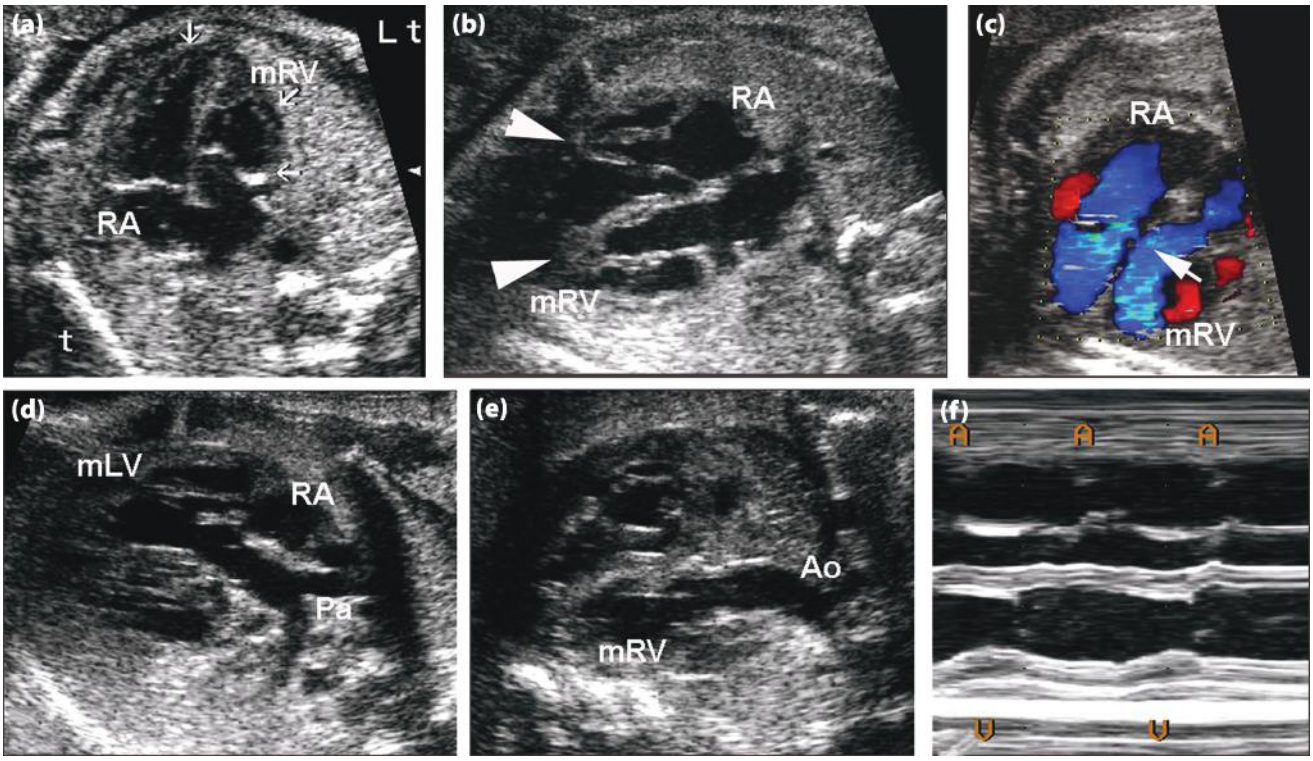


Figure 5.62 Corrected transposition of the great arteries (cTGA), 31 weeks of gestation. (a) On the four-chamber view, the morphologic right ventricle (mRV) is connected with the left atrium, and, vice versa, the morphologic left ventricle is connected with the right atrium. Note the moderator band in the mRV and the Ebstein-like appearance of the left-sided tricuspid valve. (b) On the transverse four-chamber view, the differential insertion of the papillary muscles is evident: the tricuspid ones attach to the apex of the ventricle, whereas the mitral one attaches to the lateral free ventricular wall. (c) Color Doppler is used to demonstrate a small VSD not visible on grayscale ultrasound (arrow). (d) The right outflow tract view demonstrates the pulmonary artery (with the bifurcation) arising from the right-sided left ventricle. (e) The left outflow tract view demonstrates the aorta arising from the left-sided mRV. (f) A complete heart block can sometimes appear in the third trimester. Note the dissociation between the atrial (A) and ventricular (V) frequencies.

Definition Corrected transposition of the great arteries (cTGA) features atrioventricular and ventriculoarterial discordance. The double discordance functionally corrects the circulation.

Anatomy. The key anomaly is the double (atrioventricular and ventriculoarterial) discordance, with the left atrium connected via a tricuspid valve to a morphologically right ventricle from which the aorta emerges; conversely, the right atrium is connected via the mitral valve to a morphologically left ventricle from which the pulmonary artery emerges. The discordance between cardiac situs and position is frequently associated, with dextrocardia in situs solitus and levocardia in situs inversus. Other major cardiac lesions, involving VSDs, Ebstein-like attachments of the left-sided tricuspid valve, pulmonary outflow obstruction, and/or rhythm disturbances, are frequently associated.

Ultrasound diagnosis. Unlike the other conotruncal anomalies, the key plane for the diagnosis of cTGA is the *four-chamber view*, in which the atrioventricular discordance is diagnosed (Figure 5.62a and b). In particular, the atrioventricular discordance is diagnosed when the morphologically right ventricle, with the moderator band and a trabecular wall, is connected to the left atrium, and conversely, the left ventricle, forming the apex of the heart, is connected to the right atrium. Additional features that may increase the confidence of the diagnosis are the different attachments of the chordae tendinae of the two atrioventricular valves: the left-sided tricuspid valve papillary muscles attach to the ventricular apex, whereas the right-sided mitral valve papillary muscles attach to the lateral free wall (Figure 5.62b). Assessment of the *outflow views* demonstrates the pulmonary artery arising from the right-sided left ventricle (Figure 5.62d) and the aorta connected with the left-sided right ventricle (Figure 5.62e). Recognition of dextrocardia in situs solitus should always prompt assessment of central connections to exclude the presence of cTGA. Anomalies of the tricuspid valve, VSDs (Figure 5.62c), pulmonary and aortic outflow obstruction, and complete heart block are

frequently and variously associated (Figure 5.62f). On rarer occasions, a double-outlet left-sided right ventricle can be present. The heart block is progressive, frequently appearing only in the third trimester or after birth, and is due to the abnormal position of the conduction tissue [65]. Color Doppler may be helpful in the assessment of the spatial relationship of TGA and in the detection of the VSD. Spectral Doppler may be used to quantify the transvalvular gradient in the case of pulmonary stenosis. Four-dimensional echocardiography has a limited role.

Differential diagnosis. This includes principally TGA, from which cTGA is easily distinguished by the double discordance. The abnormal arrangement of the great vessels may sometimes need to be differentiated from a DORV.

Prognostic indicators. Severe anomalies of the atrioventricular valves, which are responsible for ventricular hypoplasia, represent ominous prognostic signs.

Association with other malformations. Renal anomalies are the extracardiac malformations most frequently associated with cTGA [65].

Risk of chromosomal anomalies. This is virtually absent. Also cTGA, like TGA and cardiosplenic syndromes, seems to *protect* from aneuploidy [65].

Risk of nonchromosomal syndromes. This is virtually absent.

Obstetric management. Fetal karyotyping is not indicated, owing to the extremely low risk of chromosomal anomalies. Delivery should take place in a tertiary referral center if there is evident outflow obstruction, major atrioventricular anomalies, or congenital heart block with low cardiac output.

Postnatal therapy. If it is not associated with other major anomalies, cTGA does not need to be operated upon. The optimal management of cTGA is controversial, with pros and cons regarding the submission of patients with cTGA to the double (atrial and arterial) switch operation. However, the midterm results of this complex surgical procedure seem good, with 94%–100% survival at ten years [66]. However, as expected, at 20 years, survival was 83%, with 86% of patients in NYHA class I/II [67].

Prognosis, survival, and quality of life. The overall prognosis of cTGA is one of the most controversial and debated issues in pediatric cardiology. The frequency and severity of the associated cardiac lesions represent the most important determinants of survival and mortality. In particular, severe insufficiency of the left-sided tricuspid valve and impaired systolic function of the right (systemic) ventricle are the main indicators of a poor prognosis: by 45 years of age, 67% of individuals with associated lesions showed heart failure, in comparison with 25% of individuals with isolated cTGA [68].

hETERo TAxy syNdroMEs

Incidence. These account for about 4% of CHDs at birth.

Ultrasound diagnosis. Any arrangement of the internal organs other than situs solitus or situs inversus: heart and stomach on opposite sides, abnormal relationship of the abdominal aorta and inferior vena cava, and a midline liver. Almost always associated with major CHD.

Risk of chromosomal anomalies. Extremely low.

Risk of nonchromosomal syndromes. Virtually absent.

Outcome. Depends on the type and severity of the associated cardiac malformations. *Right atrial isomerism*: increased mortality in the case of obstructed pulmonary veins with the presence of a right outflow tract obstruction. *Left atrial isomerism*: increased mortality when complete heart block is present.

Definition Situs anomalies are often considered confusing, in part because of the overlapping features of some anomalies, such as situs ambiguous with polysplenia and situs ambiguous with asplenia. The literature also contributes to this confusion, because some authors use the terms "situs inversus" and "situs ambiguous" interchangeably. Greater understanding can be achieved by defining the terms commonly used to describe situs anomalies. The term *situs* refers to the position of the heart and viscera relative to midline. The normal anatomic configuration of the viscera (with the liver, vena cava, and trilobed lung

on the right, and the spleen, abdominal aorta, and bilobed lung on the left) and of the atria (the atrium morphologically right located on the right, and the atrium morphologically left located on the left) is called *situs solitus*. In *situs inversus*, there is usually a mirror-like position of the organs. A position of the organs different from situs solitus and situs inversus is called *situs ambiguous* or *heterotaxy*. Situs ambiguous or heterotaxy is not characterized by a single set of abnormalities but by a spectrum of abnormalities. The two major subcategories of situs ambiguous are situs ambiguous with polysplenia and situs ambiguous with asplenia.

Anatomy. Situs ambiguous with polysplenia (also known as bilateral left-sidedness or left atrial isomerism) is associated with paired left-sided viscera, while right-sided viscera may be absent. Bilateral morphological left atrial digit-like appendages, multiple cardiac anomalies, congenital heart block, bilateral morphologic left (bilobed) lungs, multiple splenules, a malpositioned stomach, a midline liver, and an interruption of the inferior vena cava with azygos continuation are all associated with left isomerism. In contrast, situs ambiguous with asplenia (bilateral right-sidedness or right atrial isomerism) features paired right-sided viscera, while left-sided viscera may be absent. Typical fin - ings are bilateral morphologic right atrial wide-based appendages, multiple cardiac anomalies, bilateral morphologic right (trilobed) lungs, an absent spleen, and a midline liver. A malpositioned inferior vena cava and aorta are frequently seen. Cardiac malformations are more complex in right isomerism postnatally. The most common cardiac and/or venous anomalies associated with *right atrial isomerism* [24] are abnormal axis and heart position (often opposite to the stomach), abnormal pulmonary venous return, a common atrium, an unbalanced AVSD, abnormal ventriculoarterial connection (mainly DORV or TGA), a TAPVC, stenosis or atresia of the pulmonary artery, and an inferior vena cava and abdominal aorta located either on the same side of the spine or centrally (the vena cava is always anterior to the aorta). The most common cardiac and/or venous anomalies associated with *left atrial isomerism* [24,69] are a shift of the cardiac axis or abnormal position of the heart, an unbalanced AVSD, ASD, absence of the intrahepatic tract of the inferior vena cava with azygos continuation, a bilateral superior vena cava, hepatic veins draining directly into the right atrium, a DORV, pulmonary outflow obstruction, and complete heart block.

Ultrasound diagnosis. The US markers for immediate evaluation of this syndrome are as follows [24,69]:

Left atrial isomerism

- Interruption of the intrahepatic tract of the inferior vena cava with azygos continuation (100%; Figure 5.63a and b);
- Complete unbalanced AVSD (68%; Figure 5.36);
- Viscerocardiac heterotaxy (54%): contralateral and not homolateral position of the heart with respect to the stomach (heart on the right—stomach on the left, and vice versa);
- Complete heart block (38%);
- Right ventricular outflow tract obstruction (35%);
- DORV (23%);
- Left ventricular outflow tract obstruction (21%);
- Total anomalous pulmonary vein drainage (5%).

When interruption of the inferior vena cava with azygos continuation is present, on the *axial view of the abdomen*, the azygos is close and lateral to the abdominal aorta (and not anterior, as with the inferior vena cava) (Figure 5.63b). This latter anomaly is also evident on the *four-chamber view*: behind the left atrium, two vessels (rather than one) of similar size but different pulsatility are identified (Figure 5.64). The azygos continuation usually drains into the superior vena cava in the upper mediastinum.

Right atrial isomerism

- Contralateral rather than ipsilateral position of the heart with respect to the stomach (heart on the right—stomach on the left, and vice versa; Figure 5.65);
- Anomalous position of the abdominal aorta and the inferior vena cava, both positioned centrally or on the same side of the spine (Figure 5.63c);
- Unbalanced AVSD (Figure 5.36) or other structural heart disease.

Color Doppler can be used to characterize the major cardiac anomalies and to trace the course of the abnormal pulmonary or systemic venous returns (Figure 5.26b) and to detect atrioventricular insufficiency or ductus dependence. Spectral Doppler may be used to support the identification of abnormally located pulmonary venous returns. Four-dimensional echocardiography has been employed in identification of atrial appendages' morphology (Figure 5.66) [63,70], and it can be of help in locating the normal and abnormal pulmonary veins [71]. It is also very useful to define the liver morphology, which is abnormal in both left and right isomerism (Figure 5.65).

Differential diagnosis. Isomerisms must be differentiated from situs inversus, where all the organs have a mirror image with respect to the norm, and from

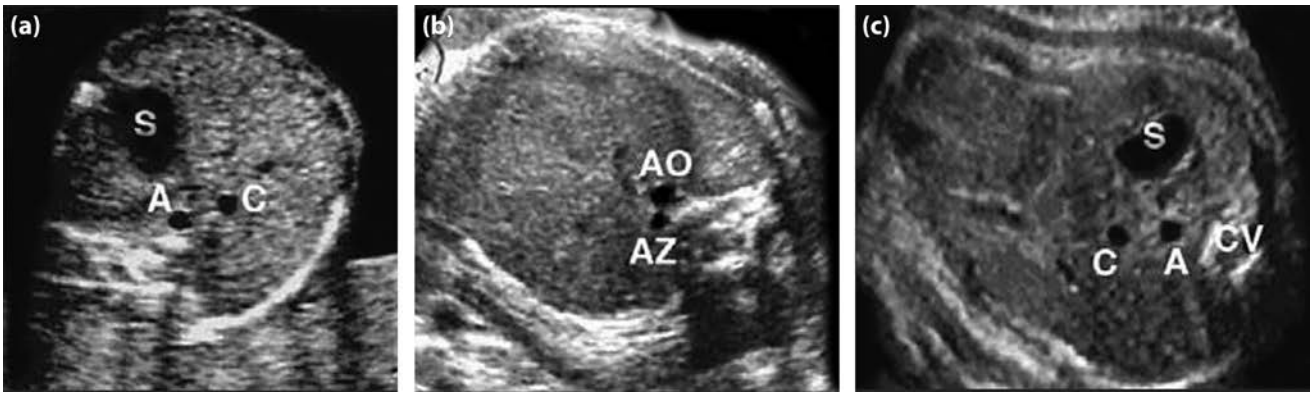


Figure 5.63 Cardiosplenic syndromes. (a) Situs solitus: the abdomen is seen in cross-section at the level of the stomach (S). The normal relationship of the aorta (A) and inferior vena cava (C) in the upper abdomen is seen. (b) In left atrial isomerism, interruption of the intrahepatic tract of the inferior vena cava with azygos continuation: axial view of the abdomen. The azygos vein (AZ) is close and lateral to the abdominal aorta (AO) (and not anterior, as with the inferior vena cava). (c) In right atrial isomerism: an anomalous position of the abdominal aorta (A) and the inferior vena cava, both of which are positioned on the same side of the spine. S: stomach.

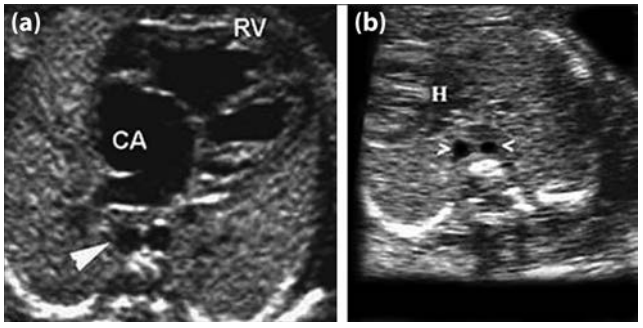


Figure 5.64 Left atrial isomerism. (a) Unbalanced atrioventricular septal defect. Note the azygos continuation (arrowhead) close to the descending aorta. CA: common atrium; RV: right ventricle. (b) On the four-chamber view, behind the left atrium, two (rather than one) vessels (arrowheads) of equal size are identifi d. H: heart.

isolated dextrocardia, where the other organs are arranged normally and associated cardiac malformations may be absent.

Prognostic indicators. The worst prognostic indicator is association of complete heart block with AVSD, which often leads to intrauterine demise. The prognosis is also unfavorable in a significant percentage of cases characterized by obstructed TAPVC and stenosis or atresia of the pulmonary artery.

Association with other malformations. Intestinal malrotation is frequent in both types of isomerism, occasionally with signs of occlusion.

Risk of chromosomal anomalies. Only one case of association with the 22q11 microdeletion has been reported. Otherwise, the cardiosplenic syndromes are not associated with chromosomal anomalies.

Risk of nonchromosomal syndromes. Sporadic cases of syndromes have been described featuring isomerism-like visceral arrangement. In addition, a recessive autosomal inheritance pattern with reduced penetrance has been reported in a few cases of isomeric syndromes.

Obstetric management. Among fetuses with structural cardiac anomalies, abnormal visceral situs is strongly predictive of a normal karyotype. Delivery must take place in any case in a tertiary referral center, in order to transfer the newborn to a pediatric cardiology or cardiosurgery unit for final diagnosis and adequate neonatal management.

Postnatal treatment. In some cases of left atrial isomerism, there is no need for any treatment, because the associated anomalies may be of limited clinical significance Surgery is needed for newborns with complex lesions—who account, unfortunately, for the majority of cases. The main indication for early correction is in those cases where a TAPVC is present, typically right isomerism, and often burdened by obstructive problems. The percentage of success increases in cases of biventricular correction, whereas it is significantly lower for univentricular correction mainly submitted to a Fontan-type treatment. In these cases, the presence of a double superior vena cava in the absence of a communicating vein requires a Glenn operation, which leads to an increase in morbidity. In addition, the visceral anomalies may adversely affect

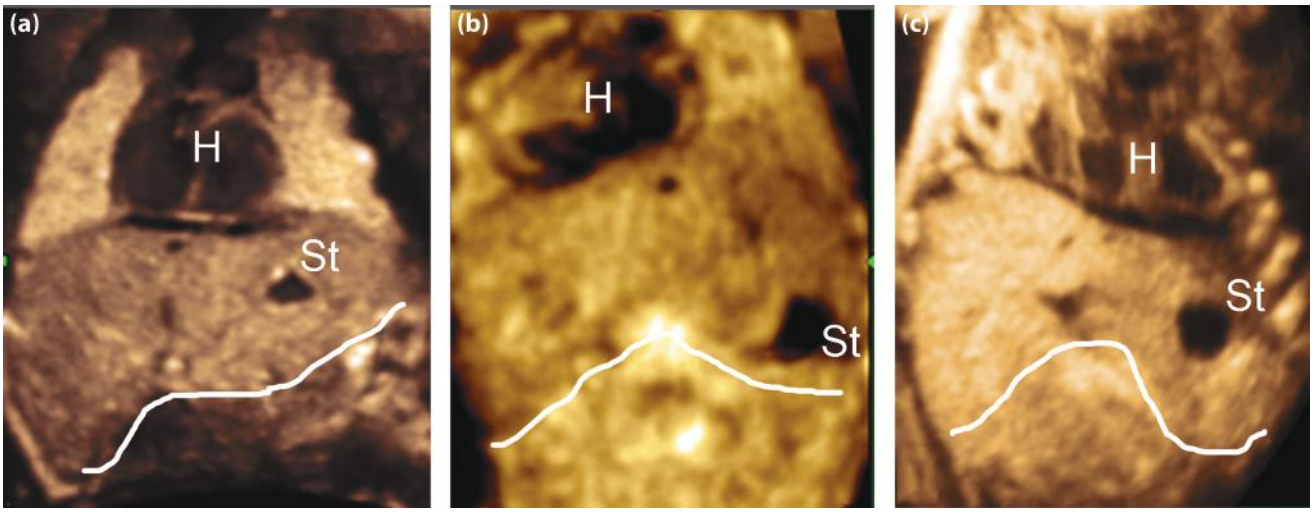


Figure 5.65 Visceral heterotaxy. Three-dimensional (3D)-derived coronal view of the fetal trunk in situs solitus and ambiguous. (a) In situs solitus, the heart appears centralized, because the plane is almost prevertebral, and the cardiac apex is out of the image. Note the stomach in the left hemiabdomen, and the normal outline of the liver (lower aspect), highlighted by the white line. (b) In right isomerism, the heart is on the right, and the shape of the liver is abnormal, bilobed, as there are two morphologically right liver lobes; and (c) also in left isomerism, the shape of the liver is abnormal. These findings can be assessed only with 3D ultrasound.

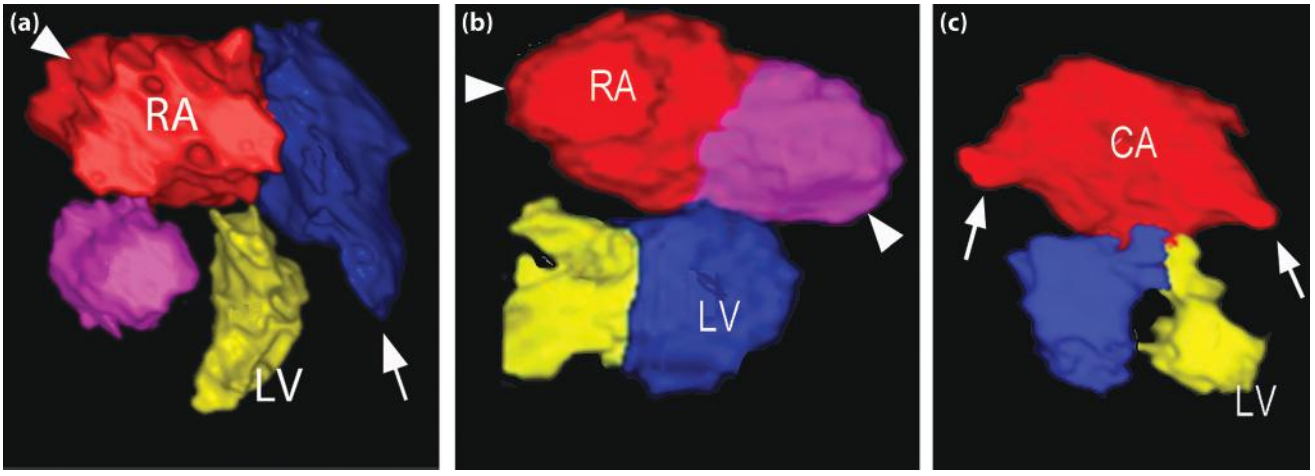


Figure 5.66 Atrial isomerism. Sono-AVC (a 3D-derived technique) is able to reconstruct casts of the cardiac chambers from 4D volume data sets. (See this chapter's text and Massoudy et al. [63].) In this way, it is possible to demonstrate the shape of the atrial appendages. (a) A normal heart. The right atrial appendage has a wide base (arrowhead), whereas the left one is digit-like (arrow). (b) In right atrial isomerism, both atrial appendages are wide based (arrowheads); and (c) in left atrial isomerism (atrioventricular septal defect), both atrial appendages are digit-like (arrows). CA: common atrium; LV: left ventricle; RA: right atrium.

the long-term outcome of patients with heterotaxy. Varying degrees of malrotation and malfixation of the bowel and gastric volvulus are common in both left and right isomerism, with a predominance in left isomerism. Children with right isomerism and asplenia who survive cardiac palliation are at great risk of dying from sepsis.

Prognosis, survival, and quality of life. The prognosis is certainly unfavorable in the case of right isomerism with TAPVC and stenosis or atresia of the pulmonary artery. In cases of right isomerism, Hashmi et al. [72] have reported a mortality rate of 75% in patients operated in the neonatal period and of 51% in those requiring an operation later. The prognosis is relatively better in children subjected to biventricular correction in comparison with those needing univentricular correction complicated by an anomaly of the veno-atrial connection. In cases of left isomerism, occasionally there may be no complex heart defects requiring surgery in the

neonatal period. During the postnatal period, the complexity and severity of cardiac anomalies are greater in right isomerism. The overall mortality is roughly 50% for both right and left isomerism, but it depends heavily on the type and the association of the various heart lesions.

cA rd IAc T UMors

Incidence. Very low.

Ultrasound diagnosis. On the *four-chamber view*, the tumors appear as single or multiple, usually hyperechoic nodules attached to the cardiac walls and/or septum. Tachyarrhythmias or hydrops can be associated.

Risk of chromosomal anomalies. Virtually absent.

Risk of nonchromosomal syndromes. High (rhabdomyomas with tuberous sclerosis).

Outcome. Good, unless the tumors cause valve obstruction with consequent heart failure and death. The prognosis is variable in the case of association with tuberous sclerosis.

Definition Cardiac tumors are mesenchymal or hamartomatous nodules arising from the cardiac layers and located in the heart or the pericardium.

Anatomy. *Rhabdomyoma*s are the most common tumors, accounting for two-thirds of the cardiac masses detected in the fetus and neonate [73]. These tumors are encapsulated and are often multiple. Characteristically, they are of late onset and often shrink significantly in the neonatal period [74]. *Teratomas* are the second most common histotype, accounting for about 15% of cardiac tumors. They are usually single and encapsulated, and they tend to grow within the pericardial cavity, fairly frequently leading to large pericardial effusions. Other tumors—*fibroma* , *hemangiomas*, and *myxomas*—have occasionally been described in the fetus [75]. They are usually single tumors. Myxomas are located in the atrium and have a stalk that allows free movement during the cardiac cycle.

Ultrasound diagnosis. *Rhabdomyomas* are usually detected on the *four-chamber view*: they are hyperechoic, well defined and round or oval (Figure 5.67a and b). These tumors may arise anywhere in the myocardium, and in a few cases they may completely replace some areas of the myocardium, appearing as hyperechoic regional myocardial thickening; however, in these rare cases, classic nodules are always associated and lead to the diagnosis. *Fibromas* (Figure 5.68) have sonographic characteristics similar to those of the rhabdomyoma, but they are almost always single. A cardiac *myxoma* has been described only once in the fetus, with an appearance consistent with that reported after birth: a moderately hyperechoic stalked tumor floating freely during the cardiac cycle [75]. It should be underlined that all these tumors evolve during the course of pregnancy: they appear in the late second trimester, growing steadily until 32–35 weeks, when they reach a plateau. After birth, rhabdomyomas can shrink significantly or disappear macroscopically. It has been speculated that this biphasic behavior may be related to the maternal hormonal milieu, which may stimulate tumor growth in the third trimester. After birth, the neonate is no longer in contact with maternal estrogens, and this allows the tumor to shrink as the mitotic hormonal stimulus is withdrawn. Color Doppler assessment may help in detecting dynamic outflow obstruction if the tumor is located in the ventricular outflo , and/or in checking the patency of an atrioventricular valve if the nodule is located just below the atrioventricular plane. Spectral Doppler may be used to quantify the outflow obstruction. Four-dimensional echocardiography is of little use in cases of cardiac tumors.

Differential diagnosis. This includes *hyperechogenic foci* and the rare dystrophic calcifications The differentiation from hyperechogenic foci is simple, since these do not have any continuity with the myocardium, being located on the chordae tendinae of the atrioventricular valves, and are very small. As far as the rare form of diffuse rhabdomyomatosis is concerned, this can rarely be mistaken for a cardiomyopathy, since other well-defined tumors are usually associated and lead to the final diagnosis

Prognostic indicators. The tumor volume is the main prognostic factor: it is much more common for large tumors to obstruct the atrioventricular inlets or the outflows The occurrence of *tachyarrhythmias*, which have been related to mechanical stimulation of the atrioventricular conduction system by tumors located at that level, and the possibly associated hydrops from cardiac failure are also poor prognostic factors.

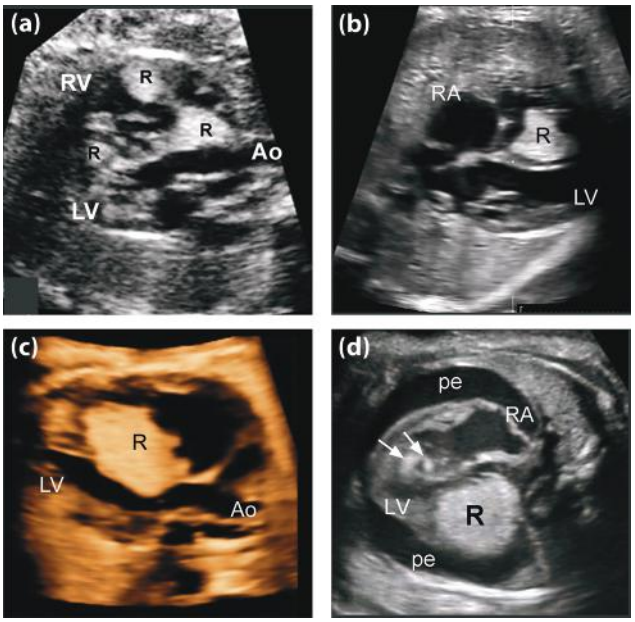


Figure 5.67 Rhabdomyomas. (a) Three tumors (R) are seen on the left outflow tract view. (b) A single tumor (R) below the tricuspid valve. (c) A single tumor (R) occupying most of the interventricular septum and partially obstructing the left outflow tract. (d) A large rhabdomyoma (R; 34 weeks) associated with other two small nodules (arrows). Pericardial effusion (pe) is associated. Ao: aorta; LV: left ventricle; pe: pericardial effusion; RA: right atrium; RV: right ventricle.

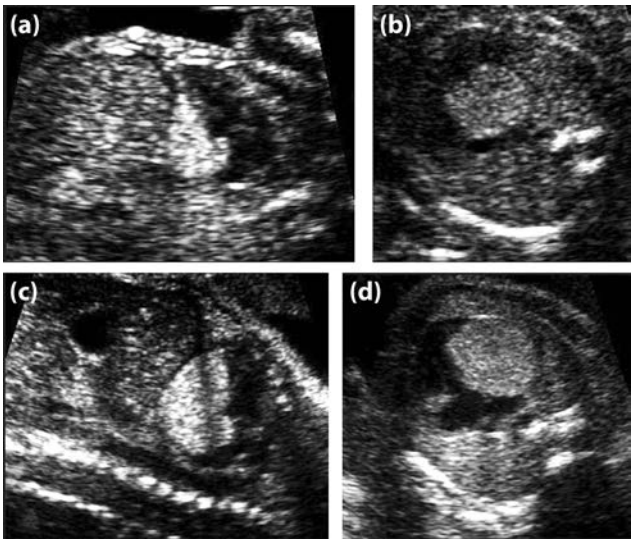


Figure 5.68 Cardiac fibroma at 22 weeks (a,b) and 30 weeks (c,d) of gestation. (a) Sagittal view, showing the relationships between the homogeneously hyperechoic tumor mass, the liver, the diaphragm, and the cardiac chambers. (b) Axial view of the base of the heart. The round shape of the tumor is evident. (c) At 30 weeks of gestation, the sagittal view shows the increased size of the tumor. (d) The axial view confirms the increased volume of the tumor.

Association with other malformations. No association has been reported, with the significant exception of tuberous sclerosis (TS) tumoral lesions if this congenital disorder is associated (see the "Risk of nonchromosomal syndromes" subsection below).

Risk of chromosomal anomalies. This is virtually absent.

Risk of nonchromosomal syndromes. This is extremely high for multiple—and, to a lesser extent, for single—rhabdomyomas, which account for 90% of all cases, but it is absent for the other histotypes.

Tuberous sclerosis (OMIM 191100—see Chapter 10) is a dominantly inherited disorder showing genetic heterogeneity and high penetrance. It is characterized by the presence of hamartomas in multiple organ systems (Chapter 10, Figure 10.43). Clinically, epilepsy, learning difficulties, behavioral problems, and skin lesions are the most commonly encountered problems. Renal angiomyolipomas may cause renal compression and hemorrhage. In utero, cerebral calcifications and subependymal nodules (Figure 10.43), possibly responsible in the neonate for epilepsy, seizures, and hydrocephalus, have occasionally been described on MRI and US in fetuses with rhabdomyomas. Mental retardation of variable degrees complicates 20%–30% of cases. TS can be diagnosed at birth, with recognition of the typical *café-au-lait spots*, but in other cases the disease may also appear late in infancy (up to 18 months of life). Ninety percent of fetuses diagnosed with multiple rhabdomyomas will eventually develop TS after birth.

Obstetric management. Karyotyping is not mandatory, as the risk of chromosomal anomalies is low. However, prenatal genetic counseling and genetic assessment of the parents are indicated in order to disclose a possible, previously unknown presence of TS in one of them. Obstetric management is based on follow-up of the tumors: if these show active growth and threaten to cause complete valve obstruction, then early delivery may be a valid option. If tachyarrhythmia is associated, transplacental antiarrhythmic therapy with digoxin should be attempted, although rhythm disturbances secondary to cardiac tumors are often unresponsive. Delivery should be organized in a tertiary referral center, in order to provide cardiologic and respiratory assistance if needed.

Postnatal therapy. Cardiac tumors do not require any medical or surgical treatment in 85% of cases, due to the significant regression of the lesions that occurs postnatally. In the case of multiple rhabdomyomas, examination including cerebral MRI, electroencephalography, renal US, and an ocular fundus examination

should be scheduled and serially repeated in order to disclose or confirm the presence of TS. The remaining 15% of cases are symptomatic at birth, and as such they may need medical and/or surgical intervention. In particular, in the case of *tumors causing severe pleuro-pericardial effusions*, which are responsible for cardiac tamponade and low cardiac output, an emergency pericardiocentesis should be performed, followed by surgical resection of the pericardial tumor. In the case of *tumor-induced tachyarrhythmias*, medical antiarrhythmic treatment is indicated (digoxin, flecainide or sotalol), and, if the rhythm disturbance is unresponsive, surgical removal of the tumor(s) is carried out. In the limited number of cases in which the tumors (rhabdomyomas) cause hemodynamically significant valve obstruction, surgical resection of the mass is always indicated.

Prognosis, survival, and quality of life. The surgical mortality rate for cardiac tumors is extremely low. Survival rates are high, and deaths (due to refractory cardiac failure and tachyarrhythmias) are usually confined to the first months of life. The long-term prognosis is guarded in the case of TS because of the 30% risk of mental retardation and the other possible sequelae possibly requiring repeated surgery.

cArd Io Myop ATh IEs

Incidence. Extremely low.

Ultrasound diagnosis. On the *four-chamber view*, concentric, biventricular thickening of the myocardial walls with variable impairment of cardiac function.

Risk of chromosomal anomalies. Virtually absent.

Risk of nonchromosomal syndromes. Variable (Noonan syndrome).

Outcome. Extremely variable. Depends on the degree of compromise of cardiac function and on possible underlying genetic disorders.

Definition The term *cardiomyopathy* (CMP) identifies a primary or secondary disorder of the myocardium that causes impairment of cardiac function of variable severity. Most CMPs have neonatal onset, but in a few cases they may arise in the late third trimester.

Anatomy. Primary CMPs are due to an architectural anomaly of the myocytes. The final consequence is compromise of cardiac diastolic and/or systolic function of variable degree. In the fetus, a detailed diagnosis of the type of CMP is not possible, and only an initial assessment of these disorders, mainly based on the sonographic appearance of the myocardium, is feasible. The primary forms that have been described in the fetus are familial hypertrophic CMP, dilated CMP, and spongious CMP (or myocardial dysplasia). Among the secondary forms, those most frequently seen in utero are the high-output CMP of the recipient twin in monochorionic pregnancies complicated by twin-to-twin transfusion syndrome and the CMP that is frequently observed in severe renal malformations (autosomal recessive polycystic renal disease, bilateral renal agenesis, etc.). Rarely, CMPs secondary to storage diseases are detected in the late third trimester.

Ultrasound diagnosis. The diagnosis is made on the *transverse four-chamber view*, since the thickness of free myocardial walls is best appreciated if displayed at 90° to the insonating beam. CMPs are easy to detect when severe, since in these cases cardiac function is highly depressed. What is extremely difficult is early recognition of a CMP when myocardial function is still apparently normal: it is the authors' personal experience that in a small number of cases that have later developed frank CMP, in the second-trimester scan, the myocardium appeared *very bright*, although of normal thickness and contractility (Figure 5.69a); then, in the early third trimester, the myocardial walls thickened and acquired the classic aspect of CMP (Figure 5.69b). Color Doppler may help to detect small VSDs, which are sometimes associated with CMPs, and to evaluate the outflows to exclude dynamic subaortic stenosis due to the thickened myocardium, which may obstruct the aortic outflo during systole. In CMP, the degree of cardiac function impairment benefits from the use of 4D echocardiography, which, especially with the inversion mode, is able to show in detail the degree of diastolic underfil - ing or systolic compromise (Figure 5.69c). In the few cases in which a storage disease shows prenatal onset, the cardiac findings are unmistakable (Figure 5.70a).

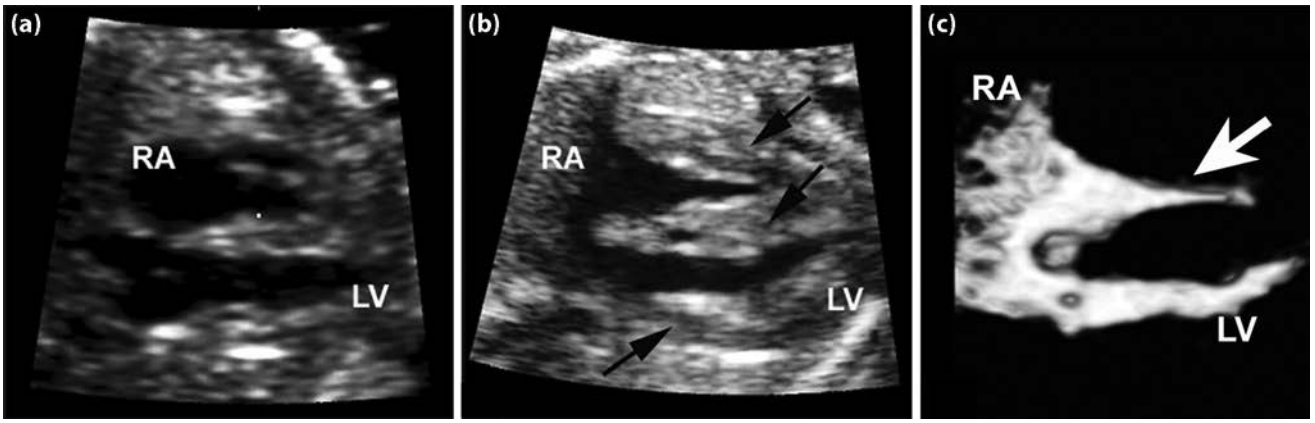


Figure 5.69 Familial hypertrophic cardiomyopathy: four-chamber view. (a) At 23 weeks of gestation, the only abnormal finding was a mildly bright aspect of the myocardium (not easily detected on the image). (b) At 35 weeks of gestation, the severe hypertrophy involving the free walls and the septum is evident (arrows). (c) 3D inversion-mode image demonstrating a significant impairment of ventricular relaxation, evidenced by the extremely reduced amount of blood in the ventricles (arrows).

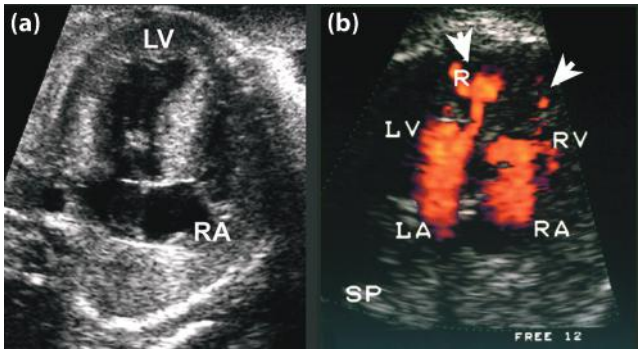


Figure 5.70 Cardiomyopathies. (a) Storage disease cardiomyopathy at 38 weeks of gestation. Note the severe thickening of the myocardial walls and septum. (b) Spongious cardiomyopathy (or myocardial dysplasia, noncompaction of the myocardium) at 36 weeks of gestation. Note the presence of several myocardial recesses (arrows) highlighted by the power Doppler. LA: left atrium; LV: left ventricle; RA: right atrium; RV: right ventricle; R and arrows: myocardial recesses.

Spongious CMP, which has also been referred to as noncompaction of the ventricle or myocardial dysplasia, can also have a fetal onset (Figure 5.70b).

Differential diagnosis. CMP should be differentiated from the mild hypertrophy of the right ventricle that is sometimes detected in the fetus late in gestation and that regresses shortly after birth. However, the key feature of most CMPs is that the myocardial thickening involves both ventricles. Also, in the case of CHD characterized by severe pressure or volume overload, myocardial thickening is typically unilateral, whereas the contraction of the contralateral ventricle is generally unremarkable.

Prognostic indicators. The degree of impairment of systolic function is the most important prognostic factor: cases that are associated with severe pump failure and that are often complicated by hydrops have a very high perinatal mortality rate. The association of tachyarrhythmias, due to compression and involvement of the conduction system, is also an ominous finding

Association with other malformations. No significant association with extracardiac anomalies has been described, unless the CMP is in a syndromic context.

Risk of chromosomal anomalies. This is virtually absent.

Risk of nonchromosomal syndromes. This is relatively low, if the extremely rare cases in which a storage disease has a prenatal onset are excluded. Three of the conditions that can present with CMP are Noonan syndrome and the extremely rare Toriello–Carey syndrome and Leopard syndrome (the latter is not diagnosable in the fetus):

- *Noonan syndrome [12]:* look for ► *CMP* + pulmonary outflow obstruction + nuchal edema (formerly enlarged nuchal translucency [NT]);
- *Toriello–Carey syndrome [12,76]:* look for ► *CMP* + corpus callosum agenesis + positive family history.

Obstetric management. Fetal karyotyping is not indicated, because of the extremely low risk of chromosomal anomalies and the usual late onset of CMPs. Early delivery may be considered in selected cases showing initial heart failure when pulmonary maturation is virtually guaranteed. In these rare cases, a Cesarean

section at 34–36 weeks of gestation may allow neonatal cardiac assistance and resuscitation with improved survival. In the case of arrhythmias, transplacental therapy should be attempted, although rhythm disturbances associated with CMP are usually refractory to antiarrhythmic drugs. Delivery should be organized in a tertiary referral center where these described neonatal procedures are available.

Postnatal therapy. Aortopulmonary shunting is necessary only if severe dynamic subaortic stenosis is detected after birth. If cardiac decompensation is refractory to all remedies, cardiac transplantation may represent the only option to save the infant's life.

Prognosis, survival, and quality of life. Survival rates and overall prognosis are extremely variable, and they depend mainly upon the degree of impairment of cardiac function and the etiology of the myocardial lesion. Storage diseases are almost invariably lethal in a few years; familial hypertrophic CMP has a variable phenotypic expression even within the same family, with cases requiring early cardiac transplantation and cases who manage to reach adulthood in acceptably good condition and in NYHA functional class I/II. Of note, in familial hypertrophic CMP, significant clinical improvements and, in selected cases, complete regression of the hypertrophy have been obtained with the beta-blocker propranolol [77].

FETAL Arrhy Th MIAs

Heart rate and rhythm. The fetal *heart rate* changes significantly across pregnancy. At six weeks of gestation, when the very early heartbeat is recognized, the heart rate is about 60–80 bpm, and it increases to 170 bpm in a few days; at 11–14 weeks, it averages 150–170 bpm, to remain in the range of 120–170 bpm thereafter; during fetal movements, the heart rate may reach 180–190 bpm to return promptly less than 170 bpm.

The *rhythm* is rather regular with minor, physiological, beat-to-beat variations.

The conduction system. This includes the sinus node, located at the level of the right atrium; the internodal pathway; the atrioventricular node; and the atrioventricular bundle, with the right and left bundle branches (Figure 5.71).

Techniques for cardiac rhythm assessment. Cardiac rhythm can be studied basically with two approaches, PWD and M-mode. With both, the sampling should include an atrial and a ventricular element, be it the wall motion (with M-mode) or the blood motion determined by atrial or ventricular contraction (with PWD). In this way, the relationship between atrial and ventricular contractions can be adequately assessed. However, with both techniques, care should be taken to adapt the sweep of the M-tracing or the Doppler strip to the overall heart rate of the examined fetus, which can vary from as low as 50 bpm to more than 300 bpm with heart block and atrial flutter, respectively. In addition, the magnification of the M-mode strip should be enough to permit visual evaluation of the contraction events that take place at the atrial and ventricular levels.

- *M-mode echocardiography (Figure 5.72)*: For the ideal sampling site, which corresponds to the classic postnatal one, the M-mode cursor is placed across the left ventricular free wall, the aortic valve, and the posterior wall of the right atrium on a long-axis view of the left ventricle (Figure 5.72a); simplifying this approach, one of the atrial walls and one of the ventricular walls should be sampled, regardless of the presence of the aorta in the middle. M-mode is simple to use in cases of good acoustic window; if the image quality is poor due to maternal habitus, polyhydramnios, or fetal crowding, then PWD is preferable. Recently, the possibility to reconstruct the M-mode signal from an oblique virtual M-mode cursor also has become available in some US systems (Figure 5.72b). This facilitates the evaluation of those cases in which only a suboptimal alignment with the cardiac chamber is possible due to an unfavorable fetal position.
- *PWD (Figure 5.73)*: If PWD is used for assessing fetal heart rhythm, then two settings should be preliminarily checked: (1) the sample volume should be wide (3 mm or even more, according to gestational age); and (2) the sweep of the spectral strip should be enough to clearly display atrial and ventricular events without overlapping. There are two techniques that are easy and reliable: one requires the five-chamber view of the fetal heart and does not need a color Doppler guide (Figure 5.73a). On this view, the atrial contraction is represented by the transmitral blood flow signal (A-wave), whereas the ventricular contraction is represented by the transaortic blood flow signal. The second technique consists of recording the signal from a pulmonary arterial branch and

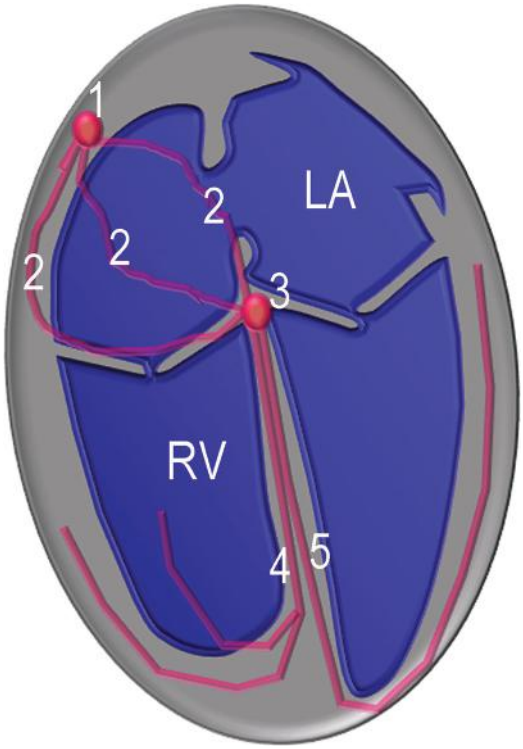


Figure 5.71 The cardiac conduction system. (1) sinus atrial node; (2) internodal pathway; (3) atrioventricular node; (4) right bundle branch; and (5) left bundle branch.

the adjacent pulmonary venous branch, virtually anywhere in the lung (Figure 5.73b); this latter technique requires a color Doppler guide to correctly place the PWD sample volume on the small arterial and venous branches of the pulmonary circulation [78]. In this case, the systolic peak corresponds to the ventricular contraction, whereas the negative A-wave of the pulmonary vein indicates the atrial contraction.

Definition of fetal arrhythmia. Fetal rhythm abnormalities are commonly divided into three categories: irregular rhythm (with a normal overall rate), tachycardias, and bradycardias. Unfortunately, there is no definition of the two latter abnormalities that is accepted worldwide. Normal range cutoffs vary from 100–200 bpm to 120–180 bpm, with some recent articles recommending 160 bpm as an upper cutoff (!). Frankly, we think that setting the cutoff as low as 160 bpm would trigger a plethora of referrals for alleged tachycardias that have nothing to do with real sustained fetal arrhythmias. This is why—as experts—we recommend using in clinical practice the former definition of bradycardia for heart rates less than 110 bpm and tachycardias for heart rates more than 180 bpm.

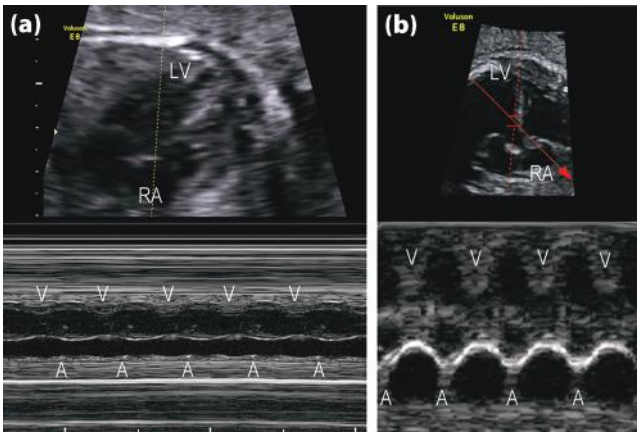


Figure 5.72 M-mode echocardiography. The aim is to display on the M-mode tracing the atrial and the ventricular contractions. (a) This is usually achieved on the five-chamber view of the fetal heart. This technique can be obtained on the native image, if the angle of insonation is favorable. (b) With newer scanners, also positioning of an oblique M-mode cursor is possible, in case of an unfavorable fetal position. In this case, the M-mode tracing is reconstructed by the scanner. A: atrial contraction; LV: left ventricle; RA: right atrium; V: ventricular contraction.

Irregular rhythm disturbances. This category comprises ≈90% of all fetal arrhythmias. The arrhythmia is caused by an ectopic beat (extrasystole) that may originate in atria or, more rarely, in ventricles, with its origin not bearing any prognostic significance (Figure 5.74). It represents a common occurrence, especially in the third trimester of pregnancy. What is currently debated is whether detection of such ectopic beats represents an indication to fetal echocardiography or not. In fact, on one hand, ectopics are associated with major CHDs in roughly 2% of cases and, in the same percentage, can trigger a reentry tachycardia, especially in cases with reduced ventricular rate [79]; on the other hand, in the overwhelming majority of cases, these ectopic beats (premature atrial or ventricular contractions) are benign and disappear within a few weeks or at birth. A final worldwide accepted recommendation is not available, but it can be reasonably suggested to refer these cases only if ectopics intensify or determine a bradycardia because they are coupled (bigeminy), monitoring the heart rate through cardiotocography.

Tachycardias. Moderate sinus tachycardia is associated with active fetal movements, maternal hyperpyrexia, or maternal beta-mimetics administration. However, this type of tachycardia is benign and does not affect the cardiac output, because the heart rate remains well below 200 bpm.

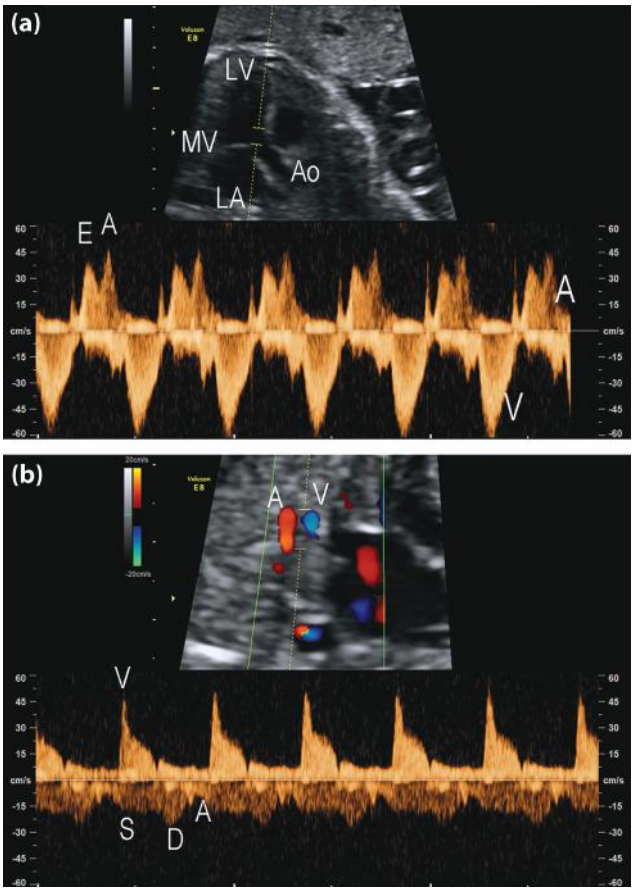


Figure 5.73 Pulsed-wave Doppler echocardiography. (a) The classic recording is carried out on the left outflow tract view. The transmitral inflow corresponds to the atrial contraction, whereas the transaortic outflow represents the ventricular contraction. (b) More recently, also the pulmonary intraparenchymal simultaneous sampling of a pulmonary arterial and venous branch has been described as a reliable and simple way to assess the relationships of atrial and ventricular contraction. A: atrial contraction; Ao: ascending aorta; EA: *e*arly and *a*trial components of the mitral spectral waveform; LA: left atrium; LV: left ventricle; M: mitral flow; RA: right atrium; V: ventricular contraction.

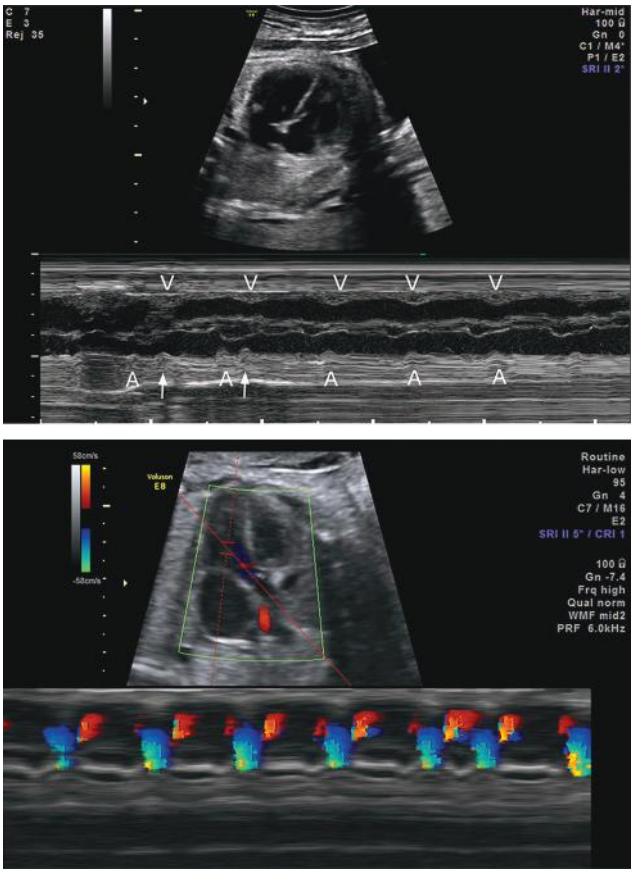


Figure 5.74 Premature atrial contraction (extrasystole). Upper panel: M-mode tracing of benign premature atrial contractions (arrows). A: atrial contraction; V: ventricular contraction. Lower panel: a different mode of investigating fetal arrhythmias is through color M-mode; the tracing shows ventricular inflows (diastole) in red and ventricular outflows (systole) in blue. At the end of the tracing, the ectopic atrial beat.

The most common pathological tachycardia is **supraventricular parossistic tachycardia (SVPT)**, which accounts for 70%–90% of all pathological tachycardias in the fetus [80]. This rhythm disturbance is characterized by a heart rate of more than 200 bpm and a 1:1 atrioventricular conduction ratio (Figure 5.75). Pathogenetically, SVPT is in most cases a reentry tachycardia, a condition in which an accessory atrioventricular conduction pathway allows retrograde passage of the electrical impulse from the ventricles to the atria, establishing a reentry circuit. This warrants a roughly constant heart rate of 220–240 bpm. More rarely, SVPT is due to other mechanisms, including atrial ectopic tachycardia and junctional reciprocating tachycardia. The assessment of the time interval between atrial and ventricular contraction allows one to hypothesize the mechanism of the tachycardia, contributing to an adequate selection of the antiarrhythmic drug.

Atrial flutter is much rarer than SVPT, accounting for not more than 10%–15% of all tachyarrhythmias. It is characterized by an atrial rate of 350–500 bpm and a halved ventricular rate, due to the presence of a 2:1 or variable atrioventricular block, because the atrial contractions are so frequent that at least half of them occur during the refractory period and, hence, are not conducted to the ventricle. It has been suggested that this tachyarrhythmia is much more difficult to convert to sinus rhythm with antiarrhythmic drugs than SVPT and is more often associated with hydrops from heart

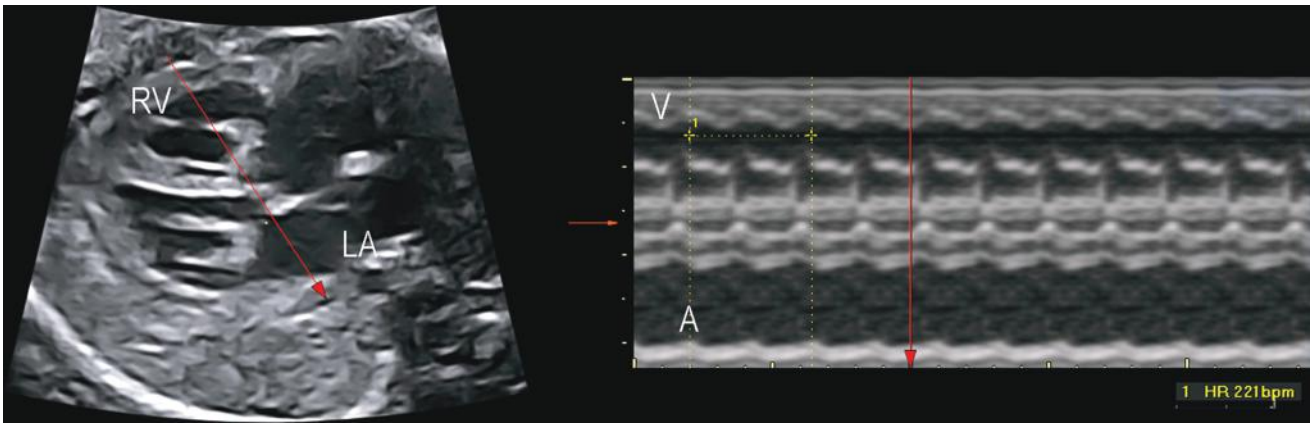


Figure 5.75 Supraventricular parossistic tachycardia (SVPT) at 28 weeks of gestation. The M-mode tracing demonstrates a 1:1 atrioventricular conduction ratio with a heart rate of 221 bpm, consistent with SVPT. A: atrial contraction; LA: left atrium; RV: right ventricle; V: ventricular contraction.

decompensation, even though both these findings were not confirmed in a detailed meta-analysis of fetal atrial flutter [81].

Management of fetal tachycardias. Four options are available for fetuses diagnosed with tachycardias: (1) delivery and plan for postnatal treatment; (2) drug treatment through administration of antiarrhythmic drugs to the mother; (3) direct (invasive) fetal treatment, with delivery of the antiarrhythmic drug directly into the fetal circulation; (4) close monitoring with no active intervention.

As a general rule, preterm delivery of a sick hydropic fetus should be avoided; similarly, most experts agree on not treating a fetus with an intermittent tachycardia and no signs of fetal heart failure.

In most cases, maternal administration of antiarrhythmic drugs is effective in the majority of cases, with few fetuses being refractory to this approach. If maternal administration of antiarrhytmic drugs fails, then direct fetal therapy or delivery should be considered. When using the former approach, it should be considered that hydropic fetuses tend to respond less than nonhydropic ones, probably because hydrops reduces the transplacental transfer of the drug. However, the need for direct fetal therapy due to failed transplacental conversion to sinus rhythm occurs in a very limited number of fetuses [80]. In general, most fetuses (>80%) with tachyarrhythmias are delivered in sinus rhythm without signs of hydrops [80]. Hydrops represents a poor prognostic sign because it is associated with a decrease in survival rate (73% vs. 96% in nonhydropic fetuses), a higher incidence of preexcitation on neonatal electrocardiography (ECG) (16% vs. 4%), and a higher chance of long-term postnatal antiarrhythmic therapy [80].

Antiarrhythmic drugs most commonly used in the fetus include digoxin, flecainide, and sotalol; much less used are amiodarone and adenosine, the former for the significant risk it poses of fetal hypothyroidism. Most groups agree on using digoxin in monotherapy as the first line of therapy for all nonhydropic fetuses, but note that the same drug is much less effective in hydropic ones because of impaired placental transfer. If digoxin is used, maternal ECG and digoxinemia should be checked weekly, both to maintain an adequate blood level of the drug and to disclose possible signs of digoxin intoxication. The problem is that the therapeutic index in these cases is very narrow and difficult to maintain, because of the high glomerular filtration rate of pregnant women and the consequent need for full dosage administration. The protocol usually requires an initial loading dose followed by a maintaining regimen. If effective, conversion of the SVPT back to sinus rhythm should be achieved in less than one week. In hydropic fetuses, flecainide or sotalol in monotherapy or in association with digoxin has been used [81]. Flecainide is a class 1c (Na^+ channel block) antiarrhythmic drug, initially associated with some adverse fetal effects and a maternal proarrhythmic effect. Sotalol is a beta-blocker with some class III action (K^+ channel block). Both of these drugs, as well as digoxin, have been used for direct fetal intravenous administration through the cord. A therapeutic flow chart for fetal tachyarrhythmias is reported in Figure 5.76.

Bradycardias. Fetal bradycardias include multiple blocked atrial ectopic beats, sinus bradycardia, and atrioventricular block. The first two entities are rare. **Multiple blocked atrial ectopics** represent a benign arrhythmia that often resolves spontaneously

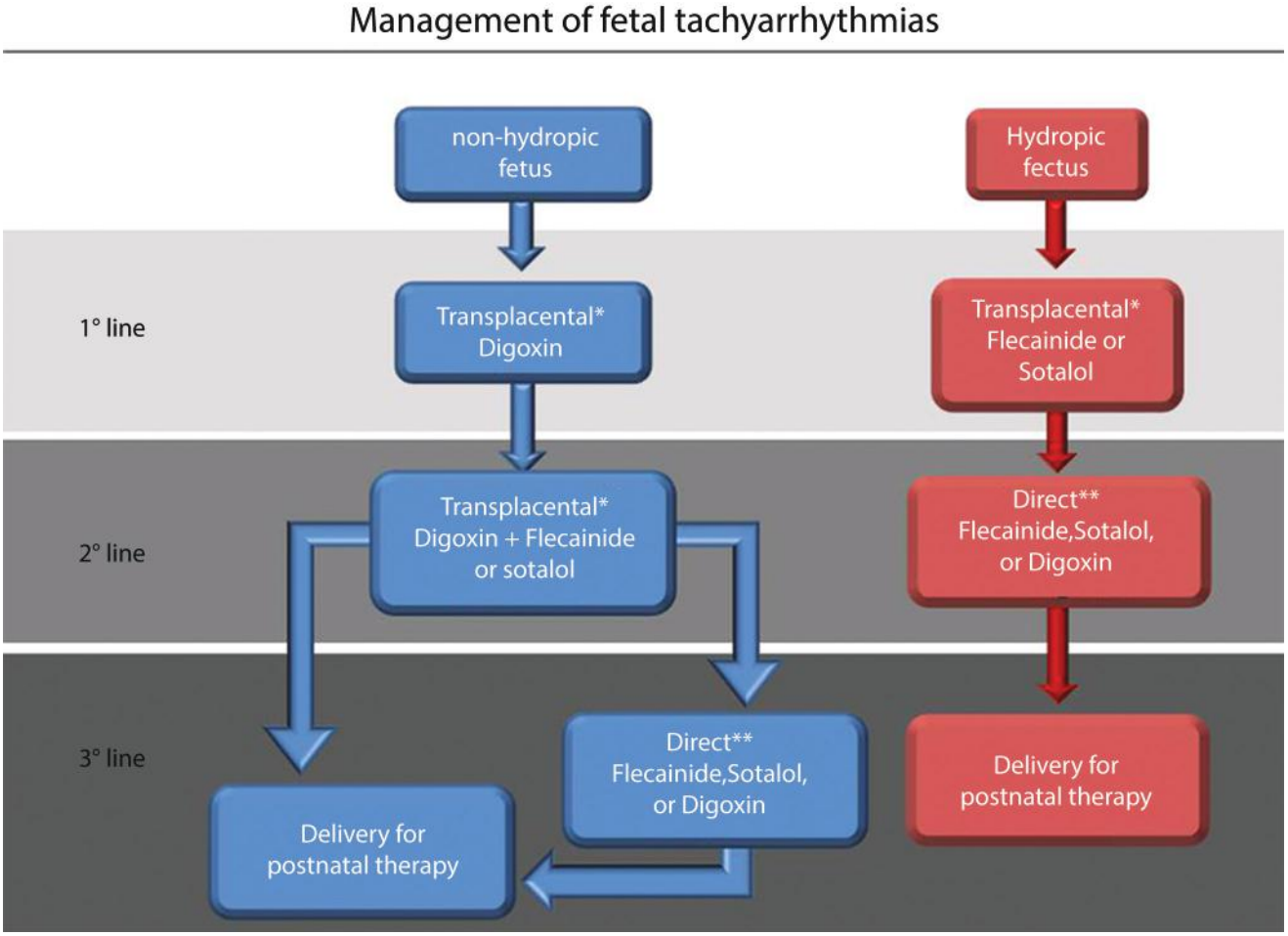


Figure 5.76 Flowchart for management of fetal tachyarrhythmias. In the nonhydropic fetus, the first-line treatment is transplacental digoxin, followed, if conversion to sinus rhythm is not achieved within seven to ten days, by association with flecainide or sotalol. Only in refractory cases should direct fetal drug administration or delivery be considered. In the hydropic fetus, monotherapy with digoxin is likely to be ineffective due to impaired transplacental transfer. Therefore, a direct approach with flecainine or sotalol is used by most groups. As for the nonhydropic fetus, direct administration of the drug in the fetal circulation or delivery is considered only in cases of failed conversion. *Through maternal administration of the drug; **through cord or intramuscular injection.

after a few weeks. **Sinus bradycardia** is a rare condition that can be associated with left atrial isomerism, due to involvement of the sino-atrial node. If sequential cardiac anatomy is unremarkable, the only significant condition that has been associated with sinus bradycardia in the fetus is the long QT syndrome [82].

Atrioventricular block is the most common pathological bradyarrhythmia. It is classified into three degrees. In first-degree heart block, there is prolongation of the mechanical PR interval (or atrioventricular interval). In second-degree heart block, there is either a fixed 2:1 or 3:1 ratio of atrial-to-ventricular contractions, or progressive prolongation of the PR interval until an atrial beat is nonconducted (Wenckebach). In complete (or third-degree) heart block (CHB), there is complete dissociation between atrial and ventricular contractions (Figure 5.77).

CHB can occur as an isolated anomaly or be associated with CHD, namely, left isomerism or corrected transposition of great arteries. If isolated, it may be due to maternal autoimmune diseases (Lambert–Eaton myasthenic syndrome, Sjogren syndrome, etc.) associated with the production of anti-Ro or anti-La (Sjogren syndrome type A antigen and type B antigen, respectively) autoantibodies. In particular, what causes CHD is the transplacental passage of maternal autoantibodies directed against 48 kD (La), 52 kD (52Ro), and 60 kD (60Ro) components of the Ro particles. A recent report shows that the risk of

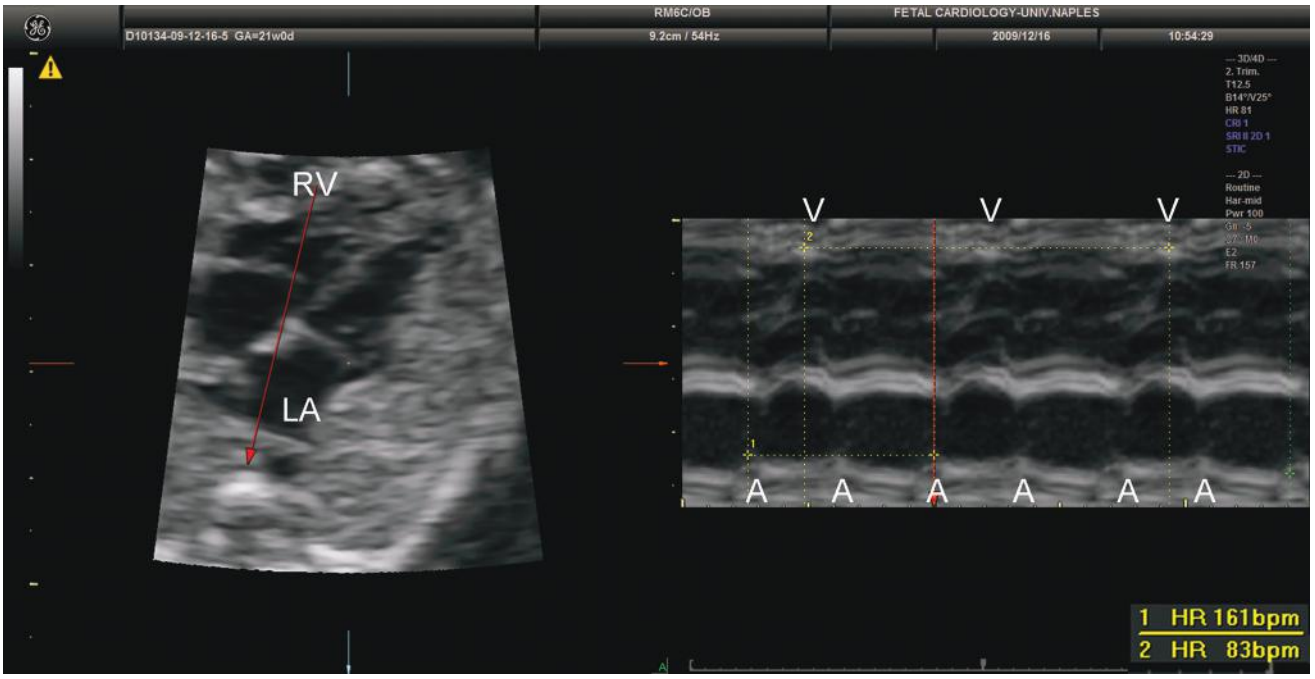


Figure 5.77 Complete heart block. In this fetus at 21 weeks of gestation, complete heart block is found. On the reconstructed M-mode strip from a 4D volume data set, the atrial rate is 161 bpm (in yellow, lower right end corner of the image, measurement 1), while the ventricular rate is 83 bpm (in yellow, lower right end corner of the image, measurement 1). A: atrial contraction; LA: left atrium; RV: right ventricle; V: ventricular contraction.

developing fetal CHB is less than 5% and 0% for pregnancies with anti-Ro enzyme-linked immunosorbent assay (ELISA) levels of more than 100 U/mL and less than 50 U/mL [83]. The mechanism through which anti-Ro antibodies seem to damage primarily (but not uniquely) the fetal conduction system is the following. Apparently, Ro and La proteins are located on the cell surface, where they are involved in the normal developmental apoptosis of cardiac cells. Here, they bind the anti-Ro antibodies, with consequent impairment of the physiological apoptosis, attraction of macrophages, and production of cytokines. Inflammation, fibrosis, and calcification in the conducting system and, more rarely, in the myocardium may then lead to heart block and/or endocardial fibroelastosis.

In most cases, CHB is diagnosed in the second trimester, at 18–24 gestational weeks. Poor prognostic factors indicating a relatively high risk of perinatal death include fetal hydrops, endocardial fibroelastosis, and ventricular escape rates less than 55 bpm. Neonatal survival rates range from 66% to 86%, with a 5%–10% risk of developing late-onset congestive heart failure due to dilated cardiomyopathy (and, apparently, this risk is not altered by any kind of prenatal therapy).

In fact, the effectiveness of **CHB prenatal treatment** has always been controversial. The rationale of such treatment is to (1) reduce damage to the conduction system and the myocardium through anti-inflammatory agents, such as steroids; and (2) increase the ventricular heart rate to above 60 bpm in cases characterized by a very low (<55 bpm) ventricular escape rate through the administration of beta-agonists. Regarding the former aspect, both dexamethasone and betamethasone have been used; robust data in favor of such long-term treatment are not available, but concerns about fetal and maternal side effects of steroid therapy have been raised. Both salbutamol and terbutaline have been used to increase the fetal cardiac output through an increase in heart rate associated with a reduction in peripheral resistance. Such treatment is indicated if the heart rate falls below 55 bpm and/or in cases of impaired cardiac contractility. In these cases, both drugs—if administered at high dosages (a maximum of 40 mg/day for salbutamol and 30 mg/day for terbutaline)—are effective in increasing the heart rate by 5–10 bpm. Common maternal side effects include tremors, tachycardia, and sweating, which usually disappear with continuation of therapy. Rarely, serious effects

such as pulmonary edema, myocardial ischemia, and arrhythmias have been described. As for all betamimetics, the pros and cons of such treatment in women with diabetes, hypertension, or hyperthyroidism should be evaluated.

In conclusion, there is no evidence of the effectiveness of any transplacental drug treatment in improving the survival rates of fetuses and neonates with CHB.

EAr Ly scr EENING ANd dIAGNos Is o F chd

Screening. The widespread application of the 11–14 weeks combined screening for aneuploidies and the concurrent discovery that an increased NT thickness is also associated with cardiac defects, even in euploid fetuses [84], have brought about the potential for an early detection of CHD. Indeed, it has been known for ten years that the cardiac defects are also associated with two additional first-trimester US markers of aneuploidy: tricuspid valve regurgitation (TR) and reversed A-wave in the ductus venosus (DV) flow velocity waveform [85–87]. And the definition of the methodology for TR assessment has represented the first step toward the routine evaluation of the four-chamber view by experienced sonographers in first-trimester scans.

The need for further cardiac investigation in the presence of these ultrasonographic markers (increased NT with normal karyotype, TR, and reversed DV A-wave) has led to the inclusion of these findings among the list of indications to fetal echocardiography at 18–22 weeks of gestation. Along these lines, an early echocardiography (at 14–16 gestational weeks) has been proposed in cases of NT measurements more than 99th centile (3.5 mm) or for the presence of two ultrasonographic markers simultaneously. However, the increased skills of the operators together with the availability of higher resolution US equipment have led to an even earlier assessment of the fetal heart, at the very same time as the NT screening. In fact, several studies have been conducted on first-trimester echocardiography, initially in high-risk fetuses [88–91] and, subsequently, even in unselected populations, reporting satisfactory feasibility, sensibility, and high specificity [38,92,93].

A screening strategy—including a routine screening at 11–14 weeks for NT with tricuspid valve, DV, and direct fetal heart evaluation, and a subsequent 14–16 weeks and/or 18–22 weeks echocardiography in case of any abnormal findings—can increase significantly, together with the classic mid-trimester anomaly-screening scan, our ability to detect CHD. However, before this potential boost in the prenatal CHD detection rate can be implemented in clinical practice, a detailed assessment of the cost–benefit ratio should be made, considering that none of these studies has reported how much additional time was required to carry out the cardiac screening at the time of the first-trimester US screening.

While awaiting a cost-effectiveness evaluation and an unbiased evaluation of the extra time needed to carry out this additional screening procedure, it should anyway be considered that a suspicious four-chamber view in the first-trimester screening seems to be the single most sensitive and specific first-trimester marker of CHD. Combined to NT, TR, and examination, this finding can potentially lead to the early detection of about 70% of major cardiac defects [38].

Early fetal echocardiography. The direct cardiac examination requires a rather different set of echocardiographic views from the second-trimester one. The principal first-trimester views should include the following:

- A *four-chamber view (Figure 5.78)*, preferably with the cardiac apex at the top of the screen. On this view, assessment of the cardiac situs and its relation with the fetal stomach should be carried out. Also, an evaluation of the two atrioventricular connections by 2D US and color flow mapping should be performed;
- *Left outflow tract view (Figure 5.79)*;
- *Crossover view*: this view is referred to in the first trimester as the "X-sign" [93] or "anterior V-sign" [38] on color flow mapping (Figure 5.80). However, it should be considered that the two great arteries lie on different planes, although by a few millimeters, and, therefore, the crossover cannot be documented with a single image;
- *Three-vessel and trachea view*: the ductal and aortic arches are depicted on color flow mapping as a posterior "V-sign" (Figure 5.80).

When performing an early fetal echocardiography, the natural history of CHDs should be considered; in fact, some major cardiac abnormalities are indeed detectable at 12–14 weeks, while other similarly important defects cannot be detected at this early gestational age.

In fact, although most types of CHD occur during the first eight weeks of embryonic development, many of these lesions progress significantly to become

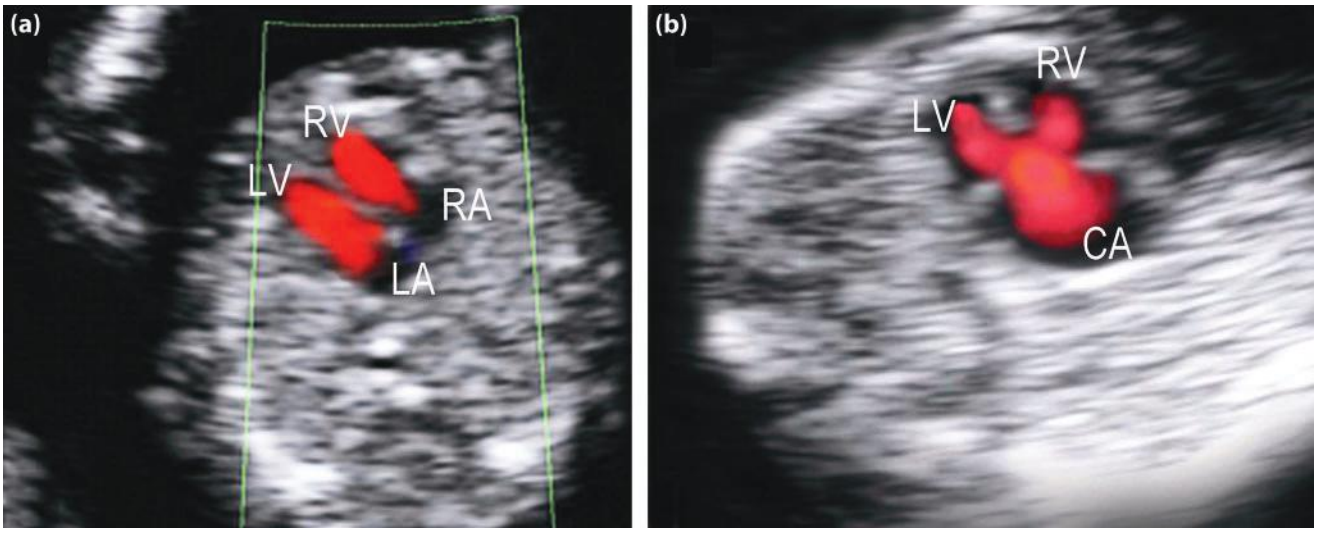


Figure 5.78 Early echocardiography: transabdominal ultrasound, four-chamber view. (a) Color Doppler image of an apical four-chamber view at 12 weeks of gestation demonstrates normal atrioventricular fillings: the right and left ventricle separated by the interventricular septum can be clearly identified, as well as the two atria. (b) Color Doppler image of an apical four-chamber view in a fetus with complete atrioventricular septal defect at 14 weeks of gestation. A single inflow is demonstrated, with the blood flow bifurcating beyond the atrioventricular plane at the level of the interventricular septum. The color signal is Y-shaped. CA: common atrium; LA: left atrium; LV: left ventricle; RA: right atrium; RV: right ventricle.

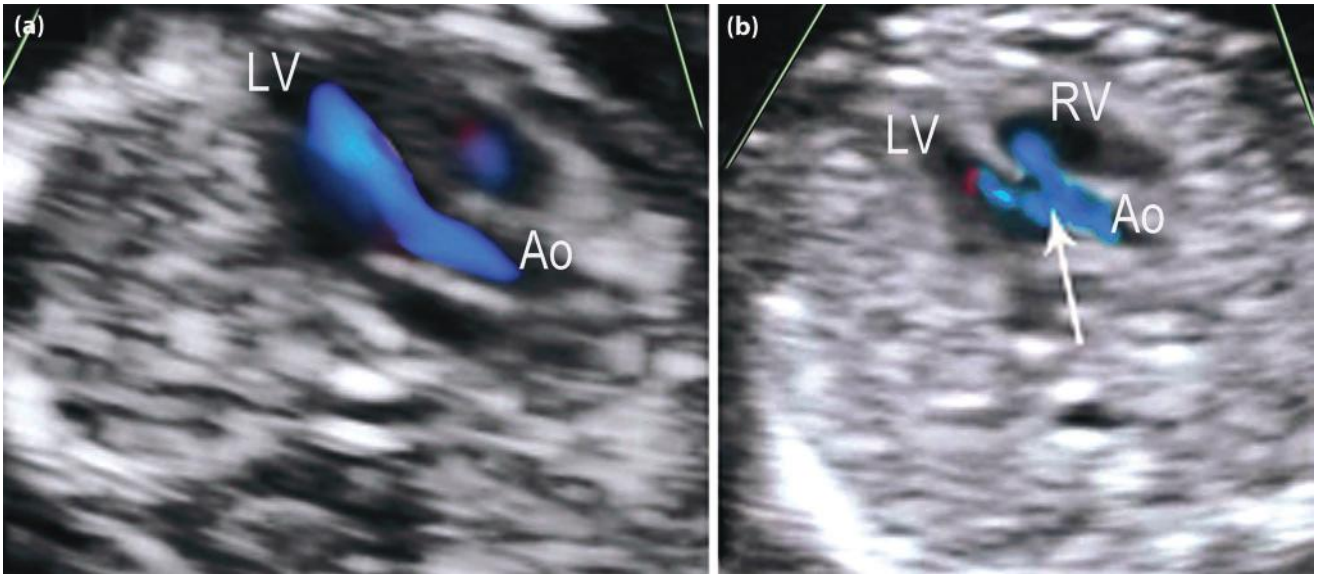


Figure 5.79 Early echocardiography: transabdominal ultrasound, left outflow tract view (13 weeks of gestation). (a) Color Doppler image showing the normal left outflow tract; the aorta arising from the left ventricle and the presence of septoaortic continuity are demonstrated. (b) Color Doppler image demonstrating malaligment ventricular septal defect with overriding aorta: the outflow color Doppler signal is Y-shaped because the aorta receives blood from both ventricles, across the malalignment ventricular septa defect. Ao: ascending aorta; LV: left ventricle; RV: right ventricle. (Modified from Volpe P et al. *Prenat Diagn* 2011; 31: 1054–61.)

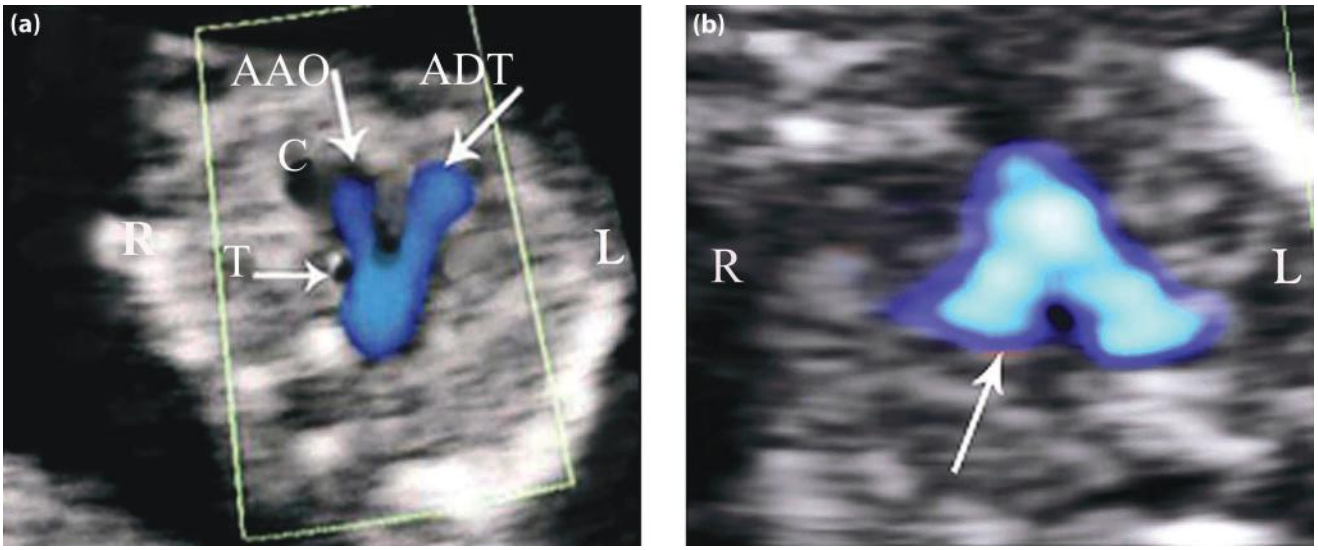


Figure 5.80 Early echocardiography: transabdominal ultrasound, three-vessel views. (a) Three-vessel trachea view demonstrating the ductal arch (ADT) and aortic arch (AAO) (posterior V-sign), merging together into the descending aorta, to the left of the trachea (T). The superior vena cava (C) is located to the right of the aortic arch. L: left; R: right. (b) Anterior V-sign: the left branch of the V corresponds to the ductal arch, whereas the somewhat shorter right branch corresponds to the ascending aorta (arrow), imaged just prior to the curvature of the aortic arch. L: left; R: right. (Modified from Volpe P et al. *Prenat Diagn* 2011; 31: 1054–61.)

sonographically detectable only with advancing gestation [94–97]. In this regard, it has been shown that CHD progression is much more pronounced between 11–14 and 18–22 weeks than from 22 weeks onward [38]. Therefore, it must be underscored that, although first-trimester echocardiography is feasible at the time of the NT evaluation and can achieve an early detection of at least 50% of major cardiac disease, some heart defects may develop and become apparent only later in gestation.

rEFE r ENc Es

1. Carvalho JS, Ho SY, Shinebourne EA. Sequential segmental analysis in complex fetal cardiac abnormalities: a logical approach to diagnosis. *Ultrasound Obstet Gynecol* 2005; 26: 105–11.
2. Yoo SJ, Lee YH, Cho KS, et al. Sequential segmental approach to fetal congenital heart disease. *Cardiol Young* 1999; 9: 430–44.
3. Carvalho JS, Allan LD, Chaoui R, et al. ISUOG Practice Guidelines (updated): sonographic screening examination of the fetal heart. *Ultrasound Obstet Gynecol* 2013; 41: 348–59.
4. Gonçalves LF, Lee W, Chaiworapongsa T, et al. Four-dimensional ultrasonography of the fetal heart with spatio-temporal image correlation. *Am J Obstet Gynecol* 2003; 189: 1792–802.
5. Chaoui R, Hoffmann J, Heling KH. Three-dimensional (3D) and 4D color Doppler fetal echocardiography using spatio-temporal image correlation (STIC). *Ultrasound Obstet Gynecol* 2004; 23: 535–45.
6. Paladini D, Vassallo M, Sglavo G, et al. The role of spatio-temporal image correlation (STIC) with tomographic ultrasound imaging (TUI) in the sequential analysis of fetal congenital heart disease. *Ultrasound Obstet Gynecol* 2006: 27: 555–61.
7. Volpe P, Campobasso G, De Robertis V, et al. Two- and four-dimensional echocardiography with B-flow imaging and spatiotemporal image correlation in prenatal diagnosis of isolated total anomalous pulmonary venous connection. *Ultrasound Obstet Gynecol* 2007; 30: 830–7.
8. Darling RC, Rothney WB, Craig JM. Total pulmonary venous drainage into the right side of the heart. Report of 17 autopsied cases not associated with other major cardiovascular anomalies. *Lab Invest* 1957; 7: 44–64.
9. Valsangiacomo ER, Hornberger LK, Barrea C, et al. Partial and total anomalous pulmonary venous connection in the fetus: two-dimensional and Doppler echocardiographic findings *Ultrasound Obstet Gynecol* 2003; 22: 257–63.
10. Volpe P, Buonadonna AL, Campobasso G, et al. Cat-eye syndrome in a fetus with increased nuchal translucency: three-dimensional ultrasound and echocardiographic evaluation of the fetal phenotype. *Ultrasound Obstet Gynecol* 2004; 24: 485–7.
11. Vassallo M, Pascotto M, Pisacane C, et al. Right superior vena cava draining into the left atrium: prenatal diagnosis and postnatal management. *Ultrasound Obstet Gynecol* 2006; 27: 445–8.
12. Jones KL. *Smith's Recognizable Patterns of Human Malformation*, 6th edn. Philadelphia: WB Saunders, 2006.
13. Ferencz C, Rubin DJ, Loffredo AC, et al., eds. *Epidemiology of Congenital Heart Disease. The Baltimore–Washington Infant Study 1981–1989*. Perspectives in Pediatric Cardiology, Vol 4. New York: Mount Kisco Futura, 1993.
14. Allan LD, Sharland GK, Milburn A, et al. Prospective ultrasound diagnosis of 1006 consecutive cases of congenital heart disease in the fetus. *J Am Coll Cardiol* 1994; 23: 1452–8.
15. Paladini D, Russo M, Teodoro A, et al. Prenatal diagnosis of congenital heart disease in the Naples area during the years 1994–1999—the experience of a joint fetal–pediatric cardiology unit. *Prenat Diagn* 2002; 22: 545–52.

16. Paladini D, Palmieri S, Lamberti A, et al. Characterization and natural history of ventricular septal defects in the fetus. *Ultrasound Obstet Gynecol* 2000; 16: 118–22.
17. Axt-Fliedner R, Schwarze A, Smrcek J, et al. Isolated ventricular septal defects detected by color Doppler imaging: evolution during fetal and first year of postnatal life. *Ultrasound Obstet Gynecol* 2006; 27: 266–73.
18. Paladini D, Russo MG, Vassallo M, et al. The "in-plane" view of the interventricular septum. A new approach to the characterization of ventricular septal defects in the fetus. *Prenat Diagn* 2003; 23: 1052–5.
19. Yagel S, Valsky DV, Messing B. Detailed assessment of fetal ventricular septal defect with 4D color Doppler ultrasound using spatio-temporal image correlation technology. *Ultrasound Obstet Gynecol* 2005; 25: 97–8.
20. Hoffman JIE, Rudolph AM. The natural history of ventricular septal defects in infancy. *Am J Cardiol* 1965; 16: 634–53.
21. Kirklin JW, Barratt-Boyes BG. *Cardiac Surgery*, 2nd edn. New York: Churchill Livingstone, 1993.
22. Huggon IC, Cook AC, Smeeton NC, et al. Atrioventricular septal defects diagnosed in fetal life: associated cardiac and extra-cardiac abnormalities and outcome. *J Am Coll Cardiol* 2000; 36: 593–601.
23. Allan LD. Atrioventricular septal defect in the fetus. *Am J Obstet Gynecol* 1999; 181: 1250–3.
24. Berg C, Geipel A, Smrcek J, et al. Prenatal diagnosis of cardiosplenic syndromes: a 10-year experience. *Ultrasound Obstet Gynecol* 2003; 22: 451–9.
25. Paladini D, Volpe P, Sglavo G, et al. Partial atrioventricular septal defect in the fetus: diagnostic features and associations in a multicenter series of 30 cases. *Ultrasound Obstet Gynecol* 2009; 34: 268–73.
26. Paladini D, Marasini M, Volpe P. Severe ductal constriction in the third-trimester fetus following maternal self-medication with nimesulide. *Ultrasound Obstet Gynecol* 2005; 25: 357–61.
27. Faiola S, Tsoi E, Huggon C, et al. Likelihood ratio for trisomy 21 in fetuses with tricuspid regurgitation at the 11 to 13+6-week scan. *Ultrasound Obstet Gynecol* 2005; 26: 22–7.
28. Todros T, Paladini D, Chiappa E, et al. Pulmonary stenosis and atresia with intact ventricular septum during prenatal life. *Ultrasound Obstet Gynecol* 2003; 21: 228–33.
29. Salvin JW, McElhinney DB, Colan SD, et al. Fetal tricuspid valve size and growth as predictors of outcome in pulmonary atresia with intact ventricular septum. *Pediatrics* 2006; 118; e415–20.
30. Daubeney PEF, Sharland GK, Cook AC, et al., for the UK and Eire Collaborative Study of Pulmonary Atresia with Intact Ventricular Septum. Pulmonary atresia with intact ventricular septum. Impact of fetal echocardiography on incidence at birth and postnatal outcome. *Circulation* 1998; 98: 562–6.
31. Simpson JM. Hypoplastic left heart syndrome. *Ultrasound Obstet Gynecol* 2000; 15: 271–8.
32. Allan LD, Sharland G, Tynan MJ. The natural history of the hypoplastic left heart syndrome. *Int J Cardiol* 1989; 25: 341–3.
33. Lowenthal A, Kipps AK, Brook MM, et al. Prenatal diagnosis of atrial restriction in hypoplastic left heart syndrome is associated with decreased 2-year survival. *Prenatal Diagnosis* 2012; 32: 485–90.
34. Rychik J, Szwast A, Natarajan S, et al. Perinatal and early surgical outcome for the fetus with hypoplastic left heart syndrome: a 5-year single institutional experience. *Ultrasound Obstet Gynecol* 2010; 36: 465–70.
35. Galindo A, Nieto O, Villagrá S, et al. Hypoplatic left heart syndrome diagnosed in fetal life: associated findings pregnancy outcome and results of palliative surgery. *Ultrasound Obstet Gynecol* 2009; 33: 560–6.
36. Simpson JM, Sharland GK. Natural history and outcome of aortic stenosis diagnosed prenatally. *Heart* 1997; 77: 205–10.
37. McCaffrey FM, Sherman FS. Prenatal diagnosis of severe aortic stenosis. *Pediatr Cardiol* 1997; 18: 276–81.
38. Volpe P, De Robertis V, Campobasso G, et al. Diagnosis of congenital heart disease by early and second-trimester fetal echocardiography *JUM* 2011; 31: 563–8.
39. Makikallio K, McElhinney DB, Levine JC, et al. Fetal aortic valve stenosis and the evolution of hypoplastic left heart syndrome: patient selection for fetal intervention. *Circulation* 2006; 113: 1401–5.
40. McElhinney DB, Marshall AC, Wilkins-Haug LE, et al. Predictors of technical success and postnatal biventricular outcome after in utero aortic valvuloplasty for aortic stenosis with evolving hypoplastic left heart syndrome. *Circulation* 2009; 120: 1482–90.
41. Brierley J, Redington AN. Aortic coarctation and interrupted aortic arch. In: Anderson RH, Macartney FJ, Shinebourne EA, et al. eds. *Paediatric Cardiology*. Edinburgh: Churchill Livingstone, 2001: 1523–58.
42. Sharland GK, Chan KY, Allan LD. Coarctation of the aorta: difficulties in prenatal diagnosis *Br Heart J* 1994; 7: 70–5.
43. Paladini D, Volpe P, Russo MG, et al. Aortic coarctation: prognostic indicators of survival in the fetus. *Heart* 2004; 90: 1348–9.
44. Volpe P, Marasini M, Caruso G, et al. Prenatal ultrasound diagnosis of interruption of the aortic arch and its association with deletion of chromosome 22q11. *Ultrasound Obstet Gynecol* 2002; 20: 327–31.
45. Volpe P, Tuo G, De Robertis V, et al. Fetal interrupted aortic arch: 2D-4D echocardiography, associations and outcome. *Ultrasound Obstet Gynecol* 2010; 35: 302–9.
46. Chaoui R, Schneider MBE, Kalache KD. Right aortic arch with vascular ring and aberrant left subclavian artery: prenatal diagnosis assisted by three-dimensional power Doppler ultrasound. *Ultrasound Obstet Gynecol* 2003; 22: 661–3.
47. Volpe P, Marasini M, Caruso G, et al. 22q11 deletions in foetuses with malformations of the outflow tracts or interruption of the aortic arch: impact of additional ultrasound signs. *Prenat Diagn* 2003; 23: 752–7.
48. Chaoui R, Kalache KD, Heling KS, et al. Absent or hypoplastic thymus on ultrasound: a marker for deletion 22q11.2 in fetal cardiac defects. *Ultrasound Obstet Gynecol* 2002; 20: 546–52.
49. Achiron R, Rotstein Z, Heggesh J, et al. Anomalies of the fetal aortic arch: a novel sonographic approach to in-utero diagnosis. *Ultrasound Obstet Gynecol* 2002; 20: 553–7.
50. Yoo SJ, Min JY, Lee YH, et al. Fetal sonographic diagnosis of aortic arch anomalies. *Ultrasound Obstet Gynecol* 2003; 22: 535–46.
51. Volpe P, Paladini D, Marasini M, et al. Characteristics, associations and outcome of absent pulmonary valve syndrome in the fetus. *Ultrasound Obstet Gynecol* 2004; 24: 623–8.
52. Hornberger LK, Sanders SP, Sahn DJ, et al. In utero pulmonary artery and aortic growth and potential for progression of pulmonary outflow tract obstruction in tetralogy of Fallot. *J Am Coll Cardiol* 1995; 25: 739–45.
53. Escribano D, Herraiz I, Granados M, et al. Tetralogy of Fallot: prediction of outcome in the mid-second trimester of pregnancy. *Prenat Diagn* 2011; 31: 1126–33.
54. Paladini D, Rustico MA, Todros T, et al. Conotruncal anomalies in prenatal life. *Ultrasound Obstet Gynecol* 1996; 8: 241–6.
55. Lev M, Eckner FA. The pathologic anatomy of tetralogy of Fallot and its variants. *Disease Chest* 1964; 45: 251–61.
56. Razavi RS, Sharland GK, Simpson JM. Prenatal diagnosis by echocardiogram and outcome of absent pulmonary valve syndrome. *Am J Cardiol* 2003; 91: 429–32.
57. Lagopoulos ME, Manlhiot C, McCrindle BW, et al. Impact of prenatal diagnosis and anatomical subtype on outcome in double outlet right ventricle. *Am Heart J* 2010; 160: 692–700.
58. Collet RW, Edwards JE. Persistent truncus arteriosus: a classification according to anatomic types. *Surg Clin North Am* 1949; 29: 1245–70.

59. Volpe P, Paladini D, Marasini M, et al. Common arterial trunk in the fetus: characteristics, associations, and outcome in a multicentre series of 23 cases. *Heart* 2003; 89: 1437–41.
60. Baker EJ. Tetralogy of Fallot with pulmonary atresia. In: Anderson RH, Macartney FJ, Shinebourne EA, et al. eds. *Paediatric Cardiology*. Edinburgh: Churchill Livingstone, 2001; 1251–79.
61. Bonnet D, Coltri A, Butera G, et al. Detection of transposition of the great arteries reduces neonatal morbidity and mortality. *Circulation* 1999; 99: 916–18.
62. Paladini D, Volpe P, Sglavo G, et al. Transposition of the great arteries in the fetus: assessment of the spatial relationships of the arterial trunks by four-dimensional echocardiography. *Ultrasound Obstet Gynecol* 2008; 31: 271–6.
63. Massoudy P, Baltalarli A, de Laval MR, et al. Anatomic variability in coronary arterial distribution with regard to the arterial switch procedure. *Circulation* 2002; 106: 1980–4.
64. Jouannic JM, Gavard L, Fermont L, et al. Sensitivity and specificity of prenatal features of physiological shunts to predict neonatal clinical status in transposition of the great arteries. *Circulation* 2004; 110: 1743–6.
65. Paladini D, Volpe P, Marasini M, et al. Diagnosis, characterization and outcome of congenitally-corrected transposition of the great arteries in the fetus. A multicenter series of 30 cases. *Ultrasound Obstet Gynecol* 2006; 27: 281–5.
66. Ly M, Belli E, Leobon B, et al. Results of the double switch operation for congenitally corrected transposition of the great arteries. *Eur J Cardiothorac Surg* 2009; 35: 879–83.
67. Hiramatsu T, Matsumura G, Konuma T, et al. Long-term prognosis of double-switch operation for congenitally corrected transposition of the great arteries. *Eur J Cardiothorac Surg* 2012; 42: 1004–8.
68. Graham TP, Bernard YD, Mellen BG, et al. Long-term outcome in congenitally corrected transposition of the great arteries. *J Am Coll Cardiol* 2000; 36: 255–61.
69. Pepes S, Zidere V, Allan LD. Prenatal diagnosis of left atrial isomerism. *Heart* 2009; 95; 1974–7.
70. Paladini D, Sglavo G, Masucci A, et al. Role of four-dimensional ultrasound (spatiotemporal image correlation and sonography-based automated volume count) in prenatal assessment of atrial morphology in cardiosplenic syndromes. *Ultrasound Obstet Gynecol* 2011; 38: 337–43.
71. Volpe P, Campobasso G, Stanziano A, et al. A novel approach to enhance the assessment of sources of pulmonary blood flow and the identification of the anatomy of pulmonary arteries in foetuses with pulmonary atresia with ventricular septal defect: 4D-US with B-flow imaging and spatiotemporal image correlation. *Ultrasound Obstet Gynecol* 2006; 28: 40–46.
72. Hashmi A, Abu-Sulaiman R, McCrindle BW, et al. Management and outcomes of right atrial isomerism: a 26-year experience. *J Am Coll Cardiol* 1998; 31: 1120–6.
73. Groves AM, Fagg NL, Cook AC, et al. Cardiac tumours in intrauterine life. *Arch Dis Chil* 1992; 67: 1189–92.
74. Paladini D, Palmieri S, Russo GM, et al. Cardiac multiple rhabdomyomatosis: prenatal diagnosis and natural history. *Ultrasound Obstet Gynecol* 1996; 7: 84–5.
75. Paladini D, Tartaglione A, Vassallo M, et al. Prenatal ultrasonographic findings of a cardiac myxoma. *Obstet Gynecol* 2003; 102: 1174–6.
76. Paladini D, Russo MG, Tartaglione A, et al. Prenatal ultrasound diagnosis of Toriello-Carey syndrome. *Prenat Diagn* 2002; 22: 1185–7.
77. Dimitrow PP, Kizanowski M, Nizankowski R, et al. Comparison of the effect of verapamil and propranolol on response of coronary vasomotion to cold pressor test in symptomatic patients with hypertrophic cardiomyopathy. *Cardiovasc Drug Ther* 2000; 14: 643–50.
78. Carvalho JS, Prefumo F, Ciardelli V, et al. Evaluation of fetal arrhythmias from simultaneous pulsed wave Doppler in pulmonary artery and vein. *Heart* 2007; 93: 1448–53.
79. Simpson J, Yates RW, Sharland GK. Irregular heart rate in the fetus—not always benign. *Cardiol Young* 1996; 6: 28–31.
80. Simpson JM, Sharland GK. Fetal tachycardias: management and outcome of 127 consecutive cases. *Heart* 1998; 79: 576–81.
81. Krapp M, Kohl T, Simpson JM, et al. Review of diagnosis, treatment, and outcome of fetal atrial flutter compared with supraventricular tachycardia. *Heart* 2003; 89: 913–17.
82. Hofbeck M, Ulmer H, Beinder E, et al. Prenatal findings in patients with prolonged QT interval in the neonatal period. *Heart* 1997; 77: 198–204.
83. Hutter D, Silverman ED, Jaeggi ET. The benefits of transplacental treatment of isolated congenital complete heart block associated with maternal anti-Ro/SSA antibodies: a review. *Scand J Immunol* 2010; 72: 235–41.
84. Hyett J, Perdu M, Sharland G, et al. Using fetal nuchal translucency to screen for major congenital cardiac defects at 10–14 weeks of gestation: population based cohort study. *BMJ* 1999; 318: 81–5.
85. Huggon IC, DeFigueiredo DB, Allan LD. Tricuspid regurgitation in the diagnosis of chromosomal anomalies in the fetus at 11–14 weeks of gestation. *Heart* 2003; 89: 1071–3.
86. Matias A, Gomes C, Flack N, et al. Screening for chromosomal abnormalities at 10–14 weeks: the role of ductus venosus blood flo . *Ultrasound Obstet Gynecol* 1998; 12: 380–4.
87. Borrell A, Martinez JM, Serés A, et al. Ductus venosus assessment at the time of nuchal translucency measurement in the detection of fetal aneuploidy. *Prenat Diagn* 2003; 23: 921–6.
88. Carvalho JS. Fetal heart scanning in the first trimester. *Prenat Diagn* 2004; 24: 1060–7.
89. Haak MC, Twisk JW, Van Vugt JM. How successful is fetal echocardiographic examination in the first trimester of pregnancy? *Ultrasound Obstet Gynecol* 2002; 20: 9–13.
90. Makrydimas G, Sotiriadis A, Ioannidis JP. Screening performance of first-trimester nuchal translucency for major cardiac defects: a meta-analysis. *Am J Obstet Gynecol* 2003; 189: 1330–5.
91. Bellotti M, Fesslova V, De Gasperi C, et al. Reliability of the first-trimester cardiac scan by ultrasound-trained obstetricians with high-frequency transabdominal probes in fetuses with increased nuchal translucency. *Ultrasound Obstet Gynecol* 2010; 36: 272–8.
92. Volpe P, Ubaldo P, Volpe N, et al. Fetal cardiac evaluation at 11–14 weeks by experienced obstetricians in a low-risk population. *Prenat Diagn* 2011; 31: 1054–61.
93. Persico N, Moratalla J, Lombardi CM, et al. Fetal echocardiography at 11–13 weeks by transabdominal high-frequency ultrasound. *Ultrasound Obstet Gynecol* 2011; 37: 296–301.
94. Axt-Fliedner R, Kreiselmaier P, Schwarze A, et al. Development of hypoplastic left heart syndrome after diagnosis of aortic stenosis in the first trimester by early echocardiography. *Ultrasound Obstet Gynecol* 2006; 28: 106–9.
95. Gardiner HM. Progression of fetal heart disease and rationale for fetal intracardiac interventions. *Semin Fetal Neonatal Med* 2005; 10: 578–85.
96. Trines J, Hornberger LK. Evolution of heart disease in utero. *Pediatr Cardiol* 2004; 25: 287–98.
97. Yagel S, Weissman A, Rotstein Z, et al. Congenital heart defects: natural course and in utero development. *Circulation* 1997; 96: 550–5.

Chapter 6
Thoracic anomalies

Normal anatomy of the thorax: ultrasound approach, scanning planes, and diagnostic potential

The thorax has a conotruncal shape. Its upper borders are represented by the clavicles and the neck; it is limited inferiorly by the diaphragm, laterally by the ribs, and anteriorly by the sternum. Posteriorly, the shoulder blades can be seen in strict relationship with the ribs and the clavicles. In the thorax, the following regions/organs can be identified: the *lungs*, which extend from the diaphragm to the upper border, just below the clavicles; the *heart*, which is located in the lower mediastinum and lies on the surface of the diaphragm; and the *mediastinum*, with the great vessels and the thymus, larger in the fetus than in the neonate. The bony outline, represented by the rib cage, and the overlying soft tissues complete the thoracic area. In this chapter, normal and abnormal anatomy of thoracic viscera are described. The heart and the great vessels are described in Chapter 5.

Timing of examination. Ultrasound (US) assessment of the thorax can be carried out easily until 25–26 weeks of gestation. After this period, the increased mineralization of the ribs leads to significant acoustic shadowing, which limits the display of intrathoracic organs, especially if coronal or sagittal views are sought (see below). Besides, it must be emphasized that a good number of thoracic anomalies evolve, that is, they can appear only in the third trimester or, on the contrary, they can regress before birth. Therefore, if an initial assessment of the thorax and the heart can be performed as early as 12–14 weeks of gestation, it should be noted that, in order to follow up abnormal cases, late third-trimester scans may be needed.

US approach and scanning planes (views). The regular shape of the thorax lends itself easily to a standardized US approach. However, it should be noted that the key view for the assessment of intrathoracic anatomy is the classic *four-chamber view* of the fetal heart. In fact, in this plane, most thoracic viscera can be displayed, including the ribs, the sternum, and the cutaneous outline. This is why numerous scientific societies refer to the four-chamber view as the key view to assess intrathoracic anatomy. However, if the results from this view are abnormal, and a thoracic lesion is found, this should be explored further using coronal and sagittal views, as reported below. The *midsagittal* and *parasagittal views* allow display of the diaphragm as a hypoechoic layer below the basal aspects of the lungs and the heart, and above the liver and the stomach. The diaphragm shows a curved outline, convex toward the thorax. With regard to the other anatomic districts, because the anatomic scan is usually carried out (in most countries), at 18–22 weeks of gestation, all normal planes shown in the figures in this chapter refer to second-trimester fetuses.

Axial four-chamber view (Figures 6.1 and 6.2). As already mentioned, this represents the fundamental plane where heart and lung anatomy is assessed. On this view, the following structures can and should be checked (Figure 6.1), in addition to the cardiac anatomy described in Chapter 5: the thoracic outline, consisting of the two displayed ribs and the overlying soft tissues and skin; the two lungs, shown in cross-section; the thoracic aorta, lying in the prevertebral area just left of the midline and behind the left atrium (if the situs is *solitus*); and one thoracic vertebra, on the midline, posteriorly. The sternum begins to show mineralization in the late second trimester, sometimes earlier. In the latter case, the shadowing from the upper sternal ossification nucleus may hamper the visualization of the thorax and the heart. A useful hint to get a perfectly axial four-chamber view is to look at the two displayed ribs, considering that in the fetus, unlike the adult, the

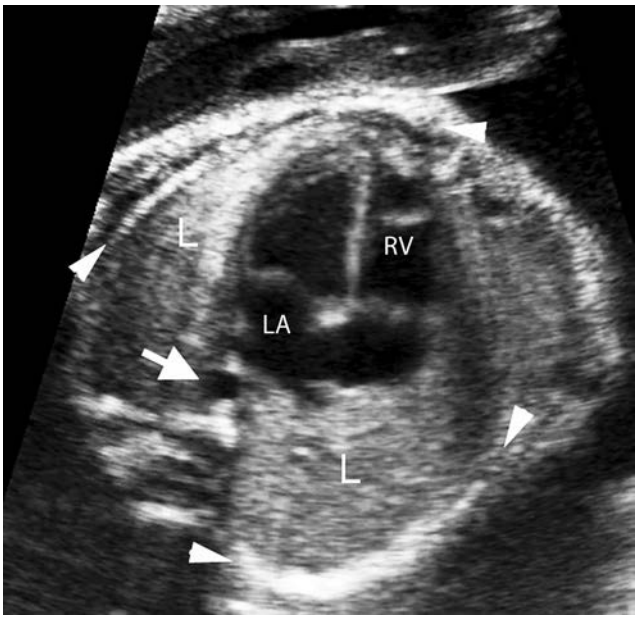


Figure 6.1 Axial view of the thorax: Four-chamber view. In this view, the two lung fields (L: lung), the heart (LA: left atrium; RV: right ventricle), and the descending thoracic aorta (arrow) behind the left atrium are visible. Laterally, two complete ribs are evident (arrowheads); posteriorly, one thoracic vertebra can be seen. The cutaneous outline, outside the rib-cage, is also evident. Note that the right lung appears larger than the left lung.

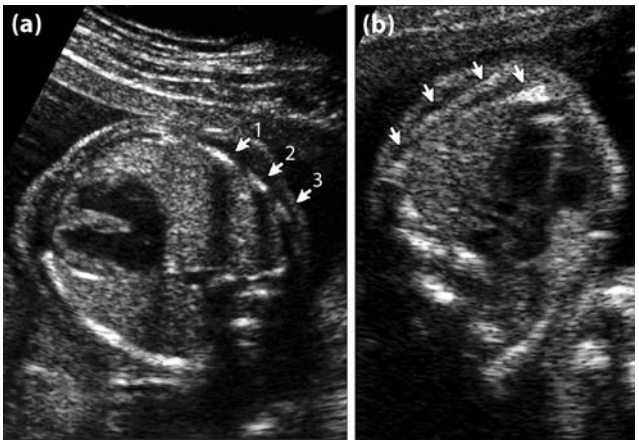


Figure 6.2 Four-chamber view: Abnormal alignment. The ribs represent a good marker to assess the adequacy of the scanning plane. (a) If the axial alignment is unbalanced in the anteroposterior plane, then several indented rib segments will be visible (arrows 1, 2, 3). (b) If the axial alignment is unbalanced in the latero-lateral plane, several whole ribs will appear (arrows).

ribs are perfectly horizontal: if the whole length of the ribs is visible, then the orientation of the transducer is correct. If, on the contrary, more than one rib is displayed, then the plane is malaligned either in the anteroposterior axis (a few segments of different ribs: Figure 6.2a) or in the latero-lateral one (a few almost complete and parallel ribs: Figure 6.2b). On the correct axial plane, the two lungs appear as solid, homogeneous, weakly hyperechoic structures that almost completely surround the heart. Because the heart is mainly located in the left hemithorax, the right lung will appear larger than the left one (Figure 6.1). In the normal fetus, the pleural cavity is virtual, and does not show up; on the contrary, a film of fluid is often seen within the pericardium, especially if insonated with high-frequency transducers.

Axial view of the mediastinum (three-vessel view) (Figure 6.3) [1]. This plane is parallel to the four-chamber view, but more cranial. It is routinely sought in fetal echocardiography in order to demonstrate the aortic and pulmonary arches and the corresponding flows on color Doppler, for the detection of aortic branching anomalies and of ductus dependence (Chapter 5). A description of this view is included in this chapter because it allows one to visualize the thymus and study its relationship with the great vessels. The thymus, which is easier to recognize from the late second trimester onward, when it starts to undergo significant hypertrophy, appears as a well-defined roundish solid structure interposed between the great vessels, in the prevertebral region, and the sternum. It is weakly hypoechoic in comparison with the surrounding lungs (Figure 6.3a and b), although it should be emphasized that the different echogenicity is not easy to pick up, especially if high-frequency (>5 MHz) transducers are not employed. An additional feature that makes identification of the thymus easier is the fact that the thymus is located on top of the heart and, therefore, unlike the lungs, it shows transmitted movements synchronous with the cardiac cycle. Recently, another technique has been proposed to identify the thymic area, especially at earlier gestational ages, the so-called *thy-box*. This expression [1] is based on the fact that the thymus is bordered laterally by the two internal mammary arteries; hence, by tracing these two arteries with power Doppler or low PRF color Doppler, the thymic area can be easily identified on an axial view of the upper mediastinum (Figure 6.3c). Behind the thymus and in front of the vertebra, the great vessels, the trachea, and, with some difficulty, the esophagus can be seen.

Right parasagittal view (Figure 6.4). The midsagittal view does not give significant information regarding the lungs, because it is occupied mainly by the heart.

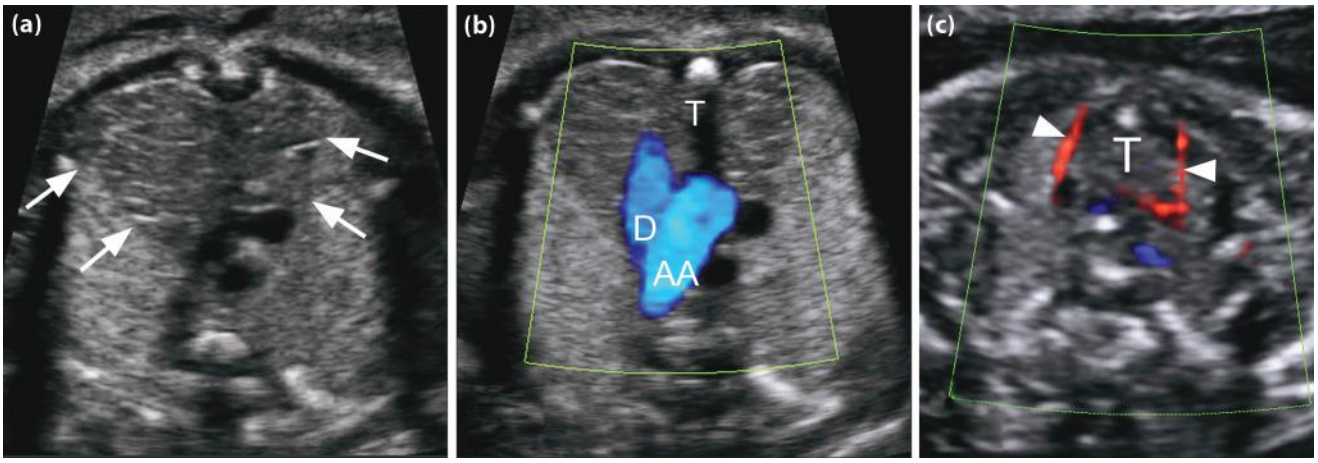


Figure 6.3 Axial view of the upper mediastinum. (a) The thymus (arrows), which is weakly hypoechoic in comparison with the lungs, can be seen in the middle of the thorax (27 weeks of gestation; (b) On a parallel plane, just caudal to the former one, the great vessels with the pulmonary artery and the ductus arteriosus (D) on the left, the aortic arch (AA) in the middle, and the superior vena cava on the right can be seen, all behind the thymus (27 weeks of gestation); (c) The *thy-box* technique (20 weeks of gestation): with power Doppler, the two internal mammary arteries (arrowheads) are sought on an axial view of the upper thorax. These vessels will identify the lateral borders of the thymic area (T). (See ref.1)

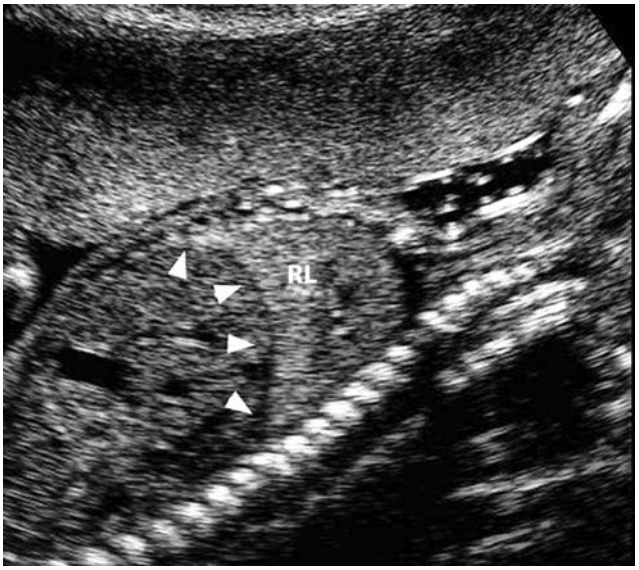


Figure 6.4 Right parasagittal thoracic view. This view allows detection of the hypoechoic muscular layer represented by the diaphragm (arrowheads), just below the right lung (RL).

In contrast, on the right parasagittal view, the whole of the right lung comes into view. The heart is not visible, being in the left hemithorax. On this view, the diaphragmatic hypoechoic layer can be seen below the right lung. Care should be taken to consider the identification of the diaphragmatic plane in this view as a demonstration of an intact diaphragm: if the hernia is located on the other side, as in the Bochdalek type (see below), the contour of the right hemidiaphragm is normal. Also, it is important to note that this view can be employed advantageously to disclose the severe thoracic hypoplasia typical of lethal skeletal dysplasia (Chapter 9).

Us dIFFEr ENTIAL dIAGNos Is o F Thor Ac Ic A No MALIEs

Following the practical approach typical of this book—from US finding to diagnosis—and noting that the reference view for the diagnosis of thoracic anomalies is the four-chamber view, we believe that a classification of the various thoracic lesions according to their US appearance on this view may help in differential diagnosis. Hence, we have distinguished them according to their position and echogenicity (Figure 6.5): lateral versus central (median); hypo- or anechoic versus hyperechoic; and bilateral versus unilateral. The final assessment regards those cases in which there is clear disproportion between the thorax and the heart; in such circumstances, the operator should always consider whether it is the heart that is enlarged (cardiomegaly

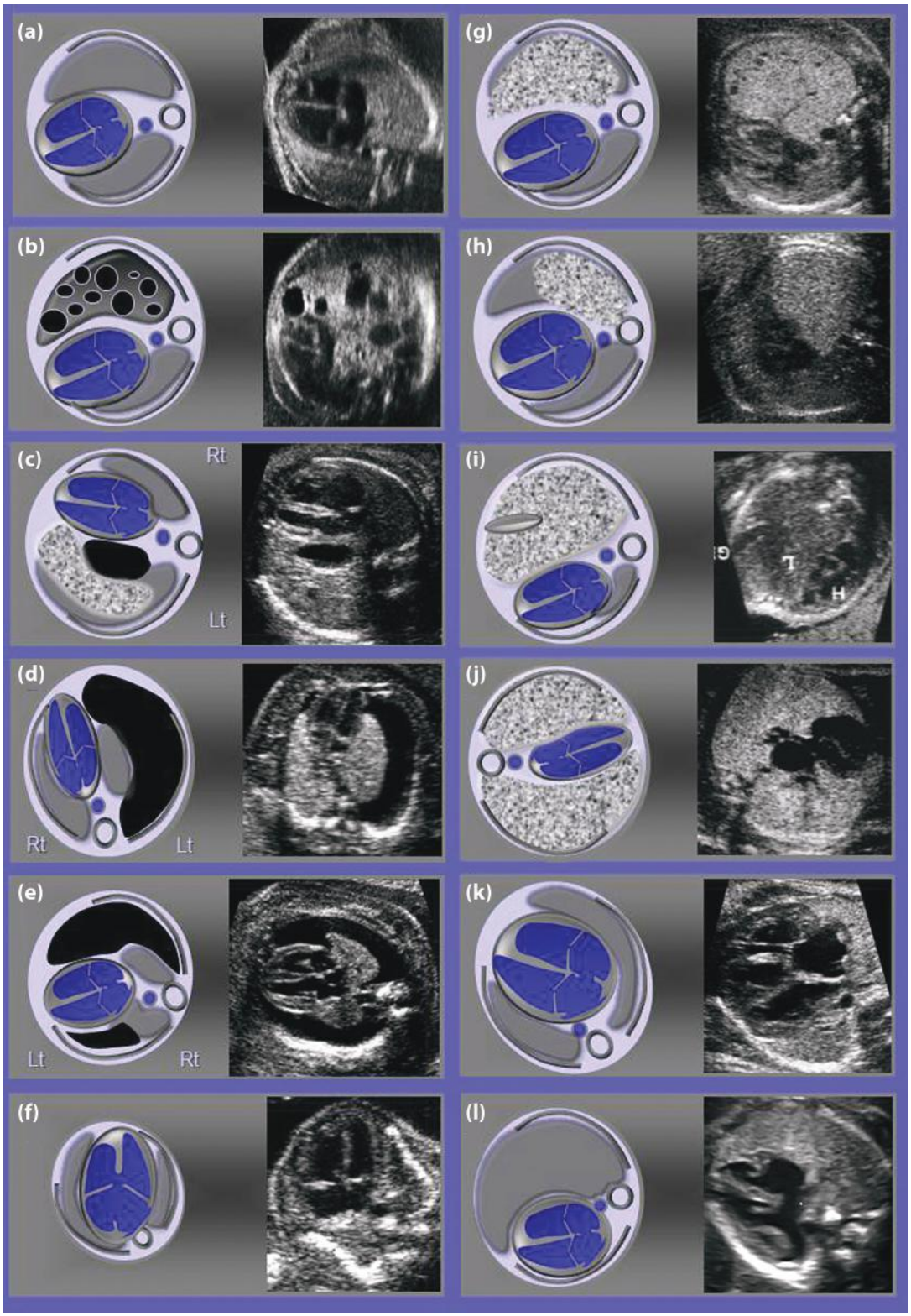


Figure 6.5 Summary of the different types of thoracic abnormalities, classified according to their laterality (unilateral vs. bilateral) and echogenicity (fluid vs. solid): (a) normal thorax; (b) Cystic adenomatoid malformation of the lung (CAML), macrocystic type; (c) congenital diaphragmatic hernia (CDH), left-sided; (d) hydrothorax, unilateral; (e) hydrothorax, bilateral; (f) thoracic hypoplasia; (g, h) pulmonary sequestration/CAML microcystic type; (i) CDH, right-sided; (j) laryngeal atresia; (k) cardiomegaly; (l) right lung agenesis.

and cardiomyopathies) or the rib cage that is too small (thoracic/pulmonary hypoplasia).

- **Unilateral, anechoic lesions**
  - *Congenital diaphragmatic hernia, left-sided (Figure 6.5c)*: Only in left posterolateral hernia, Bochdalek type, can the stomach migrate into the left hemithorax, especially if there are no ileal loops in the thorax at the same time. The heart will be displaced contralaterally, or in the center of the thorax. The stomach appears as a round or oval, anechoic, well-defined area.
  - *Cystic adenomatoid malformation of the lung (CAML) type I, macrocystic variant (Figure 6.5b)*: In this case, the anechoic cystic structure can be single or multiple, but is located in one hemithorax only—Cystic adenomatoid malformation of the lung (CAML) is almost always unilateral. The heart is displaced contralaterally.
  - *Unilateral hydrothorax (pleural effusion) (Figure 6.5d)*: A unilateral pleural effusion can appear as an anechoic moon-shaped area of variable size, according to the severity of the hydrothorax. Characteristically, in the middle of the anechoic area, the ipsilateral lung, showing movements synchronous with the heartbeats, can be identified. Rarely, the amount of fluid within the pleural space is so large as to increase the intrathoracic pressure severely; in such rare cases, all viscera, including the ipsilateral compressed lung, are pushed into the other hemithorax. After birth, most of these hypertensive unilateral pleural effusions turn out to be chylothoraces.
- **Unilateral hyperechoic lesions**
  - *CAML type III, solid (Figure 6.5g and h)*: The solid subtype of CAML appears as a homogeneously highly hyperechoic pulmonary mass. Although, by definition, CAML almost always involves one lobe only, the volume of the mass does not allow the remaining intact lobe(s) to be displayed on US. If the volume of the lesion is large enough, the mediastinum shifts toward the contralateral hemithorax.
  - *Pulmonary sequestration (Figure 6.5g and h)*: This shares with CAML type III the same highly hyperechoic US aspect. Differential diagnosis relies on the identification, with power or color Doppler, of the feeding vessels originating from the descending aorta in the pulmonary sequestration. As with CAML, pulmonary sequestration is virtually always unilateral (prevalently on the left side).
  - *Congenital diaphragmatic hernia (CDH), right-sided (Figure 6.5i)*: In right-sided hernias, as well as in eventration, which is an upward displacement of the abdominal contents secondary to a congenitally thin hypoplastic diaphragm, the right lobe of the liver is displaced upward, into the right hemithorax, and pushes the heart and the mediastinum into the left hemithorax. Identification of the gallbladder, and/or of the hepatic colonic flexure, in the right hemithorax leads to the diagnosis. Also, in a minority of cases of left posterolateral hernias in which the stomach does not migrate into the thorax, the appearance of the ileus and the spleen in the thorax may be that of an inhomogeneous hyperechoic mass in the left hemithorax.
  - *Tumors*: The same tumors that usually arise in the mediastinum can, very rarely, arise from the lateral walls of the thorax.
- **Bilateral hyperechoic lesions**
  - *Congenital high airway obstruction syndrome (CHAOS) (laryngeal atresia) (Figure 6.5j)*: There is virtually only one entity that can appear as a bilateral hyperechoic lesion, namely laryngeal atresia. Obstruction of the high airways causes hyperplasia of the alveolar units, which are filled with fluid. Severely increased lung volume results from this hyperplasia together with the entrapment of a significant amount of fluid within the lungs. The severely enlarged lungs deform the thorax, which becomes bell-shaped as the diaphragmatic convexity is reversed and the lower more mobile ribs are displaced laterally; the heart is squeezed into the middle of the thorax and the cardiac angle is reduced (sometimes to zero) by high intrathoracic pressure. Ascites is constantly associated.
- **Bilateral anechoic lesions**
  - *Bilateral hydrothorax (pleural effusion) (Figure 6.5e)*: If pleural effusion is bilateral, two moon-shaped anechoic areas surrounding the mediastinum are evident.
- **Median anechoic lesions**
  - *Congenital diaphragmatic hernia (Figure 6.5c)*: In the left posterolateral subtype (Bochdalek type) of CDH, the stomach, appearing as a round well-defined anechoic structure, is frequently displaced into the center of the thorax; the heart is consequently pushed into the right hemithorax.
  - *Absent pulmonary valve syndrome*: In this rare anomaly, usually associated with tetralogy of Fallot, the anechoic mediastinal structure is represented by an extremely dilated pulmonary trunk and branches—results of the severe pulmonary valve insufficiency (Chapter 5).
- **Median hyperechoic lesions**
  - *Mediastinal tumors*: A large mediastinal hyperechoic mass, located in the upper mediastinum,

is often consistent with a mesenchymal tumor, such as a teratoma or a hemangioma.

- **Increased cardiothoracic ratio: enlarged heart**
  - *Isolated cardiomegaly (Figure 6.5k)*: If the cardiomegaly is not associated with congenital heart disease, it can be related to incipient heart failure from arteriovenous fistulas (placental chorioangioma, twin-to-twin transfusion syndrome [TTTS], sacrococcygeal teratoma, etc.), or increased intraventricular pressure, as in ductus arteriosus constriction/closure.
  - *Atrioventricular valve insufficiency*: Cardiac enlargement can also be determined by congenital heart diseases associated with severe atrioventricular valve insufficiency: the consequent severe atriomegaly is responsible for the cardiomegaly (Chapter 5). Cardiomyopathies characterized by severe pump failure may also be associated with cardiomegaly, because of the dilatation of the ventricular chambers and of the severe myocardial hypertrophy.
- **Increased cardiothoracic ratio: hypoplastic thorax**
  - *Skeletal dysplasia featuring thoracic hypoplasia (Figure 6.5f)*: Severe hypoplasia of the rib cage (sternum, ribs, and spine) can be associated with some lethal skeletal dysplasias (asphyxiating thoracic dystrophy [Jeune syndrome]), thanatophoric dysplasia, achondrogenesis, short-rib-polydactyly syndrome, and the fetal akinesia deformation sequence (FADS) group (Chapters 9 and 10). In the presence of severe thoracic hypoplasia, the midsagittal scan of the fetus at low magnification often shows a dip at the junction between the thorax and the abdomen.
  - *Primary lung hypoplasia (Figure 6.5l)*: This is a very rare anomaly of the thorax, due to a severe arrest of lung development; if it affects both lungs, it is lethal. In the case of bilateral lung hypoplasia, the thorax is virtually occupied by the heart only.

ThE r oLE oF Thr EE-dIMENsIo NAL Us IN ThE Ass Ess MENT oF Thor Ac Ic ABNor MALITIEs

Premises. There are four areas in which the use of three-dimensional (3D) US may improve the characterization of thoracic and thoracoabdominal malformations. In particular, 3D renderings may contribute to the assessment of: (1) the liver position in CDH; (2) tracheal and esophageal abnormalities; (3) liver outline, relationships with the heart, and position of abdominal vessels in cardiosplenic syndromes

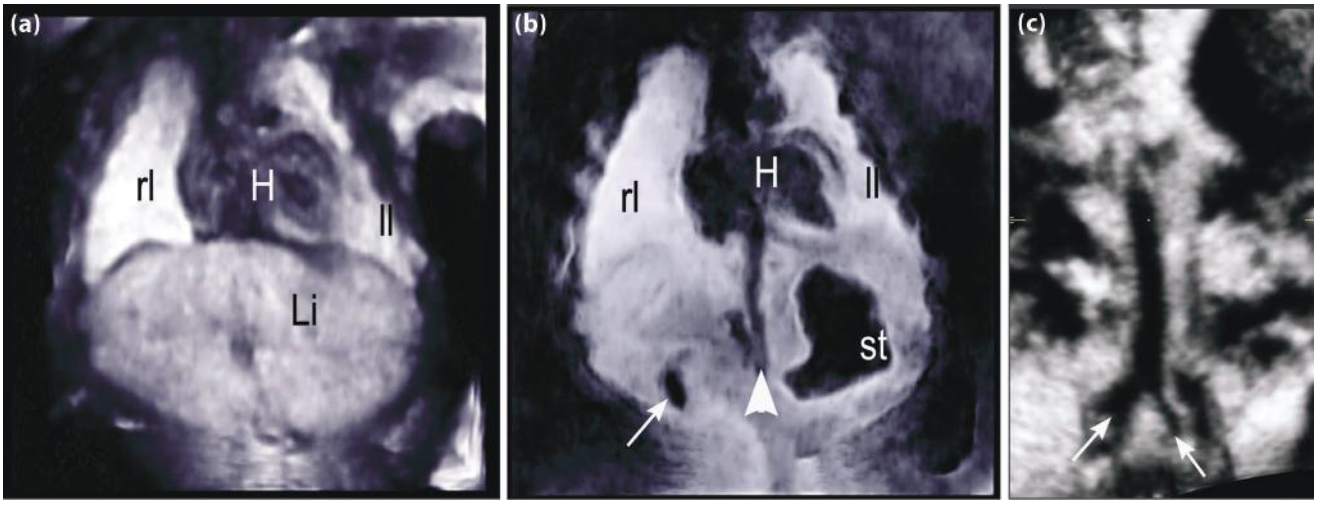


Figure 6.6 Three-dimensional assessment of the normal thorax (26 weeks of gestation). Reconstruction of the coronal plane + volume contrast imaging (thick-slice technique). (a) Surface-mode rendering of the reconstructed coronal plane demonstrates the relationships between the heart (H) in levocardia and the lungs (ll: left lung; rl: right lung); the normal appearance of the upper liver margin (Li) is also visible, thanks to the natural contrast created by the hypoechoic diaphragmatic lining and the thoracic viscera. (b) Same view with minimum mode rendering. In this case, the hollow structures are highlighted: the heart (H), in levocardia, the stomach (st), also in the left part of the abdomen, the gallbladder (arrow), at the lower right margin of the liver, and the inferior vena cava (arrowhead) which enters the heart. (c) A high magnification coronal view (minimum mode + volume contrast imaging) of the trachea, with the carina and the two main bronchi (arrows).

(see Chapter5); and (4) the degree of thoracic hypoplasia and the presence of rib anomalies in skeletal dysplasias (see Chapter 9). Prior to describing the relative techniques, it should be emphasized that there is still no scientific evidence in the literature of this diagnostic superiority of 3D US, with only a few papers worth mentioning [2,3]. However, it is experience of the authors that all areas mentioned above benefit from a 3D US assessment, either with a multiplanar correlation approach (trachea-bronchial and esophageal anomalies) or with the reconstruction of the coronal view of thorax and abdomen (diaphragmatic hernia and cardiosplenic syndromes). The issue of skeletal dysplasias will be dealt with in Chapter 9. It is also important to emphasize that, as explained more thoroughly in the corresponding section, all efforts aimed at the assessment of lung volume in diaphragmatic hernia have been replaced with magnetic resonance imaging (MRI), which suffers no limitation from rib shadowing, as is the case with US (see Appendix Table A.19). The use of 3D US in the evaluation of the normal thorax is shown in Figure 6.6.

chArAcTErIzATIoN oF MAjor A NoMALIEs

coNGENITAL dIAphr AGMATIc hEr NIA (cdh)

Incidence. Common.

Ultrasound diagnosis. Stomach in the thorax (left-sided hernias); right liver lobe in the thorax (right-sided hernias); heart displaced in right hemithorax or hyper-rotated in the left hemithorax, respectively. Sometimes, ileal loops and/or the spleen in the thorax as well.

Risk of chromosomal anomalies. Relatively high (5%–15%): trisomies 18 and 21.

Risk of nonchromosomal syndromes. High (25%–30%): Fryns, Pallister–Killian, Beckwith–Wiedemann.

Outcome. Extremely poor in syndromic cases. Overall survival rate of 40%–60% in nonsyndromic cases; prenatal endoscopic approach seems to improve survival in cases with the poorest prognosis.

Definition The term *congenital diaphragmatic hernia* encompasses a range of closure defects of the diaphragm. Because the intra-abdominal pressure is higher than the intrathoracic pressure, in the presence of a diaphragmatic defect the abdominal viscera located near the defect migrate into the thorax. CDHs are classified according to the site of the defect: 75%–85% of cases involve the left posterolateral area (*Bochdalek type:* Figure 6.7); 10%–15% of cases involve the right hemidiaphragm; and 3%–4% of cases are bilateral hernias.

Etiology and pathogenesis. Embryologically, CDHs originate if normal closure of primary pleuroperitoneal channels does not occur. At 12 weeks of gestation, when the physiologic umbilical hernia disappears, the intra-abdominal pressure increases and may force the abdominal viscera through the hernia, if this is present. From a prognostic standpoint, the main problem of a CDH is not the defect itself, but rather the occurrence and degree of pulmonary damage. This consists of severe alveolar hypoplasia induced by the long-term compression of the lungs exerted by the migrated abdominal viscera. After birth, the onset of pulmonary hypertension can further complicate the situation. The association of pulmonary hypoplasia with pulmonary hypertension represents the main determinant of death in neonates with nonsyndromic CDH [4].

Ultrasound diagnosis. The US diagnosis of CDH is, in most instances, indirect: what is detected is the abnormal intrathoracic position of the stomach and/or the other migrated viscera and the displacement of the heart and the mediastinum. These findings indirectly demonstrate the existence of the diaphragmatic defect. The intrathoracic migration of the abdominal viscera is recognized on the *four-chamber view*.

Left posterolateral CDH (Figures 6.7 through 6.10). On the four-chamber view, the stomach is found either in the left hemithorax or in the mediastinal area (Figure 6.8). In most instances, a few ileal loops can be found near the stomach, while the heart and the mediastinum are displaced contralaterally. Much more rarely, the spleen and/or the left liver lobe may migrate as well (Figure 6.9a). In left-sided hernias, the stomach is found in the thorax in most cases (about 90%). In a minority of cases, only some ileal loops and/or the left hepatic lobe migrate into the thorax (Figure 6.9b and c). If this is the case, only the dextrocardia and

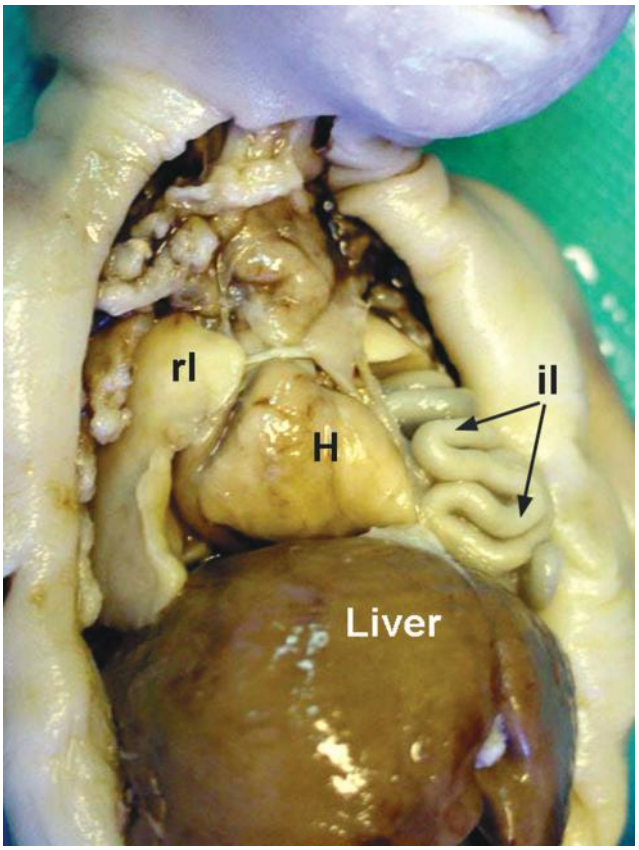


Figure 6.7 Congenital diaphragmatic hernia, Bochdalek type (left, posterior). This specimen (22 weeks of gestation) shows herniation into the left hemithorax of ileal loops (il), which hide the stomach. The heart (H) is displaced into the right hemithorax, where it compresses the right lung (rl). The liver is visible below.

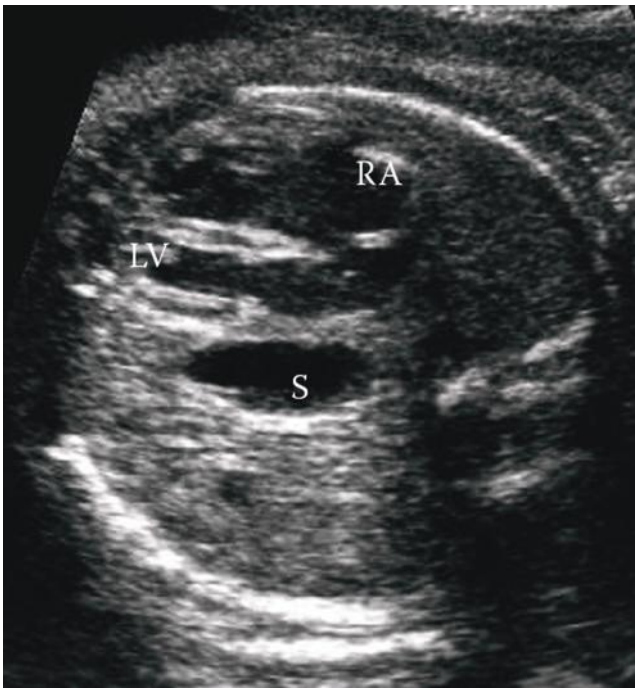


Figure 6.8 Congenital diaphragmatic hernia, Bochdalek type. In this variant of CDH, the stomach (S) is visible in the middle of the thorax, or in the left hemithorax, while the mediastinum, with the heart, is shifted contralaterally. RA: right atrium; LV: left ventricle.

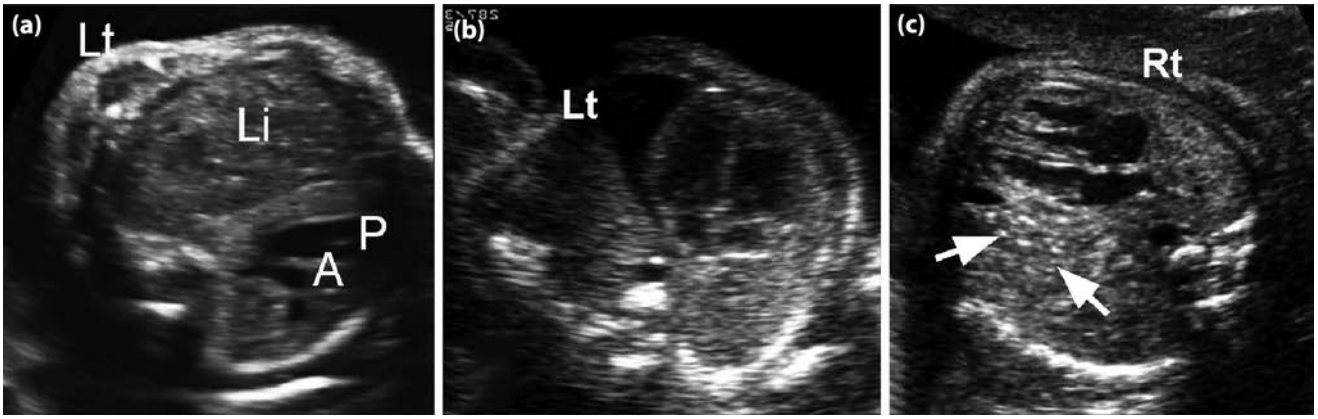


Figure 6.9 Congenital diaphragmatic hernia, Bochdalek type. (a) In rarer cases, rather than the stomach, the spleen, ileal loops, and/or the left hepatic lobe (Li) can also migrate into the thorax (Lt: left; Rt: right). (b) In some cases, the first sign, in the second trimester, of a CDH may be a dextrocardia, possibly associated with fluid collection, as in this case. (c) After 3 weeks, the hernia has become evident, although only some bowel loops (arrows) and not the stomach have herniated into the left hemithorax.



Figure 6.10 Congenital diaphragmatic hernia, Bochdalek type. The right parasagittal thoracic view can contribute to direct detection of the defect in the diaphragm ("???"). However, this sign should not be considered as a primary finding; the most important clues to the diagnosis of CDH are the intrathoracic location of abdominal viscera and dextrocardia.

the unusual dyshomogeneous appearance of the left hemithorax may lead to the diagnosis (Figure 6.9c). It should be emphasized that even though the diaphragmatic defect occurs at 12 weeks of gestation, the moment at which the viscera herniate is extremely variable and ranges from the early second trimester to the first hours of life; in the latter instance, it is the first breaths that determine the migration of the viscera. Hence, CDH can be considered an "evolving" lesion, which has obvious medicolegal implications. This process is responsible for the fact that only 50%–60% of CDHs are diagnosed prenatally [4,5]. The *longitudinal views (ventral approach)* allow one to detect additional signs that may confirm the existence of the hernia: a tortuous aspect of the inferior vena cava and the absence of the hypoechoic contour of the diaphragm (Figure 6.10). However, care should be taken not to diagnose a CDH only on the grounds of the longitudinal views; the evidence of intrathoracic viscera on the four-chamber view is the basic requirement, in our opinion, for a correct diagnosis of CDH.

Right-sided CDH (Figure 6.11). These represent about 10% of all CDHs at birth. In the case of right-sided hernia, the US diagnosis is more challenging because the main finding leading to the final diagnosis of CDH in most instances, the intrathoracic displacement of the stomach, is absent, being the defect on the other side of the diaphragm. Nonetheless, there are some features that allow one to recognize a right-sided hernia in utero. The first is represented by an extreme leftward rotation of the heart, with a consequent abnormal increase in the cardiac axis: the heart appears squeezed toward the lateral wall of the thorax (Figure 6.11a through c). The second hint for diagnosis of a right CDH is the upward displacement of the right hepatic lobe: this is pushed upward by the absence of the counter pressure represented by the diaphragm and can be detected in the right hemithorax (Figure 6.11b). However, the latter finding is sometimes difficult to identify, because the echogenicity of the lung and the liver are quite similar. High-frequency transducers and the use of power or color Doppler to identify the suprahepatic veins "in the thorax"—once

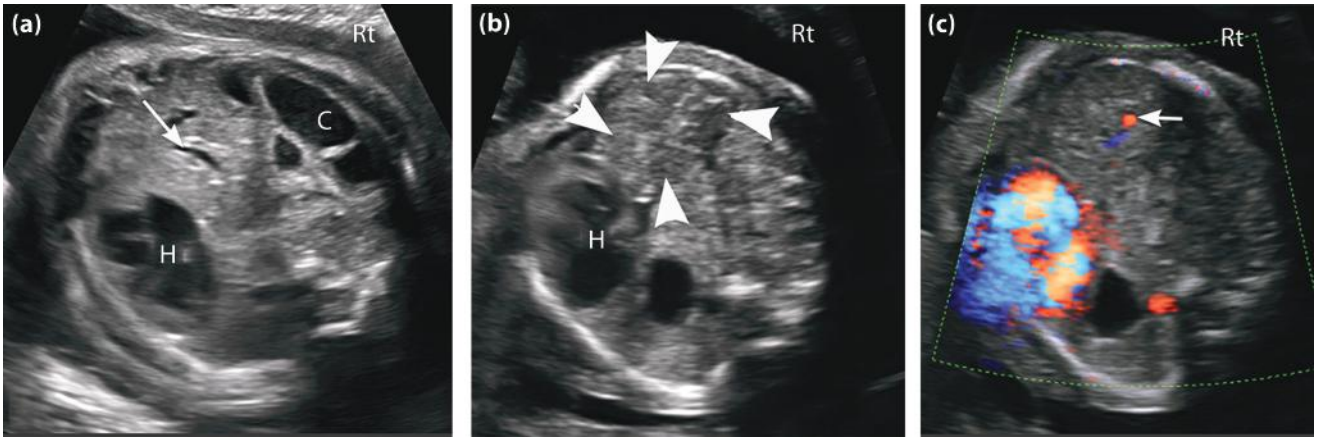


Figure 6.11 Congenital diaphragmatic hernia, right-sided (third trimester). In 10% of cases, the diaphragmatic defect involves the right hemidiaphragm. In this case, the right hepatic lobe (and sometimes the gallbladder, as well) may migrate into the thorax. (a) On gray-scale ultrasound, the evidence of the hepatic flexure of the colon in the thorax (C) may contribute to the diagnosis (H: heart; Rt: right side); (b) on rare occasions, the right lobe itself (arrowheads) becomes evident in the right hemithorax; (c) color or power Doppler may be used to confirm the presence of the suprahepatic veins (arrow) in the thorax, if the gray scale image (see corresponding arrow in [a] is not self-explanatory.

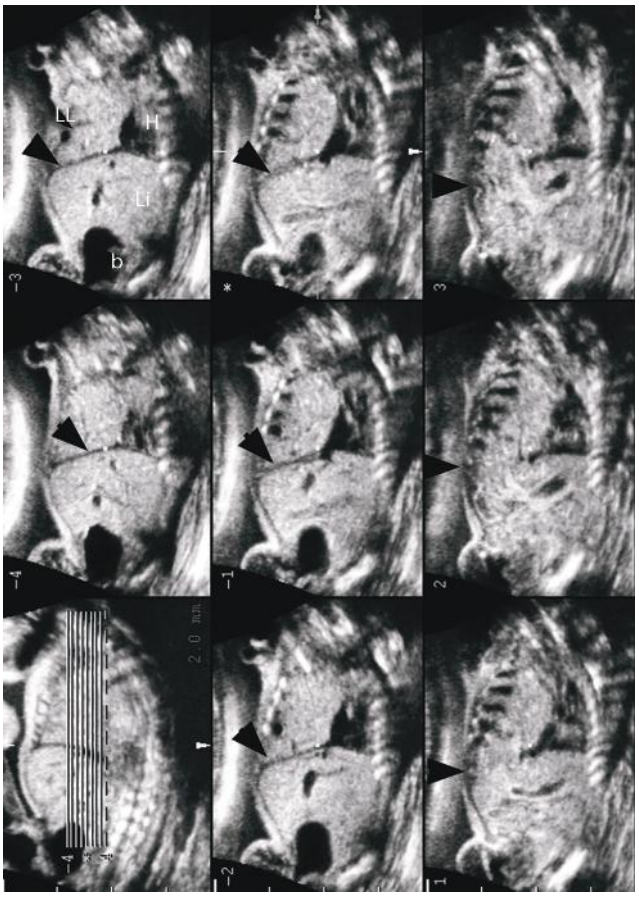


Figure 6.12 Congenital diaphragmatic hernia, Bochdalek type. Three-dimensional ultrasound (TUI). The use of three-dimensional ultrasound with the tomographic approach (TUI) may be of help in the evaluation of the diaphragmatic defect. In particular, by displaying the coronal plane of the thorax and abdomen, it is possible to assess the size and the site of the defect: the diaphragm (arrowheads) appears present in all the windows on the left and the middle rows, whereas its contour is lost in all of the right-row images. b: bladder; H: heart; LL: left lung.

a suspicion of right CDH has been raised—help identify the intrathoracic position of the right hepatic lobe (Figure 6.11c).

Three-dimensional US. As already mentioned, the assessment of the thorax and, in particular, of the lungs, may benefit from a 3D US approach. In particular, the diaphragmatic defect itself is effectively studied both with surface-renderings of the reconstructed coronal view and with tomographic ultrasound imaging (TUI). The latter imaging modality allows one to display on a single panel a variable number of reconstructed two-dimensional (2D) sections, as in a computed tomography (CT) or MRI scan. Using this approach, the reconstructed coronal plane is used to display the extent and the site of the diaphragmatic defect (Figure 6.12). In Figure 6.13, the coronal approach is used to evaluate the migration of the liver and/or other abdominal viscera in the thorax. However, the doubts regarding the need for 3D US in the assessment of CDH are shown in Figure 6.14, where with a simple parasagittal view a right-sided CDH is clearly depicted.

Differential diagnosis *(Figure 6.5)*. For left-sided CDH, the differential diagnosis includes the macrocystic subtype of ACML, because the stomach might, at least theoretically, resemble the dominant cyst in a macrocystic CAML. Right-sided CDH should be differentiated from the solid, microcystic variant of CAML and pulmonary sequestration: The echogenicity of the intrathoracic liver/intestine should be differentiated from the highly hyperechoic CAML, although the difference in "brightness" is usually significant

Prognostic indicators. The most important prognostic factor for fetuses with CDH is the possible association with chromosomal anomalies and/or syndromes. In the case of isolated CDH, several US features have been assessed over the years for their capacity to predict the neonatal occurrence of lethal pulmonary hypoplasia and of pulmonary hypertension: early gestational age at diagnosis, presence of a mediastinal shift, higher pulmonary artery resistance at Pulsed Wave Doppler [6], intrathoracic position of the liver (*liver up*), lung-to-head ratio (LHR) [7–10], and observed/expected LHR (o/e LHR) [11]. Of these, only the last three have proved acceptably reproducible and of sufficient although not exceptional, prognostic value. However, in a logistic regression analysis, the *liver up* position apparently loses its independent prognostic significance when compared with the o/e LHR [11]. As for the LHR, this can be calculated by multiplying the two orthogonal diameters of the right lung, which is located between the rib cage and the heart in the right hemithorax (Figure 6.15), and dividing the result by the head circumference. The measurements can be done in three ways: (1) measuring the longest lung diameter and the longest perpendicular diameter; (2) measuring the anteroposterior diameter of the lung at the midclavicular line by the perpendicular diameter at the midpoint of the anteroposterior diameter; (3) tracing manually the limits of the lungs. The last method has shown the highest reproducibility [12], also because it can be more easily used in cases in which it is difficult to measure the lung. Currently, the procedure of choice to predict the risk

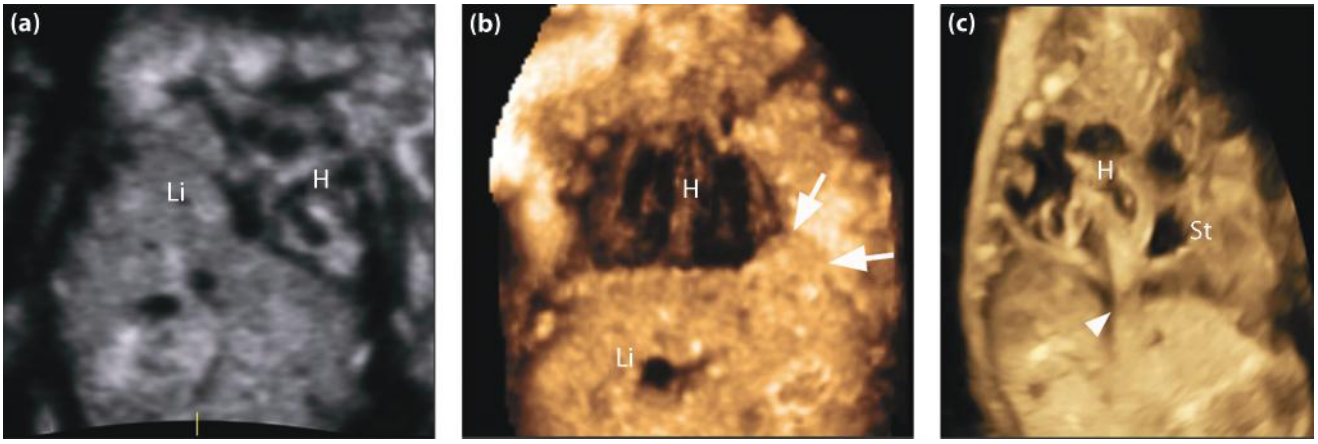


Figure 6.13 Congenital diaphragmatic hernia. Three-dimensional ultrasound (surface-rendering + VCI). Three-dimensional ultrasound may also be used to reconstruct the coronal view of the fetal trunk. The concurrent use of surface-rendering and volume contrast imaging (VCI, thick-slice technique) may contribute to assessing the site, as well as the extent and content of the hernia. (a) Right-sided hernia: the whole right hemithorax is occupied by the right liver lobe (Li); (b) anterior Morgagni hernia: the heart (H) is in mesocardia, and the small anterior hernia is shown by the arrows; (c) left-sided hernia, with the stomach (st) and some ileal loops (arrowhead) in the thorax.

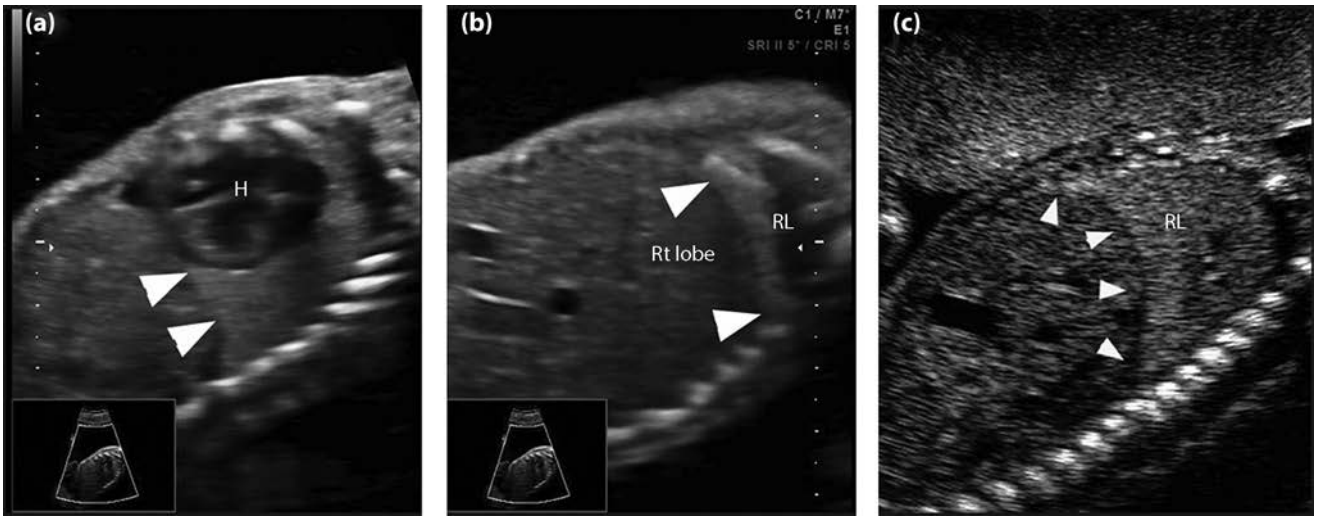


Figure 6.14 Congenital diaphragmatic hernia, right-sided. Two-dimensional ultrasound. On this figure, the limited value of the three-dimensional approach is shown in a 26-week-old fetus with a right-sided CDH: (a) left parasagittal view, showing the normal outline of the diaphragm (arrowheads) and the moderately hyperechoic left lung behind the heart (H); (b) the corresponding right parasagittal view shows the absence of the hypoechoic diaphragmatic lining and the right lobe of the liver displaced upwardly into the thorax. The compressed right lung (RL) is evident as is the differential echogenicity of liver and lung (arrowheads); (c) in comparison, the right parasagittal view of a normal fetus, showing the whole uncompressed right lung (RL), the complete hypoechoic lining of the diaphragm, and the right lobe well below.

of death from pulmonary hypoplasia/hypertension in fetuses with isolated CDH is as follows [13]:

1. Select the axial four-chamber view of the fetal thorax, taking care in displaying the right side of the fetus closer to the transducer, for better measurements, and avoiding shadowing from the ribs.
2. Magnify the image so that the axial view of the thorax occupies the whole screen.
3. Select the method of choice for measurement of the lung, taking into consideration that the manual tracing has shown the highest reproducibility [18].
4. Divide the area of the lung (in squared millimeters) by the head circumference (in millimeters),

Table 6.1 Formulae to calculate the expected LHR ratio in left- and right-sided congenital diaphragmatic hernia (CDH), using different methods for measurement of the lung area, based on gestational age (GA) in weeks with decimals

Lung area measurement	Right LHR in left CDH	Left LHR in right CDH
Longest diameter method	$-3.4802 + (0.3995 \times GA) - (0.0048 \times GA^2)$	$-2.5957 + (0.3043 \times GA) - (0.0042 \times GA^2)$
Anteroposterior diameter method	$-3.1597 + (0.3615 \times GA) - (0.0041 \times GA^2)$	$-1.0224 + (0.1314 \times GA) - (0.0011 \times GA^2)$
Tracing method	$-2.3271 + (0.27 \times GA) - (0.0032 \times GA^2)$	$-1.4994 + (0.1778 \times GA) - (0.0021 \times GA^2)$

Source: Modified from Jani JC et al., *Ultrasound Obstet Gynecol* 39, 2–6, 2012.

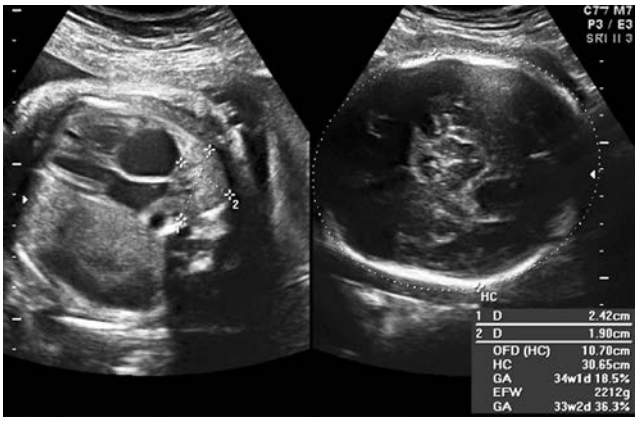


Figure 6.15 Calculation of the lung-to-head ratio (LHR). This is performed by multiplying the two orthogonal diameters (D1 and D2) of the right lung, which is located behind the heart, in a left-sided hernia. This value is then divided by the head circumference (CC) (see text).

to obtain the LHR. Care should be taken not to include the myocardium in the measurement.

5. Then, the *observed* LHR should be divided by the *expected* LHR to derive the o/e LHR according to Table 6.1 [13].

The only method that has shown a higher accuracy in the measurement of lung volume is MRI [14], and this technique is currently used for preoperative assessment of the cases undergoing prenatal fetoscopic tracheal occlusion (see below).

Another prognostic indicator has recently been reported in the literature, and has still to be validated by other researchers: It seems that fetuses with CDH and a formerly increased nuchal translucency (NT) have a poorer outcome than those with a normal NT [15]. In particular, in this retrospective series of 80 cases with CDH and NT measurement 7/9 (78%) fetuses with CDH + NT > 95° died in the neonatal period versus only 24/62 (35%) of those with CDH and a normal NT (P = 0.035). The authors speculated that early intrathoracic compression by the herniated abdominal viscera is responsible for a venous or lymphatic congestion in the head and neck, leading ultimately to the enlargement of the NT.

Association with other malformations. In addition to the cases associated with syndromes, CDH can be associated with congenital heart disease, and gastrointestinal and central nervous system (CNS) anomalies.

Risk of chromosomal anomalies. This risk is relatively high (5%–15%). CDH is mainly associated with trisomies 21 and 18.

Risk of nonchromosomal syndromes. This risk is high (25%–30%). A summary of the most important monogenic conditions that may present with CDH is shown in Table 6.2 [16]. Among these, those that may be considered to be detectable in utero are

- *Fryns syndrome [16,17]*: look for ► *CDH* + unilateral cleft lip/palate + micrognathia + CNS anomalies;
- *Pallister–Killian syndrome [18]*: look for ► *CDH* + abnormal profile ("small" nose and thin upper lip) + mesomelic hypoplasia;
- *Beckwith–Wiedemann syndrome [17]*: look for ► *CDH* + macroglossia + somatic hemihypertrophy + polycystic kidneys + exomphalos (Chapter 10).

Obstetric management. Should CDH be diagnosed in a fetus, karyotyping is mandatory because of the relatively high risk of aneuploidy. In addition, a thorough anatomic scan should be performed by an expert, in order to detect major and/or minor signs possibly leading to the diagnosis of one of the above-mentioned syndromes. As to the timing and mode of delivery, in the past, it had been apparently shown that delivery by Cesarean section was associated with a better outcome.

Table 6.2 Monogenic syndromic conditions frequently associated with congenital diaphragmatic hernia

Syndrome	OMIM	Inheritance	Locus	Phenotype
Cornelia de Lange syndrome	122470	AD	5p13	IUGR, micromelia, facial dysmorphsms, mental retardation, hirsutism
	300560	XL	Xp11.2	
Cranio-fronto-nasal dysplasia	304110	XL	Xq12	Craniosynostosis, hypertelorism, bifid nose muscolo-skeletal anomalies
Donnai–Barrow syndrome	222448	AR	2q24.3 3-2q31	Hypertelorism, corpus callosum agenesis, neurosensorial deafness, developmental delay, proteinuria
Fryns syndrome	229650	?	?	typical facies, CNS anomalies, genito-urinary anomalies, CHD, distal digital hypoplasia
Matthew Wood syndrome	601186	AR	14q24.1	Microphthalmia, CHD, genito-urinary anomalies
Spondylo-costal dysostosis (Jarcho–Levin syndrome)	277300	AR	19q13	Short stature, hemivertebrae, vertebral fusion, costal abnormalities
Simpson–Golabi–Behmel	312670	XL	Xq26	Accelerated growth, abnormal facies, vertebral anomalies, acral anomalies, renal anomalies

Source: Modified from Pober BR *Clin Genet* 74, 1–15, 2008.
AD: autosomal dominant; AR: autosomal recessive; XL: X-linked; CHD: congenital heart disease; CNS: central nervous system; OMIM (*Online Mendelian Inheritance in Men*) website.

However, none of the more recent studies has confirmed this apparent advantage of the operative delivery. As a result, currently there is no recommendation to deliver fetuses with CDH by Cesarean section [4]. There are also some interesting data (which need be confirmed by larger trials) regarding the timing of delivery. In a recent study, survival was significantly higher for deliveries occurring later than 40 weeks of gestation than for those occurring at 38–40 weeks [19].

Postnatal therapy. Prior to addressing the postnatal treatment issue, it should be emphasized that CDH is one of the few anomalies for which fetal surgery has been attempted. In particular, the U.S. West coast group of Harrison et al. [20] was the first to try to devise an intrauterine surgical approach to CDH with poor prognostic indicators (LHR < 1.0 and/or liver up). The original technique consisted of direct closure of the diaphragmatic defect by suture or patch, after hysterotomy and exposure of the fetal chest; on completion of the hernia repair, the fetus was repositioned in utero, and the amniotic membranes and the hysterotomy were sutured. However, this approach showed mortality and prematurity rates that were not significantly different from those seen with conventional postnatal surgery, and the costs were extremely high. As a result, this approach was abandoned even by those who had first proposed it. More recently, another less invasive procedure for the treatment of CDH with poor prognostic signs was devised. The original idea came from the observation that fetuses with laryngeal atresia had significantly enlarged lungs with histologic signs of alveolar hyperplasia. The new approach consists of the creation of an iatrogenic obstruction of the high airways achieved with the insertion of a balloon catheter in the fetal trachea; the balloon is left in place for several weeks, during which it stimulates alveolar growth, and is eventually removed just prior to delivery. The procedure, which was originally performed with a surgical approach, is currently done under fetoscopic guidance, which reduces invasiveness, risks, and costs [20,21]. The name of the procedure is FETO (fetal endoscopic tracheal occlusion), which denotes the limited invasiveness of the endoscopic approach. The latest update on the results of this procedure are the following [21]: on the basis of stratified data from the Antenatal CDH Registry, FETO seems to increase survival in severe cases with left-sided CDH from 24.1% to 49.1% and with right-sided CDH from 0% to 35.3% ($P < 0.001$). The strongest predictors of survival were o/e LHR prior to the procedure (odds ratio = 1.490, $P = 0.019$) and gestational age at delivery (odds ratio = 1.024, $P = 0.007$). Currently, two randomized trials have started enrolling patients, one in severe cases and one in moderately

severe cases. The latter is based on the hypothesis that FETO will lead to less bronchopulmonary dysplasia in survivors. It compares expectant management during pregnancy with late (30–32 weeks) FETO; the former trial concerns fetuses with severe pulmonary hypoplasia (from o/e LHR) and will compare FETO at 27–30 weeks with expectant management. In all cases, the balloon is removed at 34 weeks of gestation. In summary, so far no type of prenatal approach has yet been proved to be superior to the conventional postnatal approach in randomized trials, though there is mounting evidence in this direction. The final answer will be provided in a few years by the two aforementioned trials.

In the conventional perinatal management of neonates with CDH, a very important role is played by in utero transport to referral centers and by resuscitation and stabilization protocols. After delivery, immediate resuscitation should proceed with respiratory support, including intubation, and circulatory support as needed. In this regard, although there is no single study demonstrating higher survival for severe cases if Extra-Corporeal Membrane Oxygenation (ECMO) is employed, it is advised that ECMO be available in all neonatal intensive care units. Briefly, this technique employs a heart-lung machine to oxygenate the blood in those cases in which the alveolar units are severely damaged or hypoplastic. However, regardless of the technique used, currently the most crucial issue in the early neonatal management seems to be *gentle ventilation*, in other words, ventilation allowing mild hypercapnea; this has proven more advantageous than the aggressive ventilation used until 1995 [4]. Once the neonate has been stabilized, surgery is performed. The timing of the surgical intervention depends on the severity of the desaturation (O_2) and on the presence of pulmonary hypertension. The surgical approach usually involves the use of a synthetic patch when the diaphragmatic defect is too large to be closed by primary tissue approximation. Occasionally, rotational muscle flaps can be used to repair the defect. Unfortunately, because prosthetic patches do not grow with the neonate, reherniation will occur in a significant number of survivors.

Prognosis, survival, and quality of life. If CHD is associated with aneuploidy or nonchromosomal syndromes, survival is very poor, because of the high lethality of the above-described syndromic conditions. In the case of isolated nonsyndromic CDH, the major determinant of death is the degree of pulmonary hypoplasia and the occurrence of severe pulmonary hypertension, considering that moderate pulmonary hypertension is ubiquitous in neonates with CDH. For left-sided CDH, survival rates range between 30% and 80%, with a median of 50%–60%. Quality of life is generally good, especially when primary closure of the defect has been achieved. However, long-term sequelae have been reported in a significant number of cases. First of all, some authors have reported signs of cortical and basal ganglia damage on MRI scans in neonates with repaired CDH discharged from hospital in apparently good condition [22]. Even though it is still unclear whether these worrying signs of cerebral damage on MRI are indeed responsible for functional neurologic deficits this finding should warrant further investigation and long-term follow-up: If the occurrence of long-term damage should be confirmed in other series, this possibility should be mentioned during prenatal counseling. Other fairly frequent but less important long-term sequelae include growth retardation (18%), gastroesophageal reflux (27%), chronic lung disease (22%), and, rarely, oxygen requirement (2%) [23].

cYSTIc AdENoMATodId MALFoRMATIoN oF THE LUNG (cAML)

Incidence. Relatively rare.

Ultrasound diagnosis. On the *4-chamber view*, unilateral uni- or multilocular cystic lung mass; unilateral, homogeneously hyperechoic lung mass.

Risk of chromosomal anomalies. Extremely low.

Risk of nonchromosomal syndromes. Extremely low.

Outcome. Good/very good, with spontaneous complete regression or surgical removal after birth.

Definition Cystic adenomatoid malformation of the lung (CAML) is a developmental anomaly of the lung characterized by a mass of disordered pulmonary parenchyma with proliferation of terminal respiratory bronchioles and a lack of normal alveoli, thought to represent a hamartomatous lesion. It is unilateral in 97% of cases. Histologically, the original Stocker classification [24] recognizes three subtypes differentiated

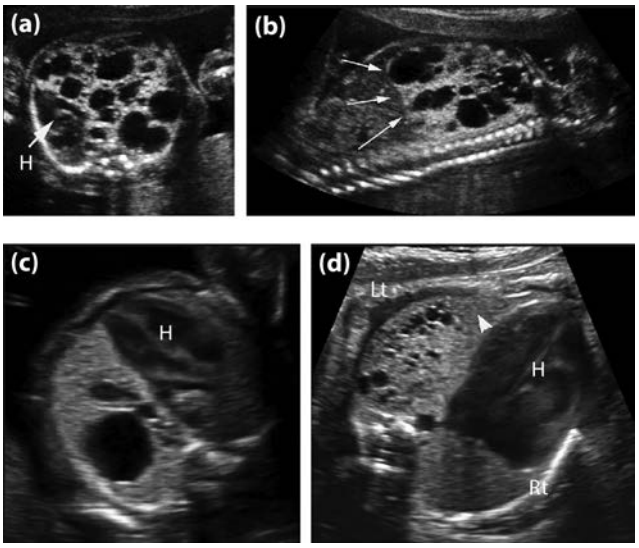


Figure 6.16 Cystic adenomatoid malformation of the lung (CAML), macrocystic type (22 weeks of gestation). The macrocystic type is characterized by one or more cysts of various sizes. (a) and (b) In this case, the lesion was so large as to compress the heart (H) against the left thoracic wall (a) and distend the diaphragm (arrows, in b); (c) another case of left-sided macrocystic CAML characterized by a single dominant cyst. The heart (H: heart) is displaced contralaterally; (d) in this case, the lesion corresponds to type II of the Stocker classification (in between the macrocystic and solid, microcystic types). It is homogeneously hyperechoic, but shows small multiple cysts, and involves only part of the lung (arrowhead: unaffected lung tissue), determining moderate mediastinal shift. H: heart.



Figure 6.17 Cystic adenomatoid malformation of the lung (CAML), solid or microcystic type (26 weeks of gestation). If the lesion appears homogeneously hyperechoic, with no visible cysts, the CAML is defined as microcystic, and has to be differentiated from pulmonary sequestration, which has similar sonographic features (see Figure 6.19). Lt: left side; H: heart; Rt: right side.

according to the dimensions of the cysts: type I, with large cysts (2–10 cm); type II, with small cysts (0.5–2 cm); and type III, solid or microcystic (<0.5 cm).

Etiology and pathogenesis. The etiology of CAML is unknown. As already mentioned, this lesion represents a developmental anomaly. Histologically, it involves one lobe only, although on US it appears to extend to the whole lung, due to its usually large dimensions. It is interesting to note that, on histology slides following surgical removal of the mass, CAML is found to be associated with pulmonary sequestration or segmentary bronchial atresia in a not insignificant percentage of cases. On the basis of these findings it has been hypothesized that a common pathogenetic mechanism may be responsible for the three different anomalies.

Ultrasound diagnosis. This is performed on the classic *four-chamber view*. Because the histologic Stocker classification cannot be applied to the US appearance, a simpler US-based classification was developed by Wilson et al. [25], which recognizes a cystic and a solid variant or microcystic. The US appearance is completely different for the two types of lesion: The cystic variant appears as a multilocular lesion with cysts of various sizes from a few millimeters to more than 10 mm, which show bright contours due to the posterior wall US enhancement (Figure 6.16). In contrast, the solid, microcystic variant appears as a well-defined homogeneously hyperechogenic mass (Figure 6.17). Both types are unilateral by definition (only 3% of CAML cases involve both lungs), and usually of large volume, which causes a contralateral shift of the mediastinum and the heart. In the case of right-sided CAML, there is an abnormally increased cardiac axis, due to the extreme levorotation (Figure 6.16a). Three-dimensional US may be used to evaluate better the volume of the mass and, possibly, to assess the net volume of the cystic component.

Differential diagnosis (Figure 6.5). The differential diagnosis should consider, for the cystic variant, CDH, as already mentioned: the intrathoracic stomach may, to some extent, resemble a single cyst in a CAML. With regard to the solid variant, the most difficult diagnosis to differentiate CAML from is pulmonary

sequestration. The only US feature that may allow discrimination between the two lesions, which share a highly hyperechoic and homogeneous appearance and mainly unilateral involvement, is the feeding artery, which is ubiquitous in pulmonary sequestration. This is detectable in most cases of pulmonary sequestration using power Doppler or color Doppler with a low pulse repetition frequency in order to visualize low-velocity vessels: the artery feeding the sequestration is commonly seen branching off the descending aorta. Theoretically, also, a right-sided hernia with liver up should be differentiated from the solid, microcystic variant of CAML; however, in this case, the weak echogenicity of the liver is significantly different from the bright appearance of the CAML.

Prognostic indicators. CAML is not usually associated with syndromes, and, therefore, the risk of more severe underlying conditions of prognostic significance is not an issue. The only significant prognostic factor, which allows identification of cases at high risk of perinatal demise, is the occurrence of hydrops (ascites and/or hydrothorax) at the time of diagnosis or during follow-up. It has been hypothesized that the development of hydrops is a consequence of central venous compression, but direct vena caval obstruction is not found in all cases with hydrops. Fortunately, this poor prognostic sign is found in less than 10% of the cases at diagnosis [26], although it can develop in another 30% of cases during follow-up [27]. If hydrops is present, the chances of survival are very low, with perinatal demise being by far the most frequent outcome [28]. Recently, another promising prognostic index derived from 3D assessment of CAML has been investigated: the *CAM volume ratio (CVR)* [27]. This parameter is calculated by dividing the volume of the CAML lesion by the circumference of the head, similarly to LHR in CDH. In a prospective study [27], the incidence of hydrops was 75% for CVR > 1.6 and 17% for CVR < 1.7; the latter value dropped to 2.3% if cases with a dominant cyst were excluded. Hence, it seems that for the cystic subtype of CAML, regardless of the volume of the mass, hydrops is more likely to occur if there is a dominant cyst (Figure 6.16c).

Association with other malformations. There is a strict histologic and pathogenetic relationship with pulmonary sequestration, with the two lesions often being found at histology in the same gross pulmonary lesion. CAML may also be associated with other pulmonary or thoracic anomalies, such as CDH, duplication cysts, tracheoesophageal fistulas and pulmonary artery branching abnormalities.

Natural history. It is important to underscore that CAML represents an evolving lesion with peculiar features. First of all, the growth of the mass shows a predictable course, with rapid growth occurring between 20 and 26 weeks of gestation. After that period, the volume of the mass plateaus, in a significant percentage of cases, tends to regress or sonographically disappear during the third trimester of pregnancy. Therefore, since the volume of the mass is not expected to grow further after 26 weeks, if there is no hydrops by that gestational age, then it is highly unlikely that this will develop afterward. In addition, it has to be emphasized that, in a significant proportion of apparently vanished lesions, the mass is still present and can be detected by MRI: it has only become invisible on US since it has become isoechogenic with adjacent normal lung parenchyma [28]. Overall, 10%–20% of cases really do regress almost completely during the third trimester of pregnancy.

Risk of chromosomal anomalies. This is extremely low (anecdotal reports only). In all reports in which a slight increase in the risk of chromosomal anomalies was detected, extrapulmonary malformations were constantly associated.

Risk of nonchromosomal syndromes. This risk is extremely low.

Obstetric management. Should a CAML be detected in a fetus, it is of the utmost importance to search further for very early signs of hydrops. As far as karyotyping is concerned, considering what has already been expressed, we deem this necessary only if other extrapulmonary anomalies are found. An important issue, in our opinion, is to accurately emphasize during prenatal counseling sessions, the relatively high rate of spontaneous regression and the consequently very good outcome that these lesions show [26]. The above-mentioned prognostic tools (i.e., CVR and presence of hydrops) may be employed at diagnosis and at follow-up US examinations, to predict the risk of developing hydrops and consequently identify the fetuses who can benefit from intrauterine treatment. This treatment should be limited to those cases in which hydrops develops as a result of increased intrathoracic pressure; it may consist of simple cyst aspiration or, more often, placement of a thoracoamniotic shunt (Figure 6.18), and relies on the fact that all of the cysts communicate with one another. Both procedures have been demonstrated to improve significantl the outcome of fetuses with CAML complicated by hydrops [29].

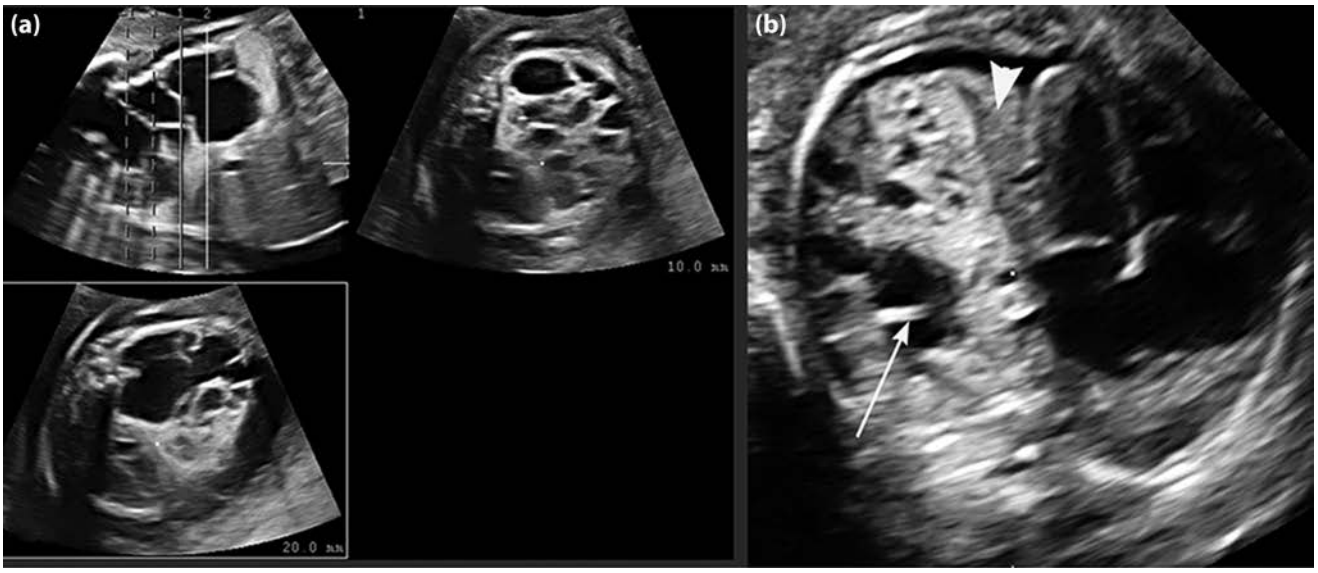


Figure 6.18 Cystic adenomatoid malformation of the lung (CAML, 26 weeks), shunt placement. (a) Tomographic imaging (TUI) demonstrates the huge volume of the lesion, responsible for the hydrops (ascites + hydrothorax + polyhydramnios); (b) the placement of a thoracoamniotic shunt within the main cyst (arrow) has determined dramatic shrinkage of the CAML. The normal decompressed lung tissue is also visible, after shunting (arrowhead). In two weeks, the hydrops disappeared completely.

Postnatal therapy. The first step is to confirm the volume of the lesion by MRI. Although there is no general agreement among pediatric surgeons about the need to resect the affected lobe, most of them believe that the CAML should be removed, even if asymptomatic, by 12 months of age. The need to resect the nonfunctioning lobe is based on the high incidence of infection and on the very low risk of neoplastic transformation, although, as for other types of lesions, if a genetic predisposition to neoplastic transformation is thought to be present in the alveolar epithelium, the resection of the CAML alone would not prevent the neoplasia from originating in the adjacent lung parenchyma. The standard surgical procedure consists of thoracotomy and lobectomy, though the less invasive endoscopic approach is gaining popularity in recent years.

Prognosis, survival, and quality of life. If hydrops is absent, survival is generally unaffected, with no functional limitations, regardless of the possible need for lobectomy. On the contrary, neonatal death is almost certain if hydrops is present and no intrauterine procedure has succeeded in reversing it. Overall survival rates for prenatally diagnosed CAML are greater than 80% in most series.

pULMoNAr y sEqUEsTr ATIo N (ps)

Incidence. Rare.

Ultrasound diagnosis. On the *4-chamber view*, homogeneously hyperechoic unilateral (left-sided in 90% of cases) lesion, sometimes extending below the diaphragm; presence of feeding artery on power/color Doppler.

Risk of chromosomal anomalies. Very low.

Risk of nonchromosomal syndromes. Very low.

Outcome. Good/very good in most instances, with spontaneous regression, selective embolization of the feeding artery, or surgical resection.

Definition Pulmonary sequestration (PS) consists of an island of lung parenchyma that does not communicate with the bronchial tree and is fed by the systemic rather than the pulmonary circulation. There are two types of PS: intralobar and extralobar. Prenatal diagnosis concerns the latter type only, because intralobar

sequestration is not visible on US, despite accounting for three quarters of the PS cases detected after birth. The extralobar variant is further subdivided into a supradiaphragmatic and a subdiaphragmatic subtype, the former accounting for 90% of extralobar PS and the latter for the remaining 10%. The lesion is characteristically unilateral, and involves the left lower lobe in 90% of cases. In general, PS shows a roughly triangular shape, with the apex pointing toward the mediastinum. Typically, extralobar sequestrations present a feeding artery branching off the descending thoracic or abdominal aorta.

Etiology and pathogenesis. The etiology of PS is unknown, although it has been suggested that it might share the same pathogenesis with CAML, due to the fact that the two lesions are frequently associated.

Ultrasound diagnosis. This is carried out on the *four-chamber view*, given that the lesion often involves the left lower lobe, which is at the same level as the heart, or just below. PS appears as a well-defined homogeneously hyperechoic, roughly triangular mass, often involving the lower part of the left lung (Figure 6.19a and b). Only small instances of PS and the subdiaphragmatic variant may not be readily recognizable on the four-chamber view, and instead require a lower axial view, at the level of the diaphragm (Figure 6.19c and d). To complete the US assessment, it is necessary to switch to *sagittal views*, because only these allow: (1) assessment of the caudal extension of the mass (Figure 6.19b); (2) detection and characterization of subdiaphragmatic extralobar sequestrations (Figure 6.19d); and (3) recognition, on power or color Doppler, of the feeding artery branching off the descending aorta (Figure 6.20). Finally, the possible association of ipsilateral hydrothorax (Figure 6.21), frank hydrops, or other thoracic malformations (e.g., a CDH) should be excluded (Figure 6.22).

Differential diagnosis (Figure 6.5). As already mentioned, the only difficult differential diagnosis is with the solid, microcystic variant of CAML, due to the very similar echogenicity of the mass. However, a more triangular shape, a location in the left lower lung area, and, above all, the recognition of the feeding vessel (Figure 6.20) all favor a PS. With the rare subdiaphragmatic subtype of PS, the differential diagnosis should include rare tumors (e.g., hemangiomas and neuroblastomas). It should be noted that in the very rare instance in which a feeding vessel is identified entering the solid component of a prevalently cystic CAML, the lesion is probably a rare case of mixed CAML + PS lesion.

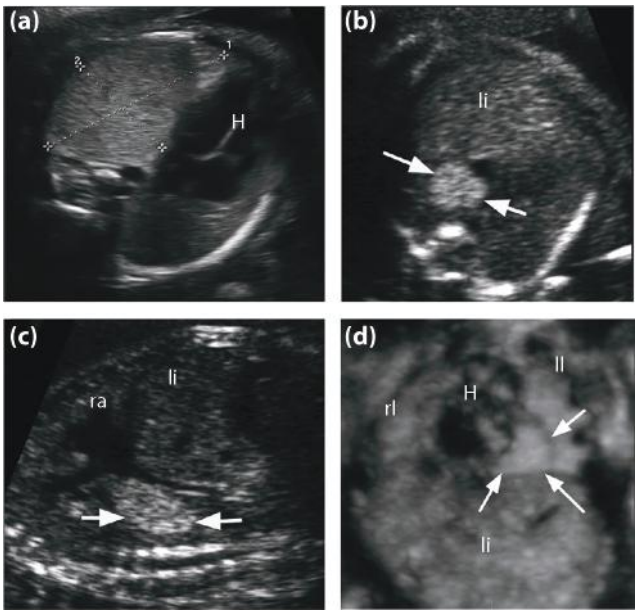


Figure 6.19 Pulmonary sequestration, extralobar. This anomaly has a hyperechoic aspect and, often, a triangular shape. It can be located in the thorax or below the diaphragm. (a) Supradiaphragmatic pulmonary sequestration (25 weeks of gestation): the axial view of the thorax demonstrates the homogeneously hyperechoic lesion of the left lung (calipers); the heart (H) is displaced in the right hemithorax; (b, c) subdiaphragmatic pulmonary sequestration (22 weeks of gestation): (b) on the axial view of the abdomen, just below the diaphragm, it is possible to locate the small hyperechoic lesion (arrows), on the right side of the midline; (c) the right parasagittal thoracic view confirms the abdominal location of the sequestration (arrows); (d) another case of extralobar supradiaphragmatic sequestration (21 weeks of gestation): the coronal view reconstructed from the three-dimensional volume shows the two lungs and the small sequestration (arrows). H: heart; li: liver; ll: left lung; rl: right lung; ra: right atrium.

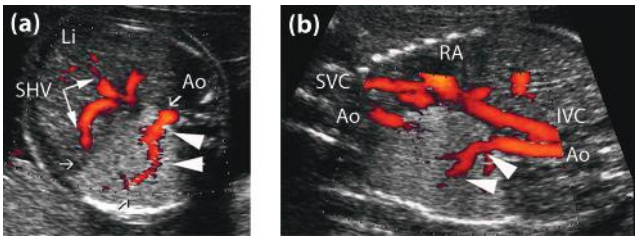


Figure 6.20 Pulmonary sequestration, extralobar. The vascular pedicle can be recognized in all cases. Color or power Doppler with a low pulse repetition frequency are used to locate the feeding artery, which, in most instances, branches off the thoracic or abdominal aorta. (a) Axial abdominal view: the feeding artery (arrowheads) is seen branching off the abdominal aorta. (b) On the longitudinal view, the inferior and superior vena cava (IVC and SVC) are seen draining into the right atrium (RA); the descending aorta is partially hidden by the sequestration, and the feeding vessel (arrowhead) is clearly visible. Ao: aorta; Li: liver; SHV: suprahepatic veins.

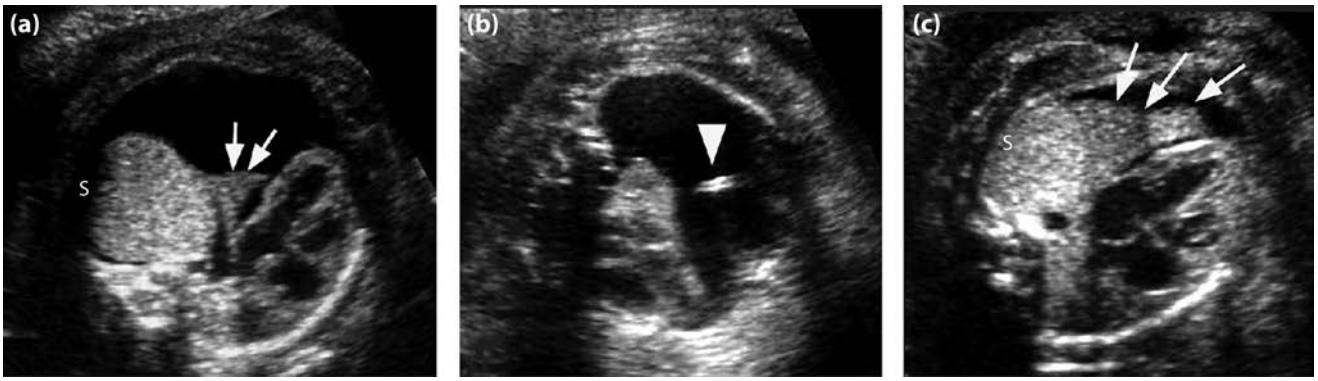


Figure 6.21 Pulmonary sequestration, extralobar. In some cases, pulmonary sequestration is associated with hydrops. In these cases, a single tap or the placement of a thoracoamniotic shunt may resolve the hydrops due to venous compression. (a) The supradiaphragmatic pulmonary sequestration (S) is associated with a severe hypertensive hydrothorax, severely compressing the left lung (arrows). (b) This image shows the tip of a needle (arrowhead) inserted to drain the pleural effusion. (c) After drainage of the fluid collection, the left lung re-expands (arrows). The different echogenicities of the sequestration (S) and the lung are also evident. Also note the heart displaced in the right hemithorax.

Prognostic indicators. As for CAML, the occurrence of hydrops is the most ominous prognostic indicator. However, there have been cases (although rare) in which with the spontaneous regression of the PS, the hydrops has also disappeared, with a good perinatal outcome.

Association with other malformations. The close histologic and pathogenetic relationship with CAML has already been emphasized. PS, like CAML, may also be associated with other pulmonary or thoracic anomalies, such as CDH (Figure 6.22), duplication cysts, tracheoesophageal fistulas and pulmonary artery branching abnormalities.

Natural history. The tendency to regress and even disappear during the third trimester has also been reported for PS, which further supports the close pathogenetic links with CAML. In some series, this tendency has been shown to be even more pronounced than that reported for CAML, occurring in 30% of cases [30,31].

Risk of chromosomal anomalies. This risk is extremely low.

Risk of nonchromosomal syndromes. This risk is extremely low.

Obstetric management. Given that the risk of chromosomal anomalies is low, karyotyping is not mandatory in the case of isolated PS. What should be monitored is the possible presence/onset of hydrothorax or hydrops. In most cases, the hydrops is a consequence of the hypertensive hydrothorax that can occasionally complicate PS. In fact, the hydrops often disappears after placement of a thoracoamniotic shunt, which reduces the high intrathoracic pressure. The possibility of spontaneous regression and a good outcome also in cases complicated by hydrops should be communicated to the parents during prenatal counseling [26].

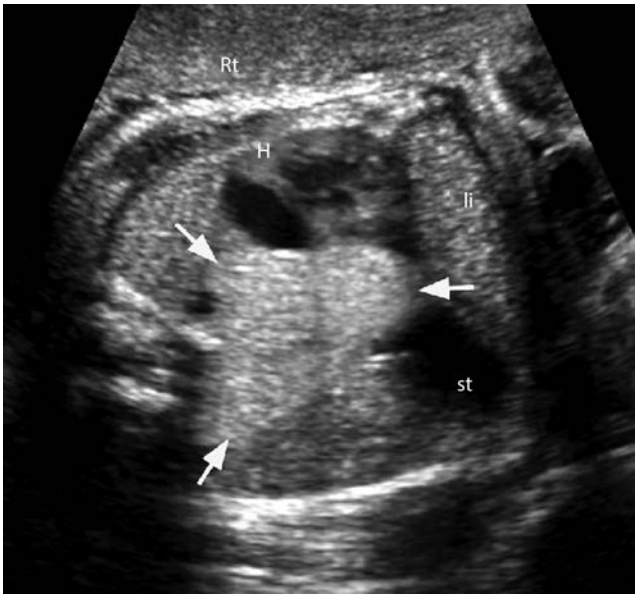


Figure 6.22 Pulmonary sequestration, extralobar, associated with CDH. In rare cases, pulmonary sequestration may be associated with other pulmonary lesions. In this case (at 28 weeks of gestation), the sequestration (arrows) is associated with a left-sided diaphragmatic hernia. H: heart; li: liver; Rt: right side; st: stomach.

Postnatal therapy. This consists of surgical or endoscopic removal of mass [32] or, alternatively, of selective embolization of the feeding artery under catheterization [33].

Prognosis, survival, and quality of life. The survival rate of prenatally detected cases is very high [30,31]. As already noted, the possibility of active prenatal management (by drainage and thoracoamniotic shunt placement) of cases associated with hydrops contributes significantly to the extremely good survival rates

Bro Nch IAL ATr Es IA

Incidence. Extremely rare.

Ultrasound diagnosis. Severely enlarged and hyperechoic lung, unilateral. Possible partial bronchogram (abnormal dilatation of the distal bronchus).

Risk of chromosomal anomalies. Extremely low.

Risk of nonchromosomal syndromes. Extremely low.

Outcome. The outcome is generally favourable for distal atresia, whereas mainstem bronchial atresia is associated with a poorer prognosis.

Definition and anatomy. *Bronchial atresia* is defined as a focal obliteration of a proximal segmental or subsegmental bronchus that lacks communication with the central airways. Generally, a distal segment persists, and it may dilate as a consequence of entrapment of the fluid produced by the alveoli

Etiology and pathogenesis. The more accepted pathogenetic theory for this kind of lesion implicates the impaired blood supply during the embryogenetic period, which may have prevented the normal development of the affected bronchial segment.

Ultrasound diagnosis. This is carried out on the axial four-chamber view of the thorax. The heart and the mediastinum are severely displaced contralaterally by a huge pulmonary hyperechoic mass (Figure 6.23). The lung tissue is hyperechoic due to entrapment of the fluid produced by the alveoli, and, in some cases, the distal segments of the bronchus, dilated by the entrapped fluid are visible, too (Figure 6.23).

Differential diagnosis (Figure 6.5). Both the microcystic, solid variant of CAML and PS should be differentiated from bronchial atresia, due to the homogeneously increased echogenicity of the lung mass. However, in bronchial atresia the volume of the mass is generally larger than with the other two entities, and, in addition, part of the distal bronchus is visible as a sonolucent segment (Figure 6.23), in most cases.

Prognostic indicators. Should ascites be associated, this represents a sign of central venous compression and, as such, it bears a poor prognostic sign (Figure 6.23b).

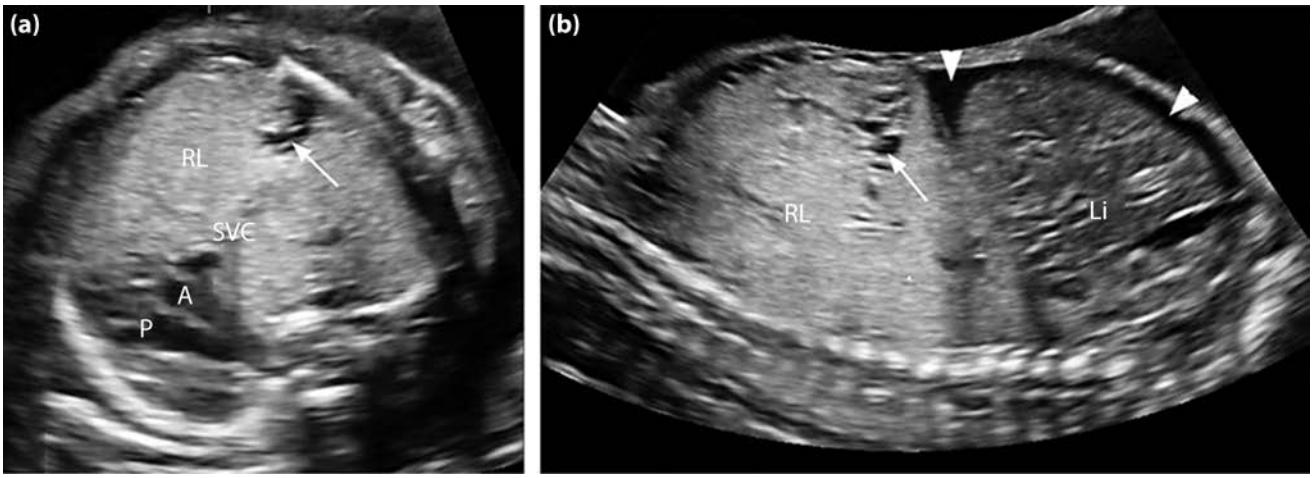


Figure 6.23 Bronchial atresia (25 weeks of gestation). (a) On the axial three-vessel view, the severe mediastinal shift is evident, with the whole thorax occupied by the grossly enlarged and hyperechoic right lung (RL). Dilatation of distal bronchi is also visible (arrow); (b) on a right parasagittal view of the fetal trunk, the huge mass is seen indenting the diaphragm; ascites (arrowheads) from central venous compression is also evident. A: aortic arch; Li: liver; P: pulmonary artery and ductal arch; SVC: superior vena cava.

Association with other malformations. Developmental anomalies involving other parts of the bronchial tree and/or esophageal abnormalities may be associated.

Risk of chromosomal anomalies. This risk is extremely low.

Risk of nonchromosomal syndromes. This risk is extremely low.

Obstetric management. Karyotyping is not indicated, because of the low risk of aneuploidy. Delivery should take place in a referral center, due to the possible need for immediate postnatal resuscitation and intubation.

Postnatal therapy. If not symptomatic at birth, bronchial atresia may remain asymptomatic for years. However, dyspnea, pneumonia, and bronchial asthma have been reported [34]. Recently, a successful prenatal fetoscopic approach to bronchial atresia has been described [35].

Prognosis, survival, and quality of life. Mainstem bronchial atresia is associated with a relatively high rate of perinatal mortality, due also to the concurrent hydrops. More distal atresias are symptomatic later in life but they tend to escape prenatal diagnosis.

LAr yNGEAL ATr Es IA—ch Aos

Incidence. Extremely rare.

Ultrasound diagnosis. On the *4-chamber view*, Severely enlarged and hyperechoic lungs. Bronchogram (abnormal dilatation of the bronchial tree); ascites constantly associated.

Risk of chromosomal anomalies. Extremely low.

Risk of nonchromosomal syndromes. Extremely high: Fraser syndrome.

Outcome. Extremely unfavorable. The very few survivors have been managed with the EXIT procedure.

Definition Laryngeal atresia is an exceedingly rare anomaly consisting of three possible lesions: agenesis of the glottis, agenesis of the larynx, or agenesis of both. As a result of any of the three anomalies, the high airways are completely obstructed, and this leads to the inclusion of laryngeal atresia among the lesions causing CHAOS. The other oropharyngeal and neck anomalies responsible for the CHAOS sequence are illustrated in Chapter 3. Here, we describe the laryngeal and tracheal atresias, because these two entities are not distinguishable on US and are detected on the basis of the unmistakable intrathoracic signs. Furthermore, both bear the same ominous prognosis.

Etiology and pathogenesis. The more accepted pathogenetic theory for this kind of lesion implicates the impaired blood supply during the embryogenetic period, which may have prevented the normal development of the trachea/larynx.

Ultrasound diagnosis. As already pointed out, differentiation between laryngeal and tracheal atresia is not feasible on US. The diagnosis is made on the *four-chamber view of the fetal heart*. Typically, *both* lungs appear severely enlarged and highly hyperechoic (Figure 6.24). Owing to the exceedingly high intrathoracic pressure, the heart is squeezed in between the lungs, and appears smaller than it really is due to the degree of pulmonary enlargement. It shows a reduced (sometimes to zero) cardiac axis (Figure 6.24a). Relatively often, some fluid is trapped in the bronchial tree and is responsible for the bronchogram (dilatation of the trachea and bronchi by the entrapped fluid) that can sometimes be present. In this case, the swollen trachea appears as a small round sonolucent area behind the heart (Figure 6.24c). The bronchogram, if present, is better displayed with a *coronal approach*: on this view, the dilated trachea is seen bifurcating at the level of the carina in the two bronchi. On the coronal view of the fetal thorax and abdomen, at low magnification the severe bell-shaped distortion of the thorax, the flattening or inversion of the diaphragmatic convexity, and the ubiquitous ascites can be appreciated (Figure 6.24b).

Differential diagnosis (Figure 6.5). There is virtually no differential diagnosis to be made, since laryngeal atresia represents an absolutely unique lesion on US. Seen once, it will never be forgotten! The extremely rare cases (<3%) of bilateral, solid, microcystic ACML would not show the severely increased lung volume typical of laryngeal atresia.

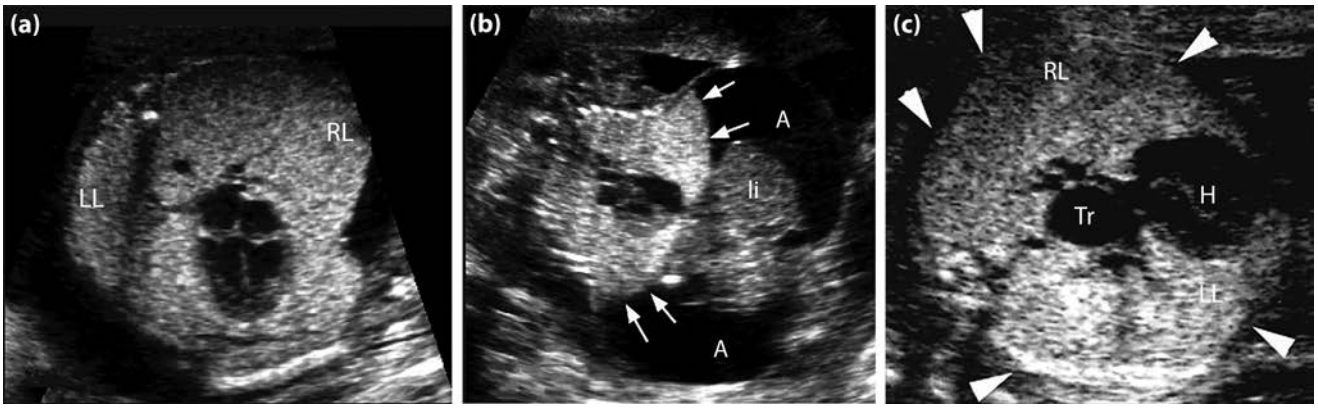


Figure 6.24 Laryngeal atresia (22 weeks of gestation). (a) On the axial four-chamber view, the highly hyperechoic lungs appear severely enlarged. The (normal) heart is squeezed into the mediastinum. (b) The coronal view of the fetal trunk demonstrates eversion of the diaphragm (arrows), due to the massive enlargement of the lungs, and ascites, which is almost ubiquitous in laryngeal atresia. (c) Another case, associated with Fraser syndrome, in which the four-chamber view demonstrates tracheal dilatation often found in these cases. A: ascites; li: liver; LL: left lung; H: heart; RL: right lung; Tr: trachea.

Prognostic indicators. The lethality of this condition makes the identification of poor prognostic signs irrelevant. If anything, the detection of severe oligoamnios due to concurrent renal agenesis together with other major anomalies characterizing *Fraser syndrome* makes the prognosis even worse than it already is, considering that the latter is transmitted as an autosomal recessive trait [36].

Association with other malformations. Developmental anomalies involving the bronchial tree and the esophagus may be associated.

Risk of chromosomal anomalies. This risk is extremely low.

Risk of nonchromosomal syndromes. This risk is high. A significant proportion of cases of laryngeal atresia are associated with Fraser syndrome:

- *Fraser syndrome [36]*: look for ► *laryngeal atresia* + cleft lip/palate + congenital heart disease + microphthalmia + external ear anomalies + bilateral renal agenesis (Chapter 10).

Obstetric management. The possibility of additional anomalies indicating the likely presence of Fraser syndrome should be investigated. In fact, isolated laryngeal atresia is a sporadic malformation, whereas Fraser syndrome shows autosomal recessive inheritance. Karyotyping is not indicated, because of the low risk of aneuploidy and the very high mortality rate.

Postnatal therapy. The only available option to try salvaging a fetus with laryngeal atresia is the *EXIT procedure* (ex utero intrapartum treatment; Chapter 3). As of 2006, even with this technique, there are fewer than five surviving cases of laryngeal atresia reported in the literature. Recently, an additional four survivors have been reported after EXIT procedure [37].

Prognosis, survival, and quality of life. Except for the above-mentioned cases, and those that undergo termination of pregnancy, the prognosis is exceedingly poor, and early neonatal death is the rule.

Bro Ncho GENIc cys T

Incidence. Extremely rare.

Ultrasound diagnosis. On the *4-chamber view*, Single large cyst in the lung. Very rarely, hyperechoic lung lesion may turn out to be obstructive and be diagnosed after birth as a bronchogenic cyst.

Risk of chromosomal anomalies. Extremely low.

Risk of nonchromosomal syndromes. Extremely low.

Outcome. Generally good.

Definition and anatomy. Bronchogenic cysts result from an anomalous development of the ventral foregut. More commonly, they are single, but multiple cysts also have been described postnatally. They can occur along the whole tracheoesophageal course, but with a predilection for the area around the carina. Those in the mediastinum are frequently adherent to the tracheobronchial tree, but do not communicate with it. Bronchogenic cysts have also been described in unusual locations, such as the neck, abdomen, and retroperitoneal space.

Etiology and pathogenesis. Bronchogenic cysts arise from anomalous airway buds that contain nonfunctional pulmonary tissue.

Ultrasound diagnosis. In most cases, the cysts are large enough to be detected on the four-chamber view, where they appear as large, sometimes bilobed anechoic lesions (Figure 6.25). However, it should be noted that, very rarely, bronchogenic cysts appeared prenatally as hyperechoic lesions [38].

Differential diagnosis. Theoretically, a cystic thoracic lesion might be a CAML with a dominant cyst or the herniated stomach in CDH. However, in CAML the tissue surrounding the mass is hyperechoic, which is not the case for the bronchogenic cyst, which represents an isolated lesion; and the presence of the stomach in its normal subdiaphragmatic location rules out CDH.

Association with other malformations. Developmental anomalies involving the bronchial tree and the esophagus may be associated.

Risk of chromosomal anomalies. This risk is extremely low.

Risk of nonchromosomal syndromes. This risk is extremely low.



Figure 6.25 Bronchogenic cyst (29 weeks of gestation). On the axial three-vessel view of the thorax, the large cyst (C) is visible. It displaces the mediastinum and the heart contralaterally, and is not associated with lung hyperechogenicity. (A: aortic arch; P: pulmonary artery and ductal arch)

Obstetric management. Karyotype is not indicated, because the risk of aneuploidy is virtually nonexistent. Delivery should take place in a referral center, because of the possible need for emergency intubation at birth [38].

Postnatal therapy. In cases where there is prenatal evidence of bronchial obstruction, fetuses should be delivered with the *EXIT procedure* (ex utero intrapartum treatment; Chapter 3) [38]. In the remaining cases, the need for surgical removal of the cyst should be assessed on the basis of the symptoms.

Prognosis, survival, and quality of life. Except for the above-mentioned cases in which there is early tracheobronchial obstruction, bronchogenic cysts may remain asymptomatic for years.

LUNG AGENESIS–APLASIA–HYPOPLASIA

Incidence. Extremely rare.

Ultrasound diagnosis. Diagnosis on the *4-chamber view* of the fetal heart. *Lung agenesis:* completely absent lung, unilateral. Pronounced mediastinal shift. *Lung hypoplasia:* Mesocardia. If on the right side, it may be a part—together with partial abnormal pulmonary venous return—of scimitar syndrome.

Risk of chromosomal anomalies. Extremely low.

Risk of nonchromosomal syndromes. Extremely low, with the exception of the *scimitar syndrome.*

Outcome. *Lung agenesis:* better for left than for right lung agenesis.

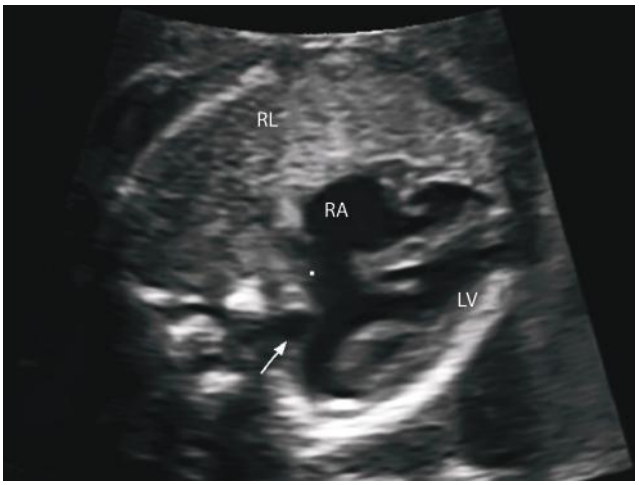


Figure 6.26 Lung agenesis, left. Axial four-chamber view of the thorax. Note the evident mediastinal shift toward the left, with the heart completely in the left hemithorax. The left lung is absent, and the right lung (RL) is larger than normal, occupying completely the right hemithorax. Arrow: descending aorta; LV: left ventricle; RA: right atrium.

Definition and anatomy. The various degrees of pulmonary underdevelopment have been classified into three groups [39]: In group 1, bronchus and lung are absent (agenesis); in group 2, a rudimentary bronchus is present and limited to a pouch without lung tissue (aplasia); in group 3, there is bronchial hypoplasia with variable reduction of lung tissue (hypoplasia). Most cases of right lung hypoplasia are associated with scimitar syndrome, a rare anomaly in which a moderate-to-severe degree of lung hypoplasia is associated with partial abnormal venous return into the inferior vena cava.

Etiology and pathogenesis. Lung agenesis is usually unilateral and it occurs at approximately 4 weeks of gestation, when the primitive lung is forming. The etiology of this anomaly is unknown. However, >50% of children with pulmonary agenesis have associated congenital anomalies that involve the cardiovascular, gastrointestinal, skeletal, and genitourinary systems, with most of the limb and spinal anomalies occurring ipsilaterally to the pulmonary agenesis. The contralateral lung is normal in structure but has compensatory hypertrophy.

Ultrasound diagnosis. *Lung agenesis*: the diagnosis is made on the *axial four-chamber view* of the fetal thorax. The first impression is that of a CDH, due to the extreme displacement of the mediastinum and the heart (Figure 6.26). Once the sonologist notes that there are no abdominal viscera in the thorax and that one of the lung fields is absent, the diagnosis is made. Color

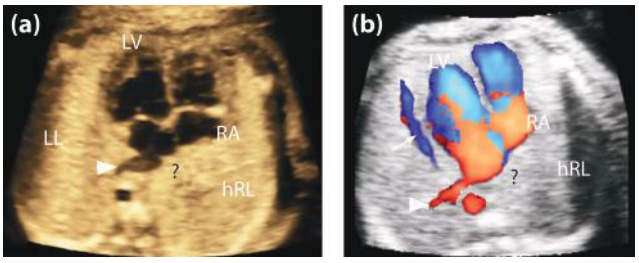


Figure 6.27 Lung hypoplasia, in scimitar syndrome (21 weeks of gestation). (a) Four-chamber view. Note the mesocardia and the absence of the right inferior pulmonary vein (?); (b) on direction power Doppler, the absence of the right pulmonary venous drainage (?) is confirmed. Arrow: left inferior pulmonary vein intraparenchymal; arrowhead: right inferior pulmonary vein drainage into the left atrium; hRL: hypoplastic right lung; LL: left lung; LV: left ventricle; RA: right atrium.

Doppler may be used to detect the concurrent absence of the ipsilateral pulmonary branch. *Lung hypoplasia:* in most of the cases detected in the fetus, this anomaly is part of the scimitar syndrome. The reader is referred to Chapter 5 in the abnormal pulmonary venous return section for further description. In brief, on the *four-chamber view* the right lung is smaller than normal, which determines a shift toward the midline/right hemithorax of the heart (mesocardia or dextrocardia; Figure 6.27a). The inferior right pulmonary vein (Figure 6.27b) or both pulmonary veins are absent, and replaced with a collecting vertical vein (not visible on this view) which drains abnormally into the inferior vena cava. The 3D aspect of this abnormal drainage resembles a scimitar and, hence, the name of the condition. (see also Figure 5.27 in chapter 5)

Obstetric management. There is no need for karyotyping, due to the very low risk of association with chromosomal abnormalities. Delivery should take place in a referral center, because early neonatal intubation may be needed in rare cases of lung agenesis, due to tracheal malposition. In scimitar syndrome, only very rarely does the neonate need an early intervention or ventilatory assistance.

Survival, prognosis, and quality of life. Patients with right lung agenesis have been shown to have a shorter life expectancy than those with left-lung agenesis, probably because of a greater degree of heart and mediastinum displacement, with corresponding distortion of blood vessels and bronchi. As for scimitar syndrome, a recent multicenter report has shown hospital mortality as low as 5.9% and a late mortality of 3.1% due to severe pulmonary hypertension. The main poor prognostic feature was the need for right pneumonectomy or lobectomy [40].

hydro Thor Ax

Incidence. Common.

Ultrasound diagnosis. On the *4-chamber view* of the fetal heart, Anechoic moon-shaped area, unilateral or bilateral, with the lung in the middle.

Risk of chromosomal anomalies. High.

Risk of nonchromosomal syndromes. High.

Outcome. Depends on etiology. Good in isolated chylothorax.

Definition This is a fluid pleural effusion. It can be unilateral or bilateral, isolated, or in the context of generalized hydrops.

Etiology and pathogenesis. The etiology is extremely variable, including at one end of the spectrum thoracic causes, such as in chylothorax, and at the other, classic nonimmune hydrops fetalis (NIHF) (Chapter 4). Thus, hydrothorax shares its pathogenesis with that of NIHF, if the pleural effusion represents one of the signs of hydrops. On the contrary, if the pleural effusion is isolated and no other chromosomal or nonchromosomal anomalies are associated, it may be due to a malformation (atresia or fistula) of the thoracic duct (chylothorax).

Ultrasound diagnosis. Hydrothorax can be diagnosed on the *four-chamber view*, as a unilateral or bilateral anechoic area. It usually has a roughly moon-shaped appearance, due to the fact that it surrounds the lung, except for the hilum (Figure 6.28). The *hydrothorax* is defined as hypertensive if the intrathoracic pressure is high and all viscera are pushed into the contralateral hemithorax (Figure 6.29a). A significant proportion of isolated, hypertensive, unilateral hydrothoraces are actually chylothoraces [41]. If the pleural effusion is part of general NIHF, the severe edema of the subcutaneous thoracic tissue can be seen on the four-chamber view (Figures 6.28 and 6.29).

Prognostic indicators. The most important prognostic factor in fetuses with hydrothorax is the association with NIHF, because in these cases the outcome is generally very poor, with a few exceptions described in Chapter 4. Another poor prognostic indicator is the association with anomalies at high risk of chromosomal anomalies, such as congenital heart disease or CNS malformations. The absence of any associated malformation and/or of any other fluid effusion possibly indicative of concurrent hydrops is the only good

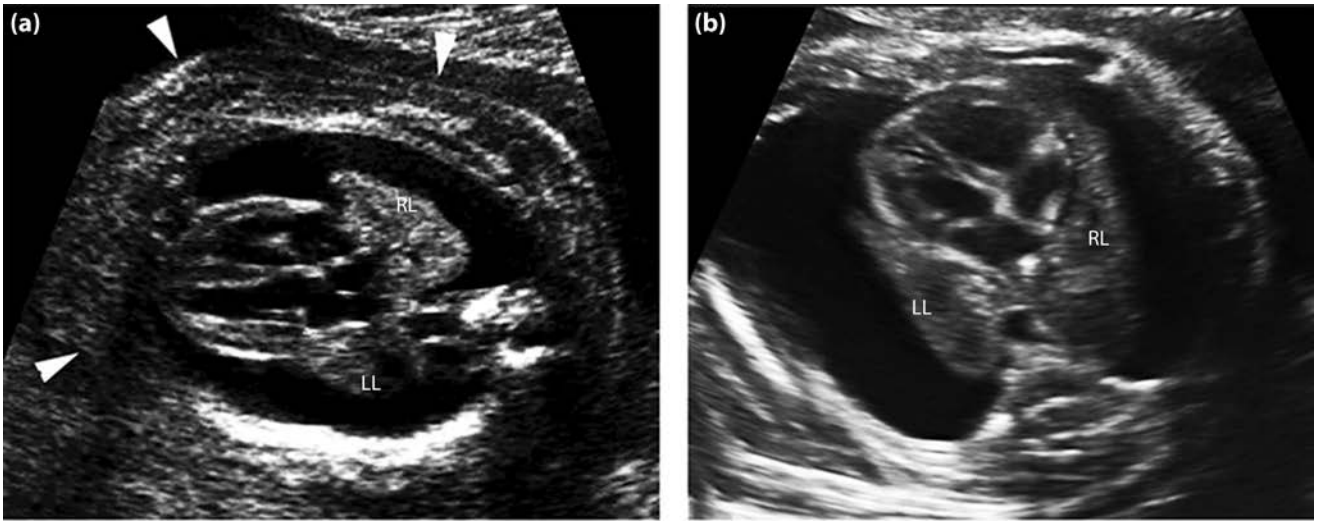


Figure 6.28 Hydrothorax, bilateral. Hydrothorax appears as a moon-shaped anechoic image encircling the ipsilateral lung. (a) in this case (22 weeks of gestation), the pleural effusion was associated with general hydrops: note the severe edema of the subcutaneous tissues (arrowheads); (b) in this other case, bilateral pleural effusion was an isolated finding at 33 weeks of gestation. LL: left lung; RL: right lung.

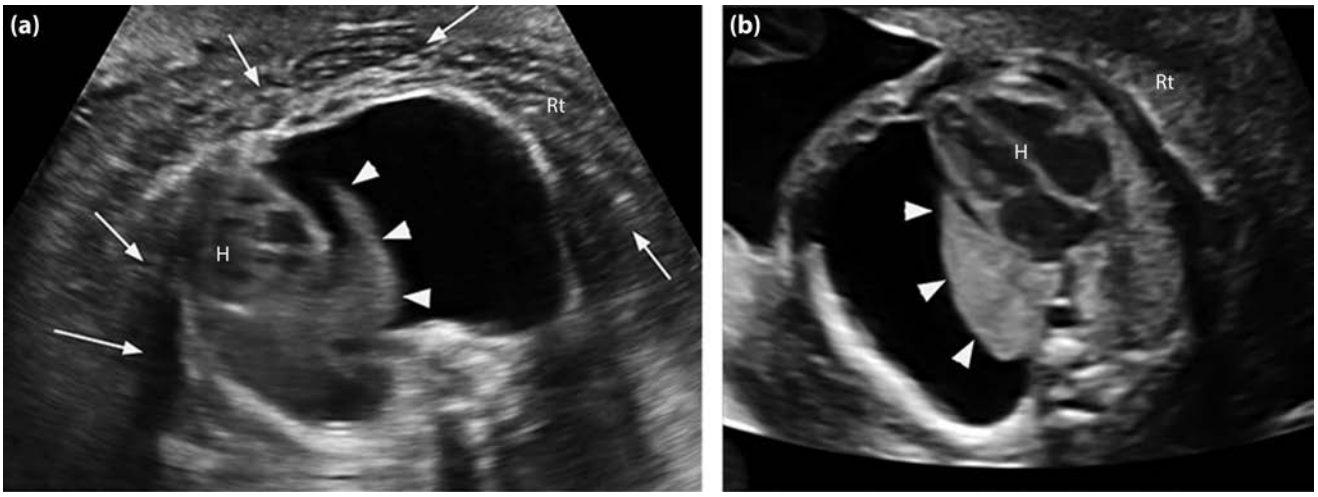


Figure 6.29 Hydrothorax, unilateral, hypertensive. (a) The increased intrathoracic pressure is demonstrated by the fact that both the mediastinum and the lung ipsilateral to the effusion (arrowheads) are pushed into the left hemithorax. This was associated with massive hydrops and severe subcutaneous edema (arrows). (b) As a comparison, note the relatively normal expansion of the lung (arrowheads) in a case of unilateral nonhypertensive hydrothorax. H: heart.

prognostic factor; in fact, in isolated hydrothorax, the placement of a thoracoamniotic shunt has been demonstrated to improve the outcome of hypertensive cases.

Association with other malformations. Congenital heart disease and ipsilateral pulmonary malformations may be associated.

Natural history. Chylothorax can regress in 10%–25% of cases, spontaneously or after a single drainage [41,42].

Risk of chromosomal anomalies. This risk is high. The risk applies also to isolated transient hydrothorax, be it of early or late third-trimester onset, and concerns mainly trisomy 21 and Turner syndrome (monosomy X). Isolated chylothorax has also been shown to bear a not insignificant risk of aneuploidy (1%–6%)

Risk of nonchromosomal syndromes. This risk is high, especially if NIHF is associated. There are several syndromes that may feature hydrothorax. These may be associated with other sonographically detectable anomalies, or, in a few instances, the hydrothorax may represent the only prenatally recognizable sign.

Obstetric management. Should a pleural effusion be diagnosed in a fetus, karyotyping is mandatory, due to the high risk of associated chromosomal anomalies. In addition, a thorough anatomic scan should be performed by an expert, in order to detect major and/or minor signs possibly indicative of a syndromic context. If the hydrothorax is isolated, and karyotyping has ruled out any underlying chromosomal aberration, its evolution should be carefully monitored: The detection of signs possibly indicating elevated intrathoracic pressure, such as flattening of the ipsilateral lung and/or evident mediastinal and heart displacement into the contralateral hemithorax (Figure 6.28), may represent an indication for a single drainage and/or the placement of a thoracoamniotic shunt. In fact, these procedures have been demonstrated to be able to prevent or reverse the occurrence of hydrops if it is due to the hydrothorax. In particular, it has been shown that if the hydrops is a direct consequence of the hypertensive hydrothorax, the placement of a thoracoamniotic shunt increases the overall survival rate from 10% to 60% [41,42].

Postnatal management. This depends on the cause of the hydrothorax. Virtually no treatment is possible for NIHF, if idiopathic. On the contrary, in many cases of congenital chylothorax, resolution of the effusion occurs spontaneously with time, probably because collateral lymphatic channels develop. In cases with respiratory distress, placement of chest tube drainage and mechanical ventilation may be needed. If drainage remains persistent and copious, surgery, consisting of ligation of the thoracic duct, may be necessary.

Prognosis, survival, and quality of life. The overall prognosis is guarded and survival exceptional in cases associated with NIHF. The only case in which hydrothorax may have a good outcome, as already noted, is chylothorax.

INcr EAsEd cArd IoThor AcIc rATIo: cArd IoMEGALy

Incidence. Relatively common.

Ultrasound diagnosis. On the *4-chamber view*: increased heart circumference or area (>95th percentile), with thoracic circumference or area within the normal range.

Risk of chromosomal anomalies. Low.

Risk of nonchromosomal syndromes. Low.

Outcome. Depends on etiology, but generally guarded.

Definition Cardiomegaly consists of an increased cardiac volume (circumference or area).

Etiology and pathogenesis. In general, cardiomegaly is a sign of cardiac overload, which may or may not evolve into frank hydrops from heart failure. The cause of the cardiomegaly can be cardiac or extracardiac. All conditions associated with arteriovenous fistulas such as sacrococcygeal teratoma, aneurysm of the vein of Galen, placental chorioangioma, and TTTS (Figure 6.30), can result in cardiomegaly as a sign of cardiac overload. The same is true for conditions leading to severe fetal anemia, such as parvovirus B19 infection. In such cases, the pathogenesis of the cardiomegaly is insufficient emptying of cardiac chambers due to the venous engorgement (preload increase) associated with elevated intraventricular pressure: this leads to systolic dysfunction and ultimately to cardiac failure. Alternatively, cardiomegaly can result from primary heart diseases. Cardiomyopathies inducing myocardial dysfunction (pump failure) and/or congenital heart diseases associated with severe atrioventricular valve insufficiency may be responsible for the development of cardiomegaly (see Chapter 5). Premature constriction/closure of the ductus arteriosus, both spontaneous and induced by cyclooxygenase inhibitors such as indomethacin and nimesulide [43], is another rare but serious cause of cardiomegaly and heart failure.

Ultrasound diagnosis. This is made on the *four-chamber view*. Except for very severe cases of cardiomegaly, such as those characterizing the worst cases of Ebstein's anomaly (Chapter 5), it is necessary to quantify the degree of cardiac enlargement by measuring the cardiothoracic ratio: this is the ratio between the cardiac circumference (or area) and the thoracic circumference (or area) (Figure 6.31). The cardiothoracic ratio in these cases is increased because the numerator (cardiac circumference or area) is increased [44] (Figure 6.31a). On the contrary, in thoracic and/or pulmonary hypoplasia, the cardiothoracic ratio is similarly elevated, but due to a decrease in the denominator (Figure 6.31b). Therefore, to assess whether it is the heart that is enlarged or the thorax that is hypoplastic, the thoracic circumference or area should be plotted against the nomograms for gestational age (see the Appendix Table A.18).

Prognostic indicators. These are related to the cause of the cardiomegaly and the presence or absence of concurrent hydrops. Clearly, if the cardiomegaly is due to treatable conditions, such as supraventricular tachycardia or parvovirus B19 infection, the prognosis is better, even in hydropic cases; in fact, with transplacental antiarrhythmic therapy and intrauterine blood transfusions, respectively, the hydrops from cardiac failure can disappear completely. If, on the contrary, hydrops is associated with other nontreatable conditions, then the prognosis is generally very poor.

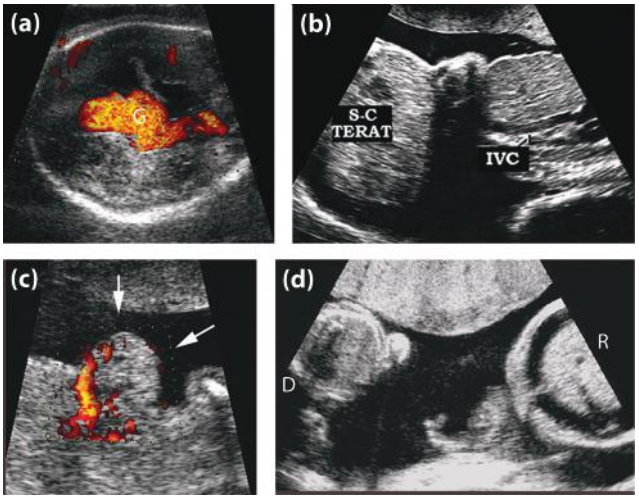


Figure 6.30 Abnormalities causing cardiomegaly due to high-output cardiac failure. (a) Aneurysm of the vein of Galen, demonstrated on power Doppler (G). (b) Sacrococcygeal teratoma: note the enlargement of the inferior vena cava (IVC), which drains the large tumor. (c) Placental chorioangioma (arrows). (d) Twin-to-twin transfusion syndrome. Note the discrepant biometry between the donor (D) and recipient (R) twins. The latter had already developed ascites as a sign of high-output cardiac failure.

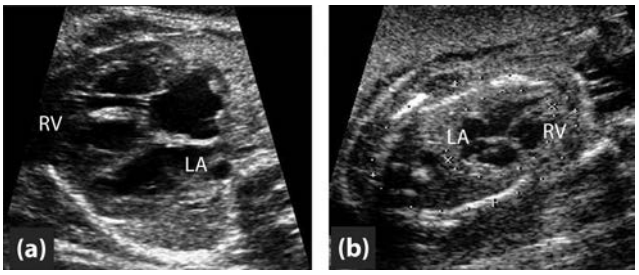


Figure 6.31 Abnormal cardiothoracic ratio. The cardiothoracic ratio can be abnormal due to cardiomegaly or thoracic hypoplasia. (a) In this case, the cardiac enlargement was due to premature constriction of the ductus arteriosus, at 36 weeks of gestation. (b) Lethal skeletal dysplasias and the fetal akinesia deformation sequence (FADS) can be associated with severe thoracic hypoplasia. This case was in the context of FADS.

Association with other malformations. These include congenital heart disease, TTTS, conditions associated with arteriovenous fistulas

Risk of chromosomal anomalies. This risk is low. It depends on the cause of the cardiomegaly.

Risk of nonchromosomal syndromes. This risk is low. It depends on the cause of the cardiomegaly.

Obstetric management. Should cardiomegaly be detected, fetal echocardiography should be carried out to confirm or rule out the existence of congenital heart disease or cardiomyopathy as the primary cause of the cardiomegaly. In addition, a thorough anatomic scan should be performed by an expert, in order to detect possible lesions associated with arteriovenous fistulas If potentially treatable conditions are found, then the intrauterine treatment of choice should be performed. This includes antiarrhythmic therapy for tachyarrhythmias and intrauterine blood transfusions for parvovirus B19 infections. With regard to the former, the first-line drug is digoxin, which can be administered by a transplacental route (oral maternal therapy) or, in highly hydropic fetuses, by direct intravenous fetal therapy (umbilical vein). The intrauterine therapy of conditions associated with arteriovenous fistulas is another important issue. Laser coagulation of arteriovenous anastomoses between the two placental sides of a monochorionic twin pregnancy complicated by TTTS is well-established, and has reduced the risk of cerebral damage in surviving TTTS fetuses [45]. In sacrococcygeal teratomas, there have been some attempts at reducing the hemodynamic impact of the mass by fetal debulking, drainage of the cystic component, and/or direct ethanol treatment of the main feeding vessels of the tumor; the results are controversial [46].

Prognosis, survival, and quality of life. The prognosis depends on the cause of the cardiomegaly. As already mentioned, good survival can be achieved in cases benefiting from intrauterine therapy (antiarrhythmic transplacental or direct therapy for tachyarrhythmias; intrauterine blood transfusions for parvovirus B19 infections; and placental laser treatment of arteriovenous fistulas in TTTS).

INcr EAsEd cArd IoThor AcIc rATIo: Thor AcIc hypop LAsIA

Incidence. Very rare.

Ultrasound diagnosis. On the *4-chamber view*: normal heart circumference or area with thoracic circumference/area below the fifth percentile.

Risk of chromosomal anomalies. Low.

Risk of nonchromosomal syndromes. Very high (mainly, skeletal dysplasia).

Outcome. Invariably fatal for severe cases.

Definition This is a reduced volume of the ribcage (ribs and sternum), due to primary bone diseases (skeletal dysplasias) or secondary to severe bilateral pulmonary hypoplasia. The minor forms of thoracic hypoplasia that are compatible with survival are rarely detected by US in the fetus.

Etiology and pathogenesis. In most instances, severe thoracic hypoplasia is an integral feature of a number of lethal skeletal dysplasias. Secondary thoracic hypoplasia may also be due to severe bilateral pulmonary hypoplasia. The latter occurs very rarely as a primary disease, while it is much more often the consequence of a long-lasting oligohydramnios from very premature rupture of membranes. The pathogenesis of thoracic hypoplasia, when this represents a sign of syndromes and/or skeletal dysplasias, involves underdevelopment of the ribs and the sternum. In those cases in which a neuromuscular disease

is present, as in the FADS, the thoracic hypoplasia is the effect of the fixed contractures of the diaphragm and the intercostal muscles (Chapter 10). In all these conditions, lethal pulmonary hypoplasia is invariably associated with thoracic hypoplasia.

Ultrasound diagnosis. The US diagnosis is made on the *four-chamber view*. Similarly to what is seen in cardiomegaly, the heart will appear to fill the whole thorax, but the sonographer should be able to appreciate that in this case it is the thorax that is smaller while the heart is not affected (Figure 6.31b). As already mentioned, there are nomograms in the literature both for the cardiothoracic ratio [44] and for the thoracic circumference versus gestational age (see Appendix Table A.18). On the low-magnification *midsagittal view of the fetal trunk*, a dip can be seen on the anterior contour of the fetal trunk at the passage between thorax and abdomen; this is due to the exceedingly different circumferences of a hypoplastic thorax and the normal abdomen (Figure 9.7c). The same sign, but due to gross hepatomegaly, can sometimes be seen in severe intrauterine cytomegalovirus infection (Chapter 7).

Prognostic indicators. When severe, thoracic hypoplasia is invariably lethal, since it is associated with severe bilateral pulmonary hypoplasia.

Risk of chromosomal anomalies. This risk is very low.

Risk of nonchromosomal syndromes. This risk is high, especially if the frequently associated skeletal dysplasias are considered as syndromes. The syndromes detectable in utero that can be associated with severe thoracic hypoplasia are as follows:

- *Achondrogenesis*: look for ► *thoracic hypoplasia* + micromelia + micrognathia + hypomineralization (Chapter 9);
- *FADS* (including *Pena–Shokeir syndrome*): look for ► *thoracic hypoplasia* + diffuse joint contractures + micrognathia + clubfeet + ulnar deviations of the hands + extremely reduced fetal movements (Chapter 10);
- *Hypophosphatasia*: look for ► *thoracic hypoplasia* + micromelia + hypomineralization (clavicles excluded) (Chapter 9);
- *Short-rib-polydactyly syndrome(s)*: look for ► *thoracic hypoplasia* + micromelia + polydactyly + congenital heart disease (Chapter 9);
- *Thanatophoric dysplasia*: look for ► *thoracic hypoplasia* + micromelia and cloverleaf skull (Chapter 9);
- *Asphyxiating thoracic dystrophy (Jeune syndrome)*: look for ► *thoracic hypoplasia* + rhizomelia (moderate), polydactyly + renal anomalies (Chapter 9).

  Also, fetuses with achondroplasia and – more rarely – those with trisomy 21 may show from moderate to moderately severe thoracic hypoplasia.

Obstetric management. Should severe thoracic hypoplasia be detected, a thorough anatomic scan should be performed by an expert, in order to assess the other abnormal features that in most instances allow one to reach a final diagnosis of skeletal dysplasia or neuromuscular syndrome. The importance of a correct diagnosis is not in the context of the current pregnancy, given that this is unfortunately destined to end in termination or perinatal demise, but rather with regard to future pregnancies. Some of the lethal conditions featuring thoracic hypoplasia may not occur sporadically but exhibit autosomal recessive inheritance.

Prognosis, survival, and quality of life. The prognosis is very poor in all cases associated with severe thoracic (and pulmonary) hypoplasia (see Chapter 9).

THYMUS HYPOPLASIA/APLASIA

Incidence. Relatively uncommon.

Ultrasound diagnosis. *Three-vessel view*: non-visualization of the thymus in the upper mediastinum, or thymus diameters less than 5th percentile. To be sought only in fetuses with congenital heart disease possibly at risk of microdeletion 22q11 (mainly conotruncal anomalies).

Risk of chromosomal anomalies. Very high (microdeletion 22q11), trisomy 21.

Risk of nonchromosomal syndromes. Low.

Outcome. Depends on the severity of the associated cardiac defect and on the expression of the 22q11 microdeletion, which is variable.

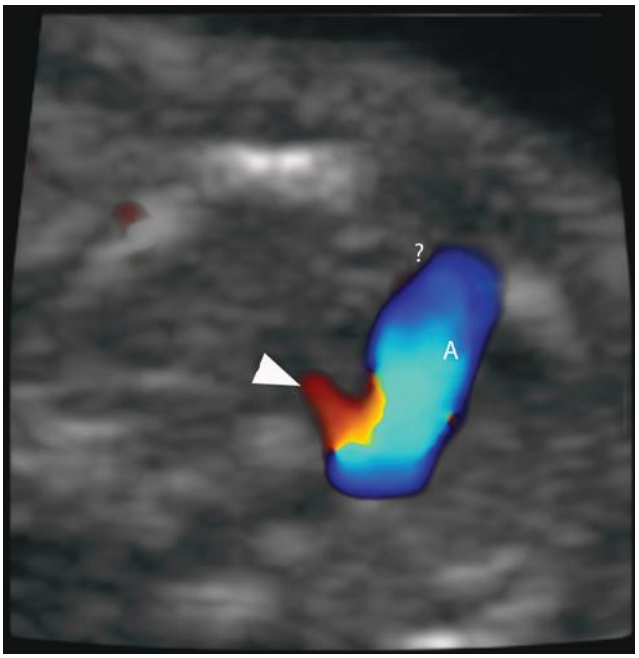


Figure 6.32 Thymus aplasia. This 21-week fetus was diagnosed with pulmonary atresia + ventricular septal defect and thymic hypoplasia, due to microdeletion 22q11. The color Doppler axial three-vessel view demonstrates the reverse blood flow across an extremely hypoplastic and atretic pulmonary artery/ductus arteriosus (arrowhead) and the absence of the thymus: the aortic arch (A) is displaced forwardly just behind the sternum and the thymus cannot be seen in its usual position.

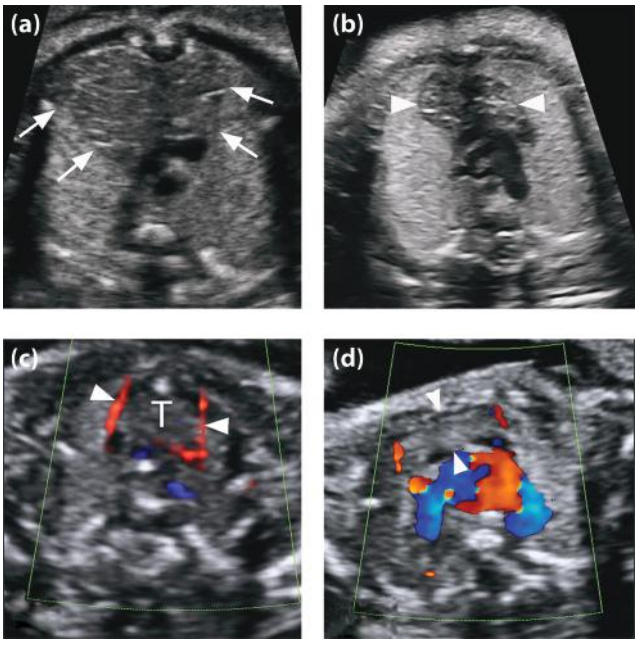


Figure 6.33 Thymus hypoplasia: Three-vessel view. (a) normal thymus at 32 weeks of gestation (arrows); (b) Thymic hypoplasia at 32 weeks of gestation in a fetus with microdeletion 22q11 and tetralogy of Fallot. Note the evident discrepancy in the size of the thymus; (c) normal thymus (T) at 21 weeks of gestation, as highlighted by the internal mammary arteries (thy-box); (d) thymic hypoplasia (arrowheads) in a 21-week fetus with common arterial trunk and microdeletion 22q11. (From Paladini D, *Ultrasound Obstet Gynecol* 37, 488–92, 2011.)

Definition This is complete absence or hypoplasia of the thymus. It is virtually always associated with congenital heart disease at risk of 22q11 microdeletion [47] (Chapter 5), even though recently, thymus hypoplasia has also been described in fetuses with trisomy 21 [48,49].

Etiology and pathogenesis. The thymus defect is due to an abnormal development of the third and fourth branchial arches which, in turn, depends on the absent migration of neural crest cells toward these embryological structures [50–52]. The genetic derangement responsible for this lack of migration is a microdeletion in the so-called *DiGeorge critical region (DGCR)*, which maps to chromosome 22, locus q11 (see Chapter 10).

Ultrasound diagnosis (Figures 6.3, 6.32, and 6.33) [1]. The diagnosis of thymus aplasia/hypoplasia has only been described fairly recently [47], and is made on the upper mediastinal *three-vessel view*, which is an axial view of the mediastinum at the level of the ductal and aortic arches (Figure 6.3b), and/or just cranial to this, in which only the thymus is seen, between the lungs (Figure 6.3a). In the former view, the thymus appears as a well-defined weakly hypoechoic roundish solid structure interposed between the great vessels, in the prevertebral region, and the sternum. Thymic aplasia is diagnosed when the thymus cannot be visualized and the great vessels appear to be displaced just behind the sternum (Figure 6.32). If the thymus is present but its diameters are below the 5th percentile, then thymic hypoplasia is present (Figure 6.33b). The occurrence of thymic hypoplasia may also be derived by calculation of the thymic-thoracic ratio, which provides an accurate estimate of the thymic versus thoracic volumes [49]. The importance of this finding is related to its capacity to accurately predict the risk of 22q11 microdeletion in fetuses previously diagnosed with conotruncal anomalies [47]. Therefore, it should be emphasized that checking for the presence of the thymus is not a standard US procedure; it should be performed only in fetuses with conotruncal anomalies and/or, regardless of the occurrence of CHD, if one of the parents has the microdeletion, since in this case the transmission risk is 50% (autosomal dominant).

Recently, variable degrees of thymic hypoplasia also have been found in fetuses with trisomy 21 [48,49].

Prognostic indicators. The occurrence of thymus hypoplasia/aplasia is electively sought in fetuses at risk of

22q11 microdeletion. Hence, if the thymus is indeed absent or hypoplastic, the presence of the microdeletion is very likely (>90% probability), and this, of course, represents per se a poor prognostic sign. An additional poor prognostic sign in this context may be a conotruncal anomaly with an unfavorable anatomy, such as tetralogy of Fallot with absent pulmonary valve or common arterial trunk with aortic arch interruption (Chapter 5).

Association with other malformations. In the context of 22q11 microdeletion, thymic anomalies are associated with cardiac defects, renal anomalies, fetal growth restriction (FGR), and polyhydramnios (Chapter 10).

Risk of chromosomal anomalies. This is very high in view of the virtually ubiquitous presence of the 22q11 microdeletion. To a much lesser extent, it is associated with trisomy 21.

Risk of nonchromosomal syndromes. This risk is low.

Obstetric management. Should thymus hypoplasia/aplasia be detected in a fetus at risk for 22q11 microdeletion, a thorough anatomic scan should be performed by an expert, in order to assess the other abnormal features (renal anomalies, FGR, and polyhydramnios) that increase the likelihood of the microdeletion even more. As pointed out above, the associated cardiac defect should have already been diagnosed and characterized by fetal echocardiography. Fetal karyotyping with fluorescence in situ hybridization (FISH) analysis for the DGCR is mandatory, because only about 5%–10% of the microdeletions are long enough to show up on conventional G-banding. Should the FISH analysis reveal the presence of the microdeletion, parental assessment for the DGCR should be carried out to confirm or rule out the presence of the microdeletion [50–52]. As for trisomy 21, thymic hypoplasia cannot be considered a significant marker, despite its association with Down syndrome [48,49].

Prognosis, survival, and quality of life. The final prognosis and quality of life depend on the phenotypic expression of the microdeletion, which is extremely variable, as well as on the severity of the associated cardiac defect (see Chapter 10).

MEdIAsTINAL TUMors/ cys Ts

Incidence. Relatively rare.

Ultrasound diagnosis. *Four-chamber view/three-vessel view.* Cystic or solid mass, and if large, possibly associated with mediastinal shift.

Risk of chromosomal anomalies. Low.

Risk of nonchromosomal syndromes. Low.

Outcome. Depends on the final diagnosis and the size of the mass, but generally good, with the possible exception of thoracic lymphangioma. Large tumors may create high airway obstruction, with possible need for EXIT procedure.

Definition In this section, we thought to include cystic or solid mediastinal lesions not belonging to the heart, the gastrointestinal tract, or the tracheobronchial tree. Hence, most of these lesions are represented by simple cysts (pericardial or neurenteric), or by benign tumors, such as lymphangiomas or teratomas [53,54].

Etiology and pathogenesis. These are either developmental anomalies (e.g., neurenteric cyst) or benign mesenchymal tumors (e.g., lymphangioma or teratoma).

Ultrasound diagnosis (Figures 6.34 and 6.35). The diagnosis of mediastinal tumors is made on the two major axial planes of the thorax, the *four-chamber view,* and/or the *three-vessel view.* The site of the tumor dictates the diagnostic view, though it should be considered that in most cases these tumors are large enough to be visible on all thoracic views. Thoracic **lymphangioma** (Figure 6.34) need to be differentiated from the macrocystic type of CAML; however, the former is often large enough to present with bilateral cystic areas, which is very unusual for CAML, which is bilateral only in 3% of cases. Solid tumors, such as teratomas (Figure 6.35), may be associated with a pericardial effusion (Figure 6.35b).

Prognostic indicators. As for all thoracic and neck masses, the poorest prognostic factors are represented by central venous compression leading to hydrops or

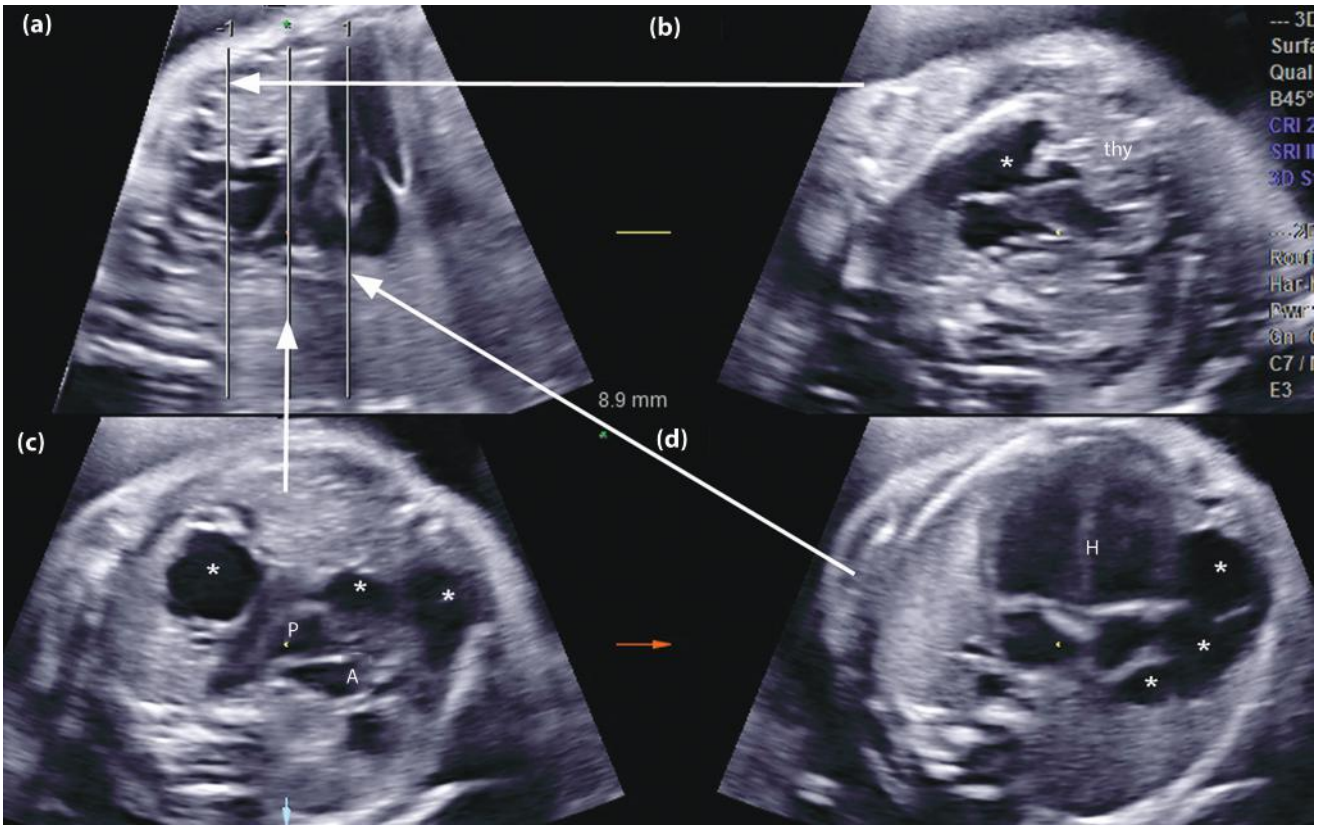


Figure 6.34 Thoracic lymphangioma (29 weeks of gestation). Three-dimensional tomographic ultrasound imaging (TUI) mode: (a) shows the sagittal view with the lines indicating the three planes shown in (b)–(d). On these, the cystic areas of the large lymphangioma are marked by asterisks. A: ascending aorta; H: heart; P: pulmonary artery; thy: thymus.

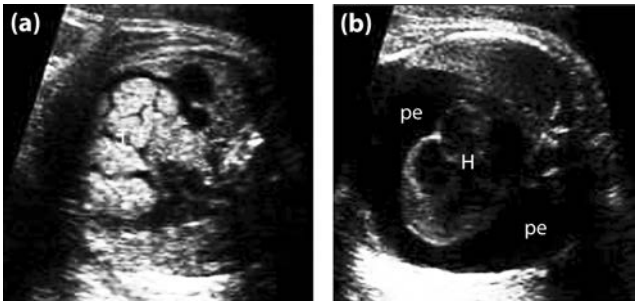


Figure 6.35 Mediastinal teratoma (32 weeks of gestation). (a) On a cranial view of the thorax, the mediastinum appears completely occupied by a large lobular hyperechoic tumor (T), revealed after birth to be a teratoma. The sonolucent area in the upper part of the screen is part of a huge pericardial effusion, visible in (b). (b) On the four-chamber view level, the huge associated pericardial effusion (pe) is visible, with the normal heart (H) in the middle.

high airway compression, which would require an EXIT procedure at birth (see CHAOS).

Association with other malformations. Lymphangiomas, as well as hemangiomas, may have multiple locations, often subcutaneous.

Risk of chromosomal anomalies. This risk is low.

Risk of nonchromosomal syndromes. This risk is low.

Obstetric management. In nonobstructive lesions, the final diagnosis will be made after birth. MRI may help in challenging cases to differentiate thoracic lymphangiomas from CAML, macrocystic type. In case of cystic lesions leading to hydrops from increased central venous pressure, placement of a thoracoamniotic shunt may represent an option for consideration. The most important task is to define prenatally whether there is a need for an EXIT procedure due to high airway obstruction [37] and, if so, proceed to in utero transfer to a referral center where this complicated and costly procedure is available.

Prognosis, survival, and quality of life. The final prognosis and quality of life depend on the final diagnosis, and on the absence/presence of hydrops from cardiac failure or high airway obstruction by the time of birth. Some mesenchymal lesions may also regress spontaneously, at least in part, after birth.

rEFE r ENc Es

1. Paladini D. How to identify the thymus in the fetus: the thy-box. *Ultrasound Obstet Gynecol* 2011; 37: 488–92.
2. Achiron R, Gindes, L, Zalel Y, et al. Three- and four-dimensional ultrasound: new method for evaluating fetal thoracic anomalies. *Ultrasound Obstet Gynecol* 2008; 32: 36–43.
3. Gindes L, Benoit B, Pretorius DH, et al. Abnormal number of ribs on three-dimensional ultrasound: associated anomalies and outcome in 75 fetuses. *JUM* 2008; 27: 1263–71.
4. Downward CD, Wilson JM. Current therapy of infants with congenital diaphragmatic hernia. *Semin Neonatol* 2003; 8: 215–21.
5. Grandjean H, Larroque D, Levi S. The performance of routine ultrasonography screening of pregnancies in the Eurofetus study. *Am J Obstet Gynecol* 1999; 181: 446–54.
6. Fuke S, Kanzaki T, Mu J, et al. Antenatal prediction of pulmonary hypoplasia by acceleration time/ejection time ratio of fetal pulmonary arteries by Doppler blood flow velocimetry. *Am J Obstet Gynecol* 2003; 188: 228–33.
7. Metkus AP, Filly RA, Stringer MD, et al. Sonographic prediction of survival in fetal diaphragmatic hernia. *J Pediatr Surg* 1996; 31: 148–51.
8. Lipshultz GS, Albanese CT, Feldstein VA, et al. Prospective analysis of lung-to-head ratio predicts survival for patients with prenatally diagnosed congenital diaphragmatic hernia. *J Pediatr Surg* 1997; 32: 1634–6.
9. Sbragia L, Paek BW, Filly RA, et al. Congenital diaphragmatic hernia without herniation of the liver: does the lung-to-head ratio predict survival? *J Ultrasound Med* 2000; 19: 845–8.
10. Heling KS, Wauer RR, Hammer H, et al. Reliability of the lung-to-head ratio in predicting outcome and neonatal ventilation parameters in fetuses with congenital diaphragmatic hernia. *Ultrasound Obstet Gynecol* 2005; 25: 112–8.
11. Jani J, Nicolaides KH, Keller RL, et al. Observed to expected lung area to head circumference ratio in the prediction of survival in foetuses with isolated diaphragmatic hernia. *Ultrasound Obstet Gynecol* 2007; 30: 67–71.
12. Peralta CFA, Cavoretto P, Csapo B, et al. Assessment of lung area in normal foetuses at 12–32 weeks. *Ultrasound Obstet Gynecol* 2005; 26: 718–24.
13. Jani JC, Peralta CFA, Nicolaides KH. Lung-to-head ratio: a need to unify the technique. *Ultrasound Obstet Gynecol* 2012; 39: 2–6.
14. Jani J, Cannie M, Sonigo P, et al. Value of prenatal magnetic resonance imaging in the prediction of postnatal outcome in fetuses with diaphragmatic hernia. *Ultrasound Obstet Gynecol* 2008; 32: 793–9.
15. Spaggiari E, Stirnemann J, Ville Y. Outcome in fetuses with isolated congenital diaphragmatic hernia with increased nuchal translucency thickness in first trimester. *Prenat Diagn* 2012; 32: 268–71.
16. Pober BR. Genetic aspects of human congenital diaphragmatic hernia. *Clin Genet* 2008; 74: 1–15.
17. Lyons Jones K. *Smith's Recognizable Patterns of Human Malformation*. 6th edn. Philadelphia, PA: WB Saunders; 2006.
18. Paladini D, Borghese A, Arienzo M, et al. Prospective ultrasound diagnosis of Pallister–Killian syndrome in the second trimester of pregnancy: the importance of the fetal facial profile *Prenat Diagn* 2000; 20: 996–8.
19. Stevens TP, Chess PR, McConnochie KM, et al. Survival in early and late-term infants with congenital diaphragmatic hernia treated with extracorporeal membrane oxygenation. *Pediatrics* 2002; 110: 590–6.
20. Harrison MR, Sydorak RM, Farrell JA, et al. Fetoscopic temporary tracheal occlusion for congenital diaphragmatic hernia: prelude to a randomized controlled trial. *J Pediatr Surg* 2003; 30: 1012–20.
21. Deprest J, Nicolaides KH, Done' E, et al. Technical aspects of fetal endoscopic tracheal occlusion for congenital diaphragmatic hernia. *J Pediatr Surg* 2011; 46: 22–32.
22. Hunt RW, Kean MJ, Stewart MJ, et al. Patterns of cerebral injury in a series of infants with congenital diaphragmatic hernia utilizing magnetic resonance imaging. *J Pediatr Surg* 2004; 39: 31–6.
23. Jaillard SM, Pierrat V, Dubois A, et al. Outcome at 2 years of infants with congenital diaphragmatic hernia: a population-based study. *Ann Thorac Surg* 2003; 75: 250–6.
24. Stocker JT, Madewell JE, Drake RM. Congenital cystic adenomatoid malformation of the lung. Classification and morphologic spectrum. *Hum Pathol* 1977; 8: 155–71.
25. Wilson RD, Hedrick HL, Liechty KW, et al. Cystic adenomatoid malformation of the lung: review of genetics, prenatal diagnosis, and in utero treatment. *Am J Med Genet* 2006; 140A: 151–5.
26. Monni G, Paladini D, Ibba RM, et al. Prenatal ultrasound diagnosis of congenital cystic malformation of the lung: a report of 26 cases and review of the literature. *Ultrasound Obstet Gynecol* 2000; 16: 159–62.
27. Crombleholme TM, Coleman B, Hedrick H, et al. Cystic adenomatoid malformation volume ratio predicts outcome in prenatally diagnosed cystic adenomatoid malformation of the lung. *J Pediatr Surg* 2002; 37: 331–8.
28. Adzick NS, Harrison MR, Crombleholme TM, et al. Fetal lung lesions: management and outcome. *Am J Obstet Gynecol* 1998; 179: 884–9.
29. Schrey S, Kelly N, Langer JC, et al. Fetal thoraco-amniotic shunting for large macrocystic congenital cystic adenomatoid malformations of the lung. *Ultrasound Obstet Gynecol* 2012; 39: 515–20.
30. Lopoo JB, Goldstein RB, Lipshultz GS, et al. Fetal pulmonary sequestration: a favourable congenital lung lesion. *Obstet Gynecol* 1999; 94: 567–71.
31. Pumbergera W, Hörmann M, Deutingerc J, et al. Longitudinal observation of antenatally detected congenital lung malformations (CLM): natural history, clinical outcome and long-term follow-up. *Eur J Cardiothorac Surg* 2003; 24: 703–11.
32. de Lagausie P, Bonnard A, Berrebi D, et al. Video-assisted thoracoscopic surgery for pulmonary sequestration in children. *Ann Thorac Surg* 2005; 80: 1266–9.
33. Lee BS, Kim JT, Kim EA, et al. Neonatal pulmonary sequestration: clinical experience with transumbilical arterial embolization. *Ped Pulmon* 2008; 43: 404–13.
34. Avni EF, Vanderelst A, Van Gansbeke D, et al. Antenatal diagnosis of pulmonary tumors: report of two cases. *Pediatr Radiol* 1986; 16: 190–2.
35. Martínez JM, Prat J, Gómez O, et al. Decompression through tracheobronchial endoscopy of bronchial atresia presenting as massive pulmonary tumor: a new indication for fetoscopic surgery. *Fetal Diagn Ther* 2013; 33: 69–74.
36. Maruotti GM, Paladini D, Agangi A, et al. Prospective prenatal ultrasound diagnosis of Fraser syndrome variant in a family with negative history. *Prenat Diagn* 2004; 24: 69–70.
37. Saadai P, Jelin EB, Nijagal EB, et al. Long-term outcome after fetal therapy for congenital high airway obstructive syndrome. *J Ped Surg* 2012; 47: 1095–100.
38. Levine D, Jennings R, Barnewolt C, et al. Progressive fetal bronchial obstruction caused by a bronchogenic cyst diagnosed using prenatal MR imaging. *AJR* 2001; 176: 49–52.

39. Schneider P, Schwalbe E. Die morphologic der missbildungen des menschen und der thiere. *Jena: Fischer* 1912; 3: 812–22.
40. Vida VL, Padalino MA, Boccuzzo G, et al. Scimitar syndrome: a European Congenital Heart Surgeons Association (ECHSA) multicentre study. *Circulation* 2010; 122: 1159–66.
41. Longaker MT, Laberge JM, Dansereau J, et al. Primary fetal hydrothorax: natural history and management. *Pediatr Surg* 1989; 24: 573–6.
42. Aubard Y, Derouineau I, Aubard V, et al. Primary fetal hydrothorax: a literature review and proposed antenatal clinical strategy. *Fetal Diagn Ther* 1998; 3: 325–33.
43. Paladini D, Marasini M, Volpe P. Severe ductal constriction in the third-trimester fetus following maternal self-medication with nimesulide. *Ultrasound Obstet Gynecol* 2005; 25: 357–61.
44. Paladini D, Chita SD, Allan LD. Prenatal measurement of cardiothoracic ratio in the evaluation of heart disease. *Arch Dis Child* 1990; 65: 20–3.
45. Senat MV, Deprest J, Boulvain M, et al. Endoscopic laser surgery versus serial amnioreduction for severe twin-to-twin transfusion syndrome. *N Engl J Med* 2004; 351: 136–44.
46. Hedrick HL, Flake AW, Crombleholme TM, et al. Sacrococcygeal teratoma: prenatal assessment, fetal intervention, and outcome. *J Pediatr Surg* 2004; 39: 430–8.
47. Chaoui R, Kalache KD, Heling KS, et al. Absent or hypoplastic thymus on ultrasound: a marker for deletion 22q11.2 in fetal cardiac defects. *Ultrasound Obstet Gynecol* 2002; 20: 546–52.
48. De Leon-Luis J, Santolaya J, Gamez F, et al. Sonographic thymic measurements in Down syndrome fetuses. *Prenatal Diagn* 2011; 31: 841–5.
49. Karl K, Heling KS, Sarut Lopez A, et al. The thymic-thoracic ratio in foetuses with trisomy 21, 18 and 13. *Ultrasound Obstet Gynecol* 2012; 40: 412–7.
50. Paladini D, Pacileo G, Palmieri S, et al. Prenatal diagnosis of 22q11 microdeletion in a fetus with a conotruncal heart defect. *Ultrasound Obstet Gynecol* 1998; 11: 68–70.
51. Volpe P, Marasini M, Caruso G, et al. 22q11 deletions in foetuses with malformations of the outflow tracts or interruption of the aortic arch: impact of additional ultrasound signs. *Prenat Diagn* 2003; 23: 752–7.
52. Volpe P, Marasini M, Caruso G, et al. Prenatal ultrasound diagnosis of interruption of the aortic arch and its association with deletion of chromosome 22q11. *Ultrasound Obstet Gynecol* 2002; 20: 327–31.
53. Bernasconi A, Yoo SJ, Golding F, et al. Etiology and outcome of prenatally detected paracardial cystic lesions: a case series and review of the literature. *Ultrasound Obstet Gynecol* 2007; 29: 388–94.
54. Merchant AM, Hedrick HL, Johnson MP, et al. Management of fetal mediastinal teratoma. *J Pediatr Surg* 2005; 40: 228–31.

Chapter 7
Anomalies of the gastrointestinal tract and of the abdominal wall

Normal anatomy of the gastrointestinal tract and abdominal wall: ultrasound approach, scanning planes, and diagnostic potential

The main differential feature of the gastrointestinal (GI) tract in comparison with other organ systems is that its ultrasound (US) appearance varies significantly during pregnancy and also, for some sites, in the course of the same US examination, due to the physiology of swallowing, stomach emptying, and intestinal peristalsis. It is therefore necessary to become acquainted with the whole range of anatomic correlates.

It should be underlined that the detection of an intra-abdominal abnormality can become particularly challenging due to the variety of systems and organs that could be involved, including the GI tract, genitourinary system, adrenal glands, spleen, liver, pancreas, and lungs. Many of these abnormalities do not give a direct sonographic sign, but they may be suspected on the basis of the observation of indirect abnormal findings. Topography of the observed abnormality, fetal sex, and gestational age are significantly useful to determine their possible origin [1].

Another feature of the GI tract pathologies that renders their antenatal diagnosis a difficult task is the frequent absence of any sonographic evidence before the third trimester. Furthermore, some abnormalities may not give any sonographic sign during the whole pregnancy, such as an esophageal atresia (EA) with tracheal fistula; in this case, there is usually an almost normally fluid-filled stomach.

Timing of examination. As mentioned in this chapter, the US appearance of the various GI tract changes significantly with advancing gestational age. In the third trimester, the density of the intestinal content at the level of the colon increases and becomes hypoechoic in comparison with the intestinal walls. This allows identification of the whole course of the colon, from the cecum to the rectum (Figure 7.1). It is also important to consider that the sonographic echogenicity of the intestinal walls changes significantly with the emission frequency of the transducer: higher frequencies (6–7 MHz) make the interfaces between the solid intestinal walls and the fluid content much brighter, with a consequent overall increase in intestinal echogenicity.

US approach and scanning planes (views). A complete US assessment of the GI tract requires a series of views targeted at the various segments that have to be visualized, from the mouth to the rectum. Some of these views have already been described in Chapters 3 and 6. To these views, those necessary to explore the intra-abdominal intestinal tract, the liver, and the spleen should be added.

Cranial views (mouth, pharynx, and esophagus). These views have been described in Chapter 3, and the reader may refer to that chapter for full descriptions. These views are summarized below.

- *Lips*: oblique view (Figure 7.2a);
- *Tongue and pharynx*: axial view (Figure 7.2b);
- *Neck (pharynx and esophagus)*: sagittal view (Figure 7.3a);
- *Thorax (esophagus)*: parasagittal view (Figure 7.3b);
- *Thorax (esophagus)*: axial view (four-chamber view) (Figure 7.3c).



Figure 7.1 Axial view of the abdomen in a 35-week-old fetus. Note the dilation of the colon with the haustra. This finding may be indicative of an obstruction or may be completely normal, as it happened to be in this case.

Abdominal views (the stomach, ileum, jejunum, colon, liver, spleen, and abdominal wall). The scanning views are as follows:

- *Axial view of the upper abdomen*: stomach, spleen, intrahepatic tract of umbilical vein (UV), right hepatic lobe, and gallbladder (Figures 7.4a,b and 7.5a);
- *Axial view of the lower abdomen*: small bowel (Figure 7.4b);
- *Midsagittal view of the abdomen*: cord insertion and rectal pouch in the pelvis (Figure 7.6a and b);
- *Left parasagittal view*: spleen (Figure 7.5b);
- *Right parasagittal view*: right hepatic lobe (Figure 7.6c);
- *Coronal view (volume contrast imaging, or VCI-C)*: general approach (Figure 7.7).

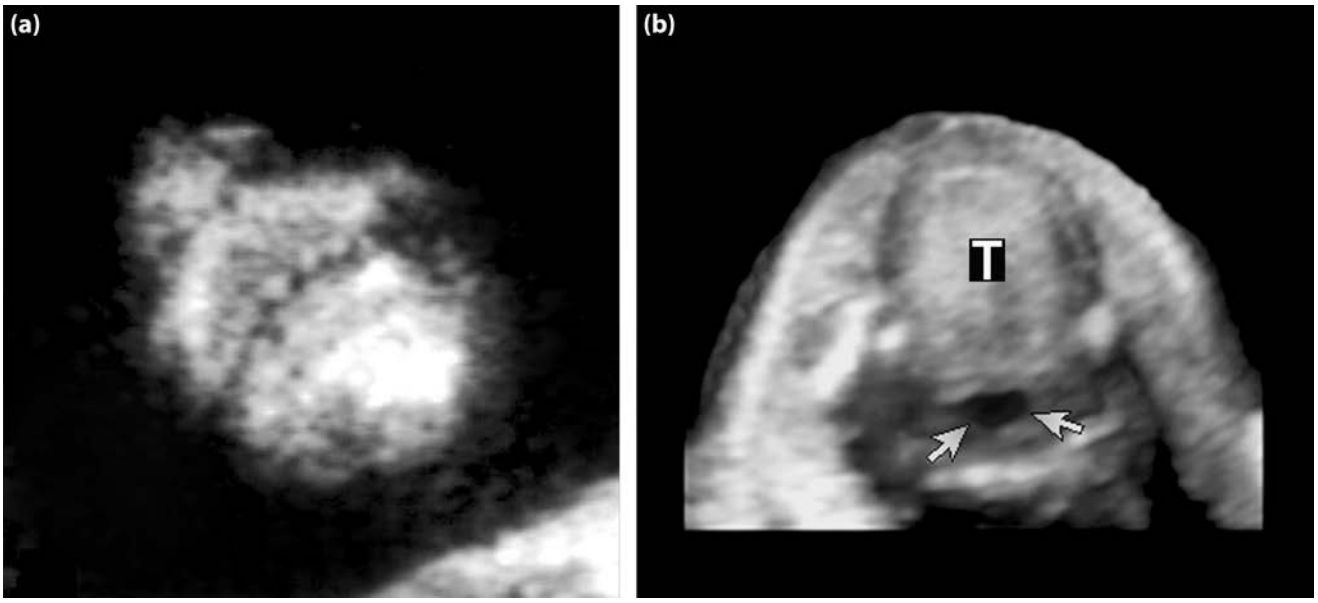


Figure 7.2 Cranial views for the assessment of the upper gastrointestinal tract (mouth and pharynx). (a) Oblique view of the lips. (b) Axial view of the mouth with the tongue (T) and, behind, the oropharynx (arrows).

GAsTro INTEsTINAL Tr AcT ANd ABdo MINAL WALL ANo MALIEs By sc ANNING VIEW

Cranial views and related malformations. We describe again the cranial views in order to underline the normal US appearance of the esophagus. The esophagus presents three portions: cervical, thoracic, and abdominal. The cervical portion may be difficult to visualize, while the thoracic portion, which is the less difficul one to recognize, can be seen behind the trachea, immediately anterior to the descending aorta; whereas the two upper portions of the esophagus run in front of the spine, the abdominal portion is deviated to the left. In fact, the esophagus may be visualized in a near-midsagittal plane with the abdominal portion deviated to the left. Some authors have described the sonographic aspect of this organ, when empty, as a

tubular structure composed of four parallel echogenic lines corresponding to the apposition of the anterior and posterior walls of the esophagus [2] (Figure 7.3a). After fetal swallowing, the esophagus fills with amniotic fluid and it can appear as an anechoic structure (Figure 7.3b). The thoracic tract may resemble a vessel. Power or color Doppler may be used to exclude its vascular origin. Also on the four-chamber view, the cross-sectional appearance of the esophagus distended by some amniotic fluid may be mistaken for that of an abnormal vessel, as in abnormal pulmonary or systemic (azygos continuation) venous return. This artifact is shown in Figure 7.3c.

Axial view of the abdomen and related malformations (Figure 7.4). This represents the classic view for measurement of the abdominal circumference (Figure 7.4a). On this view, the following structures can be recognized: on the left, the gastric bubble, appearing as a well-defined anechoic, round, or oval area (although, in some circumstances, particulate matter can be seen floating in it); on the right, most of the liver, which shows a weakly hyperechogenic echostructure, and the intrahepatic tract of the UV, anechoic with evident walls. On the right of the UV, the gallbladder can also be seen in the right upper quadrant next to the liver. The gallbladder has a variable shape and volume, as in postnatal life, and it usually has an anechoic content (Figure 7.4a).

With minor tilting of the transducer, sometimes it is possible to visualize the spleen behind the stomach (Figure 7.5a). However, it should be kept in mind that the spleen is difficult to visualize since it lies below the shadows of the lower ribs and has an echodensity that is rather similar to that of the liver and the lung.

Nomograms of the normal gastric biometry versus gestational age are available in the literature [3] (see Appendix Table A.20). The GI anomalies that can be recognized on this view are as follows:

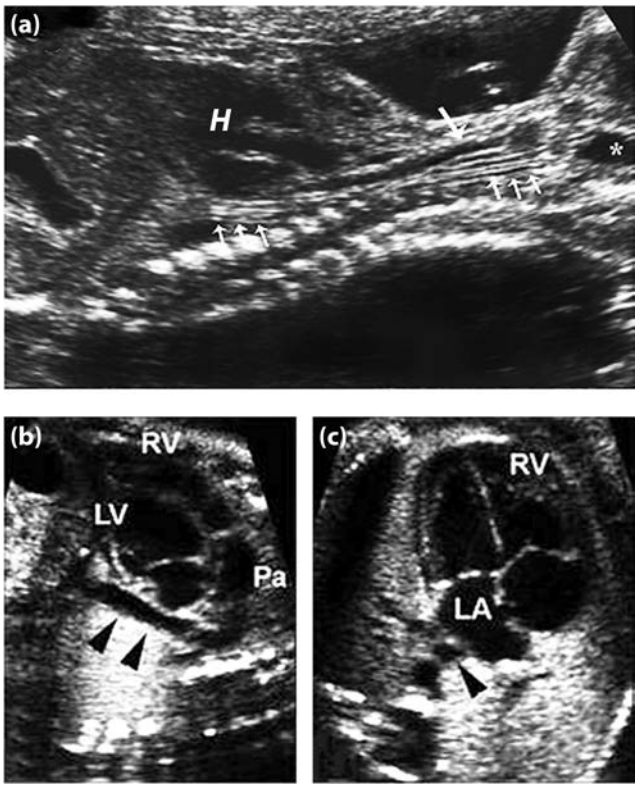


Figure 7.3 Ultrasound views of esophagus. (a) Sagittal view of the fetal neck, thorax, and upper abdomen, showing the course of an empty esophagus (small arrows), behind the trachea (big arrow). H: heart; *: pharynx. (b) The parasagittal view of the thorax demonstrates a distended esophagus behind the left atrium (arrowheads). LV: left ventricle; RV: right ventricle; Pa: pulmonary artery. (c) Axial view of the thorax: behind the left atrium (LA), a distended esophagus (arrowhead) can be seen; in this case, it is necessary to differentiate the temporary dilation of the esophagus from an abnormal venous return (systemic or pulmonary). If the anechoic area is due to esophageal dilation, it disappears after a few minutes; in addition, the use of color or power Doppler may easily confirm or rule out a cardiovascular anomaly.

Esophageal atresia. Nonvisualization of the gastric bubble.

Duodenal atresia or stenosis. Double bubble.

Choledochal cyst. An anechoic cystic structure just below the liver.

Hepatomegaly. Increased liver volume.

Splenomegaly. Increased splenic volume.

Nonvisualization of the gastric bubble (Figure 7.8). Following the spirit of this book—from US sign to diagnosis—we believe it is useful to define a diagnostic algorithm to apply in case of small or absent gastric bubble. The importance of this algorithm lies in the fact that absent or small gastric bubble has been identified not only in case of esophageal atresia but also in a heterogeneous group of other conditions. First, it has to be excluded that the stomach is not visible because it has just emptied in the duodenum following its physiologic emptying cycle. To confirm or exclude this frequent cause of nonvisualization of the gastric bubble, it is sufficient to rescan the woman after 60–80 min; in fact, the physiologic filling–emptying cycle of the stomach lasts about 50–60 min [1]. In cases of severe oligohydramnios from premature rupture of membranes and, to a

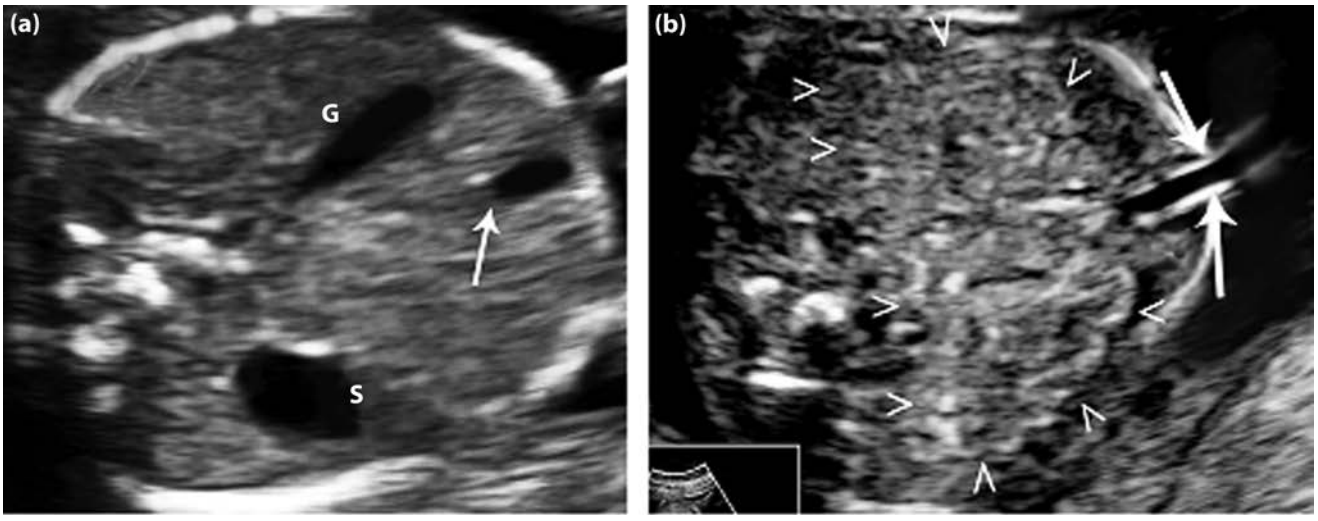


Figure 7.4 Axial abdominal views (stomach, bowel, liver, and gallbladder). (a) Axial view of the upper abdomen: the stomach (S) is visible on the left, the right hepatic lobe and gallbladder (G) on the right, and the intrahepatic tract of the umbilical vein (arrow) on the midline. (b) Axial view of the lower abdomen (ventral approach): the bowel (ileum and jejunum) (arrowheads) and the cord insertion (arrows) are visible.

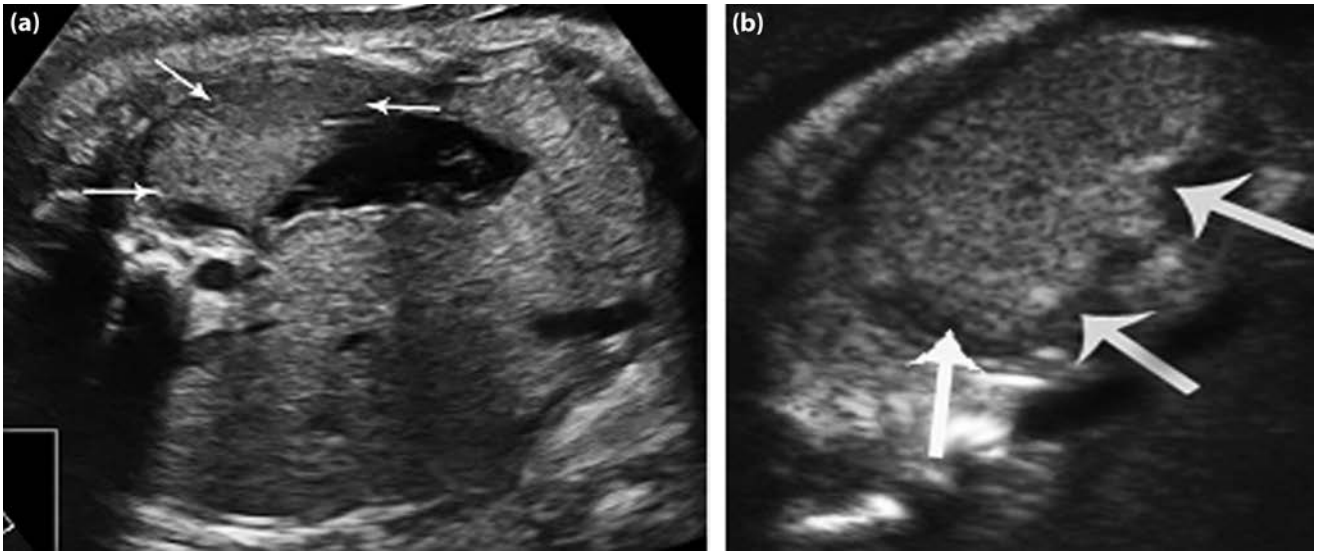


Figure 7.5 (a) Axial view of the upper abdomen. The spleen (arrows) can be clearly seen behind the stomach. (b) Left parasagittal view of the abdomen showing the spleen (arrows).

lesser extent, from severe fetal growth restriction (FGR), the stomach could be empty or its size could be small, since the amount of residual amniotic fluid may not be enough to ensure a sufficient filling to be recognizable on US. Other very severe conditions that may result in absent or small stomach bubble are the fetal akinesia deformation sequence (FADS) and the other neuro-arthrogryposes (Chapter 10): here, the swallowing reflex is blocked due to contracture of the masseters and the pharyngeal muscles. This leads to polyhydramnios on the one hand and to nonvisualization of the stomach on the other. In addition, it seems that the increased incidence of nonvisualization of the gastric bubble reported in cases of complex facial clefts is due to the fact that the palatal anomaly renders deglutition ineffective. The stomach may also be impossible to visualize in its usual position due to migration, as in left-sided congenital diaphragmatic hernia (CDH). Finally, there is an extremely rare congenital anomaly, microgastria, which represents an arrest in the development of the stomach. A diagnostic flow chart to be applied in the case of nonvisualization or small size of the stomach is shown in Figure 7.8.

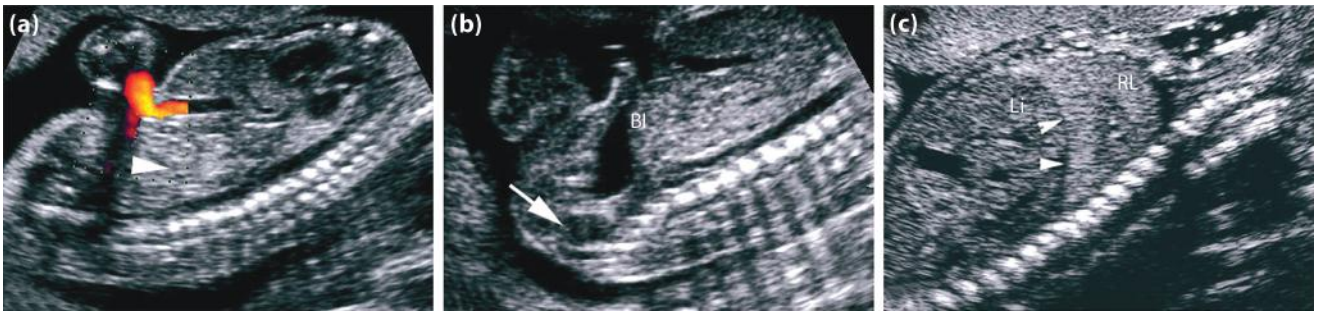


Figure 7.6 Abdominal views (liver, abdominal wall, and rectum). (a) Midsagittal view of the abdomen: the cord insertion, highlighted by power Doppler, and part of the small bowel (arrowhead) are visible. (b) With small movements of the transducer, it is possible to visualize, in the pelvis, the bladder (BI) and, behind it, the rectal pouch (arrow). (c) Right parasagittal view of the abdomen: the right hepatic lobe (Li), just below the hypoechoic layer of the diaphragm (arrowheads), and some ileal loops are visible. RL: right.



Figure 7.7 Coronal view of thorax and abdomen: volume contrast imaging (VCI-C): 3D ultrasound allows reconstruction of the coronal view of the fetal body, which is rather difficult to obtain with 2D ultrasound. On this view, the spatial relationships among the thoracic and the abdominal viscera can be studied in detail. The diaphragm appears as a hypoechoic layer (arrowhead). In the thorax, the lungs (LL: left lung; RL: right lung) and the heart (H), in the left hemithorax, are clearly displayed. Below the diaphragm, the liver is visible, with its left lobe (LL: left lobe) above the gastric bubble (St) and the right lobe (RL); the arrow indicates the gallbladder.

Axial view of the lower abdomen and related malformations (Figure 7.4b). On this view, which is parallel and caudal to the axial view discussed in this chapter, the small bowel, the transverse colon, and, in some cases, the cord insertion can be recognized. The ileal loops appear weakly hyperechoic in comparison with the relatively hypoechoic colon. The major anomalies that may be detected on this view are as follows:

Omphalocele. Defect of the anterior abdominal wall, presenting as a sac containing bowel and/or liver, which bulges out from the cord insertion area.

Gastroschisis. Ileal loops floating freely in the amniotic fluid.

Small-bowel atresia. Severe dilation of ileal loops proximal to the atretic tract.

Meconium ileus. Diffuse hyperechogenicities and calcifications within the intestinal lumen, sometimes associated with small-bowel obstruction.

Midsagittal view of the abdomen and related malformations (Figure 7.6a and b). This view allows one to assess the outline of the abdominal wall and the cord insertion site. In addition, in the pelvis, it is possible to identify the rectal pouch behind the bladder: it appears as a hypoechoic structure that becomes particularly

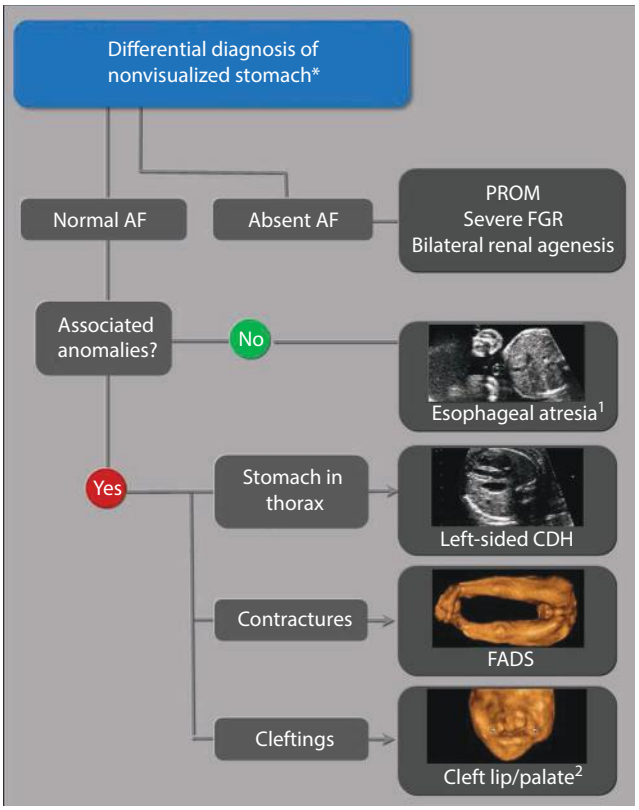


Figure 7.8 Nonvisualization of fetal stomach. AF: amniotic fluid; CDH: congenital diaphragmatic hernia; FADS: fetal akinesia deformation sequence; FGR: fetal growth restriction; PROM: premature rupture of membranes; *after exclusion of normal transient depletion; [1]only complete atresias with no tracheoesophageal fistula; [2]complex cleftings are sometimes associated with impaired swallowing.

evident in the third trimester, when it is full with meconium. In this view, abdominal wall defects—namely, the omphalocele, gastroschisis, and, in some cases, bladder and cloacal exstrophy—can be detected.

Left parasagittal view and related malformations. This view is parallel and to the left of the midsagittal one. On this view, the stomach and the spleen (Figure 7.5b) can be seen, although the spleen is very difficult to visualize for the reasons already described. With color or power Doppler, using an axial approach, it is possible to locate the vascular hilum of the spleen. Nomograms reporting the two maximum splenic diameters versus gestational age have been published and are reported in the Appendix Table A.22. However, it should be noted that, when conspicuous, such as in the case of severe cytomegalovirus (CMV) infection, splenomegaly cannot be missed.

Right parasagittal view and related malformations (Figure 7.6c). If the transducer is moved contralaterally, toward the right part of the abdomen, the right lobe of the liver comes into view, appearing as a solid, weakly hyperechoic structure located between the hypoechoic diaphragmatic contour upward and the ileal loops (and the hepatic flexure of the colon in the third trimester) downward. It is on this view that the degree of hepatomegaly, if present, is best appreciated (see Appendix Table A.21).

Coronal view of the abdomen and related malformations (Figure 7.7). This plane represents a low-magnification view of the whole abdomen and, as such, allows one to get a fair idea of the topographic location of cysts or bowel dilation. With two-dimensional (2D) US, obtaining this view may require significant manual skills; the use of three-dimensional (3D) US makes the display of this plane much easier, since it can be reconstructed from a previously acquired volume using VCI-C. The major anomalies that may be detected on this view are as follows:

Esophageal atresia. Absent or small size of the gastric bubble.

Duodenal atresia or stenosis. Double-bubble sign.

Hepatomegaly. Increased volume of the liver.

Choledochal cyst. Round cystic structure under the liver.

Enteric duplication cyst. Round cystic structure adjacent to the stomach.

Splenomegaly. Increased volume of the spleen.

Small-bowel atresia. Severe dilation of the ileal loops proximal to the atretic tract.

Meconium ileus. Diffuse hyperechogenicities and calcifications within the intestinal lumen, sometimes associated with small-bowel obstruction.

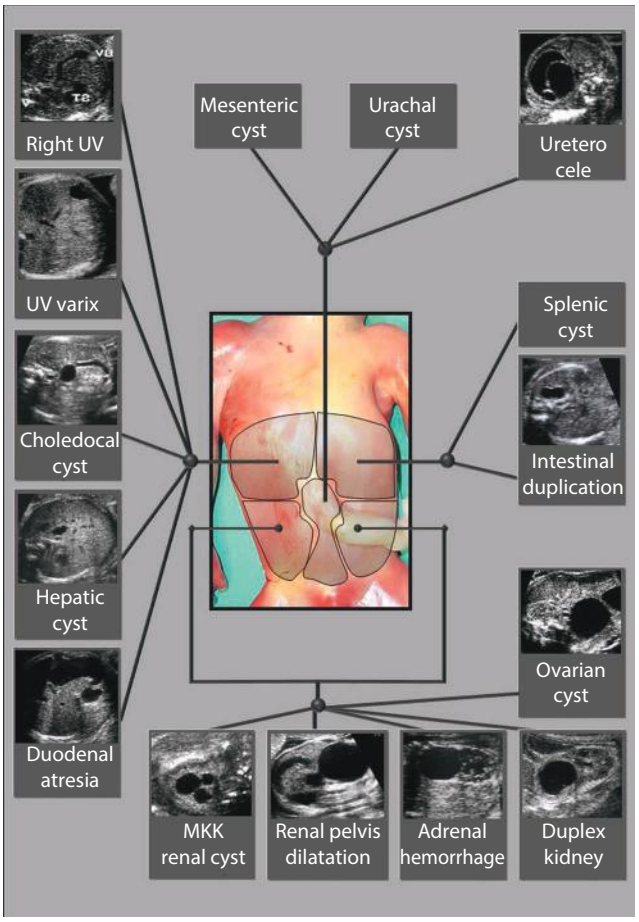


Figure 7.9 Differential diagnosis of abdominal cystic masses.

Cystic intra-abdominal masses. Again following the philosophy of this book—*from US sign to diagnosis*—in this subsection, a diagnostic algorithm of cystic intra-abdominal masses is described, taking into consideration their location and aspect. In fact, in clinical practice, the detection of a cystic intra-abdominal mass comes first, followed by determination of its origin—not, unfortunately, the other way around. The proposed algorithm for the differential diagnosis of intra-abdominal cystic masses is shown in Figure 7.9: this takes into consideration the location of the mass and its US appearance. As evident, there are several possible causes of cystic intra-abdominal structures. However, using this algorithm and/or clinical experience, a final determination of the actual origin of the mass is achieved in a good number of cases.

CHARACTERIZATION OF MAJOR ANOMALIES

ESOPHAGEAL ATRESIA (EA) AND TRACHEOESOPHAGEAL (TE) FISTULA

Incidence. 1/3000–1/4000 live births.

Ultrasound diagnosis. Absent or small gastric bubble, relatively late-onset polyhydramnios. Inconstant presence of a blind-ending proximal esophagus during swallowing (pouch sign).

Risk of chromosomal anomalies. High (20%–44%): trisomies 21 and, to a lesser extent, 18.

Risk of nonchromosomal syndromes. Relatively high.

Outcome. If not associated with other malformations, generally good, but depends mainly on the birth weight and the extent of the atretic tract.

Definition In EA, the communication between the proximal and the distal tract of the esophagus is absent, due to a lack of development of the intermediate esophageal portion, mainly because of an interruption of the blood supply during organogenesis. EA can occur as an isolated anomaly or, much more frequently, be associated with a TE fistula (i.e., an abnormal communication between the trachea and the distal esophageal stump) (about 90% of cases). The frequent association with a TE fistula is responsible for the low intrauterine detection rate: this is due to the fact that some amniotic fluid may actually reach the distal esophagus and

eventually fill the stomach, just by transiting through the fistula If this is the case, then US diagnosis becomes very difficult being based on the detection of a relatively small gastric bubble. Anatomically, five types of EA are recognized, according to the Gross classific - tion [4], on the bases of the anatomy and site of the TE fistula

- *Type A*: no fistula (7% of cases);
- *Type B*: EA with proximal TEF (2%);
- *Type C*: EA with distal TEF (86%);
- *Type D*: EA with proximal and distal TEF (1%);
- *Type E*: TEF without concomitant EA (4%).

Only type A is reliably detectable in the fetus by the nonvisualization of the gastric bubble.

Etiology and pathogenesis. The etiology of the defect is unknown. It originates when, at eight weeks of gestation, the primitive foregut does not divide into the ventral trachea-bronchial part and the dorsal digestive part.

Ultrasound diagnosis. The prenatal diagnosis of EA is challenging. The lack of persistent patency of the esophageal lumen, and the close proximity of this organ to anatomical structures of similar tissue texture, render the sonographic evaluation of the fetal esophagus a difficult task [2]. In addition, it should be underlined that most of the cases of EA are extremely difficult to detect in utero due to the presence of a concurrent TE fistula: usually, this fistula does not prevent a nearly normal stomach filling; in less frequent cases, a constantly small gastric size is found.

In fact, the combination of a small or absent fetal stomach (Figure 7.10a) with polyhydramnios (Figure 7.10b), which are the most common indirect US findings when EA is suspected prenatally, has a low positive predictive value of between 40% and 56% in diagnosing esophageal obstruction [5–7], with a high false-positive rate.

In addition, as also shown in Figure 7.8, a wide range of pathologic conditions may be associated with absent or small gastric bubble, and all of these should be ruled out prior to reaching a definite diagnosis of EA. The fact that these anomalies include very severe or lethal conditions, such as FADS, has led some authors to identify persistent nonvisualization of the gastric bubble as a poor prognostic sign per se, being associated with a poor pregnancy outcome in roughly 50% of the cases, regardless of its cause. As reported here, the other sign possibly indicative of EA is polyhydramnios, which becomes clearly evident only in the late second or the third trimester (Figure 7.10b). It can be associated with FGR; it should be underlined that

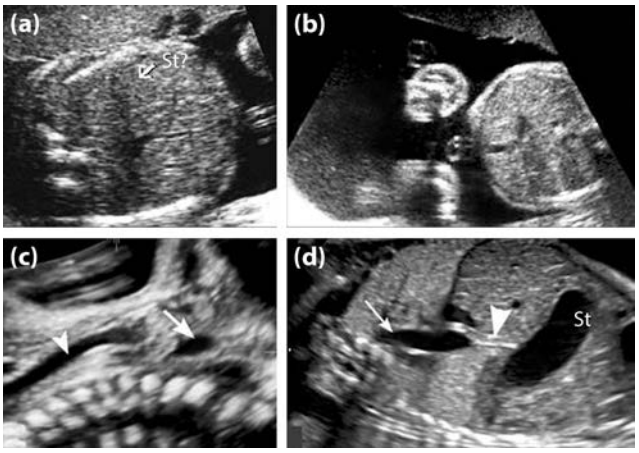


Figure 7.10 Esophageal atresia. (a) At 23 weeks of gestation, a suspicion of EA (without TE fistula—see this chapter's text) arises due to persistent nonvisualization of the gastric bubble in the abdomen. The amount of amniotic fluid is normal. (b) At 30 weeks of gestation, polyhydramnios has developed, and the stomach is still not visualized: the diagnosis of EA is confirmed. (c) A dilation of the proximal blind-ending esophagus (esophageal pouch) (arrow) can be clearly seen in the fetal neck. (d) In this case of EA associated with a gastrointestinal obstruction, the pouch (arrow) is located in the thoracoabdominal tract of the esophagus.

the association between FGR and polyhydramnios is uncommon, the latter usually being associated with fetal macrosomia. The development of FGR, which is present in 35%–40% of fetuses with EA, has been thought to be an effect of the reduced intestinal absorption of the proteins present in the amniotic fluid (due to lack of swallowing), which at term can be as high as 2 g protein per day. Another interesting feature is that 50% of the EAs associated with Down syndrome are type A (i.e., without a TE fistula); this is why in the fetus, the recognition of an EA based on absent gastric bubble implies a very high risk of chromosomal anomalies.

More recently, visualization of the dilation of the blind-ending esophagus (esophageal pouch) (Figure 7.10c) in the fetal neck or upper mediastinum during fetal swallowing has been reported and proposed as a reliable sign for predicting EA. In fact, more than 85% of EA are type C of the Gross classification, with a blind ending of the proximal part of the esophagus.

Unfortunately, this ultrasound sign is uncommon before 23 weeks and inconstant in the third trimester. Its identification can imply a detailed and long sonographic examination and depends on the presence of fetal swallowing during examination. Consequently, failure to identify a pouch in the fetal neck does not exclude EA. However, the association of absent or

small gastric bubble, polyhydramnios, and the presence of a pouch, especially if they persist in successive examinations, can significantly increase the likelihood of EA [5].

The accuracy of the prenatal diagnosis of EA might be further improved by 3D US and by magnetic resonance imaging (MRI) [8,9].

Differential diagnosis. This includes all conditions possibly associated with absent or small gastric bubble. These are shown in Figure 7.8: severe oligohydramnios (and consequent lack of amniotic fluid ingestion) in the case of premature rupture of membranes or bilateral renal agenesis, FADS and related syndromes, diaphragmatic hernia, and cleft lip and palate.

Prognostic indicators. Association with other major anomalies, which is fairly common, represents the most important poor prognostic sign, since the occurrence of concurrent anomalies makes surgical correction of the defect more difficult In addition, the frequent occurrence of a low birth weight, as a result of FGR, may render the outcome even more guarded.

Association with other malformations. Major anomalies are associated in 40%–70% of the cases, with prevalence, in decreasing order, of GI tract (28%) (Figure 7.10d), cardiovascular (24%), genitourinary (13%), and osteomuscular (11%) malformations. The *VA(C)TER(L) association* (see Chapter 10), the "TE" of which stands for TE fistula (as mentioned in "Risk of Nonchromosomal Syndromes" in this section), accounts for a significant number of these anomalies

Risk of chromosomal anomalies. This is high, reaching 20%–44% of cases in the fetus, with a prevalence of trisomies 21 and 18. This high risk is related to the fact that mainly type A EA (atresia without concurrent TE fistula) which is the one most frequently associated with Down syndrome, is usually diagnosable in utero.

Risk of nonchromosomal syndromes. This is relatively high:

- *VA(C)TER(L) association*: look for ► *EA (TE fistula)* + vertebral anomalies + anorectal atresia + cardiac, renal anomalies + limb anomalies (Chapter 10).

Obstetric management. Should EA be suspected in a fetus, a thorough anatomic scan should be performed by an expert in order to detect major and/or minor signs possibly leading to the diagnosis of one of the associated anomalies discussed in this chapter. Fetal karyotyping is also mandatory, because of the high risk of Down syndrome and, to a lesser extent, of trisomy 18. The delivery should take place in a tertiary referral center where a neonatal intensive care unit (NICU) and pediatric surgery are available. The need for *in utero* transport arises from various considerations: (1) the consistent risk of associated FGR (40% of cases) and prematurity (due to polyhydramnios), which may require NICU admission; (2) the possibility that other major anomalies overlooked at prenatal US may be present; (3) the need for adequate preoperative nutrition; and (4) the need for early corrective surgery.

Postnatal therapy. This obviously consists of surgical reconstruction of the esophagus and may be carried out in a single intervention or require a two-stage procedure, according to the length of the atretic segment.

The primary repair of the EA–TE fistula abnormality is considered the preferred surgical option and achieves the best results [10]. The fistula is divided a few millimeters distal to its entry in the trachea, and the defect is closed with interrupted sutures. In a second step, the proximal blind end of the esophagus is mobilized sufficiently to allow a tension-free anastomosis with the lower esophageal segment [10]. In repairs with tension at the level of the anastomosis, the infant would be paralyzed for five days to prevent swallowing and upward movements of the proximal esophagus. Infants with isolated EA usually have a long gap between the ends of the esophagus precluding early primary repair. The infant would be brought to the operating theater for the creation of a feeding gastrostomy and an assessment of the gap between the ends of the esophagus. Options for treatment beyond this stage include attempted delayed primary anastomosis at around six to eight weeks, or substitution of the esophagus with stomach, small bowel, or large bowel in later infancy [10].

Prognosis, survival, and quality of life. The prognosis depends on the presence of associated malformations, especially congenital heart diseases and VA(C)TER(L) association; on the birth weight; and on the length of the esophageal defect.

The survival rate of the EA–TE fistula repair in a term baby with no associated anomalies is about 95% [10]. The analysis of risk factors revealed two important predictors of outcome: birth weight of less than 1500 g and the presence of major congenital cardiac disease. However nowadays, in patients with low birth weight or cardiac anomalies, the survival has increased from 60% (in the 1980s) to more than 80%.

The final outcome of fetuses with EA is quite different if neonatal series are compared with fetal series, as for congenital heart disease. This is due to the fact that the cases with poorer prognosis, due to association with syndromic and/or chromosomal anomalies,

die prior to their enrollment in neonatal series. For these reasons, the prognosis of the fetus with EA, with a mortality rate as high as 75% [7], is radically different from that of the neonate.

In the surviving cases, the most frequent long-term complication is gastroesophageal reflux, which, if severe, may also be life threatening because of the possibility of *ab ingestis* lung infection, followed by esophageal restenosis, which occurs in about 30% of cases. Tracheomalacia is another complication that affects approximately 10%–20% of infants with EA–TE fistula.

dUod ENAL ATr EsIA

Incidence. 1/2500–1/10,000 live births.

Ultrasound diagnosis. Double bubble, with communication between the two parts; late polyhydramnios.

Risk of chromosomal anomalies. High (20%–50%): mainly trisomy 21.

Risk of nonchromosomal syndromes. Low.

Outcome. Mainly good if isolated.

Definition In duodenal atresia, the tract between the proximal and distal portions of the duodenum is atretic. In most cases (80%), the obstruction is due to complete atresia and is caudal to the ampulla of Vater. In the remaining 20% of cases, the obstruction can be due to a diaphragm or membrane located within the lumen of the duodenum, and it can be complete or partial (stenosis).

Etiology and pathogenesis. The etiology of the defect is unknown. The pathogenetic mechanism involves an interruption of blood supply during the organogenetic period, as for most GI tract atresias. According to another theory, the defect may be due to a lack of duodenal recanalization, which is always during early embryogenesis.

Ultrasound diagnosis. This is based upon recognition of the classic double bubble, associated with polyhydramnios, which often develops in the late second and early third trimesters. Usually, when the midtrimester anomaly scan is carried out (at 19–21 weeks of gestation in most countries), polyhydramnios is absent and the double bubble has not yet completely developed: the only finding can consist of an evidently dilated stomach, with a mild dilation of the duodenum (Figure 7.11). During follow-up scans, which should always be scheduled if the stomach presents the features of enlargement and evidence of pylorus, the classic double bubble becomes clearly visible (Figure 7.11). Care should be taken in demonstrating a communication between the two anechoic bubbles, to obtain confirmation that the second bubble is actually the dilated proximal duodenum (Figure 7.11): only by demonstrating this communication can the rare occurrence of enteric duplication cysts or other upper abdominal cysts be ruled out. Furthermore, it should be noted that, in the less common cases of duodenal stenosis, most of which are not diagnosed prenatally, the double bubble may become visible only late in gestation or may even never occur, with a constantly dilated stomach with evidence of the pylorum being the only sign of the partial obstruction. Finally, it should be underlined that in the extremely rare cases in which duodenal atresia is associated with

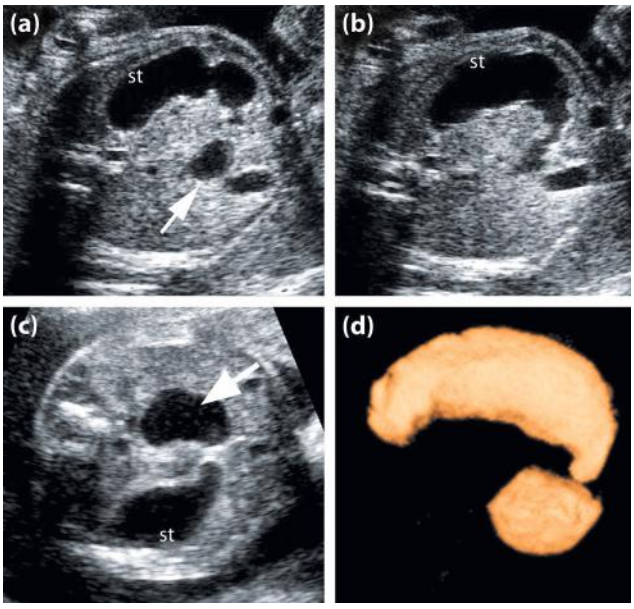


Figure 7.11 Duodenal atresia. (a) At 23 weeks of gestation, initial evidence of a double bubble is detected (arrow). (b) After a few minutes, intestinal peristalsis demonstrates the communication between the stomach and the dilated proximal duodenum. (c) Later in gestation, a clear double bubble (arrow) has developed, confirming the suspicion of duodenal atresia. (d) Three-dimensional ultrasound with inversion mode rendering: the site of the obstruction is clearly visible.

EA, the overdistension of the stomach and proximal duodenum is massive.

Differential diagnosis. This should include all other conditions featuring a cystic structure in the middle or right upper abdomen (Figure 7.9): choledochal cysts, enteric duplication cysts, and hepatic cysts. The differential diagnosis is made by simply demonstrating the communication between the right-sided anechoic structure and the stomach: if this communication exists, then the diagnosis can only be duodenal atresia.

Prognostic indicators. The association with other anomalies, which is relatively frequent, represents the main poor prognostic sign.

Association with other malformations. Major anomalies are associated with duodenal atresia in 40%–50% of cases, with a prevalence (in decreasing order) of other GI tract, vertebral (about 33%), and cardiac anomalies (30%), related to the close association with Down syndrome. In particular, the rate of association with intestinal malrotation reaches 40%, but more severe anomalies of the biliary tract and of the pancreas (annular pancreas), which may have a negative impact on prognosis, are also not uncommon. These latter anomalies are virtually impossible to be detected in utero: an US-detectable sign (i.e., nonvisualization of the gallbladder), which would be indicative of life-threatening biliary atresia, has a low diagnostic specificity due to its frequent occurrence in the normal fetal population.

Risk of chromosomal anomalies. This is high. Overall, 40% (range 20%–50%) of cases of duodenal atresia are associated with Down syndrome. Conversely, 5%–15% of neonates with trisomy 21 have duodenal atresia.

Risk of nonchromosomal syndromes. This is low.

Obstetric management. Should duodenal atresia be diagnosed in a fetus, karyotyping is mandatory because of the high risk of trisomy 21. In addition, a thorough search for associated malformations (including fetal echocardiography) should be carried out. With the caveats discussed in this chapter, the gallbladder should be searched as well. There is also a consistent risk of preterm delivery because of the severe polyhydramnios, which constantly develops by the early third trimester. In very carefully selected cases, this may benefit from amniodrainage. Delivery should take place in a tertiary referral center where a NICU and pediatric surgery are available. In fact, it has been demonstrated that in utero transport to tertiary referral centers as a result of prenatal diagnosis of duodenal atresia has contributed significantly to improving the final outcome of such fetuses [11].

Postnatal therapy. The surgical approach to this anomaly is carried out just after birth. The operative management of duodenal atresia is determined by the anatomic findings and the associated anomalies noted at laparotomy. Bypass procedures for duodenal atresia or stenosis include duodeno-duodenostomy or duodeno-jejunostomy. Additional surgical procedures may be needed in the case of associated intestinal, pancreatic (annular pancreas), and/or biliary malformations.

Prognosis, survival, and quality of life. The final outcome of fetuses diagnosed with duodenal atresia is generally good, except for the cases in which severe biliary tract anomalies are present. These are responsible for the 20%–40% neonatal mortality rate reported in most series. If only isolated cases are considered, then overall survival is extremely good, with an early postoperative mortality rate of 3%–5% and a late mortality rate that does not exceeds 6% [12]. Hence, about 90% of neonates with isolated duodenal atresia survive. Of these, 25% will require an additional surgical procedure, which is needed to remove a restenosis or postoperative complications such as gastroesophageal reflux by 6 years of age. Late-onset sequelae are represented by megaduodenum, duodenogastro esophageal reflux and peptic ulcers. The quality of life is normal in the overwhelming majority of cases.

SMALL-BOWEL ATRESIA

Incidence. 1/2500–1/5000 live births.

Ultrasound diagnosis. Severe late-onset dilation of the ileal loops proximal to the obstruction. Late-onset polyhydramnios.

Risk of chromosomal anomalies. Low.

Risk of nonchromosomal syndromes. Low.

Outcome. Generally good, but guarded in apple-peel variant and multiple-site atresia.

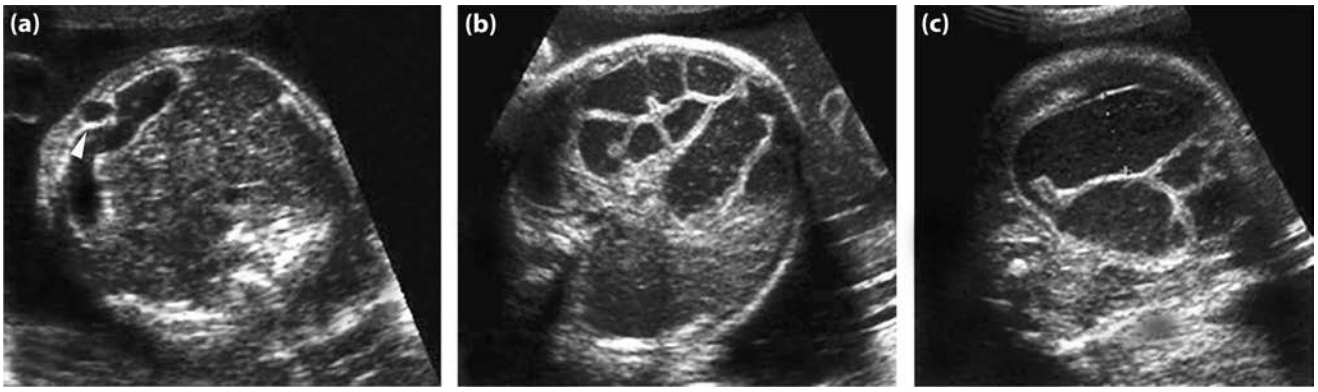


Figure 7.12 Ileal atresia. (a) Before 24 weeks of gestation, there is hardly any evidence of intestinal dilation. The only doubtful sign is represented by a moderate dilation (7 mm) of a single ileal or jejunal loop, possibly associated with the hyperechoic aspect of the wall (arrowheads). (b) In the 3rd trimester, the obstruction becomes evident, with moderately severe dilation of various loops. In the dilated bowel loops cranial to the obstruction, increased intestinal peristalsis is seen, with the intestinal content moving from one loop to the adjacent one. (c) At 36 weeks, by following the course of the dilated loops, it is possible to demonstrate the communication between the various dilated segments (the maximum transverse diameter of the loops was 23 mm).

Definition Small-bowel atresia can be single or multiple. According to the surgical classification system there are more types:

- Type I (20% of cases) is membranous, due to an intraluminal diaphragm or web, with no mesenteric defect and normal bowel lenght;
- Type II (32% of cases) features blind ends separated by a fibrous cord but no mesenteric defect and normal bowel lenght; type III includes two variants;
- Type IIIa (20% of cases) which shows blind ends with complete separation, mesenteric gap and short bowel lenght; type IIIb (11% of cases) known as "apple peel or christmas tree" affects long segment of the bowel with large mesenteric defect, more likely familial;
- Type IV (17% of cases)represents multiple atresias. As far as the anatomic site of the atresia is concerned, the jejunum only is involved in 50% of cases, the ileum only in 43% of cases, and both intestinal tracts in the remaining 7% of cases. The anatomic site of the lesion is important, since there are some differences related to the site of the atresia. Ileal atresias are more often single, show a higher tendency to perforation in utero, and are associated with a higher neonatal mean weight and more advanced gestational age at delivery. In contrast, jejunal atresias are more often multiple, tend to dilate rather than perforate, and show a significantly lower neonatal mean weight and less advanced gestational age at delivery in comparison with ileal atresias.

Etiology and pathogenesis. The etiology of the defect is unknown. Investigations in animal models and in humans have demonstrated that in most cases, intestinal atresia is due to a vascular insult, consisting of an atresia or torsion of the feeding artery during the rotation of the midgut. The apple-peel variant has been hypothesized to be the effect of vascular occlusion of a superior mesenteric artery branch.

Ultrasound diagnosis. US diagnosis is based mainly on the detection of the severe dilation of the intestinal loops proximal to the obstruction, which is absent in most cases prior to 25 weeks of gestation. The polyhydramnios is also of late onset. Hence, the first sonographic evidence of a possible small-bowel atresia is the isolated dilation of an ileal loop, showing a transverse diameter of greater than 7 mm (Figure 7.12a), according to the published nomograms [13], which are given in the Appendix. Additional signs that contribute to confirming the diagnosis are a centro-abdominal location of the affected loop, its hyperechoic walls (Figure 7.12b), increased peristalsis, and the presence of endo-abdominal calcifications that are possibly indicative of a meconium ileus. In the late second or early third trimester, the malformation is fully demonstrated by US, with severe dilation of the ileal and jejunal loops proximal to the obstruction, showing particulate matter moving with the increased peristaltic waves (Figure 7.12c). It should be underlined that it is not possible to identify the real site of the obstruction (ileal or jejunal). The only features that may point toward one of the two sites are the evidence of intestinal

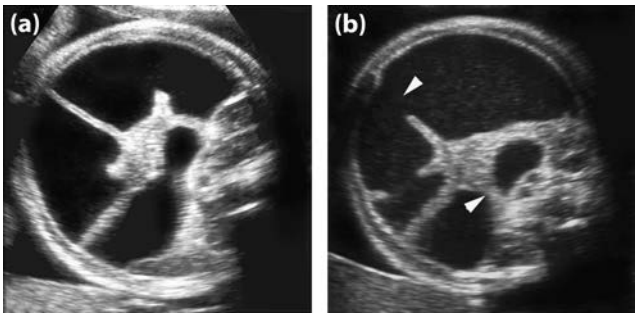


Figure 7.13 Jejunal atresia (37 weeks of gestation). Note the extremely severe dilation without evidence of perforation (absence of meconium peritonitis). The arrowheads indicate the site of the peristaltic wave, opening and closing the communication between adjacent loops from (a) to (b).

perforation (ascites with particulate matter and/or calcifications) for the ileus or extreme dilation without perforation for the jejunum (Figure 7.13).

Differential diagnosis. It should be pointed out that the US signs of small-bowel atresia are virtually the same as those characterizing *Hirschsprung's disease* (*aganglionic megacolon*) and *volvulus*. Therefore, a differential diagnosis among these three completely different causes of intestinal obstruction cannot be carried out in most instances. Only the timing and the rapidity of the appearance of the loop dilation may be roughly indicative of the likely diagnosis: it is gradual for atresia and sudden (in three–four days) for volvulus. In addition, the differentiation from meconium ileus, which is characterized by a mechanical intraluminal obstruction due to the increased consistency of the meconium, is similarly rather challenging, if not impossible. The evidence of diffuse intra-abdominal calcifications would suggest the occurrence of meconium peritonitis, which follows intestinal perforation. FGR can be associated, especially if the atresia is in the jejunum, due to the consequent consistent protein malabsorption.

Prognostic indicators. The detection of intra-abdominal calcifications possibly suggesting the presence of a meconium ileus complicated by perforation and meconium peritonitis, represents one of the most important poor prognostic signs. The poorer prognosis is related to the poor outcome of the cases complicated by perforation and to the fact that, in the case of meconium ileus, the risk of underlying cystic fibrosis is very high (90%). According to a recent retrospective report, another prognostic factor seems to be polyhydramnios [14]. Its presence would indicate a higher risk of delayed anastomosis and a longer hospital stay, due to an increased rate of surgical complications.

Association with other malformations. In about 25% of cases, it can be associated with other intestinal anomalies such as malrotation, and intussusception intestinal duplication, and volvulus. Extraintestinal anomalies are rarely associated with intestinal atresias.

Risk of chromosomal anomalies. This is low.

Risk of nonchromosomal syndromes. This is relatively low. There is a 10% risk of cystic fibrosis; however, if meconium peritonitis is associated, the risk of cystic fibrosis reaches 90%

- *Feingold syndrome*: look for ► *GI atresias* + microcephaly + sindactyly or clinodactyly.

Obstetric management. Should ileo-jejunal atresia be diagnosed in a fetus, karyotyping is not recommended, because of the low risk of chromosomal aberrations. With regard to perinatal management, it should be noted that the risk of preterm delivery is significant due to the ubiquitous occurrence of late-onset but severe polyhydramnios. Amniodrainage may be an option in very carefully selected cases, in order to reduce the uterine overdistension and the associated risk of preterm delivery. The delivery should be planned in a tertiary referral center. Although there is no indication for Cesarean section, the rate of malpresentation is increased by the common occurrence of severe polyhydramnios. The need for in utero transport derives from the increased risk of preterm delivery and FGR. Furthermore, surgery has to be carried out immediately after birth in most cases.

Postnatal therapy. The surgical procedure includes removal of the atretic tract(s) and end-to-end intestinal anastomosis. Only in selected, more complex cases does the procedure involve a two-step procedure with an initial ileostomy followed by anastomosis.

Prognosis, survival, and quality of life. The final outcome of fetuses with ileo-jejunal atresias is generally good, except for the relatively rare cases of apple-peel atresia or multiple atresias (types IIIB and IV, respectively). In fact, in these cases, the total length of the intestine is significantly reduced, and this leads to malabsorption (*short bowel syndrome*). Also, the association with volvulus, perforation, and meconium peritonitis, which complicates fewer than 10% of the cases, negatively affects the survival rate, being responsible for a 10% increase in postoperative mortality.

hyp Er Echo GENIc Bo WEL

Definition Echogenic bowel is not a truly pathological feature but a nonspecific US sign; it is commonly observed in normal fetuses. However, its detection is important because it can be found in association with other anomalies in about 27%–34% of cases [15,16].

Etiology and pathogenesis. The hyperechogenic bowel etiology is unclear, but explanations include alteration in the meconium with increased protein content and/or decreased water content, swallowed blood following intra-amniotic hemorrhage, intestinal wall edema, and ischemia. Decreased water content is the most frequent alteration observed in fetuses with hyperechogenic bowel and may derive from hypoperistalsis secondary to decreased bowel function or vascular injury. In fetuses with trisomy syndromes, and cystic fibrosis, the reduction of microvillar enzymes leads to constipation and thickened calcified meconium. In cases of growth-restricted fetuses, hyperechogenic bowel may occur as a result of impaired bowel function secondary to hemodynamic redistribution and consequent mesenteric ischemia [15,16]. In cases of infections, the hyperechogenic bowel is due to the fluid inside or outside the intestine and to the consequent different acoustic impedance of the adjacent media (intestinal tissue versus fluid) The prevalence of echogenic bowel on routine second-trimester US ranges from 0.2% to 1.8% [17].

Ultrasound diagnosis. The normal echogenicity of the bowel changes along pregnancy: instead of the late second trimester (19–25 weeks), a mild hyperechogenicity is normally seen in the first trimester and in the early midtrimester. Hyperechogenic bowel can be diffuse or focal. Because the definition and interpretation of hyperechogenic bowel are subjective, various grading systems have been proposed in order to minimize subjectivity; one of the most used is the following grading system [17]:

- *Grade 1*: mildly echogenic and typically diffuse;
- *Grade 2*: moderately echogenic and typically focal;
- *Grade 3*: very echogenic, similar to that of fetal bone.

Transducer frequency should be 5 MHz or less. To reduce subjectivity, we consider only bowel that appears as bright as fetal bone (Figure 7.14).

Differential diagnosis. This includes echogenic intra-abdominal masses such as dysplastic kidneys, intra-abdominal extrathoracic pulmonary sequestration, duplication cyst, and meconium peritonitis, which will be discussed in this chapter.

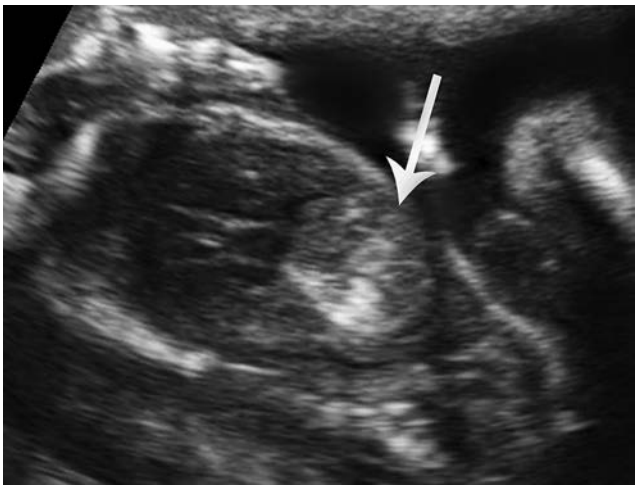


Figure 7.14 Hyperechogenic bowel at 20 weeks of gestation.

Prognostic indicators. The prognosis depends on the underlying condition.

Association with other malformations. Hyperechogenic bowel is found in association with other anomalies in about 27%–34% [15,16] of cases: fetal aneuploidy (especially trisomy 21), congenital infection, cystic fibrosis intrauterine growth restriction, gastrointestinal obstruction, thalassemia, intramniotic bleeding, and fetal demise. The likelihood of association between hyperechogenic bowel and cystic fibrosis increases with the degree of intestinal echogenicity.

Risk of chromosomal anomalies. About 9% of fetuses with hyperecogenic bowel have chromosomal anomalies [15].

Risk of nonchromosomal syndromes. About 2%–3% of fetuses with hyperecogenic bowel have cystic fibrosis [15].

Obstetric management. Karyotype, screening for maternal serological infections, and screening for cystic fibrosis should be offered in the presence of hyperechogenic bowel. Hyperechogenic bowel is associated with aneuploidy, especially trisomy 21; therefore, increased intestinal echogenicity is actually considered a soft marker for fetal aneuploidy.

Prognosis, survival, and quality of life. The clinical presentation depends on the cause of hyperechogenic bowel.

MEco NIUM ILEUs

Incidence. Unknown in the fetus.

Ultrasound diagnosis. Mechanical ileal obstruction due to the increased consistency of the meconium; significant risk of perforation and consequent meconium peritonitis.

Risk of chromosomal anomalies. Relatively low.

Risk of nonchromosomal syndromes. If cystic fibrosis is considered here, the risk is extremely high (>90%).

Outcome. Depends on the underlying cystic fibrosis and its phenotypic expression.

Definition Meconium ileus is characterized by an ileal mechanical obstruction caused by thickened meconium. The meconium is thicker than normal due to a high protein content, the primary cause of which is cystic fibrosis which is associated with most cases of meconium ileus. This obstruction leads relatively often to ileal perforation and, consequently, meconium peritonitis. In some cases, the obstruction occurs more distally, in the colon, where the meconium causes a *mucus plug* that obstructs the rectum. Also in this case, the risk of underlying cystic fibrosis is high

Etiology and pathogenesis. As mentioned in this section, cystic fibrosis is associated in more than 90% of cases. In the few cases not associated with this genetic condition, the etiology of the intestinal obstruction remains unclear. The pathogenetic mechanism leading to the obstruction is represented by the significan changes in the components of the meconium caused by cystic fibrosis: this shows a very high protein content and, at the same time, less fluids due to their impaired intraluminal secretion. This leads to a significant inspissation, which in turn delays and eventually blocks the intraluminal transit of the meconium along the relatively narrow ileal lumen. Once the obstruction occurs, the loops proximal to the obstruction dilate and, due to the weak elasticity of the ileal walls, often perforate, with the thick meconium spilling into the abdominal cavity, with a consequent severe adhesive peritonitis.

Ultrasound diagnosis. This is based upon recognition of an ileal obstruction, with one or multiple dilated loops that characteristically show hyperechoic content and similarly hyperechoic walls (Figure 7.15). In meconium ileus, the obstruction is usually of late onset, becoming evident in the late second trimester, after 24–25 weeks of gestation. The US appearance is pleomorphic. The dilated ileal loops may show hyperechoic content or, in other cases, meconium or fluid levels; the walls may appear normal or thickened and hyperechoic. The situation is further complicated by the frequent occurrence of meconium peritonitis, which is characterized by diffuse intra-abdominal calcifications and less frequently by a meconium pseudocyst. If the obstruction involves the ileus, the colon is typically empty, since meconium transit is blocked. As mentioned under "Definition in this section, in a minority of cases, the obstruction involves the colon, with evidence of a distal mucus plug. The association with cystic fibrosis is also present for this variant, although at a lower rate (25%). In a significan number of cases, the first evidence of meconium ileus at US consists of the so-called *echogenic bowel*. This finding as mentioned in this section, in the early–mid second trimester may have different underlying causes (see "Hyperechogenic Bowel").

Differential diagnosis. The differential diagnosis with simple small-bowel atresia may be impossible. The detection of a highly hyperechoic meconium within the ileal loops and/or of intra-abdominal calcifications due to the meconium peritonitis may point toward meconium ileus as the most likely diagnosis.

Prognostic indicators. If an intestinal obstruction is possibly identified as meconium ileus, this is itself a poor prognostic sign, especially if it is associated with meconium peritonitis. This is due to the extremely strong association with cystic fibrosis which affects the mid- to long-term prognosis; and to the surgical difficulties encountered in dealing with the meconium peritonitis, which may require multiple bowel resections.

Association with other malformations. This is unknown.

Risk of chromosomal anomalies. This is relatively low. However, considering that the first evidence of a meconium ileus may be an echogenic ileus, it should be remembered that this soft marker carries a risk of chromosomal anomalies of 9% (see "Hyperechogenic Bowel").

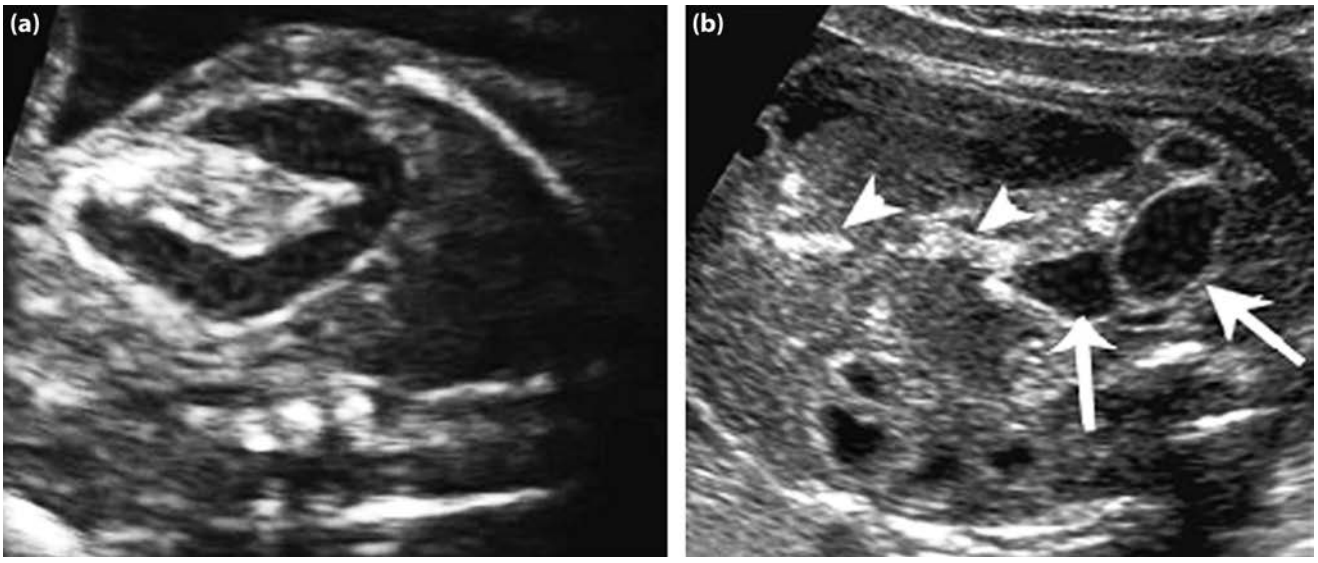


Figure 7.15 Meconium ileus. (a) Axial view of the fetal abdomen showing an obstructed loop with hyperechoic content and hyperechoic walls in the middle of the abdomen at 26 weeks of gestation. (b) At 29 weeks of gestation, some ileal loops are dilated and show hyperechoic walls (arrows). The presence of macrocalcifications (arrowheads) demonstrates the perforation and the consequent meconium peritonitis.

Risk of nonchromosomal syndromes. This is extremely high, if the almost ubiquitous cystic fibrosis is considered as a syndrome.

Obstetric management. If meconium ileus is detected in a fetus, the option of an amniocentesis performed to obtain fetal DNA for cystic fibrosis testing should be discussed with the parents. In fact, the diagnosis of meconium peritonitis is usually made after 24 weeks of gestation, which is the limit for termination of pregnancy in those countries in which there is a time limit for this option. Therefore, in these countries, DNA testing will not alter the course of pregnancy if, as is highly probable, the results of the test will become available in the early third trimester of pregnancy. On the other hand, in countries in which termination for serious fetal conditions is permitted until delivery, this caveat does not apply, and DNA testing may be easily carried out. As mentioned here, if the US finding is an *echogenic ileus* but not yet meconium ileus, then karyotyping is justified by the 9% risk of chromosomal anomalies associated with this finding Regardless of the results of DNA testing, in the case of meconium ileus, the fetus should be delivered in a tertiary referral center in order to optimize neonatal management, which includes surgery for the bowel obstruction and, if not already performed, DNA testing for cystic fibrosis In this regard, the helpful role of prenatal MRI has been underlined: this technique can improve the low diagnostic yield of prenatal US for meconium peritonitis [18].

Postnatal therapy. The postnatal workup should include a contrast computed tomography (CT) scan in order to ascertain persistent intestinal perforation that is invisible on prenatal US. The timing of surgery depends on the clinical presentation. If bowel atresia is associated, bowel resection with end-to-end anastomosis should be carried out soon after birth. If the ileus is not associated with anatomic atresia, then a simple saline, water-soluble contrast enema or *N*-acetylcysteine therapy may induce meconium passage. Clearly, the long-term prognosis depends on the clinical expression of the underlying cystic fibrosis

Prognosis, survival, and quality of life. The outcome of fetuses diagnosed with meconium ileus is extremely variable, depending on the abdominal situation (concurrence of ileal atresia or of meconium peritonitis) and on the association with cystic fibrosis Survival and quality of life depend directly on the severity of the cystic fibrosis The early surgical mortality rate has been reported to be as low as 2% [19], which underlines once more that survival is dependent almost entirely on the clinical severity of the underlying cystic fibrosis

ANAL ATRESIA AND OTHER ANORECTAL ABNORMALITIES

Incidence. About 1/5000 live births.

Ultrasound diagnosis. Late-onset dilation of the sigmoid colon and rectum, often with hyperechoic meconium. Normal amniotic fluid.

Risk of chromosomal anomalies. High: trisomies 18 and 21.

Risk of nonchromosomal syndromes. High: predominantly associated with various expressions of the caudal regression sequence.

Outcome. Good in mild forms, if isolated. If syndromic, it depends on the associated malformations (as in caudal regression).

Definition Anorectal malformations (ARMs) represent a spectrum of abnormalities ranging from mild anal anomalies to complex cloacal malformations. ARMs incidence is approximately 1 in 5000 live births.

Etiology and pathogenesis. In most cases, the etiology of ARMs remains unclear and is likely multifactorial. However there are reasons to believe that there is a genetic component [1].

During the fourth week of human embryonic development, the urogenital and gastrointestinal systems empty into a common draining structure—the cloaca—consisting of the distal hindgut and allantois.

Subsequently, the cloaca is divided into an anterior part (the urogenital sinus, which develops into the urinary bladder and urethra) and posterior part (the rectum and the proximal part of the anal canal) by the developing urorectal septum. The urorectal septum fuses with the cloacal membrane by the seventh week of development at what then becomes the perineal body. After eight weeks of development, the ventral urogenital portion acquires an external opening and the dorsal anal membranes normally rupture, creating communications between the anorectal tract and the amniotic cavity.

Interferences with anorectal structural development at different stages (abnormal formation of the urorectal septum, ectopic location of the anal opening, and excessive obliteration of the dorsal cloaca) commonly lead to various anomalies, ranging from mild or moderate anorectal anomalies (i.e., imperforate anus) to complex cloacal malformations such as persistent cloaca. In this last case, the urinary, genital, and intestinal tracts converge into a cloacal canal with a single opening at the perineum.

Ultrasound diagnosis. Prenatal diagnosis of ARMs can be suspected when an overdistension of the rectum and, to a lesser extent, the sigmoid colon (Figure 7.16a) is detected. Although case reports of ARMs at as early as 12 weeks of gestation have been described [20], the majority of ARMs, especially in cases of imperforate anus, are missed prenatally. Occasionally, the meconium in the dilated rectosigmoidal intestinal tract or in the dilated rectal pouch becomes hyperechoic (Figure 7.16b) either proximally or distally to the site of obstruction. Intraluminal calcifications can result from prolonged stasis of the meconium and/or indicate the presence of alkaline urine derived from an urorectal fistula (Figure 7.16c). It is likely that a change of pH causes precipitation of the calcium salt [21].

Usually, in cases of isolated anal malformations, the amount of amniotic fluid is unchanged. On the contrary, if the anorectal atresia is associated with an urorectal fistula, the amniotic fluid is reduced. If polyhydramnios is noted in association with anorectal atresia, this can be due to associated anomalies of other organs.

In more complex cases, such as *persistent cloaca*, commonly seen in the female fetus, prenatal US findings may vary considerably and encompass the presence of septated or bilateral fetal pelvic cystic mass (Figures 7.17 and 7.18), usually represented by hydrocolpos or hydrometrocolpos and bladder obstruction. Often, the hydrometrocolpos can compress the bladder, causing partial bladder outlet obstruction. Ascites (caused by drainage of the urine into the abdominal cavity via the vagina) (Figures 7.17 and 7.18), bilateral hydronephrosis, dysplastic kidneys, intraluminal colonic calcifications, reduction in amniotic fluid volume, growth retardation, and vertebral anomalies can also be present.

Differential diagnosis. This includes mainly the upper bowel obstructions; the site and the hyperechoic meconium in the rectal pouch may help in reaching the diagnosis. It should be underlined that under normal conditions, some meconium does fill the rectal pouch, especially in the third trimester. However, the maximum diameter of the rectum does not exceed that of

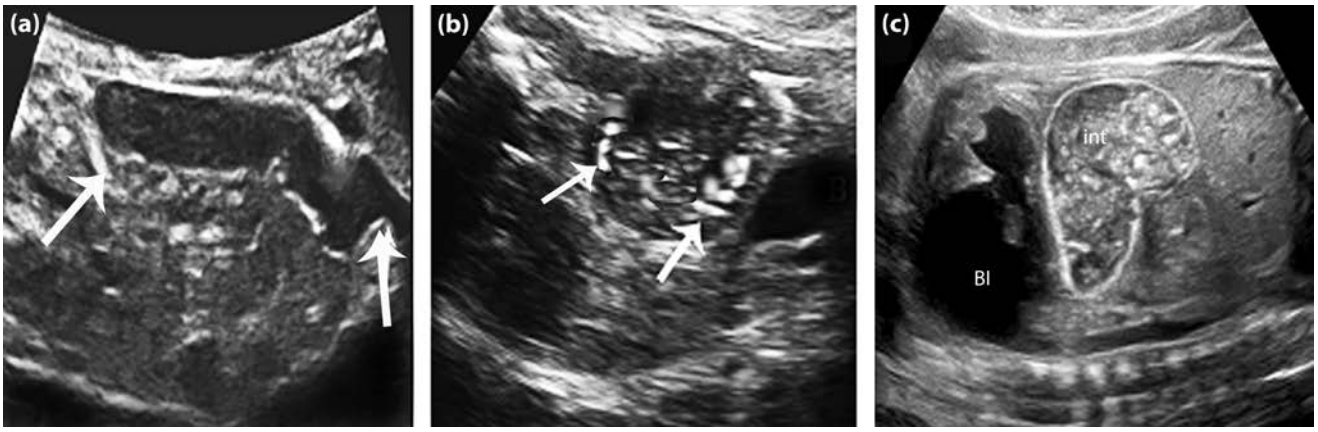


Figure 7.16 Anorectal atresia. (a) Axial view of the fetal lower abdomen showing the dilation of the rectosigmoidal intestinal tract (arrows). (b). Axial view of the fetal lower abdomen and pelvis showing a dilated lower tract of intestine with intraluminal calcifications representing enterolithiasis (arrows) (c). Sagittal view of the fetal lower abdomen showing a dilated intestinal tract (Int) with enterolithiasis and a dilated bladder containing meconium in a case of a rectovesical fistula. With the passage of urine to the bladder, a swirling of this sediment can be seen.

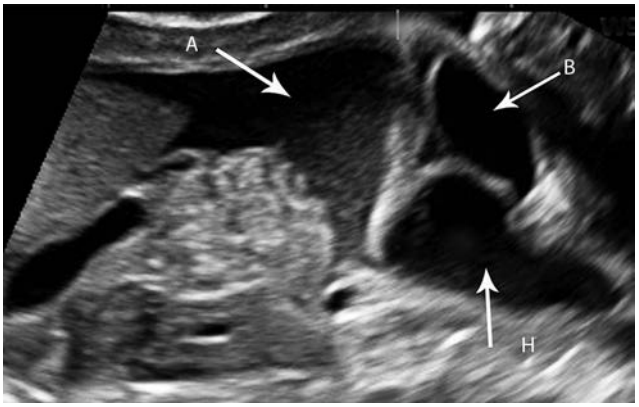


Figure 7.17 Persistent cloaca. Sagittal view of the fetal abdomen and pelvis at 28 weeks of gestation showing a large pelvic cystic structure. The anterior cystic space is the bladder (B), and the posterior is the hydrocolpos (H). A: ascites.

the adjacent full bladder under normal conditions. If the rectal pouch is larger than the full bladder, then anorectal obstruction is likely.

Association with other malformations. An association with other anomalies is a relatively common finding in cases of anorectal atresia (up to 70%): these are mainly urogenital malformations because of their common embryologic origin (in the cloaca and urogenital sinus). Other commonly associated malformations involve vertebral anomalies, the GI tract, and the central nervous system (CNS).

Risk of chromosomal anomalies. This is high (trisomies 18 and 21).

Risk of nonchromosomal syndromes. This is high. The syndromes detectable in utero that can be associated with anorectal atresia are as follows:

- *VA(C)TER(L)*: look for ► *anorectal malformation* + vertebral anomalies + cardiac defects + EA (TE fistula) + renal agenesis + limb anomalies (Chapter 10);
- *Caudal regression syndrome*: look for ► *anorectal malformation* + renal agenesis + sacral agenesis + lumbar vertebral anomalies + femoral hypoplasia + talipes (Chapter 10);
- *MURCS syndrome*: look for ► *anorectal malformation* + renal aplasia + cervico-thoracic somite dysplasia;
- *OEIS syndrome*: look for ► *anorectal malformation* + omphalocele + bladder exstrophy + spinal defects;
- *Klippel–Feil syndrome*: look for ► *anorectal malformation* + fusion of cervical vertebrae + scoliosis + renal and heart anomalies;
- *Sirenomelia*: look for ► *anorectal malformation* + fusion of inferior limbs + renal agenesis + severe vertebral anomalies + genital anomalies (Chapter 10).

Obstetric management. If anorectal atresia is diagnosed in the third trimester, a careful assessment of fetal anatomy should be performed in order to exclude associated anomalies, especially urogenital malformations. The clinical situation is completely different if the possibility of an anorectal malformation arises following the diagnosis, in the early second trimester, of caudal regression syndrome or, worse, sirenomelia. In such circumstances, the diagnosis of anorectal malformation is of no prognostic significance since these two anomalies are already

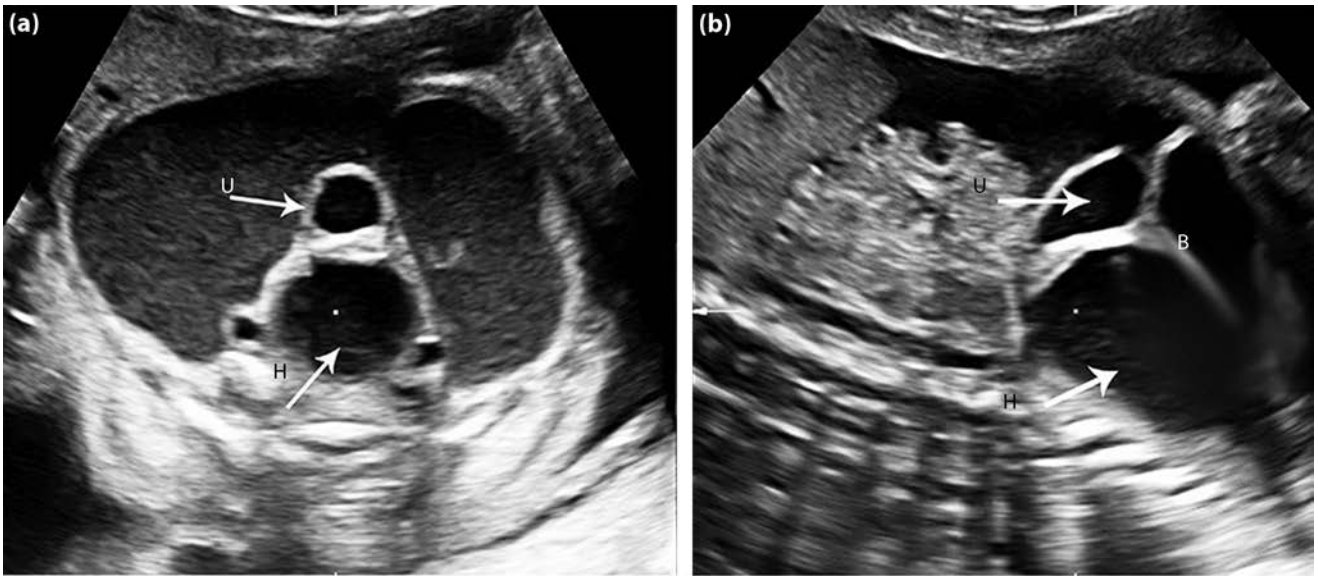


Figure 7.18 Persistent cloaca. Axial (a) and sagittal (b) views of the fetal abdomen at 30 weeks of gestation showing a hydrocolpos (H) and a distended uterus (U). Ascites is also present. B: urinary bladder. In (a) the two dilated ureters lateral to the hydrometrocolpos can be clearly seen.

lethal due to the associated bilateral renal agenesis. In the case of anorectal malformation, delivery should be planned in a tertiary referral center in order to ensure the best possible perinatal management of the lesion, which usually comprises a diagnostic workup and a surgical approach to the distal bowel obstruction.

Postnatal therapy. All patients must be evaluated at birth to rule out urogenital defects. In addition, the presence of a single perineal orifice is clinical evidence of a persistent cloaca. In patients with a persistent cloaca, an abdominal examination may reveal an abdominal mass, which likely represents a distended vagina (present in about 50% of cases). A plain radiograph of the spine is also suggested to rule out spinal anomalies [22].

The surgical approach to repairing anorectal malformation changed in 1980 with the introduction of the posterior sagittal approach, which allowed surgeons to view the anatomy of these defects clearly, to repair them under direct vision, and to learn about the complex anatomic arrangement of the junction of the rectum and genitourinary tract. It has become the predominant surgical method for anorectal anomalies [22].

Prognosis, survival, and quality of life. If the anorectal malformation is isolated, the prognosis and overall survival are good. However, not all neonates undergoing posterior sagittal anorectoplasty achieve fecal continence. Postoperatively, the patients can be categorized into three groups with different treatment options for the management of postoperative problems: *group I* includes patients with poor anatomy, flat bottom, poor-quality muscle, sacral defect, and urinary incontinence. In these cases, muscle transfers and/or definitive colostomy are considered. *Group II* includes patients with good-quality muscle and sacrum but misplaced bowel. In these cases, the option to consider is repositioning of the bowel. Finally, *group III* includes patients suffering from constipation. These patients can be managed with enemas, suppositories, or anterior resection. In contrast, if other major anomalies are present, then the final prognosis depends mainly on the severity of these anomalies.

The prognosis is poor in most cases presenting with multiple anomalies within the broad spectrum of the V(A)CTER(L)–caudal regression syndrome.

INTr A-ABdo MINAL c ys Ts ANd dIFFE r ENTIAL dIAGN os Is

Most of the GI tract is located in the abdominal cavity, which contains the other GI-tract-related structures such as the liver, choledochal system, pancreas, mesentery and omentum, and non-GI-tract-related organs, such as the kidneys, adrenals, spleen, and the ovaries in females. One of the main difficulties in the sonographic examination of the fetal abdomen is to establish the origin of an intra-abdominal cyst detected



Figure 7.19 Choledochal cyst. Axial view of the fetal abdomen showing a choledochal cyst (arrow) located adjacent to the gallbladder.

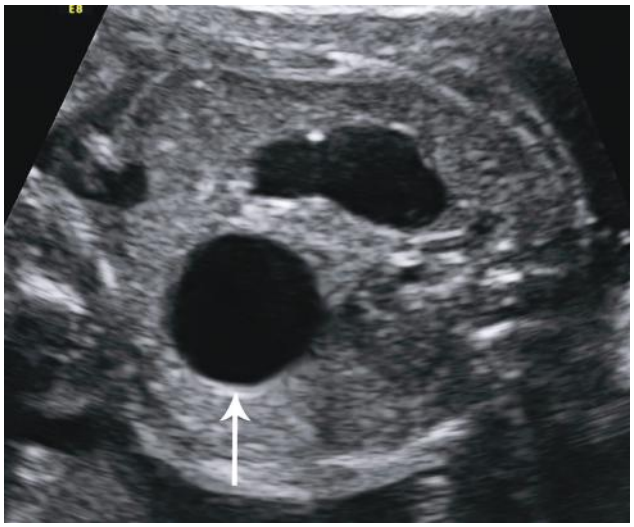


Figure 7.20 Hepatic cyst. Axial view of the fetal abdomen at 26 weeks of gestation showing a hepatic cyst (arrow).

during an examination, which could be any of the structures mentioned here or, moreover, early embryonic structures not normally developed and embryonic abdominal toti-potential cells such as teratomas.

Location, sonographic appearance, associated anomalies, gestational age, and fetal sex provide important information to orient toward a possible diagnosis. In many cases, it will remain difficult to be certain about the origin of the detected mass even until the end of the pregnancy. Topographic assessment of an intra-abdominal cystic mass can be useful to exclude noncompatible hypotheses about its origin or even lead to a diagnostic clue, as in cases of choledochal (Figure 7.19), hepatic (Figure 7.20), splenic (Figure 7.21), or renal cysts; duplex or multicystic kidney; and so on. A topographic approach for differential diagnoses between the most frequent intra-abdominal fetal masses is proposed in Figure 7.9.

Assessment of the fetal sex is mandatory when an abdominal cyst is detected, as some cystic masses are sex related (ovarian cysts or hydrometrocolpos occur exclusively in females) or may present a sex predominance (choledochal cysts are more frequent in female fetuses).

Finally, a cyst may be differentiated by the assessment of its sonographic appearance (shape, echogenicity, or other specific features) and it is mandatory a careful examination to detect other possible associated sonographic findings. The use of color Doppler allows examination of the vascular supply for the intra-abdominal cyst, its anatomic relations with the abdominal blood vessels, and the diagnosis of its possible vascular origin. This is helpful, for instance, in cases of UV varix (Figure 7.22) or hepatic arteriovenous malformation.

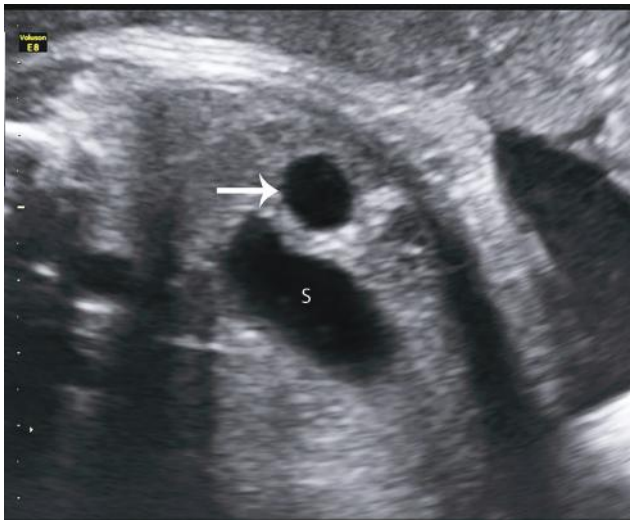


Figure 7.21 Splenic cyst. Axial view of the fetal abdomen at 23 weeks of gestation showing a splenic cyst (arrow). S: stomach.

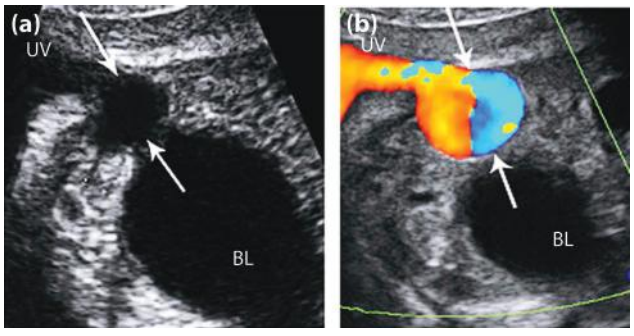


Figure 7.22 (a) Axial view of the fetal abdomen showing an extrahepatic varix (arrows) of the umbilical vein (UV) in a two-dimensional image. Color Doppler image (b) of the umbilical vein varix (arrows). Bl: bladder.

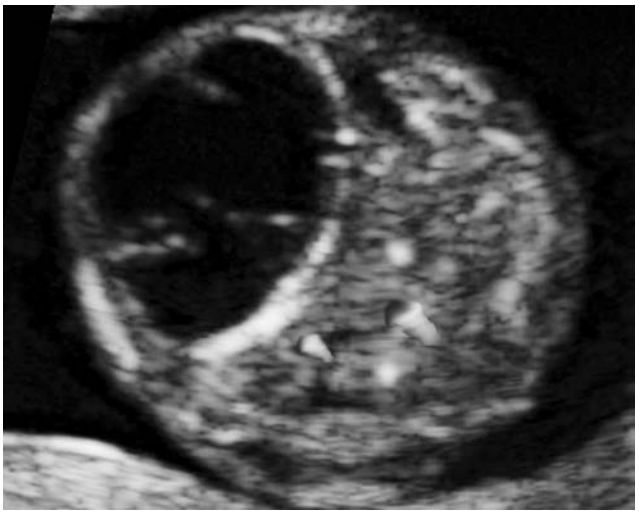


Figure 7.23 Meconium pseudocyst. Axial view of the fetal abdomen showing a cyst with irregular echogenic borders and calcifications of the wall associated to diffuse intra-abdominal calcifications.



Figure 7.24 Duplication cyst. Esophageal duplication cyst. Oblique view of the fetal upper abdomen showing the stomach (S) and a cyst (C) close to the collapsed esophagus (arrows). DA: descending aorta.

MECONIUM PSEUDOCYST

This is not a distinct disease process but a common endpoint for any condition resulting in prenatal bowel perforation. Usually, it has irregular echogenic borders with calcifications of its walls (Figure 7.23), presenting a gradual reduction in size and a contemporary increase of the calcifications in the follow-up scans; it is associated with echogenic foci anywhere in the peritoneal cavity and with bowel dilation. Ascites and polyhydramnios may be also present.

DUPLICATION CYST

Intra-abdominal duplications can be found at any point along the GI tract, as they can originate from any part of it GI tract. It has been proposed that these cysts arise from a failure of separation between the notochord and endoderm, and this may explain their association with vertebral anomalies. These anomalies are either spherical or tubular structures, usually sharing a common wall with the normal GI tract. They may be anechoic (Figure 7.24) or hyperechoic.

The differential diagnosis includes other abdominal cysts, such as choledochal cysts, urachal cysts, ovarian cysts, splenic cysts, renal cysts, and mesenteric cysts, as well as intestinal obstructions.

MESENTERIC CYST

A mesenteric cyst may indicate impaired lymphatic functioning. It is so named because it develops in the mesentery, that area of the peritoneum that encompasses the GI tract.

Mesenteric cysts are commonly found in the small-bowel mesentery and, together with omental and retroperitoneal cysts, often represent lymphangiomas. This cyst is most frequently seen as a unilocular

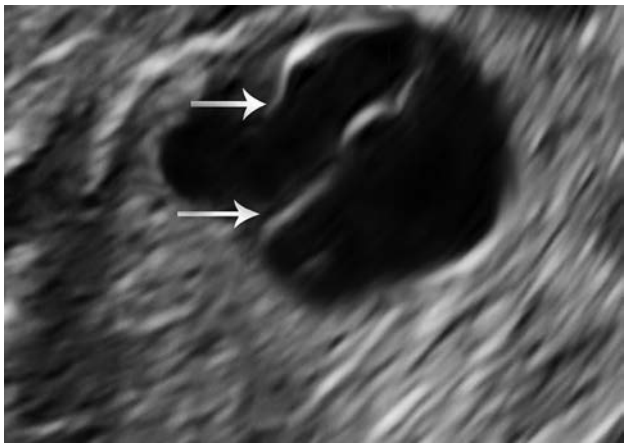


Figure 7.25 Mesenteric cyst. Parasagittal view of a fetal abdomen showing a mesenteric cyst. Several septations (arrows) can be seen within an otherwise anechoic cyst.

(Figure 7.25) or multilocular hypoechogenic cystic mass with variable size and morphology. Sonographic imaging of these lesions shows very thin walls and no peristalsis. The differential diagnosis includes other abdominal cysts, such as choledochal cysts, urachal cysts, ovarian cysts, splenic cysts, and renal cysts, as well as bowel obstructions or duplications.

spLENIc cysT

Congenital splenic cysts are very rare and include serous, vascular, and dermoid cysts; hemangiomas; and lymphangiomas. Approximately 25% of congenital splenic cysts remain of unknown origin. Splenic cysts are commonly observed in the upper left quadrant of the fetal abdomen from 18–20 gestational weeks onwards (Figure 7.21).

The differential diagnosis of fetal splenic cyst can include renal, ovarian, adrenal, duplication, and mesenteric cysts.

cho LEdoch AL cysT

Choledochal cysts are very rare: their incidence in Western countries is around 1 in 100,000, with a 3 to 4:1 ratio between females and males, while a much higher incidence has been observed in Japan, with an equal ratio between sexes.

A recent classification of choledochal cysts has been proposed by Visser et al. [23] in an attempt to simplify the numbering system by introducing a nomenclature that follows a pathogenetic approach that distinguishes four entities: choledochal cyst, choledochocele, choledochal diverticulum, and Caroli disease.

Choledochal cyst is the most frequent antenatally diagnosed type. It is detected as a simple cystic mass in the upper or right upper quadrant of the abdomen near the gallbladder (Figure 7.19). The identification of the biliary ducts leading to the cystic mass could allow a definitive diagnosis of a choledochal cyst. Antenatal detection has been reported from 20 weeks of gestation.

The differential diagnosis includes cystic biliary atresia, hepatic cysts, gallbladder duplication, ovarian cysts, and enteric duplication cysts. In a series of 13 cases of biliary abnormalities, the correct diagnosis was made in only 15%, whereas other types of cystic mass were erroneously defined in the remaining cases. An antenatal differential diagnosis between cystic biliary atresia and choledochal cyst is not feasible, and it remains difficult to distinguish the two conditions even after birth.

For a discussion of renal and ovarian cysts, see Chapter 8.

hypEr EchoIc INTrA-ABdoMINAL MAss

The most common causes of intra-abdominal calcifications include meconium peritonitis, hepatic calcifications, and enterolithiasis.

MEcoNIUM pErIToNITIs

Incidence. Rare. 1/35,000 live births, but higher in utero.

Ultrasound diagnosis. Peritoneal calcifications can appear as a continuous line on the border of the peritoneum, as scattered calcifications throughout the peritoneum, or as a focal calcification with shadowing.

Risk of chromosomal anomalies. Low.

Risk of nonchromosomal syndromes. High if cystic fibrosis is considered as a syndrome.

Outcome. In the presence of simple peritonitis, generally the outcome is good and surgical intervention is not necessary. In cases of complex peritonitis, the outcome is more guarded.

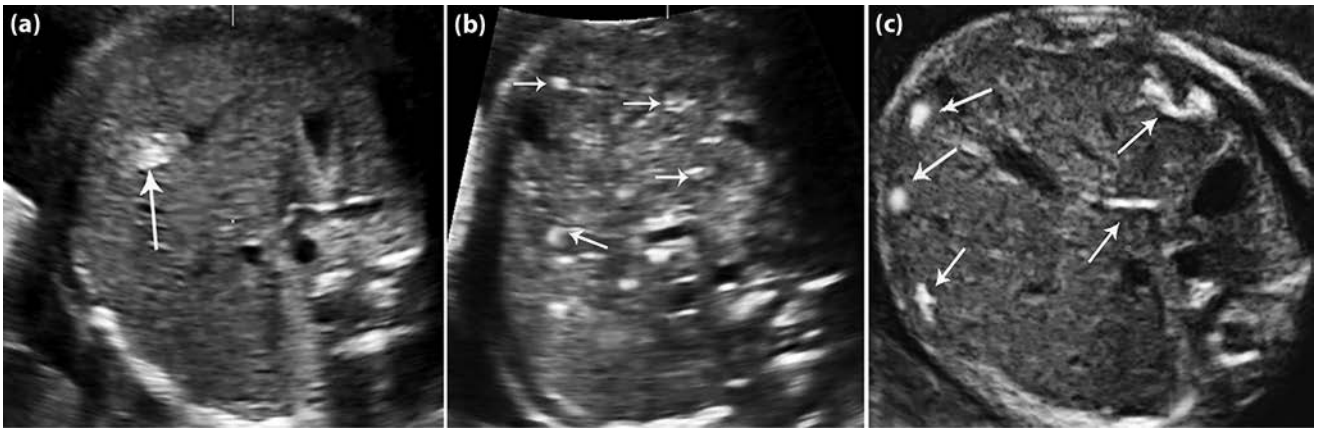


Figure 7.26 Hepatic calcifications. Axial view of the fetal abdomen showing (a) an isolated intrahepatic calcification (arrow); (b) multiple intraparenchymal calcifications (arrows) due to a varicella infection; and (c) multiple calcifications (arrows) along the liver capsule due to meconium peritonitis.

Definition Meconium peritonitis is a common endpoint for any conditions that result in prenatal bowel perforation. It is a rare condition, with an incidence of 1 in 35,000 live births. The peritonitis can be diffuse or localized, and can lead to a fibrotic reaction with intraperitoneal calcification Sometimes a fibrous wall may form around the leaked meconium, creating a pseudocyst. Ascites and polyhydramnios can be associated. However, in certain cases, the perforation heals spontaneously.

Etiology and pathogenesis. The etiology of meconium peritonitis includes bowel atresia, meconium ileus, gastroschisis, volvulus, intussusceptions, internal intestinal hernia, and intrauterine fetal infections, especially CMV and parvovirus B19. However, in some cases, the cause of meconium peritonitis cannot be identified because spontaneous healing of the perforation occurs in utero.

Ultrasound diagnosis. It has been proposed to classify meconium peritonitis into two types: simple and complex. The former is diagnosed only if peritoneal calcifications are seen (Figure 7.26a); and the latter when peritoneal calcifications are associated with ascites, a meconium pseudocyst (Figure 7.23), and/or bowel dilation (Figure 7.15b). For these reasons, the sonographic findings can be represented by either isolated intra-abdominal calcifications or a combination of these calcifications associated with a spectrum of other sonographic findings already mentioned [24]. Extraluminal abdominal calcifications can appear as a continuous line on the border of the peritoneum, as scattered calcifications throughout the peritoneum, or as a focal calcification with shadowing

Differential diagnosis. This should include all other conditions featuring intra-abdominal calcifications, such as hepatic calcifications and enterolithiasis. Hepatic calcifications can be divided into three categories: peritoneal, vascular, and parenchymal.

In contrast to vascular and parenchymal calcifications, peritoneal hepatic calcifications are usually due to meconium peritonitis.

Enterolithiasis is characterized by calcifications within the bowel lumen, whereas in meconium peritonitis the calcifications are outside the lumen, within the visceral or parietal peritoneum.

Prognostic indicators. The presence of other sonographic findings associated with calcifications such as bowel dilation, ascites, or pseudocyst in the case of complex peritonitis, represents a bad prognostic sign. Sometimes, simple meconium peritonitis can evolve into a complex case. If there is associated meconium ileus, this is itself a poor prognostic sign due to its strong association with cystic fibrosis

Association with other malformations. The association with extra-GI tract malformations is low.

Risk of chromosomal anomalies. This is low.

Risk of nonchromosomal syndromes. This is high if cystic fibrosis is considered as a syndrome. The incidence of cystic fibrosis in neonatal meconium peritonitis ranges from 15% to 40%. It is less frequent in fetal series. In cases of simple peritonitis, it is uncommon.

Obstetric management. Once a diagnosis of intra-abdominal calcifications is made, a pertinent laboratory workup should be requested to establish the underlying pathologic process, which includes infections (especially CMV or parvovirus B19) or meconium ileus due to fetal cystic fibrosis If the above workup yields negative

results, the most likely diagnosis is bowel obstruction from small bowel atresia, volvulus, internal intestinal hernia, or intussusceptions [22].

Postnatal therapy. In cases of complex peritonitis, such as bowel dilation or pseudocyst, surgical intervention is usually required at birth.

Prognosis, survival, and quality of life. In cases of simple peritonitis, generally the outcome is good and surgical intervention is not necessary. In cases of complex peritonitis, such as bowel dilation, ascites, or pseudocyst, the outcome is more guarded, surgical intervention may be required at birth, and the risk increases with the number of associated findings detected

hEpATIc cALcIFIcATIoNs

Incidence. Infrequent.

Ultrasound diagnosis. One or more calcified foci can be visualized, or even a diffuse calcification of the liver or of its peritoneum.

Risk of chromosomal anomalies. Low if the calcifications are isolated.

Risk of nonchromosomal syndromes. Low if the calcifications are isolated.

Outcome. Good if the maternal serology is negative, the fetal karyotype is normal, and no other fetal anomalies are associated.

Definition Hepatic calcifications may represent a transient phenomenon without any clinical consequences, or they may be the epiphenomenon of an underlying pathology. They can be divided, as mentioned in the "Meconium Peritonitis" section, into three main categories: peritoneal, parenchymal, and vascular (Figure 7.26).

Etiology and pathogenesis. Peritoneal hepatic calcifications are commonly due to meconium peritonitis. Parenchymal calcifications are usually due to the presence of either an intrauterine infection (rubella, CMV, and herpes simplex virus 2; parvovirus and varicella-zoster virus) or a tumor. Hepatic calcifications due to vascular abnormalities result from thromboembolism of hepatic and portal veins.

Ultrasound diagnosis. One or more calcified foci (Figure 7.26a and b) can be visualized, or even a diffuse calcification of the liver (Figure 7.26b) or of its peritoneum (Figure 7.26c).

Differential diagnosis. In cases of hepatic calcification their location and a pertinent laboratory workup may allow one to make the correct diagnosis. Peritoneal hepatic calcifications located on the surface of the liver are commonly associated with meconium peritonitis. Calcifications spread throughout the liver parenchyma (Figure 7.26b) are the result of more widespread ischemia and necrosis that may occur consequently to fetal infections. When calcifications are located within the bowel lumen, enterolithiasis is the most common cause.

Prognostic indicators. The final prognosis depends mainly on the cause of the hepatic calcifications

Risk of chromosomal anomalies. Low in cases of isolated hepatic calcifications

Risk of nonchromosomal syndromes. Low in cases of isolated hepatic calcifications

Obstetric management. Once a diagnosis of hepatic calcifications is made, a detailed sonographic evaluation of the fetal anatomy is recommended. A pertinent laboratory workup should be requested to establish the underlying pathologic process, which includes infections or, in cases of associated meconium ileus, cystic fibrosis mutation testing

Because of the reported associations with aneuploidy, amniocentesis should be offered when other fetal anomalies are present.

Postnatal therapy. In cases of isolated calcification no surgical intervention may be required.

Prognosis, survival, and quality of life. If the maternal serology is negative, the fetal karyotype is normal, and no other fetal anomalies are associated (including meconium ileus and an intrahepatic or adrenal gland mass), the overall prognosis for the fetus is good.

ENTEROLITHIASIS

Incidence. Rare.

Ultrasound diagnosis. Dilated bowel loops associated with multiple endoluminal small calcifications.

Risk of chromosomal anomalies. High.

Risk of nonchromosomal syndromes. High.

Outcome. Poor: mostly attributed to associated anomalies.

Definition Enterolithiasis is a rare US finding characterized by the presence of multiple calcifications of the intraluminal meconium.

Etiology. It has been reported that both the prolonged stasis of the meconium and the interaction between urine (due to the presence of rectourethral fistula) and meconium play significant roles in the pathogenesis of enterolithiasis. However, it can occur in the absence of a rectourethral fistula as a result of stasis and low intraluminal pH [21]

Ultrasound diagnosis. This is based upon recognition of dilated bowel loops associated with multiple endoluminal small calcifications (Figure 7.16b and c). Urinary tract dilation also can be present.

Differential diagnosis. The differential diagnosis with meconium peritonitis is possible. In fact, in contrast to meconium peritonitis, enterolithiasis is characterized by calcifications within the bowel lumen; in meconium peritonitis, the calcifications are outside the lumen, within the visceral or parietal peritoneum, and often linear or curvilinear on the border of the peritoneum. In recto-anal atresia, the calcifications are usually located in the lumen of the colon, and are possibly associated with rectourethral fistula

Prognostic indicators. The presence of the most severe forms of anorectal malformation, such as cloacal malformation, represents a poor prognostic sign.

Association with other malformations. It is commonly associated with anorectal malformations; however, small-bowel atresia or stenosis and Hirschsprung disease association have been reported.

Risk of chromosomal anomalies. This is high because of the association with anorectal malformations.

Risk of nonchromosomal syndromes. This is high because of the association with anorectal malformations.

Obstetric management. Should enterolithiasis, which is associated with an anorectal malformations, be diagnosed in a fetus, karyotyping is recommended, because of the considerable risk of chromosomal anomalies. With regard to perinatal management, it should be noted that the risk of preterm delivery can be increased, in case of the occurrence of late-onset polyhydramnios. The delivery should be planned in a tertiary referral center.

Postnatal therapy. The postnatal workup should include adequate gastrointestinal and urologic studies to help delineate the underlying etiology and the presence of a rectourethral fistula a persistent cloaca, an imperforate anus, or intestinal atresia.

Prognosis, survival, and quality of life. Prenatal diagnosis of enterolithiasis carries a severe prognosis [21]. It is a warning sign for large-bowel obstruction, often due to anorectal malformations, with or without enterourinary fistula There is a significant mortality rate in the reported cases, mostly attributed to associated anomalies, and all the survivors require neonatal surgery.

HEPATOMEGALY AND SPLENOMEGALY

Incidence. Rare; often due to severe fetal infections.

Ultrasound diagnosis. Enlarged liver or spleen.

Risk of chromosomal anomalies. Low, except for the myeloproliferative disease typical of trisomy 21.

Risk of nonchromosomal syndromes. Relatively low. Hepatomegaly can be associated with the Beckwith–Wiedemann and Zellweger syndromes.

Outcome. Depends on the underlying cause.

Definition Hepatomegaly is defined as an increased volume of the liver. Similarly, splenomegaly refers to an increased volume of the spleen. They may be associated or occur independently.

Etiology and pathogenesis. The etiology of *hepatomegaly* comprises a wide spectrum of causes. *Intrauterine fetal infections* are among the most common causes of hepatomegaly. CMV infection, when severe, is commonly associated with hepatosplenomegaly. The well-known myeloproliferative disease associated with Down syndrome may be responsible, in some cases, for moderate to severe hepatomegaly. Also, rare benign and malignant hepatic tumors, such as hemangioma or hepatoblastoma, may induce hepatomegaly. It should also be noted that the hepatomegaly due to venous congestion is often present in those cardiac and extracardiac conditions possibly causing heart failure. In fact, the first step of cardiac failure in the fetus is an increase in central venous pressure, which in turn causes venous congestion in the liver, due to the fact that because of the patency of the two shunts (foramen ovale and ductus arteriosus), all increases in cardiac pressure are reflected in the right heart. Finally, there are two very rare syndromic conditions, the Beckwith–Wiedemann and Zellweger syndromes, which can be associated with hepatomegaly.

Fetal infections are also the primary cause of splenomegaly, with or without hepatomegaly. In particular, CMV infection, when severe, is typically associated with splenomegaly, as well as hepatomegaly and ascites, in addition to other signs of infection (CNS calcifications, etc.). Other rather unusual causes of late-onset splenomegaly are storage diseases, such as the Gaucher and Niemann–Pick syndromes, which, in the late third trimester, may lead to splenomegaly.

Ultrasound diagnosis. If the enlargement of the spleen and/or liver is severe, the diagnosis of these conditions is straightforward, because the two organs will occupy most of the abdomen. The recognition of hepatomegaly and splenomegaly is made even simpler if ascites, which acts as an intra-abdominal contrast medium, is associated (Figures 7.27 and 7.28). If hepatomegaly is very pronounced, the prominence of the liver deforms the anterior abdominal wall, causing a dip at the thoracoabdominal junction, similarly to what happens in cases of severe thoracic hypoplasia, although in this case it is the abdomen that is enlarged rather than the thorax that is hypoplastic (Figure 7.27). Nomograms of the maximum diameters of the liver and the spleen have been published [25] and are shown in the Appendix Table A.21 and A.22. Nomograms giving liver and

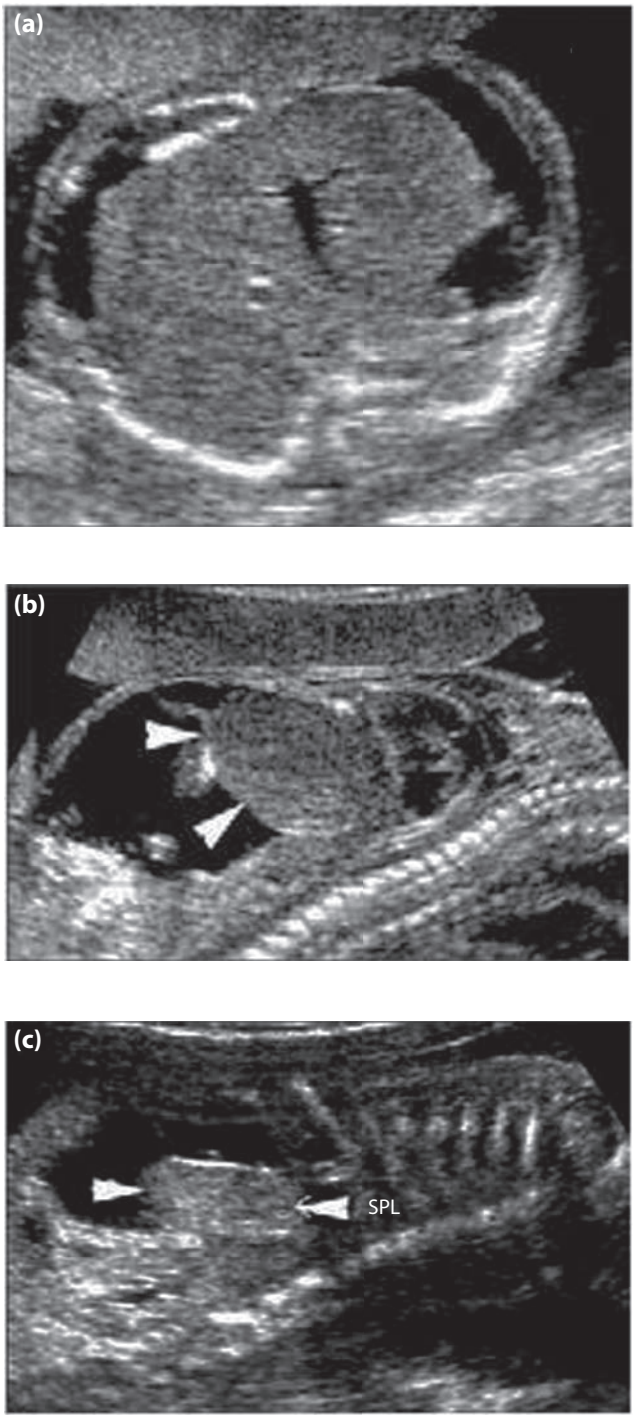


Figure 7.27 Hepatomegaly. This patient had serologically confirmed hepatitis A infection in the first trimester. At 19 weeks, ultrasound demonstrated the following: (a) Axial view: evident hepatomegaly, with capsular macrocalcification and moderate ascites. (b) Left parasagittal view: ascites and moderate enlargement of the left hepatic lobe (LL; arrowheads) are shown; in such a situation, the left hepatic lobe should not be mistaken for the spleen, which was normal in this case. (c) Spleen (SPL and arrowheads).

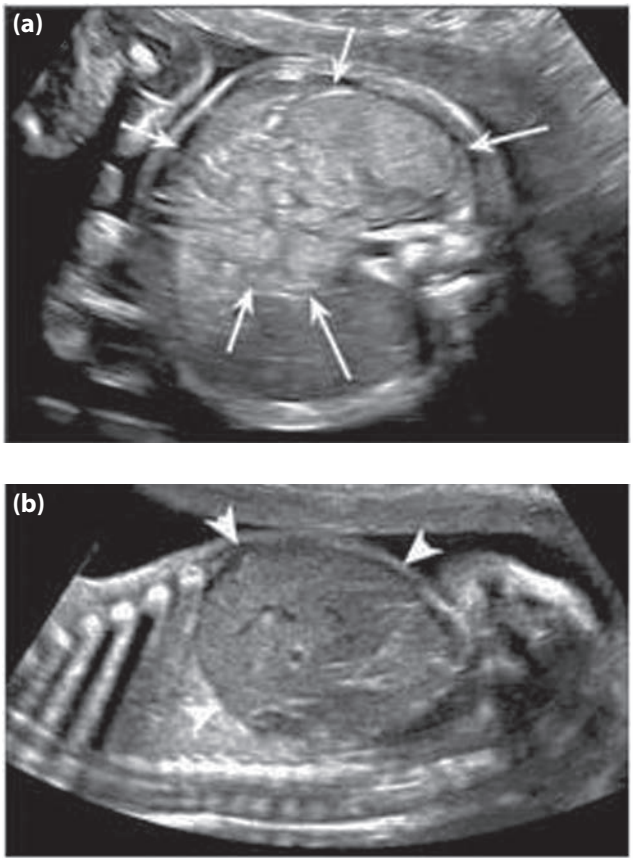


Figure 7.28 Severe hepatomegaly due to CMV infection. (a) On the axial view of the upper abdomen, it is possible to recognize the enlarged, hyperechoic, and rather inhomogeneous liver (arrows). (b) On the right parasagittal view, the degree of hepatomegaly is easily evaluated, and the prominence of the abdomen in comparison with the normal thorax is evident (arrowheads).

spleen volumes versus gestational age have been published, due to the widespread use of 3D US. However, we feel that the measurement of the two cross-sectional diameters of the viscera remains easier and faster (Figure 7.29). It should be underlined that, especially in the case of CMV infection, the involvement of the spleen is predominant (Figure 7.30).

Differential diagnosis. Virtually nonexistent. Care needs only be taken not to mistake the left hepatic lobe, which is larger in utero than in postnatal life, for the spleen.

Prognostic indicators. Clearly, the final prognosis depends mainly on the cause of the hepatomegaly and splenomegaly. If other signs of severe fetal infection, such as cerebral calcification or ascites, are present, then these are highly indicative of a poor prognosis.

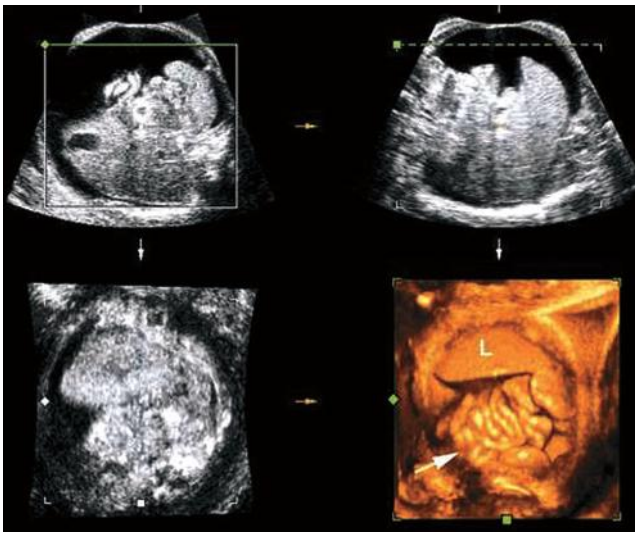


Figure 7.29 Hepatomegaly. The simultaneous presence of ascites acts as a natural contrast medium, allowing 3D ultrasound (surface rendering) to visualize the enlarged liver (L), the spleen (on the left), and the bowel (arrow). However, in this case, the diagnostic role of 3D imaging is limited.

Association with other malformations. The enlargement of the liver and/or the spleen does not itself represent a malformation; it is rather an acquired lesion due to environmental factors (e.g., infections).

Risk of chromosomal anomalies. This is virtually absent except for the already-mentioned myeloproliferative disease that, in a minority of Down syndrome fetuses, leads to evident hepatomegaly.

Risk of nonchromosomal syndromes. This is relatively low. Hepatomegaly can be associated with the following:

- *Beckwith–Wiedemann syndrome*: look for ► *hepatomegaly* + omphalocele + body hemihypertrophy + macroglossia (Chapter 10);
- *Zellweger syndrome*: look for ► *hepatomegaly* + polycystic kidney + agenesis of the corpus callosum.

Obstetric management. Should hepatomegaly or splenomegaly be diagnosed in a fetus, the first issue to consider is a possible infective cause. Therefore, a careful interview with the mother with the aim of disclosing any possible infectious episodes, which in most cases are also simple flulike events, should be carried out. Maternal serologic evidence of recent CMV or other hepatotropic infections should be sought. In addition, a thorough US assessment searching for additional signs of fetal infection (cerebral calcification hydrocephalus, ascites, and cardiomegaly (myocarditis) should be performed by an expert.

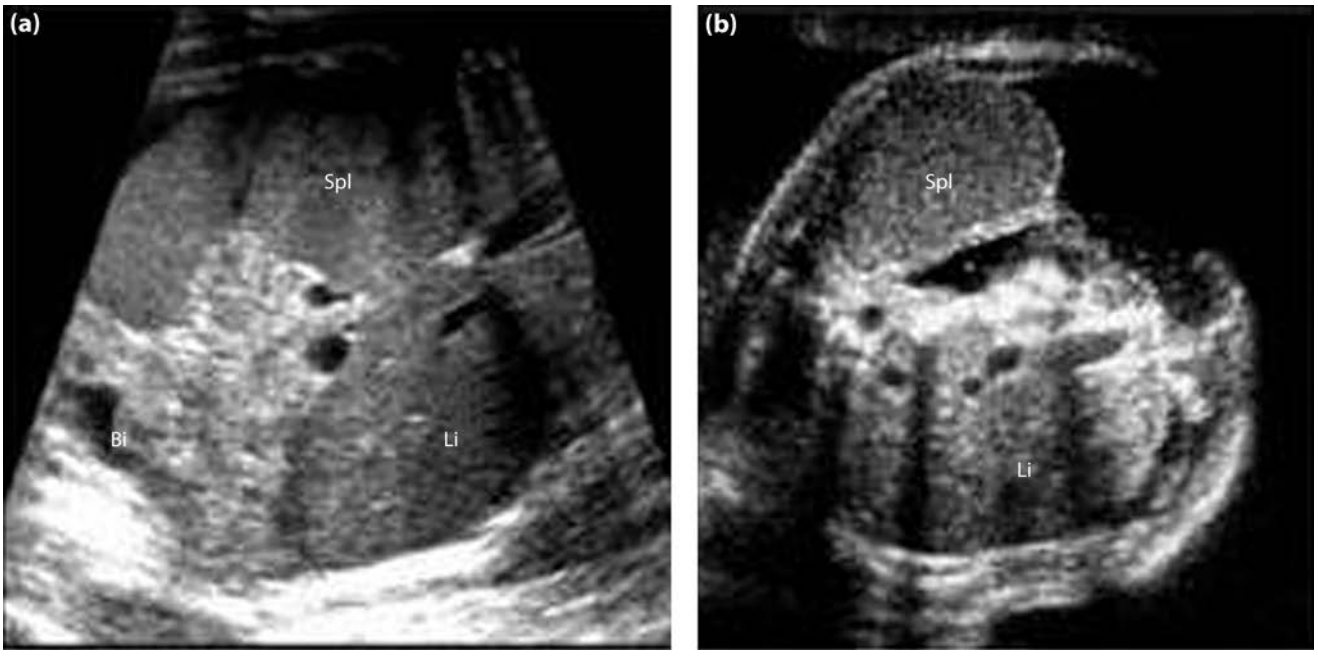


Figure 7.30 Splenomegaly in two cases of severe fetal CMV infection. (a) On the coronal view, at 37 weeks of gestation, it is possible to recognize the severely enlarged spleen (Spl), the lower pole of which reaches the bladder (Bl) and a concurrent similarly severe hepatomegaly (Li). (b) A similar case, at 36 weeks of gestation, showing severe hepatosplenomegaly, ascites, and intra-abdominal calcifications. Both neonates died of widespread CMV infection.

Despite the fact that only a minority of Down syndrome fetuses present hepatosplenomegaly, a karyotyping should be recommended in those cases in which all other causes have been excluded.

Postnatal therapy. This is directly related to the underlying cause of the hepatomegaly or splenomegaly.

Prognosis, survival, and quality of life. The prognosis of the hepatomegaly or splenomegaly also depends on its cause. Storage diseases are usually lethal within a few months or years of life. In cases due to intrauterine infections, the neonatal outcome will depend upon the type of infection and on its severity. In cases of CMV infection, fetal involvement may range from a limited hepatitis of moderate severity to very important sequelae such as hearing loss or neurologic damage. Early perinatal demise may also occur in severe CMV infection.

UMBILIc AL, por TAL, ANd hEpATIc V ENo Us sys TEMs

The venous perfusion of the liver in utero is substantially different from the one after birth. While postnatally all venous blood is supplied by the portal vein, during fetal life the liver receives venous blood from both the portal and UVs. In fact, the venous perfusion of the fetal liver is supplied by two embryologically and functionally different blood systems: the umbilical and the portal-vitelline systems.

The UV enters the fetal abdomen within the falciform ligament, ascending steeply toward the liver. It enters the liver anteriorly and runs along its inferior surface in a cephalad direction. It then joins a confluence of vessels named the portal sinus (PS). The PS is a wide L-shaped vessel at the terminal end of the UV, connecting two main vessels (the right and left intrahepatic portal veins) perfusing the right and left hepatic lobes (i.e., the "afferent venous system"; Figure 7.31a). While 20% to 30% of the umbilical venous blood leaves the intra-abdominal UV and enters the PS to reach the ductus venosus (DV), the fetal liver receives the remaining 70% to 80% of the venous return from the placenta. There are a number of vessels arising from the left and right hepatic lobes converging into the three main (right, middle, and left) hepatic veins (the "efferent venous system"; Figure 7.31b). The right, middle, and left hepatic veins appear to have the same caliber. They join the inferior vena cava (IVC) (Figure 7.31b) and the DV in the subdiaphragmatic vestibulum, an inverted funnel-shaped vascular space just below the diaphragm.

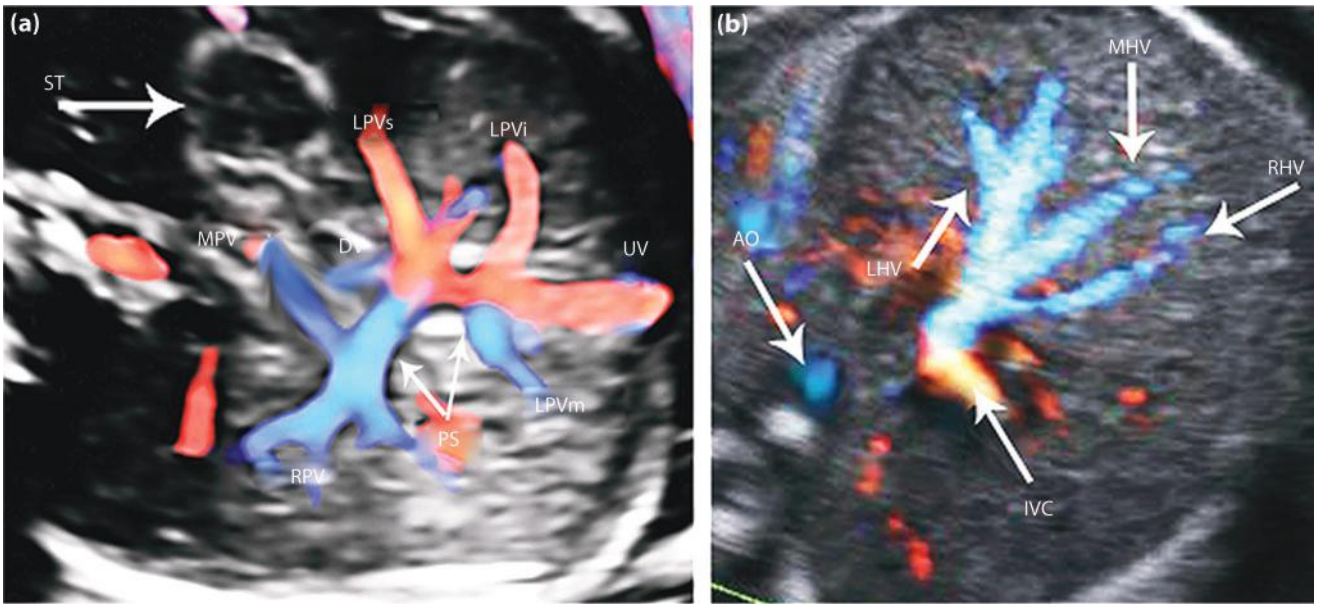


Figure 7.31 Transverse fetal abdominal sections at 23 weeks of gestation, showing details of a normal umbilical-portal venous system. (a) Afferent venous system: three-dimensional ultrasound using render mode with glass body showing how the umbilical vein (UV) joins the left portal vein (LPV), dividing into three branches: the inferior (LPVi) and superior (LPVs) branches, which supply the left lobe, and the medial branch (LPVm). The LPV continues as the L-shaped portal sinus (PS). The ductus venosus (DV) emerges just before the LPV turns to the right to continue as the right portal vein (RPV). The main portal vein (MPV) is seen joining the portal sinus (PS) from left to right. Ao: aorta; St: stomach. (b) Efferent venous system: color flow map of the fetal abdomen and thorax showing the three main (right, middle, and left) hepatic veins arising from the left and right hepatic lobes joining the inferior vena cava (IVC) in the subdiaphragmatic vestibulum. The vestibulum continues through the diaphragm and joins the right atrium. LHV: left hepatic vein; RHV: right hepatic vein; MHV: middle hepatic vein; AO: descending aorta.

The vestibulum continues through the diaphragm and joins the right atrium.

The fetal DV is a slender trumpet-like shunt, connecting the intra-abdominal UV to the IVC (Figure 7.32a) at its inlet to the heart.

As the well-oxygenated blood from the DV is loaded with the highest kinetic energy in the IVC, it will predominantly be this blood that presses and opens the foramen ovale valve to enter the left atrium, thus forming the "preferential streaming" of the *via sinistra*.

UMBILICAL AND PORTAL VENOUS SYSTEMS MALFORMATIONS

AGENESIS OF DUCTUS VENOSUS

Incidence. Agenesis of ductus venosus (ADV) is an infrequent anomaly.

Ultrasound diagnosis. The diagnosis of ADV is established by color Doppler demonstration of an absence of DV in optimal scanning planes for the visualization of ductal blood flow.

Risk of chromosomal anomalies. High, if associated with other anomalies.

Risk of nonchromosomal syndromes. High, if associated with other anomalies.

Outcome. When chromosomal abnormality, structural abnormality, and effusion or hydrops are excluded, ADV may not be associated with an increased risk of adverse outcome.

Definition and anatomy. As described above, the fetal umbilical–portal venous system (UPVS) is derived from two different embryological precursors, the portal-vitelline and UVs. It comprises the portal system, the UV, and the DV. In recent years, improvements of color Doppler technology and increasing interest in the fetal venous systems have enabled extensive investigation of fetal venous anomalies [26–30], leading to greater

insight into prenatal diagnosis of the different types of UPVS malformations, and a better understanding of their pathophysiology and clinical implications.

These anomalies often affect the hemodynamics of fetal circulation and, in particular, the DV that shunts well-oxygenated blood through the foramen ovale toward the left atrium and left ventricle, and to the fetal cerebral and coronary circulation.

Two different routes for umbilical venous return have been described in fetuses with ADV:

- Extrahepatic umbilical venous drainage bypassing the liver [27–30]: the UV directly connects to the iliac vein, the IVC, the renal vein, the right atrium, or the coronary sinus;
- Intrahepatic umbilical venous drainage without liver bypass [27–30]: the UV connects to the PS in its usual way without giving rise to the DV.

In a certain number of the aforementioned cases, it is possible to find a partial or total congenital agenesis of the portal venous system (CAPVS—a rare anomaly, in which the portal blood bypasses the liver, completely or in part, through a splenomesenteric shunt to the systemic circulation) [27–30]. In cases of extrahepatic umbilical venous drainage, it also has been reported that the development of a portal system may be related to the dimensions of the shunt at the point of UV connection [29]. When this connection is wide (and its diameter may equal that of the UV), this may lead to incomplete or anomalous development of the portal system.

Etiology and pathogenesis. During the fifth week of gestation in normal embryonic development, the embryonic venous system has three pairs of veins running into the cardiac sinus: the cardinal veins, the UVs (bringing the blood from the trophoblast), and the vitelline or omphalo-mesenteric veins (taking the blood from the yolk sac to the fetal heart). Development of the liver plays a role in modifying the primitive vitelline and umbilical systems to their final form. In fact, the vitelline veins (VVs) and UVs connect to the liver before entering the sinus venosus. During their course through the liver, they are interrupted by the hepatic sinusoids and linked to them. The right UV and the part of the left UV between the liver and the sinus venosus disappear, and the remaining part of the left UV carries all the blood from the placenta to the fetus. The portal vein develops from three main anastomoses between the VVs at the caudal end of the liver; gradually, these anastomoses form the portal vein, which passes dorsal to the duodenum and branches to form the splenic vein and mesenteric vein, which run ventral to the duodenum. Thus, the VV anastomoses around the gut are established, and the portal vein anlage is present at the 35-day stage, connected to the superior mesenteric vein and emptying into the left UV in the liver. The left proximal and right distal VVs disappear.

A direct communication between the left UV, the IVC, and the DV, bypassing the liver sinusoids, is later established. The DV links the portal and umbilical venous circulation with that of the IVC. Failure of this obliteration of primitive veins or nondevelopment of new vessels and anastomoses can produce abnormalities of umbilical-portal circulation (e.g., CAPVS), often associated with ductal agenesis.

Ultrasound diagnosis. The diagnosis of ADV is established by color Doppler demonstration of an absence of DV in the optimal scanning planes for the visualization of ductal blood flo .

- In cases of extrahepatic umbilical venous drainage bypassing the liver, the UV directly connects to the iliac vein, the IVC, the renal vein, the right atrium (Figure 7.32b) or left atrium, or the coronary sinus;
- In cases of intrahepatic umbilical venous drainage without liver bypass, the UV connects to the PS without giving rise to the DV (Figure 7.32c).

While ADV with extrahepatic umbilical venous drainage could be detected by visualization of the aberrant course of the intra-abdominal UV on grayscale sonography, ADV without liver bypass is only reliably diagnosed by detailed evaluation by color Doppler of the umbilico-portal circulation.

Differential diagnosis. Virtually nonexistent.

Prognostic indicators. Association with structural and chromosomal anomalies, which is fairly common, represents the most important poor prognostic sign. In cases without structural and chromosomal anomalies associated, the presence of hydrops represents the most important poor prognostic sign.

Associated anomalies. ADV is significantly associated with other anomalies, especially fetal hydrops, congenital heart defects, and gastrointestinal defects [27–30]. An association with Noonan syndrome also has been described, and mutations of the PTPN11 gene can be detected in some affected individuals. Fetuses with liver bypass have an additional risk of developing congestive heart failure, which can affect the outcome, even in those with otherwise normal fetal anatomy.

In addition, the association with partial or total agenesis of the portal venous system has been reported [30]. However, because prenatal diagnosis

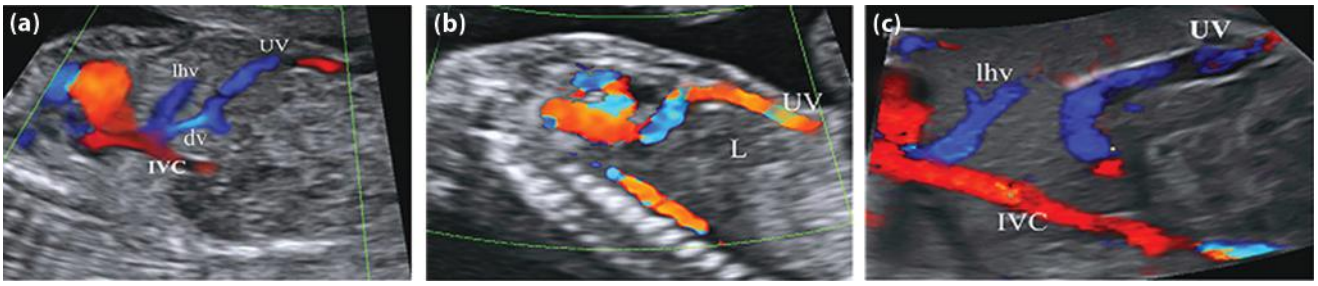


Figure 7.32 (a) Color flow map of the fetal abdomen and thorax in a sagittal view at 24 weeks of gestation. The fetal ductus venosus (dv) can be clearly seen joining the inferior vena cava (IVC). UV: umbilical vein; lhv: left hepatic vein. (b) Color flow map of the fetal abdomen and thorax in a median sagittal view at 23 weeks of gestation in a fetus with agenesis of ductus venosus and extrahepatic umbilical venous drainage to the right atrium. UV: umbilical vein; L: liver. (c) Color flow map of the fetal portal circulation in a sagittal view at 30 weeks of gestation in a fetus with agenesis of ductus venosus and intrahepatic umbilical venous drainage. No connection between the umbilical vein and the inferior vena cava (IVC) can be demonstrated. UV: umbilical vein; lhv: left hepatic vein.

of CAPVS is difficult, most reported cases of CAPVS appear only in the pediatric literature. For this reason, it is unknown what proportion of CAPVS is associated with ADV.

Risk of chromosomal anomalies. High, if associated with other anomalies (especially trisomies 21 and 18 and Turner syndrome).

Risk of nonchromosomal syndromes. High, if associated with other anomalies.

- *Noonan syndrome*: look for ► *ADV* + congenital heart disease (CHD) + cystic hygroma + facial anomalies + fetal growth retardation (Chapter 10);
- *Isomerism*: look for ► *ADV* + duplication of structures typical of one side of the body on the other side + CHD + gastrointestinal anomalies.

Obstetric management. Although knowledge of the mechanisms involved in the genesis of these anomalies is limited, in cases of prenatal diagnosis of DV agenesis, fetal karyotyping, is recommended especially if associated with other anomalies, due to the important association with aneuploidies. Careful serial sonographic evaluation of the fetal anatomy (including the entire UPVS) should be recommended, and, in the presence of severe heart failure, delivery may need being anticipated.

Postnatal therapy. In some cases, a persistent postnatal porto-systemic shunt may require the placement of an occlusion device.

Prognosis, survival, and quality of life. When chromosomal abnormality, structural abnormality, and effusion or hydrops are excluded, the ADV may not be associated with an increased risk of adverse outcome. Hydrops (and cardiac failure) has been reported, especially in association with extrahepatic bypass due to hemodynamics (hyperdynamic circulation) as combined cardiac output is markedly elevated in some cases of extrahepatic shunt [26]. However, the strong association with genetic and chromosomal anomalies in which abnormalities of the lymphatic system are present may play a role in the pathogenesis of hydrops in these cases. The clinical significance of CAPVS has to be better understood as the fetal cases described so far are still few [30]. However, it seems that in contrast to complete CAPVS, partial CAPVS may have an almost normal outcome.

UMBILICAL VEIN VARIX

Incidence. Relatively frequent: about 1:1000.

Ultrasound diagnosis. A sonographic anechoic cyst is seen between the abdominal wall and the lower liver edge. Color, power, and pulsed Doppler examination indicate umbilical venous flow within the cystic intra-abdominal mass.

Risk of chromosomal anomalies. Low, if isolated.

Risk of nonchromosomal syndromes. Low, if isolated.

Outcome. When the diagnosis of fetal umbilical vein varix is made after 26 weeks and the varix is isolated, the outcome is usually good.

Definition Fetal umbilical vein varix is a focal dilation, usually involving the intra-abdominal part of the vein, with an incidence in utero of about 1:1000.

Etiology. An umbilical vein (UV) varix is a developmental rather than an embryologic anomaly. The extrahepatic intra-abdominal portion of the UV has the weakest supporting structure of the whole umbilical circulation. Therefore, any condition that increases venous pressure could potentially dilate this portion of the UV, resulting in an UV varix.

Ultrasound diagnosis. This anomaly is diagnosed when a sonographic anechoic cyst is seen between the abdominal wall and the lower liver edge (Figure 7.22a). Color, power, and pulsed Doppler examination indicate umbilical venous flow within the cystic intra-abdominal mass (Figure 7.22b). The UV is considered dilated when the measurement is above two standard deviations of the mean for gestational age. The maximum diameter of most of the varices ranges between 10 and 15 mm.

Differential diagnosis. Several differential diagnoses can be considered when US examination reveals an intra-abdominal cystic mass. However, if flow is noted on Doppler US examination, the suspicion of a nonvascular structure (choledochal cyst, hepatic cyst, mesenteric cyst, or enteric cyst duplication) can be excluded.

Prognostic indicators. When the diagnosis of umbilical vein varix is made before 26 weeks [31], increased incidences of fetal death and obstetrical complication have been reported.

Associated anomalies. Associated abnormalities are reported in about 32% of cases, most commonly anomalies of the cardiovascular system and chromosomal abnormalities.

Risk of chromosomal anomalies. A recent publication reports that the overall incidence of aneuploidies is about 10%, the majority being trisomy 21 or 18; in all except one reported case, associated sonographic abnormalities were present [31].

Risk of nonchromosomal anomalies. Syndromal abnormalities were present in two of 91 cases reported in the literature [31]. In both cases, associated structural abnormalities were present.

Management. In the presence of UV varix, fetal echocardiography and detailed US study of fetal anatomy are needed to exclude associated anomalies. Karyotyping should be offered when additional fetal abnormalities are detected. Serial US scans should be performed to assess fetal cardiac function, using color Doppler in order to exclude thrombosis of the UV.

Prognosis, survival, and quality of life. When other associated anomalies are present, nearly 30% of cases have a normal outcome [31]. In isolated cases, the prognosis is better: in 75% of cases, no clinical fin - ings are associated. However, 8.1% of cases result in intrauterine death with no specific cause [31]. The risk of fetal death and obstetrical complications is higher if the diagnosis of FUV varix is made before 26 weeks. The outcome seems to be much better if FUV varix is detected later in pregnancy.

pErs IsTENT r IGhT UMBILIc AL VEIN (pr UV)

Incidence. Relatively frequent: 1:500/1200.

Ultrasound diagnosis. Sonographic finding of the umbilical vein curving to the left toward the stomach, usually connecting to the right portal vein rather than to the left portal vein.

Risk of chromosomal anomalies. Low, if isolated.

Risk of nonchromosomal syndromes. Low, if isolated.

Outcome. Good, if isolated.

Definition and Incidence. Persistent right umbilical vein (PRUV) is a relatively common variation in which the left UV becomes occluded and the right vein persists, remaining patent. It can be intra- or extrahepatic. The former is much commoner (about 95% of cases). The prevalence of PRUV ranges from 1:526 to 1:1228 [32].

Etiology. The right UV starts obliterating around the fourth week of pregnancy, and it disappears by the seventh week of gestation. Its persistence does not alter the blood flow distribution to the fetus. In the vast majority of cases, it replaces the left UV; in a few cases, it is found as a supernumerary vein. Thromboembolic events arising from the placenta may induce PRUV.

Ultrasound diagnosis. The US appearance is characteristic, with the UV curving to the left and toward the stomach, usually connecting to the right portal vein

rather than to the left portal vein. The gallbladder will be on the left of the UV (between the stomach and the UV) (Figure 7.33). In some cases, it may bypass the liver and portal system (extrahepatic type) and may abnormally drain into the IVC or directly into the fetal heart.

Differential diagnosis. Virtually nonexistent.

Prognostic indicators. Associated anomalies and abnormal draining (extrahepatic type of PRUV) into the fetal heart or IVC represent bad prognostic signs.

Associated anomalies. PRUV is associated with other anomalies in about 25% of cases [32]. When the course of PRUV is extrahepatic, an associated abnormality is usually present. Gastrointestinal malformations, heart anomalies, urinary tract malformations, and single umbilical artery have been reported in association with PRUV.

Risk of chromosomal anomalies. When associated with other anomalies, an underlying chromosomal abnormalities in 8% of cases has been reported.

Risk of nonchromosomal syndromes. Relatively high in cases of extrahepatic type of PRUV, which is commonly associated with other anomalies.

Obstetric management. US finding of PRUV is an indication for a targeted fetal sonography.

Postnatal therapy. None is needed, if isolated.

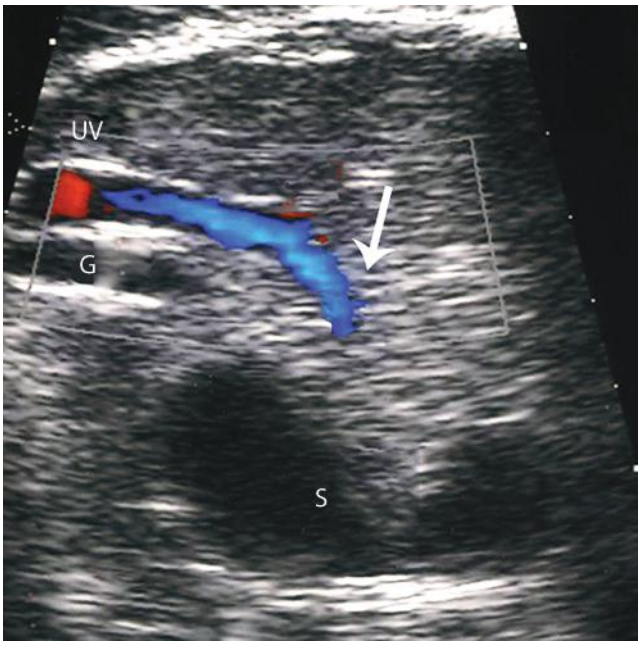


Figure 7.33 Axial view of the fetal abdomen showing a persistent right umbilical vein (UV). The portal vein is curving toward rather than away from the stomach (S). G: gallbladder.

Prognosis, survival, and quality of life. When isolated and connected to the portal system, PRUV represents a normal anatomical variant with no clinical significance

OMPHALOCELE

Incidence. Relatively infrequent. 1/3000 live births, but higher in utero.

Ultrasound diagnosis. On *sagittal and axial views* of the abdomen: midline abdominal wall defect, with herniation of abdominal content. Round, solid mass that deforms the anterior abdominal wall, usually containing some bowel loops and/or right hepatic lobe. The cord insertion is on the mass.

Risk of chromosomal anomalies. High (from 15% to 40%): trisomies 18 and 13 and triploidy.

Risk of nonchromosomal syndromes. Relatively high: Beckwith–Wiedemann syndrome and pentalogy of Cantrell (PC).

Outcome. Good if the lesion is isolated and the liver is not completely herniated. Very poor in the case of associated malformations and/or chromosomal aberrations.

Definition Omphalocele is a defect in the closure of the abdominal wall that also involves the cord insertion. It results from the failure of loops of bowel to return to the abdominal cavity after physiological herniation into the umbilical cord from the sixth to tenth week of development [33,34]. The herniated organs are wrapped in a two-layered sac, with the two layers being the peritoneum and the amnion. It is the commonest abdominal wall defects, with an incidence of 1 in 3000 live births [35].

The incidence of omphalocele is higher in the first trimester, about 1 in 384 at 11–14 weeks, according to a recent publication [36]; this can be explained by its strong association with chromosomal abnormalities and other structural anomalies related to a higher rate of spontaneous fetal loss or termination of pregnancy.

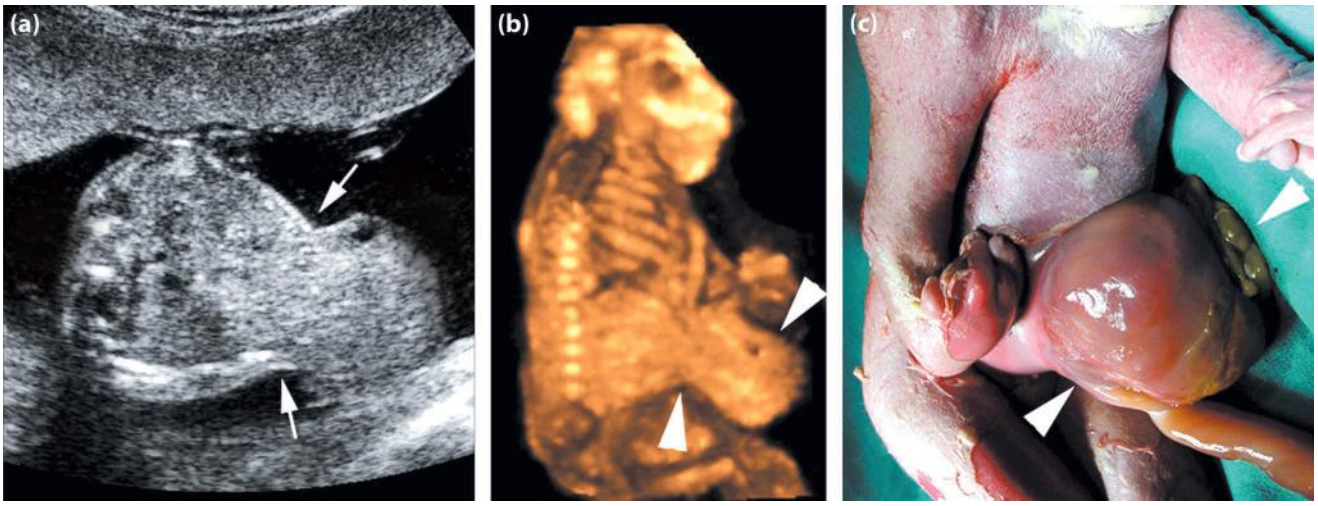


Figure 7.34 Omphalocele in a fetus with multiple anomalies (anencephaly, omphalocele, and bilateral aplasia radii). (a) At 23 weeks of gestation, the axial view of the abdomen demonstrates a large omphalocele containing the liver (the arrows indicate the large wall defect). (b) 3D low-magnification maximum-mode rendering showing the anencephaly and the omphalocele (arrowheads). (c) The stillborn fetus: the omphalocele (arrowhead), with the cord insertion, and the aplasia radii with ectrodactyly are shown.

Anatomy. The cord insertion is located on the top of the sac. Two variants of omphalocele exist, according to the presence or absence of the liver in the sac. The two variants have a different embryogenesis and may have a completely different prognosis, due to the differential risk of associated chromosomal anomalies. Rupture of the two-layered membranes occurs in about 10% of cases. In this rare circumstance, as reported in this section, the differential diagnosis with gastroschisis may be difficult

Ultrasound diagnosis. An omphalocele is sonographically represented by a bulging structure that (1) arises from the anterior abdominal wall, (2) contains some abdominal viscera (liver and/or bowel), and (3) presents the cord insertion on its convexity (Figures 7.34 and 7.35). The presence of the UV within the omphalocele is an indirect sign of the fact that this anomaly represents a primary closure defect of the abdominal wall (Figure 7.36). In some cases, ascites may also be associated, and care should then be taken not to mistake the ascites for amniotic fluid (Figure 7.36), as this would lead to an erroneous diagnosis of gastroschisis. In addition, it should be noted that polyhydramnios, possibly secondary to bowel obstruction at the level of the wall defect or within the omphalocele, may complicate one-third of cases. If the liver is detected within the omphalocele (Figure 7.37a), the diagnosis is certain also early in gestation; if, on the contrary, only some bowel loops are seen in it (Figure 7.37b), care should be taken to differentiate a real omphalocele from the physiologic herniation of the intestine within the cord that is frequently seen

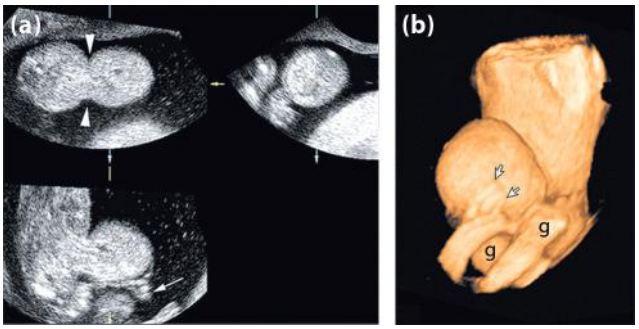


Figure 7.35 Omphalocele. 3D ultrasound. (a) Multiplanar imaging, showing the omphalocele on the three orthogonal planes, which enables assessment of its content and extension (arrowheads indicate the abdominal wall defect; the arrow indicates cord insertion). (b) Surface rendering demonstrates the cord insertion on the top of the omphalocele (arrows), in between the two knees (g).

until the 11th week of gestation. Therefore, if an omphalocele containing only ileal loops is identified earlier than the 12th week of gestation, the fetus should be rescanned in a week's time: if the herniation persists, then it is an omphalocele; if it has disappeared, then it was a physiologic transient herniation of the intestine in the cord.

Differential diagnosis. The differential diagnosis should include other abdominal wall defects and the physiologic herniation in the cord that disappears completely after the 11th completed week of gestation. The differences with gastroschisis are evident: in an omphalocele, there is a sac containing the viscera, whereas in gastroschisis,

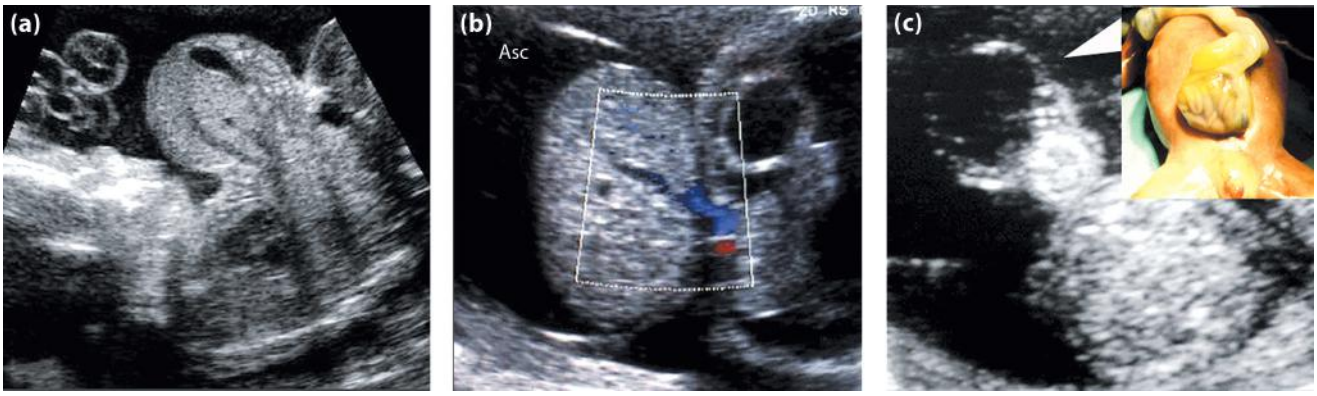


Figure 7.36 Omphalocele. (a) Midsagittal view of the abdomen: a case of omphalocele containing the liver at 29 weeks of gestation (normal karyotype). (b) Rarely, ascites can be associated with the omphalocele and can be detected in the sac (Asc); color Doppler shows the umbilical vein. (c) A small omphalocele, containing only some bowel loops (19 weeks of gestation) in a fetus with trisomy 18. Note the concurrent cord cyst (arrowhead), which is also often associated with trisomy 18. The inset shows the specimen with the small omphalocele and the bowel loops visible under the omphalocele membranes.

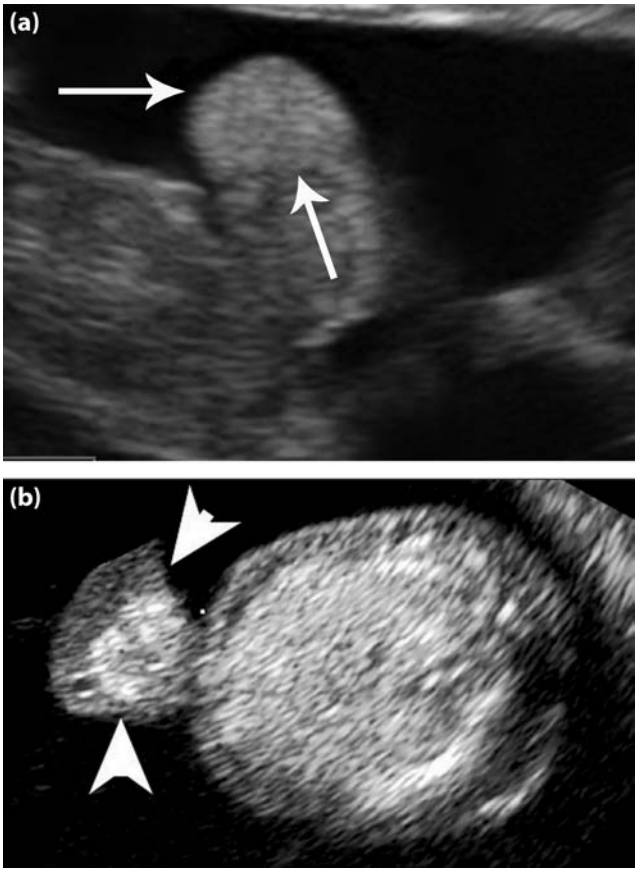


Figure 7.37 Omphalocele. (a) At 11 weeks of gestation, an omphalocele can reliably be diagnosed only if it contains the liver (arrows). (b) In fact, if the omphalocele contains bowel loops only, as in this case (arrowheads), to confirm the diagnosis and rule out physiologic herniation of intestine in the cord, it is necessary to wait until the 12th completed week of gestation.

the bowel float freely in the amniotic fluid In addition, the cord insertion is normal in gastroschisis, the defect of which is paramedian, while in an omphalocele, it inserts on the top of the sac. If a large omphalocele contains the whole of the liver, this should be differentiated from the so-called *limb–body–wall complex* (LBWC), which is characterized by major distortion of the body anatomy, with severe scoliosis and limb and skull abnormalities. Another entity that should be differentiated from isolated omphalocele is cloacal exstrophy, in which omphalocele extends caudally and is associated with bladder exstrophy and anomalies of the external genitalia. This anomaly is described in Chapter 8. In the case of omphalocele, the recognition of a normal bladder in the pelvis rules out this very rare possibility.

Association with other malformations. CHDs and urogenital and GI tract malformations are often associated with omphalocele. When the fetus with omphalocele has increased nuchal translucency (NT), there is a stronger association with cardiac defects than with other malformations [37].

Risk of chromosomal anomalies. This is high, from 15% to 40% (mainly trisomies 18 and 13, and, in a few cases, triploidy, trisomy 21, and Turner syndrome), in particular when the omphalocele is associated with other major structural abnormalities or with increased NT in the first trimester [37]

It should be underlined that the chromosomal risk is higher in the case of a small omphalocele containing only bowel loops. Huge omphaloceles containing the liver are less frequently associated with chromosomal anomalies. However, a recent study has shown that when the diagnosis is made in the first trimester, the

risk of aneuploidy is no different when the sac contains only bowel compared with when it contains the liver; on the contrary, if NT is increased, the risk is significantly higher [38].

Risk of nonchromosomal syndromes. This is high. The most common syndromes detectable in utero that can be associated with omphalocele are as follows:

- *Beckwith–Wiedemann syndrome*: look for ► *omphalocele* + macroglossia + somatic hemihypertophy + polycystic kidney (Chapter 10);
- *Pentalogy of Cantrell*: look for ► *midline anterior ventral wall defect* + diaphragmatic defect + cleft distal sternum + defect of the apical pericardium with communication into the peritoneum + CHD;
- *Cloacal exstrophy*: look for ► *omphalocele* + exstrophy of the urinary bladder + anorectal malformations + spinal defects.

Obstetric management. Should an omphalocele be diagnosed in a fetus, karyotyping is mandatory because of the high risk of chromosomal anomalies, especially if the defect is small and contains bowel only. In addition, fetal echocardiography and a thorough anomaly scan should be performed to detect possibly associated defects. With regard to delivery, there is no consensus on the need for Cesarean section, which is advocated by some authors to reduce the risk of traumatic rupture of the sac during passage through the birth canal. Empirically, it has been suggested that a Cesarean section may be indicated in cases presenting with huge (5 cm) omphalocele, with spontaneous delivery recommended for smaller lesions.

Postnatal therapy. Surgical correction of the defect may be performed in a single intervention or may require a two-step procedure, according to the size of the omphalocele. In fact, in those cases in which the whole liver has herniated, the limited intra-abdominal pressure is insufficient to allow normal growth of the abdomen. As a result, there is no space left in the abdomen to accommodate the large volume of the liver. In these cases, the defect is only partially closed, and the viscera remaining outside the abdomen are wrapped up in a sterile silastic bag (or spring-loaded silos). The final closure is delayed until the growth of the abdominal wall will allow complete closure without an abnormal increase in intra-abdominal pressure. Alternatively, rotational muscular flaps may be used to increase the surface of the anterior abdominal wall.

Prognosis, survival, and quality of life. Early neonatal mortality is generally due to the associated anomalies, and it may be as high as 80% in the case of multiple anomalies or even 95%–100% in the case of severe aneuploidies or syndromes. On the contrary, if the omphalocele is isolated and the liver is not in the sac, the prognosis is excellent, at least in pediatric series. Should the liver be in the sac, the prognosis is relatively poor and significant respiratory sequelae have been reported. As for other malformations, prenatal series yield very different results, with significantly lower survival rates and much poorer quality of life [39].

pENTALo Gy o F cANT r ELL (pc)

Incidence. Rare: 5.5 per 1 million live births.

Ultrasound diagnosis. Midline anterior ventral wall defect, diaphragmatic defect, cleft distal sternum, defect of the apical pericardium with communication into the peritoneum, and CHD.

Risk of chromosomal anomalies. Relatively low. Abnormalities of chromosomes 13 and 18 have been reported.

Risk of nonchromosomal syndromes. Pentalogy of Cantrell is a syndrome by itself.

Outcome. Poor, especially in cases with the presence of the complete pentad of features of the PC and severe intracardiac defects.

Definition This is a rare form of abdominal wall defect that consists of five associated anomalies: a midline anterior ventral wall defect, a diaphragmatic defect, a cleft distal sternum, a defect of the apical pericardium with communication into the peritoneum, and an intracardiac defect [40]. Several variants, characterized by the presence of all or at least three of these five anomalies, have been reported. Pentalogy of Cantrell is also known as "thoracoabdominal ectopia cordis" and is in part a misnomer, given that the heart is always outside of the thorax in the latter case.

Etiology and pathogenesis. PC is a complex congenital abnormality that occurs as a result of embryonic failure in the development of the septum transversum.

Ultrasound diagnosis. The sonographic features of PC are the typically supra-umbilical omphalocele and cardiac defects (in most of cases, septal defects and tetralogy of Fallot).

The presence of a pericardial effusion implies a communication between the pericardial sac and the exomphalos. The visualization of a transient pericardial effusion with the presence of an omphalocele is typical of PC. The sternal and the anterior diaphragmatic defect may be difficult to detect. In PC, usually there is a shift in cardiac axis with the apex oriented vertically at the superior edge of the abdominal wall defect. In contrast to *ectopia cordis*, which is characterized by an abnormal position of the heart outside of the chest, in PC the heart is positioned within the chest. However, recently several cases of PC with a significant degree of protrusion of the heart outside the chest, before 20 weeks of gestation, have been reported (Figure 7.38). In all these cases, after 20 weeks the heart appeared to be contained within the thorax [40].

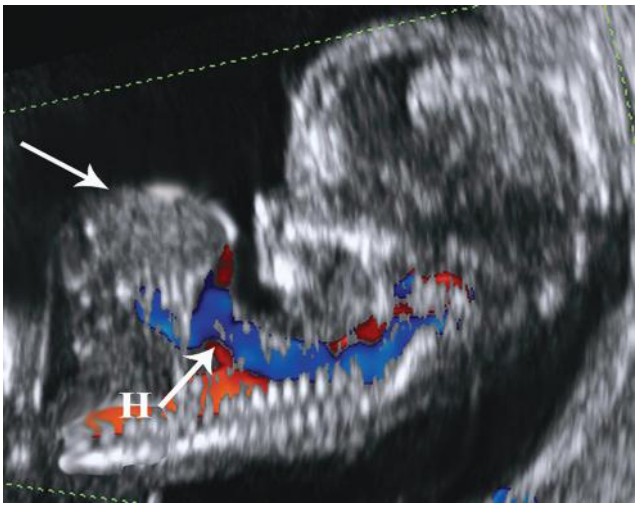


Figure 7.38 Pentalogy of Cantrell (13 weeks of gestation): the typically supra-umbilical omphalocele (arrow) and a slight degree of protrusion of the heart (H) outside the chest can be clearly seen.

Differential diagnosis. The differential diagnosis in PC includes isolated omphalocele, Limb-Body-Wall Complex (see Chapter 1), and ectopia cordis. In ectopia cordis, often used interchangeably with PC, the heart protrudes through a cleft sternum and no other defects are associated; in LBWC, a severely distorted fetus is adherent to the placenta and no free-floating cord is present; in isolated omphalocele, the fetus lacks cardiac and diaphragmatic abnormalities.

Prognostic indicators. Presence of a severe heart defect represents a bad prognostic sign.

Association with other malformations. It can be associated with other midline ventral defects such as exencephaly and cleft lip or palate.

Risk of chromosomal anomalies. Abnormalities of chromosomes 13 and 18 have been reported in association with PC.

Risk of nonchromosomal syndromes. PC is a syndrome.

Obstetric management. Karyotyping and a careful search for other anomalies are recommended. Delivery in a tertiary referral center is recommended.

Postnatal therapy. Treatment by multiple operations for both cardiac and extracardiac anomalies is required.

Prognosis, survival, and quality of life. Survival for patients with the complete pentad of features of PC is low (8%–37%) [41]. In cases with variants of the syndrome, the survival has been reported to be 60% [41]. The prognosis is also correlated with the type and extent of the torachoabdominal defects and the severity of the heart defects.

However, all survivors have experienced prolonged hospitalization and a significant degree of long-term disability.

GASTROSCHISIS

Incidence. Rare. In the last two decades, the incidence of gastroschisis has increased from 0.29 to 1.66 per 10,000 live births in the developed world [42]. It occurs frequently in young mothers, often those from small communities, smokers, and illicit drug users.

Ultrasound diagnosis. Bowel loops freely floating in the amniotic fluid. Para-umbilical wall defect. Normal cord insertion.

Risk of chromosomal anomalies. Very low.

Risk of nonchromosomal syndromes. Low. Concurrent joint contractures of the legs with hypoplastic lower limb muscles indicate the presence of congenital amyoplasia.

Outcome. Very good, unless rare complications including perforation, infarction, or infection of the herniated loops occur.

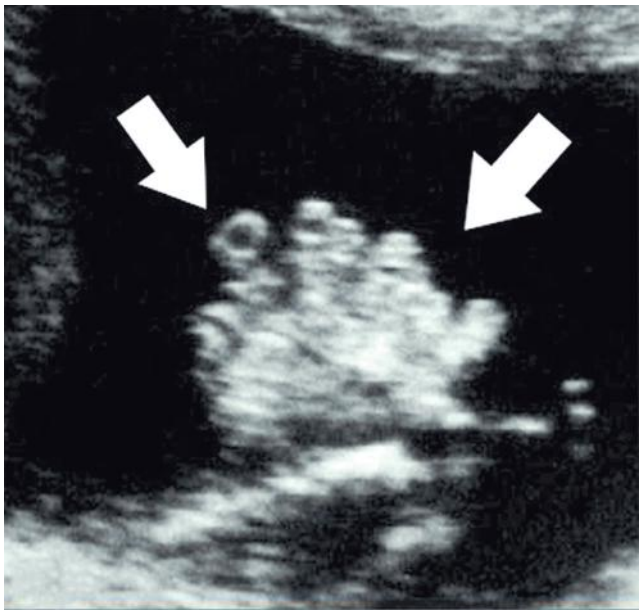


Figure 7.39 Gastroschisis (arrows) at 12 weeks of gestation.

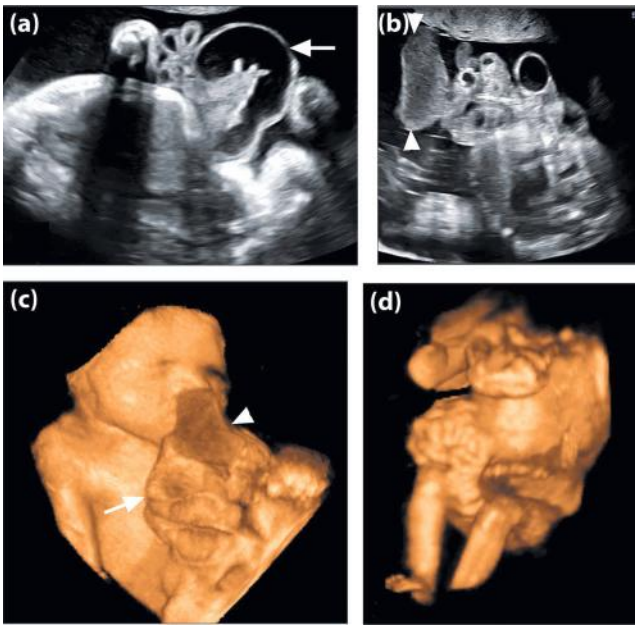


Figure 7.40 Gastroschisis at 31 weeks of gestation. The appearance of bowel dilation in the 3rd trimester represents a complication, indicating a likely obstruction. This situation may evolve with perforation and/or necrosis of one or more bowel loops. (a) Sagittal view of the fetal trunk showing some normally sized loops close to the fetal arm and one severely dilated tract (arrow). (b) Axial view also demonstrating some meconium blocked in the dilated loop (arrowhead). (c) Surface rendering demonstrating the dilated loop (the same as in (b)). (d) Below the dilated loop, most of the herniated bowel is of normal size.

Definition Gastroschisis is characterized by a para-umbilical defect of the abdominal wall through which bowel loops herniate to float freely in the amniotic fluid

Anatomy. The defect involves all layers of the abdominall wall, and the herniated viscera consist, in the overwhelming majority of cases, of bowel loops only; in very rare circumstances, the stomach and, exceptionally, urogenital structures may herniate as well. As was pointed out in this chapter, there is no membrane wrapping the herniated viscera, as in omphalocele, and these float freely in the amniotic fluid This very fact increases the likelihood of chemically induced infla - mation of the herniated bowel loops, which may lead to perforation. The pathogenetic mechanism leading to the para-umbilical defect involves an abnormal regression of the right UV or, alternatively, a vascular accident during embryogenesis.

Ultrasound diagnosis. The US diagnosis is straightforward and relies on the recognition of freely floa - ing bowel outside the fetal abdomen (Figure 7.39). Once the suspicion of gastroschisis has been raised, a closer inspection may lead to identification of the right para-umbilical wall defect through which the bowel herniates. Usually, the defect is small (2 cm), and this is responsible for the occurrence of bowel infarction due to torsion and/or compression of the mesenteric pedicle on the rim of the defect. In some cases, during the third trimester, thickening and edema of the intestinal walls, possibly associated with dilation (Figure 7.40), may indicate the onset of obstruction and/or of even worse complications such as infarction. Some authors have described how, in extremely rare cases, after severe dilation of an ileal loop due to obstruction, the dilation may completely disappear due to complete necrosis of the affected loop (*vanishing gut*).

Differential diagnosis. The differential diagnosis with omphalocele has already been addressed in detail in the "Omphalocele" section. The only other condition that may, to a limited extent, mimic gastroschisis is the LBWC, especially if this is due to amniotic bands. In such a rare circumstance, the damage created by the amniotic band may extensively involve the abdominal wall, with consequent herniation of bowel and other viscera. However, in this lethal condition, there are other major anomalies of the spine, the limbs, and possibly the skull, which lead to the diagnosis.

Association with other malformations. Intestinal perforation and consequent peritonitis represent complications rather than associated malformations.

Gastroschisis is rarely associated with non-GI tract anomalies. The only severe condition that would significantly worsen the prognosis, if present, is the so-called congenital amyoplasia, which is characterized by absence of limb muscles, which are replaced by fibrous and fatty tissue

Risk of chromosomal anomalies. This is extremely low.

Risk of nonchromosomal syndromes. This is extremely low, except for the rare association with the above-mentioned congenital amyoplasia.

Obstetric management. Should gastroschisis be detected in a fetus, karyotyping is not mandatory, because of the low risk of chromosomal anomalies. Similarly, the risk of associated nonchromosomal anomalies is low, and the only issue that needs to be addressed is the presence and function of the lower limb muscles. Serial follow-up scans should be scheduled in order to detect possible local complications, such as dilation, wall edema, or perforation. With regard to the mode of delivery, no definite conclusion has been reached on the real need for Cesarean section in order to avoid tearing on the mesenteric pedicle of the herniated bowel. In fact, almost the same risk applies for delivery of the fetal abdomen with gastroschisis in the course of Cesarean section. The only aspect for which the operative modality of delivery would be preferable is the possible risk of infection of the bowel exposed to the bacteria of the birth canal.

Postnatal therapy. As for omphalocele, surgical reduction of the defect may be carried out in a single operation or approached with a two-step procedure, according to the state and amount of herniated bowel. The same silastic bag (or spring-loaded silos) mentioned for omphalocele may be used for gastroschisis in those cases in which the single-step closure of the defect would dangerously increase the intra-abdominal pressure. Regardless of the procedure, the outcome is very good in the overwhelming majority of cases.

Prognosis, survival, and quality of life. In isolated gastroschisis the postoperative mortality rate has been reported to be 15%. Causes of death are sepsis and the complications of mesenteric ischemia. However, in more recent series, the survival rate exceeds 90%.

In up to 40% of cases a significant morbidity is present. This is mainly due to GI tract complications, including bowel necrosis due to constriction at the level of the abdominal wall defect, hypoperistalsis due to prenatal exposure of the bowel to the amniotic fluid, and abdominal compartment syndrome due to excessive intra-abdominal pressure at the time of surgical repair [43–44]. The presence of bowel pathology at birth, such as bowel atresia, malrotation, volvolus, infarction, perforation, and stenosis, affects the prognosis of these babies and reduces the survival rate to 28%, whereas affected neonates without bowel complications can survive in almost 100% of cases [45].

rEFE r ENc Es

1. Volpe P. Paladini D, De Robertis V, et al. Fetal gastrointestinal anomalies. In: Fleischer AC, Toy E, Lee W, et al., eds. *Sonography in Obstetrics & Gynecology*, 7th edn. New York: McGraw-Hill; 2010.
2. Malinger G, Levine A, Rotmensch S. The fetal esophagus: anatomical and physiological ultrasonographic characterization using a high-resolution linear transducer. *Ultrasound Obstet Gynecol* 2004; 24: 500–5.
3. Goldstein I, Reece EA, Yakoni S, et al. Growth of the fetal stomach in normal pregnancies. *Obstet Gynecol* 1987; 70: 641–4.
4. Gross RE. *The Surgery of Infancy and Childhood*. Philadelphia, PA: WB Saunders; 1953.
5. Has R, Guenay S, Topuz S, et al. Pouch sign in prenatal diagnosis of esophageal atresia. *Ultrasound Obstet Gynecol* 2004; 23: 523–4.
6. Langer JC, Hussain H, Khan A, et al. Prenatal diagnosis of esophageal atresia using sonography and magnetic resonance imaging. *J Pediatr Surg* 2001; 36: 804–7.
7. Stringer MD, McKenna KM, Goldstein RB, et al. Prenatal diagnosis of esophageal atresia. *J Pediatr Surg* 1995; 30: 1258–63.
8. Yagel S, Sonigo P, Rousseau V, et al. Esophageal atresia diagnosed with three-dimensional ultrasonography. *Ultrasound Obstet Gynecol* 2005; 26: 307–8.
9. Salomon LJ, Sonigo P, Ou P, et al. Real-time fetal magnetic resonance imaging for the dynamic visualization of the pouch in esophageal atresia. *Ultrasound Obstet Gynecol* 2009; 34: 471–4.
10. Houben CH, Curry JI. Current status of prenatal diagnosis, operative management and outcome of esophageal atresia/tracheo-esophageal fistula *Prenat Diagn* 2008; 28: 667–5.
11. Romero R, Jeanty P, Pilu GL, et al. The prenatal diagnosis of duodenal atresia. Does it make any difference? *Obstet Gynecol* 1988; 71: 739–41.
12. Escobar MA, Ladd AP, Grosveld JL, et al. Duodenal atresia and stenosis: long-term follow up over 30 years. *J PediatrSurg* 2004; 39: 867–71.
13. Paralekar S. Sonography of normal fetal bowel. *J Ultrasound Med* 1991; 10: 211–13.
14. Iacobelli BD, Zaccara A, Spirydakis I, et al. Prenatal counseling of small bowel atresia: watch the fluid! *Prenat Diagn* 2006; 26: 214–17.
15. Sepulveda W, Sebire NJ. Fetal echogenic bowel: a complex scenario. *Ultrasound Obstet Gynecol* 2000; 16: 510–14.
16. Goetzinger KR, Cahill AG, Macones GA et al. Echogenic bowel on second-trimester ultrasound: evaluating the risk of adverse pregnancy outcome. *Obstet Gynecol* 2011; 117: 1341–8.

17. Bronshtein M, Blazer S, Zimmer EZ. The gastrointestinal tract and abdominal wall. In: Callen, PW. ed. *Ultrasonography in Obstetrics and Gynecology*. Philadelphia, PA: Saunders Elsevier; 2008: 587–639.
18. Cham KL, Tang MHY, Tse HY, et al. Meconium peritonitis: prenatal diagnosis, postnatal management and outcome. *Prenat Diagn* 2005; 25: 676–82.
19. Mushtaq I, Wright VM, Drake DP, et al. Meconium ileus secondary to cystic fibrosis The East London experience. *Pediatr Surg Int* 1998; 13: 365–9.
20. Taipale P, Rovamo L, Hiilesmaa V. First-trimester diagnosis of imperforate anus. *Ultrasound Obstet Gynecol* 2005; 25: 187–8.
21. Lubusky M, Prochazka M, Dhaifalah I, at al. Fetal enterolithiasis: prenatal sonographic and MRI diagnosis in two cases of urorectal septum malformation (URSM) sequence. *Prenat Diagn* 2006; 26: 345–9.
22. Levitt MA, Peña A. Anorectal malformations. *Orphanet J Rare Dis* 2007, 2: 33.
23. Visser BC, Suh I, Way LW, et al. Congenital choledochal cysts in adults. *Arch Surg* 2004; 139: 855–60.
24. Zangheri G, Andreani M, Ciriello E, et al. Fetal intra-abdominal calcifications from meconium peritonitis: sonographic predictors of postnatal surgery. *Prenat Diagn* 2007; 27: 960–3.
25. Roberts AM, Mitchell JM, Pattison NS. Fetal liver length in normal and isoimmunized pregnancies. *Am J Obstet Gynecol* 1989; 161: 42–6.
26. Volpe P, De Robertis V, Campobasso G, et al. Four D and 2D echocardiographic evaluation of anomalies of the venous connections. In: Rizzo G, Arduini D, eds. *Four Dimensional Fetal Echocardiography*. Bentham Books, 2010; 85–94.
27. Berg C, Kamil D, Geipel A, et al. Absence of ductus venosus: importance of umbilical venous drainage site. *Ultrasound Obstet Gynecol* 2006; 28: 275–81.
28. Volpe P, Marasini M, Caruso G, et al. Prenatal diagnosis of ductus venosus agenesis and its association with cytogenetic/congenital anomalies. *Prenat Diagn* 2002; 22: 995–1000.
29. Shen O, Valsky DV, Messing B, et al. Shunt diameter in agenesis of the ductus venosus with extrahepatic portosystemic shunt impacts on prognosis. *Ultrasound Obstet Gynecol* 2011; 37: 184–90.
30. Achiron R, Gindes L, Kivilevitch Z, et al. Prenatal diagnosis of congenital agenesis of the fetal portal venous system. *Ultrasound Obstet Gynecol* 2009; 34: 643–52.
31. Fung TY, Leung TN, Leung TY, et al. Fetal intra-abdominal umbilical vein varix: what is the clinical significance? *Ultrasound Obstet Gynecol* 2005; 25: 149–54.
32. Weichert J, Hartge D, Germer U, et al. Persistent right umbilical vein: a prenatal condition worth mentioning? *Ultrasound Obstet Gynecol* 2011; 37: 543–48.
33. Sadler TW, ed. Body cavities. In: *Langman's Medical Embryology*, Baltimore, MD: Lippincott, Williams and Wilkins; 2010: 155–64.
34. Kilby MD, Lander A, Usher-Somers M. Exomphalos (omphalocele). *Prenat Diagn* 1998; 18: 1283–8.
35. Mann S, Blinman TA, Douglas Wilson R. Prenatal and postnatal management of omphalocele. *Prenat Diagn* 2008; 28: 626–32.
36. Kagan KO, Staboulidou I, Syngelaki A, et al. The 11–13-week scan: diagnosis and outcome of holoprosencephaly, exomphalos and megacystis. *Ultrasound Obstet Gynecol* 2010; 36: 10–14.
37. Khalil A, Arnaoutoglou C, Pacilli M, et al. Outcome of fetal exomphalos diagnosed at 11–14 weeks of gestation. *Ultrasound Obstet Gynecol* 2012; 39: 401–6.
38. Iacovella C, Contro E, Ghi T, et al. The effect of the contents of exomphalos and nuchal translucency at 11–14 weeks on the likelihood of associated chromosomal abnormality. *Prenat Diagn* 2012; 32: 1066–70.
39. Brantberg A, Blaas HGK, Haugen SE, et al. Characteristics and outcome of 90 cases of fetal omphalocele. *Ultrasound Obstet Gynecol* 2005; 26: 527–37.
40. Zidere V, Allan LD. Changing findings in pentalogy of Cantrellin fetal life. *Ultrasound Obstet Gynecol* 2008; 32: 835–7.
41. Vasquez-Jiminez JF, Muehler EG, et al. Cantrell's syndrome: a challenge to the surgeon. *Ann Thorac Surg* 1998; 65: 1178–85.
42. Loane M, Dolk H, Bradbury I. Increasing prevalence of gastroschisis in Europe 1980–2002: a phenomenon restricted to younger mothers? *Paediatr Perinat Epidemiol* 2007; 21: 363–9.
43. Contro E, Fratelli N, Okoye B, et al. Prenatal ultrasound in the prediction of bowel obstruction in infants with gastroschisis. *Ultrasound Obstet Gynecol* 2010; 35: 702–7.
44. Tower C, Ong SS, Ewer AK, et al. Prognosis in isolated gastroschisis with bowel dilatation: a systematic review. *Arch Dis Child Fetal Neonatal* 2009; 94: 268–74.
45. Lao OB, Larison C, Garrison MM, et al. Outcomes in neonates with get a gastroschisis in U.S. children's hospitals. *Am J Perinatol* 2010; 27: 97–101.

Chapter 8
Anomalies of the urinary tract and of the external genitalia

Normal anatomy of the urogenital tract: ultrasound approach, scanning planes, and diagnostic potential

The urogenital system develops from the intermediate mesoderm. During folding of the embryo in the horizontal plane, this mesoderm is carried ventrally; then, a longitudinal ridge of mesoderm, the urogenital ridge, forms on each side of the dorsal aorta. This structure will eventually give rise to parts of the urinary and genital tract. The part of the urogenital ridge giving rise to the urinary system is the nephrogenic cord; the part giving rise to the genital system is the genital ridge [1]. The urinary system begins to develop prior to the genital system. Three regions of excretory kidney develop in the human embryo: the pronephros, mesonephros, and metanephros. These arise sequentially from the intermediate mesoderm beginning at days 19–21 of development. The pronephros and mesonephros degenerate, while the metanephros will develop into the adult kidney. The metanephros begins to develop during the fifth week of development and starts to be functionally active five weeks later. Initially, it consists of two cell types: the epithelium of the ureteric bud and the mesenchyme of the metanephric blastema. A series of reciprocal interactions between these two structures causes the ureteric bud to repeatedly branch to form the ureter, the renal pelvis, the calices, and the collecting tubules. Concurrently, the mesenchyme, induced by the adjacent ureteric bud branch tips, undergoes a transformation to form the nephrons. The first glomeruli develop by eight–nine weeks, and the nephrogenesis continues in the cortex of the fetal kidney until 34–36 weeks. The bladder develops from the urogenital sinus, and the first stage of bladder development involves division of the cloaca into the anorectal and urogenital regions. Initially, the bladder is in continuity with the allantois, but eventually this structure regresses, converting into a thick fibrous cord, the urachus, which connects the bladder with the umbilicus. The mature human kidney contains about a million nephrons, consisting of specialized segments, including glomeruli, proximal tubules, the loop of Henle, and the distal tubule, connected to the tree-like collecting duct system, intimately associated with the vascular supply.

Timing of examination. Ultrasound (US) screening of urinary tract anomalies is generally performed at 19–21 weeks of gestation, despite the fact that at this gestational age a significant number of late-onset renal diseases, such as most forms of hydronephrosis, cannot yet be identified In fact, the incidence of prenatally detected urinary tract malformations depends also on the timing of the scan: the later the ultrasound examination is performed, the higher the percentage of urinary tract anomalies detected.

Ultrasound approach and scanning planes (views).

Kidneys. Anatomic assessment of the kidneys can be made on two scanning planes: axial and longitudinal. On *axial views*, the kidneys appear as two round paravertebral structures with the pelvis oriented toward the midline. On *longitudinal views*, they appear elliptic. The adrenal glands are located just cranial to the kidneys and, in cases of renal agenesis, can be mistaken for the kidneys. On the *axial view* of the kidney, it is possible to measure its width and thickness. The length of the kidney, from the upper to the lower pole, can be measured on the *longitudinal view*. Nomograms for kidney size at different gestational ages are given in the Appendix Table A.23–A.24. The ratio between the renal circumference and abdominal circumference

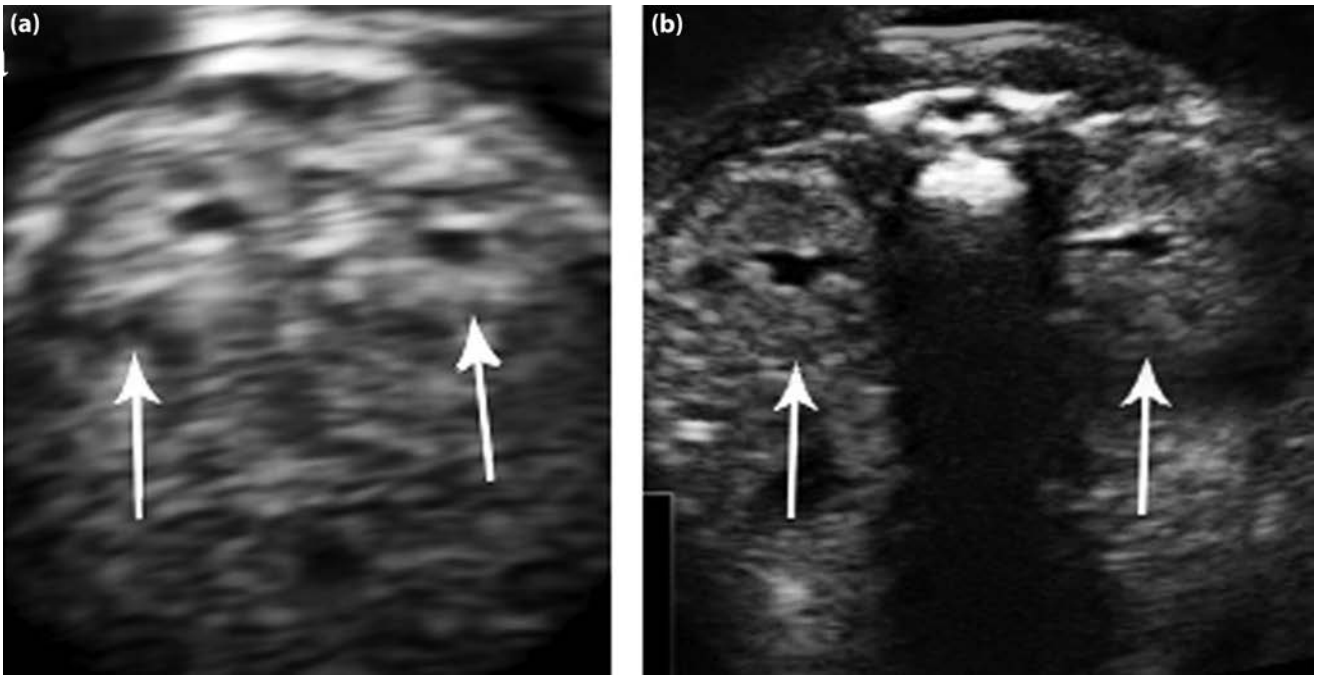


Figure 8.1 (a) Normal fetal kidneys at 13 weeks of gestation. At this stage, the kidneys appear as bilateral hyperechoic structures in the paravertebral regions (arrows). (b) Normal fetal kidneys at 22 weeks. The kidneys appear less echoic (arrows) than in the 1st trimester; the renal pelvis is seen centrally.

is approximately 0.27–0.30 and remains constant throughout pregnancy. The fetal kidneys can be visualized on ultrasound in most cases by the end of the first trimester (11–12 weeks), when they appear as two hyperechoic paravertebral structures (Figure 8.1a); in the second trimester, they lose their hyperechoic appearance (Figure 8.1b), and by the third trimester, it is possible to distinguish between the cortex and the medulla; the renal pyramids appear hypoechoic, while the pelvis appears as a small medial sonolucent area (Figure 8.2). The cortex is peripheral to the medulla and is slightly more echogenic. The size of the pelvis in axial sections (Figure 8.3) should not exceed 4 mm before the 32nd week and 7 mm from the 33rd week until term [2].

Bladder. The bladder can be visualized as soon as urine production begins, at about ten weeks of gestation. On US, the bladder can always be visualized by 12 weeks in the middle of the fetal pelvis as a circular anechoic structure with echoic walls. The ultrasound aspect of the bladder does not change during gestation, and, under physiological conditions, the thickness of its walls should never exceed 2–3 mm (Figure 8.4a). The perivesical arteries, which run laterally to the bladder (Figure 8.4b), are easily detected on color Doppler, and they represent useful landmarks that can help to differentiate the bladder from other cystic formations that might be present in the fetal pelvis.

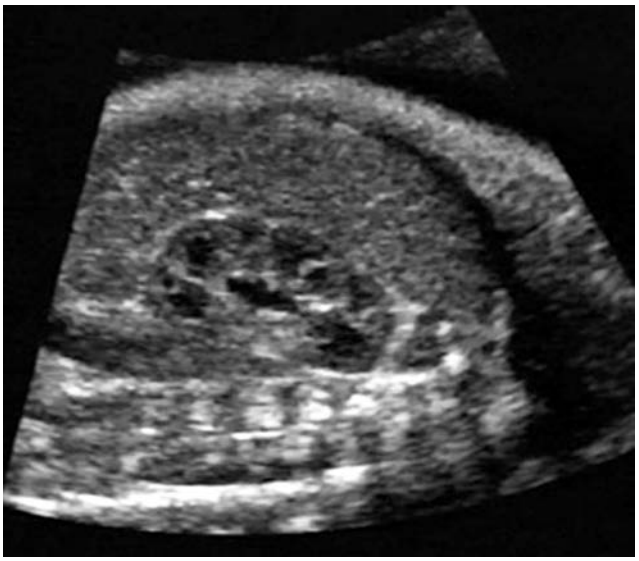


Figure 8.2 Ultrasound appearance of the fetal kidney at 28 weeks of gestation: the renal pyramids may be seen as hypoechoic structures within the renal parenchyma; the renal pelvis may be seen as an echo-free area medially.

Ureters and urethra. Both of these structures are not visible prenatally, except in cases of disease. Figure 8.5 shows the main embryologic events occurring during the definitive formation of the kidneys

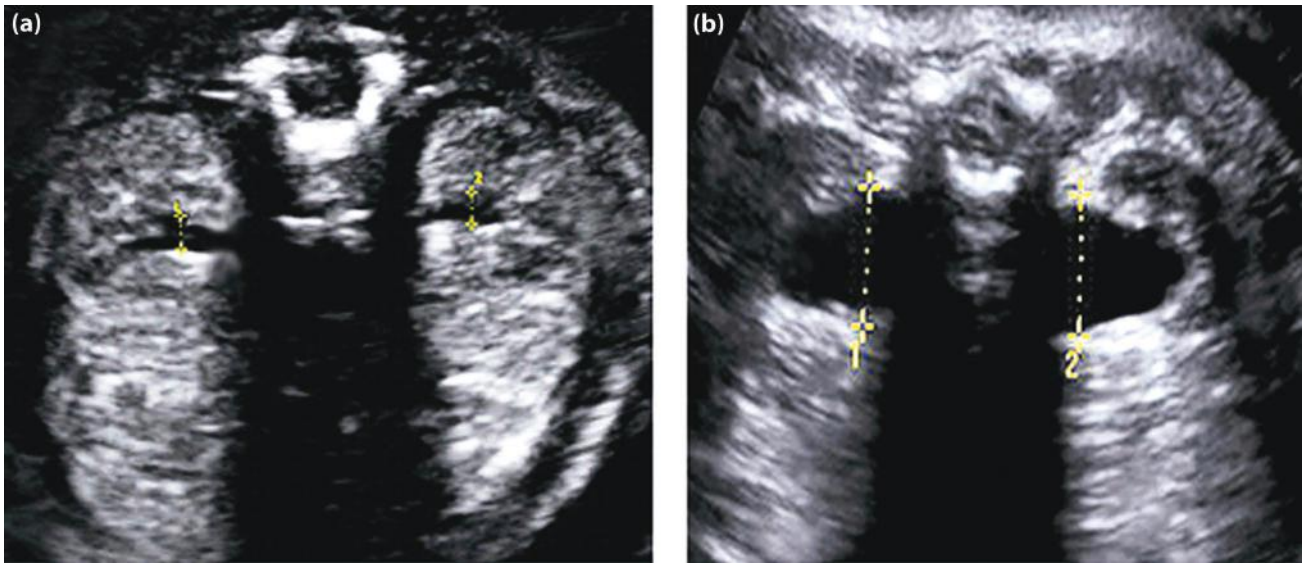


Figure 8.3 Axial scan through the fetal abdomen, showing measurement of the normal (a) and enlarged (b) renal pelvises.

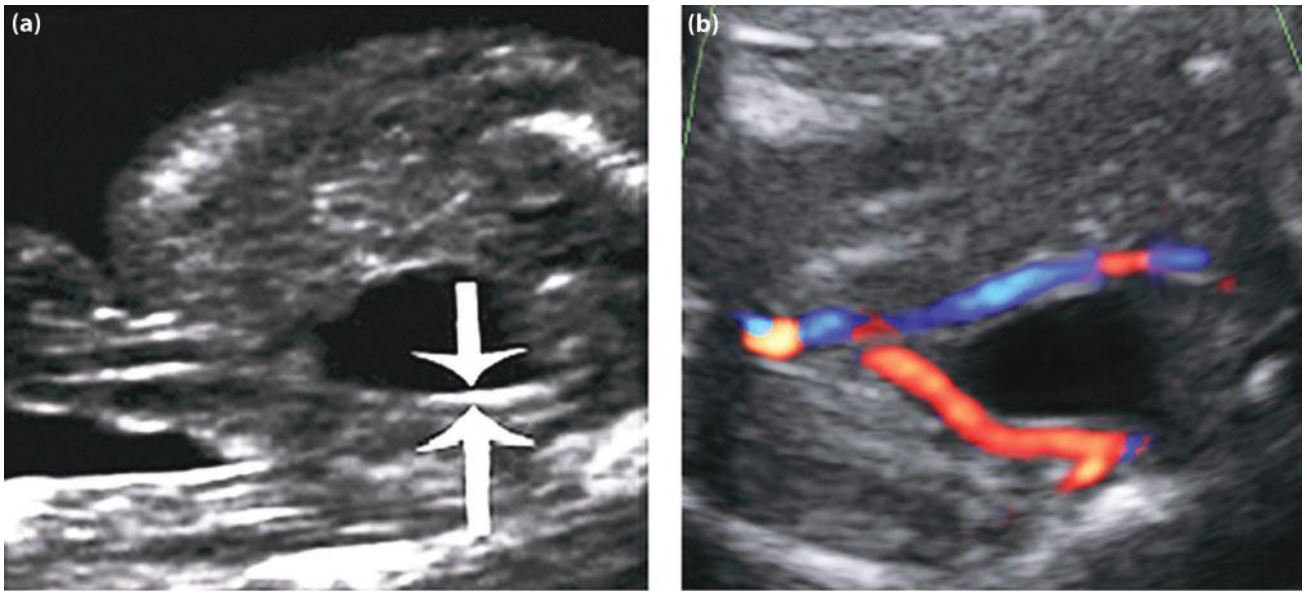


Figure 8.4 (a) Axial scan through the fetal pelvis showing the bladder wall (arrows). (b) Color flow Doppler image showing both perivesical arteries separating around the bladder (arrow).

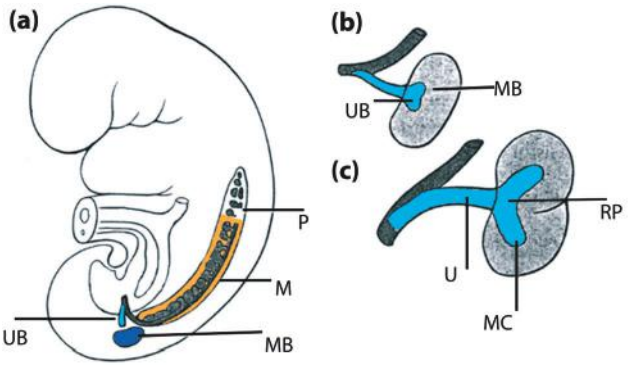


Figure 8.5 Development of the kidney. (a) Sketch of a lateral view of a five-week embryo, showing the primordium of the metanephros. (b,c) Sketches showing successive stages in the development of the metanephric diverticulum or ureteric bud (fifth to sixth weeks). Observe the development of the ureter, renal pelvis, and major calices. UB: ureteric bud; P: remnant of pronephros; M: mesonephros; MB: metanephric blastema; RP: renal pelvis; U: ureter; MC: major calyx.

dIFFE r ENTIAL dIAGN os Is o F Ur INAr y Tr Ac T ANo MALIEs

A systematic approach to the fetal urinary tract requires ultrasound assessment of the bladder, both kidneys, and the amount of amniotic fluid.

Absent kidney. If one of the two kidneys is not found on ultrasound in its proper location, then it may be ectopic or completely absent (unilateral agenesis). In the former case, the most common ectopic site is represented by the pelvis, in the presacral area or in the iliac fossa; alternatively, and, much more rarely, the ectopic kidney can be fused with the contralateral one (simple or fused crossed renal ectopia). If the kidney cannot be found in ectopic sites, then a putative diagnosis of *unilateral renal agenesis* can be made after excluding the possibility of severe renal hypoplasia. If both kidneys are absent (bilateral agenesis), the bladder cannot be visualized, and only after 16 weeks of gestation will severe oligohydramnios be associated.

Abnormal renal echogenicity and size (Figure 8.6).

- If both kidneys appear hyperechoic in comparison with the liver or spleen, and larger than normal, this will point toward a diagnosis of polycystic kidneys. If additional extra-renal abnormalities are associated (especially of the skeleton and central nervous system [CNS], then the kidney anomaly is likely to be part of a well-defined syndrome.
- If the kidneys are small and hyperechoic, then this may indicate the presence of Potter type IV cystic renal dysplasia.
- If the kidneys are hyperechoic and normal in size and no associated extra-renal anomalies are found, the picture may simply represent a variant form of normal kidney development, although some authors have included this feature (i.e., a normally sized hyperechoic kidney) among the soft markers of aneuploidy.
- If parenchymal cysts of various sizes are detected, and the overall renal volume is increased, a diagnosis of multicystic kidney can be made if the cysts

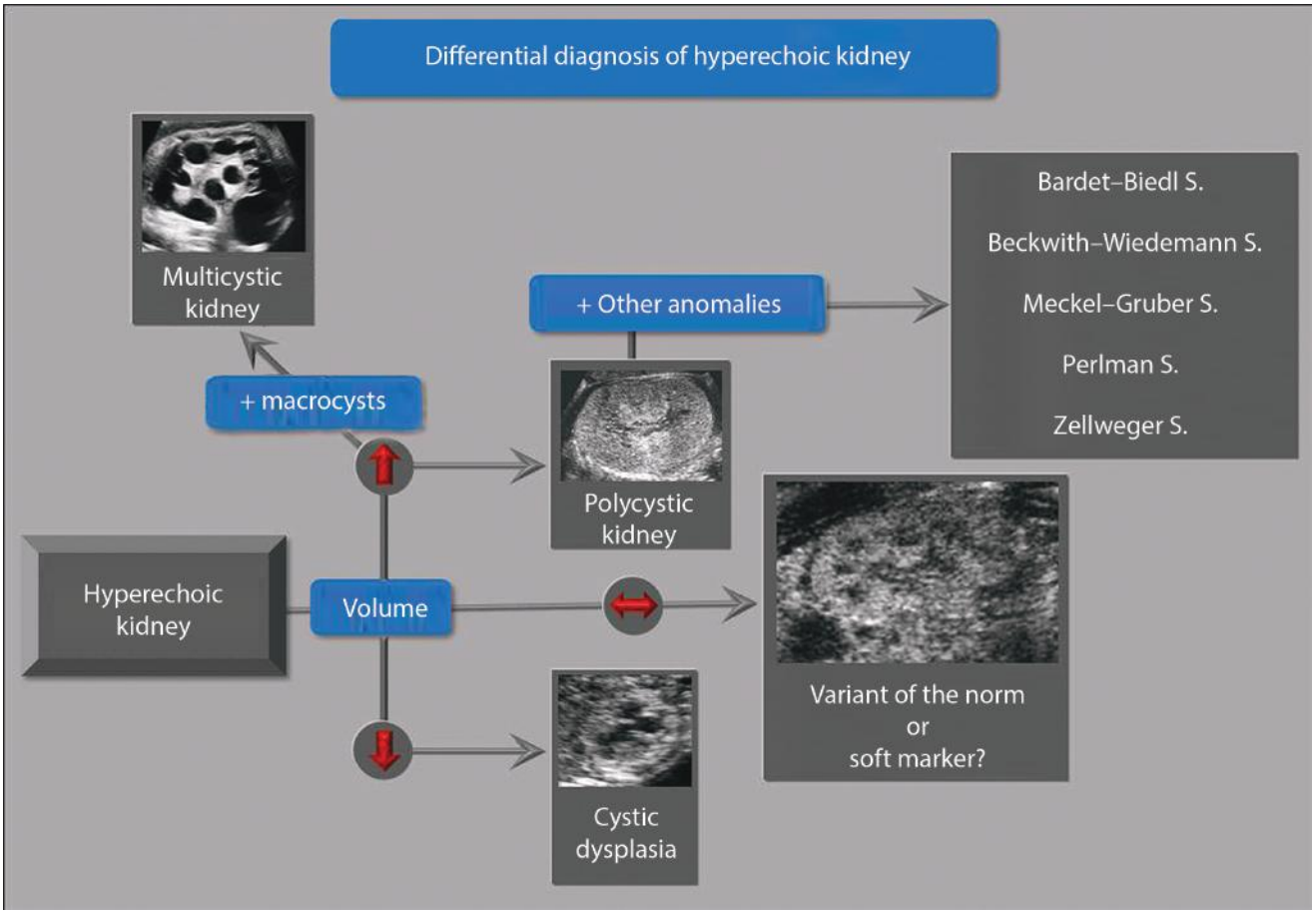


Figure 8.6 Algorithm to be applied in the case of hyperechoic kidneys.

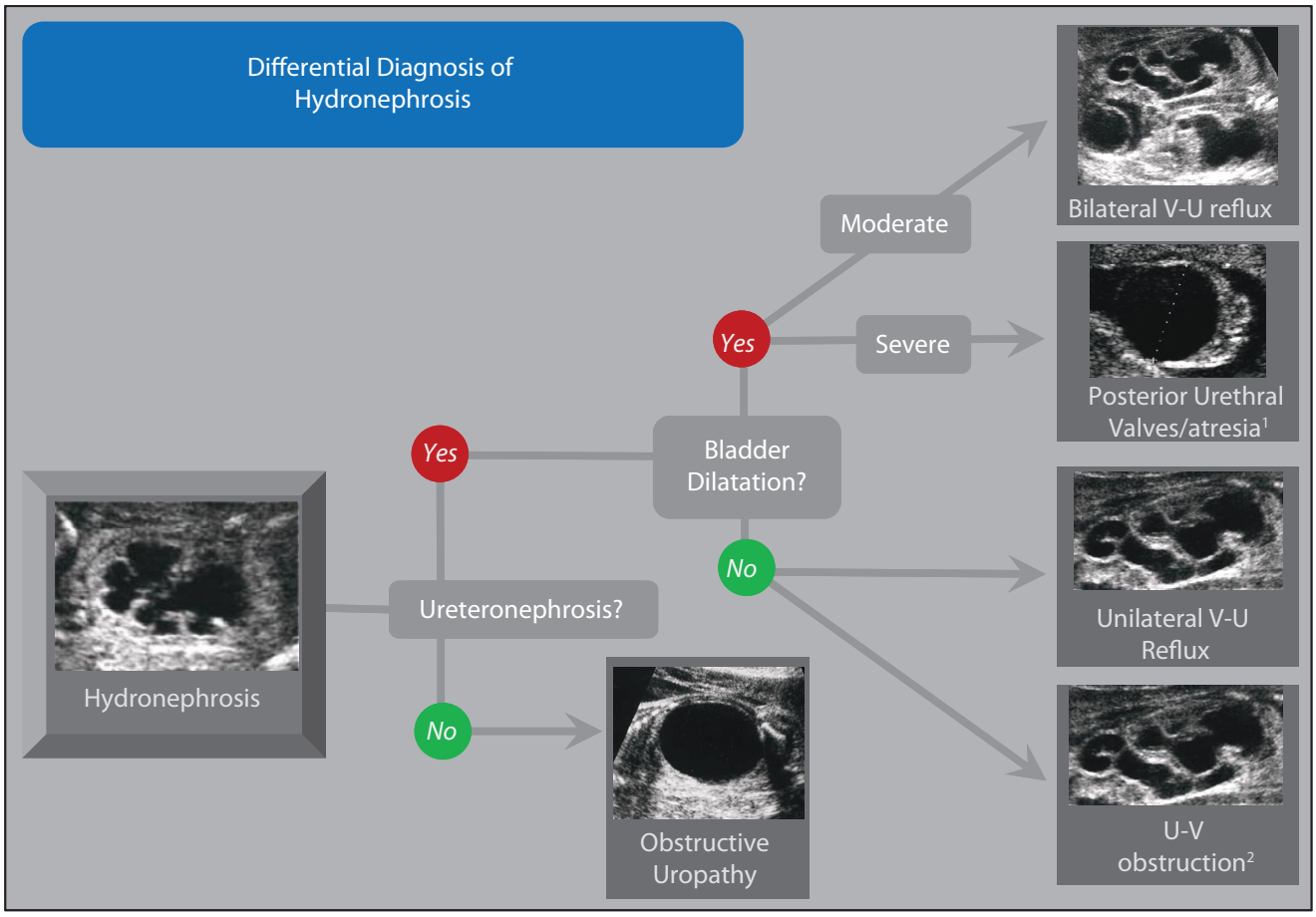


Figure 8.7 Differential diagnosis of hydronephrosis. [1]If the obstruction is complete, the amniotic fluid is absent after 16 weeks. [2]Often associated with duplex kidney.

do not communicate with one another; otherwise, it could be a case of severe hydronephrosis. In both cases, it is of the utmost importance, for prognostic purposes, to make a careful assessment of the contralateral kidney, as described in this chapter.

- If unilateral calicopyelic dilation is present (Figure 8.7), then the hydronephrosis may be due to obstruction or vesicoureteral reflux (VUR). The operator should check for signs of dilation of the ureter to exclude the possibility of pyelo-ureteral junction obstruction, thereby hypothesizing that an obstruction of the vesicoureteral junction or a reflux might be present.
- If bilateral hydroureteronephrosis is present together with mild distension of the bladder but with normal thickness of the bladder walls and a normal amount of amniotic fluid, then the most likely diagnosis is that of bilateral VUR.
- Conversely, if the bladder is clearly dilated with thickened and hyperechoic walls, and significant oligohydramnios is associated, then this points toward a diagnosis of lower urinary tract obstruction. In this case, hydroureteronephrosis and / or increased echogenicity of the renal parenchyma (Potter type IV cystic dysplasia) may be present.
- If the fetal bladder cannot be seen, then the diagnostic algorithm shown in Figure 8.8 should be applied, and a firm diagnosis made only after weighing up all of the parameters listed here.

chArAcTErIzATIoN oF MAjor A NoMALIEs

In most renal abnormalities, the prognosis is worse if the lesion is bilateral and/or if it is associated with extra-renal anomalies. In fact, bilateral renal malformations often cause renal insufficiency, which in turn is responsible for severe oligohydramnios. This may induce Potter sequence anomalies, including the

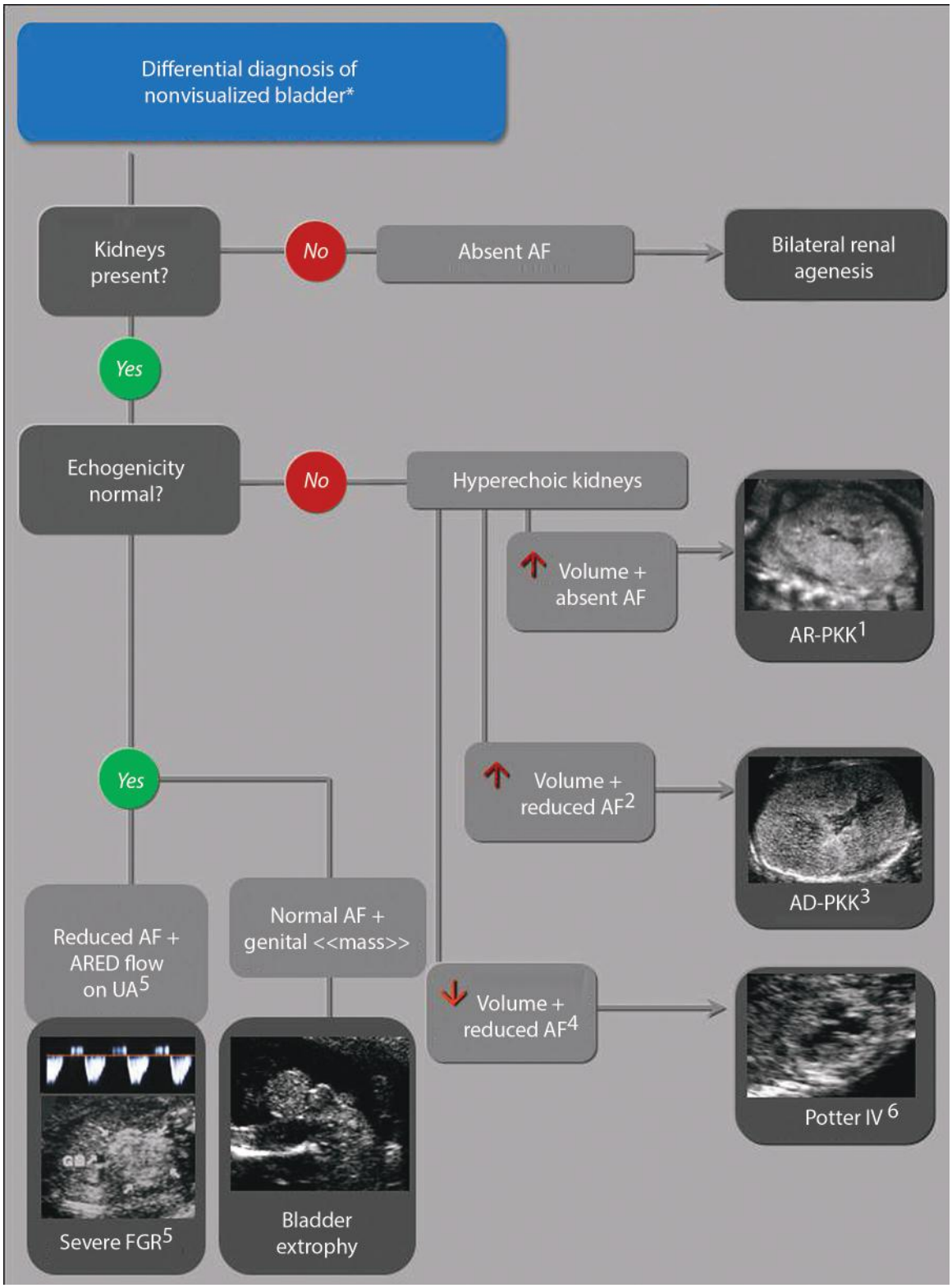


Figure 8.8 Differential diagnosis for "non visualization of the fetal bladder" (AF: amniotic fluid; ARED: absent or reversed end-diastolic flow; FGR: fetal growth restriction; UA: umbilical artery). *After exclusion of normal transient depletion from micturition; [1]autosomal recessive polycystic kidney (infantile type); [2]reduced amniotic fluid may be present, more frequently in the third trimester; [3]autosomal dominant polycystic kidney (adult type); [4]if bilateral, reduced amniotic fluid; [5]often associated with hyperechoic ileus from mesenteric ischemia; [6]cystic obstructive dysplasia

Potter facies, clubfeet, and other skeletal deformities. The association of extra-renal anomalies increases the risk of chromosomal and nonchromosomal syndromic conditions.

rENAL AGENESIS

Incidence. 1–2/1000 for the unilateral form and 1/3000–4000 for the bilateral form.

Ultrasound diagnosis. *Bilateral form*: lack of visualization of the kidneys and bladder associated with severe oligohydramnios (after the 16th week). *Unilateral form*: lack of visualization of one kidney, with normal bladder and amniotic fluid.

Risk of chromosomal anomalies. Low risk in isolated unilateral forms (<1%); slightly higher risk in isolated bilateral renal agenesis.

Risk of nonchromosomal syndromes. High: 20%–25%.

Outcome. Bilateral form: uniformly fatal. Unilateral form: good, if isolated.

Definition Renal agenesis is defined as the complete absence of one or both kidneys (unilateral or bilateral renal agenesis).

Etiology and pathogenesis. This anomaly is due to failure of the development of the ureteric bud or of any interaction with the metanephric blastema [3]. The incidence is 1–2/1000 for the unilateral form and 1/3000–4000 for the bilateral form.

Ultrasound diagnosis. Sonographic diagnosis of bilateral renal agenesis is based on the impossibility of visualizing the kidneys and the bladder, associated with severe oligohydramnios after the 16th week of gestation. In these cases, it is important not to mistake the adrenal glands for the kidneys (Figure 8.9a and b). The lack of an acoustic window, due to the severe oligohydramnios, can make the diagnosis challenging in some cases. In addition, the adrenal glands may be mistakenly interpreted as kidneys: in fact, due to the absence of the kidneys, these glands sometimes appear merely rounder than normal and fil the renal fossa in what has been termed the "lying down" adrenal sign (Figure 8.9). Although amnioinfusion has been proposed as a diagnostic aid, it is generally sufficien to employ color or power Doppler to confirm the absence of the renal arteries, a feature consistent with the diagnosis of bilateral renal agenesis (Figure 8.10). The course of the superior vesical arteries can also help to confirm the

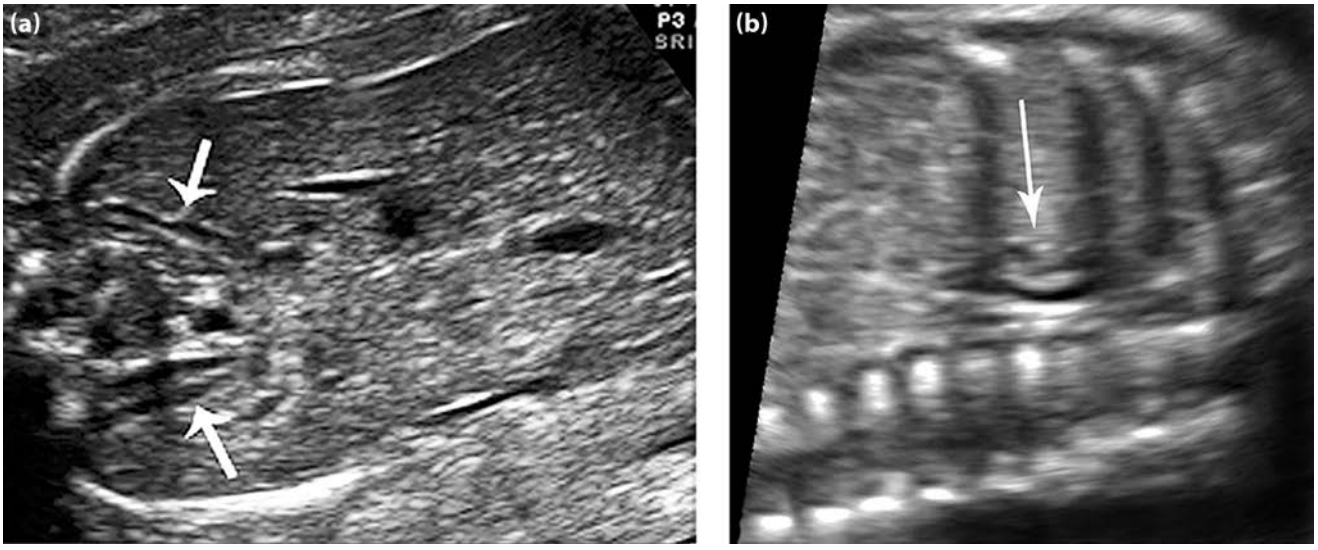


Figure 8.9 Bilateral renal agenesis. (a) The absence of both kidneys is evident despite the associated oligohydramnios; the arrows indicate both adrenal glands in the paraspinal regions. (b) The right adrenal gland (arrowhead) fills the renal fossa; the typical "ice cream sandwich" appearance of the adrenal gland is characterized by the hypoechoic cortex and hyperechoic medulla; this is quite different from the normal kidney. The image also depicts the "lying down" adrenal sign.

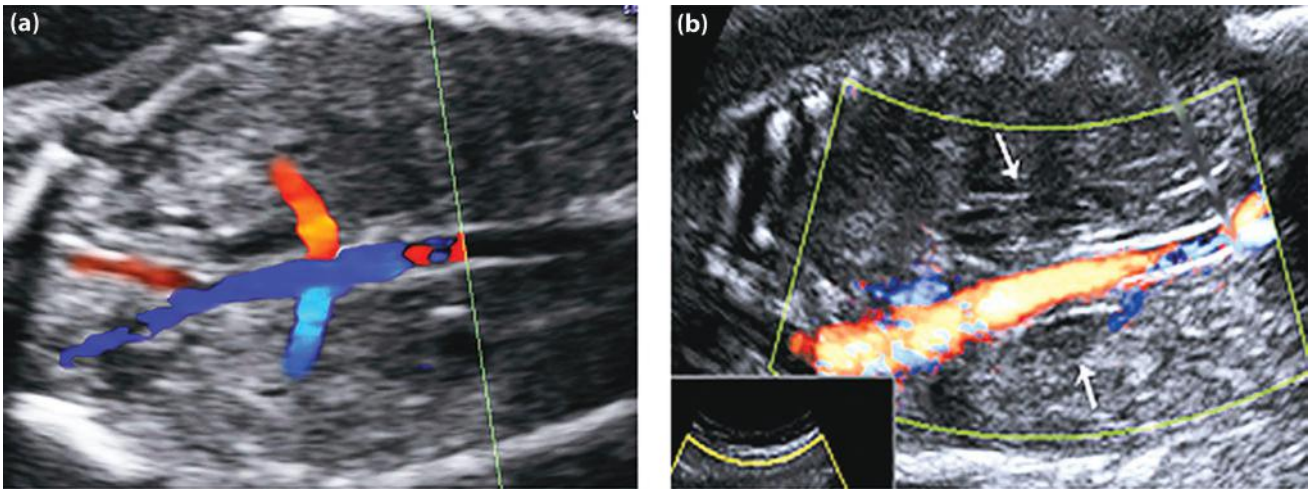


Figure 8.10 (a) Color flow Doppler shows both renal arteries in a 22-week fetus. (b) Absence of the renal arteries is noted in a case of bilateral renal agenesis, while the aorta is clearly shown; the arrows indicate the adrenal glands.

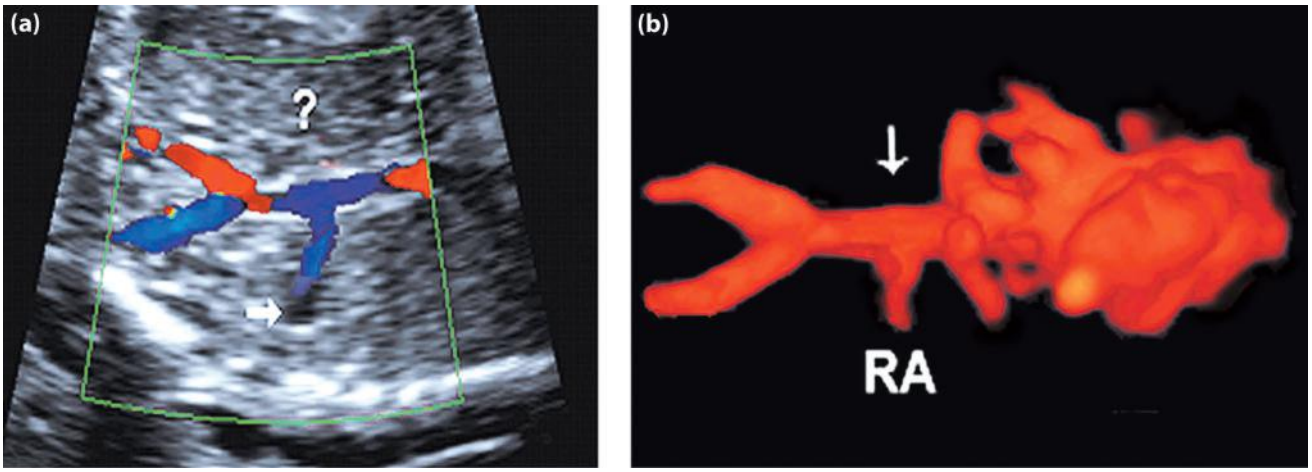


Figure 8.11 Unilateral renal agenesis. (a) Color Doppler image demonstrating a single renal artery. The arrow indicates the pelvis of the single kidney; ? indicates the empty contralateral renal area. (b) 3D power Doppler of the same case, showing a single renal artery (RA) branching off the abdominal aorta; the arrow indicates the absence of a contralateral renal artery.

absence of the bladder. Fetal biometry and Doppler evaluation of the umbilical artery velocity waveform rules out another cause of nonvisualization of the fetal bladder and oligohydramnios: fetal growth restriction (FGR). Most cases of *unilateral renal agenesis* escape prenatal diagnosis because the bladder and amount of amniotic fluid are normal, and so there are no indirect signs raising the suspicion of renal disease. Moreover, in the same way as in bilateral agenesis, the presence of the adrenal gland in the ipsilateral renal loggia may resemble the kidney. Color Doppler can be used in doubtful cases to confir the absence of the ipsilateral renal arteries (Figure 8.11). However, prior to a definite diagnosis of unilateral kidney agenesis, care should be taken to rule out the more frequent presence of an ectopic kidney (or of renal hypoplasia). In the third trimester, the findings of an enlarged kidney contralateral to the empty renal fossa can assist in diagnosing in utero the absence of the other kidney. In fact, unilateral renal agenesis can cause compensatory hypertrophy of the contralateral kidney.

Artifacts. As just underlined, there is a risk of mistaking the adrenal glands for the missing kidney(s), considering also the impaired acoustic window. The features that may help in differentiating the adrenals from the kidneys are as follows: the adrenal glands are smaller and oblong, and (in contrast to the renal medulla) the adrenal medulla is hyperechoic rather than hypoechoic. Finally, the renal pelvis cannot be visualized (Figure 8.9).

Differential diagnosis. In cases of bilateral renal agenesis, the differential diagnosis should include other

conditions possibly responsible for severe oligohydramnios: severe FGR and rupture of the membranes. In the presence of severe FGR, umbilical artery velocimetry is usually abnormal, while the presence of a normal bladder can help orientating the diagnosis towards rupture of the membrane, testifying a normal renal function.

Association with other malformations. The anomalies most frequently associated with unilateral renal agenesis [3] affect the contralateral kidney and the internal genital organs (which cannot be visualized in the prenatal period). Extra-renal anomalies often associated with bilateral renal agenesis include cardiac, cerebral, and skeletal malformations.

Risk of chromosomal anomalies. This is relatively low in isolated bilateral forms (1%–5%) and even lower in unilateral forms (<1%).

Risk of nonchromosomal syndromes. This is high (20%–25%). Renal agenesis can be the main sign of more than 40 different syndromes [3]. The most common syndromes and associations are as follows:

- *Fraser syndrome [3]*: look for ► *renal agenesis* + laryngeal atresia + cryptophthalmos + syndactyly (Chapter 10);
- *VA(C)TER(L) association [3]*: look for ► *renal agenesis* + vertebral anomalies + anal atresia + congenital heart disease (CHD) + tracheoesophageal fistula + limb anomalies (Chapter 10);
- *Caudal regression syndrome [3]*: look for ► *renal agenesis* + sacral agenesis + lumbar vertebral anomalies + femoral hypoplasia (Chapter 10);
- *Sirenomelia [3]*: look for ► *renal agenesis* + fusion of the lower limbs + anal atresia + vertebral anomalies + genital anomalies (Chapter 10);
- *Cerebro-oculo-facial-skeletal syndrome [3]*: look for ► *renal agenesis* + microcephaly + micrognathia + joint contractures;
- *Otocephaly [3]*: look for ► *renal agenesis* + agnathia + microstomia + holoprosencephaly + cleft lip and palate.

If renal agenesis is isolated, the empiric risk of recurrence is 3.5%, whereas if it is one sign of a syndrome, the risk of recurrence is obviously the risk associated with the underlying syndrome.

Obstetric management. Karyotyping is not mandatory for the unilateral form. Although the association with chromosomal anomalies is not considered to be high in the bilateral form, some authors advise karyotyping [4], especially in cases associated with other malformations, to help estimate the recurrence risk. US investigation of the parents' kidneys is necessary in cases of unilateral agenesis, in view of the autosomal dominant inheritance pattern of the condition. Postnatally, scintigraphy should be performed to gain confirmation of the renal agenesis and to assess the residual renal function.

Postnatal therapy. No treatment is available for bilateral renal agenesis: one-third of fetuses die in utero, and the remaining two-thirds die immediately after birth due to severe pulmonary hypoplasia.

Prognosis, survival, and quality of life. Bilateral renal agenesis is always lethal, due to the associated severe pulmonary hypoplasia. In fact, apart from provoking the typical Potter sequence (Potter facies, deformation of hands and feet, etc.), severe oligohydramnios induces lethal pulmonary hypoplasia. In fact, the compression of the fetal chest by the uterine walls and the absence of amniotic fluid impairs pulmonary development. In cases of unilateral agenesis, if the contralateral kidney is unaffected, the prognosis is good and the survival and quality of life are normal.

rENAL EcTopIA

This features an abnormal position of the kidney, which in most cases is located in the pelvis (Figure 8.12). The ectopic kidney can be positioned either ipsilaterally or contralaterally (crossed renal ectopia).

pELVIc kIdNEy

Incidence. 1/700 newborns.

Ultrasound diagnosis. Visualization of the kidney in the pelvis, beside the bladder.

Risk of chromosomal anomalies. Low.

Risk of nonchromosomal syndromes. Low.

Outcome. Good in isolated forms.

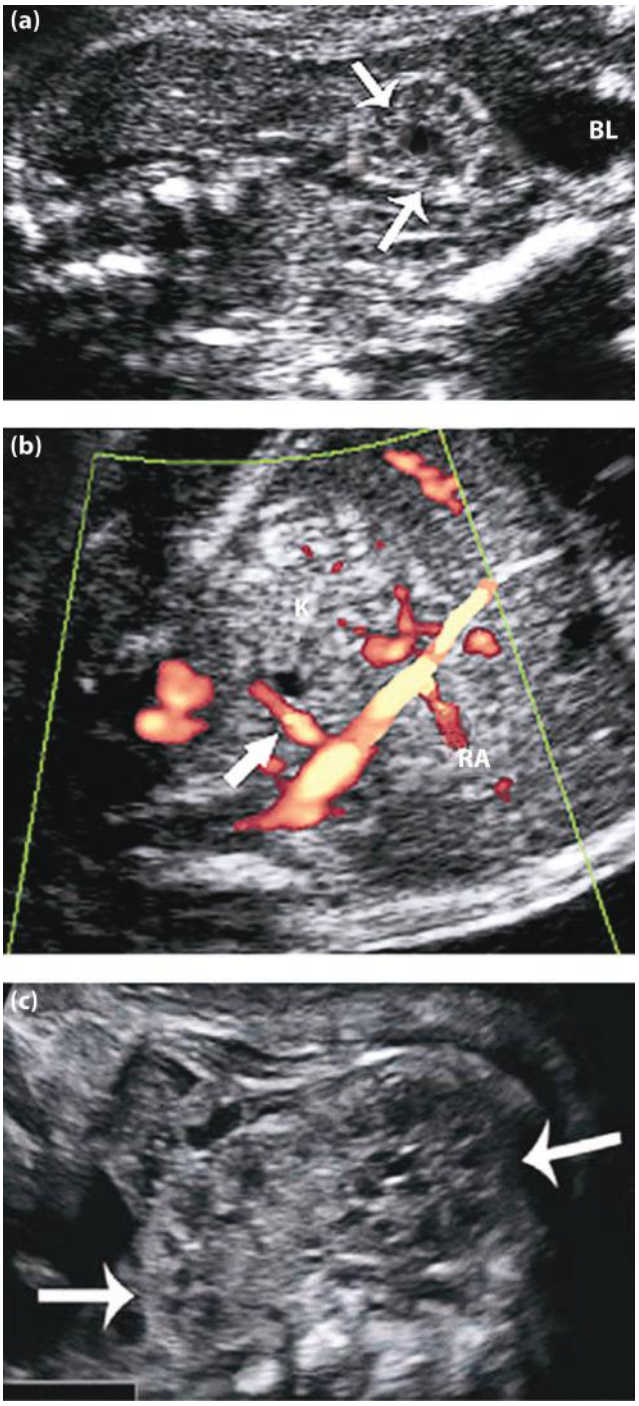


Figure 8.12 Pelvic kidney. (a) Oblique scan through the fetal pelvis. The kidney (arrows) is seen within the pelvis, lying superior to the bladder (BL). (b) Color flow Doppler shows the pelvic kidney artery (arrow), which originates from the aorta at a more caudal level than the contralateral renal artery (RA). K: pelvic kidney. (c) Crossed fused renal ectopia. Note the two fused kidneys (arrows); the lower pole of the upper one is fused with the upper pole of the lower one. In these cases, the kidneys are also abnormally rotated, as in horseshoe kidney.

Definition The kidney is positioned in the fetal pelvis, below the aortic bifurcation, on the midline in the presacral area.

Etiology and pathogenesis. The kidney fails to migrate up into the lumbar region between the sixth and tenth weeks of gestation [1]. The incidence of this anomaly is approximately 1/700 live-borns.

Ultrasound diagnosis. The kidney is not visible in its usual location. Only the adrenal gland is visible, and it can sometimes be mistaken for the kidney; instead, the kidney is positioned in the pelvis beside the bladder (Figure 8.12a), usually below the level of the aortic bifurcation. The amount of amniotic fluid and the filling of bladder are normal. In some cases, the vascularization renal artery of the pelvic kidney branches off as a tributary of the iliac arteries, rather than of the descending abdominal aorta (Figure 8.12b). A pelvic kidney is also frequently hypoplastic.

Differential diagnosis. A pelvic kidney must be differentiated from unilateral agenesis and from crossed renal ectopia, in which both kidneys are present, often partly fused (crossed fused ectopia), in the same half of the abdomen; one kidney is usually at the normal level, and the second is inferior to it. The fused kidneys commonly have a globular appearance. Color Doppler may help to visualize the separate vessels supplying the kidneys.

It should be underlined that the visualization of a pelvic kidney is often hampered by interposition of bowel loops and shadowing from the iliac wings. Color Doppler may be useful to locate the hilum of the ectopic kidney.

Association with other malformations. Apart from anomalies of the genital tract, which in any case cannot be identified in the prenatal period, the pelvic kidney can be associated with gastrointestinal and cardiac anomalies.

Risk of chromosomal anomalies. This is low.

Risk of nonchromosomal syndromes. This is low.

Obstetric management. An accurate anatomic scan should be performed by an expert in order to exclude the presence of associated anomalies. US examination of the parents' kidneys is recommended. Serial US follow-up is warranted in order to detect possible late-onset hydronephrosis, which is not uncommon.

Postnatal therapy. No treatment is needed, unless other abnormalities, such as vesico-ureteral reflux are present.

Prognosis, survival, and quality of life. In isolated forms, the prognosis is good. VUR and uretero-pelvic junction (UPJ) obstruction are frequently present.

FUSION ANOMALIES

HORSESHOE KIDNEY

Incidence. 1/400 newborns.

Ultrasound diagnosis. In axial scans, the isthmus linking the two inferior poles of the kidneys can be seen in front of the descending aorta.

Risk of chromosomal anomalies. High: Turner syndrome and trisomy 18.

Risk of nonchromosomal syndromes. Moderately high: 12%–16%.

Outcome. In isolated forms, horseshoe kidney is asymptomatic in about one-third of cases. Increased incidence of infections, nephrolithiasis, and vesico-ureteral reflux.

Definition The kidneys are fused, with an equal amount of renal tissue on each side of the midline. The inferior poles of the kidneys are linked by an isthmus of fibrous tissue or parenchyma. The ureters do not cross the midline before entering the renal sinuses.

Etiology and pathogenesis. Horseshoe kidney is the most common type of fusion anomaly. The anomaly originates after the interaction of the ureteral buds with the metanephric blastema, but before the migration and rotation processes [3]. The horseshoe kidney is usually positioned lower than normal because its ascent in the normal position is impeded by the emergence of the inferior mesenteric artery. In fact, the inferior poles are joined at an isthmus commonly located below the inferior mesenteric artery. The incidence is 1/400 newborns and is higher in males. This anomaly has a heterogeneous etiology. About 10% of parents of individuals with horseshoe kidney were found to have renal anomalies.

Ultrasound diagnosis. On transverse or oblique views of the fetal abdomen, the isthmus connecting the inferior poles of the two kidneys can be seen in front of the descending aorta; the kidneys appear medially and anteriorly rotated. In this scanning plane, it is also possible to see the two renal pelvises (Figure 8.13a), which have a more anterior location and are often slightly dilated. In the coronal plane, the shape of a horseshoe is clearly visualized (Figure 8.13b).

Association with other malformations. The anomalies most frequently associated include hydronephrosis (possibly due to vesico-ureteral reflux or ureteral obstruction) and genital anomalies (unrecognizable in the fetus). In one-third of the cases, extra-renal anomalies (CNS, cardiac, and skeletal malformations) are associated [3]. Association with Wilms' tumor in the prenatal period has also been described.

Risk of chromosomal anomalies. High. Horseshoe kidney is present in 30% of cases of Turner syndrome and about 20% of trisomy 18.

Risk of nonchromosomal syndromes. This is relatively high (12%–16%). The best-known syndromes possibly associated with horseshoe kidney are as follows:

- *Caudal regression syndrome [3]*: look for ► *horseshoe kidney* + sacral agenesis + lumbar vertebral anomalies + femoral hypoplasia (Chapter 10);
- *Otocephaly [3]*: look for ► *horseshoe kidney* + agnathia + CHD + cleft lip and palate;
- *Oro-cranio-digital syndrome [3]*: look for ► *horseshoe kidney* + cleft lip and palate + microcephaly + hypoplastic thumbs + elbow deformities.

Obstetric management. An accurate anatomic scan should be performed by an expert in order to exclude the presence of associated anomalies. Karyotyping is indicated. Serial US monitoring should be warranted to detect the possible late onset of hydronephrosis, which is not uncommon.

Postnatal therapy. Postnatal treatment may be indicated in the presence of hydronephrosis and nephrolithiasis.

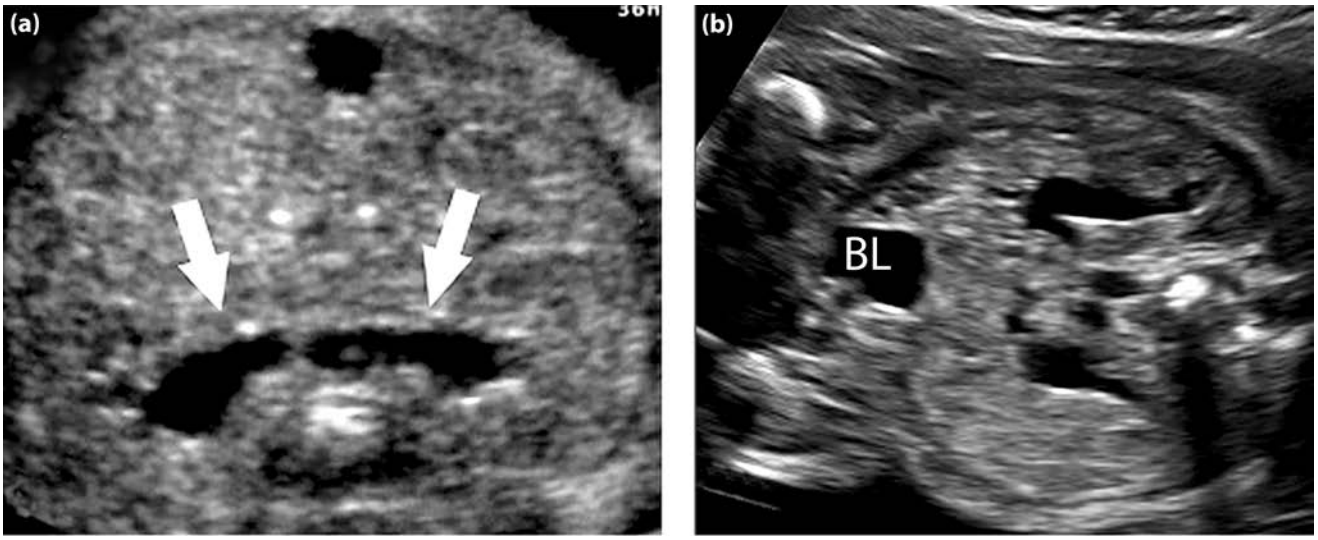


Figure 8.13 Horseshoe kidney. Ultrasound images showing (a) both renal pelvises (arrows), which have a more anterior location than normal; and (b) the slightly lower than normal location of the horseshoe kidney. The arrows indicate the renal pelvises; BL: bladder.

Prognosis, survival, and quality of life. In about one-third of the isolated forms, the anomaly is asymptomatic. Postnatal follow-up is advised because of the significant association with infections, nephrolithiasis, hematuria, and hydronephrosis. Prognosis, survival, and quality of life are poorer if the disease is associated with other anomalies, especially in the context of a syndrome. In isolated forms, the prognosis is better.

hyp Er Echo Ic kI d NEys

One of the prenatal US renal findings that can represent a difficult diagnosis is the bright or hyperechoic kidney. While increased echogenicity is a subjective assessment, kidneys that are brighter than liver or spleen after 15–17 weeks are considered to be hyperechoic. Hyperechogenicity of both kidneys (Figure 8.14) represents a dilemma, especially in the presence of a normal amniotic fluid volume. In fact, while the increased echogenicity of the renal parenchyma can be a normal variant, it can also result from the presence of dysplasia often associated with genetic syndromes (Table 8.1). Recently, the study of fetal renal disease in animal models, along with molecular biologic studies, has allowed investigation of the relationship between specific renal histological lesions and the underlying molecular mechanisms of disease [5]; this may help achieve a better comprehension of kidney diseases and their sonographic features.

The term *dysplastic kidney* is used to encompass a heterogeneous group of disorders due to abnormal development and differentiation of the metanephric mesenchyme, and to abnormal interaction with the ureteric bud. In a relevant proportion of cases,

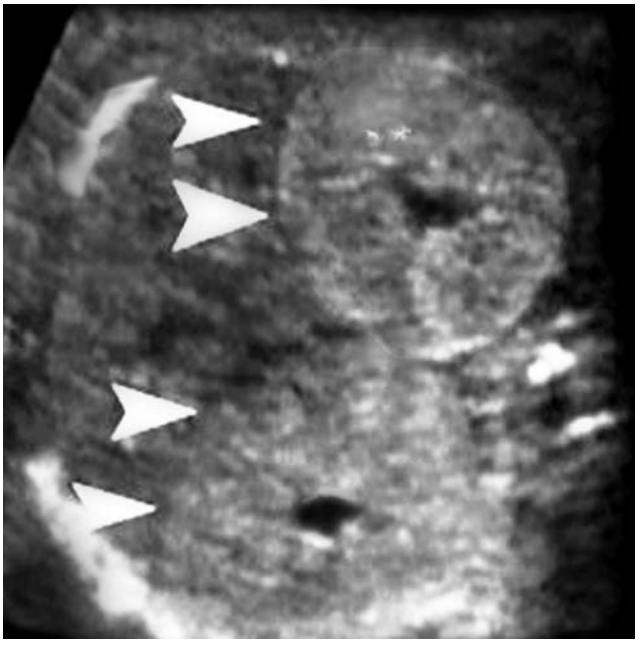


Figure 8.14 Coronal view of two hyperechoic kidneys in a 22-week fetus.

Table 8.1 Conditions associated with bright kidneys

Condition	Amniotic fluid	Renal macrocysts	Associated anomalies	Inheritance	Kidney volume
ARPKD	Decreased/absent	-	-	AR	Increased
ADPKD	Normal/decreased	±	-	AD	Increased
Beckwith–Wiedemann syndrome	Normal/increased	-	+	AD/sporadic	Increased
Perlman syndrome	Increased/decreased	-	+	AR	Increased
Trisomy 13	Normal/decreased	-	+	Sporadic	Increased
Bardet–Biedl syndrome	Normal	-	+	AR	Increased
Meckel–Gruber syndrome	Decreased	+	+	AR	Increased
Zellweger syndrome	Normal	-	+	AR	Normal
Elejalde syndrome	Decreased	-	+	AR	Increased
Cystic dysplasia (Potter IV)	Decreased/absent	±	-	10% AD	Normal/ decreased

ARPKD: autosomal recessive polycystic kidney disease; ADPKD: autosomal dominant polycystic kidney disease; AR: autosomal recessive; AD: autosomal dominant.

dysplastic kidneys are associated with ectopic placement of ureteric orifices, and/or with abnormalities of the urinary tract, leading to unilateral, bilateral, or focal obstruction of urine flow. Dysplastic organs often contain cysts, usually deriving from dilated terminal ampullae of the ureteric bud. As a general rule, severely dysplastic kidneys have no excretory function, are usually attached to atretic or absent ureters, and remain asymptomatic only if unilateral. On ultrasound, as reported elsewhere in this chapter, the increased echogenicity of the renal parenchyma can be related to the dysplasia and/or multiple microscopic cysts, although it does not represent a specific sign, since at times it is also present in the absence of dysplasia. Sometimes, even if the parenchyma is not hyperechoic, the dysplasia may still be present. Kidneys with focal dysplastic lesions may exhibit an almost normal function and may be diagnosed later in life owing to the late onset of signs and/or symptoms related to their larger size, or to the occurrence of frequently relapsing infections.

In the case of hyperechoic kidney ± renal macrocysts, US examination of the parents and grandparents is useful. Kidney morphology must be evaluated, and their size compared with the reference table. An accurate anatomic scan should be performed in order to exclude or detect other malformations, and karyotyping should be discussed, especially if other anomalies are present. An accurate fetal anatomic scan, family history, and adequate counseling are mandatory also in the case of apparent isolated large kidney. In fact, it can occur as a normal variant, a compensatory hypertrophy (if the contralateral kidney is absent), or, less frequently, a component of a genetic syndrome.

AUTOSOMAL RECESSIVE POLYCYSTIC KIDNEY DISEASE (ARPKD): POTTER TYPE I

Incidence. 1/20,000–40,000 newborns.

Ultrasound diagnosis. Both kidneys are increased in volume and are hyperechogenic. The bladder cannot be visualized, and severe oligohydramnios is present.

Risk of chromosomal anomalies. The pathology is monogenic (a single-gene disorder with multiple mutant alleles).

Risk of nonchromosomal syndromes. High, if the polycystic aspect (and not the genetic cause) is considered.

Outcome. Unfavorable, due to associated severe pulmonary hypoplasia.

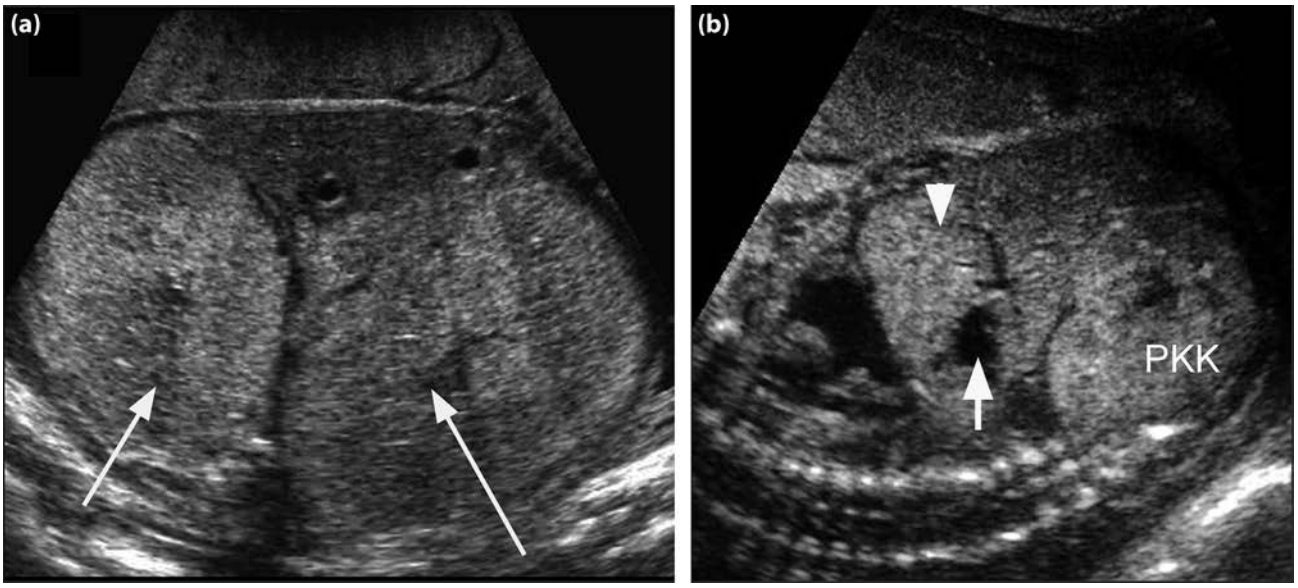


Figure 8.15 Autosomal recessive polycystic kidney disease (ARPKD): Potter type I. (a) Axial scan through the fetal abdomen showing the enlarged hyperechoic kidneys (arrows). (b) Sagittal scan of the fetal abdomen (another case) showing the increased echogenicity of the liver due to cystic fibrosis (arrowhead: cystic fibrosis; arrow: single large cyst; PKK: affected polycystic kidney).

Definition This is a bilateral anomaly mainly characterized by fusiform cystic dilations of the collecting ducts. The kidneys appear spongy, and there is no clear separation between cortex and medulla. The cut surface demonstrates the cortical extension of fusiform or cylindrical spaces arranged radially throughout the renal parenchyma from the medulla to the cortex [6,7]. It is an inherited disorder with an autosomal recessive inheritance pattern [6]. The disease is associated with portal and interstitial fibrosis of the liver. According to the time of onset, which is a function of the proportion of dilated renal ducts, autosomal recessive polycystic kidney disease (ARPKD) is subdivided into perinatal, neonatal, infantile, and juvenile forms.

Etiology and pathogenesis. The disease is caused by mutations in the *PKHD1* gene on chromosome 6p21 [6]. The protein encoded by the *PKHD1* gene is known as polyductin or fibrocystin and it is characterized by a single transmembrane segment and a short cytoplasmic C-terminal portion. However, significant genetic heterogeneity is present. Primary anomalies of the tubular cilia are clearly involved in the pathogenesis of the disease. The incidence is 1/20,000–1/40,000 newborns.

Ultrasound diagnosis. On US, ARPKD is characterized by increased volume and hyperechogenicity of both kidneys. These two signs result from the insonation of interfaces provided by the walls of the microcysts (Figure 8.15). The bladder cannot be seen, and severe oligohydramnios is usually present, starting from 16 weeks onward. Despite the fact that in a significant number of cases the disease becomes sonographically recognizable in the third trimester only, in more than 70% of cases the diagnosis can be made in the second trimester. Repeated sonographic measurements of kidney length appear to be the most useful parameter. In addition, unlike in the normal kidney, in the third trimester it will not be possible to differentiate the cortex from the medulla because cortico-medullary differentiation is less defined or completely lacking [6,7] (Figure 8.15). In some cases, densely echogenic renal pyramids or macrocysts are present. In milder forms, which have been demonstrated to involve only part of the nephrons, prenatal US diagnosis may be very challenging.

Differential diagnosis. This includes mainly the autosomal dominant form of polycystic kidney disease (ADPKD, Potter type III). The latter is generally associated with a normal quantity of amniotic fluid and a normal bladder (Table 8.1). Moreover, the differentiation between the cortex and the medulla is more pronounced in comparison with ARPKD, because the cortex tends to be hyperechoic whereas the medulla is normally hypoechoic, probably due to confinement of the microcysts to the cortical region [7] (Figure 8.16). However, the family history and a rapid US assessment of the parents' kidneys often solve any diagnostic doubt, because of the different inheritance pattern of the two diseases (autosomal recessive for ARPKD and autosomal dominant for the adult form).

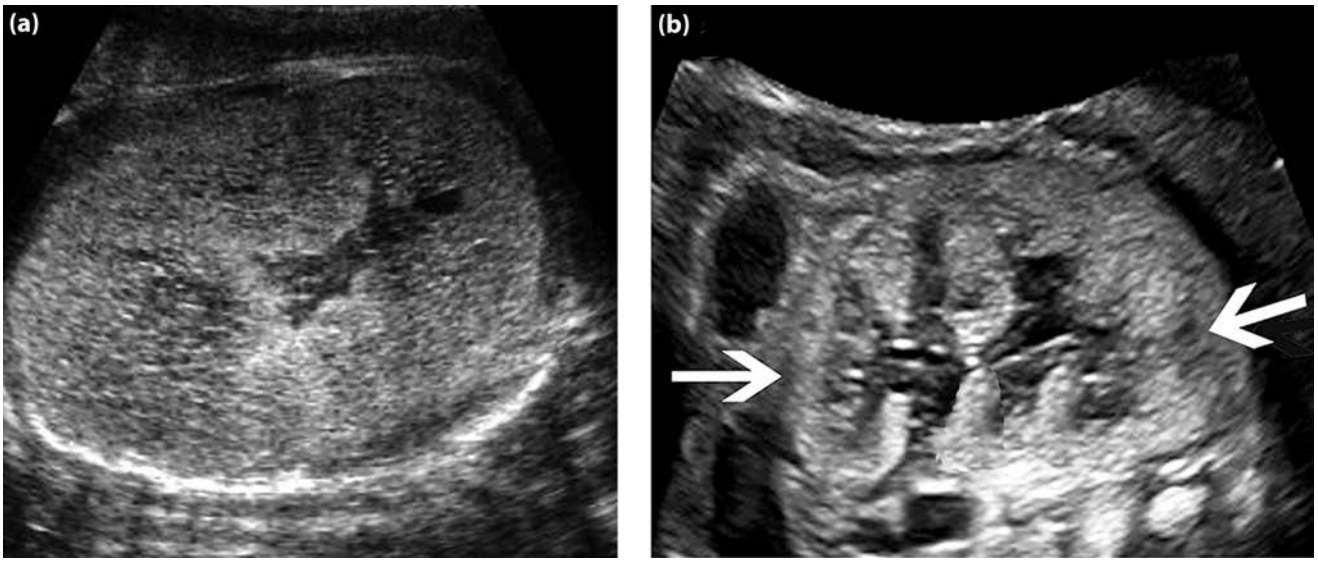


Figure 8.16 Polycystic kidney disease. (a) In ARPKD, there is no clear separation between cortex and medulla; thus, the kidney appears homogeneously hyperechoic. (b) In ADPKD, on the other hand, there is a more evident differentiation between the cortex and medulla.

Association with other malformations. These include cystic fibrosis of the liver (Figure 8.15), pulmonary hypoplasia, and the Potter phenotype (the last two linked to severe oligohydramnios sequence). It should be noted that in ARPKD, the disease spectrum ranges from mild kidney alterations with severe liver involvement to the reverse picture or inverse?

Risk of chromosomal anomalies. The condition is a single-gene disorder, not associated with karyotypic alterations.

Risk of nonchromosomal syndromes. Enlarged and hyperechoic kidneys can be found in a relatively high number of syndromic conditions [7] (Table 8.1). In Bardet–Biedl syndrome, as in ARPKD, there is little or no cortico-medullary differentiation; however, polydactyly is present, and the quantity of amniotic fluid and bladder filling is usually normal. In Meckel–Gruber syndrome, the markedly increased kidney volume is generally apparent even earlier, macrocysts are present, and CNS anomalies and polydactyly are associated in most cases, although they are difficult to recognize because of the common occurrence of severe oligohydramnios. The presence of the extra-renal findings is sufficient to make a differential diagnosis in the two aforementioned syndromes and in other rarer conditions characterized by enlarged and hyperechoic kidneys (Table 8.1):

- *Meckel–Gruber syndrome [3]*: look for ► *enlarged and hyperecoic (with macrocysts) kidneys* + cephalocele + microcephaly + polydactyly (Chapter 10);
- *Bardet–Biedl syndrome [3]*: look for ► *enlarged and hyperecoic kidneys* + polydactyly + genital anomalies;
- *Beckwith–Wiedemann syndrome [3]*: look for ► *enlarged and hyperecocic kidneys* + macroglossia + omphalocele + hemihypertrophy (Chapter 10);
- *Perlman syndrome [3]*: look for ► *enlarged and hyperecoic kidneys* + diaphragmatic hernia + macrosomia + cleft palate + dextrocardia;
- *Elejalde syndrome [3]*: look for ► *enlarged and hyperecoic kidneys* + omphalocele + corpus callosum agenesis + macrosomia + craniosynostosis + skeletal dysplasia.

Obstetric management. After the 24th week of gestation, management is conservative. Molecular typing of polycystic kidneys has yielded a better understanding of the disease, but the possibility of making an early genetic diagnosis of the disease during the prenatal period is still very limited. In the case of ARPKD, mutations of the *PKHD1* gene are responsible for the disease, but there is a high rate of allelic heterogeneity and a high frequency of missense mutations, whose identificatio usually requires gene sequencing. For this reason, in sporadic cases identified in the prenatal period, it is unlikely that the specific mutation will be identified within a reasonable time frame. However, when other cases have occurred in the family, there are much more technical possibilities, because linkage analysis (individualizing the haplotype associated with the disease) can be performed under suitable conditions (informed consent of the family and available DNA from a previously affected

family member). In doubtful cases in which other anomalies are associated, karyotyping may be advisable.

Postnatal therapy. No treatment is possible.

Prognosis, survival, and quality of life. Up to 40%–50% of affected individuals die in the early neonatal period due to respiratory insufficienc , and the majority of surviving infants develop hypertension. Progression to end-stage renal disease occurs in 50% of the remaining cases within ten years, but a proportion maintain renal function into adulthood, where complications of liver disease predominate.

MULTIcys TIc dysp LAs TIc k Id NEy d Is EAs E (Mckd): po TTEr Typ E II

Incidence. 1/1000–5000 live births; unilateral in approximately 75%–80% of cases.

Ultrasound diagnosis. *Unilateral*: the kidney is increased in volume, with multiple noncommunicating cysts of variable size; the parenchyma is hyperechoic; there is a normal amount of amniotic fluid and bladder is visualized. *Bilateral*: same as above + severe oligohydramnios and inability to visualize bladder.

Risk of chromosomal anomalies. Relatively low in isolated unilateral forms (2%–4%); reaches 15%–18% in bilateral forms and 25%–28% when associated with other anomalies.

Risk of nonchromosomal syndromes. 5%–10%.

Outcome. *Unilateral form*: involution of the kidney, resulting in hypoplastic kidney in a significant percentage of cases within the first two years of life. *Bilateral form*: unfavorable prognosis.

Definition It is an enlarged kidney whose parenchima is replaced by multiple, non communicating macrocysts of variable size and number.

Etiology and pathogenesis. This is due to an abnormal development, associated in a significant percentage of cases with early obstruction (atretic ureters) [3]. It is unilateral in approximately 75%–80% of cases, but it may also be bilateral or segmented, in which case small areas of renal parenchyma are also present. The incidence is 1/1000–5000 births. It is usually sporadic, but recurrence has been described in 1%–2% of cases.

Ultrasound diagnosis. In the majority of cases, the US diagnosis can be made in the second trimester, and it relates to a single kidney with multiple noncommunicating cysts of variable size mixed with hyperechogenicity of the parenchyma (Figure 8.17). The dimensions of the kidney are often significantl increased and depend on the number and dimensions of the cysts that do not communicate with a renal pelvis (Figure 8.17). The bladder and quantity of amniotic fluid are usually normal. The volume of multicystic kidneys is often increased, and for this reason multicystic dysplastic kidney disease (MCKD) represents one of the most common causes of abdominal mass in the neonate. A variety with reduced volume is also described, as is the possibility of evolution into renal hypoplasia [8]. In rare cases, the cystic element may only involve part of the kidney, particularly when associated with the presence of a duplex kidney. The ipsilateral renal artery may be absent or small, with the presence of Doppler velocity waveform anomalies. When, less frequently, both the kidneys are multicystic, severe oligohydramniosis is present and the bladder cannot be visualized [8]. In sporadic cases, the multicystic kidney may also have an ectopic site.

Differential diagnosis. This mainly involves severe hydronephrosis. When the position of the cysts resembles that of a calicopyelic dilation, the presence of anomalous renal tissue between the cysts and the lack of communication between the cysts indicate a diagnosis of multicystic kidney. If the differential diagnosis is particularly difficult some authors have suggested aspiration of the cystic fluid which, in the case of multicystic kidney, shows high phosphate levels. When both kidneys are multicystic, the differential diagnosis should be made with Meckel–Gruber syndrome. However in the latter, extrarenal anomalies are always present [8].

Association with other malformations. Children with unilateral MCKD have an increased risk of abnormalities of the contralateral kidney and the lower urogenital tract; heart, CNS, and gastrointestinal problems have frequently been reported in association.

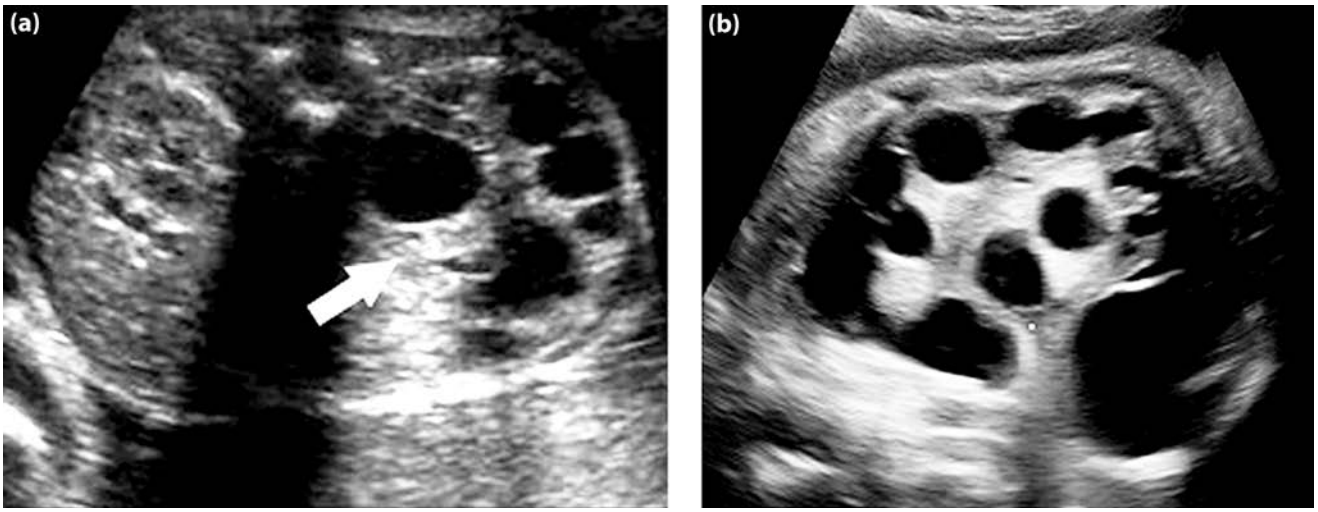


Figure 8.17 Multicystic dysplastic kidney disease (MCKD): Potter type II. (a) Axial scan through the fetal abdomen showing an enlarged right kidney (arrow) with multiple cysts within the hyperechoic parenchyma; the contralateral kidney is normal. (b) Coronal scan through the fetal abdomen showing an enlarged kidney with increased echogenicity and numerous noncommunicating cysts.

Risk of chromosomal anomalies. This is relatively low (2%–4%), but it reaches 15%–18% in bilateral forms and 25%–28% when associated with other anomalies.

Risk of nonchromosomal syndromes. This is 5%–10%. The most common syndromes possibly associated with MCKD are as follows:

- *Brachio-otorenal syndrome [3]*: look for ► *multicystic kidney* + pre-auricular tags + branchial cleft-fistulas;
- *Cerebro-reno-digital syndrome [3]*: look for ► *multicystic kidney* + digital and limb anomalies + CNS malformations;
- *VA(C)TER(L) association [3]*: look for ► *multicystic kidney* + vertebral anomalies + anal atresia + CHD + tracheo-esophageal fistula + limb anomalies (Chapter 10);
- *Short-rib polydactyly syndrome [3]*: look for ► *multicystic kidney* + narrow thorax + polydactyly;
- *Meckel–Gruber syndrome [3]*: look for ► *enlarged and hyperecoic (with macrocysts) kidneys* + cephalocele + microcephaly + polydactyly.

In isolated forms, the risk of recurrence is 3%; in syndromic forms, it is that of the underlying syndrome.

Obstetric management. In the case of unilateral involvement, serial US scans should be arranged in order to follow-up the lesion during gestation, as it may sometimes reduce in volume; at the same time, the onset of hydronephrosis (up to 40% of cases) on the contralateral kidney should be verified In the case of unilateral MCKD, meticulous long-term (pre- and postnatal) screening of the entire urinary tract is warranted. In bilateral forms, the prognosis is unfavorable due to the presence of oligohydramnios, due to complete renal insufficienc , which may result in the Potter sequence and death from lethal pulmonary hypoplasia.

Postnatal therapy. After birth, scintigraphy is recommended to confirm the type of lesion in doubtful cases and to evaluate residual renal function. During the early years of life, serial US follow-up must be carried out. Evaluation of the contralateral kidney is important, to ascertain the possible presence of associated anomalies and/or an infection. Nephrectomy is recommended if the multicystic kidney is symptomatic, being responsible for hypertension, hematuria, or infection. In this regard, it must be remembered that during the first two years of life, there is a high chance of involution of the multicystic kidney.

Prognosis, survival, and quality of life. Although occasional cases of infection or hypertension associated with multicystic kidneys have been reported, prognosis, survival, and quality of life are good in the majority of cases of isolated forms. When the multicystic disease is bilateral, a conservative approach is recommended after the 24th week, due to the unfavorable prognosis.

AUTosoMAL doMINANT poLycys TIc kIdNEy dIsEAsE (Adpkd): poTTEr Typ E III

Incidence. Affects approximately 1/1000 people.

Ultrasound diagnosis. Kidneys moderately increased in volume, hyperechogenic (often the cortex only), with visible pelvises; the bladder can be visualized and the amniotic fluid is normal or slightly reduced.

Risk of chromosomal anomalies. The anomaly is monogenic.

Risk of nonchromosomal syndromes. Relatively high, if the polycystic aspect (and not its cause) is considered.

Outcome. Although the symptoms usually occur in the third to fifth decades of life, the prognosis is apparently worse in the prenatally detected forms.

Definition This is a bilateral anomaly mainly characterized by cysts that arise from all areas of the nephron or collecting duct. The disease is inherited with an autosomal dominant pattern. It is typically of adult onset, becoming symptomatic usually in the third to fifth decades of life [3], but it can be identified in the fetus in families at risk. In prenatal life, ADPKD is characterized by the presence of enlarged kidneys that also show increased parenchymal echogenicity (often involving the outer layer only) due to the presence of microcysts. In ADPKD, initial nephron and collecting duct formation is unremarkable, but cystic dilation of these structures then ensues, causing secondary loss of adjacent normal parenchyma. According to some authors, the cases identified in the fetus have a poorer prognosis

Etiology and pathogenesis. This is the most common hereditary kidney disorder, with an incidence of 1/1000 in the general population. Mutations of two genes on chromosome 16 have been found to be responsible for the disease. Mutations of the *PKD1* gene, encoding polycystine 1, are responsible for approximately 85% of cases, whereas mutations of the *PKD2* gene, encoding polycystine 2, are responsible for approximately 10%–12% of cases; the latter mutations are responsible for the less severe cases occurring later in life. It is probable that there is also a third gene responsible for the remaining cases, but it has not yet been identified. Both polycystines are located in the primary cilia of the renal tubules and are involved in regulation of the cell cycle and in the intracellular transport of calcium (voltage-activated calcium channels). The prevailing pathogenetic hypothesis is the so-called *second-hit theory*: the genetic defect causes the focal formation of cysts, which initially involve less than 5% of the nephrons; a subsequent somatic mutation in the normal allele causes full expression of the disease later in life. The considerable variation in the phenotypic expression of the disease within individual families, and the variability of extra-renal events, suggests interaction between environmental factors and other modifying genes in modulation of the clinical expression.

Ultrasound diagnosis. The kidneys are hyperechoic (often in the cortical region only) and moderately increased in volume. The bladder and quantity of amniotic fluid are usually normal. Typically, and unlike ARPKD, the pelvises can be visualized. Furthermore, corticomedullary differentiation is increased in a discrete number of cases because the cortical is hyperechoic whereas the medulla is regularly hypoechoic, probably due to the selective presence of microcysts in the cortical region [6,7] (Figure 8.18). Less frequently, as in the autosomal recessive variety, the kidneys are considerably increased in size, and corticomedullary differentiation is absent or decreased or macrocysts may be present. The US picture described above frequently follows a normal result during the second-trimester scan. In addition, a normal US result during the prenatal period does not exclude the presence of this disease. On the contrary, in some affected families, the sonographic signs of renal disease are evident as early as the 15th week. In few cases the presence of macrocysts has been also described

Differential diagnosis. The differential diagnosis of the two polycystic kidney variants is based on a positive family history and on the recognition, in the autosomal dominant variant, of moderately enlarged kidneys with normal bladder and amniotic fluid [7] (Table 8.1). Furthermore, corticomedullary differentiation is frequently increased in ADPKD, while it is lost in ARPKD (Figure 8.16). In a minority of cases of ADPKD, the kidneys are severely enlarged and show loss of corticomedullary differentiation. In a few cases, ADPKD may also feature late-onset oligohydramnios and a reduced filling of the bladder. Enlarged and hyperecoic kidneys can also be present in a number of syndromic conditions, which are described in the "Risk of nonchromosomal Syndromes" section.

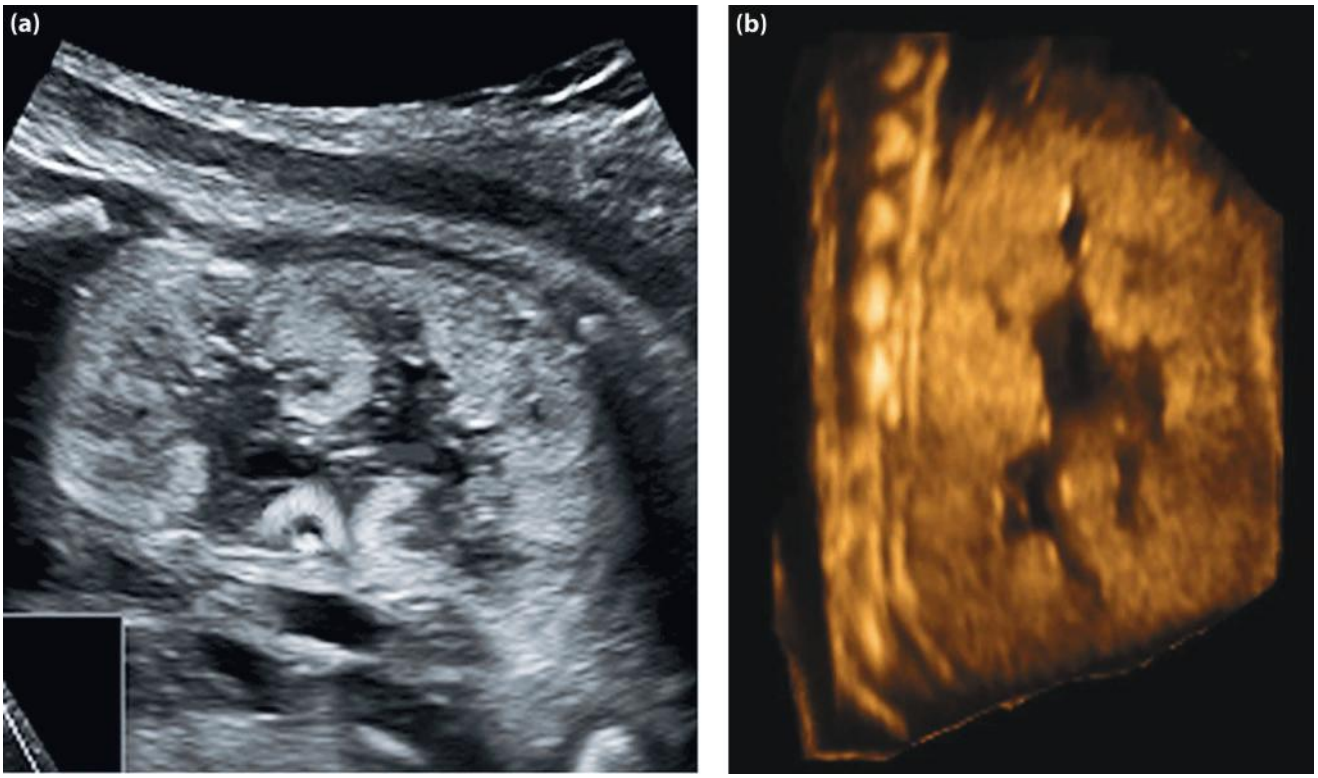


Figure 8.18 Autosomal dominant polycystic kidney disease (ADPKD): Potter type III. (a) Ultrasound image showing an enlarged kidney with increased differentiation between the cortex and the medulla. (b) 3D surface rendering of the same case.

Risk of chromosomal anomalies. The disease is monogenic.

Risk of nonchromosomal syndromes. The following syndromic conditions may have a enlarged and hyperecoic kidneys among their typical features (Table 8.1):

- *Meckel–Gruber syndrome [3]*: look for ► *Enlarged and hyperecoic (with macrocysts) kidneys* + encephalocele + microcephaly + polydactyly;
- *Bardet–Biedl syndrome [3]*: look for ► *enlarged and hyperecoic kidneys* + polydactyly and genital anomalies;
- *Beckwith–Wiedemann syndrome [3]*: look for ► *enlarged and hyperecoic kidneys* + macroglossia + omphalocele + hemihypertrophy;
- *Perlman syndrome [3]*: look for ► *enlarged and hyperecoic kidneys* + diaphragmatic hernia + macrosomia + cleft palate + dextrocardia;
- *Elejalde syndrome [3]*: look for ► *enlarged and hyperecoic kidneys* + omphalocele + agenesis of the corpus callosum + macrosomia + craniosynostosis + skeletal dysplasia.

Obstetric management. Once ADPKD has been diagnosed in a fetus, serial US monitoring is necessary in order to assess changes in the amount of amniotic fluid which reflects renal function. If the prenatal diagnosis is prospective (in the absence of a known family history), US examination of the parents' kidneys is indicated, given the autosomal dominant pattern of inheritance. The genetic diagnosis in ADPKD appears complex, due to the genetic heterogeneity (with two genes identified *PKD1* and *PKD2*) and to the sizes of the genes themselves, which make a direct search for the mutations both long and expensive; hence, in these cases, pedigree-based linkage analysis usually represents the only possible choice. However, it should be noted that the very late onset of kidney failure in this disorder and the possible treatment (dialysis and transplant) reduce the yield of genetic prenatal diagnosis. In families at risk, serial fetal US monitoring allows disclosure during the second trimester of the fetuses affected with ADPKD, with the earliest evidence being at 15 weeks in selected cases.

Postnatal therapy. Dialysis and transplant are the treatment options when the pathology becomes symptomatic (usually the third to fifth decades of life)

Prognosis, survival, and quality of life. Generally, the disease becomes clinically evident during the third to fifth decades of life. However, it has recently been

reported that prenatal recognition of the disease is a bad prognostic sign, since some of these neonates are apparently likely to develop hypertension during the first year of life

oBsTrUcTIVE cys TIc dysp LAsIA: poTTEr Typ E IV

Incidence. The bilateral form is more frequent.

Ultrasound diagnosis. Kidney(s) of normal or reduced dimensions with increased echogenicity of the parenchyma and presence of cysts in variable positions (frequently pericortical). If bilateral, oligohydramnios and a dilated bladder with thick walls are present.

Risk of chromosomal anomalies. 5%–10% in isolated forms; higher if associated with other anomalies (15%–25%).

Risk of nonchromosomal syndromes. 3%–6% in isolated forms.

Outcome. In isolated forms, this depends on the severity of the obstruction and the extent of the dysplasia.

Definition Potter type IV cystic dysplasia is due to early and severe obstruction of the collecting system. This may cause the formation of cysts, which are variously distributed in the renal parenchyma, with prevalence in the cortical part; the kidney volume is often decreased.

Etiology and pathogenesis. Potter type IV cystic dysplasia is commonly secondary to an early and severe obstruction of the urinary tract (mainly the lower urinary tract) that results in an abnormal environment during nephrogenesis, lasting for the rest of the gestational period [3].

Ultrasound diagnosis. The US diagnosis of renal cystic dysplasia (Potter type IV) secondary to early and severe obstruction of the urinary tract is based on the recognition of increased echogenicity of the renal parenchyma usually associated with cysts, which are often pericortical (Figure 8.19). The increased echogenicity of the renal parenchyma is related to the dysplasia, although it does not represent a specific sign: in fact, the kidneys can be hyperechoic but not dysplastic or, conversely, can show normal echogenicity and impaired function.

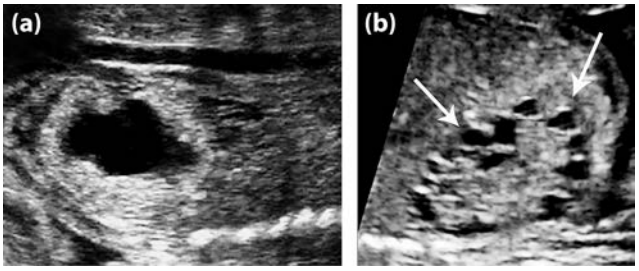


Figure 8.19 Obstructive renal cystic dysplasia: Potter type IV. (a) Longitudinal scan through the fetal abdomen showing a hydronephrotic kidney with echogenic parenchyma. (b) Ultrasound image of the cystic kidney showing several subcortical small cysts (arrows).

In its bilateral form, Potter type IV cystic dysplasia is associated with early and severe obstruction of the urethra that is responsible for severe oligohydramnios and thickening of the bladder walls (Figure 8.20).

Differential diagnosis. The main conditions to be distinguished from Potter type IV cystic dysplasia are shown in Table 8.1.

Association with other malformations. A significant association with cardiac and cerebral malformations has been reported.

Risk of chromosomal anomalies. This is 5%–10% in isolated forms, but it is higher (15%–25%) if associated with other anomalies.

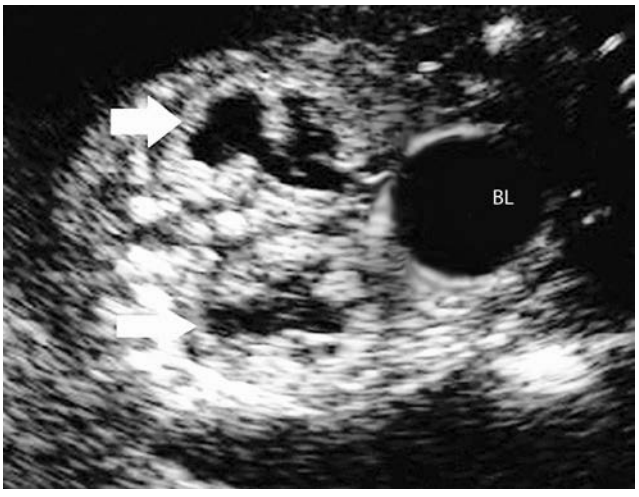


Figure 8.20 Obstructive renal cystic dysplasia: Potter type IV. Coronal scan of the fetal abdomen showing a distended urinary bladder (BL) and hydronephrotic kidneys with an echogenic cortex (arrows).

Risk of nonchromosomal syndromes. This is 5%–10%. The most common syndromes possibly associated with cystic renal dysplasia are as follows:

- *VA(C)TER(L) association [3]*: look for ► *renal cystic dysplasia* + vertebral anomalies + anorectal atresia + tracheoesophageal fistula + CHD + limb anomalies;
- *Cerebrorenodigital syndrome [3]*: look for ► *renal cystic dysplasia* + digital and limb anomalies + CNS malformations;
- *Tuberous sclerosis [3]*: look for ► *renal cystic dysplasia* + cardiac rhabdomyomas + intracranial calcifications.

Obstetric management. In the unilateral variety, which is less frequent, it is of the utmost importance to monitor the sonographic aspect and function of the contralateral kidney, in order to exclude the occurrence of concurrent diseases that might worsen the prognosis. In the bilateral form, termination of pregnancy or conservative treatment after 24 weeks of gestation may be advised.

Postnatal therapy. Surgical removal of the obstruction is relevant only in those cases in which residual renal function has been confirmed

Prognosis, survival, and quality of life. In bilateral forms, the prognosis is unfavorable; in the majority of cases, neonatal death is due to pulmonary hypoplasia, as a consequence of the severe oligohydramnios. In the unilateral form, the outcome depends on the presence of contralateral kidney anomalies and on possible associated anomalies.

HYDRONEPHROSIS, HYDROURETERONEPHROSIS, AND BLADDER DILATATION

Hydronephrosis, hydroureteronephrosis, and bladder dilatation can be associated or not with obstructions of the urinary tract. In this section, these three US findings will be examined and related to their most common causes. Hydronephrosis and hydroureteronephrosis will be dealt with together because of their relatively similar characteristics. The prognosis and treatment of these three abnormal renal findings will be discussed at the end of the section.

HYDRONEPHROSIS

Incidence. 1–5/500 newborns.

Ultrasound diagnosis. Dilatation of the collecting system of the kidney.

Risk of chromosomal anomalies. Low in isolated cases: 1%–3%.

Risk of nonchromosomal syndromes. Relatively low: 6%–8%.

Outcome. In the first two years of life: spontaneous regression in approximately 40%–50% of cases and need for surgery in 20%–30% of cases, according to the grade of hydronephrosis present during the prenatal period. In bilateral forms associated with oligohydramnios, unfavorable prognosis with the possibility, in very selected cases, of in utero therapy.

Definition Hydronephrosis is characterized by dilatation of the collecting system of the kidney. Fetal hydronephrosis is usually the expression of an obstruction of the urinary tract (Table 8.2) and, less frequently, of a nonobstructive pathology. In addition, in some cases, it may represent a transient finding related to the normal development of the urogenital system. Paradoxically, an obstructive lesion of the urinary tract may not show any sign of hydronephrosis and may be recognized only by the presence of renal dysplastic modifications frequently associated with oligohydramnios. Generally speaking, the severity of the US findings and the clinical situation are dependent upon the severity of the obstruction, its time of onset, and its duration. As a result, the US evaluation of a fetus with abnormal dilatation of the urinary tract must take into consideration various parameters: the volume of amniotic fluid the level and degree of dilation, the time of onset, the unilateral or bilateral nature of the damage, and finally the association with other malformations. An important and controversial issue is the cutoff used to differentiate the diameter of a normal renal pelvis from an abnormally dilated one.

Table 8.2 Causes of hydronephrosis

Uretero-pelvic junction (UPJ) obstruction (unilateral or bilateral)
• Vesico-ureteric junction obstruction
• Megaureter (with or without reflux) (unilateral or bilateral)
• Cloacal dysgenesis
• Complicated duplex kidney (unilateral or bilateral)
• Bladder and urethral obstruction (e.g., posterior urethral valves)
• Vesico-ureteric reflux (VUR) (unilateral or bilateral
• Megacystis microcolon intestinal hypoperistalsis syndrome
• Hydrometrocolpos
• Abdomino-pelvic masses

The confusion arises from the fact that a slight dilation of the renal pelvis can also been encountered in normal fetuses. In fact, even if mild dilation of the renal pelvis may represent the first evidence of more severe obstructions, in most instances, mild second-trimester renal pyelectasis will resolve either in utero or within the first year of postnatal life [9,10]. In fact, renal pelvis dilation is observed in 1% to 5% of pregnancies; however, in only about 30%–50% of pregnancies with renal pelvis dilation is a urinary abnormality confirmed in the neonatal period. The likelihood of underlying urinary tract anomalies increases with the degree of dilation. Of the various cutoff values proposed by different authors, one of the more widely accepted is the following: the anteroposterior diameter of the pelvis on a transverse view of the abdomen should not, under normal conditions, exceed 4 mm up to 32 weeks of gestation and 7 mm from the 33rd week onwards [2]. The confusion has increased, however, since the discovery that in more than 50% of the cases examined in one study, the pelvic diameter showed significant variations below and above the 4 mm cutoff over an observation period of approximately 2 h [11]. Factors influencing the diameter of the fetal pelvis include the state of hydration of the mother, the grade of distension of the fetal bladder, and recent emptying of the bladder itself. On the contrary, what is highly indicative of an obstructive lesion is the associated dilation of the renal calices. However, as reported, thresholds for renal pelvis dilation that represent a measurement of potential postnatal disease have been established to help in counseling families and guiding pre- and postnatal management. Hydronephrosis with or without dilation of the ureters accounts for approximately 50% of all prenatally detected renal abnormalities [12]. Its incidence is 1–5 per 500 newborns. Together with transient forms, the most common causes of hydronephrosis are UPJ obstruction and VUR (Table 8.2).

Etiology and pathogenesis. The response of the kidney to obstruction of urinary flow during the prenatal period will depend on the time of onset and the severity of the obstruction. Very early obstructions may lead to renal dysplasia (poor branching of the collecting ducts and deficient formation of glomeruli and tubules), associated with abnormal differentiation (transformation of tubular epithelial cells into myocytes and chondrocytes). Late or partial obstruction delays maturation of the nephrons, and it may result in a reduced number of nephrons at birth (variously associated with atrophy and fibrosis) The functional damage caused by the obstruction usually leads to a progressive dilation of the pelvis, the calices, and the ureters, which act as a "compensation chamber" to reduce the intra-renal pressure. In severe and early obstruction, the consistently increased intraluminal pressure upstream of the obstruction results in an irreversible loss of nephrons due to ischemic damage. In contrast, in the case of incomplete but long-lasting obstruction, vasoactive amines released by the tubules cause a decrease in urine production and an increase in ureteral peristalsis. Recent evidence, from both animal models and newborns, has demonstrated the involvement of the renin–angiotensin system, with angiotensin-dependent renal vasoconstriction proportional to the severity of the obstruction. At least in animals, inhibition of the renin–angiotensin system with angiotensin-converting enzyme (ACE) inhibitors can reduce renal damage and preserve renal function at birth. Furthermore, it seems that renal damage occurring in obstructive uropathies is not limited to the tubules but extends to the glomeruli, with consequent activation of apoptosis. On the other hand, these experimental findings cannot be translated, at least for the time being, into clinical practice, as the marked inhibition of the renin–angiotensin system during nephrogenesis is accompanied by widespread tubular and vascular abnormalities and a decrease in the expression of growth factors critical for development of the fetus.

- *Unilateral hydronephrosis:* This can be due to an obstruction of the UPJ, in which the ureter is unaffected; VUR; or an obstruction of the vesicoureteral junction, in which both hydronephrosis and ureteronephrosis are usually present (Table 8.2).
- *Bilateral hydronephrosis:* This can be due to bilateral VUR and urethral obstruction, which is usually associated with evident ureteral dilation. Bladder overdistension may be present in both conditions, although it is more often found in cases of

urethral obstruction. Less frequently, it can be due to bilateral UPJ obstruction (20%–30% of all cases of UPJ obstructions).
- *Association with other malformations*. These relate mainly to the contralateral kidney and are represented by multicystic kidney, ectopia, and renal agenesis. Associations with extra-renal anomalies include CHD, skeletal dysplasias, and spine anomalies, usually within a syndromic context.

Table 8.2 shows the principal causes of hydronephrosis.

Ultrasound diagnosis. Hydronephrosis is diagnosed if the dilatation involves the renal collecting system only, with normal ureters and bladder. With time, some cases of mild pyelectasis evolve into moderate or severe hydronephrosis. The grade of dilatation may increase with advancing gestation, resulting in a reduction of the cortical thickness (Figure 8.21), or it may remain unchanged. The likelihood of a postnatal pathology increases with the degree of renal pelvis dilatation: 12%–14% with mild (4 to 7 mm in the second trimester and 7 to 9 mm in the third trimester), 45% with moderate, (7 to 10 mm in the second trimester and 9 to 15 mm in the third trimester) and nearly 90% with severe renal pelvis dilatation (> 10 mm in the second trimester and > 15 mm in the third trimester).

It is important to underline that hydronephrosis is considered moderate to severe when a significant dilatation of the pelvis and calyces is associated with normal renal parenchymal thickness (grade III hydronephrosis) or when the renal pelvis is so dilated as to cause cortical thinning (grade IV hydronephrosis), respectively. In the latter instance, calyces may or may not be evident. When the dilatation is confined to the renal pelvis, it is considered grade I hydronephrosis; if calyces are visible and a moderate dilatation of pelvis and calyces is present but confined within the renal border, the hydronephrosis is considered grade II. This grading system was developed by the Society for Fetal Urology for use in children but is often applied in prenatal diagnosis [15].

In rare cases, the extremely dilated collecting system may perforate, with the formation of a paranephric pseudocyst, an urinoma, which is associated with poor or absent renal function.

In the case of unilateral hydronephrosis, it is important to evaluate the contralateral kidney to exclude associated anomalies. The amount of amniotic fluid may be normal or even increased due to a reduction in the ability of the obstructed kidney to concentrate urine; in the case of bilateral obstruction, the amniotic volume may be normal only if the onset of the obstruction is recent or incomplete; otherwise, there is severe oligohydramnios.

Risk of chromosomal anomalies. This is low in isolated forms. Some studies have shown an increased incidence of aneuploidy among fetuses with mild bilateral pyelectasis. However, due to the high prevalence of this sign in the fetus, we believe that fetal karyotyping should be considered *only if* another major anomaly or other risk factors are present at the same time.

Risk of nonchromosomal syndromes. This is relatively low: 6%–8%. The syndromes most frequently associated with hydronephrosis are as follows:

- *VA(C)TER(L) association [3]*: look for ► *hydronephrosis* + vertebral anomalies + anorectal atresia + tracheoesophageal fistula + cardiac defects + limb anomalies (Chapter 10);
- *Schinzel–Giedion syndrome [3]*: look for ► *hydronephrosis* + midface retraction + skull anomalies + talipes + cardiac anomalies;
- *Camptomelic dysplasia [3]*: look for ► *hydronephrosis* + bowed tibiae and femurs + scapular hypoplasia + micrognathia + sex reversal in males.

hydro Ur ETEro NEphros Is

Definition This is dilation of the renal pelvis associated with dilation of the ureter. The main causes are obstruction of the vesicoureteral junction, VUR, obstruction secondary to ureterocele, and ectopic ureter.

Etiology and pathogenesis. In obstruction of the *vesicoureteral junction*, the distal part of the ureter is usually reduced in size. VUR involves a continuous or intermittent retrograde flow of urine from the bladder into the upper urinary tract. Most neonates with prenatally diagnosed reflux are males. A possible explanation may be the increased voiding pressure required in males, which in utero would compress the vesicoureteral junction, leading to the reflux [12]. A less common cause of hydroureteronephrosis in the fetus is *ectopic ureterocele*, which is a cystic dilation of the distal end of the ureter, associated in nearly 90% of cases with *duplex kidney*. In this case, the lower pole ureter inserts laterally into the bladder trigone and has a shortened intravesical segment that may result in VUR. The upper pole ureter inserts medially and inferiorly to the lower pole ureter, near the bladder base, and forms an intravesical uretrocele that causes obstruction. Less frequently, an ectopic ureter may insert outside of the bladder.

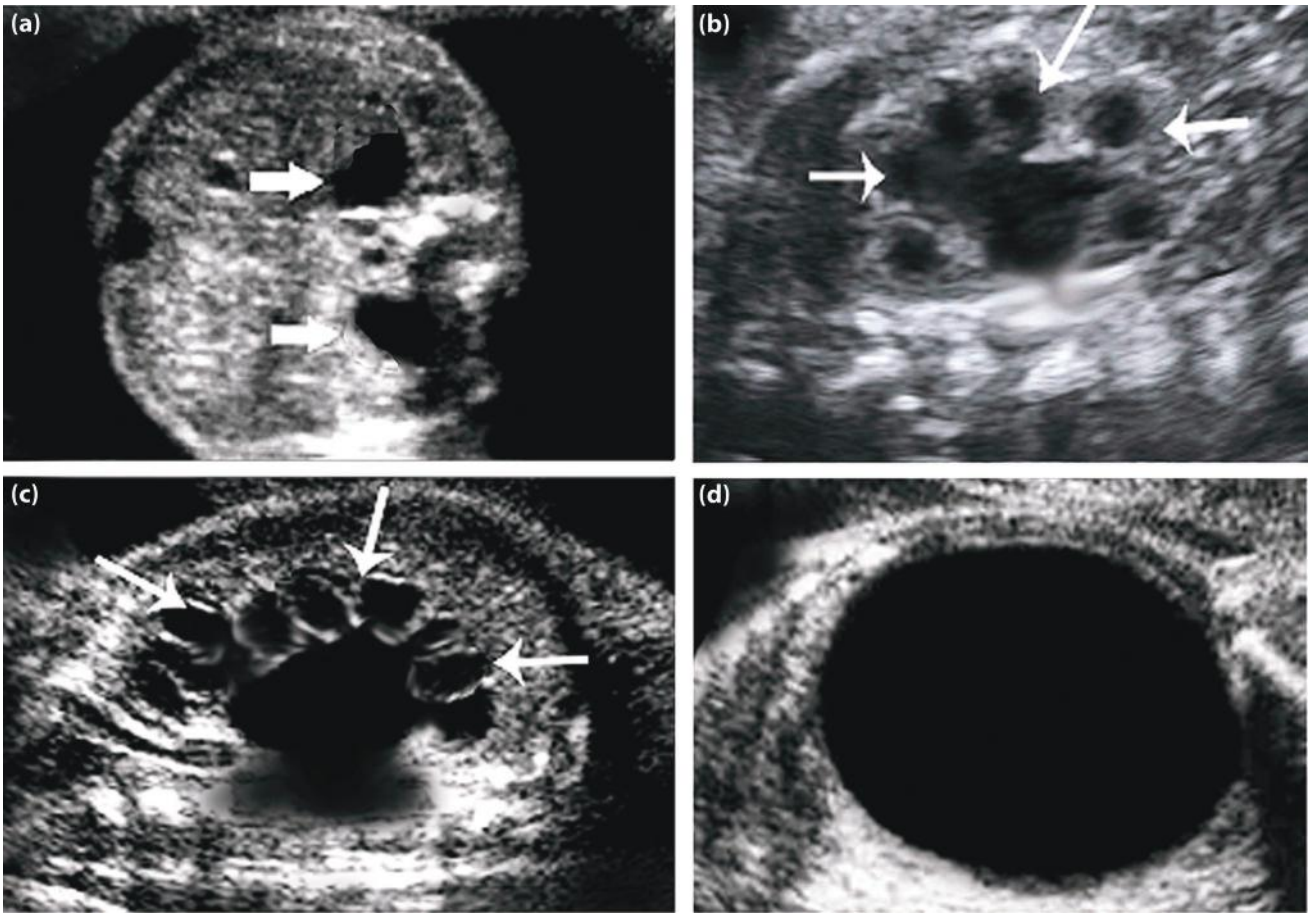


Figure 8.21 Ultrasound images showing several different degrees of hydronephrosis. (a) The kidneys show a mild bilateral pyelectasis. (b) Coronal scan of a hydronephrotic fetal kidney in a 32-week fetus, showing dilation of the pelvis (P); the calyces are visible but not significantly dilated (arrows). (c) Coronal scan of the kidney in a 30-week fetus showing a significant dilation of the pelvis (P) and calyces (arrows); the renal cortex is clearly visible. (d) Severe UPJ obstruction presenting as an abdominal cyst; the renal cortex is thinned to a few millimeters.

Ultrasound diagnosis. The ultrasound aspect of ureteral dilation is that of a tubular, tortuous anechoic structure (Figure 8.22) with a diameter ranging from a few millimeters up to 2–3 cm and extending from the renal pelvis to the retrovesical region. Hydronephrosis is associated. In unilateral forms, the bladder and the amount of amniotic fluid are normal. Sometimes, in severe bilateral VUR, the association of severe hydroureteronephrosis with moderate to severe bladder distension may mimic the presence of lower urinary tract obstruction. In the case of bilateral severe obstruction, the amount of amniotic fluid may be decreased. When the cause of the obstruction is an ectopic ureterocele associated with duplex kidney, characterized by separated upper and lower pole moieties, each drained by a ureter, the US picture is usually based on the presence of dilation of one (upper pole) or both renal pelvises, with an intervening band of renal tissue. When only the upper pole pelvis is dilated (Figure 8.23), if the hydronephrosis is severe, cystic dilation of the upper pole may dislocate and hide the normal morphology of the lower pole, complicating the US diagnosis. In these cases, the only hint leading to the diagnosis of a duplex kidney is the intravesical ureterocele associated with the hydroureteronephrosis. However, the ureterocele may be difficult to detect: with an empty bladder, the ureterocele itself may be mistaken for the bladder or vice versa, with a full bladder, the ureterocele may flaten along the bladder wall due to the high intraluminal pressure, becoming sonographically unrecognizable. Finally, it should be noted that not all duplex kidneys are associated with ureteral dilatation.

Differential diagnosis. In the bilateral form, upper causes of hydroureteronephrosis should be differentiated from lower urinary tract obstruction (Table 8.3). In the unilateral form, the differential diagnosis includes unilateral obstruction of the UPJ, in which there is no ureteral

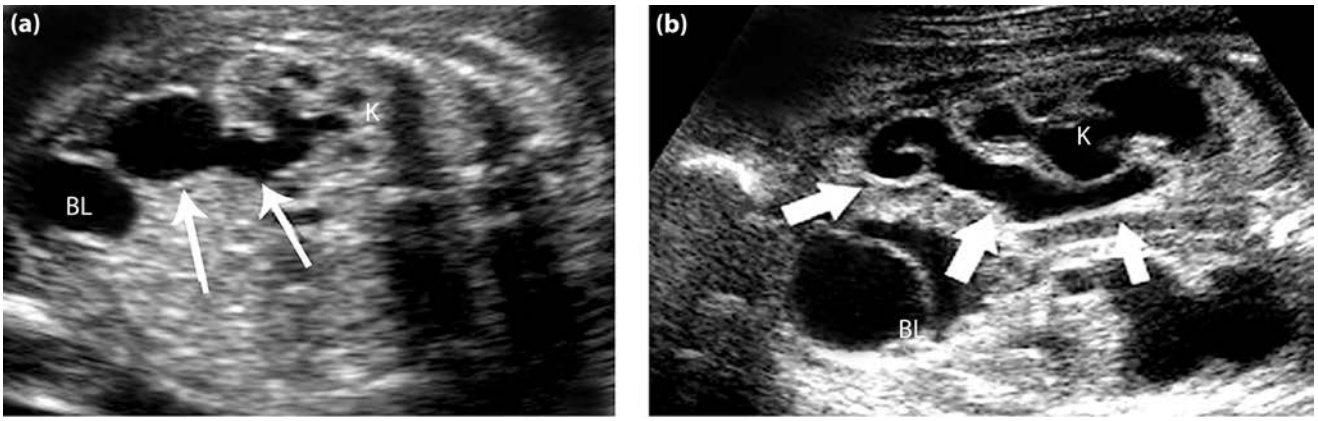


Figure 8.22 Vesico-ureteric junction obstruction. (a) Hydronephrosis and dilation of the ureter (arrows) are present. K: kidney; BL: bladder. (b) Hydroureteronephrosis and ureterocele in a duplex kidney: ultrasound image showing a tubular anechoic formation, with a tortuous path, corresponding to a dilated ureter (arrows), which extends from the renal pelvis to the retrovesical region. Hydronephrosis is associated. Note the ureterocele within the bladder (BL).

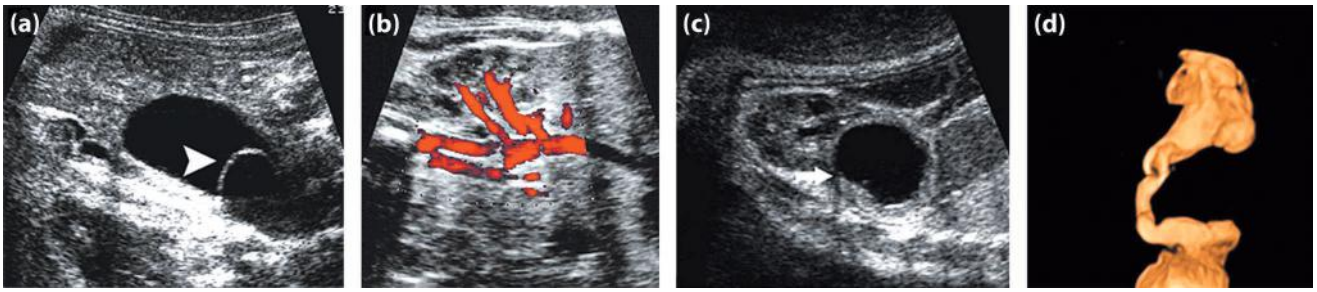


Figure 8.23 Duplex kidney with two collecting systems and ectopic ureterocele. (a) The arrowhead indicates the ureterocele within the bladder. (b) Color Doppler flow demonstrating two renal artery branches. (c) Ultrasound image showing hydronephrosis of the upper pole only (arrow). (d) Surface rendering of the same case, demonstrating the duplex kidney with a dilated ureter.

dilation. In the case of a duplex kidney with ectopic ureterocele, the presence of the ureterocele protruding into the vesical lumen identifies this type of lesion

Association with other malformations. In the unilateral form, contralateral kidney anomalies are frequently associated.

dILATEd BLAdd Er

Incidence. 1/2000–4000 newborns.

Ultrasound diagnosis. Dilatation of the bladder associated with hydroureteronephrosis (or hydronephrosis).

Risk of chromosomal anomalies. Relatively high.

Risk of nonchromosomal syndromes. Relatively high.

Outcome. If the lesion is isolated and the amount of amniotic fluid is within the normal range, the prognosis may be favorable; if, on the other hand, oligohydramnios is already present before the 24th week of gestation and the kidneys are hyperechoic (with or without cysts), the prognosis is unfavorable.

Definition In this section, we will illustrate all anomalies associated with a dilated bladder and, usually, hydroureteronephrosis or hydronephrosis.

Etiology and pathogenesis. A dilated bladder may be due to obstructive or nonobstructive anomalies. The first group comprises posterior urethral valves (typical

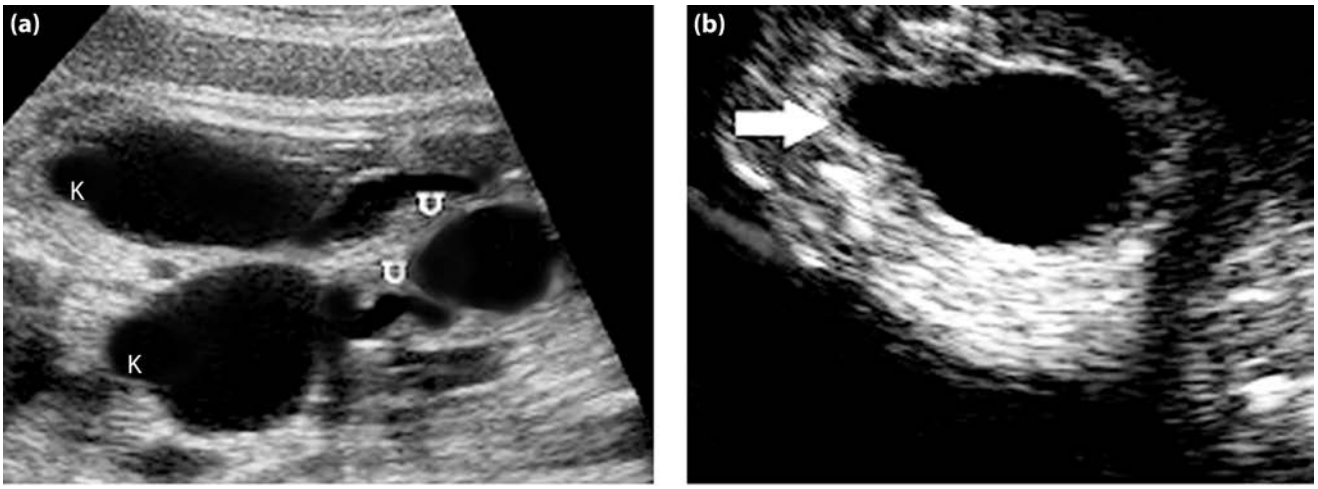


Figure 8.24 Posterior urethral valve. (a) Ultrasound image showing the moderately distended bladder and dilated ureters (U). In this case a partial urethral stenosis was present. (K: kidneys). (b) In a 14 weeks fetus, a significant dilatation of the bladder and of the proximal part of urethra (arrow) is clearly seen.

Table 8.3 Differential diagnosis of distended bladder: breakdown of ultrasound signs by type of lesion

Diagnosis	Amniotic fluid volume	Kidneys	Ureters	Bladder
Posterior urethral valves (PUV)	Normal or reduced	Hydronephrosis, or echogenic cortex ± small cysts	Dilated	Distended, thick walled
Urethral atresia	Markedly reduced or absent	Small and echogenic		Distended, thin walled
Primary reflu	Normal	Hydronephrosis	Dilated or normal	Distended bladder, normal walled
Cloacal dysgenesis	Normal or reduced	Hydronephrosis	Dilated	Distended bladder, normal or thick walled (usually female)

of male fetuses), urethral steno-atresia, and cloacal dysgenesis (mainly female). In the second group, the bladder dilation is not due to obstruction but rather to abnormalities of the vesical tone (atonia), frequently related to neurologic, genetic (e.g., megacystis microcolon intestinal hypoperistalsis [MMIH] syndrome), or chromosomal disorders. Early and complete obstruction (urethral atresia and complete posterior urethral valves) may result in conspicuous dilation of the bladder, with elevation of the diaphragm and distension and thinning of the abdominal wall. The consequent deficit of abdominal wall muscles, together with megaureter and cryptorchidism, completes the clinical condition known as *prune belly syndrome*, which can occur as a primary lesion or be secondary to various causes, with urethral obstruction being the most common.

Ultrasound diagnosis. An enlarged bladder detected at US may simply be a transient phase in the normal voiding cycle, or, if persistent and/or severe, it may be secondary to reflux or obstructive, neurogenic, or myopathic causes. US diagnosis of lower urinary tract obstruction is based on visualization of a dilated bladder with thick and hyperechoic walls, sometimes associated with bladder neck and proximal urethral distension; hydroureteronephrosis, when present, is usually bilateral (Figure 8.24). In the case of urethral atresia, the early onset of the obstruction, which dates back to organogenesis, is responsible for a severe dilation of the bladder, which frequently occupies the whole abdomen as early as the 13th week of gestation (Figure 8.25 and Table 8.3). If mild to moderate vesical dilation is present as early as the 10th–14th week (Figure 8.26), with a longitudinal bladder diameter of 7–15 mm, 23% of

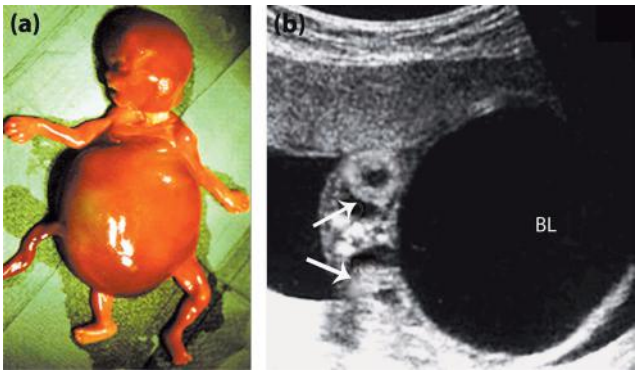


Figure 8.25 Urethral atresia. (a) Gross pathology shows a very distended abdomen and small chest. The lack of musculature gives the abdominal wall a flaccid, wrinkled appearance—hence the name "prune belly syndrome." (b) Ultrasound image showing massive dilation of the bladder and hyperechoic kidneys (arrows).



Figure 8.26 Sagittal scan through the abdomen of a 13-week fetus showing mild distension of the bladder (longitudinal bladder diameter of 10.9mm).

the fetuses have a chromosomal anomaly. However, if the karyotype is normal, spontaneous resolution of the megacystis occurs in most of cases. If the longitudinal diameter of the bladder is greater than 15 mm, the risk of aneuploidy is about 10%, and in the chromosomally normal group, the condition is usually associated with progressive obstructive uropathy [16]. The commonly associated hydroureteronephrosis is due to the increased intravesical pressure. Reflux and urinary sequestration increase the intra-renal pressure, leading to a dilation of the collecting system and impairing, by compression, the blood flow to the proximal renal tubules. The consequent parenchymal damage results in a loss of proteins, which are no longer reabsorbed, in the fetal urine. Sometimes, the VUR resulting from the obstruction may cause massive unilateral hydronephrosis that can totally destroy the kidney, decompressing the contralateral kidney, which may only show moderate hydronephrosis. The extremely high intraluminal pressures



Figure 8.27 Rupture of an obstructed bladder (arrow) may occur, producing urinous ascites, as shown in this ultrasound image.

may also lead to rupture of the bladder; in this case, urinous ascites and decompression of the collecting system will occur (Figure 8.27). Spontaneous decompression takes place in approximately 10% of the cases. The US picture will depend on the duration and degree of the obstruction. In the case of incomplete obstruction, as in some cases of posterior urethral valves, the amniotic fluid will be normal or slightly decreased. On the contrary, in most cases of complete posterior urethral valves, the early and long-lasting obstruction can lead to severe cystic dysplasia with complete loss of renal function. As a result, the production of urine will be extremely reduced. In this case, the sonographic findings will consist of hyperechoic kidneys, possibly with small pericortical cysts (Figure 8.19) and severe oligohydramnios. It is also necessary to underline that the compressive action of the increased intraluminal pressure on the tubules may precede sonographic evidence of hydronephrosis by days or weeks. In contrast, the absence or disappearance of pelvic dilation, in the presence of a hyperechoic, structurally disorganized, or frankly dysplastic kidney, may represent the final result of a protracted period of endoluminal hypertension. The conclusion to be drawn about the US diagnosis of obstructive urinary lesions is that a correct diagnosis requires longitudinal observation.

Differential diagnosis. Posterior urethral valves must be differentiated from severe VUR. Bladder dilation and hydroureteronephrosis may be present in both; however, posterior urethral valves are usually associated with thickened bladder walls (greater than 2 mm) and dilation of the proximal urethra, which are absent in VUR. In several cases of posterior urethral valves, with complete and early onset of the obstruction, the sonographic evidence is remarkable from the end of

the first trimester, featuring a severely dilated bladder occupying the whole abdomen and moderate oligohydramnios. In this regard, it must be underlined that the amniotic fluid will reduce or disappear completely by the 16th weeks of gestation, when its production will be accounted for by the fetal kidney only. Hydronephrosis is more frequently associated with incomplete rather than complete urethral obstruction. In lower urinary tract obstruction presenting in the first and second trimesters, hyperechoic kidneys are predictive of severe renal dysplasia in the vast majority of cases. Finally, it should be noted that bladder dilation (megacystis) can also be associated with nonobstructive disorders, usually in the context of genetic syndromes, as in case of the *MMIH* (Megacystis, Microcolon, Intestinal Hypoperistalsis) *syndrome*, in which the amount of amniotic fluid is usually increased and dilation of the stomach is frequently present (Figure 8.28).

Association with other malformations. An association with cardiac anomalies and anal atresia has been described.



Figure 8.28 Megacystis microcolon intestinal hypoperistalsis syndrome. Ultrasound image showing severely dilated bladder (megacystis), hydronephrotic kidneys, and polyhydramnios.

Risk of chromosomal anomalies. This is relatively high: 8%–20%.

Risk of nonchromosomal syndromes. This is relatively high.

oB s TETr Ic M ANAGEMENT, pos TNATAL Th Er Apy, ANd pro GNos Is o F hydro NEphros Is, hydro Ur ETEro NEphros Is, ANd B LAdd Er dILATIo N

US monitoring of fetuses with urinary obstruction, together with the study of animal models, has expanded the understanding of the natural history of this disease, and has allowed the definition of some general diagnostic criteria and algorithms for pre- and postnatal management of such patients. However, several aspects of the physiopathology of fetal obstructive uropathies remain unresolved, which in turn limits both diagnostic and therapeutic approaches. The first crucial point is the inability of the sonographic examination to fully define the extent and severity of parenchymal damage and to forecast its outcome at the time of initial diagnosis, with the possible exception of the most severe forms of cystic dysplasia, which are associated with severe oligohydramnios. The technical feasibility of in utero vesico-amniotic shunting, to be performed in selected cases to relieve prenatal urinary tract obstruction, has led to research into sensitive biochemical markers that might accurately reflect the (residual) fetal renal function. Unfortunately, this approach has been unsuccessful so far for a number of reasons. First, the biochemical function of the fetal kidney is only partially known, and it depends largely on gestational age. Second, the fetal blood or urine concentration of any putative biochemical marker of renal function is strongly influenced by its transplacental passage. Last, with the limitations cited here, it appears infeasible to define cutoff values that can reliably forecast the progression of renal damage, thereby justifying intrauterine interventions. To a certain extent, the same applies to the adult patient, as demonstrated by the unresolved debate around the no-return value of serum creatinine predicting the progression toward end-stage renal disease. Based on the available evidence, it is reasonable to adopt the following schedule for the management of fetal hydronephrosis. Following identification of urinary tract dilation, a detailed anatomic scan should be performed to exclude the presence of associated extra-renal anomalies. In the case of unilateral obstruction, a reduction of the ipsilateral glomerular filtration rate and a compensatory increase in the function of the contralateral kidney are the expected responses, with a presumably near-normal global excretory function. Management should therefore be limited to serial US follow-up, prolonged at least through the first year of age, associated with postnatal biochemical evaluation of renal function. This approach is based on the apparent sonographic normality of the contralateral kidney and the urinary tract, on the lack of oligohydramnios, and on the presence of urine in the fetal bladder; as such, it is limited by the fact that the assessment of renal function relies exclusively on the sonographic appearance. A detailed analysis of subjects with unilateral dysplastic kidneys diagnosed in utero showed that the usually hypertrophic

contralateral kidney was also prone to hydronephrosis, urolithiasis, and infection during postnatal life in about 30% of cases. Furthermore, uncomplicated fetal unilateral hydronephrosis has been reported in a few cases to progress to irreversible uremia early in postnatal life. This may simply be the effect of a significant reduction in the number of nephrons, despite the compensatory hypertrophy of the contralateral kidney during fetal life: accordingly, renal insufficiency would develop when the already reduced renal functional reserve has to cope with an increased functional demand over the years in postnatal life. However, recent research has revealed that the picture is far more complex: it has been demonstrated that unilateral obstruction can lead to activation of a number of hemodynamic mechanisms, such as the renin–angiotensin system, which account for functional and eventually structural modifications of the contralateral kidney. Then, unilateral obstruction may trigger an array of metabolic and immunologic mechanisms that may involve the contralateral kidney and eventually lead to uremia. Despite all of the concerns reported here, the lack of conclusive evidence and a favorable cost–benefit judgment supports a conservative approach to the fetus with unilateral obstruction. In the case of bilateral obstruction, the first step is always to rule out the simultaneous existence of other major lethal anomalies. Termination of pregnancy may be an option, where legally allowed, in these unfortunate cases. If the association with other significant anomalies (including chromosomal abnormalities) has been excluded, and the amniotic fluid is normal, then a conservative US follow-up is required, with surgical correction usually being postponed until birth. All the concerns and limitations reported for unilateral obstruction are even more compelling in this case. After the 24th week of gestation, the detection of oligohydramnios, at the time of diagnosis or thereafter, requires a more accurate evaluation of renal function. The sonographic recognition of bilateral renal dysplasia is an indication of an unfavorable outcome. Nevertheless, renal function should be explored with more invasive procedures. Fetuses with renal damage have hypertonic urine with a higher concentration of proteins as compared with normal fetuses or fetuses with low urinary tract obstruction and a good outcome. It should be recalled that up to the 20th week of gestation, fetal urine is isotonic with plasma, owing to the immaturity of tubular function. At this early stage, the fetal blood concentration of $ß_2$-microglobulin may be a valuable marker of renal function. Urinalysis should be performed on the urine collected after prolonged bladder drainage of 48–72 h, and the results should be confirmed at least thrice. Fetal urine electrolytes—Na > 100 mmol/L, Cl > 90 mmol/L, Ca > 95th centile, $ß_2$-microglobulin > 6, and Osm > 210—are associated with an abnormal renal function. The severity of urine hypertonicity correlates with the severity and extent of renal damage. In the case of severe renal damage, the degree of hypertonicity remains stable or tends to increase. At the opposite end of the spectrum, in fetuses that may benefit from intrauterine surgery, the degree of urine hypertonicity tends to decrease toward the normal range over time. In conclusion, fetuses with bilateral hydronephrosis, oligohydramnios, and bladder enlargement; associated with a normal karyotype and without coexisting malformations; and in whom urine hypertonicity tends to decrease over time are candidates for in utero surgery (placement of a vesico-amniotic shunt, cystoscopy with ablation of the posterior urethral valve, etc.). Conversely, if sonographic and biochemical findings indicate an unfavorable outcome, then termination of pregnancy or no intervention are the only possible options. In very carefully selected cases, in the presence of lung maturity and acceptable renal function, preterm delivery with early ex utero surgery may be considered. It should also be noted that some reports have described how, in a few circumstances, a single tap of a dilated bladder has unblocked the obstruction, resolving the hydronephrosis. The suggested mechanism behind these events is that the reduction in intraluminal pressure may allow the opening of a functional valve or resolve a sphincteral spasm, in this way removing an apparent obstruction.

BLAdd Er ANd cL o Ac AL Exs Trophy

Incidence. Bladder exstrophy: 1/30,000 live births. Cloacal exstrophy: 1/200,000–1/400,000 live births.

Ultrasound diagnosis. *Bladder exstrophy*: failure to visualize the bladder in the pelvis. Presence of a small mass on the lower abdominal wall. *Cloacal exstrophy*: Infra-umbilical anterior abdominal wall defect with the presence of omphalocele and cystic anterior abdominal wall structure in contact with the amniotic fluid.

Risk of chromosomal anomalies. Relatively low.

Risk of nonchromosomal syndromes. Relatively low.

Outcome. The survival rate is about 90%–95% in the case of bladder exstrophy, but it decreases to 70%–80% for cloacal exstrophy. The quality of life depends on the success of surgical correction.

Definition Bladder exstrophy is a rare midline defect and exists as part of a larger spectrum of abdominal-pelvic fusion abnormalities, known collectively as the exstrophy-epispadias complex (EEC). The open bladder can be seen everting through a lower abdominal wall defect [3,17]. The defect is associated with separation of the pubic bones, a low-set umbilicus, and abnormal genitalia. Bladder exstrophy may occur as an isolated anomaly or be part of a still more complex situation represented by exstrophy of the cloaca, in which a large infra-umbilical anterior abdominal wall defect with herniation of bowel between two halves of the bladder, a protruding omphalocele that forms the upper part of the defect, anal atresia, and malformed genitalia are also present. Spina bifida may be associated. The term "OEIS complex" (i.e., omphalocele, exstrophy of the bladder, imperforate anus, and spinal defects) is used to describe the spectrum of malformations in cloacal exstrophy. In fact, many authors consider OEIS to be synonymous with cloacal exstrophy. However, it also has been reported that cloacal exstrophy and OEIS are different expressions of a primary developmental fiel defect [18]. We think that only future research and identification of the gene or genes associated with this condition will enable us to prove or rule out this suggestion.

Etiology and pathogenesis. While some authors state that exstrophy of cloaca and exstrophy of bladder constitute two distinct disorders, others consider them as part of a "continuum" representing different levels of severity within the same spectrum. The molecular basis for the defective development in cloacal exstrophy is not known. It is presumed that maldevelopment of the cloacal membrane prevents, between weeks four and eight, migration of mesenchymal tissue located between the genital tubercles and body stalk, resulting in lack of a normal lower abdominal wall. Rupture of the cloacal membrane without a supporting abdominal wall leads to exstrophy of the cloaca. The timing of the rupture of the cloacal membrane determines the extent of the defect. Failure of fusion of the pubic rami and the genital tubercles occurs as part of the anterior midline defect.

The incidence of cloacal exstrophy is about 1/200,000–1/400,000 live births; bladder exstrophy incidence is about 1/30,000 births.

Ultrasound diagnosis. The US signs (Figure 8.29) of bladder exstrophy are nonvisualization of the bladder in the pelvis and recognition of a small moderately echoic solid mass, representing the posterior bladder wall, bulging from the lower abdominal wall. The amniotic fluid volume is normal [14] (Figure 8.8). Minor findings often difficult to identify, include a low insertion of the umbilical cord, widening of the iliac

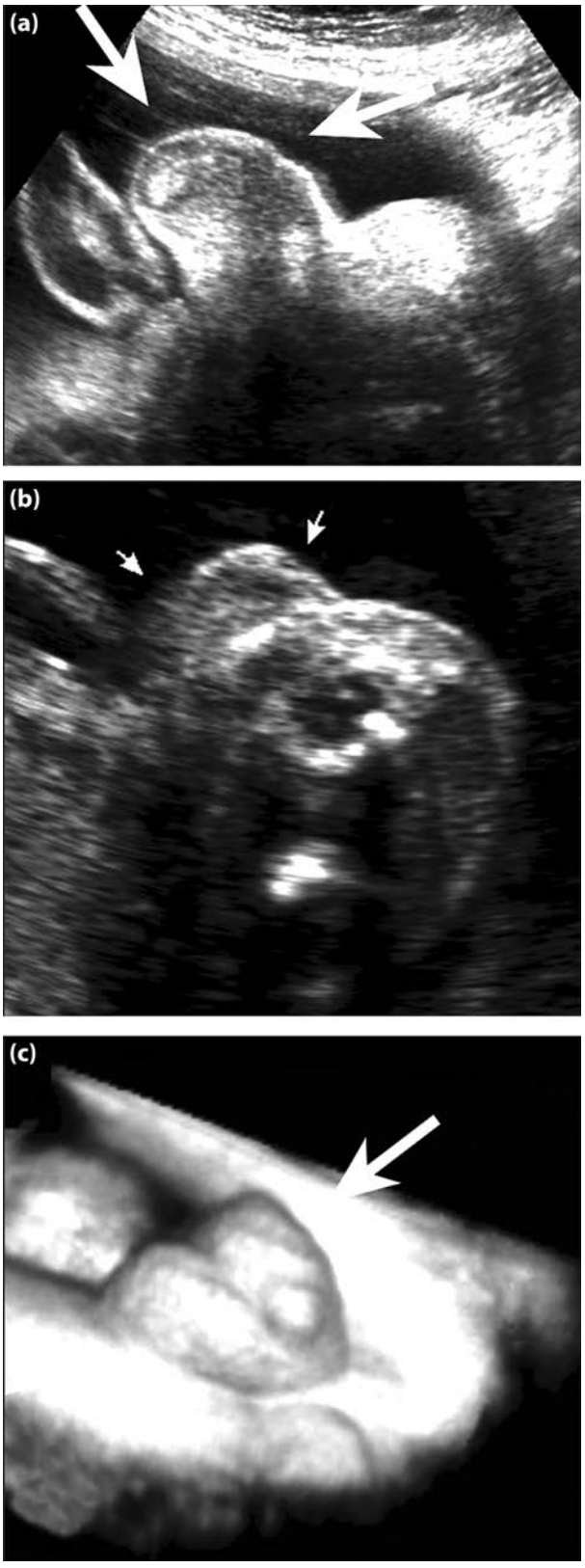


Figure 8.29 Bladder exstrophy (a,b) Ultrasound images showing an exteriorized bladder (arrows). (c) 3D surface rendering of the exteriorized bladder (arrows). Associated epispadia is evident.

crests, and abnormal external genitalia (including a small penis and epispadia in males and a cleft clitoris in females). A hint that may lead to a diagnosis of bladder exstrophy is a parallel course of the intra-abdominal umbilical arteries: in the case of bladder exstrophy, the two umbilical arteries are adjacent to one another and have a parallel (i.e., not converging) course.

In cloacal exstrophy, nonvisualization of the fetal bladder is associated with the recognition of a large infra-umbilical anterior abdominal wall defect with herniation of bowel between two halves of the bladder and a protruding omphalocele that forms the upper part of the defect. Sometimes a cystic pelvic mass, representing a persistent cloacal membrane, can be seen (Figure 8.30). Spinal defects, renal anomalies, and abnormalities of the lower limbs are often found.

Differential diagnosis. For cloacal exstrophy, the main differential diagnosis is with simple omphalocele. However, in the latter, the bladder can always be visualized in the fetal pelvis and omphalocele is usually more cephalad on the abdomen. With regard to the differential diagnosis between the two forms of exstrophy, the omphalocele is absent in isolated bladder exstrophy, and associated spinal dysraphisms are uncommon.

Association with other malformations. Generally, only genital abnormalities are associated with bladder exstrophy; on the contrary, as mentioned in this chapter, cloacal exstrophy is frequently associated with genital, neural tube, gastrointestinal (including anal atresia), and cardiac anomalies.

Risk of chromosomal anomalies. This is low in both defects.

Risk of nonchromosomal syndromes. This is relatively low in both defects.

Obstetric management. If bladder or cloacal exstrophy is detected in a fetus, a thorough anatomic scan should be performed by an expert in order to recognize possible associated anomalies, especially in the case of cloacal exstrophy. Their diagnosis is of key importance in order to accurately assess the surgical procedures needed to correct the defect. Delivery should take place in a tertiary referral center in order to provide adequate perinatal management of the different anomalies present. As far as the mode of delivery is concerned, fetuses with bladder exstrophy may be delivered spontaneously. The same considerations as for omphalocele apply to cloacal exstrophy: it may be appropriate to deliver by Cesarean section those cases in which the abdominal mass is larger than 5 cm.

Postnatal treatment. In the case of bladder exstrophy, restoration of bladder function after surgical correction occurs in a significant percentage of cases. Multiple surgical procedures are needed in the case of cloacal exstrophy. The main goals of reconstruction include secure abdominal wall and bladder closure, preservation of renal function, prevention of short gut syndrome, creation of functionally and cosmetically acceptable genitalia. The objectives of the surgical approach are to achieve bowel control, urinary control, and normal sexual function. All three goals may be achieved; or only two, one, or none of them (occasionally) may be possible. Although various operative algorithms have been published, all approaches begin with initial separation of the intervening cecal plate from the two bladder halves, closure of the omphalocele, and hindgut preservation.

Prognosis, survival, and quality of life. The prognosis for bladder exstrophy is better if it is isolated, with about a 90%–95% survival rate. Until a few decades ago, the prognosis for cloacal exstrophy was very poor. Advances in surgical techniques have resulted in an improved survival rate (approximately 80–90% of cases). The functional prognosis with fecal and urine depends on the complexity of the defect and the status of the spine length greater than 3 cm.

rENAL TUMors

Incidence. Extremely rare in the fetus. 1/125,000 during childhood.

Ultrasound diagnosis. The lesion is usually unilateral. The kidney is partly or totally replaced by a mass with ill-defined margins and high vascularization. It may or may not have a capsule.

Risk of chromosomal anomalies. Low.

Risk of nonchromosomal syndromes. Low.

Outcome. Depends on histology, but is generally good.

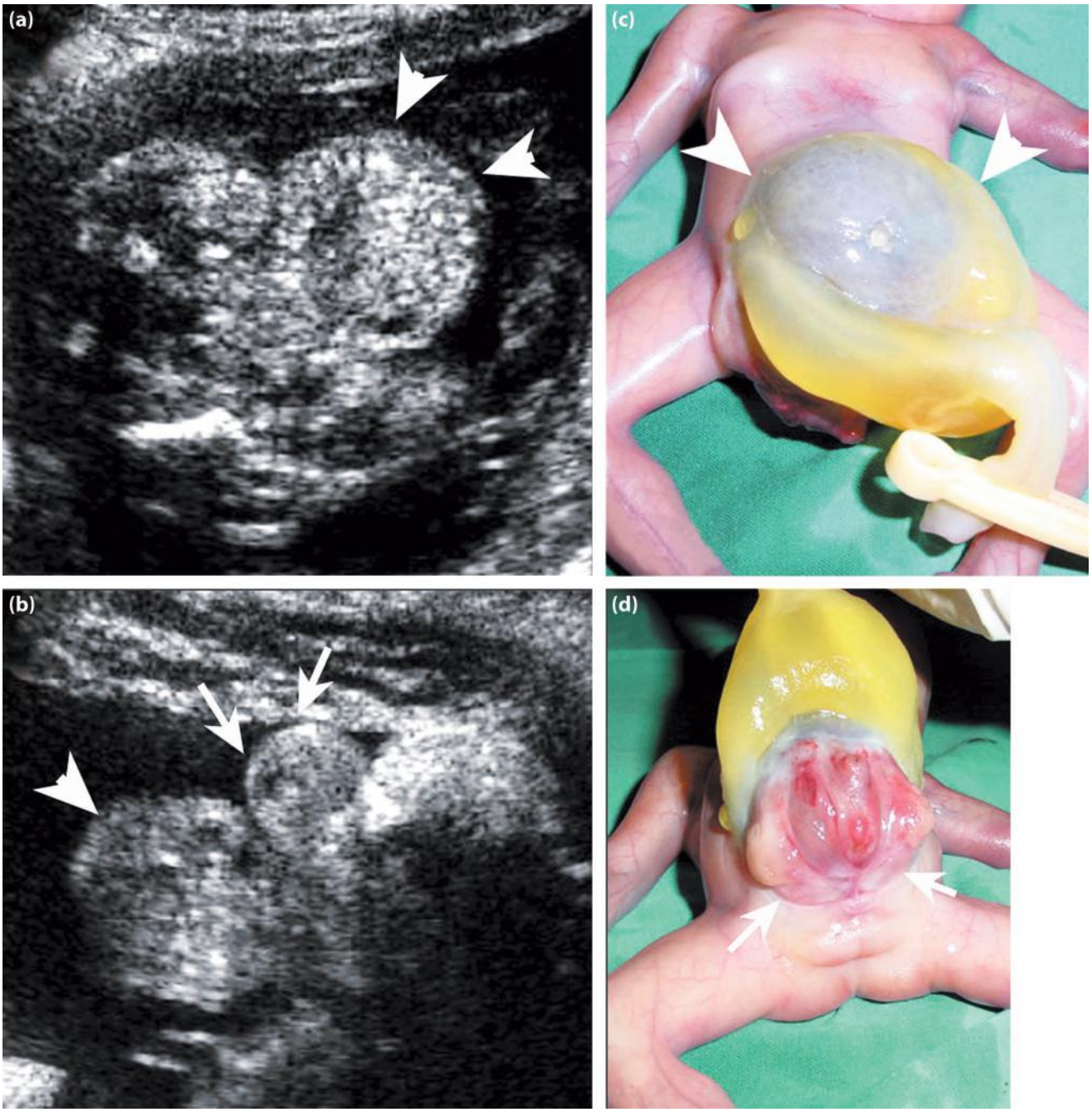


Figure 8.30 Cloacal exstrophy. (a) Axial view of a large omphalocele (arrowheads). (b) Sagittal view of the lower body, showing the omphalocele (arrowhead) and the bladder exstrophy (arrows). (c) The fetus after termination of pregnancy. Frontal view of the large omphalocele. Note the cord insertion on the top of the sac. (d) Lifting the sac of the omphalocele, the concurrent extrofied cecum and ileal segment flanked by two hemi-bladders (arrows), can be seen.

Definition Renal tumors are benign or malignant neoplasms arising in the fetal kidney. Prenatal recognition is extremely rare.

Etiology and pathogenesis. Mesoblastic nephroma, which is a benign lesion, is the most common tumor in the fetus, followed by the malignant Wilms' tumor (nephroblastoma). Some genetic markers (*WT1* and *WT2* on chromosome 11 and *WT3* on chromosome 16p) have been identified for Wilms' tumor arising in the context of Beckwith–Wiedemann syndrome.

Ultrasound diagnosis. As for most neoplasms, the diagnosis is generally made in the third trimester.

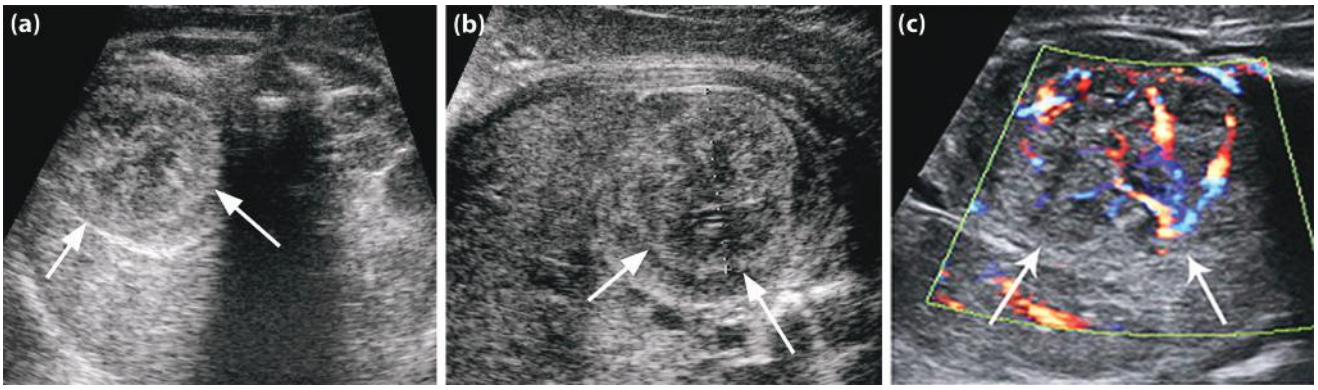


Figure 8.31 Nephroblastoma. Axial (a) and coronal (b) scans of the fetal abdomen showing a solid echogenic mass above the kidney (arrows). (c) Color Doppler shows the high vascularization of the nephroblastoma.

The tumor mass may occupy part of the kidney or replace it completely (Figure 8.31). If it is very large, a mass effect on adjacent abdominal viscera may be detected. Usually, mesoblastic nephromas show ill-defined margins due to the absence of a capsule, whereas nephroblastomas are usually capsulated. Increased vascularization may be detected on color or power Doppler.

Differential diagnosis. This includes mainly adrenal lesions, such as hemorrhage or tumors, due to the location of the mass. However, if the tumor is of renal origin, the renal parenchyma is reduced and not compressed as in adrenal tumors. In addition, adrenal tumors tend to be hypoechoic, whereas renal tumors are usually weakly hyperechoic.

Risk of chromosomal anomalies. This is very low.

Risk of nonchromosomal syndromes. This is relatively low. Nephroblastoma may be associated with the following:

- *Beckwith–Wiedemann syndrome [3]*: look for ► *nephroblastoma* + polycystic kidney + macroglossia + omphalocele + hemihypertrophy (Chapter 10);
- *Denys–Drash syndrome [3]*: look for ► *nephroblastoma* + ambiguous genitalia + diaphragmatic hernia (rare).

Obstetric management. Should a renal tumor be detected in a fetus, a thorough search for possible signs of Beckwith–Wiedemann syndrome (polycystic kidney, macroglossia, and hemihypertrophy) must be carried out. In large tumors, fetal echocardiography may be helpful to detect signs of high-output cardiac failure, which is sometimes associated with large fetal masses. Delivery should take place in a tertiary referral center in order to ensure adequate diagnostic workup, including abdominal US and magnetic resonance imaging (MRI) of the neonate. Subsequent management is determined by the final diagnosis

Postnatal therapy. Surgical removal of the tumor, or nephrectomy, may be necessary in the neonatal period.

Prognosis, survival, and quality of life. In general, the overall prognosis is good, with good survival rates. The relatively few cases in which cardiac failure develops in utero are those more likely to die after birth.

AMBIGUOUS GENITALIA

Incidence. 1/4500 newborns.

Ultrasound diagnosis. It is difficult to differentiate micropenis with cryptorchidism from clitoromegaly with normal labia; in males, the main findings are micropenis, ventral curvature of the penis, retained testicles, scrotum bifidum, and hypospadias; in females, the main finding is clitoromegaly.

Risk of chromosomal anomalies. Relatively low.

Risk of nonchromosomal syndromes. High.

Outcome. Good in isolated forms; unfavorable if associated with other anomalies.

Definition The term "ambiguous genitalia" is used when the external genitalia are different from the genetic sex, or when they are not certainly indicative of a male or female phenotype. The incidence of this anomaly is 1/4500 newborns.

Anatomy. Ambiguous genitalia is the name of a heterogeneous group of disorders with different etiologies; it frequently refers to chromosome anomalies and/or endocrine disorders [19]. Currently, there is no universally accepted classification of sexual differentiation disorders. The most widely accepted is based on the histology of the existing gonad, with an etiologic subclassification According to this gonad classification there are five main categories

I. Only an ovary is present (female pseudohermaphroditism);
II. Only a testis is present (male pseudohermaphroditism);
III. Ovary and testis are present (true hermaphroditism);
IV. Testis and gonadal "streak" are present (mixed gonadal dysgenesis);
V. Only a gonadal streak is present (pure gonadal dysgenesis).

Female pseudohermaphroditism (hyperandrogenized female). This anomaly comprises the majority of cases of ambiguity in the external genitalia. These are female individuals with a 46,XX karyotype and ovarian gonadal tissue. They have normal Müllerian duct structures (normal internal genitalia). The majority of cases are due to an accumulation of androgens upstream of the enzymatic block in the biosynthesis of cortisol. The two main enzymatic defects responsible for virilization of the female fetus are the deficiencies of 21-hydroxylase and of 11β-hydroxylase, which account for 95% of cases. The former deficiency is responsible for most cases of adrenogenital syndrome (AGS). Newborns with AGS show a degree of virilization that varies according to the severity of the enzymatic deficit. The most frequent morphologic characteristics are clitoromegaly, with a clitoris that may reach the dimensions of a phallus; the presence of a single vaginal and urethral opening (urogenital seat); and hyperpigmented labia majora characterized by roughness typical of scrotal skin, while the labia minora are fused. The pelvic organs are completely feminine and unremarkable. The diagnosis is based on the blood levels of 17-hydroxyprogesterone and 11-deoxycortisol, and the final confirmation is obtained by molecular investigation of the *CYP21* gene, the site of the mutation responsible for the enzymatic block. Deficiency of 11β-hydroxylase accounts for only 10% of the cases of congenital AGS. The *CYP11B* gene, which codes for 11β-hydroxylase, is located at chromosome 8q21 and comprises eight exons, whose sequence can be analyzed to find any mutations. Another unlikely cause of female pseudohermaphroditism is the maternal intake of androgens during pregnancy.

Male pseudohermaphroditism (hypoandrogenized male). This anomaly includes all syndromes due to a deficit in the synthesis of testosterone or to an abnormal testosterone receptor that is not able to convey the hormonal input to the target cells. Patients belonging to this group are all males with a 46,XY complement. The production of testosterone is essential for the development of the external genitalia in the male. There is a close correlation between development of the embryo and the concentration of fetal testosterone. At the sixth week of gestation, in response to a luteinizing hormone (LH) peak from the hypophysis, there is a detectable increase in the production of testosterone by the fetal testes. The concentration of fetal testosterone remains high until the 14th week of gestation. After this period, gonadal stimulation is mainly sustained by placental LH. The presence of a sufficient concentration of testosterone in the final weeks of gestation is responsible for the further growth of penile dimensions until birth. The main phenotypic characteristic of male pseudohermaphroditism is micropenis, either isolated or associated with cryptorchidism. Three enzymatic anomalies can be responsible for inadequate androgen stimulation during fetal life: (1) an enzymatic deficit in the biochemical sequence that results in the synthesis of testosterone; (2) a deficit of 5α-reductase, responsible for conversion of testosterone into dihydrotestosterone (DHT); and (3) an anomaly in the cytosome carrier protein that causes a failure of transport of DHT within the cell nucleus.

True hermaphroditism. In this extremely rare form, the chromosome complement is generally 46,XX, but there is chromatinic material from chromosome Y. Even less common is true mosaicism (46,XX and 46,XY) or male genotype. The true hermaphrodite has both testicular and ovarian tissue represented within the same gonad (ovotestis). The external genitalia are ambiguous or female.

Mixed gonadal dysgenesis. Children suffering from this anomaly show a normally differentiated testis on one side and a dysgenetic gonad on the other. The karyotype of these patients is normally characterized by mosaicism (45,X0 and 46,XY); these patients may have the classic phenotype of Turner syndrome or have ambiguous genitalia. The most significant

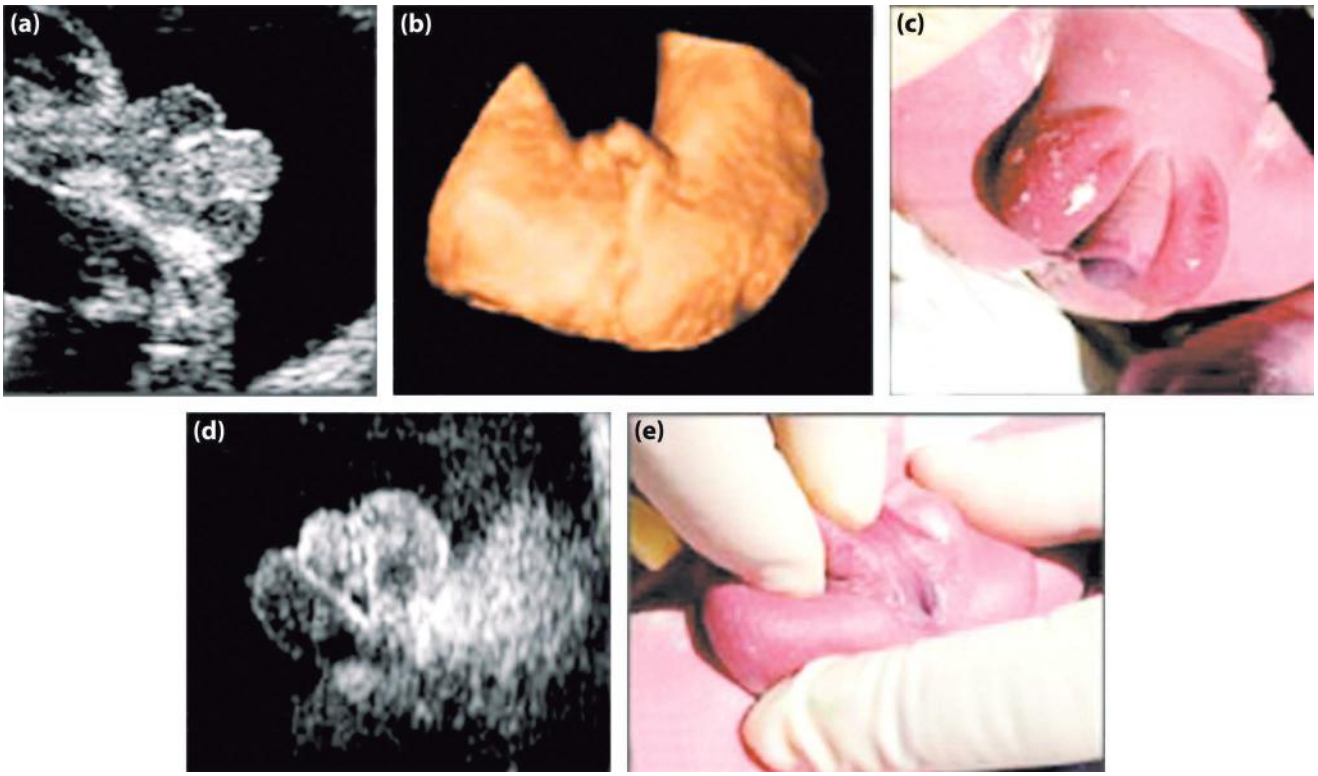


Figure 8.32 (a) Ambiguous genitalia: a small phallus is seen between a heart-shaped scrotal sac (scrotum bifidum), which mimics labia. (b) 3D surface rendering of the same finding. (c) External genitalia at birth. (d) A bifid scrotum with hypospadias is evident in this scan. (e) The external genitalia at birth: the urethral orifice and the incompletely fused scrotum are demonstrated.

characteristic of these patients is the high incidence of neoplasias of the dysgenetic gonad (gonadoblastoma). The gonadic dysgenesis also include Turner syndrome (karyotype 45,X0 and variants), characterized by dysgenetic gonads and female phenotypic appearance, and Klinefelter syndrome (karyotype 47,XXY), characterized by gonads with a testicular morphology that shows tubular dygenesis.

Pure gonadal dysgenesis. This can rarely be diagnosed during the neonatal period; the chromosome patrimony may be XY, XX, or X0, and normal female external genitalia and dysgenetic ovaries are present.

Ultrasound diagnosis. Accurate diagnosis of genital anomalies is difficult In the case of sex reversal (i.e., the phenotypic sex is the opposite of the genetic sex), diagnosis may be simple, if the fetal karyotype is available. Ambiguous external genitalia are difficult to diagnose, because a micropenis with cryptorchidism cannot always be differentiated on US from clitoral hypertrophy with normal labia. A recent investigation has reported that in more than 40% of abnormal external genitalia, the prenatal US diagnosis was not made or a significant number of false-positive results was generated [20]. In the male, the most frequent anomaly detected on US is represented by micropenis, ventral curvature of the penis, retained testes, scrotum bifidum, and hypospadias (Figures 8.32 and 8.33). In females, clitoral hypertrophy is the only finding Sex reversal may be evident in both sexes.

Association with other malformations. Facial clefts and CHD may be associated.

Risk of chromosomal anomalies. This is relatively low. The most frequent chromosomal aberrations are trisomy 13, triploidy, 13q syndrome, Xp21 duplication, 9p23 deletion, and 10q26 deletion.

Risk of nonchromosomal syndromes. High.

- *Robinow syndrome [3]*: look for ► *ambiguous genitalia (micropenis in males or hypoplastic clitoris and labia minora in females)* + short upper limbs + characteristic facies;
- *Opitz GBBB syndrome (OMIM 300000) [3]*: look for ► *hypospadias* + hypotelorism;

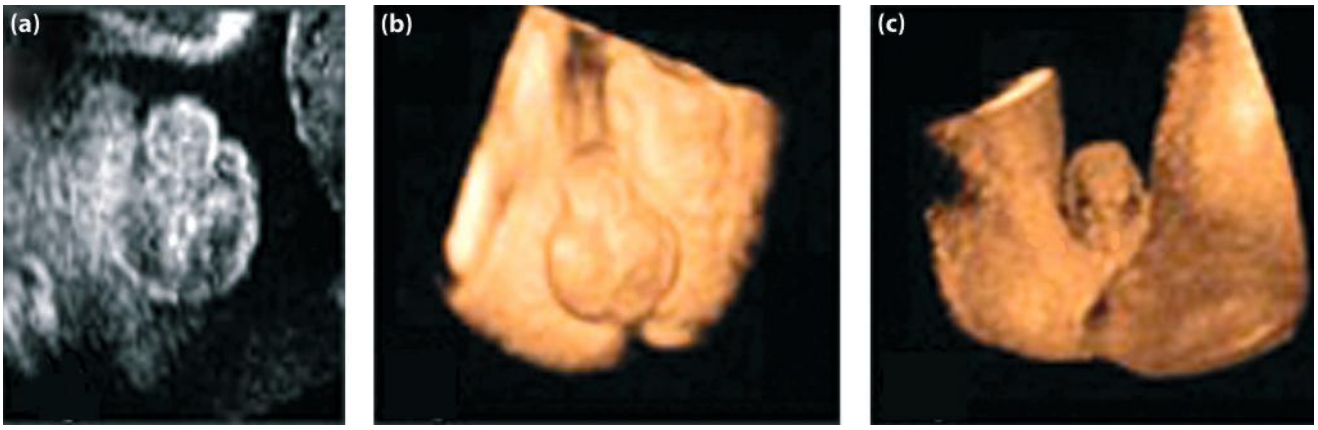


Figure 8.33 (a) 2D ultrasound of a fetal micropenis. (b,c) 3D surface rendering.

- *Smith–Lemli–Opitz syndrome (OMIM 270400) [3]*: look for ► *ambiguous genitalia* + holoprosencephaly + cleft palate + FGR;
- *Denis–Drash syndrome (OMIM 194080) [3]*: look for ► *ambiguous genitalia* + nephroblastoma + diaphragmatic hernia (rare).

Obstetric management. Should ambiguous genitalia be confidently detected in a fetus, the first tasks are to ascertain whether there are maternal signs of hyperandrogenism and to verify if there has been ingestion of progesterone or androgens during the first trimester. A complete family history should be obtained. In addition, fetal karyotyping should be performed to determine the genetic sex. The amniotic fluid should also be analyzed for the presence of 7-dehydrocholesterol, which, if elevated, is suggestive of Smith–Lemli–Opitz syndrome. Amniocytes should be saved as a source of DNA for mutational analysis of the 21-hydroxylase gene. Treatment of the fetus or neonate with ambiguous genitalia should be performed in the setting of a multidisciplinary team (genetics, neonatal endocrinology, neonatology, pediatric urology, etc.). Delivery in a tertiary center is recommended.

Postnatal treatment. The major considerations in the treatment of a newborn with ambiguous genitalia are determination of the sex of rearing and gender identity, planning for surgery if necessary, and provision of genetic counseling.

Prognosis, survival, and quality of life. It is important that the parents resolve any uncertainty about the sex of rearing of the child as soon as possible. Properly timed hormonal and surgical intervention should occur prior to and during puberty. However, several groups of adult patients currently advocate that genitalia should be left ambiguous permanently.

oVAr IAN cys T

Incidence. Most common intra-abdominal cysts in the female fetus.

Ultrasound diagnosis. Presence of abdominal anechoic or complex cyst in a female fetus, almost always in the third trimester of gestation. Presence of an abdominal cyst containing a "daughter cyst" is the best diagnostic clue.

Risk of chromosomal anomalies. Very low.

Risk of nonchromosomal syndromes. Very low.

Outcome. Very good, unless ovarian torsion occurs in the neonatal period. Most ovarian cysts regress spontaneously after birth.

Definition This is a typically benign functional cyst within the fetal ovary, although rare cases of ovarian neoplasms have been reported.

Etiology and pathogenesis. Ovarian cysts represent the response of the fetal ovary to increased circulating hormonal levels, including maternal estrogens,

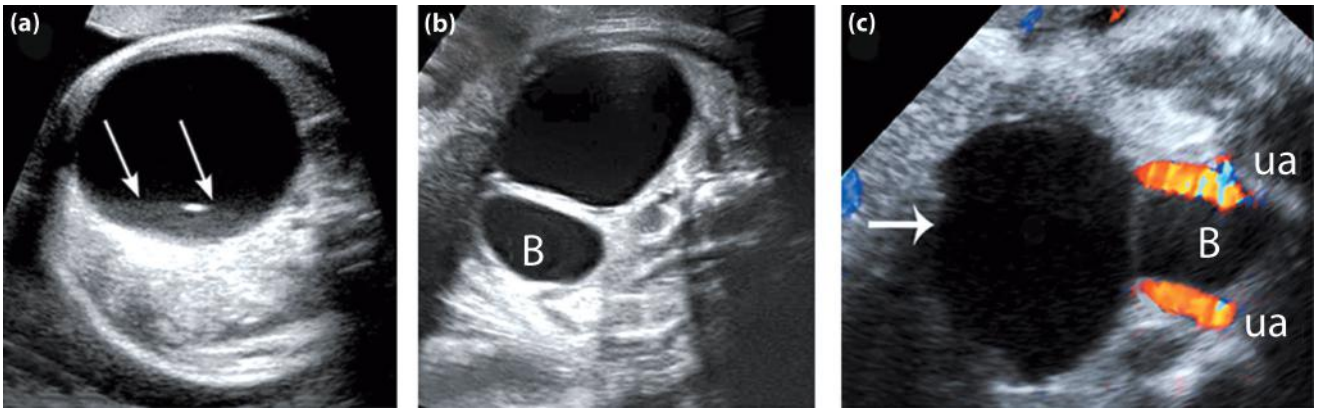


Figure 8.34 Fetal ovarian cyst. (a) Hemorrhagic ovarian cyst: axial view of the fetal abdomen showing a complex cystic mass (arrows) with an echogenic component in a 34-week female fetus. (b) Axial view of the fetal abdomen and pelvis in a 29-week female fetus, showing a unilocular and completely anechoic cyst just above the bladder (B); (c) Color Doppler demonstrates both perivesical arteries around the bladder (B). The arrow indicates the ovarian cyst.

placental human chorionic gonadotropin, and fetal gonadotropins. An increased incidence of fetal ovarian cysts has been reported in cases of maternal diabetes, Rhesus isoimmunization, and preeclampsia.

Ultrasound diagnosis. The most common finding on US is the presence of a unilocular cyst (Figure 8.34), sometimes with a daughter cyst inside [21], in the lower lateral abdomen of a female fetus during the third trimester of pregnancy. Bilateral ovarian cysts are less frequent. In rarer circumstances, the cyst is "complex": it has a hemorrhagic echogenicity, which is usually secondary to torsion (Figure 8.34). In this case, the US appearance varies according to the time elapsed from the hemorrhage: diffusely echogenic with acute hemorrhage, a fluid–flui level seen with repeated bleeds, or a clot separated from serum; sometimes, apparent septations due to fibrin strands can be seen [22]. Polyhydramnios may develop in 10% of cases. It has been suggested that this is due to partial bowel obstruction secondary to compression by a large cyst.

Differential diagnosis. Urachal, mesenteric, and enteric duplication cysts are indistinguishable from an ovarian cyst [23]. Recognition of a daughter cyst seems to be exclusive to ovarian cysts. However, it is important to consider the fetal gender (ovarian cysts can obviously be ruled out in a male fetus), confirm the presence of an unremarkable normal urinary tract (a number of cystic abdominal masses are related to the urinary tract), confirm the normal appearance of the gastrointestinal tract (a characteristic of enteric cysts is the "gut signature"), and look for cyst complications (torsion and hemorrhage).

Prognostic indicators. Torsion is the most common complication of ovarian cysts. The risk of torsion is increased if the cyst is larger than 5 cm [24].

Association with other malformations. An association with fetal hypothyroidism has been described.

Risk of chromosomal anomalies. This is very low.

Risk of nonchromosomal syndromes. This is very low.

Obstetric management. In the extremely rare circumstance in which an ovarian cyst is large enough to distend the fetal abdomen, it may cause dystocia. In this case, elective Cesarean section may be considered. In the case of complicated cyst, delivery should take place in a tertiary referral center with a pediatric surgery unit.

Postnatal therapy. After delivery, the neonate should undergo an US scan to confirm the antenatal diagnosis. Most uncomplicated ovarian cysts regress spontaneously a few weeks after birth. A surgical approach is suggested for complex cysts or cysts larger than 5 cm. Surgery should aim to preserve ovarian parenchyma (fenestration with ovarian preservation), although oophorectomy may be necessary in the case of hemorrhagic infarction due to torsion.

Prognosis, survival, and quality of life. Survival and quality of life are unaffected.

Adr ENAL GLANds A No MALIEs

Adrenal glands look like small oblong structures, with a hyperechoic central area, corresponding to the medulla, surrounded by the hypoechoic cortex (Figure 8.9). These structures are more visible in case of renal agenesis and, physiologically, during the third trimester.

Adrenal glands anomalies are extremely rare, and they include mainly cysts, hemorrhages, hypertrophy, and tumors (neuroblastoma) (Figure 8.35). In cases of hemorrhage (Figure 8.35b), the hemorrhage would be visible as a hypoechoic round-shaped lesion just above the upper pole of the kidney, which is the anatomic site of the adrenal gland. The differential diagnosis between a hemorrhage and a cyst (Figure 8.35) is based on a follow-up after a few weeks, demonstrating, in cases of hemorrhages, the typical evolution of a blood clot (organization). Hypertrophy is an extremely rare lesion that is difficult to be visualized, even if there are normal curves of adrenal glands diameters in the literature [25]. Some evidence has recently shown an increase of adrenal glands volume induced by a condition of stress related to the prolonged rupture of the membranes [26]. Multiple cysts of the adrenal glands (Figure 8.36) have been rarely described, in association with hyperechoic and enlarged kidneys, in cases of Beckwith–Wiedemann syndrome [27]. However, the most important lesion to be detected, because of its bad outcome, is the neuroblastoma.

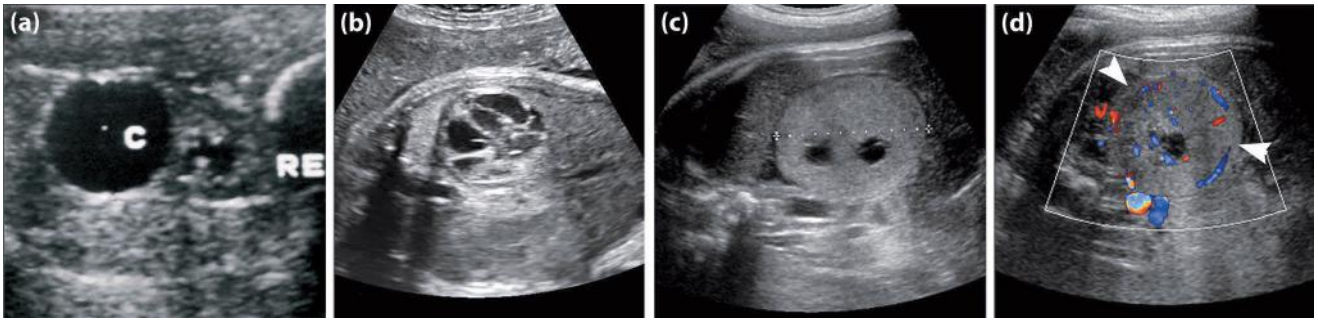


Figure 8.35 Adrenal abnormalities. (a) Adrenal cyst in a 30-week fetus. (b) Adrenal hemorrhagic cyst in a 31-week fetus. (c) Neuroblastoma. A solid suprarenal mass is clearly seen in a 33-week fetus. (d) Color Doppler shows the high vascularization of the aforementioned solid mass. C: cyst; RE: adjacent renal parenchyma.

Adr ENAL NEUro BLAs To MA

Incidence. It is the most frequent solid tumor found in childhood. The incidence is about 1/7000 – 1/10,000.

Ultrasound diagnosis. Cystic, solid, or mixed mass within an adrenal gland.

Risk of chromosomal anomalies. Chromosomal deletions of 1p, 11q, and 14q are found in up to 50% of neuroblastomas.

Risk of nonchromosomal syndromes. Almost no risk.

Outcome. If it is diagnosed in utero, and there is no N-myc amplification, there is regression in about 40% of the cases. In cases of N-myc amplification, there is higher mortality risk.

Definition The neuroblastoma is a malignant tumor originating from the neural crest cells. Both the sympathetic nervous system and the adrenal medulla originate from these same cells.

Etiology and pathogenesis. Missense mutations of the gene *KIF1B* at the level of the locus 1p36.2 have been found in a discrete number of the cases [25]. Moreover, correlation has been shown between adrenal neuroblastoma and maternal exposure during pregnancy to alcohol, diuretics, hair dye, sexual hormones, drugs, carbamazepine, and phenytoin; however, most of these associations have not been demonstrated afterward [26].

Ultrasound diagnosis. The neuroblastoma is more often found at the level of the adrenals in prenatal life rather than postnatally (60%–90% of the

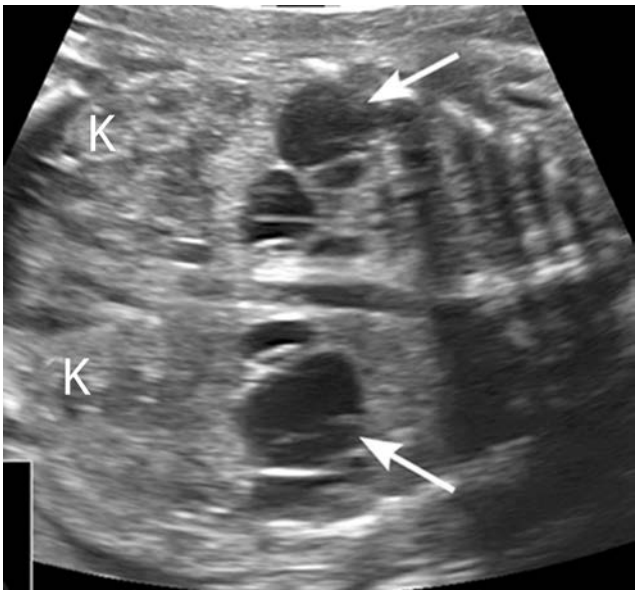


Figure 8.36 Multiple cysts of the adrenal glands associated with hyperechoic kidneys (K), in a case of Beckwith–Wiedemann syndrome.

prenatally diagnosed cases versus 35% of the postnatally diagnosed ones) [28]. This tumor looks like a mass (Figure 8.35 c,d) and is usually capsulated; less frequently, it is found as a cystic or mixed mass, because of ischemic necrosis. The underlying kidney is typically compressed and moved away from its usual position, with clear separation between the two structures. In 25% of the cases, there are already hepatic metastases at the time of the US diagnosis, even if these usually cannot be visualized; in these cases, the presence of associated hepatomegaly could suggest liver metastasis [29,30]. The vascularization of the mass is typically high (Figure 8.35d), like in all malignant tumors. Sometimes there are also maternal symptoms associated with this condition (sweating, hypertension, hot flashes etc.) that are related to increased levels of catecholamines passing through the placental barrier. Increased vanilmandelic and homovanillic acid could be found in one-third of the fetal cases, and in 85%–90% of urine samples of affected neonates [29–31].

Differential diagnosis. The mass must be differentiated from a hemorrhage, which is more frequent on the right side (Figure 8.35). The differential diagnosis could be difficult as both hemorrhages and neuroblastoma can have variable US appearance according to their evolution after a diagnosis. The high vascularization would orient the diagnosis toward the neuroblastoma. The variation of the US aspect of the hemorrhages, on the other hand, could be only due to the organization of the clots. The differential diagnosis of solid and mixed masses includes other abdominal masses with similar positions (higher part of the abdomen) such as subdiaphragmatic extralobar lung sequestration (see Chapter 6), bronchogenic cysts, renal tumors (nephroblastoma; Figure 8.31), abdominal lymphangioma, and bowel duplication cysts. However, the lung sequestrations and the bowel duplication cysts usually have a hyperechoic appearance, bronchogenic cysts are usually above the diaphragm, and the nephroblastoma is positioned within the kidney's parenchyma.

Prognostic indicators. The presence of associated hepatomegaly and a large placenta are suggestive of hepatic and placental metastasis, respectively. Therefore, these findings are associated with bad prognosis. Association with fetal hydrops has been reported. This could be due to different conditions: placental metastasis, inferior vena cava compression consequent to hepatomegaly, hypoalbuminemia related to hepatic metastasis, or cardiac failure due to severe arrhythmias consequent to increased levels of circulating catecholamines. In these cases, the hydrops could lead to fetal demise.

Association with other malformations. It has been reported in only one case. Hydrops and hepatomegaly are therefore considered as signs of metastasis rather than associated malformations.

Risk of chromosomal anomalies. Chromosomal deletions of 1p, 11q, and 14q are found in up to 50% of neuroblastoma.

Risk of nonchromosomal syndromes. Very low.

Obstetric management. Searching for vanilmandelic and homovanillic acid in the amniotic fluid could be helpful to make the diagnosis in unclear cases, even if these are not found positive in all the cases of adrenal neuroblastoma. An MRI could help to detect hepatic and placental metastasis. Delivery in a tertiary level hospital is recommended, in order to have diagnosis confirmation and subsequent optimal treatment

Therapy, prognosis, and survival. The survival rate is significantly higher in the cases diagnosed in utero, rather than the ones diagnosed after birth. There are two different types of neuroblastoma: the first one has better prognosis and is usually diagnosed in utero, with lower grade at the time of the diagnosis, and it does not have amplification of the N-myc gene. In these cases, it is possible to have complete regression of the lesion in about 40% of the cases [30, 31], using expectant management in view of possible spontaneous regression of

the lesion. However, it is considered ethically appropriate to offer the option of a surgical approach, usually decisive, especially in the cases with good prognosis. The second type of neuroblastoma has bad prognosis: it is usually diagnosed for the first time during the first year of life, its grade is more advanced at the time of the diagnosis, and there is amplification of the N-myc gene. In these cases, mortality is related to the evolution of the tumor, and mortality remains very high even after surgery and chemotherapy.

rEFE r ENc Es

1. Moore KL, Persaud TVN. *The Developing Human. Clinically Oriented Embryology*. 6th ed. Philadelphia, PA: WB Saunders; 1998: 305.
2. Corteville JE, Gray DL, Crane JP. Congenital hydronephrosis: correlation of fetal ultrasonographic findings with infant outcome. *Am J Obstet Gynecol* 1991; 165: 384–8.
3. Evans JA. Urinary tract. In: Stevenson RE, Hall JG, eds. *Human Malformations and Related Anomalies*. 2nd ed. Oxford: Oxford University Press; 2006: 1161–90.
4. Gruskin D, Kanil E, Rimoin D. Congenital disorders of the urinary tract. In: Rimoin D, Connor JM, Pyeritz RE, et al., eds. *Emery and Rimoin's Principles and Practice of Medical Genetics*. 4th ed. Edinburgh: Churchill Livingstone; 2002: 1659–743.
5. Winyard P, Chitty L. Dysplastic and polycystic kidneys: diagnosis, associations and management. *Prenat Diagn* 2001; 21: 924–35.
6. Roume J, Ville Y. Prenatal diagnosis of genetic renal disease: breaking the code. *Ultrasound Obstet Gynecol* 2004; 24: 10–18.
7. Brun M, Maugey-Laulom B, Eurin D. Prenatal sonographic patterns in autosomal dominant polycystic kidney disease: a multicenter study. *Ultrasound Obstet Gynecol* 2004; 24: 55–61.
8. Volpe P, Volpe N, De Robertis V. Multicystic dysplastic kidney. Visual Enciclopedia of Ultrasound in Obstetrics and Gynecology. 2013. Available from: www.VISUOG.org
9. Sherer DM. Is fetal hydronephrosis overdiagnosed? *Ultrasound Obstet Gynecol* 2000; 16: 601–6.
10. Siemens DR, Prouse KA, MacNeily AE, et al. Antenatal hydronephrosis thresholds of renal pelvic diameter to predict insignificant post-natal pelviectasia. *Tech Urol* 1998; 4: 198–201.
11. Persutte WH, Hussey M, Chyu J, et al. Stricking findings concerning the variability in the measurement of the fetal renal collecting system. *Ultrasound Obstet Gynecol* 2000; 15: 186–90.
12. Mouriquand PDE, Whitten M, Pracros JP. Pathophysiology, diagnosis and management of prenatal upper tract dilatation. *Prenat Diagn* 2001; 21: 942–51.
13. Lee RS, Cendrom M, Kinnanon DD, et al. Antenatal hydronephrosis as a predictor of postnatal outcome: a meta-analysis. *Pediatrics* 2006; 118: 586–93.
14. Nguyen HT, Herndon CD, Cooper C, et al. The Society for Fetal Urology consensus statement on the evaluation and management of antenatal hydronephrosis. *J Pediatr Urol* 2010; 6: 212–31.
15. Fernbach SK, Maizels M, Comway JJ, et al. Ultrasound grading of hydronephrosis: introduction to the system used by the Society for Fetal Urology. *Pediatr Radiol* 1993; 23: 478–80.
16. Liao AW, Sebire NJ, Geerts L, et al. Megacystis at 10–14 weeks of gestation: chromosomal defects and outcome according to bladder length. *Ultrasound Obstet Gynecol* 2003; 21: 338–41.
17. Lee EH, Shim JY. New sonographic finding for the prenatal diagnosis of bladder exstrophy: a case report. *Ultrasound Obstet Gynecol* 2003; 21: 498–500.
18. Kallen K, Castilla EE, Robert E, et al. OEIS complex—a population study. *Am J Med Genet* 2000; 92: 62–8.
19. Simpson JL. Disorders of the gonads, genital tract and genitalia. In: Emery AEH, Rimoin DL, eds. *Principle and Practice of Medical Genetics*. 4th ed. London: Churchill Livingstone; 2002: 2315–51.
20. Cheikhelard A, Luton D, Philippe-Chomette P, et al. How accurate is the prenatal diagnosis of abnormal genitalia? *J Urol* 2000; 164: 984–7.
21. Quarello E, Gorincour G, Merrot T, et al. The "daughter cyst sign": a sonographic clue to the diagnosis of fetal ovarian cyst. *Ultrasound Obstet Gynecol* 2003; 22: 433–4.
22. D'Addario V, Volpe P, Kurjak A, et al. Ultrasonic diagnosis and perinatal management of complicated and uncomplicated fetal ovarian cysts: a collaborative study. *J Perinat Med* 1990; 18: 375–81.
23. Volpe P, Paladini D, De Robertis V, et al. Fetal gastrointestinal anomalies. In: Fleischer AC, Toy E, Lee W, et al., eds. *Sonography in Obstetrics &Gynecology*. 7th ed. McGraw–Hill; 2011: 461–507
24. Dolgin SE. Ovarian masses in the newborn. *Semin Pediatr Surg* 2000; 9: 121–7.
25. Hata K, Hata T, Kitao M, et al. Ultrasonographic identification and measurement of the human fetal adrenal gland in utero: clinical application. *Gynecol Obstet Invest* 1988; 25: 16–22.
26. Buhimischi CS, Turan OM, Funai EF, et al. Fetal adrenal gland volume and cortisol/DHEAS ratio in inflammation—associated preterm birth. *Obstet Gynecol* 2008; 111: 715–22.
27. Gocmen R, Basaran C, Karcaaltincaba M, et al. Bilateral hemorrhagic adrenal cysts in an incomplete form of Beckwith–Wiedemann syndrome: MRI and prenatal US findings *Abdom Imaging* 2005; 30: 786–9.
28. Crombleholme T, Murray T, Harris B, et al. Diagnosis and management of fetal neuroblastoma. *Curr Opin Obst Gynecol* 1994; 6: 199–202.
29. Kramer S, Ward E, Meadows AT, et al. Medical and drug risk factors associated with neuroblastoma: a case-control study. *J Natl Cancer Inst* 1987; 78: 797–804.
30. Acharya S, Jayabose S, Kogan S, et al. Prenatally diagnosed neuroblastoma. *Cancer* 1997; 80: 302–10.
31. Kesrouani A, Duchatel F, Seilanian M, et al. Prenatal diagnosis of adrenal neuroblastoma by ultrasound: a report of two cases and review of the literature. *Ultrasound Obstet Gynecol* 1999; 13: 446–9.

Chapter 9
Skeletal dysplasias and muscular anomalies: A diagnostic algorithm

Normal anatomy of the fetal musculoskeletal system: ultrasound approach, scanning planes, and diagnostic potential

Ultrasound (US) assessment of the fetal musculoskeletal apparatus requires a global approach to the fetal body, given that skeletal dysplasias and neuromuscular diseases involve more or all anatomic regions simultaneously, because of the ubiquitous distribution of bones and muscles. The only exceptions are reduction defects of the limbs, congenital or acquired (amniotic band syndrome), which are regional by definition. Therefore, unlike other systems, assessment of the fetal musculoskeletal apparatus requires a multistep *total-body* US approach, which should include assessment of the following:

- Limbs: long bones and extremities;
- Spine and thorax;
- Fetal head: calvarium, central nervous system (CNS), and splanchnocranium;
- Bone mineralization;
- Any joint contractures and joint dislocations.

Each of these five points should be addressed with separate views at different degrees of magnification, which makes the evaluation of the musculoskeletal apparatus rather time-consuming and challenging. In the following sections, the diagnostic approach to the various anomalies of bones and muscles will be dealt with the help of different diagnostic flowcharts, based on the main abnormal US finding, with the intention of making the very difficult and challenging issue of differential US diagnosis easier.

Timing of examination. The US appearance of the bones changes significantly during gestation, due to progressive mineralization. It is common knowledge that in the third trimester, the posterior fossa as well as the thoracic content can hardly be evaluated due to conspicuous mineralization of the calvarium and ribs. It should also be noted that currently the suspicion of lethal skeletal dysplasias is raised often at 12–14 weeks, due to severe and early-onset micromelia, rather than at mid-trimester, as is the case for most other anomalies.

Two-dimensional (2D) US approach and scanning planes (views). In this subsection, we adopt the multistep assessment procedure described above. The standard views for suspecting or diagnosing abnormalities of the various skeletal regions are described below.

Long bones and extremities (Figures 9.1 and 9.2). To assess the anatomy of the limbs, two types of views should be sought: (1) *regional views*, aiming at visualization of the three components (rhizomelic, mesomelic, and acromelic), to ascertain whether the anomaly involves the whole limb or predominantly a part of it—this is generally carried out with low-magnification sagittal US views of the whole limb (Figure 9.1); (2) *focal, higher-magnification views*, to study in detail the anomaly of the affected segment, in order to characterize possible focal defects and/or anomalies of the extremities (Figure 9.2). The orientation of the various planes needed to carry out this task will depend on the spatial position of the limb at the time of the US examination.

Spine and thorax (Figures 9.3 and 9.4). The spine is electively evaluated using the *midsagittal view,* possibly performed with an spine up position, in order to assess the vertebral bodies and the cutaneous contour, taking care to reduce the pressure on the transducer to leave some amniotic fluid between the proximal uterine wall and the spine, which greatly enhances

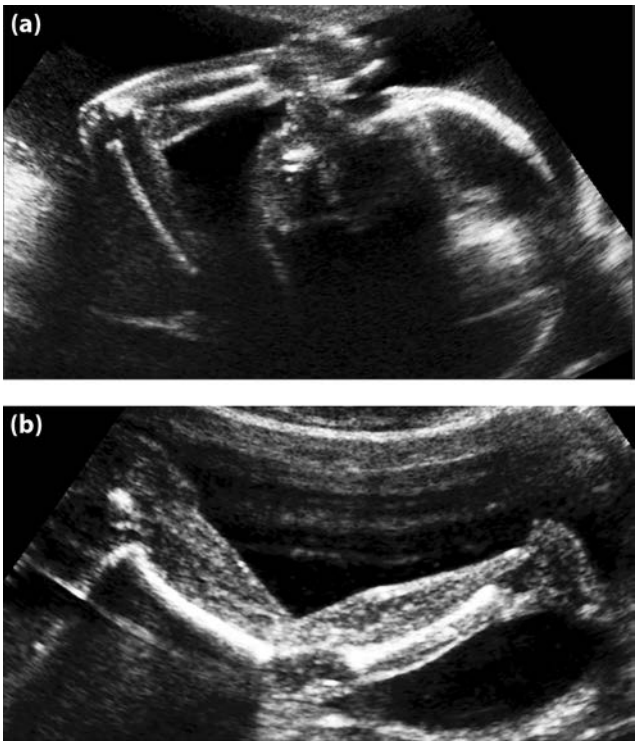


Figure 9.1 Low-magnification sagittal view of the limbs. (a) Upper limb, flexed: the image shows the rhizomelic segment (humerus), the mesomelic segment (ulna and radius), and the acromelic segment (hand). (b) Lower limb, abducted: the rhizomelic, mesomelic, and acromelic segments on the same axis (femur, tibia and fibula, and foot).

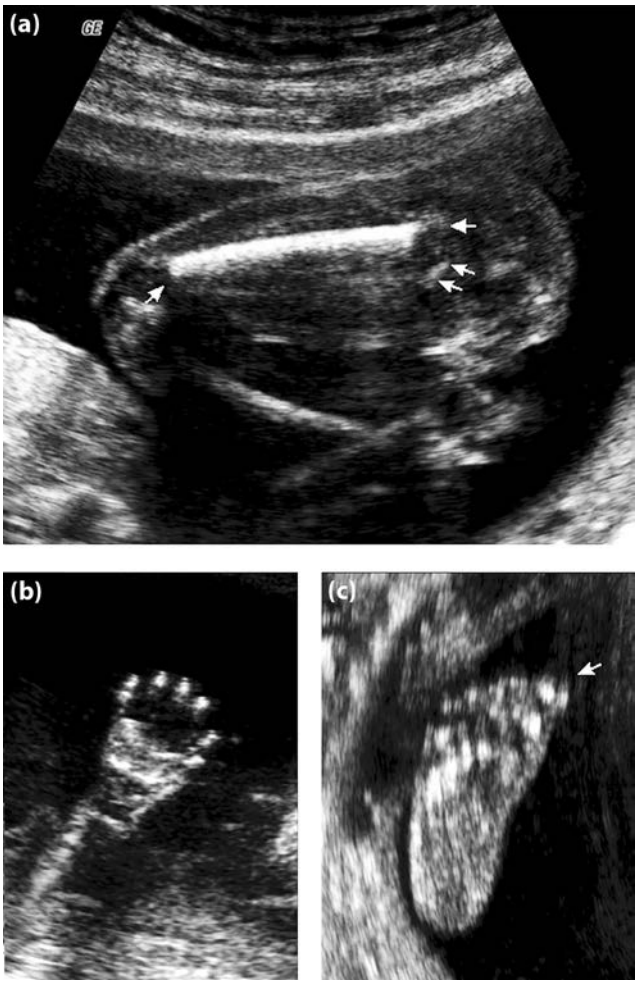


Figure 9.2 High-magnification view of a single bone segment. (a) The flexed thigh is displayed. The image shows the cutaneous contour, up to the gluteal region, the muscles of the thigh, and the shaft of the femur. The mineralization, shape, and contour of the bone should be assessed. The epiphyses are also visible (arrows) as hypoechoic round structures with hyperechoic outline at both ends of the long bone. (b) Hand, high-magnification: the five rays are visible, with all digits extended. (c) Foot, high magnification: the toe (arrow) and the other digits are visible. The calcaneus and metatarsus are also visible.

the acoustic window (Figure 9.3). This sagittal view allows display of neural tube defects (see Chapter 2), as well as possible fusions of vertebral bodies. It also allows the suspicion of scoliosis to be raised, if the axis of the spine cannot be displayed from head to breech on a single plane; if this is suspected, a *coronal view of the spine* allows one to evaluate the degree of scoliosis (Figure 9.4). Also, the *midsagittal view of the spine* allows one to identify possible focal or general mineralization defects of the vertebrae. *Parasagittal views* at the level of the outer thoracic walls are used to display, on 2D US, gross mineralization or developmental anomalies of the ribs, as well as fractures. To exclude thoracic hypoplasia, the dimensions of the thorax should be assessed on the *four-chamber view* (cardiothoracic ratio and thoracic circumference: see Chapter 6 and Appendix Table A.18) and on the *midsagittal view with ventral approach* (anteroposterior diameter of the thorax, dip at thoracoabdominal junction: Chapter 6).

Cranium (calvarium and splanchnocranium). The classic *axial transthalamic view* (Figure 9.5) is employed to detect possible deformations of the calvarial contour possibly due to early synostoses, such as in "cloverleaf skull" (thanatophoric dysplasia), although this anomaly is best displayed with a coronal approach, because the most significant deformation of the skull occurs below the transthalamic plane. The assessment of the fetal facial profile, performed on the *midsagittal view*, is needed to detect micrognathia, which is a frequent finding in skeletal dysplasias (Chapter 3).

Calvarial mineralization. The degree of mineralization is best appreciated on the *transthalamic axial*

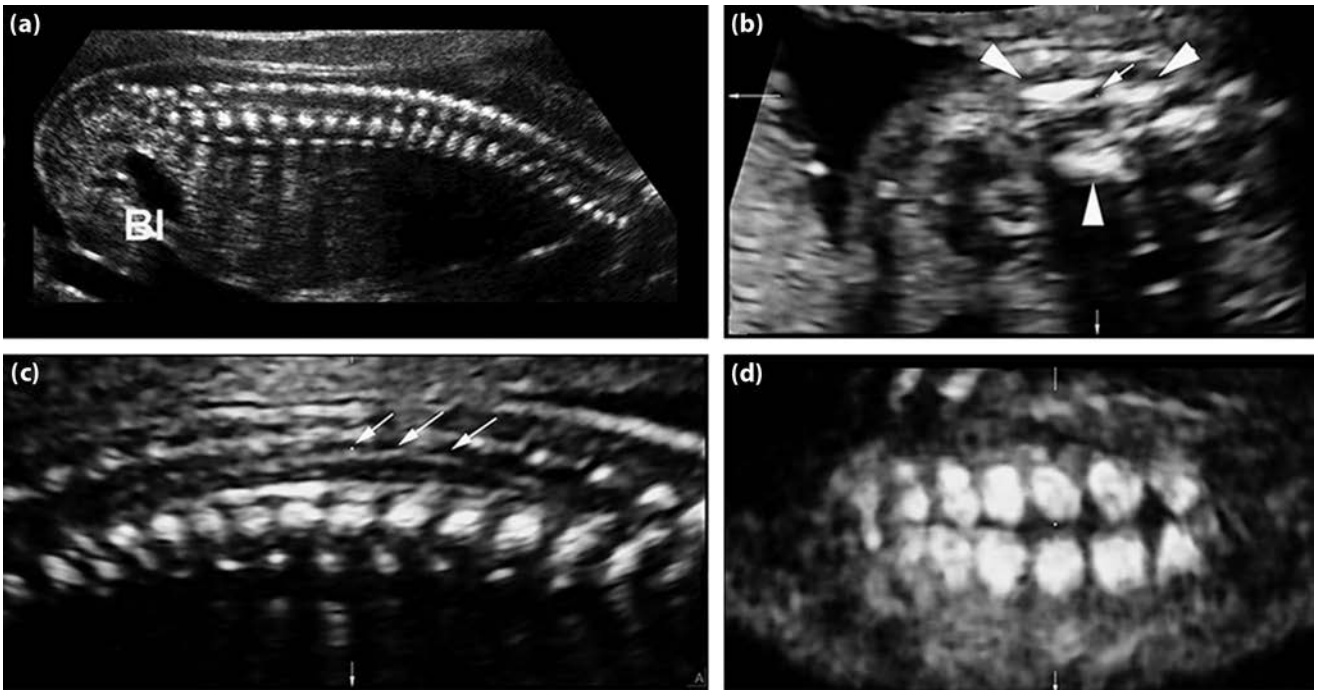


Figure 9.3 Views for the assessment of the spine. (a) Two-dimensional sagittal view: the regular aspects of all the neural arches, together with the continuous cutaneous contour, are evident. By confirming the integrity of the cutaneous contour on this view, it is possible to exclude open spina bifida. In front of the sacrum, the bladder (Bl) is visible. (b–d) Three-dimensional multiplanar imaging allows the perfect alignment of the three orthogonal planes. The cross-sectional imaging of a lumbar spine (b) demonstrates that the usual view shown in (a) is not a perfectly midsagittal one, because it cuts across one of the two posterior arches (upper arrowheads). If the plane is perfectly midsagittal, the image in (c) would result. On this, the posterior arches are not visible, but it is possible to assess in detail the course of the spinal cord (arrows) and the cauda equina; (d) this is a coronal view of the spine, further demonstrating the normal gap between the two posterior arches: correlate the position of the reference dot on the three images (b–d). The normal three vertebral ossification nuclei (vertebral body and posterior arches: arrowheads).

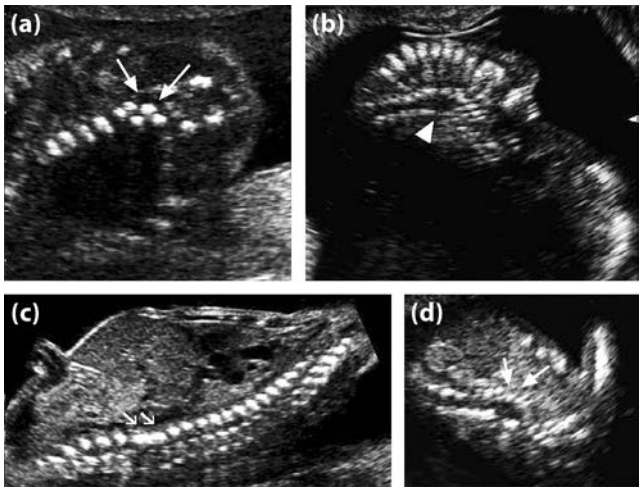


Figure 9.4 Hemivertebra (a, b) Twenty-one weeks of gestation: (a) coronal view of the spine showing the hemispondilus (arrows); (b) another case, at 16 weeks. The coronal view demonstrates the thoraco-abdominal hemispondilus; (c, d) 21 weeks of gestation; (c) is sagittal view of the thoracic spine demonstrating a rare anterior hemispondilus (arrows); (d) another coronal view, showing the distortion of the spine (arrows).

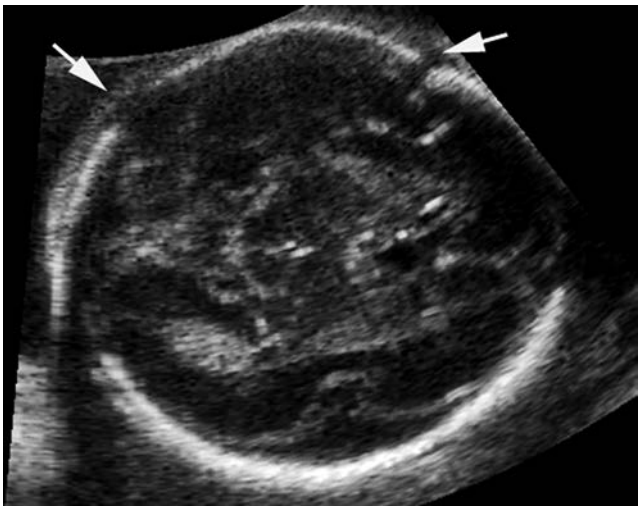


Figure 9.5 Axial transthalamic view (21 weeks of gestation). This view is also employed to assess the cranial suture on 2D ultrasound. At mid-trimester, both the coronal and parieto-occipital sutures can be identified as small sonolucent gaps along the calvarial surface (arrows).

view (Figure 9.5). Also, in the case of hypomineralization, minor pressure exerted with the transducer can produce deformation of the skull, which is very soft (see below). An important hint to enable recognition of the presence of calvarial hypomineralization is the appearance of the brain: if the ossification of the calvarium is deficient then the US waves are less absorbed by it and the usual shadowing artifact just below the proximal parietal bone is absent; as a result, both hemispheres are displayed much better than with normal calvarial ossification Therefore, the general impression, just before recognizing the bone ossification defect, is: "See how nicely this brain shows up!".

Joint contractures. The display of the fetal body *at low magnification* is the best way to recognize possible joint contractures. Alternatively, when an advanced gestational age makes such an approach impossible, separate sagittal views of the upper and lower limbs should be sought. When affected by pathologic contractures, the lower limbs often appear hyperextended and with crossed legs (scissor-like), due to the fact that the femoral extensor muscles (quadriceps) are stronger than the flexors (biceps). The reverse occurs for the upper limbs, where the flexor muscles (biceps) are stronger than the extensors (triceps): this is why, in the case of contractures, the upper limbs often appear flexed with the clenched hands lying on the thorax (Chapter 10, Figures 10.24 and 10.25). An alternative view in which it is possible to detect contractures of the upper limbs is the *axial view of the thorax* (*four-chamber view*).

No MENc LATUr E o F Bo NE dEFE c Ts

Abnormal shapes of the skull (Figure 9.6). These are mainly related to synostoses. The most evident is the so-called cloverleaf skull, which is typical of thanatophoric dysplasia type II; this is due to very premature closure of the lambdoid, coronal, and sagittal sutures. As already noted, the *coronal view of the head* is the best view in which to appreciate the cloverleaf deformation, because the parietal bones are the most severely affected.

Acrocephaly (Figure 9.6a) Acrocephaly is the presence of a pointed head (increased craniocaudal diameter), caused by premature closure of *both coronal sutures*.

Acrocephaly is typical of Apert syndrome (Chapter 10). Brachycephaly (Figure 9.6b) Brachycephaly is characterized by a reduced occipitofrontal diameter, and is often found in chromosomal anomalies, such as trisomy 18 and 21.

Scaphocephaly (Figure 9.6c) Scaphocephaly is characterized by an increased occipitofrontal diameter, due to premature closure of the sagittal suture. Plagiocephaly is usually not detected in utero; it denotes an asymmetric shape of the skull, caused by unilateral premature closure of the coronal and lambdoid sutures. Trigonocephaly indicates a triangular shape of the forehead and is due to closure of the metopic suture.

Anomalies of the spine. Platyspondyly refers to flattened vertebral bodies with reduced distance between the endplates, which is associated with some skeletal dysplasias (thanatophoric dysplasia and osteogenesis imperfecta type II) is not easily detectable by US. Therefore, we will not describe it in detail here.

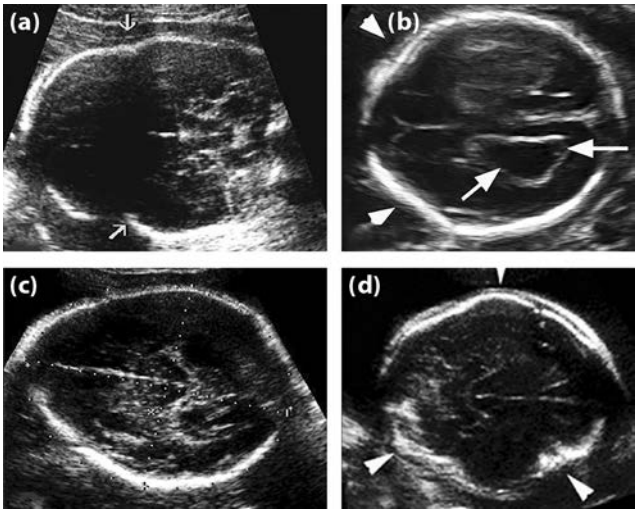


Figure 9.6 Abnormal shape of the skull. (a) In Apert syndrome, the coronal suture is already sealed at 23 weeks of gestation (arrows), causing deformation of the skull (compare with Figure 9.5). (b) In trisomy 18, one of the common findings (especially early in gestation) is a strawberry-shaped skull (arrowheads); a concurrent large choroid plexus cyst is also evident here (arrows). (c) Scaphocephaly (in this case at 32 weeks of gestation) is due to early closure of the sagittal suture, and is characterized by an increased occipitofrontal diameter. (d) In thanatophoric dysplasia type II, early abnormal closure of the coronal, lambdoid, and sagittal sutures leads to the classic cloverleaf skull; however, in type I also, there is an abnormal shape of the skull, due to abnormal incomplete closure of the same sutures.

Anomalies of the limbs. The first issue to consider is the harmonic proportion among the three segments of the limb: rhizomelic (femur/humerus); mesomelic (tibia and fibula/ulna and radius); and acromelic (foot/hand). If only one of the three segments is affected, the condition is termed *rhizomelia, mesomelia, or acromelia,* respectively. If, on the contrary, the whole length of the limb is abnormal, the condition is referred to as *micromelia*.

Anomalies of the extremities. Pathologic contractures of the ankle and the wrist are associated with *clubfoot* (*talipes*) and *ulnar deviation of the hand*, respectively. In clubfoot, the axis of the foot is no longer that of the lower leg: the foot is drawn up and bent inward (*varus),* and therefore, on the sagittal view of the leg, the sole is visible, too. In the rarer *equinus* variant, the axis is the same as that of the leg, but the foot is in fixed abnormal hyperextension, with the sole facing backward. In *ulnar deviation of the hands*, the hand appears abnormally and fixedly extrarotated on the ulnar side, with overlapping fingers

Micrognathia. Micrognathia, which is described extensively in Chapter 3, can be found in a number of skeletal dysplasias described later in this chapter (see Table 9.5).

Differential diagnosis of skeletal dysplasias

Skeletal dysplasias characterized by micromelia (Figures 9.7a and 9.8). Micromelia denotes severe hypoplasia of the three segments of the limb, and, in most cases, affects all limbs at the same time. This extreme hypoplasia of the long bones is a feature of lethal dysplasias. In general, all three bone segments are highly hypoplastic and the shafts of the long bones appear very small and curved. A diagnostic algorithm assisting in the differential diagnosis of the most common skeletal dysplasias characterized by micromelia is shown in Table 9.1, while skeletal dysplasias characterized prevalently by rhizomelia are shown in Table 9.2. Figure 9.8 shows the same information as Table 9.1, with US images.

Skeletal dysplasias characterized by thoracic hypoplasia (Figures 9.7b,c and 9.9). The US diagnosis of thoracic hypoplasia, if severe, does not offer particular difficulties provided that, when assessing the four-chamber view, the operator bears this anomaly in mind. As already pointed out, the first impression is *always* that of a very enlarged but anatomically normal heart. However, if the suspicion of a possible skeletal dysplasia has already been raised, then the diagnosis is straightforward and it becomes easy to pick up the evident disproportion between a normal-sized heart and a hypoplastic thorax (Figure 9.7b). To provide an objective impression of thoracic hypoplasia, the thoracic circumference or area and the cardiothoracic ratio should be checked against the appropriate normal ranges for gestational age, using charts published in the literature [1,2] (see Appendix Table A.18). However, it should be emphasized that the cardiothoracic ratio is abnormal (>95th percentile) both in cardiomegaly and in thoracic hypoplasia (Chapter 6), whereas by using the simple graphs of thoracic circumference or area versus gestational age, the diagnosis of thoracic hypoplasia is straightforward. In this regard, care should be taken in checking the effective gestational age of the index pregnancy, considering the difficulties related to the fact that, in skeletal dysplasias, most biometric measures are indeed below the normal range. It is useful to remember that, except for some very rare anomalies

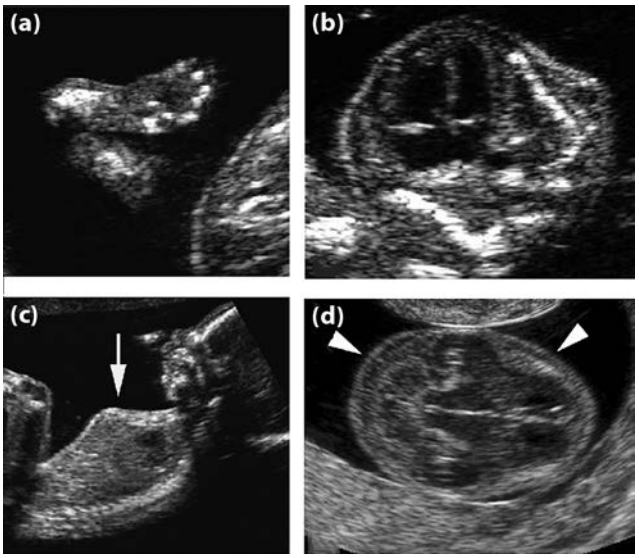


Figure 9.7 Markers of lethal skeletal dysplasias. (a) Micromelia. (b) Severe thoracic hypoplasia; note the predominance of the heart over the thorax and the abnormal shape of the ribs. (c) Severe thoracic hypoplasia. On a low magnification sagittal view of the fetal body, a dip at the thoracoabdominal junction (arrow) is a marker of severe thoracic hypoplasia. (d) Calvarial hypomineralization. Diffuse regional hypomineralization is a feature of some lethal skeletal dysplasias. Note the absence of the hyperechoic rim due to the normal mineralization of the skull and the evidence of the CNS structures (arrowheads), due to the unblocked penetration of ultrasound waves.

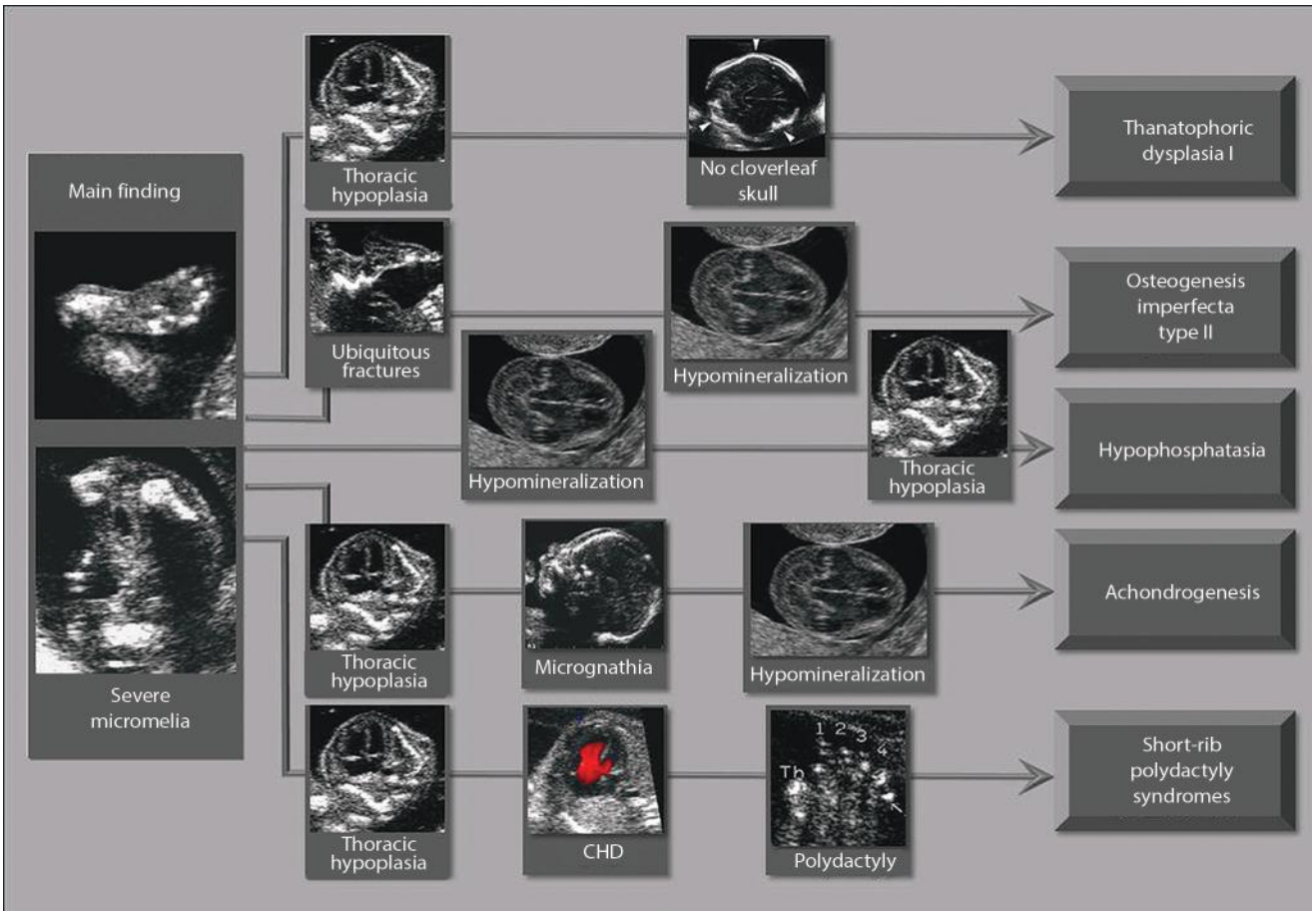


Figure 9.8 Differential diagnosis of skeletal dysplasias featuring micromelia.

Table 9.1 Ultrasound differential diagnosis of skeletal dysplasias characterized by severe micromelia (see also Figure 9.8)

Index sign	→	Severe micromelia		
Additional signs	→	Thoracic hypoplasia (no cloverleaf skull)	→	Thanatophoric dysplasia type I
Additional signs	→	Ubiquitous fractures ± hypomineralization	→	Osteogenesis imperfecta type II
Additional signs	→	Thoracic hypoplasia ± hypomineralization	→	Achondrogenesis
Additional signs	→	Severe ubiquitous hypomineralization[a]	→	Hypophosphatasia
Additional signs	→	Thoracic hypoplasia ± CHD ± polydactyly ± hypomineralization	→	Short-rib polydactyly syndrome(s)

[a] Clavicle-sparing hypomineralization.
CHD: congenital heart disease.

such as Neu–Laxova syndrome (Chapter 10), the transverse cerebellar diameter is not generally affected and its biometry gives a reliable estimate of the effective gestational age. Other findings possibly indicative of severe thoracic hypoplasia can be searched for on the *midsagittal view* of the fetal trunk obtained with a *ventral approach*. On this view, the recognition of a dip at the thoracoabdominal junction (Figure 9.7c and Chapter 6) further supports the diagnosis of severe thoracic hypoplasia. On the same view, at higher magnification, it can be appreciated that the heart occupies the whole of the anteroposterior diameter of the thorax.

Table 9.2 Ultrasound differential diagnosis of skeletal dysplasias characterized by rhizomelia of variable severity

Index sign	→	Rhizomelia		
Additional signs	→	Frontal bossing ± mild macrocrania	→	Achondroplasia
Additional signs	→	Thoracic hypoplasia ± polydactyly ± renal anomalies	→	Asphyxiating thoracic dystrophy (Jeune syndrome)
Additional signs	→	Postural deformities + 'hitch-hiker's thumb' + micrognathia	→	Diastrophic dysplasia

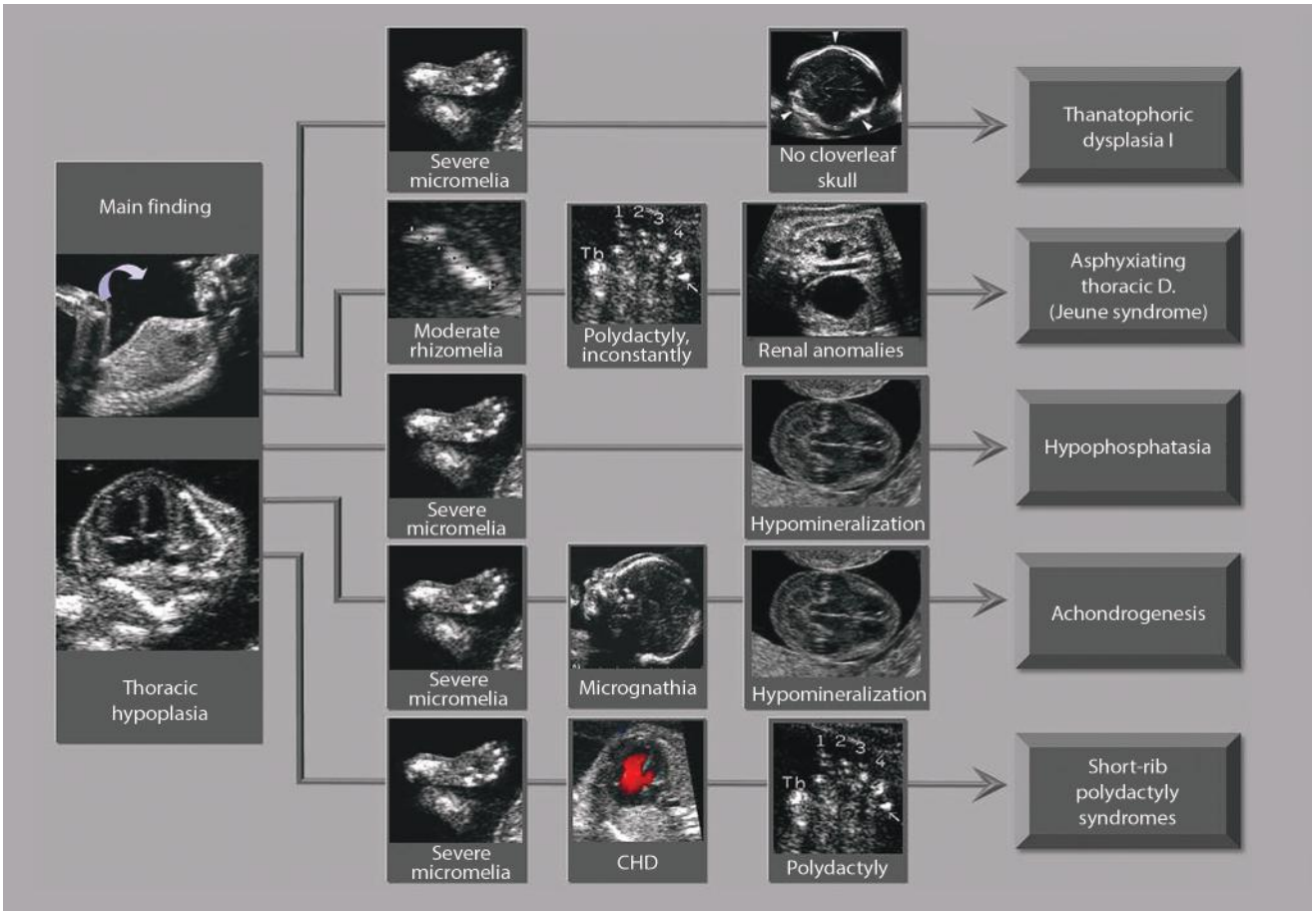


Figure 9.9 Differential diagnosis of skeletal dysplasias featuring severe thoracic hypoplasia. Note that both osteogenesis imperfecta type II and chondroectodermal dysplasia (Ellis-van Creveld) are not listed here because in these two disorders the degree of thoracic hypoplasia is variable.

Similarly to micromelia, thoracic hypoplasia, if severe, is a feature of lethal dysplasias (Table 9.3). In skeletal dysplasias associated with severe thoracic hypoplasia, death is the result of severe secondary pulmonary hypoplasia.

Skeletal dysplasias characterized by fractures. The US recognition of a fracture is straightforward in some cases, but can prove difficult and tricky in others, especially early in gestation. The positive aspect is that, if fractures have been confidently recognized, the diagnosis is made, there is virtually only one disease, and one subtype of disease, that is, associated with fractures in the second trimester, namely osteogenesis imperfecta (OI) type II! Of the other three subtypes of OI, only type III can sometimes be recognized in the third trimester, on the basis of bowed and short femurs and tibiae.

Table 9.3 Ultrasound differential diagnosis of skeletal dysplasias characterized by severe thoracic hypoplasia (see also Figure 9.9)

Index sign	→	Thoracic hypoplasia		
Additional signs	→	Micromelia (no cloverleaf skull)	→	Thanatophoric dysplasia type I
Additional signs	→	Rhizomelia ± renal anomalies /polydactyly[a]	→	Asphyxiating thoracic dystrophy (Jeune syndrome)
Additional signs	→	Micromelia ± hypomineralization	→	Achondrogenesis
Additional signs	→	Micromelia ± hypomineralization[b]	→	Hypophosphatasia
Additional signs	→	Micromelia + polydactyly + CHD ± hypomineralization	→	Short-rib polydactyly syndrome(s)

[a] Polydactyly is found only in 20% of the cases.
[b] Clavicle-sparing hypomineralization.
CHD: congenital heart disease.
Note that both osteogenesis imperfecta type II and Ellis-van Creveld syndrome are not listed here because in these two disorders, the degree of thoracic hypoplasia is variable.

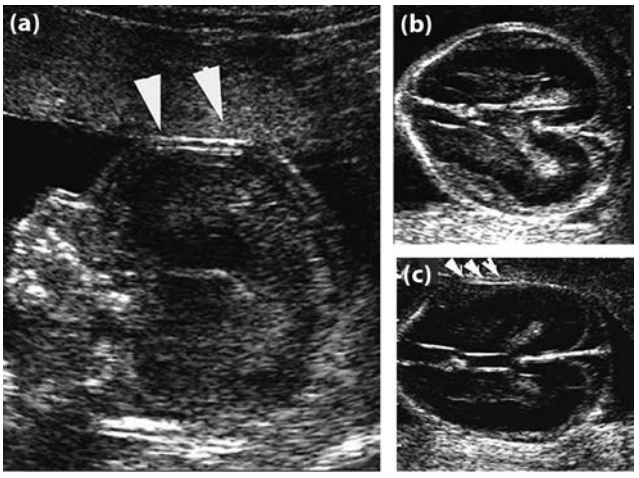


Figure 9.10 Signs of calvarial hypomineralization. In case of calvarial hypomineralization, the skull is soft and can easily be indented by applying moderate pressure with the transducer (arrowheads). (a) Sagittal view (15 weeks of gestation): note the deformation of the skull against the anterior placenta. (b) Axial view: vivid demonstration of CNS structure due to the hypomineralization of the calvarium. (c) In the same case, by applying moderate pressure with the transducer, it is possible to deform the parietal area (arrowheads).

Skeletal dysplasias characterized by hypomineralization (Figures 9.7d, 9.10, and 9.11). The US detection of hypomineralization is usually made on the axial *transthalamic view of the fetal head* (Figure 9.7d), or, alternatively, on the *midsagittal view of the fetal profile* (Figure 9.10a). A peculiar feature, in the case of hypomineralization of the calvarium, is the perfect depiction of the fetal brain ("See how nicely this brain shows up!"), due to the lack of US absorption by the underossified proximal parietal bone; in addition, the usually bright rim of the calvarium is barely visible (Figures 9.7d and 9.10). An additional feature is the softness of the calvarium: it is possible to deform the fetal head significantly by applying moderate pressure with the transducer (Figure 9.10 a-c). Once the occurrence of hypomineralization has been established, the next step is to evaluate the involved regions. The selective involvement or, on the contrary, the selective sparing of a given region may contribute to the differential diagnosis. As an example, in hypophosphatasia, the hypomineralization spares the clavicles. A flo - chart assisting in the differential diagnosis of the most common skeletal dysplasias characterized by hypomineralization is shown in Figure 9.11 (see also Table 9.4).

Skeletal dysplasias characterized by micrognathia (Figure 9.12 and Table 9.5). Given that the diagnosis of micrognathia may help in the differential diagnosis of skeletal dysplasias, a flowchart reporting the most common skeletal dysplasias characterized by this feature is shown in Figure 9.12 (see also the dedicated section in Chapter 3).

Skeletal dysplasias characterized by hydrops (Table 9.6). Usually, lethal skeletal dysplasias, especially at 12–14 weeks of gestation, can be associated with fetal hydrops or cystic hygroma. Nonimmune fetal hydrops is described in detail in Chapter 4. The most common skeletal dysplasias characterized by this feature are listed in Table 9.6.

Table 9.4 Ultrasound differential diagnosis of skeletal dysplasias characterized by diffuse hypomineralization

Index sign	→	Hypomineralization		
Additional signs	→	Micromelia + fractures	→	Osteogenesis imperfecta type II
Additional signs	→	Micromelia	→	Hypophosphatasia[a]
Additional signs	→	Micromelia + thoracic hypoplasia ± micrognathia	→	Achondrogenesis
Additional signs	→	Micromelia + CHD[b] + polydactyly	→	Short-rib polydactyly syndrome(s)[b]

[a] Clavicle-sparing hypomineralization.
[b] The presence/absence of hypomineralization in this group of syndromes varies in the four types.
CHD: congenital heart disease.

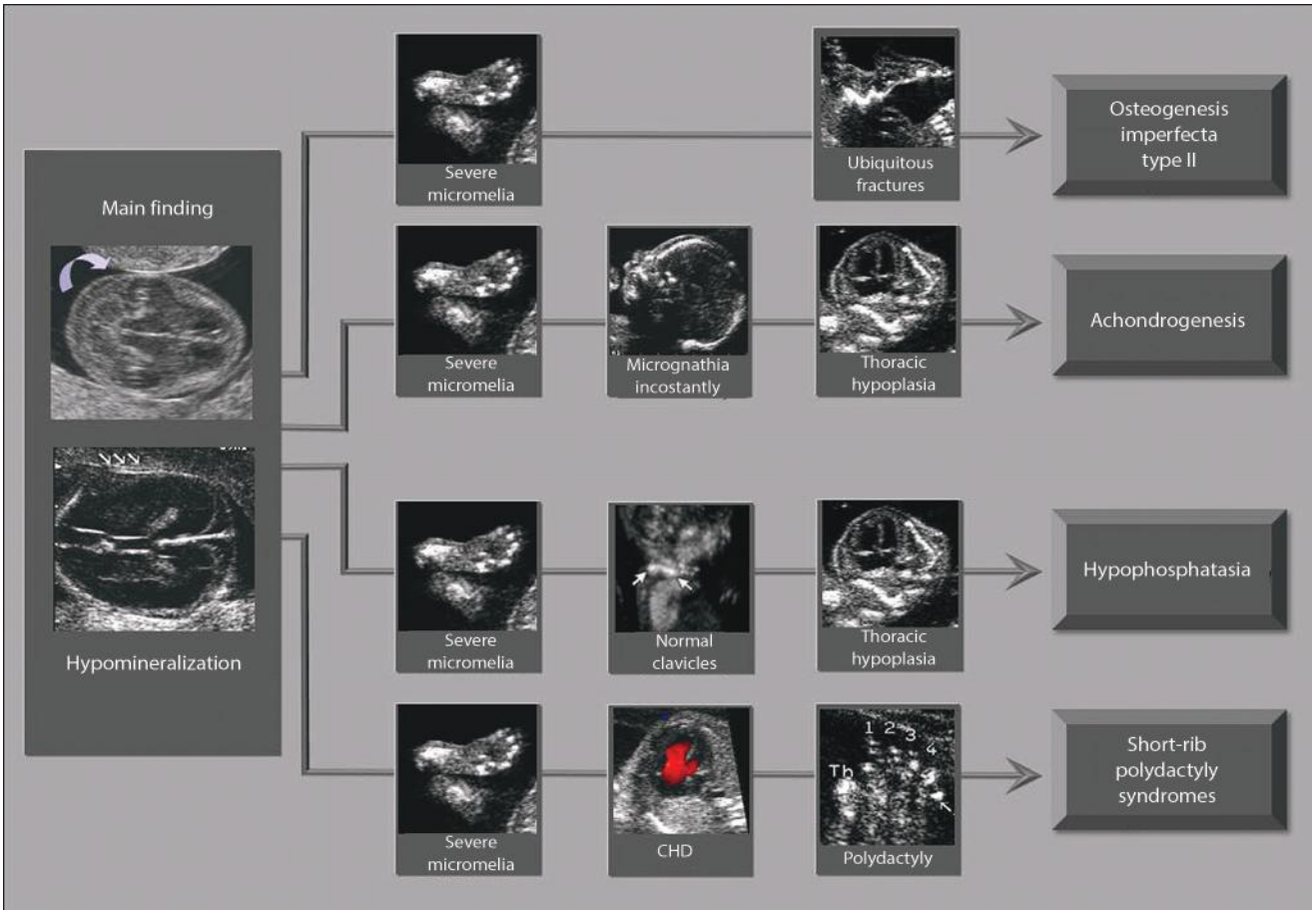


Figure 9.11 Differential diagnosis of skeletal dysplasias featuring hypomineralization.

Table 9.5 Ultrasound differential diagnosis of skeletal dysplasias featuring micrognathia

Index sign	→	Micrognathia		
Additional signs	→	Micromelia + hypomineralization + thoracic hypoplasia	→	Achondrogenesis
Additional signs	→	Bowed tibias and femurs + hypoplastic scapula	→	Campomelic dysplasia
Additional signs	→	Rhizomelia + joint contractures (hitchhiker's thumb)	→	Diastrophic dysplasia
Additional signs	→	Ubiquitous joint contractures + hydrops	→	FADS

FADS: fetal akinesia deformation sequence.

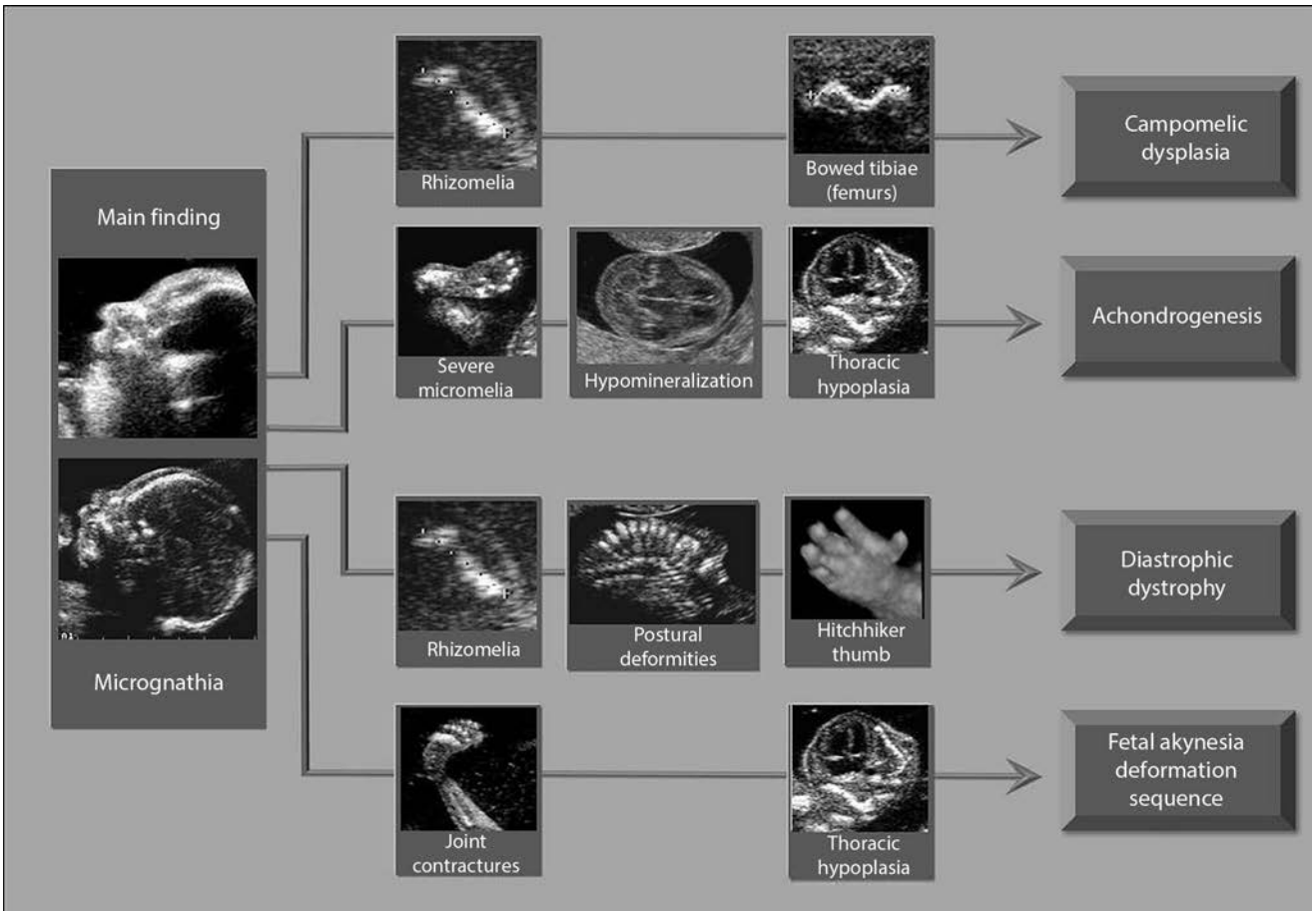


Figure 9.12 Differential diagnosis of skeletal dysplasias featuring micrognathia.

Table 9.6 Ultrasound differential diagnosis of skeletal dysplasias characterized by early hydrops/hygroma

Index sign	→	Hydrops		
Additional signs	→	Micromelia ± hypomineralization + micrognathia	→	Achondrogenesis
Additional signs	→	Micromelia (no cloverleaf skull)	→	Thanatophoric dysplasia type I
Additional signs	→	Micromelia + fractures + hypomineralization	→	Osteogenesis imperfect type II
Additional signs	→	Rhizomelia ± polydactyly[a]/renal anomalies	→	Asphyxiating thoracic dystrophy (Jeune syndrome)
Additional signs	→	Micromelia + CHD + polydactyly	→	Short-rib polydactyly syndrome(s)

[a] Polydactyly is found in only 20% of cases.
CHD: congenital heart disease.

Thr EE-dIMENsIo NAL Us IN ThE dIAGNos Is o F skELETAL dysp LAsIA ANd rELA TEd c o NdITIo Ns

Objectives. The primary objectives of three-dimensional (3D) assessment of the fetal skeleton are the following [3,4]:

- *Multiplanar imaging* of skeletal structures, aiming at the demonstration of anomalies not readily recognizable on 2D US;

- *Surface-rendering reconstructions*, to highlight abnormal postures and joint contractures;
- *Surface-rendering reconstructions*, performed mainly with the maximum mode, to better assess normal and abnormal bones, which are more difficult to explore with conventional 2D US, such as the ribs or the skull sutures (see Chapter 1).

It is important to note that the coronal volume contrast imaging (VCI-C) mode, which allows a real-time representation of the coronal plane, coupled with the transparent maximum mode, makes the assessment of the skeleton much easier and more immediate than when using the conventional procedure of acquiring a volume and then postprocessing it. By using the VCI-C mode "live," it is possible to assess normal and abnormal fetal bones quickly and efficiently.

Examination protocols. An introduction to 3D volume acquisition and processing is given in Chapter 1. We describe here the modalities with which 3D US is to be employed for the best assessment of the musculoskeletal system. As far as the rendering modes are concerned, the *transparent maximum mode* is the option of choice for assessment of the skeleton and sutures. As already mentioned, the use of the VCI-C mode reduces examination time and is the option of choice for assessment of the fetal skeleton. Once acquired, the volume may also be further postprocessed in order to improve even more the display of the region of interest. This is accomplished by adjusting the threshold and balance settings to obtain the best balance between the display of the bones and that of the overlying soft tissues. Two useful hints, for a better display of the skeleton, are to start the acquisition with a lower than normal gain setting on the 2D image and to use rather hard gray-scale settings, such as those used in fetal echocardiography.

Districts to explore.
Cranial sutures. One of most important advantages of 3D US concerns the visualization of the cranial sutures with the transparent maximum mode. In particular, with a correct orthogonal approach to the suture in question, it is possible to actually see the bony parts and the wide open sutures under normal and abnormal conditions [5–8] (see Chapter 3 for details).

Spine and ribs. The assessment of the ribcage also benefits from a 3D US approach. In addition to an overall assessment of its integrity, high-definition renderings of the cervical vertebrae and the occiput allow one to evaluate in detail possible anomalies of this tract of the spine, such as fusion of the vertebrae. However, it is in the assessment of the ribs that 3D US shows its advantages most clearly: the acquisition of a volume including the whole of the thorax and its display with the transparent maximum mode make the detection of rib number and structural anomalies much easier than with 2D US. In particular, additional ribs, rib fractures, and/or deformities are easily detected using this technique (Figure 9.13). Also, 3D renderings of the lower spine with the iliac bones are useful for the assessment

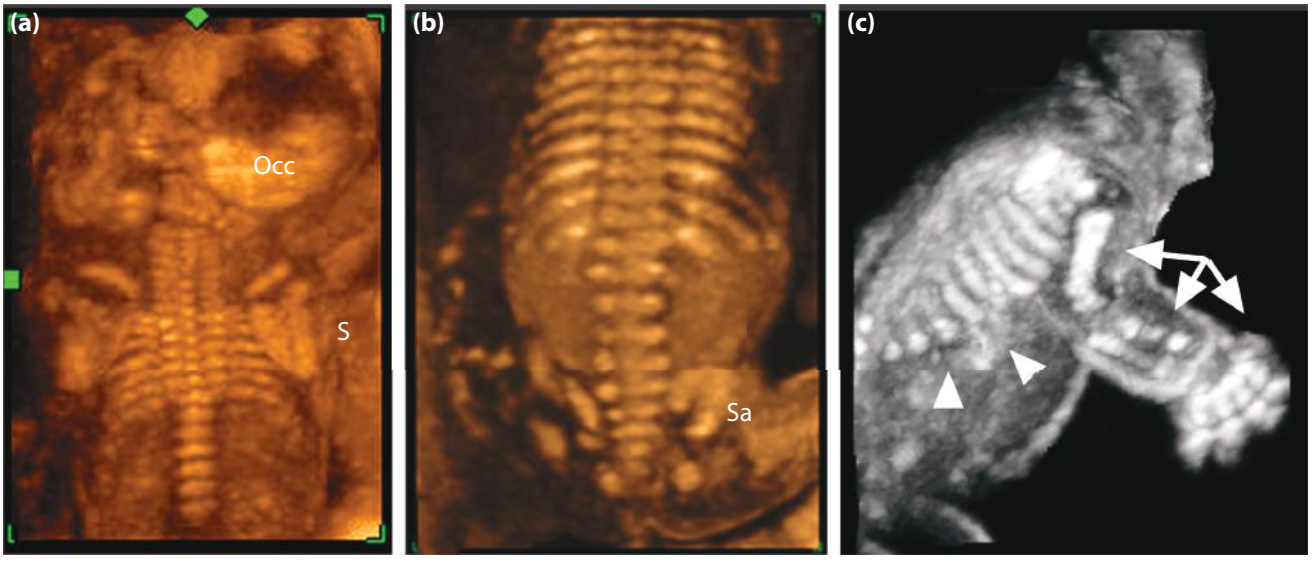


Figure 9.13 Three-dimensional maximum-mode rendering of spine and ribs. (a) Upper spine and occipital bone. The image shows the cervicothoracic spine, the ribs, the scapulae (S), the clavicles (appearing as two oblique echoic bars just above the scapulae), and the occipital bone (Occ). (b) Lower spine and sacrum. The lower ribs, the lower spine (from the thoracic to the sacral vertebrae), and the iliac wings (sa) are clearly shown. (c) Thanatophoric dysplasia type I. As an example, a lateral sagittal view of the body demonstrates on the same image the extremely short ribs (arrowheads), and the short and thickened bones (like a French telephone receiver) of the upper limb (arrows).

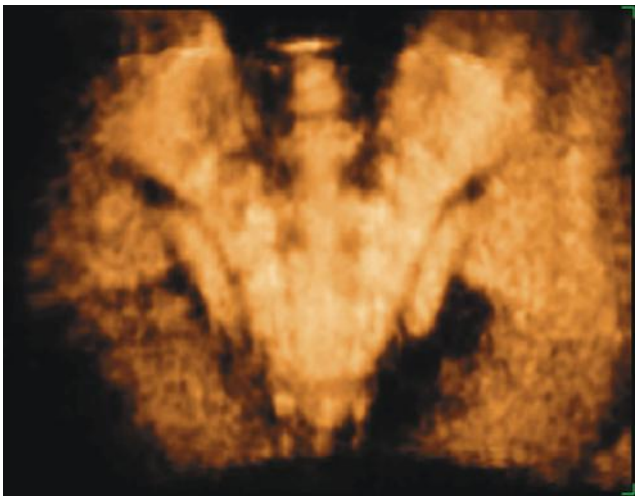


Figure 9.14 Three-dimensional maximum-mode rendering of the sacrum and the iliac bones. With an adequate insonation angle, it is possible to demonstrate the sacral vertebrae and the iliac wings.

of caudal anomalies of the spine and/or the neural tube, which are often associated in spinal dysraphisms (Figure 9.14).

Long bones and extremities. The use of 3D US in the assessment of limb anomalies includes both surface-mode and maximum-mode renderings, in order to display the overall appearance of the limb or the bony parts only (Figure 9.15). The surface-rendered appearance of a limb defect, be it a transverse defect or a clubfoot, can also be used to improve the communication of the diagnosis to the parents. On the other hand, maximum-mode renderings allow one to accurately define possible focal bony defects and/or abnormal shapes of the long bones (Figures 9.13c and 9.15c).

Anomalies detectable by 3D US only. In the case of skeletal abnormalities, it is common experience that the employment of 3D US contributes to reducing the examination time and increases the diagnostic confidence of the sonographer by enhancing the display of normal and abnormal bones. However, in addition to these advantages, there are some pathologic conditions that can be reliably diagnosed only if 3D US is used. These include delayed or abnormal ossification of the cranial sutures, anomalies of rib number or aspect (additional ribs or fusion of the ribs), fusion of vertebral bodies, and hemivertebrae. It is useful to add here that a significant number of facial anomalies (e.g., facial cleftings) are also better characterized and/or displayed by 3D US (Chapter 3).

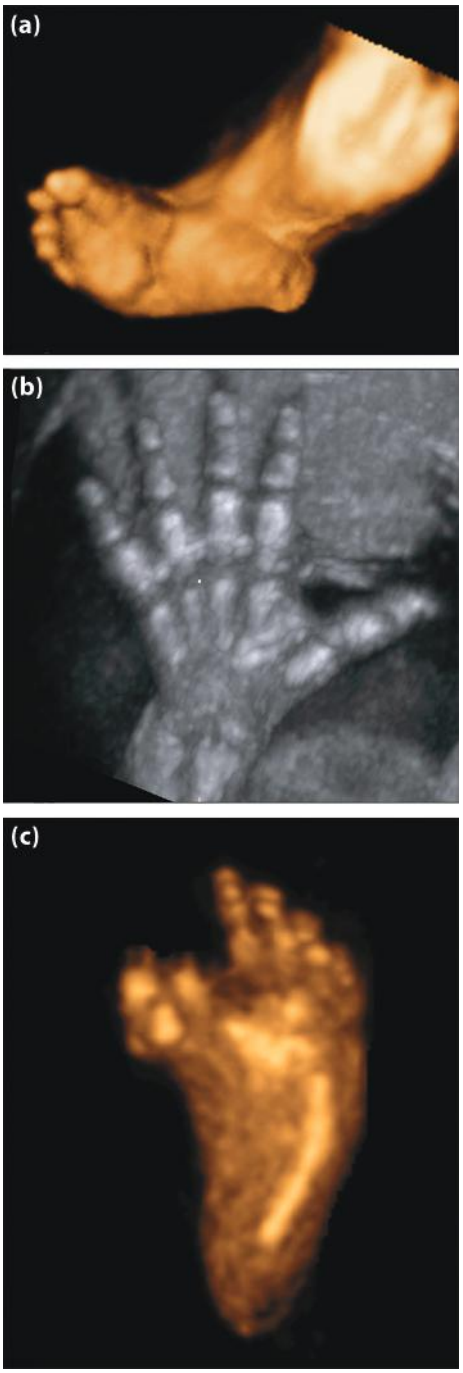


Figure 9.15 Three-dimensional image rendering of the extremities. (a) Surface rendering: clubfoot. This image shows a clubfoot in the early third trimester. Note the abnormal axis of the foot and the normal aspect of the foot and calf muscles. (b) Volume contrast imaging (VCI) plus maximum-mode rendering of a normal hand. This image demonstrates the normal bony structure of the hand at 27 weeks of gestation. Note how this image modality is able to clearly depict the bones of the metacarpus and the digits. (c) Maximum-mode rendering of an abnormal foot. This image demonstrates an abnormality of the bony structure of the toe, which is abducted and larger than normal. In this case, it was an isolated anomaly.

Table 9.7 Ultrasound differential diagnosis of conditions possibly associated with arthrogryposis (joint contractures)

Index sign	→	Arthrogryposis		
Lower limbs +	→	Micrognathia + microphthalmia	→	Cerebro-oculo-facio-skeletal syndrome
Lower limbs +	→	CHD + micrognathia + multiple anomalies	→	Trisomy 18
Upper + lower limbs +	→	Microcephaly + cataract + CNS anomalies[a] + syndactyly	→	Neu–Laxova syndrome
Upper + lower limbs +	→	Micrognathia ± hydrops	→	FADS
Upper + lower limbs +	→	Micrognathia + pterygia + hydrops	→	Multiple pterygium syndrome

[a] Corpus callosum agenesis, cerebellar hypoplasia, lissencephaly.
CHD: congenital heart disease; FADS: fetal akinesia deformation sequence; CNS: central nervous system.

differential diagnosis of joint contractures, neuromuscular diseases, and anomalies of the extremities

Arthrogryposis and joint contractures (**Table 9.7**). Arthrogryposis is a condition characterized by fixed abnormal contractures of all muscles within a given anatomic area. It can be regional, affecting only the lower or upper limbs, or ubiquitous, affecting virtually all muscles, as in the fetal akinesia deformation sequence (FADS; Chapter 10). As already mentioned, if the contractures affect the upper limbs, these will probably appear flexed, lying on the lateral walls of the thorax, and with clenched hands. In contrast, if the contractures involve the thighs, these will often lie extended and crossed, scissor-like, due to the fact that the quadriceps are more powerful than the femoral biceps. Although the neuromuscular transmission block often involves all of the muscles at the same time, in some instances the disease is confined to the lower limbs. In these rarer cases, the knee joints may also appear flexed, abducted, and crossed. It is worth noting that the time of onset of arthrogryposis is extremely variable, between 12 and 30 weeks [9]. Severe joint contractures can be associated with a number of diseases and syndromes (Table 9.7), including both chromosomal (trisomy 18) and nonchromosomal anomalies.

***Ulnar deviation* and *clubfeet* as syndromic indicators** (**Table 9.8**). Both these features may characterize some syndromes and osteomuscular disorders. It is worth noting that in *ulnar deviation*, the wrist is fixed and abnormally rotated toward the ulna; often, clenched hands and clinodactyly are associated because of the concurrent pathologic contraction of the digital flexor muscles of the forearm. In the case of *clubfoot*, the axis of the

Table 9.8 Ultrasound differential diagnosis of conditions possibly associated with clubfoot

Index sign	→	Clubfoot		
Additional signs	→	Neural tube defects + Chiari II	→	Complex spina bifid
Additional signs	→	Bowed tibias and femurs + micrognathia	→	Campomelic dysplasia
Additional signs	→	Focal femoral hypoplasia + micrognathia	→	Femoral hypoplasia–unusual facies syndrome
Additional signs	→	Arthrogryposis + pterygia	→	Multiple pterygium syndrome
Additional signs	→	Arthrogryposis + micrognathia ± hydrops	→	FADS

FADS, fetal akinesia deformation sequence.

Table 9.9 Ultrasound differential diagnosis of conditions characterized by polydactyly (see also Figure 9.16)

Index sign	→	Polydactyly		
Additional signs	→	Micromelia + thoracic hypoplasia + CHD	→	Short-rib polydactyly syndrome(s)
Additional signs	→	CHD + micrognathia + multiple anomalies	→	Trisomy 13
Additional signs	→	Thoracic hypoplasia + renal anomalies	→	Asphyxiating thoracic dystrophy (Jeune syndrome)[a]
Additional signs	→	Polycystic kidney + cephalocele	→	Meckel–Gruber syndrome
Additional signs	→	CHD + acromesomelia	→	Ellis-van Creveld syndrome

[a] Polydactyly is found in only 20% of cases.
CHD: congenital heart disease.

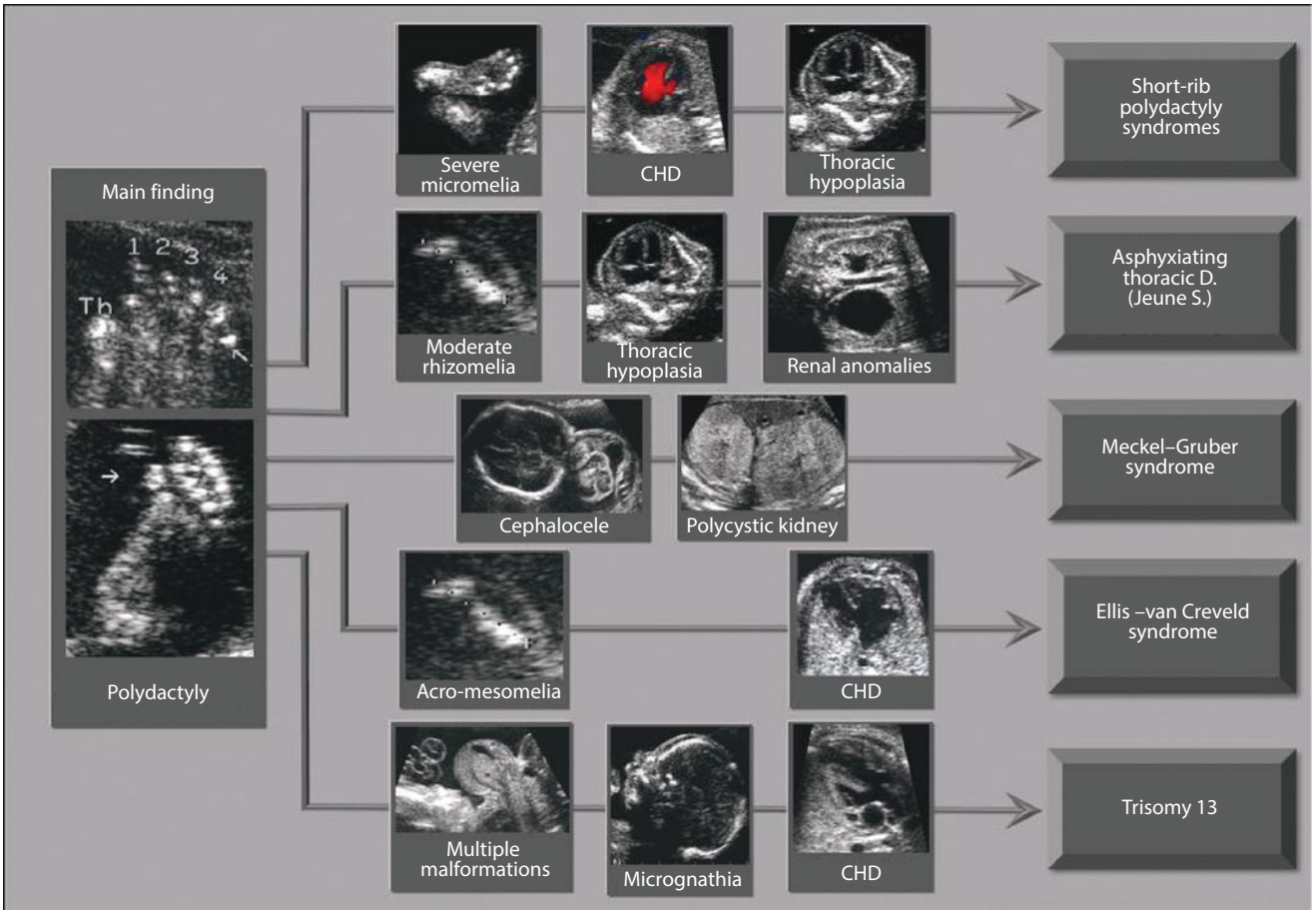


Figure 9.16 Differential diagnosis of skeletal dysplasias featuring ectrodactyly.

foot is no longer that of the lower leg, and therefore, on the sagittal view of the leg, the sole is also visible, with the foot drawn up and bent inward (Figure 9.15a).

***Polydactyly* and *ectrodactyly* as syndromic indicators (Tables 9.9 and 9.10; Figures 9.16 and 9.17).** Both of these conditions are frequently encountered in syndromes. Polydactyly is defined as *postaxial* if the sixth digit, which may or may not present a bony phalanx, is on the ulnar/fibular side, after the fift digit (Figure 9.18a through f). On the contrary, if the additional digit is located on the radial/tibial side, before the thumb/toe, which represents a much rarer finding then it is defined as *preaxial* (Figure 9.18g).

Table 9.10 Ultrasound differential diagnosis of conditions characterized by ectrodactyly (see also Figure 9.17.)

Index sign	→	Ectrodactyly		
Additional signs	→	Phocomelia + cleft lip/palate	→	Roberts syndrome
Additional signs	→	Aplasia radii + micrognathia + multiple anomalies	→	Trisomy 18
Additional signs	→	Cleft lip/palate or malar hypoplasia	→	EEC syndrome[a]
Additional signs	→	Micrognathia + external ear anomalies	→	Nager syndrome
Additional signs	→	None	→	SHFM[a]

[a] Ectrodactyly consists mainly in "lobster claw" anomaly.
EEC: ectrodactyly–ectodermal dysplasia; SHFM: Split Hand & Foot Malformation.

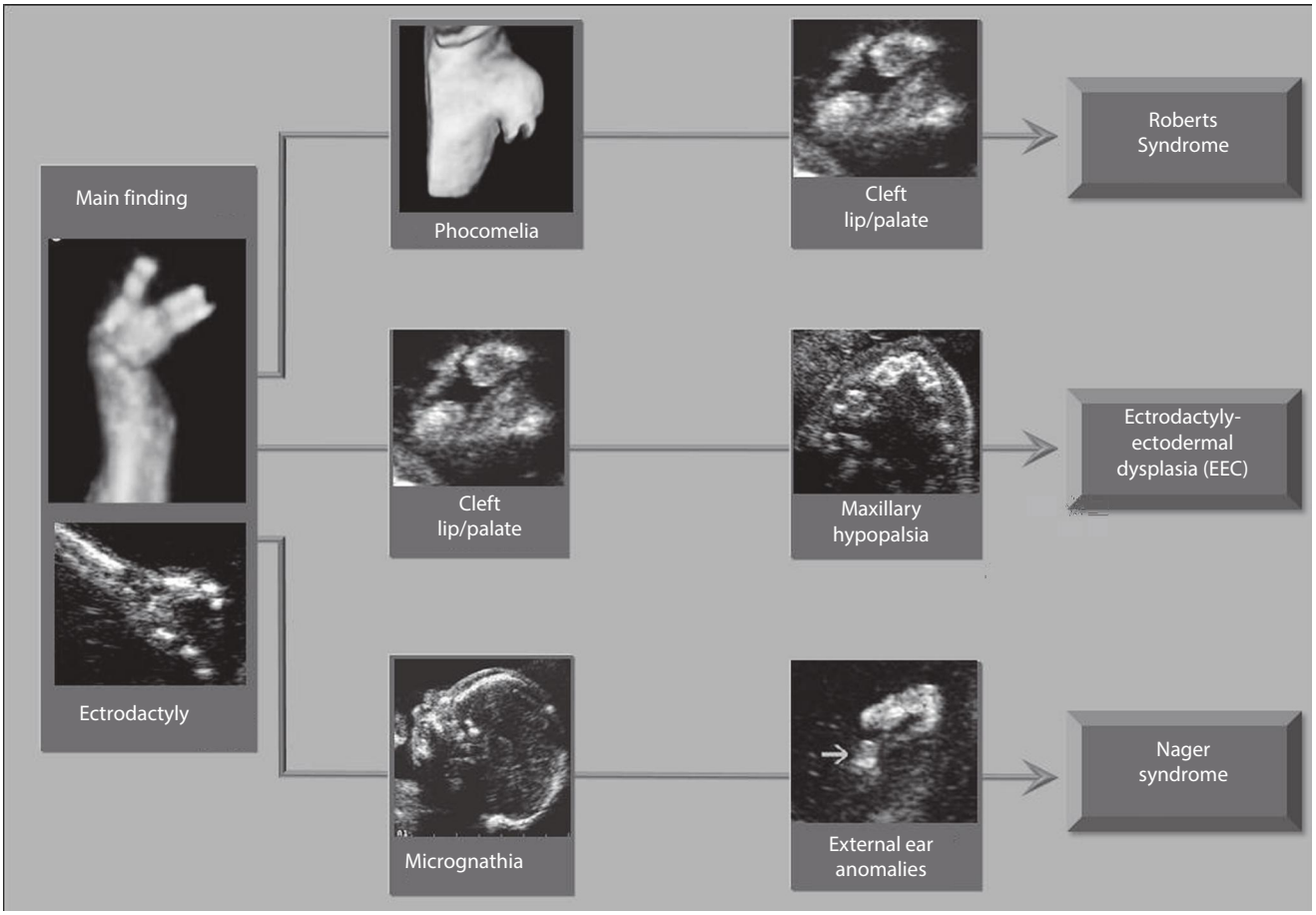


Figure 9.17 Differential diagnosis of skeletal dysplasias featuring polydactyly.

Care must be taken in the US diagnosis of suspected polydactyly. If the hand is insonated with its ulnar side proximal to the transducer, should the additional digit be represented by a soft appendix only passively floating in the amniotic fluid this may be hidden by the metacarpal bones, due to gravity (Figure 9.18d). Hence, to exclude or confirm the presence of hexadactyly, the hand has to be imaged either with the digits upward or with its radial aspect proximal to the transducer: in these positions, soft appendices would also easily be spotted on the ulnar margin of the hand.

Ectrodactyly is the absence of one or more digits, although the term is used almost synonymously with thumb aplasia, since this is the variant most commonly seen in the fetus. However, it should be emphasized that the absence of more than one digit

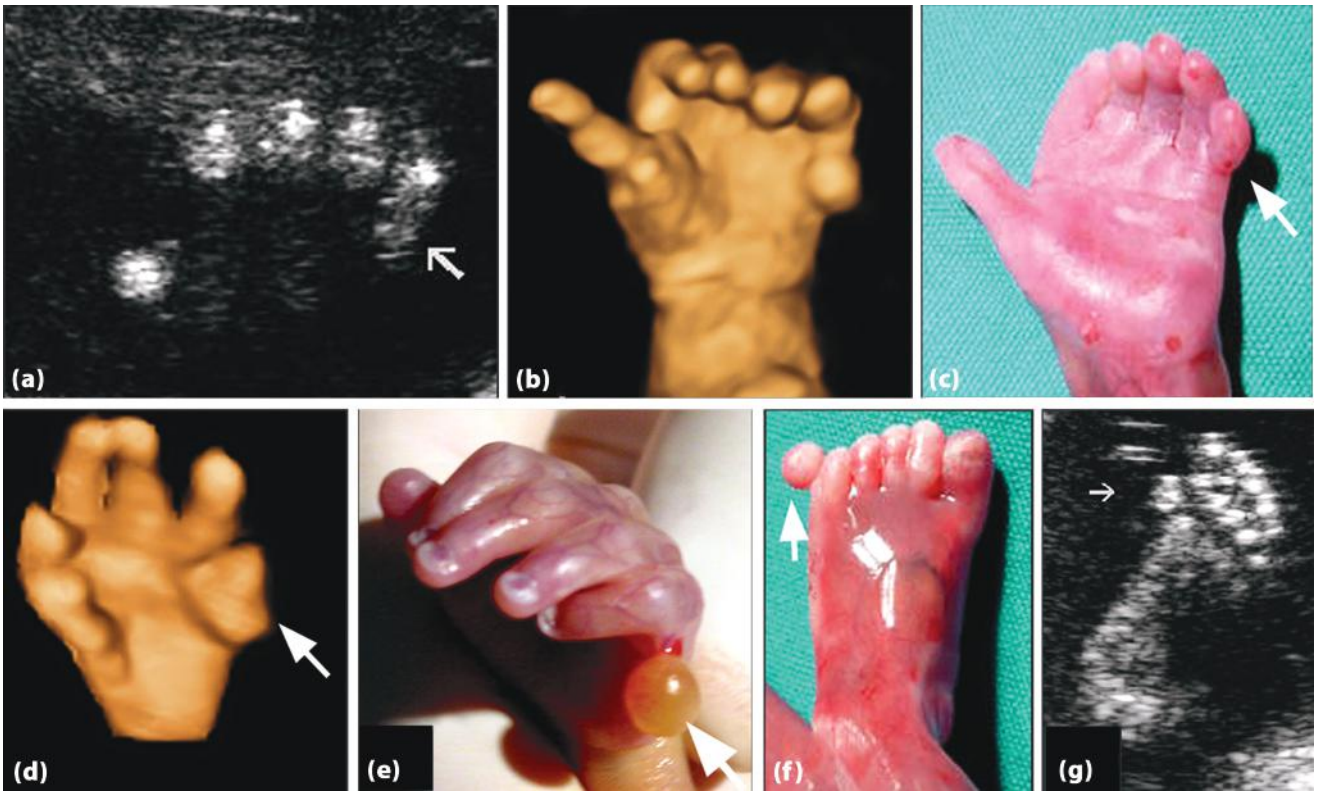


Figure 9.18 Polydactyly. (a) Postaxial polydactyly of the hand (arrow) at 20 weeks of gestation: two-dimensional imaging. (b) Three-dimensional imaging. (c) Confirmation at autopsy. (d) Postaxial polydactyly of the hand, consisting of an edematous appendix (arrow): 3D surface-rendering at 22 weeks of gestation. (e) Confirmation at autopsy. (f) postaxial polydactyly of the foot (arrow) at 21 weeks of gestation: autopsy. (g) A rare case of preaxial polydactyly of the foot, in a family with dominant inherited polydactyly (arrow).

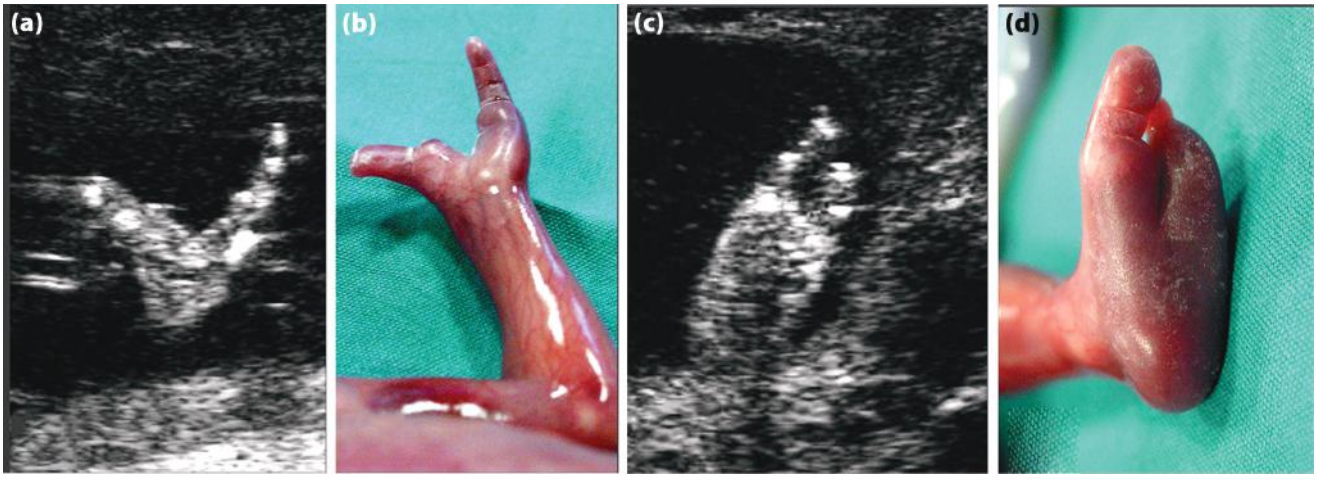


Figure 9.19 Ectrodactyly, in split hand & foot malformation (SHFM)—lobster claw anomaly. (a) On ultrasound, the hand consists of only two digits. (b) Confirmation at autopsy. (c) The foot also consists of only the toe and another large digit. (d) Confirmation at autopsy.

or the fusion of any (syndactyly) into two gross digits (lobster-claw anomaly) are highly indicative of very rare conditions such as Nager syndrome or ectrodactyly–ectodermal dysplasia (EEC) and split hand & foot malformation (SHFM), respectively (Figure 9.19).

Major skeletal dysplasias

Premises. Skeletal dysplasias include a group of diseases sharing an extremely low risk of chromosomal abnormalities and a reduced risk of associated malformations. The required obstetric management is rather limited, owing to the fact that most of the skeletal dysplasias diagnosed in the fetus are lethal, and, if diagnosed within the legal time limit for termination of pregnancy (where this is allowed), most will result in termination. Furthermore, karyotyping should be performed only in the few cases in which a differential diagnosis with aneuploidies to be carried out, as in the case of diffuse joint contractures, which may be associated with trisomies 18 and 13 and the neuroarthrogryposes (Table 9.7). Perinatal management is also rather limited, due to the fact that the nonlethal forms will need some respiratory assistance and physio-kinesiotherapy in the long-term. This is why, in this section of the chapter, the discussion of the individual dysplasias will deal only with US diagnosis, differential diagnosis, and a few notes on survival and quality of life for nonlethal conditions. It should also be noted that "Incidence" in the summarizing box at the start of each section refers not to the overall frequency of the given dysplasia, but rather to its frequency within the group of skeletal dysplasias as a whole: in fact, the overall incidence of these anomalies is rather low. In keeping with the practical approach of this book, only the most commonly detected skeletal dysplasias will be described in this chapter: in our opinion, it would be confusing for the reader to be confronted with 200 or more different diseases, over 100 of which will probably never be detected in the fetus. The reader in search of further details on skeletal dysplasias not described in this chapter (as well as any other congenital syndromic condition) may refer to the various Medline websites (www.ncbi.nlm.nih.gov), including the OMIM (Online Mendelian Inheritance in Man) database. This chapter has also been structured in such a way as to overcome the difficulties that may be encountered by operators in the differential diagnosis of skeletal dysplasias: these are listed in alphabetical order, to facilitate their retrieval, and several flowcharts supporting the differential diagnosis by the main US signs, have already been presented. Finally, it should be noted that polyhydramnios is an almost ubiquitous finding in skeletal dysplasias and neuroarthrogryposes.

Achondrogenesis (OMIM 200600, 200610)

Incidence. Rare.

Ultrasound diagnosis. Severe micromelia, with barely visible and curved bones; severe thoracic hypoplasia; diffuse hypomineralization of variable degree.

Outcome. Lethal.

Inheritance pattern and recurrence risk. Autosomal recessive (25%). *De novo* mutations with autosomal dominant inheritance.

Definition There are various subtypes of achondrogenesis that differ in inheritance pattern, genetics, and phenotype; however, the classification is continuously evolving and is not completely clear. Two main subtypes have been recognized, differing in inheritance pattern (autosomal recessive for type I and autosomal dominant for type II) and in a few sonographic aspects (see below). In type I (OMIM 200600), or Parenti-Fraccaro type, the ribs tend to be thin, often with multiple fractures, and the cranium is disproportionately large due to marked edema of soft tissues; in fact, hydrops is frequently associated. Type II (hypochondrogenesis; OMIM 200610) or Langer-Saldino type, is characterized by virtual absence of ossification in the vertebral column, sacrum, and pubic bones.

Etiology and pathogenesis. A mutation in the *COL2A1* gene coding for collagen type II has been found in some cases of type II.

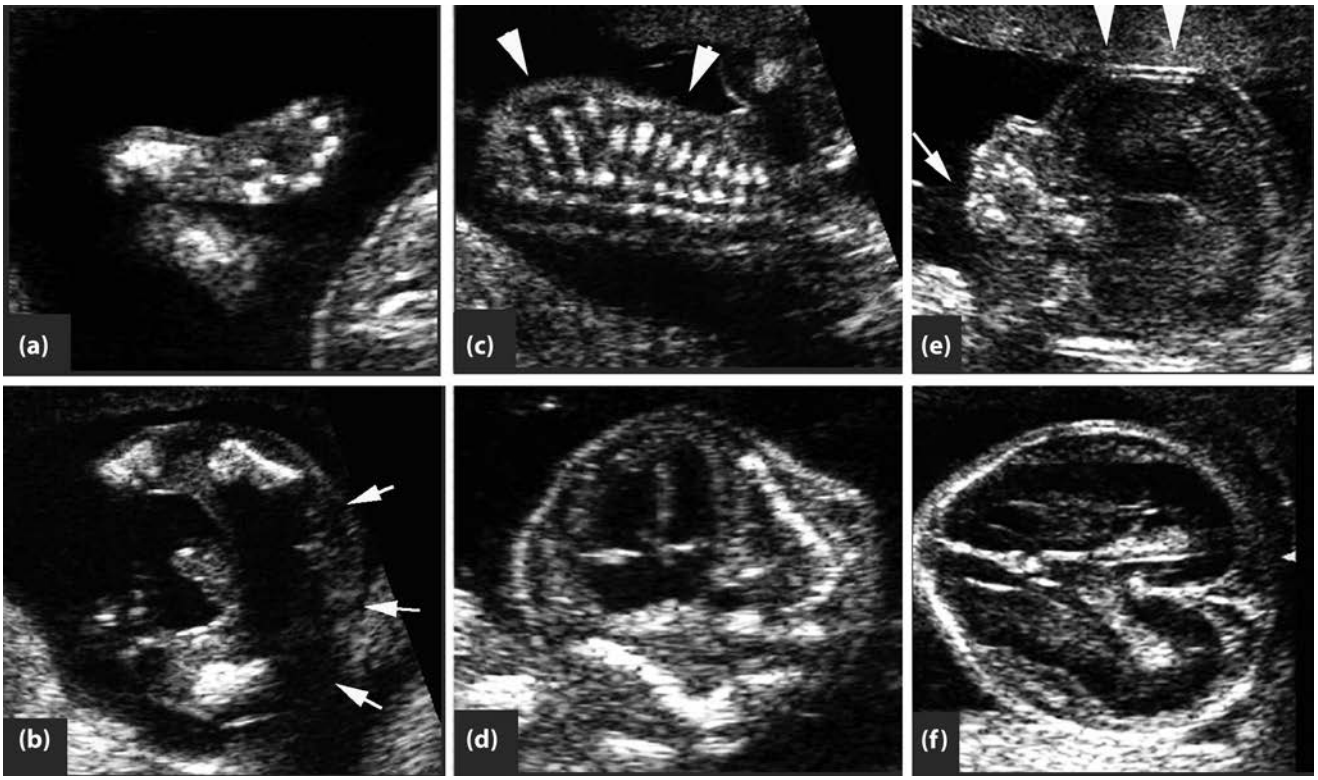


Figure 9.20 Achondrogenesis (16 weeks of gestation). (a) Micromelia. (b) Severe micromelia and hypomineralization of the sacrum (arrows). (c) Severe rib shortening (arrowheads). (d) Severe, lethal, thoracic hypoplasia. Note the heart occupying the whole of the thorax. (e) Calvarial hypomineralization. Note how the calvarium can be deformed by a moderate pressure applied with the transducer (arrowheads). Note also the significant micrognathia (arrow). (f) With a lateral approach, the usual skull hyperechoic contour is not visible and the brain shows up in detail. This is due to the severe hypomineralization of the skull.

Ultrasound diagnosis. The US diagnosis is based on the recognition of micromelia (Figure 9.20a and b), thoracic hypoplasia (Figure 9.20c and d), hypomineralization (Figure 9.20e and f), and micrognathia (Figure 9.20e). In particular, the long bones appear curved and barely visible and the thorax extremely hypoplastic due to the underdeveloped ribs. The hypomineralization predominantly involves the spine, pelvis, and calvarium. Micrognathia may be associated. If the condition is recognized at 12–14 weeks of gestation, which is likely, hydrops and diffuse subcutaneous edema ("spaceman's suit") may also be seen.

Differential diagnosis. This includes all lethal conditions characterized by micromelia plus thoracic hypoplasia plus hypomineralization (Figures 9.8, 9.9, and 9.11), such as the lethal variant of OI (type II), hypophosphatasia, and thanatophoric dysplasia. The constant occurrence of fractures in OI type II, the different pattern of hypomineralization in hypophosphatasia, and the only mild hypomineralization in thanatophoric dysplasia, which often also shows curved femurs, are the selective US findings that should contribute to reaching the correct final diagnosis

Prognosis, survival, and quality of life. Achondrogenesis is always lethal, due to the severity of the skeletal underdevelopment. The severe pulmonary hypoplasia secondary to the ribcage hypoplasia is likely to represent the actual determinant of death, should fetuses with achondrogenesis reach the neonatal period.

Recurrence risk. Achondrogenesis can behave in an autosomal dominant or recessive manner. However, autosomal dominant forms are by definition due to *de novo* mutations, because of the lethality of the condition. Therefore, only the 25% risk associated with the recessive inheritance pattern should be considered. The real issue is that it is not always possible to define exactly the type of inheritance.

Achondroplasia (OMIM 100800)

Incidence. Relatively frequent: 1/10,000 live births.

Ultrasound diagnosis. Rhizomelia, mild late-onset macrocrania, and low nasal bridge.

Outcome. Normal lifespan. No risk of mental retardation. Orthopedic and pulmonary long-term sequelae due to the relatively small thorax.

Inheritance pattern and recurrence risk. Heterozygotic: due to a *de novo* mutation, with very low recurrence risk. Autosomal dominant inheritance with high recurrence risk if one or both parents are affected (50% and 75% recurrence rates respectively).

Definition There are two types of achondroplasia (OMIM 100800) defined according to their inheritance pattern: homozygotic or heterozygotic. The former type, which is almost invariably lethal (severe pulmonary hypoplasia), is by far the rarer variant, due to the fact that it occurs *only if both parents are affected*. The heterozygotic variant is the commoner one and is the one that is usually detected at birth and, in some cases, in utero, but only in the third trimester. The incidence at birth is relatively high, considering the extremely low prevalence of other skeletal dysplasias, with 1 case per 10,000 live births.

Etiology and pathogenesis. The gene defect responsible for the disease has been identified in a *de novo* mutation of the gene for the fibroblast growth factor receptor (*FGFR3*), at chromosome 4p16.3. Ninety-seven percent of achondroplastic individuals show the same mutation, namely a guanine-to-adenine transition at nucleotide 1138 of the complementary DNA. This mutation prevents binding of FGF to its receptor, which, in turn, impairs bone growth.

Ultrasound diagnosis. The US diagnosis is difficult because the rhizomelia is of late-onset, becoming evident only at 26–28 weeks of gestation. The femur and humerus are slightly to moderately shorter than normal, showing biometry in the first to fifth percentile range; in addition, the shape of the long bones is normal, which makes the diagnosis even more difficult. In some cases, the involvement of the humerus is more severe than that of the femur. Additional criteria that, if present, may support the US diagnosis of achondroplasia are a tendency to macrocrania and a low nasal bridge. However, both of these features are difficult to diagnose (Figure 9.21a and b). To overcome this inconvenience, some authors have proposed the use of the HC/FL (head circumference/femur length) or BPD/FL (biparietal diameter/femur length) ratios, which should become abnormal earlier than the measurement of the single parameters, due to the fact that the biometric parameters nominator and denominator should deviate in opposite directions, that is, toward or above the 95th percentile for the cranial biometric variables, or toward or below the 5th percentile for the femur length (see Appendix Table A.4). In addition, a "trident" position of the hands (Figure 9.21c) has been described among the possible US features of achondroplasia. As is evident, most of the aforementioned US features, with the exception of moderate rhizomelia, are very difficult to spot and confirm These diagnostic difficulties together with the late onset of most sonographically detectable signs, are responsible for the very low prenatal detection rate of achondroplasia. To reach a definite diagnosis of achondroplasia, should short or borderline femur length and a tendency to macrocrania be detected in the second trimester, a search for the gene mutation responsible for most cases of

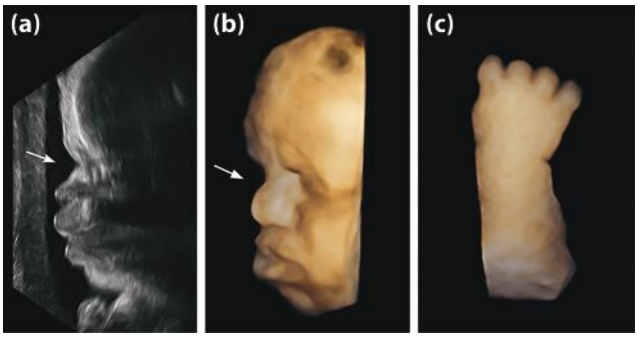


Figure 9.21 Achondroplasia (32 weeks of gestation). (a) Midsagittal two-dimensional ultrasound view of the fetal profile, showing macrocrania and the low nasal bridge (arrow). (b) Three-dimensional surface-rendering showing the same features as above; (c) three-dimensional surface-rendering showing the so-called "trident hand," which is another typical feature of achondroplasia. This is due to the fact that the skin is redundant in comparison with the short phalanges, leading the hand to have this curved appearance.

achondroplasia in fetal blood or amniocytes can be requested, although, in most cases of short femur this procedure will result only in the exclusion of achondroplasia as a likely cause of the femur growth deficit However, in pregnancies at risk for achondroplasia, such as those in which one of the parents is affected, this search may be done on the chorionic villi, so that the diagnosis of achondroplasia can be confirme or excluded at the end of the first trimester, and this possibility should be mentioned to couples with one affected individual.

Differential diagnosis. The differential diagnosis should include the other conditions possibly characterized by a borderline or short femur. The first and the easiest to rule out is trisomy 21: a simple karyotype can serve this purpose. In addition, the same cells may be used to extract the DNA needed for the diagnosis of achondroplasia. The other most important condition to rule out is early-onset atypical fetal growth restriction (FGR), the onset of which may rarely be characterized by selective underdevelopment of the long bones. The other skeletal dysplasias that may enter into the differential diagnosis, due to the presence of moderate rhizomelia (at least in the second trimester), are campomelic dysplasia, which is often characterized by micrognathia, and, always by bowed bones; chondroectodermal dysplasia (*Ellis-van Creveld syndrome*), which is associated with significant thoracic hypoplasia, polydactyly, and congenital heart disease (50% of cases); and the nonlethal variants of OI (types I, III, and IV), which may feature late-onset fractures and bowing of long bones.

Note. When assessing fetal growth and biometry one should use nomograms customized at least for the ethnic origin of the studied population: the charts for head, abdomen, and long-bone biometry usually available in most US systems are those developed many years ago by American or British authors [10–13]. If these curves are used to assess the biometry of fetuses of Asian couples, or, to a lesser extent, those of Latin origin, the number of cases featuring long-bone biometry below the fifth percentile would be higher than expected, due to the significant differences in height of the two populations. Care should be taken to use biometric charts developed from fetal populations of the same ethnic origin, or, if these are not available, from the most closely similar populations, to limit false-positive diagnoses of short femur [14].

Prognosis, survival, and quality of life. The life expectancy is virtually normal, as is the quality of life. The only difficulties that most achondroplastic individuals may encounter are related to architectural barriers, because of their short stature, and to respiratory limitations related to the small thorax. The only other significant problem concerns the stenotic vertebral canal, which is responsible in some cases for peripheral neurologic deficits Homozygous achondroplasia is lethal by definition and can only be determined if both parents are achondroplastic.

Recurrence risk. Heterozygous achondroplasia may be due to a *de novo* mutation or, much more rarely, to transmission from one of the parents. In the former case, the recurrence risk is definitely low. On the contrary, the recurrence risk reaches 50% if one parent is affected and is as high as 75% if both parents are affected, as this disorder is inherited as a dominant trait.

Asphyx IATING Thor Ac Ic dys Trophy (A Td, jEUNE sy Ndro ME—oMIM 208500, 611263)

Incidence. Rare. Two types are now described.

Ultrasound diagnosis. Thoracic hypoplasia; moderate rhizomelia to micromelia; renal anomalies; rarely, polydactyly of hands and/or feet.

Outcome. Lethal in 60% of cases, due to pulmonary hypoplasia.

Inheritance pattern and recurrence risk. Autosomal recessive; 25% recurrence risk.

Definition The name underlines the main feature of the disorder, namely the extremely small thorax, leading often to early neonatal death from lethal secondary pulmonary hypoplasia. Limb shortening of variable degree is also associated, while renal anomalies and polydactyly are inconstant features. The real incidence of the disease is not known, although it is a rare disorder.

Table 9.11 Asphyxiating thoracic dystrophy

Sign	Incidence (%)
Thoracic hypoplasia	95
Limb shortening/rhizomelia	88
Short stature	73
Renal abnormalities	29
Post–axial polydactyly: hands *or* feet (bilateral or unilateral)	14
Post–axial polydactyly: hands *and* feet (bilateral)	7

Source: Modified from Keppler-Noreuil KM et al., Incidence of the various findings in a review of 126 postnatal cases. *Am J Med Genet Part A* 155A, 1021–32, 2011.

Etiology and pathogenesis. Currently, two types are described: ATD1 (OMIM 208500) and ATD2 (OMIM 611263), corresponding to mutations on chromosome 15q13 and 3q.25.33.

Ultrasound diagnosis (Figure 9.22). The main US finding that leads to the diagnosis is the extremely severe thoracic hypoplasia (Figure 9.22a, c, and d). However, the US diagnosis of ATD may be challenging, because only severe thoracic hypoplasia is always present, while any of the other described signs may be missing, especially in the fetus (Table 9.11) [15]. The additional findings, such as moderate rhizomelia and renal anomalies, are not always easy to recognize on US (Figure 9.22b). It should be noted that this condition may escape prenatal diagnosis, especially in nonlethal cases; in fact, the long bones may be only moderately affected (moderate rhizomelia) and the thoracic hypoplasia is not always severe.

Differential diagnosis. This should take into consideration chondroectodermal dysplasia *(Ellis-van Creveld syndrome)*, because of the mild-to-moderate degree of limb shortening. However, chondroectodermal dysplasia is also characterized by frequent cardiac defects (although these are often represented by simple atrial septal defects) and by polydactyly (mainly of the hands), which is absent in Jeune syndrome. In addition, the degree of thoracic hypoplasia is higher in the latter disorder than in chondroectodermal dysplasia. To a lesser extent, the differential diagnosis may include the other skeletal dysplasias with severe thoracic dysplasia, such as achondrogenesis, thanatophoric dysplasia, hypophosphatasia, and OI type II. However, all of these disorders are also characterized by severe micromelia, which is absent in asphyxiating thoracic dystrophy.

Prognosis, survival, and quality of life. The neonatal mortality rate is 60%, with the cause of death being severe secondary pulmonary hypoplasia. Surviving neonates will have short stature, renal and (above all)

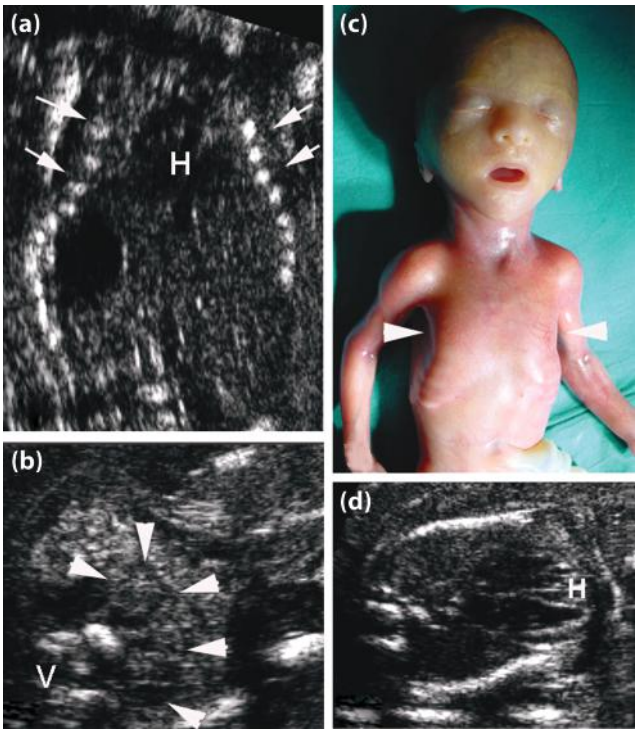


Figure 9.22 Asphyxiating thoracic dystrophy (Jeune syndrome) (20 weeks of gestation). (a) Coronal view of the thorax, showing severe thoracic hypoplasia (arrows), with the heart (H) squeezed into the center of the thorax. (b) Axial view of the abdomen, showing the horseshoe kidney (arrowheads). (c) Confirmation at autopsy. Note the severe thoracic hypoplasia (arrowheads). (d) Axial view of the thorax, confirming severe hypoplasia: the heart is almost outside the ribcage due to the extremely reduced dimensions of the thorax.

cardiovascular problems, always related to the degree of thoracic hypoplasia. Intelligence is normal.

Recurrence risk. Asphyxiating thoracic dystrophy has an autosomal recessive inheritance pattern, with a 25% recurrence rate. Therefore, in the case of termination of pregnancy, a confirmation of the US diagnosis by autopsy is of the utmost importance for correct counseling and for advising early US monitoring of the next pregnancy in referral centers.

cAMpo MELIc dysp LAsIA (oMIM 114290)

Incidence. Very rare: 0.02/10,000 live births.

Ultrasound diagnosis. Bowed tibias and, to a lesser extent, femurs; scapular hypoplasia; micrognathia; sex reversal in male fetuses.

Outcome. Lethal in most cases; rare cases of long-term survival.

Inheritance pattern and recurrence risk. Almost always due to a *de novo* mutation, with very low recurrence risk. In the rare autosomal recessive inheritance pattern, the recurrence rate is 25%.

Definition The term "campomelic" (from the ancient Greek *camptos* = *bowed*) refers to the abnormal curvature of the long bones, which is the most peculiar anomaly in this disease. The incidence of campomelic dysplasia (OMIM 114290) is low, with only 0.02 cases per 10,000 live births.

Etiology and pathogenesis. The mutation responsible for the disease, which always occurs as a *de novo* mutation, has been identified in the *SOX9* allele, which codes for the SRY-box 9 protein, expressed in the testes and the fetal skeleton. The distribution of this protein within the body explains both the bone abnormalities and the sex reversal (see below), which is typical of affected males.

Ultrasound diagnosis (Figures 9.23 and 9.24). The US diagnosis can sometimes be rather difficult because of the extreme phenotypic variability of the syndrome. The US features indicative of campomelic dysplasia are bowing of variable degree of the tibias, femurs, and humeri (Figures 9.23 and 9.24a,d), micrognathia (Figure 9.24c), which is moderate in the fetus, sex reversal in male fetuses, and scapular hypoplasia (which is difficult to detect in utero). In particular, bowing involves the tibia and, to a lesser extent, the femur; the fibula can be hypoplastic, or sometimes completely absent. Also, the humerus and the ulna may be bowed, but in a significantly smaller number of cases. Besides, it should be noted that the long bones are bowed in the sagittal plane: therefore, if the bone shaft is visualized with a lateral approach, severe bowing may not show up. Talipes and usually moderate micrognathia may be associated, while congenital heart disease is found in only one third of cases. Care should be taken in diagnosing sex reversal in male fetuses, because this may consist of a bifi scrotum with a micropenis only, or may feature real ambiguous or female-like genitalia.

Differential diagnosis. This involves mainly the nonlethal forms of OI (types I, III, and IV). In fact, in the small number of cases of nonlethal OI variants that are diagnosed in utero, the most common abnormal finding is late-onset bowing of long bones; and this is similar to what occurs in campomelic dysplasia. The detection of calvarium hypomineralization (in the OI variants) may help in the differential diagnosis; however, this is an all but inconstant finding and, in the nonlethal variants, of extremely variable degree as well. Much more rarely, campomelic dysplasia should be differentiated from incomplete variants of hypophosphatasia.

Prognosis, survival, and quality of life. Campomelic dysplasia is almost always lethal, because of the severity of the ubiquitous laryngotracheomalacia. In very rare instances, survival until adolescence has been reported, but mild-to-moderate developmental delay is present in the majority of these cases.

Recurrence risk. Because it is almost always due to a *de novo* mutation, the recurrence risk is insignificant except for the very rare cases in which an autosomal recessive inheritance pattern has been found, with a consequent 25% recurrence risk.

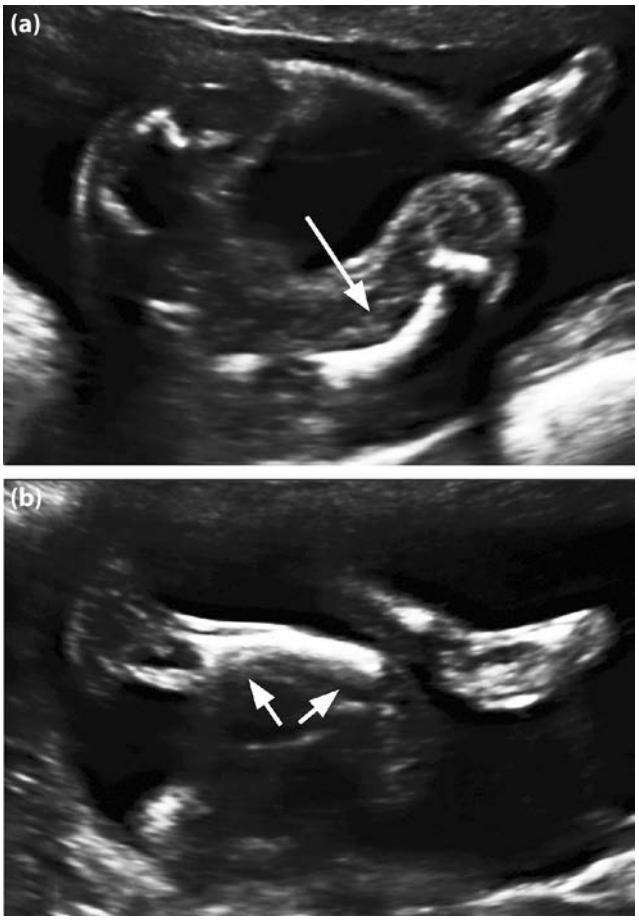


Figure 9.23 Campomelic dysplasia (22 weeks of gestation). Two-dimensional imaging (a) significantly bowed and short femur; (b) mildly bowed tibia.

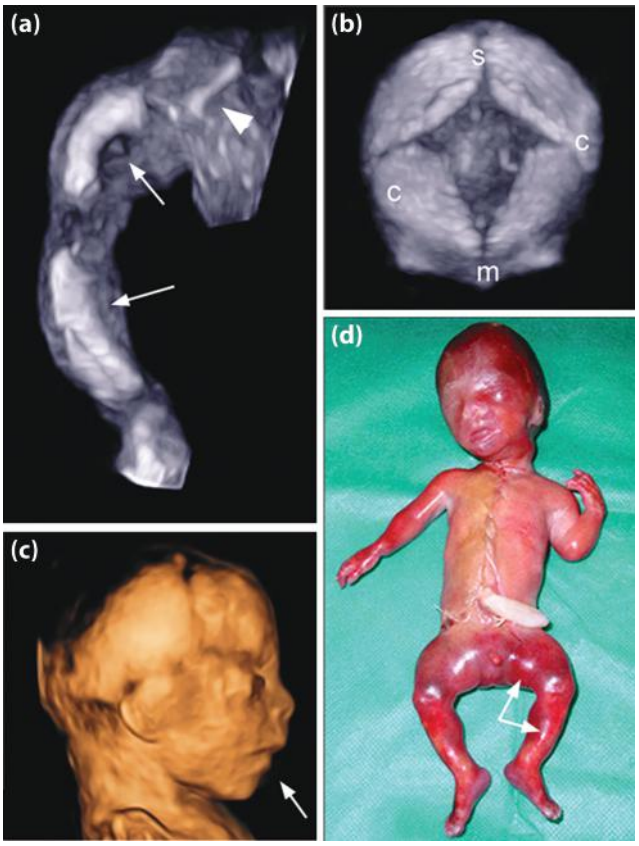


Figure 9.24 Campomelic dysplasia (22 weeks of gestation). (a) Three-dimensional maximum-mode rendering of the lower limb demonstrates evident bowing of femur and tibia (arrows). In addition, the smaller than normal iliac wing is shown; this represents an additional sign of campomelic dysplasia; (b) three-dimensional maximum mode rendering of the calvarium demonstrates a large anterior fontanelle (c: coronal suture; m: metopic suture; s: sagittal suture); (c) three-dimensional surface-rendering of the fetal profile demonstrates moderate micrognathia; (d) autoptic confirmation (arrows: bowed femur and tibia).

dIAsTroph Ic dysp LAsIA (oMIM 222600)

Incidence. Extremely rare.

Ultrasound diagnosis. "Hitch-hiker's thumb," joint contractures, micrognathia.

Outcome. Lethal in 25% of cases. In survivors, severe muscular and postural disability due to the joint contractures and the kyphoscoliosis with spinal cord compression.

Inheritance pattern and recurrence risk. Autosomal recessive: 25% recurrence risk.

Definition This extremely rare skeletal dysplasia is defined as "diastrophic" in relation to its main features: postural abnormalities and joint contractures.

Etiology and pathogenesis. The underlying genetic defect consists of a mutation in the *DTDST* gene, located on chromosome 5q32–33.1.



Figure 9.25 Diastrophic dysplasia. The left image shows the classic "hitchhiker's thumb" (arrowhead) typical of this disorder, which is due to contracture of the extensor of the thumb and the flexors of the other digits. The right image shows a less typical case on three-dimensional surface-rendering: the thumb is extended, but the other digits show only partial flexion contracture.

Ultrasound diagnosis. The key diagnostic finding on US, in addition to ubiquitous joint contractures, is the so-called "hitch-hiker's thumb," in which the first digit is fixed in extreme abduction because of the contractures of the extensor muscles, while the hand shows ulnar deviation and the other digits are clenched. (Note: the other digits are not *always* clenched.) (Figure 9.25) Other signs detectable on US are severe rhizomelia, flexion contractures of the elbows, talipes equinovarus, and micrognathia.

Differential diagnosis. This involves mainly the neuroarthrogryposes, in which the bone length is not affected.

Prognosis, survival, and quality of life. Diastrophic dysplasia is associated with a 25% infant mortality rate, mainly related to severe respiratory obstruction. Survivors experience significant limitations in physical activity due to the severe kyphoscoliosis and the joint contractures. Kyphoscoliosis may also be responsible for symptomatic spinal cord compression.

Recurrence risk. This disorder shows an autosomal recessive inheritance pattern with variable expression. This yields a 25% recurrence rate. Therefore, in the case of termination of pregnancy, confirmation of the US diagnosis by autopsy is of the utmost importance for correct counseling and for advising early US monitoring of the next pregnancy in referral centers.

ELLIs-VAN cr EVELd syNdro ME (EVc; oMIM: 225500)

Incidence. Very rare: 1/60,000 live births.

Ultrasound diagnosis. Acromesomelia and moderately severe thoracic hypoplasia. Postaxial polydactyly of hands and, rarely, of feet. Congenital heart disease (atrial septal defect).

Outcome. Lethal in 50% of cases.

Inheritance pattern and recurrence risk. Autosomal recessive: 25% recurrence risk.

Definition Currently, this skeletal condition is called Ellis-van Creveld (EVC) syndrome (OMIM 225500). It is a rare autosomal recessive condition (1/60,000 live births) with variable phenotypic expression characterized by short limbs, short ribs, postaxial polydactyly and dysplastic nails and teeth. Congenital heart disease, consisting mainly in a common atrium, occurs in 60% of cases. The former names of "six-fingered dwarfism" and chondroectodermal dysplasia are no longer in use, according to more recent recommendations.

Etiology and pathogenesis. Two mutations in two adjacent genes (EVC and EVC2) on chromosome 4p16 have been found; note that this is the same allele involved in achondroplasia.

Ultrasound diagnosis. The signs of the ectodermal dysplasia (nail dysplasia, hypodontia, and delayed eruption) are not recognizable by US. US diagnosis of EVC is based on detection of the following signs: mild-to-moderate acromesomelia; moderately severe thoracic hypoplasia

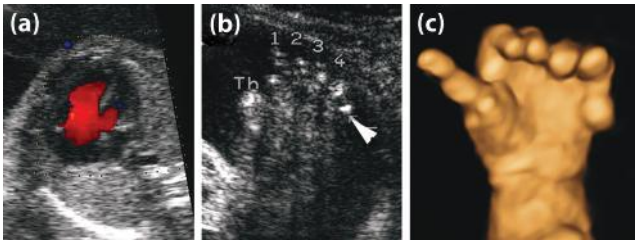


Figure 9.26 Ellis-van Creveld (EVC) syndrome (20 weeks of gestation). (a) Moderate thoracic hypoplasia and atrioventricular septal defect. (b) Two-dimensional coronal view of the hand showing postaxial polydactyly (arrowhead); (c) three-dimensional image of another case detected at 30 weeks, showing also postaxial polydactyly.

with short ribs (Figures 9.26a and 9.27a); postaxial polydactyly, which involves the hands in virtually 100% of cases and the feet in a significantly lower percentage of cases (10%–25%) (Figures 9.26 b,c and 9.27b,c); and congenital heart disease, although the heart defect most frequently associated with EVC, namely atrial septal defect, is difficult to diagnose in the fetus because of the patency of the foramen ovale (Figure 9.26a).

Differential diagnosis. This includes mainly asphyxiating thoracic dystrophy (Jeune syndrome) and the group of short-rib polydactyly syndromes (SRPS). In particular, EVC is characterized by thoracic hypoplasia of variable degree and polydactyly, whereas, in asphyxiating thoracic dystrophy, the degree of thoracic hypoplasia is significantly more pronounced and polydactyly is rare. Also, SRPS present more severe thoracic hypoplasia and, above all, micromelia, which is absent in asphyxiating thoracic dystrophy.

Prognosis, survival, and quality of life. EVC shows a 50% infant mortality rate, which is related to the severity of the thoracic hypoplasia and the consequent severe cardiopulmonary problems. Survivors have normal intelligence but short stature. The need to correct the atrial septal defect does not affect survival or quality of life, if the respiratory problems related to the thoracic hypoplasia have been overcome. The signs of the ectodermal dysplasia are easier to approach, although dentition defects often require orthodontic procedures.

Recurrence risk. The disease is inherited with an autosomal recessive pattern, which means that there is a 25% risk of recurrence after a pregnancy with an affected fetus/neonate. Therefore, in the case of termination of pregnancy, a confirmation of the US diagnosis by autopsy is of the utmost importance for correct counseling and for advising early US monitoring of the next pregnancy in referral centers.



Figure 9.27 Ellis-van Creveld (EVC) syndrome: specimen after termination of pregnancy. (a) Moderate thoracic hypoplasia (arrowheads). (b) Postaxial polydactyly of feet (arrowhead). (c) Postaxial polydactyly of hands (arrowhead).

hypophosphatasia (OMIM 241500)

Incidence. Extremely rare.

Ultrasound diagnosis. Micromelia, thoracic hypoplasia, severe hypomineralization (clavicles spared); hydrops and subcutaneous edema if detected at 12–14 weeks.

Outcome. The forms detectable in utero are always lethal.

Inheritance pattern and recurrence risk. Autosomal recessive: 25% recurrence risk.

Definition This disorder is characterized by a defect in serum and tissue alkaline phosphatase. Only the most severe, lethal form (of the three recognized) can be detected in the fetus (OMIM 241500).

Etiology and pathogenesis. The basic defect concerns the tissue nonspecific alkaline phosphatase (*TNSALP*) gene, which maps to chromosome 1p36.1–p34. Different mutations within the same locus have been described.

The degree of malfunction of the bone isoform correlates with the severity of the phenotypic expression. The severity ranges from clinically unapparent cases diagnosed only on the basis of biochemical features to lethal cases detected in the fetus, the latter showing an autosomal recessive inheritance pattern.

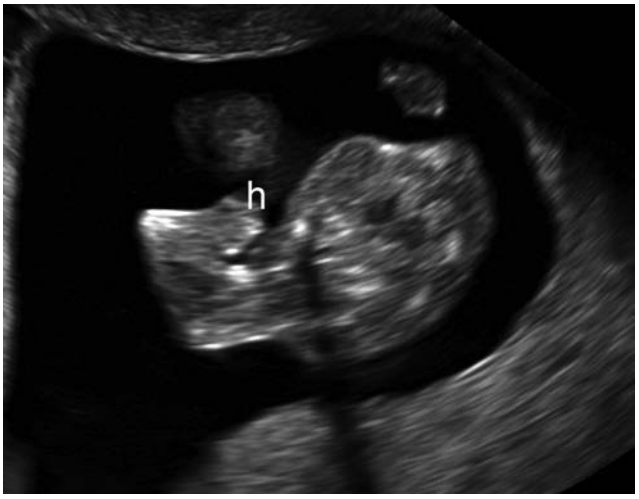


Figure 9.28 Hypophosphatasia (14 weeks of gestation). The transvaginal scan (12 MHz transducer) shows severe micromelia and hypomineralization of the upper limb. Neither the humerus nor the ulna/radius is visible in the rhizomelic and mesomelic segments of the arm, due to severe hypomineralization (h: hand).

Ultrasound diagnosis. This is based on the detection of severe micromelia (Figure 9.28), severe thoracic hypoplasia, diffuse hypomineralization involving virtually all of the bones with the exception of the clavicles (Figure 9.29), and hydrops and subcutaneous edema ("spacesuit") in the case of early (12–14 weeks) detection.

Differential diagnosis. Hypophosphatasia should be differentiated from the other lethal skeletal dysplasias presenting with micromelia and thoracic hypoplasia, namely achondrogenesis, thanatophoric dysplasia, and OI type II. It should be noted that in some cases a final diagnosis cannot be reached on the basis of the US findings In general, hypomineralization with clavicle sparing is typical of hypophosphatasia. Micrognathia, which is present in achondrogenesis, is absent in hypophosphatasia, while fractures are characteristic of OI type II.

Prognosis, survival, and quality of life. The most severe type of hypophosphatasia (the only type detectable in the fetus) is always lethal.

Recurrence risk. Hypophosphatasia has an autosomal recessive inheritance pattern, which determines the 25% recurrence rate. Therefore, in the case of termination of pregnancy, confirmation of

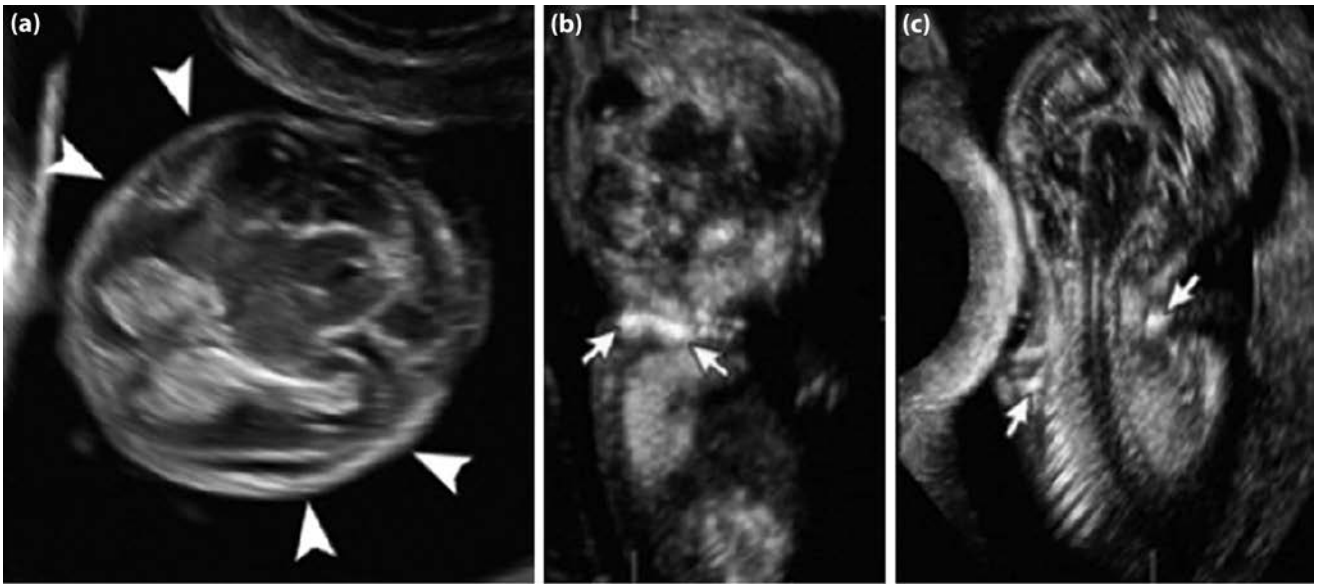


Figure 9.29 Hypophosphatasia (14 weeks of gestation). The transvaginal scan (12 MHz transducer) shows: (a) complete absence of calvarial mineralization (arrowheads); (b,c) multiplanar imaging of the fetal body demonstrating complete absence of mineralization involving virtually all districts with the significant exception of the clavicles, which are spared (arrows). In the sagittal plane (b), due to the transparent ribs, the moderately hyperechoic lung is also visible below the clavicle. On the coronal view (c), the complete absence of mineralization of the calvarium and the spine allows a neat unobscured demonstration of the spinal cord and the brain, with the two lateral ventricles and the choroid plexuses (arrows: clavicles).

the US diagnosis by autopsy is of the utmost importance for correct counseling and for advising early US monitoring of the next pregnancy in referral centers.

osteogenesis imperfecta (oi; oMIM 166210)

Incidence. Relatively frequent: 0.4/10,000 live births, 50% of which are accounted for by type II.

Ultrasound diagnosis. *Type II*: ubiquitous and diffuse fractures, thoracic hypoplasia, and hypomineralization of the calvarium. *Type III*: late onset bowing of long bones and fractures. Types I and IV are not diagnosable in the fetus.

Outcome. OI type II is lethal. Generally severe motor disability occurs in type III. Recently, therapy with bisphosphonates and stem cell transplantation has yielded good results in the nonlethal forms.

Inheritance pattern and recurrence risk. Autosomal dominant inheritance pattern. However, all cases are due to *de novo* mutations, and therefore, the recurrence risk is very low, although some authors have reported a 6% risk.

Definition OI comprises a spectrum of congenital disorders characterized by very fragile bones. Four types have been identified; of these, types I and IV are not detectable in the fetus because the associated fractures occur only after birth. Type III can sometimes be recognized in the third trimester. The lethal OI type II is the only one that can be consistently detected in utero. The incidence of OI is relatively high, with 0.4 cases per 10,000 live births, half of which are represented by type II (OMIM 166210).

Etiology and pathogenesis. OI is due to a mutation in one of the two genes involved in the production of collagen type I (*COLIA1* and *COLIA2*). Because this type of collagen is present in bones, tendons, tooth enamel, and sclera, the anomaly in collagen I is the cause of all expressions of the disease in the various subtypes.

Ultrasound diagnosis. The US findings described below refer to OI type II only. The main sonographic features of this disorder are diffuse hypomineralization of the calvarium (Figure 9.30a); thoracic hypoplasia of variable degree (Figure 9.30b), sometimes associated with rib fractures; and diffuse and early fractures, responsible for severe micromelia (Figure 9.30c and d). In the type III variant, the US diagnosis is made in only a minority of cases during the late second or early third trimester, following the recognition of late-onset bowing of long bones and, rarely, of fractures (Figure 9.31).

Differential diagnosis. OI type II should be differentiated from the other lethal skeletal dysplasias presenting with micromelia and calvarial hypomineralization, namely, achondrogenesis and hypophosphatasia. It should be emphasized that in some cases, a final diagnosis cannot be reached on the basis of the US findings In general, hypomineralization with clavicle sparing is typical of hypophosphatasia. Micrognathia, which is present in achondrogenesis, is absent in hypophosphatasia, while fractures are characteristic of OI type II.

Prognosis, survival, and quality of life. OI type II is invariably lethal. OI type III shows motor disability of variable severity (kyphosis and fractures) and worsens with age, due to the extreme fragility of the bones. By adulthood, hearing loss (otosclerosis), a need for walking aids, and dentition problems are extremely frequent. Types I and IV, which cannot be detected in the fetus, are associated with a better prognosis. In the non-lethal variants, promising results have recently been obtained with oral bisphosphonates (alendronate and pamidronate).

These are synthetic pyrophosphate analogs that seem to increase bone mineral density while decreasing bone remodeling markers, pain, and fracture rate in infants and children with OI [16]. Experimentally, transplantation of totipotent stem cells that may differentiate into osteocytes has been attempted with some success [17].

Recurrence risk. OI type II shows an autosomal dominant inheritance pattern. However, all cases are due to *de novo* mutations, and therefore, the recurrence risk is very low, although some authors have reported a 6% risk.

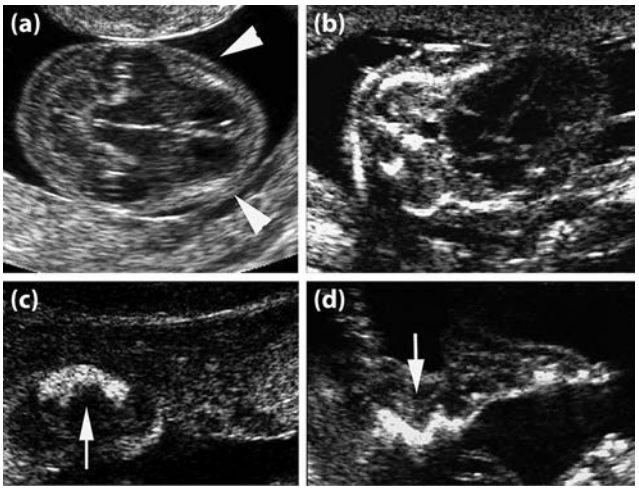


Figure 9.30 Osteogenesis imperfecta type II (lethal) (16 weeks of gestation). (a) On transvaginal ultrasound, the complete hypomineralization of the calvarium is evident (arrowheads). (b) Axial view of the thorax: abnormal ribs with thoracic hypoplasia. (c) Fractured and bowed femur (arrow). (d) Fractured tibia, with an acute angle deformation (arrow).



Figure 9.31 Osteogenesis imperfecta type III (non-lethal). Long bones' bowing from fractures occurs late in gestation. This case was referred at 35 weeks of gestation due to moderately short and bowed femurs. At examination, femurs, tibiae, and humeri showed bowing from fractures (arrow).

shor T-rIB poLyd Ac TyLy syNdro MEs

Incidence. Extremely rare; four subtypes have been identified.

Ultrasound diagnosis. Micromelia, thoracic hypoplasia with short ribs, polydactyly. In some cases, cardiac defects and/or regional hypomineralization.

Outcome. Always lethal.

Inheritance pattern and recurrence risk. Autosomal recessive: 25% recurrence risk.

Definition The SRPS comprise basically four subtypes (Saldino-Noonan, Majewski, Verma-Naumoff, and Beemer-Langer). All subtypes are characterized by micromelia and thoracic hypoplasia with short ribs; the first two only (despite the name) by postaxial polydactyly. Some feature other anomalies, including median cleft lip, congenital heart disease (transposition of the great arteries), and renal dysplasia. However, there is significant phenotypic overlap among the different subtypes and this has been controversially interpreted as being due to variable expression or to genetic heterogeneity.

Etiology and pathogenesis. The real incidence of these syndromes is not known, but they are very rare disorders. The genetic defect responsible for the SRPS remains unknown.

Ultrasound diagnosis. The US diagnosis is based on the detection of severe micromelia, severe thoracic hypoplasia with short ribs, and postaxial polydactyly (Figure 9.32). Other anomalies that may be detected by US in the various types include: congenital heart disease, median cleft lip, polycystic kidney/renal dysplasia, brain malformations (Table 9.12).

Differential diagnosis. SRPS should be differentiated from the other lethal skeletal dysplasias presenting with micromelia and thoracic hypoplasia, namely achondrogenesis, thanatophoric dysplasia, hypophosphatasia, and OI type II. However, postaxial polydactyly is present in SRPS only, and, at the same time, hypomineralization is only rarely present in some subtypes of SRPS. Another condition to be distinguished from SRPS is Ellis-van Creveld syndrome, which also

Table 9.12 Phenotypic differences among the short-rib polydactyly syndromes

SRPS type	Name	Polydactyly*	Skeletal	GI	Kidney	Genitalia	CHD	Hydrops	Other
I (263530)	Saldino-Noonan	+	Diffuse hypomineralization Severe micromelia	Atresias	PKK, atresias	–	TGA	+	–
II (263520)	Majewski	+	Micromelia, extremely hypoplastic tibia, spine	Atresias	Atresias	Ambiguous	–	–	Median CL/CP, CNS[a]
III (273410)	Verma Naumoff	–	Hypomineralization	–	PKK[b]	Ambiguous	Genitalia –	–	–
IV (269860)	Beemer-Langer	–[c]	Short, bowed limbs	–	Dysplasia	–	Genitalia –	+	Median CL/CP, CNS, anophtalmia

* Postaxial.
[a] Cerebellar vermis hypoplasia, pachygyria.
[b] Rarely, cloacal malformations.
[c] Present in some cases only.
Only features detectable prenatally are reported. All forms share severe thoracic hypoplasia with short rib, but, as reported below, not all have polydactyly, despite the name.
CHD: congenital heart disease; CL/CP: cleft lip/cleft palate; CNS: central nervous system; GI: gastro-intestinal; PKK: polycystic kidney; TGA: transposition of great arteres.

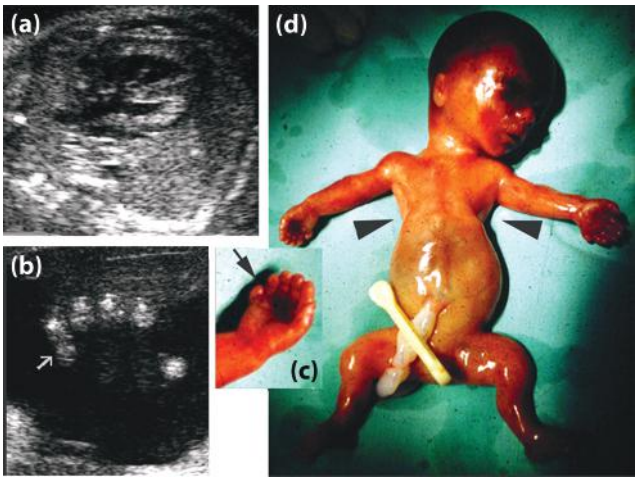


Figure 9.32 Short-rib polydactyly syndrome (20 weeks of gestation). (a) Severe thoracic hypoplasia. (b) Postaxial polydactyly of one hand (arrow). (c) Confirmation of polydactyly at autopsy. (d) Specimen after termination of pregnancy, showing severe thoracic hypoplasia (arrowheads). Note also the dip at the thoracoabdominal junction (arrowheads).

features thoracic hypoplasia and postaxial polydactyly; however, in the latter disorder, thoracic hypoplasia is less pronounced and the degree of limb shortening is lower. The occurrence of median cleft lip identifies SRPS types II and IV (Majewski and Beemer-Langer).

Prognosis, survival, and quality of life. SRPS are invariably lethal.

Recurrence risk. All SRPS have an autosomal recessive inheritance pattern, which determines the 25% recurrence rate. Therefore, in the case of termination of pregnancy, confirmation of the US diagnosis by autopsy is of the utmost importance for correct counseling and for advising early US monitoring of the next pregnancy in referral centers.

ThANATophor Ic dysp LAsIA (oMIM 187600, 187601)

Incidence. Relatively frequent (type I).

Ultrasound diagnosis. Severe limb shortening (femurs in particular); lethal thoracic (and secondary pulmonary) hypoplasia. Type I: bowed femurs and micromelia; type II: "cloverleaf skull" and straight femurs.

Outcome. Always lethal.

Inheritance pattern and recurrence risk. Both types are due to *de novo* mutations; therefore, the recurrence risk is very low.

Definition This condition is termed "thanatophoric" (or "death-bringing") to emphasize its lethality. Two subtypes of thanatophoric dysplasia have been identified: type I (OMIM 187600), which is the most frequent, is characterized by curved femurs, whereas type II (OMIM 187601) is characterized by straight femurs and the classic cloverleaf skull (see below). The reported incidence is 0.69/10,000 live births.

Etiology and pathogenesis. An anomaly of the *FGFR3* gene has been found in both subtypes of this disorder. In particular, all cases showing a Lys650Glu substitution are type II and show straight femurs and cloverleaf skull. All other types of mutations found in the same gene have bowed femurs and no cloverleaf skull (type I). The latter subtype is responsible for 80% of cases.

Ultrasound diagnosis (Figures 9.33 and 9.34). The US signs that may lead to the diagnosis of thanatophoric dysplasia are short limbs associated with severe thoracic hypoplasia. In particular, type I is characterized by bowed and extremely short femurs and humeri with metaphyseal cupping (Figure 9.33a through d). This unusual aspect has been noted as resembling the shape of a *French telephone receiver*. The ribs are very short and, on the midsagittal low-magnification view of the fetal trunk, a dip typical of severe thoracic hypoplasia can be seen at the level of the thoracoabdominal junction (Figures 9.33e and 9.34d,e). The head is large, with frontal bossing and a low nasal bridge (Figure 9.34b, c and e); no major synostoses are present in thanatophoric dysplasia type I. In contrast, in type II, there is a classic cloverleaf skull (Figure 9.34a), recognizable on a coronal view of the fetal head, which

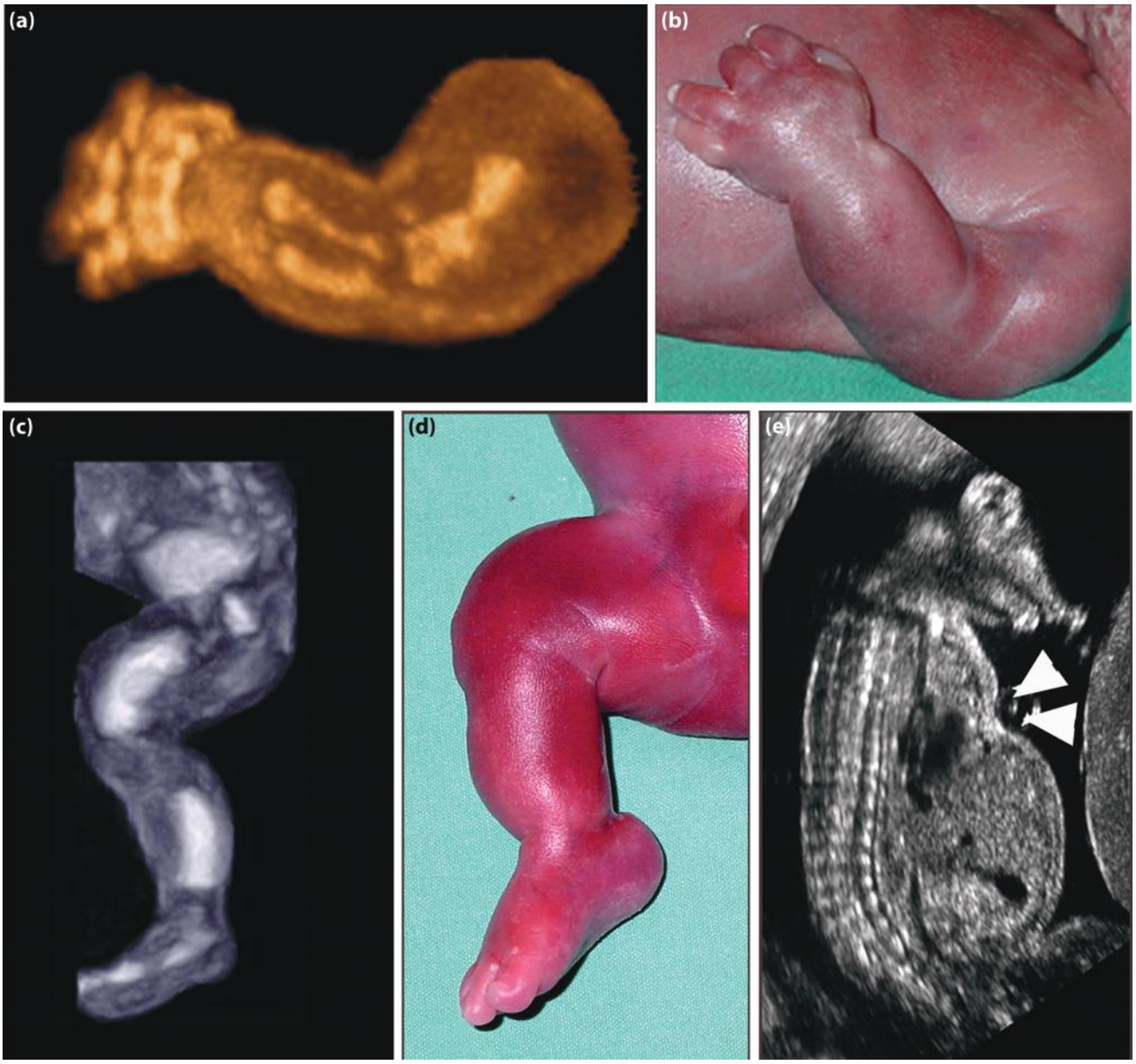


Figure 9.33 Thanatophoric dysplasia (22 weeks of gestation). (a) Three-dimensional maximum-mode rendering of the upper limb. The involvement of the three segments is evident. Note the "French telephone receiver" aspect of the humerus. (b) Confirmation of the micromelia at autopsy. (c) Maximum mode rendering of the lower limb. The thickening and shortening of the long bones is evident, together with the redundancy of the soft tissues. (d) Confirmation of the micromelia at autopsy. (e) Low magnification midsagittal view of the fetal body showing the severe thoracic hypoplasia with a dip at the thoracoabdominal junction (arrowheads).

is due to synostosis of the lambdoid, coronal, and sagittal sutures, responsible for the temporal bossing. Characteristically, in these rarer cases, the sonographer reaches the diagnosis through the impossibility of obtaining the classic axial transthalamic view for measurement of the biparietal diameter. The femurs are short, although less so than in type I, and above all, they tend to be straighter. Severe polyhydramnios is constantly associated.

Differential diagnosis. This includes the other skeletal dysplasias characterized by micromelia and severe thoracic hypoplasia, namely achondrogenesis, hypophosphatasia, and OI type II. In achondrogenesis, additional

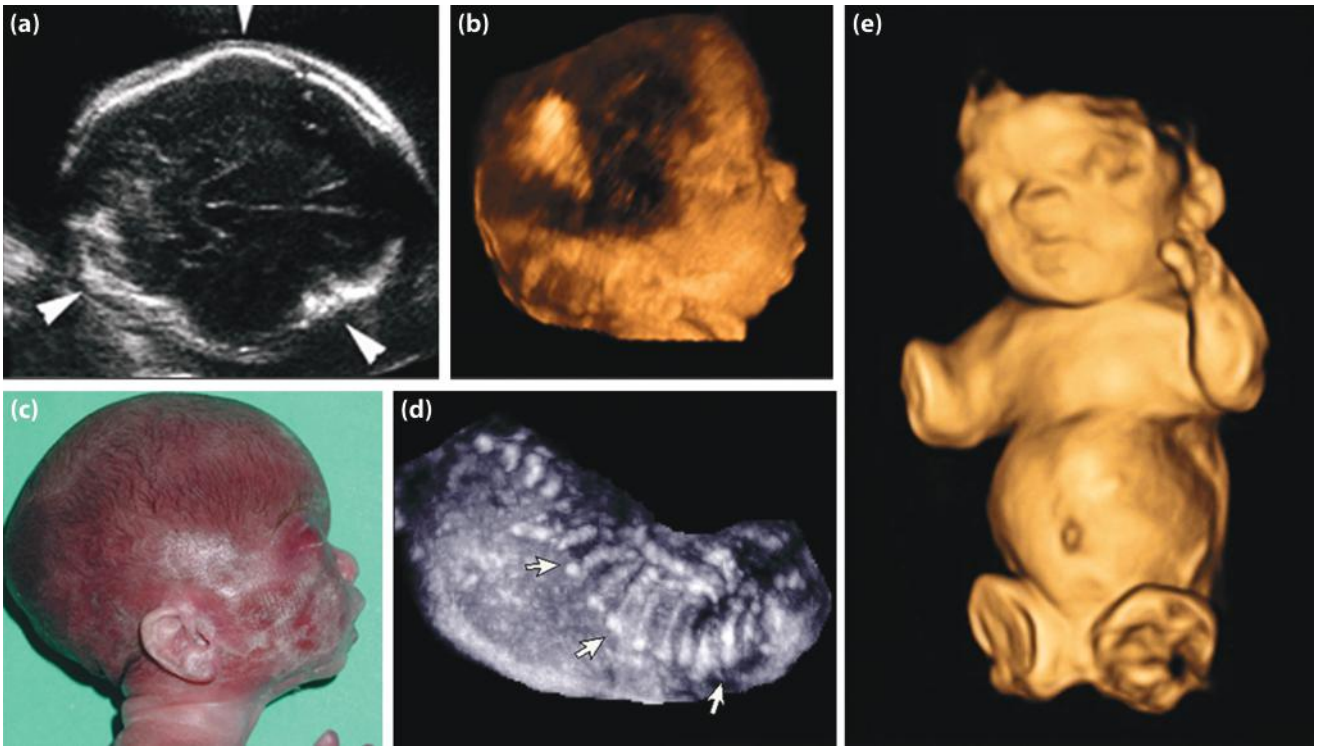


Figure 9.34 Thanatophoric dysplasia (22 weeks of gestation). (a) Axial transthalamic view demonstrating the abnormal shape of the skull and the early closure of some sutures (arrowheads). (b) Three-dimensional surface rendering of the fetal head, demonstrating moderate macrocrania, frontal bossing, and a low nasal bridge. (c) Confirmation of the macrocrania at autopsy. (d) Three-dimensional maximum-mode rendering of the fetal chest demonstrating severely hypoplastic ribs (arrows) and thorax. (e) Total body surface rendering showing: severe thoracic hypoplasia, with thoracoabdominal indentation, macrocrania, and limb shortening.

findings are micrognathia and severe hypomineralization, which are absent in thanatophoric dysplasia. Hypophosphatasia is characterized, in addition to micromelia and thoracic hypoplasia, by ubiquitous hypomineralization. Fractures are only seen in the lethal type II OI. With regard to type II thanatophoric dysplasia, the cloverleaf skull can also be present in very rare syndromes such as Pfeiffer syndrome (different skeletal anomalies) and Crouzon syndrome (no limb shortening).

Prognosis, survival, and quality of life. Thanatophoric dysplasia is always lethal, due to the severe pulmonary and thoracic hypoplasia.

Recurrence risk. Both types are due to *de novo* mutations. Therefore, the recurrence risk is trivial.

ULTr ASo UNd dIAGNos Is o F rE d Uc TIo N dEFE c Ts o F Th E LIMBs

In this section, the US diagnosis of focal and transverse defects of the limbs is described. According to the EUROCAT definition [18], an *intercalary reduction defect* is represented by a usually severe underdevelopment of one mesomelic bone segment only, whereas a *terminal transverse reduction defect* is complete absence of the terminal part of one limb (upper or lower). It is generally accepted that the latter type of defect can be congenital or acquired in utero. If congenital, it is the result of a vascular insult during organogenesis; in the very rare acquired forms, it is the result of amputation due to an amniotic band. Assessment of the reduction defects of the limbs is quite straightforward, because the differential diagnosis is limited to a small number of conditions [19]. It should be noted that nonsyndromic isolated defects of the limbs can involve all limbs at all levels. However, there are some types of defects that carry a higher syndromic risk. These include aplasia radii and focal femoral hypoplasia.

Aplasia radii. Aplasia/severe hypoplasia of the radius is commonly associated with ectrodactyly (absence of the thumb, which represents the terminal part of the radial ray). US diagnosis is straightforward: the rhizomelic

Table 9.13 Differential diagnosis of syndromes characterized by aplasia radii

Index sign	→	Aplasia radii ± ectrodactyly		
Additional signs	→	CHD[a] + multiple anomalies + micrognathia	→	Trisomy 18
Additional signs	→	Thumb present + CHD (30%) + micrognathia	→	TAR syndrome
Additional signs	→	Syndactyly + CHD	→	Holt–Oram syndrome
Additional signs	→	Phocomelia + cleft lip/palate + CHD	→	Roberts syndrome
Additional signs	→	Micrognathia + external ear anomalies	→	Nager syndrome
Additional signs	→	Vertebral + renal anomalies + gastrointestinal anomalies	→	VA(C)TER(L) association

CHD: congenital heart disease; TAR: thrombocytopenia with absent radius; VA(C)TER(L): vertebral anomalies, anal atresia, cardiac defects, tracheoesophageal fistula renal anomalies, and limb anomalies.

part of the upper limb is unremarkable, while the mesomelic component is highly abnormal: the radius can be completely absent or severely hypoplastic. The ulna can be normal or moderately hypoplastic. If radial aplasia is suspected, the hand should be carefully evaluated, because in all cases—except Thrombocytopenia Absent Radius (TAR) syndrome—the thumb is absent (Figure 9.35). The various disorders possibly associated with radial aplasia are listed in Table 9.13.

Finally, it should be noted that this anomaly is often detected at the time of the nuchal translucency scan, because in the first trimester the limbs are often stretched out, and this makes the recognition of the defect straightforward (Figure 9.36).

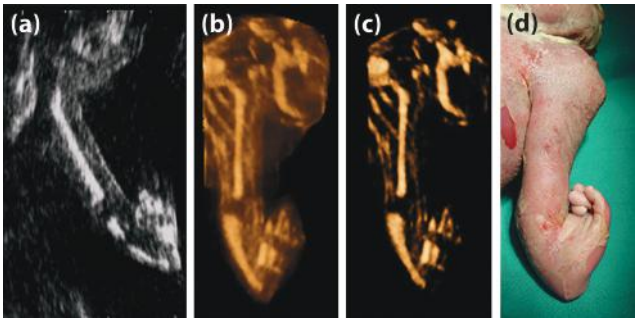


Figure 9.35 Aplasia radii (29 weeks of gestation). This is almost always associated with ectrodactyly (absence of the thumb), due to the severe hypoplasia/aplasia of the radial ray, which also causes severe ulnar deviation of the hand. (a) Two-dimensional ultrasound. (b) Three-dimensional maximum-mode demonstration with low threshold, demonstrating both the bony defect and the soft tissues. (c) Three-dimensional maximum-mode demonstration with high threshold, to highlight the bony defect. (d) Specimen after delivery (stillborn).

Femoral hypoplasia–unusual facies (femoral–facial) syndrome. Severe unilateral or bilateral focal hypoplasia of the femur(s), possibly associated with facial clefting and/or micrognathia, identifies femoral hypoplasia–unusual facies (femoral–facial) syndrome (FHUFS) [20]. Suspicion of this very rare syndrome should be raised whenever a focal defect of the femur is seen on US, especially if the pregnant woman has insulin-dependent diabetes mellitus. In fact, a relationship between maternal dysmetabolism and FHUFS has been described in the literature. FHUFS is described in detail in Chapter 10.

On the contrary, if other signs are absent, then a diagnosis of focal femoral hypoplasia can be made.

Terminal transverse reduction defects. It has been hypothesized that the cause of these not infrequent defects might be an interruption of the blood supply to the developing limb bud during organogenesis. However, if the defect involves more than one limb, then it has a syndromic context. We will briefl review this anomaly here because of its high functional

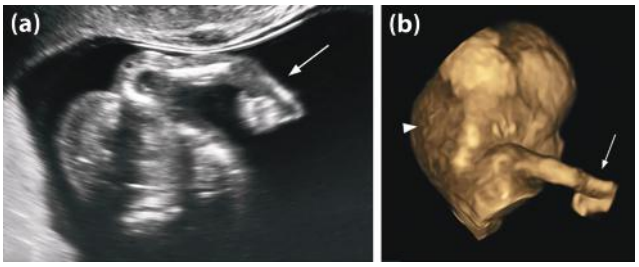


Figure 9.36 Aplasia radii (13 weeks of gestation). Transvaginal scan showing the classic aspect of aplasia radii (arrow) in a fetus with trisomy 18. (a) Two-dimensional imaging; (b) Three-dimensional surface-rendering showing also nuchal enlargement (arrowhead).

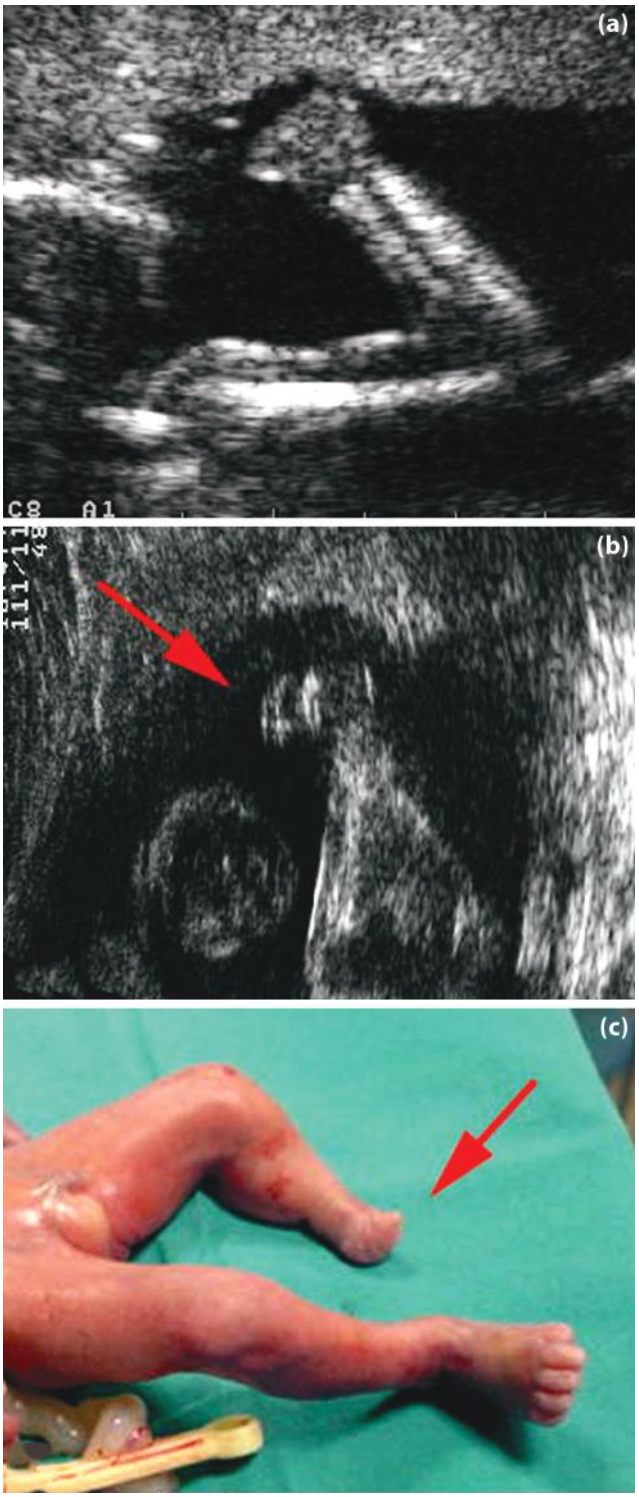


Figure 9.37 Limb reduction defects. (a) Terminal transverse reduction defect (acheiria): all digits and part of the metacarpus are completely absent. (b) Severe hypoplasia of the lower half of the calf and the foot (arrow). (c) Confirmation at autopsy: compare with the size of the normal contralateral limb and foot.

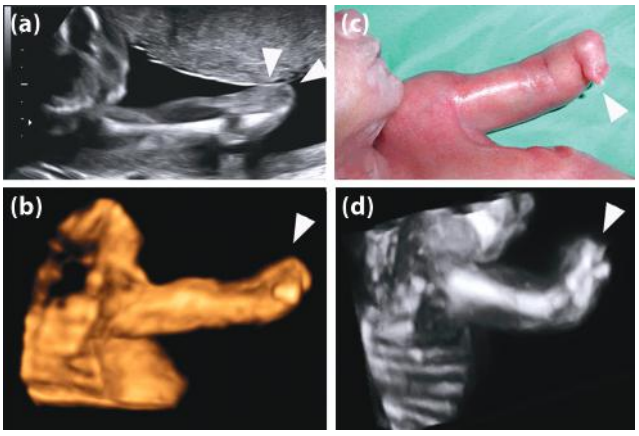


Figure 9.38 Limb reduction defects. Terminal transverse reduction defect of the upper limb (22 weeks of gestation). Sometimes, the absent part of the limb involves the hand and part of the forearm (arrowheads), as in this case. (a) Two-dimensional ultrasound. (b) Three-dimensional surface rendering of the soft tissues. (c) Confirmation at autopsy. (d) Three-dimensional maximum-mode demonstration of the bony defect.

significance and because its missed diagnosis at mid-trimester screening US represents one of the most frequent sources of medicolegal litigation. The defect can involve the hand/foot only (Figure 9.37), or a variable part of the mesomelic segment (Figure 9.38). In general, if the hand is partially absent, some hypoplastic digits are present on the terminal part of the wrist or metacarpus (Figure 9.38). An important part of the prognostic evaluation concerns the presence of the opposing digit, represented by the thumb; its absence significantly increases the functional invalidity of the hand.

Anomalies of the feet

Classic talipes. This is one of the minor anomalies most commonly encountered at birth. It comprises a spectrum of lesions characterized by contracture of variable severity of the ankle joint, possibly associated with tendon abnormalities: the two most common entities are *talipes varus* and *talipes equinus*. Talipes can occur as an isolated anomaly or can represent the effect of severe disorders of neurologic (spinal bifida), neuromuscular (FADS), or environmental (rupture of membranes, uterine hypoplasia, or twinning) origin. It is bilateral in roughly half of the cases. On US, the diagnosis is made when, on the sagittal view of the lower leg and calf, the sole, which in normal conditions is on another axis, is displayed (Figures 9.39 and 9.40). It is important to

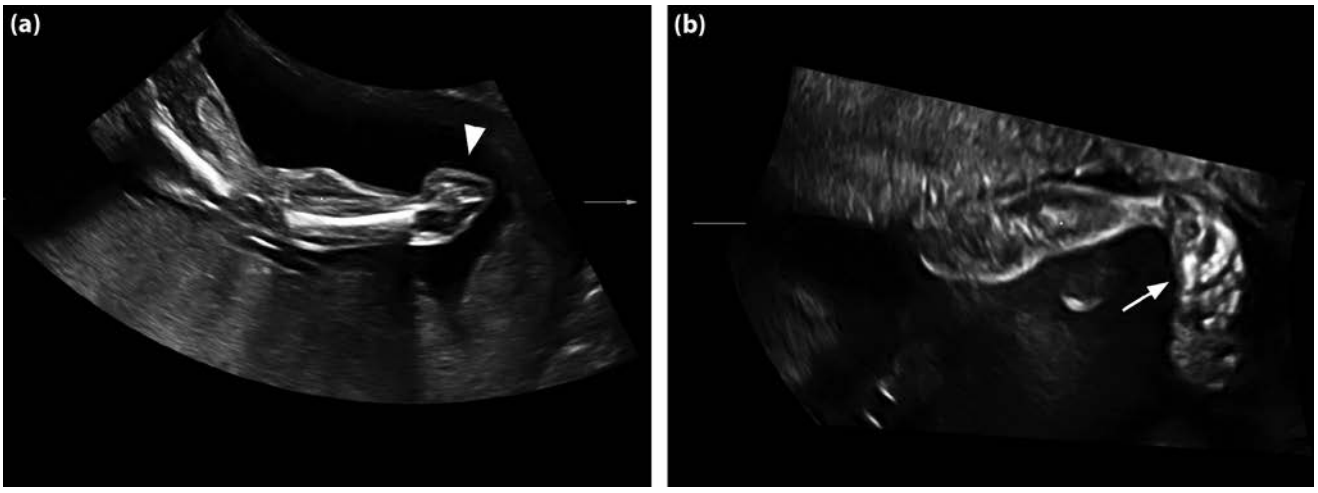


Figure 9.39 Talipes (clubfoot) (22 weeks of gestation). Two-dimensional imaging of a clubfoot: (a) the lateral view of the leg shows the bent foot sole; (b) the corresponding medial view demonstrates the foot sole, which should not be visible on this view, in normal conditions.



Figure 9.40 Talipes (clubfoot). (a) Three-dimensional maximum-mode rendering of a clubfoot in a fetus affected with myotonic dystrophy (21 weeks of gestation). Note the severe hypoplasia of the calf muscles. (b) Three-dimensional surface rendering of the same case. Note the thin aspect of the calf, also in comparison with (c) isolated clubfoot (talipes varus) at 30 weeks of gestation. Note the normal development of the calf and foot muscles.

underscore that talipes can also develop, as already mentioned, from environmental factors, such as prolonged oligohydramnios from early rupture of membranes, uterine hypoplasia, and fetal crowding from multiple pregnancies. Therefore, in a significant percentage of cases, this anomaly may be overlooked in utero and be diagnosed only at birth. Postnatal treatment depends on the cause of the deformation. With isolated talipes, the most favorable cases benefit from manipulation and casting first, followed by maintenance with strapping and splinting. If, at the end of casting (six weeks), the defect is still not corrected, this is an indication for surgery. In general, 50% of all talipes will be corrected at the end of casting at six weeks (90% of the mild form, 50% of the moderate form, and 10% of the severe form). If the defect is not corrected by the end of the casting period, surgery is needed. This consists mainly of posteromedial and subtalar release with Z-lengthening of the Achilles tendon, with a success rate of 60%–85%. In surgically corrected cases, the outcome is variable, and the condition may relapse in up to one-third of cases. However, in cases not associated with other major disorders, the outcome is generally good.

Rocker-bottom foot (congenital vertical talus). This is characterized by the following anomalies of the foot and ankle joint: calcaneus in equinus and valgus; hypoplasia and plantar flexion of the talus; abduction of the forefoot; and all dorsal tendons being tethered medial to the midline of the ankle (Figure 9.41). US diagnosis is relatively simple, relying on recognition of the anomaly of the plantar aspect of the foot, which is convex on a *sagittal view of the lower leg.* It is important to underline

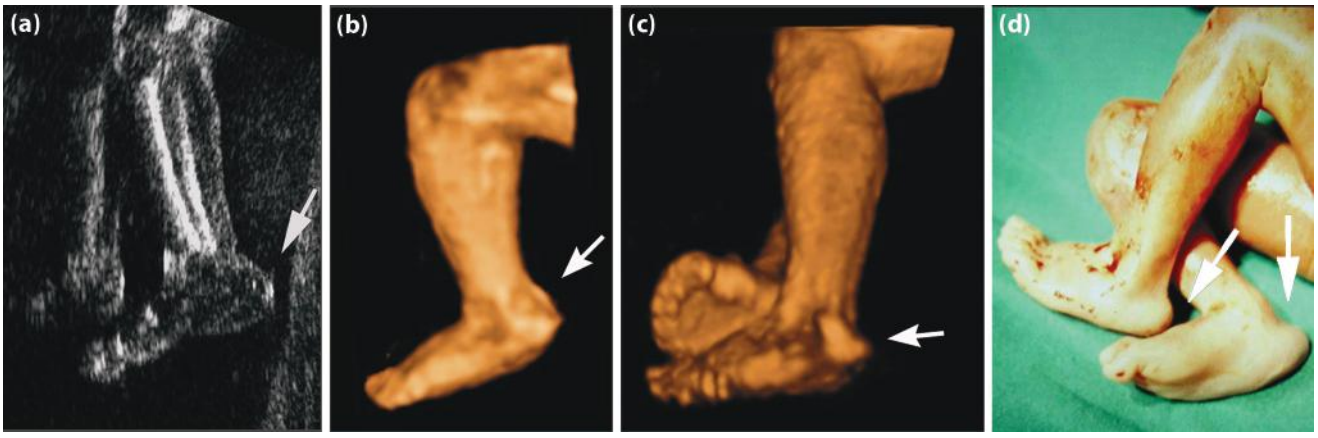


Figure 9.41 Rockerbottom foot. This deformation is typical of trisomy 18 and of other muscular and chromosomal anomalies. It is characterized by severe anomalies of the muscles and tendons of the lower leg and foot. On ultrasound, the most typical feature is the prominent calcaneus (arrow). (a) Two-dimensional imaging; (b) three-dimensional surface-rendering imaging of the same case; (c) three-dimensional imaging of another case; (d) autoptic confirmation of case a–b, which was a trisomy 18 fetus.

that this anomaly is very often associated with chromosomal aberrations, mainly trisomies 18 and 13. However, the importance of diagnosis of this anomaly is limited by the ubiquitous occurrence of other more evident and severe malformations in trisomies 18 and 13: it is highly unlikely that such chromosomal aberrations are disclosed only following the detection of rocker-bottom feet.

rEFE r ENc Es

1. Paladini D, Chita SD, Allan LD. Prenatal measurement of cardiothoracic ratio in the evaluation of heart disease. *Arch Dis Child* 1990; 65: 20–3.
2. Chitkara U, Rosenberg J, Chervenak FA, et al. Prenatal sonographic asessment of fetal thorax: normal values. *Am J Obstet Gynecol* 1987; 156: 1069–74.
3. Krakow D, Williams J 3rd, Poehl M, et al. Use of three-dimensional ultrasound imaging in the diagnosis of prenatal-onset skeletal dysplasias. *Ultrasound Obstet Gynecol* 2003; 21: 467–72.
4. Ruano R, Molho M, Roume J, et al. Prenatal diagnosis of fetal skeletal dysplasias by combining two-dimensional and three-dimensional ultrasound and intrauterine three-dimensional helical computer tomography. *Ultrasound Obstet Gynecol* 2004; 4: 134–40.
5. Faro C, Benoit B, Wegrzyn P, et al. Three-dimensional sonographic description of the fetal frontal bones and metopic suture. *Ultrasound Obstet Gynecol* 2005; 26: 618–21.
6. Chaoui R, Levaillant M, Benoit B, et al. Three-dimensional sonographic description of abnormal metopic suture in second- and third-trimester fetuses. *Ultrasound Obstet Gynecol* 2005; 26: 761–4.
7. Paladini D, Vassallo M, Sglavo G, et al. Normal and abnormal development of the fetal anterior fontanelle: a three-dimensional ultrasound study. *Ultrasound Obstet Gynecol* 2008; 32: 755–61.
8. Paladini D, Sglavo G, Penner I, et al. Fetuses with Down syndrome have an enlarged anterior fontanelle in the second trimester of pregnancy. *Ultrasound Obstet Gynecol* 2007; 30: 824–9.
9. Paladini D, Tartaglione A, Agangi A, et al. Pena–Shokeir phenotype with variable onset in three consecutive pregnancies. *Ultrasound Obstet Gynecol* 2001; 17: 163–5.
10. Chitty LS, Altman DG, Henderson A, et al. Charts of fetal size: 2. Head measurements. *Br J Obstet Gynecol* 1994; 101: 35–43.
11. Chitty LS, Altman DG, Henderson A, et al. Charts of fetal size: 3. Abdominal measurements. *Br J Obstet Gynecol* 1994; 101: 125–31.
12. Chitty LS, Altman DG, Henderson A, et al. Charts of fetal size: 4. Femur length. *Br J Obstet Gynecol* 1994; 101: 132–5.
13. Hadlock FP, Deter RL, Harris RB, et al. Fetal femur length as a predictor of menstrual age: sonographically measured. *AJR Am J Roentgenol* 1982; 138: 875–8.
14. Paladini D, Rustico MA, Viora E, et al. Fetal size charts for the Italian population. Normative curves of head, abdomen and long bones. *Prenat Diagn* 2005; 25: 456–64.
15. Keppler-Noreuil KM, Adam MP, Welch J, et al. Clinical insights gained from eight new cases and review of reported cases with Jeune syndrome (asphyxiating thoracic dystrophy). *Am J Med Genet Part A* 2011; 155A: 1021–32.
16. Forin V, Arabi A, Guigonis V, et al. Benefits of pamidronate in children with osteogenesis imperfecta: an open prospective study. *Joint Bone Spine* 2005; 72: 313–18.
17. Millington-Ward S, McMahon HP, Farrar GJ. Emerging therapeutic approaches for osteogenesis imperfecta. *Trends Mol Med* 2005; 11: 299–305.
18. EUROCAT (European Surveilance of Congenital Anomalies). *Guide 3: For the Description and Classification of Congenital Limb Defects*. 2nd ed. 2004. Available from:
19. Paladini D, Greco E, Sglavo G, et al. Congenital anomalies of upper extremities: prenatal ultrasound diagnosis, significance and outcome. *Am J Obstet Gynecol* 2010; 202: 596. e1–10.
20. Paladini D, Maruotti GM, Sglavo G, et al. Diagnosis of femoral hypoplasia-unusual facies syndrome in the fetus. *Ultrasound Obstet Gynecol* 2007; 30: 354–8.

Chapter 10
Chromosomal and nonchromosomal syndromes

dEFINITIoN

In this chapter, a limited number of chromosomal and nonchromosomal syndromic conditions will be described. There are two criteria used to define what disorders should appear in this section of the book: the first is that all syndromes described here should be reliably diagnosable by ultrasound (US), on the basis of a cluster of major and minor sonographic signs; the second is the availability of both sonographic and postmortem pictures needed to comprehensively describe the syndrome. This chapter does not claim to compete with more comprehensive textbooks and manuals of prenatal US diagnosis, fetal dysmorphology, or genetics, to which the reader may wish to refer for extensive treatment. The real aim of this chapter is to provide the reader with support in his or her daily practice by reviewing, with ample use of images, the most common chromosomal anomalies and some of the rare nonchromosomal syndromes that may be diagnosable by every professional involved in the field of prenatal US diagnosis of congenital anomalies with a little dedication and understanding.

Tr Iso My 21: doWN syNdro ME

Incidence. Very high: 1/500 at 20 weeks of gestation.

Etiology. Free trisomy of chromosome 21 (95%); trisomy from Robertsonian translocations or mosaicisms (5%).

Ultrasound diagnosis. *Major anomalies*: atrioventricular septal defect (AVSD); ventricular septal defect; gastrointestinal atresias; exomphalos. *Minor anomalies*: enlarged nuchal translucency/nuchal edema/fold; nasal bone hypoplasia; aberrant right subclavian artery; pyelectasis.

Outcome. Mental and physical developmental delays of variable degree. Overall survival reaches 50–60 years and depends on the associated anomalies.

Recurrence risk. 1% empiric risk, as for all autosomal trisomies. 25% in case of parental Robertsonian translocations.

Definition *Down syndrome* is named after John Langdon Down, the first scientist to describe the pattern of congenital anomalies characterizing individuals with trisomy 21. The overall incidence in an unselected population at 20 weeks is about 1/500.

Etiology and pathogenesis. Down syndrome is due to trisomy of chromosome 21; this is a free trisomy in 95% of the cases, while the remaining 5% are represented by Robertsonian translocation and mosaicisms of variable degree. It is well established that the occurrence of the trisomy has a positive correlation with advancing maternal age, especially after 35 years of age. Molecular biologic assays have demonstrated that in 95% of cases, the trisomy is the result of a nondisjunction during maternal meiosis (meiosis I in 75%–80% of cases). In the

remaining 5% of cases that are due to a paternal error, this occurs most frequently during meiosis II.

Genetics. The genetic defect, namely the extra copy of chromosome 21, was discovered at the end of the 1950s. The first amniocentesis leading to a diagnosis of trisomy 21 in a fetus was reported in 1968. Since then, the diagnosis of trisomy 21 has been made on chorionic villi, amniocytes, and peripheral lymphocytes through the G-banding technique.

Ultrasound diagnosis. From postnatal and prenatal data, it is evident that about 50% of individuals with Down syndrome do not show any major or minor anomaly possibly detectable in utero. The remaining 50% show one or more of the major anomalies described below, involving mainly the cardiovascular (50%) and gastrointestinal (30%) systems (Figure 10.1). As a consequence, should any of the following anomalies be detected on US, karyotyping is mandatory:

- *Esophageal atresia* is suspected on the *axial view of the upper abdomen*, where the gastric bubble cannot be visualized (Figure 10.1a). Polyhydramnios develops in the late second or early third trimester.
- *Duodenal atresia* is suspected on the *axial view of the upper abdomen*, where the classic double-bubble sign is found. However, this sign is fully appreciated after 23–24 weeks of gestation (Figure 10.1b). Also in this case, polyhydramnios develops in the late second or early third trimester.
- *Exomphalos*, especially if of small dimension and without the liver, may be associated with trisomy 21. The diagnosis is made on the *axial or sagittal view of the fetal abdomen*. At the level of the cord insertion, the exomphalos appears as a round, solid mass that deforms the anterior abdominal wall (Figure 10.1c); it may contain the right hepatic lobe and/or some ileal loops. The cord insertion is typically on the mass.
- *AVSD* is classically detected on the *four-chamber view of the fetal heart*. A common atrioventricular valve is found, and the central crux of the heart is missing (Figure 10.1d). Note that only AVSD with balanced ventricles is associated with trisomy 21 (see Chapter 5).
- *Ventricular septal defect* (VSD) is detected on the *four-chamber view of the fetal heart* or on *the left outflow tract view*, according to the site of the defect. If it involves the inlet portion of the septum, the diagnosis is made in the former view, where the defect appears as a small interruption just below the atrioventricular plane (Figure 10.1e); if, on the contrary, the VSD involves the outlet portion of the septum, then this is best appreciated on the left outflow tract view as a discontinuity of the septo-aortic tract (see Chapter 5).

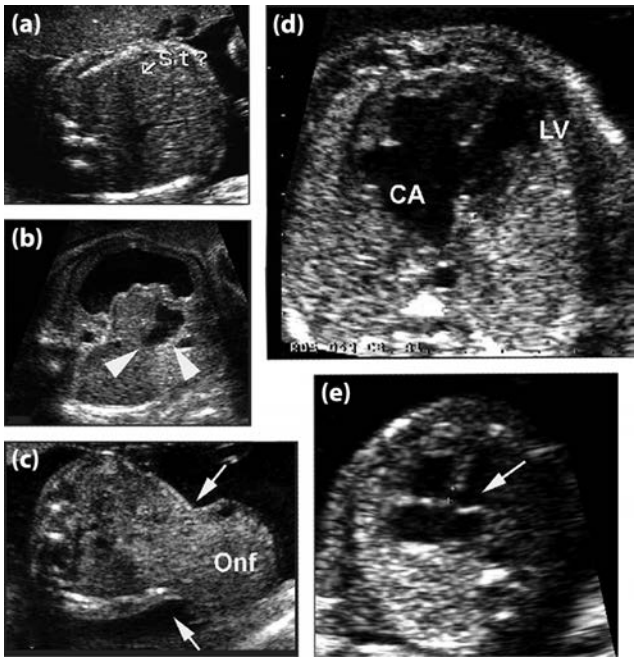


Figure 10.1 Down syndrome: major signs. Axial view of the upper abdomen. (a) Esophageal atresia: the stomach (st?) cannot be seen. (b) Duodenal atresia: the typical double bubble (arrowhead) is evident. (c) Omphalocele: the mass departing from the anterior abdominal wall (Onf) can be seen. The arrows indicate the abdominal defect. (d) Complete, balanced AVSD: a common atrium (CA) and a single atrioventricular valve are seen (LV: left ventricle). (e) Inlet VSD: small defect of the septum below the atrioventricular plane (arrow).

In addition to the described major malformations, there are a number of "minor" signs, or *soft markers*, which are associated with Down syndrome. This term refers to the fact that these signs do not represent actual malformations, but only particular findings evident on US. The detection of any of these soft markers increases the risk of trisomy 21. In this regard, it should be underlined that we do not believe that the description of all the signs that have been considered as soft markers for Down syndrome in the literature (a partial list of which is given in Table 10.1) may be of relevance here. In line with the practical approach of this book—from US sign to diagnosis—we have arbitrarily decided to include here only descriptions of the few such markers (nuchal fold thickness, aberrant right subclavian artery and hypoplastic nasal bone) that significantly increase this risk. In fact a recent meta-analysis of second trimester markers for trisomy 21 (1) reports that in the case of most isolated markers

Table 10.1 Second trimester soft markers for trisomy 21

Biometric
• Short femur and humerus
• Observed and expected femur length ratio
• Observed and expected humerus length ratio
• Pyelectasis
• Wide iliac bone wings
• Mild ventriculomegaly[a]
Morphologic
• Nuchal edema or fold[a]
• Nasal bone hypoplasia[a]
• Aberrant right subclavian artery[a]
• Intracardiac foci
• Hypoplasia second phalanx V digit
• Hyperechogenic ileus
• Sandal gap
• Macroglossia
• Small ears

[a] These are the most sensitive (see this chapter's text). For mild ventriculomegaly see Chapter 2.

there is only a small effect on modifying the pre-test odds for trisomy 21, but with ventriculomegaly, nuchal fold thickness and ARSA there is a 3–4-fold increase in risk and with hypoplastic NB a 6–7-fold increase.

- *Nasal bone hypoplasia (second trimester) (Figure 10.2a and b).* This marker should be assessed on the *midsagittal view of the fetal profile*, where the reduced longitudinal diameter of the nasal bone can be easily appreciated and checked on nomograms for the normal population (Figure 10.2a,b and c, see Appendix Table A.16). As a comparison, a normal fetus of the same gestational age as that of Figure 10.2a is shown in Figure 10.2c. This is one of the most recently described *soft marker* for the second trimester [2], which seems to have a detection rate comparable to that of the nuchal fold (described below). Two issues should be considered when measuring the nasal bone in the second trimester: (1) the insonation angle between the transducer and the nasal bone must be as close as possible to 90°, otherwise the nasal bone plate may not show up properly (the images of Figure 10.2a and b have been rotated to show the profile better, but the original scanning plane was as mentioned); and (2) as with other proposed soft markers, the incidence of apparent nasal bone hypoplasia is much higher in Asian populations and Afro-Caraibic populations, which limits to some extent the usefulness of this marker in those populations.
- *Nuchal abnormalities (Figure 10.2d and e).* We include in this paragraph both the early (12–14 weeks) anomalies, such as nuchal translucency (Figure 10.2d), and those that are visible at a later stage, which include the nuchal fold (Figure 10.2e) and nuchal edema. As far as the nuchal fold is concerned, this was described for the first time in 1985 [3]; it is found in about 40% of fetuses with trisomy 21 at 19–22 weeks of gestation. It should be measured on the modified axial view of the posterior fossa used for the assessment of cerebellar anatomy, positioning the calipers on the external echogenic rim of the skin and on the outer aspect of the occipital bone. The nuchal fold is normal if less than 6 mm. It should be underlined that an increased risk of Down syndrome remains if the nuchal fold partially regresses during the third trimester.
- *Aberrant right subclavian artery* (ARSA; Figure 10.3). This strong marker of Down syndrome was described for the first time in the fetus by Chaoui et al. [4] in 2005. Since then, several other investigators have confirmed that it represents an independent strong marker of trisomy 21 [5,6]. In particular, its incidence in euploid fetuses and in trisomic ones has been shown to be 1.2%–1.4% and 25%–37%, respectively.

In normal conditions, the right subclavian artery represents a branch of the innominate artery; when, on the contrary, it departs directly from the aortic arch, as a fourth vessel, and courses behind the trachea, it is defined as *aberrant*.

The course of the subclavian arteries should be sought with color Doppler (low PRF) on an axial view of the upper mediastinum (Figure 10.3). In normal conditions, the two subclavian arteries show an "S" course and are found just below the clavicles (Figure 10.3a); in the case of ARSA, the right subclavian artery cannot be located in its usual position, but is found at a slightly lower level, departing from the posterior aspect of the confluence of the ductal and aortic arches, and coursing behind the trachea (Figure 10.3b and c).

Differential diagnosis. This involves the other conditions in which one of the above-mentioned soft markers may be present, since the other autosomal trisomies are characterized by multiple congenital anomalies rather than soft markers only.

- *Cystic fibrosis*: look for ► *hyperechogenic ileus* + possible meconium peritonitis or ileal atresia;
- *Fetal toxoplasmosis*: look for ► *hyperechogenic ileus* + hydrocephalus or cerebral calcifications + maternal positive serology;

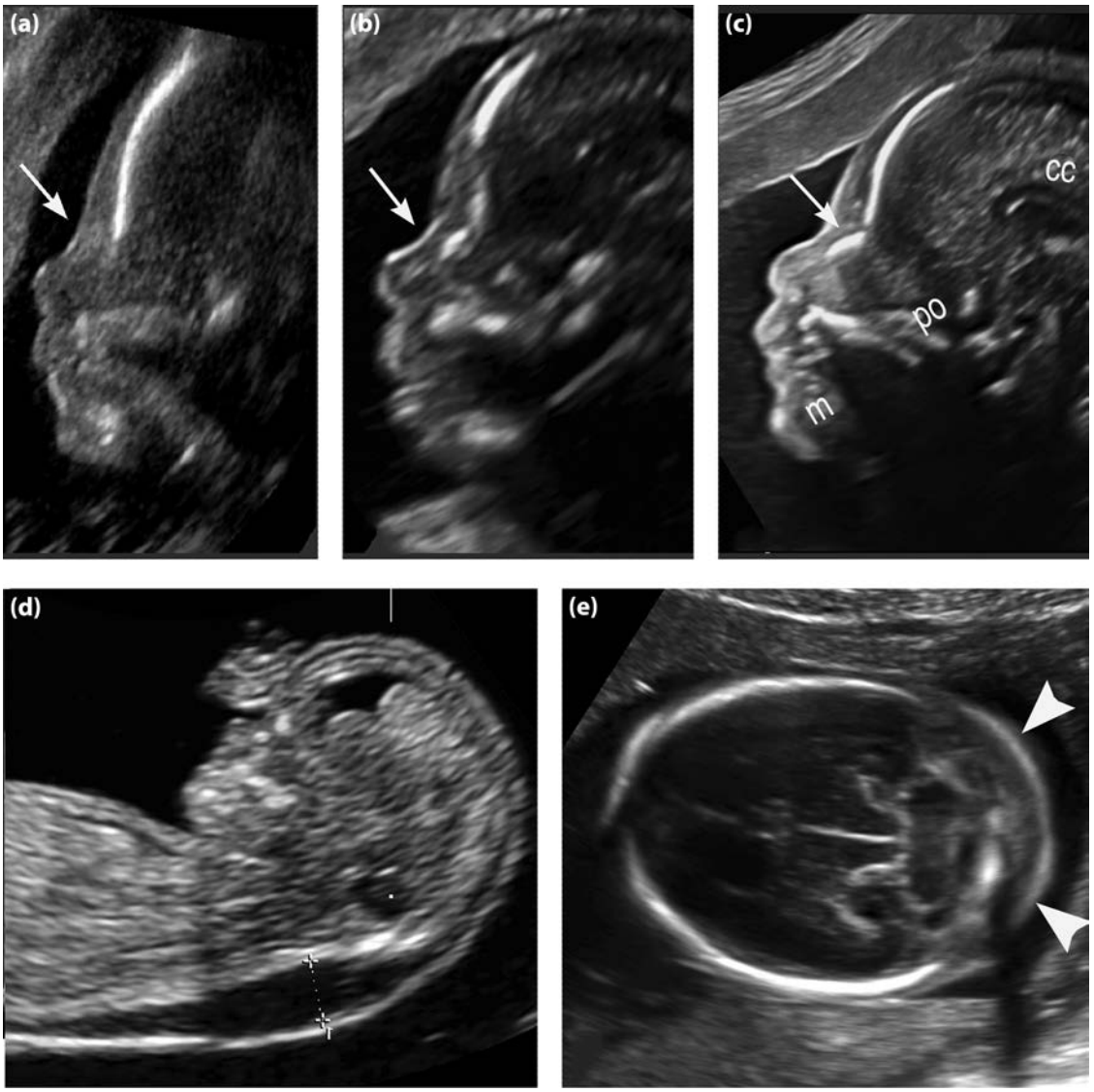


Figure 10.2 Down syndrome: minor signs (soft markers). (a) Nasal bone absence in the second trimester (arrow). (b) nasal bone hypoplasia (arrow) in the second trimester. (c) normal-sized nasal bone in a normal fetus of the same gestational age (arrow), cc: corpus callosum; m: symphisis mentis; po: bony palate. (d) Enlarged nuchal translucency (4 mm in this case). (e) Nuchal fold more than 6 mm (7 mm in this case), to be measured on the transcerebellar plane.

- *Achondroplasia*: look for ► *short femur and humerus* + moderate macrocrania + low nasal bridge;
- *Early fetal growth restriction (FGR)*: look for ► *short femur and humerus (hyperechogenic ileus)* + abnormal growth + Doppler velocimetry abnormalities (umbilical artery and ductus venosus);
- *Familial short stature*: look for ► *short femur and humerus* + parental short stature.

Prognosis, survival, and quality of life. Children with Down syndrome have decreased muscle tone, and mental as well physical development delays of variable degree. Among long-term sequelae, Down syndrome individuals may experience high-airway obstruction, which in some circumstances may be so severe as to require tracheotomy. In addition, if brachysyndactyly is severe, this may limit the functionality of the hands. Cosmetic surgery has been used in some cases to remove the facial features typical of Down syndrome if these are particularly pronounced.

Recurrence risk. This is empirically estimated at 1%. However, if the syndrome is due to a parental balanced translocation, then the recurrence risk reaches 25%, since it becomes an autosomal recessive condition.

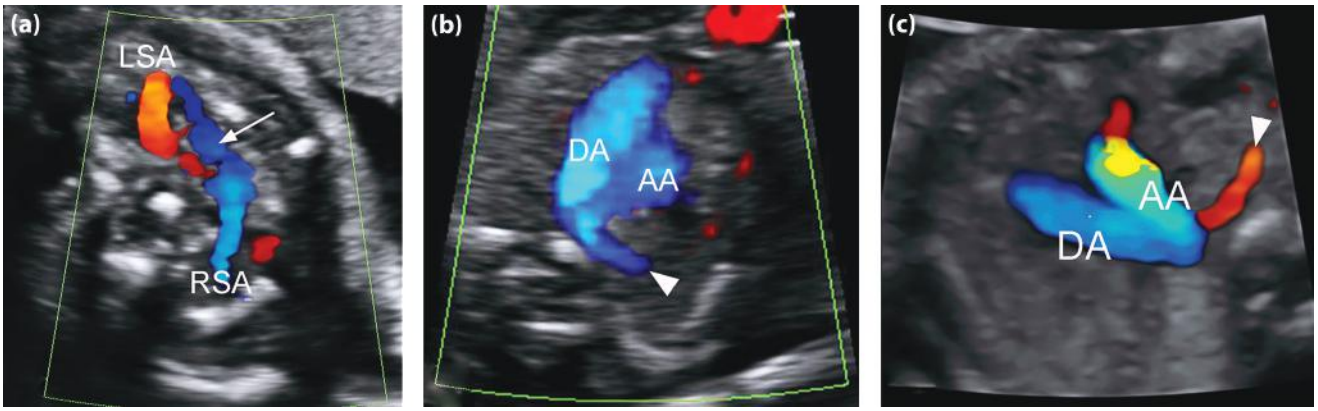


Figure 10.3 Down syndrome: aberrant right subclavian artery (ARSA). (a) Normal aortic arch branching: the two subclavian arteries are seen just below the clavicles and show an "S" shape (LSA: left subclavian artery; RSA: right subclavian artery). Often, on this view, the innominate or brachiocephalic vein (arrow) is also displayed, due to the relatively low PRF needed to demonstrate the subclavian arteries. (b) The ARSA (arrowhead) is seen departing from the confluence of the ductal (DA) and aortic (AA) arches and courses behind the trachea. If the insonation is from the fetal left side, the ARSA will show up in blue, because the blood flow will go away from the transducer. (c) On the contrary, if the thorax is insonated from the fetal right side, the arches will still appear in blue, but the ARSA (arrowhead) will take on a red color code, because the blood flow is toward the transducer. Care should be taken to insonate the three-vessel view, creating an angle more than 45° with the expected position of the ARSA; otherwise, it will not show up for the physics of Doppler.

Trisomy 18: Edwards syndrome

Incidence. 1/6000 at birth. M/F ratio 0.65.

Etiology. Free trisomy of chromosome 18 (>99%); rarely, mosaicisms or structural anomalies involving chromosome 18.

Ultrasound diagnosis. *Major anomalies*: congenital heart disease; central nervous system (CNS) anomalies; micrognathia; urinary tract malformations; radial ray anomalies; cystic hygroma; esophageal atresia; early symmetric FGR. *Minor anomalies*: enlarged nuchal translucency and choroid plexus cysts.

Outcome. High intrauterine mortality: 5% survival at birth (30% of those diagnosed in utero survive until birth). Severe psychomotor delay and mental retardation. Mean postnatal survival is 1 week (90% mortality rate within 6 months).

Recurrence risk. 1% empiric risk, as for all autosomal trisomies.

Definition Edwards syndrome was first recognized and related to an extra copy of chromosome 18 in 1960. More than 100 different malformations have been described in association with this trisomy.

Etiology and pathogenesis. Edwards syndrome is due to an extra copy of chromosome 18. In addition, rare cases of mosaicisms (with a normal second cellular line) showing extreme phenotypic variability in relation to the percentage of the trisomic line have been reported. As with Down syndrome, direct correlation with advancing maternal age has been shown for this autosomal trisomy.

Genetics. The genetic defect in Edwards syndrome, the extra copy of chromosome 18, is now easily recognizable on chorionic villi, amniocytes, and peripheral leukocytes. Molecular biologic assays have demonstrated that in 90% of cases, the trisomy is the result of a nondisjunction during maternal meiosis II. In the remaining 10% of cases, due to a paternal error, this always occurs after fertilization.

Ultrasound diagnosis. There is a wide spectrum of major anomalies that have been described in fetuses and neonates with trisomy 18 [7]. The following are the major anomalies most commonly encountered in fetuses with Edwards syndrome:

- *CNS anomalies*: neural tube defects (NTDs), agenesis of the corpus callosum, and posterior fossa anomalies (Figure 10.4a);

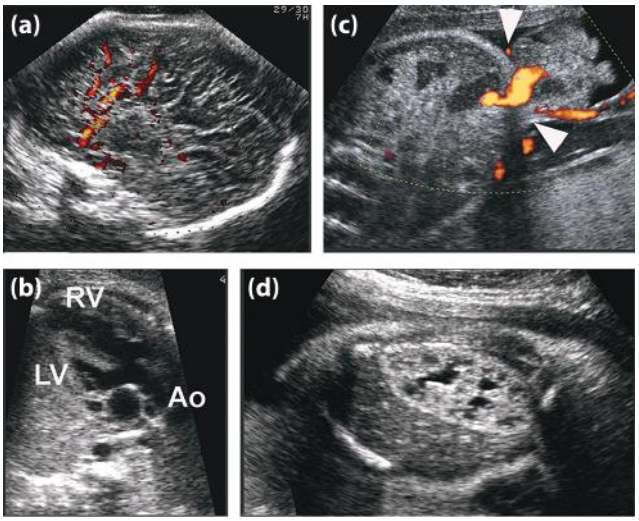


Figure 10.4 Trisomy 18. (a) Agenesis of the corpus callosum. Note the radial pattern of the fibers and the absence of the pericallosal artery on power Doppler. (b) Congenital heart disease: malalignment ventricular septal defect with overriding aorta. Ao: aorta; LV: left ventricle; RV: right ventricle. (c) Bowel-containing omphalocele (arrowheads). Note that the risk of chromosomal anomalies is maximal for small lesions without the liver in the sac. (d) Hyperechoic kidney, with or without dysplasia.

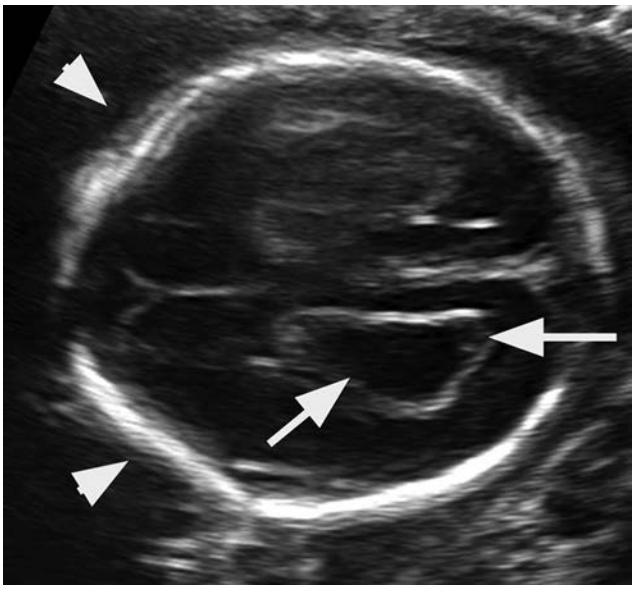


Figure 10.5 Trisomy 18. One of the additional signs, especially in the early second trimester, is the so-called strawberry-shaped skull. This anomaly is due to a reduced occipitofrontal diameter and scalloped frontal bones (arrowheads). Note the concurrent presence of a *soft marker* typical of trisomy 18, namely, a large *choroid plexus cyst* (arrow).

- *Micrognathia* of variable severity is associated with 50%–70% of cases (see Figure 3.48 and 3.49);
- *Congenital heart disease*: septation, conotruncal malformations (Figure 10.4b), and polyvalvular disease;
- *Abdominal wall anomalies:* exomphalos (Figure 10.4c);
- *Urinary tract anomalies*: cystic renal dysplasia (Figure 10.4d) and horseshoe kidney;
- *Cystic hygroma*;
- *Skeletal anomalies*: micrognathia, clenched hands with overlapping fingers, aplasia radii (Figure 9.35 and 9.36), and rockerbottom feet (Figure 9.36) [8];
- FGR, early onset.

Some of these anomalies, such as an enlarged NT or cystic hygroma, are usually detected early in gestation, while congenital heart disease and cerebral anomalies (Dandy–Walker variant and agenesis of the corpus callosum) are more commonly recognized at the midtrimester scan. FGR is already evident in the second trimester in over 50% of cases. Of the various soft markers described in association with trisomy 18, the following are worthwhile to note:

- Nuchal abnomalities: enlarged nuchal translucency (Figure 10.2d);
- Strawberry-shaped skull (Figure 10.5);
- Choroid plexus cysts (Figure 10.5).

Differential diagnosis. This includes other chromosomal anomalies characterized by multiple malformations and early FGR, as well as the group of neuroarthrogryposes:

- *Trisomy 13 [7]*: look for ► *FGR* + holoprosencephaly + microphthalmia + congenital heart disease + bilateral cleft lip and palate;
- *Triploidy [7]*: look for ► *FGR (very early)* + posterior fossa anomalies + macrophthalmia + oligohydramnios;
- *Fetal akinesia deformation sequence (FADS) [7]*: look for ► *FGR* + micrognathia + diffuse joint contractures.

Prognosis, survival, and quality of life. Trisomy 18 is a lethal condition in most cases: of the relatively few live-borns, 90% die within 6 months and less than 5% of cases reach 12 months of life. In the survivors, severe mental retardation is constantly associated. Significant hearing and sight impairment is frequent, and growth is severely compromised. In addition to the major anomalies, another determinant of mortality and morbidity is the predisposition to infections.

Recurrence risk. This is empirically estimated to comprise 1% of all autosomal trisomies.

Trisomy 13: Patau syndrome

Incidence. 1/12,500 at birth.

Etiology. Free trisomy of chromosome 13 (75%); trisomy from Robertsonian translocations (25%).

Ultrasound diagnosis. *Major anomalies*: congenital heart disease; CNS (holoprosencephaly, etc.) and craniofacial (microphthalmia and cleftings) anomalies; exomphalos; cystic renal dysplasia; postaxial polydactyly. *Minor anomalies*: enlarged nuchal translucency.

Outcome. Extremely high intrauterine mortality rate, with 2.5% of prenatally diagnosed cases reaching term. Severe psychomotor delay. 3% survival rate at 6 months of life.

Recurrence risk. This is empirically estimated to comprise 1% of all autosomal trisomies.

Definition Patau syndrome was described and related to an extra copy of chromosome 13 for the first time in 1960.

Etiology and pathogenesis. Patau syndrome is due to an extra copy of chromosome 13. In addition, rare cases of mosaicisms (with a normal second cellular line) showing extreme phenotypic variability in relation to the percentage of the trisomic line have been reported. In these cases, the recognition of a pigmentary cutaneous mosaicism may lead to disclosure of the two cellular populations. As with Down and Edward syndromes, a positive correlation with advancing maternal age has been described for trisomy 13.

Genetics. Prenatal diagnosis is feasible by G-banding of chromosomes from chorionic villi, amniocytes, and peripheral leukocytes. A free trisomy is responsible for 75% of cases, while in the remaining 25%, a Robertsonian translocation, the most common of which is rob(13q14q), is found. This is why, should a trisomy 13 be identified in a fetus, the genetic assessment should include karyotyping of both parents. Molecular biologic assays have demonstrated that in 90% of cases, the trisomy is the result of a nondisjunction during the maternal meiosis II (absence of chyasms).

Ultrasound diagnosis. There is a wide spectrum of major anomalies that can be associated with trisomy 13. The following are those most commonly encountered in the fetus:

- *CNS anomalies* (45%–55%): holoprosencephaly (Figure 10.6a), agenesis of the corpus callosum, and cerebellar malformations;
- *Craniofacial anomalies* (80%): bilateral cleft lip and palate (Figure 10.6b, e), micro- and anophthalmia, and micrognathia;
- *Congenital heart disease* (40%–50%): septation defects and absent pulmonary venous return (Figure 10.4b);
- *Urinary tract anomalies* (30%–35%): cystic renal dysplasia (Figure 10.4d);
- *Skeletal anomalies* (20%–30%): postaxial polydactyly and clenched hands [8] (Figure 10.6c and d);
- *Abdominal wall anomalies* (30%): exomphalos (Figure 10.4c);
- *FGR* (45%–55%).

Also, trisomy 13 is associated with an enlarged nuchal translucency at 12–14 weeks of gestation.

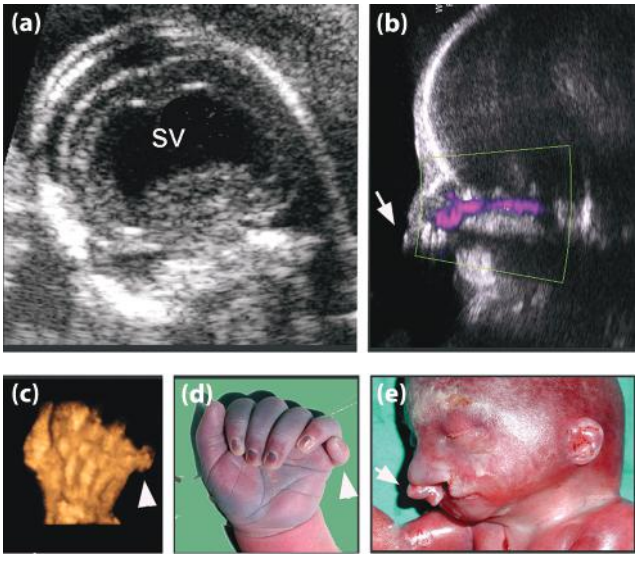


Figure 10.6 Trisomy 13. (a) Alobar holoprosencephaly: coronal view of the fetal head demonstrating a single cerebral ventricle (SV) and absence of the midline. (b) Bilateral cleft lip and palate: midsagittal view demonstrating additional tissue on the philtrum (arrow) and the cleft palate—the interruption of the bony palate is evident below the power Doppler signal in the nasal cavity. (c) Surface-rendered image of postaxial polydactyly (arrowhead). (d) Confirmation at autopsy. (e) Confirmation at autopsy of the bilateral cleft lip and palate.

Differential diagnosis. This includes mainly the following two conditions:

- *Trisomy 18 [7]*: look for ► *FGR* + CNS anomalies (not holoprosencephaly) + congenital heart disease + micrognathia + skeletal anomalies (rockerbottom feet or clenched hands with overlapping fingers, not hexadactyly);
- *Meckel–Gruber syndrome [7]*: look for ► *polycystic kidney* + cephalocele + microcephaly + polydactyly.

Prognosis, survival, and quality of life. Trisomy 13 is a lethal condition in most cases, and 95% of the survivors die within 6 months. Very rare cases without severe malformations have survived for several years. However, severe psychomotor delay is constantly associated; most survivors are also blind, due to the frequent anophthalmia, and do not thrive. Epilepsy can also be associated.

Recurrence risk. This is empirically estimated to comprise 1% of all autosomal trisomies.

MoNoSo My x: TUr NEr SyNdro ME

Incidence. Relatively rare: 1/2500–5000 at birth.

Etiology. Monosomy of chromosome X (X0).

Ultrasound diagnosis. Hydrops; cystic hygroma; left heart defects (hypoplastic left heart and aortic coarctation); short femur; renal anomalies (horseshoe kidney).

Outcome. Mental retardation of variable degrees complicates 50% of cases.

Recurrence risk. Not modified in comparison with the normal population.

Definition This syndromic condition is named after H. H. Turner, who first described its clinical features in 1938 [9].

Etiology and pathogenesis. Turner syndrome is due to complete or partial chromosome X monosomy in all or some of the body cells. The missing chromosome is usually the paternal one. No apparent relationship with advancing maternal age has been described.

Genetics. Prenatal diagnosis is based on simple G-banding of chromosomes from chorionic villi, amniocytes, and peripheral leukocytes.

Ultrasound diagnosis. Major anomalies (Figure 10.7) are present in about 50% of cases detected in utero [9]:

- *Nonimmune hydrops fetalis (NIHF)*: showing early onset and involving all districts (Figure 10.7a);
- *Cystic hygroma*: evident on the *sagittal and axial views* of the fetal head (Figure 10.7b). The hygroma is usually large and predominantly septate. It can persist or disappear during the second trimester. In the latter instance, the classic pterygium colli is found at birth;
- *Hypoplastic left heart syndrome*: recognizable on the four-chamber view of the fetal heart (Figure 10.7c);

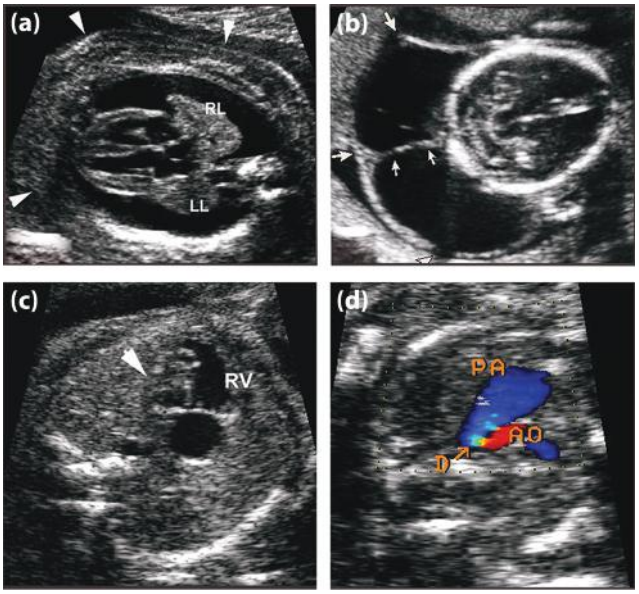


Figure 10.7 Turner syndrome. (a) Diffuse hydrops: four-chamber view showing bilateral hydrothorax (LL: left lung; RL: right lung) and severe subcutaneous edema (arrowheads) of the thorax. (b) Septate cystic hygroma (arrows). (c) Hypoplastic left heart syndrome: four-chamber view showing severe hypoplasia of the left ventricle (arrowhead) and mitral atresia. RV: right ventricle. (d) Aortic coarctation: three-vessel view showing severe hypoplasia of the aortic arch, which also shows reverse flow on color Doppler. Ao: aortic arch; D: arterial duct; PA: pulmonary artery.

- *Aortic coarctation*: directly recognizable on the *upper mediastinal three-vessel view* (Figure 10.7d).

Additional malformations that, if present, may support the US suspect of Turner syndrome are as follows:

- Renal anomalies: frequently represented by a horseshoe kidney, which, in some series, is associated in 40%–50% of cases;
- A short femur.

Differential diagnosis. An early cystic hygroma, detected at the end of the first trimester, can also be due to trisomy 21 or be of nonchromosomal origin. For small, septate hygromas, the possibility of *Noonan syndrome*, which cannot be diagnosed in utero, should also be considered. Since, in those cases in which the hygroma undergoes intrauterine regression, a pterygium is likely to remain, among the conditions to be differentiated from Turner syndrome is also the *multiple pterygium syndrome*.

Prognosis, survival, and quality of life. Most fetuses with Turner syndrome die in utero, often in the first or early second trimester. An additional group dies later due to generalized hydrops. Hence, only a minority of Turner syndrome fetuses reaches term of gestation. After birth, these females show short stature, pterygia, borderline mental retardation, and, later, amenorrhea from nonfunctioning streak gonads (primary hypogonadism). Survival is generally good, except for cases affected by hypoplastic left heart syndrome, which represents a life-threatening condition. Hearing problems are also present in a significant percentage of these women.

Recurrence risk. This is not modified in comparison with the normal population.

Triploidy

Incidence. Relatively rare: 1/2500–5000 at birth.

Etiology. An extra set of chromosomes is present (69).

Ultrasound diagnosis. Early-onset and very severe asymmetric FGR; hypotonia; CNS anomalies; congenital heart disease; syndactyly; vacuolar placenta (molar changes).

Outcome. Intrauterine demise in most cases.

Recurrence risk. Not modified in comparison with the normal population.

Definition Triploidy is due to an extra set of chromosomes of maternal or paternal origin. The incidence at birth is 1/2500–5000, and there is no relationship with advancing maternal age.

Etiology and pathogenesis. Of all triploidies, about two-thirds are 69,XXY and one-third are 69,XXX whereas in a very few cases the complement is 69,XYY. The overwhelming majority of triploidies undergo early spontaneous miscarriage.

Genetics. Prenatal diagnosis is feasible by G-banding of chromosomes from chorionic villi, amniocytes, and peripheral leukocytes.

Ultrasound diagnosis. Major anomalies are present in most cases of triploidy, but the malformative cluster differs according to the origin of the extra set of chromosomes: these differences are shown in Table 10.2. In addition, the recognition of these anomalies is often made more difficult by the frequent association of

Table 10.2 Triploidy: Breakdown by phenotype and origin of the extra set of chromosomes

Type	Provenance	FGR	Placenta	Maternal hCG
I	Paternal	Symmetric	Molar changes	High
II	Maternal	Asymmetric	Small	Unchanged

FGR: fetal growth restriction; hCG: human chorionic gonadotropin.

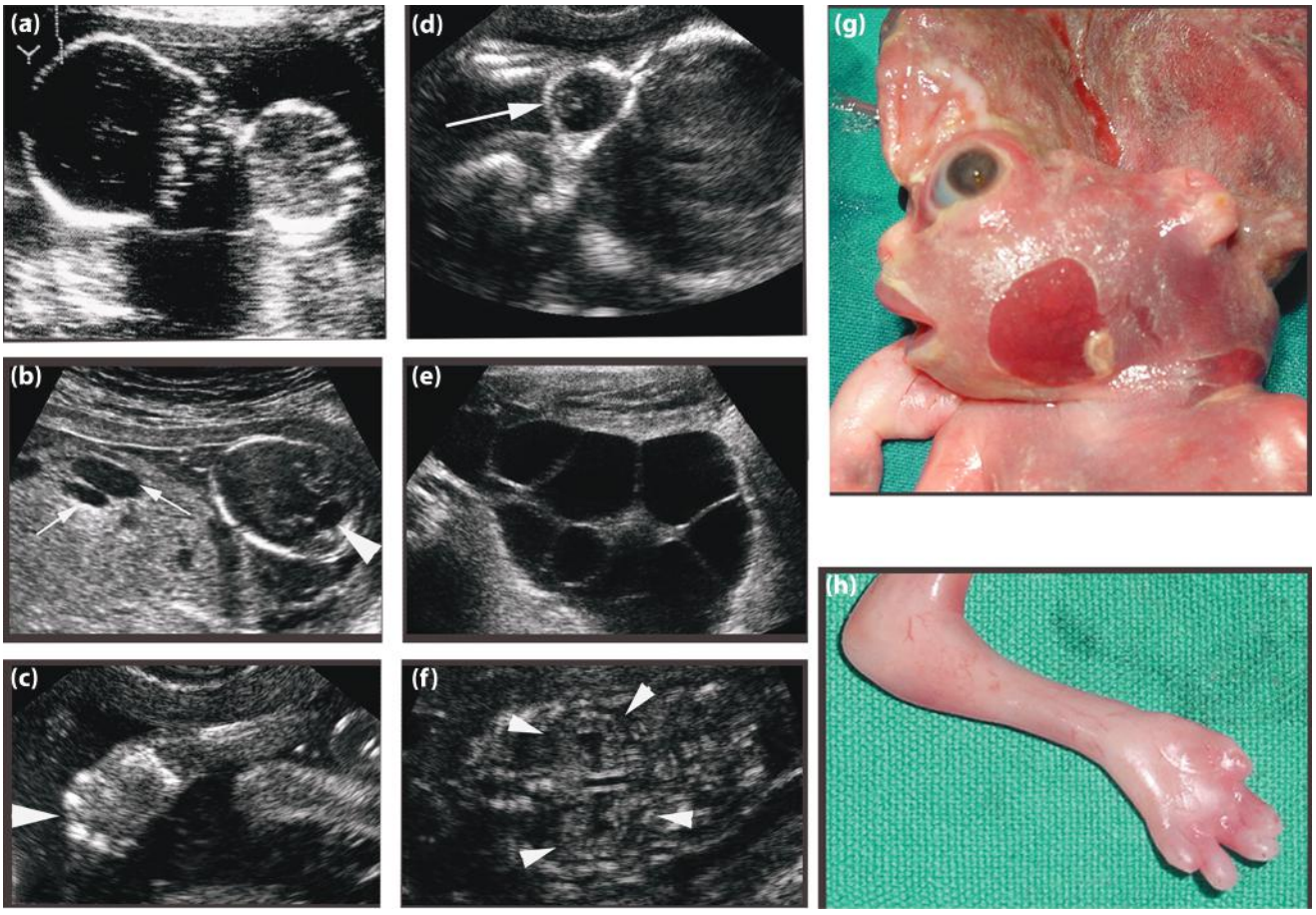


Figure 10.8 Triploidy. (a) FGR (triploidy type II). Early, severe growth retardation with generalized muscular hypotonia: often, the fetal head and the abdomen are visible on the same plane. Note the disproportion between head and abdomen, demonstrating the asymmetric type of FGR, and the ubiquitous oligohydramnios. (b) Dandy–Walker malformation (arrowhead), severe oligohydramnios, molar placenta (arrows) (triploidy type I). (c) Syndactyly: the single digits cannot be individually identified; compare with (h). (d) Macrophthalmus: a large orbit, the outline of which is outside the facial profile (pro-ophthalmus), is visible; compare with (g). (e) Ovarian hyperstimulation due to high titers of human chorionic gonadotropin (triploidy type I). (f) Cystic renal dysplasia, with parenchymal hyperechogenicity. The macerated specimen, after termination of pregnancy, demonstrates the macrophthalmos (g) and the syndactyly (h).

oligohydramnios. The most common anomalies detectable in triploidy are as follows:

- *FGR*: very early onset and severe. Characteristically asymmetric and associated with conspicuous generalized hypotonia and oligoamnios (Figure 10.8a);
- *CNS anomalies*: agenesis of the corpus callosum, hydrocephaly, Dandy–Walker variant (Figure 10.8b), and holoprosencephaly;
- *Syndactyly* (Figure 10.8c and h);
- *Craniofacial anomalies*: Micrognathia, microphthalmia, and macrophthalmia (Figure 10.8d);
- *Congenital heart disease*: VSD;
- *Renal anomalies*: cystic renal dysplasia (Figure 10.8f).

Differential diagnosis. This is virtually nonexistent, owing to the early onset and the peculiar cluster of anomalies. In rare cases, triploidy should be differentiated from other chromosomal anomalies featuring multiorgan involvement, such as trisomies 13 and 18.

Prognosis, survival, and quality of life. The overwhelming majority of cases die by the second trimester of pregnancy, and the rare cases reaching term survive for only a few hours after birth.

Recurrence risk. This is not modified in comparison with the normal population.

Microdeletion 22q11.2: diGeorge syndrome

Incidence. 1/4000–1/10,000 at birth (5%–7% of neonates with congenital heart disease).

Etiology. Microdeletion of variable extent in the locus 22q11. The deletion is recognizable in 15%–20% of cases on classic G-banded chromosomes; in most instances (80%–85%), a fluorescence in-situ hybridization (FISH) analysis is necessary. The phenotype can be due, much more rarely, to other defects such as monosomy 10p13 and deletion 18q21.33.

Ultrasound diagnosis. *Major anomalies*: conotruncal and aortic arch heart defects; thymus aplasia or hypoplasia; cleft palate; bifid uvula.

Outcome. Good survival. The most important determinants of survival are the type of heart defect and the association of T-cell immunodeficiency from thymus aplasia, associated in DiGeorge syndrome with parathyroid hypoplasia or aplasia (hypocalcemic tetany and seizures).

Recurrence risk. 50% if one of the parents is affected (5%–10% of all cases). Extremely low (<1%) in cases due to *de novo* deletions.

Definition The phenotype of the DiGeorge syndrome (OMIM 188400) was first described in 1965 by Angelo DiGeorge. In the 1990s, it was found that more than 90% of individuals diagnosed with the DiGeorge syndrome have a deletion or microdeletion of the long arm of chromosome 22 (locus 22q11.2). The same genetic defect also has been successively demonstrated in other conditions featuring craniofacial and cardiac defects, such as velocardiofacial syndrome and the conotruncal anomaly face. This is why today all of these phenotypes are considered as various expressions of the same genetic anomaly: 22q11 microdeletion.

Etiology and pathogenesis. The various phenotypes are due to microdeletions in the 22q11.2 locus. In over 80% of cases, a 3 Mb region between two repeated sequences (low copy repeats or LCRs) on chromosome 22 is deleted. The frequency of the defect is due to the fact that, because of the high homology, unequal crossing-over links occur during meiosis. The recent discovery of a rare microduplication 22q11.2 syndrome seems to confirm this pathogenetic mechanism. As mentioned in this chapter, the term "microdeletion 22q11.2 syndrome" encompasses different clinical entities, including *DiGeorge syndrome*, *Shprintzen* (*velo-cardio-facial*) *syndrome*, and *Takao* (*conotruncal anomaly face*) *syndrome*. In particular, the phenotypic expression of the 22q11.2 microdeletion is extremely variable, though in most cases, cardiac conotruncal defects, thymus hypoplasia or aplasia, parathyroid hypoplasia or aplasia, and anomalies of the palate are associated with minor craniofacial anomalies. All of these malformations involve anatomic structures developing from the third and the fourth pharyngeal arches. The underlying defect consists of an arrest in the development and migration of neural crest cells toward the pharyngeal arches [10].

Genetics. A deletion involving the locus q22.1 on chromosome 22 is present in over 90% of the cases. This lesion is rarely so large as to show up on G-banded chromosomes; this happens in only 15%–20% of cases. In most cases, to reveal the microdeletion, a FISH analysis is needed. Several manufacturers have been producing kits for FISH diagnosis of the 22q11 microdeletion (Vysis, Oncor, etc.). These kits are based on DNA probes for the locus that is usually deleted in this condition, 22q11.2. The commercial availability of these kits has allowed prenatal diagnosis of the 22q11 microdeletion. This test is now recommended in those fetuses in which a conotruncal anomaly is found [11,12]. In a very limited number of cases, the 22q11 microdeletion syndrome may be due to other chromosomal defects, such as a 10p13 monosomy or an 18q21.33 deletion. In these cases also, it has been speculated that genes involved in the neural cell migration process may be deleted. Finally, it is interesting to note that some teratogens (e.g., retinoic acid derivatives) and maternal insulin-dependent diabetes may induce a DiGeorge-like phenotype.

Ultrasound diagnosis. A significant number of the anomalies characterizing the DiGeorge syndrome and, in general, 22q11 microdeletion can be diagnosed by US:

- *Congenital heart disease of the conotruncal type (including interruption of the aortic arch type B)*: present in most cases of 22q11 microdeletion (Figures 10.9a and b), and detectable on outflow views [11,12];
- *Thymus hypoplasia or aplasia (Figure 10.9c; see also Chapter 6, Figures 6.32 and 6.33)*: always present in DiGeorge syndrome, and detectable on the *axial three-vessel view of the upper mediastinum* [11,13].

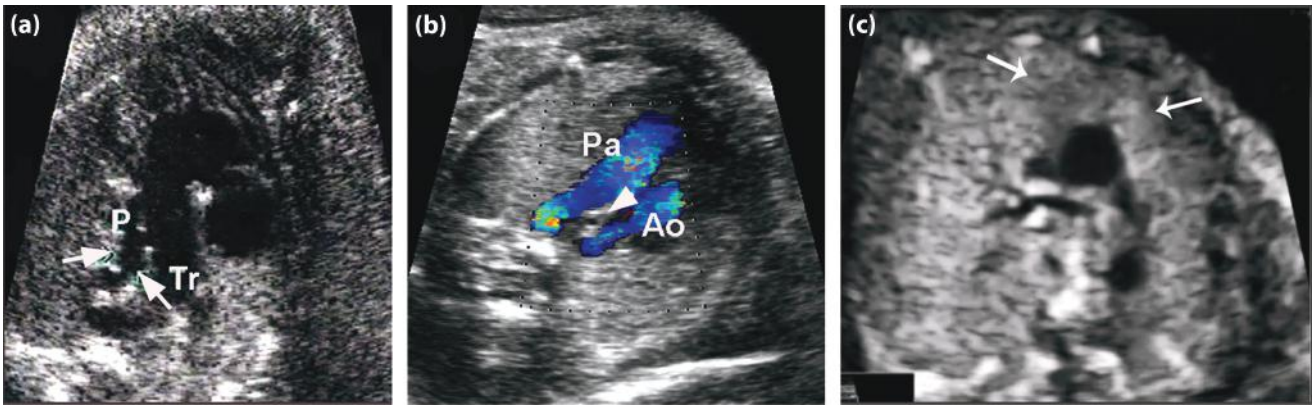


Figure 10.9 Microdeletion 22q11. Cardiovascular anomalies commonly associated with this deletion include particular conotruncal anomalies and also thymus hypoplasia or aplasia. (a) Common arterial trunk, type I: left outflow tract view showing the main pulmonary artery (P) with the branches (arrows) departing from the common arterial trunk (Tr). (b) Right aortic arch: color Doppler image of the three-vessel view showing the aortic arch located on the right of the trachea (arrowhead). In the normal left-sided arch, this is located on the left of the trachea. Ao: aortic arch; Pa: ductal arch. (c) Thymus hypoplasia at 36 weeks of gestation in a fetus with tetralogy of Fallot: a three-vessel view. Note the reduced volume of the thymus (arrows) in front of the great vessels.

Additional malformations that, if present, may support the US suspicion of 22q11 microdeletion syndrome are as follows:

- Renal anomalies: often represented by unilateral or bilateral hydronephrosis;
- Polyhydramnios;
- FGR.

Note that cleft palate, which usually involves the soft posterior palate, and minor facial dysmorphisms are not detectable in utero.

Prognosis, survival, and quality of life. The survival of individuals diagnosed with the 22q11 microdeletion depends on the phenotypic expression of the syndrome, on the severity of the associated conotruncal defect, and on the presence or absence of T-cell immunodeficiency due to thymus aplasia. Hence, if the phenotype is that of the classic DiGeorge syndrome, which also features primary hypoparathyroidism, the prognosis is guarded. As far as the quality of life and the long-term prognosis are concerned, the first issue to be considered is the fact that mental retardation of variable severity affects roughly 30% of cases and that its occurrence cannot be predicted in the fetus. This consists of borderline mental retardation (borderline IQ) in 50% of cases, mild mental retardation in 45%, and moderate or severe learning disabilities in the remaining 5% [10]. Hypocalcemic tetany and the consequent seizures may be avoided with careful supplementation.

APERT SYNDROME (OMIM 101200)

Incidence. Very rare: 1/70,000 at birth.

Etiology. Mutation of the *FGFR2* gene (98% of cases).

Ultrasound diagnosis. Turricephaly (due to synostoses) + brachysyndactyly; frontal bossing; hypertelorism; congenital heart disease; vertebral and renal anomalies.

Outcome. 50% risk of mental retardation. Motor disabilities due to the syndactyly, if particularly severe.

Recurrence risk. Extremely low. However, if one parent is affected, the transmission becomes autosomal dominant, with a 50% recurrence risk.

Definition *Apert syndrome* (OMIM 101200) is also defined as acrocephalosyndactyly to underscore the two major features of the condition: the early closure of the coronal suture, which is responsible for turricephaly,

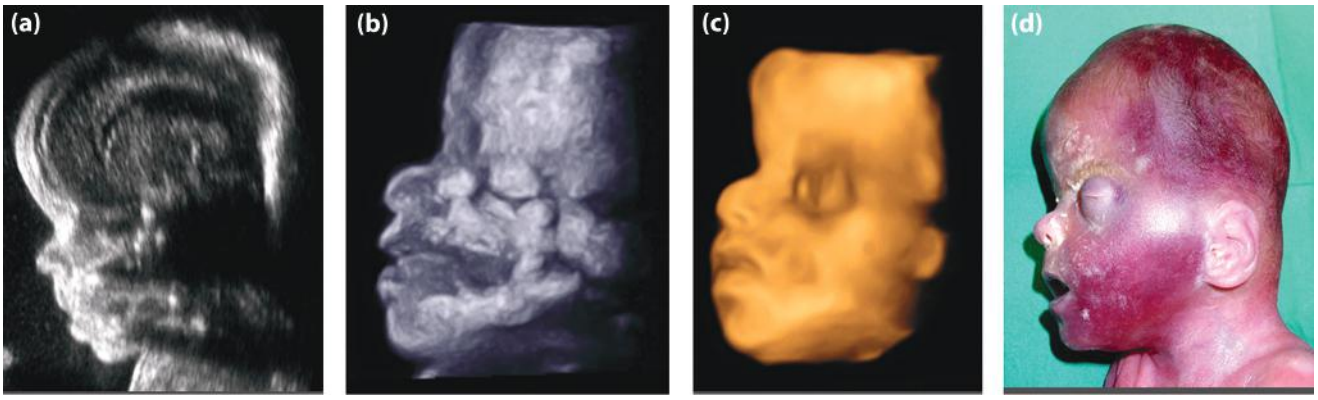


Figure 10.10 Apert syndrome: major signs. On the midsagittal view of the facial profile, the increased craniocaudal diameter of the skull (turricephaly), due to the closure of the coronal sutures, and the low nasal bridge are evident. (a) 2D imaging. (b) 3D maximum-mode image showing the sealed coronal suture (see Chapter 3 for suture abnormalities). (c) Three-dimensional surface mode image showing the characteristic features of Apert syndrome: turricephaly, low nasal bridge, and a tendency to macrophthalmia. (d) The specimen after termination of pregnancy.

hypertelorism, and frontal bossing, and the brachysyndactyly of variable severity. In addition, other major anomalies, such as congenital heart disease, fusion of the cervical vertebrae, and renal anomalies, are often associated.

Etiology and pathogenesis. One of two missense mutations of the gene coding for the fibroblast growth factor receptor 2 (*FGFR2*) is present in 98% of cases of Apert syndrome. It has been demonstrated that the pathogenetic mechanism involves an increase in the number of precursor cells entering the ostheogenic pathway, induced by the *FGFR2* mutations. This in turn leads ultimately to increased bone matrix formation and premature calvarial ossification in the fetus

Genetics. In families at risk, molecular diagnosis is feasible, through direct search for the above-mentioned mutations on DNA from chorionic villi.

Ultrasound diagnosis. Most of the anomalies characterizing Apert syndrome may be diagnosed in the fetus. The major malformations, the recognition of which leads to the diagnosis in most instances, are as follows:

- *Facial anomalies (turricephaly, depressed nasal bridge, and mandibular prognathism)*: these can be detected on the midsagittal view of the facial profile (Figure 10.10; see also Chapter 3) and on the coronal view of the face;
- *Brachysyndactyly of hands and feet*: this is usually evident and may be severe (Figure 10.11a,b and d–f);
- *Craniosynostosis of the coronal suture*: this can also be detected on two-dimensional (2D) imaging, by the indentation of the frontoparietal junction evident on the *axial transthalamic view* (Figure 10.11c and g). However, the use of three-dimensional (3D) US with the transparent maximum mode makes diagnosis of the premature closure of the coronal suture straightforward [14] (Figure 10.10b; see also Chapter 3). The early sealing of the coronal suture has a secondary effect on the ossification of the metopic one, which is significantly delayed. This phenomenon is easily assessed with 3D US, which demonstrates an abnormal "U"-shaped appearance of the metopic suture due to delayed ossification [14] (see also Chapter 3, Figure 3.58c).

Additional malformations that, if present, may support the US suspicion of Apert syndrome are as follows:

- Congenital heart disease (10% of cases) (Figure 10.12a and b): VSD in particular (Figure 10.12a);
- Fusion of cervical vertebrae (C5–C6) (Figure 10.12c);
- Renal anomalies (Figure 10.12d).

Differential diagnosis. This includes all other clinical conditions that are characterized by cranial synostoses and are due to the same missense mutations of the *FBGR2* gene, such as Carpenter, Pfeiffer, and Crouzon syndromes (in some circumstances, it is impossible to reach a definite diagnosis by US)

- *Carpenter syndrome (OMIM 201000) [7]*: look for ► *craniosynostosis* + polysyndactyly + congenital heart disease (50%);
- *Pfeiffer syndrome (OMIM 101600) [7]:* look for ► *craniosynostosis* + hypertelorism + syndactyly;
- *Crouzon syndrome (OMIM 123500) [7]:* look for ► *craniosynostosis* + maxillary hypoplasia (nonsyndactyly).

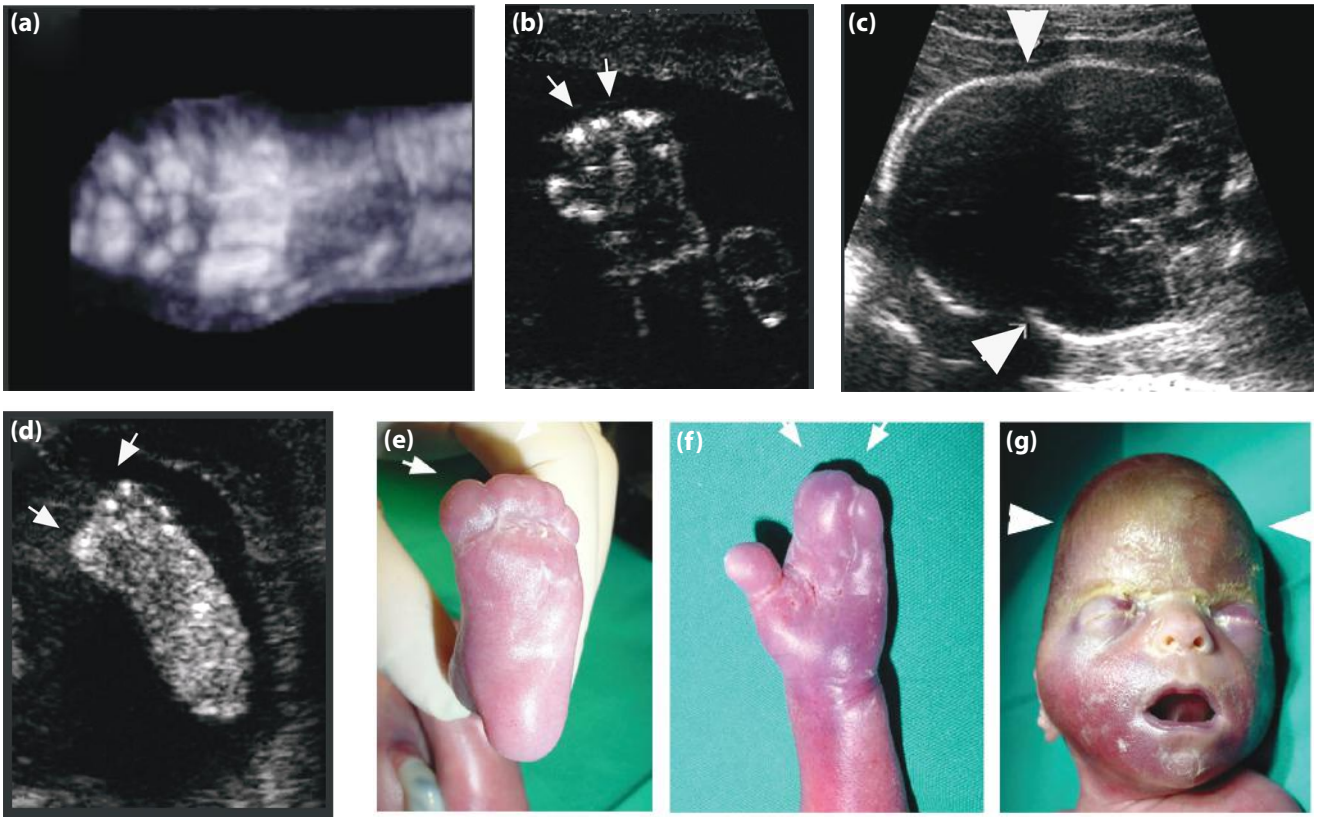


Figure 10.11 Apert syndrome: major signs. (a) 3D maximum-mode image showing syndactyly of one hand. Note the abnormal metacarpal and phalangeal bones. This image is much more informative than the 2D one (b), in which only a few of the bones can be imaged, being in different planes (arrows). With the 3D technique, it is also possible to display thicker slices, and this leads to clearer evidence of the syndactyly. (c) The closure of the coronal suture can also be detected in some cases on the 2D axial transthalamic view: the indentation at the level of the coronal suture (arrowheads) and the absence of the normal sonolucent gap between the frontal and the parietal bones are seen. (d) Syndactyly of one foot on 2D ultrasound (arrows). The external inspection of the specimen, after termination of pregnancy, demonstrates oligosyndactyly of foot (e) and hand (f), and (g) acrocephaly, due to early sealing of the coronal sutures (arrowheads).

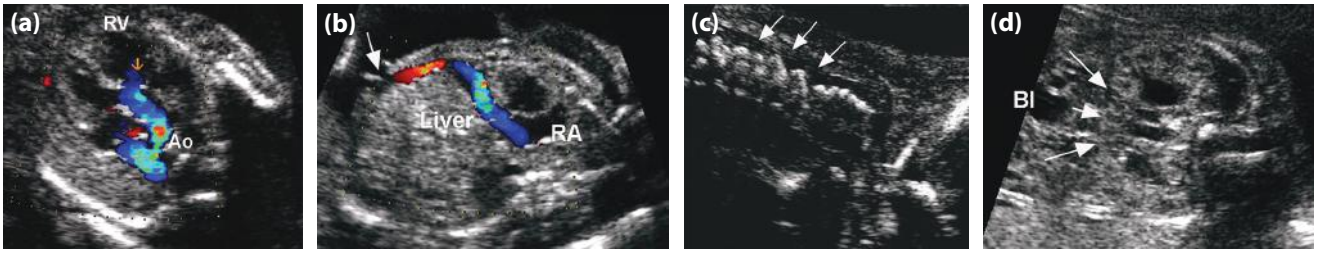


Figure 10.12 Apert syndrome: additional signs. (a) Congenital heart disease: malalignment VSD with an overriding aorta (Ao). RV: right ventricle. (b) Abnormal venous return: the ductus venosus is absent, and the umbilical vein (arrow) drains directly into the right atrium (RA) via a collector coursing on the anterior surface of the liver. (c) Fusion of the cervical vertebrae: on the midsagittal view of the spine, the spinous processes are abnormal and fused (arrows). (d) Renal anomalies: on the coronal view of the abdomen, a horseshoe kidney is found (arrows); mild pyelectasia was associated. Bl: bladder.

Prognosis, survival, and quality of life. Individuals with Apert syndrome face a 50% risk of mental retardation. Long-term sequelae also include respiratory problems due to obstruction of the high airways, which may be so severe as to require tracheotomy. Difficulties in the use of the hands may be associated if the syndactyly is severe. Cosmetic surgery is employed in cases characterized by major facial dysmorphisms.

Recurrence risk. Most cases occur sporadically, being due to *de novo* mutations, and thus the recurrence rate is extremely low. However, if one parent is affected, the transmission shows an autosomal dominant inheritance pattern, with a recurrence rate of 50%.

Beckwith–Wiedemann syndrome (OMIM 130650)

Incidence. 1/14,000.

Etiology. Structural anomalies of chromosome 11p15 (duplications, inversions). Uniparental disomy (20%). Mutations of the genes *CDKN1C* and *IGF2*. Mutations of the gene *NSD1* at 5q35.

Ultrasound diagnosis. Exomphalos; macroglossia; gigantism; polycystic kidneys; genital anomalies.

Outcome. Twenty-one percent perinatal mortality rate (preterm delivery and hypoglycemia are common); overgrowth during infancy; tendency to develop embryonal neoplasia (7%). If neonatal asphyxia due to macroglossia is prevented, the intelligence is normal.

Recurrence risk. The empiric risk, in cases with no family history, is 1%–2%. In the 15% of familial cases, the transmission is autosomal dominant with incomplete penetrance (50%).

Definition *Beckwith–Wiedemann syndrome* (BWS) (OMIM 130650) is the most common congenital disorder characterized by neonatal overgrowth and gigantism. Its most common features are macroglossia (98%), prenatal and postnatal gigantism (>90th centile) (87%), abdominal wall defects (exomphalos and diastasis recti: 77%), external ear anomalies (75%), and visceromegaly (62%). In 7% of cases, embryonal tumors may arise (Wilms' tumor, hepatoblastoma, and adrenal carcinoma).

Etiology and pathogenesis. BWS is due to genetic anomalies in chromosome 11p15. Several genes with a role in growth control are located in this region; their imbalance determines the overgrowth and the gigantism characteristic of BWS. There are three mechanisms that may cause BWS in sporadic cases: (1) chromosomal anomalies involving the 11p15 region (duplications, unbalanced translocations, and inversions; 2% of cases); (2) single-gene mutations (so-called BWS genes), for example mutations of the cyclin-dependent kinase inhibitor gene *CDKN1C*, loss of imprinting and overexpression of gene-encoding insulin-like growth factor type 2 (*IGF-2*), and methylation and silencing of the *H19* gene (5%); and (3) uniparental disomy 11p15 (20%). In some cases (2%–3%), mutations of the *NSD1* gene, mapping to 5q35, have been found; it seems that this gene controls the imprinting of the region 11p15. Familial cases (15%) are transmitted with an autosomal dominant pattern with incomplete penetrance. Genetic heterogeneity has also been found in these cases: 40% of them are due to mutations of the *CDKN1C* gene.

Genetics. Prenatal diagnosis of BWS is feasible only in those cases in which the molecular defect is known. In this regard, some genotypic–phenotypic correlations should be considered:

- *CDKN1C* gene mutations and occurrence of exomphalos;
- Uniparental disomy and defects of BWS genes and absence of exomphalos.

No correlations have been found with the tendency to develop embryonal tumors, although Wilms' tumor has been found only in patients with uniparental disomy and/or BWS gene defects.

Ultrasound diagnosis. The phenotypic expression of BWS varies significantl , and this—together with the

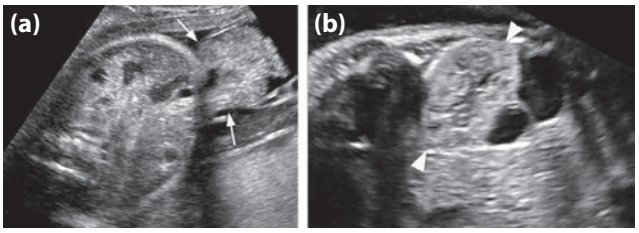


Figure 10.13 Beckwith–Wiedemann syndrome. (a) Omphalocele: the arrows point to the abdominal defect; characteristically, only bowel loops (and not the liver) have herniated. (b) Overgrown and hyperechoic kidneys (arrowheads).

genetic heterogeneity—limits the prenatal detection rate. Cases in which major abnormalities or organ overgrowth are present are those in which the diagnosis of BWS can be hypothesized prenatally [15]. Major malformations, the recognition of which leads to the diagnosis in most instances, are as follows:

- *Exomphalos* (Figure 10.13a), usually without the liver; in the case of a normal karyotype, this is the main sign that may lead to a prenatal diagnosis of BWS;
- Visceromegaly;
- Macroglossia (Figure 10.14) [15];
- Gigantism (better appreciated in the third trimester).

Additional malformations that, if present, may support the US suspicion of BWS are as follows:

- *Polyhydramnios* (usually in the third trimester);
- *Renal anomalies* (polycystic or hyperechoic kidneys: Figure 10.13b).

Differential diagnosis (Table 10.3). This should include all overgrowth syndromes, primarily those that can be hypothesized prenatally [16]:

- *Perlman syndrome (OMIM 267000)*: look for ► *visceromegaly* + gigantism + diaphragmatic hernia + micrognathia + cystic hygroma;
- *Simpson–Golabi–Behmel syndrome (OMIM 312870)*: look for ► *visceromegaly, omphalocele* + cystic hygroma + diaphragmatic hernia + enlarged or cystic kidneys + agenesis of the corpus callosum + Dandy–Walker malformation;
- *Sotos syndrome (OMIM 117550):* look for ► *macrocephaly* + brain anomalies (agenesis of corpus callosum and Dandy–Walker malformation) + coronary heart disease (CHD) (ventricular septal defects);

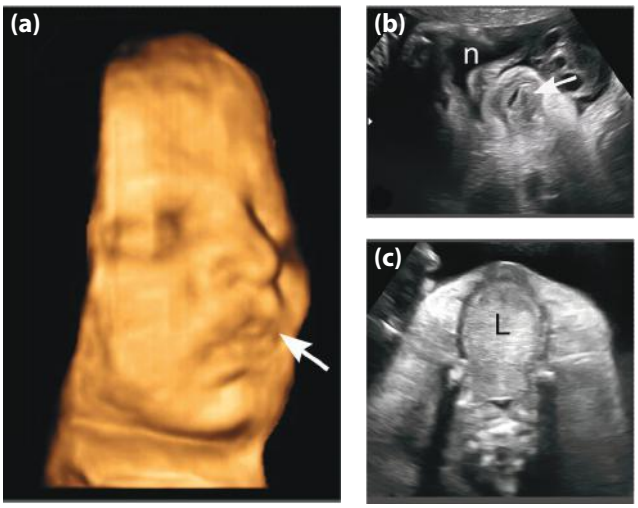


Figure 10.14 Beckwith–Wiedemann syndrome. Macroglossia (arrow) represents a more subtle and late onset sign. (a) A three-dimensional surface-rendering image; (b) two-dimensional oblique view of the lips (n: nose); and (c) axial view of the tongue.

- *Zellweger syndrome (OMIM 214100)*: look for ► *visceromegaly* + brain anomalies (agenesis of corpus callosum and migration anomalies), micrognathia + cataract + talipes + macrosomia.

In Figure 10.15 [16], a diagnostic flowchart aiming at differentiating the syndromic conditions characterized by overgrowth, some of which are described here, is shown. Finally, BWS should also be differentiated from Down syndrome, considering that exomphalos, hyperechoic (but not enlarged) kidneys, and moderate macroglossia may also be present in trisomy 21. However, a karyotype solves this simple diagnostic doubt.

Prognosis, survival, and quality of life. Fetal overgrowth and the risk of hypoglycemia may induce preterm delivery and perinatal complications, which are responsible for the 21% neonatal mortality rate. Overgrowth is associated with accelerated bone maturation, but this overgrowth is no longer evident in adulthood. The advantage of a prenatal diagnosis of BWS lies in the prevention of premature birth, hypoglycemic complications, and cerebral asphyxia due to macroglossia. At the same time, it allows one to determine an appropriate follow-up protocol aiming at early discovery of possible embryonal tumors, which arise in 7% of cases [17]. As mentioned under "Outcome" of this section, intelligence is normal.

Table 10.3 Differential diagnosis of genetic overgrowth syndromes

Syndrome	Gene location	Inheritance	Possible sonographic finding	Other aids to diagnosis
Beckwith–Wiedemann	11p15	Sporadic in 85% of cases; may also be AD, from UPD and ID	Macrosomia, polyhydramnios, omphalocele, enlarged tongue, enlarged echogenic kidneys, placentomegaly	<1% of BWS have cytogenetically detectable abnormalities; examination of parents by clinical geneticist
Pallister–Killian	Tetrasomy 12p	Sporadic	Rhizomelic micromelia, CHD, CDH, enlarged polyhydramnios, NT, facial abnormalities (small nose)	Karyotype + FISH probes for 12p
Sotos	*NSD1* on 5q35	Sporadic in 95% of cases	Macrocephaly, ventriculomegaly	Karyotype, FISH for 5q35, *NSD1* sequencing
Perlman	Unknown	AR	Polyhydramnios, macrosomia, visceromegaly, enlarged echogenic kidneys, cystic hygroma	None
Simpson–Golabi–Behmel	*GPC3* on Xp26	X-linked recessive	Polyhydramnios, omphalocele, cystic hygroma, CDH, enlarged or cystic kidneys, brain anomalies (ACC, DWM), macrosomia, placentomegaly	Elevated MSAFP level: examination of mother by clinical geneticist; determine fetal gender, GPC3 sequencing

Source: Modified from Vora N, Bianchi D, *Prenat Diagn* 29, 923–9, 2009.
ACC: agenesis of corpus callosum; AD: autosomal dominant; AR: autosomal recessive; BWS: Beckwith–Wiedemann syndrome; CDH: congenital diaphragmatic hernia; CHD: congenital heart disease; DWM: Dandy–Walker malformation; FISH: fluorescent *in-situ* hybridization; ID: imprinting defects; MSAFP: maternal serum alpha-fetoprotein; NT: nuchal translucency; UPD: uniparental disomy.

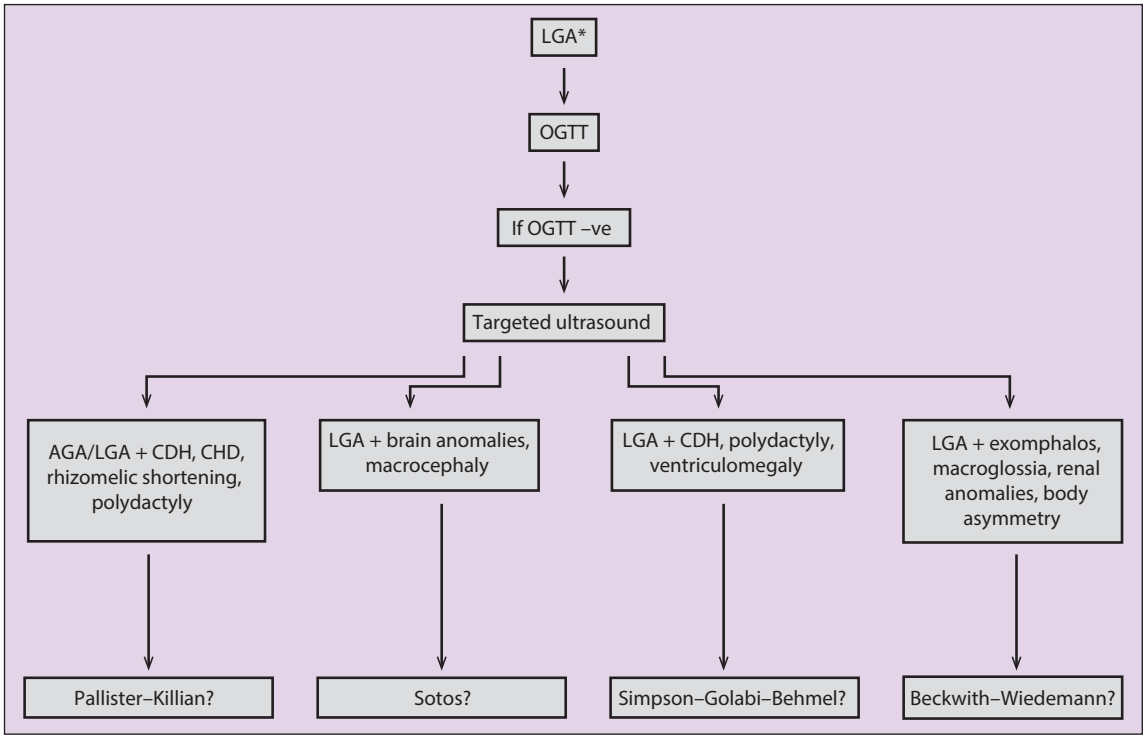


Figure 10.15 Diagnostic flowchart of the fetus with overgrowth and congenital anomalies. * >90° centile; AGA: adequate for gestational age; CDH: congenital diaphragmatic hernia; CHD: congenital heart disease; LGA: large for gestational age; OGTT: oral glucose tolerance test. (Modified from Vora N, Bianchi D, *Prenat Diagn* 29, 923–9, 2009.)

BINdEr syNdro ME (oMIM 155050)

Incidence. Rare.

Etiology. Hetereogeneous disorder due to different causes, from vitamin K deficiency to chondrodysplasia punctata.

Ultrasound diagnosis. Flat profile, vertical barely visible nose, increased maxillary convexity. Possibly associated signs of chondrodysplasia punctata (stippled epiphyses).

Outcome. 20% infant mortality rate. Mild to moderate developmental delay in 60% of cases; severe in 5%–8%.

Recurrence risk. Autosomal dominant or multifactorial.

Definition Binder syndrome (OMIM 155050) is a rare disorder also called maxillo-nasal dysplasia. It is characterized by midfacial hypoplasia with absence of the *spina nasalis*. This leads to the typical phenotypic feature represented by a small vertical nose with a flat nasal bridge, short columella, and acute naso-labial angle; the upper lip is convex, and there is a tendency to class III malocclusion [18]. It can occur as an isolated anomaly or be associated with various types of chondrodysplasia punctata, metabolic abnormalities, or vitamin K deficienc (warfarin syndrome).

Etiology and pathogenesis. These are uncertain; some isolated cases represent developmental anomaly of the maxilla and the nasal complex, whereas others may be part of metabolic diseases involving the bone metabolism.

Genetics. Due to the genetic heterogeneity, there is no candidate gene to be employed in prenatal diagnosis.

Ultrasound diagnosis. The diagnosis is made on the *mid-sagittal view of the profil* : a small, vertical nose is barely visible, with an acute naso-labial angle (Figure 10.16). When this diagnosis is made, care should be taken in assessing the long bones longitudinally, aiming at the

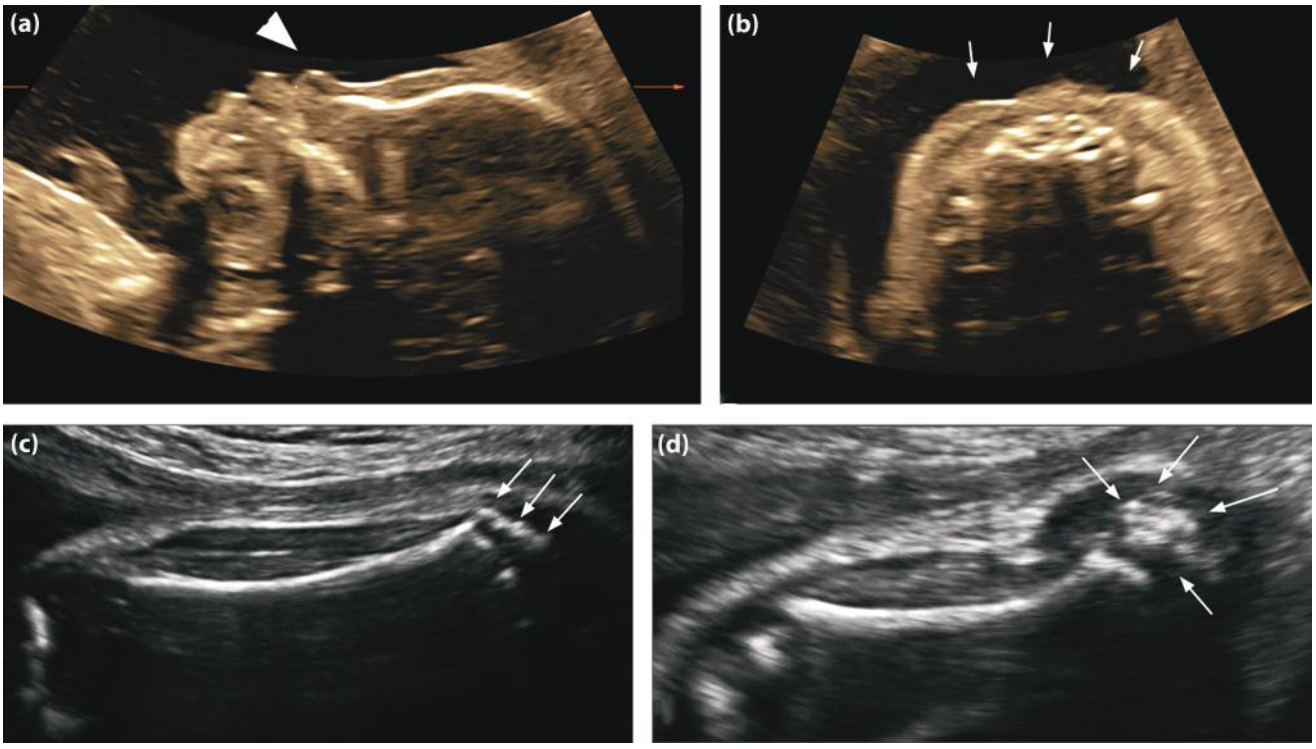


Figure 10.16 Binder syndrome (24 weeks of gestation). (a) A flat facial profile, with the small, vertical nose (arrowhead) typical of this condition; (b) flatness of the premaxillary curve (arrows); (c) stippled femoral epiphysis (arrows); and (d) stippled humeral epiphysis (arrows).

detection of signs of an underlying X-linked chondrodysplasia punctata (see Chapter 9), such as stippled epiphyses (Figure 10.16 c,d) [21], brain anomalies, or micrognathia. Also, considering the association with vitamin K deficiency (fetal warfarin syndrome) [19], the possible presence of other major malformations often seen in this condition should be evaluated (cerebral malformations, congenital cataract, and congenital heart disease), because stippled epiphyses also may be present in the latter condition.

Differential diagnosis. This includes Down syndrome, because a flat profile with a small nose is present also in trisomy 21 (see Chapter 3). However, in the latter it is associated in most cases with hypoplastic nasal bones, whereas in Binder syndrome the nasal bones are relatively normal (or only slightly hypoplastic), only verticalized, and it is the *spina nasalis* that is absent. Should any doubt persist, a simple karyotype may solve the issue. Note that a few true cases of Binder phenotype have been found associated with Down syndrome [19,20].

Obstetric management. An interview to the mother should be conducted to ascertain whether there might have been exposure to warfarin in the embryonic period. Recently, it has also been suggested that incoercible maternal vomiting in pregnancy or malabsorption from untreated celiac disease or short bowel syndrome may determine vitamin K deficiency [19]. The same authors [19] suggest vitamin K supplementation in early pregnancy in case of incoercible maternal vomiting. It should be considered that phenytoin exposure, maternal alcoholism, and maternal autoimmune diseases also may create a vitamin K deficienc status.

Prognosis, survival, and quality of life. The prognosis of Binder syndrome depends on the final diagnosis. If it represents an isolated condition, the outcome may be normal; however, both in cases of type 1 rhizomelic chondrodysplasia punctata and in cases of the X-linked recessive type, the outcome is poor, with a high risk of mortality by the age of 2 and of mental retardation, in addition to significant skeletal problems

cAT-EyE syNdro ME (cEs; oMIM 115470)

Incidence. Rare.

Etiology. Presence of a marker extra chromosome: inv/dup (22).

Ultrasound diagnosis. CHD (60%) (mainly abnormal pulmonary return), urogenital (70%), gastrointestinal, and facial (pre-auricular tags in >80%) anomalies.

Outcome. Twenty percent infant mortality rate. Mild to moderate developmental delay in 60% of cases; severe in 5%–8%.

Recurrence risk. Extremely low in cases with no family history. If one parent is affected, the recurrence risk becomes 50%, but the reproductive function of the affected individuals is severely compromised.

Definition CES (OMIM 115470) is a rare disorder with variable expression characterized by five types of anomalies: (A) pre-auricular tags, (B) anorectal malformations, (C) urogenital malformations, (D) ocular colobomas, and (E) congenital heart disease.

Etiology and pathogenesis. CES is due to the presence of a supernumerary bisatellited chromosome, resulting from an inversion or duplication of the regions 22q11.1 and 22q11.21 (inv/dup(22)). According to the break point, two types of CES have been identified (CES I and II). No correlation has been found between the subtype of CES and the phenotypic expression.

Genetics. The original genetic defect was identified for the first time in 1965 and thoroughly described in 1981. Prenatal diagnosis of CES is feasible on fetal cells harvested with chorionic villus sampling (CVS), amniocentesis, or cordocentesis. A FISH analysis with probes specific for chromosome 22 is needed for the final diagnosis

Ultrasound diagnosis. Only a few of the numerous malformations characterizing CES are recognizable at

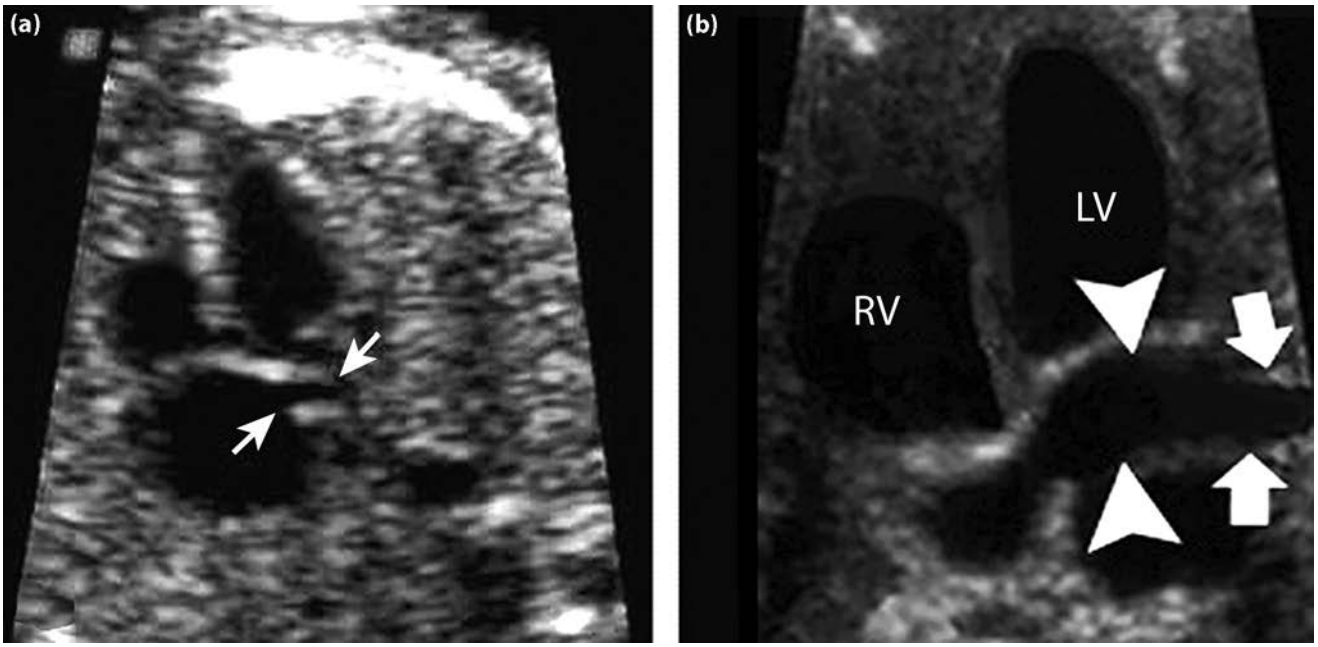


Figure 10.17 Cat-eye syndrome. Partial abnormal pulmonary venous return. (a) Normal size of the coronary sinus (arrows). (b) Abnormal drainage of one pulmonary vein (arrows) into the coronary sinus, which is consequently dilated (arrowheads). (Modified from Volpe P et al., *Ultrasound Obstet Gynecol* 24, 485–7, 2004.)

midtrimester US. The major malformations, the recognition of which leads to the diagnosis in most cases, are as follows [21]:

- Congenital heart disease (Figure 10.17), in particular abnormal pulmonary venous return. It should be underlined that the prospective diagnosis of this anomaly requires a highly experienced fetal cardiologist, an optimal acoustic window, and a favorable fetal lie;
- Anorectal atresia; this is not always diagnosable prenatally;
- Pre-auricular tags (Figure 10.18); these can be more easily recognized on 3D US (see also Chapter 3, Figure 3.53);
- Urogenital anomalies.

Differential diagnosis. The association of pre-auricular tags and abnormal pulmonary venous return is typical of CES. However, in most cases, the diagnosis is made as an incidental finding during karyotyping performed for other indications.

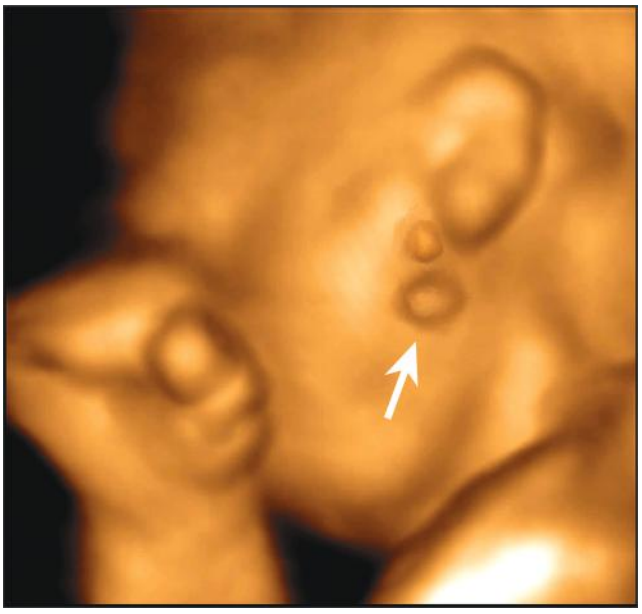


Figure 10.18 Cat-eye syndrome. 3D rendering of the lateral aspect of the fetal face, showing two pre-auricular tags (arrow). (Modified from Volpe P et al., *Ultrasound Obstet Gynecol* 24, 485–7, 2004.)

Prognosis, survival, and quality of life. CES has an infant mortality rate of 20%, mainly due to cardiac failure and recurrent infections. Mental retardation occurs in 50% of cases and is severe in 5%–8% of the cases only. In cases with no family history, the recurrence risk is extremely low. However, if one parent is affected, the risk becomes 50%, although the reproductive function of the affected individuals is severely compromised.

Cornelia De Lange Syndrome (OMIM 122470 and D 608667)

Incidence. Extremely rare.

Etiology. Mutations of the NIPBL gene have been found in 50%–60% of the cases.

Ultrasound diagnosis. Intrauterine growth restriction (IUGR), polyhydramnios, upper limb anomalies (radial aplasia and oligosyndactyly), micrognathia, prefrontal edema, synorphrys. Less often: diaphragmatic hernia.

Outcome. Poor. Severe mental retardation in most cases. Hearing loss.

Recurrence risk. Sporadic.

Definition Cornelia de Lange syndrome (also called Brachmann–de Lange syndrome) (OMIM 122470) is a multisystem malformation syndrome. The major diagnostic features are not detectable at US: typical facies with low anterior hairline, arched eyebrows, synophrys, anteverted nares, prognathism, long filtrum, thin lips, and "carp" mouth. Hypertrichosis leads to one of the typical facial signs, the two eyebrows meeting on the midline, at the level of the base of the nose (synorphrys).

Etiology and pathogenesis. A mutation in the NIPBL gene, located at 5p13.2, which encodes components of the cohesion complex has been found in 50%–60% of the cases. A remaining 5%–10% present other mutations that are always related to the cohesin complex but located elsewhere (they are X-linked, but their etiology is unknown).

Genetics. Prenatal genetic diagnosis is theoretically possible, but it has not yet been reported, possibly due to the extremely variable phenotype.

Ultrasound diagnosis. The main facial features, which represent the basis for the diagnosis of the syndrome postnatally, are not promptly recognizable in utero, despite 3D US, also because most of them would be late onset. Hence, the prospective diagnosis of Cornelia de Lange syndrome in a fetus should rely on the recognition of other abnormalities, the most common of which are listed here (Figures 10.19 and 10.20):

- IUGR with polyhydramnios, which represents an unusual and alarming sign;
- Prefrontal edema; this aspecific finding is detected on the *midsagittal view of the fetal profile* (Figure 10.19a through c);
- Micrognathia; detected on the midsagittal view of the fetal profile (Figure 10.19b);
- Congenital diaphragmatic hernia;
- Congenital heart disease;
- Micromelia, oligosyndactyly, and clinodactyly (Figure 10.19d and e).

In addition, only if: [1] other major anomalies are already present and consistent with a possible diagnosis of Cornelia de Lange syndrome, and [2] the examination is carried out in the advanced second trimester (>21–22 weeks), then additional facial signs of the syndrome may be searched, with the help of 3D imaging:

- Anteverted nares with a long philtrum (Figure 10.19a through c);
- Early appearance of eyebrows or long eyelashes (Figures 10.19b,c and 10.20).

Differential diagnosis. The main differential diagnosis is with trisomy 13 and 18, because growth restriction, oligosyndactyly, radial aplasia, clinodactyly, micrognathia, diaphragmatic hernia, and heart defects may occur in all three conditions. However, a karyotype will easily rule out the other two options. Other much rarer conditions that should be considered are Holt–Oram syndrome, Fanconi anemia, and thrombocytopenia-absent radius (TAR) syndrome, due to the presence of radial aplasia in all. In these cases, the family history will help, because these conditions are inherited with an autosomal dominant (Holt–Oram) or recessive (Fanconi and TAR) trait [22].

Prognosis, survival, and quality of life. Survival may be long, but growth is severely impaired also after birth, also because these neonates fail to thrive. Furthermore, the large majority of individuals with Cornelia de Lange syndrome suffer from severe neurodevelopmental delay.

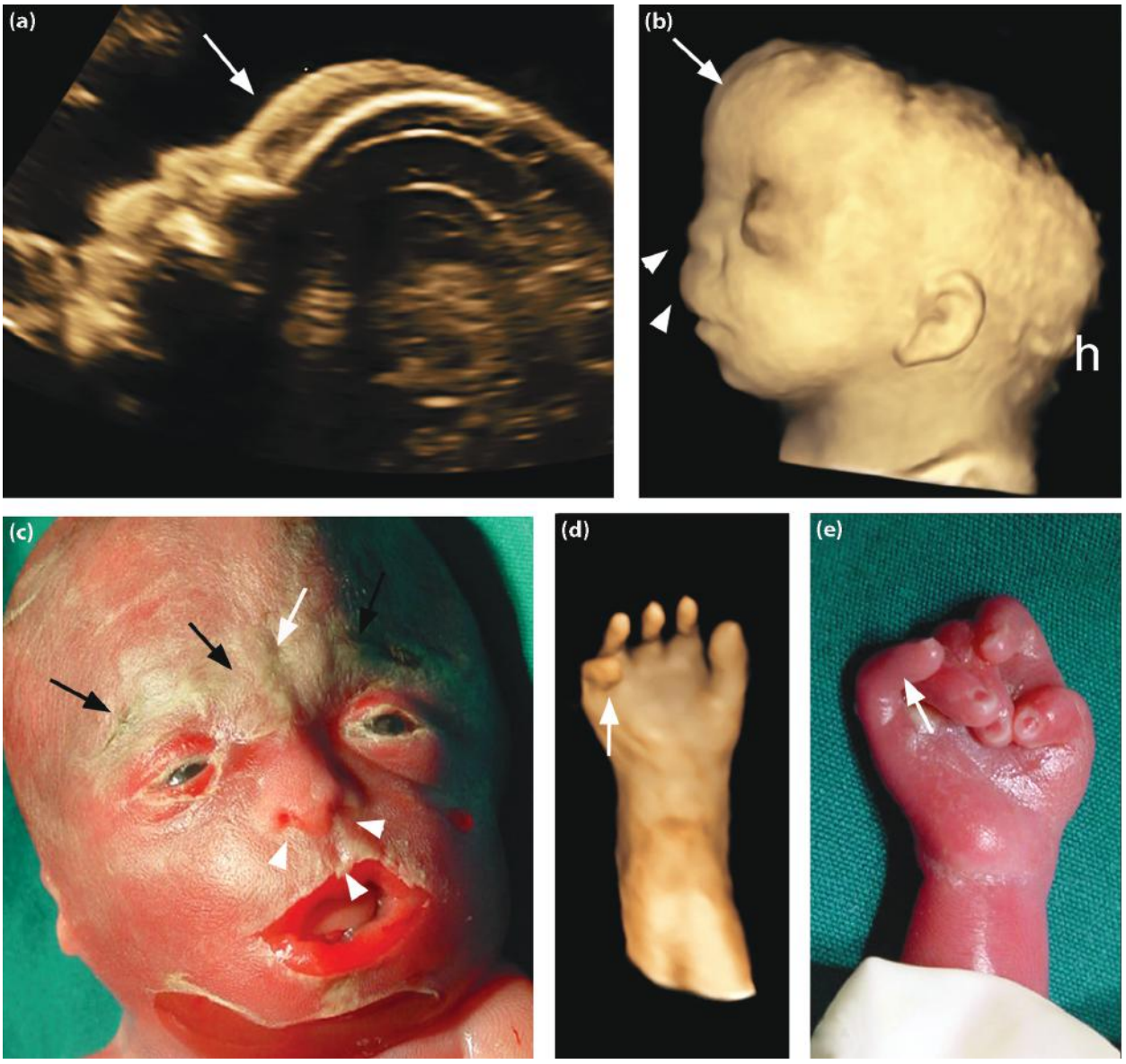


Figure 10.19 Cornelia de Lange syndrome (22 weeks of hair gestation). (a) Midsagittal 2D imaging showing prefrontal edema; (b) a 3D surface rendering of the face showing the long philtrum and the anteverted nares (arrowheads); with the ridge corresponding to the prefrontal edema of (a) and (c); moderate micrognathia; hairs (h) on the occipital bone (absent in normal cases at this gestational age). (c) The specimen after termination of pregnancy; arrows and arrowheads as in (a) and (b). The black arrows point to the early presence of eyebrows already meeting in the midline (synophrys). (d) A 3D surface-rendering image of clinodactyly (arrow); and (e) autoptic confirmation (arrow).

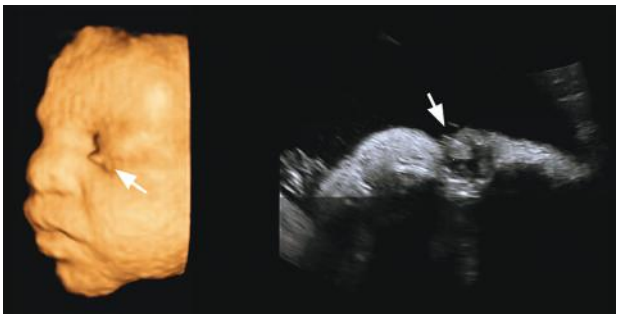


Figure 10.20 Cornelia de Lange syndrome (27 weeks of gestation). Another case in which long eyelashes (arrow) were evident at 27 weeks. (Left) 3D ultrasound; and (right) 2D ultrasound.

Femoral hypoplasia/unusual facies syndrome (FHUFS; OMIM 134780)

Incidence. Extremely rare.

Etiology. Unknown. The syndrome is often associated with maternal insulin-dependent diabetes mellitus.

Ultrasound diagnosis. Focal femoral hypoplasia, uni- or bilateral, possibly associated with fibular hypoplasia; micrognathia; cleft lip and palate; and mandibular asymmetry.

Outcome. Normal survival and intelligence. Motor disabilities due to the femoral hypoplasia.

Recurrence risk. Sporadic.

Definition The definition of FHUFS (OMIM 134780) is based upon two major signs: focal femoral hypoplasia and the characteristic unusual face, characterized by a small nose, possible cleft lip and palate, and micrognathia. FHUFS was described for the first time in 1975. It is also called *femoral-facial syndrome*.

Etiology and pathogenesis. The etiology is unknown. However, a significant association with maternal insulin-dependent diabetes mellitus has been reported.

Genetics. Prenatal genetic diagnosis is not possible, since the involved gene(s) are unknown.

Ultrasound diagnosis (Figures 10.21 and 10.22). The two main features, both of which can be recognized on US, are as follows [23,24]:

- *Micrognathia*: this is detected on the midsagittal view of the fetal profile (Figure 10.21a and b);
- *Focal femoral hypoplasia*: this is of variable degree, uni- or bilateral; sometimes it is associated with fibular hypoplasia (Figures 10.21c–e and 10.22c,d).

Additional findings include the following:

- *Cleft lip and palate*: inconstantly associated (Figure 10.22a and b);
- *Mandibular asymmetry*: very difficult to detect.

If the femoral hypoplasia is found in association with one of the other features reported above, the diagnosis of FHUFS is virtually certain. This unusual syndromic association can also be detected in the first trimester, considering that the degree of femoral hypoplasia is significant [23,24].

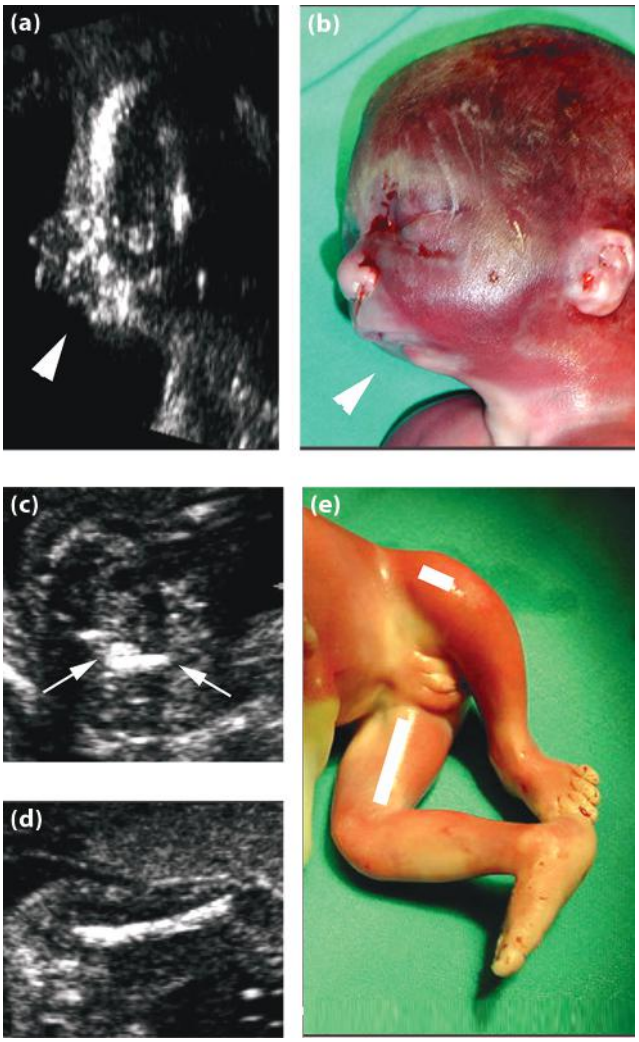


Figure 10.21 Femoral hypoplasia/unusual facies syndrome (21 weeks of gestation). (a) Severe micrognathia (arrow). (b) Confirmation, at autopsy, showing also the long philtrum and the thin upper lips, which are typical features of this syndrome. (c) Focal femoral hypoplasia (arrows). (d) The contralateral femur, showing normal length. (e) Confirmation at autopsy: the white bars indicate the size and position of the femurs.

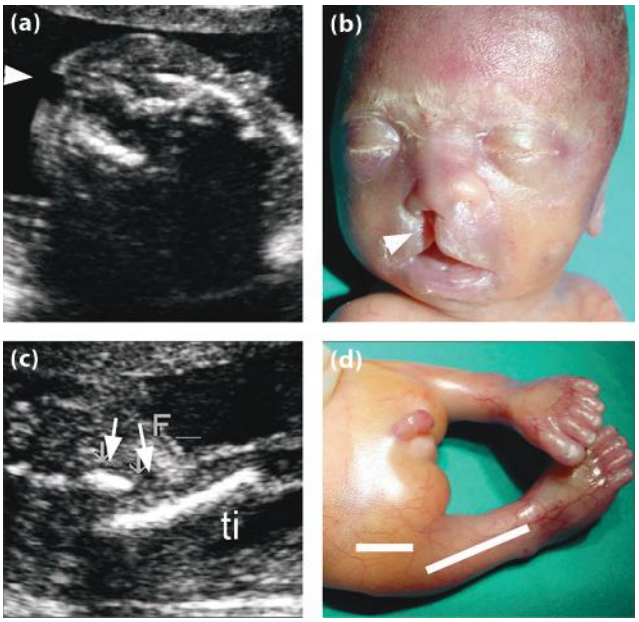


Figure 10.22 Femoral hypoplasia/unusual facies syndrome (22 weeks of gestation). (a) Axial view of the mandible, demonstrating a unilateral cleft lip and palate (arrowhead); (b) autoptic confirmation, showing also the long philtrum and the thin upper lip, which are typical features of this syndrome; (c) focal femoral hypoplasia (arrows); (d) confirmation at autopsy: the white bars indicate the size and position of the hypoplastic femur and the tibia.

Differential diagnosis. The differential diagnosis is rather limited, because of the rarity of the focal femoral hypoplasia. If no craniofacial anomalies are detected in association, the occurrence of a focal ischemic event during embryogenesis may be considered.

Prognosis, survival, and quality of life. Survival and intelligence are normal. The only major disability is physical and is due to the femoral hypoplasia, which impairs ambulation.

FETAL AkINESIA dEFor MATIoN sEqUENcE (FAds; oMIM 208150)

Incidence. Variable, according to diagnostic criteria.

Etiology. Unknown.

Ultrasound diagnosis. Diffuse joint contractures with extended and crossed legs, flexed and adducted arms, talipes, and clenched hands with overlapping fingers; lethal thoracic hypoplasia; micrognathia.

Outcome. Lethal in the majority of cases.

Recurrence risk. Autosomal recessive inheritance pattern, with a 25% recurrence risk. Sporadic cases have also been described.

Definition The FADS (OMIM 208150) includes a large group of syndromic conditions characterized by fixe joint contractures. The list of anomalies included in this group featuring joint contractures varies among the different textbooks and web resources. In our opinion, the easiest way to deal with these entities is as follows. There is a first group of disorders strictly related to the occurrence of diffuse and total neuromuscular block. These share a very high perinatal mortality rate, mainly due to the lethal pulmonary hypoplasia induced by the ubiquitous thoracic hypoplasia. This group comprises the classic FADS (including also *arthrogryposis multiplex congenita* and *Pena–Shokeir syndrome*), *Neu–Laxova syndrome* (OMIM 256520), *multiple pterygium syndrome* (OMIM 253290), and *cerebro-oculofacioskeletal* (*COFS*) *syndrome* (OMIM 214150). A second group of conditions is characterized by joint contractures of variable severity and different etiologies. This larger group includes *congenital myotonic dystrophy* (OMIM 214150), *restrictive dermopathy*, *Alpers syndrome* (OMIM 203700), and *Gaucher storage disease* (OMIM 231000). In the acronym FADS, the word "sequence" is appropriate since, according to numerous authors, this sequence of events represents the common *final pathway* of completely different pathogenetic mechanisms rather than a single neuromuscular disease. In this section, FADS will be described in detail, while in the following sections, most of the other prenatally recognizable disorders mentioned here will be illustrated. However, the description of conditions characterized by joint contractures that may not be diagnosed in the fetus will not be described here. The reader may wish to consult more comprehensive textbooks and/or websites on neonatal genetic diseases in order to find additional information regarding these conditions (Gaucher storage disease, restrictive dermopathy, etc.).

Etiology and pathogenesis. The basic defect of FADS and related conditions is the presence of severe and progressive contractures involving virtually all muscles. From the etiological standpoint, two findings are important to underscore: the first is that high maternal titers of autoantibodies directed against the muscular acetylcholine receptor (AChR), which are usually detected in patients with acquired myasthenia gravis, have been repeatedly found in families with multiple reproductive failures due to the recurrence of FADS. However, in these cases, the mothers were asymptomatic, and the antibodies were directed against different domains of the receptor compared with the autoantibodies usually associated with myasthenia gravis [25]. The second issue regards the genetic basis of this group of diseases. In fact, there is mounting evidence that null mutations of several genes involved in the neuromuscular transmission pathway are present in families with a positive history of FADS and related disorders [26]. The etiopathogenetic mechanism that begins to be uncovered is as follows: FADS and related disorders can be considered synaptopathies in which one of the genes encoding either the subunits of the AChR (CHRNA1, CHRNB1, CHRND, CHRNG, or CHRNE) or one of the proteins involved in its anchoring to the cell membranes (DOK7 or RAPSN) presents nonsense mutations. It seems that if these mutations occur as a heterozygous trait, this will cause postnatal forms of myasthenic syndromes, with muscular hypotonia and increased fatigue. On the contrary, homozygous mutations would lead to lethal forms of FADS or multiple pterygium syndrome [26]. According to this hypothesis, the various FADS phenotypes (from the lethal multiple pterygium syndrome to the mild form of arthrogryposis multiplex congenita) would be all but prenatal myasthenic syndromes that warrant further genetic and functional diagnostic investigations of the AChR pathway [26]. The only rather important limitation is that, until now, these mutations have been found only in a very limited subset of these families and fetuses (from 3% to 27%). Another interesting result of the molecular studies carried out in recent years is that it seems that in multiple pterygium syndrome, the pterygia are not the result of the fetal akinesia, as postulated before, but the consequence of early hydrops. In fact, fetuses with mutations in CHRNA1 and CHRND showed the lethal form of the disease with very early prenatal onset, featuring gross hydrops, pterygia, and contractures; on the other hand, fetuses with novel recessive missense RAPSN mutations showed the classic FADS with pulmonary hypoplasia, leading to early life-threatening respiratory distress, if born at term [26].

Genetics. Considering the genetic heterogeneity and the limited number of FADS cases in which these mutations have been found so far, prenatal molecular diagnosis is not possible. In addition, if an "early" prenatal diagnosis on chorionic villi might be hypothesized in the few families studied in detail, it should be considered that the results would be available when the most severe cases would already be detectable by US [27,28].

Deformation sequence (Figure 10.23). Regardless of the time of onset and of the underlying cause, the ubiquitous contractures of all muscles result in a particular position of the limbs, due to different opposing forces. As far as posture is concerned (see also Chapter 9), the lower limbs are in fixed extension and crossed, since the quadriceps (extensors) are more powerful than the femoral biceps (flexors) Talipes are often associated. In contrast, the upper limbs show flexion deformities and appear adducted on the thorax, because of the prevalence of the flexors (biceps) over the extensors (triceps). The hands often show ulnar deviation, with clenched and overlapping fingers The contractures of the diaphragm and the intercostal muscles lead to frequently lethal *thoracic hypoplasia*. Finally, the impairment of the swallowing reflex and the contracture of the masseter are responsible for *micrognathia* (and polyhydramnios). Sometimes, the contractures may involve the lower limbs only, and in these cases the knees appear flexed

Ultrasound diagnosis. All of the above-mentioned signs are detectable in the fetus. In this regard, it should be noted that the onset of the contracture is variable (from 12 to 30 weeks of gestation), also in consecutive pregnancies of the same couple [27]. The major signs, the recognition of which may lead to the diagnosis, are as follows (Figures 10.24 through 10.26):

- *Complete absence of active fetal movements (akinesia)*: this is due to complete motor paralysis. If the US examination is performed midway through the development of the akinesia, it is possible to spot *en bloc* movements of the limbs, which show no joint articulation;
- *Limb contractures*: involving the arms and legs (Figures 10.24b, d and 10.25a–d);
- *Micrognathia*: this is due to the block of the temporomandibular joint (Figures 10.24a and 10.25e,f);
- *Abnormal positioning of hands and feet*: ulnar deviation, clenched and overlapping fingers, and talipes (Figures 10.24b and d and 10.25a–d);
- *Thoracic hypoplasia*: this is due to the fixed contractures of the diaphragm and the intercostal muscles (Figure 10.23);
- *Severe polyhydramnios*: this is due to the absence of swallowing.

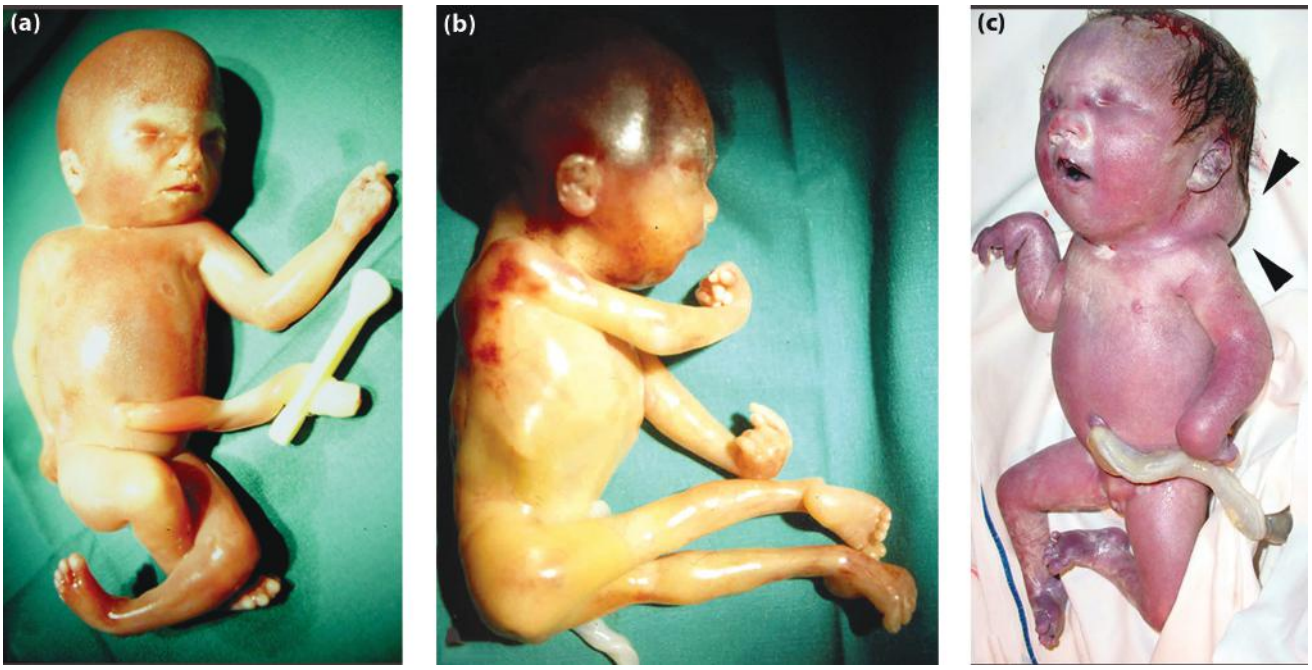


Figure 10.23 Fetal akinesia deformation sequence (FADS). The specimens shown here demonstrate how joint contractures may variously affect the limbs. (a) A 21-week-old fetus: predominant involvement of the lower limbs, which appear flexed and crossed, with talipes. Clinodactyly of the hands and low-set ears are also present. (b) A 19-week-old fetus: classic FADS, with the lower limbs extended and crossed scissors-like, while the upper limbs appear adducted and flexed. Talipes and ulnar deviation of the clenched hands are also evident. Note the severe hypoplasia of all muscles, defined as congenital amyoplasia, which is the result of prolonged akinesia. (c) Neonate dead just after birth: diffuse contractures, ulnar deviation of the hands, microstomia (small mouth), and cystic hygroma (arrowheads) are seen (this is the same case as in Figure 10.24 and 10.26).

Additional, inconstant signs include the following:

- *Microstomia*: this is due to the masseter contracture (Figure 10.26);
- *Cystic hygroma* or *nuchal edema* may be associated with FADS in some cases (Figures 10.23c, 10.24c);
- *Nonvisualization of the gastric bubble*: this is due to the absence of swallowing.

Differential diagnosis. The first entity to be ruled out is trisomy 18, because contractures of the legs are relatively often present in this aneuploidy. The recognition of major anomalies possibly associated with trisomy 18 and, above all, fetal karyotyping may help rule out trisomy 18. In addition, a differential diagnosis with the other neuroarthrogryposes should be carried out, although this procedure does not have an important prognostic role, since all of these disorders are almost invariably lethal, with the exception of a few cases of late-onset FADS. The features to consider in the differential diagnosis of the various neuroarthrogryposes are as follows:

- *Multiple pterygium syndrome [7]*: look for ► *arthrogryposis* + pterygia + edema + cystic hygroma (see the "Multiple pterygium syndrome" section in this chapter and Figure 10.34);

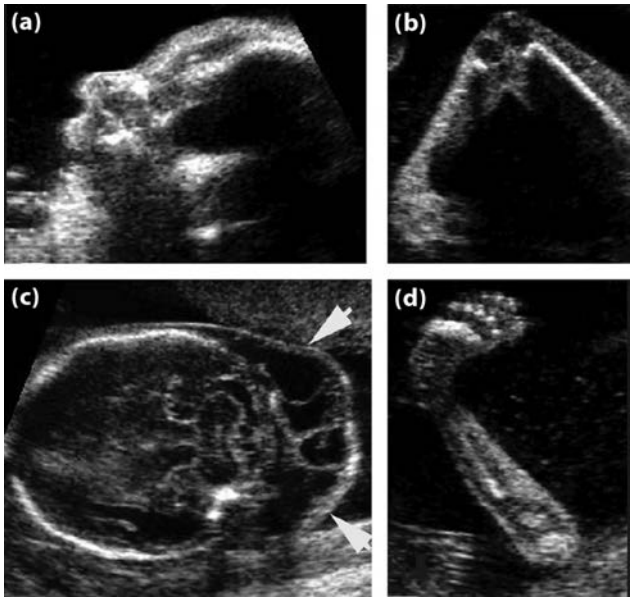


Figure 10.24 Fetal akinesia deformation sequence (FADS). In this case (the same as in Figure 10.23c), the following anomalies can be seen: (a) micrognathia, due to paralysis of the masseter (blocked temporomandibular joint); (b) arthrogryposis of the upper limbs, which appear flexed and adducted; (c) cystic hygroma (arrows), which is inconstantly associated with FADS: and (d) arthrogryposis of the lower limbs, with talipes.

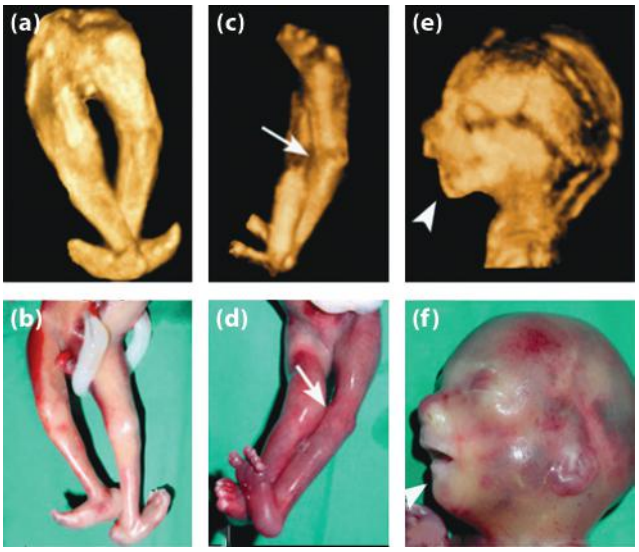


Figure 10.25 Fetal akinesia deformation sequence (FADS). Two cases of FADS at 21 (a,b) and 19 weeks (c–f) of gestation. (a) Arthrogryposis of the lower extremities, with the legs fixed in extension and abnormal feet; (b) confirmation at autopsy; (c) in this case, the legs appear extended and crossed, scissor-like (note also the dislocation of the knee; see arrow); (d) confirmation at autopsy; (e) severe, early onset micrognathia (arrowhead), due to the block of the temporomandibular joint, from paralysis of the masseter; and (f) confirmation at autopsy.

- *Neu–Laxova syndrome [7]*: look for ► *arthrogryposis* + microcephaly + hypertelorism + cataract + micrognathia + CNS anomalies + syndactyly + subcutaneous edema (see the corresponding section in this chapter and Figures 10.35 and 10.36);
- *COFS syndrome [7,28]*: look for ► *arthrogryposis* + anophthalmia or microphthalmia + cataract + micrognathia + CNS anomalies + scoliosis.

Prognosis, survival, and quality of life. Most FADS cases reach term, although preterm delivery may occur because of the severe associated polyhydramnios. However, after birth, death ensues within a range from a few minutes to some hours due to the lethal pulmonary hypoplasia. The extremely rare late-onset cases, in which the pulmonary hypoplasia is not so severe as to be lethal, may survive the neonatal period. However, the quality of life is often extremely poor because of the severe contractures requiring multiple orthopedic surgical procedures to release the hypoplastic tendons and long-term physiotherapy. Significant respiratory complications can also occur. In a small subset of these cases, the outcome may be fair, after surgery and physiotherapy.

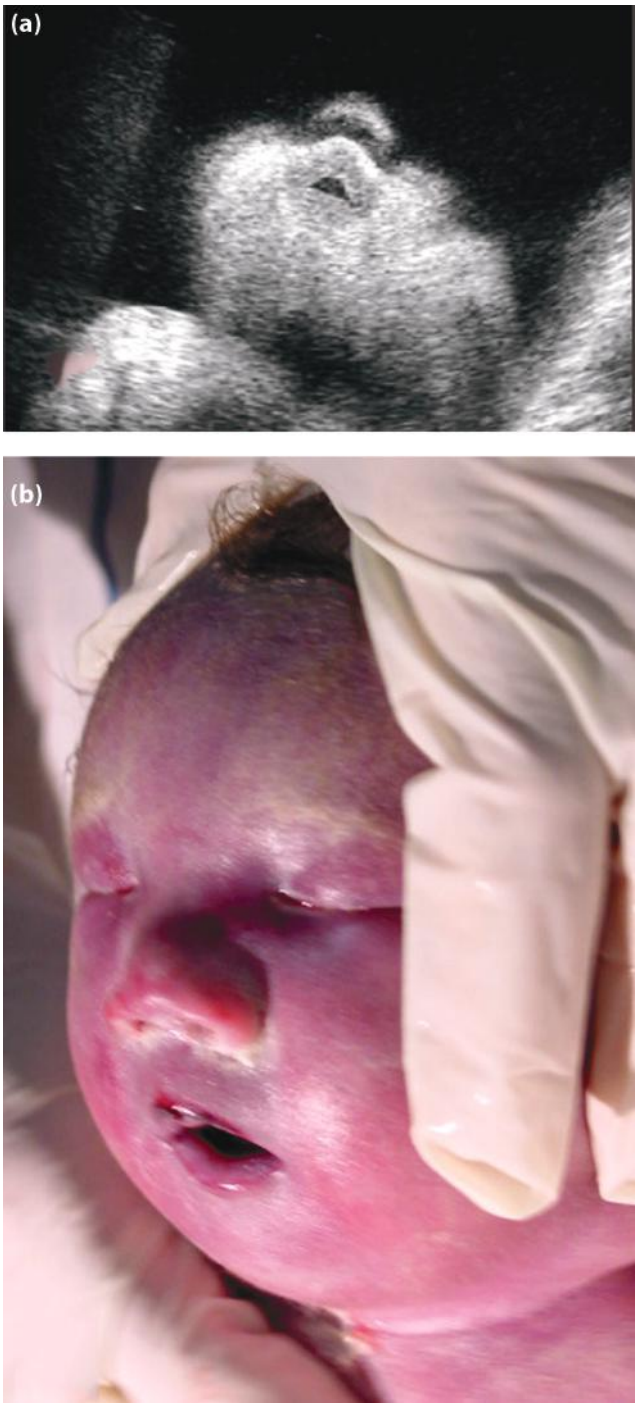


Figure 10.26 Fetal akinesia deformation sequence (FADS). In some cases, the neuromuscular block of the masseter and of the orbicular muscles impairs the normal development of the mouth, eventually leading to a smaller than normal mouth (microstomia). (a) On the oblique view of the lips, the small size of the mouth is evident. Note the concurrent polyhydramnios, which is constantly associated and is due to lack of swallowing. (b) Confirmation at autopsy following birth. This is the same case as in Figures 10.23c (c) and 10.24.

Recurrence risk. FADS is mainly transmitted with an autosomal recessive inheritance pattern, which implies a 25% recurrence risk. Rarer X-linked and sporadic cases have also been described.

FRASER SYNDROME (OMIM 219000)

Incidence. Extremely rare: 1/200,000 at birth.

Etiology. Unknown.

Ultrasound diagnosis. Laryngeal atresia; cleft lip and palate; congenital heart disease; microphthalmia; bilateral renal agenesis; syndactyly.

Outcome. Lethal. A few reports of survivors after an ex utero intrapartum treatment (EXIT) procedure.

Recurrence risk. Autosomal recessive inheritance, with a 25% recurrence risk. Sporadic cases have also been described.

Definition *Fraser syndrome* (OMIM 219000), which shows an extremely variable phenotypic expression, is named after the author who first described the cluster of anomalies in 1962. The malformations that characterize Fraser syndrome are laryngeal atresia, cleft lip and palate, congenital heart disease, microphthalmia, bilateral renal agenesis, and syndactyly.

Etiology and pathogenesis. In a few families with Fraser syndrome, a missense mutation of the *FRAS1* gene, at chromosome 4q21, has been described. This gene encodes a putative extracellular matrix (ECM) protein.

Genetics. Prenatal genetic diagnosis is not available.

Ultrasound diagnosis. In the fetus, the malformation that in most cases leads to the suspicion or diagnosis of Fraser syndrome is laryngeal or tracheal atresia, due to the frequent association of bilateral renal agenesis and consequently of severe oligohydramnios, which makes the assessment of fetal anatomy very difficult [29]. Major anomalies, the recognition of which may lead to the diagnosis of Fraser syndrome, are as follows:

- *Laryngeal atresia*: this can be diagnosed on the *axial and coronal views of the fetal thorax* (Figure 10.27; see also Chapter 6, Figures 6.5 and 6.24). Both lungs are severely enlarged and hyperechoic; the heart is squeezed into the center of the thorax. Inconstantly,

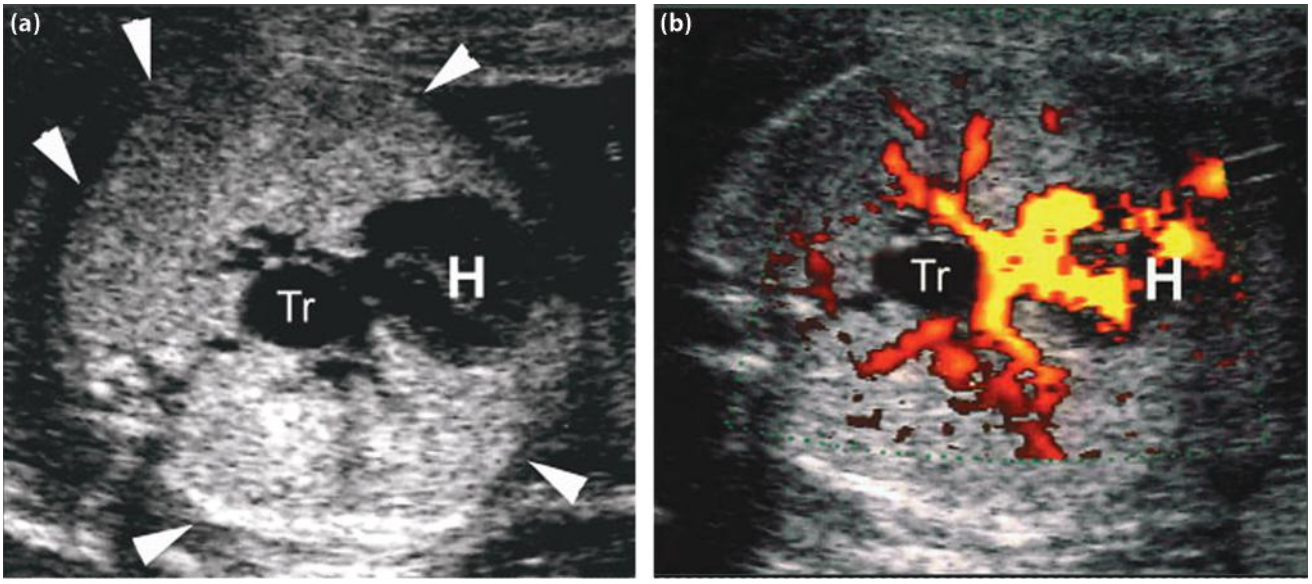


Figure 10.27 Fraser syndrome: laryngeal atresia. (a) On the axial view of the thorax, the severely enlarged and hyperechoic lungs (arrowheads) are visible. The heart (H) is squeezed into the mediastinum by compression from the lungs. Behind the heart, the trachea (Tr) can be seen: the whole bronchial tree is dilated due to the fluid trapped below the atretic larynx (bronchogram). (b) Power Doppler examination demonstrating that the hollow structure behind the heart is not of cardiovascular origin. It should be noted that, for a diagnosis of Fraser syndrome, other major anomalies should be present.

a bronchogram (dilatation of the trachea and bronchi by the entrapped fluid) is seen;
- *Bilateral renal agenesis*: this is responsible for the frequently associated severe oligohydramnios;
- *Congenital heart disease*: this is constantly associated;
- *Microphthalmia*: this is detected on the axial view of the orbits.

Additional anomalies, the detection of which is hampered by the severe oligohydramnios, are as follows:

- Syndactyly;
- Cleft lip and palate.

Differential diagnosis. This is virtually nonexistent, due to the peculiarity and the rarity of the malformations, especially laryngeal atresia. It should be pointed out that laryngeal atresia is not always present, but this is the only anomaly that may lead to the diagnosis in the fetus, because of the difficulties in recognizing the other craniofacial and/or skeletal signs due to the constant oligohydramnios (renal agenesis). The differential diagnosis of laryngeal atresia is described in Chapter 6.

Prognosis, survival, and quality of life. Fraser syndrome is almost always lethal, due to the bilateral renal agenesis and laryngeal atresia. There are a few descriptions of survivors following an EXIT procedure (see Chapters 3 and 6). In these cases, the microphthalmia and syndactyly, if severe, represent the main problems.

Recurrence risk. Fraser syndrome is transmitted with an autosomal recessive inheritance pattern, which implies a 25% recurrence risk. However, a few sporadic cases have been described.

hEMIFAcIAL MIcrosoMIA (GoLdENhAr syNdroME; oMIM 164210)

Incidence. 1/3000–5000 at birth.

Etiology. Unknown.

Ultrasound diagnosis. Hemifacial microsomia; cleft lip and palate; external ear anomalies; vertebral anomalies.

Outcome. Relatively good survival. Intelligence is normal in most cases. High cosmetic impact.

Recurrence risk. The empiric recurrence risk, in the absence of a positive family history, has been set at 2%. Families with autosomal dominant and recessive inheritance patterns have been described (50% and 25% recurrence risk, respectively).

Definition Recently, the name "hemifacial microsomia" has replaced in the OMIM website (http://omim.org/entry/164210?search=goldenhar&highlight=goldenhar) the former ones of Goldenhar syndrome and oculo-auriculo-vertebral spectrum (OAVS). Regardless of how the reader wants to refer to it, this disorder represents a cluster of malformations due to abnormal development of the first and second branchial arches, associated in some cases with ocular and vertebral anomalies. According to some authors, the association of an epibulbar dermoid with vertebral anomalies specifically identifies Goldenhar syndrome within AVS spectrum.

Etiology and pathogenesis. The etiology is unknown. Pathogenetically, a derangement in the development of the neural crest has been discovered in hemifacial microsomia (OAVS or Goldenhar), which links this malformative cluster with the CHARGE (coloboma, heart defects, atresia of choanae, retarded growth, and genital anomalies) association. Hemifacial microsomia shows genetic heterogeneity, since linkage analysis has shown possible involvement of the chromosome 14q32 region in one family but not in others.

Genetics. Prenatal genetic diagnosis is still not available, because of the above-mentioned genetic heterogeneity.

Ultrasound diagnosis. Most malformations characterizing hemifacial microsomia can be recognized prenatally [30–32]; those more commonly detected in the fetus are the facial and cerebral ones, which are both present in more than 50% of reported cases [32]. Major anomalies, the recognition of which may lead to the diagnosis of hemifacial microsomia, are as follows:

- *Cleft lip and palate (Figure 10.28a)*: this is detected on the axial and oblique *views of the lips and palate* and/or on 3D surface-rendered images of the fetal face;

- *Hemifacial microsomia (Figure 10.28a and b)*: this becomes evident on the coronal view of the face and/or 3D surface-rendered images of the fetal face;
- *Unilateral microphthalmia (Figure 10.28a and b)*: this is detected on the axial view of the orbits;
- *Unilateral external ear anomalies (Figure 10.28c)*: these are detected on the *parasagittal view of the head* for the external ear or, more advantageously, 3D surface-rendered images of the fetal face;
- *Vertebral anomalies*: often involving the cervical and thoracic region, these are recognized on the sagittal view of the spine.

Additional anomalies include the following:

- *Congenital heart disease (Figure 10.28d)*: these often involve the interventricular septum;
- *Urinary tract anomalies*;
- *CNS anomalies*: these are most often agenesis of the corpus callosum and cerebellar abnormalities (also hemihypoplasia) [30].

Differential diagnosis. This includes the CHARGE association and Treacher Collins syndrome:

- *Treacher Collins syndrome*: look for ► *cleft lip and palate* + mandibular hypoplasia + external ear anomalies;
- *CHARGE association*: look for ► *external ear anomalies* + ocular anomalies + congenital heart disease + urinary tract anomalies + FGR.

Prognosis, survival, and quality of life. Survival is normal. The risk of mental retardation is relatively low, with 13% of affected individuals showing an IQ < 85. Usually, individuals with mental retardation also have microtia. Hearing loss may also be present, due to the involvement of the external ear. Cosmetic surgery is indicated in all cases to reduce the aesthetic impact of hemifacial microsomia.

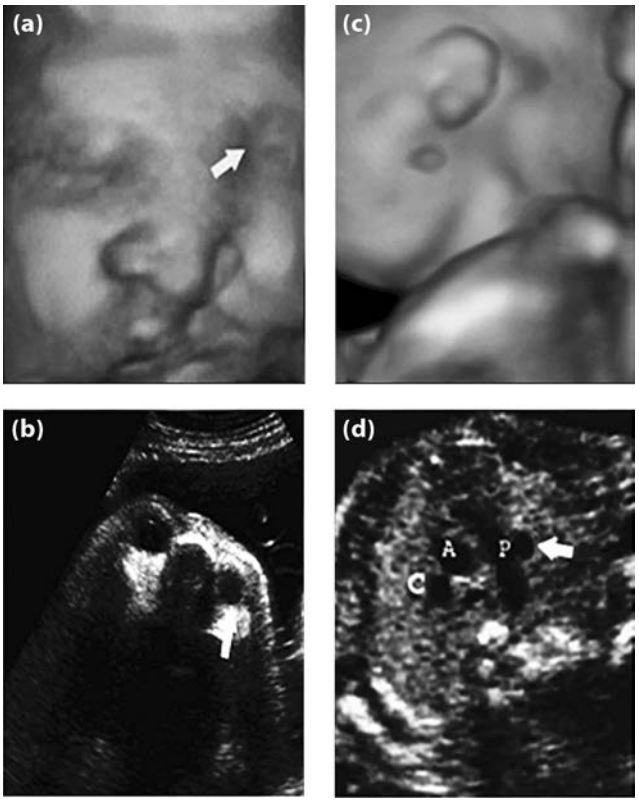


Figure 10.28 Hemifacial microsomia (Goldenhar syndrome or oculo-auriculo-vertebral spectrum [OAVS]). (a) A 3D surface-rendered image of the fetal face showing cleft lip and palate and hemifacial microsomia (note the hypoplastic orbit on the same side of the clefting). (b) Axial view of the orbits showing unilateral microphthalmia. (c) Pre-auricular tag. (d) Left superior vena cava (arrow); A: aorta; C: right superior vena cava; P: pulmonary artery. (Modified from Volpe P, et al. *Ultrasound Obstet Gynecol* 2004; 24: 798–800).

jA rcho–L EVIN sy Ndro ME (oMIM 277300)

Incidence. Extremely rare.

Etiology. The most common mutation regards the *DLL3* gene, located on chromosome 19q13.

Ultrasound diagnosis. Abnormal and/or fused ribs; hemivertebrae, vertebral fusion, and abnormal mineralization of the spine.

Outcome. Most cases die in the first year of life from intractable and recurrent respiratory infections.

Recurrence risk. Autosomal recessive. In milder cases, autosomal dominant.

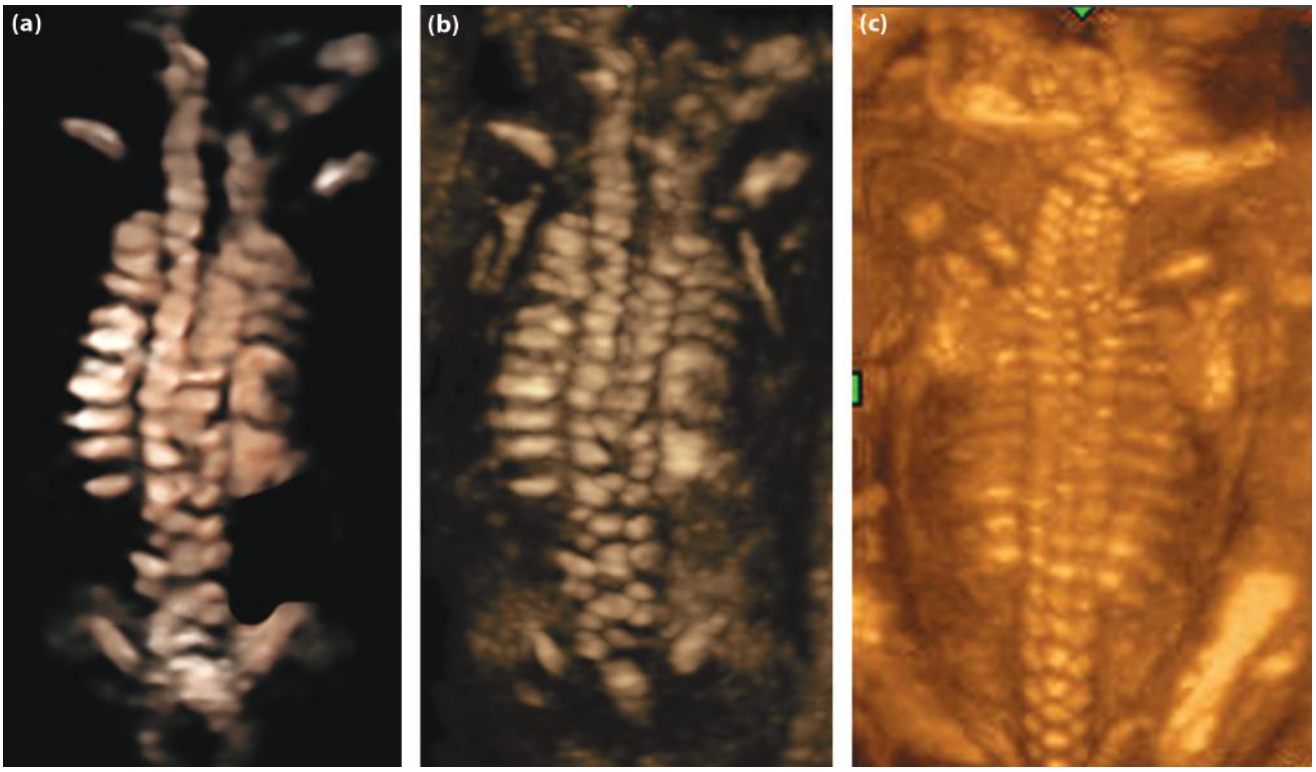


Figure 10.29 Jarcho–Levin syndrome (spondylocostal dysostosis, 22 weeks of gestation). (a and b) Three-dimensional rendering with different filters of the whole spine and ribs highlights the severe costal and vertebral defects (see this chapter's text); and (c) for comparison, a normal spine at the same gestational age.

Definition Jarcho–Levin syndrome (OMIM 277300) is also called spondylocostal dysostosis, type 1. The number differentiates the severe form, which is detectable in utero, from the less severe ones, which are compatible with a normal lifespan. Also, it refers to the subtype with a symmetric "crablike" involvement of the ribs and spine.

Etiology and pathogenesis. The most common mutation regards the *DLL3* gene, located on chromosome 19q13. However, genetic heterogeneity is high.

Genetics. Prenatal genetic diagnosis is not possible, due to the high genetic heterogeneity.

Ultrasound diagnosis. The main features of the syndrome are recognizable on US from the late first trimester

- *Abnormal and/or fused ribs*: this is detected on the *parasagittal and coronal views of the thorax*; the abnormalities are even more evident with 3D US, because, due to the distortion of the spine, the thorax is twisted and especially the ribcage cannot be assessed thoroughly in a single 2D plane (Figure 10.29);
- *Abnormal spine and hemivertebrae*: these are best seen on the midsagittal view of the spine with a posterior approach (fetus with an anterior spine) (Figures 10.29 and 10.30).

In cases at risk, the anomaly is recognizable at the nuchal translucency scan (12–14 weeks—see Figure 10.30).

Differential diagnosis. The differential diagnosis is rather limited, because of the peculiar aspect of the spine and the ribcage. Furthermore, the absence of limb shortening or bowing represents an important differential diagnostic sign in relation to the other skeletal dysplasias characterized by a small, hypoplastic thorax (see Chapter 9).

Prognosis, survival, and quality of life. Most cases die in the first year of life from intractable and recurrent respiratory infections.

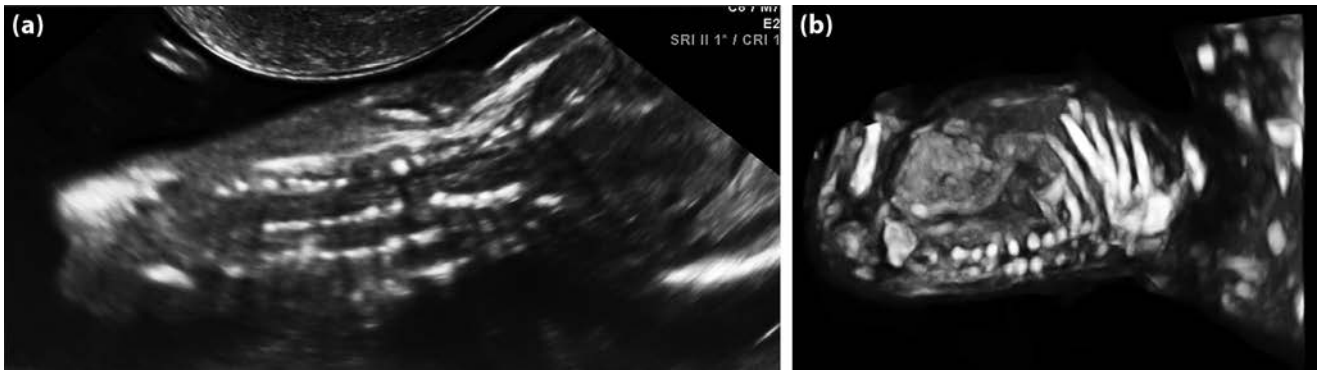


Figure 10.30 Jarcho–Levin syndrome (spondylocostal dysostosis, 14 weeks of gestation). This condition can be detected as early as the 14th week of pregnancy. At transvaginal high-frequency (6–12 MHz volumetric transducer) ultrasound, the severely abnormal development of the ribs and spine is clearly evident at both (a) 2D and (b) 3D ultrasound.

kLIppEL–Tr ENAUNAy–WEBEr syNdro ME (kTWs; oMIM 149000)

Incidence. Extremely rare.

Etiology. Unknown.

Ultrasound diagnosis. Abnormal contour of one or more limbs due to large hemangiomas, sometimes also involving the trunk. Hypertrophy and microcystic appearance of soft tissues.

Outcome. Depends on the site and extent of the hemangiomas. These undergo significant regression after birth.

Recurrence risk. Extremely low. Most cases are sporadic, although families with an autosomal dominant inheritance pattern, implying a 50% recurrence risk, have been described.

Definition KTWS (OMIM 149000) was described by Klippel and Trenaunay in 1900 and by Weber in 1907. It is characterized by multiple hemangiomas variously involving the limbs, the trunk, and the internal organs (CNS, abdominal, etc.).

Etiology and pathogenesis. A mutation of the *VG5Q* gene, at chromosome 5q13.3, has been found in a few cases. This mutation results in increased production of the protein coded by the malfunctioning gene, which is a potent angiogenic factor found in endothelial cells, myocytes, and osteoblasts.

Genetics. Prenatal genetic diagnosis is possible if the *VG5Q* mutation has been identified in the affected family.

Ultrasound diagnosis. US diagnosis is straightforward because of the uniqueness of the sonographic appearance of the hemangiomas. The only issue to consider is that, due to the rarity of KTWS, most sonographers have never seen such lesions on US and therefore may reach the diagnosis only if they recall it from textbooks. The US signs of KTWS are as follows [33]:

- *Hemangiomas involving one or more limbs*: these have an abnormal cutaneous contour and diffuse microcystic changes of the subcutaneous tissue, with some calcified spots (Figures 10.31a and 10.32a);
- *Soft tissues and bone hypertrophy, at the level of the affected limb*: the degree of hypertrophy can be appreciated by comparing the cross-sectional views of the two limbs—the affected and the normal (Figure 10.31b);
- *Trunk involvement* (less evident and less common): at this level, the hemangiomatosis can appear as

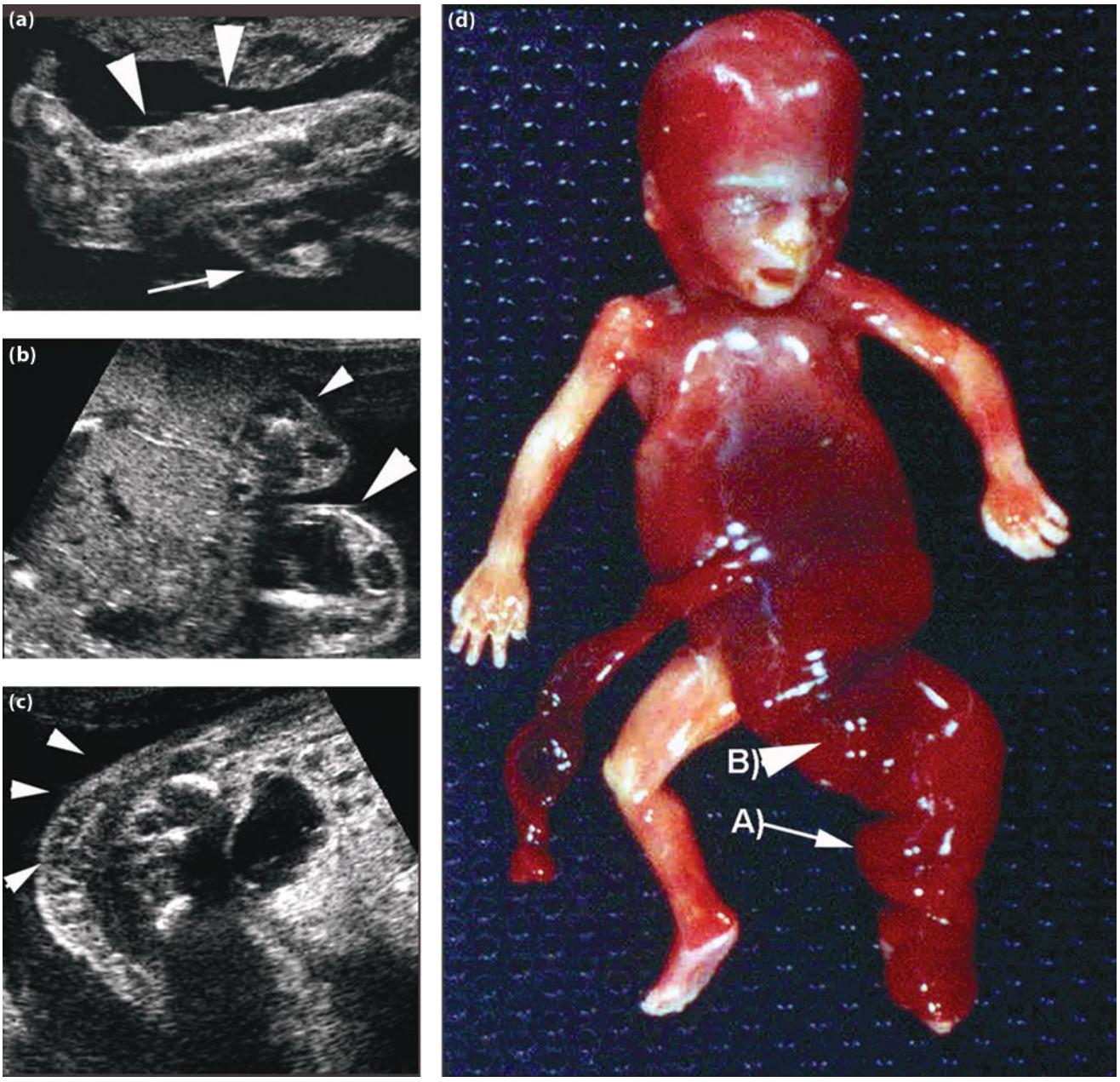


Figure 10.31 Klippel–Trenaunay–Weber syndrome at 19 weeks of gestation. (a) The thigh shows an irregular cutaneous outline, both on the anterior aspect (arrowhead) and posteriorly, at the popliteal region, where a conspicuous hemangioma (arrow) is visible. (b) Axial view of the lower limbs at the level of the middle part of the femur showing an evident discrepancy in size due to bone and soft tissue hypertrophy (arrowheads) and to hemangiomatosis (hypoechoic areas). (c) Arrowheads indicate the involvement of the gluteal region, which appears as a spongious aspect of the subcutaneous tissue. (d) Autopsy after termination of pregnancy showing diffuse hemangiomatosis; the letters relate to the sonographic findings in parts (a) and (b).

regional thickening of the subcutaneous tissues, with or without a microcystic subcutaneous mass (Figures 10.31c and 10.32b). When involving internal organs, the lesion shows the classic microcystic aspect.

Like most conditions characterized by hyperplasia of mesenchyme-derived tissues, KTWS changes during the course of gestation. The lesions tend to increase in size and extend to the trunk, with new hemangiomas possibly appearing at a later stage. If the number and/or

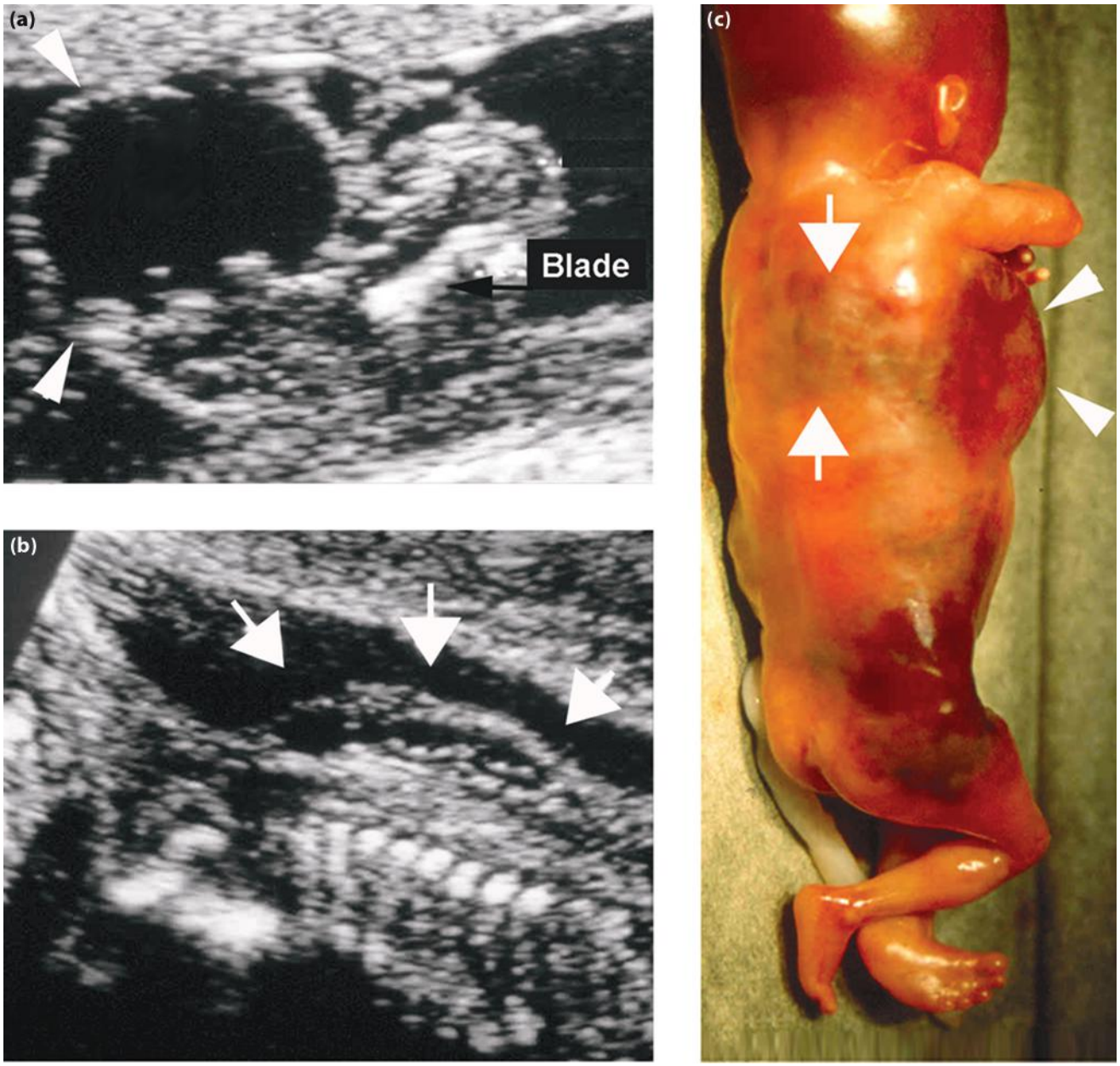


Figure 10.32 Klippel–Trenaunay–Weber syndrome at 20 weeks of gestation. (a) Huge hemangioma of the axilla, appearing as a cystic mass; arrowheads to be compared with the arrowheads on the specimen in (c). (b) Involvement of the lateral aspect of the fetal trunk; arrows to be compared with the arrows on the specimen in (c). (c) Specimen after termination of pregnancy: note the various hemangiomas and the involvement of the right pelvic area.

extent of the lesions are significant, cardiac decompensation due to high-output failure may develop [33]. However, as reported in this section, all lesions tend to significantly regress with time.

Differential diagnosis. In most cases, the hemangioma is sonographically indistinguishable from a lymphangioma. However, the latter is frequently single and localized, whereas in KTWS the hemangiomas are multiple and/or massive, involving large areas of a limb. Another condition that should be differentiated from KTWS is Beckwith–Wiedemann syndrome [7]: both share hypertrophy and hyperplasia of bone and soft tissues. However, Beckwith–Wiedemann syndrome is characterized also by exomphalos and macroglossia, both of which are absent in KTWS. Also, the Proteus syndrome (OMIM 176920) shows hemihypertrophy and macroglossia; in addition, the Proteus syndrome may show lymphangiomas. Thus,

this is the single disorder that is most difficult to differentiate from KTWS. However, the multiple location of the hemangiomas and the absence of real hemihypertrophy may allow one to recognize KTWS.

Prognosis, survival, and quality of life. As already pointed out, the hemangiomas of KTWS show a significant tendency to regress after birth. The size of the lesions may shrink dramatically in a few months. However, the fina prognosis is highly variable and depends mainly on the size and the location of the hemangiomas: cerebral hemangiomas may induce seizures or epilepsy, and they can bleed or may cause severe cerebral atrophy, which, although rare, is one of the most ominous sequelae. Thrombocytopenia can also be associated owing to the platelet sequestration within the hemangiomas. If the hemangiomas involve only superficial areas, such as the limbs or the trunk, to a certain extent the prognosis is more favorable, and, in selected cases, resection or plastic surgery may be considered. Laser treatment may lead to improvement of the superficial hemangioma component of the affected areas.

Recurrence risk. KTWS is generally a sporadic condition, but a few cases with autosomal dominant inheritance, with a 50% recurrence risk, have been described.

Meckel–Gruber syndrome (OMIM 249000)

Incidence. Frequent: 1/9000 live births.

Etiology. The involved gene maps to chromosome 17q21–24, but there is genetic heterogeneity.

Ultrasound diagnosis. The phenotypic expression of the syndrome is variable, as a consequence of its genetic heterogeneity. The three signs that usually lead to the diagnosis—occipital cephalocele, cystic renal dysplasia, and postaxial polydactyly—are present in 60% of cases. Additional anomalies include CNS, craniofacial, and gastrointestinal malformations.

Outcome. Lethal.

Recurrence risk. Autosomal recessive inheritance pattern, with a 25% recurrence risk. Rare sporadic cases have been described.

Definition The original malformative cluster of Meckel–Gruber syndrome (OMIM 249000) was first described by Meckel in 1822, although the number of anomalies found in Meckel–Gruber syndrome is huge. The three classic signs (occipital cephalocele, cystic renal dysplasia, and postaxial polydactyly) are present in 60% of cases. Other malformations found in this syndrome involve the CNS (Dandy–Walker complex, cerebellar hypoplasia, and hydrocephaly), gastrointestinal tract (exomphalos, asplenia, splenomegaly, and imperforate anus), and cardiovascular system (septal defects).

Etiology and pathogenesis. A significant number of cases show mutations at chromosome 17q21–24, but the genetic heterogeneity is high, with other cases mapping to different loci. This leads to the variable clinical expression of the syndrome.

Genetics. This is not available, due to the high genetic heterogeneity.

Ultrasound diagnosis. There are three anomalies that lead to the diagnosis in most of the cases detected in utero:

- *Occipital cephalocele*: the detection of this may be difficult due to the frequently associated severe oligohydramnios (Figure 10.33a and b);
- *Cystic renal dysplasia, with enlarged and hyperechoic kidneys*: this is the sign that is most promptly detected, since the kidneys fill most of the fetal abdomen (Figure 10.33c and d);
- *Postaxial polydactyly*: also in this case, recognition of the anomaly is hampered by the severe oligohydramnios. If the fetal lie is favorable, the bony phalanges may be recognized, and this may lead to a diagnosis of polydactyly (Figure 10.33e and f). In a few cases, the extra digit may also be preaxial. In the rare cases in which a definite diagnosis is not reached due to concomitant severe oligohydramnios, unfavorable fetal lie, or maternal obesity, both a transvaginal approach and a diagnostic amnioinfusion may solve the problem. In families at risk (with a positive history), US diagnosis of Meckel–Gruber syndrome has been reported as early as 12–13 weeks of gestation.

Differential diagnosis. The differential diagnosis includes different conditions according to the sign considered. The most important one to address, since it may also occur in other syndromic disorders, is cystic renal dysplasia. The sonographic appearance of the kidney is often indistinguishable from that of classic

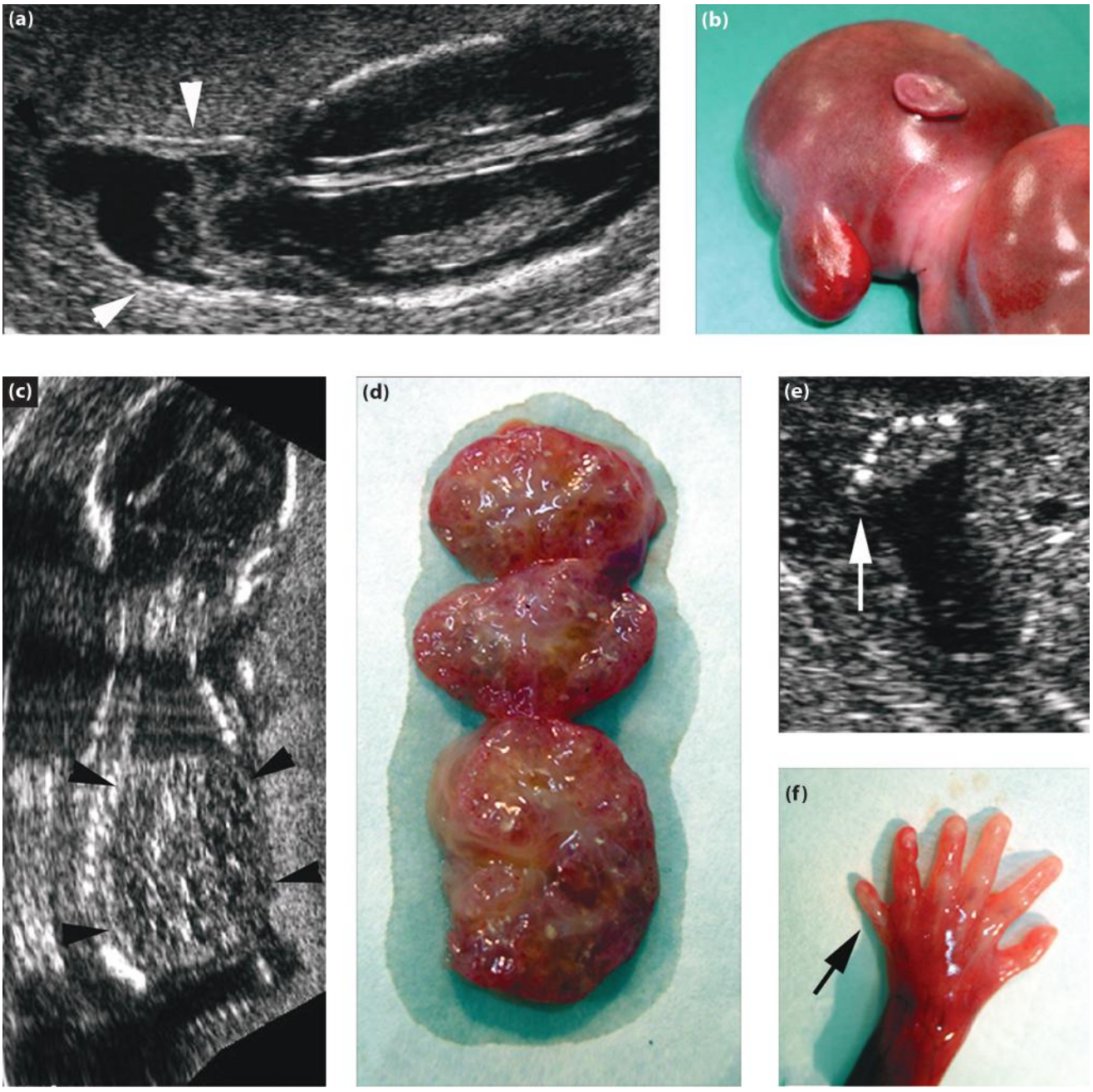


Figure 10.33 Meckel–Gruber syndrome at 19 weeks of gestation. (a) Occipital encephalocele: axial transventricular view showing the large occipital bone defect through which the meninges and the cerebral parenchyma (arrowheads) have migrated. (b) Confirmation at autopsy. (c) Cystic renal dysplasia: low-magnification view of the fetus showing that the whole abdomen is occupied by the severely enlarged polycystic kidneys (arrowheads). Note also the severe thoracic hypoplasia. (d) Specimen of the polycystic kidney, showing the parenchymal cysts. (e) Polydactyly of one foot. (f) Postaxial polydactyly of one hand at autopsy.

autosomal recessive polycystic kidney disease. The same enlarged and hyperechoic kidneys are also characteristic of other syndromes: a thorough description is given in Chapter 8. If multiple anomalies involving the CNS and the heart are found, one of the other conditions to be ruled out is trisomy 13, in which polydactyly, renal dysplasia, and CNS and cardiac anomalies can be found.

Prognosis, survival, and quality of life. Meckel–Gruber syndrome is invariably lethal, due to the severe pulmonary hypoplasia induced by the oligohydramnios.

Recurrence risk. Meckel–Gruber syndrome has an autosomal recessive inheritance pattern, with a 25% recurrence risk, although rare sporadic cases have been described. Therefore, a correct diagnosis is of the utmost importance in order to allow early US assessment of any following pregnancy.

MULTIPLE PTERYGIUM SYNDROME (OMIM 253290)

Incidence. Extremely rare.

Etiology. Unknown. It belongs to the neuroarthrogryposes (FADS).

US signs. Ubiquitous and severe joint contractures; multiple pterygia at elbows and knees; cystic hygroma.

Outcome. Invariably lethal.

Recurrence risk. Autosomal recessive inheritance pattern, with a 25% recurrence risk.

Definition Different variants of this syndrome (OMIM 253290) have been described according to the lethality and to the diffusion of the pterygia. The lethal form is included in the group of neuroarthrogryposes (FADS), together with Neu–Laxova syndrome, the COFS syndrome, and classic FADS (or Pena–Shokeir syndrome). In multiple pterygium syndrome, the four limbs are flexed from the early weeks, and this leads to the development of the pterygia at the level of the main joints. Facial abnormalities (cleftings), cystic hygroma, early and severe FGR, and polyhydramnios complete the prenatal appearance.

Etiology and pathogenesis. Being considered part of the FADS spectrum, it shares at least in part the genetic background of this group of synaptopathies. Please refer to the corresponding heading under the "Fetal akinesia deformation sequence" section for details regarding molecular genetics. As far as the development of the pterygia is concerned, recent studies have apparently demonstrated that it derives not from the long-lasting akinesia but from the severe early hydrops that is often associated with this disorder; the hydrops then regresses, leaving the pterygia, especially at the level of the neck, axillae, antecubital, popliteal, and intercrural areas.

Genetics. Prenatal diagnosis is not available.

Ultrasound diagnosis. The sonographic features are striking:

- *Arthrogryposis*: this involves all muscles, with flexed and adducted limbs, deformed extremities, and clinodactyly (Figure 10.34);
- *Multiple pterygia*: these are difficult to recognize, due to the fixed adduction of all limbs;
- *Cystic hygroma-lymphangiomas*: these are of early onset and severe (Figure 10.35);
- *Craniofacial anomalies*: these comprise mainly cleft lip and palate and micrognathia (Figure 10.34c and d);
- *FGR*: this is severe, symmetric, and of early onset.

Differential diagnosis. A differential diagnosis is limited to the other neuroarthrogryposes and to cystic hygroma. The second issue is the most important one, due to the completely different recurrence risk shown by the two conditions: 25% for the autosomal recessive inherited multiple pterygium syndrome, compared with the 1% recurrence rate of cystic hygroma, if due to aneuploidy.

Prognosis, survival, and quality of life. This syndrome is invariably lethal.

Recurrence risk. There is an autosomal recessive inheritance pattern, with a 25% recurrence risk.

NEU–LAXOVA SYNDROME (OMIM 256520)

Incidence. Extremely rare.

Etiology. Unknown. It belongs to the neuroarthrogryposes (FADS).

Ultrasound diagnosis. Microcephaly; CNS anomalies; macrophthalmia and proptosis; external ear anomalies; micrognathia; arthrogryposis; lymphedema of the limbs and extremities; ichthyosis; FGR.

Outcome. Invariably lethal.

Recurrence risk. Autosomal recessive inheritance pattern, with a 25% recurrence risk.

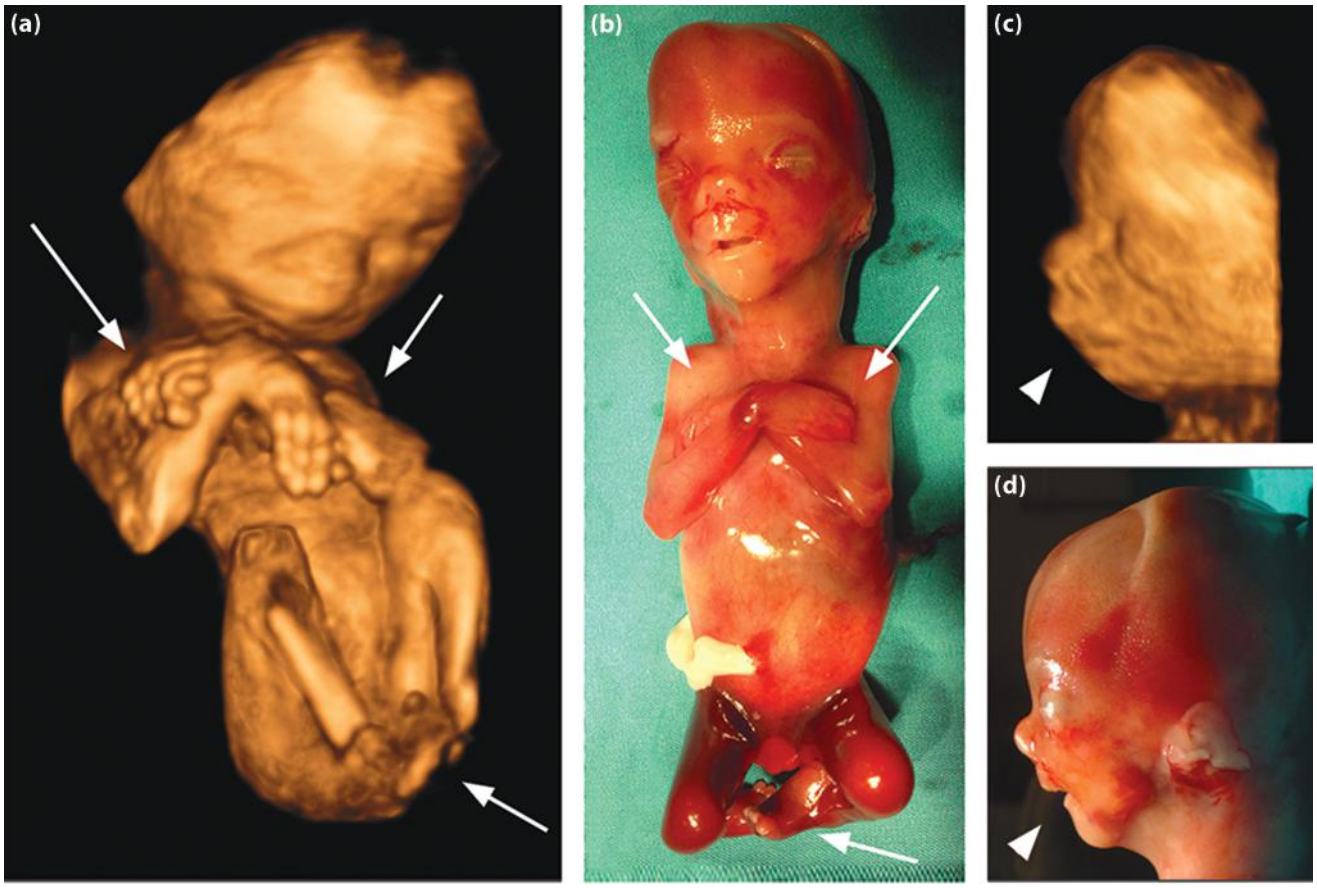


Figure 10.34 Multiple pterygium syndrome (15 weeks of gestation). (a) Three-dimensional rendering of the fetal body showing the arthrogryposis, with the four limbs in flexed, fixed contracture (arrows); and (b) autoptic confirmation. The pterigya form at the level of the neck, axillae, antecubital, popliteal, and intercrural areas and are thought to be related to regression of very early hydrops rather than to contractures (see this chapter's text); (c) 3D surface rendering of the fetal profile showing evident micrognathia (arrowhead) already at this relatively early gestational age; and (d) autoptic confirmation.

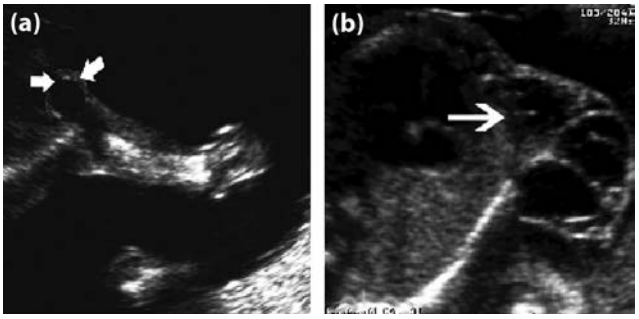


Figure 10.35 Multiple pterygium syndrome (21 weeks of gestation). (a) Lymphangioma of the knee (arrow), which, after regressing, transforms into a pterygium; and (b) lymphangioma of the antero-lateral thoracic wall (arrow).

Definition Neu–Laxova syndrome (OMIM 256520) is named after the two authors who first described the condition in 1971–1972. This syndrome is included in the group of neuroarthrogryposes (FADS), together with multiple pterygium syndrome, COFS syndrome, and classic FADS (or Pena–Shokeir syndrome). In addition to the diffuse and severe arthrogryposis, the following malformations are also present: severe CNS anomalies (extreme cerebellar hypoplasia, Dandy–Walker complex, and agenesis of the corpus callosum); severe early-onset microcephaly; proptosis and corneal opacities; diffuse edema of the limbs and, especially, of the extremities, which appear severely distorted; early-onset symmetric FGR; and polyhydramnios. There are also two other abnormalities, which are not detected on US in most cases (at least in the second trimester): lissencephaly and ichthyosis.

Etiology and pathogenesis. The etiology is unknown. Neo–Laxova syndrome, like the multiple pterygium syndrome, is considered to be a neurogenic arthrogryposis.

Genetics. This is not available.

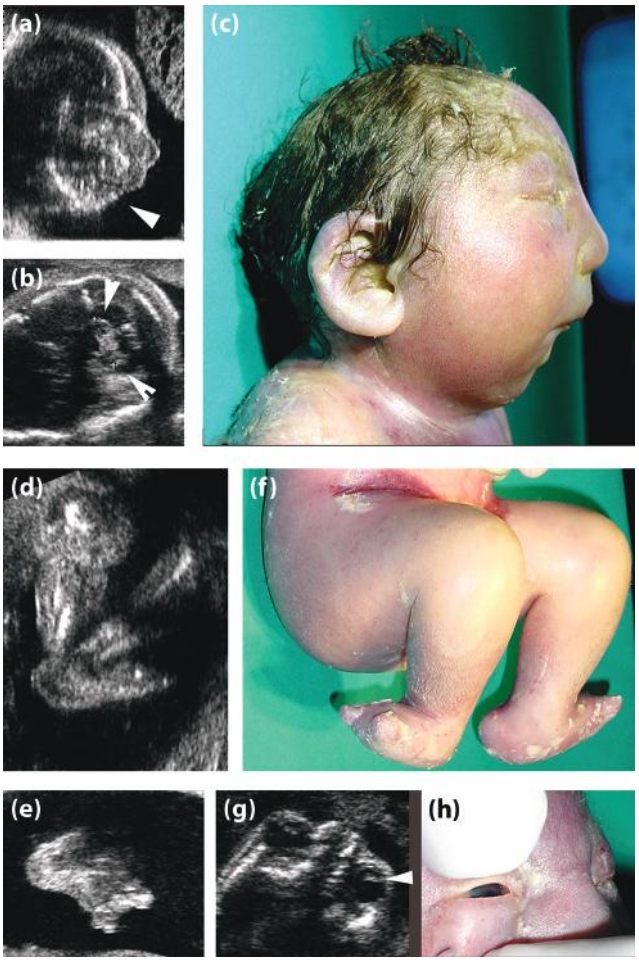


Figure 10.36 Neu–Laxova syndrome. (a) Severe micrognathia; compare with (c). (b) Severe cerebellar hypoplasia and microcephaly; compare with (c). (c) Specimen after birth showing severe microcephaly (sloping forehead), facial soft tissue edema, and micrognathia. (d) Diffuse joint contractures, with abnormal posture of the heel; compare with (f). (e) Edema of foot and toes; compare with (f). (f) Specimen after birth showing arthrogryposis and the abnormal posture of the edematous feet. (g) Corneal opacity (arrowhead). (h) Confirmation at autopsy.

Ultrasound diagnosis. The US appearance of Neu–Laxova syndrome is striking, with multiple severe anomalies present at the same time:

- *Microcephaly* (severe and of early onset): This is subjectively detectable by assessing the *midsagittal view of the fetal profile*, on which the severely slanting forehead, macrophthalmia, and micrognathia are evident at the same time (Figures 10.36a–c and 10.37);
- *CNS anomalies*: these include extremely severe cerebellar hypoplasia (Figure 10.36b);
- *Micrognathia*: this is subjectively detectable on the *midsagittal view of the fetal profile*, on which the severely slanting forehead, macrophthalmia, and micrognathia are evident at the same time (Figures 10.36a,c and 10.37);
- *Arthrogryposis*: this involves all of the muscles, with fixed and adducted limbs and distorted and edematous extremities (Figure 10.36d and f);
- *Edema of the extremities*: this may give a false impression of ectrodactyly, due to the swelling of the digits (Figure 10.36e and f);
- *Proptosis and corneal opacities*: these are recognized on the coronal view of the orbits and the face (Figure 10.36g and h);
- *FGR*: this is severe, symmetric, and of early onset;
- *Lissencephaly*: this can be suspected on US only in the third trimester, when gyri and sulci become evident. In the case of lissencephaly, the outer surface of the brain is smoother.

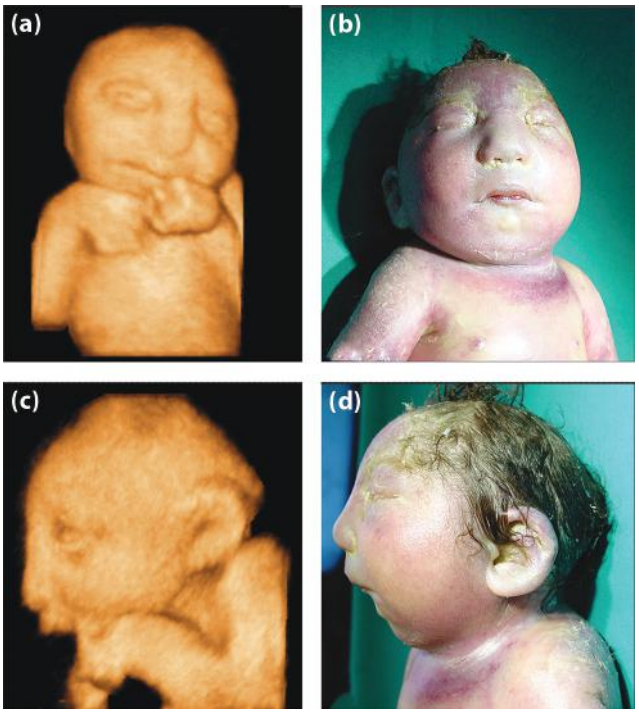


Figure 10.37 Neu–Laxova syndrome. (a) 3D rendering of the fetal head and trunk demonstrating microcephaly, macrophthalmia, and arthrogryposis of the upper limbs, which appear adducted and with clenched hands. (b) Confirmation at autopsy. (c) 3D rendering of the fetal profile demonstrating microcephaly, low-set ears, and micrognathia. (d) Confirmation at autopsy.

Differential diagnosis. This is limited to the other neuroarthrogryposes. However, none of these is associated with so many and so severe anomalies at the same time.

Prognosis, survival, and quality of life. This condition is invariably lethal.

Recurrence risk. Neu–Laxova syndrome has an autosomal recessive inheritance pattern, with a 25% recurrence risk.

Noonan syndrome (NS; OMIM 163950)

Incidenza. Relatively common: 1/1000–1/2500 live-borns.

Etiology. In roughly 50% of the cases, mutations on the PTPN11 on chromosome 12q.24.1 have been found.

Ultrasound diagnosis. Cystic hygroma or enlarged nuchal translucency in the first trimester; late-onset CHD (pulmonary stenosis or cardiomyopathy); abnormal course of ductus venosus.

Outcome. Good survival and virtually normal quality of life. Psychomotor delay with usually moderate mental retardation in 30% of the cases.

Recurrence risk. Sporadic. A minority of autosomal dominant familial cases, with prevalence of maternal transmission, have been described.

Definition NS (OMIM 163950) is a dysmorphic syndrome characterized after birth by hypertelorism, a downward eye slant, low-set posteriorly rotated ears, short stature, a webbed neck, cardiac anomalies, deafness, motor delay, and a bleeding diathesis. The final diagnosis of NS is challenging also in postnatal life, and it is based on clinical features due to its genetic heterogeneity; several scoring systems have been used [34].

Etiology and pathogenesis. NS shows significant genetic heterogeneity, but 50% of the cases have a missense mutation in the *PTPN11* gene on chromosome 12, which encodes the nonreceptor protein tyrosine phosphatase SHP-2. A significant correlation has been found postnatally between the presence versus absence of the *PTPN11* mutation and the type of CHD: patients with the mutation tend to have pulmonary stenosis, whereas those without mainly have cardiomyopathy.

Genetics. Prenatal diagnosis is possible, but it is limited by the above-mentioned genetic heterogeneity to 50%. *PTPN11* gene mutations have been found postnatally in 59% of the familial cases and in 37% of the sporadic ones. Prenatally, mutations of the *PTPN11* gene were found in 11% of cases with cystic hygroma and in 37% of those with cystic hygroma + CHD [35].

Ultrasound diagnosis (Figure 10.38). An US diagnosis is virtually impossible, due to the subtle facial signs and the late onset of the CHD. The diagnosis of NS can only be hypothesized in cases of US detection of the following:

- *Cystic hygroma/nuchal edema/enlarged NT* with normal karyotype, in the first or early second trimester (Figure 10.2d and e);

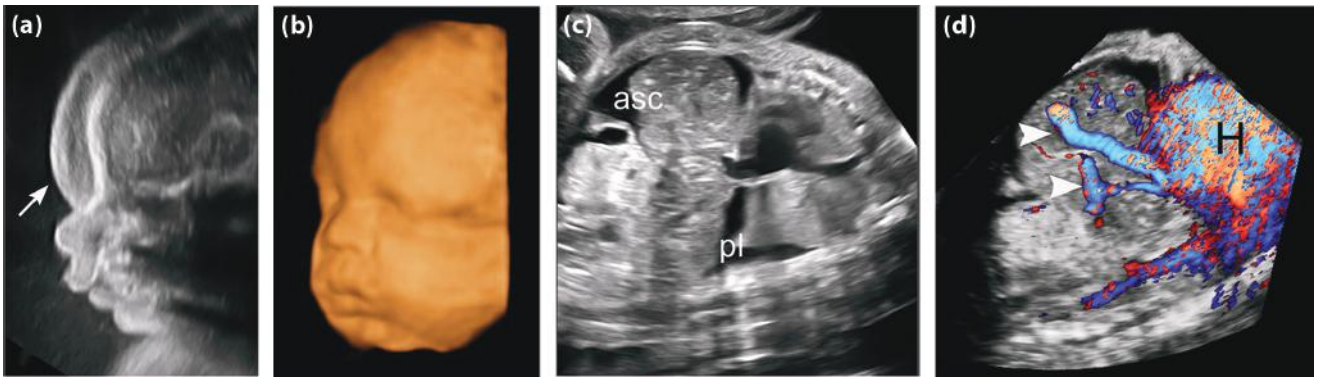


Figure 10.38 Noonan syndrome (30 weeks of gestation). The fetus had been found with an enlarged nuchal translucency in the first trimester (4.1 mm), but the karyotype on chorionic villi was normal. The 20 weeks' anomaly scan was unremarkable. At 30 weeks, the patient was referred for the onset of ascites. The following signs were found at targeted ultrasound: (a) a 2D view of the fetal profile, demonstrating prefrontal edema (arrow); (b) a 3D surface rendering of the face, showing probably the *coarse* facies described postnatally, together with the prefrontal edema; (c) the sagittal view of the fetal trunk demonstrates ascites (asc) and pleural effusion (pl); and (d) the 3D glass-body image of the fetal trunk demonstrates the abnormal course of the ductus venosus (arrowheads), which in part drains directly into the right atrium and in part in the portal system (H: heart).

- *Congenital heart disease:* cardiomyopathy (20% of the cases) or pulmonary stenoses (50%–62% of the cases), both appearing late in pregnancy. As mentioned here, the former is more common in cases with a *PTPN11* gene mutation, and the latter in those without. Much rarer are VSDs (5%–10%);
- *Abnormalities of the ductus venosus* may also be present: agenesis of the ductus venosus or other abnormalities of the porto-umbilical system (Figure 10.38d) [36];
- *Pleural effusion, ascites*, also late onset (Figure 10.38c);
- *Renal anomalies* (hydronephrosis);
- *Polyhydramnios*.

Three-dimensional assessment of the fetal face may sometimes show the typical *coarse facies* described postnatally (Figure 10.38a and b), even though it should be underlined that this feature is so subjective and also so much affected by the acoustic window that it should not be relied upon at all. In this regard, it is important to underscore once more that the diagnosis of NS is (1) clinical, and (2) postnatal. In utero, one can only hypothesize the presence of NS in those fetuses who present with the above-mentioned US signs. In these cases, invasive testing is of limited value because it could confirm the diagnosis in the 50% of the cases showing the *PTPN11* gene [35].

Differential diagnosis. It depends on the availability of a karyotype and the index sign. As for all hydropic cases, especially if late onset, Down and Turner syndrome should be considered if a karyotype is still unknown. If the index sign is the late-onset cardiomyopathy, then attention should be focused on a significant number of nonchromosomal syndromic conditions sharing this anomaly. If the index sign is valvular pulmonary stenosis, then also infections come into discussion, because rubella or cytomegalovirus (CMV) infections can lead to the late development of semilunar valvular stenoses, due to valvulitis followed by inflammatory sealing of the cusps.

Prognosis, survival, and quality of life. Individuals with NS may have a normal life expectancy [35]. In case of cardiac problems, these should be dealt with accordingly. Only the neonates born with hydrops or cardiomyopathy with severe cardiac dysfunction may face an early demise. Psychomotor delay affects 25%–30% of the cases, but it is usually of moderate entity, and it has been demonstrated to improve with time.

Recurrence risk. NS may occur as a sporadic disorder or be autosomal dominant with a predominance of maternal transmission. In the latter case, the recurrence risk is 50%.

Restrictive Dermopathy (OMIM 275210)

Incidence. Extremely rare.

Etiology. A mutation in the *LMNA* and *ZMPSTE24* genes has been found in some cases. It is included in the group of the neuroarthrogriposes with the FADS.

Ultrasound diagnosis. Eyes and mouth wide open; micrognathia; multiple contractures; extended fingers; early IUGR; polyhydramnios.

Outcome. Invariably lethal.

Recurrence risk. The inheritance pattern is autosomal recessive (25% recurrence risk).

Definition Restrictive dermopathy (OMIM 275210) or lethal tight skin contracture syndrome is characterized by ubiquitous contractures and the skin stretched tightly across the face and the body, determining a typical facies.

Etiology and pathogenesis. Mutations of the genes encoding for the zinc metalloproteinase STE24 (ZMPSTE24) and for the lamin A/C (LMNA) have been found in some cases. Histologically, the skin is abnormal, with hyperkeratosis, absence of elastin, and delayed maturation of the pilosebaceous and eccrine sweat apparatus. The epidermis and subcutaneous fat layer are thickened, while the dermis is thin, with dense, thin collagen fibers in parallel with the epidermis.

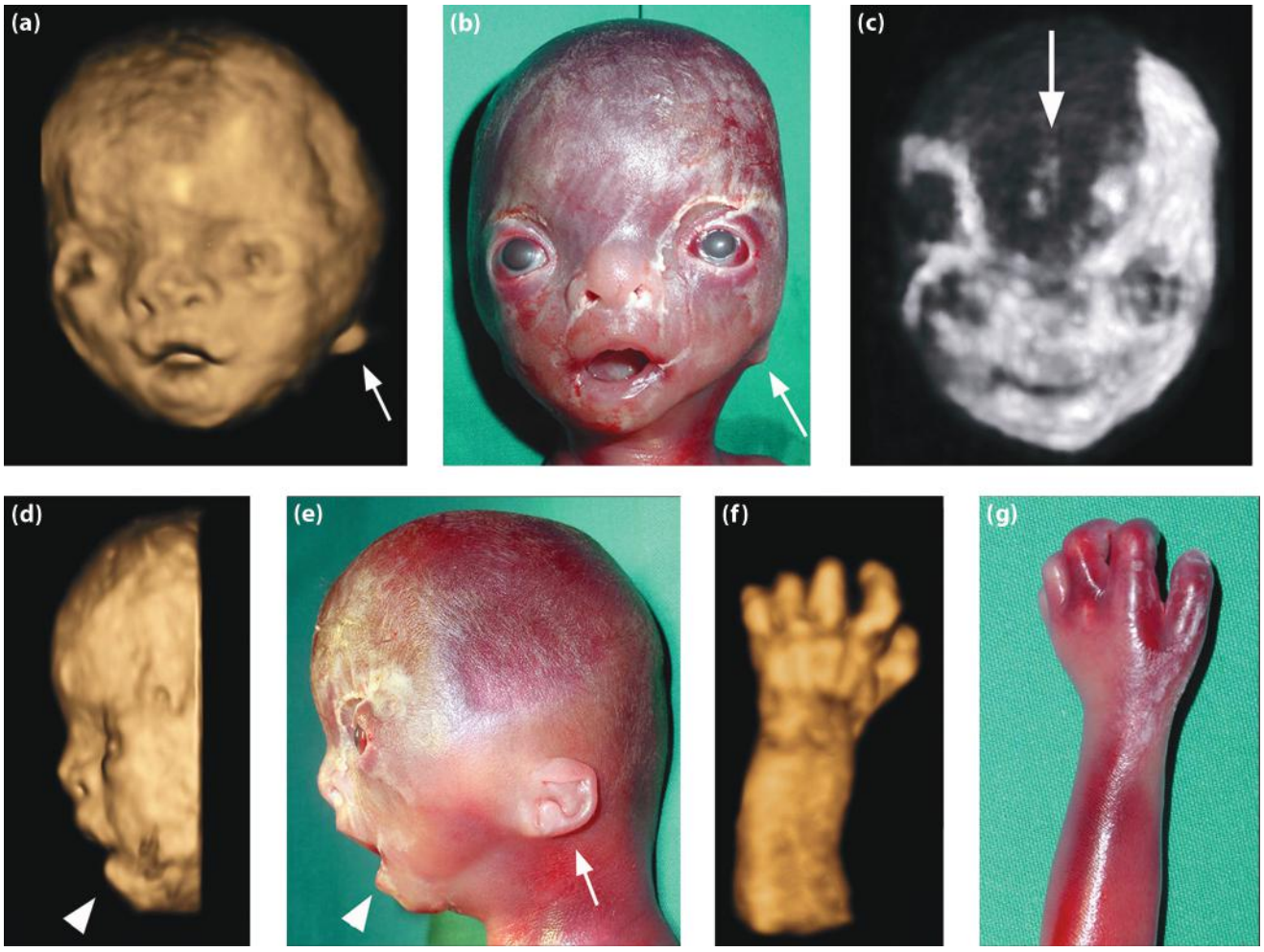


Figure 10.39 Restrictive dermopathy (21 weeks of gestation). (a) Three-dimensional rendering of the face. Because the skin is drawn tightly over the face, the eyelids are retracted, with the eyes wide open; the nose is small; and the lips are similarly retracted, which leads to a permanently open mouth and microstomia. Note also the low-set ear (arrow); (b) autoptic confirmation (note the stretched skin all over the face); (c) three-dimensional maximum-mode imaging shows the severely delayed ossification of the metopic suture and the anterior fontanelle (arrow); (d) a three-dimensional surface-rendered view of the profile demonstrates the small nose and micrognathia (arrowhead); (e) autoptic confirmation (the arrow indicates the low-set and wrinkled ear); (f) 3D surface rendering shows the fixed contracture of one hand, permanently halfway open; and (g) autoptic confirmation.

Genetics. Despite the recognition of these mutations, prenatal diagnosis still relies upon US.

Ultrasound diagnosis (Figure 10.39). Restrictive dermopathy can be recognized from the early second trimester, due to very peculiar signs:

- *Hypertelorism*: this is seen on the axial view of the orbits (Figure 3.34);
- *Persistently open eyes and mouth*: visible also on 2D imaging, but 3D rendering gives a better idea of the severity of the condition (Figure 10.39a, b). This is due to the stretched inextensible skin;
- *Delayed calvarial mineralization, with wide fontanelles and sutures*: These may be seen on 3D US (Figure 10.39c; see also Chapter 2);
- *Micrognathia*: this may be detected on the midsagittal view of the fetal profile (Figure 10.39d and e);
- *Persistently open or semiclenched hands*; these are related to the contractures and the tightness of the skin on the single digits (Figure 10.39f and g);
- *Polyhydramnios*: this is usually severe, due to impaired swallowing.

Differential diagnosis. The findings are very typical, but two conditions should be mentioned. The first is

congenital ichtyosis (*harlequin fetus*), but in this exceedingly rare disease, the lips and orbits are much thicker than in restrictive dermopathy. The second group of conditions is represented by the FADS group, because restrictive dermopathy is included in the neuroarthrogryposes (synaptopathies; see the section on FADS). It shares with FADS the severe and ubiquitous muscular contractures, but in none of the other syndromes in this group are the facial features of restrictive dermopathy found.

Prognosis, survival, and quality of life. Restrictive dermopathy is always lethal.

Recurrence risk. The inheritance pattern is autosomal recessive (25% recurrence risk).

Rubinstein–Taybi syndrome (RSTS; OMIM 180849)

Incidence. Extremely rare.

Etiology. In 20% of cases, a mutation of the gene-encoding CBP, a transcriptional coactivator, mapping to chromosome 16p13.3, has been found.

Ultrasound diagnosis. Wide and abducted thumbs and toes; CNS anomalies; beaked nose; small mouth.

Outcome. Moderate risk of neonatal death. Survivors show moderate-severe mental retardation (mean IQ 51) and a tendency to develop neoplasias.

Recurrence risk. Most cases are sporadic. In the 20% in which the above-mentioned mutation is found, the inheritance pattern becomes autosomal dominant (50% recurrence risk).

Definition Rubinstein–Taybi syndrome (RSTS; OMIM 180849) is named after the two authors who independently described the condition in 1963. It is characterized by moderate-severe mental retardation, microcephaly and other CNS anomalies, and a peculiar facies with a beaked nose and a small mouth. However, the most typical feature of the syndrome, which can be recognized on US, is the presence of wide and abducted thumbs and toes. Inconstantly, clinodactyly and polydactyly can be associated.

Etiology and pathogenesis. A mutation of the gene encoding the transcriptional coactivator CBP (CREB-binding protein, where CREB is cAMP response-element-binding protein), mapping to chromosome 16p13.3, has been found in 20% of individuals affected with RSTS. According to the studies reporting this genetic anomaly, it seems that both a microdeletion and a mutation with gene amputation are sufficient to cause the syndrome.

Genetics. Genetic diagnosis might be performed in cases with a mutation of the CBP gene, which account for 20% of all RSTS. Hence, a positive result may confirm the diagnosis, but a negative one cannot exclude it.

Ultrasound diagnosis (**Figure 10.40**). RSTS can be suspected on US if CNS anomalies are found in association with the above-mentioned abnormalities of the extremities [37]:

- *Microcephaly*: this may also be of late onset; it is detectable on the axial transthalamic view;
- *Other CNS anomalies*: these may include cerebellar hypoplasia and agenesis of the corpus callosum;
- *Wide fontanelles*: these may be seen on 3D US (see Chapter 2);
- *Micrognathia, of variable degree*: this may be detected on the midsagittal view of the fetal profile (Figure 10.40a and b);
- *Wide and abducted thumbs and toes* (Figure 10.40c and d);
- *Beaked nose*: this may be detected on the midsagittal view of the fetal profile (Figure 10.40a and b);
- *Polyhydramnios*, of variable degree.

Differential diagnosis. This is limited to diastrophic dysplasia, which is characterized by the typical "*hitchhiker's* thumb." However, in this disorder, the thumbs are of normal dimensions and there are other anomalies of the osteomuscular apparatus that may help in reaching the correct diagnosis (Chapter 9).

Prognosis, survival, and quality of life. RSTS is not always lethal. If the neonate does not die within the first few weeks of life, the chances of reaching adulthood are high. With regard to the overall prognosis,

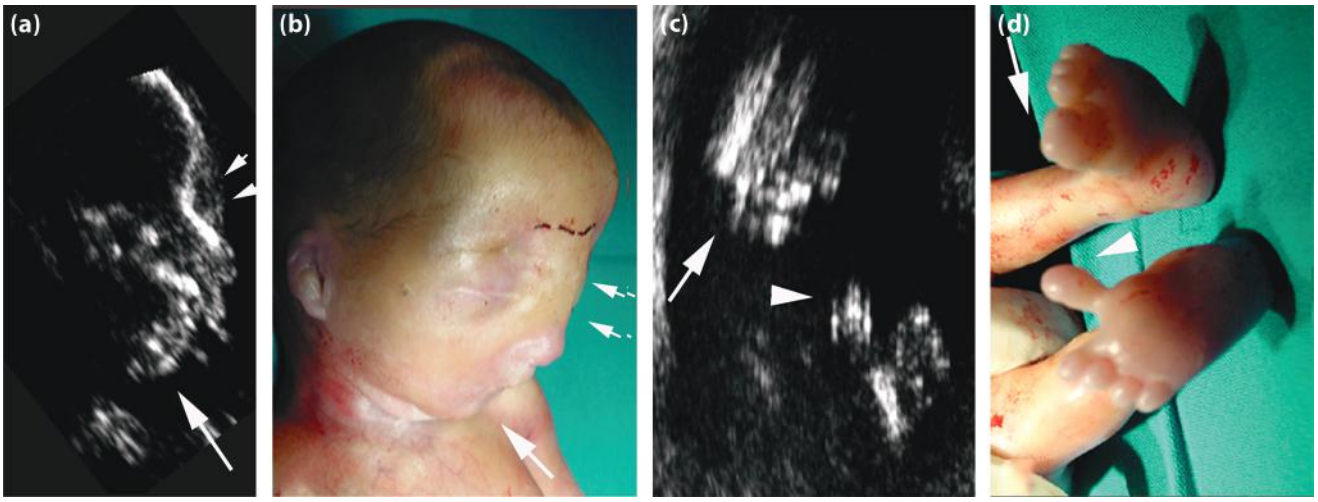


Figure 10.40 Rubinstein–Taybi syndrome. (a) Midsagittal view of the facial profile showing a beaked nose (consider the outline of the soft tissue (arrowheads), not the nasal bones) and the micrognathia (arrow). (b) Confirmation at autopsy. (c) Feet showing the enlarged and abducted toes. (d) Confirmation at autopsy, with the right toe abducted and the left toe enlarged.

it should take into account that RSTS individuals are subjected to failure to thrive, moderately severe mental retardation (with a mean IQ of 51), and a tendency to develop neoplasias.

Recurrence risk. Most cases are sporadic. Those in which the CBP mutation is found show an autosomal dominant transmission pattern, with a 50% recurrence risk.

sMITh–LEMLI–opITz syNdro ME (sLos; oMIM 270400)

Incidence. Extremely rare.

Etiology. It is caused by a mutation in the gene-encoding sterol delta-7-reductase (DHCR7), on chromosome 11q13, which determines deficiency of 7-dehydrocholesterol reductase and, consequently, low cholesterol plasma levels.

Ultrasound diagnosis. Thickened nuchal translucency in the first trimester; microcephaly; hydrocephalus; micrognathia; congenital heart disease (VSD); renal anomalies; ambiguous genitalia; postaxial polydactyly; talipes.

Outcome. Poor. High mortality rate, from intrauterine to neonatal. Moderate to severe mental retardation in survivors.

Recurrence risk. SLOS is an autosomal recessive syndrome. As such, the risk of recurrence is 25%.

Definition Smith–Lemli–Opitz syndrome is a multiple congenital malformation syndrome, a very unique metabolic syndromic condition responsible for the development of fetal anomalies (discussed further here). It is characterized by moderate to severe mental retardation and by the inconstant presence of several subtle signs, few of which are detectable at US.

Etiology and pathogenesis. SLOS is caused by a homozygous or compound heterozygous mutation in the gene-encoding sterol delta-7-reductase (DHCR7), on chromosome 11q13. The consequent deficiency of the 7-dehydrocholesterol reductase blocks its biosynthesis pathway, with low levels of cholesterol and elevated levels of its precursor, 7-dehydrocholesterol. The unavailability of free plasma cholesterol determines the phenotype, considering that cholesterol is extremely important in fetal development. In fact, it is involved in cell and mitochondrial membranes, and it represents a key component in the myelination process of the CNS.

Genetics. Prenatal diagnosis of SLOS is possible on the basis of measurements of 7-dehydrocholesterol in amniotic fluid as reported for the first time in 1994 [38,39]

Table 10.4 Postmortem and postnatal findings versus prenatal ones in 27 SLOS cases

Type of malformation	Autopsy/postnatal	Antenatal detection
Cardiac malformations (AVSD, VSD, HLH, HCMP, PDA, AoCo, and PAVD)	15/27 (55.5%)	3/15 (20.0%)
Renal malformations (horseshoe kidney, hypoplasia or agenesis, and hydronephrosis)	13/27 (48.1%)	4/13 (30.7%)
Polydactyly (postaxial polydactyly, hand or foot)	14/27 (51.8%)	3/14 (21.4%)
Ambiguous genitalia	8/27 (29.6%)	2/8 (25.0%)
Microcephaly at birth (<third centile)	13/20 (65.0%)	0/13 (0)
Cerebral malformations (ACC and holoprosencephaly)	5/27 (18.5%)	3/5 (60.0%)
Total	68 malformations	15/68 (22.1%)

Source: Modified from Goldenberg A et al., *Am J Med Genet A* 124A, 423–6, 2004.
ACC: agenesis of corpus callosum; AoCo: aortic coarctation; AVSD: atrioventricular septal defect; HCMP: hypertrophic cardiomyopathy; HLH: hypoplastic left heart syndrome; PAVD: pulmonary abnormal venous return; PDA: patent ductus arteriosus (two cases); VSD: ventricular septal defect.

Ultrasound diagnosis. SLOS can be hypothesized prenatally on the basis of US signs, but the detection rate of this important syndromic condition is very low, because the spectrum of congenital anomalies that these fetuses and neonates have is wide, and in the majority of cases only subtle signs, almost impossible to detect with US, are present [40] (Table 10.4). Nonetheless, it should be considered that if a fetus has IUGR (sometimes already in the second trimester) and one or more of the major anomalies among those listed below, SLOS is certainly a possibility worth investigating (cholesterol in amniotic fluid or chorionic villi)

- *IUGR*: early or, more commonly, late onset and of variable degree (Figure 10.41);
- *Microcephaly*: this is usually late onset (Figure 10.41); it is detectable on the axial transthalamic view;
- *Other CNS anomalies* (less frequent): holoprosencephaly, agenesis of the corpus callosum, and cerebellar hypoplasia;
- *Micrognathia*: this may be detected on the midsagittal view of the fetal profile;
- *Congenital heart disease*: AVSD, VSD, coarctation of the aorta, and anomalous pulmonary venous return;
- *Renal anomalies*: horseshoe kidney, hypoplasia or agenesis, and hydronephrosis;
- *Ambiguous genitalia*: sex reversal in males;
- *Polydactyly*: postaxial and more frequently of hands than feet;
- *Thickened nuchal translucency* [41];
- *Low maternal estriol level on the triple test*: hence, in cases in which the triple test analyte results are particularly low (<30 MoM), an amniocentesis to investigate the possibility of SLOS is certainly indicated, especially if targeted US has demonstrated one or more anomalies [42].

An issue to remember is that a significant number of malformations described in this condition involve the midline (agenesis of corpus callosum, holoprosencephaly, encephalocele, micrognathia, horseshoe kidney, and ambiguous genitalia).

Also, it is important to underline that a thickened nuchal translucency has been found at 13 weeks in fetuses and neonates subsequently found to have SLOS [41]. This is of crucial importance because in the families with a positive history, the recognition of a nuchal translucency >95th centile at the time of the CVS (to check cholesterol on the villi) represents a high risk factor for SLOS.

Differential diagnosis. This is a challenging task. In the limited cases in which there is IUGR + a major cardiac or cerebral malformation, the much more common autosomal trisomies 13 and 18 should be ruled out, making an amniocentesis. Secondarily, in the much rarer cases in which there is IUGR + microcephaly or cataract (very rarely associated with SLOS), CMV infection should also be considered and ruled out by checking maternal serology (immunoglobulin G and M [IgG and IgM, respectively] and Ig avidity). Finally, SLOS shares with campomelic dysplasia (see Chapter 9) micrognathia + ambiguous genitalia. However, bowed and short femurs (and tibiae) are present in the vast majority of cases in the latter disease but not in SLOS.

Prognosis, survival, and quality of life. The perinatal mortality rate is relatively high. The survivors experience moderate to severe mental retardation, while

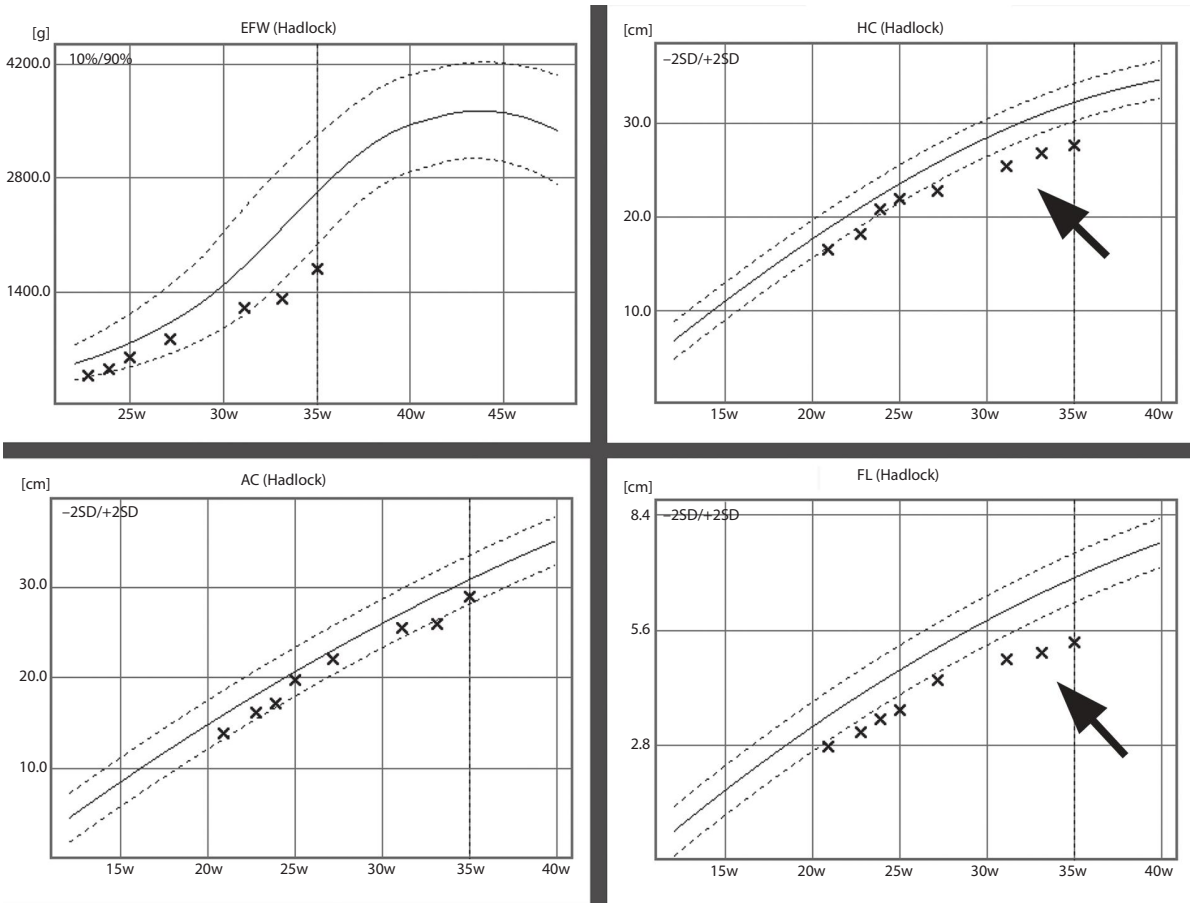


Figure 10.41 Smith–Lemli–Opitz syndrome (SLOS). The four graphs demonstrate how both microcephaly and femur shortening were late onset (arrows). The abdominal circumference remained within the normal range throughout gestation. AC: abdominal circumference; EFW: estimated fetal weight; HC: head circumference; FL: femur length.

the initial muscular hypotonia turns to hypertonia with time. Feeding difficulties are also a frequent problem

Recurrence risk. SLOS is inherited as an autosomal recessive trait, with a 25% recurrence risk.

TUBERo Us scLEros Is coMpLEx (Tsc; oMIM 191100)

Incidence. Rare.

Etiology. In most cases, TSC is due to two mutations in either the *TSC1* or *TSC2* genes, mapping respectively on chromosome 9q34.13 and 16p13.

Ultrasound diagnosis. Cardiac rhabdomyomata; brain tuberi (late onset).

Outcome. High risk of moderate to severe mental retardation, epilepsy, and autism. Ubiquitous hamartomata.

Recurrence risk. TSC is inherited as an autosomal dominant trait, so the risk of recurrence is 50%, if one of the parents is affected. *De novo* mutations are responsible for two-thirds of cases.

Definition TSC (OMIM 191100) is a multisystem disorder inherited with autosomal dominant inheritance pattern. It is characterized by a wide clinical spectrum, with individuals who barely have cutaneous signs and other individuals with severe neurologic problems (epilepsy, developmental delay, mental

retardation, and autism) and with hamartomas in multiple organ systems, including the brain, skin, heart, kidneys, and lung.

Etiology and pathogenesis. Two-thirds of cases represent *de novo* mutations, while the remainder is inherited from one parent. Ten to thirteen percent of cases are associated with a mutation in the *TSC1* gene (encoding hamartin), located on chromosome 9q34.13, whereas 75%–80% of sporadic cases are associated with a mutation in the *TSC2* gene (encoding tuberin), located on chromosome 16p13. The protein products of the two genes, hamartin and tuberin, act together to regulate cell growth. Only 10%–20% of the cases do not have a specific mutation, and these are deemed to be due to mosaicism. Individuals with *TSC2* mutations have a more severe form of the disorder than those with *TSC1* mutations, and the degree of mental retardation is much higher.

Genetics. Prenatal diagnosis of TS is therefore possible by searching for the *TSC1* and *TSC2* mutations [43]. Usually, this is performed in case of family history or on detection of cardiac rhabdomyomata.

Ultrasound diagnosis (Figures 10.42 and 10.43). US findings that can support the diagnosis of TSC are as follows:

- *Cardiac rhabdomyomata (Figure 10.42)*, detected on the four-chamber view of the fetal heart (see Chapter 5);
- *Structural brain abnormalities (Figure 10.43)*: tubers, subependymal nodules, and subependymal giant cell astrocytomas (SEGAs).

Natural history. A diagnosis of TSC cannot be established on sonographic criteria in all cases, because of the natural history of TCS (described in this chapter). Only when cardiac rhabdomyomata are found in association with brain lesions can a diagnosis of TSC be made with US. However, in most cases this occurs in the third trimester only. In most cases not referred because of a positive family history, the finding that prompts further evaluation is the recognition of rhabdomyomata, which usually appear from 22 gestational weeks onward [44]. At that time, brain lesions are absent in the overwhelming majority of cases. To understand the evolving prenatal presentation of TS, the following issues should be considered:

- The number of cardiac rhabdomyomata may increase with advancing gestational age [44];

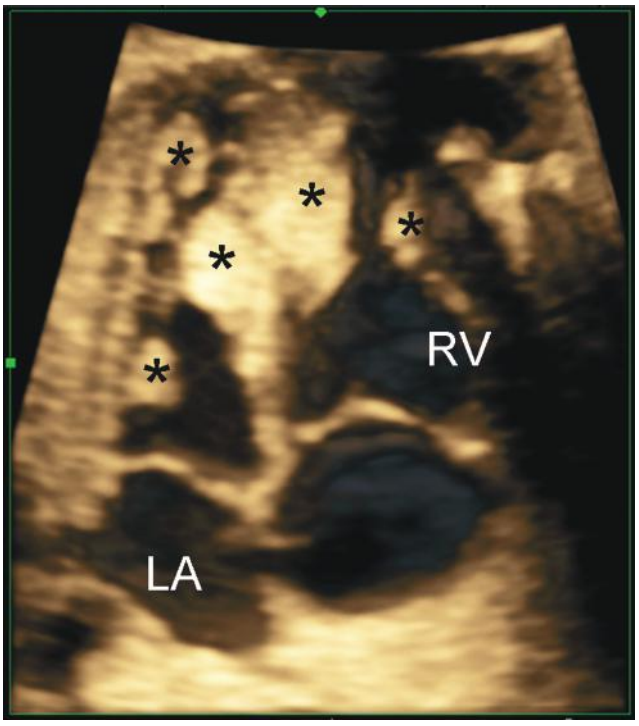


Figure 10.42 Tuberous sclerosis complex (33 weeks of gestation). 3D rendering of the four-chamber view showing five rhabdomyomata (asterisks). LA: left atrium; RV: right ventricle. Three more were evident on the outflow tract views.

- The size of cardiac rhabdomyomata usually increases until 32–35 weeks, then plateaus and eventually regresses significantly after birth [45]. It has been speculated that this biphasic behavior is due to the fact that tumor growth would be due to the maternal hormonal milieu;
- Brain lesions may be absent at presentation in the second trimester, and arise only on follow-up [46,47];
- The risk of TSC is significantly different for single and multiple rhabdomyomata. Overall, the association with TSC ranges from 50% to 79% [44,48]. Multiple tumors seem to have a much higher association with TSC than a single tumor: 95% versus 23%–42% [48].

Differential diagnosis. This is limited to the cardiac tumors, because in virtually all cases the recognition of the brain lesions follows the diagnosis of the rhabdomyomata, to support TCS as the underlying cause of both. The only differential diagnosis of a cardiac rhabdomyomata is with the fibroma However, this will apply only in the minority of cases in which the rhabdomyomata is single, because only these tumors may be multiple, but not the fibromas or other histotypes. Fibromas are much

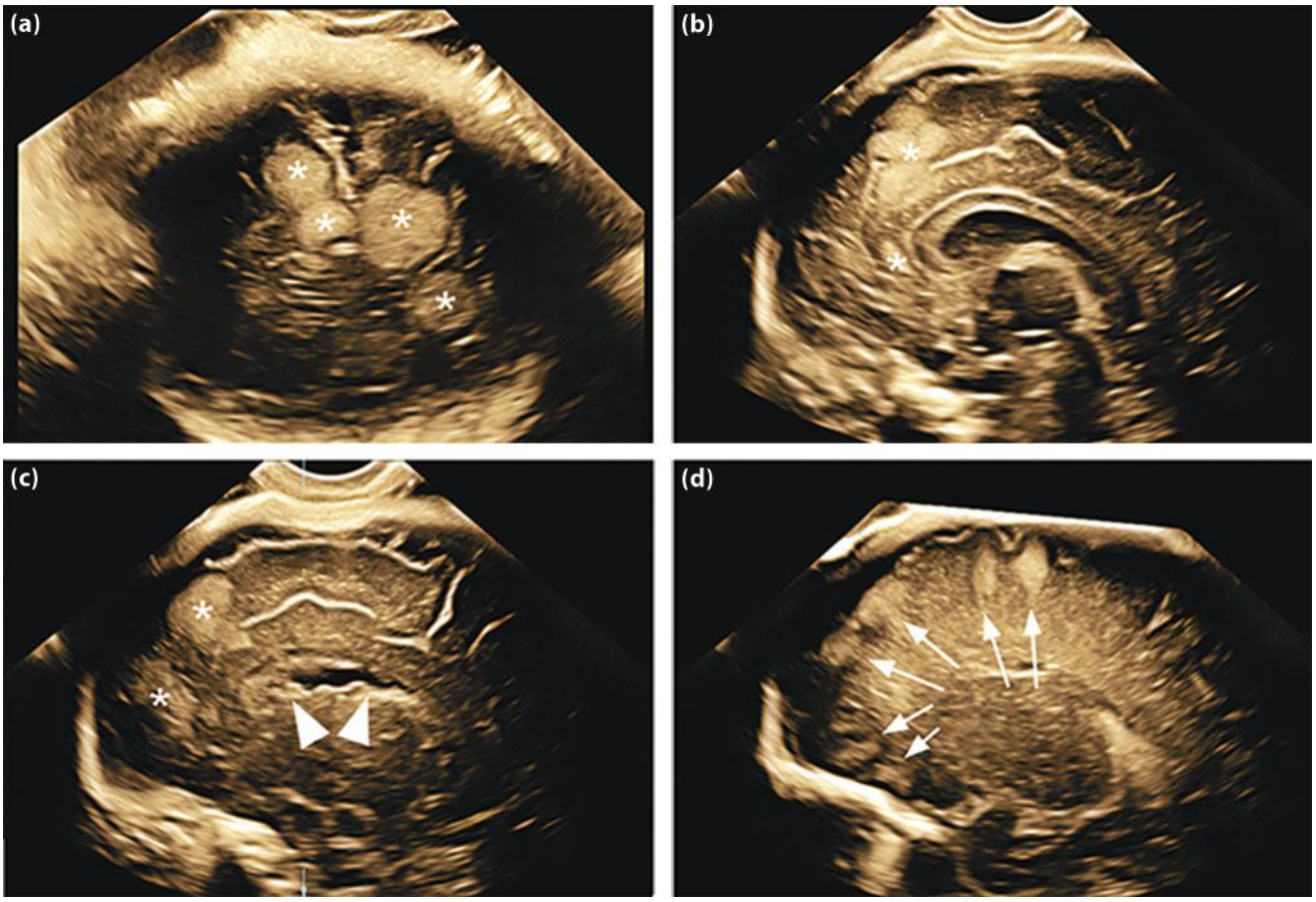


Figure 10.43 Tuberous sclerosis complex (33 weeks of gestation). Several brain lesions are evident on the coronal view of the frontal lobes (a) and the sagittal views of both hemispheres (b–d). Note the multiple tubers (arrows and asterisks) and the subependymal nodules (arrowheads).

rarer than rhabdomyomata, they may be associated with a pericardial effusion, and they are usually larger.

Prognosis, survival, and quality of life. An unknown percentage of TSC individuals dies by the age of 20 from intractable epilepsy, lung, or renal problems. Survivors experience neurologic problems in roughly 30% of cases, with developmental delay, epilepsy (often drug refractory), and autism. Astrocytomas may obstruct the foramen of Monro, determining an obstructive hydrocephalus. Renal problems include hemorrhage and renal insufficiency from progressive compression from the angiomyolipomas. In this regard, preclinical studies have shown the efficacy of mTOR inhibitors in inhibiting the tumor growth in animal models of TSC. In the clinical setting, mTOR inhibitors (rapamycin and sirolimus) have shown promising efficacy in patients with TSC-associated angiomyolipomas and subependymal giant cell astrocytomas. Hence, mTOR inhibitor therapy as a systemic therapeutic approach to treat the underlying cause of TSC is under investigation worldwide. The drawbacks of this pharmacological therapy are that (1) it is effective as long as it is administered, with the hypothetical need for a lifelong therapy; and (2) the drug is toxic, causing apthous ulceration, interstitial pneumonitis, and hyperlipidemia.

Recurrence risk. If one of the parents is affected, the recurrence risk is 50%, TSC being an autosomal dominant disease. However, familial cases account for only one-third of all TSC cases, most being due to *de novo* mutations. In the latter case, the recurrence should be very low. Nonetheless, it has happened that apparently healthy couples have had more than one affected child, which has been explained with an increased incidence of gonadal mosaicism in TSC. Gonadal mosaicism is the situation where an apparently unaffected parent has a population of affected cells confined to his or her gonads, and therefore he or she is liable to have more than one affected child.

VATER (VACTER) Association

Incidence. Rare.

Etiology. Unknown. More common in cases of maternal insulin-dependent diabetes.

Ultrasound diagnosis. Vertebral anomalies; anal anomalies; cardiac defects; tracheoesophageal fistula; renal anomalies; limb anomalies (aplasia radii).

Outcome. Depends on the severity of the various anomalies.

Recurrence risk. Most cases are sporadic.

Definition In 1972, this malformative cluster of various apparati was defined as VATER–VACTER–VACTERL (OMIM 192350), according to the different anomalies present at the same time. The original acronym (VATER) refers to the nonrandom association of the following malformations: vertebral anomalies (fusion, hemivertebrae, and scoliosis), anal anomalies (anorectal atresia), tracheoesophageal fistulae and renal anomalies (dysplasia, hydronephrosis, and ectopia). Then, the "C" (for cardiac defects: VSD, tetralogy of Fallot, and transposition of the great arteries) and the "L" (for limbs: aplasia radii and polydactyly) were added if necessary. Also, a variant named VACTERL-H association has been described, wherein the "H" stands for hydrocephalus.

Etiology and pathogenesis. The etiology is unknown. A significant association has been found with maternal diabetes.

Genetics. This is not available.

Ultrasound diagnosis (Figures 10.44 through 10.46). The diagnosis is difficult because of the wide spectrum of anomalies that can be present for each apparatus (Table 10.5) [7,49]. The major anomalies most frequently recognized in the fetus are as follows:

- *Scoliosis or hemivertebrae*: this is evident on the *coronal view of the spine* (Figures 10.44a, 10.45d, and 10.46a);
- *Cardiac defects*: these include various types of congenital heart defects (TGA, Fallot, and VSD);
- *Renal anomalies*: these include agenesis, ectopia, hydronephrosis (Figure 10.45b and c; Figure 10.46, inset), and horseshoe kidney;
- *Limb anomalies*: the most common of these is aplasia radii (Figure 10.45a; see also Figure 9.35).

In Table 10.5, a list of the various anomalies found postnatally in patients with VACTERL association is shown. As evident, the spectrum of possible anomalies

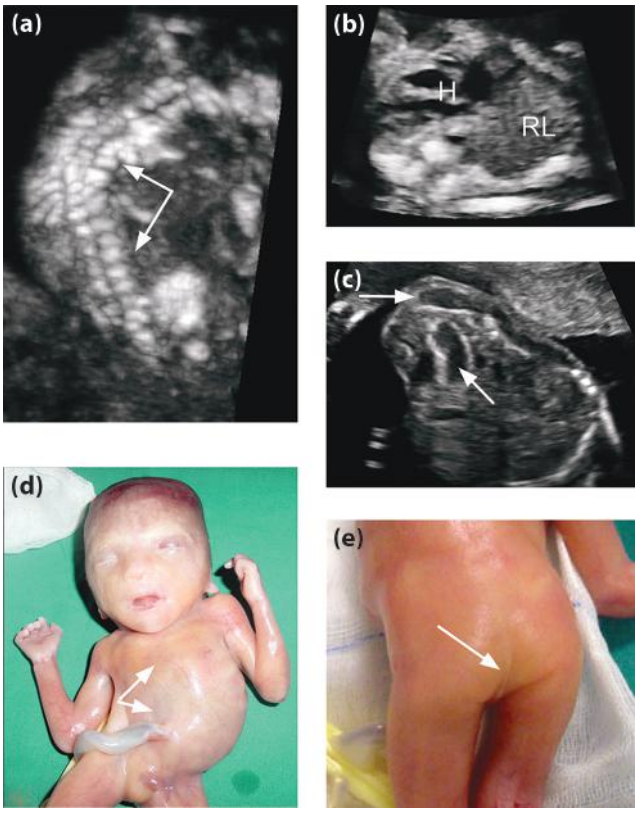


Figure 10.44 VA(C)TER(L) association (21 weeks of gestation). (a) Severe scoliosis and thoracic deformation (arrows) due to multiple vertebral anomalies, including a hemivertebra, and the ribs also are abnormal; (b) left lung agenesis was associated; (c) in the pelvis, the rectum is abnormally dilated (arrows), which was a sign of anorectal atresia; (d) autoptic confirmation: note the severe scoliosis and consequent marked asymmetry of the thorax (arrows); and (e) the posterior view of the pelvis confirms anal atresia.

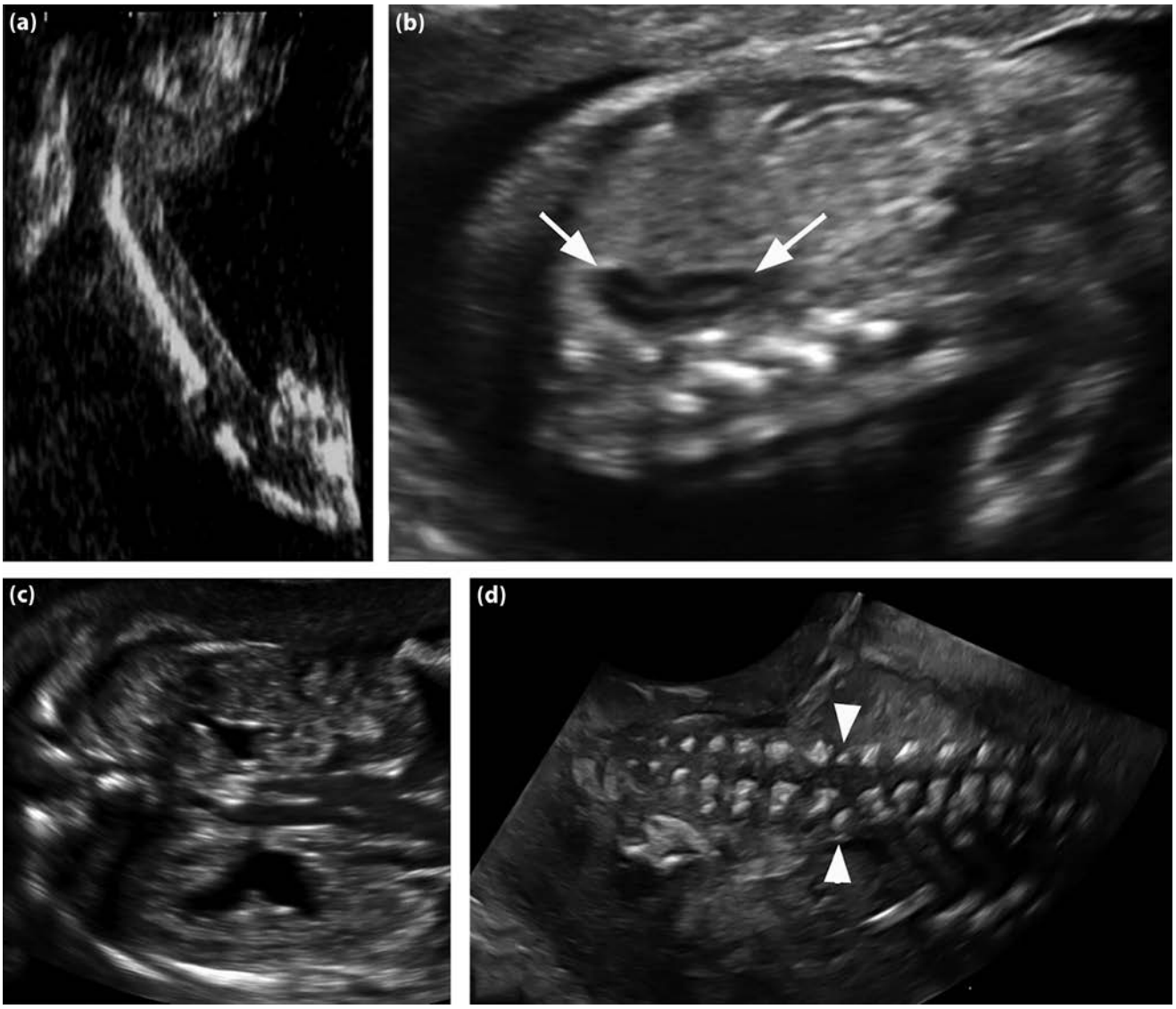


Figure 10.45 VA(C)TER(L) association. Other signs possibly indicative of this nonrandom association of congenital anomalies are (a) aplasia radii; (b) unilateral renal agenesis (note the verticalized adrenal gland; see arrows); (c) hydronephrosis; and (d) an abnormal spine, with wedge vertebrae (arrowhead) or hemispondilus.

per anatomical system varies significantly; in relation to the prenatal diagnosis issue, three categories can be identified: (1) very subtle malformations, the diagnosis of which also represents a challenge postnatally (vertical vertebral clefts, anal stenosis, etc.); (2) major malformations that cannot be diagnosed prenatally or are recognized only late in pregnancy (tracheoesophageal atresia, anal atresia (Figure 10.44c and e), some VSDs, and vertebral fusion); and (3) major malformations that can be adequately diagnosed prenatally (TGA, Fallot, radial aplasia, hemivertebrae, cystic renal dysplasia, unilateral renal agenesis, and ectopia).

A comment should be made regarding the feasibility of prenatal diagnosis of VACTERL association, because a significant number of colleagues have been sued worldwide for missing a prenatal diagnosis of such a malformation cluster. Table 10.5 demonstrates irrefutably that only a very minority of cases with VACTERL association can be diagnosed prenatally. The fact that only a few case reports have been published in the last 20 years, and no major case series, is a further confirmation.

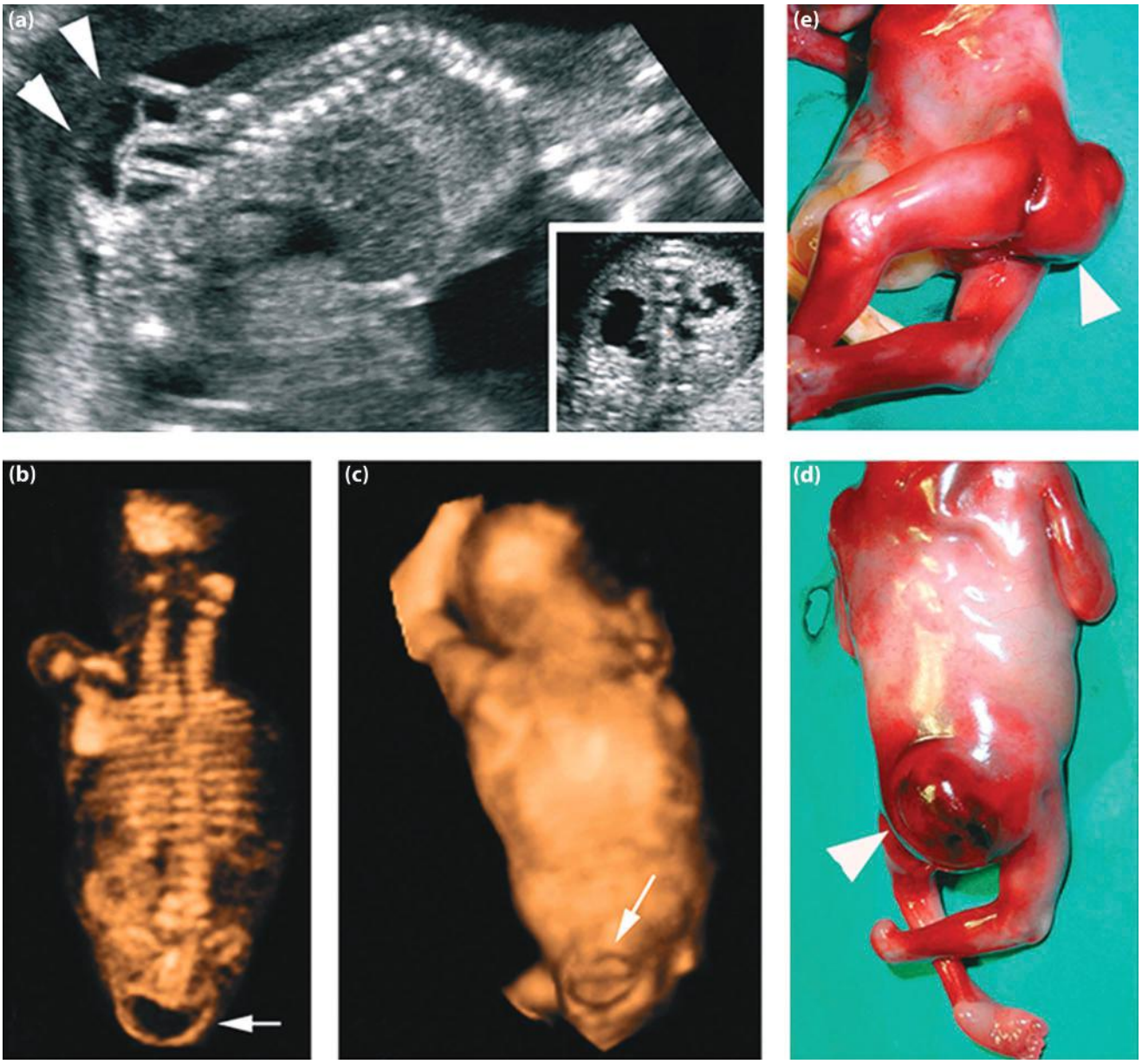


Figure 10.46 VA(C)TER(L) association (22 weeks of gestation). An unusual case sharing some features with the caudal regression sequence complex. (a) A large defect of the caudal part of the spine involving the lumbar and sacral tracts (arrowheads). The inset shows bilateral renal dysplasia. (b) 3D maximum-mode rendering demonstrating the vertebral anomalies and the wide sacral defect (arrow). (c) The same image, but with surface-rendering mode showing the cystic sacral lesion (arrow). (d and e) Autoptic confirmation; compare with (b) and (c).

Differential diagnosis. Considering the wide range of malformations that involve several organ systems, the differential diagnosis issue is a complicated one for the VACTERL association. The simple task is to rule out the autosomal trisomies 13 and 18 by doing a karyotype in those cases in which malformations such as VSD, tetralogy of Fallot, or aplasia radii are diagnosed. The more difficult part would be to differentiate VACTERL association from other rare, nonchromosomal syndromic conditions that may feature some of the malformations present in VACTERL association (Table 10.6) [49]. Note that for aplasia radii, the differential diagnosis includes Fanconi anemia, TAR syndrome, and trisomy 18 (Chapter 9).

Table 10.5 Congenital anomalies present in VA(C)TER(L) association

Vertebral anomalies	**60–80%**
Hemivertebrae	
Butterfl vertebrae[a]	
Wedge vertebrae[a]	
Vertebral fusion[a]	
Vertebral dysplasia[a]	
Scoliosis	
Congenital heart disease	**40–80%**
TGA	
Tetralogy of Fallot	
VSD	
Anal atresia[a]	**55–90%**
Tracheoesophageal fistul [a]	**50–80%**
Radial ray defects	**40–50%**
Radial aplasia and hypoplasia	
Radio-ulnar synostosis[a]	
Thumb hypoplasia[a], syndactyly, pre-axial polydactyly	
Renal anomalies	**50–80%**
Unilateral agenesis, horseshoe kidney, ectopia	
Cystic dysplasia	
Hydronephrosis	
Ectopia	
Single umbilical artery	**35%**

Source: Modified from Jones KL, *Smith's Recognizable Patterns of Human Malformation*, 6th edn., WB Saunders, Philadelphia, PA, 2006; Solomon BD, *Orphanet J Rare Dis* 6, 56, 2011.

[a] Not detectable prenatally in most cases.

TGA: transposition of the great arteries; VSD: ventricular septal defects.

Prognosis, survival, and quality of life. The outcome depends obviously on the severity and the time-lined management of the various abnormalities. Heart defects (TGA and Fallot), anorectal malformations, tracheoesophageal fistulae and tethered cord (associated with vertebral defects) require an early surgical approach. Functional impairment may represent a problem for individuals with scoliosis (from hemivertebrae) or severe radial defects. Mental retardation is not expected in VACTERL association.

Recurrence risk. VACTERL association is a sporadic anomaly, and therefore the recurrence risk is extremely low.

Table 10.6 Differential diagnosis of VA(C)TER(L) association

• Alagille syndrome
• Baller–Gerold syndrome
• CHARGE syndrome
• Currarino syndrome
• 22q11 microdeletion
• Fanconi anemia
• Feingold syndrome
• Fryns syndrome
• Hemifacial microsomia[a]
• Holt–Oram syndrome
• MURCS association
• Opitz G/BBB syndrome
• Pallister–Hall syndrome
• Townes–Brocks syndrome

[a] Also known also as Goldenhar syndrome or oculo-auricolo-vertebral spectrum (OAVS).

CHARGE: *C*olobomata, *H*eart anomaly, choanal *A*tresia, *R*etardation of growth and development, *G*enital anomalies, *E*ar anomalies; MURCS: Müllerian duct aplasia, *R*enal aplasia, and *C*ervico-thoracic *S*omite dysplasia, also known as Mayer–Rokitansky–Küster–Hauser syndrome type II.

References

1. Agathokleous M, Chaveeva P, Poon LCY, et al. Meta-analysis of second trimester markers for trisomy 21. *Ultrasound Obstet Gynecol* 2013; 41: 247–261.
2. Odibo AO, Sehdev HM, Gerkowicz S, et al. Comparison of the efficiency of second-trimester nasal bone hypoplasia and increased nuchal fold in Down syndrome screening. *Am J Obstet Gynecol* 2008; 199: 281.
3. Benacerraf FR, Barss VA, Laboda LA. A sonographic sign for the detection in the second trimester of the fetus with Down syndrome. *Am J Obstet Gynecol* 1985; 151: 1078–80.
4. Chaoui R, Heling KS, Sarioglu N, et al. Aberrant right subclavian artery as a new cardiac sign in second- and third-trimester fetuses with Down syndrome. *Am J Obstet Gynecol* 2005; 192: 257–63.
5. Paladini D, Sglavo G, Pastore G, et al. Aberrant right subclavian artery: incidence and correlation with other markers of Down syndrome in second-trimester fetuses. *Ultrasound Obstet Gynecol* 2012; 39: 191–5.
6. Borenstein M, Minekawa R, Zidere V, et al. Aberrant right subclavian artery at 16 to 23 + 6 weeks of gestation: a marker for chromosomal abnormality. *Ultrasound Obstet Gynecol* 2010; 36: 548–52.
7. Jones KL. *Smith's Recognizable Patterns of Human Malformation*, 6th edn. Philadelphia, PA: WB Saunders; 2006.
8. Paladini D, Greco E, Sglavo G, et al. Congenital anomalies of upper extremities: prenatal ultrasound diagnosis, significance and outcome. *Am J Obstet Gynecol* 2010; 202: 596.
9. Surerus E, Huggon IC, Allan LD. Turner's syndrome in fetal life. *Ultrasound Obstet Gynecol* 2003; 22: 264–7.
10. Goldmunts E. DiGeorge syndrome: new insights. *Clin Perinatol* 2005; 32: 963–78.
11. Volpe P, Marasini M, Caruso G, et al. Prenatal ultrasound diagnosis of interruption of the aortic arch and its association with deletion of chromosome 22q11. *Ultrasound Obstet Gynecol* 2002; 20: 327–31.
12. Paladini D, Russo M, Teodoro A, et al. Prenatal ultrasound diagnosis of congenital heart disease in the Naples area during the years 1994–1999 – the experience of a joint fetal–pediatric cardiology unit. *Prenat Diagn* 2002; 22: 545–52.
13. Chaoui R, Kalache KD, Heling KS, et al. Absent or hypoplastic thymus on ultrasound: a marker for deletion 22q11.2 in fetal cardiac defects. *Ultrasound Obstet Gynecol* 2002; 20: 546–52.
14. Faro C, Chaoui R, Wegrzyn P, et al. Metopic suture in foetuses with Apert syndrome at 22–27 weeks of gestation. *Ultrasound Obstet Gynecol* 2006; 27: 28–33.
15. Williams DH, Gauthier DW, Maizels M. Prenatal diagnosis of Beckwith–Wiedemann syndrome. *Prenat Diagn* 2005; 25: 879–84.
16. Vora N, Bianchi D. Genetic considerations in the prenatal diagnosis of overgrowth syndromes. *Prenat Diagn* 2009; 29: 923–9.
17. Rump P, Zeegers MPA, van Essen AJ. Tumor risk in Beckwith–Wiedemann syndrome: a review and meta-analysis. *Am J Med Genet* 2005; 136A: 95–104.

18. Binder KH. Dysostosis maxilla-nasalis, ein arhinencephaler missbildungskomplex. *Deutsch Zahnaerztl DZZ* 1962; 17: 438–44.
19. Levaillant JM, Moeglin D, Zouiten K, et al. Binder phenotype: clinical and etiological heterogeneity of the so-called Binder maxillonasal dysplasia in prenatally diagnosed cases, and review of the literature. *Prenat Diagn* 2009; 29: 140–50.
20. Delaire J, Tessier P, Tulasne JF, et al. Clinical and radiological aspects of maxillonasal dysostosis (Binder syndrome). *Head Neck Surg* 1980; 3: 105–22.
21. Volpe P, Buonadonna AL, Campobasso G, et al. Cat-eye syndrome in a fetus with increased nuchal translucency: three-dimensional ultrasound and echocardiographic evaluation of the fetal phenotype. *Ultrasound Obstet Gynecol* 2004; 24: 485–7.
22. Pajkrt E, Griffin DR, Chitty LS. Brachmann–de Lange syndrome: definition of prenatal sonographic features to facilitate definitive prenatal diagnosis *Prenat Diagn* 2010; 30: 865–72.
23. Paladini D, Maruotti GM, Sglavo G, et al. Diagnosis of femoral hypoplasia-unusual facies syndrome in the fetus. *Ultrasound Obstet Gynecol* 2007; 30: 354–8.
24. Nowaczyk MJ, Huggins MJ, Fleming A, et al. Femoral-facial syndrome: prenatal diagnosis and clinical features. Report of three cases. *Am J Med Genet A* 2010; 152A: 2029–33.
25. Brueton LA, Huson SM, Cox PM, et al. Asymptomatic maternal myasthenia as a cause of the Pena–Shokeir phenotype. *Am J Med Genet* 2000; 92: 1–6.
26. Michalk A, Stricker S, Becker J, et al. Acetylcholine receptor pathway mutations explain various fetal akinesia deformation sequence disorders. *Am J Human Genet* 2008; 82: 464–76.
27. Paladini D, Tartaglione A, Agangi A, et al. Pena–Shokeir phenotype in three consecutive pregnancies. *Ultrasound Obstet Gynecol* 2001; 17: 163–5.
28. Paladini D, D'Armiento MR, Ardovino I, et al. Prenatal diagnosis of the cerebro-oculo-facio-skeletal (COFS) syndrome. *Ultrasound Obstet Gynecol* 2000; 16: 91–3.
29. Maruotti GM, Paladini D, Agangi A, et al. Prospective prenatal diagnosis of Fraser syndrome variant in a family with negative history. *Prenat Diagn* 2004; 24: 69–70.
30. Martinelli P, Maruotti GM, Agangi A, et al. Prenatal diagnosis of hemifacial microsomia and ipsilateral cerebellar hypoplasia in a fetus with oculo-auricolo-vertebral spectrum. *Ultrasound Obstet Gynecol* 2004; 24: 199–201.
31. Volpe P, Gentile M. Three-dimensional diagnosis of Goldenhar syndrome. *Ultrasound Obstet Gynecol* 2004; 24: 798–800.
32. Castori M, Brancati F, Rinaldi R, et al. Antenatal presentation of the oculo-auriculo-vertebral spectrum (OAVS). *Am J Med Genet* 2006; 140A: 1573–9.
33. Paladini D, Morra T, Teodoro A, et al. Prenatal diagnosis and hemodynamic evaluation of Klippel–Trenaunay–Weber syndrome. *Ultrasound Obstet Gynecol* 1998; 11: 215–17.
34. Van der Burgt I. Noonan syndrome. *Orphanet J Rare Dis* 2007; 2: 4.
35. Lee KA, Williams B, Roza K, et al. PTPN11 analysis for the prenatal diagnosis of Noonan syndrome in fetuses with abnormal ultrasound findings *Clin Genet* 2009; 75: 190–4.
36. Volpe P, Marasini M, Caruso G, et al. Prenatal diagnosis of ductus venosus agenesis and its association with cytogenetic/congenital anomalies. *Prenatal Diagn* 2002; 22: 995–1000.
37. Greco E, Sglavo G, Paladini D. Prenatal sonographic diagnosis of Rubinstein-Taybi syndrome. *J Ultrasound Med* 2009; 28: 669–72.
38. Johnson JA, Aughton DJ, Comstock CH, et al. Prenatal diagnosis of Smith-Lemli-Opitz syndrome, type II. *Am J Med Genet* 1994; 49: 240–3.
39. Dallaire L, Mitchell G, Giguere R, et al. Prenatal diagnosis of Smith-Lemli-Opitz syndrome is possible by measurement of 7-dehydrocholesterol in amniotic fluid *Prenatal Diag* 1995; 15: 855–8.
40. Goldenberg A, Wolf C, Chevy F, et al. Antenatal manifestations of Smith-Lemli-Opitz (RSH) syndrome: a retrospective survey of 30 cases. *Am J Med Genet A* 2004; 124A: 423–6.
41. Hyett JA, Clayton PT, Moscoso G, et al. Increased first trimester nuchal translucency as a prenatal manifestation of SmithLemli-Opitz syndrome. *Am J Med Genet* 1995; 58: 374–6.
42. Shinawi M, Szabo S, Popek E, et al. Recognition of Smith-Lemli-Opitz syndrome (RSH) in the fetus: utility of ultrasonography and biochemical analysis in pregnancies with low maternal serum estriol. *Am J Med Genet A* 2005; 138: 56–60.
43. Milunsky A, Ito M, Maher TA, et al. Prenatal molecular diagnosis of tuberous sclerosis complex. *Am J Obstet Gynecol* 2009; 200: 321
44. Bader RS, Chitayat D, Kelly E, et al. Fetal rhabdomyomata: prenatal diagnosis, clinical outcome, and incidence of associated tuberous sclerosis complex. *J Pediatr* 2003; 143: 620–4.
45. Paladini D, Palmieri S, Russo MG, et al. Cardiac multiple rhabdomyomatosis: prenatal diagnosis and natural history. *Ultrasound Obstet Gynecol* 1996; 7: 84–5.
46. Saada J, Hadj Rabia S, Fermont L, et al. Prenatal diagnosis of cardiac rhabdomyomatas: incidence of associated cerebral lesions of tuberous sclerosis complex. *Ultrasound Obstet Gynecol* 2009; 34: 155–9.
47. Levine D, Barnes P, Korf B, et al. Tuberous sclerosis in the fetus: second-trimester diagnosis of subependymal tubers with ultrafast MR imaging. *AJR Am J Roentgenol* 2000; 175: 1067–9.
48. Tworetzky W, McElhinney DB, Margossian R, et al. Association between cardiac tumors and tuberous sclerosis in the fetus and neonate. *Am J Cardiol* 2003; 92: 487–9.
49. Solomon BD. VACTERL/VATER association. *Orphanet J Rare Dis* 2011; 6: 56.

Chapter 11
Ultrasound in fetal infection

rATIONALE Approach ANd dIAGNostIc poTENTIAL

For the new edition of this book, we decided to add a few chapters, and the one that we believed was needed is this one covering the role of ultrasound (US) in fetal infection. However, having always in mind what inspired us—*from the sign to the diagnosis*—we have decided to split the chapter into two sections: (1) US signs possibly indicative of a fetal infection, and (2) the signs that can be expected if a fetus is infected or at high risk of being infected. In most cases, in our routine work at the screening level, we face the former scenario: we perform an US scan and find a suspicious sign in the fetus of a patient who is not known to be at risk (or whom we do not know to be at risk). In this situation, the US finding represents the fulcrum of the whole diagnostic flowchart: what are the chances that this sign is indicative of an infection or a malformation, or—in the case of a soft marker, such as hyperechogenic ileus—indicates that the fetus is perfectly healthy? Second, if we consider an infection likely, what is going to be the prognosis—and, consequently, the diagnostic flowchart? The second scenario is usually seen only in tertiary-care centers where a patient is referred due to seroconversion or risk of vertical transmission for a viral, bacterial, or protozoan infection. In this case, we already know, or come to know, that the fetus we are going to scan is indeed infected. Hence, the scan is targeted to ascertain whether specific or aspecific signs of infection and, more importantly, damage are present or not. This type of scan—often together with a late magnetic resonance imaging (MRI) (28–30 weeks of gestation)—is of crucial importance in the evaluation of the prognosis, even though, as we will see, its predictive value is somewhat limited. US signs possibly indicative of fetal infection are summarized in Table 11.1. As the reader will see from reading this chapter, these do not change significantly by the type of infection [1].

In this introduction, we would also like to underline that this section does not represent a thorough assessment on the issue of vertical transmission of maternal infection in pregnancy. Several textbooks have been published on this topic, and the reader is referred to them for insight into this complex diagnostic and prognostic problem.

cyTomEGALoVIrUs

Cytomegalovirus (CMV) is a DNA virus of the herpes family. In developed countries, the incidence of congenital CMV infection ranges from 0.3% to 2.4% of live-borns, and in the overwhelming majority of cases, it is the effect of primary maternal CMV infection [2]. The vertical transmission rate is 40%, with a range of 24%–75%, according to the time of infection and maternal serological status. Timing of maternal infection is linearly correlated with the chances of fetal infection and inversely correlated with the severity of feto-neonatal infection (Table 11.2). In a very limited number of cases, congenital CMV infection may derive from a nonprimary infection (e.g., a reinfection from a different strand or reactivation)[3]. In this case, the vertical transmission rate is much lower than that of primary maternal infection, ranging from 1% to 2.2%. However, there is mounting evidence that, contrary to what was believed until a few years ago, nonprimary CMV infection also may determine symptomatic and severe congenital infection.

Diagnosis of maternal infection. Most women who are infected in pregnancy remain asymptomatic; less than 5% report aspecific symptoms and signs such as arthralgia, low fever, moderate lymph node swelling, and mononucleosis-like syndrome. Since preconceptional and early-pregnancy CMV screening is not offered in most countries, the infection is often suspected when fetal signs are detected at US. The most reliable method to assess the possibility of fetal CMV

Table 11.1 US signs of fetal infection

• Aspecific signs of fetal infectio
• Intrauterine growth restriction (IUGR)
• Oligohydramnios
• Hyperplacentosis
• Hyperechoic ileus
• Specific signs of fetal infectio
• Brain lesions (including calcifications
• Hydrops (including ascites, pleural effusion, subcutaneous and prefrontal edema, and enlarged nuchal translucency)
• Hepatomegaly, splenomegaly, and abdominal calcification
• Myocarditis
• Anemia
• Cataract

infection, when a formal serology maternal evaluation is not available, is the anti-IgG avidity test, because it has been repeatedly shown that immunoglobulin M (IgM) may persist in maternal blood up to one year after the end of the acute phase of primary infection. A high avidity stands in favor of a past infection, and if this occurs at 12–16 weeks, it virtually excludes the possibility of vertical transmission. Primary infection is detected in the presence of IgM associated with low IgG avidity (usually <30%). If a high IgG avidity is found in association with positive IgM, it denotes reinfection.

Diagnosis of fetal infection. Vertical transmission is thought to occur hematogenously, through infected maternal leucocytes that pass the placental barrier. In suspected cases, fetal infection is established by means of amniocentesis carried out more than 6 weeks after the primary infection and, anyway, after 21 weeks of gestation. This is due to the fact that six–eight weeks are needed after maternal infection for the virus to be excreted in fetal urine [4] and that fetal disease is more likely to be severe if the infection is contracted before the 16th week of pregnancy. Direct virus search can be done, but it shows relatively low sensitivity (70%–80%); on the contrary, both qualitative and, above all, quantitative polymerase chain reaction (PCR) for viral DNA are highly accurate (90%–98% sensitivity and 92%–98% specificity for qualitative PCR). Furthermore, the quantitative evaluation also shows prognostic significance: a viral load of less than 10^3 copies/mL is associated with favorable neonatal outcome and no severe damage [5,6]. On the contrary, viral loads of more than 10^3 and 10^5 denote infected fetuses and symptomatic fetuses, respectively [6].

In general, after a primary maternal infection, most neonates are asymptomatic (85%–90%); 30%–40% show signs of fetal infection, but only 10%–15% are symptomatic. In the last group, 90% show severe complications and 20%–30% die of infection [7].

Ultrasound. US signs possibly indicative of fetal CMV can be classified into cerebral and extracerebral, due to the frequent involvement of the brain in severe CMV infection [8–12]. Extracerebral signs are rather aspecific being similarly found in other viral and nonviral infections of the fetus (Table 11.3). Cerebral signs are shown in Figures 11.1 through 11.4. Most findings are related

Table 11.2 Cytomegalovirus infection in pregnancy: relationships between time of maternal infection, incidence of transmission to the fetus, and severity of feto-neonatal infection

Time of maternal infection	Probability of vertical transmission	Feto-neonatal infection[a]
First trimester	14%	Severe
Second trimester	29%	Moderate
Third trimester	60%	Mild

[a] Overall, 4% of infected fetuses and neonates die or develop severe neurologic impairment.

Table 11.3 US lesions and signs associated with Citomegalovirus (CMV) infection

- Cerebral
  - Brain atrophy (microencephaly, microcephaly) (Figure 11.2a and b)
  - Secondary ventriculomegaly (hemorrhage)
  - Obstructive hydrocephalus
  - Cortical calcifications (Figure 11.2)
  - Candlestick calcifications of caudate nucle
  - Subependymal edema (halo) (Figure 11.1)
  - Fibrin strands in the occipital horn (Figure 11.1b)
  - Subependymal cysts (Figure 11.3)
  - Periventricular focal pattern (hyperechogenicity + cysts)
  - Hemorrhage (supra- or infratentorial) (Figure 11.4)
  - Destruction of corpus callosum
- Extracerebral
  - Face and neck
    - Edema, prefrontal or diffuse
    - Cataract
  - Thorax and heart
    - Pleural effusion (Figure 11.5a)
    - Myocarditis (Figure 11.5b)
  - Abdominal
    - Hepatomegaly (Figure 11.6b)
    - Splenomegaly (Figure 11.6b)
    - Liver calcification
    - Echogenic ileus (Figure 11.6a)
    - Ascites
  - Adnexa
    - Thickened placenta (Figures 11.5a and 11.7)
    - Oligohydramnios

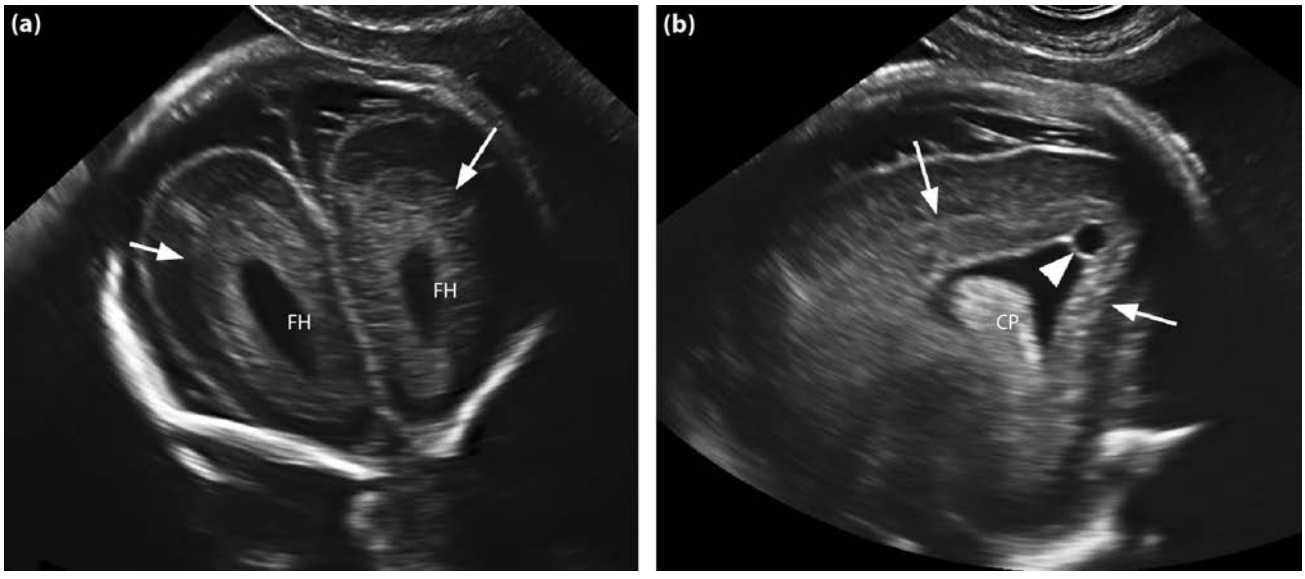


Figure 11.1 Cytomegalovirus infection at 22 weeks of gestation. One of the cerebral signs is the presence of a subependymal halo (arrows), due to inflammatory infiltration and, on some occasions, cortical necrosis. (a) A coronal view at the level of the frontal horns (FH) showing the periventricular subependymal halo (arrows); and (b) a sagittal view of the occipital horn showing the same pattern (arrows) and, in addition, a fibrin strand (arrowhead) typical of the acute inflammatory process. CP: choroid plexus.

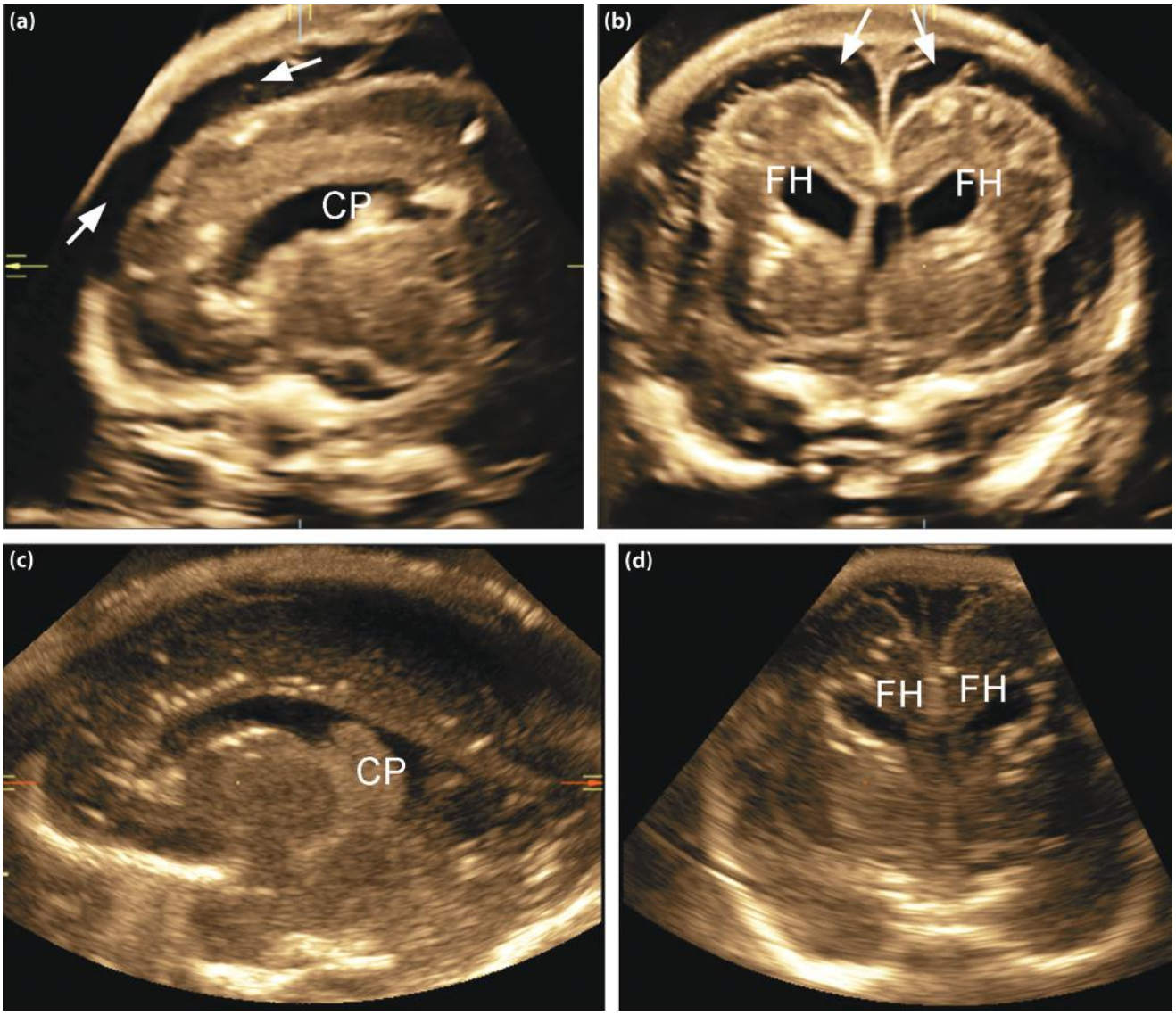


Figure 11.2 Cytomegalovirus infection at 22 (a and b) and 32 (c and d) weeks of gestation. Diffuse calcifications are seen in both cases, but in (a) and (b) also microencephaly is evident. (a) A sagittal view of the lateral ventricle showing diffuse calcifications and widened subdural spaces (arrows); (b) a coronal view at the level of the frontal horns (FH) showing the same findings (note the large subdural spaces (arrows) due to the concurrent microencephaly; the brain is small due to early neuronal loss from severe CMV infection); (c) a sagittal view of the lateral ventricle showing diffuse calcifications; and (d) a coronal view at the level of the frontal horns (FH) showing diffuse calcification and a normal ratio between brain volume and subdural spaces. CP: choroid plexus.

to ventriculitis and encephalitis, leading to inflamm - tory reaction of the ependyma and the subependymal layers (Figure 11.1) [9,10]. Diffuse calcifications are also very common, and they usually follow the vascular distribution (Figure 11.2). Less frequently, subependymal cysts (Figure 11.3) and hemorrhages (Figure 11.4) also can be seen in fetuses infected with CMV, with the latter probably favored by the thrombocytopenia that complicates the most severe cases [11,12].

Extracerebral signs include a variable combination of cataract, pleural effusions (Figure 11.5a), myocarditis (Figure 11.5b), echogenic ileus (Figure 11.6a), hepatosplenomegaly (with spleen enlargement prevailing on liver enlargement; Figure 11.6b), thickened placenta, and oligohydramnnios (Figure 11.7).

As is evident, brain signs are more specific, even though they can be found in other viral infections, such as rubella. However, they are much more specific

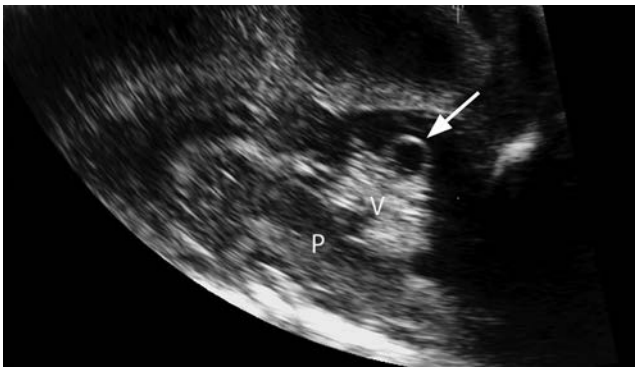


Figure 11.3 Cytomegalovirus infection at 32 weeks of gestation. In this case, in addition to diffuse cerebral calcification (see Figure 11.3), a cerebellar cyst also (arrow) was present. P: pons; V: vermis.

than the extracerebral ones, which may trigger an infinite round of differential diagnoses: let us only think about the echogenic ileus, which is associated with cystic fibrosis, Down syndrome, ileal atresia, and so on.

US has repeatedly been demonstrated to yield suboptimal accuracy in the prediction of symptomatic and severe infection at birth (Table 11.3). The apparent discrepancy in the results is due also to the fact that different outcome measures were considered in the various studies: in fact, symptomatic infection is not synonymous with poor (neurological) outcome in all cases.

MRI. Few papers have recently been published on the role of MRI in predicting symptomatic neonatal infection and poor outcome, comparing its performance to that of US [13–16]. They have almost the same sample sizes (38, 38, 38, 49 cases) and come almost to the same conclusions, with some caveats. In general, it seems that the addition of MRI to US increases the positive predictive value but cannot replace US [13,14]. At the same time, it seems that subtle MRI findings should not be considered as worrying in the absence of major MRI or US ones [15]. However, the major result shared by all groups is that fetuses with negative US and negative MRI are highly likely to be asymptomatic and well after birth [13–16]. A comment is needed regarding the timing of the MRI examination: in three-fourths of the studies, this was carried out between 28 and 34 weeks, with the last reporting a median gestational age of 25 weeks at first MRI [14]. This represents an important detail, because it means that what was said in this chapter does not apply to a midtrimester MRI evaluation

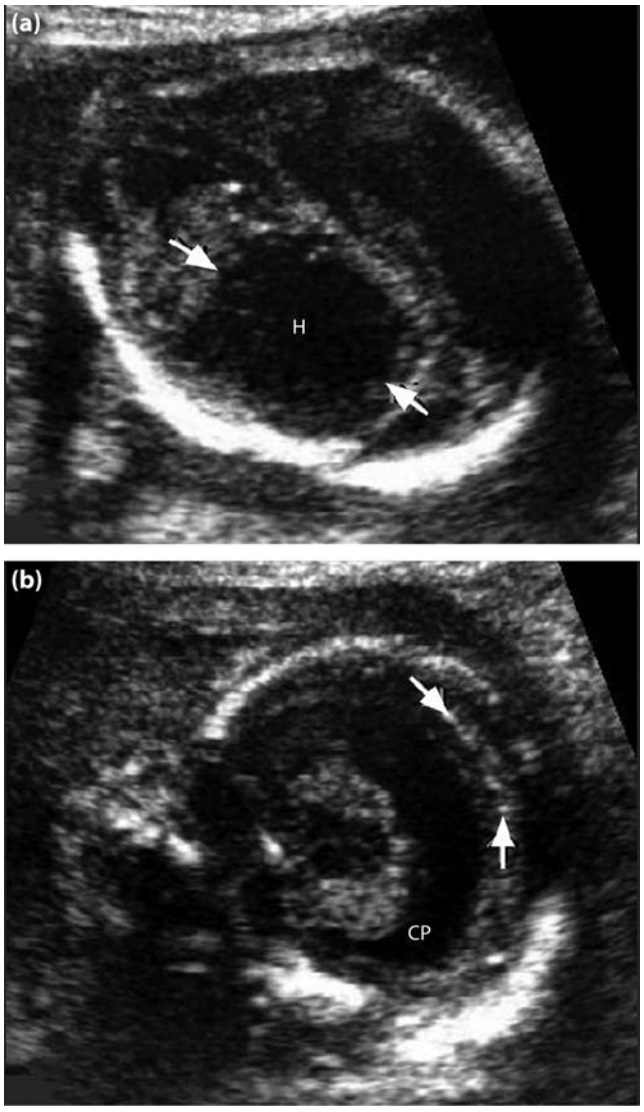


Figure 11.4 Cytomegalovirus infection at 24 weeks of gestation. (a) The axial view of the brain shows severe parenchymal hemorrhage of the parietal lobe (H and arrows); and (b) the slightly parasagittal view of the brain demonstrates the associated calcifications. CP: choroid plexus.

that may be completely useless in those countries in which termination of pregnancy is allowed only up to 23 weeks of gestation.

Outcome. Overall, the outcome of fetal CMV infection is the following: 80–90% will be completely asymptomatic; and, of the remainder, 5%–10% will have moderate symptoms (hepatosplenomegaly, thrombocytopenia, hepatitis, and meconium peritonitis), and 5%–10% will develop severe sequelae (cerebral lesions, hearing

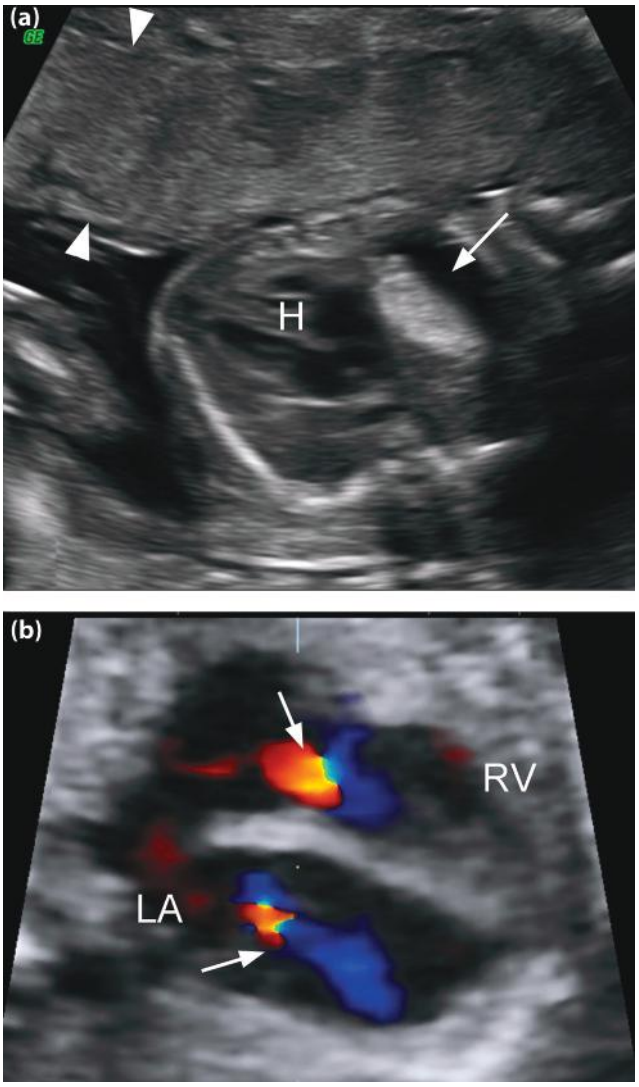


Figure 11.5 Cytomegalovirus infection at 24 weeks of gestation. (a) The four-chamber view demonstrates right pleural effusion (arrow), associated with a lung echogenic lesion, and thickened placenta (arrowheads); and (b) the magnified color Doppler image shows moderate cardiomegaly and bilateral atrioventricular regurgitation (arrows), due to viral myocarditis (LA: left atrium; RV: right ventricle).

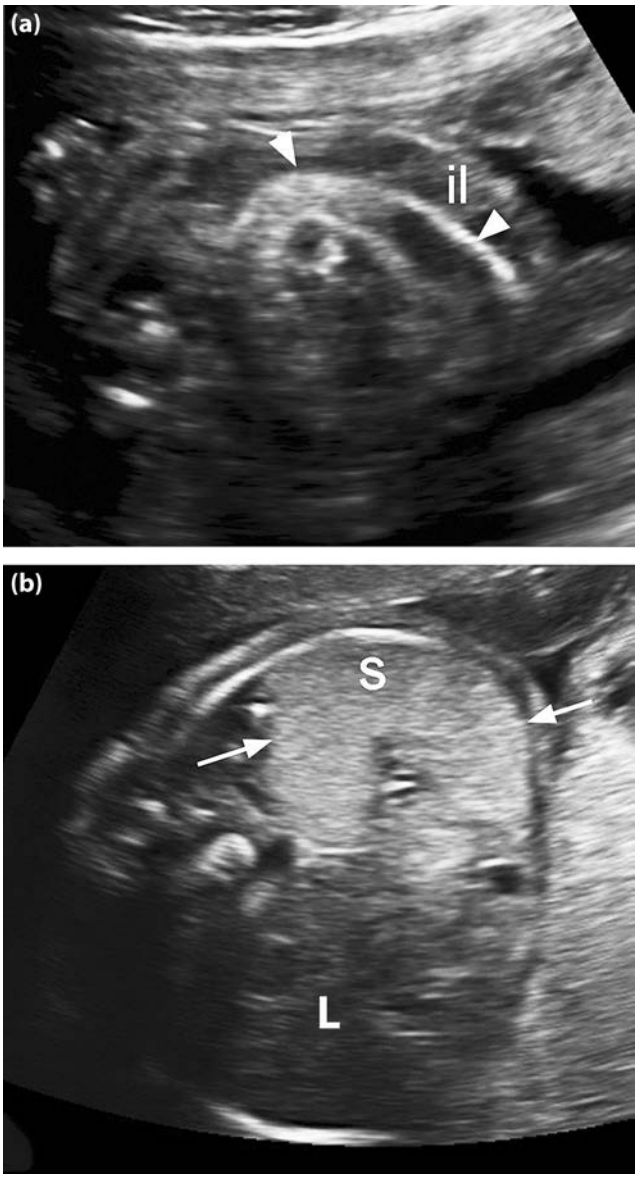


Figure 11.6 Cytomegalovirus infection. Additional extracerebral, rather aspecific signs are (a) echogenic ileus (il: arrowheads); and (b) splenomegaly (S: arrows) and hepatomegaly (L), with the former prevailing on the latter.

loss, and severe psychomotor delay). Some therapeutic attempts have been made, so far with limited success, using Valacyclovir, and a randomized trial is currently underway in France.

In conclusion, the following should be remembered:

1. The timing of maternal infection is linearly correlated with the chances of fetal infection (14, 29, and 60% in the first, second, and third trimesters, respectively) and inversely correlated with a poor outcome (highest risk in first-trimester infections).
2. The method of choice for diagnosing fetal infection is an amniocentesis performed after 21 completed gestational weeks, on which both a quantitative PCR for the viral DNA and an amniotic fluid culture are done.
3. Eighty to 90% of infected neonates are asymptomatic at birth, with only 10%–15% showing mental retardation or hearing loss.
4. If brain lesions are demonstrated by US and/or MRI in a fetus known to be infected (or at high risk

of being infected) with CMV, the outcome is likely to be poor and the neonate highly symptomatic.

5. In contrast, if both US and MRI are normal, the outcome is highly likely to be good, with an asymptomatic infection in the neonate and a normal outcome.
6. However, hearing loss and mental retardation also have been found in cases with isolated abdominal signs (echogenic ileus and/or hepatosplenomegaly) and no brain lesions.
7. An early prediction of outcome—in the course of the second trimester—remains a major challenge.

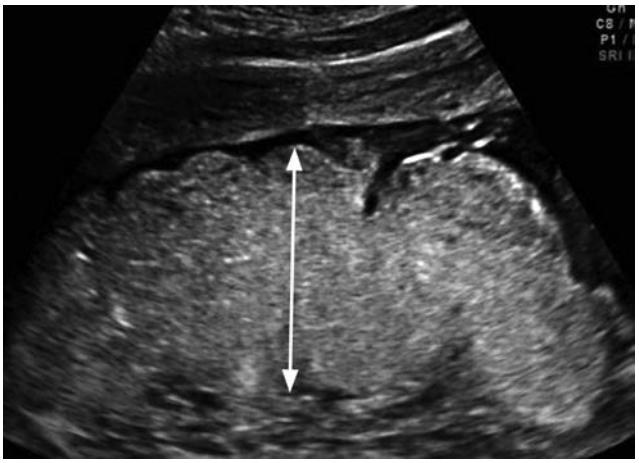


Figure 11.7 Cytomegalovirus infection. Aspecific signs also include thickened placenta (arrows) and oligohydramnios. Both are evident in this image.

pAr Vo VIr Us B19

Parvovirus B19 is a single-stranded DNA virus of the Parvoviridae family. It was isolated for the first time in 1975, and it was called B19 because it was found in Panel B, Sample 19, of the laboratory testing kit. In children, it is responsible for the *fifth disease* (slapped face disease, or erythema infectiosum), whereas in adults it is asymptomatic in about 50% of cases, being responsible for aspecific symptoms in the remainder (fever, arthralgia, and headache). The onset of symptoms, when present, corresponds to the appearance of IgM in the maternal blood (viremia). At this time, the vertical transmission is maximal, around 25% [17]. The incidence of feto-neonatal mortality and morbidity decreases with advancing gestational age, probably in relation to passive transfer of maternal IgG after 25 weeks of gestation [18].

Diagnosis of maternal infection. In general, 15%–50% of women of childbearing age are susceptible to Parvovirus B19 infection, but few become infected. The real problem is that, as said in this chapter, about 50% of infected women are asymptomatic, and the remainder usually do not seek specialized medical advice other than for treating headache and/or "fl - like" symptoms. Hence, the more common scenario for suspecting maternal Parvovirus B19 infection is when fetal hydrops associated with fetal anemia is detected. When the fetus is referred for specialized assessment and management, the maternal infection is discovered by checking the IgG and IgM on maternal blood. Much more rarely, the mother reports for assessment after contact with a child known to have developed the fifth disease. Whatever the path leading to maternal blood testing, the serology status of the mother needs to be interpreted:

1. IgG positive and IgM negative demonstrate an "absence of recent infection."
2. IgG and IgM negative demonstrate maternal susceptibility and warrant further testing in three–four weeks.
3. IgG positive or negative and IgM positive confirm maternal infection with Parvovirus B19.

Confirmed maternal infection in the absence of fetal signs should prompt biweekly US monitoring of fetal conditions and Doppler assessment of the middle cerebral artery peak systolic velocity (MCAPSV), which has been shown to be the best way to noninvasively detect fetal anemia from whatever cause [19], including Parvovirus B19 infection [20].

Diagnosis of fetal infection. In the fetus, Parvovirus B19 infection causes severe anemia due to massive destruction of red blood cell precursors. As mentioned in this chapter, in most cases the pregnancy is referred for expert assessment when fetal hydrops or ascites is detected on standard US scans. In the expert setting, the anemic status is confirmed by checking the MCAPSV on spectral Doppler. This often triggers an emergency intrauterine transfusion due to the deteriorated fetal conditions, and only when the transfusion is initiated is a small fetal blood sample taken to check the fetal red blood cell and platelet counts and to look for viral DNA in amniotic fluid by PCR. The presence of maternal

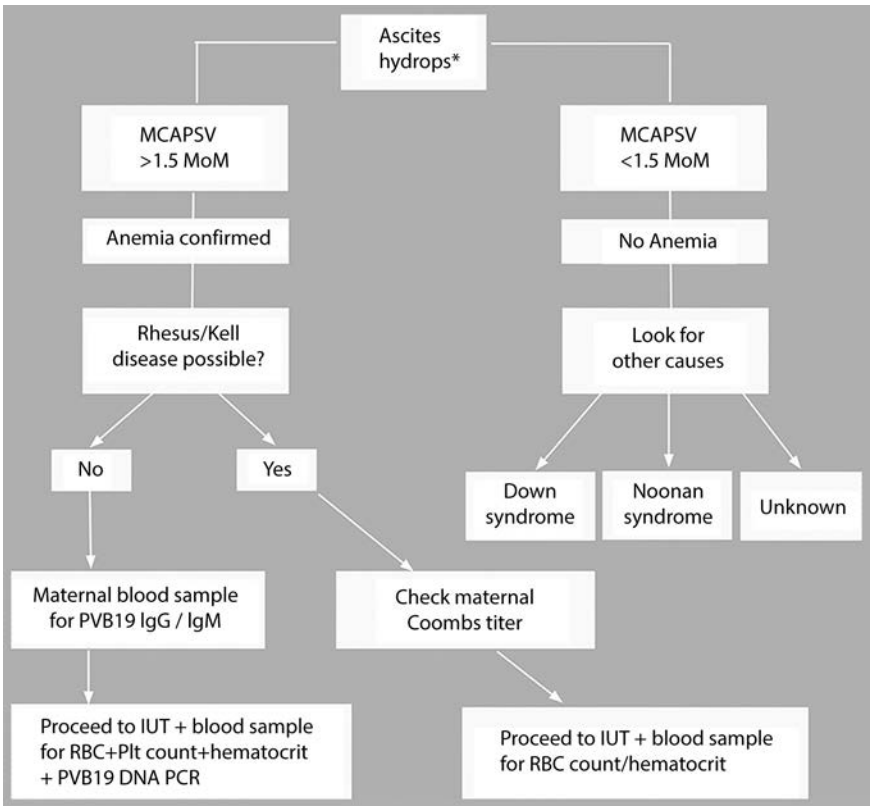


Figure 11.8 Diagnostic flowchart for late-onset hydrops or ascites. See this chapter's text for details. *Late onset; IUT: intrauterine transfusion; PCR: polymerase chain reaction; PVB19: Parvovirus B19; RBC: red blood cell.

IgM and fetal anemia (MCAPSV > 1.5 MoM) [20] in a hydropic fetus is virtually synonymous with Parvovirus B19 fetal infection.

Note that the fetus is much more likely to be infected and to develop a symptomatic infection in the second than in the third trimester. It has been speculated that this change of susceptibility is determined by the reduced expression of the cytotrophoblast P antigen in the third trimester; this is a glycolipid (globoside) that the virus uses to pass the placental barrier [21]. Finally, it should also be considered that Parvovirus B19 may destruct not only red blood cell precursors but platelet ones as well, with a consequent risk of severe thrombocytopenia. Hence, when preparing for intrauterine transfusion (as discussed in this chapter), it is always advisable to have a platelet unit ready also, should the blood count show significant platelet reduction.

Ultrasound. In Figure 11.8, a diagnostic flowchart is shown. Unlike those published in other textbooks and reviews, the entering point of this graph is hydrops or ascites, because this is the most common scenario encountered in real life, not the monitoring of patients exposed to the virus; the latter also occurs in real life, but it is much less common.

Moving to the US signs, it should be considered that the more common sign of the anemia associated with Parvovirus B19 fetal infection is ascites, which rapidly progresses, if untreated, to severe hydrops, with pericardial effusion, subcutaneous edema, and placental thickening (Figure 11.9). Hence, when assessing a fetus with hydrops or also isolated ascites, it is always mandatory to check the MCAPSV to diagnose possible fetal anemia (Figure 11.10) [20,21]; usually, the cutoff for intrauterine transfusion is set at an MCAPSV > 1.5 MoM. Once Rhesus disease is ruled out, Parvovirus B19 infection becomes the most likely cause of the fetal anemia. Myocardial damage occurs less often (Figure 11.11), but it can be life-threatening also in the absence of fetal hydrops. Interestingly, 15% of myocardial biopsies from fetuses and neonates dead from cardiomyopathy have tested positive for Parvovirus B19 inflammation [22].

Treatment. Once the diagnosis is suspected, US is employed to warrant needle access to the umbilical vein, to proceed with the blood sample and the transfusion. For the latter, packed red blood cells are used, with a hematocrit of 75%–80%. Among the various formulas published, we found the one by Moise et al. [23] particularly useful. It should also be considered that

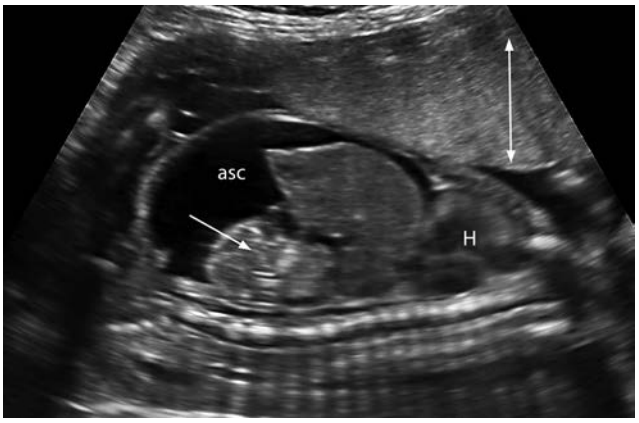


Figure 11.9 Parvovirus B19 infection in a fetus at 22 weeks of gestation. The low-magnification sagittal view of the fetal body demonstrates severe ascites (asc), an echogenic ileus (arrow), and a thickened placenta (double pointed arrow). Note also the grossly enlarged heart (H).

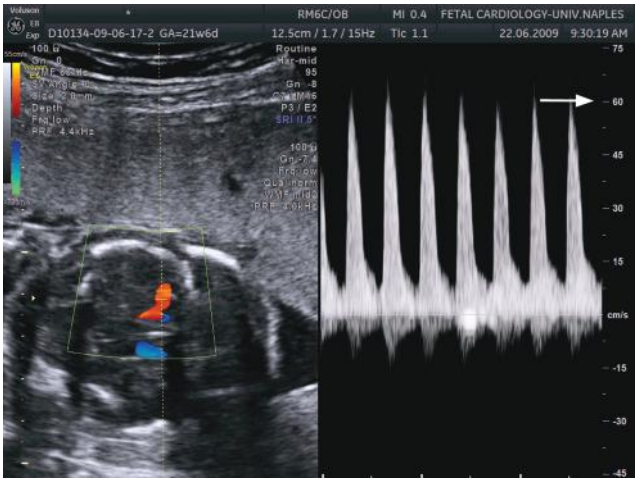


Figure 11.10 Parvovirus B19 infection. Assessment of the middle cerebral artery peak systolic velocity (MCAPSV) in the same hydropic fetus at 22 weeks of gestation shows a value of 60 cm/s (arrow), which corresponds to >2 MoM according to reference ranges from 20. (Cosmi E et al., *Am J Obstet Gynecol* 187, 1290–3, 2002; Jordan JA, DeLoia JA, *Placenta* 20, 103–8, 1999.) Note also the relatively thickened placenta.

if the fetus is extremely anemic, the initial hematocrit should not be increased by more than fourfold to allow the fetal cardiovascular system to compensate for the acute change in viscosity [24]. At the same time, as mentioned in this chapter, a platelet unit should be ready, because Parvovirus B19 infection may cause also severe thrombocytopenia.

Outcome. The mortality risk in fetuses that have undergone intrauterine transfusion(s) has been considered to be 6% [25]. However, the risk of death depends on the



Figure 11.11 Parvovirus B19 infection. The four-chamber view demonstrates moderately thickened myocardial walls and bilateral atrioventricular regurgitation (blue jets). Both are signs of myocarditis and may progress to cardiomyopathy.

degree of hydrops and cardiac decompensation at the time of the transfusion, because—especially in smaller fetuses—the amount of transfused blood has a huge impact on the already depressed cardiac function.

As for the outcome, the overwhelming majority of fetuses that tolerate the transfusion will be completely asymptomatic at birth. The only concern regards those cases in which the degree of anemia at the time of the transfusion was extremely severe (hematocrit < 15%), because in these cases the possibility of brain ischemic lesions is higher. There has been only one paper published so far that raises serious concerns about the outcome of fetal Parvovirus B19 infection: in this paper, reporting on the outcome of a group of 23 infected cases from 1997 to 2005, the rate of perinatal death was as high as 30%, and, of the survivors, approximately 30% had delayed psychomotor development at long-term follow-up [26].

In conclusion, the following should be remembered:

1. Parvovirus B19 is one of the three causes of fetal hydrops that are potentially treatable in utero, the others being Rhesus isoimmunization and tachyarrhythmias.
2. Fetal infection occurs mostly in the second trimester, and very rarely in the third trimester.
3. Positive maternal IgM (with positive or negative IgG) + evidence of fetal anemia (ascites or

hydrops + MCAPSV > 1.5MoM) are highly indicative of fetal infection with Parvovirus B19.

4. Usually, a single intrauterine transfusion is needed to help the fetus overcome the acute phase of the infection.
5. Neonatal outcome is very good in most cases, with a possible but very limited risk of brain or cardiac damage in cases with extremely severe anemia at the time of transfusion (hematocrit < 15%).
6. The expected mortality after transfusion is 6%–10%.
7. If the infection occurs very late in pregnancy, consider delivery. However, if the fetus is hydropic, intrauterine transfusion is a better option.

rUBELLA

Rubella virus belongs to the Togaviridae family. In children, it is responsible for a mild disease. This is characterized by the classic nonconfluent maculopapular rash, which appears on the face first and then disseminates to the trunk and limbs. In the adult, the disease may be more severe, with significant arthralgia, cough, conjunctivitis, and headache.

The risk of transmission is up to 80% if the infection is acquired in the first trimester, with 85% of the infected fetuses developing severe infection and/or malformations. Multiple defects are more common for infections acquired in the first eight weeks of pregnancy. After 12 weeks, the risk of vertical transmission decreases rapidly, to re-increase after 30 weeks of gestation (60%).

Diagnosis of maternal infection. If the pregnant woman has a rash consistent with rubella infection, the following should be checked: (1) if a previous rubella antibody test is available (which occurs in most cases, due to widespread maternal screening), and (2) when the onset of maternal symptoms occurred. If these data are known, a simple blood sample allows definition of the situation. In fact, positive IgM and positive or negative IgG (if both were negative on the initial pregnancy rubella test) indicate current infection. A second blood sample taken after seven to ten days will show increase in the IgG levels and confirm the IgM positivity. In the absence of a former rubella test, the IgG avidity should be assessed: if the avidity is high, the infection is older than six months; and if it is low, then it has occurred in the past three months.

If the pregnant woman has had contact with a rubella-like illness, and if she is susceptible to rubella from her initial pregnancy testing, then IgG and IgM levels should be assessed on her serum for a few weeks, to check whether she may show seroconversion.

A significant increase in the IgG levels in a woman with already positive IgG who has had contact with a rubella-like illness stands in favor of reinfection.

Diagnosis of fetal infection. There are two issues that make prenatal diagnosis and US in rubella infection different from those for CMV and Parvovirus B19: (1) an initial pregnancy rubeo-test is available in the overwhelming majority of cases; and (2) most cases are referred because of maternal rubella or contact with a rubella-like illness. Therefore, in this case both prenatal diagnosis and US are carried out in a fetus known to be at risk for the disease.

Prenatal diagnosis is carried out by checking the presence of the viral DNA by PCR on the amniotic fluid more than 7–8 weeks after maternal infection and anyway after the 21st week of gestation. Reverse transcription PCR (RT-PCR) on multiple samples should be used. However, the patient should be aware that false negative results may occur, although on exceedingly rare occasions. Main indications to prenatal diagnosis are represented by the following [27]: (1) equivocal IgM results in the first trimester, which do not allow one to rule out maternal infection; (2) when, more frequently, maternal rubella infection is confirmed by the lab to have occurred in the first 12 weeks of pregnancy; and (3) when rubella reinfection is confirmed to have occurred in the first 12 weeks of pregnancy.

Ultrasound. The sonographic assessment of a fetus with rubella infection may disclose two different patterns, according to the time of infection. If this has occurred in the first trimester, then major congenital anomalies may be present; if, on the other hand, infection has occurred later, and also in some of the earlier infections, then signs of congenital *infection* but not malformations may be present. Malformations associated with rubella infection in the first 12 weeks of gestation (especially the first eight weeks) include cerebral, eye, cardiac, and skeletal anomalies. In particular, cerebral abnormalities include microcephaly, leukoencephalopathy, and basal ganglia calcifications. Neuronal loss may lead to severe mental retardation. In addition, central or neurosensory hearing loss is also frequent in congenital rubella syndrome.

At US, signs of cerebral involvement are similar to those seen with CMV infection: periventricular halo (Figure 11.12), basal ganglia calcifications (candlestick aspect), and microcephaly (late onset). Eye anomalies detectable at US include microphthalmos and cataract

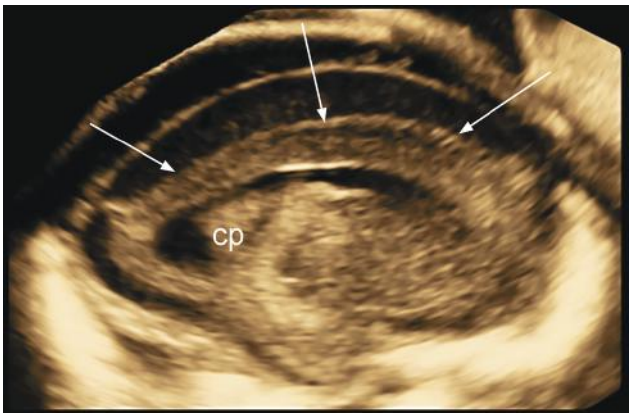


Figure 11.12 Rubella infection. In this case of confirmed rubella infection at 28 weeks, the parasagittal view of the cerebral hemisphere demonstrates the periventricular halo (arrows). This is quite similar to that visible in CMV infection (see Figure 11.1).

(Figure 11.13). The more common type of congenital heart disease seen in congenital rubella infection is a patent ductus arteriosus, which, by definition, is not detectable in utero; this represents 30% of all cardiac defects seen in congenital rubella. The second most common cardiac anomaly that can be diagnosed with US is pulmonary artery stenosis or atresia (Figure 11.14). Aspecific signs of infection include growth restriction, echogenic ileus, and placentitis.

Outcome. The outcome of rubella infection is poor, especially if contracted in the first 12 weeks of gestation: an 80% vertical transmission rate with 85% of malformations in infected fetuses. This is why termination of pregnancy is often chosen on confirmation of fetal infection.

In conclusion, the following should be remembered:

1. Rubella infection in the first trimester is associated with an 80% rate of vertical transmission and 85% incidence of severe malformations in infected fetuses.

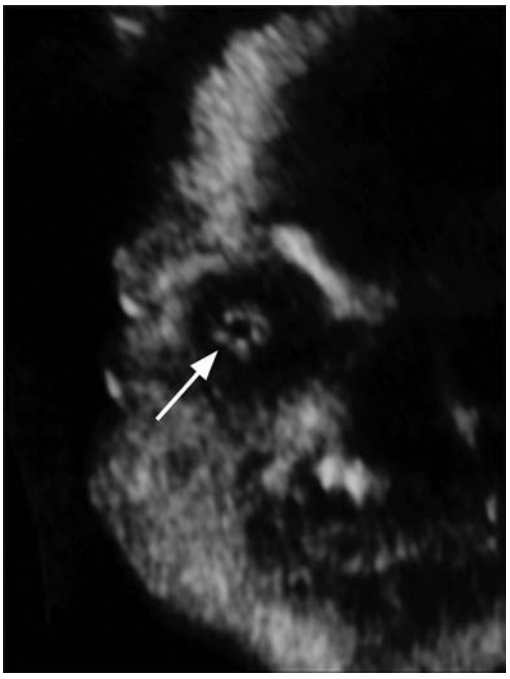


Figure 11.13 Rubella infection (same case as in Figure 11.12). The coronal view of the fetal face demonstrates the opacity of the lens (cataract: arrow).

2. Unlike other infections, an early rubeo-test (IgG and IgM levels) is available in most cases, which allows adequate assessment of the timing of infection and likelihood of fetal infection.
3. If needed, amniocentesis with an RT-PCR search of viral DNA should be performed after seven–eight weeks from primary infection and after 21–22 weeks of gestation.
4. In consideration of the extremely high risk of severe sequelae, the termination of pregnancy may be offered if the fetus is shown to be infected on amniocentesis, or if major malformations are already evident at US.

Toxop LAsMA Go Nd II

The protozoan *Toxoplasma gondii (TG)* is an obligate intracellular parasite that completes its sexual cycle in the feline intestinal epithelium; oocysts are then shed in feces for several weeks. Oocysts can be ingested from contaminated water or fruits, raw or undercooked meat, and gardening in contaminated soil. The prevalence of the disease varies significantly, with the highest rates in central Africa, Central America, and France, where 1% of all pregnancies are infected with TG. The prevalence in the United States is one-tenth of that in France.

Vertical transmission occurs with maternal primary infection. The risk of transmission is linearly correlated with gestational age: it is about 15% in the first trimester, 30% in the second, and 60% in the third trimester [28]. Fetuses infected in the first trimester show more severe disease than those infected later in pregnancy; third-trimester fetal infection often results in an asymptomatic form at birth.

Diagnosis of maternal infection. In adults, TG infection is asymptomatic in more than 90% of cases.

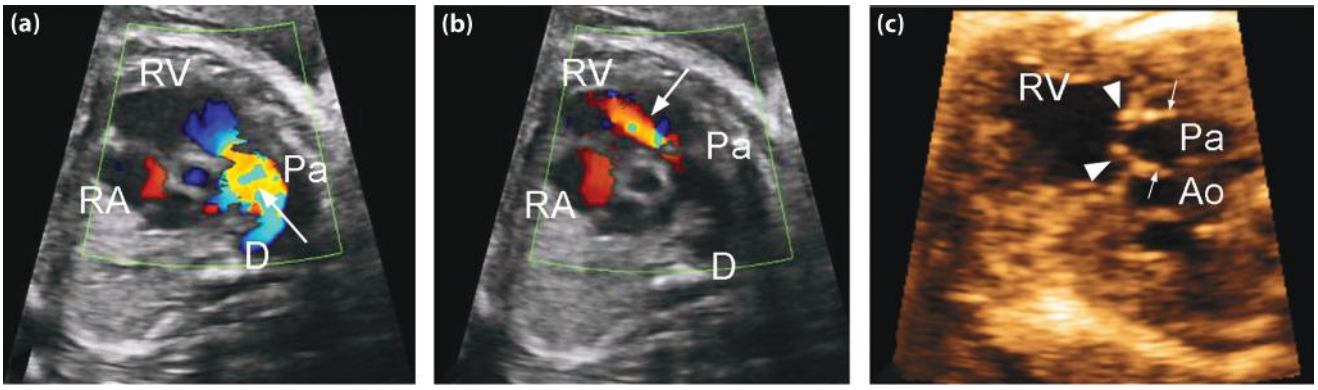


Figure 11.14 Rubella infection (same case as in Figures 11.12 and 11.13). Fetal echocardiography demonstrates the presence of moderately severe pulmonary stenosis, due to a inflammatory process that reduces the normal excursion of the semilunar valve cusps, leading to stenosis and, progressively, to atresia (from sealing of the cusps). The short-axis view of the right ventricle demonstrates (a) on color Doppler, during systole, the incompletely open cusps are visible and determine significant stenosis of the lumen. Aliasing and turbulence, due to high velocity of the jet across the valve, are also visible (arrow). (b) During diastole, a regurgitant jet across the hypomobile valve is visible (arrow); and (c) on three-dimensional surface rendering, the restricted valvar orifice (arrowheads) and the poststenotic moderate dilatation (arrows) of the main pulmonary artery are visible. Ao: ascending aorta; D: ductus arteriosus; Pa: main pulmonary artery; RA: right atrium; RV: right ventricle.

The remaining 10% complain of fatigue, fever, malaise, and laterocervical lymphadenopathy (typical of TG infection). Primary infection leads to lifelong immunity, with the presence of IgG. As for the IgM, it has been demonstrated that these antibodies may persist years after the end of the primary infection, making the ascertainment of the exact time of infection sometimes challenging. In those European countries in which nationwide early-pregnancy screening is covered by their respective National Health Services, such as France or Italy, the availability of a Toxo-test in early pregnancy (IgG and IgM) makes assessment of the situation in cases of primary maternal infection in pregnancy easier than it is in countries in which such health policy is not in place (e.g., the United States). Seroconversion is defined as the appearance of IgM and IgG in a susceptible woman. Care should be made in diagnosing a recent infection if both IgG and IgM are positive, because, as mentioned in this chapter, IgM may persist for years after the end of the primary infection. Hence, if a former negative Toxo-test (IgG and IgM negative) is not available, then to ascertain whether the infection is recent or not, the IgG avidity should be performed in reliable reference laboratories. A high avidity indicates an old infection (usually older than six months), whereas a low avidity indicates an infection in the last three months.

Diagnosis of fetal infection. If maternal infection is confirmed and there is risk of fetal infection, or if signs indicative of infection are found on US (see the next paragraph on US), prenatal invasive diagnosis of TG fetal infection is indicated. This is usually performed through an amniocentesis, carried out after >18–19 weeks gestation and at least five–six weeks after the estimated date of maternal infection. The presence of the protozoal DNA in the amniotic fluid is searched with a PCR. However, the accuracy of the test is limited and is highly dependent on the quality of the laboratory performing the PCR: the sensitivity ranges from 40% to 92% and the negative predictive value is 96%–98% [29,30], which means that a negative test is not always synonymous with absence of infection. Therefore, even though recommendations should be based on the diagnostic performance of the local lab, it is also generally advisable to prolong maternal treatment in case of a negative PCR on amniotic fluid

Ultrasound. US signs of TG infection of the fetus overlap significantly with those of CMV infection [1]. These include cerebral and extracerebral signs. To the former group belong ventriculomegaly (Figures 11.15a), calcifications (Figures 11.15 and 11.16), and microcephaly. Noncerebral signs include cataract (Figure 11.17a), hepatosplenomegaly (Figure 11.17b), liver calcifications and echogenic ileus. Among noncerebral signs, liver calcifications are more likely to be associated with TG, while intestinal dilatation is more frequent in CMV infection. Overall, abdominal signs are more frequent in TG than in CMV fetal infection [1].

Treatment [28]. If maternal infection occurs up to the 18th week of gestation, administration of oral Spiramycin (1 g every 8 h) has been shown to prevent transmission of the infection to the fetus. Spiramycin is a macrolide antibiotic that does not cross the placenta, so it cannot be used for fetal treatment in case

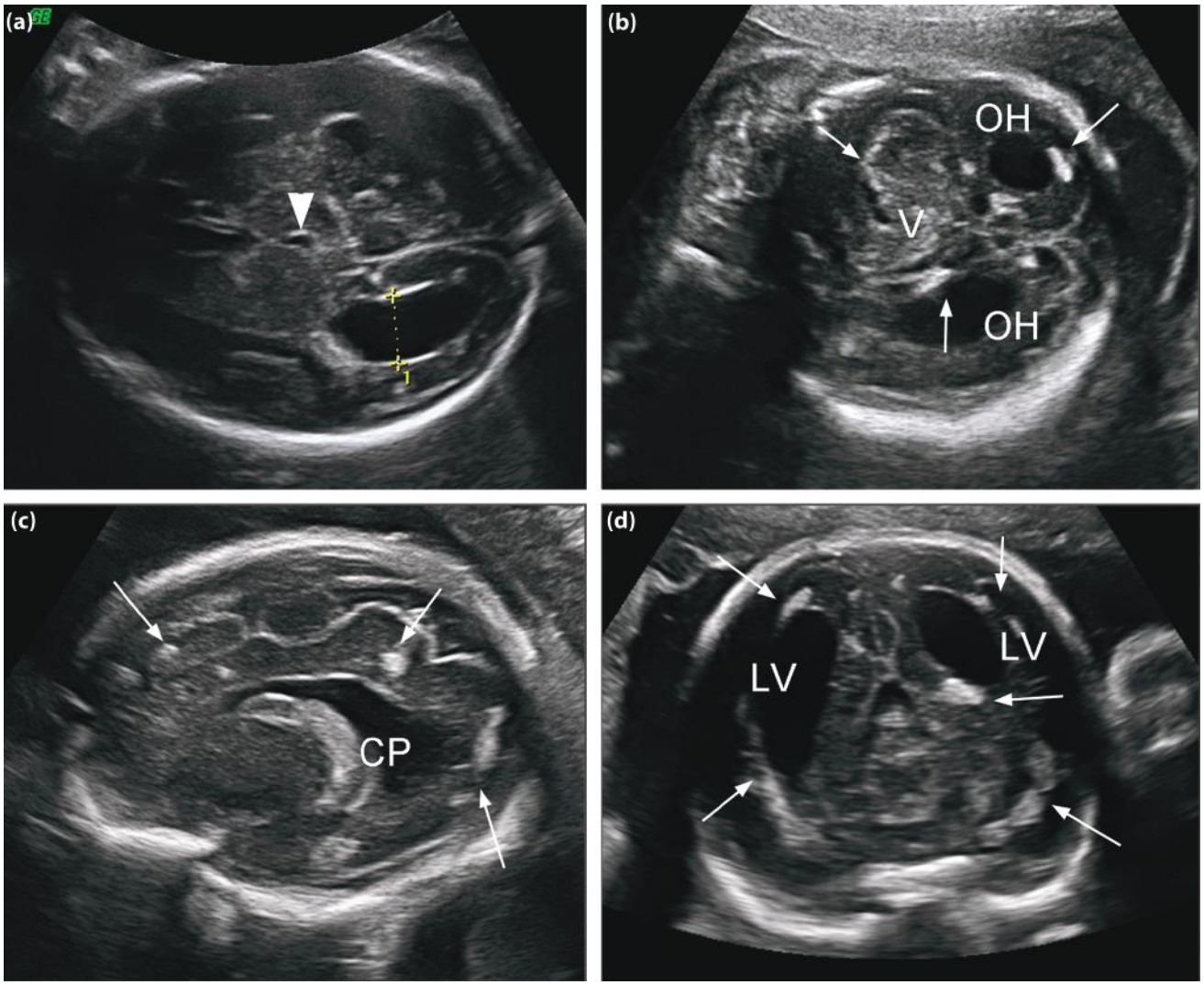


Figure 11.15 *Toxoplasma gondii* infection. In this case (30 weeks of gestation), a neurosonology examination demonstrates moderate ventriculomegaly (the width of the atrium was 13 mm, in (a)) and diffuse calcifications (arrows in b–d): (a) a transthalamic view (arrowhead; moderately dilated third ventricle); (b) a coronal view of the occipital horns (OH); (c) a parasagittal view of the hemisphere and the lateral ventricle (CP: choroid plexus); and (d) a coronal view of the lateral ventricles (LV).

of confirmed fetal infection. In the absence of signs of fetal infection, Spiramycin should be continued until delivery. It is safe for the fetus and may cause only mild gastrointestinal side effects.

On the other hand, if seroconversion occurs after 18 weeks or fetal infection is confirmed by PCR or US findings, the treatment changes and consists of pyrimethamine 50 mg twice daily for two days followed by 50 mg per day, sulfadiazine 75 mg/kg per day in two divided doses for two days followed by 50 mg/kg twice daily, and folinic acid 10 to 20 mg per day. This schedule has been shown effective in preventing congenital infection and also treating the fetus. Caution should be used in administering pyrimethamine, because this drug is a folic acid antagonist and, as such, is teratogenic during the first weeks of pregnancy. Since it may cause significant bone marrow depression, repeated red blood cell counts should be scheduled during treatment. The concurrent administration of folinic acid is meant to prevent hematologic toxicity.

Outcome. The maternal seroconversion rate in pregnancy is about 1%–3% in Europe and much lower in the United States. The overall risk of vertical transmission is 10%. Thirty percent of untreated infected infants develop serious lesions after birth, including chorioretinitis, seizures, encephalitis, and hydrocephalus; and a significant number of neonates who are asymptomatic at birth develop chorioretinitis by adulthood, leading to severe visual impairment

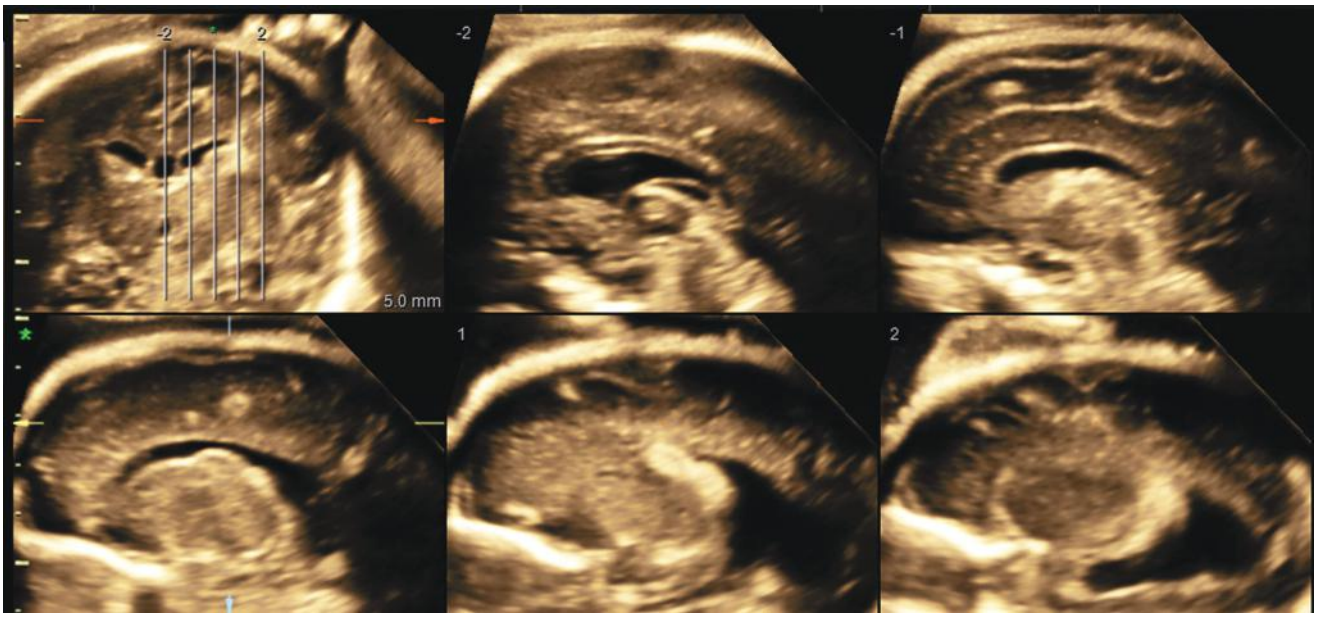


Figure 11.16 *Toxoplasma gondii* infection. In another case at 28 weeks of gestation, three-dimensional tomographic ultrasound imaging (TUI) demonstrates strikingly similar findings, with diffuse macrocalcifications. The top-left panel is the reference image showing the positions of the planes displayed in the other five panels (–2, –1, *, +1, and +2).

in half of them [31]. On the contrary, if long-term antibiotic therapy is administered just after birth, most remain asymptomatic (74%) and the rate of chorioretinitis halves (26%). Only 1% of cases are expected to have serious brain damage [32]. The evidence that prenatal treatment decreases serious neurological consequences is high. A recent study from the European Multicentre Study on Congenital Toxoplasmosis (EMSCOT) group [33] reported a four-year follow-up of 293 fetuses (including nine terminations of pregnancy), 37 of whom had serious neurological sequelae (including severe visual impairment from chorioretinitis). Factors that strongly predicted serious neurological sequelae included gestational age at maternal seroconversion, prenatal treatment, and abnormal US findings In particular, the adjusted odds ratio for any prenatal treatment compared with no treatment was 0.236 (95% CI, 0.071–0.708). At ten weeks, the estimated risk of severe neurological sequelae in fetuses of treated women was 25.7% (12.9%–43.0%) and in untreated women was 60.0% (27.6%–85.9%). The number of mothers to treat to prevent a single case of severe neurological sequelae was three in the first trimester, six at 20 weeks, and 18 at 30 weeks. What remains controversial is the need to switch the treatment schedule from Spiramycin to pyrimethamine + sulfadiazine in cases of confirme fetal infection. There are several studies that failed to confirm any difference in the degree of neonatal infection if the infected fetus was treated with one or the other regimen [33–35], yet the general recommendation is in favor of moving from the much less toxic Spiramycin to the pyrimethamine + sulfadiazine association in high-risk cases. High-risk cases include the following: (1) a positive PCR on amniotic fluid confirmed fetal infection; (2) maternal infection occurred at or after 18 weeks of gestation; and (3) a fetal infection is probable due to abnormalities consistent with TG infection detected on US.

In conclusion, the following should be remembered:

1. The timing of maternal infection is linearly correlated with the chances of fetal infection (15, 30, and 60% in the first, second, and third trimesters, respectively) and inversely correlated with a poor outcome (highest risk is in first-trimester infections).
2. Diagnosis of maternal infection is based on seroconversion or positive IgM and IgG, with low IgG avidity due to the sometimes long persistence of IgM in the maternal blood.
3. The method of choice for diagnosing fetal infection is an amniocentesis performed at after 18–19 weeks of gestation, and at least 5–6 weeks after the estimated date of maternal infection.
4. The accuracy of the PCR is highly dependent upon the quality of local laboratories, and therefore treatment should not be discontinued after a negative result.

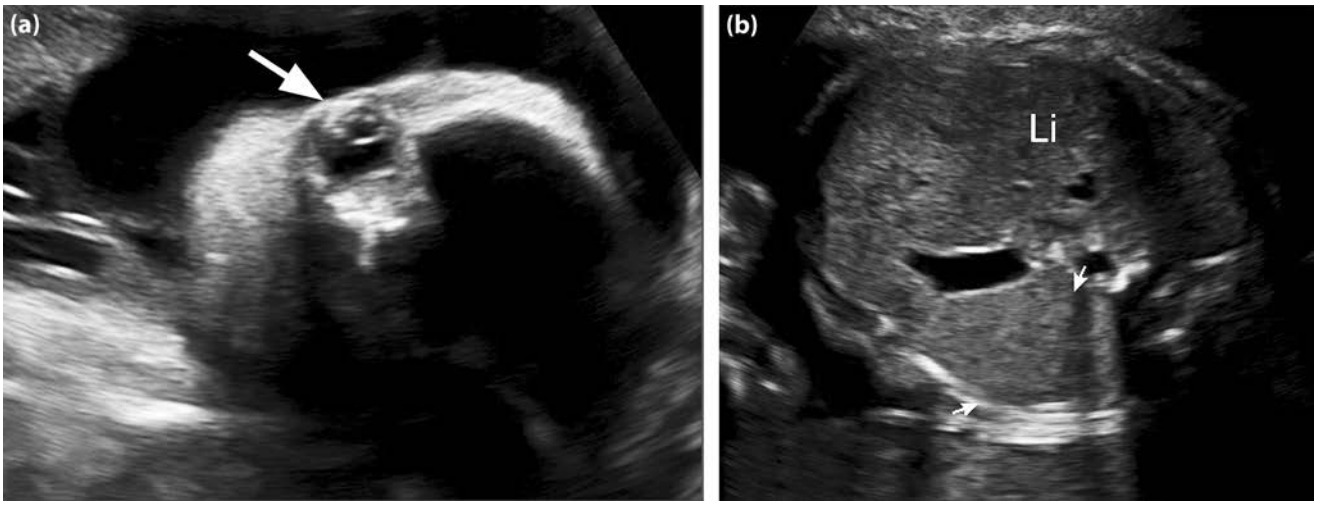


Figure 11.17 *Toxoplasma gondii* infection (same case as in Figure 11.16). In this case, extracerebral signs included cataract and hepatosplenomegaly. (a) The coronal view of the fetal face demonstrates a hyperechoic and irregular rim of the lens, consistent with a cataract (arrow); and (b) the axial view of the upper abdomen demonstrates enlarged liver (Li) and spleen (small arrows).

5. Sonographically detectable brain lesions overlap significantly with CMV ones, but liver calcifications are much more common in TG than in CMV infection.
6. Antibiotic treatment has repeatedly been shown to significantly reduce the risk of severe neurological sequelae in neonates and therefore is mandatory.
7. The antibiotic treatment regimen consists of Spiramycin in low-risk cases and before 18 weeks, and pyrimethamine + sulfadiazine after 18 weeks, although no difference in the prevention of severe neurological sequelae has been demonstrated between the two.

rEFE r ENc Es

1. Beke A, Latkòczy K, Nagy GR, Dudnyikova A, Csaba A, Szabò I, et al. Comparison of prevalence of toxoplasma and cytomegalovirus infection in cases with fetal ultrasound markers in the second trimester of pregnancy. *Prenat Diagn* 2011; 31: 945–8.
2. LazzarottoT, Guerra B, Lanari M, Gabrielli L, Landini MP. New advances in the diagnosis of congenital cytomegalovirus infection. *J Clin Virol* 2008; 41: 192–7.
3. Boppana SB, Fowler KB, Britt WJ, Stagno S, Pass RF. Symptomatic congenital cytomegalovirus infection infants born to mothers with pre-existing immunity to cytomegalovirus. *Pediatrics* 1999; 104: 55–60.
4. Ruellan-Eugene G, Barjot P, Campet M, Vabret A, Herlicoviez M, Muller G, et al. Evaluation of virological procedures to detect fetal human cytomegalovirus infection: avidity of IgG antibodies, virus detection in amniotic fluid and maternal serum. *J Med Virol* 1996; 50: 9–15.
5. Lazzarotto T, Varani S, Guerra B, Nicolosi A, Lanari M, Landini MP. Prenatal indicators of congenital cytomegalovirus infection. *J Pediatr* 2000; 137: 90–5.
6. Guerra B, Lazzarotto T, Quarta S, Lanari M, Bovicelli L, Nicolosi A, et al. Prenatal diagnosis of symptomatic congenital cytomegalovirus infection. *Am J Obstet Gynecol* 2000; 183: 476–82.
7. Yinon Y, Farine D, Yudin MH. Screening, diagnosis, and management of cytomegalovirus infection in pregnancy. *Obstet Gynecol Survey* 2011; 65: 736–43.
8. Guerra B, Simonazzi G, Puccetti C, Lanari M, Farina A, Lazzarotto T, et al. Ultrasound prediction of symptomatic congenital cytomegalovirus infection. *Am J Obstet Gynecol* 2008; 198: 380.e1–7.
9. Simonazzi G, Guerra B, Bonasoni P, Pilu G, Lazzarotto T, Santini D, et al. Fetal cerebral periventricular halo at midgestation: an ultrasound finding suggestive of fetal cytomegalovirus infection. *Am J Obstet Gynecol* 2010; 202: 599.e1–5.
10. Malinger G, Lev D, Zahalka N, Ben Aroia Z, Watemberg N, Kidron D, et al. Fetal cytomegalovirus infection of the brain: the spectrum of sonographic findings *Am J Neuroradiol* 2003; 24: 28–32.
11. Ortiz JU, Ostermayer E, Discher T, Kuschel B, Rudelius M, Shneider KTM. Severe fetal cytomegalovirus infection associated with cerebellar hemorrhage. *Ultrasound Obstet Gynecol* 2004; 23: 402–6.
12. Moinuddin A, McKinstry RC, Martin KA, Neil JJ. Intracranial hemorrhage progressing to porencephaly as a result of congenitally acquired cytomegalovirus infection—an illustrative report. *Prenat Diagn* 2003; 23: 797–800.
13. Benoist G, Salomon LJ, Mohlo M, Suarez B, Jacquemard F, Ville Y. Value of prenatal ultrasound and magnetic resonance imaging in assessment of congenital primary cytomegalovirus infection. *Ultrasound Obstet Gynecol* 2008; 32: 900–5.
14. Doneda C, Parazzini C, Righini A, Rustico M, Tassis B, Fabbri E, et al. Early cerebral lesions in cytomegalovirus infection: prenatal MR imaging. *Radiology* 2010; 255: 613–21.

15. Lipitz S, Hoffmann C, Feldman B, Tepperberg-Dikawa M, Schiff E, Weisz B. Value of prenatal ultrasound and magnetic resonance imaging in assessment of congenital primary cytomegalovirus infection. *Ultrasound Obstet Gynecol* 2010; 36: 709–17.
16. Picone O, Simon I, Benachi A, Brunelle F, Sonigo P. Comparison between ultrasound and magnetic resonance imaging in assessment of fetal cytomegalovirus infection. *Prenat Diagn* 2008; 28: 753–8.
17. Nunoue T, Kusuhara K, Hara T. Human fetal infection with parvovirus B19: maternal infection time in gestation, viral persistence and fetal prognosis. *Pediatr Infect Dis J* 2002; 21: 1133–6.
18. Enders M, Weidner A, Zoellner I, Searle K, Enders G. Fetal morbidity and mortality after acute human parvovirus B19 infection in pregnancy: prospective evaluation of 1018 cases. *Prenat Diagn* 2004; 24: 513–18.
19. Mari G, Deter RL, Carpenter RL, Rahman F, Zimmerman R, Moise KJ Jr, et al. Noninvasive diagnosis by Doppler ultrasonography of fetal anemia due to maternal red-cell alloimmunization. Collaborative Group for Doppler Assessment of the Blood Velocity in Anemic Fetuses. *N Engl J Med* 2000; 342: 9–14.
20. Cosmi E, Mari G, Delle Chiaie L, Detti L, Akiyama M, Murphy J, et al. Noninvasive diagnosis by Doppler ultrasonography of fetal anemia resulting from parvovirus infection. *Am J Obstet Gynecol* 2002; 187: 1290–3.
21. Jordan JA, DeLoia JA. Globoside expression within the human placenta. *Placenta* 1999; 20: 103–8.
22. Bultmann BD, Klingel K, Nabauer M, Wallwiener D, Kandolf R. High prevalence of viral genomes and inflammation in peripartum cardiomyopathy. *Am J Obstet Gynecol* 2005; 193: 363–5.
23. Moise KJ. Management of Rhesus alloimmunization in pregnancy. *Obstet Gynecol* 2002; 100: 600–11.
24. Radunovic N, Lockwood CJ, Alvarez M, Plecas D, Chitkara U, Berkowitz RL. The severely anemic and hydropic isoimmune fetus: changes in fetal hematocrit associated with intrauterine death. *Obstet Gynecol* 1992; 79: 390–3.
25. Rodis JF, Borgida AF, Wilson M, Egan JF, Leo MV, Odibo AO, et al. Management of parvovirus infection in pregnancy and outcomes of hydrops: a survey of members of the Society of Perinatal Obstetricians. *Am J Obstet Gynecol* 1998; 179: 985–8.
26. Nagel HT, de Haan TR, Vandenbussche FP, Oepkes D, Walther FJ. Long-term outcome after fetal transfusion for hydrops associated with parvovirus B19 infection. *Obstet Gynecol* 2007; 109: 42–7.
27. Best JM. Rubella. *Semin Fetal Neonatal Med* 2007; 12: 182–92.
28. Montoya J, Remington J. Management of Toxoplasma gondii infection during pregnancy. *Clin Infect Dis* 2008; 47: 554–66.
29. Thalib L, Gras L, Romand S, Prusa A, Bessieres MH, Petersen E, et al. Prediction of congenital toxoplasmosis by polymerase chain reaction analysis of amniotic fluid *BJOG* 2005; 112: 567–74.
30. Wallon M, Franck J, Thulliez P, Huissoud C, Peyron F, Garcia-Meric P, et al. Accuracy of real-time polymerase chain reaction for Toxoplasma gondii in amniotic fluid *Obstet Gynecol* 2010; 115: 727–33.
31. Koppe JG, Loewer-Sieger DH, de Roever Bonnet H. Results of 20-year follow up of congenital toxoplasmosis. *Lancet* 1986; 1: 254–6.
32. Berrébi A, Assouline C, Bessières MH, Lathière M, Cassaing S, Minville V, et al. Long-term outcome of children with congenital toxoplasmosis. *Am J Obstet Gynecol* 2010; 203: 552.e1–6.
33. Cortina-Borja M, Tan HK, Wallon M, Paul M, Prusa A, Buffolano W, et al. Prenatal treatment for serious neurological sequelae of congenital toxoplasmosis: an observational prospective cohort study. *PLoS Med* 2010; 7: e1000351.
34. The SYROCOT Study Group, Thiebaut R, Leproust S, Chene G, Gilbert RE. Effectiveness of prenatal treatment for congenital toxoplasmosis: a metaanalysis of individual patients' data. *Lancet* 2007; 369: 115–22.
35. Gras L, Gilbert RE, Ades AE, Dunn DT. Effect of prenatal treatment on the risk of intracranial and ocular lesions in children with congenital toxoplasmosis. *Int J Epidemiol* 2001; 30: 1309–30.

Chapter 12
Ultrasound in multiple pregnancy

rA TIo NALE Appro Ach ANd dIAGN os TIc po TENTIAL

For this new version of the book, we also decided to add this chapter on malformations in twins and multiple pregnancies. However, because this text is *malformation oriented*, we have concentrated on congenital anomalies, leaving out most of the important issues related to the genetics of twinning and risk of preterm delivery. Hence, in this chapter, we will deal with the following questions: (1) when is the risk of finding a congenital anomaly increased in twins; (2) what type(s) of anomalies are more likely to be present; and (3) is there any anomaly specifically related to the developmental pathology of twinning?

Comprehensive textbooks and manuals have been published covering all the issues of multiple pregnancies, and the reader is referred to them for insight into this complex diagnostic and prognostic problem.

Epidemiology: Zygosity and chorionicity. Twinning occurs in roughly 2%–3% of pregnancies, and it has almost doubled over the past 20 years due to increasing use of assisted reproduction techniques. Spontaneous conceptions result in 70% dichorionic twins and 30% monochorionic ones, whereas the overwhelming majority of multiple pregnancies from assisted reproduction techniques are obviously dichorionic or polychorionic. However, the use of in vitro fertilization (IVF) also has led to a significant increase of monochorionic pregnancies, although the mechanism behind this increase remains all but unknown. Monochorionic monoamniotic pregnancies are extremely rare, totaling no more than 1% of all monochorionic pregnancies.

Multiple pregnancies may be monozygotic, dizygotic, or polyzygotic; the first leads to identical twins, and the second and third lead to fraternal twins. The former occurs when two embryos derive from the same ovum, and the latter when separate ova are fertilized, usually at the same time. If the pregnancy is polyzygotic, each zygote will develop its own amnion, chorion, and placenta. On the contrary, if the pregnancy is monozygotic, then two embryos are formed from splitting of the same zygote. Different theories have been published to explain this phenomenon, the most credited being the "splitting theory" and the "codominant axis theory" [1]. The pattern of placentation in monozygotic pairs depends upon the timing of the splitting: very early (≤3 days from fertilization) division results in a dichorionic placenta, which is the rarest occurrence; division from day four to days seven–nine (according to different authors) results in a monochorionic, diamniotic placenta; and division after day nine results in a monochorionic, monoamniotic placenta [2].

In relation to the fetal sex, all monozygotic pregnancies and 50% of dizygotic ones result in same-sex twins. Considering the relative frequencies of chorionicity in dizygotic and monozygotic pregnancies, and considering that ultrasound (US) may detect chorionicity but not, obviously, zygosity, it can be calculated that dichorionic pregnancies—which account for 80% of all twin pregnancies—include 35% different-sex dizygotic-dichorionic twins, 35% same-sex dizygotic-dichorionic twins, and 10% same-sex monozygotic-dichorionic pairs. The remaining 20% of twin pregnancies will be monozygotic-monochorionic (same-sex) pairs.

Determining chorionicity: Why and how? The need to define chorionicity is due to the strikingly different rates of complications and malformations in monochorionic versus dichorionic pregnancies. With the exception of a limited risk of preterm delivery, which is increased in dichorionic pregnancy too, virtually all risks are increased in monochorionic pregnancies only (Table 12.1) [3,4]. This is mainly related to two factors: (1) the occurrence of pathologies typical of monochorionic pregnancies, such as twin-to-twin transfusion syndrome or twinning abnormalities (twin reverse arterial perfusion syndrome [TRAP] and conjoined twins [CTs]); and (2) an increased incidence

Table 12.1 Rates of pregnancy complications, dichorionic versus monochorionic pregnancy

Complication	Dichorionic pregnancy	Monochorionic pregnancy
Miscarriage (<24 weeks)	1.8%	12.2%
Fetal anomalies (vs. singletons)	1:1	3:1
Perinatal mortality (>24 weeks)	1.6%	2.8%
Preterm delivery (<32 weeks)	5.5%	9.2%
Fetal growth restriction	12.0%	21.0%
Birth weight <5 centile in both twins	1.7%	7.5%

Source: Modified from Sebire NJ et al. *Br J Obstet Gynaecol* 104, 1203–7, 1997.

of congenital anomalies, mainly involving midline structures.

US can be employed to define chorionicity, and it has been repeatedly shown that the highest accuracy is obtained before 15 weeks of pregnancy [5,6], when sensitivity and specificity in correctly assessing chorionicity are 89.8% and 99.5%, respectively [5]. After 14 completed weeks, the accuracy decreases rapidly (sensitivity of 88.0% and specificity of 94.7%) [6]. Note that both a bipartite placenta and discordant sex have been reported in monochorionic pregnancies [7].

The sonographic method to distinguish dichorionic versus monochorionic placentation in twin pregnancies is based on the differential development and anatomy of the inter-twin membrane: in dichorionic pregnancies, this is composed of four layers (two from each pregnancy, juxtaposed: amnion + chorion leave + chorion leave + amnion), whereas in monochorionic ones the membrane has only two layers (amnion + amnion). In addition, due to the absence of chorion in the membrane in monochorionics, the membrane insertion onto the placenta plate differs: in monochorionic diamniotic pregnancies, it is inserted at roughly a 90° angle, whereas in dichorionic pregnancies, the membrane insertion is wedge shaped. This differential insertion appearance has been referred to as a "T" or "lambda" (the Greek letter λ) sign in monochorionic and dichorionic pregnancies, respectively [5] (Figure 12.1). After 14 weeks, the sensitivity of US in differentiating a dichorionic from a monochorionic twin pregnancy decreases, as mentioned in this section. A list of differential signs is shown in Table 12.2.

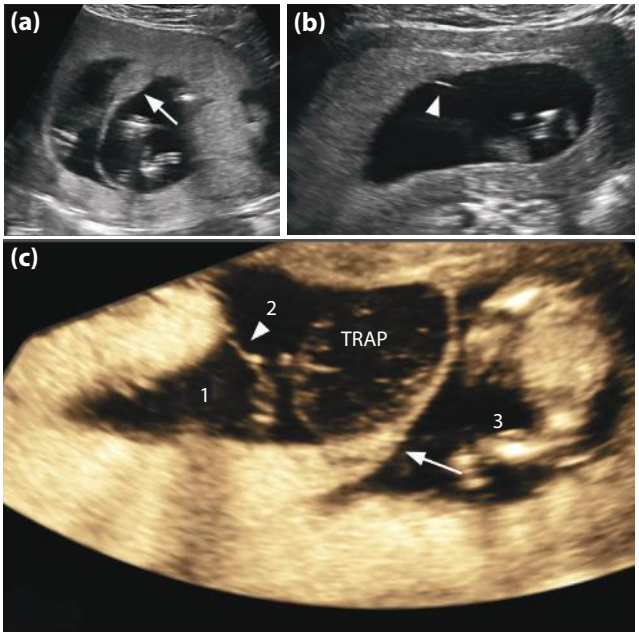


Figure 12.1 Diagnosis of chorionicity in the first trimester is based on the sonographic appearance of the inter-twin membrane. In dichorionic pregnancies, the membrane insertion onto the placental plate is wedge shaped (λ, or lambda); conversely, in monochorionic diamniotic pregnancies, its insertion is at about a 90° angle (a "T" sign). Furthermore, the membrane is thicker in dichorionic than in monochorionic pregnancies. (a) Dichorionic pregnancy; (b) monochorionic diamniotic pregnancy; and (c) triplets with a dichorionic + a monochorionic diamniotic pregnancy with a twin reversed arterial perfusion (TRAP) sequence. Arrows: lambda (λ) sign; arrowheads: "T" sign; numbers identify the three sacs in the triplet pregnancy.

Pathology of monochorionic twins. Pathological entities that can complicate monochorionic pregnancies include (A) malformations deriving from an abnormal splitting mechanism (e.g., CTs or TRAP); (B) malformations that show an increased incidence in monochorionic pregnancies (e.g., right heart defects) (Table 12.3); and (C) particular conditions such as twin-to-twin transfusion syndrome and selective intrauterine growth restriction (sIUGR).

When a malformation affects both twins, it is called *concordant*; if it occurs in one twin only, it is called *discordant*. The latter situation is much more frequent, accounting for 70%–80% of all malformations in twins, and this figure does not change with zygosity.

Table 12.2 Ultrasound signs of chorionicity after 14 weeks of pregnancy[a]

Sign	Dichorionic pregnancy	Monochorionic pregnancy
Fetal gender	Different	Same
Placenta	Double	Single
Inter-twin membrane	Thick	Thin

[a] None of these sign is 100% reliable.

Table 12.3 Congenital anomalies showing an increased incidence in monochorionic twins

- CNS
  - NTD (including anencephaly, cephalocele, and spina bifida
  - HPE
  - Cerebellar anomalies
  - ACC
- Facial
  - Ocular
  - Cleft palate (± cleft lip)
- Heart
  - ASD[a]
  - CAT
  - Pulmonary stenosis[b]
  - TOF
  - Univentricular heart
- G-I
  - G-I atresias
  - Wall defects
  - Diaphragmatic hernia
- G-U
  - Hypospadia
  - Epispadia
  - UPJ and urethral obstructions
  - Cloacal or bladder exstrophy

[a] Not diagnosable in utero.
[b] Late onset; more frequent in TTTS.

However, care should be taken in defining a malformation as discordant, because on some occasions the severity of the anomaly may be different in the two fetuses, and the operator should be careful not to overlook a subtle, less obvious form of the same anomaly in the co-twin [8].

The importance of defining chorionicity in a multiple pregnancy with a discordant fetal anomaly is because the management of a selective termination is completely different in dichorionic versus monochorionic pregnancies. In the former, a simple intracardiac injection of KCl is effective and, at the same time, safe for the co-twin; the risk of co-twin demise is 8%, and that of miscarriage or very early preterm birth (<32 weeks) around 12% [9]. On the contrary, if the discordant anomaly occurs in a monochorionic pregnancy, then other more complicated procedures are required to carry out a selective termination. This is due to the presence of vascular anastomoses that are responsible for an acute ex-sanguino in case of intrauterine monochorionic twin death that, in turn, may lead to death or severe brain damage of the co-twin. To avoid this severe event, selective termination of pregnancy in monochorionic twins is carried out by direct cord clamping under US or fetoscopic guidance. In this way, regardless of the technique (radiofrequency ablation, bipolar laser coagulation, etc.), the acute ex-sanguino is prevented. However, the risks of co-twin death and premature rupture of membranes are significant, averaging 20%–25% and 20%, respectively.

ABNor MALITIEs o F TWINNING

Conjoined twins. Probably the earliest reference to CTs dates back to the early pre-Colombian Moche civilization of Peru; it passes through the European Middle Ages and is emphasized in the 19th-century kingdom of Siam, where one of the most famous sets of CTs—the Bunker twins, Chang and Eng—was born. In fact, the term "Siamese twins" was coined as a reference to them when they became famous working in an international circus. They were considered thoracopagus, as they were joined at the lower thorax by soft tissue and shared a common liver.

The incidence of this exceedingly rare developmental accident is roughly 1:50,000 to 1:100,000 births. The pathogenetic mechanism is still unclear, although the "fission" theory is now more widely accepted than the "fusion" theory. The former postulates that CTs originate from an incomplete split of the embryonic axis. Most CTs are symmetrical, and this would support the "fission" rather than the "fusion" theory. A simplified classification is shown in Table 12.4 [10].

Table 12.4 Classification of conjoined twins (CTs)

Type	Definitio
Cephalopagus	There are two faces joined from the top of the head to the umbilicus.
Thoracopagus	These CTs are joined face to face from the upper thorax to the upper part of the abdomen, and they always share the heart.
Omphalopagus	The fusion includes the umbilicus region frequently at the lower thorax, but never the heart.
Ischiopagus	The union usually includes the lower abdomen and duplicated fused pelvic bones, and the external genitalia and anus are always involved.
Parapagus	These CTs are laterally joined and regularly share the pelvis. Varieties of parapagus conjoined twins are parapagus dithoracic (separated thoraces), parapagus dicephalus (one trunk but two separate heads), and parapagus diprosopus (one trunk, one head, and two faces).
Craniopagus	Joined by the skull, share meninges but rarely the brain surface, and do not include the face and trunk.
Pygopagus	These CTs are dorsally fused, sharing the perineal and sacrococcygeal areas; they have only one anus but two rectums.
Rachipagus	These CTs are dorsally fused; the defect may involve the dorsolumbar vertebral column and rarely the cervical vertebrae and the occipital bone.
Other symmetrical	Includes CTs that some authors classify differently and also a variety of rare types of symmetrical CT.
Asymmetric	Parasitic CTs and fetus in fetu.

Source: Modified from Mutchinick OM et al. *Am J Med Genet Part C* 157, 274–87, 2011.
CT: conjoined twins.

Ultrasound diagnosis is possible as early as the ninth week of pregnancy, with most cases being detected usually before the midtrimester anomaly scan. When scanning a monochorionic monoamniotic pregnancy, it is always mandatory to check that fetal bodies and heads are well apart and moving independently. Most of the reported cases are thoracopagus or omphalopagus, reflecting the higher frequency of these types of CTs, but also US diagnosis of the rarer types has been described [11]. The US images are often unclear in the second trimester, but they are much more comprehensible in the first (Figures 12.2 and 12.3).

The ***outcome*** of CTs depends on the type and the parental attitude toward termination of pregnancy, considering that in most developed countries the diagnosis is made early enough to allow such an option in those countries, such as Italy, where termination of pregnancy is possible until 23 weeks of pregnancy. Despite an early diagnosis and a poor outcome, a significant number of CTs still seem to reach term. In fact, in a recent report from the International Clearinghouse for Birth Defects Surveillance and Research [11], the percentage of live-born CTs averages 46%. However, this report is based on national or regional registries for congenital anomalies, and in these registries cases undergoing termination of pregnancy are often not reported. In fact, data from fetal referral centers and medicine units demonstrate that the rates of pregnancy terminations and of stillbirths are significant. If the former cannot be ascertained with certainty due to the limitation mentioned here [11], the stillbirth rate is as high as 27%. The mortality rate is also very high in all cases in which surgical separation of the CTs is attempted.



Figure 12.2 Conjoined twins at 14 weeks. In this case of thoraco-omphalopagus twins, transvaginal ultrasound demonstrates continuity at the level of the cord insertion (double arrow). The liver was shared by the two twins. (Left) A coronal view; and (right) three-dimensional surface rendering.



Figure 12.3 Conjoined twins. Necropsy specimen after termination of pregnancy at 19 weeks. The image shows a pair of thoraco-omphalopagus twins, very similar to (but not the same as) those shown in Figure 12.2.

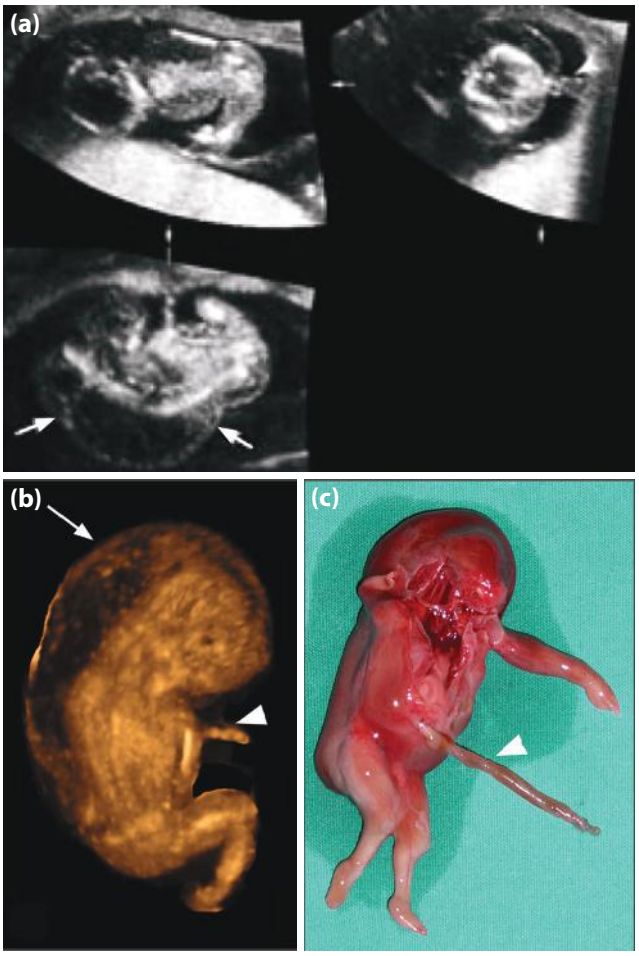


Figure 12.4 TRAP sequence at 14 weeks (acephalus–anceps type). (a) Multiplanar imaging showing the near-normal body of the parasitic twin, with severe edema of the trunk (arrows); (b) three-dimensional surface rendering demonstrating the same features (arrows: trunk edema) and, in addition, the cord insertion (arrowhead); and (c) autoptic confirmation (arrowhead: cord insertion). The patient had opted for termination of pregnancy.

TRAP Sequence. Historically, the first reference to this twinning abnormality dates back to 1500, although detailed anatomical studies were only published three centuries later, in 1800. In this rare anomaly, one of the twins is incompletely developed. The heart is always missing—and this is why this condition is also called acardius and holoacardius. In addition, several parts of the body can be missing, more often the head and the upper thorax rather than the pelvis and the lower limbs. The most used classification (Table 12.5) is that by Phelan and Hall [12]. The more widely accepted pathogenetic theory postulates a primary vascular abnormality leading to the development of artery–artery and vein–vein anastomoses and the reverse arterial perfusion sequence that allows the acardiac twin to grow as a parasite of the pump twin. Chromosomal abnormalities have been reported not infrequently in TRAP sequence, notably with three cases of trisomy 2. The pump twin, in addition to the cardiac overload that frequently leads to in utero demise if not treated (discussed in this chapter), has an increased risk of congenital anomalies, reported to be around 10% [12]. These include anencephaly, gastroschisis, and renal and skeletal abnormalities [13]. Interestingly, the racial incidence of the TRAP sequence follows that of CTs, which is likely to be due to the fact that both represent abnormalities of monochorionic twinning [13].

Ultrasound diagnosis is feasible from the first trimester (Figure 12.4). First, the diagnosis of monochorionic pregnancy is made based upon the recognition of the "T sign"; then, the absence of a heartbeat in the holoacardius is detected. Care should be taken, especially in the first trimester and in cases of near-normal anatomy of the holoacardius, not to mistake a TRAP sequence for a monochorionic pregnancy with the early demise of one fetus (Figure 12.4). The parasitic twin can appear as an amorphous, edematous mass (see the *amorphous* type of Table 12.5), as a partially formed

Table 12.5 Classification of the twin reverse arterial perfusion (TRAP) sequence

Definitio	Description
Acephalus	Absent or rudimentary cephalic structures. Limbs and trunk are more or less developed. Most frequent form (>70%).
Anceps	Some cranial structures and/or neural tissue are present. It is sometimes included in the acephalus type.
Acormus	Head and cephalic structures are present but with limited or no truncal development. The head is usually attached directly to the placenta via a cord. Very uncommon.
Amorphus	Little evidence of cephalic and truncal differentiation, with very few recognizable structures such as limbs. Can resemble a teratoma, but unlike teratoma, skeletal structures and an umbilical cord is present. May represent 20% of acardia.

Source: Modified from Phelan MC, Hall JG, Acardia. In: Stevenson RE, Hall JG, eds. *Human Malformations and Related Anomalies, 2nd edn., Oxford* University Press, New York, 1394–6, 2006.

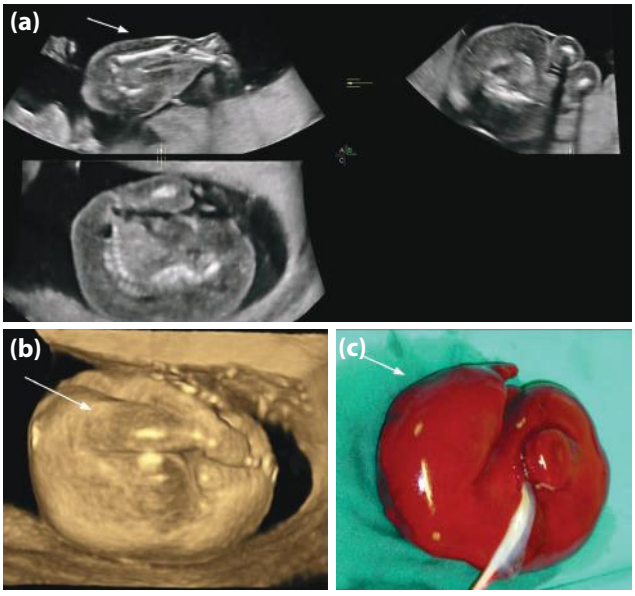


Figure 12.5 TRAP sequence at 19 weeks (acephalus–anceps type). (a) Multiplanar imaging showing crossed and edematous inferior limbs (arrow) and, in the coronal plane, the tortuous spine; (b) three-dimensional surface rendering demonstrating the whole body of the parasitic twin (arrow: inferior limbs); and (c) autoptic confirmation (arrow: inferior edematous limbs). Note also the cord insertion. The patient had opted for termination of pregnancy due to an abnormal karyotype (trisomy 21).

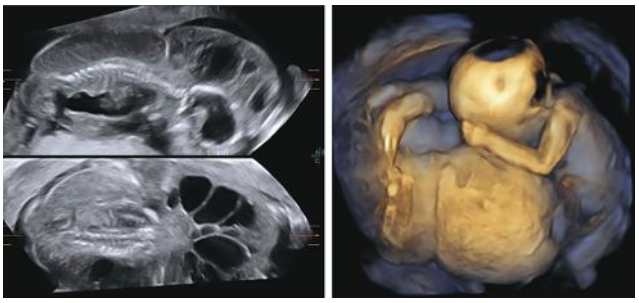


Figure 12.6 TRAP sequence at 20 weeks. Left: Multiplanar imaging demonstrating the severe trunk and head edema and the spine; and right: three-dimensional surface rendering. The pump fetus is "hugging" the large parasitic co-twin. In this case, cord coagulation under ultrasound guidance allowed the pregnancy to reach term uneventfully.



Figure 12.7 TRAP sequence at term (amorphous type). In this case, the pregnancy went to term. The parasitic twin was huge, and only some anatomic structures are recognizable.

fetus (Figure 12.5), or as a fetus with an almost normal body, usually with abnormalities of the cephalic pole (the *acephalus* Table 12.5) with no heart or heartbeat (Figures 12.6, 12.7). Since it may have some basic neural development, on very rare occasions the acardiac twin may show active movements of the limbs, if these are present. Color Doppler may contribute to reach the final diagnosis and characterize the cord pattern. In particular, it is helpful in demonstrating the presence of blood vessels inside the TRAP fetus (despite the absence of the heartbeat…), these being often located alongside a bladder-like structure in the pelvis and continuing with an aorta toward the upper part of the body, if the latter is present. Directional color or Power Doppler may also be employed to demonstrate the reverse perfusion of the cord and the cord pattern:

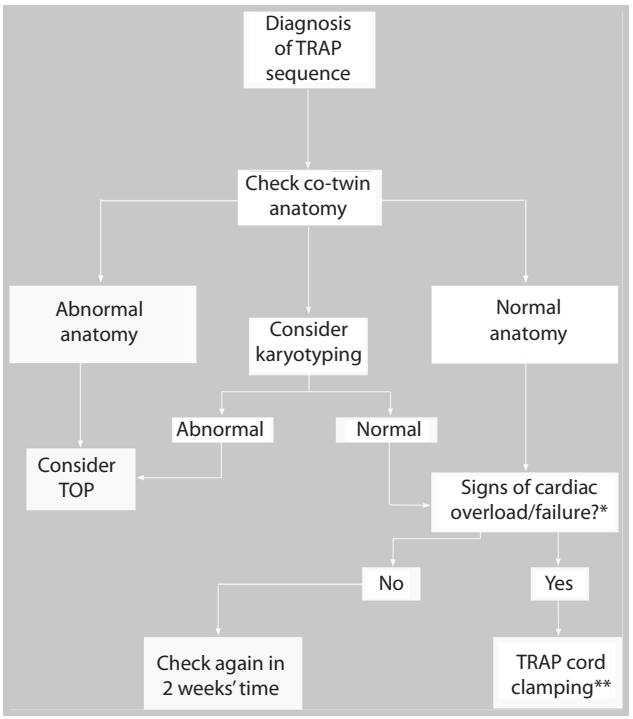


Figure 12.8 Management flowchart for the TRAP (twin reversed arterial perfusion) sequence. *These include cardiomegaly, polyhydramnios, hydrops, and tricuspid regurgitation; **cord occlusion can be obtained through bipolar coagulation or radiofrequency.

in fact, in this rare splitting anomaly, the cord may be Y shaped, it may show a velamentous insertion and, rarely, it may show up to 5 vessels in a single section.

Once the TRAP sequence is diagnosed, a stepwise protocol should be used to characterize the condition and assess the need for in utero treatment, which is needed in most cases. This stepwise protocol is shown in Figure 12.8. The pump twin should be assessed thoroughly because it has a 10% risk of major malformations, including anencephaly and renal and skeletal anomalies [12]. Fetal echocardiography should assess the cardiac functional status to ascertain whether there may be an impending risk of high-output cardiac failure. If this is the case, a cord occlusion procedure should be performed (discussed in this chapter).

The only *differential diagnosis* is with a twin pregnancy in which one of the fetuses has died in utero; however, the severe edema usually associated with the acardiac twin and the abnormal body allows one to distinguish the two conditions easily.

An important task for the sonologist, in cases undergoing cord occlusion procedures, is to define the cord path; in fact, both Y-shaped cords (with five vessels departing from the placental insertion) and sequential distribution (one cord from the placenta to the pump twin, and the second cord from the pump twin to the acardiac one), with or without velamentous cord insertion, have been described [14].

The ***outcome*** of the TRAP sequence was dismal until cord occlusion techniques were employed to interrupt the vicious circle leading to the death of the pump twin from cardiac failure; in the pre-occlusion era, survival was roughly 50% [13]. Fortunately, cord occlusion techniques have been dramatically successful in increasing the survival rate of the pump twin: in a recent meta-analysis, it has been demonstrated that when cord occlusion is performed after 18 weeks, survival is as high as 94% (16/17) [15]. If the cord occlusion is done at less than or equal to 18 weeks, mortality increases to 31% (4/13). Another review showed that in early procedures, radiofrequency ablation is probably better than bipolar coagulation, whereas the reverse is true for procedures carried after 18 weeks, because neither radiofrequency nor neodymium-doped yttrium aluminum garnet (Nd:YAG) lasers are able to coagulate thicker cords. The success of the cord occlusion technique is due to the fact that it blocks the growth of the acardiac twin, avoiding at the same time the risk of acute blood imbalance between the two fetuses. The only risk for the procedure is premature rupture of membranes, which occurs in about 20% of the cases.

Twin-to-twin transfusion syndrome. This represents one of the most severe complications of twinning. Untreated, twin-to-twin transfusion syndrome (TTTS) is associated with more than 80% perinatal mortality and a significant rate of severe brain damage, especially in the case of survival of one twin only [16]. TTTS complicates 15%–20% of monochorionic diamniotic pregnancies, with exceedingly rare cases described in monochorionic monoamniotic ones.

Pathogenesis. Vascular anastomoses connecting the two fetuses are always present on the chorionic plate of monochorionic pregnancies, insuring balanced blood exchange between the two fetuses (Figure 12.9a). TTTS is characterized by imbalance of this blood exchange, with one fetus (the recipient) receiving more blood than the other (the donor). The consequence of this imbalance is that the recipient twin becomes polyuric, while the donor becomes oligoanuric (Figure 12.9b). Progressively, the donor twin develops the classic growth restriction sequence of placental ischemia, whereas the recipient may develop high-output cardiac failure, with severe hydrops. The onset of TTTS is unpredictable, and this is why most guidelines advise biweekly monitoring with US and Doppler for monochorionic diamniotic pregnancies, at least between 16 and 34 weeks of gestation [9,16].



Figure 12.9 Twin-to-twin transfusion syndrome (TTTS). Pathology findings postmortem. Left: Close-up of placental surface showing two large veno-venous anastomoses (arrows). Arteries cross over veins, and *in vivo* they are darker due to unoxygenated blood. Postmortem, blood remains in the vein preferentially; and (right) during abortive labor induction (maternal decision), the donor (D) died first, causing an acute *ex-sanguino* from the recipient (R). This explains the plethoric aspect of the donor and the anemic aspect of the recipient, which is the reverse of the *in vivo* condition.

Ultrasound and Doppler diagnosis. Most cases of TTTS are diagnosed at 19–22 weeks, although both first- and third-trimester cases have been described. A staging system (Table 12.6) [18] has been used since its publication in 1999 by Quintero et al. [17] and, despite some evident inadequacies, is still being used. The advantage of using a staging system is the possibility to compare data among centers, although it has become clear since its firs appearance that prognosis is often not correctly reflecte by this staging system, because the natural history of TTTS is still unclear and does not follow an orderly progression through the stages over time, with many stages that do not progress to more advanced stages and others that even regress [18]. Some modifications of the Quintero staging system have been proposed, mainly to take into account and grade the cardiac dysfunctional status of the recipient twin, but so far they have not contributed significantly to preoperative staging

Ultrasound diagnosis of TTTS is based upon the criteria set in 2004 by the Eurofetus consortium [19] (Figure 12.10): (1) a polyuric recipient twin with a distended bladder; (2) an oligoanuric donor twin with a small or empty bladder; (3) polyhydramnios in the recipient sac, defined as the deepest vertical pocket of ≥ 8 cm at ≤ 20 weeks, and ≥ 10 cm after 20 weeks; and (4) oligohydramnios in the donor sac, defined as the deepest vertical pocket of ≤ 2 cm. Sometimes, detecting the inter-twin membrane may be challenging because it is wrapped closely around the body of the donor (the so called "*stuck twin*"). In this case, the operator should check the areas close to the fetal limbs where the membrane may create foldings (Figure 12.11).

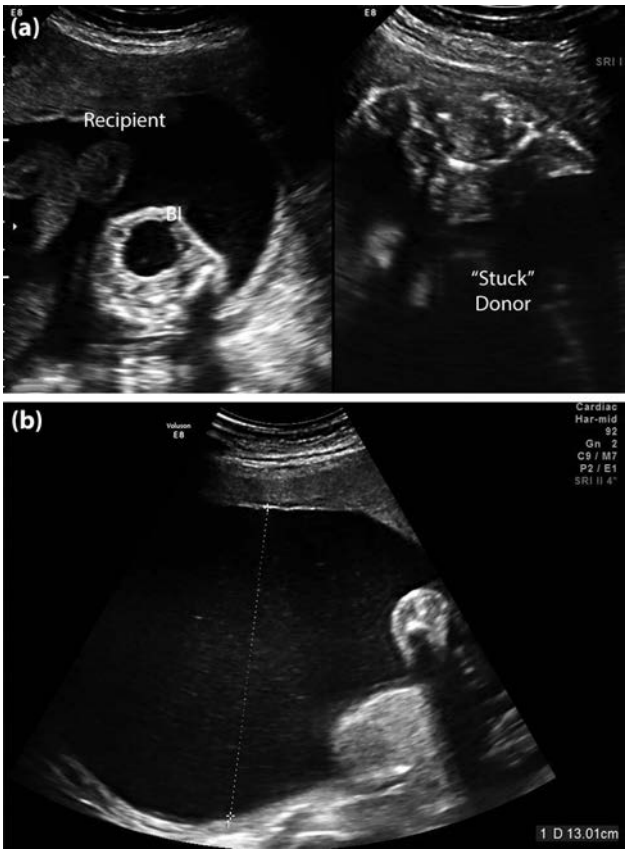


Figure 12.10 Twin-to-twin transfusion syndrome (TTTS). (a) Ultrasound diagnosis is based on a polyuric recipient twin with a distended bladder, and an oligoanuric donor (right panel) twin with a small or empty bladder; and (b) polyhydramnios in the recipient sac is defined as the deepest vertical pocket of ≥ 8 cm at ≤ 20 weeks and of ≥ 10 cm after 20 weeks; oligohydramnios in the donor sac is defined as the deepest vertical pocket of ≤2 cm; in most severe cases, the donor becomes "stuck" due to a total absence of amniotic fluid, as in the present case.

Also, care should be taken in assessing possible signs of cardiac decompensation in the recipient, such as severe cardiomegaly or cardiomyopathy, tricuspid or bilateral atrioventricular regurgitation, subcutaneous edema, ascites, and pleural effusion (Figure 12.12). Pulsed-wave Doppler is then used to sample the umbilical artery and vein, ductus venosus, and the middle cerebral artery of both fetuses (Figure 12.13). The umbilical arteries are sampled in the perivesical tract, to avoid mistaking one cord for the other in fetuses with relatively normal amniotic fluid. Any Doppler abnormality corresponds to Quintero stage III (Table 12.6).

MRI. This technique may be employed at diagnosis and/or follow up of TTTS cases. In particular, MRI may advantageously define - earlier than US - the type and extent of brain damage in the unfortunate cases in which there is demise of one twin prior to treatment.

Table 12.6 Ultrasound staging for TTTS

Stage	Classificatio
I	Discrepancy in amniotic fluid volume with oligohydramnios of a maximum vertical pocket (MVP) ≤2 cm in one sac and polyhydramnios in other sac (MVP ≥ 8 cm). The bladder of the donor twin is visible, and Doppler studies are normal.
II	The bladder of the donor twin is not visible (during the length of the examination, usually around 1 h), but Doppler studies are not critically abnormal.
III	Doppler studies are critically abnormal in either twin and are characterized as abnormal or reversed end-diastolic velocities in the umbilical artery, reverse flow in the Ductus venosus or pulsatile umbilical venous flo .
IV	Ascites, pericardial, or pleural effusion; scalp edema; or overt hydrops is present.
V	One or both fetuses are dead.

Source: Yamamoto M et al., *Am J Obstet Gynecol* 193, 1110–16, 2005.



Figure 12.11 Twin-to-twin transfusion syndrome (TTTS). Sometimes, the membranes are wrapped up around the donor twin. If this is the case, the areas close to the fetal limbs should be checked because here the membranes may be visible, as in this image, because they create foldings (arrows).

Also, it is commonly employed in referral centers in the follow up of cases undergoing Lasercoagulation of placental anastomoses (see below).

Treatment. Over the years, treatment of TTTS has moved from the less invasive amnioreduction or septostomy to the current gold standard of fetoscopic selective laser coagulation of placental vascular anastomoses (SLPVA); the use of cord occlusion techniques is limited to selected and very advanced cases (discussed further in this chapter). Currently, Quintero stages II or higher represent worldwide indication to SLPVA in the 16–26 gestational weeks' range. On the contrary, TTTS stage I is considered an indication to laser ablation by some but not all fetoscopy centers, and a randomised trial is currently ongoing to solve this issue. The superiority of SLPVA over amnioreduction (and, indirectly, septostomy) was demonstrated by a randomized controlled trial in 2004 [17]. In this trial, it was undeniably shown that the likelihood of at least one twin surviving to 28 days of age was significantly higher in the SLPVA group than in the amnioreduction one (76% vs. 56%; relative risk of the death of both fetuses, 0.63; 95% CI, 0.25–0.93; $P = 0.009$). Furthermore, not only was survival higher but also the rate of severe neurological sequelae was much lower in the laser group: the incidence of periventricular leukomalacia halved (6% vs. 14%), and the overall incidence of neurological complications (at 6 months) decreased significantly in the laser group (31% vs. 52%). A recent meta-analysis further supported the striking superiority of SLPVA over amnioreduction as the treatment of choice for TTTS [15]. And the reduced incidence of neurological damage for the laser option remained stable with long-term follow-up [20].

Laser photocoagulation technique. The SLPVA technique was first pioneered by De Lia in 1990 [21], and it was subsequently standardized and simplified by Ville et al. [22]. Two millimeter fetoscopes are used for procedures more than 20 weeks of pregnancy, and 1.2 mm ones are used for earlier procedures. Both diode and Nd:YAG lasers can be used, but most operators use the former. These lasers convert chemical or electrical energy into light energy, and their energy absorbance is very high for the spectrum of hemoglobin. The energy is absorbed by both the vascular wall and the red blood cells within the vessels, leading to injury and retraction of blood vessels that become white after coagulation.

Briefly, the procedure includes the following steps (Figure 12.14):

- US identification of the two cords' insertions and of the dividing membrane, paying attention to possible velamentous insertion;
- Identification of the best entry position, which should ideally be at a 90° angle with the donor longitudinal axis;

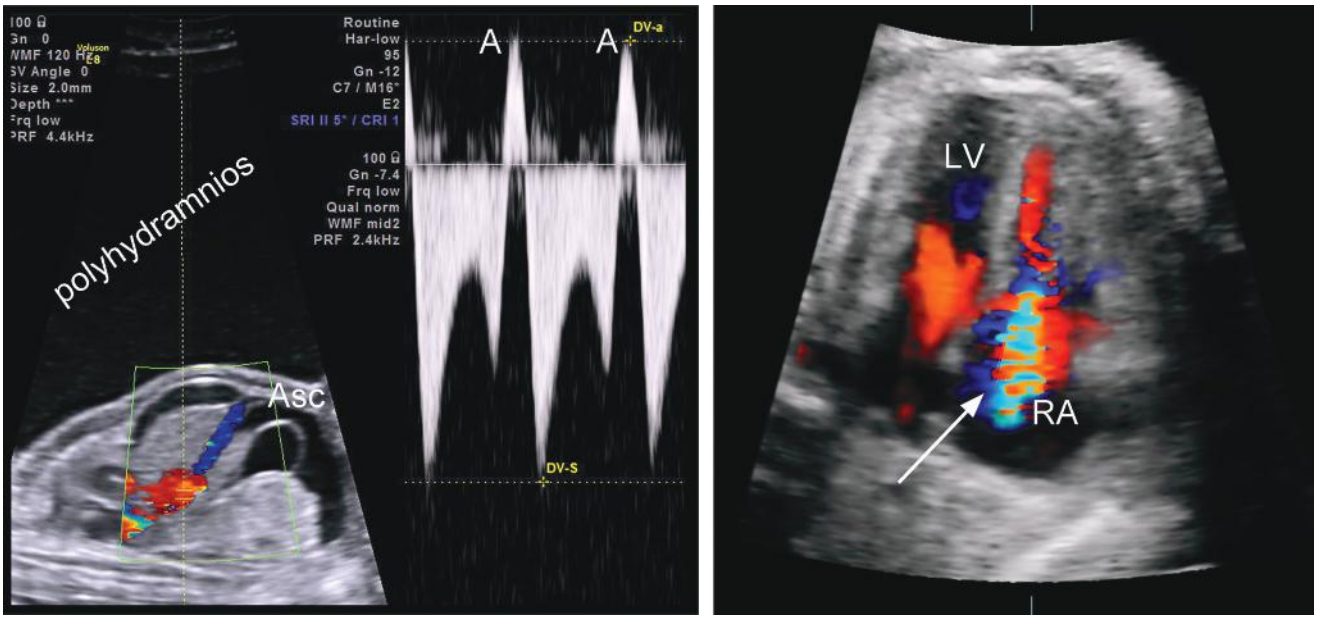


Figure 12.12 Twin-to-twin transfusion syndrome (TTTS). Signs of cardiac decompensation and an advanced Quintero stage include the following: (Left) ascites (asc), subcutaneous edema, ductus venosus abnormal velocity waveform with a negative A wave, and severe polyhydramnios; and (right) cardiomegaly, and cardiomyopathy with tricuspid regurgitation. Arrow: tricuspid regurgitation; LV: left ventricle; RA: right atrium.

- Maternal local anesthesia is administered (1% xylocaine or lidocaine) from the subcutaneous tissue to the myometrium, under US guidance, if needed;
- The fetoscope is then inserted into the amniotic cavity under US guidance, either directly or through a trocar (Figure 12.14a);
- A laser fiber, connected to the laser unit, is then passed through the fetoscope, with its red tip visible in the field of view (Figure 12.14c);
- The inter-twin membrane insertion and the cord insertion of the recipient twin are visualized (Figure 12.14b), and then the area in between is inspected, to locate the vascular anastomoses (Figure 12.14c);
- These are then coagulated only if they are found to connect the two circulations (selective ablation), not if they belong to the same fetus (Figure 12.14d);
- The optimal angle for a correct coagulation is 90°;
- When the lasering is completed, amnioreduction (to a maximum vertical pocket of 5–6 cm) is performed, to avoid leakage of amniotic fluid from the trocar insertion site;
- The trocar is then removed under US guidance, after confirming absence of bleeding at the insertion site.

The optimal conditions for SLPVA are not encountered in all cases. In case of an anterior placenta, the procedure may be challenging because of the need to perforate the placenta with the trocar or endoscope, and because the angle of the laser to the placental plate will be unfavorable, with limited energy absorbed by the blood vessels. Despite the employment of curved endoscopes, in these cases the procedure is often nonselective.

An alternative technique, the so-called Solomon technique, is currently under investigation in a randomized trial. This consists of connecting the ablation sites with the laser, photocoagulating the whole vascular equator of the placenta. The rationale of this technique is to coagulate also those anastomoses that are not visualized because they are closed due to the high pressure of the polyhydramnios and that may reopen after surgery, leading to recurrence (discussed further in this chapter). Initial reports on the use of this modified technique, ie Solomon technique, have yielded results apparently superior to those obtained so far with the conventional one. In particular, an initial trial (23) has reported a statistically significant increase in both double survival (from 46% to 85%) and overall survival (from 61% to 86%). In addition, no cases of recurrent TTTS or TAPS were reported, even though the difference was not statistically significant due to the relatively small numbers.

This technique (SLPVA) is not devoid of complications. Maternal ones have been described very rarely, but they may be important (placental abruption, septic complications, pulmonary edema, etc.). Procedure-related complications include a 20%–30% risk of premature rupture of membranes and an 18% risk of surgical failure, defined as postoperative symptomatic patent anastomoses [24]. Residual patent anastomoses may be

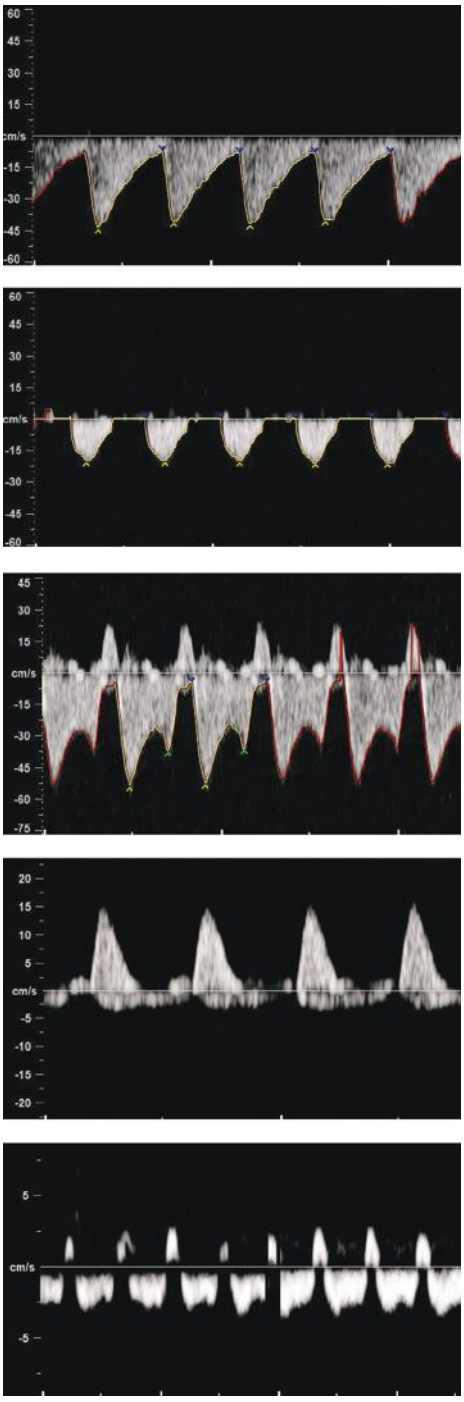


Figure 12.13 Twin-to-twin transfusion syndrome (TTTS). Doppler evaluation (from top to bottom): increased pulsatility index (PI) with diastolic flow on the umbilical artery in the donor; absent diastolic blood flow on the umbilical artery in the donor; reversed A wave on the ductus venous of the recipient; the waveforms resemble the inferior vena cava's ones, but were actually derived from the ductus venosus; absent diastolic blood flow on the umbilical artery and umbilical vein pulsations in the donor; and reversed blood flow on the umbilical vein in the agonic recipient. All but the first findings corresponds to Quintero stage ≥III (see this Chapter's text).

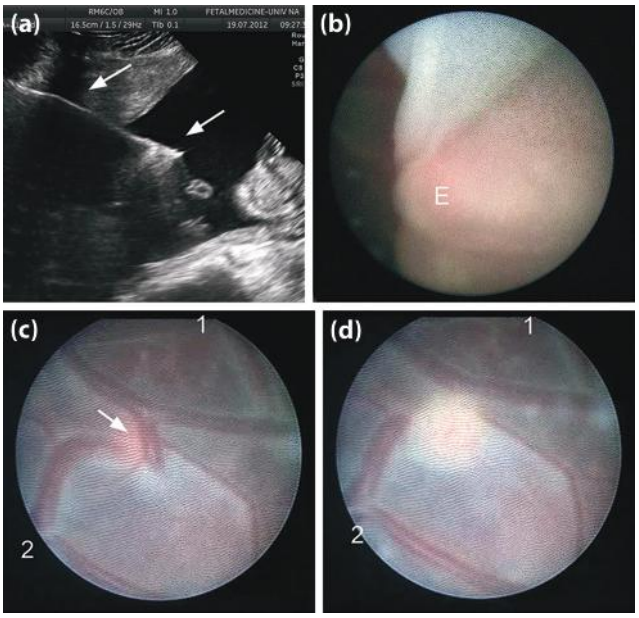


Figure 12.14 Twin-to-twin transfusion syndrome (TTTS). Laser photocoagulation of placental anastomoses. (a) Endoscope insertion under ultrasound guidance; (b) fetoscopic demonstration of a membrane folding around the fetal limbs (E: elbow); (c) the red guiding light of the laser (arrow) is visible at a large placental anastomosis, just prior to coagulation; and (d) the same site after coagulation (1 and 2: position of the two sacs).

responsible for recurrence or inversion of TTTS, the twin anemia–polycythemia sequence (TAPS), the intrauterine demise of both twins, or hypotensive sequelae in a surviving twin [25]. TAPS [26] is diagnosed when a significant discordance is found in the measurement of the peak systolic velocity in the middle cerebral artery (PSVMCA), with a PSVMCA > 1.5 MoM in one twin (anemic) and <0.8 MoM in the co-twin (polycythemic). TTTS recurrence occurs in about 10% of the cases and represents a challenging therapeutic problem. Depending on the placental location, conditions of the fetuses, technical factors, and gestational age treatment, options vary and include amniodrainage, repeat lasering, and selective cord occlusion; in recurrent TTTS, the expected survival rate is 50%. Finally, on very rare occasions, limb ischemia (from pseudoamniotic bands), aplasia cutis congenits, and bowel atresia also have been described.

Amnioreduction should be considered as a second choice in cases of laser photocoagulation failure or in cases diagnosed where no fetoscopic expertise is available onsite or nearby. In view of the results of a randomized trial [19] and the successive Cochrane review [28], amnioreduction can no longer be considered as a treatment of choice for TTTS.

Cord occlusion. This is reserved for selected cases in which one of the twins is pre-agonic or agonic. It has

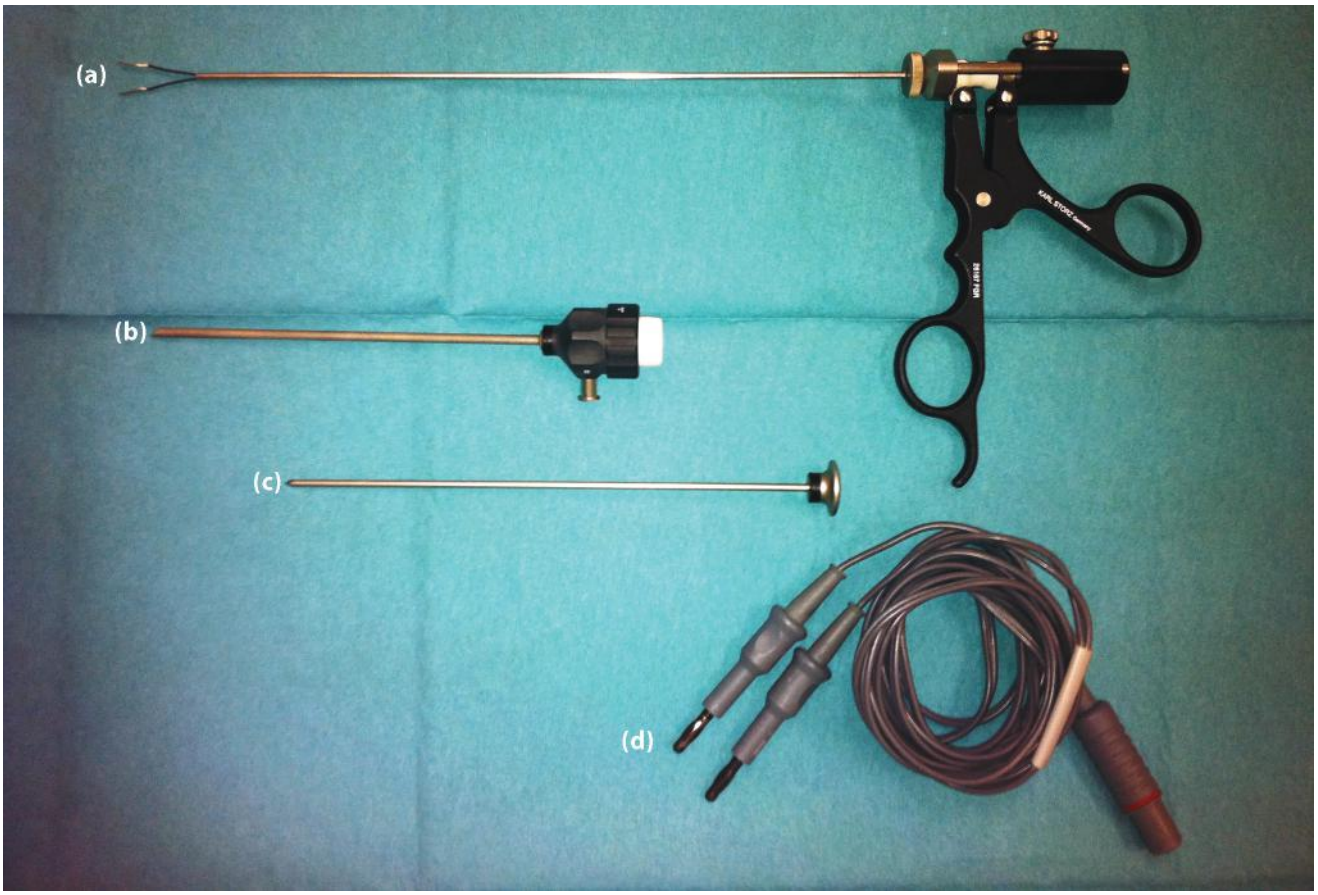


Figure 12.15 The most commonly used technique for cord occlusion is bipolar forceps coagulation under ultrasound guidance. In this image, the bipolar forceps (a), the trocar (b and c), and the connecting wire (d) are shown.

been employed both as a primary therapeutic approach and as a second-line one after laser photocoagulation failure. Cord occlusion can be obtained with different techniques; those more commonly employed are bipolar coagulation, radiofrequency ablation, and Nd:YAG laser coagulation. The last two procedures can be used up to the 18th week of pregnancy, because after this period the cord is too thick to be fully coagulated from either technique. From 19 gestational weeks onward, the technique of choice is bipolar coagulation. The procedure is carried out under US guidance. Briefly, the technique is as follows: after maternal local anesthesia, a 3-mm port is inserted under US guidance into the sac of the agonic twin. Amnioinfusion may be required in cases of oligohydramnios, in order to adequately visualize the cord. A bipolar coagulation forceps is then passed through the port and used to grasp the cord (Figure 12.15). Once cessation of blood flow is demonstrated with color Doppler, the cord is coagulated three times with bipolar energy (20–50 W) for 60 seconds at two or three sites, to ensure complete occlusion. The risk of iatrogenic rupture of membranes is 20%–30%. The survival rate of the co-twin is 75%–85%, with a 2.6% chance of neurological injury [15,27].

Post-Laser follow up. Once the SLPVA has been carried out, the pregnancy should initially (72h) undergo close monitoring with the aim of assessing the success/failure of the procedure and to detect early onset complications (i.e., rupture of membranes, abruptio, fetal death). Mid- and long-term follow up includes clinical, laboratory (white blood cell counts and C-reactive protein [PCR]) and ultrasound (greyscale and Doppler), in order to pick up other complications (i.e., TTTS recurrence or reversal, TAPS, rupture of membranes, chorioamnionitis). MRI is usually employed (according to most fetal surgery centers) as a routing procedure to confirm absence of CNS damage after SLPVA. A strong indication to MRI is death of one twin after the procedure, to rule out ischemic lesions in the survivor from incomplete dichorionization. In this case, it should be considered that possible CNS lesions in the survivor would not be visible at US before three weeks and MRI before 10 days from the event. Of note that most recent reports

seem to demonstrate that Diffusion weighted Sequence MRI is a very sensitive tool, capable of demonstrating brain lesions after only a few days from the death of the co-twin [28].

Outcome. In general, survival figures (with SLPVA) are as follows: double survival in one-third of all cases, single survival in one-third, and double demise in one-third. In earlier stages, figures shift toward double survival, and the reverse is true for advanced stages. A detailed Cochrane review of all available randomized trials [28] demonstrated that laser photocoagulation is associated with an overall death rate of 48%, (perinatal death 26% and neonatal death 8%); at least one infant dies in 58% of cases, whereas both twins die in 24% of the cases. Neurological morbidity was reduced to 5%. Laser photocoagulation of placental anastomoses is then to be considered the treatment of choice for TTTS between 17 and 26 weeks of gestation. As already mentioned, it seems from the preliminary results [23] - that using the Salomon technique may improve significantly these results through a reduction of failures.

Selective IUGR. The term sIUGR applies only to monochorionic pregnancies and is used to define cases with an estimated fetal weight (EFW) of less than the 10th percentile in one fetus. Often, this condition is associated with an inter-twin EFW discordance of more than 25%, calculated as [(larger twin–smaller twin)/larger twin] [30]. sIUGR complicates 10%–15% of monochorionic diamniotic pregnancies and is responsible for a significant share of the perinatal mortality and morbidity of monochorionic diamniotic twins.

Pathogenesis and implications for Doppler evaluation. The cause of sIUGR is a significantly unequal sharing of the placenta between the two fetuses. A velamentous or eccentric cord insertion, which is found in up to 45% of the smaller twins, is a cofactor in the pathogenesis of sIUGR [31] of this condition. However, there is another important key factor that plays a major role in the type and progression of the growth restriction in monochorionic pregnancy, namely, the presence, type, and number of vascular anastomoses between the two placental territories. In fact, it has been shown that the extent and degree of interference with the natural history of growth restriction are consequences of the relationships between the placental territory and the anastomotic pattern. If there are few anastomoses and a severely unbalanced placenta, the IUGR fetus will behave as a dichorionic one (or a singleton with placental insufficiency), and, as such, the deterioration of the fetal conditions will be predictable on the basis of the umbilical artery, ductus venosus, and middle cerebral artery Doppler velocimetry changes. On the other end, on few occasions, there is a single major arterio-arterial anastomosis. In these cases, the advantage is that the large anastomosis will cause large amounts of blood to be shifted from the normally growing co-twin to the IUGR one, reducing the severity of the growth impairment. The significant disadvantage is that this anastomosis creates a very unstable hemodynamic system, with a higher risk of acute feto-fetal transfusion episodes, especially during episodes of bradycardia of the IUGR twin. In these cases, the deterioration of the IUGR condition is not predictable by Doppler velocimetry, because the large arterio-arterial anastomosis plays a robust role in the shift of significant amounts of blood from one twin to the other. The result is that in this case, the incidence of unpredictable fetal death is higher [30].

In any event, the concurrence of placental imbalance and vascular anastomoses does not allow one to assign the same clinical significance to the deterioration of vascular indexes as is assigned to singletons with growth disturbance.

Ultrasound and Doppler. As mentioned here, the diagnosis of sIUGR in monochorionic pregnancies relies on the demonstration of an EFW <10th centile for only one of the two twins. In most cases, there will also be an inter-twin EFW discordance of more than 25%, calculated as [(larger twin–smaller twin) / larger twin] [30]. Once the diagnosis of sIUGR is made, Doppler velocimetry should be used to assess fetal well-being. In this regard, it should be considered that, due to the peculiar aspects of monochorionic placentas (described in this chapter) and the consequent significant inter-twin shunt, three different categories of sIUGR have been identified on the basis of the umbilical artery Doppler velocimetry (Figure 12.16) [30]; these three types of sIUGR have significantly different risks of death and neurological damage (Table 12.7) [30,31]. In *type I*, diastolic forward flow is present (Figure 12.16). This represents the best type in terms of outcome. *Type II* is characterized by absent or reversed umbilical artery diastolic flow (AREDF) (Figure 12.16); this type of sIUGR is associated with higher mortality and morbidity. However, in this group, fetal deaths never occur unexpectedly. *Type III* is the most dangerous group because this type of sIUGR represents the peculiar situation described in the pathogenesis section, where a single large arterio-arterial anastomosis is present. In this case, the clinical evolution is very unpredictable, with an incidence of unexpected fetal deaths as high as 15% and an incidence of brain injury of 20% [30]. This type is associated with an intermittent absent or reversed umbilical artery diastolic flow (iAREDF; Figure 12.17, upper panel). In this case, by reducing the sweep speed of the

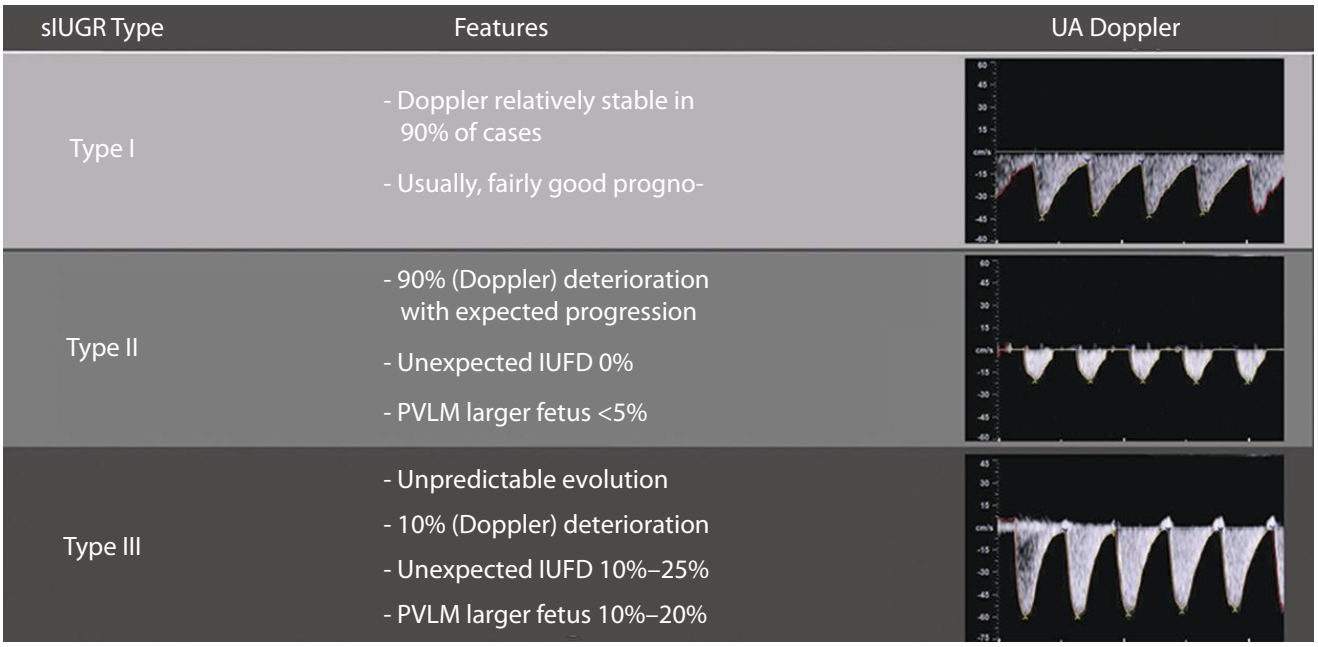


Figure 12.16 Classification of selective IUGR (sIUGR) after Gratacos. Main features. Type III is due to a large arterio-arterial anastomosis (see this Chapter's text). (From Valsky DV et al., *Prenat Diagn* 30, 719–26, 2010.)

Table 12.7 Types of selective IUGR in monochorionic twins

Parameter	Normal	Type I	Type II	Type III
GA at diagnosis (weeks)	—	23	20	22
GA at delivery (weeks)	35	35	31*	32*
Fetal deterioration[a] (%)	—	0	90**	11
uIUFD[b] (%)				
Larger twin	—	3	0	6
Smaller twin	—	3	0	15***[c]
Brain injury (%)				
Larger twin	—	0	3	20***
Smaller twin	—	0	15****	2

Source: Modified from Valsky DV et al., *Prenat Diagn* 30, 719–26, 2010; Machin GA, *J Reprod Med* 42, 785–9, 1997.
GA: gestational age.
[a] Defined as ultrasound and Doppler findings dictating active managemen
[b] Unexpected intrauterine fetal death.
[c] In four of these cases, also the larger twin died; and in an additional two, brain lesions developed.
* $p < 0.0001$ vs. uncomplicated and Type I; ** $p < 0.0001$ vs. Type I and Type III; *** $p < 0.05$ vs. Type I and Type II; **** $p < 0.05$ vs. Type 1.

spectral Doppler strip to show several cardiac cycles, cyclic or intermittent absence or reverse diastolic flow is found on the umbilical artery. This pattern reflects the existence of a large arterio-arterial anastomosis, which can often be located on the placental surface. If this vessel is sampled with spectral Doppler, the periodic bidirectional pattern typical of an arterio-arterial anastomosis is found (Figure 12.17 mid and lower panels).

Management. Biweekly follow-up of monochorionic twins, which is recommended by most national societies of US in obstetrics and gynecology [9,16], ensures prompt detection of growth discordance, IUGR, and referral for expert opinion. Doppler velocimetry of the umbilical artery will then allow one to define the type of sIUGR, after Gratacos' classification [31]. In *sIUGR type I*, the evolution is favorable, with good outcomes

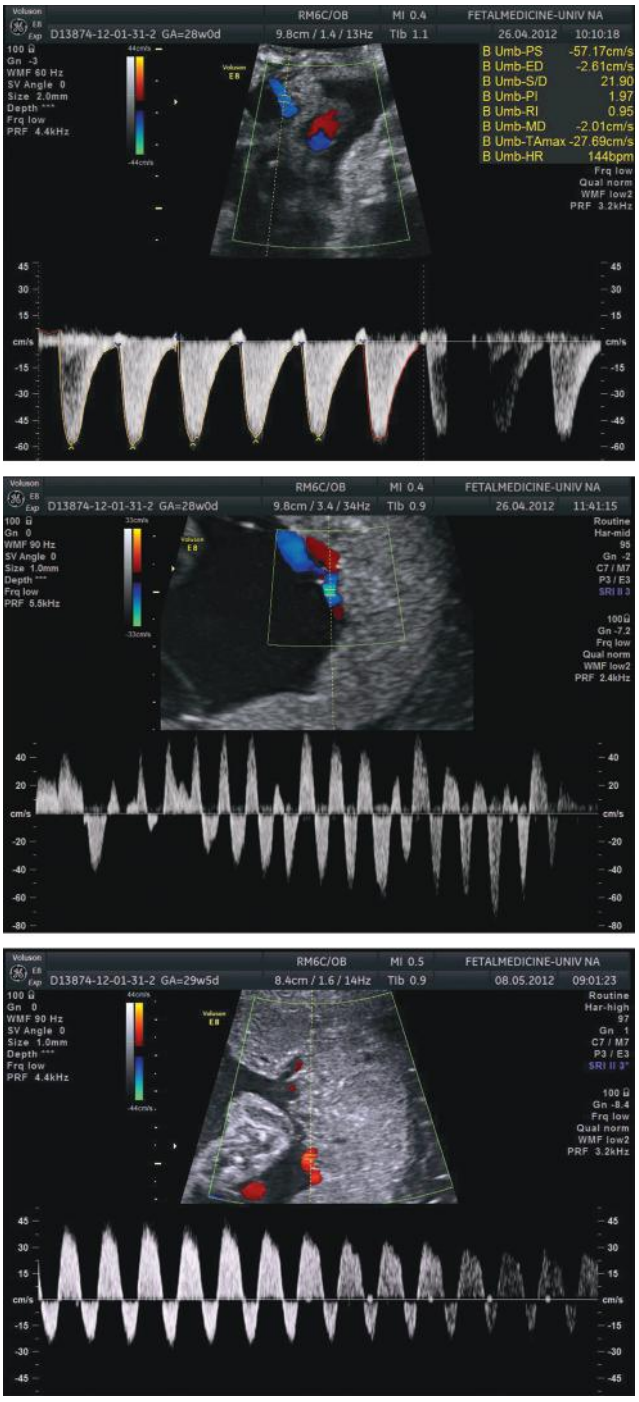


Figure 12.17 Selective IUGR in monochorionic biamniotic pregnancy. Type III after Gratacos et al. (ref. 30 and Table 12.7). Upper panel: umbilical artery velocimetry showing the variability of the waveform from present (left) to reverse (central) end-diastolic flow. This pattern is due to the presence of a large arterio-arterial anastomosis on the placental surface. In the middle and lower panels, the greyscale image shows the sampling site and the location of this anastomosis on the placental plate, while the spectral Doppler strip demonstrates the typical bi-directional sinusoid pattern of the blood flow.

in most cases. Progression to type II, due to the disappearance of the umbilical artery diastolic blood flow, is rare. Therefore, most cases will uneventfully reach the 32–34-week period, when delivery can be planned without major concerns. *sIUGR type II* is completely different in terms of outcome (Table 12.7), and therefore a strict monitoring (including Doppler velocimetry of the umbilical artery and ductus venosus) should be warranted, in order to pick up the appearance of zero or negative flow on the A wave of the ductus venosus. This finding, together with progressive deterioration of the umbilical artery Doppler (reversed end-diastolic flow), will identify cases with an impending risk of death that need active management. According to gestational age, EFW, conditions of the co-twin, and computerized cardiotocograph tracing (if applicable), management will consist of delivery after steroid prophylaxis for respiratory distress syndrome (RDS) or cord occlusion (only in countries where such an option is legally feasible in the third trimester, for progressive deterioration leading to a significant risk of death is exceedingly rare prior to 23 weeks). Management of *sIUGR type III* represents a challenge in most cases, because it is difficult to find an acceptable compromise between the risk of unexpected intrauterine death and the relatively good conditions. Venous Doppler is unlikely to deteriorate in these cases, and the decision on the management should be done together with the parents. Negative prognostic factors indicating a higher risk of unexpected death are represented by (1) an early diagnosis of sIUGR; (2) a high degree of inter-twin EFW discordance; (3) prominent intermittent reverse flow in the smaller twin; and (4) a short distance between the placental cord insertions. If all or most of these factors are present, in those countries in which late termination of pregnancy is allowed, cord occlusion should be discussed. In the remaining countries, the two options are delivery and laser coagulation of placental anastomoses. As to the former, timing of the delivery should result from a compromise between the fetal conditions, gestational age, performance of the local Neonatal Intensive Care Unit, and will of the parents. In these cases—and in these countries—since the risk of co-twin death or severe brain damage is significant, it is advisable to have the parents sign a written informed consent on the chosen management (active or conservative). Alternatively, laser coagulation of placental anastomoses should be considered. In this setting—sIUGR type III—a small series [32] has shown that lasering results in a high incidence of death of the smaller twin (67%), which was higher than the mortality rate of conservative management in the same group (19%). However, the risk of concomitant death of the larger twin was significantly lower (0% vs. 50%, $p = 0.02$), with a trend toward reduced incidence

of periventricular leukomalacia (6% vs. 14%) in comparison with the cases managed conservatively. When this option is considered, technical feasibility should be evaluated, because relatively advanced gestational age, an anterior placenta, and large arterio-arterial anastomoses or very close cord insertions may render the procedure impossible.

In cases without the negative prognostic determinants discussed in this chapter, it is reasonable to proceed to elective delivery at 32–34 weeks of gestation.

rEFE r ENc Es

1. Hall JG. Twinning. *Lancet* 2003; 362: 735–43.
2. Benirschke K, Kim CK. Multiple pregnancy. *N Eng J Med* 1973; 288: 1276–84.
3. Sebire NJ, Snijders RJ, Hughes K, et al. The hidden mortality of monochorionic twin pregnancies. *Br J Obstet Gynaecol* 1997; 104: 1203–7.
4. Oldenburg A, Rode L, Bødker B, et al. Influence of chorionicity on perinatal outcome in a large cohort of Danish twin pregnancies. *Ultrasound Obstet Gynecol* 2012; 39: 69–74.
5. Sepulveda W, Sebire NJ, Hughes K, et al. The lambda sign at 10–14 weeks of gestation as a predictor of chorionicity in twin pregnancies. *Ultrasound Obstet Gynecol* 1996; 7: 421–3.
6. Lee YM, Cleary-Goldman J, Thaker HM, et al. Antenatal sonographic prediction of twin chorionicity. *Am J Obstet Gynecol* 2006; 195: 863–7.
7. Lopriore E. Twin pregnancies with two separate placental masses can still be monochorionic and have vascular anastomoses. *Am J Obstet Gynecol* 2006; 194: 804–8.
8. Maruotti GM, Agangi A, Martinelli P, et al. Early prenatal diagnosis of concordant posterior urethral valves in male monochorionic twins. *Prenat Diagn* 2006; 26: 67–70.
9. Vayssière C, Benoist G, Blondel B, et al. Twin pregnancies: guidelines for clinical practice from the French College of Gynaecologists and Obstetricians (CNGOF). *Eur J Obstet Gynecol Reprod Biol* 2011; 156: 12–17.
10. Mutchinick OM, Luna-Mun L, Amar E, et al. Conjoined twins: a worldwide collaborative epidemiological study of the international clearinghouse for birth defects surveillance and research. *Am J Med Genet Part C* 2011; 157: 274–87.
11. Maruotti GM, Paladini D, Napolitano R, et al. Prenatal 2D and 3D ultrasound diagnosis of diprosopus: case report with post-mortem magnetic resonance images (MRI) and review of the literature. *Prenat Diagn* 2009; 29: 992–4.
12. Phelan MC, Hall JG. Acardia. In: Stevenson RE, Hall JG, eds. *Human Malformations and Related Anomalies*, 2nd edn. New York: Oxford University Press 2006; 1394–6.
13. Botto LD, Feldkamp ML, Amar E, et al. Acardia: epidemiologic findings and literature review from the International Clearinghouse of Birth Defects Surveillance and Research. *Am J Med Genet Part C* 2011; 157: 262–73.
14. Martinelli P, Paladini D, Nicotra A, et al. Holoacardius: antenatal diagnosis and pathogenetic evaluation: a case report. *Eur J Obstet Gynecol Reprod Biol* 1990; 36(1–2): 153–9.
15. Rossi AC, D'Addario V. Umbilical cord occlusion for selective feticide in complicated monochorionic twins: a systematic review of literature. *Am J Obstet Gynecol* 2009; 200: 123–9.
16. Neilson JP and Kilby MD on behalf of the Royal College of Obstricians and Gynaecologists. Management of monochorionic twin pregnancy. Green-top Guidelines no.51, 2008.
17. Quintero RA, Morales WJ, Alien MH, et al. Staging of twin-twin transfusion syndrome. *J Perinatol* 1999; 19: 550–5.
18. Yamamoto M, El Murr L, Robyr R. Incidence and impact of perioperative complications in 175 fetoscopy-guided laser coagulation of chorionic plate anastomoses in Feto-Fetal Transfusion syndrome before 26 weeks of gestation. *Am J Obstet Gynecol* 2005; 193: 1110–16.
19. Senat MV, Deprest J, Boulvain M, et al. Endoscopic laser surgery versus serial amnioreduction for severe twin-to-twin transfusion syndrome. *N Engl J Med* 2006; 8: 136–44.
20. Salomon LJ, Ortqvist L, Aegerter P, et al. Long-term developmental follow-up of infants who participated in a randomized clinical trial of amniocentesis versus laser photocoagulation for the treatment of twin-to-twin transfusion syndrome (TTTS). *Am J Obstet Gynecol* 2010; 203: 444e1–7.
21. De Lia JE, Cruikshank DP, Keye WR. 1990. Fetoscopic neodymium: YAG laser occlusion of placental vessels in severe twin-twin transfusion syndrome. *Obstet Gynecol* 75: 1046–53.
22. Ville Y, Hyett J, Hecher K, et al. Preliminary experience with endoscopic laser surgery for severe twin-twin transfusion syndrome. *N Engl J Med* 1995; 332: 224–7.
23. Ruano R, Rodo C, Peiro JL, Shamshirsaz AA, Haeri S, Nomura ML, Salustiano EM, de Andrade KK, Sangi-Haghpeykar H, Carreras E, Belfort MA. Fetoscopic laser ablation of placental anastomoses in twin-twin transfusion syndrome using 'Solomon technique'. *Ultrasound Obstet Gynecol* 2013; 42(4): 434–9.
24. Chalouhi GE, Stirnemann JJ, Salomon LJ, et al. Specific complications of monochorionic twin pregnancies: twin-twin transfusion syndrome and twin reversed arterial perfusion sequence. *Semin Fetal Neonatal Med* 2010; 15: 349–56.
25. Chalouhi GE, Essaoui M, Stirnemann J, et al. Laser therapy for twin-to-twin transfusion syndrome (TTTS). *Prenat Diagn* 2011; 31: 637–46.
26. Slaghekke F, Kist WJ, Oepkes D, et al. Twin anemia-polycythemia sequence: diagnostic criteria, classification perinatal management and outcome. *Fetal Diagn Ther* 2010; 27: 181–90
27. O'Donoghue K, Rutherford MA, Engineer N, et al. Transfusional fetal complications after single intrauterine death in monochorionic multiple pregnancy are reduced but not prevented by vascular occlusion. *BJOG* 2009; 116: 804e12.
28. Roberts D, Gates S, Kilby M, et al. Interventions for twin–twin transfusion syndrome: a Cochrane review. *Ultrasound Obstet Gynecol* 2008; 31: 701–11.
29. Weisz B, Hoffmann C, Ben-Baruch S, Yinon Y, Gindes L, Katorza E, Shrim A, Bar Yosef O, Schiff E, Lipitz S. Early Detection of Severe Brain lesions After Fetoscopic Laser Treatment in Twin-Twin Transfusion Syndrome by Diffusion weighted Sequence MRI. *Ultrasound Obstet Gynecol* 2013; doi: 10.1002/uog.13283.
30. Valsky DV, Eixarch E, Martinez JM, et al. Selective intrauterine growth restriction in monochorionic diamniotic twin pregnancies. *Prenat Diagn* 2010; 30: 719–26.
31. Machin GA. Velamentous cord insertion in monochorionic twin gestation. An added risk factor. *J Reprod Med* 1997; 42: 785–9.
32. Gratacos E, Antolin E, Lewi L, et al. Monochorionic twins with selective intrauterine growth restriction and intermittent absent or reversed end-diastolic flow (Type III): feasibility and perinatal outcome of fetoscopic placental laser coagulation. *Ultrasound Obstet Gynecol* 2008; 31: 669–75.

Appendix

Table A.1 Nomograms (centiles) for the Italian population: biparietal diameter (mm)

Gestational age (weeks)	3rd	5th	10th	25th	50th	75th	90th	95th	97th
17	35.8	36.2	36.7	37.7	**38.8**	39.9	40.8	41.4	41.8
18	38.4	38.9	39.6	40.7	**42.0**	43.3	44.5	45.2	45.6
19	41.1	41.6	42.4	43.7	**45.2**	46.7	48.0	48.9	49.4
20	43.7	44.2	45.2	46.7	**48.3**	50.0	51.5	52.4	53.0
21	46.3	46.9	47.9	49.6	**51.4**	53.2	54.9	55.9	56.5
22	48.9	49.6	50.6	52.4	**54.4**	56.4	58.2	59.2	59.9
23	51.5	52.2	53.3	55.2	**57.3**	59.4	61.3	62.5	63.2
24	54.0	54.8	56.0	58.0	**60.2**	62.4	64.4	65.6	66.4
25	56.6	57.4	58.6	60.7	**63.0**	65.3	67.4	68.6	69.4
26	59.1	59.9	61.2	63.4	**65.7**	68.1	70.2	71.5	72.3
27	61.6	62.4	63.7	65.9	**68.4**	70.8	73.0	74.3	75.1
28	64.0	64.9	66.2	68.5	**70.9**	73.4	75.6	76.9	77.8
29	66.5	67.3	68.7	70.9	**73.4**	75.9	78.1	79.5	80.3
30	68.9	69.7	71.1	73.3	**75.8**	78.2	80.5	81.9	82.7
31	71.2	72.0	73.4	75.6	**78.1**	80.5	82.8	84.1	84.9
32	73.5	74.3	75.7	77.9	**80.3**	82.7	84.9	86.2	87.1
33	75.8	76.6	77.9	80.0	**82.4**	84.8	86.9	88.2	89.0
34	78.0	78.8	80.0	82.1	**84.4**	86.7	88.8	90.0	90.8
35	80.1	80.9	82.1	84.1	**86.3**	88.5	90.5	91.7	92.5
36	82.2	83.0	84.1	86.0	**88.1**	90.2	92.1	93.3	94.0
37	84.3	85.0	86.0	87.8	**89.8**	91.8	93.6	94.7	95.3
38	86.3	86.9	87.9	89.6	**91.4**	93.2	94.9	95.9	96.5
39	88.2	88.8	89.7	91.2	**92.9**	94.5	96.1	97.0	97.5
40	90.0	90.5	91.4	92.7	**94.2**	95.7	97.1	97.9	98.4
41	91.8	92.3	93.0	94.2	**95.5**	96.7	97.9	98.6	99.1
42	93.5	93.9	94.5	95.5	**96.6**	97.6	98.6	99.2	99.6

Source: Paladini D et al., *Prenat Diagn* 25, 456–64, 2005.

Table A.2 Nomograms (centiles) for the Italian population: head circumference (mm)

Gestational age (weeks)	3rd	5th	10th	25th	50th	75th	90th	95th	97th
17	125.6	127.1	129.7	133.8	**138.4**	143.0	147.1	149.7	151.2
18	138.0	139.7	142.3	146.7	**151.5**	156.4	160.7	163.4	165.1
19	150.2	151.9	154.7	159.3	**164.4**	169.4	174.0	176.8	178.6
20	162.0	163.9	166.8	171.6	**176.9**	182.2	187.0	189.9	191.7
21	173.6	175.5	178.5	183.5	**189.1**	194.6	199.6	202.7	204.6
22	184.7	186.7	189.9	195.1	**200.9**	206.6	211.9	215.1	217.0
23	195.6	197.6	200.9	206.4	**212.3**	218.3	223.8	227.1	229.1
24	206.0	208.1	211.6	217.2	**223.4**	229.6	235.3	238.7	240.8
25	216.0	218.2	221.8	227.7	**234.1**	240.5	246.4	249.9	252.1
26	225.7	227.9	231.6	237.7	**244.3**	251.0	257.0	260.7	263.0
27	234.9	237.2	241.0	247.3	**254.1**	261.0	267.3	271.1	273.4
28	243.6	246.0	250.0	256.4	**263.5**	270.6	277.0	281.0	283.4
29	251.9	254.4	258.4	265.1	**272.4**	279.7	286.3	290.4	292.9
30	259.7	262.3	266.4	273.3	**280.8**	288.3	295.1	299.3	301.9
31	267.0	269.7	273.9	281.0	**288.7**	296.4	303.4	307.7	310.3
32	273.8	276.5	280.9	288.1	**296.1**	304.0	311.2	315.6	318.3
33	280.1	282.9	287.4	294.8	**302.9**	311.0	318.4	322.9	325.7
34	285.8	288.7	293.3	300.8	**309.2**	317.5	325.1	329.7	332.6
35	290.9	293.9	298.6	306.4	**314.9**	323.4	331.2	335.9	338.8
36	295.5	298.5	303.3	311.3	**320.0**	328.7	336.7	341.5	344.5
37	299.5	302.6	307.5	315.6	**324.5**	333.5	341.6	346.5	349.6
38	302.8	306.0	311.0	319.3	**328.4**	337.5	345.8	350.9	354.0
39	305.6	308.8	313.9	322.4	**331.7**	341.0	349.5	354.6	357.8
40	307.7	310.9	316.2	324.8	**334.3**	343.8	352.4	357.7	360.9
41	309.1	312.4	317.7	326.5	**336.2**	345.9	354.7	360.1	363.4
42	309.8	313.2	318.6	327.6	**337.5**	347.3	356.3	361.7	365.1

Source: Paladini D et al., *Prenat Diagn* 25, 456–64, 2005.

Table A.3 Nomograms (centiles) for the Italian population: abdominal circumference (mm)

Gestational age (weeks)	3rd	5th	10th	25th	50th	75th	90th	95th	97th
17	113.3	114.8	117.3	121.4	**125.9**	130.4	134.5	137.0	138.5
18	122.0	123.8	126.7	131.6	**137.0**	142.3	147.2	150.1	152.0
19	130.6	132.7	136.1	141.7	**147.9**	154.0	159.6	163.0	165.1
20	139.3	141.7	145.5	151.8	**158.7**	165.6	171.9	175.7	178.1
21	148.0	150.6	154.8	161.7	**169.3**	176.9	183.9	188.1	190.7
22	156.7	159.5	164.1	171.6	**179.8**	188.1	195.6	200.2	203.0
23	165.4	168.4	173.3	181.3	**190.2**	199.0	207.1	212.0	215.0
24	174.0	177.2	182.4	191.0	**200.4**	209.7	218.3	223.5	226.7
25	182.7	186.0	191.5	200.5	**210.4**	220.2	229.2	234.7	238.1
26	191.2	194.8	200.5	209.9	**220.2**	230.5	239.9	245.6	249.1
27	199.8	203.5	209.4	219.1	**229.8**	240.5	250.3	256.2	259.9
28	208.3	212.1	218.2	228.2	**239.3**	250.3	260.4	266.5	270.3
29	216.7	220.6	226.9	237.2	**248.5**	259.8	270.2	276.4	280.3
30	225.1	229.1	235.5	246.0	**257.5**	269.1	279.6	286.0	290.0
31	233.4	237.5	243.9	254.6	**266.4**	278.1	288.8	295.3	299.3
32	241.7	245.7	252.3	263.1	**275.0**	286.8	297.6	304.2	308.3
33	249.8	253.9	260.5	271.4	**283.3**	295.3	306.1	312.7	316.8
34	257.9	262.0	268.6	279.5	**291.4**	303.4	314.3	320.9	325.0
35	265.8	269.9	276.5	287.4	**299.3**	311.3	322.1	328.7	332.8
36	273.7	277.7	284.3	295.1	**307.0**	318.8	329.6	336.2	340.2
37	281.4	285.4	291.9	302.6	**314.3**	326.1	336.7	343.2	347.2
38	289.0	293.0	299.4	309.9	**321.4**	333.0	343.5	349.9	353.8
39	296.5	300.4	306.6	316.9	**328.3**	339.6	349.9	356.1	360.0
40	303.9	307.6	313.7	323.8	**334.8**	345.8	355.9	362.0	365.8
41	311.1	314.7	320.6	330.4	**341.1**	351.8	361.5	367.4	371.1
42	318.1	321.7	327.4	336.7	**347.0**	357.3	366.7	372.4	375.9

Source: Paladini D et al., *Prenat Diagn* 25, 456–64, 2005.

Table A.4 Nomograms (centiles) for the Italian population: femur length (mm)

Gestational age (weeks)	3rd	5th	10th	25th	50th	75th	90th	95th	97th
17	20.1	20.6	21.4	22.6	**24.0**	25.4	26.7	27.4	27.9
18	23.2	23.6	24.4	25.6	**27.0**	28.3	29.6	30.3	30.8
19	26.1	26.6	27.3	28.5	**29.9**	31.2	32.4	33.2	33.6
20	28.9	29.4	30.1	31.4	**32.7**	34.0	35.2	36.0	36.4
21	31.7	32.1	32.9	34.1	**35.4**	36.8	38.0	38.7	39.2
22	34.3	34.8	35.5	36.8	**38.1**	39.4	40.7	41.4	41.9
23	36.9	37.3	38.1	39.3	**40.7**	42.0	43.3	44.0	44.5
24	39.3	39.8	40.6	41.8	**43.2**	44.6	45.8	46.6	47.1
25	41.7	42.2	42.9	44.2	**45.6**	47.0	48.3	49.1	49.6
26	43.9	44.4	45.2	46.5	**48.0**	49.4	50.7	51.5	52.0
27	46.1	46.6	47.4	48.8	**50.3**	51.7	53.1	53.9	54.4
28	48.1	48.6	49.5	50.9	**52.4**	54.0	55.4	56.3	56.8
29	50.0	50.6	51.5	53.0	**54.6**	56.2	57.6	58.5	59.1
30	51.9	52.5	53.4	54.9	**56.6**	58.3	59.8	60.7	61.3
31	53.6	54.2	55.2	56.8	**58.6**	60.3	61.9	62.9	63.5
32	55.3	55.9	56.9	58.6	**60.5**	62.3	64.0	65.0	65.6
33	56.8	57.5	58.6	60.3	**62.3**	64.2	66.0	67.0	67.7
34	58.3	59.0	60.1	62.0	**64.0**	66.0	67.9	69.0	69.7
35	59.6	60.4	61.5	63.5	**65.6**	67.8	69.8	70.9	71.7
36	60.9	61.6	62.9	65.0	**67.2**	69.5	71.6	72.8	73.6
37	62.0	62.8	64.1	66.3	**68.7**	71.1	73.3	74.6	75.4
38	63.0	63.9	65.3	67.6	**70.1**	72.7	75.0	76.4	77.2
39	64.0	64.9	66.4	68.8	**71.5**	74.1	76.6	78.0	79.0
40	64.8	65.8	67.4	69.9	**72.7**	75.6	78.1	79.7	80.6
41	65.6	66.6	68.2	71.0	**73.9**	76.9	79.6	81.3	82.3
42	66.2	67.3	69.0	71.9	**75.0**	78.2	81.0	82.8	83.8

Source: Paladini D et al., *Prenat Diagn* 25, 456–64, 2005.

Table A.5 Nomograms (centiles) for the Italian population: tibia length (mm)

Gestational age (weeks)	3rd	5th	10th	25th	50th	75th	90th	95th	97th
17	16.9	17.5	18.4	20.0	**21.7**	23.4	25.0	25.9	26.5
18	19.7	20.3	21.2	22.7	**24.3**	26.0	27.5	28.4	28.9
19	22.5	23.0	23.9	25.3	**26.9**	28.5	29.9	30.8	31.4
20	25.1	25.7	26.5	27.9	**29.4**	31.0	32.4	33.2	33.7
21	27.7	28.2	29.0	30.4	**31.9**	33.4	34.7	35.6	36.1
22	30.2	30.7	31.5	32.8	**34.3**	35.7	37.1	37.9	38.4
23	32.6	33.1	33.8	35.2	**36.6**	38.1	39.4	40.2	40.7
24	34.8	35.3	36.1	37.4	**38.9**	40.3	41.6	42.4	42.9
25	37.0	37.5	38.3	39.6	**41.1**	42.5	43.8	44.6	45.1
26	39.1	39.6	40.4	41.7	**43.2**	44.6	46.0	46.8	47.3
27	41.1	41.6	42.4	43.8	**45.3**	46.7	48.1	48.9	49.4
28	43.0	43.5	44.4	45.8	**47.3**	48.8	50.1	51.0	51.5
29	44.8	45.4	46.2	47.6	**49.2**	50.8	52.2	53.0	53.6
30	46.6	47.1	48.0	49.5	**51.1**	52.7	54.1	55.0	55.6
31	48.2	48.7	49.7	51.2	**52.9**	54.6	56.1	57.0	57.6
32	49.7	50.3	51.3	52.9	**54.6**	56.4	58.0	58.9	59.5
33	51.1	51.8	52.8	54.5	**56.3**	58.1	59.8	60.8	61.5
34	52.5	53.1	54.2	56.0	**57.9**	59.9	61.6	62.7	63.4
35	53.7	54.4	55.5	57.4	**59.5**	61.5	63.4	64.5	65.2
36	54.8	55.6	56.8	58.8	**60.9**	63.1	65.1	66.3	67.0
37	55.9	56.7	58.0	60.1	**62.4**	64.7	66.8	68.0	68.8
38	56.9	57.7	59.0	61.3	**63.7**	66.2	68.4	69.7	70.6
39	57.7	58.6	60.0	62.4	**65.0**	67.6	70.0	71.4	72.3
40	58.5	59.4	61.0	63.5	**66.2**	69.0	71.5	73.0	74.0
41	59.2	60.2	61.8	64.5	**67.4**	70.3	73.0	74.6	75.6
42	59.7	60.8	62.5	65.4	**68.5**	71.6	74.4	76.2	77.2

Source: Paladini D et al., *Prenat Diagn* 25, 456–64, 2005.

Table A.6 Nomograms (centiles) for the Italian population: humerus length (mm)[a]

Gestational age (weeks)	3rd	5th	10th	25th	50th	75th	90th	95th	97th
17	20.1	20.6	21.3	22.6	**23.9**	25.2	26.5	27.2	27.7
18	22.6	23.1	23.8	25.0	**26.3**	27.7	28.8	29.6	30.0
19	25.1	25.5	26.2	27.4	**28.7**	30.0	31.2	31.9	32.4
20	27.4	27.9	28.6	29.7	**31.0**	32.3	33.5	34.2	34.6
21	29.7	30.1	30.8	32.0	**33.3**	34.6	35.7	36.5	36.9
22	31.9	32.3	33.0	34.2	**35.5**	36.8	37.9	38.7	39.1
23	34.0	34.4	35.1	36.3	**37.6**	38.9	40.1	40.8	41.3
24	36.0	36.4	37.2	38.4	**39.7**	41.0	42.2	42.9	43.4
25	37.9	38.4	39.1	40.3	**41.7**	43.0	44.2	45.0	45.4
26	39.7	40.2	40.9	42.2	**43.6**	45.0	46.2	47.0	47.4
27	41.4	41.9	42.7	44.0	**45.4**	46.8	48.1	48.9	49.4
28	43.1	43.6	44.4	45.7	**47.2**	48.6	50.0	50.8	51.3
29	44.6	45.1	45.9	47.3	**48.8**	50.4	51.7	52.6	53.1
30	46.0	46.5	47.4	48.8	**50.4**	52.0	53.4	54.3	54.9
31	47.3	47.9	48.8	50.3	**51.9**	53.6	55.1	56.0	56.5
32	48.5	49.1	50.0	51.6	**53.3**	55.0	56.6	57.6	58.2
33	49.6	50.2	51.2	52.8	**54.6**	56.4	58.1	59.1	59.7
34	50.5	51.2	52.2	53.9	**55.8**	57.7	59.5	60.5	61.1
35	51.3	52.0	53.1	54.9	**56.9**	58.9	60.7	61.8	62.5
36	52.1	52.8	53.9	55.8	**57.9**	60.0	61.9	63.1	63.8
37	52.6	53.4	54.6	56.6	**58.8**	61.0	63.0	64.3	65.0
38	53.1	53.9	55.2	57.3	**59.6**	61.9	64.0	65.3	66.1
39	53.4	54.2	55.6	57.8	**60.3**	62.7	64.9	66.3	67.1
40	53.6	54.5	55.9	58.2	**60.8**	63.4	65.8	67.2	68.1
41	53.6	54.5	56.1	58.5	**61.2**	64.0	66.4	67.9	68.9
42	53.5	54.5	56.1	58.7	**61.6**	64.4	67.0	68.6	69.6

[a] Paladini D et al., *Prenat Diagn* 25, 456–64, 2005.

Table A.7 Nomograms (centiles) for the Italian population: ulna length (mm)

Gestational age (weeks)	3rd	5th	10th	25th	50th	75th	90th	95th	97th
17	19.9	20.3	20.9	21.9	**22.9**	24.0	25.0	25.6	26.0
18	21.9	22.3	23.0	24.0	**25.2**	26.4	27.5	28.1	28.5
19	23.9	24.3	25.0	26.2	**27.4**	28.7	29.8	30.5	31.0
20	25.8	26.3	27.0	28.3	**29.6**	30.9	32.2	32.9	33.4
21	27.7	28.2	29.0	30.3	**31.7**	33.1	34.4	35.2	35.7
22	29.6	30.1	30.9	32.3	**33.8**	35.3	36.6	37.4	38.0
23	31.4	32.0	32.8	34.2	**35.8**	37.3	38.8	39.6	40.2
24	33.2	33.7	34.6	36.1	**37.7**	39.4	40.9	41.7	42.3
25	34.9	35.5	36.4	38.0	**39.7**	41.3	42.9	43.8	44.4
26	36.6	37.2	38.2	39.8	**41.5**	43.3	44.8	45.8	46.4
27	38.2	38.8	39.8	41.5	**43.3**	45.1	46.8	47.8	48.4
28	39.8	40.5	41.5	43.2	**45.0**	46.9	48.6	49.6	50.3
29	41.4	42.0	43.1	44.8	**46.7**	48.7	50.4	51.5	52.1
30	42.9	43.5	44.6	46.4	**48.4**	50.3	52.1	53.2	53.9
31	44.3	45.0	46.1	48.0	**50.0**	52.0	53.8	54.9	55.6
32	45.7	46.4	47.6	49.4	**51.5**	53.6	55.4	56.6	57.3
33	47.1	47.8	49.0	50.9	**53.0**	55.1	57.0	58.1	58.8
34	48.4	49.2	50.3	52.3	**54.4**	56.5	58.5	59.7	60.4
35	49.7	50.5	51.7	53.6	**55.8**	57.9	59.9	61.1	61.9
36	51.0	51.7	52.9	54.9	**57.1**	59.3	61.3	62.5	63.3
37	52.2	52.9	54.1	56.2	**58.4**	60.6	62.6	63.8	64.6
38	53.3	54.1	55.3	57.4	**59.6**	61.8	63.9	65.1	65.9
39	54.4	55.2	56.4	58.5	**60.8**	63.0	65.1	66.3	67.1
40	55.5	56.3	57.5	59.6	**61.9**	64.2	66.2	67.5	68.3
41	56.5	57.3	58.5	60.6	**62.9**	65.2	67.3	68.6	69.4
42	57.5	58.3	59.5	61.6	**63.9**	66.2	68.3	69.6	70.4

Source: Paladini D et al., *Prenat Diagn* 25, 456–64, 2005.

Table A.8 Nomograms (centiles) for the Italian population: radius length (mm)

Gestational age (weeks)	3rd	5th	10th	25th	50th	75th	90th	95th	97th
17	17.2	17.5	18.0	18.9	**19.8**	20.7	21.5	22.0	22.3
18	19.2	19.5	20.1	21.0	**22.0**	23.1	24.0	24.6	24.9
19	21.1	21.4	22.1	23.1	**24.3**	25.4	26.4	27.1	27.5
20	22.9	23.3	24.0	25.2	**26.4**	27.7	28.8	29.5	29.9
21	24.7	25.1	25.9	27.1	**28.5**	29.8	31.1	31.8	32.3
22	26.4	26.9	27.7	29.0	**30.5**	31.9	33.3	34.1	34.6
23	28.1	28.6	29.4	30.9	**32.4**	34.0	35.4	36.2	36.8
24	29.7	30.2	31.1	32.6	**34.3**	35.9	37.4	38.3	38.9
25	31.2	31.8	32.8	34.3	**36.1**	37.8	39.4	40.3	40.9
26	32.7	33.3	34.3	36.0	**37.8**	39.6	41.3	42.3	42.9
27	34.1	34.8	35.8	37.6	**39.4**	41.3	43.1	44.1	44.8
28	35.5	36.2	37.3	39.1	**41.0**	43.0	44.8	45.9	46.5
29	36.8	37.5	38.7	40.5	**42.5**	44.6	46.4	47.5	48.2
30	38.1	38.8	40.0	41.9	**44.0**	46.1	48.0	49.1	49.9
31	39.3	40.0	41.2	43.2	**45.3**	47.5	49.5	50.6	51.4
32	40.4	41.2	42.4	44.4	**46.6**	48.8	50.9	52.1	52.8
33	41.5	42.3	43.6	45.6	**47.9**	50.1	52.2	53.4	54.2
34	42.6	43.4	44.6	46.7	**49.0**	51.3	53.4	54.7	55.5
35	43.5	44.3	45.6	47.8	**50.1**	52.5	54.6	55.9	56.7
36	44.5	45.3	46.6	48.7	**51.1**	53.5	55.7	57.0	57.8
37	45.3	46.1	47.5	49.7	**52.1**	54.5	56.7	58.0	58.8
38	46.1	47.0	48.3	50.5	**52.9**	55.4	57.6	58.9	59.8
39	46.9	47.7	49.1	51.3	**53.7**	56.2	58.4	59.8	60.6
40	47.5	48.4	49.8	52.0	**54.5**	57.0	59.2	60.6	61.4
41	48.2	49.0	50.4	52.7	**55.1**	57.6	59.9	61.3	62.1
42	48.8	49.6	51.0	53.2	**55.7**	58.2	60.5	61.9	62.7

Source: Paladini D et al., *Prenat Diagn* 25, 456–64, 2005.

Table A.9 HC/AC, HC/FL, and BPD/FL ratios (centiles) for the diagnosis of microcephaly

Gestational age (weeks)	HC/AC			HC/FL			BPD/FL		
	5th	50th	95th	5th	50th	95th	5th	50th	95th
14	1.13	1.23	1.34	4.93	5.51	6.16	1.75	1.92	2.11
15	1.12	1.22	1.33	4.73	5.29	5.92	1.66	1.82	2.00
16	1.11	1.21	1.32	4.57	5.11	5.71	1.58	1.74	1.91
17	1.10	1.20	1.31	4.43	4.95	5.54	1.52	1.67	1.83
18	1.09	1.19	1.30	4.32	4.83	5.40	1.47	1.61	1.77
19	1.08	1.18	1.29	4.23	4.73	5.29	1.42	1.56	1.71
20	1.07	1.17	1.28	4.16	4.65	5.20	1.39	1.52	1.67
21	1.06	1.17	1.27	4.11	4.59	5.13	1.36	1.49	1.64
22	1.05	1.16	1.26	4.07	4.55	5.08	1.34	1.47	1.61
23	1.04	1.15	1.25	4.04	4.52	5.05	1.32	1.45	1.59
24	1.03	1.14	1.24	4.03	4.50	5.03	1.30	1.43	1.57
25	1.02	1.13	1.23	4.02	4.50	5.03	1.29	1.42	1.56
26	1.01	1.12	1.22	4.03	4.50	5.03	1.29	1.41	1.55
27	1.00	1.11	1.21	4.04	4.51	5.04	1.28	1.41	1.54
28	0.99	1.10	1.20	4.05	4.53	5.06	1.28	1.40	1.54
29	0.98	1.09	1.19	4.07	4.55	5.09	1.28	1.40	1.54
30	0.97	1.08	1.18	4.10	4.58	5.12	1.27	1.40	1.53
31	0.96	1.07	1.17	4.12	4.61	5.15	1.27	1.40	1.53
32	0.95	1.06	1.16	4.15	4.64	5.18	1.27	1.39	1.53
33	0.94	1.05	1.16	4.17	4.67	5.22	1.27	1.39	1.52
34	0.94	1.04	1.15	4.20	4.69	5.24	1.26	1.38	1.52
35	0.93	1.03	1.14	4.21	4.71	5.27	1.25	1.37	1.51
36	0.92	1.02	1.13	4.23	4.73	5.28	1.24	1.36	1.50
37	0.91	1.01	1.12	4.23	4.73	5.29	1.23	1.35	1.48
38	0.90	1.00	1.11	4.23	4.73	5.29	1.21	1.33	1.46
39	0.89	0.99	1.10	4.22	4.71	5.27	1.19	1.30	1.43
40	0.88	0.98	1.09	4.19	4.69	5.24	1.16	1.28	1.40

Source: Modified from Snijders RJM Nicolaides KH, *Ultrasound Obstet Gynecol* 4, 34–8, 1994.
HC: head circumference; AC: abdominal circumference; FL: femur length; BPD: biparietal diameter.

Table A.10 Nomograms (centiles): transverse cerebellar diameters (mm) for the diagnosis of cerebellar hypoplasia

Gestational age (weeks)	5th	50th	95th
15	12	14	15
16	13	15	17
17	14	16	18
18	10	17	19
19	16	18	21
20	17	19	22
21	19	21	24
22	20	22	25
23	21	24	27
24	22	25	28
25	24	26	30
26	25	28	31
27	26	29	33
28	27	31	34
29	29	32	36
30	30	33	37
31	31	35	39
32	32	36	40
33	34	37	42
34	35	39	43
35	36	40	44
36	37	41	46
37	38	42	47
38	39	43	48
39	40	44	49
40	41	45	51

Source: Modified from Goldstein L et al. *Am J Obstet Gynecol* 156, 1065–71, 1987.

Table A.11 Percentile measurements of cerebellar vermis (supero-inferior diameter) according to gestational age

GA (weeks)	Patients	Supero-inferior diameter (mm)				
	n	5th	25th	50th	75th	95th
19–20	18	6.5	9.1	9.5	10.0	11.1
21–22	114	10.1	10.9	11.7	12.1	13.2
23–24	82	11.4	12.3	13.0	13.6	15.2
25–26	20	13.1	14.3	14.8	15.4	16.4
27–28	15	15.3	16.0	16.8	17.9	18.6
29–30	11	15.6	17.5	18.5	20.3	20.9
31–32	13	17.2	19.6	20.1	20.7	21.0
33–34	14	18.3	20.6	21.5	22.8	24.0

Source: Modified from Achiron Z et al., *Ultrasound Obstetric Gynecol* 24, 506–10, 2004.

Table A.12 Mean ± SD measurements obtained by volume contrast imaging in the coronal plane of the cerebellar vermis in 203 normal fetuses

Gestational age (weeks)	Patients (n)	Craniocaudal diameter (mm)	Anteroposterior diameter (mm)
18–19	10	10.5 ± 1.3	8.3 ± 0.8
20–21	19	12.7 ± 1.4	9.1 ± 1.6
22–23	46	14.2 ± 1.6	10.5 ± 1.7
24–25	45	15.8 ± 1.6	12 ± 1.4
26–27	28	17.6 ± 1.7	13.5 ± 1.8
28–29	19	19.6 ± 1.7	13.9 ± 1.1
30–31	16	20.9 ± 1.5	15.5 ± 1.6
32–33	20	22.8 ± 1.6	18.2 ± 1.7

Source: Modified from Vinals F et al., *Ultrasound Obstet Gynecol* 26, 622–62, 2005.

Table A.13 Length of fetal corpus callosum by gestational age

Gestational age (weeks)	Observations (n)	Lower (95% CI)	Mean length (mm)	Upper (95% CI)
16	4	2.95	3.75	4.55
17	8	4.77	6.24	7.70
18	7	10.04	12.51	14.99
19	18	14.51	15.78	17.05
20	21	18.13	18.95	19.77
21	21	19.54	20.38	21.23
22	18	21.53	22.39	23.24
23	22	23.19	24.45	25.72
24	18	26.32	27.61	28.90
25	23	28.66	29.65	30.64
26	18	29.91	31.44	32.98
27	12	32.75	34.33	35.92
28	9	32.30	34.44	36.59
29	10	34.21	36.40	38.59
30	12	37.14	38.33	39.52
31	10	36.18	37.30	38.42
32	7	38.37	40.43	42.49
33	4	31.44	38.50	45.56
34	6	41.40	42.50	43.60
35	5	40.82	45.60	50.38
36	2	40.00	44.00	45.00
37	3	42.5	44.67	46.84

Source: Modified from Achiron R, Achiron A, *Ultrasound Obstet Gynecol* 18, 343–7, 2001.
CI: confidence interval

Table A.14 Width of fetal corpus callosum by gestational age

Gestational age (weeks)	Observations (n)	Lower (95% CI)	Mean width (mm)	Upper (95% CI)
16	4	1.61	2.38	3.14
17	8	2.08	2.63	3.17
18	7	2.82	3.99	5.15
19	18	3.80	4.18	4.55
20	21	3.93	4.43	4.93
21	21	4.40	5.02	5.64
22	18	4.56	4.99	5.43
23	22	4.90	5.39	5.88
24	18	5.49	6.16	6.83
25	23	5.26	5.68	6.11
26	18	5.74	6.40	7.06
27	12	5.72	6.69	7.66
28	9	6.50	7.19	7.88
29	10	5.35	6.18	7.01
30	12	6.45	7.16	7.87
31	10	5.92	6.63	7.34
32	7	5.43	6.61	7.80
33	4	4.81	6.58	8.34
34	6	5.90	7.32	8.73
35	5	5.43	7.16	8.89
36	2	5.60	8.60	8.80
37	3	2.98	7.67	12.36

Source: Modified from Achiron R, Achiron A,. *Ultrasound Obstet Gynecol* 18, 343–7, 2001.
CI: confidence interval

Table A.15 Nomograms (centiles) of binocular (BOD), interocular (IOD), and ocular (OD) diameters (mm) for the diagnosis of hypertelorism, hypotelorism, and microphthalmia

Gestational age (weeks)	BOD			IOD			OD		
	5th	50th	95th	5th	50th	95th	5th	50th	95th
11	5	13	20	—	—	—	—	—	—
12	8	15	23	4	9	13	1	3	6
13	10	18	25	5	9	14	2	4	7
14	13	20	28	5	10	14	3	5	8
15	15	22	30	6	10	14	4	6	9
16	17	25	32	6	10	15	5	7	9
17	19	27	34	6	11	15	5	8	10
18	22	29	37	7	11	16	6	9	11
19	24	31	39	7	12	16	7	9	12
20	26	33	41	8	12	17	8	10	13
21	28	35	43	8	13	17	8	11	13
22	30	37	44	9	13	18	9	12	14
23	31	39	46	9	14	18	10	12	15
24	33	41	48	10	14	19	10	13	15
25	35	42	50	10	15	19	11	13	16
26	36	44	51	11	15	20	12	14	16
27	38	45	53	11	16	20	12	14	17
28	39	47	54	12	16	21	13	15	17
29	41	48	56	12	17	21	13	15	18
30	42	50	57	13	17	22	14	16	18
31	43	51	58	13	18	22	14	16	19
32	45	52	60	14	18	23	14	17	19
33	46	53	61	14	19	23	15	17	19
34	47	54	62	15	19	24	15	17	20
35	48	55	63	15	20	24	15	18	20
36	49	56	64	16	20	25	16	18	20
37	50	57	65	16	21	25	16	18	21
38	50	58	65	17	21	26	16	18	21

Source: Modified from Romero R et al., *Prenatal Diagnosis of Congenital Anomalies*, Appleton & Lange, Norwalk, CT, 1988, 83.

Table A.16 Nomograms (centiles) for external ear length (mm)

Gestational age (weeks)	5th	50th	95th
15	7	9	11
16	8	10	12
17	9	11	13
18	10	12	14
19	11	13	16
20	11	15	17
21	12	16	18
22	13	17	19
23	14	18	21
24	15	19	22
25	16	20	24
26	17	22	26
27	18	23	27
28	18	24	28
29	19	25	29
30	20	26	30
31	21	27	31
32	22	28	32
33	22	28	33
34	23	29	34
35	24	30	35
36	25	30	36
37	25	31	37
38	26	31	37
39	27	32	38
40	27	32	38

Source: Modified from Chitkara U et al., *Am J Obstet Gynecol* 183, 230–4, 2000.

Table A.17 Nomograms (centiles) for nasal bone length (mm) for the diagnosis of nasal bone hypoplasia in Down syndrome

Gestational age (weeks)	5th	50th	95th
14	3.3	4.2	5.0
16	3.1	5.2	1.3
18	5.0	6.3	1.6
20	5.1	1.6	9.5
22	6.0	8.2	10.4
24	6.8	9.4	12.0
26	1.2	9.1	12.3
28	1.8	10.1	13.6
30	8.3	11.3	14.4
32	8.0	11.6	15.2
34	1.5	12.3	11.0

Source: Modified from Guis F et al., *Ultrasound Obstet Gynecol* 5, 304–7, 1995.

Table A.18 Nomograms (centiles) for thoracic circumference (cm) for the diagnosis of thoracic hypoplasia

Gestational age (weeks)	5th	50th	95th
16	6.4	9.1	11.9
17	7.3	10.0	12.8
18	8.2	11.0	13.7
19	9.1	11.9	14.6
20	10.0	12.9	15.5
21	11.0	13.7	16.4
22	11.9	14.6	17.3
23	12.8	15.5	18.2
24	13.7	16.4	19.1
25	14.6	17.3	20.0
26	15.5	18.2	21.0
27	16.4	19.1	21.9
28	17.3	20.0	22.8
29	18.2	21.0	23.7
30	19.1	21.9	24.6
31	20.0	22.8	25.5
32	20.9	23.7	26.4
33	21.8	24.6	27.3
34	22.8	25.5	28.2
35	23.7	26.4	29.1
36	24.6	27.3	30.0
37	25.5	28.2	30.9
38	26.4	29.1	31.9
39	27.3	30.0	32.8
40	28.2	30.9	33.7

Source: Modified from Chitkara U et al., *Am J Obstet Gynecol* 156, 1069, 1987.

Table A.19 Nomograms (centiles) for the measurement of lung volume (cm^3) by three-dimensional ultrasound

Gestational age (weeks)	5th	50th	95th
14	0.3	3.9	11.6
15	0.7	5.3	14.1
16	1.2	6.8	16.9
17	2.0	8.6	20.0
18	2.9	10.6	23.3
19	3.9	12.8	26.8
20	5.1	15.2	30.7
21	6.5	17.8	34.7
22	8.1	20.7	39.0
23	9.8	23.7	43.6
24	11.7	26.9	48.4
25	13.7	30.4	53.5
26	16.0	34.0	58.9
27	18.3	37.9	64.5
28	20.9	42.0	70.3
29	23.6	46.2	76.4
30	26.5	50.7	82.7
31	29.5	55.4	89.3
32	32.8	60.3	96.2
33	36.1	65.4	103.3
34	39.7	70.7	110.7
35	43.4	76.2	118.3
36	47.3	82.0	126.2
37	51.3	87.9	134.3
38	55.5	94.0	142.7
39	59.9	100.4	151.3
40	64.4	107.0	160.2

Source: Modified from Lee A et al., *Am J Obstet Gynecol* 175, 588–92, 1996.

Table A.20 Nomograms (centiles) for fetal stomach diameters: anteroposterior (AP), laterolateral (LL), and supero-inferior (SI)

Gestational age (weeks)	AP diameter (mm)			LL diameter (mm)			SI diameter (mm)		
	5th	50th	95th	5th	50th	95th	5th	50th	95th
13–15	3	4	5	4	6	8	6	9	12
16–18	4	6	8	6	8	10	9	13	17
19–21	6	8	10	7	9	11	11	16	21
22–24	6	9	12	15	18	21	13	19	25
25–27	5	10	15	14	19	24	13	23	33
28–30	9	12	15	12	16	20	18	23	28
31–33	11	14	17	12	16	20	18	23	28
34–36	10	14	18	12	16	20	19	28	37
37–39	12	16	20	16	20	24	23	32	41

Source: Modified from Goldstein I et al., *Obstet Gynecol* 70, 641–4, 1987.

Table A.21 Nomograms (centiles) for right liver lobe length (mm) for the diagnosis of hepatomegaly

Gestational age (weeks)	5th	50th	95th
13	10	13	16
14	11	14	18
15	13	16	19
16	13	17	21
17	14	19	23
18	16	20	25
19	18	22	28
20	18	24	30
21	20	26	32
22	22	28	34
23	23	29	36
24	25	31	38
25	26	33	41
26	28	35	43
27	29	37	45
28	30	39	47
29	32	40	50
30	33	42	52
31	34	43	53
32	35	45	55
33	36	46	56
34	37	47	58

Table A.21 (*Continued*) Nomograms (centiles) for right liver lobe length (mm) for the diagnosis of hepatomegaly

Gestational age (weeks)	5th	50th	95th
35	38	48	60
36	38	49	62
37	39	50	63
38	39	50	63
39	40	51	64
40	40	51	64

Source: Modified from Roberts AB et al., *Am J Obstet Gynecol* 161, 42–6, 1989.

Table A.22 Nomograms (centiles) for spleen length (mm) for the diagnosis of splenomegaly

Gestational age (weeks)	5th	50th	95th
18	7	14	21
20	11	18	26
22	15	22	29
24	19	25	32
26	20	27	34
28	24	31	38
30	27	34	41
32	31	28	45
34	35	43	50
36	41	48	55
38	47	54	62
40	55	62	70

Source: Modified from Schmidt W et al., *J Ultrasound Med* 4, 667–9, 1985.

Table A.23 Nomograms (centiles) for longitudinal diameter of the kidney (mm) for the diagnosis of renal hypoplasia/dysplasia

Gestational age (weeks)	5th	50th	95th
20	16	21	29
22	20	25	33
24	24	29	36
26	27	32	40
28	30	35	42
30	32	38	45
32	34	40	47
34	36	41	48
36	37	42	50
38	38	43	50

Source: Modified from Gloor JM et al., *Mayo Clin Proc* 72, 124–9, 1997.

Table A.24 Nomograms (centiles) for kidney volume (cm^3), calculated by three-dimensional ultrasound, for the diagnosis of renal hypoplasia/dysplasia

Gestational age (weeks)	Right			Left		
	5th	50th	95th	5th	50th	95th
20	0.3	1.5	2.7	0.6	1.8	3.0
21	0.8	2.2	3.6	1.2	2.6	4.0
22	1.4	3.0	4.6	1.7	3.3	4.9
23	1.9	3.7	5.5	2.3	4.1	5.9
24	2.4	4.5	6.5	2.8	4.8	6.9
25	3.0	5.2	7.4	3.4	5.6	7.8
26	3.5	5.9	8.4	4.0	6.5	9.0
27	4.0	6.7	9.3	4.5	7.1	9.8
28	4.5	7.4	10.3	5.0	7.9	10.8
29	5.1	8.2	11.2	5.6	8.7	11.7
30	5.6	8.9	12.2	6.1	9.4	12.7
31	6.1	9.6	13.1	6.7	10.2	13.7
32	6.7	10.4	14.1	7.2	10.9	14.6
33	7.2	11.1	15.0	7.8	11.7	15.6
34	7.7	11.9	16.0	8.3	12.5	16.6
35	8.3	12.6	16.9	8.9	13.2	17.6
36	8.8	13.3	17.9	9.4	14.0	18.5
37	9.3	14.1	18.9	10.0	14.7	19.5
38	9.8	14.8	19.8	10.5	15.5	20.5
39	10.4	15.6	20.7	11.1	16.3	21.4
40	10.9	16.3	21.7	11.8	17.2	21.7

Source: Modified from Yu C et al., *Ultrasound Med Biol* 26, 1253–6, 2000.

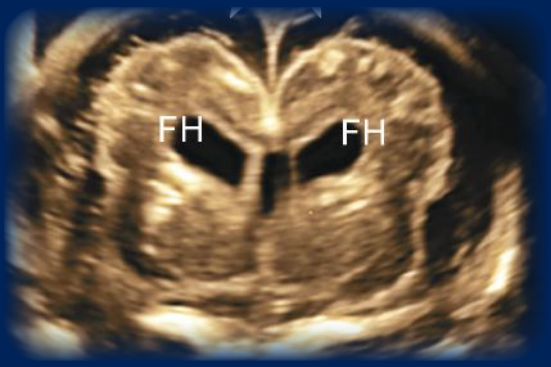
MEDICINE / OBSTETRICS AND GYNECOLOGY

SECOND EDITION

ULTRASOUND OF CONGENITAL FETAL ANOMALIES

Differential Diagnosis and Prognostic Indicators

This extensively illustrated book guides readers through the use of ultrasound (including 3D images) to detect and identify birth defects in utero, with correlated clinical images where appropriate. Up-to-date advice is offered on the differential diagnosis of a wide range of fetal abnormalities. Each anomaly is discussed in a standardized, easy-to-follow format that covers characteristic features, pathogenesis and etiology, differential diagnosis, prognosis, and management. New to this edition are important chapters on first trimester detection, on infection, and on multiple pregnancy, with significant additional material also on cardiac anomalies.



Contents: Anatomic survey of the fetus and early diagnosis of fetal anomalies * Central and peripheral nervous system anomalies * Craniofacial and neck anomalies * Cystic hygroma and nonimmune hydrops fetalis * Congenital heart disease * Thoracic anomalies * Anomalies of the gastrointestinal tract and of the abdominal wall * Anomalies of the urinary tract and of the external genitalia * Skeletal dysplasias and muscular anomalies: a diagnostic algorithm * Chromosomal and nonchromosomal syndromes * Ultrasound in fetal infection * Ultrasound in multiple pregnancy

Dario Paladini, MD, Head, Fetal Medicine and Surgery Unit, Gaslini Childrens' Hospital, Genoa, Italy

Paolo Volpe, MD, Head, Fetal Medicine Unit, Department of Obstetrics and Gynecology, Hospitals Di Venere and Sarcone, Bari, Italy

Foreword by Yves Ville

CRC Press
Taylor & Francis Group
an informa business
www.crcpress.com

6000 Broken Sound Parkway, NW
Suite 300, Boca Raton, FL 33487
711 Third Avenue
New York, NY 10017
2 Park Square, Milton Park
Abingdon, Oxon OX14 4RN, UK

K20928
ISBN-13: 978-1-4665-9896-6
90000
9 781466 598966